ORGANOMETALLICS

Volume 5, Number 1, January 1986

Reactivity Patterns of Heterobinuclear Carbonyls: Site Selectivity in Substitution Reactions of $(CO)_4Ru(\mu\text{-}PPh_2)Co(CO)_3$ with Phosphines and the X-ray Structure of $(Ph_3P)Ru(CO)_3(\mu\text{-}PPh_2)Co(CO)_3$

Rachid Regragui and Pierre H. Dixneuf*

Laboratoire de Chimie de Coordination Organique, Université de Rennes, Campus de Beaulieu, 35042 Rennes Cedex, France

Nicholas J. Taylor and Arthur J. Carty*

(GWC)², Waterloo Campus, Chemistry Department, University of Waterloo, Waterloo, Ontario, Canada N2L 3G1

Received March 12, 1985

The substitution behavior of the phosphido-bridged heterobinuclear carbonyl $(CO)_4Ru(\mu\text{-}PPh_2)Co(CO)_3$, **1**, toward phosphines L [PPh_2H, PMe_3, PMe_2Ph, $PPhMe_2$, $PPh_2C{\equiv}CR$ (R = *t*-Bu, Ph), PPh_3] has been investigated. A series of monosubstitution products $(L)(CO)_3Ru(\mu\text{-}PPh_2)Co(CO)_3$, **2**, and of disubstitution products $L_2(OC)_2Ru(\mu\text{-}PPh_2)Co(CO)_3$, **3**, has been characterized by spectroscopic methods including variable-temperature ^{31}P NMR spectroscopy. The crystal structure of $(PPh_3)(CO)_3Ru(\mu\text{-}PPh_2)Co(CO)_3$ has been determined. Crystal data: monoclinic space group $P2_1/n$, a = 13.669 (2) Å, b = 11.583 (3) Å, c = 20.908 (5) Å, β = 95.72 (2)°, Z = 4. The structure was solved by heavy-atom methods and refined anisotropically to R and R_w values of 0.025 and 0.028, respectively. The phosphine is located on the ruthenium atom trans to the Ru–Co bond and equatorially cis to the μ-PPh_2 group. The Ru–Co distance is 2.7681 (4) Å, and the Ru–P (1)–Co angle at the phosphido bridge is 75.5 (0)°. The ruthenium atom has quasi-octahedral stereochemistry while the cobalt atom coordination sphere can be described as a severely distorted square pyramid. ^{31}P NMR studies have demonstrated that monosubstitution occurs exclusively on the ruthenium atom and at equatorial sites generating mixtures of two geometrical isomers readily distinguishable in solution. Selectivity toward substitution on the ruthenium atom has also been observed for disubstitution. The product $(PPh_2H)_2(CO)_2Ru(\mu\text{-}PPh_2)Co(CO)_3$, **4** (L = PPh_2H), has an exceedingly complex ^{31}P NMR spectrum in solution due to the presence of four isomeric structures arising from the mutual arrangement of two phosphines and a phosphido bridge around the ruthenium atom. A complete analysis of the spectrum of **4** (L = PPh_2H) by the COSY NMR technique is presented.

A topic of considerable importance in the chemistry of mixed-metal systems is the extent to which different metals exhibit site selectivity toward particular substrates. Although many heteropolymetallic compounds have now been synthesized, information on this key point is generally lacking[1] even for the simplest substitution reactions. From the relatively few detailed studies which have appeared to date[1,2-8] there is some evidence that a kinetically labile metal may exert an activating influence on a second metal, which in mononuclear compounds might be considered kinetically stable. The presence of such cooperative effects implies that the substitution behavior of heteronuclear species might not be readily predictable from the chemistry of the individual metals. However, Vahrenkamp[9] has recently shown that for the mixed cluster $Ru_2Co_2(CO)_{13}$, the

(1) (a) For a recent review of mixed-metal compounds see: Roberts, D. A.; Geoffroy, G. L. In "Comprehensive Organometallic Chemistry"; Wilkinson, G., Stone, F. G. A., Abel, E. W., Eds.; Pergamon Press: Oxford, 1982; Chapter 40. (b) For a recent discussion of metal carbonyl substitution reactions see: Atwood, J. D. "Inorganic and Organometallic Reaction Mechanisms"; Brooks/Cole: Belmont, CA, 1985.

(2) (a) Fawcett, J. P.; Poe, A. J. *J. Chem. Soc., Dalton Trans.* **1976**, 2039. (b) Sonnenberger, D.; Atwood, J. D. *J. Am. Chem. Soc.* **1980**, *102*, 3484. (c) Fawcett, J. P.; Poe, A. J.; Sharma, K. R. *J. Am. Chem. Soc.* **1976**, *98*, 1401.

(3) Langenbach, H. J.; Vahrenkamp, H. *Chem. Ber.* **1979**, *112*, 3773.

(4) Cooke, G. C.; Mays, M. J. *J. Chem. Soc., Dalton Trans.* **1975**, 455.

(5) Huie, B. T.; Knobler, C. B.; Kaesz, H. D. *J. Am. Chem. Soc.* **1978**, *100*, 3059.

(6) Teller, R. G.; Wilson, R. D.; McMullen, R. D.; Koetzle, T. F.; Bau, R. *J. Am. Chem. Soc.* **1978**, *100*, 3071.

(7) Fox, J. R.; Gladfelter, W. L.; Wood, T. G.; Smegal, J. A.; Foreman, T. K.; Geoffroy, G. L.; Tavaniepour, I.; Day, V. W.; Day, C. S. *Inorg. Chem.* **1981**, *20*, 3214.

(8) Breen, M. J.; Shulman, P. M.; Geoffroy, G. L.; Rheingold, A. L.; Fultz, W. C. *Organometallics* **1984**, *3*, 782.

(9) Roland, E.; Vahrenkamp, H. *Organometallics* **1983**, *2*, 183.

0276-7333/86/2305-0001$01.50/0

heterosite specificity toward H_2 and acetylenes as substrates is exactly that predictable from the known affinity of cobalt for acetylenes and ruthenium clusters for hydrogen. A further complicating factor for mixed-metal di- or polynuclear compounds is the possibility of metal–metal bond cleavage with ligand association[10] sometimes followed by isomerization as has been found for example in Me_2As-bridged binuclear systems.[3]

We have recently described a new synthesis of mixed Ru/Co compounds involving reactions of $Co_2(CO)_8$ with (arene)$RuCl_2(Ph_2PX)$ (X = H, Cl).[11] Via this route, quantities of the binuclear, phosphido-bridged complex $(CO)_4Ru(\mu\text{-}PPh_2)Co(CO)_3$ (1) became available for reactivity studies. In this paper we report the synthesis of monosubstitution $(L)(CO)_3Ru(\mu\text{-}PPh_2)Co(CO)_3$ (2) (L = PPh_2H, PMe_3, $PPhMe_2$, PPh_2Me, $PPh_2C{\equiv}CR$ (R = *t*-Bu, Ph), PPh_3) products and their complete characterization by spectroscopic methods including variable-temperature ^{31}P NMR spectroscopy. The structure of $(Ph_3P)(CO)_3Ru(\mu\text{-}PPh_2)Co(CO)_3$, a monosubstitution product, has been determined by single-crystal X-ray diffraction. It is evident from ^{31}P NMR data that the parent carbonyl $(CO)_4Ru(\mu\text{-}PPh_2)Co(CO)_3$ exhibits considerable site selectivity toward phosphines, with substitution on ruthenium being overwhelmingly favoured. It is significant that $(Ph_3P)(CO)_3Ru(\mu\text{-}PPh_2)Co(CO)_2(PPh_3)$, a compound prepared serendipitously via another route,[12] does not appear to be accessible via direct substitution on $(CO)_4Ru(\mu\text{-}PPh_2)Co(CO)_3$.

Experimental Section

General Procedure for the Synthesis of $L_n(CO)_{4-n}Ru(\mu\text{-}PPh_2)Co(CO_3)$ (n = 1, 2). Complex 1[11] (0.54 g, 1 mmol) and phosphorus derivative L (1 mmol) were dissolved in 60 mL of THF under nitrogen and heated at 50–65 °C for several hours. The course of the reaction was followed by analysis of the reaction products using silica gel thin-layer chromatography (C_6H_{14}). The starting complex 1 migrates first, followed by the orange, monosubstitution products (n = 1) and then by the orange-red disubstitution compounds (n = 2). After complex 1 had almost completely disappeared, the solvent was removed and ether (10 mL) was added to the oily products which then solidified. The solid products were chromatographed on a column of Florisil to eliminate the residual starting complex and separate mono- and disubstitution products.

$(PPh_3)(CO)_3Ru(\mu\text{-}PPh_2)Co(CO)_3$ (2a). 1 (0.54 g) and PPh_3 (0.30 g) in 60 mL of THF were heated at 50 °C for 12 h. The reaction products were then chromatographed on a Florisil column (eluant CH_2Cl_2–hexane). Crystallization from dichloromethane–ether afforded dark red crystals (0.62 g, 80%): mp 195–198 °C. Anal. Calcd for $C_{36}H_{25}O_6P_2CoRu$: C, 55.75; H, 3.25; P, 7.98. Found: C, 56.07; H, 3.25; P, 7.70. IR (C_6H_{12}, cm^{-1}): 2076 (sh), 2017 (s), 2004 (vs), 1981 (m), 1950 (s, br). ^1H NMR (CD_2Cl_2, δ): 7–8 (m, C_6H_5). ^{31}P NMR (32.38 MHz, CD_2Cl_2, 193 K, δ): trans isomer, 183.6 (d, μ-PPh_2) and 32.5 (d, PPh_3), $^2J_{PP}$ = 104.2 Hz; cis isomer, 170.3 (s, μ-PPh_2) and 37.1 (s, PPh_3).

$(Ph_2PC{\equiv}C\text{-}t\text{-}Bu)(CO)_3Ru(\mu\text{-}PPh_2)Co(CO)_3$ (2b) and $(Ph_2PC{\equiv}C\text{-}t\text{-}Bu)_2(CO)_3Ru(\mu\text{-}PPh_2)Co(CO)_3$ (3b). 1 (0.54 mg) and $Ph_2PC{\equiv}C$-*t*-Bu (0.35 g, 1.3 mmol) were heated in refluxing THF (60 mL) for 6 h. The products were chromatographed on a Florisil column (eluant CH_2Cl_2–hexane). The product from the first fraction was crystallized in dichloromethane–hexane to afford small, brown crystals of **2b** (0.47 g, 60%). The residue obtained from the second fraction was crystallized in dichloromethane–hexane to give thin, dark-red crystals of **3b** (0.26 g, 25%).

2b: mp 125–130 °C. Anal. Calcd for $C_{36}H_{29}O_6P_2CoRu$: C, 55.46; H, 3.75; P, 7.95. Found: C, 55.60; H, 3.64; P, 7.70. IR (C_6H_{12}, cm^{-1}): ν(CO) 2078 (sh), 2017 (s), 2005 (vs), 1982 (m), 1950 (s, br); ν(C≡C) 2174 (w). ^1H NMR ($CDCl_3$, 300 K, δ): 7–8 (m, C_6H_5); 1.4 (s, *t*-Bu). ^{31}P NMR (101.2 MHz, $CDCl_3$, 223 K, δ): trans isomer, 189.4 (d, μ-PPh_2) and 3.1 (d, $Ph_2PC{\equiv}C$-*t*-Bu), $^2J_{PP}$ = 103.8 Hz; cis isomer, 173.2 (d, μ-PPh_2) and 4.8 (d, $Ph_2PC{\equiv}C$-*t*-Bu), $^2J_{PP}$ = 2.4 Hz.

3b: mp 170–173 °C. Anal. Calcd for $C_{53}H_{48}O_5P_3CoRu$: C, 62.54; H, 4.75; P, 9.13. Found: C, 62.32; H, 4.72; P, 9.07. IR (C_6H_{12}, cm^{-1}): ν(CO) 2041 (w), 1994 (s), 1973 (vs), 1940 (m), 1925 (m); ν(C≡C), 2167 (w). ^1H NMR ($CDCl_3$, 300 K, δ): 7–8 (m, C_6H_5), 1.54 and 1.48 (s, *t*-Bu). ^{31}P NMR (32.38 MHz, 223 K, δ): 183.4 (d, μ-PPh_2) and 8.6 (d, *trans*-$Ph_2PC{\equiv}C$), $^2J_{PP}$ = 109 Hz; 11.7 (s, *cis*-$Ph_2PC{\equiv}C$-*t*-Bu).

$(Ph_2PC{\equiv}CPh)(CO)_3Ru(\mu\text{-}PPh_2)Co(CO)_3$ (2c) and $(Ph_2PC{\equiv}CPh)_2(CO)_2Ru(\mu\text{-}PPh_2)Co(CO)_3$ (3c). 1 (0.54 g) and $Ph_2PC{\equiv}CPh$ (0.37 g, 1.3 mmol) were heated in THF (60 mL) at reflux for 6 h. Chromatography on a column of Florisil (eluant CH_2Cl_2–C_6H_{14}) afforded a first red fraction from which were obtained brown cystals of **2c** (0.48 g, 60%) and a second red fraction which yielded dark red crystals of **3c** (0.26 g, 25%) after crystallization in a dichloromethane–hexane mixture.

2c: mp 115–120 °C. Anal. Calcd for $C_{38}H_{25}O_6P_2CoRu$: C, 57.08; H, 3.15; P, 7.75. Found: C, 57.20; H, 3.18; P, 7.50. IR (C_6H_{12}, cm^{-1}): ν(CO) 2079 (sh), 2018 (s), 2006 (vs), 1983 (m), 1952 (s, br); ν(C≡C) 2174 (w). ^1H NMR ($CDCl_3$, 300 K δ): 7–8 (m, C_6H_5). ^{31}P NMR (32.38 MHz, $CDCl_3$, 223 K, δ): trans isomer, 190.6 (d, μ-PPh_2) and 5.4 (d, $Ph_2PC{\equiv}CPh$), $^2J_{PP}$ = 102 Hz; cis isomer, 174.0 (s, μ-PPh_2), and 6.9 (s, $Ph_2PC{\equiv}CPh$).

3c: mp 135–140 °C. Anal. Calcd for $C_{57}H_{40}O_5P_3CoRu$: C, 64.72; H, 3.81; P, 8.78. Found: C, 64.34; H, 3.79; P, 8.63. IR (C_6H_{12}, cm^{-1}): ν(CO) 2040 (sh), 1995 (s), 1973 (vs), 1941 (m), 1927 (m); ν(C≡C) 2167 (w). ^1H NMR ($CDCl_3$, 300 K, δ): 7–8 (m, C_6H_5). ^{31}P NMR (32.38 MHz, $CDCl_3$, 223 K, δ): 185.2 (d, μ-PPh_2) and 10.3 (d, *trans*-$Ph_2PC{\equiv}CPh$), $^2J_{PP}$ = 110 Hz; 12.0 (s, *cis*-$Ph_2PC{\equiv}CPh$).

$(PPh_2Me)(OC)_3Ru(\mu\text{-}PPh_2)Co(CO)_3$ (2d) and $(PPh_2Me)_2(OC)_2Ru(\mu\text{-}PPh_2)Co(CO)_3$ (3d). 1 (0.54 g) and PPh_2Me (0.3 g, 1.5 mmol) in 50 mL of THF were heated at 60–65 °C for 8 h. Chromatography of the reaction products on a column of Florisil (eluant CH_2Cl_2–hexane) afforded two red fractions. From the first fraction light red crystals of **2d** were obtained after crystallization in CH_2Cl_2/hexane (0.11 g, 15%). From the second fraction red crystals, crystallized from CH_2Cl_2–hexane, of **3d** were obtained (0.53 g, 60%).

2d: mp 110–115 °C. Anal. Calcd for $C_{31}H_{23}O_6P_2CoRu$: C, 52.19; H, 3.25; P, 8.68. Found: C, 52.00; H, 3.28; P, 8.08. IR (C_6H_{12}, cm^{-1}): ν(CO) 2076 (w), 2013 (m), 2005 (vs), 1982 (m), 1950 (m), 1935 (m). ^1H NMR ($CDCl_3$, 300 K, δ): 7.5–8.0 (m, C_6H_5), 2.20 (d, *trans*-P*Me*Ph_2, $^2J_{PH}$ = 7.5 Hz), 1.60 (s, br, *cis*-P*Me*Ph_2). ^{31}P NMR (32.38 MHz, $CDCl_3$, 213 K, δ): trans isomer, 185.1 (d, μ-PPh_2), 12.2 (d, *trans*-$PMePh_2$), $^2J_{PP}$ = 102.5 Hz; cis isomer, 171.1 (s, μ-PPh_2), 15.4 (s, *cis*-$PMePh_2$).

3d: mp 150–155 °C. Anal. Calcd for $C_{43}H_{36}O_5P_3CoRu$: C, 58.31; H, 4.10; P, 10.49. Found: C, 58.23; H, 4.00; P, 10.32. IR (C_6H_{12}, cm^{-1}): ν(CO) 2033 (w), 1992 (vs), 1963 (s), 1938 (m), 1921 (w). ^1H NMR ($CDCl_3$, 213 K, δ) 7.2–8.0 (m, C_6H_5), 2.20 (d, *trans*-P*Me*Ph_2, $^2J_{PH}$ = 7.6 Hz), 1.80 (d, *cis*-P*Me*Ph_2, $^2J_{PH}$ = 8.0 Hz). ^{31}P NMR (32.38 MHz, $CDCl_3$, 213 K, δ): 178.4 (d, μ-PPh_2), 10.2 (d, *trans*-$PMePh_2$), $^2J_{PP}$ = 107.4 Hz; 15.0 (s, *cis*-$PMePh_2$).

$(PMe_2Ph)(CO)_3Ru(\mu\text{-}PPh_2)Co(CO)_3$ (2e) and $(PMe_2Ph)_2(CO)_2Ru(\mu\text{-}PPh_2)Co(CO)_3$ (3e). 1 (0.54 g) and PMe_2Ph (0.20 g, 1.5 mmol) in 50 mL of THF were heated at 60–65 °C for 8 h. By chromatography of the reaction products on thick-layer silica gel plates (eluant C_6H_{14}–Et_2O) two fractions were obtained and their corresponding products were crystallized from dichloromethane–ether mixtures. From the first, orange-red fraction, cubic crystals of **2e** (0.07 g, 10%) were obtained, whereas from the second, red fraction light red crystals of **3e** (0.54 g, 70%) were isolated.

(10) See for example: (a) Huttner, G.; Schneider, J.; Muller, H. D.; Mohr, G.; von Seyerl, J.; Wohlfahrt, L. *Angew. Chem., Int. Ed. Engl.* **1979**, *18*, 76. (b) Vahrenkamp, H.; Wolters, D. *Organometallics* **1982**, *1*, 847. (c) Johnson, B. F. G.; Lewis, J.; Nelson, W. J. H.; Nicholls, J. N.; Vargas, M. D. *J. Organomet. Chem.* **1983**, *249*, 255 and references therein. (d) MacLaughlin, S. A.; Taylor, N. J.; Carty, A. J. *Organometallics* **1983**, *2*, 1194. (e) Field, J. S.; Haines, R. J.; Smit, D. N.; Natarajan, K.; Scheidsteger, O.; Huttner, G. *J. Organomet. Chem.* **1982**, *240*, C23.

(11) (a) Regragui, R.; Dixneuf, P. H. *J. Organomet. Chem.* **1982**, *239*, C12. (b) Regragui, R.; Dixneuf, P. H.; Taylor, N. J., Carty, A. J. *Organometallics* **1984**, *3*, 1020.

(12) Foley, H. C.; Finch, W. C.; Pierpont, C. G.; Geoffroy, G. L. *Organometallics* **1982**, *1*, 1379.

2e: mp 118–120 °C. Anal. Calcd for $C_{26}H_{21}O_6P_2CoRu$: C, 47.94; H, 3.25; P, 9.51. Found: C, 47.75; H, 3.22; P, 9.40. IR (C_6H_{12}, cm^{-1}): ν(CO) 2074 (w), 2010 (s), 2004 (vs), 1988 (sh), 1982 (m, br), 1950 (m, br), 1929 (m, br). ^1H NMR ($CDCl_3$, 300 K, δ): 7.5 (m, C_6H_5); trans isomer, 2.1 (d, PMe_2Ph, $^2J_{PH}$ = 8.4 Hz); cis isomer, 1.4 (s, br, PMe_2Ph). ^{31}P NMR (32.38 MHz, $CDCl_3$, 223 K, δ): *trans isomer*, 183.5 (d, μ-PPh_2), −6.1 (d, PMe_2Ph), $^2J_{PP}$ = 97.6 Hz; cis isomer, 171.8 (s, μ-PPh_2), −2.1 (s, PMe_2Ph).

3e: mp 148–152 °C. Anal. Calcd for $C_{33}H_{32}O_5P_3CoRu$: C, 52.05; H, 4.23; P, 12.20. Found: C, 52.26; H, 4.09; P, 12.43. IR (C_6H_{12}, cm^{-1}): ν(CO) 2034 (w), 1989 (s), 1963 (vs), 1934 (m), 1911 (m). ^1H NMR ($CDCl_3$, 300 K, δ): 7–7.5 (m, C_6H_5), 1.95 (d) and 1.93 (d) (*trans*-PMe_2Ph, $^2J_{PH}$ = 8.5 Hz); 1.51 (d, *cis*-PMe_2Ph, $^2J_{PH}$ = 9 Hz). ^{31}P NMR (32.38 MHz, $CDCl_3$, 213 K, δ) 176.0 (d, μ-PPh_2) and −4.1 (d, *trans*-PMe_2Ph), $^2J_{PP}$ = 105 Hz; 1.9 (s, *cis*-PMe_2Ph).

$(PMe_3)(CO)_3Ru(\mu\text{-}PPh_2)Co(CO)_3$ (2f). 1 (0.54 g) and PMe_3 (0.1 g, 1.3 mmol) in 50 mL of THF were heated at 50 °C for 5–6 h. Chromatography on Florisil (eluant CH_2Cl_2–C_6H_{14}) afforded a red fraction from which dark red crystals of **2f** (0.47 g, 80%) were obtained after crystallization in CH_2Cl_2–hexane and then an orange-red fraction containing traces of disubstitution products.

2f: mp 115–118 °C. Anal. Calcd for $C_{21}H_{19}O_6P_2CoRu$: C, 42.80; H, 3.35; P, 10.51. Found: C, 42.65; H, 3.25; P, 10.62. IR (C_6H_{12}, cm^{-1}): ν(CO) 2100 (w), 2005 (s), 1987 (m), 1958 (m), 1930 (w). ^1H NMR ($CDCl_3$, 300 K, δ): 7.5 (m, C_6H_5), 1.7 (d, PMe_3, $^2J_{PH}$ = 9 Hz). ^{31}P NMR (32.38 MHz, $CDCl_3$, 223 K, δ): +182.4 (μ-PPh_2), −15.2 (d, PMe_3), $^2J_{PP}$ = 95 Hz.

$(PPh_2H)_2(CO)_2Ru(\mu\text{-}PPh_2)Co(CO)_3$ (4). Complex 1[11] (0.54 g, 1 mmol) and diphenylphosphine (0.26 g, 1.4 mmol) in 60 mL of THF were heated at 60 °C for 12 h. The color of the solution changed from dark red to light red. The solvent was removed under vacuum, and the products were chromatographed on thick layers of silica gel (eluant ether). A minor, orange fraction migrates first, corresponding probably to the monosubstitution product. From the major, orange fraction which migrated slowly (CH_2Cl_2–ether), brillant, red crystals of **4** (0.5 g, 60%) were isolated after crystallization in CH_2Cl_2–ether.

4: mp 165–170 °C. Anal. Calcd for $C_{41}H_{32}O_5P_3CoRu$: C, 57.42; H, 3.76; P, 10.83. Found: C, 57.21, H, 3.72; P, 9.29. IR (C_6H_{12}, cm^{-1}): ν(CO) 2032 (w), 2020 (m), 2015 (m), 1995 (m), 1991 (m), 1981 (vs), 1956 (s), 1939 (s), 1929 (s), 1925 (s). ^1H NMR (CD_2Cl_2, 300 K, δ): 7–7.5 (m, C_6H_5), 6.8 (md, Ph_2PH, $^1J_{PH}$ = 360 Hz).

Spectroscopic Measurements. Infrared spectra were recorded on Perkin-Elmer 457 and 180 instruments as Nujol mulls or as solutions in cyclohexane using 0.5-mm matched sodium chloride cells. ^1H NMR spectra at 80 MHz and ^{31}P spectra at 32.38 MHz were obtained on a Bruker WP-80 FT spectrometer in the Centre de Mésures de l'Ouest à l'Université de Rennes. Higher field ^{31}P spectra were measured at 101.20 and 161.90 MHz on Bruker AM-250 and WH-400 spectrometers in the Guelph-Waterloo Centre for Graduate Work in Chemistry. The WH-400 instrument is a part of the Southwestern Ontario Regional NMR Centre. Chemical shifts for ^1H are relative to internal Me_4Si and for ^{31}P with respect to external 85% H_3PO_4. Microanalytical data were obtained from Le Laboratoire de Microanalyse du CNRS à Villeurbanne.

X-ray Structural Analysis of $RuCo(CO)_6(\mu\text{-}PPh_2)(PPh_3)$. A deep red crystal was rounded into a sphere by partial dissolution in CH_2Cl_2–ether, attached to a eucentric goniometer head, and mounted on a Syntex $P2_1$ diffractometer for preliminary examination. Fifteen strong reflections well dispersed in reciprocal space were centered and used to generate unit cell vectors. The Syntex autoindexing and cell refinement procedures generated the monoclinic unit cell listed in Table I. A systematic check of absences $0k0$, $k = 2n + 1$, and $h0l$, $h + l = 2n + 1$, confirmed the space group assignment.

Intensity data were collected at 297 ± 2 K by using graphite-monochromated Mo Kα radiation with θ–2θ scans (Table I). Data were corrected for Lorentz and polarization effects.

The two heavy atoms were located in a Patterson synthesis and all other non-hydrogen atoms via Fourier maps. R values ($R = \sum||F_o| - |F_c||/\sum|F_o|$) at various stages of refinement are given in Table I. Several cycles of full-matrix least-squares refinement with anisotropic parameters for all non-hydrogen atoms gave R = 0.039, and a difference Fourier synthesis revealed positions for all hydrogen atoms in the molecule. These were included and refined isotropically in subsequent cycles. The final R and R_w ($R_w = [\sum w(|F_o| - |F_c|)^2/\sum w(|F_o|)^2]^{1/2}$ values were 0.025 and 0.028 with $\sum w(\Delta|F|)^2$ being the function minimized. Scattering factors used were those listed in the ref 13. Corrections for the real and imaginary components of anomalous scattering were included for Ru and Co. Computations were carried out on IBM 4341 systems in the University of Waterloo Computing Centre using programs described elsewhere.[14] Table II contains atomic positions and Table III a selection of bond lengths and angles. Thermal parameters (Table S1) and other bond lengths and angles (Table S2) have been deposited with structure factors (Table S3).

Table I. Crystal Data, Intensity Collection, Reduction, and Refinement for $RuCo(CO)_6(\mu\text{-}PPh_2)(PPh_3)$

formula	$RuCoP_2O_6C_{36}H_{25}$
mol wt	775.55
cryst class	monoclinic
space group	$P2_1/n$
a, Å	13.669 (2)
b, Å	11.583 (3)
c, Å	20.908 (5)
β, deg	95.72 (2)
V, Å^3	3301 (1)
Z	4
ρ_{measd}, g cm^{-3}	1.56
ρ_{calcd}, g cm^{-3}	1.560
$F(000)$	1560
μ(Mo Kα), cm^{-1}	11.13
cryst size, mm	spherical 0.33 diameter
transmissn factors	0.73–0.78
radiatn	Mo Kα (λ = 0.710 69 Å)
max 2θ, deg	45.0
scan speed, deg min^{-1}	variable; 2.93–29.3
scan width, deg	0.8 below Kα_1 to 0.8 above Kα_2
stds (every 100 measurements)	621, 138
variance of stds	±2%
reflctns measd	4347
reflctns obsd ($I \geq 3\sigma(I)$)	3371
R (metal atoms only)	0.37
R(isotropic)	0.058
R(anisotropic)	0.039
final R	0.025
R_w	0.028
w^{-1}	$1.48 - 0.011|F_o| + 0.0013|F_o|^2$
max residuals, e Å^{-3}	0.31

Results and Discussion

Synthesis and Characterization of Phosphine Substitution Products of 1: $L(CO)_3Ru(\mu\text{-}PPh_2)Co(CO)_3$ (2) and $L_2(CO)_2Ru(\mu\text{-}PPh_2)Co(CO)_3$ (3 and 4). The phosphido-bridged heterobimetallic complex 1[11] does not react with tertiary phosphines at room temperature. However, heating mixtures of 1 and ligand for several hours at 50–65 °C in THF leads to the displacement of one or two carbonyls affording mono- and disubstitution products, readily separable by column chromatography on Florisil. In this paper we focus on the characterization of these compounds by microanalysis, infrared spectroscopy, and variable-temperature ^{31}P NMR studies in solution. A parallel kinetic study of these displacement reactions will be reported elsewhere.

Treatment of 1 with 1 equiv of PPh_3 at 50 °C until starting material had been consumed (12 h) gave an 80% yield of monosubstitution product **2a** (L = PPh_3) together with traces of the disubstituted species **3a** (Scheme I).

Under similar conditions but with a 1.3–1.5 molar excess of ligand the phosphinoalkynes $Ph_2PC{\equiv}C\text{-}t\text{-}Bu$ and $Ph_2PC{\equiv}CPh$ afforded **2b** and **2c** (60%) and the disubstituted derivatives **3b** and **3c** (25%) while $PMePh_2$,

(13) "International Tables for X-ray Crystallography"; Kynoch Press, Birmingham, England, 1974.

(14) Carty, A. J.; Mott, G. N.; Taylor, N. J.; Yule, J. E. *J. Am. Chem. Soc.* **1978**, *100*, 351.

Table II. Final Positional Parameters (Fractional × 10^4) and Esd's for $(PPh_3)(CO)_3Ru(\mu\text{-}PPh_2)Co(CO)_3$

(a) Heavy Atoms

atom	x	y	z	atom	x	y	z
Ru	2130.4 (2)	1407.0 (2)	259.5 (1)	C(15)	1933 (3)	5972 (4)	372 (2)
Co	2507.9 (4)	1647.7 (4)	1578.2 (2)	C(16)	2132 (3)	6601 (4)	926 (2)
P(1)	3070.3 (7)	2782.1 (8)	880.9 (4)	C(17)	2601 (3)	6085 (4)	1455 (2)
P(2)	2153.0 (7)	1792.9 (8)	-855.0 (4)	C(18)	2884 (3)	4934 (4)	1443 (2)
O(1)	874 (2)	-762 (3)	315 (2)	C(19)	3397 (2)	1759 (3)	-1106 (2)
O(2)	314 (2)	2846 (3)	490 (1)	C(20)	3658 (3)	1071 (3)	-1603 (2)
O(3)	3925 (2)	-156 (3)	184 (1)	C(21)	4621 (3)	1066 (4)	-1760 (2)
O(4)	4246 (2)	1690 (4)	2481 (2)	C(22)	5318 (3)	1755 (4)	-1434 (2)
O(5)	1067 (2)	3132 (3)	2101 (2)	C(23)	5067 (3)	2437 (4)	-943 (2)
O(6)	1934 (4)	-738 (3)	1766 (2)	C(24)	4111 (3)	2443 (3)	-777 (2)
C(1)	1330 (3)	53 (4)	275 (2)	C(25)	1677 (2)	3191 (3)	-1142 (2)
C(2)	993 (3)	2334 (3)	391 (2)	C(26)	723 (3)	3493 (3)	-1043 (2)
C(3)	3282 (3)	434 (3)	226 (2)	C(27)	345 (3)	4544 (4)	-1237 (2)
C(4)	3571 (3)	1650 (4)	2114 (2)	C(28)	900 (3)	5317 (4)	-1541 (2)
C(5)	1602 (3)	2543 (4)	1877 (2)	C(29)	1833 (3)	5026 (4)	-1660 (2)
C(6)	2150 (4)	194 (4)	1675 (2)	C(30)	2228 (3)	3963 (4)	-1463 (2)
C(7)	4404 (2)	2915 (3)	876 (2)	C(31)	1488 (3)	795 (3)	-1422 (2)
C(8)	4849 (3)	3927 (4)	705 (2)	C(32)	1484 (4)	-366 (4)	-1285 (2)
C(9)	5858 (3)	3988 (4)	698 (2)	C(33)	1036 (5)	-1135 (5)	-1739 (3)
C(10)	6433 (3)	3050 (4)	857 (2)	C(34)	612 (4)	-746 (5)	-2313 (3)
C(11)	6003 (3)	2038 (4)	1028 (2)	C(35)	604 (4)	394 (5)	-2449 (2)
C(12)	4996 (3)	1974 (4)	1036 (2)	C(36)	1046 (3)	1172 (4)	-2014 (2)
C(13)	2691 (2)	4298 (3)	883 (2)				
C(14)	2217 (3)	4818 (3)	349 (2)				

(b) Hydrogen Atoms and Isotropic Thermal Parameters

atom	x	y	z	U, Å^2	atom	x	y	z	U, Å^2
H(8)	444 (2)	455 (3)	61 (1)	38 (10)	H(23)	556 (3)	294 (3)	-69 (2)	63 (13)
H(9)	611 (3)	465 (4)	60 (2)	56 (14)	H(24)	395 (2)	290 (3)	-43 (2)	39 (10)
H(10)	714 (3)	310 (4)	85 (2)	72 (13)	H(26)	35 (2)	296 (3)	-83 (2)	41 (10)
H(11)	641 (2)	141 (3)	116 (1)	41 (9)	H(27)	-30 (3)	474 (3)	-117 (2)	62 (12)
H(12)	474 (2)	132 (3)	117 (2)	42 (11)	H(28)	59 (3)	608 (3)	-167 (2)	65 (12)
H(14)	211 (3)	437 (3)	-5 (2)	53 (11)	H(29)	216 (3)	549 (3)	-187 (2)	48 (11)
H(15)	156 (3)	634 (3)	-2 (2)	48 (12)	H(30)	285 (3)	379 (3)	-155 (2)	50 (11)
H(16)	201 (3)	741 (3)	93 (2)	55 (10)	H(32)	179 (3)	-67 (3)	-89 (2)	56 (13)
H(17)	274 (3)	651 (4)	183 (2)	73 (13)	H(33)	114 (3)	-187 (4)	-161 (2)	75 (15)
H(18)	321 (3)	462 (3)	181 (2)	54 (13)	H(34)	28 (4)	-127 (5)	-260 (3)	116 (20)
H(20)	319 (2)	58 (3)	-182 (1)	36 (9)	H(35)	28 (3)	69 (4)	-284 (2)	69 (15)
H(21)	479 (3)	57 (3)	-204 (2)	51 (12)	H(36)	104 (3)	197 (3)	-212 (2)	50 (12)
H(22)	600 (3)	170 (3)	-155 (2)	60 (12)					

Scheme I

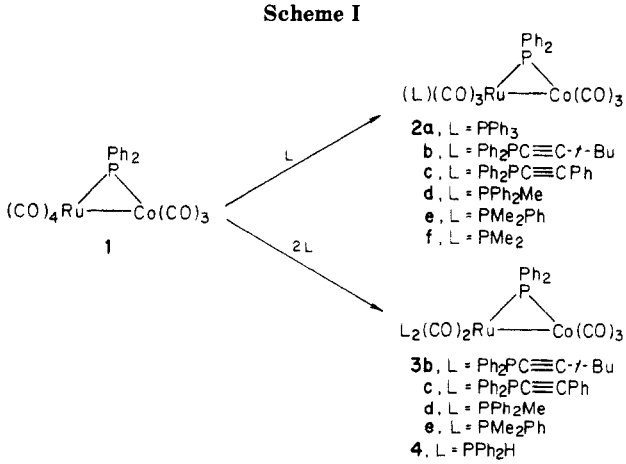

PMe_2Ph, and PMe_3 gave **2d** (15%) and **3d** (60%), **2e** (10%) and **3e** (70%), **2f** (80%) and **3f** (traces), respectively, all yields being those of crystallized compounds.

The reaction of **1** with the secondary phosphine PPh_2H followed a different course. Treatment of **1** in THF for 12 h with 1.2 equiv of PPh_2H gave only the disubstituted complex **4** in 60% yield along with recovered **1** and traces of the monosubstituted material. Microanalysis confirmed that crystalline **4** contained two molecules of phosphine. The $^{31}P\{^1H\}$ NMR spectrum of this compound is complex but can be interpreted (vide infra) in terms of the presence of four different isomers in solution.

The phosphine derivatives **2** and **3** exhibit only terminal ν(CO) bands in their solution IR spectrum and can be readily distinguished by their characteristic band patterns and frequencies. The highest frequency ν(CO) band at 2107 cm^{-1} in **1** is shifted ~30 cm^{-1} to lower frequency in **2** and ~70 cm^{-1} to lower frequency in **3**. Careful examination of the ν(CO) region for the monosubstitution products **2** (Figure 1) also reveals significant variations in intensity and frequency which can be attributed to the presence of isomers arising from the cis and trans disposition of the phosphine coordinated to ruthenium with respect to the phosphido bridge. These changes correlate well with isomer populations established by ^{31}P NMR studies (vide infra).

For the heterobinuclear molecule $(CO)_4Ru(\mu\text{-}PPh_2)Co(CO)_3$ (**1**) substitution of CO by a phosphine might occur at any of the seven different sites in the molecule. Thus in principle a number of isomers could result depending on whether substitution on cobalt or ruthenium, cis or trans to the μ-PPh_2 group occurred. In order to establish the site of substitution in a typical derivative, an X-ray study of **2a** was undertaken.

Description and Discussion of the Structure of $RuCo(CO)_6(\mu\text{-}PPh_2)(PPh_3)$. An ORTEP plot of the molecular structure is shown in Figure 2. There are several significant structural features. (i) The phosphine is coordinated to the ruthenium atom with the $Ru(CO)_3(PPh_3)$ and $Co(CO)_3$ fragments joined by a metal–metal bond (Ru–Co = 2.7681 (4) Å) and a phosphido bridge; the Ru–

Table III. A Selection of Important Bond Distances and Angles for $(PPh_3)(CO)_3Ru(\mu\text{-}PPh_2)Co(CO)_3$

	A. Bond Distances (Å)		
Ru–CO	2.7681 (4)	Ru–P(1)	2.3556 (9)
Bu–P(2)	2.3760 (8)	Ru–C(1)	1.916 (4)
Ru–C(2)	1.934 (4)	Ru–C(3)	1.946 (4)
Co–P(1)	2.161 (1)	Co–C(4)	1.747 (4)
Co–C(5)	1.777 (4)	Co–C(6)	1.771 (5)
P(1)–C(7)	1.834 (3)	P(1)–C(13)	1.831 (4)
P(2)–C(19)	1.834 (3)	P(2)–C(25)	1.825 (3)
P(2)–C(31)	1.833 (4)	C(1)–O(1)	1.140 (5)
C(2)–O(2)	1.139 (5)	C(3)–O(3)	1.125 (5)
C(4)–O(4)	1.141 (5)	C(5)–O(5)	1.137 (5)
C(6)–O(6)	1.139 (6)		
	B. Bond Angles (deg)		
Co–Ru–P(1)	49.1 (0)	Co–Ru–P(2)	159.8 (0)
Co–Ru–C(1)	96.7 (1)	Co–Ru–C(2)	82.9 (1)
Co–Ru–C(3)	91.3 (1)	P(1)–Ru–P(2)	110.7 (0)
P(1)–Ru–C(1)	145.8 (1)	P(1)–Ru–C(2)	87.1 (1)
P(1)–Ru–C(3)	90.6 (1)	P(2)–Ru–C(1)	103.5 (1)
P(2)–Ru–C(2)	97.2 (1)	P(2)–Ru–C(3)	89.0 (1)
C(1)–Ru–C(2)	88.9 (1)	C(1)–Ru–C(3)	89.7 (1)
C(2)–Ru–C(3)	173.8 (1)	Ru–Co–P(1)	55.5 (0)
Ru–Co–C(4)	134.4 (1)	Ru–Co–C(5)	109.9 (1)
Ru–Co–C(6)	89.5 (1)	P(1)–Co–C(4)	95.8 (1)
P(1)–Co–C(5)	101.0 (1)	P(1)–Co–C(6)	140.9 (1)
C(4)–Co–C(5)	109.9 (1)	C(4)–Co–C(6)	98.7 (2)
C(5)–Co–C(6)	107.7 (2)	Ru–P(1)–CO	75.5 (0)
Ru–P(1)–C(7)	122.9 (1)	Ru–P(1)–C(13)	120.7 (1)
Co–P(1)–C(7)	118.5 (1)	Co–P(1)–C(13)	117.5 (1)
C(7)–P(1)–C(13)	101.7 (1)	Ru–P(2)–C(19)	112.4 (1)
Ru–P(2)–C(25)	116.8 (1)	Ru–P(2)–C(31)	117.5 (1)
C(19)–P(2)–C(25)	103.7 (1)	C(19)–P(2)–C(31)	102.6 (1)
C(25)–P(2)–C(31)	102.0 (1)	Bu–C(1)–C(1)	176.5 (1)
Ru–C(2)–O(2)	176.9 (1)	Ru–C(3)–O(3)	176.9 (1)
Co–C(4)–O(4)	176.8 (1)	Co–C(5)–O(5)	175.5 (1)
Co–C(6)–O(6)	176.9 (2)		

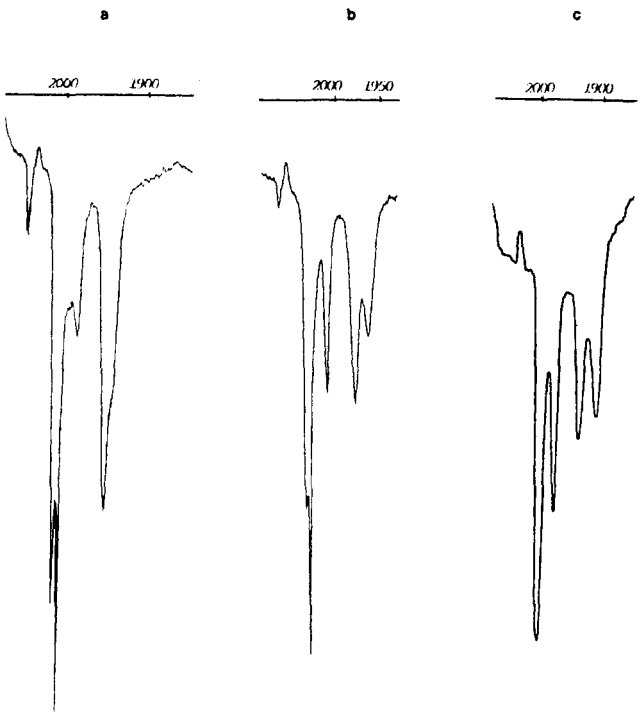

Figure 1. Infrared spectra of the monosubstituted compounds (a) $(PPh_3)(CO)_3Ru(\mu\text{-}PPh_2)Co(CO)_3$, (b) $(PPh_2Me)(CO)_3Ru(\mu\text{-}PPh_2)Co(CO)_3$, and (c) $(PMe_3)(CO)_3Ru(\mu\text{-}PPh_2)Co(CO)_3$ in C_6H_{12} solution. In (a) the cis isomer predominates, in (b) the trans isomer predominates, and in (c) only the trans isomer is present.

P(1)–Co angle is acute (75.5 (0)°). (ii) The coordination geometry around the ruthenium atom is quasioctahedral with the triphenylphosphine ligand occupying a site cis to the μ-PPh_2 group and approximately trans to the Ru–Co bond. The carbonyl groups C(2)–O(2) and C(3)–O(3) are

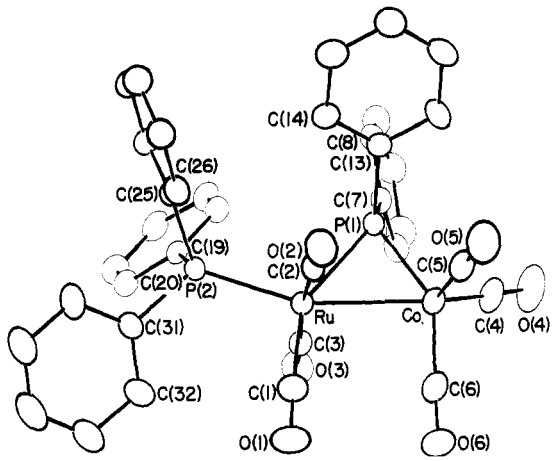

Figure 2. An ORTEP view of the molecular structure of $(PPh_3)(CO)_3Ru(\mu\text{-}PPh_2)Co(CO)_3$ showing the atomic numbering.

mutually trans and approximately perpendicular to the plane defined by Ru–P(1)–P(2) and Co. (iii) The stereochemistry of the cobalt atom is less clearly defined, the most appropriate description being distorted square pyramidal with the carbonyl group C(5)–O(5) occupying the apical site and P(1), Ru, C(4), and C(6) basal. Several heterobinuclear (Ru–Co) molecules containing phosphido bridges have recently been synthesized.[11b,12,15] Structural data are compared in Table IV. There is an interesting comparison with $(Ph_3P)(CO)_3Ru(\mu\text{-}PPh_2)Co(CO)_2(PPh_3)$[12] synthesized from $Ru(H)Cl(CO)(PPh_3)_3$ and $Na[Co(CO)_4]$ by Geoffroy et al. The latter is formally a Ph_3P substitution product of $RuCo(CO)_6(\mu\text{-}PPh_2)(PPh_3)$; however, the ruthenium-bound PPh_3 group is trans to the Ru–PPh_2 bond, with the second PPh_3 ligand coordinated to cobalt cis to the Co–PPh_2 group. Also, in $(Ph_3P)(CO)_3Ru(\mu\text{-}PPh_2)Co(CO)_2(PPh_3)$ the cobalt stereochemistry more closely resembles a trigonal bipyramid with the ruthenium atom and triphenylphosphine apical (Ru–Co–P(3) = 160.87 (7)°). The metal–metal distances in these two compounds (Ru–Co = 2.7681 (4) Å in $(Ph_3P)(CO)_3Ru(\mu\text{-}PPh_2)Co(CO)_3$ vs. 2.750 (1) Å in the bis(phosphine) compound[12]) are quite similar, as are the Ru–P–Co angles [75.5 (0) vs. 74.6 (1)°] and the metal–phosphorus distances to the phosphido bridge [Ru–P(PPh_2) = 2.3556 (9) Å vs. 2.359 (2) Å and Co–P(PPh_2) = 2.161 (1) Å vs. 2.173 (13) Å].

In the trinuclear cluster $RuCo_2(CO)_9(\mu\text{-}CO)(PPh_3)$[16] where the PPh_3 group on ruthenium is trans to an unbridged Ru–Co bond, the Ru–Co bond length is 2.7591 (8) Å. Significantly shorter phosphido-bridged Ru–Co bond lengths have been found in $RuCo_2(CO)_8(\mu\text{-}PPh_2)_2$ (2.7073 (7) Å)[11b] and in the butterfly cluster $RuCo_3(CO)_9(\mu\text{-}PPh_2)(t\text{-}BuC{\equiv}CH)$ (2.552 (1) Å)[15] where phosphines are absent but where the Ru–Co bond is also bridged by a cobalt carbonyl moiety. Thus while phosphine substitution may cause an overall Ru–Co bond lengthening, as has been observed for closed-shell systems,[17] the structural data for $(Ph_3P)(CO)_3Ru(\mu\text{-}PPh_2)Co(CO)_3$ and $(Ph_3P)(CO)_3Ru(\mu\text{-}PPh_2)Co(CO)_2(PPh_3)$ suggest that the Ru–Co bond lengths are relatively insensitive to cis or trans substitution with respect to the metal vector.

An interesting feature of the chemistry of $(CO)_4Ru(\mu\text{-}PPh_2)Co(CO)_3$ is that thermal substitution of a second CO molecule by a phosphorus group L occurs exclusively on

(15) Jones, D. F.; Dixneuf, P. H.; Benoit, A.; LeMarouille, J. Y. *J. Chem. Soc., Chem. Commun.* **1982**, 1217.
(16) Jones, D. F.; Dixneuf, P. H.; Taylor, N. J.; Carty, A. J., to be submitted for publication.
(17) See for example: Carty, A. J.; MacLaughlin, S. A.; Taylor, N. J.; Sappa, E. *Inorg. Chem.* **1981**, *20*, 4437.

Table IV. Structural Data for $Ru(\mu\text{-}PPh_2)Co$ Complexes

	Ru–P, Å	Co–P, Å	Ru–Co, Å	Ru–P–Co, deg	$^{31}P\{^1H\}$ NMR, δ
$(PPh_3)(CO)_3Ru(\mu\text{-}PPh_2)Co(CO)_3$ (**2a**)	2.3556 (9)	2.161 (1)	2.7681 (4)	75.5 (0)	170.3
$(PPh_3)(CO)_3Ru(\mu\text{-}PPh_2)Co(CO)_2(PPh_3)$[12]	2.359 (2)	2.173 (13)	2.750 (1)	74.6 (1)	139.7
$RuCo_2(\mu\text{-}PPh_2)_2(CO)_8$[11b]	2.318 (1)	2.183 (2)	2.7073 (7)	73.9 (0)	180.4
$RuCo_3(\mu\text{-}PPh_2)(\mu\text{-}\eta^2\text{-}t\text{-}BuC{\equiv}CH)(CO)_9$[15]	2.328 (1)	2.131 (1)	2.552 (1)	69.8 (3)	222.0

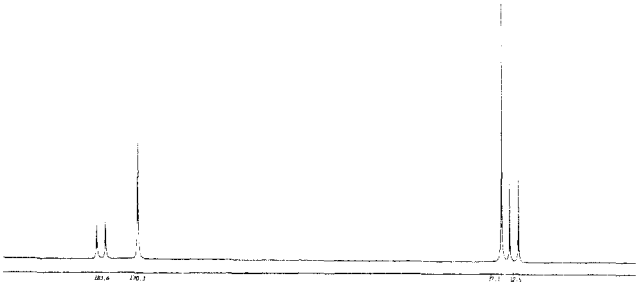

Figure 3. The $^{31}P\{^1H\}$ NMR spectrum of $(PPh_3)(CO)_3Ru(\mu\text{-}PPh_2)Co(CO)_3$ at 32.38 MHz in CD_2Cl_2 at 193 K.

the ruthenium atom (vide infra), there being no ^{31}P spectroscopic evidence for isomers with phosphines coordinated to cobalt despite the fact that $(Ph_3P)(CO)_3Ru(\mu\text{-}PPh_2)Co(CO)_2(PPh_3)$ has been synthesized via another route.[12] Several observations are pertinent to these apparently anomalous facts. (i) Examination of Figure 2 suggests that substitution of C(4)–O(4), formally cis to the phosphido bridge by PR_3 would lead to unfavorable steric interactions between the phosphido bridge and the phosphine. It is significant that in $(Ph_3P)(CO)_3Ru(\mu\text{-}PPh_2)Co(CO)_2(PPh_3)$ the $(Ph_2P)P\text{–}Co\text{–}PPh_3$ angle is 109.1 (1)° with the PPh_3 group trans to the Ru–Co bond. The stereochemistry of the cobalt atom in the latter is also significantly different from that in **2a**. (ii) Substitution of C(6)–O(6) by PPh_3 might lead to unfavorable steric interactions with C(1)–O(1) and C(3)–O(3) on the ruthenium atom. (iii) The formal 18-electron requirements of the cobalt atom demand a donation of two electrons from the μ-PPh_2 group. Thus the phosphido bridge acts as a phosphine toward Co. Increased back-donation to the terminal carbonyls may increase the Co–CO bond order and inhibit CO substitution. It is of course also possible that the presence of a metal–metal bonded $Co(CO)_3$ group *labilizes* CO groups on the ruthenium atom an effect, which, if proven, could have important consequences for bi- and polynuclear chemistry.

^{31}P NMR Studies: The Nature of $(L)(CO)_3Ru(\mu\text{-}PPh_2)Co(CO)_3$ (2) and $(L)_2(CO)_2Ru(\mu\text{-}PPh_2)Co(CO)_3$ (3 and 4) in Solution. $(PPh_3)(CO)_3Ru(\mu\text{-}PPh_2)Co(CO)_3$ (2a). The $^{31}P\{^1H\}$ NMR spectrum of **2a** at 193 K, which exists in the solid state as the ruthenium-substituted cis (to PPh_2) equatorial isomer consists of a doublet (δ +183.6) and a singlet (δ 170.3) at low field together with a corresponding doublet (δ 32.5) and singlet (δ 37.1) at high field (Figure 3). At 300 K the low field resonances broaden markedly whereas those at high field remained sharp. The chemical shifts of the low field resonances are typical of phosphido bridges across a metal–metal bond[18] and can be confidently assigned to the μ-PPh_2 group bridging the Ru–Co vector in **2a**. The precursor **1** exhibits a singlet ^{31}P resonance in the same region (+187.7 ppm).[11] Broadening of these PPh_2 resonances at higher temperatures can be attributed to the quadrupolar affect of the ^{59}Co ($I = {}^7/_2$) nucleus. The ^{31}P resonances at high field which do not exhibit quadrupolar broadening are due to the phosphine coordinated to ruthenium. The presence of two doublets and two singlets in the spectrum of **2a** suggests the presence of two different isomers in solution with the two doublets arising from the AB pattern of strongly coupled

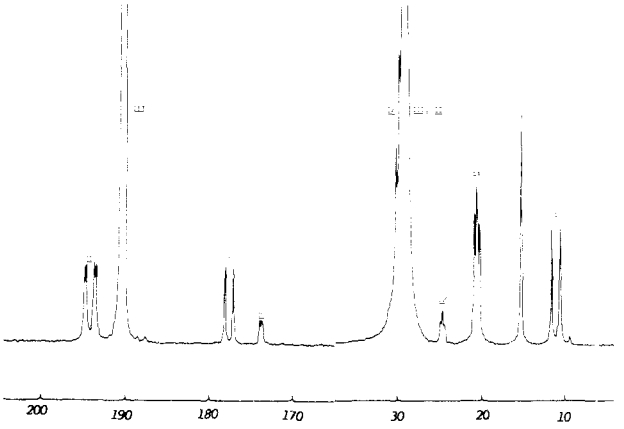

Figure 4. The $^{31}P\{^1H\}$ NMR spectrum of $(PPh_2H)_2(CO)_2Ru(\mu\text{-}PPh_2)Co(CO)_3$ at 101.20 MHz in CD_2Cl_2 at 213 K.

trans PPh_3 and μ-PPh_2 groups and the two singlets from an isomer with mutually cis phosphorus atoms. Support for this assignment derives from an analysis of the $^{31}P\{^1H\}$ spectrum of the binuclear compound $(Ph_2PC{\equiv}C\text{-}i\text{-}Pr)(CO)_2Ru(\mu\text{-}PPh_2)(\mu\text{-}C{\equiv}C\text{-}i\text{-}Pr)Ru(CO)_3$[18a,19] which also exists as cis and trans isomers in solution and for which $^2J_{PP'}$ is large (215 Hz) in the trans isomer and small (17 Hz) in the cis species. Similarly, for $(PPh_3)(CO)_2Fe(\mu\text{-}PPh_2)(\mu\text{-}C{\equiv}CPh)Fe(CO)_3$ $^2J_{PP'}$ for the trans isomer,[20] which is formed exclusively, is 90 Hz. Evidence for the formation of **2a** together with **1** in solution via the carbonylation of $(PPh_3)(CO)_3Ru(\mu\text{-}PPh_2)Co(CO)_2(PPh_3)$ has previously been presented by Geoffroy and co-workers.[12] However, it is clear that the ^{31}P spectral data given do not correspond to a mixture of **2a** and **1** but to the cis and trans isomers of **2a** alone.[11b]

Integration of the resonances for the cis and trans isomers of **2a** established an isomer ratio of ~60:40 at 193 K. At 300 K the separate resonances due to PPh_3 in the cis and trans isomers had coalesced to a single broad peak, indicating that at this temperature site exchange was occurring on the NMR time scale.

$(L)(CO)_3Ru(\mu\text{-}PPh_2)Co(CO)_3$ (L = $Ph_2PC{\equiv}C\text{-}t\text{-}Bu$, $Ph_2PC{\equiv}CPh$, $PMePh_2$, PMe_2Ph, PMe_3) (2b–2f). The $^{31}P\{^1H\}$ NMR spectra of the monosubstituted derivatives **2b–2c** closely resemble those of **2a**, with distinct resonances observable for the cis and trans (to PPh_2) phosphine substitution products. Spectral data are gathered in Table V. The spectrum of **2b**, which exhibited only two singlets for the cis isomer at 32.38 MHz, showed a cis coupling $^2J_{PP'}$ of 2.4 Hz under the superior resolution of the AM-250 instrument operating at 101.2 MHz for ^{31}P. Variable-temperature studies for **2b** showed that the cis:trans isomer ratio varied from 40:60 at 213 K to 85:15 at 300 K, indicating that the isomers cis and trans are in equilibrium in solution. For the remaining compounds **2c–f** the cis:trans isomer ratio as measured by NMR at 223 K decreased with increasing ligand donor character: **2c** (38:62); **2d** (11:89), **2e** (5:95), **2f** (0:100). The trimethylphosphine derivative

(18) (a) Carty, A. J. *Adv. Chem. Ser.* **1982**, *No. 196*, 163. (b) Mott, G. N.; Carty, A. J. *Inorg. Chem.* **1983**, *22*, 2726. See also ref 7, 8, 10, and 11.
(19) MacLaughlin, S. A. Ph.D. Thesis, University of Waterloo, 1983.
(20) Smith, W. F.; Yule, J. E.; Taylor, N. J.; Paik, H. N.; Carty, A. J. *Inorg. Chem.* **1977**, *16*, 1593.

Table V. $^{31}P\{^1H\}$ NMR Data at 32.38 MHz for the Complexes $(L)(CO)_3Ru(\mu\text{-}PPh_2)Co(CO)_3$ (2a–f) and $L_2(CO)_2Ru(\mu\text{-}PPh_2)Co(CO)_3$ (3b–e)

L	isomer	$\delta_P(\mu\text{-}PPh_2)$	δ_P(trans-eq)	δ_P(cis-eq)	$^2J_{PP'}$, Hz
CO[a]	1	187.7			
PPh_3[a]	**2a**-trans	183.6	32.5		104.2
	2a-cis	170.3		37.1	
$Ph_2PC{\equiv}C\text{-}t\text{-}Bu$	**2b**-trans	189.4	3.1		103.8
	2b-cis	173.2		4.8	2.4[b]
$Ph_2PC{\equiv}CPh$	**2c**-trans	190.6	5.4		102.0
	2c-cis	174.0		6.9	
$PMePh_2$	**2d**-trans	185.1	12.2		102.5
	2d-cis	171.1		15.4	
PMe_2Ph	**2e**-trans	183.5	−6.1		97.6
	2e-cis	171.8		−2.1	
PMe_3	**2f**-trans	182.4	−15.2		95.0
$Ph_2PC{\equiv}C\text{-}t\text{-}Bu$	**3b**-eq,eq	183.4	8.6	11.7	109.0
$Ph_2PC{\equiv}CPh$	**3c**-eq,eq	185.2	10.3	12.0	110.0
$PMePh_2$	**3d**-eq,eq	178.4	10.2	15.0	107.4
PMe_2Ph	**3e**-eq,eq	176.0	−4.1	1.9	105.0

[a] In CD_2Cl_2 (193 K) at 32.38 MHz. [b] $^2J_{PP'}$ observed at 101.2 MHz.

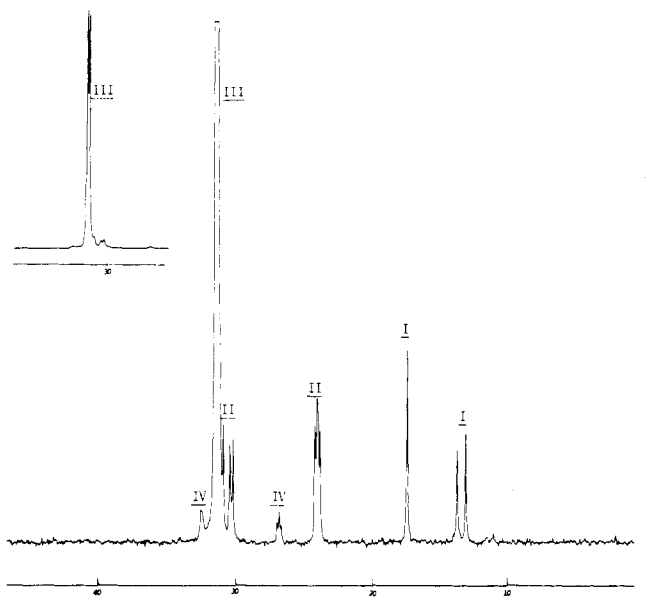

Figure 5. The $^{31}P\{^1H\}$ NMR spectrum of $(PPh_2H)_2(CO)_2Ru(\mu\text{-}PPh_2)Co(CO)_3$ at 161.90 MHz in $CDCl_3$ at 213 K. Only peaks due to the phosphines PPh_2H are shown.

Scheme II

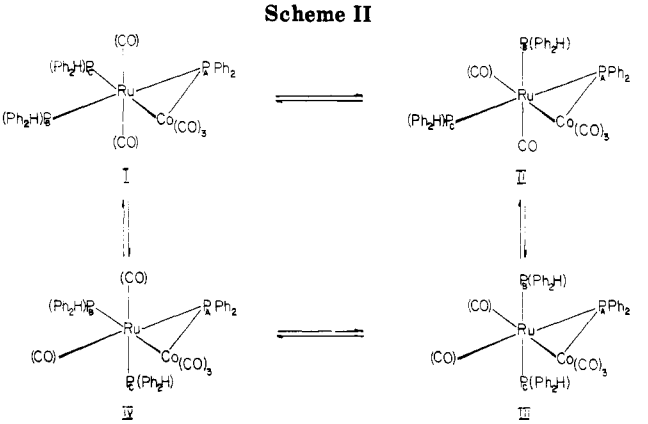

2f exhibited only two doublets over the temperature range 213–300 K, indicating the exclusive formation of the trans species in this case.

$(PPh_2H)_2(CO)_2Ru(\mu\text{-}PPh_2)Co(CO)_3$ (4). The $^{31}P\{^1H\}$ spectrum of this compound at 32.38 MHz and 223 K is complex and second order. At 101.25 MHz (Figure 4) the spectrum is considerably simplified, and at 161.9 MHz additional information is available from the resonances grouped around +31.0 ppm (Figure 5). A complete

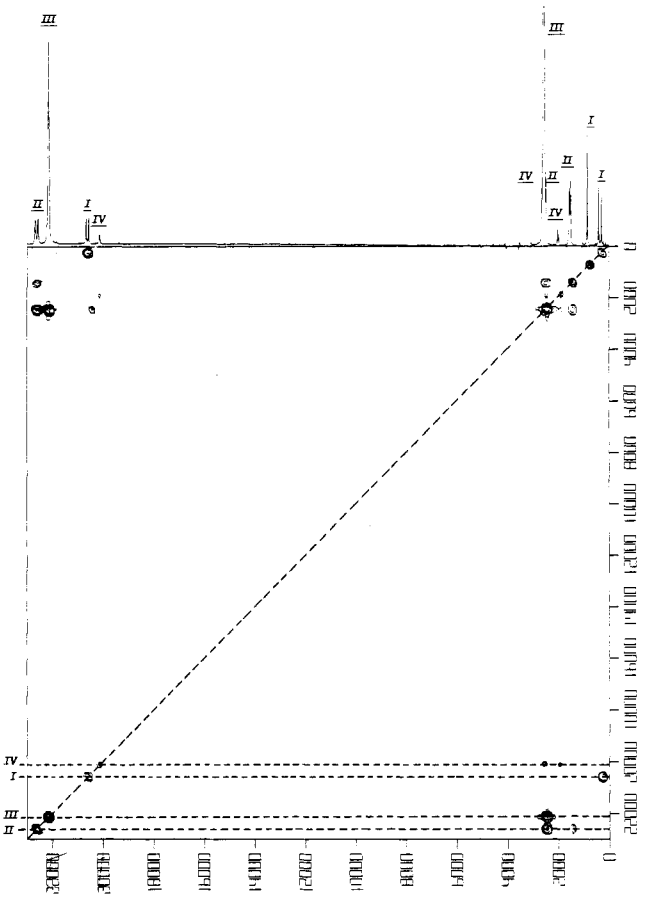

Figure 6. A COSY NMR plot of the spectrum of $(PPh_2H)_2(CO)_2Ru(\mu\text{-}PPh_2)Co(CO)_3$ at 101.20 MHz in CD_2Cl_2 at 213 K. Off-diagonal elements indicate coupled nuclei.

analysis of this spectrum was facilitated by a 2D COSY[21] plot which is essentially a contour diagram relating spin–spin coupled nuclei (Figure 6). Diagonal elements of this plot represent the chemical shifts of all ^{31}P nuclei while off-diagonal elements appear only when nuclei are spin coupled. The entire set of spectra can be elegantly interpreted in terms of the existence of four isomers I→IV derived from the parent $(CO)_4Ru(\mu\text{-}PPh_2)Co(CO)_3$ by substitution of two carbonyl groups on the ruthenium atom by PPh_2H. These isomers, which differ by virtue of their

(21) (a) Macura, S.; Wuthrich, K.; Ernst, R. R. *J. Magn. Reson.* **1982**, *47*, 351. (b) Nagayama, K.; Wuthrick, K.; Ernst, R. R. *Biochim. Biophys. Res. Commun.* **1979**, *90*, 305.

Table VI. $^{31}P\{^1H\}$ NMR Spectra (101.2 MHz) of the Isomers of $(PPh_2H)_2(CO)_2Ru(\mu\text{-}PPh_2)Co(CO)_3$ at 213 K in CD_2Cl_2

	isomer								
	P_C	P_B	$\delta_P(\mu\text{-}PPh_2)^a$	δ_P(trans-eq)^a	δ_P(cis-eq)^a	δ_P(cis-ax)^a	$J_{P_\mu\text{-}P_{tr}}{}^b$	$J_{P_\mu\text{-}P_{ax}}{}^b$	$J_{P_{ax}\text{-}P_{eq}}{}^b$
I	eq-cis	eq-trans	179.4 (d)	13.2 (d)	17.1		105		
II	eq-trans	ax-cis	196.1 (dd)	30.6 (dd)^c		22.2 (dd)	116	25	38
III	ax-cis	ax-cis	192.3 (t)			31.2 (d)		30–25	
IV	ax-cis	eq-cis	175.6 (d)		32.5 (d)^c	26.5 (t)		30	30

$^a\delta_P/H_3PO_4$. $^bJ_{PP}$ (Hz). $^c\delta_P$ observed at 161.9 MHz in $CDCl_3$ at 213 K.

axial/equatorial and cis/trans stereochemistry at the pseudooctahedral ruthenium atom, are illustrated in Scheme II. Although interconversion of these isomers is slow on the NMR time scale at 223 K, they can be related to one another by turnstile or trigonal rotation about axes passing through faces of the ruthenium-based octahedron remote from the cobalt and diphenylphosphido groups. In isomer I, both phosphines are equatorial; they differ by virtue of their positions trans to the phosphido bridge (P_B) and the cobalt atom (P_C). Isomer II has one phosphine axial and the other equatorial and trans to P_A. Assuming, as seems reasonable, that the two axial positions in the octahedron are not differentiated, i.e., there is a symmetry plane through P_A, Co, and Ru, isomer II will have a relative weight of two with respect to I. The axial/axial isomer III has a weight of one, and IV, an equatorial/axial species with the equatorial ligand trans to Co, has a weight of two.

The full assignment for isomers I–IV is given in Table VI. In each case the ^{31}P resonances of the phosphido bridges (175.6–196.1 ppm) are well shifted from those of the terminal ligands (13.2–32.5 ppm). Isomer I has the simplest ^{31}P spectrum with a doublet at δ 179.4 due to the phosphido bridge phosphorus atom P_A coupled only to the trans PPh_2H group P_B. The magnitude of this trans coupling (105 Hz) is typical for this stereochemistry. The corresponding coupled resonance of P_B occurs at 13.2 ppm, an assignment confirmed by the off-diagonal element in the COSY spectrum (Figure 6). We assign the singlet resonance at 17.1 ppm to the equatorial ligand P_C trans to Co; this nucleus is not coupled to either P_B or P_A in cis equatorial positions, a feature consistent throughout this analysis.

Assignment of the spectrum of isomer IV is also straightforward. The phosphido bridge resonance P_A at 175.6 ppm, a doublet, is coupled to only the axial phosphine P_C with a cis coupling of 30 Hz. It is clear from both relative intensities and the COSY plot that the corresponding P_C resonance is at 26.5 ppm and is an apparent triplet as a result of coupling to both P_A and the other axial phosphine P_B. Although not evident at either 32.38 or 101.2 MHz, the P_B resonance is nicely resolved at 161.9 MHz as a doublet at 32.5 ppm. As expected from the triplet P_C resonance, $J_{P_B\text{-}P_C}$ is 30 Hz. It is notable that isomer IV is a relatively minor component of the solution.

The spectrum of isomer II is more complex than I or IV owing to the presence of both trans P_A–P_C and cis P_A–P_B coupling. The PPh_2 resonance is a pair of doublets centered at 196.1 ppm with a large trans coupling of 116 Hz (cf. I) and a smaller axial/equatorial P_B–P_B coupling of 25 Hz. The corresponding P_B resonance is at 22.2 ppm as a doublet of doublets. From this resonance a coupling $J_{P_B\text{-}P_C}$ of 38 Hz was apparent. At 101.2 MHz the resonance, an expected doublet of doublets appeared to be hidden under a very intense absorption at ~32 ppm but at 161.9 MHz the expected pattern clearly emerged.

Assignment of lines and coupling constants for the last isomer III follows directly from the rationale presented above.

From Table VI a consistent pattern of coupling constants emerges. Trans $J_{P(PPh_2)\text{-}P(PR_3)}$ couplings are of the order of 100–120 Hz. Cis axial/equatorial $J_{P(PPh_2)\text{-}P(PR_3)}$ couplings are small (20–30 Hz) as are axial/equatorial $J_{P(PR_3)\text{-}P(PR_3)}$ couplings. In contrast cis equatorial–equatorial couplings involving either two phosphines or a phosphido bridge and a phosphine are very small.

$(L)_2(CO)_2Ru(\mu\text{-}PPh_2)Co(CO)_3$ (3b–e). Interpretation of the spectra of these compounds follows directly from that above for **4**. In contrast to **4**, however, the ligands occupy equatorial sites cis and trans to the phosphido bridge. The trans $^2J_{PP}$ values vary from 95 to 110 Hz with the small cis couplings not resolved at 32.38 MHz (Table V).

Conclusion

In summary it is evident that ^{31}P NMR is a powerful tool for elucidating the stereochemistry of phosphine substitution products from phosphido-bridged heterometallics. The present study has provided valuable but unexpected evidence for site selectivity in such substitution reactions, and it will be interesting to compare this behavior with that exhibited toward unsaturated ligands.

Acknowledgment. We are grateful to NSERC (A.J.C.) and the CNRS (P.H.D.) for financial support of this work. R.R. thanks the University of Waterloo for facilities provided during a 4-month visit in 1983. The help of Dr. R. E. Lenkinski with ^{31}P NMR measurements on the Southwestern Ontario Regional High Field NMR facility is appreciated.

Registry No. 1, 82544-75-0; *trans*-**2a**, 99094-58-3; *cis*-**2a**, 99094-59-4; *trans*-**2b**, 98990-29-5; *cis*-**2b**, 99094-60-7; *trans*-**2c**, 98990-31-9; *cis*-**2c**, 99147-23-6; *trans*-**2d**, 98990-32-0; *cis*-**2d**, 99094-61-8; *trans*-**2e**, 98990-34-2; *cis*-**2e**, 99095-20-2; *trans*-**2f**, 98990-35-3; **3b**, 98990-30-8; **3c**, 99016-46-3; **3d**, 98990-33-1; **3e**, 98990-37-5; **4** (isomer I), 98990-36-4; **4** (isomer II), 99094-62-9; **4** (isomer III), 99094-63-0; **4** (isomer IV), 99094-64-1; PPh_3, 603-35-0; $Ph_2PC{\equiv}C\text{-}t\text{-}Bu$, 33730-51-7; $Ph_2PC{\equiv}CPh$, 7608-17-5; PPh_2Me, 1486-28-8; PMe_2Ph, 672-66-2; PMe_3, 594-09-2; PPh_2H, 829-85-6.

Supplementary Material Available: Table S1, anisotropic thermal parameters, Table S2, remaining bond distances and angles, and Table S3, structure factors for $(Ph_3P)(CO)_3Ru(\mu\text{-}PPh_2)Co(CO)_3$ (19 pages). Ordering information is given on any current masthead page.

Ring Opening of Dihydro-2(3*H*)-thiophenethione on Complexation to Molybdenum–Molybdenum Bonded Complexes

Howard Alper,*†[1a] Frederick W. B. Einstein,[1b] Frederick W. Hartstock,[1a] and Anthony C. Willis[1b]

Departments of Chemistry, University of Ottawa, Ottawa, Ontario, Canada K1N 9B4, and Simon Fraser University, Burnaby, British Columbia, Canada V5A 1S6

Received April 2, 1985

Dihydro-2(3*H*)-thiophenethione reacts with the metal–metal triple-bonded complexes $(RC_5H_4)_2Mo_2(CO)_4$ (R = H, CH_3) to form the interesting ring-opened complexes $[S(CH_2)_3CS]Mo_2(CO)_4(C_5H_4R)$. The latter were identified on the basis of analytical and spectral data, as well as an X-ray analysis of the R = CH_3 compound. Crystal data: space group $P2_1/c$, a = 8.057 (1) Å, b = 29.857 (a) Å, c = 7.992 (3) Å, V = 1849.8 Å^3, Z = 4; final R_F = 0.0185.

Novel complexes have been synthesized by the reaction of organic sulfur compounds with cyclopentadienylmolybdenum dicarbonyl dimer (1, R = H) and related complexes containg a metal–metal triple bond. For example, carbon disulfide reacts with 1, R = H, affording $C_5H_5(CO)_2Mo$–$Mo(CO)_2(C_5H_5)(\eta^2$-$CS_2)$ which contains a nonbridging, terminal η^2-CS_2 ligand.[2] Another heteroallene, methyl isothiocyanate, gives traces of a dithiocarbamate complex, $C_5H_5(CO)_2MoS_2CNHCH_3$, on treatment with 1, R = H. An interesting desulfurization product results using (pentamethylcyclopentadienyl)molybdenum dicarbonyl dimer as the reactant.[3]

Treatment of thioketones with metal–metal triple bonded complexes at room temperature affords complexes of structural type 2 (M = Mo, W).[4] The gross structure of complexes obtained from thiolactones [e.g., dihydro-2-(3*H*)-furanthione, 3] and thio esters is similar to those

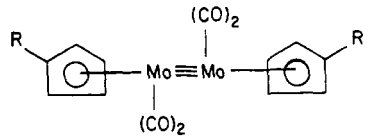

1

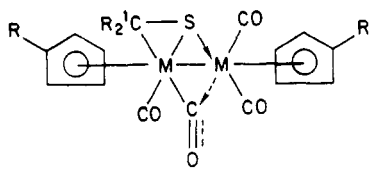

2

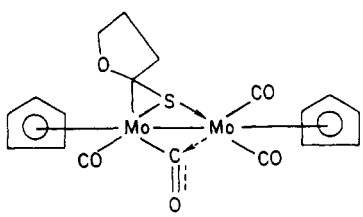

3

derived from thioketones, but there are interesting differences in detail.[5] Both 2 and 3 have semibridging carbonyl groups, and the thiocarbonyl function is bonded to one of the two metals, with the sulfur donor bound to the other metal atom. It has recently been reported that the use of dithio esters as reactants with 1, M = Mo, in refluxing toluene or xylene affords a new class of organosulfur–metal compounds 4, containing a symmetrically bridging thioacyl function and a bridging thioalkyl group.[6]

A complex similar to 2 is formed at room temperature.

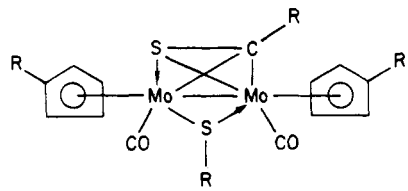

4

It was of interest to react a dithiolactone with 1 in order to determine if one could achieve ring opening by cleavage of the carbon–sulfur single bond or whether the dithio analogue of 3 would be formed by complexation of the thione unit to the metal. In the event that carbon–sulfur bond cleavage occurs, the presence of the alkyl chain may influence the bonding situation relative to 4. We now describe the results of this investigation.

Results and Discussion

When the in situ generated (methylcyclopentadienyl)-molybdenum dicarbonyl dimer 1 (M = Mo, R = CH_3) and dihydro-2(3*H*)-thiophenethione (5) were refluxed overnight in toluene, the ring-opened complex 6 was obtained and characterized on the basis of spectral data and an X-ray crystal structure. The parent triple-bonded complex (M = Mo, R = H) reacts similarly affording 6, R = H. The infrared spectra of 6 [R = H, CH_3 (KBr)] shows two in-

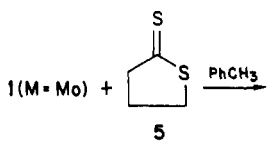

5

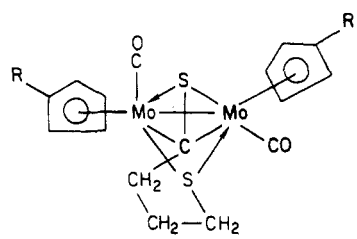

6

† John Simon Guggenhein Fellow, 1985–1986.

(1) (a) University of Ottawa. (b) Simon Fraser University.
(2) Brunner, H.; Meier, W.; Wachter, *J. J. Organomet. Chem.* **1981**, *210*, C23.
(3) Brunner, H.; Buchner, H.; Wachter, J.; Bernal, I.; Ries, W. H. *J. Organomet. Chem.* **1983**, *244*, 247.
(4) Alper, H.; Silavwe, N. D.; Birnbaum, G. I.; Ahmed, F. R. *J. Am. Chem. Soc.* **1979**, *101*, 6582.
(5) Alper, H.; Einstein, F. W. B.; Nagai, R.; Petrignani, J. F.; Willis, A. *Organometallics* **1983**, *2*, 1291.
(6) Alper, H.; Einstein, F. W. B.; Hartstock, F.; Willis, A. C. *J. Am. Chem. Soc.* **1985**, *107*, 173.

0276-7333/86/2305-0009$01.50/0

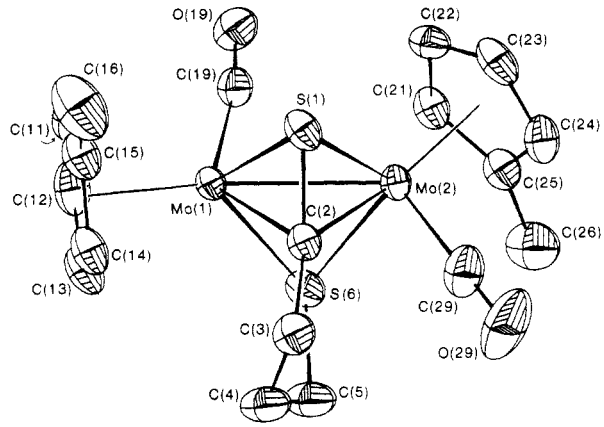

Figure 1. A view of the $Mo_2(C_5H_4CH_3)_2(CO)_2(SCC_3H_6S)$ molecule showing the atom-labeling scheme. Thermal ellipsoids enclose 50% probability levels. Hydrogen atoms have been deleted for clarity.

Table I. Crystal Data

formula	$C_{18}H_{20}Mo_2O_2S_2$	V, Å^3	1849.8
cryst system	monoclinic	Z	4
space group	$P2_1/c$	fw	524.36
a, Å	8.057 (1)	ρ_{obs} g cm^{-3}	1.86[a]
b, Å	29.857 (2)	ρ_{calc} g cm^{-3}	1.883
c, Å	7.992 (3)	μ, cm^{-1}	15.50
β, deg	105.80 (2)		

[a] By flotation in aqueous $ZnBr_2$ solution.

tense carbonyl stretching bands at 1881–1889 and 1849–1852 cm^{-1}. In contrast, complexes of structural type **4** display three carbonyl stretching bands instead of the anticipated two absorptions.[6] The carbon-13 nuclear magnetic resonance spectrum of **6**, R = H, gave the expected signals for the two different cyclopentadienyl rings and the organic ligand, as well as two carbonyl carbon resonances. The molecular ion was observed in the mass spectrum of **6** (R = H, CH_3), with loss of the carbon monoxide ligands being a significant fragmentation pathway.

The X-ray crystal structure of **6**, R = CH_3, was determined and a thermal ellipsoid diagram is shown in Figure 1. Crystal data, data collection information, atomic coordinates, and selected interatomic distances and angles are given in Tables I–IV.

The complex consists of two $Mo(C_5H_4CH_3)CO$ units connected by a Mo–Mo single bond with two sulfur atoms and one α-C atom bonded to both Mo atoms. In contrast to **4**, the α-C atom is linked to the nonadjacent S atom by an alkyl chain. Comparison[7] of the bond lengths in **4**[6] and **6** indicates that the Mo–Mo and Mo–C(2) distances are shorter in **6** (and the former is also shorter than in related metal carbonyl complexes which range from 2.95 to 3.25 Å)[6] and the four Mo–S bonds, which are very similar to each other, tend to be slightly longer. The magnitudes of these differences between **4** and **6** are small.

The effect the linking alkyl group has upon the central core of the molecule is significant and is best observed by considering the dihedral angles between planes of the type Mo(1)–Mo(2)–X, where X is a donor atom of the ligand. In particular, the angle between planes Mo(1)–Mo(2)–C(2) and Mo(1)–Mo(2)–S(6) is 96.7 (1)° for **6** cf. 111.1 (1)° for **4**, showing that C(2) and S(6) subtend a smaller angle than when they belong to separate ligands. A consequence of decreasing the effective bite of $\overline{C(2)\text{–}S(6)}$ is for there to be more space on the opposite side of the Mo–Mo bond for the carbonyl C(19)–O(19) to approach Mo(2) than in **4**, giving rise to a shorter Mo(2)···C(19) distance [3.078 (2) Å cf. 3.171 (2) Å] and therefore a more bent Mo–C–O angle [169.4 (2)° cf. 172.5 (2)°]. Nevertheless, this carbonyl should still be regarded as being intermediate between true semibridging and simple terminal bonding.

The S(1)–C(2) distance is shorter than in **4**[6] or the thiocamphor[4] or thiolactone[5] complexes studied previously [respectively 1.769 (6), 1.807 (6), and 1.790 (11) Å], suggesting an increased C=S double-bond character and so a greater ($\sigma + \pi$) contribution to bonding of the thione to the Mo atoms. Each Mo atom completes a six-membered chelate ring with C(2), C(3), C(4), C(5), and S(6). The ring with Mo(1) is in a boat conformation, and that with Mo(2) is a chair. Linking C(2) to S(6) also causes angles Mo(n)–C(2)–C(3) and Mo(n)–S(6)–C(5) to be smaller in **6** than in **4**.

(7) For comparative purposes, the atoms in **4** are relabeled according to the scheme used in **6**. In general, X($1n$) are renamed X($2n$) and vice versa.

Table II. Data Collection and Refinement

diffractometer	Enraf-Nonius CAD4F
radiation	Mo Kα, graphite monochromator
λ of radiation, Å	0.709 30 (α_1); 0.713 59 (α_2)
scan mode	coupled ω–2θ
ω scan width, deg	0.55 plus α_1–α_2 dispersion
ω scan speed, deg min^{-1}	4–0.57
bkgd	scan extended by 25% on each side
cryst size, mm	0.017 × 0.020 × 0.036
2θ range, deg	0–50
total no. of reflns	3258
obsd reflns[a]	2984
no. of variables	298
final R_F[b]	0.019[c]
final R_{wF}[d]	0.025[c]
final GOF[e]	1.81[c]

[a] Reflections with $I > 2.3(\sigma(I))$. [b] $R_F = \sum||F_o| - |F_c||/|F_o|$. [c] Observed reflections only. [d] $R_{wF} = [\sum w(|F_o| - |F_c|)^2/\sum F_o^2]^{1/2}$. [e] GOF = $[\sum w(|F_o| - |F_c|)^2/(\text{no. of obs} - \text{no. of vars})]^{1/2}$.

Table III. Fractional Atomic Coordinates and B_{eq} (Å^2) of the Non-Hydrogen Atoms[a]

atom	x	y	z	B_{eq}, Å^2
Mo(1)	0.26019 (3)	0.162059 (7)	0.52659 (3)	1.98
Mo(2)	0.09020 (3)	0.111900 (7)	0.23592 (3)	2.08
S(1)	0.37089 (8)	0.14860 (2)	0.27388 (8)	2.70
C(2)	0.3389 (3)	0.10582 (8)	0.4079 (3)	2.36
C(3)	0.4461 (4)	0.06803 (10)	0.5059 (4)	3.43
C(4)	0.3753 (4)	0.05277 (11)	0.6556 (4)	4.04
C(5)	0.1810 (4)	0.04974 (11)	0.6169 (4)	3.98
S(6)	0.05625 (8)	0.10073 (2)	0.52907 (8)	2.75
C(11)	0.3717 (4)	0.22648 (11)	0.6722 (4)	4.24
C(12)	0.2829 (4)	0.20300 (11)	0.7739 (4)	4.11
C(13)	0.3725 (4)	0.16245 (11)	0.8260 (3)	3.54
C(14)	0.5154 (4)	0.16182 (11)	0.7580 (4)	3.43
C(15)	0.5172 (4)	0.20131 (10)	0.6636 (3)	3.65
C(16)	0.6538 (6)	0.21426 (23)	0.5772 (6)	6.47
C(19)	0.0669 (3)	0.20131 (8)	0.4200 (3)	2.69
O(19)	−0.0367 (3)	0.22923 (6)	0.3774 (3)	3.81
C(21)	−0.1869 (9)	0.14290 (9)	0.1541 (3)	2.81
C(22)	−0.0884 (4)	0.16486 (10)	0.0580 (4)	3.05
C(23)	−0.0444 (4)	0.13358 (11)	−0.0524 (3)	3.48
C(24)	−0.1151 (4)	0.09221 (10)	−0.0259 (4)	3.31
C(25)	−0.2044 (3)	0.09729 (9)	0.1019 (3)	2.85
C(26)	−0.3099 (5)	0.06249 (14)	0.1609 (5)	4.80
C(29)	0.1637 (4)	0.05203 (11)	0.1982 (4)	4.28
O(29)	0.2038 (4)	0.01603 (8)	0.1735 (4)	8.05

[a] Esd's refer to last digit printed. B_{eq} is the arithmetic mean of the principal axes of the thermal ellipsoid.

Experimental Section

General Data. Melting point determinations were made on a Fisher-Johns apparatus. A Nicolet MX-1 Fourier transform

Table IV. Selected Interatomic Distances (Å) and Angles (deg)[a]

Bond Distances			
Mo(1)-Mo(2)	2.790 (1), 2.796[b]		
Mo(1)-S(1)	2.453 (1), 2.462[b]	Mo(2)-S(1)	2.456 (1), 2.462[b]
Mo(1)-C(2)	2.109 (2), 2.115[b]	Mo(2)-C(2)	2.107 (3), 2.110[b]
Mo(1)-S(6)	2.464 (1), 2.471[b]	Mo(2)-S(6)	2.454 (1), 2.462[b]
Mo(1)-C(11)	2.300 (3), 2.313[d]	Mo(2)-C(21)	2.339 (3), 2.345[d]
Mo(1)-C(12)	2.289 (3), 2.303[d]	Mo(2)-C(22)	2.341 (3), 2.349[d]
Mo(1)-C(13)	2.316 (3), 2.327[d]	Mo(2)-C(23)	2.354 (3), 2.361[d]
Mo(1)-C(14)	2.362 (3), 2.370[d]	Mo(2)-C(24)	2.361 (3), 2.366[d]
Mo(1)-C(15)	2.372 (3), 2.381[d]	Mo(2)-C(25)	2.364 (3), 2.368[d]
Mo(1)-C(19)	1.950 (3), 1.953[e]	Mo(2)-C(29)	1.932 (3), 1.950[e]
S(1)-C(2)	1.730 (3), 1.737[c]	C(5)-S(6)	1.853 (3), 1.859[c]
C(2)-C(3)	1.505 (4), 1.509[c]	C(4)-C(5)	1.514 (5), 1.517[c]
C(3)-C(4)	1.528 (5), 1.533[c]	Mo(2)···C(19)	3.078 (2)
C(11)-C(12)	1.407 (5), 1.419[d]	C(21)-C(22)	1.407 (4), 1.417[d]
C(12)-C(13)	1.413 (5), 1.425[d]	C(22)-C(23)	1.395 (4), 1.403[d]
C(13)-C(14)	1.400 (5), 1.412[d]	C(23)-C(24)	1.400 (4), 1.409[d]
C(14)-C(15)	1.402 (4), 1.414[d]	C(24)-C(25)	1.408 (4), 1.417[d]
C(15)-C(11)	1.410 (5), 1.421[d]	C(25)-C(21)	1.420 (4), 1.428[d]
C(15)-C(16)	1.500 (5), 1.513[d]	C(25)-C(26)	1.498 (4), 1.508[d]
C(19)-O(19)	1.163 (3), 1.170[f]	C(29)-O(29)	1.155 (4), 1.173[f]
Bond Angles			
Mo(2)-Mo(1)-S(1)	55.43 (2)	Mo(1)-Mo(2)-S(1)	55.31 (2)
Mo(2)-Mo(1)-C(2)	48.53 (7)	Mo(1)-Mo(2)-C(2)	48.61 (6)
Mo(2)-Mo(1)-S(6)	55.28 (2)	Mo(1)-Mo(2)-S(6)	55.61 (2)
Mo(2)-Mo(1)-C(19)	78.82 (7)	Mo(1)-Mo(2)-C(29)	121.6 (9)
Mo(2)-Mo(1)-Cp(1)[g]	170.99	Mo(1)-Mo(2)-Cp(2)[g]	129.60
S(1)-Mo(1)-C(2)	43.78 (7)	S(1)-Mo(2)-C(2)	43.74 (7)
S(1)-Mo(1)-S(6)	106.12 (3)	S(1)-Mo(2)-S(6)	106.31 (3)
S(1)-Mo(1)-C(19)	99.49 (8)	S(1)-Mo(2)-C(29)	96.95 (10)
S(1)-Mo(1)-Cp(1)	119.63	S(1)-Mo(2)-Cp(2)	125.50
C(2)-Mo(1)-S(6)	72.24 (7)	C(2)-Mo(2)-S(6)	72.48 (7)
C(2)-Mo(1)-C(19)	125.74 (10)	C(2)-Mo(2)-C(29)	75.20 (11)
C(2)-Mo(1)-Cp(1)	122.48	C(2)-Mo(2)-Cp(2)	169.21
S(6)-Mo(1)-C(19)	89.72 (8)	S(6)-Mo(2)-C(29)	98.14 (10)
S(6)-Mo(1)-Cp(1)	124.76	S(6)-Mo(2)-Cp(2)	116.15
C(19)-Mo(1)-Cp(1)	110.03	C(29)-Mo(2)-Cp(2)	108.59
Mo(1)-C(19)-O(19)	169.4 (2)	Mo(2)-C(29)-O(29)	178.4 (3)
Mo(1)-S(1)-Mo(2)	69.26 (2)	Mo(1)-S(6)-Mo(2)	69.11 (2)
Mo(1)-S(1)-C(2)	57.49 (8)	Mo(1)-S(6)-C(5)	108.63 (11)
Mo(2)-S(1)-C(2)	57.32 (8)	Mo(2)-S(6)-C(5)	106.46 (11)
Mo(1)-C(2)-Mo(2)	82.86 (9)		
Mo(1)-C(2)-S(1)	78.73 (10)	Mo(2)-C(2)-S(1)	78.94 (10)
Mo(1)-C(2)-C(3)	124.3 (2)	Mo(2)-C(2)-C(3)	135.5 (2)
C(2)-C(3)-C(4)	110.2 (2)	S(1)-C(2)-C(3)	135.6 (2)
C(3)-C(4)-C(5)	116.4 (3)	C(4)-C(5)-S(6)	116.9 (2)
C(15)-C(11)-C(12)	108.8 (3)	C(25)-C(21)-C(22)	108.2 (2)
C(11)-C(12)-C(13)	107.4 (3)	C(21)-C(22)-C(23)	108.1 (3)
C(12)-C(13)-C(14)	107.8 (3)	C(22)-C(23)-C(24)	108.1 (3)
C(13)-C(14)-C(15)	109.1 (3)	C(23)-C(24)-C(25)	108.9 (3)
C(14)-C(15)-C(11)	106.9 (3)	C(24)-C(25)-C(21)	106.7 (3)
C(14)-C(15)-C(16)	125.5 (4)	C(24)-C(25)-C(26)	126.8 (3)
C(11)-C(15)-C(16)	127.5 (4)	C(21)-C(25)-C(26)	126.3 (3)

[a] Bond lengths corrected for thermal motion area given following the corresponding uncorrected values. [b] Rigid body: Mo(1), S(1), C(2), S(6), Mo(2). [c] Rigid body: Mo(1), S(1), C(2), C(3), C(4), C(5), S(6), Mo(2). [d] Rigid body: Mo(n), C(n1)-C(n6). [e] Riding motion of C atom on Mo atom. [f] From the distances Mo···O (corrected for motion of O riding on Mo) and Mo–C (corrected for motion of C riding on Mo) and the angle Mo–C–O. [g] Cp(n) is the centroid of C(n1)-C(n5).

infrared spectrometer was used for infrared spectra, while mass spectral analyses were determined on a VG Micromass 7070E spectrometer. An EM-360 (Varian) spectrometer was used for proton NMR spectra, and carbon-13 spectra were recorded in the fully and partially decoupled modes with a Varian XL-300 spectrometer. Elemental analyses were carried out by MHW Laboratories, Phoenix, AZ. Dicyclopentadienyldimolybdenum hexacarbonyl was purchased from Strem Chemicals and used as received, and bis(methylcyclopentadienyl)dimolybdenum hexacarbonyl was prepared according to a literature procedure.[8]

All reactions were effected under a dry nitrogen atmosphere, using vacuum line and Schlenk techniques as well as pure solvents.

(8) Wilkinson, G. *J. Am. Chem. Soc.* **1954**, *76*, 209.

Dihydro-2(3*H*)-thiophenethione (5). The procedure of Lawesson and co-workers[9] was modified as follows: a mixture of 2.04 g (20 mmol) of dihydro-2(3*H*)-thiophene and 12 mmol of Lawesson reagent [2,4-bis(4-methoxyphenyl)-1,3,2,4-dithiaphosphetane 2,4-disulfide] in toluene (70 mL) was refluxed for 3 days. The solution was concentrated by rotary evaporation and chromatographed on silica gel. Elution with 2:1 ether/hexane gave dithiobutyrolactone as a clear oil in quantitative yield: mass spectrum, m/e 118 $[M]^+$. The proton NMR gave signals at somewhat higher field than reported by Lawesson and co-workers:[9] $\delta(CDCl_3)$ 2.30 (m, 2 H, CH_2), 2.98 (t, 2 H, CH_2CS), 3.53 (t, 2 H, CH_2S).

Reaction of Dihydro-2(3*H*)-thiophenethione (5) with 1 (M = Mo, R = H). The triple-bonded complex was generated by refluxing 0.98 g (2.0 mmol) of $[C_5H_5Mo(CO)_3]_2$ in toluene (30 mL) overnight. Dihydro-2(3*H*)-thiophenethione (0.23 g, 2.00 mmol) was added, and refluxing of the stirred solution was continued for another 18 h. The solution was cooled, and toluene was removed by flash evaporation. Silica gel chromatography of the residue, using ethyl acetate as the eluant, gave 0.43 g (43%) of dark red **6**, R=H: mp 63–65 °C; IR ν_{CO} (KBr) 1889, 1849 cm^{-1}; ^{13}C NMR ($CDCl_3$) δ 27.07, 31.23, 31.56 (methylene carbons), 91.25 (C_5H_5), 94.16 (C_5H_5), 136.69 (CS), 233.70, 239.61 (CO); mass spectrum, m/e 496 $[M]^+$, 468 $[M - CO]^+$, 440 $[M - 2CO]^+$. Complex **6** is quite stable in the solid state but decomposes rapidly in solution (becomes green).

Anal. Calcd for $C_{16}H_{16}Mo_2O_2S_2$: C, 38.72; H, 3.25. Found: C, 38.55; H, 3.37.

Reaction of Dihydro-2(3*H*)-thiophenethione (5) with 1 (M = Mo, R = CH_3). Utilization of the same procedure as that described for 1 (M = Mo, R = H) gave 0.40 g (38%) of red **6**, R = CH_3: mp 115–116 °C; IR ν_{CO} (KBr) 1881, 1852 cm^{-1}; ^1H NMR ($CDCl_3$) δ 2.00 (s, 3 H, CH_3), 2.02 (s, 3 H, CH_3), 2.0–3.3 (m, 6 H, methylene protons), 5.03 (m, 4 H, C_5H_4), 5.08 (m, 4 H, C_5H_4); mass spectrum, m/e 524 $[M]^+$, 496 $[M - CO]^+$, 468 $[M - 2CO]^+$.

Anal. Calcd for $C_{18}H_{20}Mo_2O_2S_2$: C, 41.23; H, 3.84. Found: C, 40.75; H, 3.95.

X-ray Analysis. A dark red crystal of **6**, R = CH_3, was sealed in a thin-walled glass capillary and mounted on the diffractometer. Accurate cell dimensions and the orientation matrix were determined by least-squares analysis of the setting angles of 23 accurately centered reflections ($29° < 2\theta < 32°$) widely separated in reciprocal space. Crystal data are given in Table I.

The intensities of a unique data set ($\pm h,k,l$) were collected as outlined in Table II. Examination of the data revealed systematic extinctions $h0l$, $l = 2n + 1$, and $0k0$, $k = 2n + 1$, determining the space group to be $P2_1/c$. Two standards monitored after every hour of X-ray exposure time varied from their respective averages by <2% and showed no systematic trends, so data were not rescaled. An analytic absorption correction was applied to all data (T = 0.740–0.784).

Mo and S atoms were located in an E map phased by MULTAN.[10,11] All remaining non-H atoms were located in a subsequent electron density difference map. Least-squares refinement of the heavy atoms with anisotropic temperature factors and including non-methyl H atoms at their calculated positions (parameters not varying) converged to R_F = 0.021. All six methyl H atoms were located in an inner-data difference map. An extinction parameter was included, H atom positional parameters were allowed to vary in subsequent cycles, and then H atom isotropic temperature factors were also allowed to refine. All shift-to-error ratios in the final cycle <0.02, R_F = 0.0185. The biggest features in a final difference map <0.29 (6) e Å^{-3}.

Refinement throughout was by the full-matrix least-squares method minimizing $\sum w(|F_o| - |F_c|)^2$ where w = 1 in the early stages of refinement and $w = [(\sigma(F_o))^2 + pF_o^2]^{-1}$ in the final cycles. The

(9) Scheibye, S.; Kristensen, J.; Lawesson, S. O. *Tetrahedron* **1979**, *35*, 1339.

(10) DeMeulenaer, J.; Tompa, H. *Acta Crystallogr.* **1965**, *19*, 1014.

(11) (a) Germain, G.; Main, P.; Woolfson, M. *Acta Crystallogr., Sect. A: Cryst. Phys., Diffr., Theor. Gen. Crystallogr.* **1971**, *A27*, 368. (b) Larson, A. C.; Gabe, E. J. "Computing in Crystallography"; Schenk, H., Olthof-Hazenkamp, R., Van Koningsveld, H., Bassi, G. C., Eds.; Delft University: Press: Delft, Holland, 1978; p 81. (c) Larson, A. C.; Lee, F. L.; LePage, Y.; Gabe, E. J. "The N.R.C. VAX Crystal Structure System"; Chemistry Division, N.R.C.: Ottawa, 1983.

parameter p was adjusted to give minimum variation in average $w(|F_o| - |F_c|)^2$ as a function of $|F_o|$ and $(\sin\theta)/\lambda$; final $p = 0.0001$. Neutral atom scattering factors with anomalous dispersion corrections were used throughout.[12] Computer programs were run on a VAX 11/750 machine.[11,13]

A thermal ellipsoid diagram[14] of the molecule showing the atomic labeling scheme is given in Figure 1. Final coordinates of the non-H atoms are given in Table III and selected interatomic distances and angles in Table IV.

Thermal motion corrections (Table IV) were derived by two methods: various rigid-body models[15] for distances involving $Mo_2(C_5H_4CH_3)_2(SCC_3H_6S)$ and riding motion[16] for the carbonyls. The rigid-body models involving only the atoms of the central core of the molecule fitted the experimental parameters well, but, as expected, agreement was less satisfactory for models involving more peripheral atoms. Nevertheless they do give an *estimate* of the correction that should be applied to these outer bond lengths. Corrections to angles have not been listed. In the main they are <1 esd's but always <0.10°. The C–O corrections were calculated by assuming that both the C and O atoms ride on the Mo atoms and correcting for the nonlinearity of the Mo–C–O angle. Once again, this is an estimate rather than a rigorously derived value.

Acknowledgment. We are grateful to the Natural Sciences and Engineering Research Council for support of this research. Mr. Hartstock is indebted to NSERC for a predoctoral fellowship.

Registry No. 1 (R = H), 56200-27-2; 1 (R = Me), 69140-73-4; 5, 82357-67-3; 6 (R = H), 98194-43-5; 6 (R = Me), 98194-44-6; dihydro-2(3*H*)-thiophenone, 1003-10-7; $[C_5H_5Mo(CO)_3]_2$, 12091-64-4.

Supplementary Material Available: Tables of hydrogen atom parameters, anisotropic thermal parameters of the nonhydrogen atoms, interatomic distances and angles involving the hydrogen atoms, and weighted least-squares planes and selected torsion angles as well as a listing of observed and calculated structure factors for $Mo_2(C_5H_4CH_3)_2(CO)_2(SCC_3H_6S)$ (30 pages). Ordering information is given on any current masthead page.

(12) "International Tables for X-ray Crystallography"; Kynoch Press: Birmingham, England, 1974; Vol. 4, pp 99, 149.
(13) Watkin, D. J.; Carruthers, J. R. "CRYSTAL User Guide", Chemical Crystallography Laboratory, University of Oxford, 1981.
(14) Davis, E. K. "CHEMGRAF User Guide", Chemical Crystallography Laboratory, University of Oxford, 1983.
(15) (a) Cruickshank, D. W. J. *Acta Crystallogr.* **1956**, *9*, 754. (b) Schomaker, V.; Trueblood, K. N. *Acta Crystallogr., Sect. B: Struct. Crystallogr. Cryst. Chem.* **1968**, *B24*, 63.
(16) Busing, W. R.; Levy, H. A. *Acta Crystallogr.* **1964**, *17*, 142.

Binuclear Oxidative Addition of Alkynes to Phosphido-Bridged Dirhodium and Diiridium 1,5-Cyclooctadiene Complexes

Tom S. Targos and Gregory L. Geoffroy*

Department of Chemistry, The Pennsylvania State University, University Park, Pennsylvania 16802

Arnold L. Rheingold

Department of Chemistry, The University of Delaware, Newark, Delaware 19716

Received April 26, 1985

Reaction of $Rh_2(\mu\text{-}PPh_2)_2(COD)_2$, (1, COD = 1,5-cyclooctadiene) and $Ir_2(\mu\text{-}PPh_2)_2(COD)_2$ (2) with $CH_3O_2CC{\equiv}CCO_2CH_3$ gives the adduct complexes $M_2(\mu\text{-}PPh_2)_2(\mu\text{-}CH_3O_2CC{\equiv}CCO_2CH_3)(COD)_2$ (M = Rh, 3; M = Ir, 4). Complex 3 has been crystallographically characterized: $P2_1/c$, $a = 17.718$ (4) Å, $b = 12.345$ (2) Å, $c = 20.047$ (5) Å, $\beta = 113.34$ (2)°, $V = 4026$ (2) Å^3, $Z = 4$, $R_F = 0.063$, and $R_{wF} = 0.071$ for 4737 reflections with $F_o > 3\sigma(F_o)$. The two Rh atoms are bridged both by the two PPh_2 ligands and the alkyne, with the latter bonded in a cis-dimetalated olefin mode. The alkyne C–C bond is parallel to the Rh–Rh single bond (Rh–Rh = 2.687 (1) Å). Each Rh is further coordinated by one COD ligand in an approximately trigonal-bipyramidal coordination geometry. The low-temperature synthesis of the unstable complex $Rh_2(\mu\text{-}PPh_2)_2(\text{norbornadiene})_2$ is also described.

The binuclear phosphido-bridged Rh_2 and Ir_2 complexes 1 and 2 prepared by Meek and co-workers[1a] appear to be

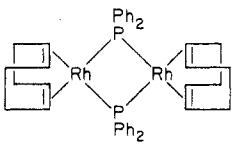

1

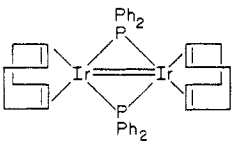

2

ideal molecules with which to explore bimetallic reactivity since (1) they contain active group 8 metals, (2) they have bridging μ-PPh_2 ligands to help maintain molecular integrity under reaction conditions, and (3) they are coordinately unsaturated and possess 1,5-cyclooctadiene (COD) ligands which should be easily removable by hydrogenation. However, relatively few reactions of these molecules have been reported. Meek and co-workers examined their phosphine substitution chemistry and found that bidentate phosphines will displace both COD ligands whereas monodentate phosphines only replace one COD.[1a-c] In related work, we have shown that both COD's can be replaced by PEt_3 ligands when the reaction is carried out under H_2 which apparently removes the COD's by hydrogenation.[2] In this regard, Meek and Kreter also demonstrated that

(1) (a) Kreter, P. E.; Meek, D. W. *Inorg. Chem.* **1983**, *22*, 319. (b) Meek, D. W.; Kreter, P. E.; Christoph, G. G., *J. Organomet. Chem.* **1982**, *231*, C53. (c) Fultz, W. C.; Rheingold, A. L.; Kreter, P. E.; Meek, D. W. *Inorg. Chem.* **1983**, *22*, 860.

(2) Burkhardt, E. W.; Mercer, W. C.; Geoffroy, G. L. *Inorg. Chem.* **1984**, *23*, 1779.

0276-7333/86/2305-0012$01.50/0

parameter p was adjusted to give minimum variation in average $w(|F_o| - |F_c|)^2$ as a function of $|F_o|$ and $(\sin\theta)/\lambda$; final $p = 0.0001$. Neutral atom scattering factors with anomalous dispersion corrections were used throughout.[12] Computer programs were run on a VAX 11/750 machine.[11,13]

A thermal ellipsoid diagram[14] of the molecule showing the atomic labeling scheme is given in Figure 1. Final coordinates of the non-H atoms are given in Table III and selected interatomic distances and angles in Table IV.

Thermal motion corrections (Table IV) were derived by two methods: various rigid-body models[15] for distances involving $Mo_2(C_5H_4CH_3)_2(SCC_3H_6S)$ and riding motion[16] for the carbonyls. The rigid-body models involving only the atoms of the central core of the molecule fitted the experimental parameters well, but, as expected, agreement was less satisfactory for models involving more peripheral atoms. Nevertheless they do give an *estimate* of the correction that should be applied to these outer bond lengths. Corrections to angles have not been listed. In the main they are <1 esd's but always <0.10°. The C–O corrections were calculated by assuming that both the C and O atoms ride on the Mo atoms and correcting for the nonlinearity of the Mo–C–O angle. Once again, this is an estimate rather than a rigorously derived value.

Acknowledgment. We are grateful to the Natural Sciences and Engineering Research Council for support of this research. Mr. Hartstock is indebted to NSERC for a predoctoral fellowship.

Registry No. 1 (R = H), 56200-27-2; 1 (R = Me), 69140-73-4; 5, 82357-67-3; 6 (R = H), 98194-43-5; 6 (R = Me), 98194-44-6; dihydro-2(3*H*)-thiophenone, 1003-10-7; $[C_5H_5Mo(CO)_3]_2$, 12091-64-4.

Supplementary Material Available: Tables of hydrogen atom parameters, anisotropic thermal parameters of the nonhydrogen atoms, interatomic distances and angles involving the hydrogen atoms, and weighted least-squares planes and selected torsion angles as well as a listing of observed and calculated structure factors for $Mo_2(C_5H_4CH_3)_2(CO)_2(SCC_3H_6S)$ (30 pages). Ordering information is given on any current masthead page.

(12) "International Tables for X-ray Crystallography"; Kynoch Press: Birmingham, England, 1974; Vol. 4, pp 99, 149.
(13) Watkin, D. J.; Carruthers, J. R. "CRYSTAL User Guide", Chemical Crystallography Laboratory, University of Oxford, 1981.
(14) Davis, E. K. "CHEMGRAF User Guide", Chemical Crystallography Laboratory, University of Oxford, 1983.
(15) (a) Cruickshank, D. W. J. *Acta Crystallogr.* **1956**, *9*, 754. (b) Schomaker, V.; Trueblood, K. N. *Acta Crystallogr., Sect. B: Struct. Crystallogr. Cryst. Chem.* **1968**, *B24*, 63.
(16) Busing, W. R.; Levy, H. A. *Acta Crystallogr.* **1964**, *17*, 142.

Binuclear Oxidative Addition of Alkynes to Phosphido-Bridged Dirhodium and Diiridium 1,5-Cyclooctadiene Complexes

Tom S. Targos and Gregory L. Geoffroy*

Department of Chemistry, The Pennsylvania State University, University Park, Pennsylvania 16802

Arnold L. Rheingold

Department of Chemistry, The University of Delaware, Newark, Delaware 19716

Received April 26, 1985

Reaction of $Rh_2(\mu\text{-}PPh_2)_2(COD)_2$, (1, COD = 1,5-cyclooctadiene) and $Ir_2(\mu\text{-}PPh_2)_2(COD)_2$ (2) with $CH_3O_2CC{\equiv}CCO_2CH_3$ gives the adduct complexes $M_2(\mu\text{-}PPh_2)_2(\mu\text{-}CH_3O_2CC{\equiv}CCO_2CH_3)(COD)_2$ (M = Rh, 3; M = Ir, 4). Complex 3 has been crystallographically characterized: $P2_1/c$, $a = 17.718$ (4) Å, $b = 12.345$ (2) Å, $c = 20.047$ (5) Å, $\beta = 113.34$ (2)°, $V = 4026$ (2) Å^3, $Z = 4$, $R_F = 0.063$, and $R_{wF} = 0.071$ for 4737 reflections with $F_o > 3\sigma(F_o)$. The two Rh atoms are bridged both by the two PPh_2 ligands and the alkyne, with the latter bonded in a cis-dimetalated olefin mode. The alkyne C–C bond is parallel to the Rh–Rh single bond (Rh–Rh = 2.687 (1) Å). Each Rh is further coordinated by one COD ligand in an approximately trigonal-bipyramidal coordination geometry. The low-temperature synthesis of the unstable complex $Rh_2(\mu\text{-}PPh_2)_2(\text{norbornadiene})_2$ is also described.

The binuclear phosphido-bridged Rh_2 and Ir_2 complexes 1 and 2 prepared by Meek and co-workers[1a] appear to be

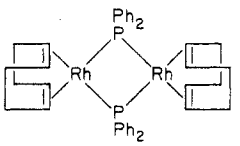

1

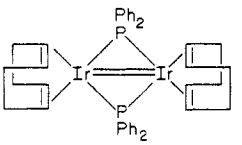

2

ideal molecules with which to explore bimetallic reactivity since (1) they contain active group 8 metals, (2) they have bridging μ-PPh_2 ligands to help maintain molecular integrity under reaction conditions, and (3) they are coordinately unsaturated and possess 1,5-cyclooctadiene (COD) ligands which should be easily removable by hydrogenation. However, relatively few reactions of these molecules have been reported. Meek and co-workers examined their phosphine substitution chemistry and found that bidentate phosphines will displace both COD ligands whereas monodentate phosphines only replace one COD.[1a-c] In related work, we have shown that both COD's can be replaced by PEt_3 ligands when the reaction is carried out under H_2 which apparently removes the COD's by hydrogenation.[2] In this regard, Meek and Kreter also demonstrated that

(1) (a) Kreter, P. E.; Meek, D. W. *Inorg. Chem.* **1983**, *22*, 319. (b) Meek, D. W.; Kreter, P. E.; Christoph, G. G., *J. Organomet. Chem.* **1982**, *231*, C53. (c) Fultz, W. C.; Rheingold, A. L.; Kreter, P. E.; Meek, D. W. *Inorg. Chem.* **1983**, *22*, 860.

(2) Burkhardt, E. W.; Mercer, W. C.; Geoffroy, G. L. *Inorg. Chem.* **1984**, *23*, 1779.

0276-7333/86/2305-0012$01.50/0

1 is an active olefin hydrogenation catalyst or catalyst precursor.[1a]

The molecular structures of complexes 1 and 2 have not been determined, although spectroscopic data are consistent with the structures drawn above. The ^{31}P NMR chemical shifts of the μ-PPh_2 ligands imply that complex 1 has no Rh–Rh bond (δ – 71.7) whereas complex 2 does (δ 166).[1a,3,4] Complex 2 is further assumed to have a double bond in order to give a satisfactory electron count, and it is similar to other diphosphido-bridged Ir_2 complexes for which double-bond formulations have been given.[5]

Alkynes are interesting substrates with which to investigate the chemistry of complexes 1 and 2 since these ligands can react in a variety of ways.[6] Alkynes can coordinate as two- or four-electron donors to one metal center or can bridge the two metals with the alkyne C–C bond parallel or perpendicular to the metal–metal vector. Since complexes 1 and 2 are coordinately unsaturated, alkynes could add without displacing the COD ligands or could substitute for one or both COD's. Insertion of alkyne into the M–PPh_2 bonds to give modified phosphine ligands is also a possible reaction.[7]

We have studied the chemistry of 1 and 2 with alkynes and find that binuclear oxidative addition of alkyne occurs across the bimetallic framework to give complexes with cis-dimetalated olefin formulations. These are the first examples of such a binuclear oxidative-addition reaction of phosphido-bridged compounds, although this type of reaction has considerable precedent in the chemistry of A-frame complexes[8-10] and $Ir_2(\mu\text{-SR})_2$ complexes.[11] These reactions are described herein as well as the synthesis and properties of the previously unreported complex $Rh_2(\mu\text{-}PPh_2)_2(NBD)_2$ (NBD = norbornadiene).

Results and Discussion

Reaction of $M_2(\mu\text{-}PPh_2)_2(COD)_2$ (M = Rh, Ir) with $CH_3O_2CC{\equiv}CCO_2CH_3$. The binuclear complex $Rh_2(\mu\text{-}PPh_2)_2(COD)_2$ (1) does not react with electron-rich alkynes such as $PhC{\equiv}CCH_3$ and $PhC{\equiv}CPh$. However, reaction does occur with the electron-withdrawing alkyne $CH_3O_2CC{\equiv}CCO_2CH_3$ to give complex 3 (eq 1). The corresponding diiridium complex 2 reacts in an analogous fashion to yield a similar complex 4. Excess alkyne must be used to drive these reactions to completion (by ^{31}P NMR), but the excess alkyne complicates the workup and purification of the products as it does not separate well from 3 and 4 upon chromatography. Furthermore, chromatography induces slow decomposition of 3 and rapid decomposition of 4. Thus neither complex was isolated in analytically pure form, but the X-ray structural analysis for 3 (see below) and the spectroscopic data for both confirm that the formulations given in eq 1 are correct. Both complexes show parent ions in their mass spectra corresponding to the indicated formulations. The $^{31}P\{^1H\}$ NMR spectrum of 3 shows a triplet at δ 176 assigned to the two equivalent μ-PPh_2 ligands with $J_{P\text{–}Rh}$ = 100 Hz. The downfield chemical shift implies that the μ-PPh_2 ligands bridge two Rh centers joined by a Rh–Rh bond,[3,4] consistent with the determined structure (Rh–Rh = 2.687 (1) Å). Likewise, the $^{31}P\{^1H\}$ NMR spectrum of 4 shows a downfield singlet at δ 111 implying two equivalent μ-PPh_2 ligands bridging two Ir atoms jointed by an Ir–Ir bond. The reaction of the Ir_2 complex 2 with $CH_3O_2C\text{-}C{\equiv}CCO_2CH_3$ is the first reported reaction of this complex with any substrate. Earlier, Meek and Kreter[1a] had shown that 2 does not react with CO nor with bidentate phosphines under any conditions examined.

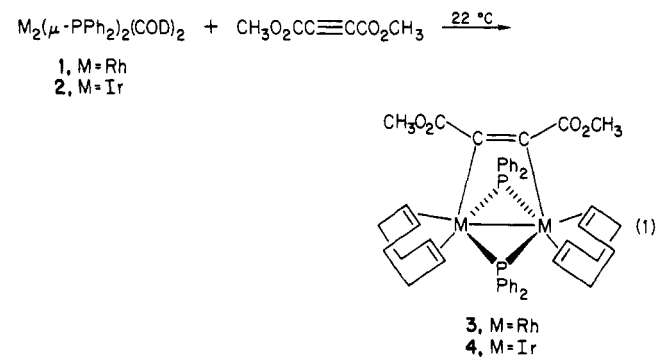

The structural data, see below, imply that the alkyne ligand in complex 3 is best formulated as a cis-dimetalated olefin, similar to a number of other binuclear alkyne complexes.[8-17] A similar formulation is implied for the Ir_2 complex 4. In forming complexes 3 and 4 the alkyne has oxidatively added across the two metal centers in 1 and 2. Such a one-electron oxidative addition to each Rh center in 1 creates two 17e metals which then form a metal–metal bond to achieve a satisfactory electron count. Alkyne addition to 2 to give 4 represents a one-electron oxidative addition to each metal across the metal–metal double bond. Accordingly, the metal–metal bond order is reduced to one in the final product. The observation that only alkynes with electron-withdrawing substituents capable of accepting electron density from the metals react with 1 and 2 is consistent with the view of this reaction as an oxidative-addition process. It is also interesting to note that $Rh_2(\mu\text{-}PPh_2)_2(COD)_2$ is air-sensitive but coordination of the alkyne gives complex 3 which is air-stable.

(3) Typically μ-PPh_2 ligands bridging metal–metal bonds show downfield chemical shifts (δ 50 → δ 200) whereas upfield shifts (δ 50 → δ – 200) are found when metal–metal bonds are absent. See: (a) Petersen, J. L.; Stewart, R. P., Jr. *Inorg. Chem.* **1980**, *19*, 186. (b) Carty, A. J.; MacLaughlin, S. A.; Taylor, N. J. *J. Organomet. Chem.* **1981**, *204*, C27. (c) Carty, A. J. *Adv. Chem. Ser.* **1982**, *No. 196*, 163. (d) Garrou, P. *Chem. Rev.* **1981**, *81*, 229. (e) Johannsen, G.; Steltzer, O. *Ibid.* **1977**, *110*, 3438.

(4) Exceptions to this correlation have recently appeared, and thus it must be used with caution. See: (a) Jones, R. A.; Wright, T. C.; Atwood, J. L.; Hunter, W. E. *Organometallics* **1983**, *2*, 470. (b) Rosen, R. P.; Hoke, J. B.; Whittle, R. R.; Geoffroy, G. L.; Hutchinson, J. P.; Zubieta, J. A. *Ibid.* **1984**, *3*, 346. (c) Targos, T. S.; Rosen, R.; Whittle, R. R.; Geoffroy, G. L. *Inorg. Chem.* **1985**, *24*, 1375.

(5) (a) Mason, R.; Sotofte, I.; Robinson, S. D.; Uttley, M. F. *J. Organomet. Chem.* **1972**, *46*, C61. (b) Bellon, P. L.; Benedicenti, C.; Caglio, G.; Manessero, M. *J. Chem. Soc., Chem. Commun.* **1973**, 946.

(6) Sappa, E.; Tiripicchio, A.; Braunstein, P. *Chem. Rev.* **1983**, *83*, 203.

(7) (a) Regragui, R.; Dixneuf, P. H.; Taylor, N. J.; Carty, A. J. *Organometallics* **1984**, *3*, 814. (b) Smith, W. F.; Taylor, N. J.; Carty, A. J. *J. Chem. Soc., Chem. Commun.* **1976**, 896.

(8) (a) Mague, J. T.; Klein, C. L.; Majeste, R. J.; Stevens, E. D. *Organometallics* **1984**, *3*, 1860. (b) Mague, J. T.; DeVries, S. H. *Inorg. Chem.* **1982**, *21*, 1632. (c) Mague, J. T. *Inorg. Chem.* **1983**, *22*, 1158.

(9) (a) Cowie, M.; Dickson, R. S. *Inorg. Chem.* **1981**, *20*, 2682. (b) Cowie, M.; Dickson, R. S.; Hames, B. W. *Organometallics* **1984**, *3*, 1879. (c) Sutherland, B. R.; Cowie, M. *Organometallics* **1984**, *3*, 1869. (d) Cowie, M.; Southern, T. G. *Inorg. Chem.* **1982**, *21*, 246. (e) Cowie, M.; Southern, T. G. *J. Organomet. Chem.* **1980**, *193*, C46.

(10) Balch, A. L.; Lee, C.-L.; Lindsay, C. H.; Olmstead, M. M. *J. Organomet. Chem.* **1979**, *177*, C22.

(11) (a) Devillers, J.; Bonnet, J.-J.; de Montauzon, D.; Goly, J.; Poilblanc, R. *Inorg. Chem.* **1980**, *19*, 154. (b) Giulmet, E.; Maisomot, A.; Poilblanc, R. *Organometallics* **1983**, *2*, 1123.

(12) Jarvis, A. C.; Kemmitt, R. D.; Russell, D. R.; Tucker, D. *J. Organomet. Chem.* **1978**, *159*, 341.

(13) Dickson, R. S.; Johnson, S. H.; Kirsch, H. P.; Lloyd, D. J. *Acta Crystallogr., Sect. B: Struct. Crystallogr. Cryst. Chem.* **1977**, *B33*, 2057.

(14) Dickson, R. S.; Mok, C.; Pain, G. *J. Organomet. Chem.* **1979**, *166*, 385.

(15) Davidson, J. L.; Harrison, W.; Sharp, D. W. A.; Sim, G. A. *J. Organomet. Chem.* **1972**, *46*, C47.

(16) Koie, Y.; Shinoda, S.; Saito, Y.; Fitzgerald, B. J.; Pierpont, C. G. *Inorg. Chem.* **1980**, *19*, 770.

(17) Smart, L. E.; Browning, J.; Green, M.; Laguna, A.; Spencer, J. L.; Stone, F. G. A. *J. Chem. Soc., Dalton Trans.* **1977**, 1777.

Table I. Crystallographic Data for $Rh_2(\mu\text{-}PPh_2)_2(\mu\text{-}CH_3O_2CC{\equiv}CCO_2CH_3)(COD)_2$ (3)

Crystal Data	
mol formula	$C_{40}H_{50}O_2P_2Rh_2$
cryst system	monoclinic
cryst dimensions, mm	0.08 × 0.28 × 0.35
space group	$P2_1/c$
a, Å	17.718 (4)
b, Å	12.345 (2)
c, Å	20.047 (5)
β, deg	113.34 (2)
V, Å	4026 (2)
Z	4
ρ(calcd), g cm^{-3}	1.54
μ(abs coeff), cm^{-1}	9.11
T, °C	21
Measurement of Intensity Data	
diffractometer	Nicolet R3
radiation	Mo Kα (λ = 0.71073 Å)
monochromator	graphite crystal
scan type	$\omega/2\theta$
scan speed	variable 4–20° min^{-1}
scan range	±0.9°
std reflctns	3 per 197 (no decay)
data limits	$4.0 < 2\theta < 48.0$
rflctns collected	$\pm h,k,l$
unique data	6301
obsvd data	4737 ($F_o > 3\sigma(F_o)$)
weighting factor,[a] g	0.0008
R_F[b]	0.063
R_{wF}[c]	0.071
GOF[d]	1.48

[a] $w^{-1} = \sigma^2(F_0) + gF_0^2$. [b] $\sum|\Delta|/\sum|F_0|$, $\Delta = |F_o| - |F_c|$. [c] $\sum(|\Delta|^{1/2})/\sum(|F_o|w^{1/2})$. [d] $[\sum w(\Delta^2)/(N_{obsd} - N_{par})]^{1/2}$.

Synthesis and Reactivity of $Rh_2(\mu\text{-}PPh_2)_2(NBD)_2$ (5). A complex analogous to 1 with the COD ligands replaced by NBD (norbornadiene) ligands has not been previously reported. Such a compound should be interesting since the NBD ligands should be more easily displaced than the COD ligands of 1. We have found that such a complex can be prepared at −78 °C by the reaction of $LiPPh_2$ with $Rh_2(\mu\text{-}Cl)_2(NBD)_2$ (eq 2). However, this

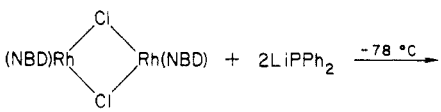

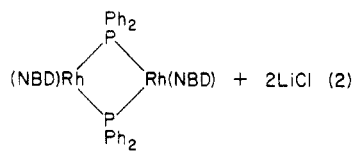

5

complex is unstable, decomposing upon warming above −10 °C, and we were unable to isolate it. The −60 °C $^{31}P\{^1H\}$ NMR spectrum of 5 shows a triplet at δ −72 ($J_{P\text{-}Rh}$ = 80 Hz) which is close to the upfield triplet observed for the COD complex 1 at δ −71.7 ($J_{P\text{-}Rh}$ = 100 Hz).[1a] The upfield position of this resonance also implies the absence of a Rh–Rh bond in 5 as in 1.[3,4] The instability of 5 has precluded an evaluation of its chemistry although it was observed to react with $PhC{\equiv}CCH_3$ and $CH_3{\equiv}CCH_3$ at low temperatures to give low yields of products whose spectroscopic data (see Experimental Section) imply formulations similar to 3.

X-ray Diffraction Study of $Rh_2(\mu\text{-}PPh_2)_2(\mu\text{-}CH_3O_2CC{\equiv}CCO_2CH_3)(COD)_2$ (3). An ORTEP drawing of complex 3 is shown in Figure 1. Crystallographic details, atomic positional parameters, and relevant bond length and bond angle data are respectively given in Tables I–III.

Table II. Atom Coordinates (×10^4) and Temperature Factors (Å^3 × 10^3)

atom	x	y	z	U
Rh(1)	2310 (1)	3403 (1)	3162 (1)	29 (1)[a]
Rh(2)	3268 (1)	3881 (1)	4541 (1)	29 (1)[a]
P(1)	2132 (1)	4070 (2)	4195 (1)	31 (1)[a]
P(2)	3412 (1)	2140 (2)	3511 (1)	34 (1)[a]
O(1)	1327 (4)	359 (5)	3040 (4)	53 (3)[a]
O(2)	462 (4)	1722 (5)	2559 (4)	62 (3)[a]
O(3)	1230 (4)	1046 (5)	4410 (3)	48 (3)[a]
O(4)	2503 (4)	415 (5)	5047 (3)	55 (3)[a]
C(1)	765 (6)	−379 (8)	2549 (6)	72 (5)[a]
C(2)	1119 (5)	1423 (6)	2976 (4)	31 (3)[a]
C(3)	1821 (5)	2071 (6)	3469 (4)	31 (3)[a]
C(4)	2256 (4)	1862 (6)	4161 (4)	26 (3)[a]
C(5)	2050 (5)	1007 (6)	4593 (4)	35 (3)[a]
C(6)	897 (6)	311 (8)	4785 (5)	57 (4)[a]
C(11)	1221 (5)	3753 (7)	2159 (4)	41 (2)
C(12)	1133 (6)	4933 (7)	1927 (5)	−50 (2)
C(13)	1717 (6)	5705 (8)	2458 (5)	56 (3)
C(14)	2529 (5)	5236 (7)	2958 (5)	43 (2)
C(15)	3009 (6)	4617 (7)	2713 (5)	46 (2)
C(16)	2812 (6)	4379 (7)	1926 (5)	52 (3)
C(17)	2304 (6)	3348 (7)	1646 (5)	47 (2)
C(18)	1739 (5)	3036 (7)	2020 (4)	41 (2)
C(21)	4193 (5)	4272 (7)	5056 (4)	37 (2)
C(22)	4570 (5)	3560 (7)	4780 (4)	39 (2)
(23)	5184 (6)	2731 (7)	5209 (5)	51 (2)
C(24)	4939 (6)	2044 (8)	5731 (5)	58 (3)
C(25)	4017 (5)	1918 (7)	5498 (5)	44 (2)
C(26)	3523 (5)	2643 (7)	5686 (4)	40 (2)
C(27)	3834 (6)	3684 (8)	6123 (5)	57 (3)
C(28)	4396 (6)	4362 (7)	5866 (5)	50 (2)
C(41)	520 (4)	3304 (5)	3896 (2)	44 (2)
C(42)	−144 (4)	3078 (5)	4081 (2)	65 (3)
C(43)	−74 (4)	3238 (5)	4792 (2)	72 (3)
C(44)	660 (4)	3624 (5)	5318 (2)	66 (3)
C(45)	1325 (4)	3851 (5)	5134 (2)	57 (3)
C(46)	1255 (4)	3691 (5)	4423 (2)	37 (2)
C(51)	1359 (3)	6067 (5)	3965 (3)	52 (2)
C(52)	1278 (3)	7175 (5)	4057 (3)	68 (3)
C(53)	1922 (3)	7749 (5)	4577 (3)	76 (3)
C(54)	2646 (3)	7215 (5)	5005 (3)	75 (3)
C(55)	2727 (3)	6107 (5)	4913 (3)	55 (3)
C(56)	2084 (3)	5533 (5)	4393 (3)	38 (2)
C(61)	2905 (4)	482 (4)	2490 (3)	56 (3)
C(62)	2737 (4)	−588 (4)	2253 (3)	76 (3)
C(63)	2794 (4)	−1409 (4)	2749 (3)	76 (3)
C(64)	3019 (4)	−1160 (4)	3481 (3)	66 (3)
C(65)	3187 (4)	−90 (4)	3718 (3)	49 (2)
C(66)	3131 (4)	731 (4)	3222 (3)	39 (2)
C(71)	4609 (4)	2906 (4)	2970 (3)	53 (2)
C(72)	5341 (4)	2810 (4)	2869 (3)	63 (3)
C(73)	5851 (4)	1917 (4)	3150 (3)	72 (3)
C(74)	5629 (4)	1121 (4)	3532 (3)	80 (3)
C(75)	4897 (4)	1217 (4)	3632 (3)	68 (3)
C(76)	4387 (4)	2109 (4)	3351 (3)	40 (2)

[a] Equivalent isotropic u defined as one-third of trace of the orthogonalized U tensor.

The two Rh atoms of complex 3 are bridged by two μ-PPh_2 ligands and the alkyne ligand. Each Rh is further coordinated by a COD ligand. The Rh_2P_2 core of the molecule is essentially planar with a [P(1)–Rh(1)–P(2)]–[P(1)–Rh(2)–P(2)] dihedral angle of 3.2°. The alkyne lies above this plane with the C–C bond parallel to the Rh–Rh axis. The coordination geometry of each Rh is approximately trigonal bipyramidal with the two phosphorus atoms and one olefinic bond of the COD ligand defining the trigonal plane. The molecule possesses approximate C_2 symmetry with the rotation axis defined by a line joining the midpoints of the Rh(1)–Rh(2) and C(3)–C(4) vectors. The Rh–Rh distance of 2.687 (1) Å in 3 is consistent with a single Rh–Rh bond as required by the 18-electron rule. This distance agrees well with other structurally characterized molecules in which a Rh–Rh single bond has been invoked (e.g., Rh_2-

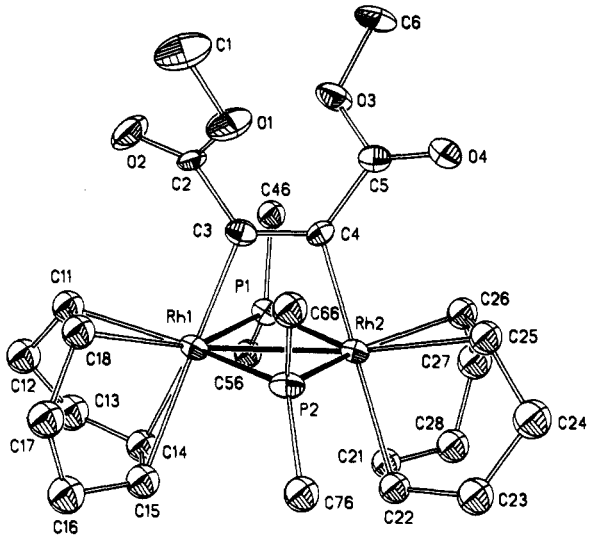

Figure 1. An ORTEP drawing of $Rh_2(\mu\text{-}PPh_2)(\mu\text{-}CH_3O_2CC{\equiv}CCO_2CH_3)(COD)_2$ (**3**). Thermal ellipsoids are drawn at the 40% probability level, and the PPh_2 phenyl rings have been omitted for clarity.

Table III. Selected Bond Distances and Angles for $Rh_2(\mu\text{-}PPh_2)_2(\mu\text{-}CH_3O_2CC{\equiv}CCO_2CH_3)(COD)_2$ (3)

Bond Distances (Å)			
Rh(1)–Rh(2)	2.687 (1)	C(4)–C(5)	1.499 (12)
Rh(1)–P(1)	2.363 (3)	C(11)–C(12)	1.519 (12)
Rh(1)–P(2)	2.377 (2)	C(12)–C(13)	1.497 (12)
Rh(2)–P(1)	2.363 (2)	C(13)–C(14)	1.506 (12)
Rh(2)–P(2)	2.363 (3)	C(14)–C(15)	1.371 (15)
Rh(1)–C(3)	2.062 (8)	C(15)–C(16)	1.502 (13)
Rh(2)–C(4)	2.072 (7)	C(16)–C(17)	1.532 (13)
Rh(1)–C(11)	2.208 (7)	C(17)–C(18)	1.520 (16)
Rh(1)–C(14)	2.360 (9)	C(21)–C(22)	1.349 (14)
Rh(1)–C(15)	2.341 (11)	C(22)–C(23)	1.493 (11)
Rh(1)–C(18)	2.153 (8)	C(23)–C(24)	1.537 (16)
Rh(2)–C(21)	2.316 (8)	C(24)–C(25)	1.520 (14)
Rh(2)–C(22)	2.319 (9)	C(25)–C(26)	1.402 (14)
Rh(2)–C(25)	2.199 (8)	C(26)–C(27)	1.530 (12)
Rh(2)–C(26)	2.177 (9)	C(27)–C(28)	1.537 (16)
C(3)–C(4)	1.318 (10)	C(28)–C(21)	1.522 (13)
C(2)–C(3)	1.480 (10)		

Bond Angles (deg)			
Rh(1)–P(1)–Rh(2)	69.3 (1)	C(4)–Rh(2)–C(26)	95.4 (3)
Rh(1)–P(2–)Rh(2)	69.1 (1)	C(4)–Rh(2)–C(25)	97.4 (3)
P(1)–Rh(1)–P(2)	110.5 (1)	C(4)–Rh(2)–C(21)	166.1 (3)
P(1)–Rh(2)–P(2)	111.0 (1)	C(4)–Rh(2)–C(22)	160.1 (3)
Rh(1)–Rh(2)–C(4)	70.4 (2)	C(3)–Rh(1)–C(11)	96.3 (3)
Rh(2)–Rh(1)–C(3)	70.8 (2)	C(3)–Rh(1)–C(18)	94.2 (3)
Rh(1)–C(3)–C(4)	109.3 (5)	C(3)–Rh(1)–C(14)	159.0 (4)
Rh(2)–C(4)–C(3)	109.2 (6)	C(3)–Rh(1)–C(15)	167.0 (4)
Rh(1)–C(3)–C(2)	124.9 (5)	C(22)–Rh(2)–C(25)	79.0 (3)
Rh(2)–C(4)–C(5)	126.0 (5)	C(21)–Rh(2)–C(26)	79.3 (3)
C(4)–C(3)–C(2)	125.7 (8)	C(15)–Rh(1)–C(18)	79.8 (3)
C(3)–C(4)–C(5)	124.8 (7)	C(14)–Rh(1)–C(11)	78.4 (3)

$(\mu\text{-}PPh_2)_2(PEt_3)_2(COD)$, 2.752 (1) Å;[1b] see also Table IV).

The bridging alkyne ligand of **3** appears best described as a cis-dimetalated olefin analogous to the formulations given for other complexes with similar geometries.[8-17] The C(3)–C(4) bond length of 1.32 (1) Å in **3** falls within the 1.27–1.34 Å range observed for other complexes with a cis-dimetalated olefin formulation (Table IV) and is comparable to a normal C=C double bond length (1.337 (6) Å.[18] By comparison, the C–C triple bond lengths of free alkynes are ca. 1.20 Å.[18] The C(4)–C(3)–C(2) and C(3)–C(4)–C(5) bond angles in **3** are 125.7 (8)° and 124.8 (7)°, respectively, consistent with the cis-dimetalated olefin coordination mode with sp^2 hybridization of the alkyne carbon atoms.

(18) "International Tables for X-ray Crystallography"; Kynoch Press: Birmingham, England, 1974; Vol. III, Table 4.2.2.

Experimental Section

All manipulations were carried out in standard Schlenk glassware under prepurified N_2. Solvents were reagent grade or better, dried by stirring over Na/benzophenone (THF, benzene, toluene, hexane) or BaO (CH_2Cl_2), followed by distillation under N_2. The compounds $Rh_2(\mu\text{-}PPh_2)_2(COD)_2$ (**1**),[1a] and $Ir_2(\mu\text{-}PPh_2)_2(COD)_2$ (**2**),[1a] $Rh_2(\mu\text{-}Cl)_2(NBD)_2$,[19] and $LiPPh_2$[20] were prepared by literature procedures. PPh_2H (Pressure Chemical Co.), *n*-BuLi, $CH_3O_2CC{\equiv}CCO_2CH_3$, $CH_3C{\equiv}CCO_2Me$, $HC{\equiv}CCO_2Me$, $PhC{\equiv}CCH_3$, $CH_3C{\equiv}CCH_3$, $PhC{\equiv}CPh$, $PhC{\equiv}CH$, and NBD (Aldrich Chemical Corp.) were purchased and used as received. Instruments used in this research have been previously described.[21] Elemental analyses were performed by Schwartzkopf Microanalytical Laboratory, Woodside, NY.

Preparation of $Rh_2(\mu\text{-}PPh_2)_2(\mu\text{-}CH_3O_2CC{\equiv}CCO_2CH_3)(COD)_2$ (3). An excess of $CH_3O_2CC{\equiv}CCO_2CH_3$ (0.108 mL, 0.76 mmol) was added via syringe to a 20 mL THF solution of $Rh_2(\mu\text{-}PPh_2)_2(COD)_2$ (0.15 g, 0.19 mmol) at 22 °C. The green solution was stirred for 1 h during which time it became dark red-brown. The solvent was evaporated, and the product was extracted into ~1 mL of CH_2Cl_2. Chromatography was conducted on silica gel under N_2 with CH_2Cl_2 as eluant. An orange band containing $Rh_2(\mu\text{-}PPh_2)_2(\mu\text{-}CH_3O_2CC{\equiv}CCO_2CH_3)(COD)_2$ was the only one to elute from the column, and 0.138 g of material slightly contaminated with free alkyne was isolated by solvent evaporation. A dark brown band remained at the top of the column. Further attempted purification failed to remove all of the excess alkyne, and the best analysis obtained corresponded to a sample containing ~67% of **3** and ~33% of free alkyne. Anal. Calcd for $C_{46}H_{50}O_2P_2Rh_2$ (**3**): C, 59.11; H, 5.35. Found: C, 56.33; H, 4.95. **3**: $^{31}P\{^1H\}$ NMR (22 °C, C_6D_6) δ 176 (t, $J_{P\text{-}Rh}$ = 100 Hz); ^1H NMR (22 °C, C_6D_6) δ 8.25–6.40 (Ph), 5.13 (br, s, olefinic CH), 2.71 (s, CO_2CH_3), 2.5–1.2 (br, m, CH_2); MS (FD), *m/z* 934 (M^+), 792 (M^+ – alkyne); IR (THF) ν_{CO} 1680 cm^{-1}.

Preparation of $Ir_2(\mu\text{-}PPh_2)_2(\mu\text{-}CH_3O_2CC{\equiv}CCO_2CH_3)(COD)_2$ (4). An excess of $CH_3O_2CC{\equiv}CCO_2CH_3$ (0.060 mL, 0.42 mmol) was added via syringe to a suspension of $Ir_2(\mu\text{-}PPh_2)_2(COD)_2$ (0.20 g, 0.22 mmol) in 25 mL of THF. The red suspension was allowed to stir for 3 days at 22 °C during which time a yellow-orange solution formed. The solution was then filtered through Celite on a glass frit and the solvent evaporated to yield 0.227 g of impure $Ir_2(\mu\text{-}PPh_2)_2(\mu\text{-}CH_3O_2CC{\equiv}CCO_2CH_3)(COD)_2$ (**4**) contaminated with free alkyne. Extensive decomposition occurred upon continued purification attempts, and analytically pure material was not obtained. **4**: $^{31}P\{^1H\}$ NMR (22 °C, THF-d_8) δ 111 (s); ^1H NMR (22 °C, THF-d_8) δ 7.98–8.01 (Ph), 4.43 (br, s, olefinic CH), 2.56 (s, CO_2CH_3), 2.28–1.73 (br m, CH_2); MS (EI), *m/z* 1114 (M^+), 1006 (M^+ – COD); IR (THF) ν_{CO} 1687 cm^{-1}.

Reaction of $Rh_2(\mu\text{-}PPh_2)_2(COD)_2$ with Nonactivated Alkynes. In separate experiments, 4 equiv of $PhC{\equiv}CH$, $PhC{\equiv}CPh$, $CH_3C{\equiv}CCH_3$, and $PhC{\equiv}CCH_3$ were added to 2 mL of 80:20 THF/benzene-d_6 solutions of $Rh_2(\mu\text{-}PPh_2)_2(COD)_2$ (0.050 g, 0.063 mmol) in 10-mm NMR tubes. Analysis of the $^{31}P\{^1H\}$ NMR spectra after the solutions were agitated for 24 h at 22 °C showed that no reaction had occurred.

Preparation of $Rh_2(\mu\text{-}PPh_2)_2(NBD)_2$ (5). One milliliter of a 75:25 THF/C_6D_6 suspension of $LiPPh_2$ (0.075 g, 0.390 mmol) in a 10-mm NMR tube was cooled to −60 °C in the NMR probe. At this temperature, a 1-mL THF/benzene-d_6 solution of $Rh_2(\mu\text{-}Cl)_2(NBD)_2$ (0.090 g, 0.195 mmol) was added. The resultant solution was allowed to spin for 20 min in the NMR probe, and then the $^{31}P\{^1H\}$ NMR spectrum was recorded: δ −72.3 (t, $J_{P\text{-}Rh}$ = 80 Hz). Upon warming to 0 °C, loss of all resonances in the $^{31}P\{^1H\}$ NMR spectrum occurred, indicating decomposition. A ^1H NMR spectrum of **5** was similarly recorded: ^1H NMR (−60

(19) Abel, E. W.; Bennett, M. A.; Wilkinson, G. *J. Chem. Soc.* **1959**, 3178.
(20) Issleib, K.; Tzschock, A. *Chem. Ber.* **1959**, *92*, 118.
(21) Breen, M. J.; Shulman, P. M.; Geoffroy, G. L.; Rheingold, A. L.; Fultz, W. C. *Organometallics* **1984**, *3*, 782.

Table IV. Structural Data for Selected Bimetallic Complexes Containing an Alkyne Ligand in a Cis-Dimetalated Olefin Coordination Mode[a]

complex	d_{M-M}, Å	$d_{C_{alk}-C_{alk}}$, Å	$C_{alk}-C_{alk}-R$, deg	ref
$Rh_2(\mu\text{-}PPh_2)_2(\mu\text{-}CH_3O_2CC{\equiv}CCO_2CH_3)(COD)_2$ (**3**)	2.687 (1)	1.32 (1)	124.8 (7) 125.7 (8)	this work
$Rh_2Cl_2(dppm)_2(\mu\text{-}CF_3C{\equiv}CCF_3)$	2.7447 (9)	1.315 (1)	127.4 (9) 128.3 (9)	9
$[Rh_2(CN\text{-}t\text{-}Bu)_4(dppm)_2(\mu\text{-}CF_3C{\equiv}CCF_3)]^{2+}$	2.9653 (6)	1.318 (9)	126.2 (5)	8
$Rh_2Cl_2(\mu\text{-}CO)(dppm)(\mu\text{-}CH_3O_2CC{\equiv}CCO_2CH_3)$	3.3542 (9)	1.32 (1)	123.8 (4)	9
$[Rh_2Cl(CNMe)_2(dppm)_2(\mu\text{-}CF_3C{\equiv}CCF_3)]^{\bullet}$	2.7091 (8)	1.32 (1)	129.3 (7) 124.9 (7)	9
$Rh_2(CO)_2Cp_2(\mu\text{-}CF_3C{\equiv}CCF_3)$	2.682 (1)	1.269 (14)	127.8 (1.1) 129.2 (1.0)	13
$Pt_2(CO)_2(PPh_3)_2(\mu\text{-}CH_3O_2CC{\equiv}CCO_2CH_3)$	2.6354 (8)	1.341 (22)	122.5 (8)	16
$[Ir_2Cl(CNMe)_2(dppm)_2(\mu\text{-}CF_3C{\equiv}CCF_3)]^{+}$	2.7793 (3)	1.344 (8)	125.4 (5) 119.5 (5)	9

[a] dppm = $Ph_2PCH_2PPh_2$, Cp = $\eta\text{-}C_5H_5$

°C, $CDCl_3$) δ 3.92 (s, bridgehead CH), 3.58 (s, olefinic CH), 1.17 (s, apex CH_2).

Reaction of $Rh_2(\mu\text{-}PPh_2)_2(NBD)_2$ with $PhC{\equiv}CCH_3$. A 20-mL THF solution of $LiPPh_2$ was cooled to −78 °C, and a 10-mL THF solution of $Rh_2(\mu\text{-}Cl)_2(NBD)_2$ (0.300 g, 0.6 mmol) and $PhC{\equiv}CCH_3$ (0.175 mL, 0.162 g, 1.40 mmol) was added by dropping funnel. The resultant deep purple solution was then stirred for 2 h at −78 °C, warmed to −20 °C, and stirred for 12 h at this temperature during which time the color changed to yellow-brown. The solution was then warmed to 22 °C, and the solvent was removed by evaporation. The brown oily product was extracted into ~50 mL of benzene and the solution was filtered through Celite on a glass frit followed by evaporation of solvent. Chromatography on SiO_2 under N_2 using neat CH_2Cl_2 as eluant gave one dark red brown band which slowly eluted from the column. Only 0.025 g of dark red-brown $Rh_2(\mu\text{-}PPh_2)_2(PhC{\equiv}CCH_3)(NBD)_2$ (**7**) was recovered (4% yield). **7**: $^{31}P\{^1H\}$ NMR (22 °C, C_6D_6) δ 188.2 (dd, J_{P-Rh} = 110, 107 Hz); MS (FD), m/z 876 (M^+), 760 (M^+ − $PhC{\equiv}CCH_3$).

Reaction of $Rh_2(\mu\text{-}PPh_2)_2(NBD)_2$ with $CH_3C{\equiv}CCH_3$. A 10-mL THF solution of $Rh_2(\mu\text{-}Cl)_2(NBD)_2$ (0.20 g, 0.434 mmol) and $CH_3C{\equiv}CCH_3$ (0.136 mL, 0.094 g, 1.73 mmole was added by dropping funnel to a 10-mL THF solution of $LiPPh_2$ (0.167 g, 0.868 mmole which had been cooled to −78 °C. After being stirred at −78 °C for 1 h, the dark purple solution was warmed to −30 °C and stirred for an additional 12 h. The solvent was then evaporated at 22 °C and the product extracted with ~30 mL of toluene which was then filtered through Celite on a glass frit. The toluene was removed by evaporation, the reaction product was dissolved in 2 g of benzene-d_6, and a $^{31}P\{^1H\}$ NMR spectrum was recorded: δ 186 (t, J_{P-Rh} = 110 Hz) plus several unresolved resonances in the δ 63–20 spectral region. Nothing would elute upon chromatography of this reaction mixture on SiO_2 even when using neat CH_2Cl_2 as eluant.

X-ray Diffraction Study of $Rh_2(\mu\text{-}PPh_2)_2(\mu\text{-}CH_3O_2CC{\equiv}CCO_2CH_3)(COD)_2$ (3). Crystals of **3** were obtained by slow evaporation of a solution under reduced N_2 pressure. A suitable crystal was mounted in an arbitrary orientation on a glass fiber which was then fixed onto an aluminum pin on a eucentric goniometer. Lattice parameters were obtained from the least-squares fit of angular settings of 25 well-centered reflections, 25° < 2θ < 30°. Data collection and refinement procedures used were as previously reported.[22] Pertinent details are provided in Table I. Lorentz and polarization corrections were applied to the data, as was an empirical (ψ-scan) absorption correction (T_{min}/T_{max} = 0.332/0.444).

The two Rh atoms were located by an automated Patterson interpretation procedure, and the remaining non-hydrogen atoms were obtained from a difference map phased by the two Rh atoms. With the incorporation of hydrogen atoms in fixed, idealized positions (d(C–H) = 0.96 Å) and rigid-body constraints on the four phenyl rings (d(C–C) = 1.395 Å), the refinement process smoothly converged to the residuals reported in Table I. The final difference map revealed no unusual or chemically relevant features (highest peak = 1.03 e/Å^3).

During all calculations the analytical scattering factors for neutral atoms were corrected for both $\Delta f'$ and $i\Delta f''$ terms. Final positional parameters are collected in Table II; thermal parameters appear in the supplementary material which also contains the structure factors and full bond length and angle data.

Acknowledgment. This research was supported by the National Science Foundation (CHE82-01160). We gratefully acknowledge Johnson-Matthey, Inc., for a loan of $RhCl_3{\cdot}3H_2O$.

Registry No. **1**, 82829-24-1; **2**, 83681-88-3; **3**, 99128-47-9; **4**, 99147-74-7; **5**, 99128-48-0; **7**, 99128-49-1; $Rh_2(\mu\text{-}Cl)_2(NBD)_2$, 12257-42-0; $Rh_2(\mu\text{-}PPh_2)_2(CH_3C{\equiv}CCH_3)(NBD)_2$, 99128-50-4; $CH_3O_2CC{\equiv}CCO_2CH_3$, 762-42-5; $LiPPh_2$, 4541-02-0; $PhC{\equiv}CCH_3$, 673-32-5; $CH_3C{\equiv}CCH_3$, 503-17-3.

Supplementary Material Available: Tables of anisotropic thermal parameters, complete bond lengths and angles, calculated hydrogen atom positions, and structure factors for **3** (33 pages). Ordering information is given on any current masthead page.

(22) Rheingold, A. L.; Sullivan, P. J. *Organometallics* **1983**, *2*, 327.

Solution and Solid-State Structures of Salts of *trans*-$HFe(CO)_3PR_3^-$ Including a Study of Alkali Cation Contact Ion Pairing

Carlton E. Ash, Terry Delord, Debra Simmons, and Marcetta Y. Darensbourg*

Department of Chemistry, Texas A&M University, College Station, Texas 77843

Received May 6, 1985

Site-specific contact ion pairing interactions have been examined by ν(CO) IR band analysis for Et_4N^+, K^+, Na^+ and Li^+ salts of *trans*-$HFe(CO)_3P^-$ (P = $P(OMe)_3$, $P(OEt)_3$, PMe_3, PEt_3, PPh_2Me, and PPh_3). Two major types of contact ion pairs were noted: one involving $^-$Fe–CO···cation$^+$ interaction and another involving $^-$Fe···cation$^+$ interaction. A combination of factors, solvent polarity, cation electrostatic potential, cation solvation, and size of the P ligand, determine the ion contact site selection. The indication of $^-$Fe···cation$^+$ interaction is supportive of a metal-based rather than hydride-based nucleophilicity in hydride/halide displacement reactions of $HFe(CO)_3P^-$ with alkyl halides. The X-ray crystal structure of $Et_4N^+HFe(CO)_3PPh_3^-$ was determined. It crystallizes in the cubic system, space group $Pa3$, with cell parameters $a = b = c = 17.670$ (8) Å, $V = 5533$ (2) Å^3, and $Z = 8$. The hydride ligand was not located but indicated to be trans to the PPh_3 in a distorted trigonal-bipyramidal coordination geometry. The equatorial CO groups are bent away from the phosphine with a P–Fe–CO angle of 99.5°.

Introduction

The site specificity of alkali cation interaction with anionic organometallics containing multiple basic sites for contact ion pairing has been effectively probed by solution infrared spectroscopy.[1] For example in THF solution ν(CO) IR analysis shows contact interaction of Na^+ with the equatorial carbonyl oxygen of trigonal-bipyramidal $Mn(CO)_5^-$.[2,3] Phosphorus-donor ligand derivatives $Mn(CO)_4PR_3^-$ are of C_{3v} symmetry; i.e., the substituent ligand is in the axial position, and the alkali cation contact interaction is again localized at the equatorial CO oxygen, or cis to the P substituent. In comparison to the all-CO anion $Mn(CO)_5^-$ the increased electron density in $Mn(CO)_4P^-$ enhances the ion pairing interaction both in terms of numbers of contact ion pairs (the K_{eq} of eq 1) as well as in the magnitude of the interaction (as reflected in force constant differences, k_{CO}, in M^-–CO vs. M^-–CO···Na^+).[2]

$$[M-]CO^- + Na^+(S)_x \overset{K_{eq}}{\rightleftharpoons} \underset{\text{cip}}{[M-]CO\cdots Na^+(S)_{x-1}} \quad (1)$$

Contact ion pairing is not spectroscopically detected with Na^+ salts of $V(CO)_6^-$ in THF.[4] This is accounted for by the greater charge delocalization of $V(CO)_6^-$ as compared to $Mn(CO)_5^-$ or $Co(CO)_4^-$, thus reducing its electrostatic potential so as to be less competitive than THF for a site in the coordination sphere of Na^+. Phosphorus donor ligand substitution, however, sufficiently increases electron density so that contact ion pairs are observed. They are of the form *trans*-$R_3PV(CO)_4CO\cdots Na^+(S)_y$.[4]

The problem of site selectivity has been extended to include anions containing hydride ligands as well as CO. With $HFe(CO)_4^-$, THF solution spectra clearly indicated Na^+ interaction with an equatorial CO oxygen.[5] The contact ion pair structure is similar to the $Na^+Mn(CO)_5^-$ and $Na^+Mn(CO)_4P^-$ structures. Sodium salts of the more charge delocalized $HM(CO)_5^-$ (M = Cr, W) systems were less clear-cut. Analysis of the ν(CO) IR spectra indicated a trans CO–oxygen interaction in the case of $Na^+HCr(CO)_5^-$, and the $HW(CO)_5^-$ anion appeared to have some interaction of Na^+ at the hydride site as well.[6] Upon synthesizing the P ligand derivatives *cis*-$HW(CO)_4PR_3^-$, both ν(CO) IR as well as ^{1}H NMR indicated contact interaction with Na^+ solely at the W–H site. The site selection was rationalized on basis of the decreased ability of H^- to serve as an electron donor in the presence of the P donor ligand. Hence the buildup of electron density on H^- has enhanced its electrostatic potential in these cases. We noted that the spectroscopic tools used could not distinguish between cation interaction at the hydride site, the metal site, or a combination M–H bond density site. Furthermore there appeared to be a correlation between site selective contact ion pairing and chemical reactivity of these highly reactive hydrides.[7]

In order to broaden these observations, we have synthesized a series of *trans*-$HFe(CO)_3PR_3^-$ complexes for comparison of ion pairing properties with the $HFe(CO)_4^-$ anion. We report herein the solid state structure of Et_4N^+*trans*-$HFe(CO)_3PPh_3^-$, first synthesized by others,[8,9] and the spectral changes (IR and NMR) associated with ion exchanging PPN^+ or Et_4N^+ by K^+, Na^+, and Li^+. A series of different PR_3 ligands is used. The $HFe(CO)_3PR_3^-$ anions are considerably more reactive as H^- transfer or reducing agents than is the parent $HFe(CO)_4^-$.[7] Some chemical properties are included also.

Experimental Section

A. Methods and Materials. An argon atmosphere glovebox and/or standard Schlenk techniques (N_2 atmosphere) were used in all reactions, sample transfers, and sample manipulations. All solvents were distilled in a N_2 atmosphere from appropriate drying agents (hexane and tetrahydrofuran (THF), from Na^0/benzophenone; diethyl ether, from lithium aluminum hydride; methanol, from MgI_2; and methylene chloride from P_2O_5) and then stored in dried, N_2-filled flasks over activated 4A molecular sieves. The crown ether 18-crown-6 was used as received. Dimethyl sulfoxide, reagent grade, was degassed prior to use. A nitrogen purge was used on these solvents prior to use, and transfers to the reaction vessels were via stainless steel cannula under a positive N_2 pressure.

(1) Darensbourg, M. Y. *Prog. Inorg. Chem.* **1985**, *33*, 221.
(2) Darensbourg, M. Y.; Darensbourg, D. J.; Burns, D.; Drew, D. A. *J. Am. Chem. Soc.* **1976**, *98*, 3127.
(3) Edgell, W. F.; Balch, T., in press.
(4) Hanckel, M.; Darensbourg, M. Y. *Organometallics* **1982**, *1*, 82.
(5) Darensbourg, M. Y.; Barros, H. L. C. *Inorg. Chem.* **1979**, *18*, 3286.
(6) Darensbourg, M. Y.; Kao, S. K.; Schenk, W. *Organometallics* **1984**, *3*, 871.
(7) Kao, S. C.; Spillett, C. T.; Ash, C.; Lusk, R.; Park, Y. K.; Darensbourg, M. Y. *Organometallics* **1985**, *4*, 83.
(8) Edens, M. W. Ph.D. Dissertation, The University of Texas, Austin, 1977.
(9) Chen, Y. S.; Ellis, J. E. *J. Am. Chem. Soc.* **1982**, *104*, 1141.

0276-7333/86/2305-0017$01.50/0

B. Instrumentation. Infrared spectra were recorded on an IBM FTIR/85 or a Perkin-Elmer 283B spectrometer using 0.1-mm sealed NaCl solution cells. Proton nuclear magnetic resonance spectra were recorded on a 90-MHz Varian EM-390 spectrophotometer. Some proton spectra as well as ^{13}C and ^{31}P NMR spectra were recorded on a Varian XL200 spectrometer.

C. Band-Shape Analysis. Infrared spectra were measured on an IBM FTIR/85. Data points in the range 4000–600 cm^{-1} were collected at an interval of 0.96 cm^{-1}. Data points in the range 2150–1760 cm^{-1} were transferred from the IBM FTIR/85 directly to a DEC VAX 11/780 where the calculations were performed.

Infrared band shapes of the carbonyl stretching vibrations were calculated. The analysis was carried out by using a program based on the work of R. N. Jones and J. Pitha of the Division of Pure Chemistry, National Research Council of Canada.[10a] The program, modified for our use,[10b] fits a Cauchy–Gauss product and/or sum function to an infrared absorption band envelope. The Cauchy–Gauss product function used for the calculation of the infrared band envelopes is given in the form described by Jones and Pitha[10a] (eq 2), where α is the base line in absorbance, χ_1 is

$$(T/T_0)_{\nu(\text{calcd})} = \exp(-2.303) \times \{\alpha + \sum_{P=1}^{M} \chi_{1(P)}[1 + \chi_{3(P)}{}^2(\nu - \chi_{2(P)})^2]^{-1} \exp[-\chi_{4(P)}{}^2(\nu - \chi_{2(P)})^2]\} \quad (2)$$

the absorbance at the band's maximum, χ_2 is the peak position in cm^{-1}, χ_3 and χ_4 together describe the half-band-width and the Cauchy–Gauss ratio, and M is the number of bands included in the analysis. The band indices $(\chi_1, \chi_2, \chi_3, \chi_4)_p$ and α were varied so as to minimize ϕ, where

$$\phi = \sum_{\text{band}} [(T/T_0)_{\nu(\text{obsd})} - (T/T_0)_{\nu(\text{calcd})}]^2 \quad (3)$$

The optimum band parameters were determined by using the product function. Then the ordinates of the band envelope were calculated for each component band in both transmittance and absorbance. Simpson's rule was used to calculate the areas under each band from the absorbance values. Most of the calculated band shapes were closer to the Cauchy than to the Gauss shape with the shape ratios, as defined by Jones and Pitha,[10a] generally being greater than 0.6. A shape ratio of unity exists for a pure Cauchy band shape, and a value of zero occurs for a pure Gauss band shape. A listing of band indices is included in the supplementary material.

D. Preparations. 1. Preparation of $PFe(CO)_4$ Complexes. One of two previously reported literature methods for these preparations was chosen according to the reported percentage yield.[11,12] For P = PPh_3 or PPh_2Me, $PFe(CO)_4$ complexes were prepared by using $CoCl_2 \cdot 2H_2O$ as the substitution catalyst for the reaction $Fe(CO)_5 + P \rightarrow PFe(CO)_4 + CO$.[11] The remainder of $PFe(CO)_4$ complexes were prepared similarly using as intermediates iron carbonyl anions prepared by sodium benzophenone ketyl reduction of $Fe(CO)_5$.[12]

2. Preparation of $[HFe(CO)_3P^-]$. (a) P = PPh_2Me, PPh_3, PEt_3, and PMe_3. The procedure of choice was adapted from that of Chen and Ellis.[9] The starting material $PFe(CO)_4$, 1 g, was typically placed in a 50-mL Schlenk flask along with 10–15 equiv of $Et_4N^+OH^-$ in MeOH (25% by weight solution). No reaction was observed until most of the MeOH was removed under vacuum.[9] A vacuum was maintained for approximately 20 h. In the case of P = PPh_3 and PPh_2Me, the resulting yellow solid was washed with three to four 10–20-mL portions of a 1:1 $MeOH/H_2O$ mixture and finally recrystallized from THF using Et_2O to precipitate the salt. Since the more reactive hydrides (P = PEt_3, PMe_3) reacted with H_2O or MeOH, the wash step was omitted. Tetrahydrofuran was added directly to the crude product and the resulting solution cannulated away from excess $Et_4N^+OH^-$ and filtered through Celite. Solutions were concentrated in vacuo and Et_2O added to effect precipitation. Yields were typically 60–80%. Anal. Found (Calcd for $Et_4N^+HFe(CO)_3PEt_3^-$): C, 52.70 (52.45); H, 9.06 (9.32).

(b) P = $P(OMe)_3$, $P(OEt)_3$, and PPh_3. In a typical preparation, 1 g of solid $PFe(CO)_4$, a 1:1 molar ratio PPNCl, and a 10:1 molar excess of KOH were added to a Schlenk flask sealed with a rubber septum. After thorough degassing, approximately 10 mL of methanol was added via cannula and the thick slurry stirred under nitrogen. For P = $P(OEt)_3$, the green liquid $PFe(CO)_4$ was added to the evacuated flask just before addition of methanol. Typically a precipitate resulted within 20 min, and the reaction was continued for 10–12 h to ensure completion. A longer reaction time was required for P = PPh_3, and there was a lower yield of hydride.

At completion of the reaction a total of approximately 70 mL of degassed H_2O was added and cannulated off under positive nitrogen pressure to remove excess KOH. The bright yellow product was dissolved in THF, filtered through Celite, and then precipitated out by the addition of diethyl ether. The yields for P = $P(OEt)_3$ and $P(OMe)_3$ are high (80–95%). Anal. Found (Calcd for $PPN^+HFe(CO)_3P(OEt)_3^-$): C, 63.92 (63.92); H, 5.12 (5.48). Found (Calcd for $PPN^+HFe(CO)_3P(OMe)_3^-$): C, 62.57 (62.78); 5.18 (5.02).

(c) Preparation of Alkali Cation Salts. The $HFe(CO)_3P^-$ anions were obtained as Na^+ or Li^+ salts by ion exchange of the isolated PPN^+ or $Et_4N^+HFe(CO)_3P^-$ salts with $KBPh_4$,[13] $NaBPh_4$ or $LiBPh_4$ in THF solution.[13] A 5-fold excess of the alkali salt was added, resulting in the formation of a white precipitate, presumably $PPN^+BPh_4^-$. Spectral measurements in THF solution were typically made on the supernatant without isolation of the Na^+, K^+, or Li^+ salts. Diethyl ether solutions of the alkali salts were prepared as follows: subsequent to vacuum removal of THF from the supernatant just described, the resulting white powder was dried in vacuo for 0.5 h to overnight and then redissolved in dry Et_2O. ^1H NMR indicated a small amount of THF remaining, on the order of 5:1 $Na^+HFe(CO)_3P^-$ to THF.

X-ray Crystal Structure Determination of $Et_4N^+HFe(CO)_3PPh_3^-$

A yellow, irregularly shaped crystal with maximum dimensions 0.28 mm × 0.32 mm × 0.40 mm was sealed in a random orientation in epoxy to prevent atmospheric contact. Intensity data were measured by using graphite monochromated Mo Kα radiation (λ = 0.71073 Å) on an Enraf-Nonius CAD-4 diffractometer. Lattice parameters were determined from 25 well-centered reflections ($2° < \theta < 7.5°$) randomly located in reciprocal space, to give the following cubic cell: $a = b = c = 17.670$ (8) Å; V = 5533 (2)Å^3. According to the systematic absences $0kl$, $k = 2n + 1$, $h0l$, $l = 2n + 1$, and $hk0$, $h = 2n + 1$, the space group was determined to be $Pa3$.

Reflection intensities were measured at room temperature by using the θ–2θ scan method for data in the range $1° < \theta < 22.5°$. A total of 4016 reflections were scanned of which 1513 had $I > 3\sigma(I)$. Periodic measurement of intensity standard reflections exhibited no significant decrease during the X-ray experiment. The intensity data were corrected for Lorentz and polarization effects to yield observed structure factors. No correction was made for absorption effects (μ = 6.2 cm^{-1}).

Structure Solution and Refinement. The structure was solved by application of the direct methods programs of the SDP crystallographic computing package, to give the Fe atom position. The remainder of the non-hydrogen atom positions were determined from subsequent difference Fourier maps. Hydrogen atoms of the phenyl rings were included in idealized, calculated positions with fixed temperature factors. It was not possible to determine the position of the hydride ligand. All non-hydrogen atoms of the anion were refined anisotropically. The NEt_4^+ cation, located on a crystallographic threefold axis, was found to be disordered. Three independent positions for the α-carbon atoms were located in the difference map and refined with arbitrary multiplicities of 0.33, 0.50, and 0.50, for C(8), C(10), and C(12), respectively, leading to a total of nine α-carbon sites. The positions for three β-carbons were located and refined (C(9), C(11), and C(13) with multiplicities of 0.33, 0.50, and 0.50, respectively). Because of this disordering, the C atoms of the cation were refined isotrop-

(10) (a) Jones, R. N.; Pitha, J., Bulletin No. 12, National Research Council of Canada, 1968. (b) Hyde, C. L.; Darensbourg, D. J. *Inorg. Chem.* **1973**, *12*, 1075.
(11) Albers, M. D.; Coville, N. J. *J. Organomet. Chem.* **1981**, *217*, 385.
(12) Butts, S. B.; Shriver, D. F. *J. Organomet. Chem.* **1979**, *169*, 191.
(13) Bhattacharyya, D. N.; Lee, C. L.; Smid, J.; Szwarc, M. *J. Phys. Chem.* **1965**, *69*, 608.

Table I. Summary of Crystallographic Data

empirical formula	$FePNC_{29}H_{36}O_3$
mol wt	533.44
cryst system	cubic
space group	Pa3
cell parameters	
$a = b = c$, Å	17.687 (8)
$\alpha = \beta = \gamma$, deg	90°
cell vol, Å^3	5533 (2)
Z	8
max cryst dimens, mm	0.28 × 0.32 × 0.40
ρ(calcd), g cm^{-1}	1.281
μ, cm^{-1}	6.48
radiatn, Å	Mo Kα (λ = 0.71073)
std reflections	142, 222, 432
2θ range, deg	2–45
total reflctns measd	4016
obsd reflctns ($I > 3\sigma(I)$)	1513
R^a	0.049
$R_w{}^b$	0.064

$^a R = \sum||F_o| - |F_c||/\sum|F_o|$. $^b R_w = [\sum w(|F_o| - |F_c|)^2/\sum w(F_o)^2]^{1/2}$.

Table II. Positional Parameters and Their Standard Deviations for $Et_4N[HFe(CO)_3PPh_3]$

atom	x	y	z
Fe	0.80442 (6)	0.8044 (0)	0.8044 (0)
P(1)	0.8758 (1)	0.8758 (0)	0.8758 (0)
O(1)	0.6746 (3)	0.7841 (4)	0.9011 (4)
N	0.3856 (4)	0.3856 (0)	0.3856 (0)
C(1)	0.7284 (5)	0.7932 (5)	0.8639 (5)
C(2)	0.9620 (4)	0.9148 (4)	0.8319 (4)
C(3)	0.9894 (5)	0.9864 (5)	0.8472 (4)
C(4)	1.0546 (5)	1.0126 (5)	0.8134 (6)
C(5)	1.0928 (5)	0.9665 (6)	0.7651 (6)
C(6)	1.0691 (5)	0.8958 (6)	0.7521 (7)
C(7)	1.0028 (5)	0.8703 (5)	0.7842 (5)
C(8)	0.468 (2)	0.429 (2)	0.374 (2)
C(9)	0.525 (2)	0.387 (2)	0.412 (2)
C(10)	0.355 (2)	0.390 (2)	0.298 (2)
C(11)	0.246 (1)	0.397 (1)	0.344 (1)
C(12)	0.414 (2)	0.430 (2)	0.324 (2)
C(13)	0.510 (1)	0.369 (1)	0.449 (1)

ically. No attempt was made to locate or place any of the hydrogen atoms of the cation.

The structure was refined by weighted ($w = 1/\sigma^2(F_o)$) full-matrix least squares based on F, minimizing the function $\sum w(|F_o| - |F_c|)^2$. Only those reflections with $F^2 > 3\sigma(F^2)$ were used in refinement. Neutral atomic scattering factors[14a] were used throughout, with anomalous dispersion corrections[12b] applied to all atoms. Refinement converged at $R = 0.049$ ($R_w = 0.064$) for 611 observations and 106 variables. The largest parameter shift during the final cycle of least squares was 0.04 times its esd. A final ΔF map had a chemically insignificant maximum residual of 0.38 e/Å^3. A summary of the crystallographic data is in Table I. Final positional parameters are given in Table II. Tables listing observed and calculated structure factors and the anisotropic thermal parameters are available as supplementary material.

Results and Discussion

Synthesis. The synthesis of the $HFe(CO)_3P^-$ anions was developed by others[8,9] and is designed according to eq 4. Making use of the well-known addition reaction of OH^-

$$PFe(CO)_4 + OH^- \rightarrow [trans\text{-}HOC(=O)Fe(CO)_3P^-] \xrightarrow{-CO_2} HFe(CO)_3P^- \quad (4)$$

to a metal-activated CO carbon, the carboxylic acid intermediate is produced and subsequently decarboxylates, yielding the hydride product. A high concentration of OH^- is essential for these preparations and is obtained in this work by using alcoholic KOH slurries. For very basic phosphines, PMe_3 or PEt_3, the preparation is successful only if the Chen and Ellis method[9] of using Et_4NOH/MeOH/$PFe(CO)_4$ slurries, evacuated to give the most concentrated solutions possible, is used.

Table III. Interatomic Distances (Å) and Angles (deg) for $HFe(CO)_3PPh_3^-$ Anion

(a) Bond Lengths (Å)			
Fe–P(1)	2.187 (1)	C(2)–C(7)	1.362 (10)
Fe–C(1)	1.719 (9)	C(3)–C(4)	1.380 (10)
P(1)–C(2)	1.844 (7)	C(4)–C(5)	1.359 (12)
C(1)–O(1)	1.169 (8)	C(5)–C(6)	1.339 (12)
C(2)–C(3)	1.381 (10)	C(6)–C(7)	1.378 (12)
(b) Bond Angles (deg)			
P(1)–Fe–C(1)	99.5 (3)	C(3)–C(2)–C(7)	117.7 (7)
C(1)–Fe–C(1)	117.3 (2)	C(2)–C(3)–C(4)	121.1 (7)
Fe–P(1)–C(2)	116.8 (2)	C(3)–C(4)–C(5)	119.0 (8)
C(2)–P(1)–C(2)	101.3 (3)	C(4)–C(5)–C(6)	120.9 (8)
Fe–C(1)–O(1)	176.5 (8)	C(5)–C(6)–C(7)	120.1 (9)
P(1)–C(2)–C(3)	123.4 (6)	C(2)–C(7)–C(6)	121.1 (8)
P(1)–C(2)–C(7)	118.9 (6)		

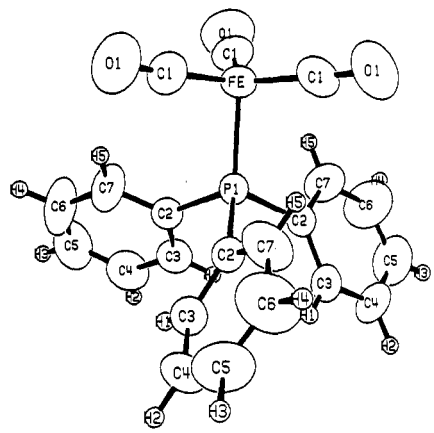

Figure 1. An ORTEP drawing of the anion of $Et_4N^+HFe(CO)_3PPh_3^-$ showing 50% probability ellipsoids of the Fe, C, O, and P atoms. Hydrogen atoms on the phenyl rings are represented as spheres in calculated positions; hydride ligand on Fe was not located.

Solid-State or Crystal Structure of $Et_4N^+HFe(CO)_3PPh_3^-$. Bond distances and angles for $HFe(CO)_3PPh_3^-$ may be found in Table III. It was not possible to locate the hydride ligand in this study; however, an ORTEP plot of the isolated anion (Figure 1) shows a distorted trigonal-bipyramidal geometry. As expected on basis of the equatorial site preference of π-accepting ligands in trigonal-bipyramidal geometry,[15] the CO groups are equatorial and the PPh_3 ligand is axial and trans to an open site where the unlocated hydride ligand is presumed to be. All Fe–CO linkages were found to be acceptably linear, and the CO groups cis to the hydride or PPh_3 are required by crystallographic symmetry to be identical. A view of the anion along the Fe–P bond axis is provided in supplementary materials and shows a staggered configuration of the P–C and Fe–C bonds. Severe disordering existed in the cation.

The distortion in the trigonal-bipyramidal geometry lies in a bending of the CO groups toward the hydride site. Despite the large steric bulk of the PPh_3 ligand this bending ($\angle P\text{–}Fe\text{–}C_{eq} = 99.5°$) is almost the same as that observed in the $HFe(CO)_4^-$ anion (the average $C_{ax}\text{–}Fe\text{–}C_{eq}$ angle was found to be 99.1°).[16] In both cases the $Fe(CO)_3L$ part of the anion has considerable tetrahedral character. The hydride ligand may be considered as buried in one face

(14) "International Tables for X-ray Crystallography"; Kynoch Press: Birmingham, England, 1975; Vol. IV; (a) Table 2.2B; (b) Table 2.3.1.

(15) Rossi, A. R.; Hoffmann, R. *Inorg. Chem.* **1975**, *14*, 365.
(16) Smith, M. B.; Bau, R. *J. Am. Chem. Soc.* **1973**, *95*, 2388.

Table IV. Comparison of Bond Distances (Å) and Angles (deg) of $LFe(CO)_4$ and $HFe(CO)_3L^-$ Taken from X-ray Data (Except Where Noted)

compd	bond angles L_{ax}–Fe–C_{eq}[a]	bond distances Fe–C_{ax}	Fe–C_{eq}	Fe–P	ref
$Fe(CO)_5$	90	1.806 (5)[b]	1.833 (4)[b]		17
$Fe(CO)_4PPh_3$	88.8 (6)	1.795 (2)	1.795 (4)	2.244 (1)	18
$HFe(CO)_4^-$	99.1 (30)	1.72 (2)	1.75 (4)		16
trans-$HFe(CO)_3PPh_3^-$	99.5 (3)		1.719 (9)	2.187 (1)	this work

[a] L_{ax} = CO or PPh_3. [b] Electron diffraction data.

of the tetrahedron, the $Fe(CO)_3$ face, and its stereochemical requirement forces an opening of that face.

There are significant differences in the structures of the anionic iron hydrides $HFe(CO)_4^-$ and *trans*-$HFe(CO)_3PPh_3^-$ and their neutral, non-hydridic counterparts $Fe(CO)_5$ and $Fe(CO)_4PPh_3$.[17,18] The latter are approximately regular trigonal bipyramids, and the former are severely distorted toward a hydride-capped tetrahedron. Conventional $d_\pi \rightarrow \pi^*$ back-bonding arguments predict shorter Fe–C bonds as electron density is increased on Fe. The bond distance data presented in Table IV (electron diffraction data for $Fe(CO)_5$)[17,19] show significant differences in the Fe–C bonds as a CO is replaced by PPh_3 and further as a CO is replaced by H^-. At 1.719 (9) Å the Fe–CO bond distances of *trans*-$HFe(CO)_3PPh_3^-$ are very short and comparable to the Fe–C distance in $Fe(CO)_4^{2-}$ as its Na^+·crypt salt.[20] Consistent with the short Fe–C bonds in $HFe(CO)_3PPh_3^-$, at 1.17 Å the C–O distances are also comparable to $Fe(CO)_4^{2-}$ and among the longest terminal CO bonds reported in carbonyl anion chemistry.[1]

Interestingly the Fe–P distance also shortens in $HFe(CO)_3PPh_3^-$ as compared to $Fe(CO)_4PPh_3$. We interpret this bond shortening to be a consequence of the geometrical difference between $Ph_3PFe(CO)_4$, a regular TBP, and $HFe(CO)_3PPh_3^-$, a distorted TBP with considerable T_d character, allowing a less hindered Fe–P contact. It should be noted that the T_d character of the hydride anion also results in more s character in the iron–phosphorus bond and, presumably, a strengthening, of the Fe–P bond. This view of the Fe–P bonding is supported by the observation that the W–P bond in the octahedral anion *cis*-$W(CO)_4(CH_3)PMe_3^-$ is somewhat *longer* than that in $W(CO)_5PMe_3$ (2.532 (3) Å vs. 2.516 Å, respectively).[21a,b] Another factor contributing to the short Fe–P bond is the π-accepting character of the PPh_3 ligand trans to strong σ-donating ligands.[22]

Solution Structure of $HFe(CO)_3P^-$: Ion Pairing as a Function of P-Donor Ligand. In accord with the C_{3v} symmetry of *trans*-$HFe(CO)_3PPh_3^-$, idealized as structure **a** in Figure 2, all of the PR_3 derivatives have two bands (A_1 + E) in the ν(CO) IR (Figure 3) when spectra are measured on non-contact ion paired forms, or symmetrically solvated anions. This is accomplished in THF solutions of PPN^+ salts, THF solutions of Na^+ salts to which good cation-complexing agents such as 18-crown-6 have been added, or CH_3CN solutions of $Et_4N^+HFe(CO)_3PPh_3^-$. Earlier conductivity measurements[2,23] suggested such so-

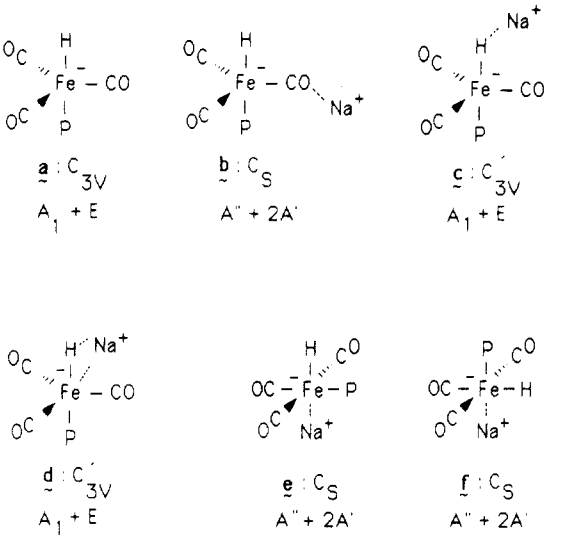

Figure 2. Possible solution forms of $HFe(CO)_3P^-$ and contact ion pairing sites. ν(CO) IR expectations are listed under each symmetry label. C_{3v}' refers to a pseudo-C_{3v} symmetry, assuming the $Na^+\cdots H^-$ (c) or $Na^+\cdots HFe^-$ (d) interaction does not significantly perturb the local trigonal symmetry of the equatorial CO's.

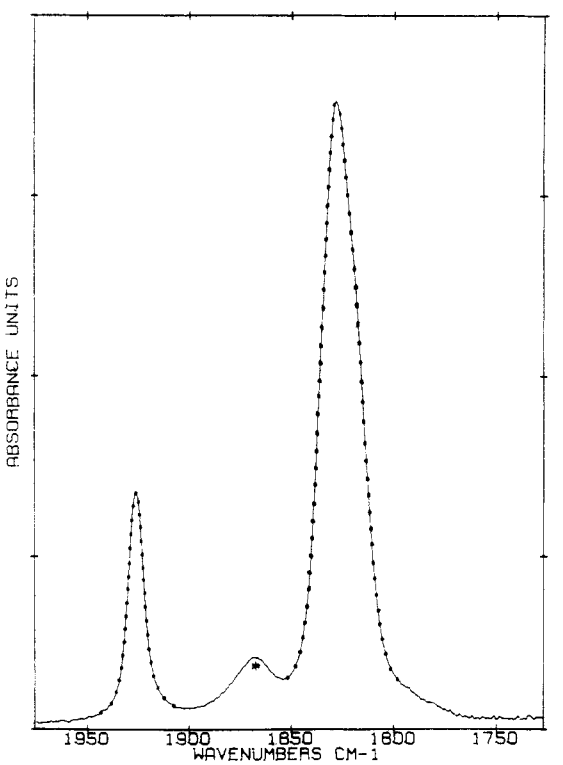

Figure 3. ν(CO) IR spectrum of $PPN^+HFe(CO)_3PPh_3^-$, 0.01 M in THF. The asterisk (*) denotes the ν(M–H). This stretch has been confirmed by deuterium substitution on pure samples and should not be mistaken here for the ν(CO) of $P_2Fe(CO)_3$ which has a similar position as seen in Figures 4 and 5.

(17) Beagley, B.; Cruickshank, D. W. J.; Pinder, P. M.; Robiette, A. G.; Sheldrick, G. M. *Acta Crystallogr., Sect. B: Struct. Crystallogr. Cryst. Chem.* **1969**, *B25*, 737.
(18) Riley, P. E.; Davis, R. E. *Inorg. Chem.* **1980**, *19*, 159.
(19) There is a low-temperature X-ray diffraction study of $Fe(CO)_5$ which reported Fe–C distances in a range of 1.79–1.84 Å; however, the structure was of insufficient quality to detect significant differences in Fe–C_{ax} and Fe–C_{eq}. Hanson, A. W. *Acta Crystallogr.* **1962**, *15*, 930.
(20) Teller, R. G.; Finke, R. G.; Collman, J. P.; Chin, H. B.; Bau, R. *J. Am. Chem. Soc.* **1977**, *99*, 1104.
(21) (a) Darensbourg, D. J.; Kudaroski, R. *J. Am. Chem. Soc.* **1984**, *106*, 3672. (b) Cotton, F. A.; Darensbourg, D. J.; Kolthammer, B. W. S. *Inorg. Chem.* **1981**, *20*, 4440.
(22) Wovkulich, M. J.; Atwood, J. L.; Canada, L.; Atwood, J. D. *Organometallics* **1985**, *4*, 867.

Table V. ν(CO) Band Positions (cm^{-1}) for Solutions[a] of Cation$^+$HFe(CO)$_3$P$^-$

P	cation$^+$	X[b]	(A′+)A$_1$	X[b]	A″	E(+X[b])	A′
P(OMe)$_3$	PPN		1941.3 (w)			1841.0 (vs)	
	Na + Cr		1941.2 (w)			1841.0 (vs)	
	Na	1953.8 (w)	1942.2 (sh)	1861.2 (s)	1852.5 (sh)	1840.95 (s)	1810.1 (w)
		[1959.6 (w)]	...	[1868.9 (s)]	...	[1843.8 (m)]	...
	Li		1942.0 (w)			1842.0 (vs)	
P(OEt)$_3$	PPN		1938.4 (w)			1836.1 (vs)	
	Na + Cr		1937.4 (w)			1837.1 (vs)	
	Na	1950.9 (w)	1939.3 (sh)	1856.4 (sh)	1847.7 (sh)	1839.0 (s)	1806.2 (w)
		[1955.7 (w)]	...	[1866.0 (s)]	...	[1839.0 (m)]	[1806.2 (sh)]
PPh$_3$	PPN		1926.8 (m)			1828.4 (vs)	
	Na + Cr		1925.8 (m)			1829.4 (vs)	
	Na		1927.7 (m)	..	1839.0 (s)	1830.0 (sh)	1795.2 (s)
		[1943.2 (m)]	...	[1953.5 (s)]	...	[1824.6 (m)]	[1790.8 (w)]
	Li	...	1927.7 (m)	..	1845.8 (sh)	1829.4 (s)	1767.7 (m)
PPh$_2$Me	Na + Cr		1922.9 (m)			1824.6 (vs)	
	Na	1936 (sh)	1924.9 (m)	...	1834.2 (s)	1822.6 (sh)	1790.8 (s)
		[1940.3 (w)]	...	[1850.6 (s)]	...	[1820.7 (m)]	[1787 (m)]
PMe$_3$	Na + Cr		1918.1 (w)			1814.9 (vs)	
	Na	1931 (bs)	1921 (br)	1836 (sh)	1830.3 (s)	1814.9 (s)	1782.0 (m)
		[1938.4 (w)]	...	[1847.7 (s)]	...	[1814.9 (m)]	[1781.2 (w)]
	Li + Cr		1918.1 (m)			1816.8 (s)	
	Li	1933.5 (sh)	1922.9 (w)	...	1838.1 (s)	1818.8 (s)	1751.3 (w)
PEt$_3$	Na + Cr		1915.2 (w)			1813.0 (vs)	
	Na	1929.7 (sh)	1920.0 (br)	...	1828.4 (s)	1812.5 (sh)	1780.2 (m)
		[1937.4 (w)]	...	[1843.8 (vs)]	...	[1812.0 (m)]	[1779.2 (m)]
	Li + Cr		1916.2 (w)			1813.9 (s)	
	Li	1930 (sh)	1918.1 (w)	...	1835.2 (s)	1816.8 (s)	1751.3 (w)

[a] THF solution spectra except where bracketed. Brackets denote Et$_2$O solution spectra. Assignments A$_1$ and E for ssip and A″ + 2A′ for cip **b**, Figure 3. [b] Bands labeled X assigned to C_s symmetry species, cip **f**, with Fe$^-$···cation$^+$ interaction.

lutions to contain the salts predominantly in the form of associated ion pairs, so that such species will be referred to as symmetrically solvated ion pairs, ssip's.

Figure 4 is the ν(CO) IR spectrum of Na$^+$HFe(CO)$_3$PPh$_3^-$ in THF solution. The spectrum was readily deconvoluted assuming only two species: the ssip with A$_1$:E intensity ratio of 1:2 as taken from spectrum 3 and another species yielding three bands. This second species has a ν(CO) absorption to lower frequencies as is typical of a μ_2-η^1-CO, i.e., Fe—C≡O···Na$^+$, and two bands to higher frequency from those of species **a**. The band pattern and positions are consistent with the expectations for C_s symmetry of structure **b** in Figure 2. Band area measurements on the resolved spectra indicated 28% of ssip and 72% of the contact ion pair (cip) of form **b**.

Yet another type of cip interaction of the Na$^+$HFe(CO)$_3$PPh$_3^-$ salt was discovered in Et$_2$O. Figure 5 represents the ν(CO) IR spectrum of Na$^+$HFe(CO)$_3$PPh$_3^-$ in Et$_2$O. The spectrum was resolved assuming the presence of two cip species. The ssip would not be expected in this low polarity solvent, nor is it indicated. The fact that the sodium salt was soluble in Et$_2$O at all suggested considerable charge neutralization to have occurred. The cip of form **b** was again indicated by a low-frequency ν(CO) band. Band analysis was completed assuming this and another three-band species. Two bands of the latter were shifted to substantially higher ν(CO) values than the parent ssip **a** or cip **b**. A notable exception was the lowest energy band of the second species (dashed line in Figure 5) which was almost degenerate with the E band position of the ssip; in fact, it was positioned just slightly below the ssip E band. Nevertheless, the overall, average shift of ν(CO) bands in this second type of cip was to higher frequency. We assigned the structure of the latter cip to one involving $^-$Fe···Na$^+$ interaction, either of form **e** or **f**, Figure 2. On basis of the isolated mixed-metal complex HFe(CO)$_3$P(OMe)$_3$W(CO)$_5^-$ whose structure is best described as a Lewis base (HFe(CO)$_3$P$^-$)/Lewis acid (W(CO)$_5^0$), Fe$^-$:→W interaction in which the P ligand is trans to the Fe–W bond and cis to the Fe–H bond,[24] cip **f** is preferred. The relative

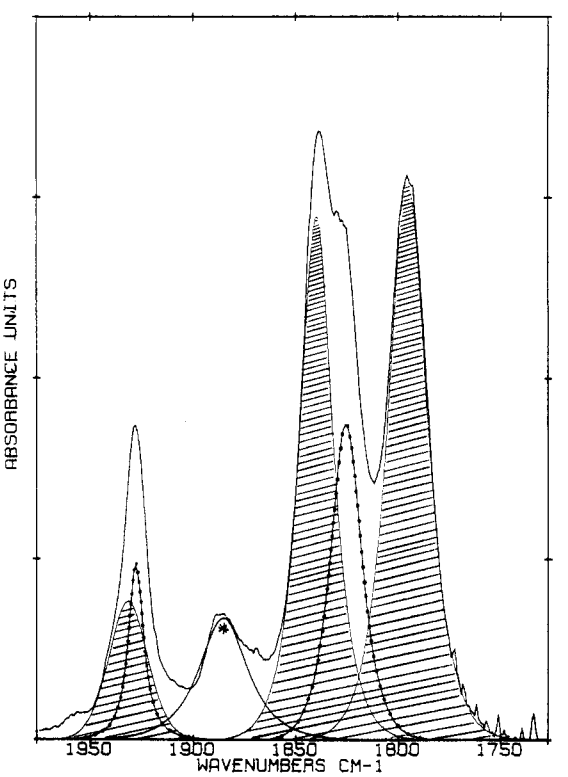

Figure 4. Na$^+$HFe(CO)$_3$PPh$_3^-$ in THF solution (0.01 M) and components as determined by band-shape analysis: ···, the symmetrically solvated anion; cross-hatches, the contact ion pair assigned to carbonyl oxygen···cation interaction, cip **b**. The asterisk (*) denotes impurity *trans*-Fe(CO)$_3$(PPh$_3$)$_2$.

(23) Darensbourg, M. Y.; Barros, H. L. C.; Borman, C. *J. Am. Chem. Soc.* **1977**, *99*, 1647.

(24) Arndt, L.; Darensbourg, M. Y.; Delord, T.; Bancroft, B. T., manuscript submitted for publication.

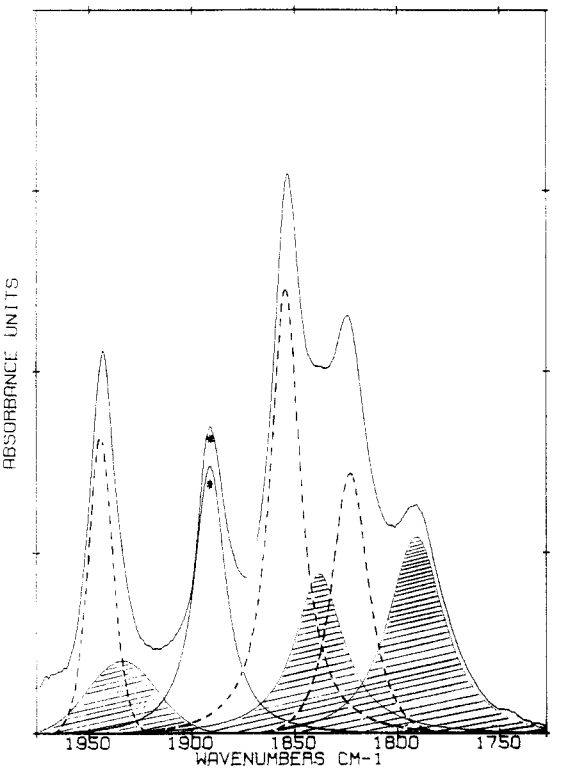

Figure 5. Band envelope observed in ν(CO) for $Na^+HFe(CO)_3PPh_3^-$ in Et_2O and its components as resolved by band-shape analysis. Cross-hatched bands are assigned to cip **b** and (- - -) bands are assigned to cip **f**. The asterisk (*) denotes impurity *trans*-$Fe(CO)_3(PPh_3)_2$.

percentages of **f** to **b** are roughly 53:47, respectively.

The $Na^+HFe(CO)_3PPh_2Me^-$ salt showed ion pairing characteristics very similar to the analogous PPh_3 salt in THF and Et_2O solution. In contrast, sodium salts of the anions containing smaller ligands, $P(OMe)_3$, $P(OEt)_3$, PMe_3, and PEt_3, existed in three ion-paired forms even in THF: ssip or **a**, cip **b**, and cip **f**. Correspondingly, in Et_2O the shift is toward more intimate ion pairs. A small amount of CO oxygen contact, cip **b**, is seen for $Na^+HFe(CO)_3PMe_3^-$ and for $Na^+HFe(CO)_3PEt_3^-$ derivatives; the predominant contact is $^-Fe\cdots Na^+$. With $P(OEt)_3$ and $P(OMe)_3$, over 90% of the ion-paired form is of the $^-Fe\cdots Na^+$ (type **f**) in Et_2O.

The two other ion-paired structures in Figure 2, interaction of Na^+ at the hydride ligand (cip **c**) or a combination Fe–H bond density site (cip **d**), would be expected not to *significantly* affect the trigonal arrangement of equatorial carbonyls and to thus yield IR expectations of A_1 and E. Our spectral interpretations, including NMR evidence (vide infra), do not include such species. Additionally there are possible triple ion structures, most plausibly of the form $Na^+\cdot\cdot[\cdot OCFe(CO)_2(H)P^-]_2^-$, that have been considered. Only in two cases, that of the Na^+ salts of $HFe(CO)_3PMe_3^-$ and $HFe(CO)_3PEt_3^-$ in Et_2O, do we have spectral evidence for such triple ion formation; those appear to be at a level of 10–15%.

Solution Structure of $HFe(CO)_3P^-$: Ion Pairing as a Function of Counterion. Despite the large sizes of both the Et_4N^+ and the PPN^+ counterions, conductivity studies have shown that both are associated with metal carbonyl anions in THF.[23] The PPN^+ counterion does not perturb the ν(CO) band pattern of such anions; hence its association is nonspecific as might be expected for such a large, charge-delocalized cation. The Me_4N^+ and Et_4N^+ cations have been noted to form both strong (i.e., large ion pair association constants) and anion-perturbing contact

Table VI. ν(CO) Band Positions (cm^{-1}) for $Et_4N^+HFe(CO)_3P^-$ in THF Solution[a]

L	A′	A″	A′
$P(OMe)_3$	1945.1 (w)	1849.6 (s)	1830.3 (m)
PPh_3	1926.8 (m)	1831.3 (s)	1813.0 (m)
PPh_2Me	1923.9 (m)	1827.5 (s)	1809.5 (m)
PMe_3	1919.1 (w)	1820.7 (s)	1805.0 (m)
PEt_3	1917.1 (w)	1816.8 (s)	1802.0 (m)

[a] Symmetry labels assigned according to C_s symmetry of cip **b**, Figure 2.

ion pairs with metal carbonylates in THF.[4,25] Similarly in THF solution Et_4N^+ is found to perturb the ν(CO) IR spectrum of $HFe(CO)_3P^-$ as compared to the CH_3CN solution spectra. The major effect is in a splitting of the E band of the ssip **a** into two, one to slightly lower and one to slightly higher values. The highest frequency band is hardly changed from that of the nonperturbed anion. Table VI lists all ν(CO) values for the Et_4N^+ salts under the symmetry labels of a C_s symmetry species corresponding to CO–oxygen contact, i.e., cip **b**. The Et_4N^+-$HFe(CO)_3P^-$ contact ion pair interaction is not changed on addition of small amounts of monodentate O-donor, cation complexing agents. Addition of 30 equiv of Me_2SO, for example, does not change the spectrum whereas much less Me_2SO is required to remove all contact interactions of Na^+ with $HFe(CO)_3P^-$. We note that the nature of the Et_4N^+ and Me_4N^+ contact with carbonylate anions has not been straightforwardly defined in earlier studies[4] and is not completely clear here as well. These cations are not likely to have only one accessible localized charge site as in $Na(THF)_y^+$ or $Li(THF)_y^+$, in which y is one less than the favored coordination number of Na^+ or Li^+. One study proposed an involvement of the Me_4N^+ in a softer, multisite, docking onto the anion.[4] We cannot rule out a combination of a CO and a hydride to be involved here, i.e., a structure akin to cip **d**.

The electrostatic potentials of the alkali cations vary $Li^+ > Na^+ > K^+$, and their tendencies to be solvated by THF vary accordingly. Hence the Li^+ salts of carbonylates typically show fewer cip's because of the stability of the symmetrical $Li(THF)_x^+$ solvate.[25] The $HFe(CO)_3P^-$ anions clearly are of great cation-attracting power. Yet for P = $P(OR)_3$ in THF, there is no cip with Li^+. For P = PPh_3 and PR_3 (R = Me, Et) there is a mixture of ssip's and cip's of type **b**. Only in the case of P = PMe_3 and PEt_3 is there any indication of some small amounts of Li^+ interaction at the Fe, cip **f**.

The K^+ salts show no solvent separated ion pairing, only contact ion pairs of type b in which there are only small splittings of the E band. In fact the effect of K^+ on the ν(CO) IR spectrum of $HFe(CO)_3P^-$ anions is similar to that of Et_4N^+. The observed relative tendencies of the alkali cations to penetrate the coordination sphere of the iron hydride, and directly interact with the Fe center, $Li^+ < Na^+ \gg K^+$, is consistent with earlier studies of Rosenblum et al. on the ion-pairing characteristics of $CpFe(CO)_2^-$.[26]

Nuclear Magnetic Resonance Spectra. Table VII lists ^1H and ^{31}P NMR data for several hydrido anions. There is a general trend for a small upfield shift of the hydride resonance as CO is replaced by the better P-donor ligands. The position of the hydride resonance for any one anion is largely independent of cation. *This result is in contrast to significant upfield shifts of the hydride resonance of cis-$HW(CO)_4PR_3^-$ as the PPN^+ or Na^+ 18-C-6*

(25) Darensbourg, M. Y.; Sackett, J. R.; Jiminez, P.; Hanckel, J. M.; Kump, R. L. *J. Am. Chem. Soc.* **1982**, *104*, 1521.
(26) Nitay, M.; Rosenblum, M. *J. Organomet. Chem.* **1977**, *136*, C23.

Table VII. NMR Spectral Data for Cation$^+$HFe(CO)$_3$L$^-$ in THF-d_8

cation$^+$	L	$\delta(^1H)^a$	$\delta(^{31}P)^b$	J_{P-H}	temp, °C
PPN	CO	-8.68			amb[c]
Na	CO	-8.70			amb
PPN	$P(OMe)_3$	-9.22	213.6	11.51	amb
		-9.26		14.85	50
		-9.20		11.92	22
		-9.07		5.06	-20
		-8.93		0.00	-60
Et_4N	$P(OMe)_3$	-9.33		8.99	22
		-9.24		3.37	-20
		-9.11		0.00	-60
Na	$P(OMe)_3$	-9.37		13.69	50
		-9.28		11.17	22
		-9.15		6.61	-20
		-9.00		0.00	-60
PPN	$P(OEt)_3$	-9.10	210.0	4.84	amb
Et_4N	PPh_3	-9.12		11.98	amb
Et_4N	PPh_2Me	-9.17		8.77	amb
Et_4N	PMe_3	-9.46	33.8	3.77	amb
Et_4N	PEt_3	-9.34	71.9	3.87	amb
		-9.37		4.93	50
		-9.33		3.24	22
		-9.18		0.00	-60

[a] Values given are for hydride resonance only, reference is δ 1.73 of THF. [b] External standard of H_3PO_4. [c] Amb refers to probe temperature, generally at 22–28 °C. Other temperature values given are ±1 °C.

cations are replaced by Na$^+$ ions (proposed to significantly interact at the W–H site) in THF solutions.[6]

The phosphorus–hydrogen scalar coupling constants are small, ranging from 4 to 12 Hz, measured at room temperature. There are few reported studies of TBP complexes containing a P-donor ligand and H trans to each other. In *trans*-$HCo(CO)_3PPh_3$ the J_{P-H} is 51 Hz.[27] In $HIr(CO)_2(PPh_3)_2$, J_{P-H} couplings of 19 and 35 Hz were ascribed to two ill-defined solution species.[28] The spectrum of the latter was determined at -70 °C in order to arrest intramolecular exchange. Indeed problems of intramolecular exchange and geometric interconversions are prominent in five-coordinate complexes so that systematic studies of coupling constants and conclusions based thereon are few and to be treated with caution. Nevertheless we note that J_{P-H} in what is generally described as TBP, five-coordinate complexes, are small (ranging from 5 to 50 Hz).[29] In contrast, J_{P-H}(trans) in analogous octahedral complexes are in the range of 80–100 Hz and the cis couplings are smaller, 20–40 Hz.[30] For example, the anionic *cis*-$HW(CO)_4PR_3^-$ complexes have J_{P-H} of 30–40 Hz.[6] Square-planar (SqPl) geometries have even larger J_{P-H} coupling constants: *trans*-$M(X)_2(P)(H)$ are up to 300 Hz and *cis*-$M(X)_2(P)(H)$ are 40–50 Hz.[30]

Since scalar coupling occurs primarily via an s orbital mechanism, the dependence of coupling constant on structure (TBP < O_h < SqPl) (TBP = trigonal-bipyramidal) may be rationalized on the basis of s orbital involvement in the two bond couplings. The axial ligands in TBP structures communicate largely via a dp hybrid set, with smaller mixing of the equatorial sp^2 set. The greater involvement of s orbital mixing in all bonds of the O_h and Sq Pl should afford larger coupling.

The dependence of J_{P-H} on temperature and cation indicated in Table VII is unusual. We have also noted a dependence of J_{P-C} and J_{H-C} on temperature. Attempts are being made to interpret these phenomena in terms of solution structural changes.

Chemical Reactivity of HFe(CO)$_3$P$^-$. All reaction probes that we have used indicate the $HFe(CO)_3P^-$ anions to be more reactive than the $HFe(CO)_4^-$ parent. All of the complexes reported here are very oxygen sensitive. Water sensitivity is not a problem (in fact H_2O is used in the purification process) except for very basic phosphines such as PMe_3 and PEt_3. The $HFe(CO)_3PR_3^-$ (R = Me, Et) anions react with H_2O or MeOH to yield a new hydride, believed to be a cluster analogous to the known $HFe_3(CO)_{11}^-$ trimer, presumably according to eq 5. This species

$$3HFe(CO)_3P^- + 2H^+ \rightarrow \text{“}HFe_3(CO)_8P_3^-\text{”} + 2H_2 + CO \quad (5)$$

has thus far eluded isolation as a pure compound. It was characterized by a hydride resonance at ca. -10.2 ppm (J_{P-H} = 61 Hz) and by two ν(CO) bands, one of medium intensity ranging from 2050 to 2067 cm^{-1} and a strong band at 1980–2000 cm^{-1}, dependent on the P-donor ligand. This species is unstable and eventually decomposes to yield $PFe(CO)_4$ and *trans*-$P_2Fe(CO)_3$. The species is observed as an intermediate in all hydride decomposition reactions and is cleanly produced upon reaction of the Lewis acid $AlMe_3$ with $HFe(CO)_3P^-$. The formation of this species as a decomposition product from the alkali-metal cation salts of $HFe(CO)_3P^-$ varies in amount of decomposition in THF: $Li^+ > Na^+ > K^+$. The decomposition to this species is even more pronounced in Et_2O where intimate ion contact increases.

Phosphine ligands in $HFe(CO)_3P^-$ may be replaced by phosphites and phosphites by CO, i.e., ligands of better π-accepting ability, as demonstrated by eq 6–10. The

$$Et_4N^+HFe(CO)_3PPh_3^- + P(OMe)_3 \rightarrow Et_4N^+HFe(CO)_3P(OMe)_3^- + PPh_3 \quad (6)$$

$$PPN^+HFe(CO)_3PPh_3^- + CO \xrightarrow[t_{1/2}= 12\ min]{} PPN^+HFe(CO)_4^- \quad (7)$$

$$PPN^+HFe(CO)_3P(OMe)_3^- + CO \not\rightarrow PPN^+HFe(CO)_4^- \quad (8)$$

$$Li^+HFe(CO)_3P(OMe)_3^- + {}^{13}CO \xrightarrow[12\ min]{} Li^+HFe(CO)_3({}^{13}CO)^- + P(OMe)_3 \quad (9)$$

$$Li^+HFe(CO)_3({}^{13}CO)^- + {}^{13}CO \xrightarrow[2\ h]{} Li^+HFe({}^{13}CO)_4^- \quad (10)$$

specific example given in eq 6 was shown to obey a first-order rate law, rate = k_1[Fe], as expected for a dissociative process. The rates of these reactions are dependent both on counterion and on the nature of P in $HFe(CO)_3P^-$. For example, PPh_3 is replaced more readily by CO than is $P(OMe)_3$. The mechanism of the cation-promoted Fe–P bond weakening is believed to occur via a polarization of electrons in π bonds, and as such the effect is expected to be larger for the better π-accepting $P(OMe)_3$ ligand.[4]

The displacement of $P(OMe)_3$ with ^{13}CO (eq 9) occurred without prior exchange of an equatorial CO with free ^{13}CO. Equations 9 and 10 demonstrate that even in the presence of Li^+ the lability of $P(OMe)_3$ is greater than that of CO.

The $HFe(CO)_3P^-$ anions will serve as hydride sources, thus reducing alkyl bromides to alkanes at ambient temperature in THF solution.[7,31] The rates are slower than analogous reactions with $HW(CO)_5^-$, $HCr(CO)_5^-$, or $CpV(CO)_3H^-$.[7] The $HFe(CO)_3P^-$ anions show a selectivity for

(27) Hieber, W.; Duchatsch, H. *Chem. Ber.* **1965**, *98*, 2933.
(28) Yagupsky, G.; Wilkinson, G. *J. Chem. Soc. A* **1969**, 725.
(29) Jesson, J. P. In “Transition Metal Hydrides”; Muetterties, E. L., ed.; Marcel Decker: New York, 1971; Vol. 1, pp 106–114.
(30) Kaesz, H. D.; Saillant, R. B. *Chem. Rev.* **1972**, *72* (3) 231.
(31) Organic halide reductions and volatile organic product analysis were conducted as described in earlier work.[7]

primary halides as demonstrated in eq 11, and the radical probe reaction, eq 12, indicated no single electron pro-

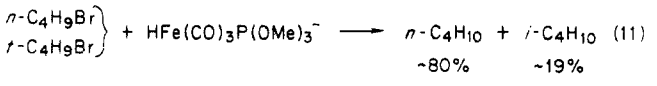

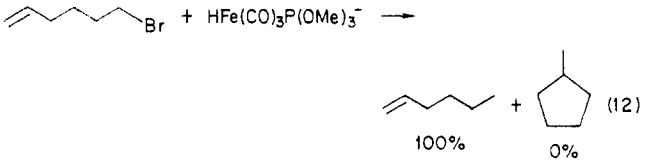

cesses.[32] The latter statement assumes the rate of cyclization for any $CH_2{=}CHCH_2CH_2CH_2CH_2\cdot$ species to be greater than the rate constant for hydrogen transfer to the linear radical.[33]

Finally, we mention that neither $HFe(CO)_4^-$ or $HFe(CO)_3P^-$ will transfer H^- to $M(CO)_6$ (M = Cr, W).[34] In fact, the new class of heterobimetallic hydrides $HFeM(CO)_9^-$ and $HFe(CO)_3PM(CO)_5^-$[24] demonstrate both the great propensity for H^- to remain associated with Fe as well as the fact that the Fe is a nucleophilic center. As indicated in structure **g**, and discussed earlier, the binuclear complex

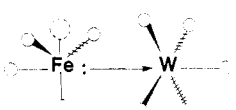

g

is viewed as containing a donor/acceptor metal–metal bond. Upon exchanging CO for $P(OMe)_3$, the Fe–W bond distance is observed to decrease, from 2.997 (2) Å in $PPN^+HFeW(CO)_9^-$ to 2.974 (5) Å in $PPN^+HFe(CO)_3P(OMe)_3W(CO)_5^-$, consistent with an enhancement of electron density at the iron for the latter.[24] These structures, together with the intimate contact ion pair observed in our solution work, i.e., cip **f** containing an $Fe^-\cdots cation^+$ interaction, leave little doubt that the iron center bears considerable negative charge. If such well-defined electrophiles as Na^+ or $W(CO)_5$ add to the Fe center, then alkyl halides should also. That is, alkyl halide reductions using $HFe(CO)_3P^-$ as hydride source involve oxidative addition of the alkyl group to Fe^-, yielding $[(H)(R)Fe(CO)_3P]$[35,36] as intermediate,[35] with subsequent reductive elimination of product RH. This interpretation contrasts with the group 6 metal hydrides where, particularly in the case of *cis*-$HW(CO)_4P^-$, negative character is associated with the hydride ligand and where oxidative addition is not favored. (Oxidative addition to W^0 in $HW(CO)_4P^-$ would break up a stable coordination geometry (d^6, O_h), whereas oxidative addition to Fe^0 in $HFe(CO)_3P^-$ would lead toward one (d^8, TBP → d^6, O_h).) It also contrasts with the reduction path adopted by $CpV(CO)_3H^-$, a radical chain process,[37] where

Scheme I. Summary of IR Spectral Results and Interpretations[a]

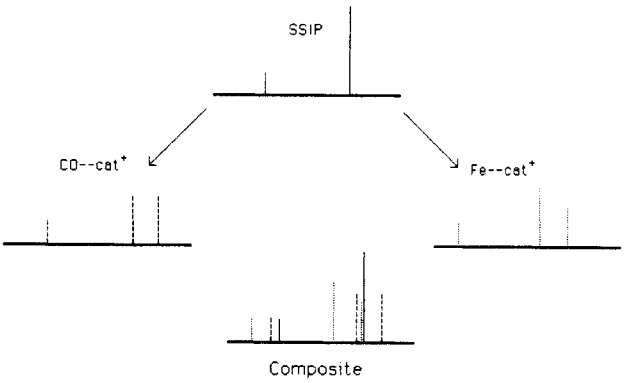

$HFe(CO)_3P^-$	PPN^+/THF Et_4N^+/CH_3CN	Et_4N^+/THF	K^+/THF	Na^+/THF	Li^+/THF	Na^+/Et_2O
PPh_3	SSIP	CIP **b**	CIP **b**	SSIP	SSIP	CIP **b**
PPh_2Me				CIP **b**	CIP **b**	CIP **f**
PMe_3	SSIP	CIP **b**	CIP **b**	SSIP	SSIP	CIP **b**
PEt_3				CIP **b**	CIP **b**	CIP **f**
				CIP **f**		Triple
$P(OMe)_3$	SSIP	CIP **b**	CIP **b**	SSIP	SSIP	CIP **f**
$P(OEt)_3$				CIP **b**		
				CIP **f**		

[a] CIP **b** refers to carbonyl-oxygen interaction with cation: $^-Fe\text{-}CO\cdots cation^+$. CIP **f** refers to interaction of cation at Fe: $^-Fe\cdots cation^+$. Triple refers to triple ion of probable form $^-Fe\text{—}CO\cdots Na^+\cdots OC\text{—}Fe^-$.

oxidative addition nor hydride transfer are particularly attractive pathways. *Certainly all three classes of hydrides $HM(CO)_5^-$, $HFe(CO)_3P^-$, and $CpV(CO)_3H^-$ are expected to be substrate responsive, reacting by alternate pathways upon strong demand.*

Summary and Comments. The original question addressed in this work was whether cation contact would be shifted from the carbonyl oxygen site, observed for $Na^+HFe(CO)_4^-$,[5] to the hydride site in Na^+[*trans*-$HFe(CO)_3P^-$]. Instead we have observed enhanced $CO\cdots cation^+$ interactions and also interaction of the Na^+ and Li^+ at the iron center, $^-Fe\cdots cation^+$. This latter type of contact ion pair has precedence in the recently prepared donor–acceptor complexes of $HFe(CO)_3LW(CO)_5^-$. The considerable metal-based nucleophilicity of the anionic iron hydride is indicated. A correlation between electron configuration and coordination number and the tendency to form such metal–metal′ interactions is suggested. For example, d^8, five-coordinate Fe^0 in $CpFe(CO)_2^-$ also shows inner-sphere alkali cation ion pair contacts,[26,38] whereas d^6, six-coordinate Mo^0 in $CpMo(CO)_3^-$ shows only CO–oxygen contacts with Na^+, Li^+, or K^+.[25]

A summary of cation interactions with various P ligand derivatives of $HFe(CO)_3P^-$ is given in Scheme I. Regardless of the ligand donor ability or the cation used, the smallest phosphines give the largest amount of $^-Fe\cdots cation^+$ interaction. The sodium ion has the greatest ability to penetrate the coordination sphere of Fe. The great oxophilicity of Li^+ renders it highly solvated, and the large K^+ lacks the requisite electrostatic potential. Sodium ion has the combination of qualities intermediate between Li^+ and K^+ to give the greatest amount of inner-sphere contact ion pairs. Nevertheless the great polarizing ability of Li^+

(32) These results are consistent with those of: Whitmire, K. H.; Lewis, E. S.; Lee, K. R. *Organometallics*, submitted for publication.
(33) Maillard, B.; Forest, D.; Ingold, K. U. *J. Am. Chem. Soc.* **1976**, *98*, 7024.
(34) Arndt, L.; Delord, T.; Darensbourg, M. Y. *J. Am. Chem. Soc.* **1984**, *106*, 456.
(35) Note that the analogous intermediate in the synthesis of aldehydes using Collman's reagent, $Fe(CO)_4^{2-}$, RX, and H^+ is $L(OC)_3Fe(C(O)R)(H)$.[36] Our approach does not permit the CO insertion process to occur.
(36) Collman, J. P.; Finke, R. G.; Cawse, J. N.; Brauman, J. I. *J. Am. Chem. Soc.* **1977**, *99*, 2515.
(37) Kinney, R. J.; Jones, W. D.; Bergman, R. G. *J. Am. Chem. Soc.* **1978**, *100*, 7902.
(38) Pannell, K. H,; Jackson, P. *J. Am. Chem. Soc.* **1976**, *98*, 4443.

imparts an eminent reactivity to its contact ion pairs. For example, even when present in such small amounts so as not to be spectroscopically observable, the contact ion pairs of Li^+ are indicated by greatly enhanced ligand lability ($Li^+HFe(CO)_4^- + {}^{13}CO \rightarrow$ rapid CO exchange). The substitution reaction is funneled through highly reactive contact ion pairs.

Acknowledgment. A grant from the National Science Foundation (CHE-8304162) supported this work. Helpful discussions with D. J. Darensbourg and K. H. Whitmire are appreciated.

Registry No. $PPn^+HFe(CO)_3P(OMe)_3^-$, 93303-97-0; $Na^+HFe(CO)_3P(OMe)_3^-$, 98942-46-2; $Li^+HFe(CO)_3P(OMe)_3^-$, 98942-47-3; $PPN^+HFe(CO)_3P(OEt)_3^-$, 98942-49-5; $Na^+HFe(CO)_3P(OEt)_3^-$, 98942-50-8; $PPN^+HFe(CO)_3PPh_3^-$, 99031-93-3; $Na^+HFe(CO)_3PPh_3^-$, 99032-51-6; $Li^+HFe(CO)_3PPh_3^-$, 99031-94-4; $Na^+HFe(CO)_3PPh_2Me^-$, 98942-51-9; $Na^+HFe(CO)_3PMe_3^-$, 98942-52-0; $Li^+HFe(CO)_3PMe_3^-$, 98942-53-1; $Na^+HFe(CO)_3PEt_3^-$, 98942-54-2; $Li^+HFe(CO)_3PEt^{3-}$, 98942-55-3; $Et_4N^+HFe(CO)_3P(OMe)_3^-$, 98942-56-4; $Et_4N^+HFe(CO)_3PPh_3^-$, 80612-33-5; $Et_4N^+HFe(CO)_3PPh_2Me^-$, 98942-58-6; $Et_4N^+HFe(CO)_3PMe_3^-$, 98942-60-0; $Et_4N^+HFe(CO)_3PEt_3^-$, 98942-62-2; $PPn^+HFe(CO)_4^-$, 56791-54-9; $Na^+HFe(CO)_4^-$, 53558-55-7.

Supplementary Material Available: Listings of structure factors, thermal parameters, positional parameters, interatomic distances and angles, and band indices for ν(CO) vibrations from band-shape analysis and an ORTEP drawing of $HFe(CO)_3PPh_3^-$ with view along the z axis (9 pages). Ordering information is given on any current masthead page.

Preparation of Molybdenum and Tungsten Neopentylidyne Complexes of the Type $M(CCMe_3)(O_2CR)_3$, Their Reactions with Acetylenes, and the X-ray Structure of the η^3-Cyclopropenyl Complex $W[C_3(CMe_3)Et_2](O_2CCH_3)_3$[1]

Richard R. Schrock,*† John S. Murdzek, John H. Freudenberger, Melvyn Rowen Churchill,*‡ and Joseph W. Ziller

Departments of Chemistry, 6-331, Massachusetts Institute of Technology, Cambridge, Massachusetts 02139, and State University of New York at Buffalo, Buffalo, New York 14214

Received March 29, 1985

$M(CCMe_3)(CH_2CMe_3)_3$ reacts with RCO_2H (R = Me, Me_2CH, Me_3C, CF_3; M = Mo, W) to give tris(carboxylate) complexes of the type $M(CCMe_3)(O_2CR)_3$; the CF_3CO_2 products are most conveniently isolated as dimethoxyethane adducts $M(CCMe_3)(O_2CCF_3)_3$(dme). $M(CCMe_3)(O_2CR)_3$ complexes ($R \neq CF_3$) react with internal acetylenes $R'C{\equiv}CR'$ to give η^3-cyclopropenyl complexes $M[C_3(CMe_3)R'_2](O_2CR)_3$ (R' = Me, Et, Ph). The $M(CCMe_3)(O_2CCF_3)_3$(dme) complexes react with internal acetylenes to give η^5-cyclopentadienyl complexes in low yield while $Mo(CCMe_3)(O_2CCF_3)_3$(dme) reacts with $RC{\equiv}CH$ (R = CMe_3, Ph) to give deprotiomolybdacyclobutadiene complexes $Mo[C_3(CMe_3)(R)](O_2CCF_3)_2$(dme). The complex $W[C_3(CMe_3)Et_2](O_2CMe)_3$ crystallizes in the centrosymmetric space group $P\bar{1}$ (No. 2) with a = 8.345 (3) Å, b = 8.379 (5) Å, c = 16.994 (6) Å, α = 77.04 (4)°, β = 76.53 (3)°, γ = 62.23 (3)°, V = 1013.2 (7) Å^3, and Z = 2. X-ray diffraction data (Mo Kα, 2θ = 4.5–45.0°) were collected on a Syntex $P2_1$ automated four-circle diffractometer, and the model was refined to R_F = 2.6% and R_{wF} = 2.8% for all 2650 unique data. The coordination geometry about the tungsten atom may be regarded as distorted pentagonal bipyramidal with the η^3-$C_3(CMe_3)Et_2$ system occupying one apical position, two acetate ligands occupying biequatorial sites, and the third acetate ligand spanning an axial (O(11)) and equatorial position. The O(11)–W–(centroid of C_3 system) angle is 169.1°. The W–C distances are approximately equivalent with W–C(4) = 2.089 (5) Å, W–C(5) = 2.114 (7) Å, and W–C(6) = 2.134 (6) Å; C–C distances within the triatomic ring are C(4)–C(5) = 1.451 (10) Å, C(4)–C(6) = 1.448 (8) Å, and C(5)–C(6) = 1.405 (11) Å.

Introduction

We have been studying reactions between alkylidyne complexes of molybdenum(VI) or tungsten(VI) and acetylenes as part of our program to elucidate the factors that determine when an alkylidyne complex will catalytically metathesize acetylenes[2] and when it will not. We have found that bulky alkoxide ligands are especially desirable for metathesis activity for both Mo[3] and W.[4] Smaller alkoxides in general encourage polymerization of the acetylene while chloride ligands (on W) allow 2 equiv of an acetylene to be incorporated to form a substituted cyclopentadienyl ring bound to a formally reduced metal.[4c] In the process of studying reactions of alkylidyne complexes with protic sources, we discovered a relatively direct route to complexes of the type $M(CCMe_3)(O_2CR)_3$, where M = Mo or W, and therefore became interested in examining the reaction of these tris(carboxylate) complexes with acetylenes. The results of this study are reported here.

† Massachusetts Institute of Technology.
‡ State University of New York at Buffalo.

(1) Multiple Metal–Carbon Bonds. 39. For part 38 see ref 3.
(2) (a) Wengrovius, J. H.; Sancho, J.; Schrock, R. R. *J. Am. Chem. Soc.* **1981**, *103*, 3932. (b) Sancho, J.; Schrock, R. R. *J. Mol. Catal.* **1982**, *15*, 75.
(3) McCullough, L. G.; Schrock, R. R.; Dewan, J. C.; Murdzek, J. S. *J. Am. Chem. Soc.* **1985**, *107*, 5987.
(4) (a) Churchill, M. R.; Ziller, J. W.; Freudenberger, J. H.; Schrock, R. R. *Organometallics* **1984**, *3*, 1554. (b) Freudenberger, J. H.; Schrock, R. R.; Churchill, M. R.; Rheingold, A. L.; Ziller, J. W. *Organometallics* **1984**, *3*, 1563. (c) Schrock, R. R.; Pedersen, S. F.; Churchill, M. R.; Ziller, J. W. *Organometallics* **1984**, *3*, 1574.
(5) Churchill, M. R.; Fettinger, J. C.; McCullough, L. G.; Schrock, R. R. *J. Am. Chem. Soc.* **1984**, *106*, 3356.

0276-7333/86/2305-0025$01.50/0

imparts an eminent reactivity to its contact ion pairs. For example, even when present in such small amounts so as not to be spectroscopically observable, the contact ion pairs of Li^+ are indicated by greatly enhanced ligand lability ($Li^+HFe(CO)_4^- + {}^{13}CO \rightarrow$ rapid CO exchange). The substitution reaction is funneled through highly reactive contact ion pairs.

Acknowledgment. A grant from the National Science Foundation (CHE-8304162) supported this work. Helpful discussions with D. J. Darensbourg and K. H. Whitmire are appreciated.

Registry No. $PPn^+HFe(CO)_3P(OMe)_3^-$, 93303-97-0; $Na^+HFe(CO)_3P(OMe)_3^-$, 98942-46-2; $Li^+HFe(CO)_3P(OMe)_3^-$, 98942-47-3; $PPN^+HFe(CO)_3P(OEt)_3^-$, 98942-49-5; $Na^+HFe(CO)_3P(OEt)_3^-$, 98942-50-8; $PPN^+HFe(CO)_3PPh_3^-$, 99031-93-3; $Na^+HFe(CO)_3PPh_3^-$, 99032-51-6; $Li^+HFe(CO)_3PPh_3^-$, 99031-94-4; $Na^+HFe(CO)_3PPh_2Me^-$, 98942-51-9; $Na^+HFe(CO)_3PMe_3^-$, 98942-52-0; $Li^+HFe(CO)_3PMe_3^-$, 98942-53-1; $Na^+HFe(CO)_3PEt_3^-$, 98942-54-2; $Li^+HFe(CO)_3PEt^{3-}$, 98942-55-3; $Et_4N^+HFe(CO)_3P(OMe)_3^-$, 98942-56-4; $Et_4N^+HFe(CO)_3PPh_3^-$, 80612-33-5; $Et_4N^+HFe(CO)_3PPh_2Me^-$, 98942-58-6; $Et_4N^+HFe(CO)_3PMe_3^-$, 98942-60-0; $Et_4N^+HFe(CO)_3PEt_3^-$, 98942-62-2; $PPn^+HFe(CO)_4^-$, 56791-54-9; $Na^+HFe(CO)_4^-$, 53558-55-7.

Supplementary Material Available: Listings of structure factors, thermal parameters, positional parameters, interatomic distances and angles, and band indices for ν(CO) vibrations from band-shape analysis and an ORTEP drawing of $HFe(CO)_3PPh_3^-$ with view along the z axis (9 pages). Ordering information is given on any current masthead page.

Preparation of Molybdenum and Tungsten Neopentylidyne Complexes of the Type $M(CCMe_3)(O_2CR)_3$, Their Reactions with Acetylenes, and the X-ray Structure of the η^3-Cyclopropenyl Complex $W[C_3(CMe_3)Et_2](O_2CCH_3)_3$[1]

Richard R. Schrock,*† John S. Murdzek, John H. Freudenberger, Melvyn Rowen Churchill,*‡ and Joseph W. Ziller

Departments of Chemistry, 6-331, Massachusetts Institute of Technology, Cambridge, Massachusetts 02139, and State University of New York at Buffalo, Buffalo, New York 14214

Received March 29, 1985

$M(CCMe_3)(CH_2CMe_3)_3$ reacts with RCO_2H (R = Me, Me_2CH, Me_3C, CF_3; M = Mo, W) to give tris(carboxylate) complexes of the type $M(CCMe_3)(O_2CR)_3$; the CF_3CO_2 products are most conveniently isolated as dimethoxyethane adducts $M(CCMe_3)(O_2CCF_3)_3$(dme). $M(CCMe_3)(O_2CR)_3$ complexes ($R \neq CF_3$) react with internal acetylenes $R'C{\equiv}CR'$ to give η^3-cyclopropenyl complexes $M[C_3(CMe_3)R'_2](O_2CR)_3$ (R' = Me, Et, Ph). The $M(CCMe_3)(O_2CCF_3)_3$(dme) complexes react with internal acetylenes to give η^5-cyclopentadienyl complexes in low yield while $Mo(CCMe_3)(O_2CCF_3)_3$(dme) reacts with $RC{\equiv}CH$ (R = CMe_3, Ph) to give deprotiomolybdacyclobutadiene complexes $Mo[C_3(CMe_3)(R)](O_2CCF_3)_2$(dme). The complex $W[C_3(CMe_3)Et_2](O_2CMe)_3$ crystallizes in the centrosymmetric space group $P\bar{1}$ (No. 2) with a = 8.345 (3) Å, b = 8.379 (5) Å, c = 16.994 (6) Å, α = 77.04 (4)°, β = 76.53 (3)°, γ = 62.23 (3)°, V = 1013.2 (7) Å^3, and Z = 2. X-ray diffraction data (Mo Kα, 2θ = 4.5–45.0°) were collected on a Syntex $P2_1$ automated four-circle diffractometer, and the model was refined to R_F = 2.6% and R_{wF} = 2.8% for all 2650 unique data. The coordination geometry about the tungsten atom may be regarded as distorted pentagonal bipyramidal with the η^3-$C_3(CMe_3)Et_2$ system occupying one apical position, two acetate ligands occupying biequatorial sites, and the third acetate ligand spanning an axial (O(11)) and equatorial position. The O(11)–W–(centroid of C_3 system) angle is 169.1°. The W–C distances are approximately equivalent with W–C(4) = 2.089 (5) Å, W–C(5) = 2.114 (7) Å, and W–C(6) = 2.134 (6) Å; C–C distances within the triatomic ring are C(4)–C(5) = 1.451 (10) Å, C(4)–C(6) = 1.448 (8) Å, and C(5)–C(6) = 1.405 (11) Å.

Introduction

We have been studying reactions between alkylidyne complexes of molybdenum(VI) or tungsten(VI) and acetylenes as part of our program to elucidate the factors that determine when an alkylidyne complex will catalytically metathesize acetylenes[2] and when it will not. We have found that bulky alkoxide ligands are especially desirable for metathesis activity for both Mo[3] and W.[4] Smaller alkoxides in general encourage polymerization of the acetylene while chloride ligands (on W) allow 2 equiv of an acetylene to be incorporated to form a substituted cyclopentadienyl ring bound to a formally reduced metal.[4c] In the process of studying reactions of alkylidyne complexes with protic sources, we discovered a relatively direct route to complexes of the type $M(CCMe_3)(O_2CR)_3$, where M = Mo or W, and therefore became interested in examining the reaction of these tris(carboxylate) complexes with acetylenes. The results of this study are reported here.

† Massachusetts Institute of Technology.
‡ State University of New York at Buffalo.

(1) Multiple Metal–Carbon Bonds. 39. For part 38 see ref 3.
(2) (a) Wengrovius, J. H.; Sancho, J.; Schrock, R. R. *J. Am. Chem. Soc.* **1981**, *103*, 3932. (b) Sancho, J.; Schrock, R. R. *J. Mol. Catal.* **1982**, *15*, 75.
(3) McCullough, L. G.; Schrock, R. R.; Dewan, J. C.; Murdzek, J. S. *J. Am. Chem. Soc.* **1985**, *107*, 5987.
(4) (a) Churchill, M. R.; Ziller, J. W.; Freudenberger, J. H.; Schrock, R. R. *Organometallics* **1984**, *3*, 1554. (b) Freudenberger, J. H.; Schrock, R. R.; Churchill, M. R.; Rheingold, A. L.; Ziller, J. W. *Organometallics* **1984**, *3*, 1563. (c) Schrock, R. R.; Pedersen, S. F.; Churchill, M. R.; Ziller, J. W. *Organometallics* **1984**, *3*, 1574.
(5) Churchill, M. R.; Fettinger, J. C.; McCullough, L. G.; Schrock, R. R. *J. Am. Chem. Soc.* **1984**, *106*, 3356.

0276-7333/86/2305-0025$01.50/0

Results

Preparation of Carboxylate Complexes and Their Reactions with Acetylenes. $W(CCMe_3)(CH_2CMe_3)_3$ and $Mo(CCMe_3)(CH_2CMe_3)_3$ react with carboxylic acids (R = Me, $CHMe_2$, CMe_3) in pentane at −30 °C to give complexes of the type $M(CCMe_3)(O_2CR)_3$ (eq 1). In the reaction

$$M(CCMe_3)(CH_2CMe_3)_3 + 3RCO_2H \xrightarrow[-30\ °C]{\text{pentane}} M(CCMe_3)(O_2CR)_3 \quad (1)$$

M = Mo, W; R = Me, Me_2CH, CMe_3

between $Mo(CCMe_3)(CH_2CMe_3)_3$ and acetic acid, 4 equiv of acetic acid are required; if only 3 equiv of acid are added some starting material remains. All pale yellow (Mo) to white (W) products are formed in high yield. All are soluble in pentane, but more so in ether. $Mo(CCMe_3)(O_2CCHMe_2)_3$ can be isolated as pale yellow cubes and $W(CCMe_3)(O_2CCMe_3)_3$ and $W(CCMe_3)(O_2CCHMe_2)_3$ as colorless crystals. Others were isolated as powders.

At 25 °C the ^1H NMR spectra all show the carboxylate ligands to be equivalent. However, at 213 K the 250-MHz ^1H NMR spectrum of a sample of $Mo(CCMe_3)(O_2CCMe_3)_3$ showed a 2:1 ratio of carboxylate *tert*-butyl groups. Inequivalent (2:1) isopropyl groups also were observed in the low-temperature spectrum of $Mo(CCMe_3)(O_2CCHMe_2)_3$. Analogous tungsten complexes behaved similarly. On the basis of this data and the crystal structure reported later, we propose that the $M(CCMe_3)(O_2CR)_3$ species are distorted pentagonal bipyramids containing two "equatorial" carboxylate ligands and a third spanning an "axial" and an "equatorial" site, viz.

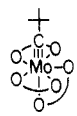

All ^{13}C NMR spectra show a signal for the neopentylidyne α-carbon atom in the range 280–310 ppm.

$Mo(CCMe_3)(O_2CR)_3$ (R = $CHMe_2$ or CMe_3) reacts with 1 equiv of MeC≡CMe or EtC≡CEt to yield pure red oils with the composition $Mo(CCMe_3)(O_2CR)_3(R'C{\equiv}CR')$ (R' = Me, Et) according to ^1H and ^{13}C NMR spectra. These oils sublime unchanged at ~60 °C and 10^{-3} μm. The reaction between $Mo(CCMe_3)(O_2CCMe_3)_3$ and PhC≡CPh produces a red crystalline product of the same type that sublimes unchanged at ~100 °C and 10^{-3} μm. Attempts to add R'C≡CR' to $Mo(CCMe_3)(O_2CCHMe_2)_3$, where R' = CMe_3, $SiMe_3$, or NMe_2, failed, while reactions between $W(CCMe_3)(O_2CCMe_3)_3$ and 2-butyne or 3-hexyne, or between $W(CCMe_3)(O_2CMe)_3$ and 3-hexyne, yielded analogous complexes. The characteristic features in the ^{13}C NMR spectra of all products are two singlets in the region 70–80 ppm, characteristic of aliphatic carbon atoms bound to a metal, not α- and β-carbon atoms in a metallacyclobutadiene complex.[4] The fact that the methylene protons in the 3-hexyne products are diastereotopic also suggests that these products cannot contain a planar metallacyclobutadiene ring. We believe that these complexes are all metallatetrahedrane or, more realistically, η^3-cyclopropenyl complexes with approximate pentagonal-bipyramidal geometries, viz.

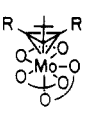

The ^1H NMR spectrum of $W[C_3(CMe_3)Me_2](O_2CCMe_3)_3$ at low temperature shows that two types of pivalate ligands are present; the two signals coalesce to one at ~230 K (250 MHz). At all temperatures, however, the two methyl groups on the WC_3 cage are equivalent on the NMR time scale. In contrast, the ^1H NMR spectrum of $Mo[C_3(CMe_3)R'_2](O_2CCMe_3)_3$ (R' = Me, Et) at 203 K showed equivalent pivalate ligands, presumably the result of rapid equilibration.

If excess 2-butyne is added to $Mo(CCMe_3)(O_2CCHMe_2)_3$, a great deal of polymer is formed along with a red-brown oil whose ^{13}C NMR spectrum shows primarily a product with signals at 121, 117, and 118 (weak) ppm characteristic of the carbon atoms in a cyclopentadienyl ring, i.e., η^5-$C_5(CMe_3)Me_4$.[4c] Unfortunately, this product could not be isolated and identified. (Cyclopentadienyl complexes containing trifluoroacetate ligands can be isolated; see below.)

Reactions between $M(CCMe_3)(O_2CR)_3$ complexes and terminal acetylenes appear to be complex compared to the results obtained for trifluoroacetate complexes (see below) where deprotiocyclobutadiene complexes can be isolated in good yield.

We were curious as to whether it would be possible to prepare $M(CCMe_3)(O_2CR)_3$ complexes from $M(CCMe_3)(OCMe_3)_3$ complexes. We found that $W(CCMe_3)(OCMe_3)_3$ complexes react with carboxylic acids to give complexes of the type $W(CHCMe_3)(O_2CR)_2(OCMe_3)_2$.[7] Analogous reactions of $Mo(CCMe_3)(OCMe_3)_3$, however, do not appear to yield *stable* neopentylidene complexes. For example, $Mo(CCMe_3)(OCMe_3)_3$ reacts with 3 equiv of isobutyric acid to give $Mo(CCMe_3)(O_2CCHMe_2)_3$ in high yield in pentane. Attempts to prepare analogous $Mo(CR')(O_2CR)_3$ (e.g., R' = Et) complexes, however, were considerably less successful, as were reactions between $Mo(CCMe_3)(OCMe_3)_3$ and other carboxylic acids.

One of the more important questions is whether the η^3-cyclopropenyl complexes can be destabilized by changing the ligand (here carboxylate) that apparently encourages formation of a tetrahedral MC_3 system to one that encourages formation of an alkylidyne complex (e.g., *tert*-butoxide). The reaction shown in eq 2 illustrates that

$$W[C_3(CMe_3)Me_2](O_2CCMe_3)_3 + 3LiOCMe_3 \xrightarrow{\text{pentane}} W(CR)(OCMe_3)_3 \quad (2)$$

R = CMe_3 (50%), Me (50%)

the MC_3 tetrahedron is destabilized in the presence of *tert*-butoxide ligands. $Mo[C_3(CMe_3)Ph_2](O_2CCHMe_2)_3$ reacts with 3 equiv of $LiOCMe_3$ in pentane to yield only $Mo(CCMe_3)(OCMe_3)_3$ and PhC≡CPh (by NMR), not what should be the thermodynamically more stable benzylidyne complex.[3] An interesting question, but one that will be difficult to answer, is whether the alkylidyne complex is formed by loss of an acetylene from the MC_3 tetrahedron or whether the complex containing the tetrahedral MC_3 form is transformed into a square-planar metallacyclobutadiene complex before loss of the acetylene. We favor the latter alternative.

The Preparation and Reactions of Trifluoroacetate Complexes. The reaction between $M(CCMe_3)(CH_2CMe_3)_3$ and CF_3CO_2H in the presence of 1,2-dimethoxyethane (dme) yields red to purple compounds of the type $M(CCMe_3)(O_2CCF_3)_3(dme)$ (eq 3). $Mo(CCMe_3)$-

$$M(CCMe_3)(CH_2CMe_3)_3 + 3CF_3CO_2H \xrightarrow[\text{pentane}]{\text{dme}} M(CCMe_3)(O_2CCF_3)_3(dme) \quad (3)$$

M = Mo, W

$(O_2CCF_3)_3(dme)$ is a purple solid that yields a red solution

in ether if concentrated to an almost yellow solution in ether if dilute. If dimethoxyethane is left out of the reaction involving $Mo(CCMe_3)(CH_2CMe_3)_3$, we obtain a red-purple solid that we assume is $Mo(CCMe_3)(O_2CCF_3)_3$. Upon recrystallization from ether, 2 equiv of ether are present (by ^1H NMR), we assume the result of formation of a bis(etherate).

Reactions between $M(CCMe_3)(O_2CCF_3)_3$(dme) and dialkylacetylenes did not produce stable η^3-cyclopropenyl complexes. $Mo(CCMe_3)(O_2CCF_3)_3$(dme) reacts with 5–20 equiv of 2-butyne to give in low yield (~10%) a diamagnetic, black crystalline complex with the apparent composition $Mo[\eta^5\text{-}C_5(CMe_3)Me_4](O_2CCF_3)_3$. The reaction between $W(CCMe_3)(O_2CCMe_3)_3$(dme) and 3-hexyne produced a related, *paramagnetic* black crystalline complex in ~20% yield that analyzes as $W[\eta^5\text{-}C_5(CMe_3)Et_4](O_2CCF_3)_4$. We conclude that reactions between internal acetylenes and neopentylidyne complexes that contain what is essentially a monodentate CF_3CO_2 ligand are relatively complex, and the end result, as with halide complexes of W,[4c] is formation of a cyclopentadienyl complex, albeit in low yield. The trifluoroacetate complexes appear to be more like halide complexes; the trifluoroacetate ligand is essentially monodentate and a relatively good electron-withdrawing ligand. Therefore, the metal is probably considerably more electrophilic than in the other carboxylate complexes and is attacked more readily by additional equivalents of dialkylacetylene. Cyclopentadienyl complexes probably are only one type out of many reaction products, judging from the low yields obtained.

$Mo(CCMe_3)(O_2CCF_3)_3$(dme) reacts with slightly more than 1 equiv of RC≡CH (R = CMe_3 or Ph) to yield what we propose are deprotonated molybdacyclobutadiene complexes $Mo[C_3(CMe_3)(R)](O_2CCF_3)_2$(dme) (eq 4) by

$$Mo(CCMe_3)(O_2CCF_3)_3(dme) \xrightarrow[-CF_3CO_2H]{+RC\equiv CH} Mo[C_3(CMe_3)(R)](O_2CCF_3)_2(dme) \quad (4)$$

R = CMe_3, Ph

comparison with related dialkoxide derivatives[3] and free CF_3CO_2H as shown by ^{19}F NMR studies. When two or more equivalents of pyridine are added to $Mo[C_3(CMe_3)(R)](O_2CCF_3)_2$(dme), bis(pyridine) adducts $Mo[C_3(CMe_3)(R)](O_2CCF_3)_2(py)_2$ can be isolated as purple-red crystals for all R (eq 5). A variety of analogous pseudo

$$Mo[C_3(CMe_3)(R)](O_2CCF_3)_2(dme) \xrightarrow[-dme]{\text{excess py}} Mo[C_3(CMe_3)(R)](O_2CCF_3)_2(py)_2 \quad (5)$$

R = CMe_3, Ph

six-, five-, or four-coordinate "deprotio" molybdacyclobutadiene[3] and tungstacyclobutadiene complexes[6] have been observed to form in reactions between alkylidyne complexes and terminal acetylenes, and one of them, $Mo[C_3(CMe_3)_2][OCH(CF_3)_2](py)_2$, has been characterized by X-ray crystallography. All show characteristic, closely spaced signals for the α- and β-carbon atoms in the region between 230 and 255 ppm.

The X-ray Structure of $W[C_3(CMe_3)Et_2](O_2CMe)_3$. The crystals of $W[C_3(CMe_3)Et_2](O_2CMe)_3$ consist of discrete molecular units separated by normal van der Waals' distances; there are no abnormally short contacts. Interatomic distances are given in Table I, interatomic angles are collected in Table II, and relevant intramolecular planes are presented in Table III. The scheme used for labeling atoms is illustrated in Figure 1, and a stereoscopic view of the molecule is provided in Figure 2.

The central tungsten atom has a very approximately pentagonal-bipyramidal coordination geometry if we count

Table I. Interatomic Distances (Å) for $W[C_3(CMe_3)Et_2](O_2CMe)_3$

(A) Distances about the Tungsten Atom			
W–O(11)	2.220 (4)	W–C(4)	2.089 (5)
W–O(12)	2.114 (4)	W–C(5)	2.114 (7)
W–O(21)	2.215 (4)	W–C(6)	2.134 (6)
W–O(22)	2.136 (5)	W···C(11)	2.536 (6)
W–O(31)	2.180 (5)	W···C(21)	2.560 (7)
W–O(32)	2.155 (4)	W···C(31)	2.565 (7)
W···centroid	1.926 (-)		
(B) Distances within the $C_3(CMe_3)Et_2$ System			
C(4)–C(5)	1.451 (10)	C(5)–C(51)	1.500 (15)
C(4)–C(6)	1.448 (8)	C(51)–C(52)	1.503 (19)
C(5)–C(6)	1.405 (11)	C(6)–C(61)	1.491 (11)
C(4)–C(41)	1.483 (9)	C(61)–C(62)	1.472 (18)
C(41)–C(42)	1.559 (12)		
C(41)–C(43)	1.538 (15)		
C(41)–C(44)	1.537 (24)		
(C) Distances within Acetate Ligands			
O(11)–C(11)	1.259 (7)	C(21)–C(22)	1.506 (12)
O(12)–C(11)	1.275 (7)	O(31)–C(31)	1.298 (8)
C(11)–C(12)	1.497 (10)	O(32)–C(31)	1.254 (9)
O(21)–C(21)	1.278 (8)	C(31)–C(32)	1.487 (14)
O(22)–C(21)	1.256 (8)		

Table II. Interatomic Angles (deg) for $W[C_3(CMe_3)Et_2](O_2CMe)_3$

(A) Selected Angles about the Tungsten Atom			
O(11)–W–O(12)	59.9 (2)	O(21)–W–O(22)	59.3 (2)
O(11)–W–O(21)	83.2 (2)	O(21)–W–O(31)	155.7 (2)
O(11)–W–O(22)	80.5 (2)	O(21)–W–O(32)	137.3 (2)
O(11)–W–O(31)	80.9 (2)	O(21)–W–centroid	94.1 (-)
O(11)–W–O(32)	85.6 (2)	O(22)–W–O(31)	134.9 (2)
O(11)–W–centroid	169.1 (-)	O(22)–W–O(32)	78.3 (2)
O(12)–W–O(21)	77.19 (15)	O(22)–W–centroid	107.3 (-)
O(12)–W–O(22)	124.06 (16)	O(31)–W–O(32)	59.6 (2)
O(12)–W–O(31)	78.88 (16)	O(31)–W–centroid	98.0 (-)
O(12)–W–O(32)	129.98 (16)	O(32)–W–centroid	103.3 (-)
O(12)–W–centroid	109.3 (-)		
(B) Internal Angles within the WC_3 Tetrahedron			
C(5)–C(4)–C(6)	58.0 (4)	W–C(5)–C(6)	71.5 (4)
C(6)–C(5)–C(4)	60.9 (5)	W–C(6)–C(4)	68.3 (4)
C(4)–C(6)–C(5)	61.1 (5)	W–C(6)–C(5)	69.9 (4)
W–C(4)–C(5)	70.7 (4)	C(4)–W–C(5)	40.4 (3)
W–C(4)–C(6)	71.6 (4)	C(4)–W–C(6)	40.1 (2)
W–C(5)–C(4)	68.9 (4)	C(5)–W–C(6)	38.6 (3)
(C) External Angles of the $W[C_3(CMe_3)Et_2]$ System			
C(5)–C(4)–C(41)	139.2 (6)	C(4)–C(41)–C(42)	109.6 (8)
C(6)–C(4)–C(41)	139.0 (6)	C(4)–C(41)–C(43)	107.9 (8)
C(4)–C(5)–C(51)	138.2 (7)	C(4)–C(41)–C(44)	110.1 (9)
C(6)–C(5)–C(51)	142.7 (7)	C(42)–C(41)–C(43)	107.8 (9)
C(4)–C(6)–C(61)	143.2 (7)	C(42)–C(41)–C(44)	108.0 (9)
C(5)–C(6)–C(61)	143.3 (7)	C(5)–C(51)–C(52)	112.4 (10)
		C(6)–C(61)–C(62)	116.3 (10)
centroid–C(4)–C(41)	150.9 (-)	W–C(4)–C(41)	141.9 (5)
centroid–C(5)–C(51)	153.9 (-)	W–C(5)–C(51)	139.4 (6)
centroid–C(6)–C(61)	159.3 (-)	W–C(6)–C(61)	136.0 (6)
(D) Angles within the Acetate Ligands			
O(11)–C(11)–O(12)	117.4 (5)	W–O(21)–C(21)	90.1 (4)
O(11)–C(11)–C(12)	122.4 (6)	W–O(22)–C(21)	94.4 (4)
O(12)–C(11)–C(12)	120.2 (6)	O(31)–C(31)–O(32)	115.0 (6)
W–O(11)–C(11)	89.2 (3)	O(31)–C(31)–C(32)	122.6 (7)
W–O(12)–C(11)	93.6 (3)	O(32)–C(31)–C(32)	122.4 (7)
O(21)–C(21)–O(22)	116.2 (6)	W–O(31)–C(31)	91.4 (4)
O(21)–C(21)–C(22)	121.4 (6)	W–O(32)–C(31)	93.9 (4)
O(22)–C(21)–C(22)	122.3 (6)		

(6) Freudenberger, J., unpublished results.
(7) Freudenberger, J. H.; Schrock, R. R. *Organometallics* **1985**, *4*, 1937.

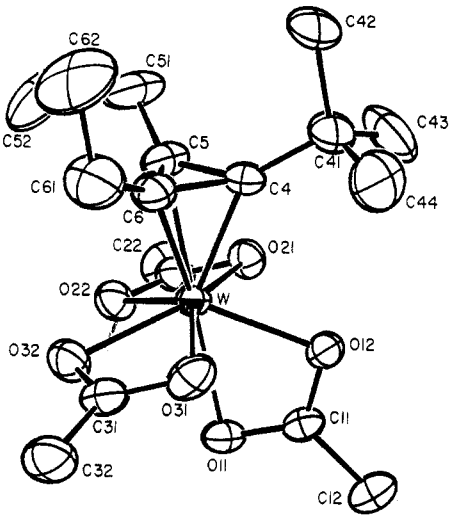

Figure 1. Labeling of non-hydrogen atoms in the $W[C_3(CMe_3)Et_2](O_2CMe)_3$ molecule (ORTEP-II diagram, 30% probability ellipsoids).

the η^3-$C_3(CMe_3)Et_2$ ligand as occupying a single coordination site. The η^3-$C_3(CMe_3)Et_2$ ligand and atom O(11) occupy the "apical" positions; O(12) and the four oxygen atoms of the remaining acetate ligands take up the five "equatorial" sites. The tungsten–oxygen distances vary appreciably, with each acetate group having slightly asymmetric W–O distances. This is most pronounced for the axial–equatorial ligand (acetate O(11), C(11), O(12)) where the axial bond (W–O(11) = 2.220 (4) Å) is 0.106 (5) Å longer than the equatorial linkage (W–O(12) = 2.114 (4) Å). However, W–O differences are also appreciable in one of the two diequatorial acetate groups—i.e., W–O(21) = 2.215 (4) Å and W–O(22) = 2.136 (5) Å (difference 0.079 (6) Å). The other acetate group is more symmetrically bound with W–O(31) = 2.180 (5) Å and W–O(32) = 2.155 (4) Å (difference 0.025 (6) Å). All acetate "bite" angles are equivalent with O(11)–W–O(12) = 59.9 (2)°, O(21)–W–O(22) = 59.3 (2)°, and O(31)–W–O(32) = 59.6 (2)°. The equatorial donor atoms are all displaced well below the tungsten atom (see Figure 2), the individual centroid–W–O angles being centroid–W–O(12) = 109.3°, centroid–W–O(21) = 94.1°, centroid–W–O(22) = 107.3°, centroid–W–O(31) = 98.0°, and centroid–W–O(32) = 103.3°. There is some ruffling of atoms within the pentagonal system.

The WO_2C systems are all close to planar—angles between the WO_2 and O_2C planes are 1.17°, 1.05°, and 3.58° for the three acetate groups. Distances and angles within the acetate groups are normal with C–O = 1.254 (9) to 1.298 (8) Å [average 1.270 (17) Å][8] and C–C(Me) = 1.487 (14) to 1.506 (12) Å [average 1.497 (10) Å] and O–C–O = 115.0 (6) to 117.4 (5)° [average 116.2 (12)°]. Angles between the η^3-C_3 plane (plane A, Table III) and the acetate groups (as defined by their O–W–O planes) are 88.48° for the O(11)–W–O(12) system, 18.57° for the O(21)–W–O(22) system, and 14.71° for the O(31)–W–O(32) system. There is also a dihedral angle of 18.33° between the planes of the two equatorial acetate ligands (i.e., O(21)–W–O(22) and O(31)–W–O(32)).

The C_3 ring is essentially symmetrically bound to the tungsten atom. The W···centroid distance is 1.926 Å. The tungsten–carbon distances to the η^3-$C_3(CMe_3)Et_2$ ligand are all substantially shorter than a normal W–C σ-bond length. Individual values are W–C(4) = 2.089 (5) Å, W–C(5) = 2.114 (7) Å, and W–C(6) = 2.134 (6) Å (average value 2.112 Å) and may be compared with W–C(sp^3) single bond distances of 2.258 (9) Å in $W(CCMe_3)(CHCMe_3)(CH_2CMe_3)(dmpe)$[9] and 2.305 (7) Å in $[W(CH_2PMe_3)(CO)_2Cl(PMe_3)_3]^+$.[10] The substituents on the η^3-$C_3(CMe_3)Et_2$ system are all bent out of the C_3 plane and away from the tungsten atom. Deviations of the α-carbon atoms from the C_3 plane (plane A, Table III) are –0.747 (7) Å for C(41), –0.669 (9) Å for C(51), and –0.548 (10) Å for C(61). These correspond to angular displacements,[11] *perpendicular* to the C_3 plane, of 30.25° for C(41), 26.50° for C(51), and 21.54° for C(61). The centroid–C(ring)–C(α) angles

Table III. Important Planes (and Atomic Deviations Therefrom) for $W[C_3(CMe_3)Et_2](O_2CMe)_3$

atom	dev, Å	atom	dev, Å
Plane A: the η^3-C_3 System			
equation: $0.1030X + 0.3426Y - 0.9338Z = -3.7225$			
C(4)*	0.000	O(11)	4.114 (4)
C(5)*	0.000	O(12)	2.608 (4)
C(6)*	0.000	O(21)	2.055 (4)
C(41)	–0.747 (7)	O(22)	2.575 (4)
C(51)	–0.669 (9)	O(31)	2.276 (5)
C(61)	–0.548 (10)	O(32)	2.485 (4)
W	1.9416 (2)		
Plane B: the O(11)–C(11)–O(12) System			
equation: $0.8517X - 0.5062Y - 0.1357Z = 1.8413$			
O(11)*	0.000	W	–0.0382 (2)
C(11)*	0.000	C(12)	–0.016 (10)
O(12)*	0.000		
Plane C: the O(11)–W–O(12) System			
equation: $0.8431X - 0.5225Y - 0.1270Z = 1.7650$			
W*	0.000	C(11)	–0.013 (6)
O(11)*	0.000	C(12)	–0.060 (9)
O(12)*	0.000		
Plane D: the O(21)–C(21)–O(22) System			
equation: $0.3678X + 0.4890Y - 0.7909Z = -0.0825$			
O(21)*	0.000	W	0.0345 (2)
C(21)*	0.000	C(22)	0.039 (9)
O(22)*	0.000		
Plane E: the O(21)–W–O(22) System			
equation: $0.3510X + 0.4951Y - 0.7948Z = -0.1115$			
W*	0.000	C(21)	0.012 (6)
O(21)*	0.000	C(22)	0.079 (9)
O(22)*	0.000		
Plane F: the O(31)–C(31)–O(32) System			
equation: $0.0042X + 0.6064Y - 0.7951Z = -1.3222$			
O(31)*	0.000	W	0.1174 (2)
C(31)*	0.000	C(32)	–0.002 (12)
O(32)*	0.000		
Plane G: the O(31)–W–O(32) System			
equation: $0.0417X + 0.5655Y - 0.8237Z = -1.2320$			
W*	0.000	C(31)	0.043 (6)
O(31)*	0.000	C(32)	0.134 (12)
O(32)*	0.000		
Interplanar Angles (deg)			
A–B	87.65	B–C	1.17
A–C	88.48	D–E	1.05
A–D	19.27	F–G	3.58
A–E	18.57	C–E	82.05
A–F	18.07	C–G	98.96
A–G	14.71	E–G	18.33

(8) Esd's on average values are, where appropriate, calculated via the scatter formula $\sigma = [\sum_N (d_i - \bar{d})^2/(N-1)]^{1/2}$.

(9) Churchill, M. R.; Youngs, W. J. *Inorg. Chem.* **1979**, *18*, 2454.
(10) Churchill, M. R.; Wasserman, H. J. *Inorg. Chem.* **1982**, *21*, 3913.
(11) Calculated as

$$\sin^{-1} = \frac{\text{deviation of } \alpha\text{-carbon atom}}{\text{C(ring)–C}(\alpha) \text{ distance}}$$

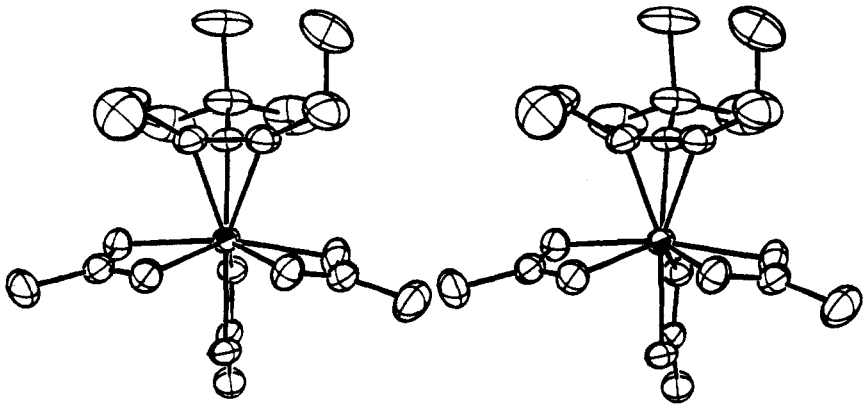

Figure 2. Stereoscopic view of the $W[C_3(CMe_3)Et_2](O_2CMe)_3$ molecule, illustrating its pentagonal-bipyramidal coordination geometry (ORTEP-II diagram, 30% probability ellipsoids).

are centroid–C(4)–C(41) = 150.9°, centroid–C(5)–C(51) = 153.9° and centroid–C(6)–C(61) = 159.3°. The supplements of these angles (i.e., 29.1°, 26.1°, and 20.7°) differ from the angular displacements listed above by being nondirectional and are therefore the composite of perpendicular and lateral displacements of the C(α) atoms from idealized radial positions.

Carbon–carbon distances within the C_3 ring are C(4)–C(5) = 1.451 (10) Å, C(4)–C(6) = 1.448 (8) Å, and C(5)–C(6) = 1.405 (11) Å; this pattern resembles that found for the C_3 ring in $W(\eta^5\text{-}C_5H_5)[C_3(CMe_3)_2Me](PMe_3)Cl_2$[5] (1.473 (8), 1.466 (7), 1.416 (8) Å), rather than that found in $W[C(CMe_3)C(Me)C(Me)](Me_2NCH_2CH_2NMe_2)Cl_3$[4c] (1.547 (10), 1.432 (10), 1.383 (9) Å). In the present molecule (as in the two previous tetrahedral WC_3 complexes that we have examined) confidence in the accuracy of the C(ring)–C(ring) distances is significantly enhanced by the agreement with known values and internal consistency of the C(ring)–C(α) distances (i.e., C(4)–C(41) = 1.483 (9) Å, C(5)–C(51) = 1.500 (15) Å, C(6)–C(61) = 1.491 (11) Å.

Attempts To Prepare $W(C_3R'_3)(O_2CR)_3$ Species by W≡W Bond Cleavage. Recently we have published a full account of the reaction between $W_2(OCMe_3)_6$ and acetylenes to give alkylidyne complexes.[12] If a W≡W bond in $W_2(O_2CR)_6$ could be cleaved by an acetylene, then $W(C_3R'_3)(O_2CR)_3$ complexes could be prepared readily.

When 2 equiv of RCO_2H are added to $W_2(OCMe_3)_6$, a compound with the formula $W_2(OCMe_3)_4(O_2CR)_2$ is formed.[18a] (A similar reaction between $Mo_2(OCMe_3)_6$ and RCO_2H gives $Mo_2(OCMe_3)_4(O_2CR)_2$, the X-ray structure of which shows that the carboxylates bridge the Mo≡Mo bond.[13]) $W_2(OCMe_3)_4(O_2CR)_2$ will not react with 3-hexyne, even at 60 °C in 16 h.

If 6 equiv of pivalic acid are added to $W_2(OCMe_3)_6$ and the solvent removed in vacuo, a complex, apparently nonhomogeneous yellow solid is obtained that we believe to be $W(OCMe_3)_x(O_2CCMe_3)_{6-x}$ where x = 2–6. If this solid is dissolved in toluene, 3-hexyne is added, and the solution is heated overnight at 60 °C, pentane-soluble blue crystals with the molecular formula $W_2(O_2CCMe_3)_6$(3-hexyne) are obtained in good yield. In a similar manner $W_2(O_2CCMe_3)_6$(2-butyne) and $W_2(O_2CCH_3)_6$(3-hexyne) have been prepared. The ^1H NMR spectra of all three change with temperature. For example, the spectrum of $W_2(O_2CCMe_3)_6$(3-hexyne) at 360 K shows a normal quartet (~4.6 ppm) and triplet (~1.4 ppm) for the ethyl group protons and a 2:1 set of singlet resonances for the pivalate ligands. At 235 K three pivalate resonances are present and the methylene protons in the ethyl group are diastereotopic. We suggest that two bridging carboxylate ligands and the acetylene bridge the W≡W bond and that the remaining carboxylate ligands take up "diequatorial" and "equatorial/axial" positions in a molecule that contains a C_2 axis, viz.

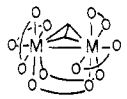

Such species evidently do not decompose to $W(CEt)(O_2CR)_3$ complexes.

Discussion

For several years the reaction between $M(CCMe_3)(CH_2CMe_3)_3$ and 3 equiv of HCl in the presence of dimethoxyethane to give $M(CCMe_3)Cl_3$(dme) has been crucial to the development of the chemistry of tungsten[18b] and molybdenum[3] alkylidyne complexes. We have been working under the assumption that $M(CCMe_3)(CH_2CMe_3)_3$ complexes are protonated at the alkylidyne α-carbon atom but that intermediate "$M(CHCMe_3)(CH_2CMe_3)_3Cl$" is unstable toward α-hydrogen abstraction[14] to give $M(CCMe_3)(CH_2CMe_3)_2Cl$. Repeated additions of HCl across the M≡$CCMe_3$ bond followed by α-hydrogen abstraction to give neopentane ultimately yields $M(CCMe_3)Cl_3$(dme). Any protonation of the neopentylidyne α-carbon atom in $M(CCMe_3)Cl_3$(dme) is reversible, and the equilibrium lies well to the side of the neopentylidyne complex. A less attractive explanation of the reaction between $M(CCMe_3)(CH_2CMe_3)_3$ and HCl is that HCl attacks the neopentyl α-carbon atoms directly. The same ambiguity exists concerning the mechanism of the reaction between $M(CCMe_3)(CH_2CMe_3)_3$ and carboxylic acids. The difference between the HCl and RCO_2H reactions is that complexation of the carboxylic acid to the metal via the carbonyl oxygen atom as a step prior to delivery of the proton seems likely.

The tetrahedral MC_3 arrangement is an alternative to the planar MC_3 ring that has been observed in four roughly trigonal-bipyramidal complexes.[4a,b,15] There is also an example of an $MC_3R'_3$ complex in which the MC_3 configuration is approximately halfway between a tetrahedron and a plane.[16] When a phosphine ligand is added to a

(12) Listemann, M. L.; Schrock, R. R. *Organometallics* **1985**, *4*, 74.
(13) Chisholm, M. H.; Huffman, J. C.; Kirkpatrick, C. C. *Inorg. Chem.* **1983**, *22*, 1704.
(14) Schrock, R. R. *Acc. Chem. Res.* **1979**, *12*, 98.
(15) (a) Pedersen, S. F.; Schrock, R. R.; Churchill, M. R.; Wasserman, H. J. *J. Am. Chem. Soc.*, **1982**, *104*, 6808. (b) Churchill, M. R.; Wasserman, H. J. *J. Organomet. Chem.* **1984**, *270*, 201. (c) Churchill, M. R.; Ziller, J. W. *J. Organomet. Chem.* **1985**, *286*, 27.
(16) (a) Churchill, M. R.; Ziller, J. W.; McCullough, L.; Pedersen, S. F.; Schrock, R. R. *Organometallics* **1983**, *2*, 1046. (b) Churchill, M. R.; Ziller, J. W. *J. Organomet. Chem.* **1985**, *279*, 403.

relative of the latter[5] or when TMEDA is added to W-$[C_3(CMe_3)Me_2]Cl_3$[4c] (one of the structurally characterized TBP complexes containing the planar MC_3 ring), an η^3-cyclopropenyl complex is formed (eq 6). Therefore, it

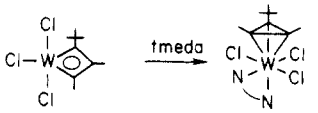

(6)

seems quite possible that planar metallacyclobutadiene rings will be found only in TBP complexes and that addition of donor ligands to such species will result in either loss of an acetylene to give an alkylidyne complex[4b] or formation of an η^3-cyclopropenyl complex. Why the η^3-cyclopropenyl complexes prepared here do not lose $Me_3CC{\equiv}CR$ to form alkylidyne complexes (eq 7) is not obvious. We speculate that an acetylene cannot be lost directly from a MC_3 tetrahedron, but only from a planar MC_3 ring.

$$M[C_3(CMe_3)R_2](O_2CR)_3 \not\rightarrow M(CR)(O_2CR)_3 + Me_3CC{\equiv}CR \quad (7)$$

It is interesting to compare the MC_3R_3 system with the $M_2C_2R_2$ system where tetrahedral M_2C_2 arrangements are the norm.[17] Only in very special circumstances is the $M_2C_2R_2$ system destabilized with respect to formation of two M≡CR complexes.[12,18a] We have proposed that M≡CR complexes can be formed only from an unobservable, planar 1,3-dimetallacyclobutadiene ring system[12] on the basis of what appears to be a more than circumstantial relationship between the chemistry of W≡C complexes and that of W≡W complexes, as far as reactions with acetylenes are concerned. The findings reported here help to strengthen and define that relationship further.

Experimental Section

General procedures can be found elsewhere.[12] $W(CCMe_3)(CH_2CMe_3)_3$[18b] and $Mo(CCMe_3)(CH_2CMe_3)_3$[3] were prepared by published methods. NMR data are listed in parts per million from Me_4Si. Obvious multiplicities and intensities and routine coupling constants are usually omitted. The solvent used for NMR studies was C_6D_6, and the temperature was ca. 298 K, unless specified otherwise.

Collection of X-ray Diffraction Data for $W[C_3(CMe_3)Et_2](O_2CMe)_3$. A carefully selected crystal of approximate dimensions 0.2 × 0.2 × 0.3 mm was sealed into a 0.2-mm diameter thin-walled glass capillary tube under an inert atmosphere (Ar) in a KSE drybox which had been specially modified (with a protruding transparent addition between the gloves) so as to allow inspection of crystals through an externally mounted binocular microscope. The capillary was then mounted (with beeswax) into an aluminum pin and inserted into a eucentric goniometer on the Syntex $P2_1$ automated four-circle diffractometer at SUNY—Buffalo. All subsequent operations (crystal alignment, determination of unit cell parameters and the crystal's orientation matrix, data collection) were performed as described previously.[19] Details appear in Table IV.

A careful analysis of the data set revealed no systematic absences nor any diffraction symmetry other than the Friedel condition. The crystal therefore belongs to the triclinic system. Possible space groups are the noncentrosymmetric $P1$ [C_1^1; No. 1] or the centrosymmetric $P\bar{1}$ [C_i^1; No. 2]. With $Z = 2$ and no expectation of a resolved chiral molecule, the latter centrosymmetric space group is far more probable[20] and was later confirmed as the correct choice by the successful solution of the structure.

Table IV. Experimental Data for X-ray Diffraction Study of $W[C_3(CMe_3)Et_2](O_2CMe)$

(A) Crystal Parameters at 23 °C (296 K)

a = 8.345 (3) Å	cryst system: triclinic
b = 8.379 (5) Å	space group: $P\bar{1}$ [No. 2; C_i^1]
c = 16.994 (6) Å	V = 1013.2 (7) Å^3
α = 77.04 (4)°	Z = 2
β = 76.56 (3)°	mol wt = 512.3 amu
γ = 62.23 (3)°	ρ(calcd) = 1.68 g cm^{-3}

(B) Data Collection

diffractometer:	Syntex $P2_1$
radiation:	Mo Kα ($\bar{\lambda}$ = 0.710 730 Å)
monochromator:	pyrolytic graphite, equatorial, 2θ(m) = 12.2°, assumed 50% perfect.
scan type:	coupled θ(crystal)–2θ(counter)
scan width:	symmetrical, [1.8 + $\Delta(\alpha_2 - \alpha_1)$]°
scan speed:	2.0 deg min^{-1}
reflctns collected:	$+h, \pm k, \pm l$ for 2θ = 4.5 – 45.0°, 2869 total yielding 2650 unique data
abs coeff:	μ = 60.6 cm^{-1}, corrected by interpolation between experimental ψ-scans, of four close-to-axial reflections (241, 254, 362, 463); filename : WAC2

The resulting unique data were corrected for the effects of absorption and for Lorentz and polarization factors and were reduced to unscaled $|F_o|$ values. All reflections with I(net) < 0 were assigned a value of $|F_o| = 0$. A Wilson plot was used to place the data on an approximate absolute scale.

Solution and Refinement of the Structure of $W[C_3(CMe_3)Et_2](O_2CMe)_3$. All calculations were performed on the SUNY—Buffalo modified version of the Syntex XTL structure solving system.[21] The analytical scattering factors for the *neutral* atoms (W, O, C, H) were corrected for both the real ($\Delta f'$) and imaginary ($i\Delta f''$) components of anomalous dispersion.[22] The function minimized during least-squares refinement was $\sum w(|F_o| - |F_c|)^2$ where $w^{-1} = [\sigma(|F_o|)]^2 + [0.015|F_o|]^2$.

The coordinates of the tungsten atom were readily determined from a three-dimensional (unsharpened) Patterson map. The remaining non-hydrogen atoms were located unambiguously from a difference-Fourier synthesis. The hydrogen atoms of the acetate groups centered on C(12), C(22), and C(32) were located on a subsequent difference-Fourier map. All other hydrogen atoms were included in calculated positions (tetrahedral geometry and idealized staggered conformation) with d(C–H) = 0.95 Å;[23] these positions were updated but were not refined. Convergence was reached with[24] R_F = 2.6%, R_{wF} = 2.8%, and GOF = 1.45 for 272 parameters refined against all 2650 unique data [R_F = 2.4% and R_{wF} = 2.8% for those 2536 data with $|F_o| > 3.0\sigma(|F_o|)$; R_F = 2.3% and R_{wF} = 2.7% for those 2431 data with $|F_o| > 6.0\sigma(|F_o|)$].

Final positional parameters are collected in Table V. Anisotropic thermal parameters (Table VS) and a table of observed and calculated structure factor amplitudes appear as supplementary material.

Preparations. $W(CCMe_3)(O_2CCMe_3)_3$. Pivalic acid (1.84 g, 18.0 mmol) was added to a solution of $W(CCMe_3)(CH_2CMe_3)_3$ (2.80 g, 6.00 mmol) in pentane (100 mL) that had been cooled to −30 °C. After the solution had warmed to room temperature, the solvent was removed in vacuo. The residue was recrystallized from pentane at −30 °C to give large colorless crystals (3.10 g, 93%): ^{1}H NMR δ 1.19 (br s, 9, O_2CCMe_3), 1.12 (br s, 18, O_2CCMe_3), 1.05 ($CCMe_3$); ^{13}C NMR (330K) δ 285.5 ($CCMe_3$), 49.4 ($CCMe_3$), 40.4 (O_2CCMe_3), 31.3 ($CCMe_3$), 26.0 (O_2CCMe_3). The O_2CCMe_3 resonance was not found. Anal. Calcd for $WC_{20}H_{36}O_6$:

(17) Hoffman, D. M.; Hoffmann, R.; Fisel, C. R. *J. Am. Chem. Soc.* **1982**, *104*, 3858.
(18) (a) Freudenberger, J. H.; Pedersen, S. F.; Schrock, R. R. *Bull. Chim. Soc. Fr.* **1985**, 349. (b) Schrock, R. R.; Clark, D. N.; Sancho, J.; Wengrovius, J. H.; Rocklage, S. M.; Pedersen, S. F. *Organometallics* **1982**, *1*, 1645.
(19) Churchill, M. R.; Lashewycz, R. A.; Rotella, F. J. *Inorg. Chem.* **1977**, *16*, 265.
(20) Nowacki, W.; Matsumoto, T.; Edenharter, A. *Acta Crystallogr.* **1967**, *22*, 935.
(21) "Syntex XTL Operations Manual", 2nd ed.; Syntex Analytical Instruments: Cupertino, CA, 1976.
(22) "International Tables for X-Ray Crystallography"; Kynoch Press: Birmingham, England, 1974; Vol. 4, pp 99–101, 149–150.
(23) Churchill, M. R. *Inorg. Chem.* **1973**, *12*, 1213.
(24) $R_F = 100[\sum||F_o| - |F_c||/\sum|F_o|]$; $R_{wF} = 100[\sum w(|F_o| - |F_c|)^2/\sum w|F_o|^2]^{1/2}$; GOF = $[\sum w(|F_o| - |F_c|)^2/(NO - NV)]^{1/2}$, where NO = number of observations and NV = number of variables.

Table V. Final Atomic Parameters for $W[C_3(CMe_3)Et_2](O_2CMe)_3$

atom	x	y	z
W	0.26592 (3)	0.21317 (3)	0.18668 (1)
O(11)	0.28291 (49)	0.39909 (54)	0.07259 (22)
O(12)	0.28578 (47)	0.45362 (49)	0.19079 (22)
O(21)	−0.02443 (47)	0.41675 (50)	0.20336 (23)
O(22)	0.06943 (52)	0.20542 (57)	0.12828 (23)
O(31)	0.56184 (50)	0.12027 (59)	0.16168 (29)
O(32)	0.43616 (54)	−0.00329 (56)	0.11347 (24)
C(11)	0.28902 (65)	0.50277 (74)	0.11403 (34)
C(12)	0.2975 (11)	0.6787 (10)	0.07636 (56)
C(21)	−0.06157 (76)	0.34273 (85)	0.15642 (34)
C(22)	−0.2510 (10)	0.4203 (12)	0.13454 (54)
C(31)	0.58107 (79)	0.00411 (85)	0.11677 (37)
C(32)	0.7614 (13)	−0.1118 (15)	0.07257 (72)
C(4)	0.25006 (76)	0.16747 (76)	0.31367 (31)
C(5)	0.15598 (83)	0.08122 (89)	0.28998 (36)
C(6)	0.34786 (81)	−0.00688 (79)	0.28330 (36)
C(41)	0.2412 (12)	0.2516 (10)	0.38356 (40)
C(42)	0.2126 (20)	0.1320 (14)	0.46517 (46)
C(43)	0.0732 (24)	0.4382 (13)	0.38276 (58)
C(44)	0.4218 (23)	0.2629 (23)	0.37878 (61)
C(51)	−0.0124 (14)	0.0503 (15)	0.32069 (52)
C(52)	−0.0176 (19)	−0.0846 (19)	0.27728 (94)
C(61)	0.5070 (14)	−0.1889 (12)	0.29384 (61)
C(52)	0.4942 (20)	−0.3059 (17)	0.3716 (10)
H(12A)	0.302 (12)	0.736 (13)	0.1138 (59)
H(12B)	0.388 (15)	0.664 (15)	0.0422 (71)
H(12C)	0.207 (10)	0.755 (10)	0.0452 (46)
H(22A)	−0.252 (12)	0.472 (13)	0.0775 (60)
H(22B)	−0.281 (13)	0.330 (15)	0.1481 (63)
H(22C)	−0.355 (13)	0.544 (15)	0.1586 (61)
H(32A)	0.786 (20)	−0.201 (22)	0.086 (10)
H(32B)	0.852 (12)	−0.049 (12)	0.0681 (57)
H(32C)	0.722 (15)	−0.074 (16)	0.0249 (74)
H(42A)	0.2036	0.1843	0.5106
H(42B)	0.3100	0.0127	0.4663
H(42C)	0.0995	0.1211	0.4693
H(43A)	0.0659	0.4955	0.4274
H(43B)	−0.0344	0.4274	0.3865
H(43C)	0.0905	0.5139	0.3330
H(44A)	0.4145	0.3188	0.4239
H(44B)	0.4399	0.3386	0.3294
H(44C)	0.5203	0.1470	0.3797
H(51A)	−0.1194	0.1663	0.3110
H(51B)	−0.0210	0.0122	0.3774
H(52A)	−0.1236	−0.1013	0.2967
H(52B)	0.0886	−0.1983	0.2862
H(52C)	−0.0098	−0.0442	0.2197
H(61A)	0.6191	−0.1672	0.2878
H(61B)	0.5321	−0.2535	0.2491
H(62A)	0.6114	−0.4192	0.3726
H(62B)	0.4004	−0.3336	0.3768
H(62C)	0.4874	−0.2474	0.4155

C, 43.18; H, 6.52. Found: C, 42.92; H, 6.66.

$Mo(CCMe_3)(O_2CCMe_3)_3$. Pivalic acid (0.40 g, 3.92 mmol) was added as a solid to a solution of $Mo(CCMe_3)Np_3$ (0.50 g, 1.32 mmol) in pentane (~30 mL) that had been cooled to −30 °C. No color change or precipitate was visible upon addition of the acid. The solution was allowed to warm to room temperature over the next 3 h. The solvent was removed in vacuo to give $Mo(CCMe_3)(O_2CCMe_3)_3$ as an off-white powder (0.56 g, 90%), which was pure by NMR and could be used without further purification in subsequent reactions. An analytical sample (white powder) was prepared by cooling a solution of it in pentane to −30 °C (~30% recovery), followed by a double sublimation at 60 °C (0.1 μm): ^1H NMR δ 1.20 (br s, 27, O_2CCMe_3), 0.94 (CMe_3); ^{13}C NMR δ 311.3 ($CCMe_3$), 196.8 (O_2CCMe_3), 53.1 ($CCMe_3$), 40.0 (O_2CCMe_3), 27.3 ($CCMe_3$), 26.3 (O_2CCMe_3). Anal. Calcd for $MoC_{20}H_{36}O_6$: C, 51.28; H, 7.75. Found: C, 50.63; H, 7.88.

$W(CCMe_3)(O_2CCHMe_2)_3$. Isobutyric acid (900 μL, 9.70 mmol) was added to a solution of $W(CCMe_3)(CH_2CMe_3)_3$ (1.50 g, 3.22 mmol) in pentane (50 mL) that had been cooled to −30 °C. The solution was warmed to room temperature, and the solvent was removed in vacuo. The resulting white powder was recrystallized from pentane at −30 °C (two crops, 1.40 g, 85%): ^1H NMR δ 2.29 (br, 3, O_2CCHMe_2)$_3$, 1.09 (s, 9, $CCMe_3$), 1.04 (br d, 18, O_2CCHMe_2); ^{13}C NMR δ 298.2 (J_{CW} = 244 Hz, $CCMe_3$), 199.8 (O_2CCHMe_2), 43.0 ($CCMe_3$), 28.7 (O_2CCHMe_2), 23.4 (Me), 8.8 (Me). Anal. Calcd for $WC_{17}H_{30}O_6$: C, 39.70; H, 5.88. Found: C, 39.42; H, 5.70.

$Mo(CCMe_3)(O_2CCHMe_2)_3$. Isobutyric acid (735 μL, 7.93 mmol, 3 equiv) was added all at once via syringe to a stirred solution of $Mo(CCMe_3)Np_3$ (1.00 g, 2.64 mmol) in pentane (~75 mL) that had been cooled to −30 °C. The reaction was allowed to warm to room temperature over a period of 2 h. Solvents were removed in vacuo, and the resulting off-white solid was crystallized from a minimum amount of ether at −30 °C to give pale yellow crystals (0.80 g, three crops, 71%): ^1H NMR δ 2.41 (sept, O_2CCHMe_2), 1.07 (d, O_2CCHMe_2), 0.94 (CMe_3); ^{13}C NMR δ 311.2 ($CCMe_3$), 195.1 (O_2CCHMe_2), 51.5 (CMe_3), 36.0 (O_2CCHMe_2), 27.3 (CMe_3), 18.0 (O_2CCHMe_2). Anal. Calcd for $MoC_{17}H_{30}O_6$: C, 47.89; H, 7.09. Found: C, 48.17; H, 7.18.

$W(CCMe_3)(O_2CCH_3)_3$. Acetic acid (1.11 mL, 19.4 mmol) was added dropwise over a period of 3 min to solution of $W(CCMe_3)(CH_2CMe_3)_3$ (3.00 g, 6.43 mmol) in pentane (75 mL) that had been cooled to −30 °C. $W(CCMe_3)(O_2CCH_3)_3$ began precipitating toward the end of the addition. The precipitate was filtered and dried in vacuo. The product was pure by ^1H NMR (2.40 g, 87%): ^1H NMR δ 1.63 (br s, 9, O_2CCH_3), 1.13 (s, 9, $CCMe_3$); ^{13}C NMR δ 286.5 ($CCMe_3$), 189.1 (O_2CMe), 49.6 ($CCMe_3$), 31.4 (Me), 22.7 (Me).

$Mo(CCMe_3)(O_2CCH_3)_3$. Acetic acid (450 μL, 10.6 mmol) was added all at once via syringe to a solution of $Mo(CCMe_3)Np_3$ (1.00 g, 2.64 mmol) in pentane (~75 mL) that had been cooled to −30 °C. The color of the solution immediately changed to a lighter yellow. The solution was allowed to warm to room temperature over a period of 2.5 h. Removing the solvent in vacuo yielded the product as an off-white powder (0.75 g, 83%): ^1H NMR δ 1.80 (br s, 9, O_2CMe), 1.00 (CMe_3); ^{13}C NMR δ 312.4 ($CCMe_3$), 188.9 (O_2CMe), 53.3 (CMe_3), 27.3 (CMe_3), 22.5 (O_2CMe).

$W(CCMe_3)(O_2CCF_3)_3$(dme). Trifluoroacetic acid (1.49 mL, 19.3 mmol) was added to a solution of $W(CCMe_3)(CH_2CMe_3)_3$ (3.00 g, 6.43 mmol) and dimethoxyethane (2.00 ml, 19.2 mmol) in pentane (150 mL) at 0 °C. The product precipitated from solution as red microcrystals (4.00 g, 91%): ^1H NMR (CD_2Cl_2) δ 4.98 (s, OCH_3), 4.18 (m, OCH_2), 3.16 (m, OCH_2), 3.45 (s, OCH_3), 1.04 (s, $CCMe_3$); ^{13}C NMR (CD_2Cl_2) δ 319.7 ($CCMe_3$), 161.6 (q, J_{CF} = 39 Hz, O_2CCF_3), 116.3 (q, J_{CF} = 289 Hz, O_2CCF_3), 116.0 (q, J_{CF} = 289 Hz, O_2CCF_3), 80.3 (OCH_3), 79.3 (OCH_2), 70.6 (OCH_2), 60.6 (OCH_3), 50.1 ($CCMe_3$), 33.2 ($CCMe_3$). Anal. Calcd for $WC_{15}H_{19}F_9O_8$: C, 26.41; H, 2.81. Found: C, 26.33; H, 2.80.

$Mo(CCMe_3)(O_2CCF_3)_3$(dme). Trifluoroacetic acid (2.40 mL, 32.3 mmol) was added all at once to a solution of $Mo(CCMe_3)Np_3$ (4.00 g, 10.6 mmol) and 1,2-dimethoxyethane (2.20 mL, 2 equiv) in pentane at −30 °C. The solution immediately turned red-purple, and a purple solid began to form. This mixture was allowed to warm to room temperature. Three hours later the solvents were removed in vacuo, and the light purple solid thus obtained was recrystallized from a minimum amount of ether at −30 °C. $Mo(CCMe_3)(O_2CCF_3)_3$(dme) was obtained as dark purple cubes (5.85 g, three crops, 93%): ^1H NMR δ 3.89 (br s, 3, $MeOCH_2CH_2OMe$), 2.65–2.63 (br, 5 total, $MeOCH_2CH_2OMe$), 2.24 (br s, 2, $MeOCH_2CH_2OMe$), 1.07 (CMe_3); ^{13}C NMR δ 341.3 ($CCMe_3$), 161.1 (br, CF_3CO_2), 116.7 (q, J_{CF} = 288 Hz, CF_3CO_2), 76.4 (br t, J_{CH} = 148 Hz, $MeOCH_2CH_2OMe$), 69.6 (br q, J_{CH} = 141 Hz, $MeOCH_2CH_2OMe$), 59.4 (br q, J_{CH} = 131 Hz, $MeOCH_2CH_2OMe$), 56.2 ($CCMe_3$), 28.3 ($CCMe_3$). Anal. Calcd for $MoC_{15}H_{19}O_8F_9$: C, 30.32; H, 3.22. Found: C, 30.09; H, 3.41.

$Mo[C_3(CMe_3)R'_2](O_2CCHMe_2)_3$ (R' = Me, Et, Ph). R = Me. 2-Butyne (20 μL, 0.256 mmol, 1 equiv) was added all at once via syringe to a pale yellow solution of $Mo(CCMe_3)(O_2CCHMe_2)_3$ (0.10 g, 0.234 mmol) in pentane (7 mL) at room temperature. The solution immediately turned red. After 2 h the solvent was removed in vacuo. The resulting dark red oil was pure by NMR: ^1H NMR δ 2.37 (m, Me_2CHCO_2), 2.34 (s, CMe), 1.28 (CMe_3), 1.08 (d, O_2CCHMe_2); ^{13}C NMR δ 192.2 (O_2CCHMe_2), 78.2 ($CCMe_3$), 72.5 (CMe), 36.1 (O_2CCHMe_2), 33.8 ($CCMe_3$), 31.0 ($CCMe_3$), 18.3 (O_2CCHMe_2), 6.1 (CMe).

R' = Et. The preparation of $Mo[C_3(CMe_3)Et_2](O_2CCHMe_2)_3$, a red oil, was analogous to that of $Mo[C_3(CMe_3)Me_2](O_2CCHMe_2)_3$: ^1H NMR δ 2.91 (m, 4, CCH_2CH_3), 2.37 (sept, O_2CCHMe_2), 1.33 (CMe_3), 1.14 (t, CCH_2CH_3), 1.08 (d, O_2CCHMe_2);

^{13}C NMR δ 192.2 (O_2CCHMe_2), 79.3 ($CCMe_3$), 77.7 (*C*Et), 36.1 (O_2CCHMe_2), 33.6 ($CCMe_3$), 31.5 ($CCMe_3$), 18.3 (O_2CCHMe_2), 16.4 (CCH_2CH_3), 15.3 (CCH_2CH_3).

R′ = Ph. Diphenylacetylene (0.21 g, 1.17 mmol, 1 equiv) was added to a pale yellow solution of $Mo(CCMe_3)(O_2CCHMe_2)_3$ (0.50 g, 1.17 mmol) in pentane (30 mL). The solution turned dark red over the next 15–20 min. After 5 h the solvent was removed *in vacuo*, leaving a dark red solid. $Mo[C_3(CMe_3)Ph_2](O_2CCHMe_2)_3$ (0.55 g, three crops, 77% of theory) was crystallized from a minimum amount of ether at −30 °C as red needles: ^1H NMR δ 7.62 (H_o), 7.15 (H_m), 6.89 (H_p), 2.09 (sept, O_2CCHMe_2), 1.56 ($CCMe_3$), 0.86 (O_2CCHMe_2); ^{13}C NMR δ 193.4 (O_2CCHMe_2), 133.8 (C_o), 131.3 (C_{ipso}), 128.8 (C_m), 128.4 (C_p), 82.0 ($CCMe_3$), 72.4 (*C*Ph), 36.6 (O_2CCHMe_2), 34.2 ($CCMe_3$), 31.7 ($CCMe_3$), 18.1 (O_2CCHMe_2). Anal. Calcd for $MoC_{31}H_{40}O_6$: C, 61.58; H, 6.67. Found: C, 62.10; H, 6.92.

$Mo[C_3(CMe_3)R'_2](O_2CCMe_3)_3$ (R′ = Me, Et, Ph). For R′ = Me or Et the dialkylacetylene (1 equiv) was added all at once via syringe to a solution of $Mo(CCMe_3)(O_2CCMe_3)_3$ (0.10 g, 0.213 mmol) in pentane (7 mL). The solution immediately turned dark red. After 3 h, the solvent was removed in vacuo, yielding $Mo[C_3(CMe_3)R'_2](O_2CCMe_3)_3$ quantitatively as a red oil.

R′ = Me: ^1H NMR δ 2.32 (CMe), 1.31 ($CCMe_3$), 1.19 (O_2CCMe_3); ^{13}C NMR δ 193.6 (O_2CCMe_3), 78.7 ($CCMe_3$), 71.3 (CCH_3), 39.7 (O_2CCMe_3), 33.8 ($CCMe_3$), 30.9 ($CCMe_3$), 26.6 (O_2CCMe_3), 5.9 (*C*Me).

R′ = Et: ^1H NMR δ 2.87 (m, CCH_2CH_3), 1.33 ($CCMe_3$), 1.18 (O_2CCMe_3), 1.13 (t, CCH_2CH_3); ^{13}C NMR δ 193.6 (O_2CCMe_3), 79.9 ($CCMe_3$), 76.5 (*C*Et), 39.7 (O_2CCMe_3), 33.6 ($CCMe_3$), 31.5 ($CCMe_3$), 26.7 (CCH_2CH_3), 15.3 (CCH_2CH_3).

R′ = Ph. Diphenylacetylene (0.19 g, 1.07 mmol, 1 equiv) was added to a stirred solution of $Mo(CCMe_3)(O_2CCMe_3)_3$ (0.50 g, 1.07 mmol) in pentane (50 mL) at 25 °C. The solution turned dark red over the next 15 min. After 4 h the solvent was removed in vacuo, leaving a red solid. The solid was dissolved in a minimum amount of a 1:1 mixture of dichloromethane and ether. Bright red needles formed at −30 °C (0.48 g, 70%, three crops): ^1H NMR δ 7.62 (H_o), 7.15 (H_m), 6.88 (H_p), 1.57 (CMe_3), 0.98 (O_2CCMe_3); ^{13}C NMR δ 194.7 (O_2CCMe_3), 133.4 (C_o), 130.9 (C_{ipso}), 127.6 (C_m), 127.5 (C_p), 80.7 ($CCMe_3$), 71.7 (*C*Ph), 39.8 (O_2CCMe_3), 33.6 ($CCMe_3$), 31.2 ($CCMe_3$), 26.1 (O_2CCMe_3). Anal. Calcd for $MoC_{34}H_{46}O_6$: C, 63.15; H, 7.17. Found: C, 63.08; H, 6.82.

$W[C_3(CMe_3)Me_2](O_2CCMe_3)_3$. 2-Butyne (141 μL, 1.80 mmol) was added to a solution of $W(CCMe_3)(O_2CCMe_3)_3$ (1.00 g, 1.80 mmol) in pentane (15 mL). The color of the solution slowly changed to deep red over a period of 4 h. The solvent was then removed in vacuo and the residue recrystallized from pentane at −30 °C to give large red prisms (two crops, 0.68 g, 62%): ^1H NMR δ 3.33 (CMe), 1.35 ($CCMe_3$), 1.14 (O_2CCMe_3); ^{13}C NMR δ 193.9 (O_2CCMe_3), 80.3 ($CCMe_3$), 68.9 (*C*Me), 40.1 (CMe_3), 33.5 (CMe_3), 33.0 ($CCMe_3$), 26.4 (O_2CCMe_3), 4.7 (*C*Me).

$W[C_3(CMe_3)Et_2](O_2CCMe_3)_3$. 3-Hexyne (51 μL, 0.45 mmol) was added to a solution of $W(CCMe_3)(O_2CCMe_3)_3$ (0.25 g, 0.45 mmol) in pentane (10 mL). The color of the solution slowly changed to deep red over a period of several hours. The solvent was removed in vacuo to give a red oil that is essentially pure product: ^1H NMR δ 4.19 (dq, 2, J_{HH} = 15.1, 7.5 Hz, $C(CH_AH_BCH_3)$), 3.74 (dq, 2, J_{HH} = 15.1, 7.5 Hz, $C(CH_AH_BCH_3)$), 1.40 ($CCMe_3$), 1.23 (t, CCH_2Me), 1.15 (O_2CCMe_3); ^{13}C NMR δ 194.0 (O_2CCMe_3), 81.5 ($CCMe_3$), 74.3 (*C*Et), 40.1 (CMe_3), 33.5 ($CCMe_3$), 31.3 (CMe_3), 26.4 (O_2CCMe_3), 17.6 (CCH_2Me), 15.2 (CCH_2Me).

$Mo[C_3(CMe_3)(Ph)](O_2CCF_3)_2(py)_2$. Excess pyridine (175 μL, 2.15 mmol, 5 equiv) was added all at once to a dark red ether solution (15 mL) of $Mo[C_3(CMe_3)(Ph)](O_2CCF_3)_2(dme)$ (0.25 g, 0.429 mmol) at −30 °C. The resulting solution darkened to purple-red, and a purple powder precipitated. The mixture was warmed to room temperature over the next 2 h, and solvents were removed in vacuo. The purple residue was recrystallized from a minimum amount of a 1:1 mixture of ether and dichloromethane at −30 °C, yielding dark purple-red cubes (0.22 g, 78%, three crops): ^1H NMR δ 8.90 (H_o-py), 8.71 (H_o-py′), 8.17 (H_o-Ph), 7.18 (H_m-Ph), 6.95 (H_p-Ph), 6.85 (H_p-py and py′), 6.58 (H_m-py), 6.53 (H_m-py′), 1.70 (CMe_3); ^{13}C NMR (CD_2Cl_2) δ 251.0 ($CCMe_3$), 245.7 (*C*Ph), 231.5 (C_β), 155.6 (q, J_{CF} = 41 Hz, CF_3CO_2), 150.8 (C_o-py), 139.7 (C_p-py), 139.4 (C_{ipso}-Ph), 133.7 (C_o-Ph), 130.3 (C_p-Ph), 129.0 (C_m-Ph), 125.6 (C_m-py), 115.6 (q, J_{CF} = 290 Hz, CF_3CO_2), 46.2 (CMe_3), 31.5 (CMe_3). Anal. Calcd for $MoC_{27}H_{24}O_4N_2F_6$: C, 49.86; H, 3.72. Found: C, 49.90; H, 3.92.

$Mo[C_3(CMe_3)_2](O_2CCF_3)_2(dme)$. $Me_3CC{\equiv}CH$ (110 μL, 0.897 mmol, 1.1 equiv was added all at once to a stirred dark red ether solution (40 mL) of $Mo(CCMe_3)(O_2CCF_3)_3(dme)$ (0.50 g, 0.841 mmol) at −30 °C. The resulting dark red solution was allowed to warm to room temperature over the next 3 h. The solvent and CF_3CO_2H were removed in vacuo to give a red solid which was recrystallized from a minimum amount of a 1:1 mixture of ether and dichloromethane at −30 °C to give red plates (0.30 g, 63%) in three crops: ^1H NMR δ 3.48 ($MeOCH_2CH_2OMe$), 3.17 ($MeOCH_2CH_2OMe$), 1.68 (CMe_3); ^{13}C NMR (CD_2Cl_2) δ 254.6 ($CCMe_3$), 243.2 (C_β), 155.5 (q, J_{CF} = 38 Hz, CF_3CO_2), 115.7 (q, J_{CF} = 290 Hz, CF_3CO_2), 72.6 ($MeOCH_2CH_2OMe$), 65.3 ($MeOCH_2CH_2OMe$), 46.2 (CMe_3), 31.5 (CMe_3).

$Mo[C_3(CMe_3)_2](O_2CCF_3)_2(py)_2$. Excess pyridine (500 μL, 6.21 mmol, 4.9 equiv) was added all at once to a stirred dark red ether solution (75 mL) of $Mo[C_3(CMe_3)_2](O_2CCF_3)_2(dme)$ (0.71 g, 1.26 mmol) at −30 °C. The resulting red-purple solution was warmed to room temperature over the next 2 h. The solvents were removed in vacuo, and the red-purple residue was recrystallized from a minimum amount of a 1:1 mixture of ether and dichloromethane at −30 °C. Small red-purple crystals (0.64 g, 80%) were isolated in three crops: ^1H NMR δ 8.82 (H_o-py), 6.82 (H_p-py), 6.56 (H_m-py), 1.63 (CMe_3); ^{13}C NMR (CD_2Cl_2) δ 252.9 ($CCMe_3$), 247.5 (C_β), 155.3 (q, $^2J_{CF}$ = 37 Hz, CF_3CO_2), 150.6 (C_o-py), 139.3 (C_p-py), 125.3 (C_m-py), 115.8 (q, J_{CF} = 290 Hz, CF_3CO_2), 46.1 (CMe_3), 31.5 (CMe_3). Anal. Calcd for $MoC_{25}H_{28}F_6O_4N_2$: C, 47.63; H, 4.48. Found: C, 47.69; H, 4.29.

$W[C_3(CMe_3)Et_2](O_2CMe)_3$. A slight excess of 3-hexyne (400 μL, 3.52 mmol) was added to a suspension of $W(CCMe_3)(O_2CMe)_3$ (1.50 g, 3.49 mmol) in ether (25 mL). After 3 h all the starting material had dissolved and the solution was a deep red. The solvent was removed from the solution in vacuo, and the residue was recrystallized from pentane at −30 °C (two crops, 1.07 g, 60%): ^1H NMR δ 4.23 (dq, 2, J_{HH} = 15.2, 7.6 Hz, $C(CH_AH_BCH_3)$), 3.94 (dq, 2, J_{HH} = 15.2, 7.6 Hz, $C(CH_AH_BCH_3)$), 1.60 (Me), 1.41 (Me), 1.25 (t, CCH_2Me); ^{13}C NMR δ 192.2 (O_2CMe), 76.9 ($CCMe_3$), 73.5 (*C*Et), 25.8 (Me), 25.5 ($CCMe_3$), 14.9 (Me), 8.6 (Me), 6.6 (CCH_2Me). Anal. Calcd for $WC_{17}H_{28}O_6$: C, 39.86; H, 5.51. Found: C, 39.64; H, 5.54.

$Mo[C_3(CMe_3)(Ph)](O_2CCF_3)_2(dme)$. Phenylacetylene (190 μL, 1.73 mmol, 1 equiv) was added all at once via syringe to a solution of $Mo(CCMe_3)(O_2CCF_3)_3(dme)$ (1.00 g, 1.68 mmol) in ether (60 mL) at −30 °C. The solution immediately darkened to purple-red. The solution was allowed to warm to room temperature. After 2 h the solvent was removed in vacuo, leaving a purple-red solid. $Mo[C_3(CMe_3)(Ph)](O_2CCF_3)_2(dme)$ was obtained as dark red needles by recrystallization from ether at −30 °C (0.80 g, 82% of theoretical 0.98 g, three crops): ^1H NMR δ 8.23 (H_o), 7.28 (H_m), 7.04 (H_p), 3.54 ($MeOCH_2CH_2OMe$), 3.21 ($MeOCH_2CH_2OMe$), 1.75 (CMe_3); ^{13}C NMR δ 252.9 (C_α), 240.5 (C_α'), 234.8 (C_β), 155.8 (q, J_{CF} = 37 Hz, CF_3CO_2), 140.3 (C_{ipso}), 131.9 (C_o), 130.0 (C_m), 128.9 (C_p), 116.1 (q, J_{CF} = 290 Hz, CF_3CO_2), 72.0 ($MeOCH_2CH_2OMe$), 64.6 ($MeOCH_2CH_2OMe$), 46.3 (CMe_3), 31.4 (CMe_3). Anal. Calcd for $MoC_{21}H_{24}O_6F_6$: C, 43.31; H, 4.15. Found: C, 42.83; H, 4.05.

$W[\eta^5\text{-}C_5(CMe_3)Et_4](O_2CCF_3)_4$. An excess of 3-hexyne (840 μL, 7.39 mmol) was added to a solution of $W(CCMe_3)(O_2CCF_3)_3(dme)$ (1.00 g, 1.47 mmol) in ether (25 mL), and the solution was stirred overnight. A black crystalline powder precipitated from solution and was collected and dried in vacuo (0.27 g, 21%). The powder could be recrystallized from dichloromethane at −30 °C to give large, black, paramagnetic crystals. Anal. Calcd for $WC_{25}H_{29}F_{12}O_8$: C, 34.54; H, 3.36. Found: C, 34.60; H, 3.39. ESR (CH_2Cl_2): g = 1.848.

$W_2(O_2CCMe_3)_6$(3-hexyne). $W_2(OCMe_3)_6$ (2.00 g, 2.48 mmol) was added to a solution of 6 equiv of pivalic acid (1.52 g, 14.9 mmol) in pentane (50 mL). The pentane was removed in vacuo from the resulting yellow-brown solution. The residue was dissolved in toluene (25 mL), and excess 3-hexyne (850 μL, 7.48 mmol) was added. The solution was placed in a Schlenk tube and heated to 60 °C overnight to give a dark blue-green solution. The solvent was removed in vacuo to leave blue crystals that were essentially pure by ^1H NMR. The product is highly soluble but

can be recrystallized from pentane at -40 °C: ^{1}H NMR (298 K) δ 5.0-4.6 (br, 4, CH_3CH_2C), 1.48 (t, 6, J = 7.3 Hz, CH_3CH_2C), 1.23 (br s, 36, O_2CCMe_3), 1.18 (s, 18, O_2CCMe_3); ^{1}H NMR (360 K) δ 4.66 (q, 4, J = 7.3 Hz, CH_3CH_2C), 1.38 (t, 6, J = 7.3 Hz, CH_3CH_2C), 1.24 (s, 36, O_2CCMe_3), 1.21 (s, 18, O_2CCMe_3); ^{1}H NMR (toluene-d_8, 235 K) δ 4.91 (m, 2, $CH_3CH_AH_BC$), 4.74 (m, 2, $CH_3CH_ACH_BC$), 1.71 (t, 6, J = 7.3 Hz, $CH_3CH_ACH_BC$), 1.24 (s, 18, O_2CCMe_3), 1.21 (s, 18, O_2CCMe_3), 1.19 (s, 18, O_2CCMe_3); ^{13}C NMR (298 K) δ 217-213 (br, O_2CCMe_3), 203-200 (br, O_2CCMe_3), 193.9 (s, CH_3CH_2C), 40.3 (s, O_2CCMe_3), 39.5 (s, O_2CCMe_3), 30.7 (CH_3CH_2C), 27.5 (O_2CCMe_3), 26.9 (O_2CCMe_3), 16.1 (CH_3CH_2C). Anal. Calcd for $W_2C_{36}H_{64}O_{17}$: C, 40.92; H, 6.11. Found: C, 41.39; H, 6.15.

$W_2(O_2CCMe_3)_6$(2-butyne). This compound was prepared in the same manner as the 3-hexyne derivative above as a blue, pure, highly crystalline solid in almost quantitative yield. It is extremely soluble in pentane and could not be recrystallized from pentane at -40 °C: ^{1}H NMR (toluene-d_8, 360 K) δ 3.78 (s, 6, CH_3C), 1.22 (s, 54, O_2CCMe_3); ^{1}H NMR (300 K) δ 3.83 (br, 6, CH_3C), 1.22 (s, 36, O_2CCMe_3), 1.20 (s, 18, O_2CCMe_3); ^{1}H NMR (toluene-d_8, 240 K) δ 3.91 (s, 6, CH_3C), 1.24 (s, 18, O_2CCMe_3), 1.17 (s, 18, O_2CCMe_3), 1.10 (s, 18, O_2CCMe_3); ^{13}C NMR (CD_2Cl_2, 225 K) δ 201.9, 196.5, 193.0, 190.8 (all singlets, O_2CCMe_3 and CH_3C); 40.3, 39.5, 38.8 (all singlets, O_2CCMe_3), 26.9, 26.2, 26.0 (all quartets, O_2CCMe_3), 17.3 (CH_3C).

$W_2(O_2CCH_3)_6$(3-hexyne). Excess acetic acid (700 μL, 12.2 mmol) was added to a solution of $W_2(OCMe_3)_6$ (1.00 g, 1.24 mmol) in dichloromethane (10 mL). The red solution immediately turned yellow. The solvent was removed in vacuo to give a yellow powder. The powder was redissolved, and an excess of 2-butyne (425 μL, 3.74 mmol) was added. The solution was heated to 60 °C overnight in a closed Schlenk tube. The solvent was removed in vacuo from the resulting solution. The product was extracted with minimal ether, and the extract was filtered through Celite in order to remove 2-butyne polymer. Cooling the filtrate to -40 °C gave dark blue prisms (0.55 g, 55%): ^{1}H NMR δ 5.1-4.5 (br, 4, CH_3CH_2C), 1.93 (br s, 12, O_2CCH_3), 1.87 (s, 6, O_2CCH_3), 1.45 (t, 6, J = 7.4 Hz, CH_3CH_2C); ^{1}H NMR (toluene-d_8, 235 K) δ 4.96 (m, 2, $CH_3CH_ACH_BC$), 4.67 (m, 2, $CH_3CH_AH_BC$), 1.89 (br s, 12, O_2CCH_3), 1.78 (s, 6, O_2CCH_3), 1.54 (t, 6, J = 7.1 Hz, $CH_3CH_AH_BC$); ^{13}C NMR δ 233-230 (br, O_2CCH_3), 198-194 (br, O_2CCH_3), 188.0 (s, CH_3CH_2C), 32.3 (CH_3CH_2C), 24.0 (O_2CCH_3), 21.3 (O_2CCH_3), 15.0 (CH_3CH_2C). Anal. Calcd for $W_2C_{18}H_{28}O_{12}$: C, 26.88; H, 3.51. Found: C, 27.12; H, 3.67.

Acknowledgment. This work was supported by NSF Grant CHE84-02892 to R.R.S. and in part by NSF Grant CHE80-23448 to M.R.C.

Registry No. $W(CCMe_3)(O_2CCMe_3)_3$, 99053-08-4; $Mo(CCMe_3)(O_2CCMe_3)_3$, 99096-78-3; $W(CCMe_3)(O_2CCHMe_2)_3$, 99053-09-5; $Mo(CCMe_3)(O_2CCHMe_2)_3$, 99053-10-8; $W(CCMe_3)(O_2CCH_3)_3$, 99053-11-9; $Mo(CCMe_3)(O_2CCH_3)_3$, 99053-12-0; $W(CCMe_3)(O_2CCF_3)_3$(dme), 99053-13-1; $Mo(CCMe_3)(O_2CCF_3)_3$(dme), 99053-14-2; $Mo[C_3(CMe_3)Me_2](O_2CCHMe_2)_3$, 99096-79-4; $Mo[C_3(CMe_3)Et_2](O_2CCHMe_2)_3$, 99053-15-3; $Mo[C_3(CMe_3)Ph_2](O_2CCHMe_2)_3$, 99053-16-4; $Mo[C_3(CMe_3)Me_2](O_2CCMe_3)_3$, 99053-17-5; $Mo[C_3(CMe_3)Et_2](O_2CCMe_3)_3$, 99053-18-6; $Mo[C_3(CMe_3)Ph_2](O_2CCMe_3)_3$, 99053-19-7; $W[C_3(CMe_3)Me_2](O_2CCMe_3)_3$, 99053-20-0; $W[C_3(CMe_3)Et_2](O_2CCMe_3)_3$, 99053-21-1; $Mo[C_3(CMe_3)(Ph)](O_2CCF_3)_2(py)_2$, 99053-22-2; $Mo[C_3(CMe_3)_2](O_2CCF_3)_2$(dme), 99053-23-3; $Mo[C_3(CMe_3)_2](O_2CCF_3)_2(py)_2$, 99053-24-4; $W[C_3(CMe_3)Et_2](O_2CMe)_3$, 99053-25-5; $Mo[C_3(CMe_3)(Ph)](O_2CCF_3)_2$(dme), 99053-26-6; $W[\eta^5\text{-}C_5(CMe_3)Et_4](O_2CCF_3)_4$, 99053-27-7; $W_2(O_2CCMe_3)_6$(B) (B = 3-hexyne), 99053-28-8; $W_2(O_2CCMe_3)_6$(B) (B = 2-butyne), 99096-80-7; $W_2(O_2CCH_3)_6$(B) (B = 3-hexyne), 99053-29-9; $W(CCMe_3)Np_3$, 68490-69-7; $Mo(CCMe_3)Np_3$, 68404-35-3; $W_2(OCMe_3)_6$, 57125-20-9; Me_3CCO_2H, 75-98-9; Me_2CHCO_2H, 79-31-2; $MeCO_2H$, 64-19-7; CF_3CO_2H, 76-05-1; MeC≡CMe, 503-17-3; EtC≡CEt, 928-49-4; PhC≡CPh, 501-65-5; $Me_3CC{\equiv}CH$, 917-92-0; PhC≡CH, 536-74-3.

Supplementary Material Available: A table of anisotropic thermal parameters (Table VS) and a listing of observed and calculated structure factor amplitudes (14 pages). Ordering information is given on any current masthead page.

Synthesis, Structural Characterization, and Regioselective Reactivity with Alkyl Iodides of the Rhodium Octaethylporphyrin-Indium Octaethylporphyrin Complex

Nancy L. Jones, Patrick J. Carroll, and Bradford B. Wayland*

Department of Chemistry, University of Pennsylvania, Philadelphia, Pennsylvania 19104

Received April 29, 1985

The complex Rh(OEP)-In(OEP) (I) has been synthesized by the reaction of [Na][Rh(OEP)] with In(OEP)(Cl). The presence of a metal-metal bond in complex I was first suggested by interpretation of ^{1}H NMR spectra and subsequently confirmed by a single-crystal X-ray diffraction study. The complex crystallizes in the monoclinic space group C_{2h}^6—$C2/c$ with four molecules in a cell of dimensions a = 18.214 (3) Å, b = 15.117 (3) Å, c = 23.540 (3) Å, β = 106.92 (2)°, and V = 6201 Å^3. The final conventional and weighted agreement indices on F_o ($F_o^2 > 3\sigma(F_o^2)$) are R = 0.047 and R_w = 0.055. The rhodium-indium metal-metal bond length is 2.584 (2) Å. The reactivity of I is consistent with the formulation of a polar covalent bond (Rh(I)$^-$:→In(III)$^+$) as manifested in the regioselective addition of alkyl iodides to I.

Introduction

Heterobimetallic complexes in which the two adjacent metal fragments have differing properties have the potential for producing selective reactivity at each metal. The unusual organometallic chemistry of the rhodium porphyrins[1-4] has prompted us to initiate a program to incorporate rhodium porphyrins into metal-metal bonded heterobimetallic complexes. Initial studies of compounds containing rhodium octaethylporphyrin (Rh(OEP)) with transition-metal species ((OEP)Rh-M'; M' = Mo-

(1) Wayland, B. B.; Woods, B. A. *J. Chem. Soc., Chem. Commun.* **1981**, 700-701.

(2) Wayland, B. B.; Woods, B. A.; Minda, V. M. *J. Chem. Soc., Chem. Commun.* **1982**, 634-635.

(3) Wayland, B. B.; Woods, B. A.; Pierce, R. *J. Am. Chem. Soc.* **1982**, *104*, 302-303.

(4) Setsune, J.-I.; Yoshida, Z.-I.; Ogoshi, H. *J. Chem. Soc., Perkin Trans. 1* **1982**, 983-987.

0276-7333/86/2305-0033$01.50/0

can be recrystallized from pentane at -40 °C: ^{1}H NMR (298 K) δ 5.0-4.6 (br, 4, CH_3CH_2C), 1.48 (t, 6, J = 7.3 Hz, CH_3CH_2C), 1.23 (br s, 36, O_2CCMe_3), 1.18 (s, 18, O_2CCMe_3); ^{1}H NMR (360 K) δ 4.66 (q, 4, J = 7.3 Hz, CH_3CH_2C), 1.38 (t, 6, J = 7.3 Hz, CH_3CH_2C), 1.24 (s, 36, O_2CCMe_3), 1.21 (s, 18, O_2CCMe_3); ^{1}H NMR (toluene-d_8, 235 K) δ 4.91 (m, 2, $CH_3CH_AH_BC$), 4.74 (m, 2, $CH_3CH_ACH_BC$), 1.71 (t, 6, J = 7.3 Hz, $CH_3CH_ACH_BC$), 1.24 (s, 18, O_2CCMe_3), 1.21 (s, 18, O_2CCMe_3), 1.19 (s, 18, O_2CCMe_3); ^{13}C NMR (298 K) δ 217-213 (br, O_2CCMe_3), 203-200 (br, O_2CCMe_3), 193.9 (s, CH_3CH_2C), 40.3 (s, O_2CCMe_3), 39.5 (s, O_2CCMe_3), 30.7 (CH_3CH_2C), 27.5 (O_2CCMe_3), 26.9 (O_2CCMe_3), 16.1 (CH_3CH_2C). Anal. Calcd for $W_2C_{36}H_{64}O_{17}$: C, 40.92; H, 6.11. Found: C, 41.39; H, 6.15.

$W_2(O_2CCMe_3)_6$(2-butyne). This compound was prepared in the same manner as the 3-hexyne derivative above as a blue, pure, highly crystalline solid in almost quantitative yield. It is extremely soluble in pentane and could not be recrystallized from pentane at -40 °C: ^{1}H NMR (toluene-d_8, 360 K) δ 3.78 (s, 6, CH_3C), 1.22 (s, 54, O_2CCMe_3); ^{1}H NMR (300 K) δ 3.83 (br, 6, CH_3C), 1.22 (s, 36, O_2CCMe_3), 1.20 (s, 18, O_2CCMe_3); ^{1}H NMR (toluene-d_8, 240 K) δ 3.91 (s, 6, CH_3C), 1.24 (s, 18, O_2CCMe_3), 1.17 (s, 18, O_2CCMe_3), 1.10 (s, 18, O_2CCMe_3); ^{13}C NMR (CD_2Cl_2, 225 K) δ 201.9, 196.5, 193.0, 190.8 (all singlets, O_2CCMe_3 and CH_3C); 40.3, 39.5, 38.8 (all singlets, O_2CCMe_3), 26.9, 26.2, 26.0 (all quartets, O_2CCMe_3), 17.3 (CH_3C).

$W_2(O_2CCH_3)_6$(3-hexyne). Excess acetic acid (700 μL, 12.2 mmol) was added to a solution of $W_2(OCMe_3)_6$ (1.00 g, 1.24 mmol) in dichloromethane (10 mL). The red solution immediately turned yellow. The solvent was removed in vacuo to give a yellow powder. The powder was redissolved, and an excess of 2-butyne (425 μL, 3.74 mmol) was added. The solution was heated to 60 °C overnight in a closed Schlenk tube. The solvent was removed in vacuo from the resulting solution. The product was extracted with minimal ether, and the extract was filtered through Celite in order to remove 2-butyne polymer. Cooling the filtrate to -40 °C gave dark blue prisms (0.55 g, 55%): ^{1}H NMR δ 5.1-4.5 (br, 4, CH_3CH_2C), 1.93 (br s, 12, O_2CCH_3), 1.87 (s, 6, O_2CCH_3), 1.45 (t, 6, J = 7.4 Hz, CH_3CH_2C); ^{1}H NMR (toluene-d_8, 235 K) δ 4.96 (m, 2, $CH_3CH_ACH_BC$), 4.67 (m, 2, $CH_3CH_AH_BC$), 1.89 (br s, 12, O_2CCH_3), 1.78 (s, 6, O_2CCH_3), 1.54 (t, 6, J = 7.1 Hz, $CH_3CH_AH_BC$); ^{13}C NMR δ 233-230 (br, O_2CCH_3), 198-194 (br, O_2CCH_3), 188.0 (s, CH_3CH_2C), 32.3 (CH_3CH_2C), 24.0 (O_2CCH_3), 21.3 (O_2CCH_3), 15.0 (CH_3CH_2C). Anal. Calcd for $W_2C_{18}H_{28}O_{12}$: C, 26.88; H, 3.51. Found: C, 27.12; H, 3.67.

Acknowledgment. This work was supported by NSF Grant CHE84-02892 to R.R.S. and in part by NSF Grant CHE80-23448 to M.R.C.

Registry No. $W(CCMe_3)(O_2CCMe_3)_3$, 99053-08-4; $Mo(CCMe_3)(O_2CCMe_3)_3$, 99096-78-3; $W(CCMe_3)(O_2CCHMe_2)_3$, 99053-09-5; $Mo(CCMe_3)(O_2CCHMe_2)_3$, 99053-10-8; $W(CCMe_3)(O_2CCH_3)_3$, 99053-11-9; $Mo(CCMe_3)(O_2CCH_3)_3$, 99053-12-0; $W(CCMe_3)(O_2CCF_3)_3$(dme), 99053-13-1; $Mo(CCMe_3)(O_2CCF_3)_3$(dme), 99053-14-2; $Mo[C_3(CMe_3)Me_2](O_2CCHMe_2)_3$, 99096-79-4; $Mo[C_3(CMe_3)Et_2](O_2CCHMe_2)_3$, 99053-15-3; $Mo[C_3(CMe_3)Ph_2](O_2CCHMe_2)_3$, 99053-16-4; $Mo[C_3(CMe_3)Me_2](O_2CCMe_3)_3$, 99053-17-5; $Mo[C_3(CMe_3)Et_2](O_2CCMe_3)_3$, 99053-18-6; $Mo[C_3(CMe_3)Ph_2](O_2CCMe_3)_3$, 99053-19-7; $W[C_3(CMe_3)Me_2](O_2CCMe_3)_3$, 99053-20-0; $W[C_3(CMe_3)Et_2](O_2CCMe_3)_3$, 99053-21-1; $Mo[C_3(CMe_3)(Ph)](O_2CCF_3)_2(py)_2$, 99053-22-2; $Mo[C_3(CMe_3)_2](O_2CCF_3)_2$(dme), 99053-23-3; $Mo[C_3(CMe_3)_2](O_2CCF_3)_2(py)_2$, 99053-24-4; $W[C_3(CMe_3)Et_2](O_2CMe)_3$, 99053-25-5; $Mo[C_3(CMe_3)(Ph)](O_2CCF_3)_2$(dme), 99053-26-6; $W[\eta^5\text{-}C_5(CMe_3)Et_4](O_2CCF_3)_4$, 99053-27-7; $W_2(O_2CCMe_3)_6$(B) (B = 3-hexyne), 99053-28-8; $W_2(O_2CCMe_3)_6$(B) (B = 2-butyne), 99096-80-7; $W_2(O_2CCH_3)_6$(B) (B = 3-hexyne), 99053-29-9; $W(CCMe_3)Np_3$, 68490-69-7; $Mo(CCMe_3)Np_3$, 68404-35-3; $W_2(OCMe_3)_6$, 57125-20-9; Me_3CCO_2H, 75-98-9; Me_2CHCO_2H, 79-31-2; $MeCO_2H$, 64-19-7; CF_3CO_2H, 76-05-1; MeC≡CMe, 503-17-3; EtC≡CEt, 928-49-4; PhC≡CPh, 501-65-5; $Me_3CC{\equiv}CH$, 917-92-0; PhC≡CH, 536-74-3.

Supplementary Material Available: A table of anisotropic thermal parameters (Table VS) and a listing of observed and calculated structure factor amplitudes (14 pages). Ordering information is given on any current masthead page.

Synthesis, Structural Characterization, and Regioselective Reactivity with Alkyl Iodides of the Rhodium Octaethylporphyrin-Indium Octaethylporphyrin Complex

Nancy L. Jones, Patrick J. Carroll, and Bradford B. Wayland*

Department of Chemistry, University of Pennsylvania, Philadelphia, Pennsylvania 19104

Received April 29, 1985

The complex Rh(OEP)-In(OEP) (I) has been synthesized by the reaction of [Na][Rh(OEP)] with In(OEP)(Cl). The presence of a metal-metal bond in complex I was first suggested by interpretation of ^{1}H NMR spectra and subsequently confirmed by a single-crystal X-ray diffraction study. The complex crystallizes in the monoclinic space group C_{2h}^6—$C2/c$ with four molecules in a cell of dimensions a = 18.214 (3) Å, b = 15.117 (3) Å, c = 23.540 (3) Å, β = 106.92 (2)°, and V = 6201 Å^3. The final conventional and weighted agreement indices on F_o ($F_o^2 > 3\sigma(F_o^2)$) are R = 0.047 and R_w = 0.055. The rhodium-indium metal-metal bond length is 2.584 (2) Å. The reactivity of I is consistent with the formulation of a polar covalent bond (Rh(I)$^-$:→In(III)$^+$) as manifested in the regioselective addition of alkyl iodides to I.

Introduction

Heterobimetallic complexes in which the two adjacent metal fragments have differing properties have the potential for producing selective reactivity at each metal. The unusual organometallic chemistry of the rhodium porphyrins[1-4] has prompted us to initiate a program to incorporate rhodium porphyrins into metal-metal bonded heterobimetallic complexes. Initial studies of compounds containing rhodium octaethylporphyrin (Rh(OEP)) with transition-metal species ((OEP)Rh-M'; M' = Mo-

(1) Wayland, B. B.; Woods, B. A. *J. Chem. Soc., Chem. Commun.* **1981**, 700-701.

(2) Wayland, B. B.; Woods, B. A.; Minda, V. M. *J. Chem. Soc., Chem. Commun.* **1982**, 634-635.

(3) Wayland, B. B.; Woods, B. A.; Pierce, R. *J. Am. Chem. Soc.* **1982**, *104*, 302-303.

(4) Setsune, J.-I.; Yoshida, Z.-I.; Ogoshi, H. *J. Chem. Soc., Perkin Trans. 1* **1982**, 983-987.

0276-7333/86/2305-0033$01.50/0

$(C_5H_5)(CO)_3$, $Mn(CO)_5$, $Ru(C_5(CH_3)_5)(CO)_2$) suggest that facile homolytic Rh–M′ bond cleavage is a dominant feature of their reactivity.[5] To explore the full scope of Rh–M′ bond cleavage reactions heterobimetallic complexes of Rh(OEP) with post-transition-metallo species are being evaluated.

Here we report on the preparation, structural characterization, and reactivity of the metal–metal bonded complex Rh(OEP)–In(OEP) (I). Thermal or photoinduced oxidative addition of methyl iodide to I is quantitatively regiospecific to produce Rh(OEP)(CH_3) and In(OEP)(I), suggesting heterolytic cleavage of the metal–metal bond.

Experimental Section

Proton NMR spectra were obtained on a Bruker WH-250 or an IBM WH-200 Fourier transform spectrometer. Chemical shifts are reported relative to tetramethylsilane. All manipulations unless otherwise stated were carried out in vacuum, under an inert atmosphere (N_2 or Ar), or in an argon-filled Vacuum Atmospheres drybox. A Viewlex projector with 500-W Sylvania projector bulb (>530 nm) or a Rayonet Photochemical Reactor (350 nm) were used for photolyses. Calcium hydride was used to dry C_6D_6. Sodium benzophenone ketyl was used to dry tetrahydrofuran (THF) and THF-d_8 and both were degassed by several freeze–pump–thaw cycles. The $NaN(Si(CH_3)_3)_2$ was purchased from Aldrich as a 1 M THF solution. The carbon monoxide (Grade 4, 67.7%)/dihydrogen (Grade 5, 32.4%) mixture was used as obtained from Airco. Methyl iodide (CH_3I, Fisher Scientific), phenylacetylene ($C_6H_5C{\equiv}CH$, Aldrich), and acrylonitrile ($CH_2{=}CHCN$, MCB) were dried over P_2O_5 and degassed by freeze–pump–thaw cycles. *n*-Butyl isocyanide (*n*-BuNC, Aldrich) was distilled onto freshly activated 4 Å-molecular sieves and degassed. Triethyl phosphite ($P(OC_2H_5)_3$, Aldrich), ethyl iodide (C_2H_5I, MCB), acids (CH_3CO_2H, CF_3CO_2H, CF_3SO_3H), and water were degassed before reaction. All liquid reagents were added by syringe or by vacuum distillation onto the metal complex. The complex Rh(OEP)(H) was prepared by a modification of the synthesis reported by Setsune and co-workers.[4] The complex In(OEP)(Cl) was prepared by the method reported by Eaton and Eaton.[6]

Synthesis of Rh(OEP)–In(OEP). To a solution of 23 mg of Rh(OEP)(H) (3.6×10^{-2} mmol) in 15 mL of THF was added 0.08 mL of $NaN(SiMe_3)_2$/THF. The mixture was stirred 1 h after which it was filtered under reduced pressure into a flask containing 18 mg of In(OEP)(Cl) (2.6×10^{-2} mmol), the frit was washed one time with THF, the washing was combined with the filtrate, and the mixture was stirred overnight. The THF was stripped off under vacuum, and the resulting dark purple solid was dried under vacuum (yield >95% Rh(OEP)–In(OEP) based on starting Rh complex, by ^1H NMR). ^1H NMR (C_6D_6): δ 9.31, 8.78 (-CH=), 4.26 (AB multiplet), 3.89 m (CH_2), 1.78, 1.72 (overlapping t) (CH_3). ^1H NMR (THF-d_8): δ 9.14, 8.54; 4.19, 4.12; 1.7. Visible spectrum (C_6H_6): λ_{max} 362, 392, 411, 522, 555 (shoulder), 579 nm.

Reaction of Rh(OEP)–In(OEP) with Other Reagents. In a typical experiment ~1 mg of Rh(OEP)–In(OEP) was placed in an NMR tube and C_6D_6 was vacuum distilled into the tube. An excess of the appropriate reagent was added, and the NMR tube was sealed off. The NMR spectra were run at room temperature, and reaction progress was followed in this way.

X-ray Diffraction Study. Red-brown crystals of the title compound were grown by slow evaporation of a C_6D_6 solution of the complex. X-ray diffraction data were collected on an Enraf-Nonius CAD-4 diffractometer, using graphite-monochromated Mo Kα radiation. The Enraf-Nonius structure determination package and PDP11/60 computer were used for all data reduction and structure refinement.[7] A numerical absorption correction was applied. A summary of crystal data and intensity collection is given in Table I.

Table I. Summary of Crystal Data and Intensity Collection for Rh(OEP)–In(OEP)

formula	$C_{72}H_{88}N_8InRh$
fw, amu	1283.28
space group	C_{2h}^6—$C2/c$
a, Å	18.214 (3)
b, Å	15.117 (3)
c, Å	23.540 (3)
β, deg	106.92 (2)
vol, Å	6201.2
Z	4
ρ(calcd), g/cm^3	1.37
temp, °C	23 ± 1 °C
cryst dimens, mm	0.20 × 0.20 × 0.08
radiatn	graphite-monochromated Mo Kα, λ(Mo Kα) = 0.71073 Å
linear abs coeff, cm^{-1}	6.7
transmissn factors	79.93–90.79
detector aperture	1.5–2.0 mm horiz, 4.0 mm vert; 37 cm from crystal
scan type	ω–2θ
scan rate	1–4°/min in ω
2θ limits	$0.0° \le 2\theta \le 55.0°$
refl measd	7698 total, 7113 unique
refl used ($F_o^2 > 3\sigma(F_o^2)$)	4323
final no. of variables	379
R (on F_o for $F_o^2 > 3\sigma(F_o^2)$)	0.047
R_w (on F_o for $F_o^2 > 3\sigma(F_o^2)$)	0.055
including unobsd data	0.092
error in observn of unit weight	1.83 electrons

The structure was solved in space group *Cc* by MULTAN 11/82 which revealed the positions of the two metal atoms. A series of weighted Fourier syntheses located the remaining atoms. At this time, it became evident that the two octaethylporphyrin units were related by a twofold symmetry axis parallel to the crystallographic *b* axis. The space group was thus changed to $C2/c$ which required the postulation of disorder for the Rh and In atoms. This model was supported by the presence of a large peak in the Patterson map corresponding to an atom–atom vector of 0.85 Å length. The crystallographic twofold axis in $C2/c$ intersects the Rh–In bond at a point midway between the two porphyrin ring systems causing the atoms in the two octaethylporphyrin units to be symmetry equivalent and leading to a 50–50 disorder of the Rh and In atoms. The non-hydrogen atoms were refined anisotropically, and the hydrogen atoms were assigned an isotropic thermal parameter of 5.0 Å and were included as fixed contributions in the anisotropic refinements. Conventional scattering factors were used for the non-hydrogen[8] and hydrogen atoms.[9] Anomalous dispersion effects were included in F_c;[10] the values of $\Delta f'$ and $\Delta f''$ were those of Cromer.[8] Agreement factors are defined as $R = \sum||F_o| - |F_c||/\sum|F_o|$ and $R_w = (\sum w(|F_o| - |F_c|)^2/\sum w|F_o|^2)^{1/2}$. The final cycle of least-squares refinement involved 379 variables and 4323 reflections ($F_o^2 > 3\sigma(F_o^2)$) and converged to final agreement indices (on F_o) $R = 0.047$ and $R_w = 0.055$. The error in an observation of unit weight is 1.83 e. Plots of $\sum w(|F_o| - |F_c|)^2$ vs. $|F_o|$, reflector order in data collection, $(\sin\theta)/\lambda$, and various classes of indices showed no unusual trends. The final positional parameters on the non-hydrogen atoms are listed in Table II. Table III[11] presents thermal parameters for the non-hydrogen atoms. Table IV[11] lists hydrogen atom positional parameters. Table V[11] lists values of $10|F_o|$ and $10|F_c|$. The root-mean-square amplitudes of vibration are presented in Table VI.[11]

Results and Discussion

Synthesis of Rh(OEP)–In(OEP) (I). The complex I has been synthesized by reaction of [Na][Rh(OEP)] with In(OEP)(Cl) in tetrahydrofuran solution. This type of synthesis by nucleophilic substitution of a metallate anion

(5) Bosch, H. W.; Wayland, B. B., submitted for publication.
(6) Eaton, S. S.; Eaton, G. R. *J. Am. Chem. Soc.* **1975**, *97*, 3660–3666.
(7) Frenz, B. A. In "Computing in Crystallography"; Schenk, H., Olthof-Hazelkamp, R., van Konigsveld, H., Bassi, G. C., Eds.; Delft University Press: Delft, Holland, 1978; pp 64–71.
(8) Cromer, D. T.; Waber, J. T. "International Tables for X-ray Crystallography"; Kynoch Press: Birmingham, England, 1974; Vol. IV.
(9) Stewart, R. F.; Davidson, E. R.; Simpson, W. T. *J. Chem. Phys.* **1965**, *42*, 3175–3187.
(10) Ibers, J. A.; Hamilton, W. C. *Acta Crystallogr.* **1964**, *17*, 781–782.
(11) See paragraph at end of paper regarding supplementary material.

Table II. Positional Parameters[a] for the Non-Hydrogen Atoms of Rh(OEP)-In(OEP)

atom	x	y	z
In	-0.04987 (3)	0.24200 (3)	0.23508 (2)
Rh	-0.09808 (3)	0.24176 (3)	0.22408 (2)
N(1)	-0.0972 (2)	0.2669 (2)	0.3093 (1)
N(2)	-0.0990 (2)	0.3739 (2)	0.2070 (1)
N(3)	-0.0982 (2)	0.2162 (2)	0.1390 (1)
N(4)	-0.0971 (2)	0.1096 (2)	0.2405 (1)
C(1)	-0.0979 (2)	0.2056 (3)	0.3522 (2)
C(2)	-0.0932 (2)	0.2512 (3)	0.4072 (2)
C(3)	-0.0901 (2)	0.3386 (3)	0.3964 (2)
C(4)	-0.0923 (2)	0.3483 (3)	0.3353 (2)
C(5)	-0.0940 (2)	0.4279 (2)	0.3057 (2)
C(6)	-0.0993 (2)	0.4408 (2)	0.2465 (2)
C(7)	-0.1105 (2)	0.5254 (2)	0.2161 (2)
C(8)	-0.1158 (2)	0.5083 (2)	0.1588 (2)
C(9)	-0.1077 (2)	0.4144 (2)	0.1532 (2)
C(10)	-0.1090 (2)	0.3683 (2)	0.1016 (2)
C(11)	-0.1039 (2)	0.2779 (2)	0.0946 (2)
C(12)	-0.1057 (2)	0.2317 (3)	0.0400 (2)
C(13)	-0.1011 (2)	0.1444 (3)	0.0522 (2)
C(14)	-0.0977 (2)	0.1344 (2)	0.1137 (2)
C(15)	-0.0951 (2)	0.0552 (2)	0.1436 (2)
C(16)	-0.0982 (2)	0.0428 (2)	0.2011 (2)
C(17)	-0.1007 (2)	-0.0425 (2)	0.2291 (2)
C(18)	-0.1049 (2)	-0.0255 (2)	0.2845 (2)
C(19)	-0.1015 (2)	0.0691 (2)	0.2920 (2)
C(20)	-0.1013 (2)	0.1153 (3)	0.3433 (2)
C(21)	-0.0924 (3)	0.2059 (3)	0.4649 (2)
C(22)	-0.0780 (3)	0.4146 (3)	0.4409 (2)
C(23)	-0.1181 (3)	0.6122 (3)	0.2447 (2)
C(24)	-0.1293 (3)	0.5751 (3)	0.1095 (2)
C(25)	-0.1136 (2)	0.2771 (3)	-0.0183 (2)
C(26)	-0.1021 (2)	0.0690 (3)	0.0103 (2)
C(27)	-0.1019 (3)	-0.1307 (3)	0.1995 (2)
C(28)	-0.1134 (3)	-0.0917 (3)	0.3300 (2)
C(29)	-0.1681 (3)	0.2097 (4)	0.4756 (2)
C(30)	-0.1479 (3)	0.4627 (4)	0.4375 (2)
C(31)	-0.1960 (3)	0.6274 (3)	0.2525 (3)
C(32)	-0.0591 (3)	0.6264 (4)	0.1092 (2)
C(33)	-0.1955 (3)	0.2985 (3)	-0.0532 (2)
C(34)	-0.1825 (3)	0.0335 (3)	-0.0182 (2)
C(35)	-0.1776 (3)	-0.1572 (3)	0.1587 (3)
C(36)	-0.1965 (3)	-0.1089 (4)	0.3260 (2)

[a] Estimated standard deviations in the least-significant figure(s) are given in parentheses in this and all subsequent tables. The estimated standard deviations must be treated with caution owing to the disorder of the two porphyrin units which yields an average porphyrin core.

on a chloroindium(III) porphyrin has been previously reported.[12] The yield of I by ^{1}H NMR spectroscopy is essentially quantitative based on starting rhodium complex. Relatively high field positions of the methine and methyl hydrogens (9.31, 8.78 ppm and 1.78, 1.72 ppm) along with two sets of well-separated AB multiplets assigned to the diastereotopic methylene hydrogens are characteristic of having two porphyrin units in close proximity (Figure 1). Comparison of this spectrum to that observed for $[Rh(OEP)]_2$ (Figure 1)[4] suggests the existence of a metal–metal bonded species which was subsequently confirmed by a single-crystal X-ray diffraction determination.

Crystal Structure of Rh(OEP)-In(OEP) (I). The molecular structure of I consists of a rhodium octaethylporphyrin group and an indium octaethylporphyrin group joined facially by a metal–metal bond (Figure 2). The two porphyrin skeletons are virtually parallel with a dihedral angle of 1.4° between the two 24-atom cores. An interplanar separation of 3.41 Å is relatively long compared to

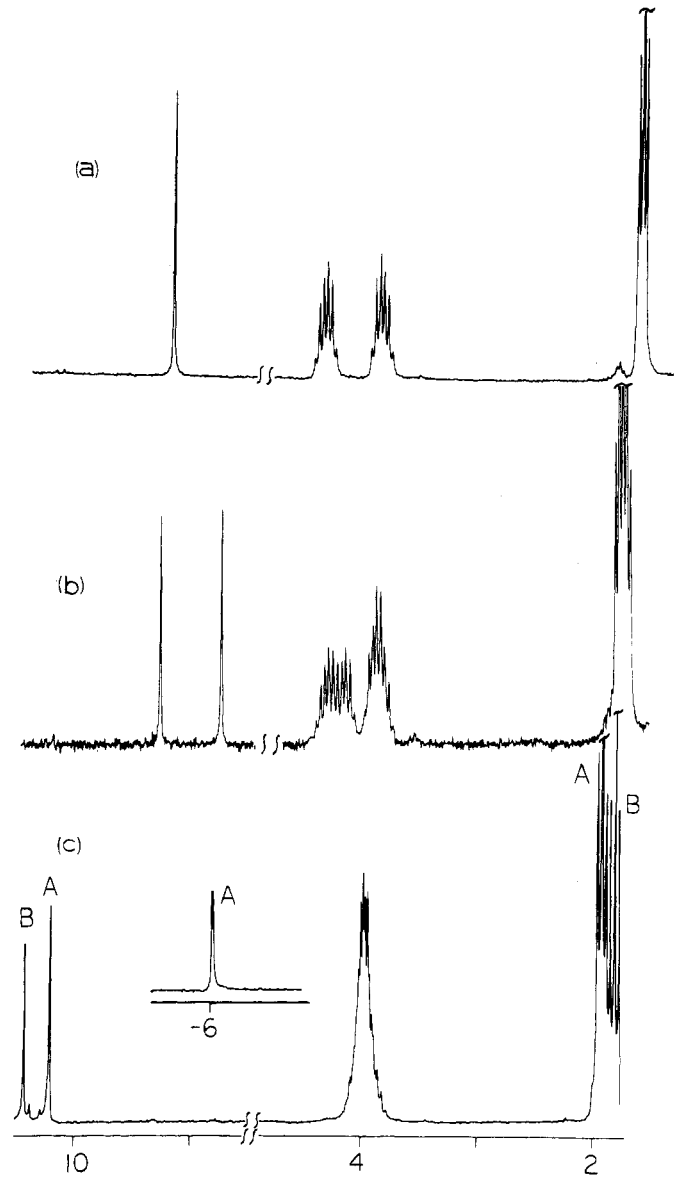

Figure 1. ^{1}H NMR spectra (C_6D_6) (a) $[Rh(OEP)]_2$, (b) Rh(OEP)-In(OEP), (c) Rh(OEP)(CH_3) (A, δ_{Rh-CH} -6.00 (J_{Rh-CH} = 3.0 Hz)), and In(OEP)(I) (B) resulting from reaction of I with CH_3I.

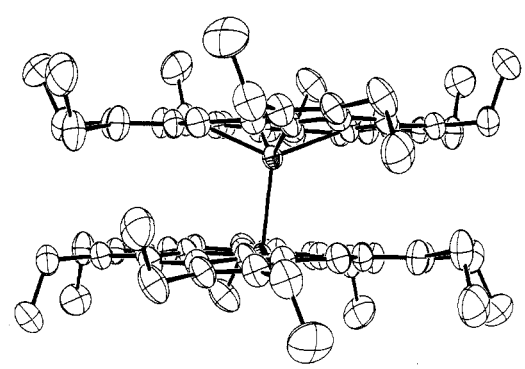

Figure 2. Drawing of Rh(OEP)-In(OEP). The hydrogen atoms have been omitted for clarity and the vibrational ellipsoids have been drawn at the 50% probability level.

that of $[Ru(OEP)]_2$ (3.26 Å),[13] indicating little interaction between the two porphyrin ligand units. The In(OEP) fragment is twisted 21.8° relative to the Rh(OEP) unit.[14]

(12) Cocolios, P.; Moise, C.; Guilard, R. *J. Organomet. Chem.* **1982**, *228*, C43–C46. Onaka, S.; Kondo, Y.; Yamashita, M.; Tatematsu, Y.; Kato, Y.; Goto, M.; Ito, T. *Inorg. Chem.* **1985**, *24*, 1070–1076.

(13) Collman, J. P.; Barnes, C. E.; Swepston, P. N.; Ibers, J. A. *J. Am. Chem. Soc.* **1984**, *106*, 3500–3510. Collman, J. P.; Barnes, C. E.; Woo, L. K. *Proc. Natl. Acad. Sci. U.S.A.* **1983**, *80*, 7684–7688.

Table VII. Comparison of Selected Metal-Porphyrin Structural Features

compd	M-N_4 plane,[a] Å	M-24-atom core,[b] Å	M-N, Å	ref
In(TPP)(CH_3)[c]	0.78 (2)	0.92 (2)	2.20 (1) (av)	15
In(OEP)(O_2CCH_3)	0.61 (2)	0.68 (2)	2.125 (20), 2.19 (2)	16
Rh(OEP)(CH_3)	0.051		2.031 (av)	17
Rh(OEP)(CHO)	0.080	0.075	2.03 (av)	18
Rh(OEP)(H)	0.010	0.024	2.02 (av)	18
Rh(OEP)-In(OEP)	Rh 0.011	0.042	2.036 (av)	this work
	In 0.832	0.882	2.202 (av)	

[a] Displacement of M from least-squares plane of four coordinated nitrogen atoms. [b] Displacement of M from least-squares plane of 24-atom skeleton. [c] TPP = tetraphenylporphyrin dianion.

Table VIII. Selected Bond Distances (Å)[a] for I

Rh-In	2.584 (1)	C(2)-C(3)	1.350 (6)
Rh-N(1)	2.037 (3)	C(7)-C(8)	1.349 (6)
Rh-N(2)	2.037 (3)	C(12)-C(13)	1.348 (5)
Rh-N(3)	2.038 (3)	C(17)-C(18)	1.353 (6)
Rh-N(4)	2.034 (3)	C_b-C_b(av)	1.350 (2)
Rh-N(av)	2.036 (3)	C(4)-C(5)	1.387 (5)
In-N(1)′	2.194 (3)	C(6)-C(5)	1.383 (6)
In-N(2)′	2.207 (3)	C(9)-C(10)	1.396 (5)
In-N(3)′	2.209 (3)	C(11)-C(10)	1.383 (5)
In-N(4)′	2.197 (3)	C(14)-C(15)	1.383 (5)
In-N(av)	2.202 (7)	C(16)-C(15)	1.384 (6)
N(1)-C(1)	1.374 (5)	C(19)-C(20)	1.394 (5)
N(1)-C(4)	1.366 (5)	C(1)-C(20)	1.380 (5)
N(2)-C(6)	1.375 (5)	C_a-C_m(av)	1.386 (6)
N(2)-C(9)	1.373 (5)	C(2)-C(21)	1.516 (6)
N(3)-C(11)	1.383 (5)	C(3)-C(22)	1.528 (6)
N(3)-C(14)	1.374 (5)	C(7)-C(23)	1.498 (6)
N(4)-C(16)	1.367 (5)	C(8)-C(24)	1.503 (6)
N(4)-C(19)	1.380 (5)	C(12)-C(25)	1.503 (6)
N-C_a(av)	1.374 (6)	C(13)-C(26)	1.505 (6)
C(1)-C(2)	1.448 (5)	C(17)-C(27)	1.502 (5)
C(4)-C(3)	1.433 (6)	C(18)-C(28)	1.506 (6)
C(6)-C(7)	1.450 (5)	C_b-C_α(av)	1.508 (10)
C(9)-C(8)	1.438 (5)	C(21)-C(29)	1.473 (7)
C(11)-C(12)	1.454 (5)	C(22)-C(30)	1.449 (8)
C(14)-C(13)	1.439 (5)	C(23)-C(31)	1.500 (8)
C(16)-C(17)	1.454 (5)	C(24)-C(32)	1.497 (7)
C(19)-C(18)	1.441 (5)	C(25)-C(33)	1.513 (6)
C_a-C_b(av)	1.445 (8)	C(26)-C(34)	1.521 (6)
		C(27)-C(35)	1.489 (6)
		C(28)-C(36)	1.512 (7)
		C_α-C_β(ethyl)(av)	1.494 (24)

[a] Primed and unprimed atoms are related by a crystallographic twofold axis.

Each porphyrin group has seven ethyl groups oriented away from the center of the molecule with no evidence for side-chain disorder. Figure 3 displays the crystal packing.[11] There is no evidence of significant intermolecular interactions as the closest intermolecular contacts are >2.2 Å (2.21 Å for H232 and H323 and 2.24 Å for H303 and H353).

The two metal atoms are displaced from the plane of the four coordinated pyrrole nitrogen atoms toward each other (0.01 Å for Rh, 0.83 Å for In). These values are comparable to other metal-nitrogen plane displacements reported for rhodium and indium porphyrin complexes (Table VII).[15-18] In particular the large out-of-plane displacement for the indium atom is comparable to that observed in In(TPP)(CH_3) (0.78 Å).[14] Figure 4 presents deviations from the 24-atom mean porphyrin planes as well as the atom numbering scheme.

The Rh-N distances (average 2.036 (2) Å) are very similar to those reported for other Rh(III)-porphyrin com-

Table IX. Selected Bond Angles (deg)[a] for I

N(1)-Rh-N(2)	90.46 (12)	C(1)-C(2)-C(3)	106.9 (4)
N(1)-Rh-N(4)	89.93 (12)	C(4)-C(3)-C(2)	107.4 (4)
N(2)-Rh-N(3)	89.67 (12)	C(6)-C(7)-C(8)	106.4 (3)
N(3)-Rh-N(4)	89.94 (12)	C(9)-C(8)-C(7)	107.5 (3)
N-Rh-N(av)	90.0 (3)	C(11)-C(12)-C(13)	107.3 (3)
N(1)-Rh-N(3)	179.6 (1)	C(14)-C(13)-C(12)	107.4 (3)
N(2)-Rh-N(4)	179.6 (1)	C(16)-C(17)-C(18)	106.7 (3)
average	179.6 (1)	C(19)-C(18)-C(17)	107.0 (3)
N(1)-Rh-In	85.69 (8)	C_a-C_b-C_b(av)	107.1 (4)
N(2)-Rh-In	91.16 (8)	N(1)-C(1)-C(20)	124.5 (3)
N(3)-Rh-In	93.96 (9)	N(1)-C(4)-C(5)	124.5 (3)
N(4)-Rh-In	88.88 (8)	N(2)-C(6)-C(5)	124.4 (3)
N-Rh-In(av)	89.9 (35)	N(2)-C(9)-C(10)	123.3 (3)
N(1)′-In-N(2)′	82.17 (11)	N(3)-C(11)-C(10)	124.6 (3)
N(1)′-In-N(4)′	81.86 (11)	N(3)-C(14)-C(15)	124.2 (3)
N(2)′-In-N(3)′	81.17 (11)	N(4)-C(16)-C(15)	124.6 (3)
N(3)′-In-N(4)′	81.55 (11)	N(4)-C(19)-C(20)	123.6 (3)
N-In-N(av)	81.7 (4)	N-C_a-C_m(av)	124.2 (5)
N(1)′-In-N(3)′	135.48 (11)	C(2)-C(1)-C(20)	126.5 (4)
N(2)′-In-N(4)′	135.13 (11)	C(3)-C(4)-C(5)	125.6 (4)
average	135.30	C(7)-C(6)-C(5)	125.5 (4)
N(1)′-In-Rh	108.23 (7)	C(8)-C(9)-C(10)	126.6 (3)
N(2)′-In-Rh	113.65 (8)	C(12)-C(11)-C(10)	126.6 (3)
N(3)′-In-Rh	116.28 (9)	C(13)-C(14)-C(15)	126.0 (3)
N(4)′-In-Rh	111.15 (8)	C(15)-C(16)-C(17)	125.3 (3)
N-In-Rh(av)	112.3 (34)	C(18)-C(19)-C(20)	126.3 (4)
Rh-N(1)-C(1)	126.8 (2)	C_b-C_a-C_m(av)	126.0 (5)
Rh-N(1)-C(4)	126.3 (2)	C(1)-C(20)-C(19)	128.0 (4)
Rh-N(2)-C(6)	126.1 (2)	C(4)-C(5)-C(6)	127.9 (4)
Rh-N(2)-C(9)	127.6 (2)	C(9)-C(10)-C(11)	127.8 (4)
Rh-N(3)-C(11)	126.5 (2)	C(14)-C(15)-C(16)	127.6 (4)
Rh-N(3)-C(14)	126.7 (2)	C_a-C_m-C_a(av)	127.8 (2)
Rh-N(4)-C(16)	126.8 (2)	C(1)-C(2)-C(21)	124.7 (4)
Rh-N(4)-C(19)	127.1 (2)	C(4)-C(3)-C(22)	124.6 (4)
Rh-N-C(av)	126.7 (5)	C(6)-C(7)-C(23)	124.7 (4)
In-N(1)′-C(1)′	124.0 (2)	C(9)-C(8)-C(24)	126.2 (4)
In-N(1)′-C(4)′	121.6 (3)	C(11)-C(12)-C(25)	123.9 (3)
In-N(2)′-C(6)′	122.9 (2)	C(14)-C(13)-C(26)	124.8 (3)
In-N(2)′-C(9)′	127.3 (2)	C(16)-C(17)-C(27)	125.1 (4)
In-N(3)′-C(11)′	125.1 (2)	C(19)-C(18)-C(28)	125.6 (4)
In-N(3)′-C(14)′	123.5 (2)	C_a-C_b-C_α(ethyl)(av)	124.9 (7)
In-N(4)′-C(16)′	124.2 (3)	C(3)-C(2)-C(21)	128.4 (4)
In-N(4)′-C(19)′	125.4 (2)	C(2)-C(3)-C(22)	127.7 (4)
In-N-C(av)	124.3 (17)	C(8)-C(7)-C(23)	128.8 (4)
N(1)-C(1)-C(2)	109.0 (3)	C(7)-C(8)-C(24)	126.3 (4)
N(1)-C(4)-C(3)	109.7 (3)	C(13)-C(12)-C(25)	128.7 (4)
N(2)-C(6)-C(7)	110.0 (3)	C(12)-C(13)-C(26)	127.8 (4)
N(2)-C(9)-C(8)	110.1 (3)	C(18)-C(17)-C(27)	128.2 (4)
N(3)-C(11)-C(12)	108.8 (3)	C(17)-C(18)-C(28)	127.3 (3)
N(3)-C(14)-C(13)	109.8 (3)	C_b-C_b-C_α(ethyl)(av)	127.9 (8)
N(4)-C(16)-C(17)	110.1 (3)	C(2)-C(21)-C(29)	111.7 (4)
N(4)-C(19)-C(18)	110.2 (3)	C(3)-C(22)-C(30)	113.0 (4)
N-C_a-C_b(av)	109.7 (5)	C(7)-C(23)-C(31)	113.8 (4)
C(1)-N(1)-C(4)	106.9 (3)	C(8)-C(24)-C(32)	113.8 (3)
C(6)-N(2)-C(9)	105.9 (3)	C(12)-C(25)-C(33)	114.3 (4)
C(11)-N(3)-C(14)	106.7 (3)	C(13)-C(26)-C(34)	112.5 (4)
C(16)-N(4)-C(19)	105.9 (3)	C(17)-C(27)-C(35)	115.1 (4)
C_a-N-C_a(av)	106.4 (5)	C(18)-C(28)-C(36)	112.2 (3)
		C_b-C_α-C_β(ethyl)(av)	113.3 (12)

[a] Primed and unprimed atoms are related by a crystallographic twofold axis.

(14) The twist angle is defined as the weighted mean of the N_x-Rh-In-N_y′ (x = 1, 4) torsion angles.

(15) Lecomte, C.; Protas, J.; Cocolios, P.; Guilard, R. *Acta Crystallogr., Sect. B: Struct. Crystallogr. Cryst. Chem.* **1980**, *B36*, 2769-2771.

(16) Cocolios, P.; Guilard, R.; Bayeul, D.; Lecomte, C. *Inorg. Chem.* in press.

(17) Takenaka, A.; Syal, S. K.; Sasada, Y.; Omura, T.; Ogoshi, H.; Yoshida, Z.-I. *Acta Crystallogr., Sect. B: Struct. Crystallogr. Cryst. Chem.* **1976**, *B32*, 62-65.

(18) Pierce, R. Ph.D Dissertation, University of Pennsylvania, 1983.

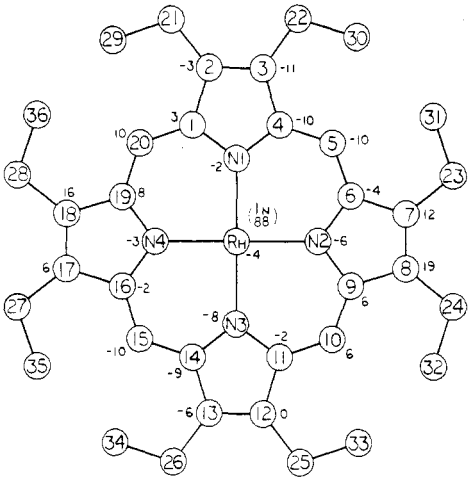

Figure 4. Displacements ($\times 10^2$ Å) of atoms from the weighted least-squares planes of the 24-atom porphyrin skeleton.

plexes (Table VII). The In–N distances (average 2.202 (2) Å) are longer than those previously reported (Table VII), as demanded by the larger displacement of the indium atom out of the N_4 plane. Intramolecular bond distances (Table VIII) and angles (Table IX) are normal.

A covalent radius for singly bonded indium(III) in a square-pyramidal geometry may be estimated from the indium–carbon distances in In(TPP)(CH_3) (2.13 (1) Å).[15,19] In this environment, a single-bond covalent radius of 1.36 Å for In(III) is suggested. The covalent radius of an octaethylporphyrin-bound rhodium atom may be approximated in a similar way (Rh–C = 2.031 Å for Rh(OEP)(CH_3)[17]) as 1.26 Å. Thus, a Rh–In single bond distance is predicted to be approximately 2.62 Å. The observed metal–metal bond length of 2.584 (2) Å is not significantly different from the value estimated for a Rh–In single bond and substantially longer than the Ru–Ru distance measured for $[Ru(OEP)]_2$ (2.408 (1) Å) where a formal metal–metal double bond is predicted.[13]

Reactivity of I. The reactivity of I has been studied by allowing I to react with an excess of the reagent in C_6D_6 (or THF-d_8) and following reaction progress by ^1H NMR spectroscopy. Complex I fails to react thermally (<125 °C) or photolytically (530–350 nm) with dihydrogen/carbon monoxide mixture, phenylacetylene, acrylonitrile, triethyl phosphite, *n*-butyl isocyanide, or dioxygen under reaction conditions where $[Rh(OEP)]_2$ is known to react.[1,3,4,20,21]

It is important to note that the ^1H NMR spectrum of I is unperturbed in the presence of donor molecules such as *n*-butyl isocyanide, triethyl phosphite, or water. In the crystal structure of I the rhodium atom lies in the porphyrin plane and the indium atom lies 0.8 Å out of the plane toward the Rh atom. This structural feature implies that only the rhodium atom is readily accessible to donor molecules. The absence of any observed donor molecule interaction with the rhodium center suggests the presence of a polar Rh–In bond in I that may be approximated by the formulation $Rh(I)^-{:}\rightarrow In(III)^+$. The $[Rh(OEP)]^-$ fragment with a filled d_{z^2} orbital would thus be expected to act as an electron donor and not as an acceptor.

The formulation $Rh(I)^-{:}\rightarrow In(III)^+$ is supported by the reactivity of I observed with alkyl iodides. Complex I reacts quantitatively with methyl iodide either thermally (125 °C) or photolytically ($\lambda > 530$ nm, 25 °C) to afford exclusively Rh(OEP)(CH_3)[22] and In(OEP)(I)[6] (eq 1) (Figure 1). Reaction of ethyl iodide proceeds more slowly but yields the analogous products. The addition of methyl iodide to a rhodium–molybdenum bond (eq 2) produces

$$\text{Rh(OEP)–In(OEP)} + CH_3I \rightarrow \text{Rh(OEP)}(CH_3) + \text{In(OEP)(I)} \quad (1)$$

$$Cp^*Rh(\mu\text{-}P(CH_3)_2)_2Mo(CO)_4 + CH_3I \rightarrow Cp^*(CH_3)Rh(\mu\text{-}P(CH_3)_2)_2Mo(CO)_3I + CO \quad (2)$$

a rhodium–methyl molybdenum–iodide complex ($Cp^* = \eta^5\text{-}C_5(CH_3)_5$), and to our knowledge is the only previously reported regioselective addition of an alkyl iodide to a heterobimetallic bond.[23] The direction of addition of CH_3I to Rh(OEP)–In(OEP) is consistent with nucleophilic substitution of iodide by $[Rh(OEP)]^-$ which is a well-established reaction for authentic $[Rh(OEP)]^-$.[24] The donor properties of the rhodium fragment are further manifested by rapid cleavage of the Rh–In bond by HX (X = O_2CCH_3, O_2CCF_3, O_3SCF_3) to yield the corresponding Rh(OEP)(H) and In(OEP)(X).

The reactivity of I is presently being explored with a broader range of electrophiles. Other Rh(OEP)–main group metal–metal bonded complexes are being studied for similar reactivity.

Acknowledgment. Support of this work by the National Science Foundation is gratefully acknowledged.

Registry No. I, 99128-05-9; Rh(OEP)(CH_3), 36643-85-3; In(OEP)(I), 99128-06-0; Rh(OEP)(H), 63372-77-0; In(OEP)(Cl), 32125-07-8; CH_3I, 74-88-4; C_2H_5I, 75-03-6; CH_3CO_2H, 64-19-7; CF_3CO_2H, 76-05-1; CF_3SO_3H, 1493-13-6; In, 7440-74-6; Rh, 7440-16-6.

Supplementary Material Available: Tables of anisotropic thermal parameters (Table III), hydrogen atom positional parameters (Table IV), the final values of $10|F_o|$ and $10|F_c|$ (Table V), and root-mean-square amplitudes of vibration (Table VI) and a stereoscopic crystal packing diagram (Figure 3) (18 pages). Ordering information is given on any current masthead page.

(19) Robinson, W. R.; Schussler, D. P. *Inorg. Chem.* **1973**, *12*, 848–854.
(20) Wayland, B. B.; Woods, B. A. *J. Chem. Soc., Chem. Commun.* **1981**, 475–476.
(21) Wayland, B. B.; Newman, A. R. *J. Am. Chem. Soc.* **1979**, *101*, 6472–6473.
(22) Ogoshi, H.; Omura, T.; Yoshida, Z. *J. Am. Chem. Soc.* **1973**, *95*, 1666–1668.
(23) Finke, R. G.; Gaughan, G.; Pierpont, C., Noordik, J. H. *Organometallics* **1983**, *2*, 1481–1483.
(24) The complexes Rh(OEP)(I) and In(OEP)(CH_3) are known[4,25] yet neither is observed spectroscopically here.
(25) Cocolios, P.; Guilard, R.; Fournari, P. *J. Organomet. Chem.* **1979**, *179*, 311–322.

Organometallic Chemistry of Fluorocarbon Acids. Synthesis and Structural and Dynamic Properties of (π-Arene)RuH(PPh_3)$_2^+$ Derivatives

A. R. Siedle* and R. A. Newmark

Science Research Laboratory, 3M Central Research Laboratories, St. Paul, Minnesota 55144

L. H. Pignolet

Chemistry Department, University of Minnesota, Minneapolis, Minnesota 55455

D. X. Wang and T. A. Albright[1]

Chemistry Department, University of Houston, Houston, Texas 77004

Received March 28, 1985

Reaction of $H_2C(SO_2CF_3)_2$ with $(Ph_3P)_4RuH_2$ in neat arene solvents produces (π-arene)RuH(PPh_3)$_2^+$-$HC(SO_2CF_3)_2^-$. The ^1H NMR spectra of these compounds indicate that substituents on the arene ring stabilize one of several ring rotational conformations. Molecular orbital calculations at the extended Hückel level were utilized to explore the structural distortion of the RuH(PPh_3)$_2^+$ units in these compounds as well as the dynamics of rotation about the arene–Ru axis. Computations on (arene)RuH(PH_3)$_2^+$ (arene = benzene, aniline, phenylborane) each showed similar distortions in the tripod portion of the molecule which can be traced to more efficient donation of electron density from the hydride to the metal compared to the phosphine ligands. The structure for each of these model compounds was optimized, and barriers to rotation about the arene–Ru bond were computed. Crystal structure determinations on (π-$PhCH_3$)-RuH(PPh_3)$_2^+HC(SO_2CF_3)_2^-$ [monoclinic, $P2_1/a$, a = 27.571 (4) Å, b = 13.620 (3) Å, c = 11.632 (3) Å, α = 90°, β = 94.05 (2)°, γ = 90°, Z = 4, R = 0.035] and (π-$PhCH_3$)RuH(PPh_3)$_2^+BPh_4^-$ [monoclinic, $P2_1/c$, a = 15.814 (2) Å, b = 16.816 (2) Å, c = 20.988 (7) Å, α = 90°, β = 103.39 (2)°, γ = 90°, Z = 4, R = 0.065] reveal rotational and metal displacement effects predicted by the calculations.

We have previously outlined the reactions of bis(perfluoroalkylsulfonyl)alkanes, exemplified by $H_2C(SO_2CF_3)_2$, **1**, with organometallic hydrides.[2,3] Generally, the reaction pattern, illustrated schematically in eq 1, consists of proton

$$M\text{–}H + H^+ \rightarrow MH_2^+ \rightarrow M^+ + H_2 \qquad (1)$$

transfer followed, in some cases, by reductive elimination of hydrogen and/or dissociation of ancillary phosphine ligands. Such protonation reactions, when carried out on a preparative scale, are usually conducted in an inert, apolar solvent such as toluene. Toluene, when present in the solvated, saltlike products, is simply incorporated into the crystal lattice. The reactions of $(Ph_3P)_4RuH_2$ with fluorocarbon acids are distinctive in that the hydrocarbon solvent is attacked and emerges bonded to ruthenium in (π-$PhCH_3$)RuH(Ph_3P)$_2^+$. This paper presents the results of a detailed investigation by NMR, X-ray crystallographic, and theoretical methods of such (π-arene)RuH(Ph_3P)$_2^+$ derivatives and the delineation of restricted arene ring rotation in this class of compounds.

Results and Discussion

Synthetic Chemistry. The reaction of $(Ph_3P)_4RuH_2$ with $H_2C(SO_2CF_3)_2$ in dry, deoxygenated toluene proceeds at room temperature to give (π-$PhCH_3$)RuH(PPh_3)$_2^+$HC-$(SO_2CF_3)_2^-$, **2a**, in 58% yield. The nature of the initial protonation product is not established but an intermediate such as $(Ph_3P)_4RuH^+$[4] may form and subsequently react with toluene. This reaction represents, when substituted benzene derivatives are employed as solvents, a general synthetic route to (arene)RuH(PPh_3)$_2^+$ compounds where the arene is benzene (**3a**), *o*-xylene (**4a**), *m*-xylene (**5a**), *p*-xylene (**6a**), ethylbenzene (**7a**), isopropylbenzene (**8a**), acetophenone (**9a**), anisole (**10a**), chlorobenzene (**11a**), fluorobenzene (**12a**), and *p*-fluorotoluene (**13a**). These compounds may be regarded as the conjugate acids of the neutral, highly reactive (arene)Ru(phosphine)$_2$ materials.[5] NMR chemical shift data for a series of $HC(SO_2CF_3)_2^-$ and Ph_4B^- derivatives are given in Table I (vide infra). In weakly coordinating solvents such as methanol, $(Ph_3P)_4RuH_2$ and $H_2C(SO_2CF_3)_2$ instead produce (π-$Ph_2PC_6H_5$)RuH(Ph_3P)$_2^+HC(SO_2CF_3)_2^-$, **14a**, in which one of the triphenylphosphine arene rings is π-bonded to ruthenium.[4,6,7] Compound **2a** is a yellow crystalline solid stable to atmospheric oxygen and water and having good solubility in polar solvents such as chloroform, acetonitrile, and ethanol, properties shared by its other arene analogues. The infrared spectrum shows a Ru–H stretching band at 2060 cm^{-1} and characteristic anion bands at 1350 and 1100 cm^{-1}. The metathetical reaction with $NaBPh_4$ in the latter solvent provides (π-toluene)RuH(PPh_3)$_2BPh_4$, **2b**. In this series of compounds, the tetraphenylborate salts **2b**–**14b** are particularly useful and readily purified by recrystallization from mixtures of dichloromethane and ethanol. Early incentive to study these arene complexes in more

(1) Camille and Henry Dreyfus Teacher-Scholar 1980–1984; Alfred P. Sloan Research Fellow 1982–1986.

(2) Siedle, A. R.; Newmark, R. A.; Pignolet, L. H.; Howells, R. D. *J. Am. Chem. Soc.* **1984**, *106*, 1510.

(3) Siedle, A. R.; Newmark, R. A.; Pignolet, L. H. *Organometallics* **1984**, *3*, 855.

(4) This cation was originally prepared by hydride abstraction from $(Ph_3P)_4RuH_2$ with Ph_3C^+: Sanders, J. R. *J. Chem. Soc., Dalton Trans.* **1973**, 743.

(5) Werner, H.; Werner, R. *Angew. Chem., Int. Ed. Engl.* **1978**, *17*, 683.

(6) McConway, J. C.; Skapski, A. C.; Phillips, L.; Young, R. J.; Wilkinson, G. *J. Chem. Soc., Chem. Comm.* **1974**, 327. Regrettably, a listing of the atomic coordinates in (π-$PhPPh_2$)RuH(PPh_3)$_2BF_4$ is unavailable and no detailed comparison with our structural data is possible.

(7) Protonation of $(Ph_3P)_3RuH(CH_3CO_2)$ with fluoboric acid also yields this arene complex: Cole-Hamilton, D. J.; Young, R. J.; Wilkinson, G. *J. Chem. Soc., Dalton Trans.* **1976**, 1995. We shall describe elsewhere a survey of the reactions of hydridometal carboxylates with fluorocarbon acids.

0276-7333/86/2305-0038$01.50/0

Table I. Observed Chemical Shifts (ppm) and Coupling Constants (Hz) of Arene Complexes (Arene)RuH(PPh_3)$_2^+$

complex (arene)	salt[a]	solvent	δ(H-2)	δ(H-3)	δ(H-4)	δ(H-5)	δ(H-6)	δ(RuH)	J(PH)	Me	J_{23}	J_{34}
2a (toluene)	HDS	CD_2Cl_2	4.66	5.28	6.35	5.28	4.66	−9.22	37.8	2.35		
2b (toluene)	BPh_4	$CDCl_3$	4.37	4.85	5.59	4.85	4.37	−9.53	37.7	2.11	6.0	5.9
3a (benzene)	HDS	$CDCl_3$	5.48	5.48	5.48	5.48	5.48	−9.09	37.0			
3b (benzene)	BPh_4	$CDCl_3$	4.96	4.96	4.96	4.96	4.96	−9.36	38.2			
4b (*o*-xylene)	BPh_4	$CDCl_3$	Me	4.17	5.35	5.35	4.17	−9.79	35.0	1.81		
5b (*m*-xylene)	BPh_4	$CDCl_3$	4.09	Me	5.06	4.75	5.06	...	...	1.84		
6b (*p*-xylene)	BPh_4	$CDCl_3$	4.50	4.50	Me	4.50	4.50	−9.99	37.6	2.18		
7b (ethylbenzene)	BPh_4	$CDCl_3$	4.16	4.80	5.77	4.80	4.16	−9.43	37.5	1.24[b]		
8b (isopropylbenzene)	BPh_4	$CDCl_3$	4.27	5.07	6.34	5.07	4.27	−9.04	37.6	1.34[b]		
9b (acetophenone)	BPh_4	$CDCl_3$	5.12	4.40	5.80	4.40	5.12	−9.59	37.7	2.10	6.3	5.8
10a (anisole)	HDS	$CDCl_3$	4.72	5.40	5.97	5.40	4.72	−9.29	36.5	3.59		
10b (anisole)	BPh_4	$CDCl_3$	4.39	4.89	5.20	4.89	4.39	−9.50	36.5	3.28	6.2	5.8
11b (chlorobenzene)	BPh_4	$CDCl_3$	4.69	4.60	5.26	4.60	4.69	−9.26	37.9		6.0	5.6
12b (fluorobenzene)[c]	BPh_4	$CDCl_3$	4.71	4.83	4.64	4.83	4.71	−9.14	36.9		5.5	5.4
13b (4-fluorotoluene)[c]	BPh_4	$CDCl_3$	4.41	4.79	F	4.79	4.41	−9.54	37.3	1.83	5.5	
14a (triphenylphosphine)	HDS	CD_2Cl_2	4.36	5.14	6.86	5.14	4.36	−8.67	38.3[d]			
14b (triphenylphosphine)	BPh_4	$CDCl_3$	4.68	4.11	5.89	4.11	4.68	−8.95	38.5[d]			

[a] HDS, $CH(SO_2CF_3)_2^-$, δ 3.92 (**2a**), 4.09 (**3a**), 4.07 (**10a**), 3.91 (**14a**). [b] CH_2, δ 2.46 in **7b**; CH, δ 2.73 in **8b**. [c] ^{19}F: δ −126.3 in **12b** and δ −131.8 in **13b**; ^3J(HRuF) = 6.4 Hz in **12b** and 5.8 Hz in **13b**; ^3J(FCH) = 4.8 Hz in **12b** and 3.6 Hz in **13b**; ^4J(FCCH) = 3.5 Hz in **12b** and 3.0 Hz in **13b**. [d] $J(HP_{arene})$ = 8.7 Hz in **14a** and 9.0 Hz in **14b**.

detail came from magnetic resonance data on **2a**.

NMR Properties. The 200-MHz proton NMR spectrum of **2a** in dichloromethane-d_2 reveals well-separated resonances at δ 4.66 (d, J_{HH} = 6 Hz, 2 H), 5.28 (t, 6 Hz, 2 H), and 6.35 (t, 6 Hz, 1 H) due respectively to the ortho, meta, and para toluene ring protons. The assignments are unambiguous since H_{ortho} is strongly coupled only to H_{meta}. The hydride resonance occurs as a triplet at −9.2 ppm (J_{PH} = 38 Hz), and the narrow band ^1H-decoupled ^{31}P spectrum comprises a doublet at 51.8 ppm, confirming the presence of a $(Ph_3P)_2RuH$ moiety. The large chemical shift dispersion for the π-arene ring protons, 1.7 ppm, is unusual in that the shielding range in such complexes is more often on the order of 0.3–0.6 ppm. A closely related example is (π-$PhCH_3$)$RuCl_2$(*n*-Bu_3P) in which the arene protons give rise to a multiplet between 5.6 and 4.96 ppm.[8] In **2a**, however, the para proton is highly deshielded and moved out of the range found in η^6-arene complexes. Since the toluene ligand in **2a** has, by NMR criteria, the same symmetry as the free arene, these data indicate operation of a dynamic process sufficiently rapid on the NMR time scale to make the symmetric protons equivalent with respect to the $(Ph_3P)_2RuH$ unit. We propose that, as a result of electronic effects, η^6-toluene in $(CH_3C_6H_5)RuH(Ph_3P)_2^+$ salts is subject to restricted rotation which is describable in terms of a double well potential. According to this scheme, two conformations, A and B, are separated by a

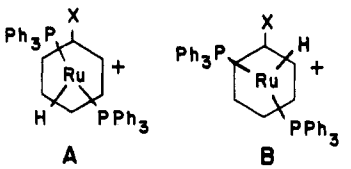

small energy barrier, on the order of several kilocalories per mole. Whether A or B is lower in energy, as well as the magnitude of the difference, will be a function of the electronic properties of the ring substituent X as will be discussed in more detail below. In conformation A, one of the ortho arene protons is in a transoid relationship to the hydride ligand on ruthenium and, since hydride is known to exert a strong trans effect, electron density at the ortho position should be reduced. Consequently, one of the ortho protons is shielded relative to its counterpart on the opposite side of the arene ring and relative to H_{para} and H_{meta}. Conversely, in conformation B, H_{meta} should be shielded relative to the other ring protons. Low-temperature ^1H NMR spectroscopic studies of **2a** reveal no apparent reduction in symmetry of the toluene ligand, indicating that A–B interconversion has a very low activation energy. Importantly, however, the shift of H_{ortho} *decreases* from 4.66 ppm at 22 °C to 4.39 ppm at −110 °C while the shift of H_{para} *increases* from 6.35 to 6.57 ppm over the same temperature range; no change occurs for the shift of H_{meta}. That H_{ortho} moves upfield on cooling while H_{para} moves downfield is indicative of a temperature-dependent conformational equilibrium resulting from the difference in energies of structures A and B; effectively, a Boltzmann-type distribution between A and B obtains and the intrinsic rotational barrier between these is quite low. Similar effects have been observed in (alkylbenzene)$Cr(CO)_3$ compounds.[9,10] In these, however, the conformational energy difference is associated with steric effects due to bulky alkyl ring substituents rather than with electronic effects as in the present case. In the corresponding benzene complex (π-C_6H_6)$RuH(Ph_3P)_2^+HC(SO_2CF_3)_2^-$, **3b**, barrier(s) to ring rotation are quite low and only a single η^6-arene proton resonance at 5.48 ppm is observed.

Since an extensive series of closely related arene ruthenium complexes was available, efforts were made to analyze their ^1H chemical shifts. To eliminate errors due to effects of variations in solvent and counterions, all the cationic materials were converted to the tetraphenylborate salts and spectra consistently obtained in deuteriochloroform. It is well-known that electron-withdrawing effects and diamagnetic anisotropy of transition metals leads to substantial upfield shifts of the protons in η^6-arene rings.[11,12] Although it is considered that these upfield shifts are due to an anisotropic effect on the shielding tensor, a precise explanation is not yet available.[13] Ring substituents on free arenes induce both upfield and downfield shifts due to inductive and resonance effects. Additional, specific deshielding in π complexes is ration-

(8) Bennett, M. A.; Smith, A. K. *J. Chem. Soc., Dalton Trans.* **1974**, 233.

(9) Jackson, W. R.; Jennings, W. B.; Rennison, S. C.; Spratt, R. *J. Chem. Soc. B* **1969**, 1214.

(10) Jackson, W. R.; Jennings, W. B.; Spratt, R. *J. Chem. Soc., Chem. Commun.* **1970**, 593.

(11) Emanuel, R. V.; Randall, E. W.; *J. Chem. Soc. A* **1969**, 3002.

(12) Wu, A.; Biehl, E. R.; Reeves, P. C. *J. Organomet. Chem.* **1971**, *33*, 53.

(13) Maricq, M. M.; Waugh, J. S.; Fletcher, J. L.; McGlinchey, M. J. *J. Am. Chem. Soc.* **1978**, *100*, 6902.

Table II. Differences between Chemical Shift (δ) of Complex (Arene)RuH$(PPh_3)_2^+$ and Chemical Shift (δ) of Free Arene after Correction for Arene Substituent Chemical Shifts

complex (arene)	salt[a]	H-2	H-3	H-4	H-5	H-6	Me
2a (toluene)	HDS	−0.59	−0.08	1.07	−0.08	−0.59	0.00
2b (toluene)	BPh_4	−0.36	0.01	0.83	0.01	−0.36	−0.24
4b (*o*-xylene)	BPh_4	Me	−0.54	0.64	0.64	−0.54	−0.45
5b (*m*-xylene)	BPh_4	−0.50	Me	−0.49	0.01	0.49	−0.47
6b (*p*-xylene)	BPh_4	−0.17	−0.17	Me	−0.17	−0.17	−0.12
7b (ethylbenzene)[b]	BPh_4	−0.57	−0.01	1.08	−0.02	−0.57	0.05
8b (isopropylbenzene)[b]	BPh_4	−0.47	0.28	1.65	0.28	−0.47	0.12
9b (acetophenone)	BPh_4	−0.35	−0.58	0.74	−0.58	−0.35	−0.49
10a (anisole)	HDS	−0.20	0.03	0.96	0.03	−0.20	−0.17
10b (anisole)	BPh_4	0.01	0.13	0.77	0.13	0.01	−0.50
11b (chlorobenzene)	BPh_4	−0.19	−0.21	0.51	−0.21	−0.19	
12b (fluorobenzene)[c]	BPh_4	0.13	−0.02	0.00	−0.02	0.13	
13b (4-fluorotoluene)[c]	BPh_4	−0.20	0.37	F	0.37	−0.20	−0.40
14a (triphenylphosphine)	HDS	−1.11	−0.33	1.39	−0.33	−1.11	
14b (triphenylphosphine)	BHp_4	−0.27	−0.84	0.94	−0.84	−0.27	

[a] HDS, $CH(SO_2CF_3)_2^-$. [b] CH_2, δ −0.07 in **7b** and −0.10 in **8b**. [c] ^{19}F, δ −13.2 in **12b** and **13b**.

alized by particular conformations of the substituted arene relative to groups attached to the metal.[9] Arene proton NMR chemical shifts for the new ruthenium compounds prepared in this work are given in Table I. Spectra of derivatives of monosubstituted arenes show three multiplets, a two proton doublet, a two proton triplet, and a one proton triplet, each with J ca. 6 Hz, assigned to the protons ortho, meta, and para, respectively, to the substituent. Spectra of the *m*- and *p*-xylene compounds **5** and **6b** may also be assigned uniquely from the observed ortho coupling constants. The *p*-fluorotoluene complex **13b** was assigned by assuming that the ortho J(HF) is larger than meta H–F coupling. The spectrum of the *o*-xylene complex **4b** was assigned from an analysis of substituent chemical shifts (vide infra). The arene protons in the π-triphenylphosphine complex **14b** showed three poorly resolved triplets having relative areas of 2, 2, and 1. The latter is due to the para proton in the η^6-arene ring, and the peaks of relative areas two were assigned by spin decoupling the para proton which collapsed the meta proton resonance to a doublet; the ortho proton gives rise to an appareent triplet due to equal H–H and H–P coupling.

These chemical shifts contain three effects: the inductive and resonance effect of the substituent(s) on the other protons in the arene ring; the shielding effect of the ruthenium atom; and specific effects due to anisotropy of the $(Ph_3P)_2$RuH moiety. The latter effect provides information about restricted arene rotation in these compounds, and, on order to extract it from gross chemical shift data, corrections must be made for substituent and metal shielding effects. The first correction was made by subtracting, for each arene proton position, the chemical shift of the free arene from that observed in the ruthenium complex. Subtracting the difference between the chemical shift of the η^6-benzene complex **3b** and free benzene compensates for the shielding effect of the phosphine ruthenium hydride unit. The resulting corrected chemical shifts are given in Table II. Negative values indicate additional shielding at a given proton position over and above that anticipated from the influence of substituents and π complexation. We shall argue that large changes in these corrected chemical shifts caused by variations in π-arene substituents reflect an electronic stabilization of the A or B rotational conformations shown above. For monosubstituted benzene derviatives, when the substituent is inductively electron releasing (X = CH_3, C_2H_5, i-C_3H_7), there is a large shielding of the ortho arene protons and a deshielding of H_{para} which we consider to indicate relative stabilization of conformation A. The fluorine substituent in (π-C_6H_5F)RuH$(PPh_3)_2BPh_4$, **12b**, has only a weak electronic effect and the π-fluorobenzene ring appears to have no strong rotational preference. When the substituent on the π-arene ring is electron withdrawing (Cl, $OCCH_3$, PPh_2), significant upfield shifts of the meta ring protons are observed, indicating increased stabilization of conformation B. The chemical shifts in the xylene complexes can be calculated, using simple additivity relationships, from the observed shifts in the toluene analogue, in agreement with results for (arene)$Cr(CO)_3$ derivatives.[14] For example, the induced shifts in **2a** indicate that the ortho, meta, and para effects of a methyl group in the η^6 ring, −0.36, +0.01, and +0.83 ppm, respectively, are over twice as large as in the analogous (toluene)$Cr(CO)_3$.[15] The calculated chemical shift for the protons in the *p*-xylene complex **6b** is the sum of an ortho and a meta effect, or −0.35 ppm. The observed shift is within 0.2 ppm of the calculated value; the calculated shifts in **4b** and **5a** are also within 0.2 ppm of those observed. They would differ by over 1.0 ppm in **4b** if the assignments of H(3,6) and H(4,5) were interchanged. In order to further explore the structure and bonding in (π-arene)RuH$(Ph_3P)_2^+$ derivatives, X-ray crystal structure determinations of the HC$(SO_2CF_3)_2^-$ and BPh_4^- salts of the toluene derviative (π-$PhCH_3$)RuH$(PPh_3)_2^+$, **2a** and **2b**, were carried out and are described in the following section.

Descriptions of the Structures

The crystal structures of **2a** and **2b** demonstrate well-separated [(π-toluene)RuH$(PPh_3)_2$]$^+$ cations and the HC$(SO_2CF_3)_2^-$ and BPh_4^- anions, respectively. The shortest interionic contacts are 3.306 (5) Å for C5···O21 in **2a** and 3.47 (1) Å for C3A···C4F in **2b**. These distances are not less than the sum of the appropriate van der Waals radii. The gross structures of the (π-toluene)RuH$(PPh_3)_2^+$ cations in both compounds are similar, exhibiting the familiar but here distorted "piano stool" architecture. However, there is a pronounced and important difference in the orientation of the toluene ring with respect to the RuH$(PPh_3)_2$ unit. This is readily apparent in Figure 1 which shows projection views of both coordination cores drawn normal to the arene rings as well as from Table III which shows a listing of selected bond distances and angles. In **2a**, the Ru–H bond lies away from the methyl group and approximately above the C3–C4 bond, nearly eclipsing C3. In **2b**, the Ru–H bond lies toward the methyl group, approximately above the C1–C6 bond and nearly eclipsing C1. These two orientations correspond to conformations

(14) Price, J. T.; Sorenson, T. S. *Can. J. Chem.* **1968**, *46*, 515.
(15) Graves, V.; Lagowski, J. J. *J. Organomet. Chem.* **1976**, *105*, 397.

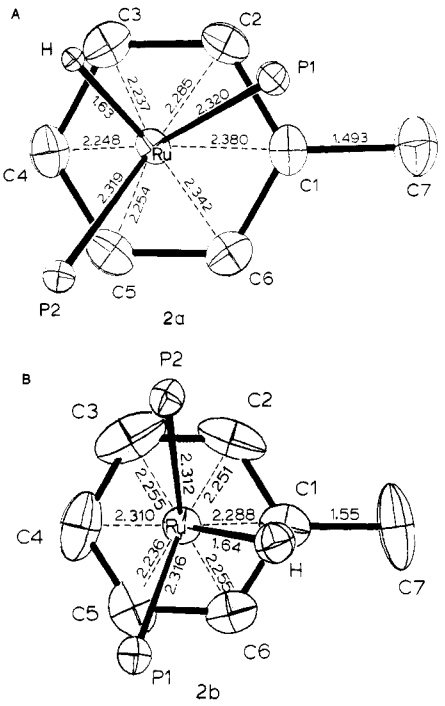

Figure 1. Projection views of the $(\pi\text{-PhCH}_3)\text{RuH}(\text{PPh}_3)_2^+$ ions in the $\text{HC}(\text{SO}_2\text{CF}_3)_2^-$ (A) and BPh_4^- (B) salts.

B and A, respectively. The two structures are not simply related by rotation of the η^6-toluene ring, and additional significant structural differences exist.

In **2a**, the ruthenium atom is not positioned over the center of the toluene ring but is displaced by approximately 0.2 Å from the ring midpoint in a direction away from the substituted arene ring carbon atom. Thus, the Ru–C1 and Ru–C6 distances [2.380 (3) and 2.342 (4) Å] are significantly longer than the average of the other Ru–C contacts [2.256 (4) Å]. In **2b**, the ruthenium atom is positioned approximately over the ring midpoint with $d(\text{Ru–C})_{av}$ = 2.267 (9) Å, $d(\text{Ru–C})_{max}$ = 2.310 (8) Å, and $d(\text{Ru–C})_{min}$ = 2.236 (8) Å. The difference in ring slippage in **2a** and **2b** is in fact close to that predicted in the calculated conformations B and A, respectively (vide infra).

The toluene ring in **2a** is slightly nonplanar with C1 and C4 being displaced by 0.020 (4) and 0.023 (4) Å, respectively, from the C1–C6 least-squares plane away from the ruthenium atom while C2 and C5 are displaced by 0.015 (4) and 0.017 (4) Å, respectively, toward the metal. This distortion corresponds to a folding of the ring about the C1–C4 vector such that the C1,C2,C3,C4 and C1,C4,C5,C6 groupings are planar within experimental error and the dihedral angle between these two planes is 3°. The π-arene ring in **2b** is planar within experimental error, but in this structure, the errors are larger and a slight ring folding would be unobservable. The C–C bond distances within the toluene rings are similar for **2a** [average 1.401 (6) Å] and **2b** [average 1.39 (1) Å] while the ring–methyl C–C bonds are slightly different [C1–C7 for **2a** is 1.493 (5) Å and for **2b**, 1.55 (1) Å].

The Ru–P and Ru–H distances in **2a** [2.320 (1) and 1.63 (4) Å] and **2b** [2.314 (2) and 1.64 (6) Å] are the same within experimental error but the P1RuP2 angle is significantly larger in **2b** [100.20 (7)°] compared with **2a** [95.20 (3)°]. The PRuH angles are the same within experimental error for the two structures. The Ru–C distances reveal a significant structural effect. The bonds which are most trans to the Ru–H vector are lengthened relative to the average Ru–C distance. This is especially evident in Figure 1 where, in **2a**, the Ru–C6 and, in **2b**, the Ru–C4 vectors are

Table III. Selected Distances and Angles

	2a	2b
	Distances, Å	
Ru–P1	2.320 (1)	2.316 (2)
Ru–P2	2.319 (1)	2.312 (2)
Ru–C1	2.380 (3)	2.288 (9)
Ru–C2	2.285 (4)	2.251 (9)
Ru–C3	2.237 (4)	2.265 (9)
Ru–C4	2.248 (3)	2.310 (8)
Ru–C5	2.254 (4)	2.236 (8)
Ru–C6	2.342 (4)	2.255 (8)
Ru–C7	3.612 (4)	3.50 (1)
Ru–H	1.63 (4)	1.64 (6)
C1–C7	1.493 (5)	1.55 (1)
C1–C2	1.431 (5)	1.41 (1)
C1–C6	1.394 (5)	1.39 (1)
C2–C3	1.394 (6)	1.41 (2)
C3–C4	1.401 (6)	1.40 (2)
C4–C5	1.385 (6)	1.34 (1)
C5–C6	1.399 (6)	1.38 (1)
P1–C1A	1.835 (3)	1.825 (7)
P1–C1B	1.844 (3)	1.847 (7)
P1–C1C	1.842 (3)	1.840 (7)
P2–C1D	1.837 (3)	1.845 (8)
P2–C1E	1.841 (3)	1.827 (8)
P2–C1F	1.840 (3)	1.843 (7)
	Angles, deg	
P1–Ru–P2	95.20 (3)	100.20 (7)
P1–Ru–H	76 (1)	77 (2)
P2–Ru–H	79 (1)	78 (2)
P1–Ru–C1	97.54 (8)	128.4 (3)
P1–Ru–C2	98.92 (9)	161.3 (3)
P1–Ru–C3	124.1 (1)	140.4 (5)
P1–Ru–C4	160.5 (1)	106.0 (4)
P1–Ru–C5	154.0 (1)	89.0 (3)
P1–Ru–C6	119.2 (1)	97.8 (2)
P2–Ru–C1	137.9 (1)	124.7 (3)
P2–Ru–C2	165.3 (1)	98.5 (3)
P2–Ru–C3	134.8 (1)	95.1 (3)
P2–Ru–C4	102.4 (1)	117.9 (4)
P2–Ru–C5	90.3 (1)	151.9 (3)
P2–Ru–C6	105.9 (1)	160.3 (3)
H–Ru–C1	143 (1)	88 (2)
H–Ru–C2	108 (1)	108 (2)
H–Ru–C3	89 (1)	143 (2)
H–Ru–C4	98 (1)	162 (2)
H–Ru–C5	130 (1)	130 (2)
H–Ru–C6	162 (1)	99 (2)
C2–C1–C7	119.9 (4)	122 (1)
C6–C1–C7	121.4 (4)	122 (1)
C1–C2–C3	120.8 (4)	122 (1)
C2–C3–C4	119.6 (4)	119 (1)
C3–C4–C5	119.4 (4)	117 (1)
C4–C5–C6	121.9 (4)	125 (1)
C5–C6–C1	119.6 (4)	120 (1)
C2–C1–C6	118.6 (3)	116 (1)

the most trans to the hydride (these H–Ru–C angles are each 162°) and are lengthened. In **2b**, this trans lengthening counters the slippage of the ruthenium atom away from the substituted arene carbon, resulting in a nearly symmetrical ring–metal interaction. In **2a**, the ring slippage is quite evident since the hydride is most trans to the ortho arene carbon atom C6. The average Ru–C(arene) bond lengths in **2a** [2.291 (4) Å] and **2b** [2.268 (9) Å] are slightly longer than those in the ruthenium arene complexes $(C_6H_6)RuCl_2(Ph_2PCH_3)$ and $(1,4\text{-}i\text{-}C_3H_7C_6H_4CH_3)\text{-}RuCl_2(Ph_2PCH_3)$.[16] In these compounds, the Ru–C bonds occur as one set of equivalent short (2.20 Å) and one set of equivalent long (2.26 Å) distances, the latter in each case

(16) Bennett, M. A.; Robertson, G. B.; Smith, A. K. *J. Organomet. Chem.* **1972**, *43*, C41.

(17) (a) Hoffmann, R. *J. Chem. Phys.* **1963**, *39*, 1397. (b) Hoffmann, R.; Lipscomb, W. N. *Ibid.* **1962**, *36*, 3179, 3489; *37*, 2872.

being trans to the phosphine ligand. The asymmetry in the arene–metal bonding was attributed to a trans bond-weakening property of the teritary phosphine.

Molecular Orbital Calculations

Calculations at the extended Hückel level[18] were utilized to probe the structural distortions observed in **2a** and **2b**. Geometric and computational details are given in the Experimental Section. The starting point is a model for the parent compound, $(C_6H_6)RuH(PH_3)_2^+$. The coordinate system and several geometrical variables are shown in **15**.

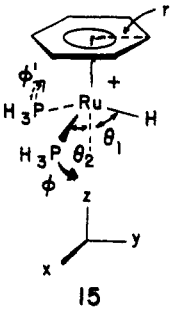

15

Here, θ_1 is the angle between the z axis and the Ru–H bond, θ_2 is the angle between the z axis and either of the two Ru–P bonds, and ϕ (along with ϕ') is the dihedral angle between the x axis and the the Ru–P bond. In all previously known 18-electron (arene)ML_3 complexes,[19] $\theta_1 \approx \theta_2 \approx 54.7°$ and $\phi = 330.0°$ ($\phi' = 210.0°$). Therefore, the metal has approximately an octahedral coordination geometry with all L–M–L angles equal to 90°. Furthermore, most complexes are very close to η^6 (r in **15** is 1.41 Å when the C–C bond lengths are 1.41 Å). It is obvious from Figure 1 that the ML_3 unit is significantly distorted from this archetypal "piano stool" arrangement. Independent optimization of θ_1, θ_2, ϕ, and r for (benzene)$RuH(PH_3)_2^+$ in the geometry shown in **15** gave values of $\theta_1 = 61°$, $\theta_2 = 55°$, $\phi = 338°$ ($\phi' = 202°$), and $r = 1.33$ Å. Thus, this compound is predicted to be slipped slightly away from a symmetric η^6 configuration, and, more significantly, the two phosphine ligands are distorted toward the T-shaped geometry evident in Figure 1. One might think that this distortion is merely a reflection of the small steric size of the hydrogen atom. However, we consider that an electronic effect must also be operative.

Figure 2 presents an interaction diagram for (C_6H_6)-$RuH(PH_3)_2^+$ in a pseudooctahedral geometry (i.e., $\theta_1 = \theta_2 = 54.7°$, $\phi = 330°$, $\phi' = 210°$). The three filled orbitals of benzene are shown on the left side of the figure. On the right side are the valence orbitals of a $RuH(PH_3)_2^+$ fragment. There is little difference compared to the normal ML_3 valence orbitals.[20,21] At low and nearly identical energies are 1a′, 1a″, and 2a′. These are the remnants of the t_{2g} set in an octahedral level splitting pattern. They overlap with the benzene orbitals to a minor extent in (polyene)ML_3 complexes[20,22] and consequently remain nonbonding in Figure 2. At high energy, the 4a′ fragment orbital is basically a metal s and p hybrid. It stabilizes the

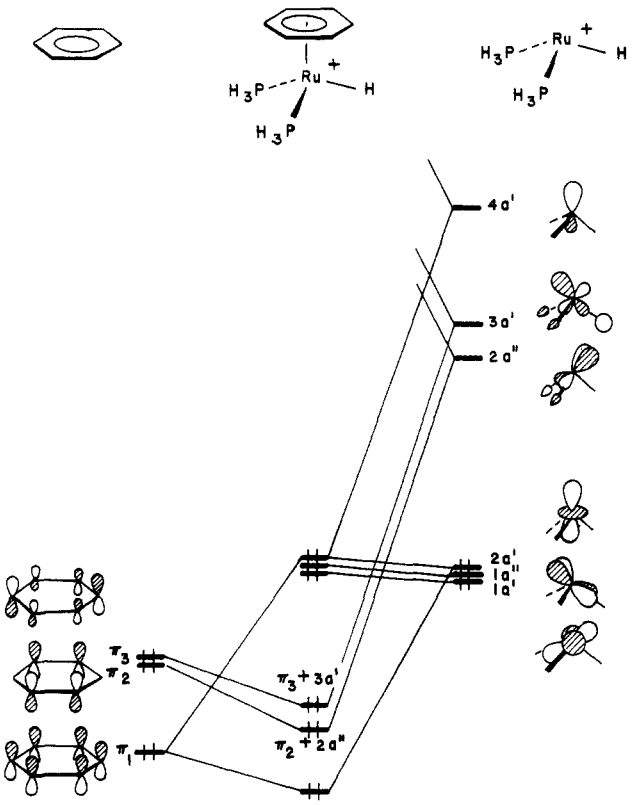

Figure 2. An orbital interaction diagram for (benzene)$RuH(PH_3)_2^+$ at the pseudooctahedral geometry.

lowest benzene π orbital π_1. The remaining two empty fragment orbitals, 2a″ and 3a′, lie at moderate energy. In a ML_3 complex where the ligands are identical, these levels are degenerate. In the pseudooctahedral configuration of the $RuH(PH_3)_2^+$ fragment, 3a′ lies 0.35 eV higher than 2a″. The reason for this derives from the fact that the hydrogen s orbital is initially higher in energy than the lone-pair hybrid of PH_3 before interaction with the metal d orbitals. Since 2a″ contains no hydrogen s character by symmetry while that in 3a′ is substantial, interaction between metal d and the ligand σ-donor functions sends 3a′ to higher energy than 2a″. A further consequence of this perturbation is that 3a′ contains significantly greater electron density at the hydrogen atom position and less at the metal compared to 2a″, which is more localized at the metal. In simplistic terms, the hydrogen behaves more like H^+ than a H^- ligand, an analogy which will be used below. The empty 2a″ and 3a′ orbitals overlap strongly with and stabilize the remaining two filled orbitals of benzene, π_2 and π_3, respectively. The resultant molecular orbitals, labeled π_2 + 2a″ and π_3 + 3a′ in Figure 2, are also nondegenerate; π_2 is stabilized more by 2a″ than π_3 is by 3a′. The reason for this is that 2a″ lies closer in energy to the degenerate π_2/π_3 set. Furthermore, because of the larger electron density at the metal in 2a′, its overlap with π_2 is larger than between 3a′ and π_3. In this geometry, the former is calculated to be 0.2313 and the latter 0.2246. Thus, for energy gap and overlap reasons, 2a″ is more strongly involved in bonding to the arene π system than is 3a′. A further consequence of this relationship is that the filled molecular orbital π_2 + 2a″ consists of 16.2% 2a″ character while there is only 8.1% 3a′ character in π_3 + 3a′. This provides the basis of the explanation of why the two phosphines move apart and approach a T-shaped $RuHP_2$ geometry.

Notice that, in Figure 2, 2a″ is antibonding between Ru and P. As ϕ in **15** increases from 330° (ϕ' decreases from 210°), the phosphine lone-pair functions move toward the

(18) Muetterties, E. L.; Bleeke, J. R.; Wucherer, E. J.; Albright, T. A. *Chem. Rev.* **1982**, *82*, 499 and references cited therein.
(19) Albright, T. A.; Hoffmann, R.; Hofmann, P. *J. Am. Chem. Soc.* **1977**, *99*, 754.
(20) (a) Elian, M.; Hoffmann, R. *Inorg. Chem.* **1975**, *14*, 1058. (b) Elian, M.; Chen, M. M. L.; Mingos, D. M. P.; Hoffmann, R. *Ibid.* **1976**, *158* 1148. (c) Burdett, J. *Ibid.* **1975**, *14*, 375.
(21) Albright, T. A.; Carpenter, B. K. *Inorg. Chem.* **1980**, *19*, 3092.
(22) (a) Radonovich, L. J.; Koch, F. J.; Albright, T. A. *Inorg. Chem.* **1980**, *19*, 3373. (b) Albright, T. A.; Hoffmann, R.; Tse, Y.-C.; D'Ottavio, T. *J. Am. Chem. Soc.* **1979**, *101*, 3801.

nodal plane at the metal. This causes 2a″ to be stabilized, and, therefore, it stabilizes π_2 more as ϕ increases than at the pseudooctahedral geometry. Counteracting the stabilization of π_2 + 2a″ along the distortion coordinate is the behavior of the 3a′ level. As ϕ increases, 3a′ rises in energy and therefore becomes a poorer acceptor. However, since 3a′ is less localized at the metal atom, the π_3 + 3a′ molecular orbital is initially not destabilized as much as π_2 + 2a″ is lowered in energy. In typical (arene)ML_3 systems where the three ligands have a more evenly balanced donor ability, the reverse situation occurs: π_3 + 3a′ is destabilized more than π_2 + 2a is stabilized and a regular piano stool geometry with ϕ = 300° and ϕ' = 210° results.

Another way to view this distortion is to consider the hydrogen ligand as H^+ interacting with Ru to a much lesser extent than do the phosphines. Consider the hypothetical $(C_6H_6)Ru(PH_3)_2$ molecule (**16**). The bonding in this type

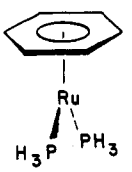

16

of 18-electron (arene)ML_2 complex has been described elsewhere.[23] These compounds, as well as their (cyclopentadienyl)ML_2 counterparts, are bases.[24] There are two high-lying occupied molecular orbitals in **16** which are shown in **17a** and **17b**. The empty s orbital of a proton,

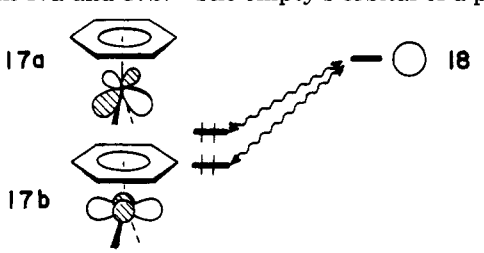

18, will maximize its overlap with **17** when the proton approaches $(C_6H_6)Ru(PH_3)_2$ in the direction shown by **19**.

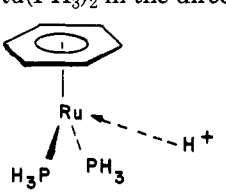

19

When the interaction between H^+ and **16** or **17** is weak, the phosphines will not bend back much from their original positions. When the interaction becomes stronger, more pyramidalization at $Ru(PH_3)_2$ occurs in turn causing **17a** and **17b** to intermix[25] so that a highly directional hybrid orbital is formed which can interact with the s orbital of the proton. The structures **2a** and **2b** can then be regarded as intermediate cases as the $Ru(PPh_3)_2$ moiety is not greatly pyramidalized (cf. Figure 1).

Our optimized structure of **15** shows the $RuH(PPh_3)_2$ unit to be slipped 0.08 Å away from an idealized η^6 position. The energy reduction associated with this distortion is quite small; the difference between the energy computed for r = 1.41 Å (at η^6) and r = 1.33 Å is only 0.2 kcal/mol. This slippage is connected with the angular distortion of

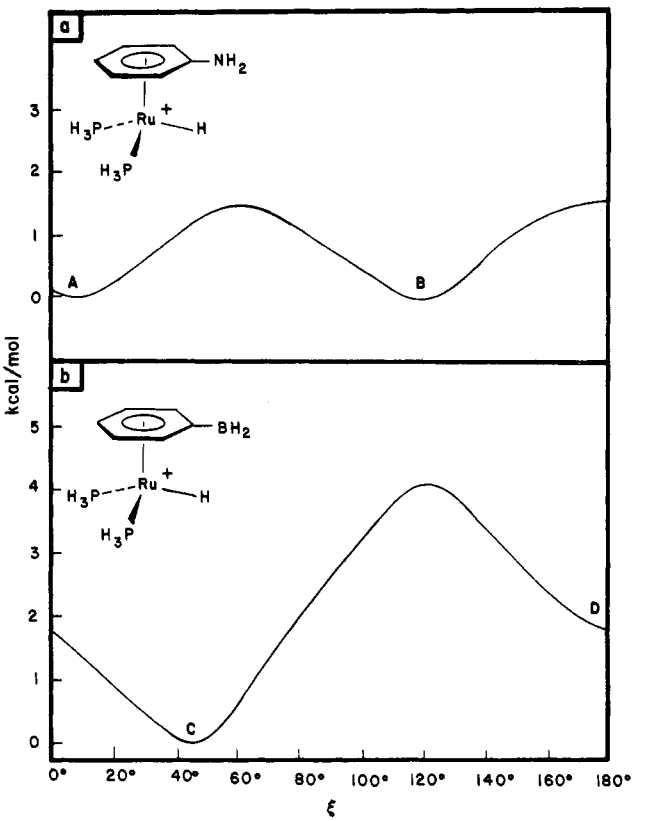

Figure 3. A plot of the relative energies vs. rotation angle, ξ, for (aniline)$RuH(PH_3)_2^+$ and (phenylborane)$RuH(PH_3)_2^+$. Here, ξ is defined as the dihedral angle made between the C–N or C–B bond and the Ru–H bonds.

the $RuH(PH_3)_2$ group and with the fact that the Ru–H and Ru–P bond energies are appreciably different. This is evidenced by the fact that in the ground-state geometries of $(C_6H_6)RuH(PH_3)_2^+$ with pseudooctahedral coordination at ruthenium ($\theta_1 = \theta_2$ = 54.74°, ϕ = 330°, ϕ' = 210°) and $(C_6H_6)Ru(PH_3)_3^{2+}$ are calculated to be at the η^6 value. In both instances, the potential for such a distortion mode is soft and it requires only approximately 2 kcal/mol to deform the structure to r = 1.33 Å.

The orbital description given for $(C_6H_6)RuH(PH_3)_2^+$ corresponds to the conformation in which the M–L bonds eclipse carbon atoms in the benzene ring. An alternative conformation exists wherein the M–L bonds are staggered and eclipse the C–C bonds, **20**. The most stable structure

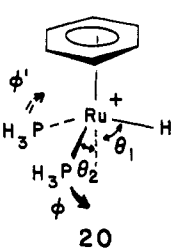

20

was found to be at the η^6 position with θ_1 = 60°, θ_2 = 55°, ϕ = 340°, and ϕ' = 200°. The total energy for it was computed to be a minuscule 0.01 kcal/mol lower than for the eclipsed conformation **14**. Here, returning to Figure 3, 3a′ interacts with π_2 and 2a″ with π_3. Since π_2 and π_3 are degenerate, these interactions are essentially identical with those described above for the eclipsed conformation. Notice that, again, the $RuH(PH_3)_2$ group is predicted to distort toward a T-shaped geometry for the same reasons given previously. Thus, the barrier to rotation in $(C_6H_6)RuH(PR_3)_2^+$ is predicted to be negligible, just as in other (benzene)ML_3 complexes.[20,25]

(23) Hofmann, P. *Angew. Chem.* **1977**, *89*, 551; Habilitationschrift, Universitat Erlangen (1978).
(24) Werner, H. *Angew. Chem., Int. Ed. Engl.* **1983**, *22*, 927.
(25) Albright, T. A. *Acc. Chem. Res.* **1982**, *15*, 149.

In the context of the NMR and structural studies reported here, it was of interest to learn how π-donor and π-acceptor substituent groups on the benzene ring would modify the conformational preference of the $RuH(PPh_3)_2$ group with respect to the arene ring. For computational efficiency, we have chosen NH_2 and BH_2 groups to model π-donor and π-acceptor groups, respectively. In each case, calculations were initially carried out by using an η^6 pseudooctahedral geometry and the rotational angle, ξ, defined as the dihedral angle between the C–R and Ru–H bonds, cf. **21**, was varied. Maxima and minima as well as

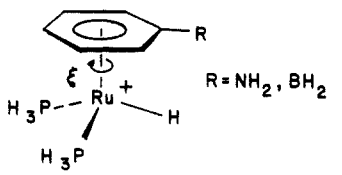

21

several points between were then reoptimized by varying θ_1, θ_2, ϕ, and ϕ' (see **14**) and slippage of the $RuH(PPh_3)_2$ group from a η^6 position. The results for (π-aniline)$RuH(PH_3)_2^+$ are shown in Figure 3a. Two minima were found, A and B, shown in a projection view in **22A** and **22B**. At

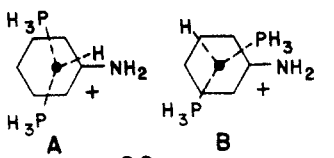

22

our computational level, they have identical energies. In **22A**, the values of θ_1, θ_2, ϕ, and ϕ' do not vary significantly from those given in the benzene system (vide supra). Importantly, while the arene in **22A** is expected to exhibit η^6 bonding, in **22B**, the $RuH(PH_3)_2^+$ unit slips 0.2 Å from η^6 in a direction away from the NH_2 substituent. In, η^6-toluene complexes, the methyl group is also a π-donor. Referring back to Figure 1, the arene conformation in (toluene)$RuH(PPh_3)_2^+BPh_4^-$, **2b**, is quite close to that calculated in **22B** and like the model structure, the metal is not significantly displaced from the ring sixfold axis. Similarly, the structure of (toluene)$RuH(PPh_3)_2^+HC(SO_2CF_3)_2^-$, **2a**, is conformationally like that of **22A**, and, as in the calculational model, the ruthenium is slipped away from the methyl substituent. As indicated by Figure 3, a relatively small barrier, 1.5 kcal/mol, connects the two ground-state conformations. Calculations on the model for an arene complex bearing a π-acceptor, (π-$PhBH_2$)-$RuH(PH_3)_2^+$, disclose that this compound also has two energy minima denoted as C and D in Figure 3b and corresponding to the conformations shown in projection view in **23C** and **23D**. Once again, the $RuH(PH_3)_2$ unit

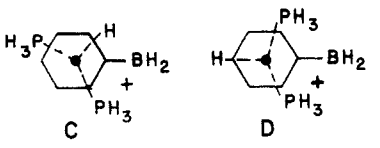

23

is distorted toward a T-shaped geometry. In **23C**, the phenylborane is η^6 bonded while in **23D**, the metal is displaced approximately 0.2 Å toward the borane group. Conformation C is calculated to be 1.8 kcal/mol more stable than D, and a 4.1 kcal/mol barrier connects the two.

The conformational preferences displayed by **22** and **23** are easily rationalized. It has been previously demonstrated in some detail that donor-substituted (arene)ML_3 complexes prefer the conformation shown in **24** while for those bearing instead acceptor substituents, conformation **25** is preferred.[19,25] A d^6 ML_3 group possesses three empty

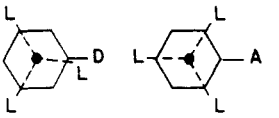

24 **25**

hybrid orbitals whose radial extent toward the arene differs little from 2a″, 3a′, and 4a′ in Figure 2 for the $RuH(PH_3)_2$ fragment. Likewise, there are three filled orbitals which match 1a′, 1a″, and 2a′ in shape. Therefore, it is not surprising that conformations **22A** and **22B** match that of **24** while **23C** and **23D** are close to **25**. An orbital analysis of these conformational preferences is totally analogous to the rationale presented elsewhere[19,25] for the generalized (arene)ML_3 system.

Experimental Section

NMR spectra were obtained on a Varian XL-200 instrument. Bis[(trifluoromethyl)sulfonyl]methane, prepared by the method of Koshar and Mitsch,[26] was the gift of R. J. Koshar, 3M Industrial and Consumer Sector Research Laboratory. Arene solvents were deoxygenated by purging with nitrogen and dried with 4A molecular sieves.

(Toluene)$RuH(PPh_3)_2^+HC(SO_2CF_3)_2^-$, 2a. Toluene, 15 mL, was added to 1.0 g of $(Ph_3P)_4RuH_2$ and 0.25 g of $H_2C(SO_2CF_3)_2$ contained in a nitrogen-filled Schlenk flask. The reaction mixture was stirred and heated at 85 °C for 16 h. After the mixture was cooled to room temperature, the light yellow solid phase was isolated by filtration and twice recrystallized by slow rotary evaporation of a dichloromethane–toluene solution. The yield of **2a** was 0.5 g (58%). Anal. Calcd: C, 55.4; H, 4.0; P, 6.2; Ru, 10.1; S, 6.2. Found: C, 55.4; H, 4.0; P, 6.3; Ru, 10.0; S, 6.4. Crystals of **2a** used for X-ray crystallography were grown by slow evaporation of a solution in dichloromethane–toluene.

Additon of ethanolic $NaBPh_4$ to a solution of **2a** in ethanol caused precipitation of the BPh_4^- salt **2b** in essentially quantitative yield. Anal. Calcd: C, 77.5; H, 5.7. Found: C, 77.2; H, 5.7. Crystals of **2b** used for X-ray crystallography were grown by slow diffusion of ethanol into a dichloromethane solution of the compound.

Other (arene)$RuH(PPh_3)_2^+$ salts reported in this paper were prepared in an analogous manner using the neat arene as solvent. The compounds were characterized by satisfactory microanalyses and ^1H NMR spectra.

Collection and Reduction of X-ray Data. A summary of crystal and intensity collection data for **2a** and **2b** is presented in Table IV. Crystals of both compounds were attached to glass fibers with fast setting epoxy resin. Both crystals were found to belong to the monoclinic crystal class by the Enraf-Nonius CAD4-SDP peak search, centering and indexing programs.[26] The space groups were chosen on the basis of systematic absences observed during data collection and were verified by successful solution and refinement. The unit cell dimensions were determined by least-squares refinement of the angular settings of 25 peaks centered on the diffractometer. The intensities of three standard reflections were measured every 1.5 h of X-ray exposure, and no decay with time was noted for either compound. The data were corrected for Lorentz, polarization, and background effects. Corrections for absorption were not made because psi scan data showed that the variation in transmission factors was less that 3% for both compounds.

Solution and Refinement of the Structures. The structures were solved by conventional heavy-atom techniques. The ruthenium atoms were located by Patterson syntheses and full-matrix least-squares refinement and difference Fourier calculations were used to locate all remaining non-hydrogen atoms. The metal hydride atoms were located in both compounds by difference Fourier analysis during the final stages of refinement. These hydride atoms were refined with use of isotropic thermal pa-

(26) Koshar, R. J.; Mitsch, R. J. *J. Org. Chem.* **1973**, *38*, 3358.

Table IV. Summary of Crystal Data and Intensity Collection

	2a	2b
	Crystal Parameters	
cryst system	monoclinic	monoclinic
space group	$P2_1/a$	$P2_1/c$
cryst dimens, mm	0.2 × 0.3 × 0.2	0.2 × 0.1 × 0.2
cell parameters		
a, Å	27.571 (4)	15.816 (2)
b, Å	13.620 (2)	16.816 (2)
c, Å	11.632 (3)	20.988 (7)
α, deg	90	90
β, deb	94.05 (2)	103.39 (2)
γ, deg	90	90
V, Å^3	4357 (3)	5430 (2)
Z	4	4
d(calcd), g cm^{-3}	1.521	1.270
abs coeff, cm^{-1}	5.92	3.79
formula	$C_{46}H_{40}F_6O_4P_2S_2Ru_1$	$C_{67}H_{59}B_1P_2Ru_1$
fw	997.97	1038.05
	Measurement of Intensity Data	
diffractometer	CAD 4	CAD 4
radiatn	Mo K$\bar{\alpha}$ (λ = 0.710 69 Å) graphite monochromatized	Mo K$\bar{\alpha}$ graphite monochromatized
scan type and range, 2θ, deg	ω–2θ, 0–50	ω–2θ, 0–46
unique reflctns measd (region)	7661 ($\pm h$,+k,+l)	8431 (+h,+k,$\pm l$)
obsd reflctns[a]	5115 [$F_o^2 > 3\sigma(F_o^2)$]	3825 [$F_o^2 > 2\sigma(F_o^2)$]
refinement of full-matrix least squares		
no. of parameters	554	337
R[b]	0.035	0.065
R_w[b]	0.046	0.065
GOF[b]	1.28	1.58
p[a]	0.04	0.04

[a] The intensity data were processed as described in: "CAD4 and SDP User's Manual"; Enraf-Nonius: Delft, Holland, 1978. The net intensity $I = [K/(\mathrm{NPI})](C - 2B)$, where K = 20.1166 × attenuator factor, NPI = ratio of fastest possible scan rate to scan rate for the measurement, C = total count, and B = total background count. The standard deviation in the net intensity is given by $[\sigma(I)]^2 = (K/(\mathrm{NPI}))^2[C + 4B + (pI)^2]$, where p is a factor used to downweight intense reflections. The observed structure factor amplitude F_o is given by $F_o = (I/Lp)^{1/2}$, where Lp = Lorentz and polarization factors. The $\sigma(I)$'s were converted to the estimated errors in the relative structure factors $\sigma(F_o)$ by $\sigma(F_o) = {}^1/_2[\sigma(I)/I]F_o$. [b] The function minimized was $\sum w(|F_o| - |F_c|)^2$, where $w = 1/[\sigma(F_o)]^2$. The unweighted and weighted residuals are defined as $R = (\sum||F_o| - |F_c||)/\sum|F_o|$ and $R_w = [(\sum w(|F_o| - |F_c|))^2/(\sum w|F_o|)^2]^{1/2}$. The error in an observation of unit weight (GOF) is $[\sum w(|F_o| - |F_c|)^2/(\mathrm{NO} - \mathrm{NV})]^{1/2}$, where NO and NV are the number of observations and variables, respectively.

Table V. Positional and Thermal Parameters and Their Estimated Standard Deviations for 2a[a]

atom	x	y	z	B(iso), Å^2	atom	x	y	z	B(iso), Å^2
Ru	0.16061 (1)	0.20431 (2)	0.23745 (3)	2.313	C4B	0.1224 (2)	0.6228 (3)	0.2755 (5)	5.023
S1	0.17135 (4)	0.22168 (8)	0.7780 (1)	3.326	C5B	0.0975 (2)	0.5770 (4)	0.3575 (5)	4.937
S2	0.18347 (5)	0.43194 (9)	0.8288 (1)	4.283	C6B	0.0855 (2)	0.4773 (3)	0.3459 (4)	3.754
P1	0.08863 (3)	0.29313 (7)	0.22833 (8)	2.066	C1C	0.0462 (1)	0.2655 (3)	0.3394 (3)	2.620
P2	0.12358 (3)	0.05196 (7)	0.24752 (8)	2.071	C2C	0.0673 (2)	0.2591 (3)	0.4514 (4)	3.737
F1A	0.2381 (1)	0.0930 (3)	0.7356 (3)	7.561	C3C	0.0379 (2)	0.2439 (4)	0.5424 (4)	5.075
F1B	0.2460 (1)	0.1516 (3)	0.9039 (3)	7.667	C4C	−0.0105 (2)	0.2341 (4)	0.5224 (4)	5.323
F1C	0.2656 (1)	0.2361 (3)	0.7633 (4)	7.612	C5C	−0.0319 (2)	0.2379 (4)	0.4119 (5)	5.073
F2A	0.1100 (2)	0.4464 (3)	0.6726 (4)	10.103	C6C	−0.0028 (2)	0.2552 (3)	0.3191 (4)	3.538
F2B	0.0937 (1)	0.4893 (3)	0.8417 (4)	9.381	C1D	0.0572 (1)	0.0382 (3)	0.2454 (3)	2.206
F2C	0.1364 (2)	0.5831 (3)	0.7420 (5)	11.383	C2D	0.0323 (1)	0.0050 (3)	0.3387 (4)	3.196
O11	0.1659 (1)	0.2434 (3)	0.6578 (3)	4.899	C3D	−0.0174 (2)	−0.0061 (4)	0.3271 (4)	3.920
O12	0.1441 (1)	0.1431 (2)	0.8231 (3)	4.551	C4D	−0.0436 (2)	0.0151 (4)	0.2262 (4)	4.154
O21	0.2152 (1)	0.4378 (3)	0.7366 (3)	5.333	C5D	−0.0194 (2)	0.0488 (3)	0.1325 (4)	3.658
O22	0.3058 (1)	0.9880 (3)	0.0686 (3)	6.370	C6D	0.0304 (1)	0.0590 (3)	0.1435 (4)	2.777
C1	0.2074 (1)	0.3120 (3)	0.3625 (4)	3.142	C1E	0.1440 (1)	−0.0181 (3)	0.3774 (3)	2.295
C2	0.2144 (1)	0.3322 (3)	0.2441 (4)	3.231	C2E	0.1638 (2)	−0.1114 (3)	0.3726 (4)	3.187
C3	0.2300 (1)	0.2589 (4)	0.1716 (4)	3.455	C3E	0.1757 (2)	−0.1640 (4)	0.4739 (4)	4.201
C4	0.2384 (1)	0.1640 (3)	0.2150 (4)	3.527	C4E	0.1686 (2)	−0.1217 (4)	0.5795 (4)	4.240
C5	0.2291 (1)	0.1434 (3)	0.3279 (4)	3.659	C5E	0.1508 (2)	−0.0286 (4)	0.5854 (4)	3.681
C6	0.2141 (1)	0.2162 (3)	0.4026 (4)	3.481	C6E	0.1388 (2)	0.0244 (3)	0.4856 (4)	3.137
C7	0.1973 (2)	0.3942 (4)	0.4423 (5)	4.775	C1F	0.1348 (1)	−0.0328 (3)	0.1291 (3)	2.329
C1A	0.0512 (1)	0.3013 (3)	0.0918 (3)	2.539	C2F	0.1092 (1)	−0.1219 (3)	0.1779 (4)	2.950
C2A	0.0613 (1)	0.2476 (3)	−0.0057 (4)	3.044	C3F	0.1182 (2)	−0.1868 (3)	0.0301 (4)	3.615
C3A	0.0330 (2)	0.2581 (4)	−0.1076 (4)	4.258	C4F	0.1521 (2)	−0.1641 (4)	−0.0467 (4)	4.306
C4A	−0.0052 (2)	0.3218 (4)	−0.1156 (4)	4.915	C5F	0.1769 (2)	−0.0779 (4)	−0.0377 (4)	4.559
C5A	−0.0159 (2)	0.3765 (3)	−0.0204 (5)	4.564	C6F	0.1684 (2)	−0.0114 (3)	0.0494 (4)	3.388
C6A	0.0123 (2)	0.3677 (3)	0.0821 (4)	3.464	C0S	0.1693 (2)	0.3187 (3)	0.8632 (4)	3.641
C1B	0.0991 (1)	0.4257 (3)	0.2506 (3)	2.494	C1S	0.2335 (2)	0.1738 (4)	0.7957 (5)	4.568
C2B	0.1232 (1)	0.4754 (3)	0.1662 (4)	3.083	C2S	0.1285 (2)	0.4903 (4)	0.7695 (6)	6.862
C3B	0.1347 (2)	0.5732 (3)	0.1800 (5)	4.340	H	0.139 (1)	0.190 (3)	0.104 (3)	4.6 (3)[b]

[a] The form of the anisotropic thermal parameter is $\exp[-(B(1,1)H^2 + B(2,2)k^2 + B(3,3)l^2 + B(1,2)hk + B(1,3)hl + B(2,3)kl)]$. [b] Refined with isotropic thermal parameter.

Table VI. Table of Positional Parameters and Their Estimated Standard Deviations for 2b[a]

atom	x	y	z	B, Å²	atom	x	y	z	B, Å²
Ru	0.25897 (5)	0.24452 (5)	0.10715 (4)	3.25 (1)	C3E	0.1821 (7)	0.4728 (7)	0.2397 (6)	7.5 (3)*
P1	0.2908 (1)	0.1747 (1)	0.2050 (1)	2.95 (5)	C4E	0.2391 (8)	0.5174 (8)	0.2853 (6)	8.5 (4)*
P2	0.3370 (2)	0.3598 (2)	0.1389 (1)	3.37 (6)	C5E	0.3242 (8)	0.5175 (8)	0.2879 (6)	8.4 (4)*
C1	0.2257 (6)	0.1953 (6)	0.0027 (5)	5.0 (3)	C6E	0.3582 (7)	0.4682 (6)	0.2447 (5)	5.6 (3)*
C2	0.2025 (7)	0.2763 (6)	0.0017 (4)	6.3 (3)	C1F	0.4563 (6)	0.3553 (5)	0.1666 (4)	4.0 (2)*
C3	0.1460 (7)	0.3063 (7)	0.0389 (5)	7.7 (3)	C2F	0.4983 (6)	0.2864 (6)	0.1877 (5)	4.3 (2)*
C4	0.1093 (6)	0.2536 (8)	0.0769 (5)	7.0 (3)	C3F	0.5894 (7)	0.2831 (6)	0.2110 (5)	5.5 (3)*
C5	0.1340 (6)	0.1772 (7)	0.0780 (5)	5.2 (3)	C4F	0.6338 (7)	0.3525 (6)	0.2102 (5)	5.6 (3)*
C6	0.1895 (6)	0.1462 (6)	0.0427 (4)	4.7 (3)	C5F	0.5952 (7)	0.4203 (6)	0.1889 (5)	5.7 (3)*
C7	0.2854 (8)	0.163 (1)	−0.0402 (5)	10.1 (5)	C6F	0.5048 (6)	0.4250 (6)	0.1659 (5)	5.2 (2)*
C1A	0.3079 (5)	0.0726 (5)	0.1813 (4)	2.9 (2)*	B	0.8246 (6)	0.1964 (6)	0.0549 (5)	3.2 (2)*
C2A	0.2438 (6)	0.0145 (5)	0.1756 (4)	3.6 (2)*	C1G	0.8883 (5)	0.1204 (5)	0.0828 (4)	3.0 (2)*
C3A	0.2526 (6)	−0.0576 (6)	0.1465 (5)	4.5 (2)*	C2G	0.8962 (6)	0.0532 (5)	0.0445 (4)	3.9 (2)*
C4A	0.3261 (6)	−0.0739 (6)	0.1253 (5)	5.1 (2)*	C3G	0.9481 (6)	−0.0112 (6)	0.0679 (5)	4.6 (2)*
C5A	0.3917 (6)	−0.0187 (6)	0.1315 (5)	5.1 (2)*	C4G	0.9959 (6)	−0.0120 (6)	0.1311 (5)	4.4 (2)*
C6A	0.3820 (6)	0.0552 (5)	0.1587 (4)	3.8 (2)*	C5G	0.9917 (6)	0.0533 (6)	0.1704 (4)	4.1 (2)*
C1B	0.3835 (5)	0.1967 (5)	0.2742 (4)	3.2 (2)*	C6G	0.9389 (5)	0.1173 (5)	0.1473 (4)	3.4 (2)*
C2B	0.3808 (6)	0.2688 (5)	0.3059 (4)	4.2 (2)*	C1H	0.8540 (5)	0.2731 (5)	0.1036 (4)	3.4 (2)*
C3B	0.4462 (6)	0.2897 (6)	0.3601 (5)	5.2 (2)*	C2H	0.9066 (6)	0.3312 (6)	0.0885 (4)	4.2 (2)*
C4B	0.5117 (6)	0.2370 (6)	0.3814 (5)	5.5 (2)*	C3H	0.9391 (7)	0.3948 (7)	0.1323 (6)	6.6 (3)*
C5B	0.5177 (7)	0.1669 (6)	0.3522 (5)	5.8 (3)*	C4H	0.9175 (7)	0.3952 (6)	0.1914 (5)	5.7 (3)*
C6B	0.4506 (6)	0.1446 (6)	0.2971 (5)	4.8 (2)*	C5H	0.8670 (6)	0.3413 (6)	0.2079 (5)	5.3 (2)*
C1C	0.2071 (5)	0.1685 (5)	0.2528 (4)	3.3 (2)*	C6H	0.8328 (6)	0.2790 (6)	0.1637 (5)	4.8 (2)*
C2C	0.2152 (6)	0.1117 (5)	0.3020 (4)	4.0 (2)*	C1I	0.8327 (5)	0.2210 (5)	−0.0197 (4)	2.9 (2)*
C3C	0.1547 (6)	0.1080 (6)	0.3416 (5)	5.0 (2)*	C2I	0.7692 (5)	0.2641 (5)	−0.0627 (4)	3.9 (2)*
C4C	0.0896 (6)	0.1639 (6)	0.3314 (5)	5.2 (2)*	C3I	0.7799 (6)	0.2921 (6)	−0.1243 (5)	5.5 (3)*
C5C	0.0823 (6)	0.2213 (6)	0.2860 (5)	5.2 (3)*	C4I	0.8547 (6)	0.2760 (6)	−0.1420 (5)	5.7 (3)*
C6C	0.1422 (6)	0.2230 (5)	0.2449 (4)	4.2 (2)*	C5I	0.9173 (6)	0.2325 (6)	−0.1027 (5)	5.4 (2)*
C1D	0.3285 (6)	0.4264 (5)	0.0679 (4)	3.9 (2)*	C6I	0.9083 (6)	0.2059 (5)	−0.0422 (4)	4.0 (2)*
C2D	0.2787 (6)	0.4944 (6)	0.0588 (5)	5.0 (2)*	C1J	0.7226 (5)	0.1721 (5)	0.0524 (4)	3.2 (2)*
C3D	0.2737 (7)	0.5403 (7)	0.0021 (6)	6.6 (3)*	C2J	0.6608 (6)	0.2289 (5)	0.0573 (4)	4.4 (2)*
C4D	0.3200 (7)	0.5210 (7)	−0.0411 (5)	6.6 (3)*	C3J	0.5722 (6)	0.2096 (6)	0.0532 (5)	5.4 (3)*
C5D	0.3708 (7)	0.4543 (7)	−0.0333 (5)	6.5 (3)*	C4J	0.5473 (7)	0.1350 (7)	0.0441 (5)	6.2 (3)*
C6D	0.3763 (6)	0.4070 (6)	0.0216 (5)	5.3 (3)*	C5J	0.6017 (7)	0.0769 (7)	0.0389 (5)	6.0 (3)*
C1E	0.3015 (6)	0.4229 (6)	0.1986 (4)	4.3 (2)*	C6J	0.6905 (6)	0.0967 (6)	0.0447 (5)	4.7 (2)*
C2E	0.2129 (7)	0.4268 (6)	0.1959 (5)	5.6 (3)*	H	0.359 (4)	0.215 (4)	0.113 (3)	4 (2)*

[a] Atoms with an asterisk were refined isotropically. Anisotropically refined atoms are given in the form of the isotropic equivalent thermal parameter defines as $(^4/_3)[a^2B(1,1) + b^2B(2,2) + c^2B(3,3) + ab(\cos\gamma)B(1,2) + ac(\cos\beta)B(1,3) + bc(\cos\alpha)B(2,3)]$.

Table VII. Parameters Used in the Extended Hückel Calculations

orbital		H_{ii}, eV	ξ_1	ξ_2	C_1[a]	C_2[a]
Ru	5s	−8.51	2.08			
	5p	−5.09	2.04			
	4d	−12.29	5.378	2.303	0.5340	0.6365
P	3s	−18.60	1.60			
	3p	−14.00	1.60			
C	2s	−21.40	1.625			
	2p	−11.40	1.625			
B	2s	−15.20	1.30			
	2p	−8.20	1.30			
N	2s	−26.00	1.95			
	2p	−13.40	1.95			
H	1s	−13.60	1.30			

[a] Contraction coefficients used in the double-ζ expansion.

rameters. All other hydrogen atoms were included in the structure factor calculations but were not refined. Their positions were calculated by use of program HYDRO[27] and a C–H distance of 0.95 Å. The atomic scattering factors were taken from the usual tabulation,[28] and the effects of anomalous dispersion were included in F_c by using Cromer and Ibers' values of $\Delta f'$ and $\Delta f''$.[29] In **2b**, a region of electron density was observed in the final difference Fourier map near a center of symmetry. The maximum peaks in this region correspond to 0.8 e Å^{-3} whereas a phenyl hydrogen atom has a height of 0.6 e Å^{-3}. Attempts to model this electron density with carbon atoms were unsuccessful, and consistently led to low occupancy factors (<0.2) and high thermal parameters ($B > 20$ Å^2). It is suspected that a small amount of residual solvent was present but since a reasonable model could not be found, no atom positions were included in the refinement or structure factor calculations. The final positional and thermal parameters of the refined atoms for **2a** and **2b** appear in Tables V and VI, respectively, and as supplementary material.[30] ORTEP drawings of the coordination cores of both compounds are shown in Figure 1, and complete labeling schemes are included as supplementary material.

Molecular Orbital Calculations. All extended Hückel calculations were carried out with the modified Wolfsberg–Helmholtz formula.[31] The H_{ii}'s and orbital exponents listed in Table V were taken from previous work.[19,32] All C–C, C–H, Ru–P, Ru–H, C–B, C–N, B–H, N–H, and P–H bond lengths were idealized at 1.41, 1.09, 2.32, 1.63, 1.41, 1.41, 1.16, 1.01, and 1.42 Å, respectively. The C–C–C–, C–C–B(N), and C–C–H angles were fixed at 120°. The distance of the ruthenium atom to the planes of the arene rings was set at 1.811 Å. Other parameters used in the extended Hückel calculations are given in Table VII.

Acknowledgment. We are grateful to the staff of the 3M Analytical and Properties Research Laboratory for the spectroscopic and analytical data, to J. R. Hill for obtaining the NMR data, and to Dr. W. Hendrickson, 3M Process

(27) All calculations were carried out on PDP 8A and 11/34 computers with use of the Enraf-Nonius CAD 4-SDP-PLUS programs. This crystallographic computing package is described by: Frenz, B. A. In "Computing in Crystallography"; Schenk, H., Olthof-Hazekamp, R., van Konigsveld, H., Bassi, G. C., Eds.; Delft University Press: Delft, Holland, 1978; pp 64–71; In "Structure Determination Package and SDP-PLUS User's Guide"; B. A. Frenz & Associates, Inc.: College Station, TX, 1982.

(28) Cromer, D. T.; Waber, J. T. "International Tables for X-Ray Crystallography"; Kynoch Press: Birmingham, England, 1974; Vol. IV, Table 2.2.4. Cromer, D. T. *Ibid.* Table 2.3.1.

(29) D. T. Cromer and J. A. Ibers in ref 27.

(30) See paragraph at end of paper regarding supplementary material.

(31) Ammeter, J. H.; Burgi, H.-B.; Thibeault, J. C.; Hoffmann, R. *J. Am. Chem. Soc.* **1978**, *100*, 3686.

(32) DuBois, D. L.; Hoffmann, R. *Nouv. J. Chim.* **1977**, *1*, 479.

Technologies Laboratory, for his seminal interpretation of the ^1H NMR spectrum of **2a**. L.H.P. acknowledges support by the National Science Foundation (Grant CHE-81-08490) of his contribution to this research. T.A.A. thanks the Robert A. Welch Foundation and the donors Petroleum Research Foundation, administered by the American Chemical Society, for generous support of his work.

Registry No. 1, 428-76-2; **2a**, 98877-86-2; **2b**, 98878-06-9; **3a**, 98877-87-3; **3b**, 98878-07-0; **4a**, 98877-89-5; **4b**, 98878-08-1; **5a**, 98877-91-9; **5b**, 98878-09-2; **6a**, 98877-93-1; **6b**, 98878-10-5; **7a**, 98877-95-3; **7b**, 98878-11-6; **8a**, 98877-97-5; **8b**, 98878-12-7; **9a**, 98877-99-7; **9b**, 98878-13-8; **10a**, 98878-01-4; **10b**, 98878-14-9; **11a**, 98878-03-6; **11b**, 98878-15-0; **12a**, 98878-05-8; **12b**, 98878-16-1; **13a**, 98901-13-4; **13b**, 98878-18-3; **14a**, 98878-19-4; **14b**, 98878-20-7; $(C_6H_6)RuH(PH_3)_2^+$, 98878-21-8; $(C_6H_5NH_2)RuH(PH_3)_2^+$, 98878-22-9; $(C_6H_5BH_2)RuH(PH_3)_2^+$, 98878-23-0; $(Ph_3P)_4RuH_2$, 19529-00-1; $C_6H_5CH_3$, 108-88-3; C_6H_6, 71-43-2; *o*-$CH_3C_6H_4CH_3$, 95-47-6; *m*-$CH_3C_6H_4CH_3$, 108-38-3; *p*-$CH_3C_6H_4CH_3$, 106-42-3; $C_6H_5C_2H_5$, 100-41-4; $C_6H_5CH(CH_3)_2$, 98-82-8; $C_6H_5COCH_3$, 98-86-2; $C_6H_5OCH_3$, 100-66-3; C_6H_5Cl, 108-90-7; C_6H_5F, 462-06-6; *p*-$FC_6H_4CH_3$, 352-32-9; Rh, 7440-16-6; Ph_3P, 603-35-0.

Supplementary Material Available: Tables of shortest interionic distances, general temperature expressions for **2a**, positional and thermal parameters for hydrogen atoms in **2a**, distances and angles within the $HC(SO_2CF_3)_2^-$ ion in **2a**, weighted least-squares planes for **2a**, general temperature factor expressions for **2b**, positional and thermal parameters for **2b**, distances and angles within the BPh_4^- ion in **2b**, weighted least-squares planes for **2b**, and observed and calculated structure factor amplitudes for **2a** and **2b** and complete labeling schemes for **2a** and **2b** and the $HC(SO_2CF_3)_2^-$ ion (55 pages). Ordering information is given on any current masthead page.

Synthesis and X-ray Crystallographic Characterization of the Binuclear Iron Complexes $(CO)_3Fe(\mu\text{-}PPh_2)(\eta^2\text{-}(C,P)\text{-}\mu\text{-}CH(CN)PPh_2)Fe(CO)_3$ and $(CO)_3Fe(\mu\text{-}PPh_2)(\eta^2\text{-}(P,P')\text{-}\mu\text{-}Ph_2PC(CN)PPh_2)Fe(CO)_3$

Yuan-Fu Yu and Andrew Wojcicki*

Department of Chemistry, The Ohio State University, Columbus, Ohio 43210

Mario Calligaris† and Giorgio Nardin

Dipartimento di Scienze Chimiche, Università di Trieste, 34127 Trieste, Italy

Received April 19, 1985

Reaction of $[(CO)_3Fe(\mu\text{-}PPh_2)(\mu\text{-}CO)Fe(CO)_2(PPh_2H)]^-$ with ICH_2CN in THF at −78 to 25 °C yielded two new binuclear iron complexes, $(CO)_3Fe(\mu\text{-}PPh_2)(\eta^2\text{-}(C,P)\text{-}\mu\text{-}CH(CN)PPh_2)Fe(CO)_3$ (**1**) and $(CO)_3Fe(\mu\text{-}PPh_2)(\eta^2\text{-}(P,P')\text{-}\mu\text{-}Ph_2PC(CN)PPh_2)Fe(CO)_3$ (**2**), in addition to $Fe_2(CO)_6(\mu\text{-}PPh_2)_2$. Complexes **1** and **2** were characterized by elemental analysis, FAB mass spectrometry, ^1H, ^{13}C, and ^{31}P NMR spectroscopy, and single-crystal X-ray diffraction techniques. Crystals of **1** are monoclinic of space group $P2_1/c$ with a = 11.070 (2) Å, b = 33.535 (6) Å, c = 17.595 (5) Å, β = 112.45 (3)°, and Z = 8. The structure was solved and refined to R = 0.053 and R_w = 0.100 by using 10,277 independent reflections. The complex is a racemate owing to the presence of a chiral carbon center, FeCH(CN)P. Two bridging ligands, PPh_2 and η^2-(*C*,*P*)-$CH(CN)PPh_2$, support an Fe–Fe bond of 2.807 (1) Å (average) in a folded arrangement of two Fe atoms and P and C donor atoms. Crystals of **2** are monoclinic, space group $P2_1/c$, with a = 13.033 (3) Å, b = 13.124 (6) Å, c = 23.929 (5) Å, β = 96.89 (2)°, and Z = 4. The structure was solved and refined to R = 0.042 and R_w = 0.054 by using 5739 independent reflections. The bridging ligands PPh_2 and symmetric η^2-(*P*,*P'*)-$Ph_2PC(CN)PPh_2$ support an Fe–Fe bond of 2.727 (1) Å. The arrangement of the two Fe and three P atoms is essentially planar.

Introduction

We have previously shown[1] that $Fe_2(CO)_6(\mu\text{-}PPh_2)_2$ reacts with $LiBEt_3H$ in THF to afford a novel binuclear anion $[(CO)_3Fe(\mu\text{-}PPh_2)(\mu\text{-}CO)Fe(CO)_2(PPh_2H)]^-$. This anion has been converted to the bridging acyl complexes $(CO)_3Fe(\mu\text{-}PPh_2)(\mu\text{-}C(R)O)Fe(CO)_2(PPh_2R)$ upon treatment with an excess of RI (R = Me and Et). In an attempt to ascertain whether binuclear iron–alkyl intermediates are formed in these reactions, we examined the behavior of $[(CO)_3Fe(\mu\text{-}PPh_2)(\mu\text{-}CO)Fe(CO)_2(PPh_2H)]^-$ toward ICH_2CN. The presence of an electron-withdrawing CN group in the CH_2CN ligand contributes to a strong M–R σ bond, and, accordingly, MCH_2CN complexes display little tendency to undergo migratory insertion reactions.[2] Such lack of reactivity suggested that a desired diiron–cyanomethyl complex might be a stable and an isolable species.

To our surprise, we discovered that, in the reaction examined, CH_2CN moiety readily loses hydrogen, and the

† Inquiries concerning the X-ray crystallographic work should be directed to the Trieste address.

(1) Yu, Y.-F.; Gallucci, J.; Wojcicki, A. *J. Am. Chem. Soc.* **1983**, *105*, 4826.

(2) (a) Ros, R.; Renaud, J.; Roulet, R. *Helv. Chim. Acta* **1975**, *58*, 133. (b) Ros, R.; Michelin, R. A.; Carturan, G.; Belluco, U. *J. Organomet. Chem.* **1977**, *133*, 213. (c) Michelin, R. A.; Ros, R. *Ibid.* **1979**, *169*, C42.

0276-7333/86/2305-0047$01.50/0

Synthesis and x-ray crystallographic characterization of the binuclear iron complexes cyclic (CO)3Fe(.mu.-PPh2)(.eta.2-(C,P)-.mu.-CH(CN)PPh2)Fe(CO)3 and cyclic (CO)3Fe(.mu.-PPh2)(.eta.2-(P,P')-.mu.-Ph2PC(CN)PPh2)Fe(CO)3

Yuan Fu. Yu, Andrew. Wojcicki, Mario. Calligaris, and Giorgio. Nardin

Organometallics, **1986**, 5 (1), 47-53• DOI: 10.1021/om00132a008 • Publication Date (Web): 01 May 2002

Technologies Laboratory, for his seminal interpretation of the ^1H NMR spectrum of **2a**. L.H.P. acknowledges support by the National Science Foundation (Grant CHE-81-08490) of his contribution to this research. T.A.A. thanks the Robert A. Welch Foundation and the donors Petroleum Research Foundation, administered by the American Chemical Society, for generous support of his work.

Registry No. 1, 428-76-2; **2a**, 98877-86-2; **2b**, 98878-06-9; **3a**, 98877-87-3; **3b**, 98878-07-0; **4a**, 98877-89-5; **4b**, 98878-08-1; **5a**, 98877-91-9; **5b**, 98878-09-2; **6a**, 98877-93-1; **6b**, 98878-10-5; **7a**, 98877-95-3; **7b**, 98878-11-6; **8a**, 98877-97-5; **8b**, 98878-12-7; **9a**, 98877-99-7; **9b**, 98878-13-8; **10a**, 98878-01-4; **10b**, 98878-14-9; **11a**, 98878-03-6; **11b**, 98878-15-0; **12a**, 98878-05-8; **12b**, 98878-16-1; **13a**, 98901-13-4; **13b**, 98878-18-3; **14a**, 98878-19-4; **14b**, 98878-20-7; $(C_6H_6)RuH(PH_3)_2^+$, 98878-21-8; $(C_6H_5NH_2)RuH(PH_3)_2^+$, 98878-22-9; $(C_6H_5BH_2)RuH(PH_3)_2^+$, 98878-23-0; $(Ph_3P)_4RuH_2$, 19529-00-1; $C_6H_5CH_3$, 108-88-3; C_6H_6, 71-43-2; *o*-$CH_3C_6H_4CH_3$, 95-47-6; *m*-$CH_3C_6H_4CH_3$, 108-38-3; *p*-$CH_3C_6H_4CH_3$, 106-42-3; $C_6H_5C_2H_5$, 100-41-4; $C_6H_5CH(CH_3)_2$, 98-82-8; $C_6H_5COCH_3$, 98-86-2; $C_6H_5OCH_3$, 100-66-3; C_6H_5Cl, 108-90-7; C_6H_5F, 462-06-6; *p*-$FC_6H_4CH_3$, 352-32-9; Rh, 7440-16-6; Ph_3P, 603-35-0.

Supplementary Material Available: Tables of shortest interionic distances, general temperature expressions for **2a**, positional and thermal parameters for hydrogen atoms in **2a**, distances and angles within the $HC(SO_2CF_3)_2^-$ ion in **2a**, weighted least-squares planes for **2a**, general temperature factor expressions for **2b**, positional and thermal parameters for **2b**, distances and angles within the BPh_4^- ion in **2b**, weighted least-squares planes for **2b**, and observed and calculated structure factor amplitudes for **2a** and **2b** and complete labeling schemes for **2a** and **2b** and the $HC(SO_2CF_3)_2^-$ ion (55 pages). Ordering information is given on any current masthead page.

Synthesis and X-ray Crystallographic Characterization of the Binuclear Iron Complexes $(CO)_3Fe(\mu\text{-}PPh_2)(\eta^2\text{-}(C,P)\text{-}\mu\text{-}CH(CN)PPh_2)Fe(CO)_3$ and $(CO)_3Fe(\mu\text{-}PPh_2)(\eta^2\text{-}(P,P')\text{-}\mu\text{-}Ph_2PC(CN)PPh_2)Fe(CO)_3$

Yuan-Fu Yu and Andrew Wojcicki*

Department of Chemistry, The Ohio State University, Columbus, Ohio 43210

Mario Calligaris† and Giorgio Nardin

Dipartimento di Scienze Chimiche, Università di Trieste, 34127 Trieste, Italy

Received April 19, 1985

Reaction of $[(CO)_3Fe(\mu\text{-}PPh_2)(\mu\text{-}CO)Fe(CO)_2(PPh_2H)]^-$ with ICH_2CN in THF at −78 to 25 °C yielded two new binuclear iron complexes, $(CO)_3Fe(\mu\text{-}PPh_2)(\eta^2\text{-}(C,P)\text{-}\mu\text{-}CH(CN)PPh_2)Fe(CO)_3$ (**1**) and $(CO)_3Fe(\mu\text{-}PPh_2)(\eta^2\text{-}(P,P')\text{-}\mu\text{-}Ph_2PC(CN)PPh_2)Fe(CO)_3$ (**2**), in addition to $Fe_2(CO)_6(\mu\text{-}PPh_2)_2$. Complexes **1** and **2** were characterized by elemental analysis, FAB mass spectrometry, ^1H, ^{13}C, and ^{31}P NMR spectroscopy, and single-crystal X-ray diffraction techniques. Crystals of **1** are monoclinic of space group $P2_1/c$ with a = 11.070 (2) Å, b = 33.535 (6) Å, c = 17.595 (5) Å, β = 112.45 (3)°, and Z = 8. The structure was solved and refined to R = 0.053 and R_w = 0.100 by using 10,277 independent reflections. The complex is a racemate owing to the presence of a chiral carbon center, FeCH(CN)P. Two bridging ligands, PPh_2 and η^2-(*C*,*P*)-$CH(CN)PPh_2$, support an Fe–Fe bond of 2.807 (1) Å (average) in a folded arrangement of two Fe atoms and P and C donor atoms. Crystals of **2** are monoclinic, space group $P2_1/c$, with a = 13.033 (3) Å, b = 13.124 (6) Å, c = 23.929 (5) Å, β = 96.89 (2)°, and Z = 4. The structure was solved and refined to R = 0.042 and R_w = 0.054 by using 5739 independent reflections. The bridging ligands PPh_2 and symmetric η^2-(*P*,*P'*)-$Ph_2PC(CN)PPh_2$ support an Fe–Fe bond of 2.727 (1) Å. The arrangement of the two Fe and three P atoms is essentially planar.

Introduction

We have previously shown[1] that $Fe_2(CO)_6(\mu\text{-}PPh_2)_2$ reacts with $LiBEt_3H$ in THF to afford a novel binuclear anion $[(CO)_3Fe(\mu\text{-}PPh_2)(\mu\text{-}CO)Fe(CO)_2(PPh_2H)]^-$. This anion has been converted to the bridging acyl complexes $(CO)_3Fe(\mu\text{-}PPh_2)(\mu\text{-}C(R)O)Fe(CO)_2(PPh_2R)$ upon treatment with an excess of RI (R = Me and Et). In an attempt to ascertain whether binuclear iron–alkyl intermediates are formed in these reactions, we examined the behavior of $[(CO)_3Fe(\mu\text{-}PPh_2)(\mu\text{-}CO)Fe(CO)_2(PPh_2H)]^-$ toward ICH_2CN. The presence of an electron-withdrawing CN group in the CH_2CN ligand contributes to a strong M–R σ bond, and, accordingly, MCH_2CN complexes display little tendency to undergo migratory insertion reactions.[2] Such lack of reactivity suggested that a desired diiron–cyanomethyl complex might be a stable and an isolable species.

To our surprise, we discovered that, in the reaction examined, CH_2CN moiety readily loses hydrogen, and the

† Inquiries concerning the X-ray crystallographic work should be directed to the Trieste address.

(1) Yu, Y.-F.; Gallucci, J.; Wojcicki, A. *J. Am. Chem. Soc.* **1983**, *105*, 4826.

(2) (a) Ros, R.; Renaud, J.; Roulet, R. *Helv. Chim. Acta* **1975**, *58*, 133. (b) Ros, R.; Michelin, R. A.; Carturan, G.; Belluco, U. *J. Organomet. Chem.* **1977**, *133*, 213. (c) Michelin, R. A.; Ros, R. *Ibid.* **1979**, *169*, C42.

0276-7333/86/2305-0047$01.50/0

resultant cyanocarbon fragments combine with bridging PPh_2. This leads to the formation of interesting binuclear complexes that incorporate CHCN and CCN, respectively, in the $CH(CN)PPh_2$ and $Ph_2PC(CN)PPh_2$ bridging ligands. This paper is concerned with the synthesis of $(CO)_3Fe(\mu\text{-}PPh_2)(\eta^2\text{-}(C,P)\text{-}\mu\text{-}CH(CN)PPh_2)Fe(CO)_3$ (1) and $(CO)_3Fe(\mu\text{-}PPh_2)(\eta^2\text{-}(P,P')\text{-}\mu\text{-}Ph_2PC(CN)PPh_2)Fe(CO)_3$ (2) and with a single-crystal X-ray diffraction study of these complexes.

Experimental Section

General Procedures and Measurements. All reactions were carried out under an atmosphere of purified N_2. Elemental analyses were done by Galbraith Laboratories, Inc., Knoxville, TN. Melting points were measured in vacuo on a Thomas-Hoover capillary melting point apparatus and are uncorrected. Infrared (IR) spectra were recorded on a Perkin-Elmer Model 283B grating spectrophotometer and were calibrated against a sharp peak (1601.4 cm^{-1}) of polystyrene film. ^1H NMR spectra were obtained on a Varian Associates EM-360 spectrometer with internal Me_4Si as a reference. ^{13}C NMR spectra were collected on a Bruker WP-80 spectrometer operating at 20.11 MHz with use of Me_4Si as an internal reference (δ 0). $^{31}P\{^1H\}$ NMR spectra were recorded on a Bruker HX-90 spectrometer at 36.43 MHz in the Fourier transform mode. Chemical shifts are given with reference to 85% H_3PO_4 and are reproducible to ±0.1 ppm. All NMR spectra were recorded at room temperature. Mass spectra were obtained by use of the fast atom bombardment (FAB) technique on a Kratos MS-30 spectrometer by Mr. C. R. Weisenberger. Samples dissolved in THF were incorporated in a matrix of tetraglyme; the bombarding gas was Xe and fluorinated kerosene was used as a reference.

Materials. THF was distilled from Na and benzophenone under an atmosphere of N_2 immediately before use. Dichloromethane and hexane were distilled from P_4O_{10} and Na, respectively, and stored over 4-Å molecular sieves. Anhydrous diethyl ether and petroleum ether (bp 30–60 °C) were used as received.

$LiBEt_3H$ (Super Hydride, 1 M in THF) and *n*-BuLi (1.64 M in hexane) were obtained from Aldrich. Iron pentacarbonyl (Alfa), chlorodiphenylphosphine, and iodoacetonitrile (Aldrich) were used as purchased commercially.

Preparation of $Fe_2(CO)_6(\mu\text{-}PPh_2)_2$. This complex was prepared by a somewhat modified procedure of Collman et al.[3] To a suspension of Na (7.5 g, 0.33 mol) in 300 mL of THF was added $Fe(CO)_5$ (40 mL, 0.30 mol) dropwise. Reaction occurred immediately with CO evolution, and the mixture was stirred at 25 °C overnight as a red slurry of $Na_2[Fe_2(CO)_8]$ appeared. To that slurry, PPh_2Cl (54 mL, 0.30 mol) was added dropwise over 2 h. The ensuing reaction was highly exothermic, and the color changed from red to brown. The resulting solution was stirred at room temperature for 2 days, solvent was removed by rotary evaporation, and the dark brown residue was extracted with petroleum ether (ca. 4 L) until the washings were essentially colorless. The yellow extracts were passed through a medium-porosity, glass filter packed with neutral alumina. The volume of the filtrate was reduced to ca. 30 mL by rotary evaporation resulting in the precipitation of yellow microcrystals which were collected by filtration. The yield was 51.6 g (53%): mp 179–180 °C; $^{31}P\{^1H\}$ NMR (THF) δ 142.5 (s). The IR and mass spectra agreed with those given in the literature.[3,4]

Reaction of $Li[(CO)_3Fe(\mu\text{-}PPh_2)(\mu\text{-}CO)Fe(CO)_2(PPh_2H)]$ with ICH_2CN. A solution of $Li[(CO)_3Fe(\mu\text{-}PPh_2)(\mu\text{-}CO)Fe(CO)_2(PPh_2H)]$,[1] prepared by treatment of 1.0 g (1.5 mmol) of $Fe_2(CO)_6(\mu\text{-}PPh_2)_2$ in 40 mL of THF with 3.0 mL (3.0 mmol) of 1 M $LiBEt_3H$ in THF at room temperature, was cooled to −78 °C. After 0.2 mL (2.8 mmol) of ICH_2CN was introduced by syringe, the resulting reaction mixture was stirred at −78 °C for 2 h and then allowed to warm to room temperature over 3 h. The solvent was removed under reduced pressure, and the dark red residue was dissolved in minimum THF. Neutral alumina (6% H_2O) was added to cover the solution, solvent was removed by rotary evaporation, and the residue was introduced onto a 1 × 20-cm column of neutral alumina (6% H_2O) in petroleum ether. Elution with 97:3 petroleum ether–Et_2O removed from the column a yellow band of $Fe_2(CO)_6(\mu\text{-}PPh_2)_2$ (0.40 g, 40%). Continued elution with petroleum ether (90–95%)–Et_2O (5–10%) gave small overlapping bands that contained insufficient amounts of material for characterization. A yellow band was then eluted down the column with petroleum ether (85–90%)–Et_2O (10–15%), and the solvent was removed to yield 0.19 g (18%) of a yellow powder. This solid, shown to be $(CO)_3Fe(\mu\text{-}PPh_2)(\eta^2\text{-}(C,P)\text{-}\mu\text{-}CH(CN)PPh_2)Fe(CO)_3$ (1), was purified further by crystallization from CH_2Cl_2–hexane: mp 206–208 °C; ^1H NMR ($CDCl_3$) δ 7.3 (m, 20 H, 4 Ph), 1.3 (dd, 1 H, $^2J_{PH}$ = 10 Hz, $^3J_{PH}$ = 4 Hz, CH); $^{13}C\{^1H\}$ NMR ($CDCl_3$) δ 219.4 (m, CO), 211.7 (t, J_{PC} = 4 Hz, CO), 135.0–127.9 (m, Ph), −19.4 (d, J_{PC} = 2 Hz, CH); ^{13}C NMR (off-resonance, partial, $CDCl_3$) δ −19.4 (d, J_{CH} = 15 Hz, CH); $^{31}P\{^1H\}$ NMR (THF) δ 176.1 (d, J_{PP} = 35.4 Hz, FePFe), 20.6 (d, J_{PP} = 35.4 Hz, CPFe); IR (THF) ν(CN) 2200 (w) cm^{-1}, ν(CO) 2059 (s), 2018 (s), 1996 (s), 1977 (s) cm^{-1}; mass spectrum, *m/e* 689 (P^+). Anal. Calcd for $C_{32}H_{21}Fe_2NO_6P_2$: C, 55.77; H, 3.07; N, 2.03. Found: C, 55.58; H, 3.17; N, 1.96.

Further elution with petroleum ether (80–85%)–Et_2O (15–20%) removed from the column an orange band, which afforded 0.08 g (6% yield based on Fe) of an orange solid upon evaporation of the solvent. Crystallization was effected from CH_2Cl_2–hexane to give analytically pure $(CO)_3Fe(\mu\text{-}PPh_2)(\eta^2\text{-}(P,P')\text{-}\mu\text{-}Ph_2PC(CN)PPh_2)Fe(CO)_3$ (2): mp 192–195 °C dec; ^1H NMR ($CDCl_3$) δ 7.5 (m, Ph); $^{31}P\{^1H\}$ NMR (THF) δ 200.6 (t, J_{PP} = 36.6 Hz, FePFe), 42.4 (d, J_{PP} = 36.6 Hz, CPFe); IR (THF) ν(CN) 2142 (w) cm^{-1}, ν(CO) 2087 (vw), 2024 (s), 1999 (s), 1971 (s) cm^{-1}; mass spectrum, *m/e* 873 (P^+). Anal. Calcd for $C_{44}H_{30}Fe_2NO_6P_3$: C, 60.46; H, 3.46. Found: C, 59.84; H, 3.56.

Reaction of $Li_2[(CO)_3Fe(\mu\text{-}PPh_2)(\mu\text{-}CO)Fe(CO)_2(PPh_2)]$ with ICH_2CN. A solution of $Li_2[(CO)_3Fe(\mu\text{-}PPh_2)(\mu\text{-}CO)Fe(CO)_2(PPh_2)]$[5] in THF was prepared in an NMR tube by treatment of 0.26 g (0.40 mmol) of $Fe_2(CO)_6(\mu\text{-}PPh_2)_2$ with 0.4 mL of 1 M (0.40 mmol) $LiBEt_3H$ in THF at 25 °C followed by cooling to −78 °C and addition of 0.25 mL of 1.64 M (0.41 mmol) *n*-BuLi in hexane. To this solution at −78 °C was added 65 μL (0.9 mmol) of ICH_2CN. The $^{31}P\{^1H\}$ NMR spectrum of the reaction mixture showed only a signal at δ 143.8, which is assigned to $Fe_2(CO)_6(\mu\text{-}PPh_2)_2$.

Crystallographic Analyses of $(CO)_3Fe(\mu\text{-}PPh_2)(\eta^2\text{-}(C,P)\text{-}\mu\text{-}CH(CN)PPh_2)Fe(CO)_3$ (1) and $(CO)_3Fe(\mu\text{-}PPh_2)(\eta^2\text{-}(P,P')\text{-}\mu\text{-}Ph_2PC(CN)PPh_2)Fe(CO)_3$ (2). Crystals suitable for X-ray diffraction were obtained by dissolving each of 1 and 2 in CH_2Cl_2 and allowing hexane slowly to diffuse into these solutions at ca. 5 °C.

Diffraction measurements were carried out on an Enraf-Nonius CAD-4 fully automated diffractometer. Cell parameters were refined from 25 randomly selected reflections in the 2θ range 24–48° obtained by using the CAD-4 automatic routines. Crystal data and data collection parameters are listed in Table I. All data processing was performed on a PDP 11/44 computer using the Enraf-Nonius SDP program library. An empirical absorption correction was applied to the data by using the ψ-scan data from close to axial (i.e., $\chi > 80°$) reflections. Neutral atom scattering factors were taken from the literature.[6a] Anomalous dispersion corrections were applied to all non-hydrogen atoms.[6b] The structure of 1 was solved by direct methods (MULTAN) which allowed location of the four crystallographically independent iron atoms. All other atoms were then located through the usual combination of structure factor calculations and Fourier syntheses.

(3) Collman, J. P.; Rothrock, R. K.; Finke, R. G.; Moore, E. J.; Rose-Munch, F. *Inorg. Chem.* **1982**, *21*, 146.

(4) Johnson, B. F. G.; Lewis, J.; Wilson, J. M.; Thompson, D. T. *J. Chem. Soc. A* **1967**, 1445.

(5) Yu, Y.-F.; Gallucci, J.; Wojcicki, A. *J. Chem. Soc., Chem. Commun.* **1984**, 653.

(6) (a) "International Tables for X-Ray Crystallography"; Kynoch Press: Birmingham, England, 1974, Vol. IV, Table 2.2.B. (b) Ibid., Table 2.1.B.

Table I. Summary of Crystal Data, Data Collection Parameters, and Structure Refinement for 1 and 2

	1	2
mol formula	$C_{32}H_{21}Fe_2NO_6P_2$	$C_{44}H_{30}Fe_2NO_6P_3$
mol wt	689.2	873.4
cryst system	monoclinic	monoclinic
space group	$P2_1/c$	$P2_1/c$
a, Å	11.070 (2)	13.033 (3)
b, Å	33.535 (6)	13.124 (6)
c, Å	17.595 (5)	23.929 (5)
β, deg	112.45 (3)	96.89 (2)
V, Å^3	6033 (3)	4063 (2)
Z	8	4
ρ_{calcd}, g cm^{-3}	1.52	1.42
μ(Mo Kα), cm^{-1}	11.1	8.7
radiatn	graphite-monochromated Mo Kα (λ = 0.710 69 Å)	
scan type	$\omega/2\theta$	$\omega/2\theta$
θ range, deg	2-30	2.5-28
scan speed, deg min^{-1}	0.6-6.7	0.6-6.7
scan range,[a] deg in ω	1.54 + 0.247 tan θ	1.2 + 0.35 tan θ
aperture width, mm	1.1 + tan θ	0.9 + tan θ
aperture height, mm	4	4
intensity monitors[b]	3	4
orientatn monitors[c]	3	5
unique data	15 139	9912
unique data with $I > 3\sigma(I)$	10 277	5739
R[d]	0.053	0.042
R_w[e]	0.100	0.054
w	$4F_o^2/[\sigma^2(I) + 0.06F_o^2]^2$	1

[a] Extended by 25% on both sides for background measurements. [b] Measured after each hour. [c] New orientation matrix, if angular change >0.1, measured after each 800 reflections. [d] $R = \Sigma(||F_o| - |F_c||)/\Sigma|F_o|$. [e] $R_w = [\Sigma w(|F_o| - |F_c|)^2/\Sigma w|F_o|^2]^{1/2}$.

The structure of **2** was solved by the heavy-atom method. Hydrogen atoms were located at calculated positions and held fixed (B = 5 Å^2) during refinement. Full-matrix least-squares refinement using anisotropic thermal parameters converged to the final R factors shown in Table I. Because of the large number of parameters to be refined for **1**, refinement was performed in alternate cycles of full-matrix least squares for the two crystallographically independent molecules. Atomic parameters of **1** are furnished in Tables II and III, whereas atomic parameters of **2** are given in Table IV. Listings of anisotropic temperature factors, fractional coordinates of hydrogen atoms, and structure factor amplitudes for both compounds are available as supplementary material.[7]

Results and Discussion

Synthesis and Spectroscopic Properties of $(CO)_3Fe(\mu\text{-}PPh_2)(\eta^2\text{-}(C,P)\text{-}\mu\text{-}CH(CN)PPh_2)Fe(CO)_3$ (1) and $(CO)_3Fe(\mu\text{-}PPh_2)(\eta^2\text{-}(P,P')\text{-}\mu\text{-}Ph_2PC(CN)\text{-}PPh_2)Fe(CO)_3$ (2). Reaction of $[(CO)_3Fe(\mu\text{-}PPh_2)(\mu\text{-}CO)Fe(CO)_2(PPh_2H)]^-$ with ICH_2CN in THF at −78 to 25 °C affords several products. Of these, three have been obtained in sufficient quantities for a complete characterization: $Fe_2(CO)_6(\mu\text{-}PPh_2)_2$ and two new binuclear complexes, **1** and **2**.

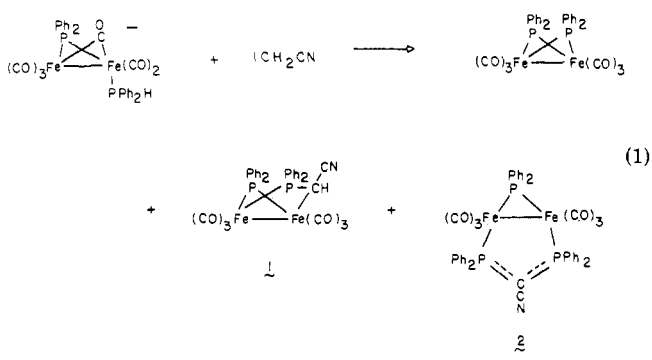

(1)

(7) See paragraph at end of paper regarding supplementary material.

Complex **1** was isolated as a yellow, air-stable solid. Its $^{31}P\{^1H\}$ NMR spectrum consists of two doublets; that at low field (δ 176.1) points to the presence of a μ-PPh_2 group in conjunction with an Fe–Fe bond,[8] whereas that at δ 20.6 is in the region typical of a coordinated PR_3.[9] The ^1H NMR spectrum shows, in addition to the resonances of Ph groups at δ 7.3, a signal of one proton at δ 1.3 coupled differently to two phosphorus nuclei ($^2J_{PH}$ = 10 Hz, $^3J_{PH}$ = 4 Hz). This signal is assigned to the FeCH proton. The resonance of the corresponding carbon atom appears in the $^{13}C\{^1H\}$ NMR spectrum at δ −19.4 (J_{PC} = 2 Hz) and is in the range found for a number of μ-CH_2PR_2 and η^2-CH_2PR_2 ligands in metal complexes.[5,10,11] The IR spectrum shows a weak ν(CN) absorption at 2200 cm^{-1}. The mass spectrum and elemental analysis of **1** are in accord with the proposed structure, which was confirmed by a single-crystal X-ray diffraction analysis (vide infra).

Although **1** represents the only known binuclear compound with the bridging system MCH(Y)P(R)$_2$M where Y = CN, related complexes have been recently reported. Geoffroy et al.[12] synthesized $(CO)_4W(\mu\text{-}PPh_2)(\eta^2\text{-}(C,P)\text{-}\mu\text{-}CH(Y)PPh_2)Os(CO)_2L$ (L = PMe_3 and $PMePh_2$; Y = OMe and OC(O)Me) by reaction of $Li[(CO)_4W(\mu\text{-}PPh_2)_2Os(CO)_2(C(O)H)L]$ with Me_3OBF_4 and MeC(O)Cl which results in coupling of a phosphido ligand with a

(8) (a) Garrou, P. E. *Chem. Rev.* **1981**, *81*, 229. (b) Carty, A. J. *Adv. Chem. Ser.* **1982**, *No. 196*, 163.
(9) Mark, V.; Dungan, C. H.; Crutchfield, M. M.; van Wazer, J. H. *Top. Phosphorus Chem.* **1967**, *5*, 227.
(10) Yu, Y.-F.; Chau, C.-N.; Wojcicki, A.; Calligaris, M.; Nardin, G.; Balducci, G. *J. Am. Chem. Soc.* **1984**, *106*, 3704.
(11) (a) Braunstein, P.; Matt, D.; Dusausoy, Y.; Fischer, J.; Mitschler, A.; Ricard, L. *J. Am. Chem. Soc.* **1981**, *103*, 5115. (b) Lindner, E.; Starz, K. A.; Eberle, H.-J.; Hiller, W. *Chem. Ber.* **1983**, *116*, 1209. (c) Al-Jibori, S.; Crocker, C.; McDonald, W. S.; Shaw, B. L. *J. Chem. Soc., Dalton Trans.* **1981**, 1572. (d) Mainz, V. V.; Andersen, R. A. *Organometallics* **1984**, *3*, 675.
(12) Rosenberg, S.; Whittle, R. R.; Geoffroy, G. L. *J. Am. Chem. Soc.* **1984**, *106*, 5934.

Table II. Positional Parameters of Non-Hydrogen Atoms of 1 (Molecule *R*) with Estimated Standard Deviations in Parentheses

	x	*y*	*z*
Fe(1)	0.36369 (7)	0.51492 (2)	0.30153 (5)
Fe(2)	0.26510 (6)	0.44085 (2)	0.32611 (4)
P(1)	0.3954 (1)	0.45478 (4)	0.25900 (8)
P(2)	0.1067 (1)	0.48089 (4)	0.24470 (8)
O(1)	0.2857 (5)	0.5853 (2)	0.3727 (3)
O(2)	0.4763 (5)	0.5614 (2)	0.2042 (3)
O(3)	0.5987 (4)	0.5069 (2)	0.4520 (3)
O(4)	0.4893 (5)	0.4170 (2)	0.4725 (3)
O(5)	0.1293 (4)	0.4338 (1)	0.4398 (3)
O(6)	0.1864 (5)	0.3625 (1)	0.2491 (3)
N	0.0752 (6)	0.5858 (2)	0.1674 (4)
C(1)	0.3106 (5)	0.5568 (2)	0.3471 (4)
C(2)	0.4339 (5)	0.5440 (2)	0.2442 (4)
C(3)	0.5062 (5)	0.5091 (2)	0.3935 (3)
C(4)	0.4064 (5)	0.4263 (2)	0.4139 (3)
C(5)	0.1800 (5)	0.4382 (2)	0.3951 (3)
C(6)	0.2146 (5)	0.3928 (2)	0.2789 (3)
C(7)	0.1838 (5)	0.5160 (2)	0.2003 (3)
C(8)	0.1221 (5)	0.5548 (2)	0.1799 (4)
C(9)	0.3504 (5)	0.4461 (2)	0.1487 (3)
C(10)	0.2325 (6)	0.4289 (2)	0.0999 (4)
C(11)	0.2001 (7)	0.4238 (2)	0.0164 (4)
C(12)	0.2854 (8)	0.4350 (2)	−0.0181 (4)
C(13)	0.4039 (7)	0.4524 (3)	0.0283 (4)
C(14)	0.4382 (6)	0.4576 (2)	0.1127 (4)
C(15)	0.5595 (4)	0.4332 (2)	0.3021 (3)
C(16)	0.6694 (5)	0.4571 (2)	0.3170 (4)
C(17)	0.7953 (5)	0.4411 (2)	0.3510 (4)
C(18)	0.8104 (5)	0.4012 (2)	0.3706 (4)
C(19)	0.7017 (6)	0.3769 (2)	0.3564 (4)
C(20)	0.5772 (5)	0.3930 (2)	0.3220 (3)
C(21)	0.0184 (5)	0.5111 (2)	0.2938 (3)
C(22)	0.0728 (5)	0.5209 (2)	0.3770 (4)
C(23)	0.0017 (6)	0.5427 (2)	0.4128 (4)
C(24)	−0.1214 (6)	0.5549 (2)	0.3664 (4)
C(25)	−0.1763 (5)	0.5467 (2)	0.2838 (4)
C(26)	−0.1079 (5)	0.5244 (2)	0.2473 (4)
C(27)	−0.0302 (5)	0.4576 (2)	0.1615 (3)
C(28)	−0.0942 (6)	0.4255 (2)	0.1794 (4)
C(29)	−0.2007 (7)	0.4084 (2)	0.1187 (5)
C(30)	−0.2447 (7)	0.4223 (2)	0.0390 (5)
C(31)	−0.1824 (7)	0.4540 (3)	0.0212 (4)
C(32)	−0.0754 (6)	0.4717 (2)	0.0811 (4)

Table III. Positional Parameters of Non-Hydrogen Atoms of 1 (Molecule *S*) with Estimated Standard Deviations in Parentheses

	x	*y*	*z*
Fe(1)	0.48137 (6)	0.19635 (2)	0.10543 (4)
Fe(2)	0.42685 (6)	0.26021 (2)	0.19011 (4)
P(1)	0.5481 (1)	0.25939 (4)	0.11320 (8)
P(2)	0.2495 (1)	0.23766 (4)	0.08556 (8)
O(1)	0.3707 (4)	0.1182 (1)	0.1213 (3)
O(2)	0.5806 (5)	0.1740 (2)	−0.0202 (3)
O(3)	0.6987 (5)	0.1708 (2)	0.2545 (3)
O(4)	0.6666 (4)	0.2594 (2)	0.3393 (3)
O(5)	0.2976 (4)	0.2531 (2)	0.3073 (3)
O(6)	0.3866 (5)	0.3461 (1)	0.1665 (3)
N	0.1669 (6)	0.1576 (2)	−0.0769 (3)
C(1)	0.4062 (5)	0.1495 (2)	0.1157 (4)
C(2)	0.5433 (5)	0.1816 (2)	0.0297 (4)
C(3)	0.6153 (6)	0.1828 (2)	0.1968 (4)
C(4)	0.5764 (5)	0.2590 (2)	0.2807 (3)
C(5)	0.3453 (5)	0.2537 (2)	0.2599 (3)
C(6)	0.4013 (5)	0.3132 (2)	0.1757 (3)
C(7)	0.3057 (5)	0.2151 (2)	0.0125 (3)
C(8)	0.2272 (5)	0.1832 (2)	−0.0385 (3)
C(9)	0.5129 (5)	0.2911 (2)	0.0227 (3)
C(10)	0.3980 (6)	0.3130 (2)	−0.0099 (4)
C(11)	0.3779 (8)	0.3383 (2)	−0.0768 (4)
C(12)	0.4704 (8)	0.3419 (2)	−0.1105 (4)
C(13)	0.5816 (7)	0.3203 (2)	−0.0800 (4)
C(14)	0.6056 (6)	0.2947 (2)	−0.0133 (4)
C(15)	0.7213 (5)	0.2700 (2)	0.1686 (3)
C(16)	0.8173 (5)	0.2425 (2)	0.1720 (4)
C(17)	0.9481 (5)	0.2515 (2)	0.2161 (4)
C(18)	0.9848 (5)	0.2872 (2)	0.2568 (4)
C(19)	0.8888 (5)	0.3148 (2)	0.2527 (4)
C(20)	0.7573 (5)	0.3068 (2)	0.2083 (4)
C(21)	0.1473 (4)	0.2002 (2)	0.1088 (3)
C(22)	0.1929 (5)	0.1787 (2)	0.1813 (4)
C(23)	0.1094 (7)	0.1519 (2)	0.1990 (4)
C(24)	−0.0154 (6)	0.1462 (2)	0.1444 (5)
C(25)	−0.0603 (6)	0.1664 (2)	0.0718 (5)
C(26)	0.0187 (5)	0.1939 (2)	0.0525 (4)
C(27)	0.1280 (5)	0.2763 (2)	0.0330 (3)
C(28)	0.0842 (5)	0.3008 (2)	0.0800 (4)
C(29)	−0.0084 (6)	0.3300 (2)	0.0422 (4)
C(30)	−0.0534 (6)	0.3352 (2)	−0.0410 (5)
C(31)	−0.0116 (7)	0.3109 (3)	−0.0880 (4)
C(32)	0.0798 (6)	0.2819 (2)	−0.0516 (4)

CH(OMe) and a CH(OC(O)Me) ligand. We reported earlier the preparation of $(CO)_3Fe(\mu\text{-}PPh_2)(\eta^2\text{-}(C,P)\text{-}\mu\text{-}CH_2PPh_2)Fe(CO)_3$[5] and $(NO)_2Fe(\mu\text{-}PPh_2)(\eta^2\text{-}(C,P)\text{-}\mu\text{-}CH_2PPh_2)Fe(NO)_2$[10] by treatment of $[(CO)_3Fe(\mu\text{-}PPh_2)(\mu\text{-}CO)Fe(CO)_2(PPh_2)]^{2-}$ and $[(NO)_2Fe(\mu\text{-}PPh_2)(\mu\text{-}NO)Fe(NO)(PPh_2)]^{2-}$, respectively, with CH_2I_2. And, very recently, Werner and Zolk[13] converted $(\eta^5\text{-}C_5H_5)_2Co_2(\mu\text{-}PMe_2)_2$ to $(\eta^5\text{-}C_5H_5)Co(\mu\text{-}PMe_2)(\eta^2\text{-}(C,P)\text{-}\mu\text{-}CH_2PMe_2)Co(\eta^5\text{-}C_5H_5)$ in two steps by use of CH_2Br_2 or CH_2I_2 and Na. In addition, a number of binuclear compounds are known in which a μ-CH(Y)PR_2 ligand bridges two metals without a supporting metal–metal bond.[11a,c,d,14]

The orange, air-stable complex **2** contains only Ph protons as shown by its ^1H NMR spectrum. The $^{31}P\{^1H\}$ NMR spectrum revealed two kinds of mutually coupled phosphorus nuclei in a ratio of 2:1. The low-field triplet (δ 200.6) again suggests that a PPh_2 group bridges over an Fe–Fe bond,[8] and a doublet at δ 42.4 is indicative of the presence of two equivalent phosphine or similar metal-bound phosphorus nuclei.[9] The IR spectrum shows a weak absorption due to ν(CN) at 2142 cm^{-1}; its lower frequency compared to the corresponding band of **1** likely arises from electron delocalization in the fragment PC(CN)P, viz., P=C(=C=N)=P (also, vide infra). The mass spectrum and elemental analysis agree with the structure assigned to **2**. This structure was established conclusively by an X-ray crystallographic determination, presented later in the paper.

Complex **2** provides the first example of a binuclear system with an η^2-(*P*,*P*′)-(R_2P=C(R′)=PR_2) bridging ligand. Stone et al.[15] deprotonated the $Ph_2PCH_2PPh_2$ in $(CO)_3Fe(\mu\text{-}Ph_2PCH_2PPh_2)(\mu\text{-}CO)Fe(CO)_3$ with MeLi, but the resultant ligand η^2-(*P*,*P*′)-μ-$Ph_2PCHPPh_2$ converted to η^3-(*P*,*C*,*P*′)-μ-$Ph_2PCHPPh_2$. In contrast, mononuclear complexes are known in which R_2PCHPR_2 functions as a P,P′-bidentate ligand.[16]

The mechanism of the formation of **1** and **2** is not clear. The complexity of the reaction in eq 1, which also produces $Fe_2(CO)_6(\mu\text{-}PPh_2)_2$ (40%) and other, unidentified compounds in trace amounts, as well as the loss of hydrogen

(13) Werner, H.; Zolk, R. *Organometallics* **1985**, *4*, 601.
(14) Klein, H.-F.; Wenninger, J.; Schubert, V. *Z. Naturforsch., B: Anorg. Chem., Org. Chem.* **1979**, *34B*, 1391.
(15) Dawkins, G. M.; Green, M.; Jeffery, J. C.; Stone, F. G. A. *J. Chem. Soc., Chem. Commun.* **1980**, 1120.
(16) (a) Cooper, G. R.; McEwan, G.; Shaw, B. L. *Inorg. Chim. Acta* **1983**, *76*, L165. (b) Karsch, H. H. *Chem. Ber.* **1984**, *117*, 783 and references therein.

Table IV. Positional Parameters of Non-Hydrogen Atoms of 2 with Estimated Standard Deviations in Parentheses

	x	y	z
Fe(1)	0.17850 (5)	0.20211 (5)	0.08198 (3)
Fe(2)	0.31107 (5)	0.12949 (5)	0.16975 (3)
P(1)	0.24343 (9)	0.36490 (9)	0.09292 (5)
P(2)	0.39478 (9)	0.27972 (8)	0.19082 (5)
P(3)	0.19662 (9)	0.04299 (9)	0.11362 (5)
O(1)	0.0050 (3)	0.2411 (4)	0.1470 (2)
O(2)	0.0215 (4)	0.2008 (5)	−0.0148 (2)
O(3)	0.3295 (4)	0.1697 (4)	0.0020 (2)
O(4)	0.4720 (3)	0.0888 (3)	0.0958 (2)
O(5)	0.3974 (4)	−0.0206 (3)	0.2522 (2)
O(6)	0.1590 (3)	0.1792 (4)	0.2467 (2)
N	0.4438 (4)	0.5505 (3)	0.1439 (2)
C(1)	0.0759 (4)	0.2264 (4)	0.1241 (3)
C(2)	0.0842 (5)	0.2040 (4)	0.0228 (3)
C(3)	0.2745 (5)	0.1816 (4)	0.0351 (2)
C(4)	0.4084 (4)	0.1051 (4)	0.1235 (2)
C(5)	0.3669 (4)	0.0390 (4)	0.2202 (2)
C(6)	0.2170 (4)	0.1620 (4)	0.2156 (2)
C(7)	0.3587 (3)	0.3731 (3)	0.1393 (2)
C(8)	0.4062 (4)	0.4709 (4)	0.1429 (2)
C(9)	0.2699 (4)	0.4081 (4)	0.0232 (2)
C(10)	0.3700 (5)	0.4149 (4)	0.0092 (2)
C(11)	0.3885 (5)	0.4390 (5)	−0.0453 (3)
C(12)	0.3075 (7)	0.4564 (5)	−0.0866 (3)
C(13)	0.2083 (7)	0.4493 (6)	−0.0734 (3)
C(14)	0.1882 (5)	0.4253 (5)	−0.0190 (3)
C(15)	0.1613 (4)	0.4680 (4)	0.1161 (2)
C(16)	0.1210 (5)	0.4581 (4)	0.1663 (3)
C(17)	0.0653 (6)	0.5364 (5)	0.1872 (3)
C(18)	0.0514 (5)	0.6251 (5)	0.1591 (4)
C(19)	0.0939 (6)	0.6395 (5)	0.1121 (4)
C(20)	0.1490 (6)	0.5620 (5)	0.0891 (3)
C(21)	0.5369 (4)	0.2663 (3)	0.1966 (2)
C(22)	0.5899 (4)	0.2965 (4)	0.1523 (2)
C(23)	0.6966 (4)	0.2850 (5)	0.1563 (3)
C(24)	0.7506 (4)	0.2434 (5)	0.2040 (3)
C(25)	0.6985 (4)	0.2129 (5)	0.2477 (3)
C(26)	0.5921 (4)	0.2238 (4)	0.2441 (2)
C(27)	0.3775 (3)	0.3279 (3)	0.2610 (2)
C(28)	0.3876 (4)	0.2644 (4)	0.3080 (2)
C(29)	0.3826 (5)	0.3022 (4)	0.3615 (2)
C(30)	0.3663 (4)	0.4051 (4)	0.3697 (2)
C(31)	0.3530 (4)	0.4685 (4)	0.3233 (2)
C(32)	0.3580 (4)	0.4320 (4)	0.2695 (2)
C(33)	0.0864 (4)	−0.0181 (3)	0.1405 (2)
C(34)	0.0972 (4)	−0.0735 (4)	0.1903 (3)
C(35)	0.0124 (5)	−0.1220 (4)	0.2082 (3)
C(36)	−0.0821 (5)	−0.1151 (5)	0.1779 (3)
C(37)	−0.0941 (5)	−0.0607 (6)	0.1286 (3)
C(38)	−0.0105 (5)	−0.0123 (5)	0.1097 (3)
C(39)	0.2431 (4)	−0.0598 (4)	0.0707 (2)
C(40)	0.3036 (5)	−0.1377 (4)	0.0977 (3)
C(41)	0.3376 (6)	−0.2165 (5)	0.0666 (3)
C(42)	0.3135 (7)	−0.2194 (5)	0.0101 (3)
C(43)	0.2531 (8)	−0.1437 (6)	−0.0171 (3)
C(44)	0.2177 (6)	−0.0637 (5)	0.0140 (3)

from the CH_2CN fragment, suggests that a radical pathway is operative. Since the reaction did not produce any observable complex with an Fe–CH_2CN bond, we attempted to prepare such a species by treatment of $[(CO)_3\overline{Fe(\mu\text{-}PPh_2)(\mu\text{-}CO)Fe(CO)_2(PPh_2)}]^{2-}$ with ICH_2CN at −78 °C. This dianion has been shown readily to react with alkyl iodides (RI) to form complexes containing P–R and Fe–R bonds.[5] However, the $^{31}P\{^1H\}$ NMR spectrum of the solution containing the binuclear dianion and ICH_2CN revealed only the resonance of $Fe_2(CO)_6(\mu\text{-}PPh_2)_2$. Thus, the presence of an electron-withdrawing CN group in the alkyl iodide exerts a striking effect on its reactivity toward $[(CO)_3\overline{Fe(\mu\text{-}PPh_2)(\mu\text{-}CO)Fe(CO)_2(PPh_2)}]^{2-}$. The iodide ICH_2CN behaves as an oxidizing agent in this apparent electron-transfer reaction.

Table V. Selected Bond Distances (Å) for 1 with Estimated Standard Deviations in Parentheses

	molecule *R*	molecule *S*
Fe(1)–Fe(2)	2.812 (1)	2.802 (1)
Fe(1)–P(1)	2.225 (1)	2.226 (1)
Fe(2)–P(1)	2.234 (1)	2.240 (1)
Fe(2)–P(2)	2.238 (1)	2.247 (1)
Fe(1)–C(1)	1.823 (4)	1.818 (4)
Fe(1)–C(2)	1.780 (4)	1.784 (4)
Fe(1)–C(3)	1.788 (4)	1.781 (4)
Fe(1)–C(7)	2.105 (3)	2.103 (4)
Fe(2)–C(4)	1.796 (4)	1.807 (4)
Fe(2)–C(5)	1.800 (4)	1.792 (4)
Fe(2)–C(6)	1.800 (4)	1.801 (4)
P(2)–C(7)	1.798 (4)	1.793 (4)
C(7)–C(8)	1.449 (5)	1.452 (5)
N–C(8)	1.145 (5)	1.137 (5)
P–C(Ph)(av)	1.823 (3)	1.833 (9)
C–O(av)	1.137 (5)	1.136 (12)

Table VI. Selected Bond Angles (deg) for 1 with Estimated Standard Deviations in Parentheses

	molecule *R*	molecule *S*
Fe(2)–Fe(1)–P(1)	51.04 (3)	51.36 (3)
Fe(2)–Fe(1)–C(1)	113.8 (1)	114.1 (1)
Fe(2)–Fe(1)–C(2)	148.1 (1)	146.1 (2)
Fe(2)–Fe(1)–C(3)	91.4 (1)	89.4 (1)
Fe(2)–Fe(1)–C(7)	81.2 (1)	82.03 (9)
P(1)–Fe(1)–C(1)	164.9 (1)	165.4 (1)
P(1)–Fe(1)–C(2)	98.4 (1)	95.5 (2)
P(1)–Fe(1)–C(3)	90.4 (1)	92.6 (1)
P(1)–Fe(1)–C(7)	87.2 (1)	87.2 (1)
C(1)–Fe(1)–C(2)	96.4 (2)	99.0 (2)
C(1)–Fe(1)–C(3)	90.5 (2)	86.8 (2)
C(1)–Fe(1)–C(7)	90.0 (2)	90.7 (2)
C(2)–Fe(1)–C(3)	98.5 (2)	100.3 (2)
C(2)–Fe(1)–C(7)	89.3 (2)	90.4 (2)
C(3)–Fe(1)–C(7)	172.1 (2)	169.3 (2)
Fe(1)–Fe(2)–P(1)	50.80 (3)	50.93 (3)
Fe(1)–Fe(2)–P(2)	68.10 (3)	66.82 (3)
Fe(1)–Fe(2)–C(4)	96.32 (1)	98.10 (1)
Fe(1)–Fe(2)–C(5)	118.88 (1)	122.50 (1)
Fe(1)–Fe(2)–C(6)	142.28 (1)	137.10 (1)
P(1)–Fe(2)–P(2)	92.46 (4)	92.29 (4)
P(1)–Fe(2)–C(4)	89.1 (1)	88.4 (1)
P(1)–Fe(2)–C(5)	167.4 (1)	170.5 (1)
P(1)–Fe(2)–C(6)	95.4 (1)	91.5 (1)
P(2)–Fe(2)–C(4)	157.7 (1)	159.0 (1)
P(2)–Fe(2)–C(5)	88.7 (1)	90.5 (1)
P(2)–Fe(2)–C(6)	102.3 (1)	100.1 (1)
C(4)–Fe(2)–C(5)	85.2 (2)	85.8 (2)
C(4)–Fe(2)–C(6)	99.7 (2)	100.8 (2)
C(5)–Fe(2)–C(6)	96.6 (2)	97.1 (2)
Fe(1)–P(1)–Fe(2)	78.20 (3)	77.72 (3)
Fe(2)–P(2)–C(7)	106.5 (1)	107.1 (1)
Fe(1)–C(7)–P(2)	94.3 (2)	92.3 (2)
Fe(1)–C(7)–C(8)	115.4 (3)	114.7 (3)
P(2)–C(7)–C(8)	116.0 (3)	117.7 (3)

Molecular Structures of $(CO)_3\overline{Fe(\mu\text{-}PPh_2)(\eta^2\text{-}(C,P)\text{-}\mu\text{-}CH(CN)PPh_2)Fe(CO)_3}$ (1) and $(CO)_3\overline{Fe(\mu\text{-}PPh_2)(\eta^2\text{-}(P,P')\text{-}\mu\text{-}Ph_2PC(CN)PPh_2)Fe(CO)_3}$ (2). Complex 1 contains a chiral center at the FeCH(CN)P carbon (C(7)). It crystallizes as a racemate with two crystallographically independent molecules per unit cell. Atomic parameters listed in Tables II and III refer to the molecules with the *R* and *S* configuration, respectively. An ORTEP drawing of one of the two molecules (*R*) is shown in Figure 1, together with the numbering scheme used to define atoms in both molecules. Selected bond lengths and angles are listed in Tables V and VI, respectively.

In each molecule the two $Fe(CO)_3$ moieties are linked by an Fe–Fe bond, supported by the bridging of a PPh_2 and a $CH(CN)PPh_2$ group. The coordination polyhedron

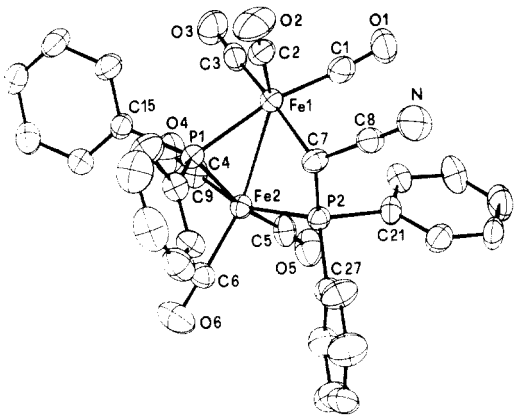

Figure 1. ORTEP drawing of molecule *R* of **1**, showing atom numbering scheme.

Table VII. Selected Bond Distances (Å) for 2 with Estimated Standard Deviations in Parentheses

Fe(1)–Fe(2)	2.727 (1)	Fe(2)–C(5)	1.785 (3)
Fe(1)–P(1)	2.301 (1)	Fe(2)–C(6)	1.792 (4)
Fe(1)–P(3)	2.224 (1)	P(1)–C(7)	1.761 (3)
Fe(2)–P(2)	2.280 (1)	P(2)–C(7)	1.762 (3)
Fe(2)–P(3)	2.199 (1)	C(7)–C(8)	1.423 (4)
Fe(1)–C(1)	1.797 (4)	N–C(8)	1.153 (4)
Fe(1)–C(2)	1.761 (4)	P–C(Ph)(av)	1.840 (9)
Fe(1)–C(3)	1.799 (4)	C–O(av)	1.141 (5)
Fe(2)–C(4)	1.809 (4)		

around each metal atom can be described as a highly distorted octahedron. The Fe(1)Fe(2)P(1)P(2)C(7) core is folded as shown by the P(1)–Fe(2)–P(2) (92.4° (average)) and P(1)–Fe(1)–C(7) (87.2° (average)) bond angles, which are close to 90°. A similar folded arrangement of the bridging ligands has been also found in the parent compound $Fe_2(CO)_6(\mu\text{-}PPh_2)_2$[17] and in its acetyl reduction derivative $(CO)_3\overline{Fe(\mu\text{-}PPh_2)(\eta^2\text{-}(C,O)\text{-}\mu\text{-}C(Me)O)Fe(CO)_2}(PMePh_2)$.[1]

The four-membered Fe(1)Fe(2)P(2)C(7) ring is puckered, with a torsion angle around the P(2)–C(7) bond of −29.8 and 32.3° in molecules *R* and *S*, respectively. The cyano group points away from the μ-PPh_2 ligand for steric reasons. The C(8)–C(7)–P(2)–C(21) torsion angle measures −25.4 and 24.9° in the *R* and *S* enantiomers, respectively. The steric overcrowding in the molecule is shown by the deviation of some bond angles involving side groups from their idealized tetrahedral values: e.g., Fe(1)–C(7)–C(8), 115.1° (average); P(2)–C(7)–C(8), 116.9° (average); Fe(2)–P(2)–C(21), 117.6° (average); Fe(2)–P(2)–C(27), 116.1° (average); and C(21)–P(2)–C(27), 101.0° (average). The Fe–Fe distances of 2.812 (1) (*R*) and 2.802 (1) Å (*S*) are comparable to the values of 2.836 (4) and 2.812 (5) Å found in the related complex $(NO)_2\overline{Fe(\mu\text{-}PPh_2)(\eta^2\text{-}(C,P)\text{-}\mu\text{-}CH_2PPh_2)Fe(NO)_2}$.[10]

The molecular structure of complex **2** is shown in Figure 2. Selected bond lengths and angles are listed in Tables VII and VIII, respectively.

The two $Fe(CO)_3$ groups are bridged by a PPh_2 ligand and a symmetric $Ph_2PC(CN)PPh_2$ ligand (vide infra) which support the Fe–Fe bond. In contrast to the puckered arrangement of Fe(1), Fe(2), P(2), and C(7) in **1**, Fe(1), Fe(2), P(1), and P(2) are coplanar within ±0.011 Å, C(7) being 0.283 Å out of this plane. As a result, the five-membered ring assumes an envelope conformation with

(17) Huntsman, J. R. Ph.D. Thesis, University of Wisconsin—Madison, 1973; quoted in Ginsburg, R. E.; Rothrock, R. K.; Finke, R. G.; Collman, J. P.; Dahl, L. F. *J. Am. Chem. Soc.* **1979**, *101*, 6550.

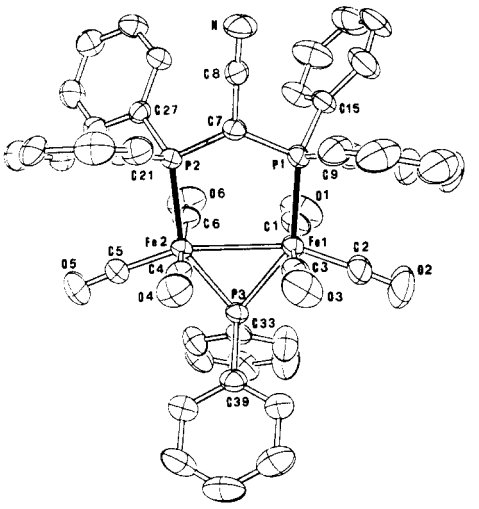

Figure 2. ORTEP drawing of **2**, showing atom numbering scheme.

Table VIII. Selected Bond Angles (deg) for 2 with Estimated Standard Deviations in Parentheses

Fe(2)–Fe(1)–P(1)	92.67 (3)	Fe(1)–Fe(2)–C(5)	157.4 (1)
Fe(2)–Fe(1)–P(3)	51.54 (2)	Fe(1)–Fe(2)–C(6)	88.3 (1)
Fe(2)–Fe(1)–C(1)	94.3 (1)	P(2)–Fe(2)–P(3)	148.51 (3)
Fe(2)–Fe(1)–C(2)	106.3 (1)	P(2)–Fe(2)–C(4)	86.4 (1)
Fe(2)–Fe(1)–C(3)	90.2 (1)	P(2)–Fe(2)–C(5)	106.3 (1)
P(1)–Fe(1)–P(3)	144.13 (3)	P(2)–Fe(2)–C(6)	90.2 (1)
P(1)–Fe(1)–C(1)	93.4 (1)	P(2)–Fe(2)–C(4)	90.5 (1)
P(1)–Fe(1)–C(2)	106.9 (1)	P(3)–Fe(2)–C(5)	105.2 (1)
P(1)–Fe(1)–C(3)	86.3 (1)	P(3)–Fe(2)–C(6)	91.9 (2)
P(3)–Fe(1)–C(1)	91.8 (1)	C(4)–Fe(2)–C(5)	92.1 (2)
P(3)–Fe(1)–C(2)	108.8 (1)	C(4)–Fe(2)–C(6)	176.4 (2)
P(3)–Fe(1)–C(3)	91.1 (1)	C(5)–Fe(2)–C(6)	89.9 (2)
C(1)–Fe(1)–C(2)	87.3 (2)	Fe(1)–P(1)–C(7)	113.8 (1)
C(1)–Fe(1)–C(3)	175.4 (2)	Fe(2)–P(2)–C(7)	111.5 (1)
C(2)–Fe(1)–C(3)	88.4 (2)	Fe(1)–P(3)–Fe(2)	76.10 (3)
Fe(1)–Fe(2)–P(2)	96.33 (2)	P(1)–C(7)–P(2)	122.3 (2)
Fe(1)–Fe(2)–P(3)	52.36 (2)	P(1)–C(7)–C(8)	115.2 (2)
Fe(1)–Fe(2)–C(4)	91.0 (1)	P(2)–C(7)–C(8)	120.5 (2)

a dihedral angle of 19.4°. The Fe(1)Fe(2)P(1)P(2) plane is nearly parallel to the plane of the three-membered Fe(1)P(3)Fe(2) ring (dihedral angle 3.1°). Thus, the molecular core Fe(1)P(1)P(2)Fe(2)P(3) is essentially planar. This contrasts with the folded arrangement of the two iron atoms and the donor atoms of the bridging ligands in the complexes $(CO)_3\overline{Fe(\mu\text{-}PR_2)(\mu\text{-}X)Fe(CO)_3}$ (and CO substitution derivatives thereof) where neutral X is formally a three-electron contributor, e.g., PR_2, C(Me)O, CH(CN)PPh_2, Cl, and C≡CPh, inter alia.[1,8b,17] The virtual planarity of the Fe(1)P(1)P(2)Fe(2)P(3) core of **2** may arise to minimize steric interactions among the bulky Ph groups or to optimize π-electron delocalization in the bridging framework formed by the two formally three-electron ligands, viz., PPh_2 and $Ph_2\ddot{P}$—C(CN)=$\dot{P}Ph_2$.

The Fe–Fe bond distance of 2.727 (1) Å in **2** is about 0.080 Å shorter than that in **1**. It seems likely that this is due to the lesser strain in the five-membered ring of **2** compared to the four-membered ring of **1**. Accordingly, bond angles at phosphorus in **2** are less distorted than in **1**: e.g., in **2**, Fe(1)–P(1)–C(7), 113.8°; and Fe(2)–P(2)–C(7), 111.5 (1)°.

The P(1)–C(7) and P(2)–C(7) bond distances of 1.761 (3) and 1.762 (3) Å, respectively, in **2** are shorter than the P(2)–C(7) bond distance in **1**, 1.795 (4) Å (average). Moreover, in **2**, the C(7)–C(8) distance of 1.423 (4) Å is shorter, and the N–C(8) distance of 1.153 (4) Å is longer, than the corresponding distances of 1.451 (5) (average) and

1.141 (5) Å (average), respectively, in **1**. The foregoing data support electron delocalization

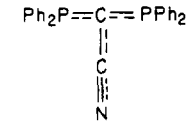

in this bridging ligand.

Acknowledgment. We gratefully acknowledge the financial support of the National Science Foundation (through Grant CHE-7911882 to A.W.), Ministero Pubblica Istruzione (Rome), and NATO (through Grant 068.81 to A.W. and M.C.). FAB mass spectra were obtained at the Ohio State University Chemical Instrument Center.

Supplementary Material Available: Listings of temperature factors, hydrogen atom coordinates, and structure factors for complexes 1 and 2 (81 pages). Ordering information is given on any current masthead page.

Syntheses, X-ray Structures, and Cis–Trans Isomerism of (Pentamethylcyclopentadienyl)dicarbonylrhenium Dihalides, $(\eta\text{-}C_5Me_5)Re(CO)_2X_2$ (X = Cl, Br, I)

Frederick W. B. Einstein, A. Hugo Klahn-Oliva, Derek Sutton,* and Kenneth G. Tyers

Department of Chemistry, Simon Fraser University, Burnaby, British Columbia, Canada V5A 1S6

Received May 24, 1985

Cis and trans isomers have been synthesized for the series of rhenium dicarbonyl dihalides $Cp^*Re(CO)_2X_2$ ($Cp^* = \eta\text{-}C_5Me_5$; X = Cl, Br, I). The cis isomers were formed by reaction of $Cp^*Re(CO)_2(N_2)$ with HX and were converted to the trans isomers by UV irradiation in hexane. The structures of the isomers have been assigned from examination of ν(CO) IR intensities and are supported by X-ray structure determinations on *cis*-$Cp^*Re(CO)_2I_2$ and *trans*-$Cp^*Re(CO)_2Br_2$. Crystal data for *cis*-$Cp^*Re(CO)_2I_2$: monoclinic $P2_1/n$, a = 7.201 (3) Å, b = 27.254 (5) Å, c = 8.682 (2) Å, β = 110.04 (4)°, U = 1600.2 (2) Å^3, D_{calcd} = 2.62 g cm^{-3}, D_{measd} = 2.64 (1) g cm^{-3}, Z = 4, λ(Mo Kα) = 0.710 69 Å, μ(Mo Kα) = 115.1 cm^{-1}, R_F = 0.046, R_{wF} = 0.058 for 1510 observed reflections (2081 measured with $3° \le 2\theta \le 45°$). Crystal data for *trans*-$Cp^*Re(CO)_2Br_2$: monoclinic $P2_1/c$, a = 8.512 (2) Å, b = 12.610 (4) Å, c = 13.794 (6) Å, β = 102.40 (3)°, U = 1446.1 (3) Å^3, D_{calcd} = 2.47 g cm^{-3}, D_{measd} = 2.43 (1) g cm^{-3}, Z = 4, λ(Mo Kα) = 0.710 69 Å, μ(Mo Kα), = 139.8 cm^{-1}, R_F = 0.043, R_{wF} = 0.054 for 1509 reflections (2008 measured with $3 \le 2\theta \le 46°$). *cis*- and *trans*-$CpRe(CO)_2Cl_2$ (the missing members of the cyclopentadienyl analogues $CpRe(CO)_2X_2$) have been synthesized from $CpRe(CO)_2(N_2)$ and Cl_2. The reaction of $Cp^*Re(CO)_3$ with I_2 in hexane yields $[Cp^*Re(CO)_3I][I_3]$ thermally and *trans*-$Cp^*Re(CO)_2I_2$ after irradiation.

Introduction

It is surprising, in view of the current activity in cyclopentadienyl and pentamethylcyclopentadienyl carbonyl chemistry in several laboratories, that prior to this work, several members of the series of simple rhenium dicarbonyl dihalides $CpRe(CO)_2X_2$ and $Cp^*Re(CO)_2X_2$ ($Cp = \eta\text{-}C_5H_5$; $Cp^* = \eta\text{-}C_5Me_5$; X = Cl, Br, I) were unknown, and reports of the others were fragmentary. In the cyclopentadienyl series, $CpRe(CO)_2Br_2$ was the first to be synthesized,[1] from the reaction of $CpRe(CO)_3$ with Br_2 in trifluoroacetic acid, and subsequently the product was shown to consist of cis (Ia) and trans (Ib) isomers (X = Br) which could be separated.[2] The iodide $CpRe(CO)_2I_2$ was not reported until

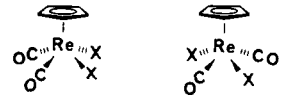

Ia Ib

1981[3,4] and could also be synthesized in cis and trans forms from the direct reaction of $CpRe(CO)_3$ with I_2 in dimethyl sulfoxide. The chloride $CpRe(CO)_2Cl_2$ was unknown. Reaction of $CpRe(CO)_3$ with Cl_2 was proposed[3] to yield the unstable salt $[CpRe(CO)_3Cl]Cl$, while reaction with $SbCl_5$ gave[5] the stable, well-characterized salt $[CpRe(CO)_3Cl][SbCl_6]$. Of the pentamethylcyclopentadienyl analogues, only $Cp^*Re(CO)_2I_2$ had been mentioned (briefly) but without details of the synthesis, characterization, or stereochemistry;[6] the dibromides and dichlorides were unknown.

We first encountered these compounds among several products, including the dinitrogen complexes $CpRe(CO)_2(N_2)$ and $Cp^*Re(CO)_2(N_2)$, formed in reactions of halides with the aryldiazenide complexes $[CpRe(CO)_2(N_2Ar)]^+$ and $[Cp^*Re(CO)_2(N_2Ar)]^+$ (Ar = aryl).[7] In this way, the dibromides and diiodides of both the Cp and the Cp* series were obtained, but notably not the dichlorides.

(1) Nesmeyanov, A. N.; Kolobova, N. E.; Makarov, Yu. V.; Anisimov, K. M. *Izv. Akad. Nauk SSSR, Ser. Khim.* **1969**, 1826.
(2) King, R. B.; Reimann, R. H. *Inorg. Chem.* **1976**, *15*, 183. King, R. B.; Reimann, R. H.; Darensbourg, D. J. *J. Organomet. Chem.* **1975**, *93*, C23.
(3) Kolobova, N. E.; Valueva, Z. P.; Kazimirchuk, E. I. *Izv. Akad. Nauk SSSR, Ser. Khim.* **1981**, 408.
(4) Dong, D. F.; Hoyano, J. K.; Graham, W. A. G. *Can. J. Chem.* **1981**, *59*, 1455.
(5) King, R. B. *J. Inorg. Nucl. Chem.* **1967**, *29*, 2119.
(6) Hoyano, J. K.; Graham, W. A. G. *J. Chem. Soc., Chem. Commun.* **1982**, 27.
(7) Barrientos-Penna, C. F.; Klahn-Oliva, A. H.; Sutton, D. *Organometallics* **1985**, *4*, 367.

0276-7333/86/2305-0053$01.50/0

1.141 (5) Å (average), respectively, in **1**. The foregoing data support electron delocalization

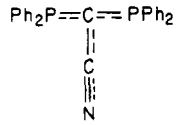

in this bridging ligand.

Acknowledgment. We gratefully acknowledge the financial support of the National Science Foundation (through Grant CHE-7911882 to A.W.), Ministero Pubblica Istruzione (Rome), and NATO (through Grant 068.81 to A.W. and M.C.). FAB mass spectra were obtained at the Ohio State University Chemical Instrument Center.

Supplementary Material Available: Listings of temperature factors, hydrogen atom coordinates, and structure factors for complexes 1 and 2 (81 pages). Ordering information is given on any current masthead page.

Syntheses, X-ray Structures, and Cis–Trans Isomerism of (Pentamethylcyclopentadienyl)dicarbonylrhenium Dihalides, (η-C_5Me_5)$Re(CO)_2X_2$ (X = Cl, Br, I)

Frederick W. B. Einstein, A. Hugo Klahn-Oliva, Derek Sutton,* and Kenneth G. Tyers

Department of Chemistry, Simon Fraser University, Burnaby, British Columbia, Canada V5A 1S6

Received May 24, 1985

Cis and trans isomers have been synthesized for the series of rhenium dicarbonyl dihalides Cp*$Re(CO)_2X_2$ (Cp* = η-C_5Me_5; X = Cl, Br, I). The cis isomers were formed by reaction of Cp*$Re(CO)_2(N_2)$ with HX and were converted to the trans isomers by UV irradiation in hexane. The structures of the isomers have been assigned from examination of ν(CO) IR intensities and are supported by X-ray structure determinations on *cis*-Cp*$Re(CO)_2I_2$ and *trans*-Cp*$Re(CO)_2Br_2$. Crystal data for *cis*-Cp*$Re(CO)_2I_2$: monoclinic $P2_1/n$, a = 7.201 (3) Å, b = 27.254 (5) Å, c = 8.682 (2) Å, β = 110.04 (4)°, U = 1600.2 (2) Å^3, D_{calcd} = 2.62 g cm^{-3}, D_{measd} = 2.64 (1) g cm^{-3}, Z = 4, λ(Mo Kα) = 0.710 69 Å, μ(Mo Kα) = 115.1 cm^{-1}, R_F = 0.046, R_{wF} = 0.058 for 1510 observed reflections (2081 measured with 3° ≤ 2θ ≤ 45°). Crystal data for *trans*-Cp*$Re(CO)_2Br_2$: monoclinic $P2_1/c$, a = 8.512 (2) Å, b = 12.610 (4) Å, c = 13.794 (6) Å, β = 102.40 (3)°, U = 1446.1 (3) Å^3, D_{calcd} = 2.47 g cm^{-3}, D_{measd} = 2.43 (1) g cm^{-3}, Z = 4, λ(Mo Kα) = 0.710 69 Å, μ(Mo Kα), = 139.8 cm^{-1}, R_F = 0.043, R_{wF} = 0.054 for 1509 reflections (2008 measured with 3 ≤ 2θ ≤ 46°). *cis*- and *trans*-$CpRe(CO)_2Cl_2$ (the missing members of the cyclopentadienyl analogues $CpRe(CO)_2X_2$) have been synthesized from $CpRe(CO)_2(N_2)$ and Cl_2. The reaction of Cp*$Re(CO)_3$ with I_2 in hexane yields [Cp*$Re(CO)_3$I][I_3] thermally and *trans*-Cp*$Re(CO)_2I_2$ after irradiation.

Introduction

It is surprising, in view of the current activity in cyclopentadienyl and pentamethylcyclopentadienyl carbonyl chemistry in several laboratories, that prior to this work, several members of the series of simple rhenium dicarbonyl dihalides $CpRe(CO)_2X_2$ and Cp*$Re(CO)_2X_2$ (Cp = η-C_5H_5; Cp* = η-C_5Me_5; X = Cl, Br, I) were unknown, and reports of the others were fragmentary. In the cyclopentadienyl series, $CpRe(CO)_2Br_2$ was the first to be synthesized,[1] from the reaction of $CpRe(CO)_3$ with Br_2 in trifluoroacetic acid, and subsequently the product was shown to consist of cis (Ia) and trans (Ib) isomers (X = Br) which could be separated.[2] The iodide $CpRe(CO)_2I_2$ was not reported until

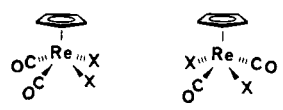

Ia Ib

1981[3,4] and could also be synthesized in cis and trans forms from the direct reaction of $CpRe(CO)_3$ with I_2 in dimethyl sulfoxide. The chloride $CpRe(CO)_2Cl_2$ was unknown. Reaction of $CpRe(CO)_3$ with Cl_2 was proposed[3] to yield the unstable salt [$CpRe(CO)_3Cl$]Cl, while reaction with $SbCl_5$ gave[5] the stable, well-characterized salt [$CpRe(CO)_3Cl$]-[$SbCl_6$]. Of the pentamethylcyclopentadienyl analogues, only Cp*$Re(CO)_2I_2$ had been mentioned (briefly) but without details of the synthesis, characterization, or stereochemistry;[6] the dibromides and dichlorides were unknown.

We first encountered these compounds among several products, including the dinitrogen complexes $CpRe(CO)_2(N_2)$ and Cp*$Re(CO)_2(N_2)$, formed in reactions of halides with the aryldiazenide complexes [$CpRe(CO)_2(N_2Ar)$]$^+$ and [Cp*$Re(CO)_2(N_2Ar)$]$^+$ (Ar = aryl).[7] In this way, the dibromides and diiodides of both the Cp and the Cp* series were obtained, but notably not the dichlorides.

(1) Nesmeyanov, A. N.; Kolobova, N. E.; Makarov, Yu. V.; Anisimov, K. M. *Izv. Akad. Nauk SSSR, Ser. Khim.* **1969**, 1826.
(2) King, R. B.; Reimann, R. H. *Inorg. Chem.* **1976**, *15*, 183. King, R. B.; Reimann, R. H.; Darensbourg, D. J. *J. Organomet. Chem.* **1975**, *93*, C23.
(3) Kolobova, N. E.; Valueva, Z. P.; Kazimirchuk, E. I. *Izv. Akad. Nauk SSSR, Ser. Khim.* **1981**, 408.
(4) Dong, D. F.; Hoyano, J. K.; Graham, W. A. G. *Can. J. Chem.* **1981**, *59*, 1455.
(5) King, R. B. *J. Inorg. Nucl. Chem.* **1967**, *29*, 2119.
(6) Hoyano, J. K.; Graham, W. A. G. *J. Chem. Soc., Chem. Commun.* **1982**, 27.
(7) Barrientos-Penna, C. F.; Klahn-Oliva, A. H.; Sutton, D. *Organometallics* **1985**, *4*, 367.

0276-7333/86/2305-0053$01.50/0

We were a little surprised to observed from an examination of the number and relative intensities of the IR ν(CO) absorptions that only the cis isomers were obtained for $Cp^*Re(CO)_2Br_2$ and $Cp^*Re(CO)_2I_2$, whereas $CpRe(CO)_2I_2$ seemed to be present only as the trans isomer and $CpRe(CO)_2Br_2$ was obtained in both forms.

This prompted us to undertake a more complete study of the synthesis and stereoisomerism of these compounds. Briefly, we set out to synthesize the missing dichlorides $CpRe(CO)_2Cl_2$ and $Cp^*Re(CO)_2Cl_2$, to determine whether the assignment of cis stereochemistry in the case of $Cp^*Re(CO)_2I_2$ (for example) produced in the manner above was supported by X-ray crystallography, to find a general method of synthesis, and to investigate whether cis–trans isomerization of these dihalides occurs under thermal or photochemical conditions.

Experimental Section

All reactions were carried out under dry N_2 in Schlenk apparatus connected to a double manifold providing low vacuum or nitrogen. Solvents were dried by conventional methods, distilled under nitrogen, and used immediately. Infrared spectra were measured by using Perkin-Elmer Model 983 or 599B instruments, usually in CaF_2 cells (solutions). ^1H and ^{13}C NMR spectra were measured by using a Bruker WM-400 instrument at 400 and 100 MHz, respectively. Mass spectra were obtained by G. Owen using a Hewlett-Packard Model 5985 mass spectrometer with electron-impact (EI) or fast-atom-bombardment (FAB; Phrasor Scientific Inc. accessory) sources. Masses are quoted for the isotopes ^{187}Re, ^{35}Cl, and ^{79}Br where present. Microanalyses were performed by M. K. Yang of the S.F.U. Microanalytical Laboratory.

Syntheses. $Cp^*Re(CO)_2(N_2)$. Method 1. An excess of solid $NaBH_4$ (15 mg) was added to a solution of $[Cp^*Re(CO)_2(p\text{-}N_2C_6H_4OMe)][BF_4]$[8] (100 mg) in acetone or acetonitrile (15 mL). An immediate intense red color formed, which gradually decreased in intensity during 1 h of stirring at room temperature. Hexane (30 mL) was then added, stirring was continued until the red color disappeared, and the supernatant was yellow. This was mainly $Cp^*Re(CO)_2(N_2)$ with some $Cp^*ReH(CO)(p\text{-}N_2C_6H_4OMe)$[8] by IR. Chromatography on a silica gel column prepared in hexane with hexane elution moved only the dinitrogen complex (45 mg, 44%). It was recrystallized from a hexane–pentane mixture at −20 °C as pale yellow crystals: mp 106–108 °C; IR (hexane) 2124 (s) (ν(NN)), 1953 (vs), 1901 (vs) (ν(CO)) cm^{-1}; ^1H NMR ($CDCl_3$) δ 2.07 (s); $^{13}C\{^1H\}$ NMR ($CDCl_3$) δ 10.36 ($C_5\mathit{Me}_5$), 96.23 (C_5Me_5), 200.08 (CO); MS (EI), m/e 406 (M^+), 378 ($M - N_2^+$).[9] Anal. Calcd for $Cp^*Re(CO)_2(N_2)$: C, 35.55; H, 3.70; N, 6.91. Found: C, 35.62; H, 3.79; N, 6.58.

Method 2. $Cp^*Re(CO)_3$ (600 mg) was irradiated in fresh distilled tetrahydrofuran (THF) for 2 h 15 min at 0 °C under N_2. (This time is sufficient to provide a reasonable conversion to the THF complex without too much ensuing decomposition.) The volume was reduced to one-third under vacuum (rotavap), and then the solution was pressurized to 1500 psi using U.S.P. grade nitrogen (Linde-Union Carbide) in a Parr bomb at room temperature for 24 h. An IR spectrum showed the disappearance of all the $Cp^*Re(CO)_2THF$ complex and ν(CO) absorption from only $Cp^*Re(CO)_2(N_2)$ and residual $Cp^*Re(CO)_3$. The brown solution was evaporated under vacuum and the residue redissolved in CH_2Cl_2 and chromatographed on a silica gel column prepared in hexane. Hexane eluted a pale yellow band from which was recovered 320 mg (53.3%) of a pale yellow solid mixture of $Cp^*Re(CO)_2(N_2)$ and $Cp^*Re(CO)_3$ in about 3:2 ratio (by IR). Next, hexane–diethyl ether (1:1) eluted a golden yellow band of Cp^*ReO_3 (formed as a result of O_2 impurity in the N_2)[10] and then an orange band containing $Cp^*_2Re_2(CO)_3$ and $Cp^*_2Re_2(CO)_5$.[6] Finally an unidentified purple band was eluted by using diethyl ether. The mixture of dinitrogen and tricarbonyl complexes could not easily be separated by column chromatography and was used as such in further reactions.

***cis*-$Cp^*Re(CO)_2Cl_2$.** The mixture of $Cp^*Re(CO)_2(N_2)$ and $Cp^*Re(CO)_3$ (method 2; 80 mg) was dissolved in diethyl ether (10 mL) at room temperature, and aqueous concentrated HCl (2 mL) was added with stirring or HCl (g) was bubbled through the solution for 3–4 min. After 10 min the yellow color began to change to red and the mixture was stirred overnight. Solvent was pumped off and the residue washed with hexane to remove the $Cp^*Re(CO)_3$ (32 mg). The red-orange residue was dissolved in CH_2Cl_2 and chromatographed on a Florisil column (prepared in hexane). Hexane was first used to elute any traces of $Cp^*Re(CO)_3$, and then the product was eluted as an orange-red band using acetone (42 mg; 79% yield) and recrystallized from CH_2Cl_2 as orange microcrystals which decomposed above 180 °C without melting: IR (CH_2Cl_2) 2037 (vs), 1958 (s) (ν(CO)) cm^{-1}; ^1H NMR ($CDCl_3$) δ 1.98 (s, C_5Me_5); $^{13}C\{^1H\}$ NMR δ 10.20 ($C_5\mathit{Me}_5$), 108.03 (C_5Me_5), 203.94 (CO); MS (EI), M^+, $M - CO^+$, $M - 2CO^+$, $M - Cl^+$. Anal. Calcd for $Cp^*Re(CO)_2Cl_2$: C, 32.14; H, 3.34. Found: C, 31.90; H, 3.17.

***trans*-$Cp^*Re(CO)_2Cl_2$.** *cis*-$Cp^*Re(CO)_2Cl_2$ (19 mg) was dissolved in $CHCl_3$ (15 mL) and irradiated for 25 min in a quartz tube. The color of the solution changed from orange to yellow. Chromatography on a Florisil column (prepared in hexane) using 1:1 CH_2Cl_2–hexane moved an orange band from which the trans isomer separated on evaporation as yellow-orange needles (12 mg, 64%) that decomposed without melting above 85 °C. Acetone moved residual cis isomer. IR (CH_2Cl_2) 2059 (s), 1986 (vs) (ν(CO)) cm^{-1}; ^1H NMR ($CDCl_3$) δ 1.89 (s) (C_5Me_5); $^{13}C\{^1H\}$ NMR ($CDCl_3$) δ 9.48 ($C_5\mathit{Me}_5$), 106.15 (C_5Me_5), 189.74 (CO); MS (EI), M^+, $M - CO^+$, $M - 2CO^+$, $M - Cl^+$. Anal. Calcd for $Cp^*Re(CO)_2Cl_2$: C, 32.14; H, 3.34. Found: C, 31.66; H, 3.44.

***cis*-$Cp^*Re(CO)_2Br_2$.** Hydrogen bromide was bubbled through diethyl ether (15 mL) for 5 min at room temperature, and then the mixture of $Cp^*Re(CO)_2(N_2)$ and $Cp^*Re(CO)_3$ (method 2; 110 mg) was added. The solution was stirred overnight and changed color slowly from yellow to red. A red solid precipitated. Solvent was removed, and the solid was washed twice with 10-mL portions of hexane to remove $Cp^*Re(CO)_3$ (47 mg), then redissolved in CH_2Cl_2, and chromatographed on Florisil. Elution with CH_2Cl_2–hexane (1:1) moved a red band which gave 76 mg (91%) of the cis isomer. Recrystallization from CH_2Cl_2–hexane gave red microcrystals which decomposed above 190 °C without melting: IR (CH_2Cl_2) 2033 (vs), 1958 (s) (ν(CO)) cm^{-1}; ^1H NMR ($CDCl_3$) δ 2.06 (s), (C_5Me_5); $^{13}C\{^1H\}$ NMR ($CDCl_3$) δ 10.42 ($C_5\mathit{Me}_5$), 106.88 (C_5Me_5), 201.52 (CO); MS (EI), M^+, $M - CO^+$, $M - 2CO^+$, $M - Br^+$. Anal. Calcd for $Cp^*Re(CO)_2Br_2$: C, 26.77; H, 2.78. Found: C, 26.83; H, 2.56.

***trans*-$Cp^*Re(CO)_2Br_2$.** *cis*-$Cp^*Re(CO)_2Br_2$ (24 mg) was dissolved in $CHCl_3$ (15 mL) and irradiated for 35 min in a quartz tube. The color changed from red to orange-yellow. Solvent was pumped off and the orange solid was dissolved in CH_2Cl_2 and chromatographed on a Florisil column prepared in hexane. Elution with CH_2Cl_2–hexane (2:3) moved an orange band which yielded the trans isomer as an orange solid. Recrystallization twice from CH_2Cl_2–heptane gave orange crystals (15 mg, 63%) which decomposed above 115 °C without melting: IR (CH_2Cl_2) 2050 (s), 1981 (vs) (ν(CO)) cm^{-1}; ^1H NMR ($CDCl_3$) δ 2.00 (s, C_5Me_5); $^{13}C\{^1H\}$ NMR ($CDCl_3$) δ 10.33 ($C_5\mathit{Me}_5$), 105.04 (C_5Me_5), 186.40 (CO); MS (EI), M^+, $M - CO^+$, $M - 2CO^+$, $M - Br^+$. Anal. Calcd for $Cp^*Re(CO)_2Br_2$: C, 26.77; H, 2.78. Found: C, 26.73; H, 2.88.

***cis*-$Cp^*Re(CO)_2I_2$.** The mixture of $Cp^*Re(CO)_2(N_2)$ and $Cp^*Re(CO)_3$ (method 2; 80 mg) was dissolved in diethyl ether (15 mL). Hydrogen iodide (2 mL of a freshly opened, colorless 47% aqueous solution (Eastman Kodak)) was added, and the two-phase mixture was stirred vigorously overnight. Ether was pumped off, and the residual aqueous HI was removed by syringe to leave a red solid which was washed with water and vacuum dried. Washing with pentane removed the $Cp^*Re(CO)_3$ component (36 mg), and the remaining red solid was dissolved in CH_2Cl_2 and chromatographed on a Florisil column eluting with CH_2Cl_2–hexane (3:2). Recrystallization from CH_2Cl_2–hexane gave red needles (67 mg, 98%) which decomposed above 210 °C without melting: IR (CH_2Cl_2) 2022 (vs), 1953 (s) (ν(CO)) cm^{-1}; ^1H NMR ($CDCl_3$) δ 2.23

(8) Barrientos-Penna, C. F.; Gilchrist, A. B.; Klahn-Oliva, A. H.; Hanlan, A. J. L.; Sutton, D. *Organometallics* **1985**, *4*, 478.

(9) Loss of N_2 was confirmed from the MS of ^{15}N-labeled $Cp^*Re(CO)_2(^{15}N{\equiv}^{14}N)$: IR (hexane) 2091 (s) ($\nu(^{15}N^{14}N)$), 1952 (vs), 1901 (vs) (ν(CO)) cm^{-1}; MS, m/e 407 (M^+), 378 ($M - {}^{15}N^{14}N^+$).

(10) Klahn-Oliva, A. H.; Sutton, D. *Organometallics* **1984**, *3*, 1313.

(s, C_5Me_5); $^{13}C\{^1H\}$ NMR ($CDCl_3$) δ 11.13 ($C_5\mathit{Me}_5$) 104.63, C_5Me_5, 199.52 (CO); MS (EI), M^+, $M - CO^+$, $M - 2CO^+$, $M - I^+$. Anal. Calcd for $Cp^*Re(CO)_2I_2$: C, 22.82; H, 2.37. Found: C, 22.95; H, 2.46.

***trans*-$Cp^*Re(CO)_2I_2$.** The cis isomer (25 mg) suspended in hexane (in which it is slightly soluble) was irradiated in a quartz tube. The resulting orange-red solution was chromatographed on Florisil using 3:2 CH_2Cl_2–hexane as eluant, to remove first the red-orange trans isomer (ca. 20% conversion) and then the red cis isomer. The trans isomer was identified by comparison with that formed from $Cp^*Re(CO)_3$ and I_2 directly (see below). Irradiation in $CHCl_3$ resulted in formation of no diiodo compounds; *trans*-$Cp^*Re(CO)_2Cl_2$ and a trace of $Cp^*Re(CO)_2ClI$ (identified by its MS) were formed instead.

Reaction of $Cp^*Re(CO)_3$ with I_2. $Cp^*Re(CO)_3$ (200 mg) was dissolved in hexane (100 mL), and an excess of I_2 in hexane was added to give an immediate dark red precipitate of $[Cp^*Re(CO)_3I][I_3]$ (see below). The suspension was rapidly stirred and irradiated for 1 h in a quartz tube. Solvent was pumped off, and the red solid residue which was a mixture of *cis*- and *trans*-$Cp^*Re(CO)_2I_2$ was chromatographed on a Florisil column prepared in hexane. A hexane wash first removed traces of unreacted $Cp^*Re(CO)_3$, and then red-orange *trans*-$Cp^*Re(CO)_2I_2$ (35 mg, 11%; decomposed without melting above 170 °C) was recovered from an orange band which was eluted using CH_2Cl_2–hexane (1:1): IR (CH_2Cl_2) 2028 (s), 1964 (vs) (ν(CO)) cm^{-1}; ^1H NMR ($CDCl_3$) δ 2.21 (s, C_5Me_5); $^{13}C\{^1H\}$ NMR ($CDCl_3$) δ 12.12 ($C_5\mathit{Me}_5$), 102.94 (C_5Me_5) 183.00 (CO); MS (EI), M^+, $M - CO^+$, $M - 2CO^+$, $M - I^+$. Anal. Calcd for $Cp^*Re(CO)_2I_2$: C, 22.82; H, 2.37. Found: C, 22.94; H, 2.34.

A red band was next eluted using CH_2Cl_2–hexane (4:1) which yielded *cis*-$Cp^*Re(CO)_2I_2$ (160 mg, 51%) as a red solid.

The precipitate of $[Cp^*Re(CO)_3I][I_3]$ was identified as follows: IR (KBr) 2087 (vs), 2045 (m) 2027 (vs) (ν(CO)) cm^{-1}; MS (FAB, xenon–sulfolane), m/e for cation $[Cp^*Re(CO)_3I]^+$ 553 (M^+), 505 ($M - CO^+$), 447 ($M - 2CO^+$), 405 ($M - 3CO^+$), 406 ($M - I^+$). Anal. Calcd for $[Cp^*Re(CO)_3I][I_3]$: C, 17.60; H, 1.69. Found: C, 17.20; H, 1.70. When stirred with hexane, the suspended solid partly redissociated to give a violet solution containing I_2 and $Cp^*Re(CO)_3$ (IR). Freshly prepared solutions in $CHCl_3$ exhibited IR bands of $[Cp^*Re(CO)_3I][I_3]$ (2099 (s), 2043 (s) (ν(CO)) cm^{-1} and $Cp^*Re(CO)_3$ (2007 (s), 1914 (s) (ν(CO)) cm^{-1}) having comparable intensities. Addition of I_2 to saturation increased the relative intensity of the former but those of $Cp^*Re(CO)_3$ were still present (though about half as intense): ^1H NMR ($CDCl_3$) δ 2.39 (s, Cp*) [at −50 °C δ 2.48 (s)]; $^{13}C\{^1H\}$ NMR ($CDCl_3$) δ 11.4 ($C_5\mathit{Me}_5$), 103.2 (C_5Me_5), 191 (br, CO). Spectra are assigned to fast exchange of $[Cp^*Re(CO)_3I][I_3]$ and $Cp^*Re(CO)_3$. Data for $Cp^*Re(CO)_3$: ^1H NMR ($CDCl_3$) δ 2.16; $^{13}C\{^1H\}$ NMR ($CDCl_3$) δ 10.64, 98.43, 198.07.

***cis*-$CpRe(CO)_2Cl_2$.** The dinitrogen complex $CpRe(CO)_2(N_2)$ (prepared by reacting $[CpRe(CO)_2(p\text{-}N_2C_6H_4OMe)][BF_4]$ (100 mg) in acetone with KI)[11] was dissolved without further purification in hexane, and a dilute solution of Cl_2 in hexane was added dropwise until all of the dinitrogen complex had reacted (by IR). The brown precipitate formed was removed, washed twice with hexane and with diethyl ether, and then recrystallized in good yield from acetone–diethyl ether (10:1) at −10 °C as red microcrystals which decomposed slowly above 170 °C without melting: IR (acetone) 2056 (vs), 1976 (s) (ν(CO)) cm^{-1}; IR ($CHCl_3$) 2061 (vs), 1988 (s) (ν(CO)) cm^{-1}; ^1H NMR (acetone-d_6) δ 6.54 (s, C_5H_5); $^{13}C\{^1H\}$ NMR (acetone-d_6) δ 98.55 (C_5H_5), 201.85 (CO); MS (EI), M^+, $M - CO^+$, $M - 2CO^+$, $M - Cl^+$, $M - CO - Cl^+$ (weak). Anal. Calcd for $CpRe(CO)_2Cl_2$: C, 22.28; H, 1.32. Found: C, 22.50; H, 1.40.

***trans*-$CpRe(CO)_2Cl_2$.** *cis*-$CpRe(CO)_2Cl_2$ was dissolved in a large excess of $CHCl_3$ (in which it is poorly soluble) and irradiated for 40 min in a quartz tube. The IR spectrum now showed only the trans isomer to be present. The red solid remaining after the solvent was pumped off was chromatographed on Florisil with CH_2Cl_2 as eluant. Recrystallization from CH_2Cl_2–diethyl ether (3:1) gave red microcrystals in approximate 70% yield which decomposed without melting above 135 °C: IR (CH_2Cl_2) 2078 (s), 2012 (vs) (ν(CO)) cm^{-1}; IR ($CHCl_3$) 2081 (s), 2017 (vs) (ν(CO)) cm^{-1}; ^1H NMR ($CDCl_3$) δ 5.69 (s, C_5H_5); $^{13}C\{^1H\}$ NMR ($CDCl_3$) δ 95.32 (C_5H_5), 185.72 (CO); MS (EI), M^+, $M - CO^+$, $M - 2CO^+$, $M - Cl^+$, $M - CO - Cl^+$. Anal. Calcd for $CpRe(CO)_2Cl_2$: C, 22.28; H, 1.32. Found: C, 22.42; H, 1.19.

X-ray Structure Determinations for *cis*-$Cp^*Re(CO)_2I_2$ (A) and *trans*-$Cp^*Re(CO)_2Br_2$ (B). It was hoped preferably to determine X-ray structures of the cis and trans isomers of a single halide for better comparison, but unfortunately no single pair could be found which gave acceptable crystals for both isomers.

Collection and Reduction of the X-ray Data. Suitable crystals of A (orange-red) and B (red) were obtained from CH_2Cl_2–hexane and were mounted on thin glass fibers with the major morphological axis aligned with the glass fiber. Preliminary oscillation photos (λ(Cu K_α) = 1.5405 Å) showed the crystals chosen to be of an acceptable quality. The crystals were then transferred to an Enraf-Nonius CAD-4 diffractometer, operating at room temperature, and the crystal class, cell dimensions, and space groups were examined in a routine manner. The same instrument was then used to collect intensity data. The crystallographic data and scan conditions are listed in Table I. The data were monitored by measuring two standard reflections every 1 h of X-ray exposure time. Only the reflections having intensities, $I > 3\sigma(I)$ were retained as observed, which after correction for Lorentz, polarization, and absorption errors (ψ scans) were used to solve and refine the structures. Densities were measured by buoyancy in $CHCl_3$–$CHBr_3$ mixtures.

Solution and Refinement of the Structures. The heavy atoms were located from a Patterson map and all other non-hydrogen atoms from a series of difference Fourier syntheses and least squares refinements. All hydrogen atoms were placed in geometrically calculated positions with d(C–H) = 0.98 Å and thermal parameters U = 0.09 $Å^2$ for *cis*-$Cp^*Re(CO)_2I_2$ (A) and U = 0.08 $Å^2$ for *trans*-$Cp^*Re(CO)_2Br_2$ (B). The disposition of the hydrogen atoms of the methyl groups was assumed to be identical with that found by Dahl.[12] The Re atom and halide ligands were refined anisotropically and all other atoms isotropically. The structures were refined by further cycles until all shift-to-error ratios were less than 0.01. For the final cycles, the weighting scheme used was $w = [\alpha(F_o)^2 + pF_o^2]^{-1}$. The value of the parameter p (= 0.0005 for A and 0.0004 for B) was that for which the variation of the averaged $\sum\{w|F_o| - |F_c|\}^2$ as a function of $|F_o|$ and $(\sin\theta)/\lambda$ was kept to a minimum. Final residuals for A were $R_F = \sum(||F_o| - |F_c||)/\sum|F_o| = 0.046$ and $R_{wF} = [\sum w(|F_o| - |F_c|)^2/\sum w(|F_o|)^2]^{1/2} = 0.058$ and for B, $R_F = 0.043$ and $R_{wF} = 0.054$. A small extinction correction (1.28×10^{-7}) was necessary for B.[13a] The largest peaks in a final difference map for A were 1.7 (2) and 1.2 (2) e $Å^{-3}$ located near the C(1)O(1) and C(2)O(2) ligands, respectively, and 2.62 Å from the Re atom. The location of the peaks was suggestive of a small disorder of I(2) with the carbonyl group C(2)O(2) and I(1) with C(1)O(1). The two peaks were refined as iodine atoms with variable occupancy and a fixed isotropic temperature factor of 0.05 $Å^2$. After several cycles, the peaks had refined to occupancies of 2.2% and 1.4%, respectively, with Re–I bond lengths of 2.65 Å. Because of the small occupancy of the partial iodine atoms this model was not pursued. A final difference map for B revealed numerous peaks and troughs of ±0.8–0.9 (2) e $Å^{-3}$ around the Re and Br atoms and a single large peak of 1.6 (2) e $Å^{-3}$ located 1.5 Å from the Re and 1.2 Å from C(1) having no apparent chemical significance. Neutral scattering factors with anomalous dispersion corrections for the non-hydrogen atoms were used.[13b] Computer programs[14] were run on an in-house VAX 11-750. Atom coordinates for A and B respectively are listed in Tables II and III and bond distances and angles in Tables IV and V. The calculated hydrogen atom coordinates, mean planes and dihedral angles, anisotropic thermal

(11) Barrientos-Penna, C. F.; Einstein, F. W. B.; Sutton, D.; Willis, A. C. *Inorg. Chem.* **1980**, *19*, 2740.

(12) Byers, L. R.; Dahl, L. F. *Inorg. Chem.* **1980**, *19*, 277.

(13) (a) Larson, A. C. "Crystallographic Computing"; Ahmed, F. R., Ed.; Munksgaard: Copenhagen, 1970; p 291. (b) "International Tables for X-ray Crystallography"; Kynoch Press: Birmingham, England, 1975; Vol. IV, Tables 2.28, 2.31.

(14) Larson, A. C.; Gabe, E. J. "Computing in Crystallography"; Schenk, H. et al., Eds.; Delft University Press: Delft, Holland, 1978. Larson, A. C.; Lee, F. L.; LePage, Y.; Gabe, E. J. "The N.R.C. Vax Crystal Structure System"; Chemistry Division, N.R.C.: Ottawa, Ontario, Canada.

Table I. Summary of Crystal Data and Data Collection Conditions

	cis-$(C_5Me_5)Re(CO)_2I_2$ (A)	*trans*-$(C_5Me_5)Re(CO)_2Br_2$ (B)
formula	$C_{12}H_{15}I_2O_2Re$	$C_{12}H_{15}Br_2O_2Re$
mol wt	631.3	537.3
space group	$P2_1/n$	$P2_1/c$
a, Å	7.201 (3)	8.512 (2)
b, Å	27.254 (5)	12.610 (4)
c, Å	8.682 (2)	13.794 (6)
β, deg	110.04 (4)	102.40 (3)
Z	4	4
cell vol, Å^3	1600.2 (2)	1446.1 (3)
d_{calcd}, g cm^{-3}	2.62	2.47
d_{measd}, g cm^{-3}	2.64 (1)	2.43 (1)
cryst dimens, mm	0.05 × 0.08 × 0.25	0.09 × 0.12 × 0.15
radiatn	Mo	Mo
μ, cm^{-1}	115.08	139.82
transmissn factors	0.565–0.996	0.679–0.988
scan speeds, deg min^{-1}	1.0–4.0	0.5–4.0
scan width, deg	0.70 + dispersion	0.75 + dispersion
data limits, 2θ, deg	3°, 45°	3°, 46°
measd reflcns	2081	2008
obsd reflcns, $I > 3.0\sigma(I)$	1510	1509
no. of variables	84	85
R_F	0.046	0.043
R_{wF}	0.058	0.054
GOF	1.83	2.05
extinctn		1.28×10^{-7}

Table II. Atom Coordinates (×10^4 for Re and I Atoms and ×10^3 for Others) and Equivalent Isotropic Temperature Factors (Å^2 × 10) for *cis*-$(C_5Me_5)Re(CO)_2I_2$

atom	x	y	z	B_{iso}, Å^2
Re	748 (1)	1315.5 (3)	2286.7 (8)	30.7 (4)
I(1)	3104 (2)	525.7 (7)	3791 (2)	70.2 (11)
I(2)	2206 (3)	1113.6 (8)	−200 (2)	79.2 (14)
C(1)	751 (4)	194 (1)	169 (3)	74 (6)
O(1)	185 (3)	227.9 (7)	130 (2)	70 (4)
C(2)	250 (4)	157.9 (9)	450 (3)	59 (5)
O(2)	311 (2)	168.2 (5)	546 (2)	49 (3)
C(3)	−205 (3)	160.6 (7)	242 (2)	43 (4)
C(31)	−236 (4)	211.0 (10)	314 (3)	78 (6)
C(4)	−240 (3)	150.5 (7)	76 (2)	41 (4)
C(41)	−307 (4)	185.4 (10)	−72 (3)	79 (7)
C(5)	−232 (3)	99.7 (7)	57 (2)	34 (3)
C(51)	−286 (4)	70.2 (9)	−107 (3)	66 (6)
C(6)	−196 (3)	76.9 (7)	207 (2)	36 (4)
C(61)	−196 (4)	22.3 (10)	242 (3)	70 (6)
C(7)	−170 (3)	115.6 (7)	328 (2)	39 (4)
C(71)	−152 (4)	108.5 (10)	502 (3)	75 (6)

Table III. Atom Coordinates (× 10^4 for Re and Br Atoms and ×10^3 for Others) and Equivalent Isotropic Temperature Factors (Å^2 × 10) for *trans*-$(C_5Me_5)Re(CO)_2Br_2$

atom	x	y	z	B_{iso}
Re	7392.4 (6)	7800.5 (5)	7093.1 (4)	31.7 (3)
Br(1)	10184 (2)	7859 (2)	6649 (1)	57.6 (11)
Br(2)	4403 (2)	7696 (2)	6207 (1)	68.3 (16)
C(1)	735 (2)	659 (1)	624 (1)	38 (3)
C(2)	719 (2)	899 (1)	621 (1)	39 (3)
O(1)	734 (1)	584 (1)	582 (1)	65 (3)
O(2)	708 (2)	974 (1)	573 (1)	65 (3)
C(3)	650 (2)	724 (1)	842 (1)	46 (3)
C(4)	819 (2)	695 (1)	860 (1)	42 (3)
C(5)	906 (2)	792 (1)	869 (1)	50 (3)
C(6)	801 (2)	878 (1)	855 (1)	39 (3)
C(7)	742 (2)	836 (1)	839 (1)	36 (3)
C(31)	514 (2)	647 (1)	846 (1)	55 (4)
C(41)	884 (2)	585 (2)	873 (1)	62 (4)
C(51)	1093 (2)	795 (2)	902 (1)	68 (5)
C(61)	850 (2)	991 (2)	863 (1)	67 (4)
C(71)	494 (2)	899 (1)	841 (1)	52 (3)

parameters, and structure factors have been deposited as supplementary material.

Results and Discussion

(a) (Pentamethylcyclopentadienyl)dicarbonyl(dinitrogen)rhenium, Cp*Re(CO)$_2$(N$_2$).

The synthesis of the dinitrogen complex $CpRe(CO)_2(N_2)$ has been described previously,[11,15] but that of the Cp* analogue Cp*Re(CO)$_2$(N$_2$) has not been. These dinitrogen complexes are

Table IV. Bond Distance (Å) and Angles (deg) for *cis*-$(C_5Me_5)Re(CO)_2I_2$

Bond Distances			
Re–I(1)	2.773 (2)	C(3)–C(4)	1.40 (3)
Re–I(2)	2.761 (2)	C(4)–C(5)	1.40 (3)
Re–C(1)	1.92 (3)	C(5)–C(6)	1.38 (2)
Re–C(2)	2.03 (3)	C(6)–C(7)	1.46 (3)
Re–C(3)	2.20 (2)	C(7)–C(3)	1.41 (3)
Re–C(4)	2.26 (2)	C(3)–C(31)	1.56 (3)
Re–C(5)	2.37 (2)	C(4)–C(41)	1.54 (3)
Re–C(6)	2.41 (2)	C(5)–C(51)	1.56 (3)
Re–C(7)	2.26 (2)	C(6)–C(61)	1.52 (3)
C(1)–O(1)	1.03 (3)	C(7)–C(71)	1.48 (3)
C(2)–O(2)	0.85 (3)	Re–Cp*(center)	1.951 (9)
Bond Angles			
I(1)–Re–I(2)	83.00 (7)	I(2)–Re–C(1)	75.3 (8)
C(1)–Re–C(2)	78.5 (10)	I(2)–Re–C(2)	122.4 (6)
I(1)–Re–C(1)	129.5 (7)	Re–C(1)–O(1)	177 (2)
I(1)–Re–C(2)	75.4 (7)	Re–C(2)–O(2)	173 (2)

Table V. Bond Distances (Å) and Angles (deg) for *trans*-$(C_5Me_5)Re(CO)_2Br_2$

Bond Distances			
Re–Br(1)	2.579 (2)	C(3)–C(4)	1.46 (2)
Re–Br(2)	2.579 (2)	C(4)–C(5)	1.42 (2)
Re–C(1)	1.93 (2)	C(5)–C(6)	1.39 (2)
Re–C(2)	1.92 (2)	C(6)–C(7)	1.43 (2)
Re–C(3)	2.25 (2)	C(7)–C(3)	1.41 (2)
Re–C(4)	2.31 (2)	C(3)–C(31)	1.52 (2)
Re–C(5)	2.36 (2)	C(4)–C(41)	1.49 (2)
Re–C(6)	2.31 (2)	C(5)–C(51)	1.56 (3)
Re–C(7)	2.33 (2)	C(6)–C(61)	1.49 (3)
C(1)–O(1)	1.10 (2)	C(7)–C(71)	1.50 (2)
C(2)–O(2)	1.15 (2)	Re–Cp*(center)	1.945 (7)
Bond Angles			
Br(1)–Re–Br(2)	138.97 (7)	Br(2)–Re–C(2)	78.1 (4)
Br(1)–Re–C(1)	76.9 (4)	C(1)–Re–C(2)	104.3 (6)
Br(1)–Re–C(2)	77.7 (4)	Re–C(1)–O(1)	174 (1)
Br(2)–Re–C(1)	77.6 (4)	Re–C(2)–O(2)	176 (1)

(15) Sellmann, D. *J. Organomet. Chem.* **1972**, *36*, C27. Sellmann, D.; Kleinschmidt, E. *Z. Naturforsch., B: Anorg. Chem., Org. Chem.* **1977**, *32B*, 795.

very convenient starting materials for the stereospecific synthesis of the dihalides since they react with halogens X_2 in hexane or with hydrogen halides HX (in the case of $Cp^*Re(CO)_2(N_2)$ to produce only the cis isomers of $CpRe(CO)_2X_2$ or $Cp^*Re(CO)_2X_2$. Previously described methods for $CpRe(CO)_2Br_2$ and $CpRe(CO)_2I_2$ produce mixtures of the cis and trans isomers.[1-3] We have prepared $Cp^*Re(CO)_2(N_2)$ by two methods here. The best for obtaining it analytically pure is method 1 (see Experimental Section) which starts from the cationic aryldiazenide complex $[Cp^*Re(CO)_2(p\text{-}N_2C_6H_4OMe)]^+$. Excess sodium borohydride first produces what we believe to be the red aryldiazene[11] complex $Cp^*Re(CO)_2(p\text{-}NHNC_6H_4OMe)$ which then generates the dinitrogen complex that is readily separated by column chromatography. Method 2, however, is a much more convenient one since it utilizes $Cp^*Re(CO)_2THF$ (readily synthesized in situ by irradiation of $Cp^*Re(CO)_3$) and dinitrogen directly. Because of their closely similar molecular weight and properties, the dinitrogen complex is difficult to separate from residual tricarbonyl. In reactions such as those described here in which the tricarbonyl is unreactive, its presence as an impurity in the dinitrogen complex is inconsequential and this is the synthetic method of choice for such preparative purposes.

$Cp^*Re(CO)_2(N_2)$ is a pale yellow microcrystalline solid, that is quite stable in air as a solid and in solution. The typical ν(NN) infrared absorption (hexane) occurs at 2124 cm^{-1} [2091 cm^{-1} in the ($^{15}N^{14}N$) compound] and ν(CO) at 1901 and 1953 cm^{-1}. These are consistently lower values than for the cyclopentadienyl analogue $CpRe(CO)_2(N_2)$ (ν(NN) 2145; ν(CO) 1920, 1974 cm^{-1} in hexane)[7,11] and are indicative of the greater electron releasing ability of the Cp* ligand. In the electron-impact mass spectrum at 70 eV the major fragmentation is the loss of the N_2 ligand, which was readily confirmed from the MS of the ($^{15}N^{14}N$) analogue synthesized from $[Cp^*Re(CO)_2(^{15}N^{14}NC_6H_4OMe)]^+$ by method 1.[9]

(b) *cis*-(Pentamethylcyclopentadienyl)dicarbonylrhenium Dihalides. The reactions of $Cp^*Re(CO)_2(N_2)$ with hydrogen halides HX (X = Cl, Br, I), produce only single products of stoichiometry $Cp^*Re(CO)_2X_2$ in good to excellent yield. Reactions with the halogens X_2 will also work but are not so clean. These red or orange-red microcrystalline solids exhibit mass spectra which typically show M^+, $M - CO^+$, $M - 2CO^+$, and $M - X^+$ peaks. The ^1H and ^{13}C NMR exhibit just the resonances expected for a single isomer. Similarly, the IR in each case consists of only two ν(CO) absorptions in the region 1950–2040 cm^{-1}, and the higher wavenumber one is much more intense. On this criterion, as well as the correspondence between our IR values and those reported for *cis*-$CpRe(CO)_2Br_2$ and *cis*-$CpRe(CO)_2I_2$,[2,3] we consider that our products are also the cis isomers. Furthermore, we have used the relative ν(CO) IR intensities to calculate the OC–Re–CO angle (2θ) using the relationship[2] $\tan^2\theta = I_{as}/I_s$ where I_{as} and I_s are the areas under the antisymmetric (lower wavenumber) and symmetric (higher wavenumber) bands, respectively. The angles thus determined by this method are 87° (Cl), 84° (Br), and 80° (I) for $Cp^*Re(CO)_2X_2$ and accord with their postulated cis structures. The X-ray structure determination for *cis*-$Cp^*Re(CO)_2I_2$ (see below) not only confirms that the cis geometry is indeed correct but also provides a value of 78 (1)° for this angle, in excellent agreement.

(c) *trans*-(Pentamethylcyclopentadienyl)dicarbonylrhenium Dihalides. Each of the above cis isomers is stable in the solid state and in solution with respect to thermal isomerization. No isomerization was observed even in boiling benzene or toluene, though the complexes do not survive for long at these temperatures. Acetone solutions of $Cp^*Re(CO)_2Cl_2$ and $Cp^*Re(CO)_2I_2$ showed no isomerization over 4 days under N_2 at room temperature nor when heated to boiling for a brief time. However, the cis isomers are readily isomerized to the trans isomers by UV irradiation. The dichlorides and dibromides may be irradiated in $CHCl_3$ with the formation of the trans isomers in 60–70% yield (the rest is decomposition) after about 30–40 min using our conditions. No formation of the dichloride via the solvent seems to occur in the latter case. However, isomerization of the cis diiodide $Cp^*Re(CO)_2I_2$ cannot be carried out in $CHCl_3$, because chlorine substitution occurs. Both *trans*-$Cp^*Re(CO)_2Cl_2$ and a trace of *trans*-$Cp^*Re(CO)_2ClI$ are formed instead. Irradiation of a suspension of *cis*-$Cp^*Re(CO)_2I_2$ in hexane for 90 min produces the trans isomer in about 20% yield, plus decomposition.

The trans isomers are recognizable by having two IR ν(CO) absorptions in which the higher wavenumber one ($\nu(CO)_{sym}$) is now the *less* intense of the pair. Both bands are also shifted to higher wavenumber by comparison with the corresponding cis isomer by amounts which increase in the order I < Br < Cl. In the diiodides the differences ($\Delta[\nu(CO)]$) are about 6 cm^{-1} for $\Delta[\nu(CO)_{sym}]$ and 11 cm^{-1} for $\Delta[\nu(CO)$ asym], while in the dichlorides they are 22 and 28 cm^{-1}, respectively. This can be understood in terms of the increased competition for rhenium d electrons between the carbonyl groups when they are mutually trans. The OC–Re–CO interbond angles, estimated from the ν(CO) intensities, are all found to be ca. 115°, some 28–35° greater than the angles in the cis compounds, and consistent with the postulated trans stereochemistry. The X-ray structure analysis for trans $Cp^*Re(CO)_2Br_2$ (see below) yields a value of 104°.

The trans isomers show considerably greater solubility than do the cis isomers, especially in hydrocarbon solvents. They also tend to be thermally less stable and decompose at considerably lower temperatures. The ^{13}C NMR chemical shift for the CO groups is smaller by ca. 15 ppm in the trans isomers. The resonances for the Cp* groups in the ^1H and ^{13}C NMR do differ also, but less consistently, in the two sets of isomers.

(d) *cis*- and *trans*-Cyclopentadienyldicarbonylrhenium Dihalides. In the same manner as was found for the Cp* compound described above, the Cp dinitrogen complex $CpRe(CO)_2(N_2)$ reacts in hexane with the halogens X_2 (X = Cl, Br, I) to afford only the cis isomers of the dihalides $CpRe(CO)_2X_2$. Interestingly, however, the hydrogen halides, e.g., HCl, appeared unreactive to $CpRe(CO)_2(N_2)$. While mixtures of both cis and trans isomers of $CpRe(CO)_2Br_2$ and $CpRe(CO)_2I_2$ have been synthesized previously from reactions of Br_2 or I_2 with $CpRe(CO)_3$ either thermally or under UV irradiation,[1-3] the present method is notable in producing solely the cis isomers. More interestingly, it provides the first synthesis of the chloride *cis*-$CpRe(CO)_2Cl_2$ (to thereby complete the series), as reactions of $CpRe(CO)_3$ with Cl_2 evidently proceed[3] only as far as the cation $[CpRe(CO)_3Cl]^+$. These cis isomers are recognized from their characteristic IR absorption intensities in the ν(CO) region, where the higher wavenumber band $\nu(CO)_{sym}$ is the more intense. For *cis*-$CpRe(CO)_2Cl_2$, ν(CO) occurs at 2037 and 1958 cm^{-1} (CH_2Cl_2), and from the intensities the OC–Re–CO interbond angle is calculated to be ca. 91°.

cis-$CpRe(CO)_2Cl_2$ does not isomerize thermally to the trans isomer in acetone at room temperature within 24 h

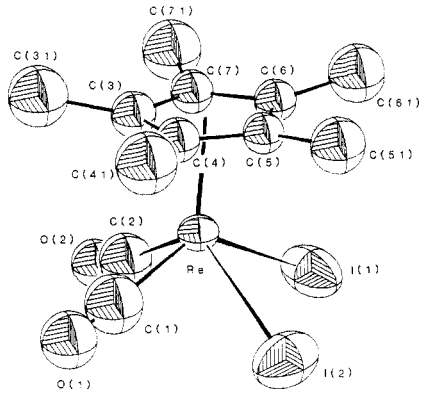

Figure 1. Perspective view (ORTEP plot) of a molecule of *cis*-$(C_5Me_5)Re(CO)_2I_2$ (A) showing the atom labeling (hydrogen atoms are omitted for clarity).

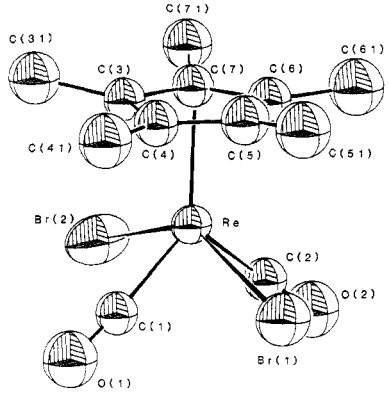

Figure 2. Perspective view (ORTEP plot) of a molecule of *trans*-$(C_5Me_5)Re(CO)_2Br_2$ (B) showing the atom labeling (hydrogen atoms are omitted for clarity).

(whereas the iodide is completely isomerized to trans in this solvent in 3 h), but when UV-irradiated in acetone, it quickly and cleanly isomerizes to *trans*-$CpRe(CO)_2Cl_2$.

(e) $[Cp^*Re(CO)_3I][I_3]$. An alternative route to *trans*-$Cp^*Re(CO)_2I_2$ is by irradiation of $Cp^*Re(CO)_3$ and I_2 in hexane. Upon addition of hexane solutions of the tricarbonyl and excess I_2 at room temperature a dark red precipitate of $[Cp^*Re(CO)_3I][I_3]$ forms (eq 1). The

$$Cp^*Re(CO)_3 + 2I_2 \rightleftharpoons [Cp^*Re(CO)_3I][I_3] \quad (1)$$

presence of the $[Cp^*Re(CO)_3I]^+$ cation in the solid is convincingly demonstrated by the FAB mass spectrum, which is exactly as expected with strong isotopic patterns at m/e 553 (^{187}Re) for the cation, m/e 505, 447, and 405 for the loss of three successive CO groups, and m/e 406 for loss of I.

The dark red solid appears to be quite stable under N_2 at room temperature, but attempts to wash it with hexane always give purple washings owing to partial reformation of iodine and $Cp^*Re(CO)_3$. An IR spectrum in KBr of the freshly washed solid contains ν(CO) absorptions of $[Cp^*Re(CO)_3I][I_3]$ at 2087, 2045, and 2027 cm^{-1} and very weak absorptions at 1994 and 1900 cm^{-1} from $Cp^*Re(CO)_3$. The spectrum is unchanged after 24 h. In solution in $CHCl_3$ or CH_2Cl_2 equilibrium is established (eq 1) and the bands for $[Cp^*Re(CO)_3I][I_3]$ (ν(CO) 2099, 2043 cm^{-1} ($CHCl_3$)) and $Cp^*Re(CO)_3$ (ν(CO) 2008, 1914 cm^{-1}) have roughly similar intensity. Even when the $CHCl_3$ solution is saturated with I_2, the absorptions for the latter are only about half as intense. Despite this, an I_2-saturated solution of $[Cp^*Re(CO)_3I][I_3]$ in $CDCl_3$ exhibits at room temperature only a sharp *single* ^1H NMR resonance at δ 2.39 (C_5Me_5) and a single set of ^{13}C NMR resonances at δ 11.4 ($C_5\mathit{Me}_5$), 103.2 (C_5Me_5), and 191 (br, CO), which we attribute to fast interconversion averaging the resonances for $[Cp^*Re(CO)_3I][I_3]$ and $Cp^*Re(CO)_3$. At −50 °C the proton resonance has broadened slightly and moved to δ 2.47. By way of contrast, in a solvent of much higher polarity (CH_3CN), the ν(CO) absorptions for $[Cp^*Re(CO)_3I][I_3]$ (2107, 2043 cm^{-1}) are about five times more intense than those of $Cp^*Re(CO)_3$ (2006, 1909 cm^{-1}).

(f) X-ray Structures of *cis*-$Cp^*Re(CO)_2I_2$ (A) and *trans*-$Cp^*Re(CO)_2Br_2$ (B). The structure determinations for *cis*-$Cp^*Re(CO)_2I_2$ (A) and *trans*-$Cp^*Re(CO)_2Br_2$ (B) were carried out to confirm the geometries deduced from the infrared ν(CO) relative intensities and to provide typical metrical data for this class of compounds, none of which has been structurally investigated before.

Both compounds occur as discrete molecules in the crystals, with no unusually short inter- or intramolecular contacts. ORTEP diagrams and atom labeling schemes for

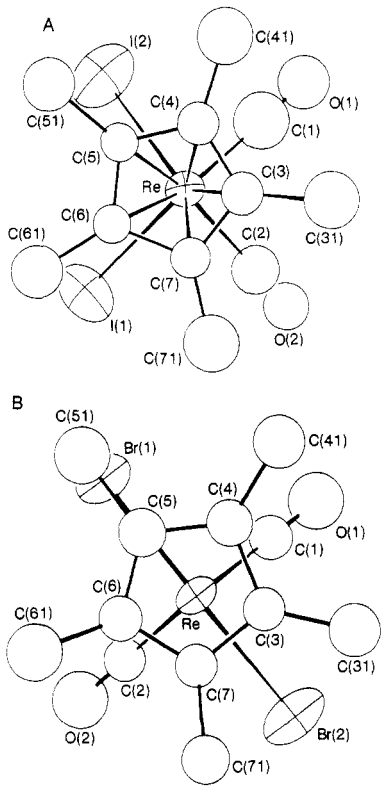

Figure 3. Views of *cis*-$(C_5Me_5)Re(CO)_2I_2$ (A) and *trans*-$(C_5Me_5)Re(CO)_2Br_2$ (B) projected onto the plane of the C5 ring showing the approximate mirror symmetry of each.

A and B are in Figures 1 and 2, respectively. Neither molecule has any crystallographically imposed symmetry in the lattice; however, both molecules (including the hydrogen atoms) possess an approximate mirror plane that is easily seen in parts A and B of Figure 3 which show the molecules in projection. In A this bisects the C_5Me_5 ligand at C(3) and C(31) and bisects the angles I(1)–Re–I(2) and C(1)–Re–C(2). In B it bisects C(5) and C(51) and both of the Re–Br bonds.

The rhenium atoms are formally in the III oxidation state and are seven-coordinate if the Cp* group is considered as a three-coordinate monoanion, and the overall geometry is that of a typical four-legged piano-stool Cp^*ML_4 complex.[16] The Re–C(CO) bond lengths in A and B are not distinguishable at this level of precision and are

(16) Kubacek, P.; Hoffmann, R.; Havlas, Z. *Organometallics* **1982**, *1*, 180.

in the range 1.9–2.0 Å that we have observed previously in $CpRe(CO)_2(\eta^2\text{-}C_2Ph_2)$[17] and in $CpRe(CO)_2(\eta^2\text{-}N_2Ph_2)$.[18] The Re–Br and Re–I bond lengths are unexceptional.

The Re–Cp* (centroid) distances of 1.945 (7) and 1.951 (9) Å in A and B are identical and evidently insensitive to the differing cis and trans arrangements of the carbonyl and halide basal ligands in the two structures. Examination of the individual Re–C bond lengths to the Cp* ligand reveals, however, differences in A and B. The individual Re–C bonds in B vary from 2.25 (2) to 2.36 (2) Å in no evidently regular manner, but in A they vary systematically in a way that is chemically sensible even though only marginally significant at the level of precision. The bonds Re–C(5) and Re–C(6) are long at 2.37 (2) and 2.41 (2) Å, Re–C(4) and Re–C(7) are intermediate at 2.26 (2) Å, and Re–C(3) is the shortest at 2.20 (2) Å. With reference to the projection in Figure 3A, it can be seen that the long Re–C bonds are "opposite" or pseudotrans to the two CO groups, while the shortest is "opposite" the iodide ligands. The asymmetry therefore follows a pattern that would be expected considering the π-acceptor properties possessed by CO ligands but not by iodide. The CO ligands withdraw π-electron density and diminish the π-contribution to the Re–C(Cp*) bonds trans to them, thereby resulting in lengthening. The asymmetry pattern also can be interpreted as a tilt of the Cp* ring away from the bulky iodide ligands. Hoffmann[16] has suggested that a degree of tilting of the Cp ring observable in some $CpML_4$ compounds is accountable by interactions involving δ orbitals of the metal and Cp ligand. In essence, it appears that (in projection) the eclipsing of a M–C(Cp) bond with a M–L bond results in a slightly long M–C(Cp) bond length, whereas when a M–C(Cp) bond is staggered between the M–L bonds, it is short. It is possible that such an effect also contributes to the pattern of Re–C(Cp*) bond lengths observed here, but it must be pointed out that in *cis*-$Cp^*Re(CO)_2I_2$ (A) none of the Re–C(Cp*) is exactly eclipsed. Nevertheless, it is true (Figure 3A) that the longer bonds that occur for Re–C(5) and Re–C(6) are the ones most nearly eclipsed by the Re–I bonds, while the shortest (Re–C(3)) is the most staggered one. In *trans*-$Cp^*Re(CO)_2Br_2$ (B) eclipsing does occur, but no significant statistical variation of the Re–C(Cp*) bond lengths is observable.

(17) Einstein, F. W. B.; Tyers, K. G.; Sutton, D. *Organometallics* **1985**, *4*, 489.
(18) Einstein, F. W. B.; Tyers, K. G.; Sutton, D., unpublished work.

The C–O bond lengths in B are in the expected range of 1.10–1.15 Å for metal carbonyl groups, but abnormally short values (0.85 (3) and 1.03 (3) Å) were obtained for A. These we consider to be invalid and to result from the 1–2% disordered iodine atom electron density contributions in these locations, causing the apparent shortening. The carbonyl group interbond angle C(1)–Re–C(2) in A is 78.5 (10)° compared with the value estimated from the infrared ν(CO) intensities of 80°. The corresponding angle in the trans isomer B is 104.3 (6)°. A rather larger angle (115°) was estimated from the ν(CO) intensities.

The C–C ring dimensions in the Cp* ligands in A and B are similar and normal, and the carbon atoms form well-defined planes with χ^2 values of 1.71 and 1.14. There is no systematic distortion from planarity such as was observed for $(C_5Me_5)Co(CO)_2$.[12] The methyl substituents are all displaced from these planes in a direction away from the rhenium atom with average deviations of 0.18 (2) Å in A and 0.17 (2) Å in B.

A survey by Dahl[12] of various (pentamethylcyclopentadienyl)metal complexes revealed this type of displacement to be general, with average deviations ranging from 0.037 to 0.205 Å. In B there are additional features to note, which are that the methyl carbon deviations conform to the approximate molecular mirror plane symmetry, and the largest deviations are displayed by the methyl groups C(31), C(51), and C(71). that are closest to eclipsing the bromine positions in projection (Figure 3B). Thus, the related pair C(41) and C(61) show very small deviations (+0.04 and +0.08 Å) while those of the pair C(31) and C(71) are much larger (+0.24 and 0.28 Å) and that of C(51) is +0.19 Å. In A the methyl carbon deviations also conform to the mirror symmetry, but C(41)–C(71) all have similar displacements of ca. 0.14–0.19 Å while that of the unique methyl group C(31) is larger at 0.28 Å.

Acknowledgment. This work was supported by N. S.E.R.C. Canada through operating grants to F.W.B.E. and D.S. The Universidad Catolica de Valparaiso, Valparaiso, Chile, is thanked for providing a leave of absence to A. H.K.-O.

Supplementary Material Available: Tables S1 (calculated hydrogen atom coordinates), S2 (calculated mean planes and dihedral angles), and S3 (anisotropic thermal parameters) for A and B and Table S4 (calculated and observed structure amplitudes for *cis*-$Cp^*Re(CO)_2I_2$ (A)) and Table S5 (calculated and observed structure amplitudes for *trans*-$Cp^*Re(CO)_2Br_2$ (B)) (28 pages). Ordering information is given on any current masthead page.

Stepwise Oxidative Cleavage of Bis(diphenylphosphino)methane in the Substituted Ruthenium Clusters $Ru_3(CO)_8(\mu\text{-}\eta^2\text{-}Ph_2PCH_2PPh_2)_2$ and $Ru_4(\mu\text{-}H)_4(CO)_{10}(\mu\text{-}\eta^2\text{-}Ph_2PCH_2PPh_2)$

Christian Bergounhou, Jean-Jacques Bonnet,* Patricia Fompeyrine, Guy Lavigne, Noël Lugan, and Frederica Mansilla

Laboratoire de Chimie de Coordination du CNRS associé à l'Université Paul Sabatier, 31400 Toulouse, France

Received March 20, 1985

Thermolysis of $Ru_3(CO)_8(\mu\text{-}\eta^2\text{-dppm})_2$ (**1**) (dppm = bis(diphenylphosphino)methane) yields the intermediate species $Ru_3(\mu\text{-H})(CO)_7(\mu_3\text{-}\eta^4\text{-}(C_6H_5)PCHP(C_6H_5)(C_6H_4))(\mu\text{-}\eta^2\text{-dppm})$ (**3**) which is subsequently converted into $Ru_3(CO)_7(\mu_3\text{-P}(C_6H_5))(\mu_3\text{-}\eta^2\text{-CHP}(C_6H_5)_2)(\mu\text{-}\eta^2\text{-dppm})$ (**4**). In the presence of molecular hydrogen, **3** yields $Ru_3(\mu\text{-H})_2(CO)_6(\mu_3\text{-}\eta^2\text{-}(C_6H_5)PCH_2P(C_6H_5)_2)$ (**5**). The X-ray structure of **3** is reported: the compound crystallizes in monoclinic system, space group $P2_1/c$, $Z = 4$, and cell dimensions $a = 12.865$ (1) Å, $b = 17.524$ (2) Å, $c = 23.661$ (2) Å, $\beta = 105.53$ (1)°. The structure, refined to $R = 0.041$, consists of the packing of four molecular cluster units. The cluster possesses an open trinuclear framework involving two metal–metal bonds (Ru(1)–Ru(2) = 2.888 (1) Å; Ru(2)–Ru(3) = 3.205 (1) Å). The latter, H-bridged, is supported by a bridging dppm ligand. The other ligand is seen on the face of the cluster during the intermediate activation step. Coordination of this fragment involves (i) terminal and bridging phosphorus atoms (P(2)–Ru(2) = 2.361 (2) Å; P(1)–Ru(1) = 2.375 (2) Å; P(1)–Ru(3) = 2.230 (2) Å), (ii) the ortho-metalated phenyl ring (Ru(1)–C(22) = 2.164 (8) Å), and (iii) unusual metalation of the carbon atom C(8) which leads to a triangular cyclometalated ring, P(1)–C(8)–Ru(3), with Ru(3)–C(8) = 2.229 (7) Å. Thermolysis of $Ru_4(\mu\text{-H})_4(CO)_{10}(\mu\text{-}\eta^2\text{-dppm})$ (**6**) yields $Ru_4(\mu\text{-H})_3(CO)_{10}(\mu_3\text{-}\eta^2\text{-}(C_6H_5)PCH_2P(C_6H_5)_2)$ (**7**), the structure of which is discussed on the basis of mass spectrometry and ^1H and ^{31}P NMR data. **7** is shown to react with CO to afford $Ru_3(\mu\text{-H})(CO)_9(\mu_3\text{-}\eta^2\text{-}(C_6H_5)PCH_2P(C_6H_5)_2)$ (**8**). Complexes **6–8** were checked by catalytic hydrogenation of cyclohexene, and their efficiency was compared with that of $Ru_4(\mu\text{-H})_4(CO)_{12}$. Under the reported experimental conditions, conversion of **6** into **7** is observed, while **8** is inactive. Catalytic hydrogenation is observed in the presence of **7** with rates matching those observed for $Ru_4(\mu\text{-H})_4(CO)_{12}$.

Introduction

Chemical reactions involving cleavage of C–H and C–P bonds in phosphine ligands are currently observed in substituted cluster complexes, where they seem to be favored by the presence of adjacent metal centers.[1] Since these intramolecular oxidative additions may occur at the expense of vacant coordination sites, a poisoning effect would be expected for catalytic systems involving phosphine-substituted metal clusters. By contrast, the organic fragments generated in such transformations may act as labile polyhapto ligands permitting coordination of various substrates via bridge-opening reactions[2-7] which may have implications in homogeneous catalysis.

We have undertaken studies aimed to clarify the intermediate steps involved in a cluster-assisted transformation of bis(diphenylphosphino)methane. Earlier work[8] showed that the substituted ruthenium cluster $Ru_3(CO)_8(\mu\text{-}\eta^2\text{-dppm})_2$ (**1**) experiences a facile thermal conversion into $Ru_3(CO)_7(\mu_3\text{-P}(C_6H_5))(\mu_3\text{-}\eta^2\text{-CHP}(C_6H_5)_2)(\mu\text{-}\eta^2\text{-dppm})$ (**4**).

More recently,[9] we found that thermolysis of **1** in the presence of H_2 yields $Ru_3(\mu\text{-H})_2(CO)_6(\mu_3\text{-}\eta^2\text{-P}(C_6H_5)\text{-}CH_2P(C_6H_5)_2)_2$ (**5**).

Clearly, intramolecular oxidative cleavage of dppm and activation of H_2 are concomitant processes in the latter reaction. We have now succeeded in isolating an intermediate complex providing insight into both of these transformations. Parallel observation of a facile thermal conversion of $Ru_4(\mu\text{-H})_4(CO)_{10}(\mu\text{-}\eta^2\text{-dppm})$ (**6**) into $Ru_4(\mu\text{-H})_3(CO)_{10}(\mu_3\text{-}\eta^2\text{-P}(C_6H_5)CH_2P(C_6H_5)_2)$ (**7**) is also reported. On the basis of the isolated species, a general scheme for the stepwise oxidative cleavage of dppm on a metal cluster is suggested. Some implications of the observed transformations in homogeneous catalysis are also examined.

Experimental Section

A. General Comments. Syntheses. All reactions were routinely conducted under N_2 atmosphere, using standard Schlenk

(1) (a) Cullen, W. R.; Harbourne, D. A.; Liengme, B. V.; Sams, J. R. *Inorg. Chem.* **1970**, *9*, 702. (b) Bradford, C. W.; Nyholm, R. S.; Gainsford, G. J.; Guss, J. M.; Ireland, P. R.; Mason, R. *J. Chem. Soc., Chem. Commun.* **1972**, 87. (c) Gainsford, G. J.; Guss, J. M.; Ireland, P. R.; Mason, R.; Bradford, C. W.; Nyholm, R. S. *J. Organomet. Chem.* **1972**, *40*, C70. (d) Bradford, C. W.; Nyholm, R. S. *J. Chem. Soc., Dalton Trans.* **1973**, 529. (e) Bruce, M. I.; Shaw, G.; Stone, F. G. A. *J. Chem. Soc., Dalton Trans.* **1973**, 1667. (f) Deeming, A. J.; Underhill, M. *J. Chem. Soc., Dalton Trans.* **1973**, 2727. (g) Fahey, D. R.; Mahan, J. E. *J. Am. Chem. Soc.* **1976**, *98*, 4499. (h) Deeming, A. J. *J. Organomet. Chem.* **1977**, *128*, 63. (i) Mason, R.; Meek, D. W. *Angew. Chem., Int. Ed. Engl.* **1978**, *17*, 183. (j) Carty, A. J.; Taylor, N. J.; Wayne, F. S.; Smith, W. F. *J. Chem. Soc., Chem. Commun.* **1979**, 750. (k) Brown, S. C.; Evans, J.; Smart, L. E. *J. Chem. Soc., Chem. Commun.* **1980**, 1021. (l) Demartin, F.; Manassero, M.; Sansoni, M.; Garlaschelli, L.; Sartorelli, U. *J. Organomet. Chem.* **1981**, *204*, C10. (m) Cook, S. L.; Evans, J.; Gray, L. R.; Webster, M. *J. Organomet. Chem.* **1982**, 236, 367. (n) Carty, A. J. *Pure Appl. Chem.* **1982**, *54*, 113. (o) McLaughlin, S. A.; Carty, A. J.; Taylor, N. J. *Can. J. Chem.* **1982**, *60*, 87. (p) McLaughlin, S. A.; Taylor, N. J.; Carty, A. J. *Inorg. Chem.* **1983**, *22*, 1411. (q) Bruce, M. I.; Nicholson, B. K.; Williams, M. L. *J. Organomet. Chem.* **1983**, *243*, 69. (r) Patel, V. D.; Taylor, N. J.; Carty, A. J. *J. Chem. Soc., Chem. Commun.* **1984**, 99. (s) See also specific references cited and discussed below.

(2) Smith, W. F.; Taylor, N. J.; Carty, A. J. *J. Chem. Soc., Chem. Commun.* **1976**, 896.

(3) Regragui, R.; Dixneuf, P. H.; Taylor, N. J.; Carty, A. J. *Organometallics* **1984**, *3*, 814.

(4) Harley, A. D.; Guskey, G. J.; Geoffroy, G. L. *Organometallics* **1983**, *2*, 53.

(5) Shyu, S. G.; Wojcicki, A. *Organometallics* **1984**, *3*, 809.

(6) Rosenberg, S.; Whittle, R. R.; Geoffroy, G. L. *J. Am. Chem. Soc.* **1984**, *106*, 5934.

(7) Lugan, N.; Bonnet, J. J.; Ibers, J. A. *J. Am. Chem. Soc.* **1985**, *107*, 4484.

(8) Lavigne, G.; Bonnet, J. J. *Inorg. Chem.* **1981**, *20*, 2713.

(9) Lavigne, G.; Lugan, N.; Bonnet, J. J. *Organometallics* **1982**, *1*, 1040.

0276-7333/86/2305-0060$01.50/0

line techniques. $RuCl_3 \cdot 3H_2O$ was generously supplied by Johnson Matthey Chemicals. Bis(diphenylphosphino)methane (dppm) was purchased from Ventron Chemicals. $Ru_3(CO)_{12}$,[10] $Ru_3(CO)_8(\mu\text{-}\eta^2\text{-dppm})_2$,[8] $Ru_4(\mu\text{-H})_4(CO)_{12}$,[11] and $Ru_4(\mu\text{-H})_4(CO)_{10}(\mu\text{-}\eta^2\text{-dppm})$[12] were prepared by published procedures. Solvents were reagent grade; they were freshly distilled prior to use.

Chromatographic Workup. Separation of all complexes was done on chromatographic columns (diameter 2.5 cm, length 40 cm) filled with silica gel (Kieselgel 60 Merck, ref 7734).

Spectroscopic Data. IR solution spectra in the ν(CO) region were recorded on a Perkin-Elmer 225 spectrophotometer. These spectra were calibrated with water vapor lines. ^1H NMR spectra were recorded on a Bruker WM 250 instrument (250.13 MHz), chemical shifts (δ) are in parts per million, relative to internal Me_4Si reference. ^{31}P NMR spectra were recorded on Bruker WH90 instrument (36.5 MHz), chemical shifts (δ) are in parts per million relative to external 85% H_3PO_4 (downfield shifts recorded as positive).

Mass Spectrometry. High-resolution mass spectra were obtained on a Varian MAT 311 A instrument with direct inlet probe (EI), temperature 160 °C. The average spectra resulting from 30 accumulations were compared with theoretical spectra by using the MASPAN program.[13] A quantitative estimate of the goodness of fit between the calculated and observed spectra is given by an R factor defined as

$$R = \sum_{i=0}^{N} |I_i^o - I_i^c| / \sum_{i=0}^{N} I_i^c$$

where N is the number of peaks in the parent ion multiplet, while I_i^o and I_i^c are the observed and calculated intensities of the ith peak, respectively.

B. Thermolysis of $Ru_3(CO)_8(\mu\text{-}\eta^2\text{-dppm})_2$ (1) and Preparation of $Ru_3(\mu\text{-H})(CO)_7(\mu_3\text{-}\eta^4\text{-}(C_6H_5)PCHP(C_6H_5)(C_6H_4))(\mu\text{-}\eta^2\text{-dppm})$ (3). Complex 1 (700 mg, 0.54 mmol) was dissolved in distilled ethoxyethanol (50 mL). The solution was carefully deareated and kept under a slow nitrogen stream. The temperature was maintained at 95 °C for 2 h. After the mixture was cooled, the solvent was evaporated and the residue was chromatographed on silica gel. Elution with toluene/heptane (1/1) gave three bands. The first band to elute yielded the yellow complex **3** and the second gave trace amounts of the orange complex **2**, while the third contained the unreacted complex **1**. Full separation of the first two fractions was extremely tedious. Separation of compounds **2** and **3** could be better achieved by crystallization: upon cooling a cyclohexane solution of a mixture of **2** and **3**, yellow crystals of **3** were obtained, while the more soluble orange complex **2** remained in solution.

The orange complex **2** was identified from its IR spectrum (ν(CO) (cyclohexane) 1995 s, 1985 vs, 1963 w cm^{-1}). It was not obtained in sufficient amount to allow further characterization.

Yellow complex $Ru_3(\mu\text{-H})(CO)_7(\mu_4\text{-}\eta^4\text{-}(C_6H_5)PCHP(C_6H_5)(C_6H_4))(\mu\text{-}\eta^2\text{-dppm})$ (**3**): 60 mg, 9%.

The experimental conditions reported for the preparation of **3** must be strictly adhered to. Longer reaction time or higher temperatures result in (i) formation of **4**, due to the facile conversion of **3** into **4** (vide infra), which elutes simultaneously with **4**, (ii) formation of traces amounts of additional products which have not been characterized, and (iii) disappearance of complex **2** due to its observed conversion into **3**.

Spectroscopic Data for 3. IR (ν(CO), cyclohexane): 2057 s, 2018 vs, 2010 vs, 1995 m, 1962 s cm^{-1}. ^1H NMR (CD_2Cl_2): the assignment of ^1H NMR signals has been established through selective homonuclear decoupling experiments from $^1H\{^{31}P\}$ data; H nuclei are labeled as H_a and H_b (methylene group of dppm), H_c (methyne group), and H_d (bridging hydride ligand); δ 7.5–5.9 (br, 34 H, C_6H_5 and C_6H_4), 3.09 (dd, H_a, $J_{H_aH_b}$ = 13.8 Hz, $J_{H_aH_d}$ = 2 Hz), 1.16 (d, H_b) 2.46 (d, Hc, $J_{H_cH_d}$ = 2 Hz), −19.27 (dd, H_d). Selective irradiation of the H_d nucleus restores a doublet for H_a and a singlet for H_c. Noticeably, coupling of the hydride nucleus with only one proton of the methylene group of dppm has been already observed and discussed.[9]

Table I. ^1H NMR Data for Complex 7

	methylene signal	hydride signals	
H nuclei	Ha, Hb	Hc	Hd, He
δ	3.92	−17.45	−19.30
^1H	dd	dd	dd
$^1H\{^{31}P\}$	s	s	s
$^1H\{^{31}P_a\}$	d (br), J_{HaPb} = J_{HbPb} = 11 Hz	d, J_{HcPb} = 39.4 Hz	d, J_{HdPb} = J_{HePb} = 17.4 Hz
$^1H\{^{31}Pb\}$	d, J_{HaPa} = J_{HbPA} = 11 Hz	br	d, J_{HdPa} = J_{HePa} = 9.8 Hz

C. Thermolysis of $Ru_3(\mu\text{-H})(CO)_7(\mu_3\text{-}\eta^4\text{-}(C_6H_5)PCHP(C_6H_5)(C_6H_4))(\mu\text{-}\eta^2\text{-dppm})$ (3). Compound **3** (50 mg) was dissolved in toluene (25 mL), and the solution was heated under reflux. Monitoring by infrared spectroscopy (ν(CO) region) showed quantitative conversion into the already reported complex $Ru_3(CO)_7(\mu_3\text{-P}(C_6H_5))(\mu_3\text{-}\eta^2\text{-CHP}(C_6H_5)_2)(\mu\text{-}\eta^2\text{-dppm})$ (**4**).[8]

D. Reaction of $Ru_3(\mu\text{-H})(CO)_7(\mu_3\text{-}\eta^4\text{-}(C_6H_5)PCHP(C_6H_5)(C_6H_4))(\mu\text{-}\eta^2\text{-dppm})$ (3) with H_2. Compound **3** (50 mg) was dissolved in toluene (25 mL). Hydrogen was then bubbled through this solution at 85–90 °C for 30 min. Monitoring by IR spectroscopy (ν(CO) region) showed complete conversion into the known complex $Ru_3(\mu\text{-H})_2(CO)_6(\mu_3\text{-}\eta^2\text{-}(C_6H_5)PCH_2P(C_6H_5)_2)_2$ (**5**).[9]

E. Preparation of $Ru_4(\mu\text{-H})_4(CO)_{10}(\mu\text{-}\eta^2\text{-dppm})$ (6). The complex was prepared by the published procedure based on radical ion catalysis.[12] $Ru_4(\mu\text{-H})_4(CO)_{12}$ (200 mg, 0.26 mmol) and dppm (105 mg, 0.26 mmol) were dissolved in tetrahydrofuran (20 mL) at 40 °C. After addition of the catalyst ($Ph_2CO^{\cdot-}$), rapid color change occurred. After being cooled, the solution was evaporated to dryness under vacuum and the solid residue was chromatographed on silica gel. Elution with heptane gave a yellow band identified as $Ru_4(\mu\text{-H})_4(CO)_{12}$ (traces). Further elution with toluene/heptane (1/1) gave a red fraction containing the substituted comples **6** which was recrystallized from dichloromethane/ethanol.

$Ru_4(\mu\text{-H})_4(CO)_{10}(\mu\text{-}\eta^2\text{-dppm})$ (**6**): 225 mg, 78%. Anal. Calcd for $C_{35}H_{26}O_{10}P_4Ru_4$: C, 39.19; H, 2.42. Found: C, 41.88; H, 2.44.

IR (ν(CO), cyclohexane) 2084 m, 2072 s, 2050 vs, 2032 vs, 2023 w, 2010 vs, 1990 w, 1978 m, 1968 m cm^{-1}. NMR spectra: $^{31}P\{^1H\}$ ($(CD_3)_2CO$ solution) δ 9.64 (s, terminal P); $^1H\{^{31}P\}$ (methylene protons are labeled as H_a and H_b) δ 7.57 (br, 20 H, C_6H_5), 4.89 (d, H_a, $J_{H_aH_b}$ = 11.8 Hz), 4.40 (d, H_b), −16.43 (s, 4 H, hydride ligands).

F. Thermolysis of $Ru_4(\mu\text{-H})_4(CO)_{10}(\mu\text{-}\eta^2\text{-dppm})$ (6) and Preparation of $Ru_4(\mu\text{-H})_3(CO)_{10}(\mu_3\text{-}\eta^2\text{-}(C_6H_5)PCH_2P(C_6H_5)_2)$ (7). A toluene solution (50 cm^3) of **6** (200 mg) was heated at 95 °C for 4 h, while a color change from red to orange was observed. After the solution was cooled the solvent was evaporated and the residue was chromatographed on silica gel. Elution with heptane gave traces of a red uncharacterized product (ν(CO) (cyclohexane) 2075 s, 2047 vs, 2029 vs, 2007 s, 1980 m, br, 1965 w, 1935 m, br cm^{-1}). Further reaction with toluene/heptane (1/1) afforded an orange band containing the main reaction product. This fraction was evaporated to dryness. Recrystallization from dichloromethane/hexane gave orange crystals **7** (145 mg, 76%) subsequently formulated as $Ru_4(\mu\text{-H})_3(CO)_{10}(\mu_3\text{-}\eta^2\text{-}(C_6H_5)PCH_2P(C_6H_5)_2)$.

Anal. Calcd for $C_{29}H_{20}O_{10}P_2Ru_4$: C, 35.02; H, 2.01. Found: C, 35.71; H, 2.08.

Spectroscopic Data for 7. Mass spectroscopy: the mass spectrum showed a parent ion consistent with the formulation $H_{20}C_{29}O_{10}P_2Ru_4$. The presence of three hydride ligands could be inferred from a detailed analysis of the parent ion multiplet by using the MASPAN program.[13] The goodness of fit between observed and calculated intensities (Table S1) was given by a satisfactory R value of 6.6%. The fragmentation pattern showed successive loss of 10 CO groups followed by loss of 3 phenyl groups. NMR spectra: phosphorus nuclei are labeled as P_a (bridging) and P_b (terminal); $^{31}P\{^1H\}$ ($CDCl_3$) δ 244.95 (d, P_a, J_{PP} = 83 Hz), 20.75 (d, P_b); ^1H NMR data are displayed in Table I.

G. Reactions of $Ru_4(\mu\text{-H})_4(CO)_{10}(\mu\text{-}\eta^2\text{-dppm})$ (6) with Carbon Monoxide. A continuous stream of carbon monoxide

(10) Mantovani, A.; Cenini, S. *Inorg. Synth.* **1976**, *16*, 47.
(11) Knox, S. A. R.; Koepke, J. W.; Andrews, M. A.; Kaesz, H. D. *J. Am. Chem. Soc.* **1975**, *97*, 3942.
(12) Bruce, M. I.; Matisons, J. G.; Nicholson, B. K. *J. Organomet. Chem.* **1983**, *247*, 321.
(13) MASPAN computer program, version 6, written by Art Cabral at UCLA in 1978 and kindly supplied by H. D. Kaesz.

Table II. Experimental Crystals and Intensity Data for 3

Crystal Data	
formula	$C_{52}H_{44}O_8P_4Ru_3$
mol wt	1247.75
crystal system	monoclinic
space group	$P2_1/c$
Z	4
unit cell parameters (at 25 °C)	
a, Å	12.865 (1)
b, Å	17.524 (2)
c, Å	23.661 (2)
β, deg	105.55 (1)
V, Å^3	5182.3
D(calcd), g cm^{-3}	1.60
μ, cm^{-1}	10.21
cryst vol, mm^3	0.343×10^{-2}
Intensity Data	
radiation	Mo Kα (λ = 0.70930 Å)
takeoff angle, deg	3.5
2θ limits, deg	3–44
scan mode	$\omega/2\theta$
scan range (θ)	0.5° below Kα_1 to 0.5° above Kα_2
ω scan speed, deg min^{-1}	2
reflctns collected	6967
unique data used	4884
final no. of variables	376
$R = \sum(\|F_o\| - \|F_c\|)/\sum\|F_o\|$	0.041
$R_w = \sum_w(\|F_o\| - \|Fc\|)^2/\sum wF_o^3)^{1/2}$	0.044

was bubbled through a toluene solution (60 mL) of **6** (100 mg) heated under reflux for 3 h. After the solution was cooled, the solvent was evaporated to dryness, and the product was chromatographed on silica gel. Elution with heptane gave two orange bands. The first band was identified as $Ru_3(CO)_{12}$ (6 mg, 10%) and the second one as $Ru_3(\mu\text{-H})(CO)_9(P(C_6H_5)CH_2P(C_6H_5)_2)$ (**8**) (40 mg, 49.7%) (**8** was previously observed in a reaction of $Ru_3(CO)_{10}(\mu\text{-}\eta^2\text{-dppm})$ with molecular hydrogen).[7] Further elution with heptane/toluene (1/1) gave an orange fraction identified as the known complex **7** (30 mg, 32.4%) (vide supra).

H. Reaction of $Ru_4(\mu\text{-H})_3(CO)_{10}(\mu_3\text{-}\eta^2\text{-P}(C_6H_5)CH_2P(C_6H_5)_2)$ (7) with CO. Under the same experimental conditions as above, starting from 100 mg of **7**, the reaction yielded three products which were separated by chromatography. The first product to elute with heptane was $Ru_3(CO)_{12}$ (12 mg, 18.7%), and the second one was a red complex (ν(CO) (cyclohexane) 2105 w, 2075 s, 2050 vs, 2017 s, 2000 m cm^{-1}) obtained at trace amounts which did not allow further characterization. The third product was the known complex $Ru_3(\mu\text{-H})(CO)_9(\mu_3\text{-}\eta^2\text{-P}(C_6H_5)CH_2P(C_6H_5)_2)$ (**8**) (vide supra; 70 mg, 80.5%).

I. Catalytic Tests. Experimental conditions for the catalytic hydrogenation of cyclohexene were as follows: SOTELEM 150B autoclave; solvent, freshly distilled tetrahydrofuran (50 cm^3); H_2 pressure, 40 bars; temperature, 80 °C; amount of catalyst, 4.3×10^{-5} mol; amount of cyclohexene, 49×10^{-3} mol; molar ratio of substrate to catalyst, 1140.

The products were analyzed by gas chromatography, using an Intersmat IGC 121 DFL equipped with a flame ionization detector and coupled with an integrator Intersmat CR 1B. The chromatographic column (3 m) was filled with 10% SE 30 on Chromosorb PAW 80/100.

J. Crystallographic Data for $Ru_3(\mu\text{-H})(CO)_7(\mu_3\text{-}\eta^4\text{-}(C_6H_5)PCHP(C_6H_5)(C_6H_4))(\mu\text{-}\eta^2\text{-dppm})$ (3). 1. Collection and Reduction of X-ray Data. Suitable crystals for X-ray diffraction were obtained by recrystallization of **3** from acetone/ethanol mixtures. Preliminary Laue and precession photographs showed **3** to crystallize in a monoclinic cell, space group C_{2h}^5—$P2_1/c$ (No. 14). The crystal selected for data collection was a lozenge-based parallelepiped with boundary planes of the form ($\bar{1}10$), ($1\bar{1}0$), (110), ($\bar{1}\bar{1}0$), (001), and (00$\bar{1}$). The distances from these planes to an arbitrary origin in the crystal were 0.067, 0.140 and 0.137 mm, respectively. The crystal was transferred to an Enraf-Nonius CAD4 diffractometer. The setting angles of the 25 reflections within the range $24 < 2\theta$ (Mo Kα) $< 26°$ were refined by least-squares procedure. The resulting cell parameters are given in Table II along with experimental data.

Table III. Atomic Coordinates for Independent Atoms in Complex 3

atom	x	y	z
Ru(1)	0.79237 (4)	0.11323 (3)	0.43202 (3)
Ru(2)	0.85733 (4)	0.12918 (3)	0.32385 (2)
Ru(3)	0.60954 (4)	0.09229 (3)	0.27022 (2)
P(1)	0.6242 (1)	0.1311 (1)	0.36553 (8)
P(2)	0.7538 (7)	0.24029 (10)	0.32427 (8)
P(3)	0.8785 (1)	0.13369 (10)	0.22815 (8)
P(4)	0.6296 (1)	0.1246 (1)	0.17558 (8)
C(1)	0.7784 (5)	0.0058 (5)	0.4147 (4)
O(1)	0.7686 (4)	−0.0583 (4)	0.4038 (3)
C(2)	0.7400 (7)	0.1105 (5)	0.5002 (4)
O(2)	0.7119 (6)	0.1107 (5)	0.5425 (4)
C(3)	0.9419 (6)	0.1095 (5)	0.4700 (4)
O(3)	1.0300 (5)	0.1063 (4)	0.4932 (3)
C(4)	0.9352 (6)	0.0356 (5)	0.3445 (4)
O(4)	0.9891 (4)	−0.0155 (4)	0.3594 (3)
C(5)	0.9781 (5)	0.1847 (4)	0.3617 (3)
O(5)	1.0527 (4)	0.2188 (3)	0.3833 (3)
C(6)	0.6098 (5)	−0.0156 (5)	0.2633 (3)
O(6)	0.6112 (4)	−0.0806 (3)	0.2606 (3)
C(7)	0.4603 (6)	0.0942 (5)	0.2512 (4)
O(7)	0.3682 (4)	0.0939 (4)	0.2414 (3)
C(8)	0.6224 (5)	0.2053 (4)	0.3145 (3)
C(9)	0.7597 (5)	0.1685 (4)	0.1748 (3)
C(21)	0.7885 (5)	0.2854 (4)	0.3956 (3)
C(22)	0.8059 (5)	0.2357 (4)	0.4427 (3)
C(23)	0.8328 (6)	0.2693 (5)	0.4979 (3)
C(24)	0.8423 (6)	0.3465 (6)	0.5056 (4)
C(25)	0.8239 (6)	0.3951 (5)	0.4587 (4)
C(26)	0.7958 (5)	0.3645 (4)	0.4025 (3)
C(10)	0.161 (2)	0.134 (2)	0.055 (1)
C(20)	0.233 (1)	0.1034 (9)	0.1043 (6)
C(30)	0.103 (1)	0.084 (1)	0.0237 (9)
O(10)	0.163 (1)	0.212 (1)	0.0186 (8)
H	0.743 (4)	0.083 (4)	0.294 (3)
H(8)	0.573 (5)	0.241 (4)	0.306 (3)
H(91)	0.773	0.161	0.137
H(92)	0.755	0.223	0.180
H(23)	0.843	0.236	0.532
H(24)	0.863	0.368	0.545
H(25)	0.832	0.450	0.464
H(26)	0.781	0.398	0.368

A total of 6967 reflections were recorded within the range $1.5° < \theta$(Mo Kα) $< 22°$. These intensities were corrected for Lorentz, polarization, and absorption effects, and reduced to observed structure factor amplitudes.[14]

2. Solution and Refinement of the Structure. The structure was solved by the heavy-atom technique.[14] Atomic scattering factors were taken from Cromer and Waber's tabulation[15] for all atoms but hydrogen, for which the values of Stewart et al. were used.[16] Anomalous dispersion terms for Ru and P atoms were included in F_c.[17] In order to reduce the number of variable parameters, six phenyl rings were treated as rigid groups, except the ortho-metalated phenyl ring. Rigid groups were constrained to D_{6h} symmetry (C–C = 1.395 Å; C–H = 0.95 Å; isotropic thermal parameters for hydrogen atoms were taken 1 Å^2 greater than those of adjacent carbon atoms and held fixed during structure refinements). All hydrogen atoms, including the

(14) The main programs used are listed below: the Northwestern absorption program, AGNOST, which includes the Coppens–Leiserowitz–Rabinovich logic for Gaussian integration and the Tompa De Meulenaur analytical method; Zalkin's FORDAP Fourier summation program; Busing's and Levy's ORFFE error function program; Iber's NUCLS full-matrix least-squares program, which in its nongroup form closely resembles the Busing–Levy ORFLS program. Johnson's ORTEP, ORNL-3794, 1965. All calculations were performed on the "Multics" computer of the C.I.C.T., the Paul Sabatier computer center.

(15) Cromer, D. T.; Waber, J. T. "International Tables for X-ray Crystallography"; Kynoch Press: Birmingham, England, 1974; Vol. IV, Table 2.2A.

(16) Stewart, R. F.; Davidson, E. R.; Simpson, W. T. *J. Chem. Phys.* **1965**, *42*, 3175.

(17) Cromer, D. T.; Waber, J. T. "International Tables for X-ray Crystallography"; Kynoch Press: Birmingham, England, 1974; Vol. IV, Table 2.3.1.

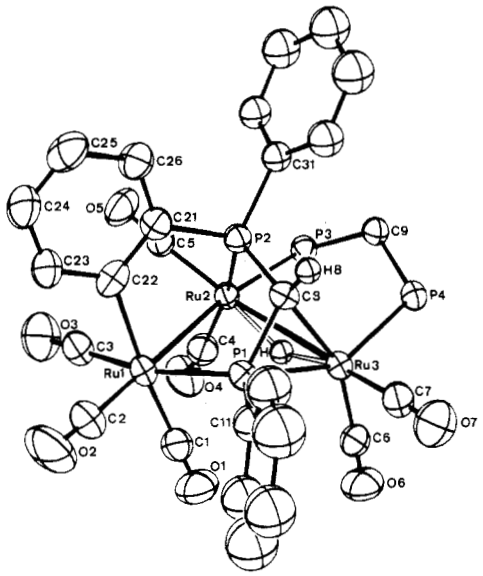

Figure 1. Geometry and labeling of the trinuclear cluster complex $Ru_3(\mu\text{-H})(CO)_7(\mu_3\text{-}\eta^4\text{-}(C_6H_5)PCHP(C_6H_5)(C_6H_4))(\mu\text{-}\eta^2\text{-dppm})$ (**3**). Thermal ellipsoids are shown at the 30% probability level; the hydrido ligand and the H atom of the methylene group are represented with dummy ellipsoids. Phenyl rings in the bridging dppm ligand have been omitted for clarity.

Table IV. Selected Interatomic Distances (Å) with Esd's for $Ru_3(\mu\text{-H})(CO)_7(\mu_3\text{-}\eta^4\text{-P}(C_6H_5)CHP(C_6H_5)(C_6H_4))(\mu\text{-}\eta^2\text{-dppm})$ (3)

Ruthenium–Ruthenium			
Ru(1)–Ru(2)	2.888 (1)		
Ru(2)–Ru(3)	3.205 (1)		
Ru(1)–Ru(3)	4.006 (1)		
Ruthenium–Carbon		Carbon–Oxygen	
Ru(1)–C(1)	1.926 (9)	C(1)–O(1)	1.15 (1)
Ru(1)–C(2)	1.890 (9)	C(2)–O(2)	1.14 (1)
Ru(1)–C(3)	1.922 (8)	C(3)–O(3)	1.14 (1)
Ru(2)–C(4)	1.924 (8)	C(4)–O(4)	1.14 (1)
Ru(2)–C(5)	1.871 (8)	C(5)-O(5)	1.14 (1)
Ru(3)–C(6)	1.899 (9)	C(6)–O(6)	1.14 (1)
Ru(3)–C(7)	1.865 (8)	C(7)–O(7)	1.15 (1)
Ru(3)–C(8)	2.229 (7)	average	1.142
Ru(1)–C(22)	2.164 (7)		
Ruthenium–Phosphorus		Phosphorus–Carbon	
Ru(1)–P(1)	2.375 (2)	P(1)–C(8)	1.771 (7)
Ru(2)–P(2)	2.361 (2)	P(2)–C(8)	1.761 (6)
Ru(2)–P(3)	2.345 (2)	P(3)–C(9)	1.840 (6)
Ru(3)–P(1)	2.230 (2)	P(4)–C(9)	1.847 (6)
Ru(3)–P(4)	2.382 (2)	P(1)–C(11)	1.771 (7)
average	2.357	P(2)–C(21)	1.821 (7)
		P(2)–C(31)	1.825 (5)
		P(3)–C(41)	1.830 (5)
Ruthenium–Hydride		P(3)–C(51)	1.839 (4)
Ru(2)–H	1.67 (6)	P(4)–C(61)	1.832 (4)
Ru(3)–H	1.69 (5)	P(4)-C(71)	1.830 (5)
Carbon–Carbon (ortho-metalated phenyl ring)		Carbon–Hydrogen (methyne group)	
C(21)–C(22)	1.39 (1)	C(8)–H(8)	0.870 (7)
C(22)–C(23)	1.40 (1)		
C(23)–C24)	1.37 (1)		
C(24)–C(24)	1.37 (1)		
C(25)–C(26)	1.40 (1)		
C(26)–C(21)	1.40 (1)		

hydride ligand, were located on a Fourier difference map. The atomic coordinates of the hydride ligand (labeled as H) and those of the hydrogen atom of the C–H group (labeled as H(8)) were refined, while hydrogen atoms of the methylene group and of the ortho-metalated phenyl ring were entered in idealized positions and held fixed during refinements. Even though all atoms of the molecular cluster unit were located, a final Fourier difference map showed four residues. The distribution of these peaks in a plane and the observed geometry were consistent with the presence of an acetone molecule in the lattice. However, attempts to refine these atoms were unsuccessfull, due to an intricate disorder problem. Consequently, this solvent molecule was not included. The final refinement, involving 376 variables from 4884 data with $F_o^2 > 3\sigma(F_o^2)$ led to $R(F) = 0.041$ and $R_w(F) = 0.044$. Final coordinates for independent atoms are listed in Table III. Anisotropic thermal parameters and rigid-group parameters are given as supplementary material in Tables S2 and S3, respectively. A listing of observed and calculated structure factor amplitudes is also available (Table S4).

Table V. Selected Bond Angles with Esd's for 3

Ru–Ru–Ru			
Ru(1)–Ru(2)–Ru(3)	82.05 (2)		
Ru–H–Ru			
Ru(2)–H–Ru(3)	144 (4)		
Ru–Ru–P			
Ru(1)–Ru(2)–P(2)	78.10 (4)	Ru(3)–Ru(2)–P(2)	70.04 (4)
Ru(2)–Ru(1)–P(1)	79.04 (4)	Ru(2)–Ru(3)–P(1)	73.26 (4)
Ru(2)–Ru(3)–P(4)	90.28 (4)	Ru(3)–Ru(2)–P(3)	87.52 (4)
Ru–Ru–C			
Ru(2)–Ru(1)–C(1)	86.4 (2)	Ru(3)–Ru(2)–C(4)	109.7 (2)
Ru(2)–Ru(1)–C(2)	174.4 (3)	Ru(3)–Ru(2)–C(5)	158.3 (2)
Ru(2)–Ru(1)–C(3)	87.2 (2)	Ru(2)–Ru(3)–C(6)	102.3 (2)
Ru(2)–Ru(1)–C(22)	88.6 (2)	Ru(2)–Ru(3)–C(7)	164.2 (3)
Ru(1)–Ru(2)–C(4)	86.3 (2)	Ru(2)–Ru(3)–C(8)	71.3 (2)
Ru(1)-Ru(2)-C(5)	90.5 (2)		
C–Ru–C			
C(1)–Ru(1)–C(2)	97.1 (4)	C(3)–Ru(1)–C(22)	86.3 (3)
C(1)–Ru(1)–C(3)	95.7 (3)	C(4)–Ru(2)–C(5)	89.9 (3)
C(2)–Ru(1)–C(3)	96.8 (4)	C(6)–Ru(3)–C(7)	91.1 (3)
C(2)-Ru(1)–C(22)	87.7 (3)	C(7)–Ru(3)–C(8)	93.1 (3)
P–Ru–P			
P(2)–Ru(2)–P(3)	99.85 (6)	P(1)–Ru(3)–P(4)	147.36 (7)
Ru–P–Ru			
Ru(1)–P(1)–Ru(3)	117.16 (8)		
P–Ru–C			
P(1)–Ru(1)–C(1)	87.9 (2)	P(1)–Ru(3)–C(6)	112.0 (2)
P(1)–Ru(1)–C(2)	96.6 (2)	P(1)–Ru(3)–C(7)	94.1 (3)
P(1)–Ru(1)–C(22)	89.0 (2)	P(1)–Ru(3)–C(8)	45.8 (2)
P(2)–Ru(2)–C(5)	88.5 (2)	P(4)–Ru(3)–C(6)	98.8 (2)
P(3)–Ru(2)–C(4)	95.8 (2)	P(4)–Ru(3)–C(7)	95.9 (3)
P(3)–Ru(2)–C(5)	99.9 (2)	P(4)–Ru(3)–C(8)	102.6 (2)
P–Ru–H			
P(2)–Ru(2)–H	87 (2)	P(1)–Ru(3)–H	82 (2)
P(3)–Ru(2)–H	84 (2)	P(4)–Ru(3)–H	90 (2)
C–Ru–H			
C(4)–Ru(2)–H	92 (2)	C(6)–Ru(3)–H	85 (2)
C(5)–Ru(2)–H	174 (2)	C(7)–Ru(3)–H	173 (2)
		C(8)–Ru(3)–H	88 (2)
Cyclometalated Ring			
P(1)–C(8)–Ru(3)	69.2 (2)	P(1)–C(8)–H(8)	124 (4)
Ru(3)–P(1)–C(8)	64.4 (2)	P(2)–C(8)–H(8)	114 (4)
P(1)–Ru(3)–C(8)	45.8 (2)	Ru(3)–C(8)–H(8)	124 (4)

Results and Discussion

A. Description of the Structure of $Ru_3(\mu\text{-H})(CO)_7((C_6H_5)PCHP(C_6H_5)(C_6H_4))$(dppm) (13). A perspective view of the molecule is given in Figure 1. Interatomic distances and selected bond angles are listed in Tables IV and V, respectively. The structure of this 50e cluster consists of a triangular array of metal atoms involving two metal–metal bonds (Ru(1)–Ru(2) = 2.888 (1) Å; Ru(2)–Ru(3) = 3.205 (1) Å) while the third metal–metal

Scheme I

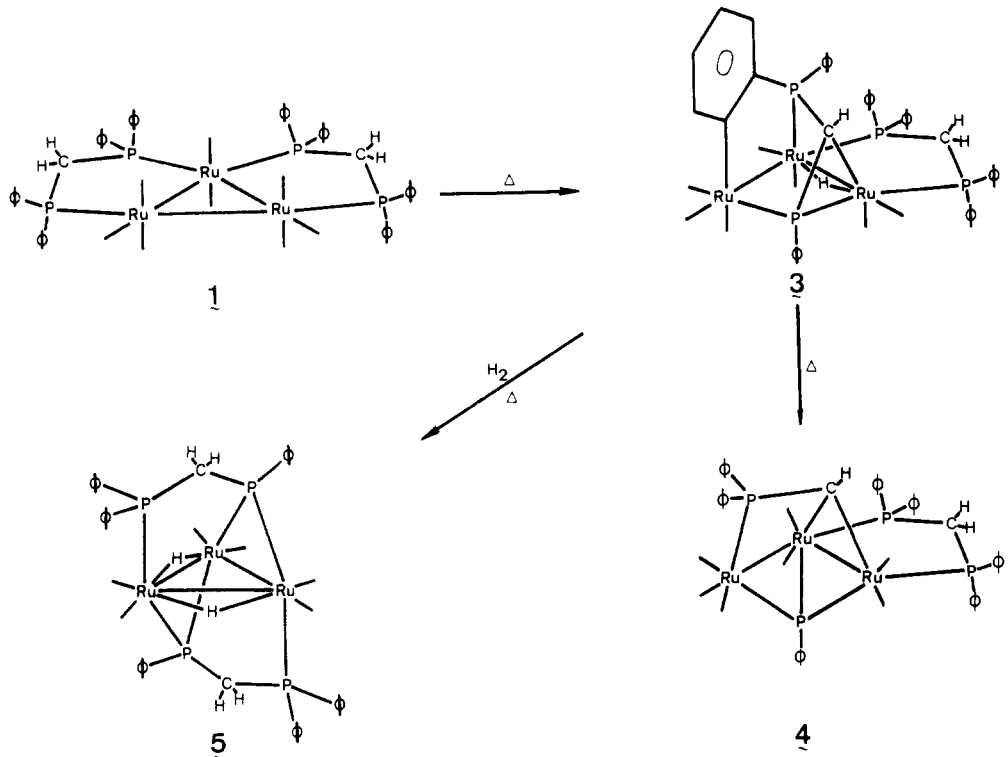

separation, Ru(1)···Ru(3) = 4.006 (1) Å, is clearly nonbonding. A dppm molecule is still bridging the metal–metal vector Ru(2)–Ru(3), in a equatorial position as referred to the parent cluster 1.[18] The second dppm molecule has provided the face-bridging organic fragment $((C_6H_5)PCHP(C_6H_5)(C_6H_4))$ which acts as a seven-electron donor through five bonds (Ru(1)–P(1) = 2.375 (2) Å; Ru(3)–P(1) = 2.230 (2) Å; Ru(3)–C(8) = 2.229 (7) Å; Ru(2)–P(2) = 2.361 (2) Å; Ru(1)–C(22) = 2.164 (7) Å). The presence of a hydride ligand bridging the metal–metal vector Ru(2)–Ru(3) may account for the unusually high metal–metal separation observed here (vide supra). The environment of metal atoms is achieved by seven carbonyl groups. The distribution and symmetry of these CO groups are similar to those found in $Ru_3(CO)_7(\mu_3\text{-}P(C_6H_5))(\mu_3\text{-}\eta^2\text{-}CHP(C_6H_5)_2)(dppm)$[8] (4) as also shown by the analogy of infrared spectra (see Experimental Section).

A salient feature in this structure is the occurrence of an unusual triangular cyclometalated ring, P(1)–C(8)–Ru(3), where adjacent phosphorus and carbon atoms P(1) and C(8) are coordinated to the same ruthenium atom Ru(3).

Spectroscopic evidence for closely related metalations has been obtained for mononuclear complexes.[19,20] A similar bonding situation was also described for the ligand $[R_2PCHPR_2]^-$.[21-23]

B. Pathways for the Cluster-Assisted Transformations of dppm. The isolation of the new cluster complex $Ru_3(\mu\text{-}H)(CO)_7(\mu_3\text{-}\eta^4\text{-}(C_6H_5)PCHP(C_6H_5)(C_6H_4))(\mu\text{-}\eta^2\text{-}dppm)$ (3) in a controlled thermolysis of $Ru_3(CO)_8(\mu\text{-}\eta^2\text{-}dppm)_2$ (1) provides a link between the parent cluster 1 and the already reported complexes 4[8] and 5[9] (Scheme I). This deserves several comments.

(i) Compound 3 illustrates a key intermediate step preceding the cleavage of a P–C bond. This is one step further than in the related species $Ru_3(CO)_9(\mu_3\text{-}\eta^3\text{-}(C_6H_5)PCH_2P(C_6H_5)(C_6H_4))$ (I) derived from $Ru_3(CO)_{10}(\mu\text{-}\eta^2\text{-}dppm)$.[7] In both intermediate species, the ortho

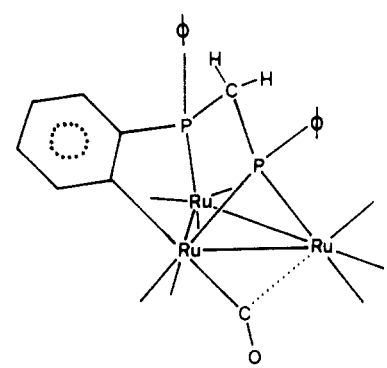

I

metalation process has provided the hydrogen atom required for the observed reductive elimination of benzene. The hydride ligand in the 50e cluster 3 is derived from the metalation of the methylene group. Though not observed in our experiment, a 48e species formulated as $Ru_3(CO)_7(\mu_3\text{-}\eta^3\text{-}(C_6H_5)PCH_2P(C_6H_5)(C_6H_4))(\mu\text{-}\eta^2\text{-}dppm)$ is believed to be the antecedent of 3.

(ii) The observation of a facile reaction of 3 with molecular hydrogen is consistent with the occurrence of two metal–carbon bonds which are prone to a demetalation process (we were not able to isolate any intermediates in the conversion of 3 into 5). This observation would also suggest that intramolecular oxidative addition of dppm has preceded oxidative addition of hydrogen in the direct reaction of 1 with molecular hydrogen.[9]

(iii) Regarding the intramolecular rearrangement of 3 into 4, there is evidence to suggest that *coordination of*

(18) Lavigne, G.; Lugan, N.; Bonnet, J. J. *Acta Crystallogr., Sect. B: Struct. Crystallogr. Cryst. Chem.* **1982**, *B38*, 1911.
(19) Rathke, J. W.; Muetterties, E. L. *J. Am. Chem. Soc.* **1975**, *97*, 3272.
(20) Harris, T. V.; Rathke, J. W.; Muetterties, E. L. *J. Am. Chem. Soc.* **1978**, *100*, 6966.
(21) Dawkins, G. M.; Green, M.; Jeffery, J. C.; Stone, F. G. A. *J. Chem. Soc., Chem. Comm.* **1980**, 1120.
(22) Dawkins, G. M.; Green, M.; Jeffery, J. C.; Sambale, C.; Stone, F. G. A. *J. Chem. Soc., Dalton Trans.* **1983**, 499.
(23) Karsch, H. H. *Angew. Chem., Int. Ed. Engl.* **1982**, *21*, 921.

adjacent phosphorus and carbon atoms to one metal center is an important transition state permitting subsequent cleavage of the phosphorus–carbon bond. The primary steps involved here must occur in some order: (a) cleavage of the phosphorus–carbon bond within the triangular cyclometalated ring P(1)–C(8)–Ru(3) (oxidative addition to the metal); (b) formation of a C–H bond resulting from a hydride shift to the ortho-metalated phenyl ring (reductive elimination).

Such a splitting of the ligand yields two organic fragments which next rearrange on the cluster faces: the phosphinidene ligand caps one of the faces, while the phosphinocarbene ligand $CHP(C_6H_5)_2$ caps the other one in compound 4.

A comparable sequence may also govern the transformation of the ligand R_2PCH_2PR in $Fe_3(\mu\text{-}H)(CO)_9(R_2PCH_2PR)$ to yield $Fe_3(CO)_9(\mu_3\text{-}PR)(R_2PCH_3)$.[24] One may also notice analogies between such transformations of phosphorus-containing ligands and the desulfurization of a thioformamido ligand in an osmium cluster.[25]

While the final steps of the transformation of dppm were clearly established in the reaction reported here (Scheme I), we were interested in clarifying the unknown initial step. Parallel studies of the thermolysis of $Os_3(CO)_{10}(dppm)$[26] provided evidence for initial orthometalation of a phenyl ring in the monohydrido cluster species $Os_3(\mu\text{-}H)(CO)_8((C_6H_5)(C_6H_4)PCH_2P(C_6H_5)_2)$. The X-ray structure of the latter complex indicated migration of the dppm ligand from the equatorial to the axial position.

In connection with this observation, we thought that oxidative cleavage of dppm could be facilitated in complexes where the bridging ligand occupies an axial position. Indeed, such a position would favor interactions between phenyl rings and metal centers. With this in mind, we prepared the complex $Ru_4(\mu\text{-}H)_4(CO)_{10}(dppm)$ (6) in which the Ru–P vectors are approximately perpendicular to a cluster face,[27] as also found in $Ru_4(\mu\text{-}H)_4(CO)_{10}(\mu\text{-}\eta^2\text{-diphos})$[28] (diphos = bis(diphenylphosphino)ethane). Thermolysis of 6 afforded $Ru_4(\mu\text{-}H)_3(CO)_{10}(\mu_3\text{-}\eta^2\text{-}(C_6H_5)PCH_2P(C_6H_5)_2)$ (7) in 76% yield. On the basis of spectroscopic data, we assign the structure shown to the new complex 7.

Indeed, (i) evidence for the presence of three hydride ligands can be obtained from mass spectrometry data. Analysis of the parent ion multiplet by using the MASPAN program[13] reveals a satisfactory estimate of the goodness of fit between observed and calculated intensities (R = 6.6%) taking into account three hydride ligands (see also Table S1).

(ii) The ^{31}P NMR spectrum exhibits a low-field signal (δ 244.95) consistent with a phosphorus atom bridging a Ru–Ru single bond and a higher signal (δ 20.75) typical for a terminal phosphorus atom.

(iii) The ^1H NMR spectrum shows equivalence of H nuclei within the methylene group, thus revealing a mirror plane symmetry for the molecule. In the high-field region, the spectrum also shows a distribution of the three hydride ligands in two sites of different symmetry. The signal at

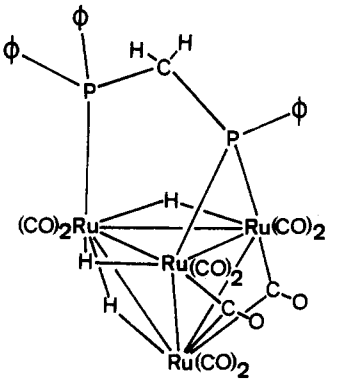

7

−17.45 ppm is assigned to a unique hydride ligand bridging the metal–metal vector trans to the terminal phosphorus atom (as evidenced by the value of the coupling constant J_{PH} of 39.4 Hz). The occurrence of a unique signal at −19.30 ppm for two other hydride ligands is consistent with the magnetic equivalence of both these atoms. Lower J_{PH} values (J_{P_aH} = 9.8 Hz; J_{P_bH} = 17.7 Hz) are interpreted as resulting from cis positions of the hydrides relative to P_a and P_b.[29]

(iv) In regards to the symmetry of the molecule inferred from NMR data, the bridging carbonyl group detected by IR spectroscopy might bridge the metal–metal vector also supported by the phosphorus atom. **Note added in proof:** By the time the paper was in press, an X-ray study[34] showed the actual structure to involve two bridging carbonyls, as indicated in the above picture.

Noticeably, the tetranuclear compound 7 reacts with CO at atmospheric pressure to yield the trinuclear compound $Ru_3(\mu\text{-}H)(CO)_9(\mu_3\text{-}\eta^2\text{-}(C_6H_5)PCH_2P(C_6H_5)_2)$ (8), while the expelled mononuclear fragment is recombined as $Ru_3(CO)_{12}$ which is detected in the reaction. Complex 8 was already reported as the main product from the reaction of $Ru_3(CO)_{10}(\mu\text{-}\eta^2\text{-dppm})$ with H_2.[7,30]

The formation of complex 7 raises several intriguing questions. (i) For unknown reasons, oxidative cleavage of C–H and C–P bonds in dppm seems easier than that for closely related ligands. Typically, thermolysis of $Ru_4(\mu\text{-}H)_4(CO)_{10}(diphos)$ yields no oxidative cleavage, but a simple rearrangement in which the initially edge-bridging diphos behaves as a chelating ligand about one ruthenium center.[28] Noticeably, we do observe traces amount of a complex which exhibits an IR spectrum similar to the species involving the chelating diphos reported by Shapley et al.[28] (see Experimental Section). However, this is a minor side reaction in the case of dppm.

(ii) The transformation of the electronically saturated species involves sequences of oxidative additions and reductive eliminations, though no evidence for formation of a vacant coordination site appears. Indeed, the reaction proceeds without CO evolution (see Experimental Section). We thus postulate that opening of the tetrahedral structure by cleavage of one metal–metal bond may provide the vacant site required for the transformation of the ligand.

Catalytic Tests. Since compounds 6 and 7 were available in good yield, we attempted an investigation of their catalytic properties. The hydrogenation of cyclo-

(24) Stelzer, O.; Hietkamp, S.; Sommer, H. *Phosphorous Sulfur* **1983**, *18*, 279.

(25) (a) Adams, R. D.; Dawoodi, Z. *J. Am. Chem. Soc.* **1981**, *103*, 6510. (b) Adams, R. D.; Dawoodi, Z.; Foust, D. F.; Segmüller, B. E. *Organometallics* **1983**, 2, 315.

(26) Clucas, J. A.; Foster, D. F.; Harding, M. M.; Smith, A. K. *J. Chem. Soc., Chem. Commun.* **1984**, 949.

(27) The X-ray structure of $Ru_4(\mu\text{-}H)_4(CO)_{10}(dppm)$ is to be published separately. Mansilla, F.; Lavigne, G.; Bonnet, J. J. *Acta Crystallogr.*, submitted for publication.

(28) Churchill, M. R.; Lashewycz, R. A.; Shapley, J. R.; Richter, S. I. *Inorg. Chem.* **1980**, *19*, 1277.

(29) Shapley, J. R.; Richter, S. I.; Churchill, M. R., Lashewycz, R. A. *J. Am. Chem. Soc.* **1977**, *99*, 7384.

(30) Bruce, M. I.; Horn, E.; Snow, M. R.; Williams, M. L. *J. Organomet. Chem.* **1984**, *276*, C53–57.

Table VI. Results of Catalytic Hydrogenation of Cyclohexene in the Presence of Various Cluster Complexes Derived from $Ru_4(\mu\text{-}H)_4(CO)_{12}$

cat. precursor	amount of cat. added, mol	cat. recovered	half-time $t_{1/2}$, min	turnover, s^{-1}
$Ru_4(\mu\text{-}H)_4(CO)_{12}$	4.30×10^{-5}	yes	120	0.566
$Ru_4(\mu\text{-}H)_4(CO)_{10}$-(dppm) (6)	4.29×10^{-5}	no	230	0.194
$Ru_4(\mu\text{-}H)_3(CO)_{10}$-($PhPCH_2PPh_2$) (7)	4.32×10^{-5}	yes	50	0.211
$Ru_3(\mu\text{-}H)(CO)_9$-($PhPCH_2PPh_2$) (8)	5.7×10^{-2}	yes		4×10^{-4}

[a] Routine experimental conditions are as follows: amount of cyclohexene, 5 cm^3; solvent THF, 50 cm^3, temperature, 80 °C, $P(H_2)$, 40 bars. Turnover is defined as the number of moles of substrate converted per mole of catalyst per unit time (second) at the origin. All catalytic runs were checked three times, leading to reproducible results.

hexene was chosen as a test reaction, and the efficiency of **6** and **7** was compared with that of the nonsubstituted cluster $Ru_4(\mu\text{-}H)_4(CO)_{12}$ which was known from earlier studies to be an efficient hydrogenation catalyst for olefins.[31,32] This conversion was made under routine experimental conditions. No attempts were made to optimize such conditions.

The results are summarized in Table VI. A kinetic study on **7** indicated first-order rate dependence in cyclohexene concentration, as shown in Figure 2. The corresponding rate constant was 8.03×10^{-3} min^{-1}. This study deserves the following comments.

(i) Compound **6** is not recovered at the end of the catalytic run, due to its expected quantitative conversion into **7** (see Experimental Section). **7** is believed to be the actual catalyst precursor. Let us recall here the related observation concerning hydroformylation of propene in the presence of $Rh_4(CO)_{10}(PPh_3)_2$ where the catalytic reaction was found to take place with transformation of the phosphine ligand.[33]

(ii) The hydrogenation of cyclohexene into cyclohexane occurs in the presence of compound **7**. At the end of a catalytic run, **7** is the only detectable Ru compound in solution; it can be recovered in 100% yield within experimental error.

Since fragmentation of **7** into the trinuclear complex **8** was observed under CO atmosphere (see Experimental Section), we examined the catalytic activity of **8** under the same conditions as for **7** and found this complex inactive. This would support the idea that the active species is a tetranuclear complex. Activation of the olefin in such a species requires prior coordinative unsaturation, which may be achieved by CO dissociation, opening of the phosphorus bridge, or reversible opening of a metal–metal bond. Mechanistic studies aimed to determine the actual process are in progress.

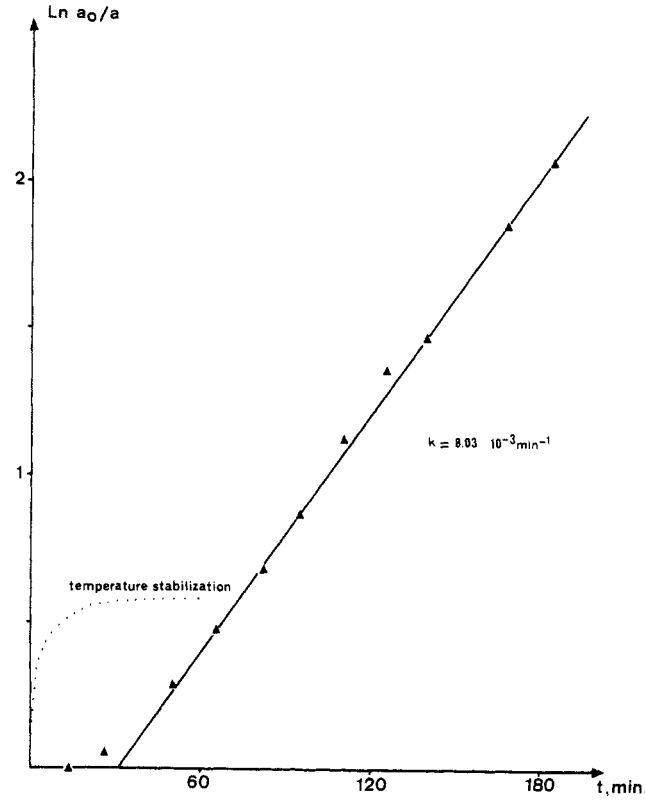

Figure 2. Kinetic study of the hydrogenation of cyclohexene in the presence of **7** [ln (a_0/a) as a function of time].

Conclusion

The cluster-assisted transformation of bis(diphenylphosphino)methane can be viewed as the result of a cooperative interaction of three metal centers. At the intermediate step, this ligand is seen to be coordinated to two metal centers, while the activation process is performed by the third one. The whole reaction involves sequences of oxidative addition/reductive elimination steps. Such transformations do not require loss of carbon monoxide; the corresponding changes in the formal oxidation state of the metal atoms are balanced by sequential rupture and formation of metal–metal bonds.

Investigators using phosphine-substituted metal clusters in catalysis should be aware that such transformations are extremely facile and may occur under the experimental conditions currently used for the hydrogenation of olefins. As demonstrated here in one case, the resulting species may act as an efficient catalyst precursor.

Acknowledgment. This work was supported by the CNRS through a "A.T.P., Chimie Fine". We wish to thank Dr. G. Commenges for fruitful discussions regarding NMR, Dr. Jean Roussel for recording mass spectra data, and Johnson Matthey for a generous loan of $RuCl_3$.

Registry No. **1**, 77611-27-9; **2**, 15243-33-1; **3**, 98944-60-6; **4**, 77611-28-0; **5**, 98944-61-7; **6**, 98976-60-4; **7**, 98976-61-5; $Ru_4(\mu\text{-}H)_4(CO)_{12}$, 34438-91-0; $(C_6H_5)_2PCH_2P(C_6H_5)_2$, 2071-20-7; cyclohexene, 110-83-8; cyclohexane, 110-82-7.

Supplementary Material Available: Table S1, mass spectrometry data, Table S2, anisotropic thermal parameters for independent atoms, Table S3, rigid-group parameters, and Table S4, listing of observed and calculated structure factor amplitudes (29 pages). Ordering information is given on any masthead page.

(31) Frediani, P.; Matteoli, U.; Bianchi, M.; Piacenti, F.; Menchi, G. *J. Organomet. Chem.* **1978**, *150*, 273.
(32) Doi, Y.; Koshizuka, K.; Keii, T. *Inorg. Chem.* **1982**, *21*, 2732 and references therein.
(33) Chini, P.; Martinengo, S.; Garlaschelli, G. *J. Chem. Soc., Chem. Commun.* **1972**, 709.
(34) Bruce, M. I., personal communication.

d^0–d^8 Heterobimetallic Complexes as Catalysts: Molecular and Crystal Structure of a Zirconium–Dirhodium Complex, $Rh_2(\mu\text{-}t\text{-BuS})_2[(\mu\text{-}Ph_2PCH_2)_2Zr(\eta\text{-}C_5H_5)_2](CO)_2$

Robert Choukroun,[1a] Danièle Gervais,*[1a] Joël Jaud,[1b] Philippe Kalck,*[1c] and François Senocq[1c]

Laboratoire de Chimie de Coordination du CNRS, Unité No. 8241 liée par convention à l'Université Paul Sabatier, 31400 Toulouse, France, GITER, CNRS, 31400 Toulouse, France, and Laboratoire de Chimie Minérale et de Cristallochimie, Ecole Nationale Supérieure de Chimie, 31077 Toulouse Cedex, France

Received April 1, 1985

Addition of the zirconium(IV) diphosphine $(\eta^5\text{-}C_5H_5)_2Zr(CH_2PPh_2)_2$ to the (μ-thiolato)dirhodium(I) complex $Rh_2(t\text{-BuS})_2(CO)_4$ results in the hydroformylation-active bimetallic species $Rh_2(\mu\text{-}t\text{-BuS})_2[(\mu\text{-}Ph_2PCH_2)_2Zr(\eta^5\text{-}C_5H_5)_2](CO)_2$, the crystal and molecular structures of which were studied by ^1H, ^{13}C, and ^{31}P NMR spectroscopy and by X-ray diffraction. The compound crystallizes in the monoclinic space group $P2_1/c$, with four molecules in a cell having dimensions a = 16.020 (4) Å, b = 16.237 (7) Å, c = 18.304 (8) Å, and β = 112.61 (3)°. The zirconium diphosphine bridges the two rhodium atoms in a cis arrangement toward the bent (μ-thiolato)dirhodium core. One of the sulfur atoms interacts with the zirconium giving a pentacoordinated 18-electron configuration. This unprecedented geometry explained the inequivalences shown in ^1H and ^{13}C spectra and is related to the stoichiometric and catalytic reactivity.

Introduction

We have recently shown[2] that hydroformylation of 1-hexene is catalyzed at low pressure and low temperature (5 bar, 80 °C) by addition of the zirconium(IV) diphosphine $(\eta\text{-}C_5H_5)_2Zr(CH_2PPh_2)_2$ to the inactive (μ-thiolato)dirhodium(I) species $Rh_2(\mu\text{-S-}t\text{-Bu})_2(CO)_4$. Comparison with the catalytic activity obtained when 1,4-bis(diphenylphosphino)butane is used instead of the zirconium diphosphine demonstrated the important role of the zirconium atom.

We have investigated the structure of the bimetallic complex $Rh_2(\mu\text{-}t\text{-BuS})_2[(\mu\text{-}(Ph_2PCH_2)_2Zr(\eta\text{-}C_5H_5)_2](CO)_2$ (1), readily obtained in the catalytic mixture as well as by mixing the two reactants in 1:1 stoichiometry in toluene at room temperature.

Spectroscopic Data

Experimental Data. All preparations were carried out under argon using Schlenk techniques. All solvents were dried and distilled under argon and degassed before use. $Cp_2Zr(CH_2PPh_2)_2$ may be prepared either as previously reported by Schore[3] or by the procedure used for $Cp_2Ti(CH_2PPh_2)_2$.[4] $Rh_2(\mu\text{-}t\text{-BuS})_2(CO)_4$ was prepared as previously reported.[5]

^1H, ^{31}P, and ^{13}C NMR spectra were recorded on Bruker WH90 and WM 250 spectrometers. Values of ^{31}P chemical shifts are positive downfield from external 85% H_3PO_4 in D_2O.

Microanalyses were performed by the Service Central de Microanalyses du CNRS.

Preparation of $Rh_2(\mu\text{-S-}t\text{-Bu})_2[(\mu\text{-}Ph_2PCH_2)_2Zr(\eta\text{-}C_5H_5)_2](CO)_2$. A solution of the dinuclear rhodium complex $Rh_2(\mu\text{-}t\text{-BuS})_2(CO)_4$ (0.383 g, 0.77 mmol) in 15 mL of toluene was added slowly at room temperature to a 15-mL toluene solution of $Cp_2Zr(CH_2PPh_2)_2$ (0.478 g, 0.77 mmol). The resulting solution was stirred for 30 min and evaporated to 5 mL. Pentane (20 mL) was added to give a yellow precipitate which was filtered, washed with pentane, and dried under vacuum: yield 85%; IR ν(CO) 1930, 1945 cm^{-1}; $^{31}P\{^1H\}$ NMR δ 53.1 (d, $^1J_{Rh\text{-}P}$ 140 Hz). Recrystallization from a saturated CH_2Cl_2 solution by slow evaporation of the solvent gave crystals suitable for X-ray analysis.

Anal. Calcd for $C_{46}H_{52}Rh_2ZrO_2P_2S_2$: C, 52.1; H, 4.9; P, 5.9; Zr, 8.6. Found: C, 52.3; H, 5.1; P. 6.2; Zr, 8.8.

Results and Discussion. From analytical data and IR and ^{31}P NMR spectra a structure could be proposed with one CO ligand per rhodium atom and two equivalent phosphorus nuclei each bonded to one rhodium atom giving a cis arrangement as seen in I.

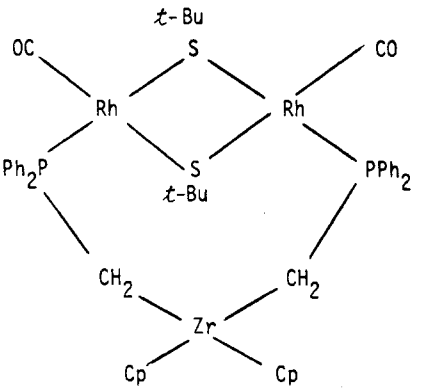

I

In the $^{13}C\{^1H\}$ spectrum (see Table I) the equivalent carbonyl groups give a doublet of doublets resulting from coupling to one rhodium and one phosphorus. The quaternary carbons and the methyl carbons of the *tert*-butyl groups give two sets of peaks due to the magnetic inequivalence of the thiolato-bridging groups (endo and exo positions) as previously reported for various complexes of general formula $[M(SR)(CO)L]_2$ with M = Rh[5] or Ir.[6]

The bridging diphosphine with the Rh–S–Rh sequence gives an eight-membered ring, and we observed that the four phenyl groups give two separate sets of peaks of equal

(1) (a) Laboratoire de Chimie de Coordination. (b) GITER. (c) Laboratoire de Chimie Minérale et Cristallochimie.

(2) Senocq, F.; Randrianalimanana, C.; Thorez, A.; Kalck, P.; Choukroun, R.; Gervais, D. *J. Chem. Soc., Chem. Commun.* **1984**, 1376.

(3) Schore, N. E.; Young, S. J.; Olmstead, M. M.; Hofmann, P. *Organometallics* **1983**, *2*, 1769.

(4) Etienne, M.; Choukroun, R.; Basso-Bert, M.; Dahan, F.; Gervais, D. *Nouv. J. Chim.* **1984**, *8*, 531.

(5) Kalck, P.; Poilblanc, R. *Inorg. Chem.* **1975**, *14*, 2779.

(6) de Montauzon, D.; Kalck, P.; Poilblanc, R. *J. Organomet. Chem.* **1980**, *186*, 121.

0276-7333/86/2305-0067$01.50/0

Table I. $^{13}C\{^1H\}$ NMR Data for $[Rh_2(\mu\text{-}t\text{-}BuS)_2\{(Ph_2PCH_2)_2Zr(\eta\text{-}C_5H_5)_2\}(CO)_2]$ and Related Derivatives

compound[a]	δ_{CO}	$^1J_{Rh-C}$, Hz	$^2J_{P-C}$, Hz	*t*-BuS δ_{S-C-C}	*t*-BuS δ_{S-C-C}
$Rh_2(\mu\text{-}t\text{-}BuS)_2[(Ph_2PCH_2)_2ZrCp_2](CO)_2$[b]	193.0	76.3	12.2	33.9 45.4	35.2 37.7
$Rh(PPh_3)_2(CO)Cl$[c]	187.4	73	16		
$Ir_2(\mu\text{-}t\text{-}BuS)_2(PMe_3)_2(CO)_2$[d]	179.67		9.3	46.37 53.29 46.90	33.48 39.66 34.55
$Rh_2(\mu\text{-}t\text{-}BuS)_2(CO)_4$[e]					
$Rh_2(\mu\text{-}t\text{-}BuS)_2[Ph_2P(CH_2)_4PPh_2](CO)_2$[f]				44.33 49.97	34.82 38.38

[a] Cp = η-C_5H_5. [b] In CD_2Cl_2. Other resonance peaks: C_5H_5, 109.7 and 112.2 ppm; phenyl C^1, 144.9 ($^1J_{PC}$ = 30.5 Hz) and 139.6 ppm ($^1J_{PC}$ = 42.7 Hz); C^2, 134.2 ($^2J_{PC}$ = 12.1 Hz) and 131.6 ppm ($^2J_{PC}$ = 12.2 Hz); C^3-C^4, multiplet 129.7-128.1 ppm. [c] From ref 7 in $CDCl_3$. [d] From ref 6 in CD_2Cl_2. [e] Measured in C_6D_6. [f] In $CDCl_3$ (Kalck, P.; Randrianalimanana, C.; Thorez, A., unpublished results).

Table II. IR and ^1H NMR Data for $Rh_2(\mu\text{-}t\text{-}BuS)_2[(Ph_2PCH_2)_2Zr(\eta\text{-}C_5H_5)_2](CO)_2$ and Related Derivatives

compound[a]	ν_{CO}, cm^{-1}	$\delta(t\text{-}BuS)$[f]	$\delta(C_5H_5)$[f]	$\delta(PCH)$[g]	$^2J_{P-H}$, Hz	$^3J_{Rh-H}$, Hz
1, $Rh_2(\mu\text{-}t\text{-}BuS)_2[(Ph_2PCH_2)_2ZrCp_2](CO)_2$	1930	1.43	5.45	1.27	17.5	1.9
	1945	2.19	6.16	2.17[h]	11.4	0
2, $Rh_2(SPh)_2(PMe_3)_2(CO)_2$[b]	1972			1.29	9.6	1.2
	1985			1.58[i]	9.6	1.2
3, $Ir_2(\mu\text{-}t\text{-}BuS)_2(PMe_3)_2(CO)_2$[c]	1942	1.58		1.39[f]	9.7	
	1956	1.92				
4, $Cp_2Zr(CH_2PPh_2)_2$[d]			5.76	0.97[f]	3	
5, $Cp_2Zr(CH_2PPh_2)_2Cr(CO)_4$[d]			5.30	1.50[f]	6	
6, $Cp_2Zr(CH_2PPh_2)_2Rh(CO)Cl$[e]			6.10	2.16[f]	3.4	0.9

[a] Cp = η-C_5H_5. [b] From ref 6. [c] From ref 7. [d] From ref 3. [e] From ref 8. [f] In C_6D_6 (or C_6H_6). [g] PCH_2 or PCH_3. [h] In toluene-d_8. [i] In CH_2Cl_2.

intensity. This is indicative of two nonequivalent kinds of phenyl bonded to the phosphorus nuclei. The cyclopentadienyl groups η^5-bonded to zirconium also clearly are nonequivalent (Table I).

In the ^1H spectrum, these inequivalences are confirmed (see Table II) and the corresponding chemical shift separation depends on the nature of the solvent (for instance, *t*-BuS, 2.19 and 1.43 ppm in C_6D_6, 2.27 and 1.52 ppm in toluene-d_8, 1.76 and 1.17 ppm in CD_2Cl; cyclopentadienyl, 6.16 and 5.45 ppm in C_6D_6, 6.26 and 5.76 ppm in toluene-d_8, 6.04 and 5.99 ppm in CD_2Cl_2). The spectrum is unaffected when the temperature is lowered to −80 °C or raised to 100 °C (in toluene-d_8). Moreover, while in the ^{13}C spectrum the methylene resonance ($Zr-CH_2-P$) could not be clearly distinguished, in the ^1H spectrum we can see a complex pattern appearing as two sets of peaks of equal intensity: a pseudotriplet and two doublets of doublets. This reveals the nonequivalence of the hydrogen nuclei of each methylene group. By irradiation techniques and ^{31}P decoupling the pseudotriplet could be attributed to H_A with δ_A 2.17 ($^2J_{H-H}$ = 11.5 Hz, ^2J_H = 11.4 Hz, $^3J_{H-Rh} \approx 0$) and the octet to H_B with δ_B 1.27 ($^2J_{H-H}$ = 11.5 Hz, ^2J_H = 17.5 Hz, ^3J_H = 1.94 Hz) (in toluene-d_8).

As the proposed structure is unprecedented and the strong magnetic inequivalences observed by NMR spectroscopy have not been described previously and lack ready explanation, it seemed necessary to investigate the crystal structure of complex 1.

X-ray Structure

Experimental Data. A green-yellow needle-shaped crystal of $C_{46}H_{52}Rh_2ZrO_2P_2S_2$ having approximate dimensions of 0.25 × 0.05 × 0.05 mm was mounted in a glass capillary, on a CAD4 Enraf-Nonius PDP 11/23 computer-controlled single-crystal diffractometer. The unit cell was refined by optimizing the setting of 25 reflections (Mo Kα radiation). The results are shown in Table III as well as the schedule for the measurement of the intensity of the reflections which were corrected for Lorentz–polarization factors; empirical absorption corrections were applied.

Table III. Crystallographic Experimental Details

A. Crystal Data

formula: $C_{46}H_{52}Rh_2ZrO_2P_2S_2$	a = 16.020 (4) Å
fw: 1056.00	b = 16.237 (7) Å
$f(000)$ = 2128	c = 18.304 (8) Å
cryst dimens: 0.25 × 0.05 × 0.05 mm	β = 112.61 (3)
Mo Kα radiatn: λ = 0.71073 Å	V = 4395.3 Å^3
temp: 20 °C ± 1°	Z = 4
monoclinic space group $P2_1/c$	ρ = 1.60 g/cm^3
	μ = 11.6 cm^{-1}

B. Intensity Measurements

instrument	Enraf-Nonius CAD4 diffractometer
monochromator	graphite crystal, incident beam
attenuator	Zr foil, factor 19.4
takeoff angle	3.2°
detector aperture	4.0 mm horizontal 4.0 mm vertical
cryst detector dist	21 cm
scan type	θ–2θ
scan rate	1–10°/min (in ω)
Scan width, deg	0.9 + 0.350 tan θ
maximum 2θ	55.0°
no of reflctn measd	8748 total, 5208 unique
correctns	Lorentz–polarization linear decay (from 0.964 to 1.177 on I) empirical absorptn

C. Structure Solution and Refinement

solution	direct methods
hydrogen atoms	included as fixed contribution to the structure factor
minimization functn	$\sum w(\lvert F_o\rvert - \lvert F_c\rvert)^2$
least-squares weights	$4F_o^2/\sigma^2(F_o^2)$
anomalous dispersn	all non-hydrogen atoms
reflections included	5080 with $I > 2\sigma(I)$
parameters refined	497
unweighted agreement factor	0.034
weighted agreement factor	0.038
high peak in final diff map	0.14 (19) e/Å^{-3}

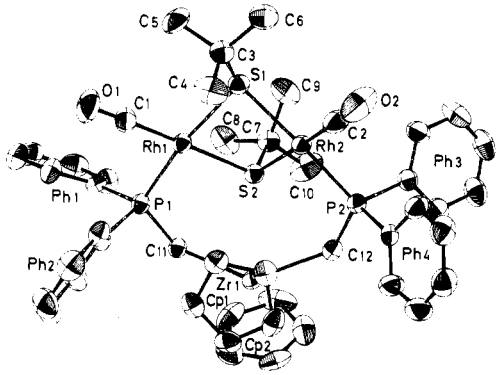

Figure 1. An ORTEP drawing of $Rh_2(S\text{-}t\text{-}Bu)_2[(Ph_2PCH_2)_2Zr(\eta\text{-}C_5H_5)_2](CO)_2$ (1) with 50% thermal ellipsoids. Cp1 and Cp2 contain the atoms C(37)–C(41) and C(42)–C(46). Ph1, Ph2, Ph3, and Ph4 contain C(13)–C(18), C(19)–C(24), C(25)–C(30), and C(31)–C(36), respectively.

Table IV. Selected Positional and Thermal Parameters for $Rh_2(\mu\text{-}t\text{-}BuS)_2[(Ph_2PCH_2)_2Zr(\eta\text{-}C_5H_5)_2](CO)_2$ (1)

atom	x	y	z	B, Å^2
Rh(1)	0.13203 (3)	0.20525 (3)	0.23440 (3)	2.501 (9)
Rh(2)	0.34976 (3)	0.19150 (3)	0.25077 (3)	2.558 (9)
Zr(1)	0.28107 (4)	0.43773 (4)	0.30387 (3)	2.34 (1)
P(1)	0.0634 (1)	0.3197 (1)	0.25514 (9)	2.44 (3)
P(2)	0.4617 (1)	0.2884 (1)	0.30011 (9)	2.63 (3)
S(1)	0.2272 (1)	0.0968 (1)	0.22525 (9)	2.74 (3)
S(2)	0.2752 (1)	0.2556 (1)	0.32719 (9)	2.53 (3)
O(1)	−0.0499 (4)	0.1487 (4)	0.1299 (4)	7.1 (2)
O(2)	0.4343 (4)	0.1090 (4)	0.1524 (3)	7.7 (2)
C(1)	0.0218 (4)	0.1692 (5)	0.1679 (4)	3.9 (2)
C(2)	0.4015 (5)	0.1426 (4)	0.1901 (4)	4.0 (2)
C(3)	0.1845 (4)	0.0412 (4)	0.1287 (4)	3.1 (1)
C(7)	0.3082 (4)	0.2040 (4)	0.4284 (3)	3.1 (1)
C(11)	0.1413 (4)	0.3965 (4)	0.3154 (3)	2.4 (1)
C(12)	0.4293 (4)	0.3768 (4)	0.3433 (4)	3.1 (1)
C(13)	−0.0193 (4)	0.2973 (4)	0.2988 (3)	2.5 (1)
C(19)	−0.0102 (4)	0.3777 (4)	0.1686 (3)	2.8 (1)
C(25)	0.5628 (4)	0.2470 (4)	0.3797 (3)	2.8 (1)
C(31)	0.5155 (4)	0.3299 (4)	0.2361 (3)	2.7 (1)
C(37)	0.2018 (4)	0.3957 (4)	0.1598 (3)	3.1 (1)
C(38)	0.2918 (4)	0.4073 (5)	0.1712 (3)	3.3 (2)
C(39)	0.3129 (5)	0.4912 (5)	0.1876 (4)	3.8 (2)
C(40)	0.2340 (5)	0.5314 (5)	0.1836 (4)	3.7 (2)
C(41)	0.1649 (4)	0.4732 (4)	0.1674 (4)	3.3 (2)
C(42)	0.2565 (5)	0.5192 (5)	0.4149 (4)	4.7 (2)
C(43)	0.2543 (5)	0.5738 (5)	0.3573 (4)	4.8 (2)
C(44)	0.3390 (6)	0.5793 (5)	0.3552 (4)	4.8 (2)
C(45)	0.3950 (5)	0.5296 (5)	0.4101 (5)	5.1 (2)
C(46)	0.3470 (7)	0.4883 (5)	0.4499 (4)	5.7 (3)

The structure was solved by direct methods. With 250 reflections (minimum E of 1.40) and 2000 relationships, a total of nine phase sets were produced. A total of 29 atoms were located from an E map prepared from the phase set.

The remaining atoms were located in succeeding difference Fourier syntheses. Hydrogen atoms were located and added to the structure factor calculations but their positions were not refined.

Scattering factors were taken from Cromer and Waber.[9] Anomalous dispersion effects were included in F_c,[10] and their values were those of Cromer and Liberman.[11] A total of 5080 reflections having intensities $I > 2$ were used in the refinements. The final cycle of refinement included 497 variable parameters and converged with unweighted and weighted agreement factors of $R_1 = 0.034$ and $R_2 = 0.038$. The highest peak in the final difference Fourier had a height of 0.14 e/Å^{-3}. All calculations were performed on a VAX-11 computer using SDP.PLUS.[12]

Table V. Selected Bond Distances (Å)[a]

atom 1	atom 2	dist	atom 1	atom 2	dist
Rh(1)	P(1)	2.264 (1)	P(1)	C(11)	1.809 (3)
Rh(1)	S(1)	2.376 (1)	P(1)	C(13)	1.827 (4)
Rh(1)	S(2)	2.412 (1)	P(1)	C(19)	1.830 (4)
Rh(1)	C(1)	1.814 (4)	P(2)	C(12)	1.808 (4)
Rh(2)	P(2)	2.294 (1)	P(2)	C(25)	1.839 (4)
Rh(2)	S(1)	2.394 (1)	P(2)	C(31)	1.829 (4)
Rh(2)	S(2)	2.398 (1)	Zr(1)	C(11)	2.423 (3)
Rh(2)	C(2)	1.806 (4)	Zr(1)	C(12)	2.413 (4)
O(1)	C(1)	1.141 (5)	Zr(1)	S(1)	5.701 (1)
O(2)	C(2)	1.152 (5)	Zr(1)	S(2)	2.995 (1)
Rh(1)	Rh(2)	3.391 (1)	Zr(1)	Cp(1)[b]	2.242 (4)
			Zr(1)	Cp(2)[b]	2.271 (4)

[a] Numbers in parentheses are estimated standard deviations in the least significant digits. [b] Centroid of the C_5H_5 ring.

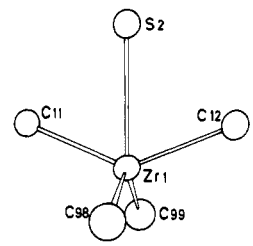

Figure 2. An ORTEP drawing showing pentacoordination around the zirconium atom in 1. C(98) and C(99) are the centroids of the η-C_5H_5 rings.

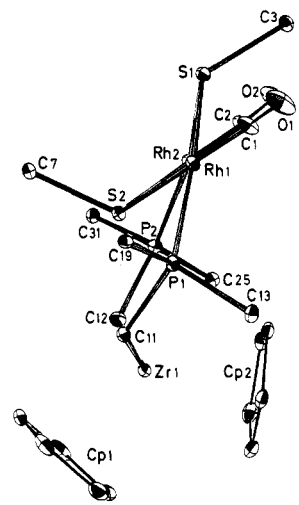

Figure 3. A view of 1 looking approximately down the Rh(1)–Rh(2) axis showing the conformation of the eight-membered ring Zr(1)–C(11)–P(1)–Rh(1)–S(1)–Rh(2)–P(2)–C(12). Phenyl rings are omitted for clarity.

Results and Discussion. An ORTEP diagram of the molecular structure of compound 1 is shown in Figure 1 and does not differ greatly from the proposed arrangement shown in I. Final positional and thermal parameters are given in Table IV. Tables V and VI list selected interatomic distances and angles. The molecule has a quasi-mirror plane containing the zirconium and the two sulfur

(7) Bresler, L. S.; Buzina, N. A.; Vashavsky, Yu. S.; Kiseleva, N. V.; Cherkasova, T. G. *J. Organomet. Chem.* **1979**, *171*, 229.
(8) Choukroun, R.; Gervais, D. *J. Organomet. Chem.* **1984**, *266*, C37.
(9) Cromer, D. T.; Waber, J. T. "International Tables for X-Ray Crystallography"; Kynoch Press: Birmingham, England, 1974; Vol. IV, Table 2.2.B.
(10) Ibers, J. A.; Hamilton, W. C. *Acta Crystallogr.* **1964**, *17*, 781.
(11) Cromer, D. T.; Liberman, D. "International Tables for X-Ray Crystallography"; Kynoch Press: Birmingham, England, 1974; Vol. IV, Table 2.3.1.
(12) Frenz, B. A. "The Enraf-Nonius CAD4 SDP (crystal determination package)" In "Computing in Crystallography"; Schenk, H., Olthof-Hazelkamp, R., Vankonigsveld, H., Bassi, G. C., Eds.; Delft University Press: Delft, Holland, 1978; pp 64–71.

Table VI. Selected Bond Angles (deg)[a]

atom 1	atom 2	atom 3	angle	atom 1	atom 2	atom 3	angle
P(1)	Rh(1)	S(1)	170.34 (3)	C(12)	Zr(1)	Cp(2)[b]	97.2 (2)
P(1)	Rh(1)	S(2)	89.76 (3)	Cp(1)[b]	Zr(1)	Cp(2)[b]	124.8 (2)
P(1)	Rh(1)	C(1)	88.1 (1)	Rh(1)	P(1)	C(11)	113.7 (1)
S(1)	Rh(1)	S(2)	80.71 (3)	Rh(1)	P(1)	C(13)	113.0 (1)
P(2)	Rh(2)	S(1)	167.32 (3)	Rh(1)	P(1)	C(19)	118.1 (1)
P(2)	Rh(2)	S(2)	87.81 (3)	Rh(2)	P(2)	C(12)	113.9 (1)
P(2)	Rh(2)	C(2)	94.0 (1)	Rh(2)	P(2)	C(25)	112.2 (1)
S(1)	Rh(2)	S(2)	80.64 (3)	Rh(2)	P(2)	C(31)	119.3 (1)
C(11)	Zr(1)	C(12)	134.2 (1)	Rh(1)	S(1)	C(3)	114.5 (1)
C(11)	Zr(1)	Cp(1)[b]	103.9 (2)	Rh(2)	S(1)	C(3)	118.1 (1)
C(11)	Zr(1)	Cp(2)[b]	96.7 (2)	Rh(1)	S(2)	C(7)	111.6 (1)
C(12)	Zr(1)	Cp(1)[b]	103.3 (1)	Rh(2)	S(2)	C(7)	111.1 (1)

[a] Numbers in parentheses are estimated standard deviations in the least significant digits. [b] Centroid of the C_5H_5 ring.

Table VII. Equation of Planes and Distances (Å) from the Planes[a]

plane no.	A	B	C	D	atom	x	y	z	dist	esd
1	−0.9937	0.0756	−0.0828	−2.2375			Atoms in Plane			
					S(1)	2.0542	1.5724	3.8062	0.000	0.002
					S(2)	2.1067	4.1500	5.5288	0.000	0.002
					Zr(1)	2.3645	7.1073	5.1346	0.000	0.001
							Other Atoms			
					Rh(1)	0.4657	3.3325	3.9608	1.699	0.001
					Rh(2)	3.8385	3.1093	4.2374	−1.693	0.001
					P(1)	−0.7805	5.1903	4.3112	3.048	0.002
					P(2)	5.2846	4.6828	5.0711	−3.080	0.002
					C(11)	0.0444	6.4372	5.3292	2.239	0.006
					C(12)	4.4625	6.1183	5.8006	−2.215	0.007
					C(1)	−0.8325	2.7479	2.8375	3.038	0.008
					C(2)	5.0948	2.3158	3.2115	−2.916	0.008
					O(1)	−1.7144	2.4148	2.1954	3.942	0.007
					O(2)	5.8850	1.7703	2.5749	−3.690	0.007
					C(3)	2.0495	0.6685	2.1748	0.071	0.007
					C(7)	1.9231	3.3126	7.2386	−0.022	0.007
					C(37)	2.1089	6.4241	2.7004	0.404	0.007
					C(38)	3.4702	6.6138	2.8926	−0.950	0.007
					C(39)	3.6931	7.9748	3.1700	−1.092	0.008
					C(40)	2.4569	8.6281	3.1021	0.191	0.008
					C(41)	1.4645	7.6832	2.8285	1.129	0.007
					C(42)	1.1899	8.4299	7.0114	1.112	0.008
					C(43)	1.5606	9.3173	6.0367	0.891	0.009
					C(44)	2.9309	9.4059	6.0019	−0.461	0.009
					C(45)	3.4423	8.5993	6.9300	−1.107	0.009
					C(46)	2.3927	7.9284	7.6025	−0.170	0.012
2	0.0606	−0.4660	−0.8827	−7.7011			Atoms in Plane			
					Zr(1)	2.3645	7.1073	5.1346	0.000	0.001
					C(11)	0.0444	6.4372	5.3292	0.000	0.006
					C(12)	4.4625	6.1183	5.8006	0.000	0.006
3	0.0680	0.9974	−0.0242	3.2597			Atoms in Plane			
					Rh(1)	0.4657	3.3325	3.9608	0.000	0.001
					Rh(2)	3.8385	3.1093	4.2374	0.000	0.001
					C(7)	1.9231	3.3126	7.2386	0.000	0.007
							Other Atoms			
					S(2)	2.1067	4.1500	5.5288	0.889	0.002
					Zr(1)	2.3645	7.1073	5.1346	3.866	0.001

Dihedral Angle between Planes 1 and 2: 91.3°

[a] The equation of the plane is of the form $Ax + By + Cz - D = 0$ where A, B, C, and D are constants and x, y, and z are orthogonalized coordinates.

atoms as well as the two centroids of the C_5H_5 rings; the quaternary carbons of the *tert*-butyl groups are nearly in the same plane since the maximum displacements are only 0.071 (7) Å for C(3) and −0.022 (7) for C(7) (Table VII). This plane is perpendicular to the plane defined by the zirconium atom and carbons C(11) and C(12) of the methylene groups of CH_2PPh_2. The dirhodium core $Rh_2(t\text{-}BuS)_2(CO)_2P_2$ is roughly comparable to the bent geometry of previously reported Rh_2 or Ir_2 systems such as $Rh_2(SPh)_2(CO)_2(PMe_3)_2$[13] (**2**) and $Ir_2(t\text{-}BuS)_2(CO)_2[P(OMe)_3]_2$[14] (**3**): the *tert*-butyl groups are in an anti configuration with respect to the Rh_2S_2 arrangement, with the *t*-Bu in the exo position lying between the phosphine ligands. The intramolecular rhodium–rhodium distance is 3.391 (1) Å (to be compared to 3.061 (1) Å in **2**).

The structural arrangement of the zirconium diphosphine part of the molecule roughly resembles those of the uncomplexed $(\eta\text{-}C_5H_5)_2Zr(CH_2PPh_2)_2$ (**4**) or the cis complex $(\eta\text{-}C_5H_5)_2Zr(CH_2PPh_2)_2Cr(CO)_4$ (**5**) previously described by Schore.[3] The more striking discrepancy is observed for the C(11)–Zr–C(12) angle which is 134.2° (1)

(13) Bonnet, J. J.; Kalck, P.; Poilblanc, R. *Inorg. Chem.* **1977**, *16*, 1514.

(14) Bonnet, J. J.; Thorez, A.; Maisonnat, A.; Galy, J.; Poilblanc, R. *J. Am. Chem. Soc.* **1979**, *101*, 5940.

in (1), a much larger value than those in 4 (100.2°) and 5 (93.5°). Pentacoordination around the zirconium atom may then be presumed by comparison to the recently reported cationic species[15] $[(\eta\text{-}C_5H_5)_2Zr(H_2O)_3]^{2+}$ (7) or the thiocarbamate complex[16] $(\eta\text{-}C_5H_5)_2ZrCl(S_2CNEt_2)$ (8) where the corresponding angles X(1)ZrX(3) (II) are 145.2°

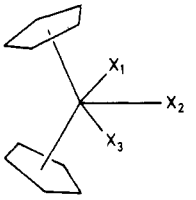

II

(2) and 137.5° (1), respectively. This is supported by the distance Zr–S(2) (2.995 (1) Å), much shorter than expected for noninteracting atoms, although significantly longer than the two Zr–S distances in the thiocarbamato complex 8:[16] 2.635 (2) and 2.723 (2) Å. Moreover, the lone pair of S(2) directly faces zirconium as demonstrated by comparing the Zr(1)–S(2) distance (2.995 Å) to the difference (2.977 Å) between the distance of Zr(1) (3.866 Å) and S(2) (0.889 Å) to the plane Rh(1)Rh(2)C(7) (Table VII) containing the three other atoms directly bonded to S(2) which is then brought to tetracoordination.

The pentacoordinated arrangement around zirconium is shown in Figure 2. The characteristic structural features of complex 1 can be seen in Figure 3 where the geometric arrangement of the eight-membered ring formed by the zirconium diphosphine bridging the Rh–S–Rh sequence is clearly visible.

Magnetic inequivalences shown in ^1H and ^{13}C NMR spectra are now explainable on account of axial and equatorial positions with respect to the ring. This holds for the phenyls bonded to each phosphorus and for the hydrogens of each methylene group as well as for the two cyclopentadienyl groups bonded to the zirconium atom.

The coordination of the sulfur atom S(2) to zirconium is certainly responsible for the stereorigidity of complex 1 even in solution up to 100 °C in toluene. It also explained the unusual chemical shift of one of the quaternary carbons (found at 33.9 ppm) due very probably to the influence of the tetracoordination of the sulfur S(2) on the C(7) carbon nucleus.

(15) Thewalt, U.; Lasser, W. *J. Organomet. Chem.* **1984**, *276*, 341.
(16) Silver, M. E.; Eisenstein, O.; Fay, R. C. *Inorg. Chem.* **1983**, *22*, 759.

Conclusions

By reacting the zirconium diphosphine $(\eta\text{-}C_5H_5)_2Zr(CH_2PPh_2)_2$ with $Rh_2(t\text{-}BuS)_2(CO)_4$, we obtained a novel bimetallic zirconium–dirhodium species, $Rh_2(\mu\text{-}S\text{-}t\text{-}Bu)_2[(\mu\text{-}Ph_2PCH_2)_2Zr(\eta\text{-}C_5H_5)_2](CO)_2$ (1), with the zirconium diphosphine bridging the two rhodium in a cis arrangement toward the retained bent dirhodium dicarbonyl bis(μ-thiolato) core.

A strong interaction between one of the sulfur atoms and the zirconium is responsible for the unprecedented inequivalences shown in the ^1H and ^{13}C spectra. It also can explain the unexpected stability of the zirconium–alkyl bond which is not cleaved by dihydrogen, carbon monoxide, olefins, or aldehydes, due probably to the saturation of the pentacoordinated 18-electron configuration of the zirconium.

In contrast to most of the previous work on bimetallic complexes, the bimetallic frame of 1 can be maintained under catalytic conditions (e.g., for hydroformylation), and this is quite unique for bimetallic species involving such an oxophilic metal as zirconium. On the other hand, the reason why the catalytic performance is improved by using the zirconium diphosphine ligand instead of the more classical 1,4-bis(phenylphosphino)butane is not completely understood. The $(\eta\text{-}C_5H_5)_2Zr$ moiety probably plays the role of an electron buffer which is able to push or pull the electron density toward or from the rhodium atoms following the successive steps of the catalytic cycle such as oxidative addition of dihydrogen, coordination of hexene, and insertion of carbon monoxide.

Acknowledgment. We wish to thank the Centre National de la Recherche Scientifique for support of this research through Greco-Oxydes de Carbone and Dr. Jean Galy for useful discussions. We also greatly acknowledge Mr. Gerard Commenges for his assitance with NMR investigations.

Registry No. $Rh_2(\mu\text{-}t\text{-}BuS)_2(CO)_4$, 54032-58-5; $Cp_2Zr(CH_2PPh_2)_2$, 74395-16-7; $Rh_2(\mu\text{-}S\text{-}t\text{-}Bu)_2[(\mu\text{-}Ph_2PCH_2)_2Zr(\eta\text{-}C_5H_5)_2](CO)_2$, 95029-92-8; $Rh_2(\mu\text{-}t\text{-}BuS)_2[Ph_2P(CH_2)_4PPh_2](CO)_2$, 95029-17-7.

Supplementary Material Available: Listings of anisotropic and isotropic general temperature factors, refined temperature factors, root mean square amplitudes of thermal vibration, bond angles, bond distances, positional parameters, and observed and calculated structure factor (51 pages). Ordering information is given on any current masthead page.

Reactions of $HC{\equiv}CCO_2Et$ with $(np_3)CoH$ and $(np_3)Ni$ [np_3 = $N(CH_2CH_2PPh_2)_3$]. Crystal Structures of the Alkenyl Complexes $[(np_3)CoC(CO_2Et){=}CH_2]BPh_4{\cdot}0.5THF$ and $[(np_3)\overline{NiCH{=}CHC(O)}OEt]BPh_4$

Claudio Bianchini,* Paolo Innocenti, Dante Masi, Andrea Meli, and Michal Sabat*

Istituto per lo Studio della Stereochimica ed Energetica dei Composti di Coordinazione, CNR, 50132 Firenze, Italy

Received April 17, 1985

The hydride $(np_3)CoH$ (**1**) [np_3 = $N(CH_2CH_2PPh_2)_3$] reacts with $HC{\equiv}CCO_2Et$ to yield the σ-alkenyl complex $(np_3)CoC(CO_2Et){=}CH_2$ (**2**) by insertion of the alkyne molecule into the Co–H bond. Addition of $NaBPh_4$ in *n*-butyl alcohol to a tetrahydrofuran solution of **2** gives the Co(II) derivative $[(np_3)CoC(CO_2Et){=}CH_2]BPh_4{\cdot}0.5THF$ (**3**). The crystal structure of **3** has been determined by standard X-ray methods. The compound crystallizes in the triclinic space group $P\bar{1}$ with a = 17.937 (6) Å, b = 15.188 (5) Å, c = 12.916 (4) Å, α = 87.00 (2)°, β = 101.37 (2)°, γ = 110.44 (2)°, and Z = 2. The structure was refined to an R factor of 0.088 (R_w = 0.087) using 3180 reflections with $I > 3\sigma(I)$. The $[(np_3)CoC(CO_2Et){=}CH_2]^+$ cation adopts the gem conformation with a Co–C distance of 1.91 (2) Å. Reaction of $HC{\equiv}CCO_2Et$ with the Ni(0) complex $(np_3)Ni$ (**4**) followed by $NaBPh_4$ addition gives the β-carbethoxyvinyl complex $[(np_3)\overline{NiCH{=}CHC(O)}OEt]BPh_4$ (**5**), the structure of which has been established by an X-ray analysis. Compound **5** crystallizes in the monoclinic space group $P2_1/a$ with a = 26.696 (7) Å, b = 14.729 (4) Å, c = 16.203 (4) Å, β = 105.50 (2)°, and Z = 4. The structure was refined to an R factor of 0.079 (R_w = 0.085) for 4933 reflections with $I > 3\sigma(I)$. The β-carbethoxyvinyl group in the $[(np_3)\overline{NiCH{=}CHC(O)}OEt]^+$ cation is chelated to Ni by its carbonyl oxygen atom and β-carbon atom forming a five-membered ring. The Ni–C and Ni–O bond distances are 1.878 (7) and 2.229 (5) Å, respectively. The reaction mechanisms for the formation of the σ-alkenyl complexes **2**, **3**, and **5** are briefly discussed.

Introduction

The reaction of transition-metal hydrides with electron-deficient acetylenes provide a well-developed method for the synthesis of σ-alkenyl complexes.[1-6] Acetylenes insert into metal–hydrogen bonds to give products with trans (I) or cis (II) stereochemistry.

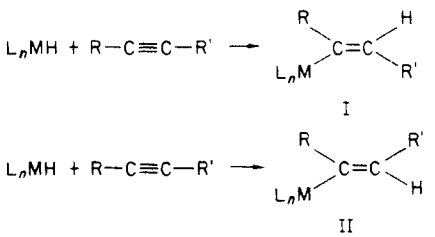

I

II

In recent years, considerable information on the insertion reactions of acetylenes into M–H bonds has become available. In particular, studies have been carried out to determine how factors like the nature of the metal fragments and of the substituents on the acetylenes may influence the stereochemistry of the products.[1,2] Structural data on σ-alkenyl complexes, however, still remain rather scarce. In an attempt to provide further information in this field, we have investigated the reactivity of the trigonal-bipyramidal Co(I) hydride $(np_3)CoH$ (**1**)[7] [np_3 = tris(2-(diphenylphosphino)ethyl)amine] toward ethyl propiolate, $HCCCO_2Et$. As a result, the two η^1-vinyl complexes $(np_3)CoC(CO_2Et){=}CH_2$ (**2**) and $[(np_3)CoC(CO_2Et){=}CH_2]BPh_4{\cdot}0.5THF$ (**3**) have been synthesized. The structure of **3** has been elucidated by means of X-ray methods.

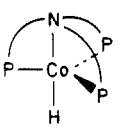

1

An alternative synthetic route to (σ-alkenyl)metal complexes is the reaction of complex anions possessing σ lone pairs with acetylenes activated by the presence of electron-withdrawing groups.[8] To get some better insight into this chemistry, we carried out the reaction of $HC{\equiv}CCO_2Et$ with the trigonal-pyramidal complex $(np_3)Ni$ (**4**).[7] The latter compound has an occupied orbital suited to transfer electron density into an appropriate empty orbital of an incoming electrophile[9] (III). Accordingly, **4** behaves as a metal base and forms strong adducts with Lewis acids such as H^+,[10] CH_3^+, $SnCl_2$, and BF_3.[11]

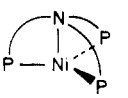

4

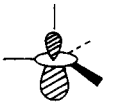

III

(1) Otsuka, S.; Nakamura, A. *Adv. Organomet. Chem.* **1976**, *14*, 245.
(2) Collmann, J. P.; Hegedus, L. S. "Principles and Applications of Organotransition Metal Chemistry"; University Science Books: Mill Valley, CA, 1980.
(3) Longato, B.; Bresadola, S. *Inorg. Chem.* **1982**, *21*, 168.
(4) Scordia, H.; Kergoat, R.; Kubicki, M. M.; Guerchais, J. E.; L'Haridon, P. *Organometallics* **1983**, *2*, 1681.
(5) Petillon, F. Y.; Le Quere, J. L.; Le Floch-Perennou, F.; Guerchais, J. E.; Gomes De Lima, M. B.; Manojlovic-Muir, L. J.; Muir, K. W.; Sharp, D. W. A. *J. Organomet. Chem.* **1984**, *255*, 231.
(6) Deeming, A. J.; Manning, P. J.; Rothwell, I. P.; Hursthouse, M. B.; Walker, N. P. C. *J. Chem. Soc., Dalton Trans.* **1984**, 2039.
(7) Sacconi, L.; Ghilardi, C. A.; Mealli, C.; Zanobini, F. *Inorg. Chem.* **1975**, *14*, 1380.
(8) Bruce, M. J.; Harbourne, D. A.; Waugh, F.; Stone, F. G. A. *J. Chem. Soc. A* **1968**, 895.
(9) Cecconi, F.; Ghilardi, C. A.; Innocenti, P.; Mealli, C.; Midollini, S.; Orlandini, A. *Inorg. Chem.* **1984**, *23*, 922.

0276-7333/86/2305-0072$01.50/0

Under suitable conditions, ethyl propiolate adds oxidatively to **4** forming a β-carbethoxyvinyl complex cation, which is stabilized by bulky anions like BPh_4^- to give the complex [(np$_3$)NiCH=CHC(O)OEt]BPh$_4$ (**5**). The crystal structure of **5** has been established by an X-ray analysis.

Results and Discussion

Reaction of HC≡CCO$_2$Et with 1. Diamagnetic brown crystals of **2** are obtained in 62% yield by treating at room temperature the hydride **1** in tetrahydrofuran with a slight excess of HC≡CCO$_2$Et (IV).

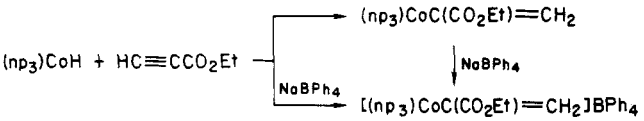

IV

Compound **2** is reasonably air stable in the solid state but slowly decomposes in solution even in an inert atmosphere. It is soluble in common organic solvents, in which it behaves as a nonelectrolyte. The reflectance spectrum consists of a band at 23 000 cm^{-1} and is fully comparable with those of five-coordinate low-spin Co(I) complexes.[12] The IR spectrum contains no ν(Co–H) vibrations, but there are two medium-strong bands at 1680 and 1540 cm^{-1}, which can be positively assigned to ν(C=O) of a carboxylate group and to ν(C=C) of an alkene moiety,[3,13,14] respectively. The IR spectrum also exhibits a strong band at 1210 cm^{-1} typical of ν(COC). The $^{31}P\{^1H\}$ NMR spectrum in benzene at 20 °C consists of a single resonance at −26.30 ppm. This pattern, unchanged also in tetrahydrofuran even at −60 °C, is consistent with rapid intramolecular exchange of the three phosphorus atoms of np$_3$ around the cobalt atom, as observed also for a variety of trigonal-bipyramidal Co(I) complexes with np$_3$.[15] The ^1H NMR spectrum in benzene at 20 °C, although poorly resolved as some decomposition occurs in solution, shows two doublets at δ 5.85 and 5.06 (1 H), a quadruplet at δ 3.68 (2 H), and a triplet at δ 0.62 (3 H). The last two resonances are typical of the ethoxy protons of carbonic esters.

The insertion of ethyl propiolate into the Co–H bond may take place giving σ-alkenyl complexes with three possible structures (V–VII).

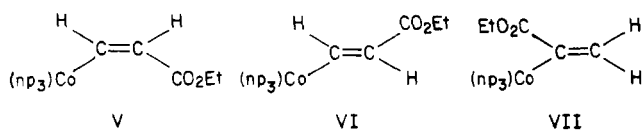

The nature of the ^1H NMR spectrum of **2** is such that it appears to be a single isomer. In particular, the two olefinic hydrogen shifts as well as the coupling constant of 2.5 Hz are strongly indicative of the gem structure VII. A similar band pattern has been observed for the insertion products of 3,3,3-trifluoropropyne into L$_n$M–H bonds (L$_n$M = Fe(CO)$_2$(C$_5$H$_5$), *cis*-PtCl(PEt$_3$)$_2$, Mn(CO)$_5$), which have been assigned structure VII.[16a] Decisive support for the proposed stereochemistry of **2** is provided by the crystal structure of compound **3**. The latter is obtained as red crystals in 70% yield by adding NaBPh$_4$ to the reaction mixture leading to **2**. Compound **3** is quite air stable in the solid state but slowly decomposes in solution unless air is excluded. It is soluble in common organic solvents, in which it behaves as a 1:1 electrolyte (molar conductance value in 10^{-3} M nitroethane solution 42 cm^2 Ω^{-1} mol^{-1}). It is paramagnetic with a magnetic moment of 2.12 μ_B corresponding to one unpaired spin. The reflectance spectrum has bands at 8000, 10800, and 20600 cm^{-1} and is fully comparable with those of five-coordinate Co(II) complexes with np$_3$, where the fifth donor atom is carbon.[12] The IR spectrum exhibits two strong bands at 1700 and 1215 cm^{-1} assigned to ν(C=O) and ν(COC) of a CO$_2$Et group, respectively. A medium band at 1555 cm^{-1} is attributed to a ν(C=C) stretching vibration. The crystal structure of **3** consists of complex cations of [(np$_3$)CoC(CO$_2$Et)=CH$_2$]$^+$ and BPh_4^- anions (see the description of the structure). The complex cation has structure VII. The same stereochemistry may be, thus, reasonably assigned to **2** when assuming that NaBPh$_4$ has the effect of promoting the stabilization of the oxidized species (IV). Indeed, it has been previously observed that a variety of trigonal-bipyramidal Co(II) complexes of general formula [(np$_3$)CoX]BPh$_4$ (X = NO,[17] CN,[11] CH$_3$[18]) can be obtained by treatment of solutions of the corresponding Co(I) derivatives with NaBPh$_4$.

Reaction of HCCCO$_2$Et with 4. Ethyl propiolate reacts almost instantaneously with the red Ni(0) complex **4** in tetrahydrofuran at room temperature to give an orange solution from which yellow orange crystals of **5** are obtained by addition of NaBPh$_4$ in *n*-butyl alcohol (yield 80%) (VIII).

$$(np_3)Ni + HC{\equiv}CCO_2Et \xrightarrow[\text{VIII}]{NaBPh_4,\ n\text{-butyl alcohol}} [(np_3)NiCH{=}CHC(O)OEt]BPh_4$$

Compound **5** is diamagnetic and air stable both in the solid state and in solution. It is soluble in common organic solvents, in which it behaves as a 1:1 electrolyte (molar conductance value in 10^{-3} M nitroethane solution 41 cm^2 Ω^{-1} mol^{-1}). The reflectance spectrum consists of a band at 25 000 cm^{-1} and is typical of five-coordinate Ni(II) complexes.[12] The IR spectrum exhibits bands at 1640, 1520, and 1210 cm^{-1}. The latter two bands are assigned to ν(C=C) of an alkene moiety and to ν(COC) of the COEt fragment, respectively. The broad medium-strong band at 1640 cm^{-1} is attributable to the CO$_2$Et carbonyl group coordinated to the nickel atom. A number of complexes have been described, in which an ester carbonyl group is coordinated to a metal atom.[3,13,16a,19] In the IR spectra of such complexes, a band in the region 1500–1600 cm^{-1} has been attributed to a coordinated ketonic carbonyl group. The $^{31}P\{^1H\}$ NMR spectrum in acetone at −60 °C consists of two resonances at 28.38 and −21.16 ppm (intensity ratio 2:1). The band pattern as well as the relative intensities are typical of metal complexes with tripodal triphosphines acting as bidentate ligands, the third

(10) Sacconi, L.; Orlandini, A.; Midollini, S. *Inorg. Chem.* **1974**, *13*, 2850.
(11) Bianchini, C.; Meli, A., to be submitted for publication.
(12) Sacconi, L.; Mani, F. *Transition Met. Chem. (N.Y.)* **1982**, *8*, 179.
(13) Booth, B. L.; Hargreaves, R. G. *J. Chem. Soc. A.* **1969**, 2766.
(14) Nakamura, A.; Otsuka, S. *J. Am. Chem. Soc.* **1972**, *94*, 1886.
(15) Bianchini, C.; Meli, A.; Scapacci, G. *Organometallics* **1983**, *2*, 1834.
(16) (a) Harbourne, P. A.; Stone, F. G. A. *Inorg. Phys. Theor.* **1968**, 1765. (b) Chen, G. J.-J.; McDonald, J. W.; Newton, W. E. *Organometallics* **1985**, *4*, 422.
(17) Di Vaira, M.; Ghilardi, C. A.; Sacconi, L. *Inorg. Chem.* **1976**, *15*, 1555.
(18) Bianchini, C.; Meli, A. *Organometallics* **1985**, *4*, 1537.
(19) (a) Dubeck, M.; Schell, R. A. *Inorg. Chem.* **1964**, *3*, 1757. (b) Canziani, F.; Garlaschelli, L.; Malatesta, M. C. *J. Organomet. Chem.* **1978**, *146*, 179. (c) Canziani, F.; Albinati, A.; Garlaschelli, L.; Malatesta, M. C. *Ibid.* **1978**, *146*, 197. (d) Carmona, E.; Gutierrez-Puebla, E.; Monge, A.; Marin, J. M.; Paneque, M.; Poveda, M. L. *Organometallics* **1984**, *3*, 1438. (e) Komiya, S.; Ito, T.; Cowie, M.; Yamamoto, A.; Ibers, J. A. *J. Am. Chem. Soc.* **1976**, *98*, 3874.

Table I. Summary of Crystal Structure Data

	3	5
formula	$C_{71}H_{69}BO_2P_3NCo \cdot 0.5C_4H_8O$	$C_{71}H_{69}BO_2P_3NNi$
M	1166.95	1130.79
cryst size, mm	0.4 × 0.15 × 0.09	0.75 × 0.22 × 0.18
cryst system	triclinic	monoclinic
space group	$P\bar{1}$	$P2_1/a$
a, Å	17.937 (6)	26.696 (7)
b, Å	15.188 (5)	14.729 (4)
c, Å	12.916 (4)	16.203 (4)
α, deg	87.00 (2)	90.0
β, deg	101.37 (2)	105.50 (2)
γ, deg	110.44 (2)	90.0
V, Å^3	3231.9	6139.4
Z	2	4
d(calcd), g cm^{-3}	1.197	1.223
μ(Mo Kα), cm^{-1}	3.81	4.37
radiatn	graphite-monochromated Mo Kα (λ = 0.710 69 Å)	
scan type	$\omega/2\theta$	$\omega/2\theta$
2θ range, deg	5-45	5-50
scan width, deg	0.9	1.0
scan speed, deg s^{-1}	0.05	0.04
total data	8275	11432
unique data $I > 3\sigma(I)$	3180	4933
no. of parameters	319	291
R	0.088	0.079
R_w	0.087	0.085
$w = 1.0[\sigma^2(F_o) + pF_o^2]^{-1}$	p = 0.0005	p = 0.001

phosphorus atom not being coordinated to the metal center.[20] The ^{1}H NMR spectrum in chloroform at 20 °C shows a doublet at δ 5.26 (1 H) (J_{H-H} = 8.4 Hz), a quadruplet at δ 3.93 (2 H), and a triplet at δ 1.14 (3 H). The latter two resonances can be positively assigned to the ethoxy protons of the CO_2Et group. The doublet seems to be half of an AB pattern, the second half of which is probably masked by the resonances of the phenyl protons. Vinylic protons of compounds with structure I (R = H), generally, give rise to AB patterns with J = 10 Hz.[13,16] One half of the AB pattern may fall in the region of phenyl hydrogens. On the basis of all of these data a structure may be assigned to **5** where nickel is five-coordinated by the nitrogen atom and two phosphorus atoms of np_3 and by a carbon and the ketonic oxygen of a HC=CH(CO_2Et) group. The two vinylic protons appear to be disposed in cis manner. The X-ray structural analysis of **5**, presented below, confirms such an arrangement of the donor atoms.

As a consequence of the reaction with HC≡CCO_2Et, the formal oxidation state of nickel is raised by two units. This may be interpreted in terms of an overall two-electron oxidative addition of the acetylene molecule to the Ni(0) complex.[2]

Description of the Structures

Compound 3. As a result of the insertion of ethyl propiolate into the Co–H bond σ-alkenyl complexes V–VII may be formed. In order to establish unambigously the conformation of the insertion product **3**, an X-ray analysis was performed. The crystal structure of **3** is composed of discrete [(np_3)CoC(CO_2Et)=CH_2]$^+$ complex cations, BPh_4^- anions, and tetrahydrofuran solvent molecules. Selected bond distances and angles are given in Table IV. The complex cation (Figure 1) adopts the gem conformation (structure VII) with both the metal fragment and the electron-withdrawing group CO_2Et bonded to the same carbon atom C(7). The coordination sphere around Co center can be described in terms of a distorted square

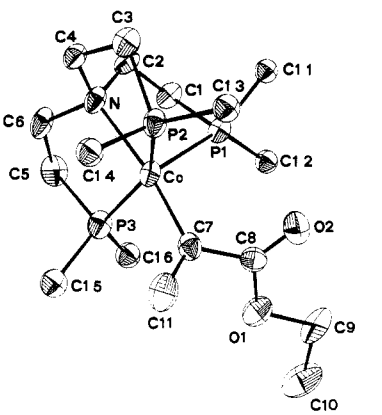

Figure 1. ORTEP drawing of the [(np_3)CoC(CO_2Et)=CH_2]$^+$ cation. Hydrogen atoms and phenyl rings of the np_3 ligand (except for the connecting C atoms) are omitted for clarity.

pyramid with the phosphorus atom P(1) in the apical position and the two other phosphorus and nitrogen atoms of the tripod ligand as well the vinyl carbon atom C(7) forming the basal plane. The distortions from square-pyramidal geometry result in closing down the P(2)–Co–P(3) and N–Co–C(7) bond angles of the basal plane to 148.8 (2) and 170.5 (7)°, respectively. The Co–P and Co–N bond lengths being significantly elongated with respect to the analogous bond distances in the trigonal-bipyramidal (np_3)CoH[7] resemble quite close those found in the square-pyramidal low-spin [(np_3)CoI]I.[21] The Co–C(7) distance of 1.91 (2) Å compares well with the Co–vinyl σ bond lengths found in other structures[22] and the Co–C(7)–C(11) bond angle of 124 (1)° may be indicative that the metal–carbon bond is single. The parameters defining the vinyl ligand geometry are quite normal. Thus, the C(7)–C(11) bond length of 1.35 (2) Å approaches that observed in the Co(III) complex with the unsubstituted vinyl group (1.33 (2) Å), while the C(7)–C(8) separation of 1.48 (2) Å is characteristic for a single bond involving sp^2-hy-

(20) Bianchini, C.; Mealli, C.; Meli, A.; Scapacci, G. *Organometallics* **1983**, *2*, 141. Bianchini, C.; Meli, A. *J. Chem. Soc., Dalton Trans.* **1983**, 2419.

(21) Mealli, C.; Orioli, P. L.; Sacconi, L. *J. Chem. Soc.* **1971**, 2691.

(22) Brueckner, S.; Calligaris, M.; Nardin, G.; Randaccio, L. *Inorg. Chim. Acta* **1968**, *2*, 416.

Table II. Final Positional Parameters (×10^4) for [(np$_3$)CoC(CO$_2$Et)=CH$_2$]BPh$_4$•0.5THF

atom	x	y	z	atom	x	y	z
Co	8069 (1)	2474 (1)	7823 (2)	C(1)5	8719 (6)	1556 (7)	10180 (10)
P(1)	8433 (2)	2466 (3)	6189 (3)	C(2)5	8115 (6)	1012 (7)	10715 (10)
P(2)	7146 (2)	3185 (3)	7578 (3)	C(3)5	8213 (6)	1130 (7)	11803 (10)
P(3)	8611 (3)	1465 (3)	8766 (4)	C(4)5	8916 (6)	1792 (7)	12356 (10)
O(1)	10282 (7)	4258 (7)	8536 (9)	C(5)5	9520 (6)	2337 (7)	11821 (10)
O(2)	9438 (7)	4604 (8)	7225 (10)	C(6)5	9422 (6)	2219 (7)	10733 (10)
N(1)	7056 (6)	1218 (8)	7257 (10)	C(1)6	9552 (6)	1289 (7)	8654 (9)
C(1)	7938 (8)	1197 (9)	5947 (12)	C(2)6	9594 (6)	389 (7)	8658 (9)
C(2)	7084 (8)	916 (10)	6164 (12)	C(3)6	10316 (6)	271 (7)	8568 (9)
C(3)	6289 (8)	2326 (10)	6738 (11)	C(4)6	10996 (6)	1053 (7)	8474 (9)
C(4)	6251 (8)	1365 (9)	7167 (11)	C(5)6	10954 (6)	1954 (7)	8469 (9)
C(5)	7840 (10)	329 (10)	8377 (13)	C(6)6	10232 (6)	2071 (7)	8559 (9)
C(6)	7027 (9)	444 (10)	8017 (14)	B	3617 (10)	1762 (10)	5964 (13)
C(7)	8888 (9)	3563 (11)	8529 (14)	C(1)7	4276 (6)	1971 (6)	5113 (8)
C(8)	9547 (12)	4190 (12)	8017 (15)	C(2)7	4474 (6)	2809 (6)	4559 (8)
C(9)	10966 (10)	4861 (14)	8059 (17)	C(3)7	4958 (6)	2941 (6)	3801 (8)
C(10)	11678 (11)	4744 (14)	8850 (16)	C(4)7	5244 (6)	2236 (6)	3597 (8)
C(11)	8916 (10)	3849 (12)	9511 (16)	C(5)7	5046 (6)	1399 (6)	4151 (8)
C(1)1	7991 (6)	2992 (5)	5063 (9)	C(6)7	4562 (6)	1266 (6)	4909 (8)
C(2)1	7739 (6)	2536 (5)	4080 (9)	C(1)8	2685 (5)	1242 (6)	5325 (7)
C(3)1	7427 (6)	2960 (5)	3199 (9)	C(2)8	2462 (5)	1408 (6)	4256 (7)
C(4)1	7366 (6)	3841 (5)	3303 (9)	C(3)8	1653 (5)	1034 (6)	3751 (7)
C(5)1	7617 (6)	4298 (5)	4287 (9)	C(4)8	1066 (5)	495 (6)	4314 (7)
C(6)1	7930 (6)	3873 (5)	5167 (9)	C(5)8	1289 (5)	329 (6)	5384 (7)
C(1)2	9423 (7)	2710 (6)	5815 (8)	C(6)8	2098 (5)	703 (6)	5889 (7)
C(2)2	9810 (7)	2049 (6)	6010 (8)	C(1)9	3703 (5)	2810 (6)	6484 (7)
C(3)2	10540 (7)	2211 (6)	5677 (8)	C(2)9	3007 (5)	2932 (6)	6679 (7)
C(4)2	10884 (7)	3034 (6)	5150 (8)	C(3)9	3065 (5)	3757 (6)	7167 (7)
C(5)2	10497 (7)	3696 (6)	4955 (8)	C(4)9	3819 (5)	4461 (6)	7460 (7)
C(6)2	9766 (7)	3534 (6)	5288 (8)	C(5)9	4515 (5)	4340 (6)	7265 (7)
C(1)3	7193 (5)	4338 (6)	7043 (8)	C(6)9	4457 (5)	3514 (6)	6777 (7)
C(2)3	6615 (5)	4414 (6)	6179 (8)	C(1)10	3895 (5)	1115 (5)	6967 (8)
C(3)3	6655 (5)	5295 (6)	5773 (8)	C(2)10	4347 (5)	1518 (5)	7941 (8)
C(4)3	7273 (5)	6101 (6)	6231 (8)	C(3)10	4596 (5)	961 (5)	8729 (8)
C(5)3	7851 (5)	6025 (6)	7095 (8)	C(4)10	4393 (5)	1 (5)	8543 (8)
C(6)3	7811 (5)	5144 (6)	7501 (8)	C(5)10	3940 (5)	-402 (5)	7570 (8)
C(1)4	6756 (6)	3184 (6)	8771 (7)	C(6)10	3691 (5)	155 (5)	6781 (8)
C(2)4	6294 (6)	3735 (6)	8876 (7)	O3	2936 (19)	1808 (22)	558 (25)
C(3)4	5956 (6)	3665 (6)	9774 (7)	C13	2730 (25)	2342 (31)	1183 (33)
C(4)4	6079 (6)	3044 (6)	10568 (7)	C14	3349 (32)	3361 (36)	1098 (41)
C(5)4	6541 (6)	2493 (6)	10464 (7)	C15	3847 (27)	3310 (32)	457 (36)
C(6)4	6879 (6)	2563 (6)	9565 (7)	C16	3507 (35)	2334 (42)	-50 (44)

bridized carbon atoms (1.46 Å). There is also a remarkable structural similarity between the σ-bonded vinyl moieties in the present complex and in an iron compound obtained by nucleophilic addition of a methyl group to the molecule of MeC≡CCO$_2$Et η^2-coordinated to the metal center.[23] To our best knowledge the compound (Cp)Fe(CO)(PPh$_3$)[C(CO$_2$Et)CMe$_2$] has been so far the only structurally authenticated example of a geminal isomer found for σ-alkenyl–transition metal systems. All structural features are virtually the same in both compounds except for somewhat different orientation of the ester group relative to the vinyl bond. This can be described by the torsion angle C=C–C–O(carbonyl) which has a value of −118.2 and 97.8° in the Co and Fe complexes, respectively. Furthermore, the observed orientation of the ester group in the Fe compound is believed to result from nonbonding interactions between the planar CO$_2$Et system and one of the phenyl rings of the PPh$_3$ ligand. However, this is not the case of the Co derivative as no analogous interactions have been found in the structure.

Compound 5. Spectroscopic studies on **5** indicated that reaction VIII may be considered as a chelate-assisted oxidative addition of the substituted acetylene to the Ni(0) complex. The results of an X-ray structure determination for **5** fully support those of the spectroscopic investigations.

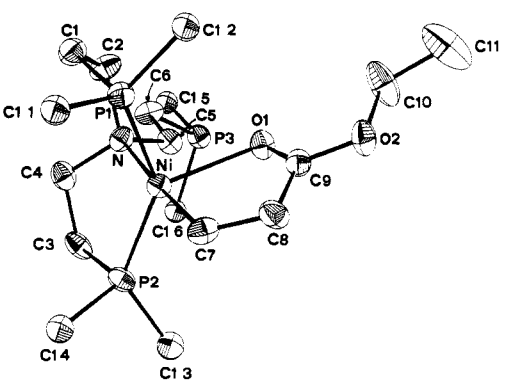

Figure 2. ORTEP drawing of the [(np$_3$)NiCH=CHC(O)OEt]$^+$ cation. Hydrogen atoms and phenyl rings of the np$_3$ ligand (except for the connecting C atoms) are omitted for clarity.

The structure of the compound consists of the [(np$_3$)NiCH=CHC(O)OEt]$^+$ complex cations and tetraphenylborate anions. Selected bond distances and angles are given in Table V. The coordination geometry around the metal atom is that of a distorted trigonal bipyramid where two phosphorus atoms of the tripod ligand are in the meridional plane and the nitrogen atom occupies the axial position. The β-carbethoxyvinyl ligand is bonded to the Ni center by its carbonyl oxygen O(1) and β-carbon atoms C(7) of the vinyl group, thus forming a five-membered chelate ring (Figure 2). The chelate ring is disposed perpendicularly to the basal plane with the vinyl carbon

(23) Reger, D. L.; McElligott, P. J.; Charles, N. G.; Griffith, E. A. H.; Amma, E. L. *Organometallics* **1982**, *1*, 443.
(24) Browning, J.; Penfold, B. R. *J. Chem. Soc., Chem. Commun.* **1973**, 198.

Table III. Final Positional Parameters ($\times 10^4$) for $[(np_3)\overline{NiCH{=}CHC(O)OEt}]BPh_4$

atom	x	y	z	atom	x	y	z
Ni	1073.7 (4)	1902 (1)	8332 (1)	C(5)4	296 (2)	4934 (4)	6539 (3)
P(1)	1624 (1)	1556 (2)	7590 (2)	C(6)4	234 (2)	4094 (4)	6898 (3)
P(2)	429 (1)	2828 (1)	8248 (2)	C(1)5	-851 (3)	-1543 (5)	7828 (4)
P(3)	-399 (1)	-735 (2)	8502 (2)	C(2)5	-1333 (3)	-1680 (5)	7990 (4)
O(1)	1389 (2)	928 (4)	9397 (4)	C(3)5	-1664 (3)	-2359 (5)	7555 (4)
O(2)	2088 (2)	919 (4)	10525 (4)	C(4)5	-1513 (3)	-2901 (5)	6957 (4)
N(1)	565 (3)	997 (4)	7607 (4)	C(5)5	-1031 (3)	-2764 (5)	6795 (4)
C(1)	1210 (3)	848 (6)	6759 (6)	C(6)5	-700 (3)	-2085 (5)	7231 (4)
C(2)	825 (4)	374 (6)	7120 (6)	C(1)6	-805 (2)	264 (4)	8533 (3)
C(3)	-99 (3)	2200 (6)	7498 (6)	C(2)6	-666 (2)	778 (4)	9283 (3)
C(4)	153 (3)	1541 (6)	7008 (6)	C(3)6	-921 (2)	1594 (4)	9335 (3)
C(5)	346 (3)	420 (5)	8193 (5)	C(4)6	-1315 (2)	1895 (4)	8638 (3)
C(6)	-48 (3)	-295 (6)	7738 (6)	C(5)6	-1454 (2)	1381 (4)	7888 (3)
C(7)	1560 (3)	2678 (6)	9046 (6)	C(6)6	-1199 (2)	565 (4)	7836 (3)
C(8)	1845 (4)	2291 (6)	9780 (6)	B	-1177 (4)	2256 (7)	4548 (7)
C(9)	1748 (3)	1328 (6)	9880 (6)	C(1)7	-527 (2)	2118 (3)	4739 (4)
C(10)	2028 (4)	-75 (7)	10581 (8)	C(2)7	-320 (2)	1279 (3)	4604 (4)
C(11)	2487 (5)	-463 (8)	11143 (9)	C(3)7	208 (2)	1202 (3)	4651 (4)
C(1)1	1860 (2)	2442 (4)	7017 (4)	C(4)7	528 (2)	1965 (3)	4832 (4)
C(2)1	2206 (2)	2244 (4)	6530 (4)	C(5)7	321 (2)	2804 (3)	4967 (4)
C(3)1	2349 (2)	2920 (4)	6035 (4)	C(6)7	-207 (2)	2881 (3)	4920 (4)
C(4)1	2146 (2)	3795 (4)	6027 (4)	C(1)8	-1475 (2)	1282 (4)	4721 (3)
C(5)1	1801 (2)	3992 (4)	6514 (4)	C(2)8	-1974 (2)	1095 (4)	4210 (3)
C(6)1	1658 (2)	3316 (4)	7009 (4)	C(3)8	-2231 (2)	310 (4)	4353 (3)
C(1)2	2189 (2)	874 (4)	8085 (4)	C(4)8	-1990 (2)	-287 (4)	5007 (3)
C(2)2	2201 (2)	-61 (4)	7955 (4)	C(5)8	-1491 (2)	-99 (4)	5518 (3)
C(3)2	2637 (2)	-564 (4)	8379 (4)	C(6)8	-1234 (2)	685 (4)	5375 (3)
C(4)2	3061 (2)	-132 (4)	8931 (4)	C(1)9	-1406 (3)	2510 (4)	3498 (4)
C(5)2	3049 (2)	804 (4)	9061 (4)	C(2)9	-1844 (3)	3057 (4)	3212 (4)
C(6)2	2613 (2)	1306 (4)	8638 (4)	C(3)9	-2055 (3)	3200 (4)	2337 (4)
C(1)3	181 (3)	3187 (5)	9120 (4)	C(4)9	-1828 (3)	2796 (4)	1748 (4)
C(2)3	-261 (3)	3734 (5)	8984 (4)	C(5)9	-1389 (3)	2249 (4)	2034 (4)
C(3)3	-431 (3)	4036 (5)	9679 (4)	C(6)9	-1178 (3)	2106 (4)	2909 (4)
C(4)3	-160 (3)	3791 (5)	10510 (4)	C(1)10	-1283 (3)	3082 (4)	5204 (3)
C(5)3	281 (3)	3243 (5)	10646 (4)	C(2)10	-1245 (3)	3992 (4)	4990 (3)
C(6)3	451 (3)	2942 (5)	9951 (4)	C(3)10	-1275 (3)	4673 (4)	5574 (3)
C(1)4	488 (2)	3916 (4)	7753 (3)	C(4)10	-1342 (3)	4443 (4)	6373 (3)
C(2)4	804 (2)	4578 (4)	8249 (3)	C(5)10	-1380 (3)	3533 (4)	6588 (3)
C(3)4	866 (2)	5418 (4)	7890 (3)	C(6)10	-1350 (3)	2853 (4)	6003 (3)
C(4)4	612 (2)	5595 (4)	7035 (3)				

atom located trans to nitrogen and the oxygen atom completing the coordination sphere in the meridional plane. Similar arrangement of the five-membered ring has previously been observed in the octahedral Ru complex with *n*-butyl methacrylate $\overline{RuH[CH{=}C(CH_3)C(O)O(n\text{-}Bu)]}(PPh_3)_3$.[19e] The Ni–C distance of 1.878 (7) Å falls within the range typical for Ni–C σ bonds, while the Ni–O interaction appears to be quite weak as shown by the relevant Ni–O distance of 2.229 (5) Å compared to 1.81 (1) Å found in $(t\text{-BuNC})_2\overline{NiC(CF_3)_2NHC(CF_3)_2O}$.[25] On the other hand, this interaction is much stronger than that existing in a related chelate system $\overline{Ni[C(Ph){=}C(H)COCH_2SiMe_3]}Cl(PMe_3)_2$,[19d] as documented by the very long Ni–O separation of 2.535 (7) Å, although the overall geometry of the five-membered ring remains rather unchanged. The geometrical parameters of the vinylic moiety in the present complex are essentially close to those revealed for the previously discussed Co compound. An interesting feature of the Ni complex is that one of the phosphorus atoms of the tripod ligand does not enter the coordination sphere. The np_3 molecule acting as a tridentate ligand, rather than using all its four donor atoms, has been observed quite frequently.[12,26] However, with one exception,[27] in all of these cases it was rather the nitrogen atom that was not coordinated to the metal center. The Ni–P distances are found to be significantly elongated in comparison with those in the parent compound $(np_3)Ni$ where all the donor atoms of the np_3 ligand are engaged in bonding to the Ni center.[7]

Conclusions

Insertion of acetylenes into metal–hydrogen bonds may occur by ionic stepwise, radical, or concerted mechanisms.[1,2] In the absence of more detailed studies, it would be hazardous to discrimate between these three pathways when considering the reaction of ethyl propiolate with the hydride **1** to give the η^1-vinyl complex **2**. The reaction conditions and the high stereospecificity observed seem to favor a concerted mechanism. Even though stereospecificity does not necessarily rule out any of the possible mechanisms; generally, however, the radical mechanism, and, to a lesser extent, the ionic one give a mixture of products. At least in principle, the occurrence of a concerted mechanism is quite reasonable since complex **1** may arrange suitable orbitals to form a transition state with an acetylene molecule. More detailed information on the electronic properties and the chemistry of $(np_3)MX$ (M = Co, Rh, Ni; X = unidentate ligand) and $(np_3)M$ complexes has been reported in a series of recent papers.[9,28]

(25) Countryman, R.; Penfold, B. R. *J. Chem. Soc., Chem. Commun.* **1978**, 1598.
(26) Bianchini, C.; Masi, D.; Mealli, C.; Meli, A. *Inorg. Chem.* **1984**, *23*, 2838.
(27) Bianchini, C.; Ghilardi, C. A.; Meli, A.; Orlandini, A. *J. Organomet. Chem.* **1984**, *270*, 251.
(28) (a) Cecconi, F.; Ghilardi, C. A.; Innocenti, P.; Mealli, C.; Midollini, S.; Orlandini, A. *Inorg. Chem.* **1984**, *23*, 422. (b) Ghilardi, C. A.; Mealli, C.; Midollini, S.; Orlandini, A. *Inorg. Chem.* **1985**, *24*, 1964. (c) Bianchini, C.; Masi, D.; Mealli, C.; Meli, A.; Sabat, M. *Organometallics* **1985**, *4*, 1014.

Table IV. Selected Bond Lengths (Å) and Angles (deg) for Compound 3

Bond Lengths			
Co–P(1)	2.331 (4)	P(3)–C(1)6	1.83 (1)
Co–P(2)	2.340 (4)	N(1)–C(2)	1.52 (2)
Co–P(3)	2.270 (4)	N(1)–C(4)	1.52 (2)
Co–N(1)	2.16 (1)	N(1)–C(6)	1.48 (2)
Co–C(7)	1.91 (2)	C(1)–C(2)	1.52 (2)
P(1)–C(1)	1.83 (1)	C(3)–C(4)	1.52 (2)
P(1)–C(1)1	1.80 (1)	C(5)–C(6)	1.51 (2)
P(1)–C(1)2	1.84 (1)	C(7)–C(8)	1.48 (2)
P(2)–C(3)	1.83 (1)	C(7)–C(11)	1.35 (2)
P(2)–C(1)3	1.83 (1)	C(8)–O(1)	1.33 (2)
P(2)–C(1)4	1.81 (1)	C(8)–O(2)	1.19 (2)
P(3)–C(5)	1.82 (2)	C(9)–O(1)	1.48 (2)
P(3)–C(1)5	1.81 (1)	C(9)–C(10)	1.53 (2)
Bond Angles			
P(1)–Co–P(2)	106.1 (2)	Co–P(3)–C(1)6	126.6 (4)
P(1)–Co–P(3)	102.6 (2)	C(5)–P(3)–C(1)5	105.9 (7)
P(2)–Co–P(3)	148.8 (2)	C(5)–P(3)–C(1)6	103.3 (7)
N(1)–Co–P(1)	85.9 (4)	C(1)5–P(3)–C(1)6	101.6 (5)
N(1)–Co–P(2)	85.3 (3)	C(2)–N(1)–C(4)	107 (1)
N(1)–Co–P(3)	84.7 (3)	C(2)–N(1)–C(6)	111 (1)
N(1)–Co–C(7)	170.5 (7)	C(4)–N(1)–C(6)	105 (1)
C(7)–Co–P(1)	103.6 (5)	P(1)–C(1)–C(2)	108.1 (9)
C(7)–Co–P(2)	91.5 (5)	C(1)–C(2)–N(1)	113 (1)
C(7)–Co–P(3)	93.6 (5)	P(2)–C(3)–C(4)	107 (1)
Co–P(1)–C(1)	95.7 (5)	C(3)–C(4)–N(1)	112 (1)
Co–P(1)–C(1)1	120.4 (3)	P(3)–C(5)–C(6)	110 (1)
Co–P(1)–C(1)2	131.8 (4)	C(5)–C(6)–N(1)	113 (1)
C(1)–P(1)–C(1)1	104.7 (6)	Co–C(7)–C(8)	122 (1)
C(1)–P(1)–C(1)2	103.1 (5)	Co–C(7)–C(11)	124 (1)
C(1)1–P(1)–C(1)2	97.3 (5)	C(8)–C(7)–C(11)	114 (2)
Co–P(2)–C(3)	101.5 (5)	C(7)–C(8)–O(1)	113 (2)
Co–P(2)–C(1)3	130.6 (4)	C(7)–C(8)–O(2)	124 (2)
Co–P(2)–C(1)4	111.4 (3)	O(1)–C(8)–O(2)	123 (2)
C(3)–P(2)–C(1)3	106.1 (6)	C(8)–O(1)–C(9)	116 (1)
C(3)–P(2)–C(1)4	102.2 (6)	O(1)–C(9)–C(10)	100 (1)
C(1)3–P(2)–C(1)4	101.8 (4)		
Co–P(3)–C(5)	102.5 (5)		
Co–P(3)–C(1)5	114.9 (4)		

There is ample experimental evidence that the hydride **1** may release H, H$^+$, or H$^-$ species depending on the particular type of reaction involved.[29] An important factor in determining the behavior of **1** is represented by the unique bonding capabilities of the ligand np$_3$. In effect, this may envelope the metal in different ways, which ultimately affect the mobility of hydrogen over the coordination sphere and hence influence the mode of rupture of the Co–H linkage.[9,28b,29] In the present reaction, the hydrogen should have hydridic nature. Such an assumption is supported by the course of the addition of the Co—H moiety across the C≡C triple bond. The Co—H, in fact, adds to the most electropositive carbon of the alkyne.

An important factor that may determine the type of addition of electrophilic acetylenes to metal hydrides is the electron availability of the C–C system.[1] The latter property strictly depends on the nature of the substituents on acetylenes. Within this context, it is interesting to compare some reactions of the hydrides **1** and HMn(CO)$_5$ with activated alkynes HC≡CR. Complexes containing the MC(R)=CH$_2$ moiety are formed by reacting **1** with HC≡CCO$_2$Et, or HMn(CO)$_5$ with HC≡CCF$_3$,[16a] whereas HMn(CO)$_5$ reacts with HC≡CCO$_2$Me to give *cis*-(CO)$_5$MnCH=CH(CO$_2$Me) by a stereospecific trans addition.[13]

As for the mechanism of the reaction of the nickel(0) complex **4** with HC≡CCO$_2$Et, we suggest an ionic stepwise mechanism to explain the formation of **5** (IX). The fact

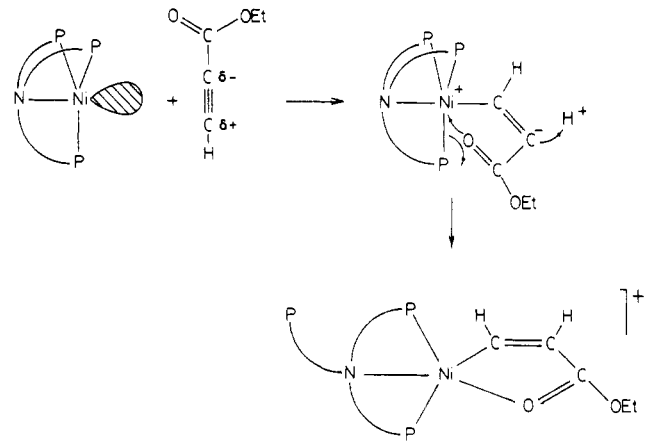

IX

that a four-centered transition state would involve the participation of a molecule of substrate makes, in fact, less probable a concerted mechanism. By contrast, the high σ basicity of **4** could easily explain the intermediacy of an ionic adduct through the formation of a bond between nickel and the most electrophilic carbon atom of ethyl propiolate. In this case, the second carbon of the acetylene moiety, bearing a negative charge, could abstract a proton from a molecule of *n*-butyl alcohol. Although alkyl propiolates are acidic compounds, *n*-butyl alcohol is the most probable hydrogen source. In fact, notwithstanding equimolecular amounts of **4** and HC≡CCO$_2$Et are used, 75–80% yields are observed. Moreover, when no alcoholic solvent is employed, the reaction of **4** with ethyl propiolate and NaBPh$_4$ does not give the alkenyl complex **5**. **5** cannot be obtained by reacting **4** with a twofold excess of ethyl propiolate. In this case, the reaction takes a different pathway, which likely involves the interaction of **4** with two or more alkyne molecules. Once the NiCH=CH(CO$_2$Et) moiety is formed displacement of one phosphorus atom of np$_3$ from nickel by the ketonic oxygen of the CO$_2$Et group may take place to give the β-carbethoxyvinyl complex **5**. The latter process involves the rupture of the five-membered metallacycle $\overline{\text{NCCPNi}}$, followed by formation of the five-membered metallacycle $\overline{\text{NiCCCO}}$. Some important factors that determine this rearrangement may be the formation of a metallacycle where, although small, some electronic delocalization occurs and the greater affinity of Ni(II) for oxygen donors than for phosphorus donors.[30]

An ionic stepwise mechanism, similar to that we suggest, has been previously reported for the formation of other alkenyl complexes, namely, *cis*-F$_3$CCH=CHRe(CO)$_5$ and *cis*-F$_3$CCH=CHFe(CO)$_2$(C$_5$H$_5$). These compounds were obtained by reaction of [Re(CO)$_5$]$^-$ and [Fe(CO)$_2$(C$_5$H$_5$)]$^-$ with HC≡CCF$_3$.[8]

Even though comparisons between organic and inorganic reactions are not always pertinent, it is interesting to note the analogies existing between the present reaction and that of PPh$_3$ with phenylacetylene in the presence of water, which gives β-styryltriphenylphosphonium hydroxide (X).[31]

$$PPh_3 + HC{\equiv}CPh \xrightarrow[X]{H_2O} (Ph_3P^+CH{=}CHPh)OH^-$$

In both cases a nucleophile possessing a σ lone pair (the nickel(0) complex **4** or PPh$_3$) attacks the most electrophilic

(29) Bianchini, C.; Masi, D.; Mealli, C.; Meli, A.; Sabat, M.; Scapacci, G. *J. Organomet. Chem.* **1984**, *273*, 91 and references therein.

(30) Ahrland, S.; Chatt, J.; Davies, N. R. *Q. Rev., Chem. Soc.* **1958**, *12*, 265.

(31) Allen, D. W.; Tebby, J. C. *Tetrahedron* **1967**, *23*, 2795.

Table V. Selected Bond Lengths (Å) and Angles (deg) for Compound 5

Bond Lengths			
Ni–P(1)	2.193 (2)	P(3)–C(1)6	1.835 (6)
Ni–P(2)	2.171 (2)	O(1)–C(9)	1.216 (8)
Ni–O(1)	2.229 (5)	O(2)–C(9)	1.331 (9)
Ni–N(1)	2.036 (6)	O(2)–C(10)	1.48 (1)
Ni–C(7)	1.878 (7)	N(1)–C(2)	1.497 (9)
P(1)–C(1)	1.825 (8)	N(1)–C(4)	1.491 (9)
P(1)–C(1)1	1.809 (6)	N(1)–C(5)	1.506 (9)
P(1)–C(1)2	1.812 (6)	C(1)–C(2)	1.49 (1)
P(2)–C(3)	1.845 (8)	C(3)–C(4)	1.52 (1)
P(2)–C(1)3	1.794 (7)	C(5)–C(6)	1.531 (9)
P(2)–C(1)4	1.818 (6)	C(7)–C(8)	1.35 (1)
P(3)–C(6)	1.856 (8)	C(8)–C(9)	1.46 (1)
P(3)–C(1)5	1.833 (7)	C(10)–C(11)	1.44 (1)
Bond Angles			
P(1)–Ni–P(2)	138.4 (1)		
P(1)–Ni–O(1)	96.1 (1)	Ni–O(1)–C(9)	104.9 (5)
P(1)–Ni–N(1)	88.4 (2)	C(2)–O(2)–C(10)	115.7 (6)
P(1)–Ni–C(7)	91.5 (2)	Ni–N(1)–C(2)	112.0 (5)
P(2)–Ni–O(1)	125.5 (1)	Ni–N(1)–C(4)	106.6 (4)
P(2)–Ni–N(1)	88.8 (2)	Ni–N(1)–C(5)	108.5 (4)
P(2)–Ni–C(7)	93.6 (3)	C(2)–N(1)–C(4)	110.7 (6)
O(1)–Ni–N(1)	94.7 (2)	C(2)–N(1)–C(5)	107.4 (6)
O(1)–Ni–C(7)	81.9 (3)	C(4)–N(1)–C(5)	111.7 (6)
N(1)–Ni–C(7)	176.5 (3)	P(1)–C(1)–C(2)	108.9 (6)
Ni–P(1)–C(1)	100.1 (3)	C(1)–C(2)–N(1)	112.7 (7)
Ni–P(1)–C(1)1	119.3 (2)	P(2)–C(3)–C(4)	107.3 (5)
Ni–P(1)–C(1)2	119.1 (2)	C(3)–C(4)–N(1)	110.9 (6)
C(1)1–P(1)–C(1)2	105.3 (9)	C(6)–C(5)–N(1)	114.7 (6)
Ni–P(2)–C(3)	100.4 (3)	P(3)–C(6)–C(5)	108.9 (5)
Ni–P(2)–C(1)3	126.1 (2)	Ni–C(7)–C(8)	114.7 (6)
Ni–P(2)–C(1)4	114.9 (2)	C(7)–C(8)–C(9)	115.6 (7)
C(1)3–P(2)–C(1)4	100.5 (3)	O(1)–C(9)–O(2)	122.8 (7)
C(6)–P(3)–C(1)5	101.5 (3)	C(8)–C(9)–O(1)	122.1 (7)
C(6)–P(3)–C(1)6	98.4 (3)	C(8)–C(9)–O(2)	115.1 (7)
C(1)5–P(3)–C(1)6	103.8 (3)	O(2)–C(10)–C(11)	110.1 (9)

carbon atom of the activated alkyne while a proton is abstracted from a weak Brønsted acid. Within this context, reaction X provides further support to the suggested reaction mechanism for the formation of **5**.

Experimental Section

All operations were routinely performed under nitrogen by using deoxygenated solvents. Reagent grade chemicals were used in the preparation of the complexes. Tetrahydrofuran (THF) was purified by distillation over $LiAlH_4$ just before use. Compounds **1** and **4** were prepared according to published procedures.[7] The solid complexes were collected on a sintered glass frit and dried in a stream of nitrogen. Infrared spectra were recorded on a Perkin-Elmer 283 spectrophotometer using samples mulled in Nujol between CsI plates. ^1H and $^{31}P\{^1H\}$ NMR spectra were taken on a Varian CFT 20 spectrometer. Peak positions are relative to tetramethylsilane and phosphoric acid, respectively, with downfield shifts positive. Ultraviolet–visible spectra were recorded on a Beckman DK-2A spectrophotometer. Magnetic susceptibilities of solid samples were measured on a Faraday balance. Conductance measurements were made with a WTW Model LBR/B conductivity bridge.

$(np_3)CoC(CO_2Et)=CH_2$ (2). Ethyl propiolate (0.07 mL, 0.6 mmol) was pipetted into a magnetically stirred solution of **1** (0.35 g, 0.5 mmol) in THF (30 mL). After 5 min the resulting solution was concentrated at ca. 10 mL under reduced pressure. Addition of *n*-butyl ether (10 mL) precipitated in a few minutes brown crystals that were filtered and washed with a 3:1 mixture of *n*-butyl ether/THF and petroleum ether; yield 62%. Anal. Calcd for $C_{47}H_{49}CoNO_2P_3$: C, 69.54; H, 6.08; Co, 7.25; N, 1.72. Found: C, 69.82; H, 5.99; Co, 7.20; N, 1.60.

$[(np_3)CoC(CO_2Et)=CH_2]BPh_4 \cdot 0.5THF$ (3). Ethyl propiolate (0.07 mL, 0.6 mmol) was pipetted into a magnetically stirred solution of **1** (0.35 g, 0.5 mmol) in THF (30 mL). The resulting mixture was then stirred for a further 40 min. Addition of $NaBPh_4$ (0.18 g, 0.6 mmol) in *n*-butyl alcohol (20 mL) precipitated red crystals that were filtered and washed with ethanol and petroleum ether; yield 70%. Anal. Calcd for $C_{73}H_{73}BCoNO_{2.5}P_3$: C, 75.12; H, 6.30; Co, 5.04; N, 1.20. Found: C, 74.80; H, 6.10; Co, 5.13; N, 1.18.

$[(np_3)NiCH=CHC(O)OEt]BPh_4$ (5). Ethyl propiolate (0.06 mL, 0.5 mmol) was added to a solution of **4** (0.35 g, 0.5 mmol) in THF (20 mL). Immediately an orange-brown solution was obtained. Addition of $NaBPh_4$ (0.18 g, 0.6 mmol) in *n*-butyl alcohol (30 mL) gave yellow-orange crystals that were filtered and washed with ethanol and petroleum ether; yield 80%. They were recrystallized from CH_2Cl_2 and ethanol. Anal. Calcd for $C_{71}H_{69}BNNiO_2P_3$: C, 75.41; H, 6.15; N, 1.23; Ni, 5.19. Found: C, 74.87; H, 6.10; N, 1.30; Ni, 5.26.

X-ray Data Collection and Structure Determination. A summary of crystal and intensity data is presented in Table I. All X-ray measurements were performed on a Philips PW1100 diffractometer using Mo Kα radiation. The intensities of three standard reflections were measured every 120 min of X-ray exposure, and no significant changes were noted for both compounds. The data were corrected for Lorentz and polarization effects. Numerical absorption corrections were applied with transmission factors ranging 0.94–0.97 for **3** and 0.91–0.94 for **5**. Atomic scattering factors were those tabulated by Cromer and Waber[32] with anomalous dispersion corrections taken from ref 33. The structures of the compounds were solved by Patterson and Fourier techniques using the SHELX76 program package.[34] Refinement was performed by full-matrix least-squares calculations, initially with isotropic and then with anisotropic thermal parameters for all non-hydrogen atoms of the complex cations but the phenyl carbon atoms. The function minimized was $\sum w(|F_o| - |F_c|)^2$. The phenyl rings were treated as rigid bodies of D_{6h} symmetry with C–C distances fixed at 1.395 Å and calculated hydrogen atom positions (C–H = 1.0 Å). Contributions from the remaining hydrogen atoms in positions fixed by geometry have also been included during final cycles of refinement. In the case of the Co compound a difference map showed a few higher peaks forming a five-membered ring of the tetrahydrofuran solvent molecule. The high thermal parameters indicated that the tetrahydrofuran positions were probably partially occupied. As a consequence the atoms of the ring were refined isotropically with occupancy factors 0.5, but no attempt was made to refine these coefficients. This approach was also in agreement with the results of the elemental analysis which demonstrated the 2:1 complex/solvent molar ratio. The final difference map for the Co compound revealed two peaks each 0.5 e/Å^3 high located near the phenyl rings 3 and 9, while in the case of the Ni complex the largest residuals were 1.2 and 0.9 e/Å^3 high and were located near the Ni atom and ring 3, respectively.

Final coordinates for all non-hydrogen atoms of **3** and **5** are reported in Tables II and III, respectively.

Registry No. **1**, 53687-39-1; **2**, 98838-13-2; **3**, 98838-16-5; **4**, 52633-73-5; **5**, 98838-18-7; $HC{\equiv}CCO_2Et$, 623-47-2.

Supplementary Material Available: Listings of anisotropic thermal parameters, supplementary distances, and observed and calculated structure factors (55 pages). Ordering information is given on any current masthead page.

(32) "International Tables for X-ray Crystallography"; Kynoch Press: Birmingham, England, 1974; Vol. IV, p 99.
(33) Reference 32, p 149.
(34) Sheldrick, G. M., SHELX76, Program for Crystal Structure Determination, University of Cambridge, Cambridge, 1976.

Structures and Energies of C_3H_3Li Isomers. Polar Organometallic Models for "Cyclopropenyl Anions"

Paul v. R. Schleyer,* Elmar Kaufmann, and Günther W. Spitznagel

Institut für Organische Chemie der Friedrich-Alexander-Universität Erlangen-Nürnberg, D-8520 Erlangen, Federal Republic of Germany

Rudolf Janoschek and Georg Winkelhofer

Institut für Theoretische Chemie der Karl-Franzens-Universität Graz, A-8010 Graz, Austria

Received May 31, 1985

As even the most stable nonplanar forms of the singlet (**1**, C_s) and triplet (**3**, C_{3v}) 3-cyclopropenyl anion are indicated not to be bound with regard to loss of an electron, the more realistic gegenion-stabilized systems are examined by ab initio molecular orbital theory at electron-correlated levels. The cyclic $(CH)_3Li$ singlet (**5**, C_s) is calculated to be more than 10 kcal/mol more stable than the best triplet (**7**, C_{3v}). Both forms have strongly nonplanar cyclopropenyl anion moieties, with all hydrogens bent out of the carbon plane on the same side away from lithium. This distortion eliminates much of the destabilizing "antiaromatic" character, and both the $C_3H_3^-$ singlet anion (**1**) and its lithium salt (**5**) are indicated to be about as stable thermodynamically as the 2-propyl anion and as 2-propyllithium, respectively. These results also indicate that, with the exception of the methyl anion, none of the simple alkyl carbanions will be bound in the gas phase. An open-chain $(CH)_3Li$ isomer (**8**, C_{2v}) is lower in energy than any of the three-membered ring forms. The beryllium analogue $(CH)_3BeH$ (**9**) has a similar $2\pi e$ structure. The calculated geometries and energies of other C_3H_3Li isomers 1-propynyllithium (**10**), allenyllithium (**11**), and 1-cyclopropenyllithium (**12**) provide further comparisons. All are considerably more stable than **5**: **10** due to the sp hybridization, **11** due to delocalization, and **12** due to its strained vinyl character which enhances the s contribution to the carbanionic orbital. The methyl group in **10** is destabilizing, **11** has a bridged structure and a strongly bent CCC backbone, and **12** has an elongated ring C^1–C^3 bond.

Introduction

As the smallest Hückel antiaromatic system with four π electrons, the 3-cyclopropenyl anion is of fundamental interest.[1,2] While experimental evidence indicates cyclopropenyl anions to be very unstable species thermodynamically,[3] the quantitative theoretical examination of 3-cyclopropenyllithium reported here challenges this commonly held expectation. Indeed, the many assumptions that have been imposed on this problem have long beclouded its essential nature. In particular, many of the earlier theoretical studies of the 3-cyclopropenyl anion assumed planar geometries and thus were basically incomplete.[4] Our recent investigation was the first to consider this problem comprehensively with regard to geometries and electronic states.[5] Neither the planar D_{3h} cyclopropenyl anion triplet favored by Hückel theory nor the Jahn–Teller distorted C_{2v} planar singlets are indicated to be minima on the potential energy surfaces. Instead, the singlet and triplet forms are much more stable (25–30 kcal/mol) in nonplanar geometries. The 3-cyclopropenyl anion has a singlet ground state; two forms are nearly comparable in energy. One of these has C_2 symmetry and the other, pertinent to the present study, has C_s symmetry (**1**). The hydrogen at the formal carbanion center is strongly bent out of the carbon plane, and the other two hydrogens extend in the opposite direction.[5] Similarly, the two lowest energy triplet cyclopropenyl anion structures have nearly the same energy. One form (**2**) also has C_s symmetry with two of the hydrogens bent into opposite directions out of the ring plane and the second isomer (**3**), C_{3v}, has all three hydrogens on the same side. The unfavorable orbital interactions associated with antiaromaticity are thus avoided or minimized by such out-of-plane distortions. Interestingly, an opened $(CH)_3^-$ anion (**4**) is indicated to be competitive in energy, or perhaps even more stable than any of the 3-cyclopropenyl anions.[5]

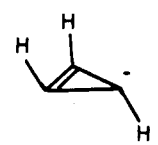

1, C_s ($^1A'$)

2, C_s ($^3A''$)

3, C_{3v} ($^3A_2$)

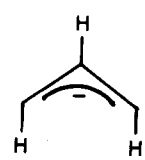

4, C_{2v} ($^1A_1$)

However, even these nonplanar cyclopropenyl anions are unlikely to be viable species as isolated entities, e.g., in the gas phase. All are indicated to be unbound; electron loss should be essentially spontaneous. In itself, this is not exceptional. The ethyl, 2-propyl, and many alkyl carbanions also are unbound.[6a,b] Chemical realistic cyclo-

(1) Breslow, R. *Acc. Chem. Res.* **1973**, *6*, 393.
(2) Borden, W. T.; Davidson, E. R. *Acc. Chem. Res.* **1981**, *14*, 69.
(3) (a) Breslow, R.; Brown, J.; Gajewski, J. J. *J. Am. Chem. Soc.* **1967**, *89*, 4383. (b) Breslow, R.; Douek, M. *Ibid.* **1968**, *90*, 2698. (c) Wasielewski, M. R.; Breslow, R. *Ibid.* **1976**, *98*, 4222.
(4) See ref 5 for a discussion of the earlier literature. Also see: Epiotis, N. D. *Nouv. J. Chim.* **1984**, *8*, 421.
(5) Winkelhofer, G.; Janoschek, R.; Fratev, F.; Spitznagel, G. W.; Chandrasekhar, J.; Schleyer, P. v. R. *J. Am. Chem. Soc.* **1985**, *107*, 332. Also see: Hess, B. A., Jr.; Schaad, L. J.; Čársky, P. *Tetrahedron Lett.* **1984**, *25*, 4721.
(6) (a) DePuy, C. H.; Bierbaum, V. M.; Damrauer, R. *J. Am. Chem. Soc.* **1984**, *106*, 4051. Also see: Tumas, W.; Foster, R. F.; Brauman, J. I. *J. Am. Chem. Soc.* **1985**, *106*, 4053. Dam Raver, R.; Danahey, S. E.; Yost, V. E. *Ibid.* **1985**, *106*, 7633. (b) Schleyer, P. v. R.; Chandrasekhar, J.; Spitznagel, G. W., submitted for publication in *Tetrahedron Lett.* (c) Bartmess, J. E.; Scott, J. A.; McIver, R. T., Jr. *J. Am. Chem. Soc.* **1979**, *101*, 6046. Bartmess, J. E.; McIver, R. T., Jr. In "Gas Phase Ion Chemistry"; Bowers, M. T., Ed.; Academic Press: New York, 1979; Vol. 2. (d) Pross, A.; Radom, L. *J. Am. Chem. Soc.* **1978**, *100*, 6572. (e) Ingemann, S.; Nibbering, N. M. M. *Can. J. Chem.* **1984**, *62*, 2273.

0276-7333/86/2305-0079$01.50/0

Table I. Total Energies (au) of C_3H_3Li Isomers and Related Species

	point group	state	3-21G//3-21G	4-31G[a]	6-31G*[a]	6-31G*//6-31G*	LSD/3-21G//3-21G	MP2/4-31G[a]
5	C_s	$^1A'$	−121.937 67	−122.454 07	−122.632 94		−122.730 75	−122.736 50
6	C_s	$^3A''$	−121.921 15	−122.441 26	−122.625 18		−122.708 99	−122.696 71
7	C_{3v}	$^3A_2$	−121.933 91	−122.453 28	−122.636 63		−122.719 60	−122.709 14
8	C_{2v}	$^1A_1$	−121.984 16	−122.503 76	−122.672 49		−122.776 87	−122.756 86
9	C_{2v}	$^1A_1$	−129.725 58					
10	C_{3v}	$^1A_1$	−122.053 61[b]	−122.571 05	−122.735 16		−122.849 30	−122.850 55
11	C_s	$^1A'$	−122.035 85	−122.553 21	−122.721 49	−122.721 87[c]	−122.833 61	−122.832 58
12	C_s	$^1A'$	−121.979 96	−122.496 30	−122.677 61[d]	−122.678 52	−122.773 12	−122.777 57
13	C_s	$^1A'$	−115.126 52	−115.605 23[e]	−115.776 32[f]			−115.845 35[g]

[a] Species 5–8 and 13 in 3-21G and 10–12 in 4-31G (ref 8, Table VI) optimized geometries. [b] Rohde, C., unpublished calculations. [c] Kos, A. J., unpublished calculations. [d] The 6-31G*//3-21G value is −122.676 81 au. [e] The 4-31+G//4-31+G value is −115.605 32 au. [f] The MP2 (frozen core) value is −116.125 23 au. [g] Frozen core.

propenyl (and alkyl) "anions" will be stabilized by association with an alkali-metal cation. The purpose of this paper is to examine such polar organometallic derivatives and to compare them with the corresponding carbanions.[5] While a number of cyclopropenyl transition-metal complexes are known,[7a] these less ionic species involve multicenter covalent bonding to a large extent. Our study includes the $(CH)_3Li$ isomers **5–7** corresponding to **1–3**, respectively, and an unusual four-membered ring (or lithium bridged) form, **8**, corresponding to **4**. Some transition-metal structures are similar.[7b] We also consider the beryllium analogue $(CH)_3BeH$ (**9**).[7c] Other C_3H_3Li isomers reported earlier,[8,9] propynyllithium (**10**), allenyllithium (**11**), and 1-cyclopropenyllithium (**12**), have also been reexamined for comparison.

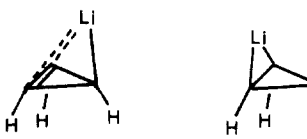

5, C_s ($^1A'$)

6, C_s ($^3A''$)

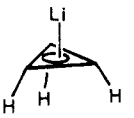

7, C_{3v} ($^3A_2$)

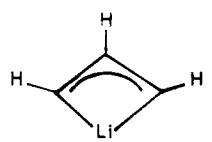

8, C_{2v} ($^1A_1$)

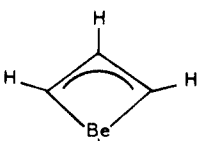

9, C_{2v} ($^1A_1$)

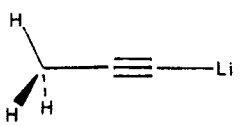

10, C_{3v} ($^1A_1$)

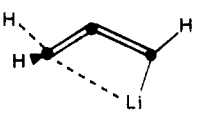

11, C_s ($^1A'$)

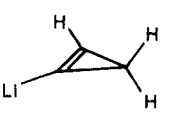

12, C_s ($^1A'$)

Methods

Ab initio calculations used the Gaussian series of programs[10] and standard 3-21G,[11] 4-31G (this implies 5-21G for lithium),[12] and 6-31G*[13] basis sets. (While diffuse function augmented basis sets, e.g., 4-31+G,[14a] are required for the energetic description of anions, they do not improve the calculational results for organolithium compounds[14b] and were not employed here.) Geometries were fully optimized within the indicated symmetry constraints. Electron correlation corrections were estimated at the second-order Møller–Plesset (MP2) level[15a] including core orbitals. The local spin density (LSD) formalism,[15b] employed in our earlier paper,[5] also was used for this purpose for comparisons. The absolute energies, coded in the usual way, are presented in Table I and relative energies in Table II. Thus, "MP2/4-31G//4-31G" denotes a single point MP2/4-31G run carried out on the geometries optimized at 4-31G. Assuming transferability of the MP2 correction at the 4-31G level, final relative energy estimates at MP2/6-31G* are derived and are given in the last column of Table II. Earlier data on **10–12** are included for comparison.[8] The geometrical details of all lithiated species at various levels are summarized in Table III.

Results

Relative Energies and Geometries of C_3H_3Li Isomers. As established in our earlier studies, 1-propynyllithium (**10**) is the lowest energy C_3H_3Li isomer.[8,9] This reflects not only the stability of the acetylenic anion but also the energy of the corresponding hydrocarbon, propyne, which is known experimentally to be 1.6 kcal/mol more stable than allene and 21.7 kcal/mol more stable than cyclopropene.[16] Our best estimates (Table II) indicate that allenyllithium (**11**) and 1-cyclopropenyllithium (**12**) are 8.7 and 35.0 kcal/mol less stable than 1-propynyllithium (**10**), respectively. The main structural features of these three

(7) (a) See: Jemmis, E. D.; Hoffmann, R. *J. Am. Chem. Soc.* **1980**, *102*, 2570. Churchill, M. R.; Fettinger, J. C.; McCullough, L. G.; Schrock, R. R. *Ibid.* **1984**, *106*, 3356. (b) See: Churchill, M. R.; Ziller, J. W.; Freudenberger, J. H.; Schrock, R. R. *Organometallics* **1984**, *3*, 1554. Freudenberger, J. H.; Schrock, R. R.; Churchill, M. R.; Rheingold, A. L.; Ziller, J. W. *Ibid.* **1984**, *3*, 1563 and ref 26. (c) For MNDO calculations on **9**, see: Bews, J. R.; Glidewell, C. *J. Organomet. Chem.* **1981**, *219*, 279.

(8) Jemmis, E. D.; Chandrasekhar, J.; Schleyer, P. v. R. *J. Am. Chem. Soc.* **1979**, *101*, 2848.

(9) Schleyer, P. v. R.; Chandrasekhar, J.; Kos, A. J.; Clark, T.; Spitznagel, G. W. *J. Chem. Soc., Chem. Commun.* **1981**, 882.

(10) GAUSSIAN 76: Binkley, J. S.; Whiteside, R. A.; Hariharan, P. C.; Seeger, R.; Pople, J. A.; Hehre, W. J.; Newton, M. D. *QCPE* **1978**, *14*, 368. GAUSSIAN 82, Release A: Binkley, J. S.; Frisch, M.; Raghavachari, K.; DeFrees, D.; Schlegel, H. B.; Whiteside, R.; Fluder, E.; Seeger, R.; Pople, J. A. Carnegie-Mellon University, 1983. This was adapted to CYBER 173 and 845 computers by A. Sawaryn.

(11) Binkley, J. S.; Pople, J. A.; Hehre, W. J. *J. Am. Chem. Soc.* **1980**, *102*, 939.

(12) Ditchfield, R.; Hehre, W. J.; Pople, J. A. *J. Chem. Phys.* **1971**, *54*, 724. Hehre, W. J.; Pople, J. A. *Ibid.* **1972**, *56*, 4233. Dill, J. D.; Pople, J. A. *Ibid.* **1975**, *62*, 2921.

(13) Hariharan, P. C.; Pople, J. A. *Theor. Chim. Acta* **1973**, *28*, 213. Dill, J. D.; Pople, J. A. *J. Chem. Phys.* **1975**, *62*, 2921.

(14) (a) Chandrasekhar, J.; Andrade, J. G.; Schleyer, P. v. R. *J. Am. Chem. Soc.* **1981**, *103*, 5609 and supplementary materials. (b) Spitznagel, G. W.; Clark, T.; Chandrasekhar, J.; Schleyer, P. v. R. *J. Comput. Chem.* **1982**, *3*, 363.

(15) (a) Møller, C.; Plesset, M. S. *Phys. Rev.* **1934**, *46*, 618. Binkley, J. S.; Pople, J. A. *Int. J. Quantum Chem.* **1975**, *9*, 229. Pople, J. A.; Binkley, J. S.; Seeger, R. *Int. J. Quantum Chem. Symp.* **1976**, *10*, 1. (b) Stoll, H.; Golka, E.; Preuss, H. *Theor. Chim. Acta* **1978**, *49*, 143.

(16) Rosenstock, H. M.; Draxl, K.; Steiner, B. W.; Herron, J. T. *J. Phys. Chem. Ref. Data* **1977**, *6*, Suppl. 1.

Table II. Relative Energies (kcal/mol) of C_3H_3Li Isomers

	3-21G//3-21G	LSD/3-21G//3-21G	4-31G[a]	MP2/4-31G[a]	6-31G*[a]	MP2/6-31G*[a,b]
10	0.0	0.0	0.0	0.0	0.0	0.0
11	11.1	9.8	11.2	11.3	8.6[c]	8.7
12	46.2	47.8	46.9	45.8	36.1[c]	35.0
8	43.6	45.5	42.2	58.8	39.3	55.9
5	72.8	74.4	73.4	71.6	64.1	62.3
7	75.1	81.4	73.9	88.7	61.8	76.6
6	83.1	88.0	81.4	96.5	69.0	84.1

[a] Species **5**–**8** in 3-21G and **10**–**12** in 4-31G[8] optimized geometries. [b] Correlation correction estimate taken from the 4-31G level, see text. [c] The 6-31G*//6-31G* values for **11** and **12** are 8.3 and 35.5 kcal/mol, respectively.

Table III. Geometries of C_3H_3Li Isomers and Related Species[a]

			3-21G	4-31G[b]	6-31G*		3-21G	4-31G[b]	6-31G*
5	C_s	C^1C^2	1.296			C^1H	1.064		
		C^1C^3	1.627			HC^1C^3	148.0		
		C^3Li	1.877			$HC^1C^3C^2$	17.0[c]		
		LiC^3O[d]	82.4			C^3H	1.085		
		C^1Li	2.330			HC^3O[d]	113.2		
6	C_s	C^1C^2	1.460			C^1H	1.070		
		C^1C^3	1.475			HC^1C^3	131.0		
		C^3Li	2.432			$HC^1C^3C^2$[e]	122.6		
		LiC^3O[d]	51.8			C^3H	1.072		
		C^1Li	2.057			HC^3O[d,e]	146.7		
7	C_{3v}	C^1C^2	1.469			C^1H	1.070		
		C^1Li	2.092			HC^1O[f]	141.2		
8	C_{2v}	C^1C^2	1.400			C^1H	1.086		
		$C^1C^2C^3$	115.3			HC^1C^2	115.1		
		C^1Li	2.039			C^2H	1.083		
		C^2Li	2.411						
9	C_{2v}	C^1C^2	1.395			C^1H	1.079		
		$C^1C^2C^3$	105.6			HC^1C^2	121.6		
		C^1Be	1.846			C^2H	1.075		
		C^2Be	2.318			BeH	1.360		
10[g]	C_{3v}	C^1C^2	1.213	1.216		C^3H	1.086	1.085	
		C^2C^3	1.468	1.461		HC^3C^2	110.9	111.4	
		C^1Li	1.912	1.896					
11[h]	C_s	C^1C^2	1.267	1.277	1.269	C^1H	1.068	1.068	1.072
		C^2C^3	1.345	1.341	1.344	HC^1C^2	131.3	130.0	127.9
		$C^1C^2C^3$	160.8	161.4	160.9	C^3H	1.076	1.075	1.077
		C^1Li	2.044	2.000	2.015	HC^3H	116.7	116.3	116.5
		C^3Li	2.409	2.469	2.402	OC^3C^2[i]	164.4	167.4	164.3
12	C_s	C^1C^2[j]	1.289	1.304	1.294	C^2H	1.060	1.063	1.071
		C^1C^3[j]	1.770	1.594	1.571	HC^2C^3	137.1	143.2	143.5
		C^2C^3[j]	1.523	1.480	1.460	C^3H	1.078	1.079	1.086
		C^1Li	1.922	1.916	1.943	HC^3H	115.7	112.9	112.1
		LiC^1C^3	76.3	144.2	137.3	OC^3C^2[i]	147.6	157.6	157.1
13	C_s	C^1C^2	1.332			$H(cis)C^1C^2$	119.5		
		C^2C^3	1.465			C^2H	1.076		
		$C^1C^2C^3$	116.7			HC^2C^1	119.5		
		$C^1H(trans)$	1.074			$C^3H(s\text{-}trans)$	1.099		
		$H(trans)C^1C^2$	122.8			$H(s\text{-}trans)C^3C^2$	109.4		
		$C^1H(cis)$	1.073						

[a] Bond lengths in Å and angles in deg. [b] 4-31G data are taken from ref 8. [c] All hydrogens lie on one side of the ring plane. [d] O is the middle of the C^1C^2 bond. [e] The hydrogens at C^1 and C^2 lie on the opposite side of the ring plane to lithium, and the hydrogen at C^3 lies on the same side. [f] O is the center of the ring. [g] 3-21G data: Rohde, C., unpublished calculations. [h] 6-31G* data: Kos, A. J., unpublished calculations. [i] OC^3 is the bisector of HC^3H. [j] Compare data for cyclopropene: C^1C^2 = 1.282 (1.276) and C^2C^3 = 1.523 (1.495) Å at 3-21G (6-31G*).[22]

isomers have been discussed earlier,[8] but two X-ray structures of allenyllithium derivatives have become available subsequently.[17] Both these are in very good agreement as far as the carbon skeleton geometries are concerned with the higher level calculated values given in Table III. Particularly noteworthy are the bent CCC angle (161°) and the different C–C bond lengths (1.27–1.28 and 1.34–1.35 Å) in **11**. Several X-ray structures of 2-substituted lithiated acetylenes have also been published recently.[18] Both dimers and tetramers (roughly tetrahedral) have been found. Association is known to lengthen the C–Li distances,[19] but the C–C bond lengths again agree with those computed for **10**.

Calculated geometries for 1-cyclopropenyllithium (**12**) (Table III) at 3-21G and at 4-31G differ significantly. The latter level indicates conventional angles at the lithiated carbon, but, at 3-21G, the lithium distorts abnormally toward the saturated C–C bond. Such bending, noted previously in the STO-3G structure of vinyllithium,[20] is a consequence of the special electronic structure of **12**

(17) See: Schleyer, P. v. R. *Pure Appl. Chem.* **1984**, *56*, 151.
(18) Schubert, B.; Weiss, E. *Chem. Ber.* **1983**, *116*, 3212; *Angew. Chem., Int. Ed. Engl.* **1983**, *22*, 496; *Angew. Chem. Suppl.* **1983**, 703. Neugebauer, W.; Schleyer, P. v. R.; Weiss, E.; Kopf, J.; Schubert, B., to be submitted for publication.
(19) Setzer, W. N.; Schleyer, P. v. R. *Adv. Organomet. Chem.* **1985**, *24*, 353.
(20) Apeloig, Y.; Clark, T.; Kos, A. J.; Jemmis, E. D.; Schleyer, P. v. R. *Isr. J. Chem.* **1980**, *20*, 43.

Table IV. Stabilization Energies (kcal/mol) of Anions and Organolithiums Relative to Methyl

R	anion[a]	organolithium[b]	estd E_a of radical[c]	exptl[c,d]
ethynyl	−47.9	−33.3		66[e]
1-propynyl	−40.3	−31.2 (**10**)		
1-cyclopropenyl	−35.2	−21.0, −22.0[f] (**12**)		
allenyl	−33.5	−21.5, −25.4[f] (**11**)		
prop-1-en-3-yliden-1-yl	−45.7[g] (**4**)	−51.5[g,h] (**8**)		
allyl	−28.0	−15.7	9.8	12.7,[e] 8.3[i]
2-propenyl	−10.5	−2.3		
vinyl	−9.7	−4.8	17	17
cis-1-propenyl	−9.3	−4.0		
trans-1-propenyl	−7.4	−4.0		
methyl	0.0	0.0		1.8[e]
cyclopropyl	1.8	2.1	1.2	8
1-propyl	2.7	4.0		
3-cyclopropenyl	5.5, 1.9[j] (**1**)	6.0 (**5**)	−9.5, −17.9[j]	
ethyl	5.6, 3.2[j]	5.0	−12.5, −10.1[k]	−9
2-propyl	5.8	8.3	−15.8	−11

[a] Equation, 1, 4-31+G//4-31+G.[9] [b] Equation 2, 4-31G//4-31G.[9] [c] See ref 6b for a detailed discussion. [d] Reference 6a. [e] Reference 6c. [f] 6-31G*//6-31G* (calculated using reference data from ref 22). [g] This work. [h] 3-21G//3-21G. [i] MP2/6-31+G*//6-31+G* (Spitznagel, G. W., unpublished calculations). [j] Reference 5. [k] Kos, A. J., unpublished calculations. [l] Oakes, J. M.; Ellison, G. B. *J. Am. Chem. Soc.* **1984**, *106*, 7734.

which is overemphasized at lower levels of theory. Lithium potential energy surfaces are often very flat, and relatively large changes in lithium positions do not change the energy to a large extent. Thus, the 6-31G*//4-31G energy of **12** is only 0.5 kcal/mol below the 6-31G*//3-21G value (Table I). Our 6-31G* optimized geometry (see Table III) should be definitive; the 4-31G parameters are in better agreement with the 6-31G* values than those at 3-21G. However, at all levels the C^1–C^3 bond in **12** is rather long (1.57–1.77 Å, Table III); the anion value is 1.666 Å (4-31+G//4-31+G).[14a] These elongations are due to an in-plane interaction,[21] which also transfers part of the negative charge to C^3 (see below).

Of the three $(CH)_3Li$ isomers **5**, **7**, and **8**, the open C_{2v} form **8** rather surprisingly is the most stable. This structure can be considered to be a derivative of singlet vinylcarbene (**13**), which is estimated to lie about 72 kcal/mol above propyne in energy (MP2/6-31G*, calculated from data of Table I and ref 22). Lithium substitution lowers this value substantially, since **8** lies 55.9 kcal/mol above **10** in energy (Table II).

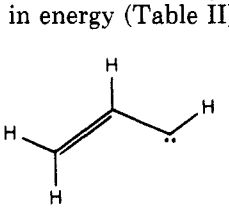

13, C_s ($^1A'$)

Since both the 1-propynyl anion and 1-propynyllithium (**10**) are favored by the sp hybridization, considerable stabilization in **8** (and the corresponding anion **4**) is indicated as well. Charge delocalization and the ability of lithium to associate with both centers is responsible. The C–C bond lengths, 1.400 Å, are like those in allyllithium (1.393 Å, also at 3-21G//3-21G).[23] The symmetrically bridged, C_{2v} structure **8** is more stable than lower symmetry alternatives. Oddly, electron correlation disfavors **8** relative to all other singlet isomers significantly.

Of the two 3-cyclopropenyllithium states, the C_s singlet **5** is significantly more stable at correlated levels than the triplet **7**. As in the corresponding singlet anion (**1**), the C^3–H hydrogen in **5** is strongly bent (66.8°) out of the carbon ring plane, but the other hydrogens bend to the *same* side (8.9°) away from the lithium. The C=C bond length in **5** (1.296 Å) is like those in **1** (1.294 Å)[5] and in cyclopropene (1.282 Å),[22] but the C^1–C^3 distance (1.627 Å) is even longer than in the anion (1.591 Å).[5]

In the singlet **5**, the lithium is bent toward the center of the ring. Starting with this geometry, optimization of the triplet led to further lithium movement; the symmetrical C_{3v} structure **7** resulted. All three hydrogens in **7** are strongly bent out of the carbon plane, 38.8° away from lithium. The C–C bond lengths, 1.469 Å, are much closer to those of *cyclopropane* (1.513 Å)[22] than to the C–C lengths of the aromatic cyclopropenyl cation (1.361 Å, 3-21G//3-21G data).[22] The C–C bond lengths and the high relative energies of **5** and **7** (Table II) reflect antiaromatic destabilization. Thus, **5** and **7** are 27.3 and 41.5 kcal/mol less stable than the isomer 1-cyclopropenyllithium (**12**). Other estimates of the antiaromatic destabilization energy are discussed below.

Stabilization Energies. The stabilities of various carbanions and their organolithium counterparts can be evaluated, relative to methyl as a standard, by means of isodesmic equations (1) and (2).[9] This corrects for the

$$RH + CH_3^- \rightarrow R^- + CH_4 \quad (1)$$

$$RH + CH_3Li \rightarrow RLi + CH_4 \quad (2)$$

different energies of the parent hydrocarbons mentioned earlier. Table IV lists values for the systems discussed in this paper as well as a few others for reference.[9] Comparisons of this type are not very sensitive to the level of theory employed (provided diffuse function-augmented basis sets are used for the anions),[14b] and the few experimental data available (for the anions)[6] are in reasonably good agreement.

It is apparent from Table IV that the stabilization energies of the anions and the corresponding lithium compounds parallel each other closely. A plot (Figure 1) gives a slope of 0.73 with only one significant deviation (for **8** vs. **4**; this reflects the exceptional stability of **8**). As we have pointed out in earlier papers,[9,17] organolithium compounds exhibit the commonly attributed "anionic" behavior. The attenuation factor of 0.73 is most simply

(21) Cf. Clark, T.; Spitznagel, G. W.; Klose, R.; Schleyer, P. v. R. *J. Am. Chem. Soc.* **1984**, *106*, 4412.
(22) Whiteside, R. A.; Frisch, M. J.; Pople, J. A. "The Carnegie-Mellon Quantum Chemistry Archive", 3rd ed.; Carnegie-Mellon University: Pittsburgh, PA, 1983.
(23) Clark, T.; Rohde, C.; Schleyer, P. v. R. *Organometallics* **1983**, *2*, 1344.

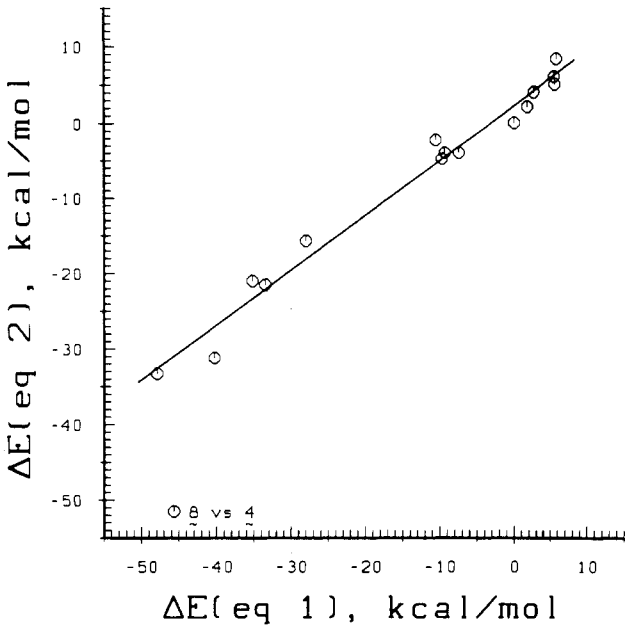

Figure 1. Plot of the methyl stabilization energies (Table IV) of carbanions (R^- vs. CH_3^-, eq 1) vs. those of the corresponding organolithium compounds (RLi vs. CH_3Li, eq 2). The slope of the least-squares correlation line, 0.73, indicates attenuation due primarily to ion pair formation. The deviation of the point for **8** (vs. **4**) shows the special stabilization of the lithiated system.

ascribed to ion pairing. Both single-coordinated (**10** and **12**) and multi-coordinated organolithium compounds (**5** and **11**) are affected similarly. Multicenter covalent interactions, if present, must contribute only modestly to the stabilization energies of these systems. While this is not the case in other instances, we need not differentiate between the carbanions and the organolithiums in the subsequent discussion.

The acetylene anionic systems have the largest stabilization energies due to their high s character (sp hybridization). In agreement with gas-phase experimental studies,[6c,d] the methyl group in **10** (and in the 1-propynyl anion) is destabilizing. The same is true when methyl groups are directly attached to carbanionic centers (ethyl vs. methyl, but 2-propyl vs. ethyl and 2-propenyl vs. vinyl are less clear-cut). In other instances, more remote methyl attachment can be stabilizing (1-propyl vs. ethyl) or somewhat destabilizing (*cis*- and *trans*-1-propenyl vs. vinyl, see Table IV and ref 9). Polarization (a size effect) helps stabilize charged species, but the four-electron hyperconjugative interactions in carbanions often are destabilizing.[24] These influences often balance.

The stabilization energies of the localized vinyl systems (vinyl, 1-propenyl, and 2-propenyl) are modest and reflect the sp^2 hybridization. Because of the high degree of s character, the vinyl hydrogens in cyclopropene are much more acidic.[25] The stabilization energies of the 1-cyclopropenyl anion and of **12** are very high, and the charge in these systems actually is delocalized: Mulliken population analysis indicates that in **12** appreciable negative charge is transferred to C^3. In fact, at all levels studied C^3 has the largest negative charge on any of the carbon atoms, including C^1, where the lithium is attached. The elongated C^1–C^3 bond (see above) results. The situation can be described by the resonance formalism.[21]

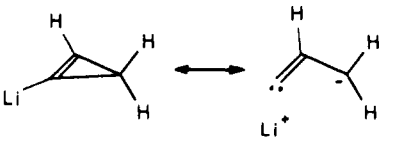

The formally delocalized species allenyl- (**11**), allyl-, and prop-1-en-3-yliden-1-yllithium (**8**) have the expected large stabilization energies. The value for allyl is exceeded by that of **8**. This latter species, as yet unknown, is an intriguing target for experimental investigations. Transition-metal derivatives resembling **8** have been reported.[7b,26]

The electronic structure of this lithiacyclobutadiene is well represented by formula **8**. Interestingly, the two electrons of the π system lie energetically *below* the two carbon–lithium σ bonds. While **8** has a formal similarity with the cyclobutadiene dication, lithium participates in the π system only to a negligible extent. That the lithium interaction is largely ionic is suggested by the Mulliken population analysis: the charges are +0.47 at lithium and −0.27 at the terminal carbons. The unique carbon atom (C^2) bears most of the negative charge, −0.46 electrons (3-21G data), reflecting the larger coefficient at C^2 in the π molecular orbital. The electronic structure of **8** with *two* π electrons is in contrast to that of the experimentally known transition-metal analogues which are apparently 4π systems.[26] Due to involvement of metal d orbitals the latter can also stabilize the π_2 orbital in a $C_3H_3^{3-}$ moiety.[26] The exceptional role of lithium in lowering the relative energy of this system is apparent from the deviation of the point for **8** from the correlation line in Figure 1.

The beryllium analogue of **8**, $(CH)_3BeH$ (**9**),[7c] is expected to be much closer in its electronic structure to the isoelectronic cyclobutadiene dication $(CH)_4^{2+}$.[27] Indeed, Mulliken population analysis indicates a slightly higher metal–carbon bond order in **9** (0.42) than in **8** (0.39). However, despite the less electropositive character of beryllium vs. lithium, the charge separation in **9** between beryllium and the terminal carbons (+0.57 and −0.32 electrons) is much larger than in **8**. This is due to the additional attachment of a "hydride" to beryllium which bears −0.16 electrons (3-21G data). This leads to an induced charge shift from the central hydrogen to the terminal carbons in the $C_3H_3^-$ moiety. The resulting dipole moment of **9** therefore is much larger than that of **8** (3.9 and 2.0 D, respectively) and may be the reason for the lower stabilization energy of **9** (−38.1 kcal/mol, evaluated by using eq 2 with BeH instead of Li).

We now turn to the central question of this paper: To what extent is the 3-cyclopropenyl anion "antiaromatic"? This depends on which of the several anionic species we take and the method of evaluation. The most stable structures, the singlet anion **1** and the organolithium **5**, show only modest destabilization energies vs. methyl (Table IV). But this does not take into account the additional strain energy present in cyclopropenyl systems compared to methyl. Thus, the fairest evaluation is, perhaps, to use cyclopropyl as a strained model (eq 3).

(24) Schleyer, P. v. R.; Kos, A. J. *Tetrahedron* **1983**, *39*, 1141. Also see: Radom, L. *J. Chem. Soc., Chem. Commun.* **1974**, 403. DeFrees, D. J.; Bartmess, J. E.; Kim, J. K.; McIver, R. T., Jr.; Hehre, W. J. *J. Am. Chem. Soc.* **1977**, *99*, 6451.

(25) Closs, G. L.; Larrabee, R. B. *Tetrahedron Lett.* **1965**, 287.

(26) Pedersen, S. F.; Schrock, R. R.; Churchill, M. R.; Wasserman, H. J. *J. Am. Chem. Soc.* **1982**, *104*, 6808. Also see: Bursten, B. E. *Ibid.* **1983**, *105*, 121 and ref 7.

(27) However, **9** prefers planarity whereas both $(CH)_4^{2+}$ (Krogh-Jespersen, K.; Schleyer, P. v. R.; Pople, J. A.; Cremer, D. *J. Am. Chem. Soc.* **1978**, *100*, 4301. Chandrasekhar, J.; Schleyer, P. v. R.; Krogh-Jespersen, K. *J. Comput. Chem.* **1981**, *2*, 356) and the isoelectronic boron analogue $1,3\text{-}(BH)_2(CH)_2$ (Krogh-Jespersen, K.; Cremer, D.; Dill, J. D.; Pople, J. A.; Schleyer, P. v. R. *J. Am. Chem. Soc.* **1981**, *103*, 2589. Schleyer, P. v. R.; Budzelaar, P. H. M.; Cremer, D.; Kraka, E. *Angew. Chem., Int. Ed. Engl.* **1984**, *23*, 374. Bodzelaar, P. H. M.; Krogn-Jespersen, K.; Clark, T.; Schleyer, P. v. R. *J. Am. Chem. Soc.* **1985**, *107*, 2773) are nonplanar.

The small destabilization found for the anion and organolithium contrasts sharply with the moderate to large stabilization energies of the 3-cyclopropenyl radical and cation.

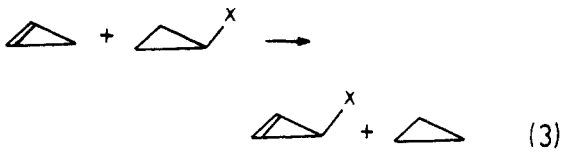

(3)

X		level
− (anion) (1)	+3.7 kcal/mol	4-31+G//4-31+G[9]
Li (5)	+3.9 kcal/mol	4-31G//4-31G[9]
· (radical)	−15 kcal/mol	expt.[28]
	−8.1 kcal/mol	6-31G*//6-31G*[5,29]
+ (cation)	−69.4 kcal/mol	6-31G*//6-31G*[22,30]

These unexpectedly low destabilizations of potentially antiaromatic species result from geometrical distortions which relieve most of the adverse electronic interactions in 1 (and 5). In the HOMO of 1, the repulsive interaction between the lone pair and the double bond is alleviated by bending.

Classical analyses of aromaticity and antiaromaticity in *n*-annulenes have assumed planarity and usually D_{nh} symmetry as well. The most stable form of $C_3H_3^-$ in D_{3h} symmetry is a triplet, which, at correlated levels, is 28 kcal/mol higher in energy than 1.[5] On this basis, eq 3 would give a destabilization energy of 32 kcal/mol. Compared to a D_{3h} singlet which is (at 3-21+G//3-21+G) 56 kcal/mol less stable than 1,[5] an antiaromatic destabilization of 60 kcal/mol can be evaluated.

We may compare the inversion barrier of the cyclopropyl anion (15.1 kcal/mol at MP2/4-31+G//4-31+G[14a]) with that of the 3-cyclopropenyl anion. Using the corresponding $^1A'$ (1) and $^1A_1$ (for the planar C_{2v} structure) states, the barrier is 28.9 kcal/mol (also at MP2/4-31+G//4-31+G).[5,14a] On this basis the repulsive interaction between the lone pair and the double bond in $C_3H_3^-$ can be estimated to be 13.8 kcal/mol.

(1,2,3-Triphenylcyclopropenyl)lithium. In our earlier paper,[5] we reported MNDO[31] calculations on the 1,2,3-triphenylcyclopropenyl anion, a system investigated experimentally in solution.[3,32] As the MNDO lithium parametrization[31b] gives generally excellent results for π-carbanionic systems in comparison with X-ray structures,[17] we have examined (1,2,3-triphenylcyclopropenyl)lithium at this level. As in the case of the parent anion,[5,32] the potential energy surface is found to be quite flat; this applies in particular to the position of the lithium counterion. The lowest energy MNDO structure we have found is shown in Figure 2. The bond lengths in the ring are quite different (1.359 Å for the essentially double bond

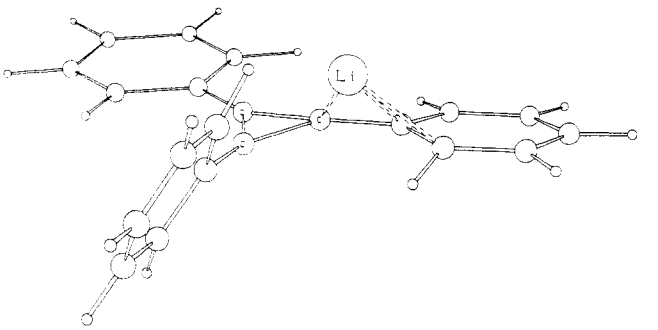

Figure 2. The MNDO[31] optimized structure of (1,2,3-triphenylcyclopropenyl)lithium. Essential distances are Li–C^3 = 2.066 Å, Li–C_{ipso} = 2.242, and Li–C_{ortho} = 2.126 Å (these distances refer to the dotted lines). The distance between Li and the ortho H at the phenyl ring attached to C^1 is 2.094 Å. The phenyl rings are bent out of the plane of the three-membered ring (5.5° up, 0.5° up, and 9.2° down for the rings at C^1, C^2, and C^3, respectively). The twist angles between the plane of the three-membered ring and the phenyl rings are 59°, 3°, and 15° (same order). The ortho H of the phenyl ring associated with Li is bent down by 20.6°. The full **Z** matrix and distance matrix for this system is available as supplementary material.

opposite the position where lithium is attached and an average of 1.493 Å for the two single bonds; this corresponds to an "en–yl" type anion with a negative charge at C^3 in contrast to the calculated structure of the parent $C_3H_3^-$ anion which gave a preference for an "allyl"-type structure). In addition, the ipso carbons of the phenyl substituents lie more or less in the three-membered ring plane. One of the phenyl rings is strongly twisted. The lithium counterion is unsymmetrically located and is associated with the phenyl as well as with the cyclopropenyl anion ring. This resembles the position of the lithium in the benzyllithium X-ray structure.[33] Additionally, an interaction between the lithium and one of the ortho hydrogens of the phenyl ring attached to C^1 may be present (see Figure 2). X-ray structural studies of such cyclopropenyl anion systems are of interest and are being undertaken.

Conclusions

Since the "cyclopropenyl anion" is an unstable, hypothetical species, it is more satisfactory, and certainly more realistic in terms of possible experimental observation, to consider the alkali-metal derivatives instead. Because of the large degree of ion pair character, the C_3H_3Li isomers mirror the relative energies of the corresponding $C_3H_3^-$ arrangements rather closely. Some exceptions, due to specific electrostatic interactions or the presence of some degree of multicenter covalent character, are noted. In particular, the open-chain $(CH)_3Li$ structure 8 as well as its beryllium analogue **9**[7c] is particularly favorable. The latter, at least, should benefit from some $2\pi e$ aromatic character. Although transition-metal analogues of 8 and 9 are known, these species have not been reported experimentally and the synthesis of derivatives of 8 and 9 would be a challenging goal. Although ring-opening reactions from possible cyclopropenyl anion precursors are forbidden by orbital symmetry considerations in a C_s pathway, the ring opening via an unsymmetrical transition state may be better; 8 is more stable than 5 by about 14 kcal/mol. The experimental determination of the structure of 1-cyclopropenyllithium (12) or its derivatives would also be interesting. Our calculations predict that 12 should

(28) DeFrees, D. J.; McIver, R. T., Jr.; Hehre, W. J. *J. Am. Chem. Soc.* **1980**, *102*, 3334.
(29) For a comprehensive recent study of the cyclopropenyl radical, see: Chipman, D. M.; Miller, K. E. *J. Am. Chem. Soc.* **1984**, *106*, 6236.
(30) See: Raghavachari, K.; Whiteside, R. A.; Pople, J. A.; Schleyer, P. v. R. *J. Am. Chem. Soc.* **1981**, *103*, 5649. Although experimental energies for the cyclopropyl cation are given in the literature, these probably refer to other species.
(31) (a) Dewar, M. J. S.; Thiel, W. *J. Am. Chem. Soc.* **1977**, *99*, 4899, 4907. (b) Thiel, W.; Clark, T., lithium parametrization, to be submitted for publication.
(32) Köser, H. G.; Renzoni, G. E.; Borden, W. T. *J. Am. Chem. Soc.* **1983**, *105*, 6359. This work inadvertently was not cited in our earlier paper.[5]
(33) Patterman, S. P.; Karle, I. L.; Stucky, G. D. *J. Am. Chem. Soc.* **1970**, *92*, 1150.

have an elongated C^1–C^3 bond.

Somewhat surprisingly, the lithium salt of the "antiaromatic cyclopropenyl anion" *is not indicated to be particularly unstable* thermodynamically. The lowest energy 3-cyclopropenyllithium form, singlet **5** with C_s symmetry, has about the same methyl stabilization energy as that of, e.g., 2-propyllithium. This possibility was considered by Wasielewski and Breslow[3c] and is due to compensating factors: some residual 4πe destabilization is balanced by the stabilization due to small-ring rehybridization and the σ inductive effects of the double bond. Nevertheless, manifestations of the expected Hückel 4π electron antiaromaticity are quite clearly evident in the strong distortions from planarity exhibited both in the singlet **5** and in the triplets **6** and **7**. These triplets are estimated to be about 10 kcal/mol less stable than the singlet **5**.

Breslow has measured the rates of base-catalyzed deuterium exchange in comparably substituted cyclopropyl and cyclopropenyl systems. The latter exchanged about 6000[3a] to 10 000[3b] times slower than the corresponding cyclopropane, thus indicating some destabilization of cyclopropenyl anion systems. With the assumption that kinetic acidities parallel thermodynamic acidities[2] an energetic difference for the proton abstraction of 5.2–6.1 kcal/mol can be evaluated. This is in reasonable good agreement with our calculated value of 3.7 kcal/mol (eq 3).[34]

Acknowledgment. This work was supported at Erlangen by the Fonds der Chemischen Industrie and the Deutsche Forschungsgemeinschaft. We also appreciate the assistance of the Regionales Rechenzentrum Erlangen and the Rechenzentrum der Universität Graz.

Registry No. **1/2/3**, 20829-57-6; **4**, 98705-30-7; **5/6/7**, 72507-54-1; **8**, 98705-27-2; **9**, 98705-28-3; **10**, 4529-04-8; **11**, 51760-92-0; **12**, 51174-22-2; **13**, 19527-08-3; CH_3Li, 917-54-4; CH_3^-, 15194-58-8; ethynyllithium, 1111-64-4; allyllithium, 3052-45-7; 2-propenyllithium, 6386-71-6; vinyllithium, 917-57-7; *cis*-1-propenyllithium, 6524-17-0; *trans*-1-propenyllithium, 6386-72-7; methyllithium, 917-54-4; cyclopropyllithium, 3002-94-6; 1-propyllithium, 2417-93-8; ethyllithium, 811-49-4; 2-propyllithium, 1888-75-1; (1,2,3-triphenylcyclopropenyl)lithium, 98705-29-4; ethynyl anion, 29075-95-4; 1-propynl anion, 31139-07-8; allenyl anion, 64066-06-4; allyl anion, 1724-46-5; 2-propenyl anion, 65887-19-6; vinyl anion, 25012-81-1; 1-propenyl anion, 65887-20-9; cyclopropyl anion, 1724-45-4; 1-propyl anion, 59513-13-2; ethyl anion, 25013-41-6; 2-propyl anion, 25012-80-0.

Supplementary Material Available: Tables of fractional coordinates and interatomic distances (5 pages). Ordering information is given on any current masthead page.

(34) In a later study using indirect methods, Breslow was able to estimate the pK_a of unsubstituted cyclopropene to be 61.3.[3c] However, no comparable value for the pK_a of cyclopropane is available.

Organotin Biocides. 4. Crystal and Molecular Structure of Tricyclohexylstannyl 3-Indolylacetate, Incorporating the First Monodentate Carboxylate Group Bonded to a Triorganotin(IV)

Kieran C. Molloy*[1] and Thomas G. Purcell

School of Chemical Sciences, National Institute for Higher Education, Glasnevin, Dublin 9, Ireland

Ekkehardt Hahn and Herbert Schumann*

Institut fur Anorganische und Analytische Chemie, Technische Universität, Strasse des 17 Juni 135, D-1000 Berlin 12, FGR

J. J. Zuckerman*

Department of Chemistry, University of Oklahoma, Norman, Oklahoma 73019

Received October 4, 1984

The crystal and molecular structure of tricyclohexylstannyl 3-indolylacetate $[(C_6H_{11})_3SnO_2CCH_2(C_8H_6N)]$ is reported. Crystal data (150 K): space group $P2_12_12_1$; a = 16.487 (6) Å, b = 10.674 (4) Å, c = 14.804 (5) Å; V = 2605.2 Å^3, Z = 4; ρ_{calcd} = 1.382 g cm^{-3}. For 2091 observed reflections $[I \geq 2\sigma(I)]$ R = 0.0351 and R_w = 0.0248. The molecule incorporates a monodentate carboxylate ligand and a tetrahedral geometry at tin. Intermolecular NH···OC hydrogen bonds propagate through the lattice to produce a "S"-shaped polymer from which the tricyclohexyltin(IV) moiety is pendant.

Introduction

Organotin compounds are now the active components in a number of biocidal formulations, finding application in such diverse areas as fungicides, miticides, molluscicides, marine antifouling paints, surface disinfectants, and wood preservatives.[2] It is currently of interest to us[3] to prepare and structurally characterize novel compounds in which the active organotin moiety is bound to a substrate which is itself active, in the hope that a combination of complimentary properties might enhance the effectiveness of the whole unit. In particular, our work is centered on derivatives of the R_3Sn residue, which are now established as having the most favorable activity patterns, and specifically in this report the tricyclohexyltin compounds

(1) Author to whom correspondence should be addressed, at current address: School of Chemistry, University of Bath, Claverton Down, Bath BA2 7AY, U.K.

(2) Davies, A. G.; Smith, P. J. In "Comprehensive Organometallic Chemistry"; Wilkinson, G., Stone, F. G. A., Abel, E. W., Eds.; Pergammon Press: Oxford, 1982; Vol. 2, p 519.

(3) (a) For previous parts to this series, see: Burke, N.; Molloy, K. C.; Purcell, T. G.; Smyth, M. R. *Inorg. Chim. Acta* **1985**, *106*, 129. (b) Molloy, K. C.; Zuckerman, J. J. *Acc. Chem. Res.* **1983**, *16*, 386.

0276-7333/86/2305-0085$01.50/0

Organotin biocides. 4. Crystal and molecular structure of tricyclohexylstannyl 3-indolylacetate, incorporating the first monodentate carboxylate group bonded to a triorganotin(IV)

Kieran C. Molloy, Thomas G. Purcell, Ekkehardt. Hahn, Herbert. Schumann, and J. J. Zuckerman

Organometallics, **1986**, 5 (1), 85-89• DOI: 10.1021/om00132a014 • Publication Date (Web): 01 May 2002

have an elongated C^1–C^3 bond.

Somewhat surprisingly, the lithium salt of the "antiaromatic cyclopropenyl anion" *is not indicated to be particularly unstable* thermodynamically. The lowest energy 3-cyclopropenyllithium form, singlet **5** with C_s symmetry, has about the same methyl stabilization energy as that of, e.g., 2-propyllithium. This possibility was considered by Wasielewski and Breslow[3c] and is due to compensating factors: some residual $4\pi e$ destabilization is balanced by the stabilization due to small-ring rehybridization and the σ inductive effects of the double bond. Nevertheless, manifestations of the expected Hückel 4π electron antiaromaticity are quite clearly evident in the strong distortions from planarity exhibited both in the singlet **5** and in the triplets **6** and **7**. These triplets are estimated to be about 10 kcal/mol less stable than the singlet **5**.

Breslow has measured the rates of base-catalyzed deuterium exchange in comparably substituted cyclopropyl and cyclopropenyl systems. The latter exchanged about 6000[3a] to 10 000[3b] times slower than the corresponding cyclopropane, thus indicating some destabilization of cyclopropenyl anion systems. With the assumption that kinetic acidities parallel thermodynamic acidities[2] an energetic difference for the proton abstraction of 5.2–6.1 kcal/mol can be evaluated. This is in reasonable good agreement with our calculated value of 3.7 kcal/mol (eq 3).[34]

Acknowledgment. This work was supported at Erlangen by the Fonds der Chemischen Industrie and the Deutsche Forschungsgemeinschaft. We also appreciate the assistance of the Regionales Rechenzentrum Erlangen and the Rechenzentrum der Universität Graz.

Registry No. **1**/**2**/**3**, 20829-57-6; **4**, 98705-30-7; **5**/**6**/**7**, 72507-54-1; **8**, 98705-27-2; **9**, 98705-28-3; **10**, 4529-04-8; **11**, 51760-92-0; **12**, 51174-22-2; **13**, 19527-08-3; CH_3Li, 917-54-4; CH_3^-, 15194-58-8; ethynyllithium, 1111-64-4; allyllithium, 3052-45-7; 2-propenyllithium, 6386-71-6; vinyllithium, 917-57-7; *cis*-1-propenyllithium, 6524-17-0; *trans*-1-propenyllithium, 6386-72-7; methyllithium, 917-54-4; cyclopropyllithium, 3002-94-6; 1-propyllithium, 2417-93-8; ethyllithium, 811-49-4; 2-propyllithium, 1888-75-1; (1,2,3-triphenylcyclopropenyl)lithium, 98705-29-4; ethynyl anion, 29075-95-4; 1-propynl anion, 31139-07-8; allenyl anion, 64066-06-4; allyl anion, 1724-46-5; 2-propenyl anion, 65887-19-6; vinyl anion, 25012-81-1; 1-propenyl anion, 65887-20-9; cyclopropyl anion, 1724-45-4; 1-propyl anion, 59513-13-2; ethyl anion, 25013-41-6; 2-propyl anion, 25012-80-0.

Supplementary Material Available: Tables of fractional coordinates and interatomic distances (5 pages). Ordering information is given on any current masthead page.

(34) In a later study using indirect methods, Breslow was able to estimate the pK_a of unsubstituted cyclopropene to be 61.3.[3c] However, no comparable value for the pK_a of cyclopropane is available.

Organotin Biocides. 4. Crystal and Molecular Structure of Tricyclohexylstannyl 3-Indolylacetate, Incorporating the First Monodentate Carboxylate Group Bonded to a Triorganotin(IV)

Kieran C. Molloy*[1] and Thomas G. Purcell

School of Chemical Sciences, National Institute for Higher Education, Glasnevin, Dublin 9, Ireland

Ekkehardt Hahn and Herbert Schumann*

Institut fur Anorganische und Analytische Chemie, Technische Universität, Strasse des 17 Juni 135, D-1000 Berlin 12, FGR

J. J. Zuckerman*

Department of Chemistry, University of Oklahoma, Norman, Oklahoma 73019

Received October 4, 1984

The crystal and molecular structure of tricyclohexylstannyl 3-indolylacetate $[(C_6H_{11})_3SnO_2CCH_2(C_8H_6N)]$ is reported. Crystal data (150 K): space group $P2_12_12_1$; a = 16.487 (6) Å, b = 10.674 (4) Å, c = 14.804 (5) Å; V = 2605.2 Å^3, Z = 4; ρ_{calcd} = 1.382 g cm^{-3}. For 2091 observed reflections $[I \geq 2\sigma(I)]$ R = 0.0351 and R_w = 0.0248. The molecule incorporates a monodentate carboxylate ligand and a tetrahedral geometry at tin. Intermolecular NH···OC hydrogen bonds propagate through the lattice to produce a "S"-shaped polymer from which the tricyclohexyltin(IV) moiety is pendant.

Introduction

Organotin compounds are now the active components in a number of biocidal formulations, finding application in such diverse areas as fungicides, miticides, molluscicides, marine antifouling paints, surface disinfectants, and wood preservatives.[2] It is currently of interest to us[3] to prepare and structurally characterize novel compounds in which the active organotin moiety is bound to a substrate which is itself active, in the hope that a combination of complimentary properties might enhance the effectiveness of the whole unit. In particular, our work is centered on derivatives of the R_3Sn residue, which are now established as having the most favorable activity patterns, and specifically in this report the tricyclohexyltin compounds

(1) Author to whom correspondence should be addressed, at current address: School of Chemistry, University of Bath, Claverton Down, Bath BA2 7AY, U.K.

(2) Davies, A. G.; Smith, P. J. In "Comprehensive Organometallic Chemistry"; Wilkinson, G., Stone, F. G. A., Abel, E. W., Eds.; Pergammon Press: Oxford, 1982; Vol. 2, p 519.

(3) (a) For previous parts to this series, see: Burke, N.; Molloy, K. C.; Purcell, T. G.; Smyth, M. R. *Inorg. Chim. Acta* **1985**, *106*, 129. (b) Molloy, K. C.; Zuckerman, J. J. *Acc. Chem. Res.* **1983**, *16*, 386.

0276-7333/86/2305-0085$01.50/0

(Cy_3SnX) which are potent acaricides while possessing tolerable mammalian toxicity.[4] Two of this class of compounds are currently marketed commercially, tricyclohexyltin hydroxide (Plictran, Dow Chemicals) and 1-(tricyclohexylstannyl)-1,2,4-triazole (Peropal, Bayer A.G.) while a third, (*O,O'*-dialkyl dithiophosphato)tricyclohexyltin, is under patent.[5]

Indole-3-acetic acid (HIAA; 1) is a naturally occurring plant growth hormone which promotes cell enlargement in shoots and lateral root initiation. Its *modus operandi*

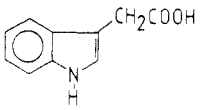

1

is unproven but is thought to stimulate polysaccharide synthesis or in some way alter the properties of existing cell wall components so that the cell wall is "loosened" and enlargement made easier.[6]

In this paper we report the synthesis and X-ray crystallographic characterization of tricyclohexylstannyl 3-indolylacetate, in which both acaricidal and growth hormonal properties are latent.

Experimental Section

General Data. 3-Indolylacetic acid was purchased from Aldrich and used without further purification. Infrared spectra were recorded on a Perkin-Elmer 1330 instrument; ^1H NMR were obtained at 60 MHz on a Perkin-Elmer R12B spectrometer. Details of our Mössbauer spectrometer and method of data collection and manipulation are described elsewhere.[7] Microanalyses were carried out by the Microanalytical Service of University College, Dublin.

Preparation of Tricyclohexylstannyl 3-Indolylacetate. A solution containing tricyclohexyltin(IV) hydroxide (3.00 g, 7.8 mmol) and 3-indolylacetic acid (1.39 g, 7.9 mmol) in toluene (100 mL) was refluxed for 45 min, and the water formed was removed azeotropically by using a Dean and Stark apparatus. The solution was allowed to cool to ca. 55 °C, filtered, concentrated to ca. half its volume, and subsequently allowed to crystallize overnight at 0 °C. The resulting crude, crystalline product was recrystallized from hot toluene to yield colorless crystals (1.25 g, 30%) of the title compound: mp 150–152 °C; IR (KBr disk) 3295 br, 1615 cm^{-1}; IR ($CHCl_3$) 3480, 1635 cm^{-1}; ^1H NMR ($CDCl_3$) δ 1.55 (m, 33 H, $(C_6H_{11})_3Sn$), 3.70 (s, 2 H, O_2CCH_2), 7.0–8.2 (m, 6 H, C_6H_4CCHNH); ^{119}Sn NMR ($CH_3C_6H_5$) δ +5.1; Mössbauer spectrum, IS = 1.55 mm s^{-1}, QS = 3.01 mm s^{-1}, fwhh = 1.01 mm s^{-1}. Anal. Calcd for $C_{28}H_{41}NO_2Sn$: C, 62.00; H, 7.63; N, 2.58. Found: C, 62.18; H, 7.77; N, 2.52.

Crystallographic Analysis. Crystals suitable for X-ray diffraction experiments were obtained through recrystallization from hot toluene. A crystal with the dimensions 0.32 × 0.40 × 0.20 mm was glued on top of a glass fiber and placed in the nitrogen stream of the diffractometer.

Preliminary crystal analysis and final data collection were performed at 150 (3) K on a Syntex $P2_1$ automatic four-circle counter diffractometer fitted with a low-temperature device. The crystal system was determined by axial photography techniques to be orthorhombic. Final cell dimensions were obtained by least-squares refinement of the angular settings of 15 accurately centered reflections. The intensities of all reflections with $2\theta < 50°$ were measured by using 1° ω scans. Two reflections were used as standard, and their intensities were monitored after each 50 observations. No significant changes in the intensities of the monitor reflections were noted.

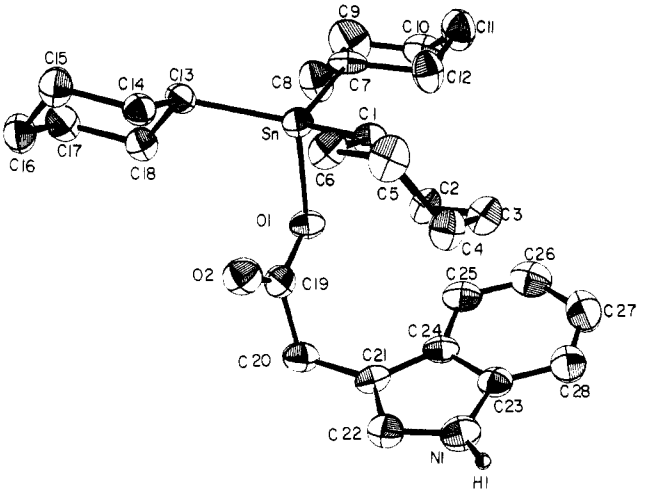

Figure 1. ORTEP drawing of one molecule of $(C_6H_{11})_3SnOC(O)CH_2(C_8H_6N)$, showing the employed numbering scheme. The thermal ellipsoids enclose 50% of the electron probability distribution for all non-hydrogen atoms. H1 is drawn on an arbitrary scale; all other hydrogen atoms have been omitted for clarity.

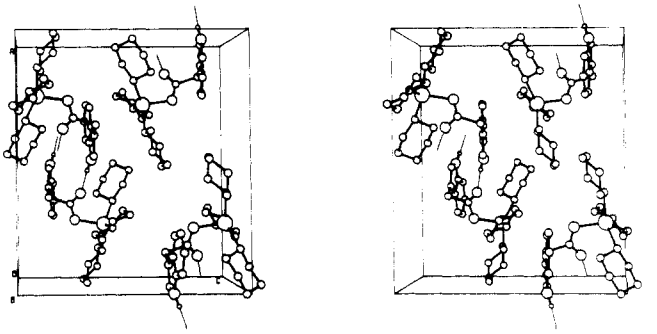

Figure 2. Stereoview of the packing, viewed down the b axis.

The raw data were converted to F_o values after correction for Lorentz and polarization effects. The esd's, σ_F, were based upon counting statistics. Due to the regular shape of the data crystal and the low absorption coefficient, no absorption correction was made (μ = 9.10 cm^{-1}; the minimum and maximum transmittances are 0.69 and 0.83, respectively). Additional crystal and data collection details are summarized in Table I.

Structure Solution and Refinement. From the systematically absent reflections the space group was determined to be $P2_12_12_1$ (no. 19). The position of the tin atom was calculated from a three-dimensional Patterson map. A difference Fourier map based on the heavy-atom phases revealed the positions of all other non-hydrogen atoms. These atoms were refined in stages by using first isotropic and latter anisotropic thermal parameters. All hydrogen positions were calculated (d(C–H) = 1.08 Å) but only the positional parameters of H1 (bonded to N) were refined in the least-squares procedure. The isotropic temperature factor for all hydrogens was held constant at U = 0.05 $Å^2$.

The maximum parameter shifts in the final cycle of refinement were 0.001 of their estimated standard deviations. A difference Fourier map calculated from the final structure factors showed no features greater than 0.44 e/$Å^3$. The strongest peaks in this map were located in the vicinity of the tin atom. The final R value is 0.0351 for the 2091 reflections ($I > 2\sigma(I)$) included in the least-squares sums (R_w = 0.0248). The correct enantiomer for the crystal selected was established by comparison of the R values for each of the two possibilities.

All calculations were performed by using the program SHELX.[8] Atomic scattering factors for C, N, and O were obtained from ref 9 and those for Sn from ref 10. The $\Delta f'$ and $\Delta f''$ components

(4) Evans, C. J. *Tin Its Uses* **1970**, *110*, 6.
(5) Baker, D. R. U.S. Patent, 3919418, 1975; *Chem. Abst.* **1976**, *84*, 85644.
(6) Corbett, J. R. "The Biochemical Mode of Action of Pesticides"; Academic Press: New York, 1974.
(7) Molloy, K. C.; Purcell, T. G.; Quill, K.; Nowell, I. W. *J. Organomet. Chem.* **1984**, *267*, 237.
(8) Sheldrick, G. M. "SHELX 76 System of Programs", 1976.
(9) Cromer, D. T.; Mann, J. B. *Acta Crystallogr., Sect. A: Cryst. Phys., Diffr., Theor. Gen. Crystallogr.* **1968**, *A24*, 321.
(10) Cromer, D. T.; Mann, J. B. *Acta Crystallogr., Sect. A: Cryst. Phys., Diffr., Theor. Gen. Crystallogr.* **1968** *A24*, 390.

Table I. Crystal and Data Collection Parameters for $(C_6H_{11})_3SnOC(O)CH_2(C_8H_6N)$[a]

formula	$C_{28}H_{41}NO_2Sn$
fw, dalt	542.30
a, Å	16.487 (6)
b, Å	10.674 (4)
c, Å	14.804 (5)
V, Å^3	2605.2
Z	4
space group[b]	$P2_12_12_1$
ρ_{calcd}, g/cm^3	1.382
μ, cm^{-1}	9.10
$F(000)$	1128
radiation, λ, Å	Mo Kᾱ, 0.71069
temp, K	150 (3)
scan technique	ω–2θ
2θ limit, deg	50
data collected	$0\rightarrow h$, $0\rightarrow k$, $0\rightarrow l$
no. of data collected	2329
no. of unique data	2306
no. of observed data	2091 ($I \geq 2\sigma(I)$)
$R = \sum\|\|F_o\| - \|F_c\|\|/\sum\|F_o\|$	0.0351
$R_w = [\sum w\|\|F_o\| - \|F_c\|\|^2/\sum w\|F_o\|^2]^{1/2}$	0.0248
$w = 2.5339/(\sigma_F)^2$	
no. of parameters	292

[a] Estimated standard deviations of the last significant digit are given in parentheses. [b] No. 19 in: "International Tables for X-ray Crystallography"; Kynoch Press: Birmingham, U.K., 1976.

Table II. Final Positional Parameters for $(C_6H_{11})_3SnOC(O)CH_2(C_8H_6N)$ ($\times 10^4$)[a]

atom	x	y	z
Sn	−2379.8 (2)	−1742.1 (4)	−4092.6 (3)
C(1)	−3328 (4)	−530 (6)	−4593 (4)
C(2)	−3632 (4)	362 (7)	−3859 (4)
C(3)	−4244 (4)	1288 (6)	−4227 (5)
C(4)	−4950 (4)	628 (6)	−4688 (4)
C(5)	−4659 (4)	−246 (7)	−5422 (4)
C(6)	−4049 (4)	−1197 (6)	−5061 (4)
C(7)	−1209 (3)	−866 (6)	−4038 (4)
C(8)	−565 (4)	−1459 (7)	−3336 (5)
C(9)	173 (4)	−832 (8)	−3312 (6)
C(10)	115 (4)	546 (7)	−3169 (4)
C(11)	−413 (4)	1164 (7)	−3880 (5)
C(12)	−1258 (4)	552 (7)	−3897 (5)
C(13)	−2264 (4)	−3714 (5)	−4410 (4)
C(14)	−3014 (4)	−4290 (6)	−4865 (4)
C(15)	−2870 (4)	−5645 (6)	−5105 (4)
C(16)	−2634 (4)	−6400 (5)	−4277 (4)
C(17)	−1890 (4)	−5846 (6)	−3806 (4)
C(18)	−2040 (4)	−4486 (6)	−3570 (4)
O(1)	−2565 (2)	−1648 (4)	−2700 (2)
O(2)	−3691 (3)	−2720 (4)	−2958 (3)
C(19)	−3255 (4)	−2131 (6)	−2453 (5)
C(20)	−3506 (4)	−1822 (7)	−1477 (4)
C(21)	−3922 (5)	−583 (7)	−1489 (4)
C(22)	−4746 (5)	−394 (7)	−1504 (4)
N	−4905 (4)	856 (6)	−1584 (4)
H(1)[b]	−539 (4)	118 (6)	−165 (4)
C(23)	−4815 (5)	1507 (7)	−1638 (4)
C(24)	−3561 (5)	624 (7)	−1574 (4)
C(25)	−2751 (5)	1054 (8)	−1634 (4)
C(26)	−2622 (6)	2299 (9)	−1752 (4)
C(27)	−3259 (6)	3155 (8)	−1811 (4)
C(28)	−4060 (5)	2774 (7)	−1756 (4)

[a] Estimated standard deviations of the last significant digit are given in parentheses. [b] H1 is bonded to N and is the only hydrogen atom with refined positional parameters. Positional parameters for H1 are multiplied by 10^3.

of anomalous dispersion for Sn are from ref 11. Final atomic positional parameters are listed in Table II. The atomic numbering scheme followed in these listings is identified in Figure 1. Figure 2 shows a stereoview of the packing. A stereoview of a part of the infinite helix formed by the title compound is shown in Figure 3. Interatomic distances and angles are listed in Tables III and IV, respectively. Tables of thermal parameters, hydrogen positions, least-squares planes, and tables of observed and calculated structure factor amplitudes are available (see supplementary material).

(11) Cromer, D. T.; Liberman, D. *J. Chem. Phys.* **1970**, *53*, 1891.

Table III. Bond Distances (Å) for $(C_6H_{11})_3SnOC(O)CH_2(C_8H_6N)$[a]

Intramolecular Bond Distances			
Sn–C(1)	2.161 (6)	C(1)–C(2)	1.529 (8)
Sn–C(7)	2.147 (5)	C(2)–C(3)	1.514 (8)
Sn–C(13)	2.165 (6)	C(3)–C(4)	1.522 (7)
Sn–O(1)	2.086 (3)	C(4)–C(5)	1.510 (8)
O(1)–C(19)	1.302 (7)	C(5)–C(6)	1.525 (8)
O(2)–C(19)	1.213 (7)	C(6)–C(1)	1.550 (8)
C(19)–C(20)	1.538 (8)	C(7)–C(8)	1.521 (7)
C(20)–C(21)	1.489 (9)	C(8)–C(9)	1.523 (8)
C(21)–C(22)	1.374 (8)	C(9)–C(10)	1.489 (9)
C(22)–N	1.365 (8)	C(10)–C(11)	1.517 (8)
C(23)–N	1.377 (8)	C(11)–C(12)	1.539 (8)
H(1)–N	0.88 (6)	C(12)–C(7)	1.530 (8)
C(23)–C(24)	1.398 (8)	C(13)–C(14)	1.537 (7)
C(24)–C(21)	1.425 (9)	C(14)–C(15)	1.508 (8)
C(24)–C(25)	1.415 (9)	C(15–C(16)	1.519 (8)
C(25)–C(26)	1.357 (8)	C(16)–C(17)	1.530 (8)
C(26)–C(27)	1.395 (9)	C(17)–C(18)	1.514 (8)
C(27)–C(28)	1.383 (9)	C(18)–C(13)	1.536 (7)
C(28)–C(23)	1.380 (9)		
Intermolecular Bond Distances			
H(1)–O(2)′[b]	2.00 (6)		

[a] Estimated standard deviations of the last significant digit are given in parentheses. [b] Primed atoms represent transformed coordinates of the type $-1 - x$, $^1/_2 + y$, $-^1/_2 - z$.

Table IV. Bond Angles (deg) for $(C_6H_{11})_3SnOC(O)CH_2(C_8H_6N)$[a]

Intramolecular Angles			
C(1)–Sn–C(7)	113.7 (2)	C(24)–C(25)–C(26)	118.3 (9)
C(1)–Sn–C(13)	124.9 (2)	C(25)–C(26)–C(27)	122.1 (9)
C(1)–Sn–O(1)	101.7 (2)	C(26)–C(27)–C(28)	121.5 (8)
C(7)–Sn–O(13)	110.6 (2)	C(27)–C(28)–C(23)	116.0 (8)
C(7)–Sn–O(1)	94.2 (2)	C(28)–C(23)–C(24)	124.0 (8)
C(13)–Sn–O(1)	105.9 (2)	C(1–)C(2)–C(3)	111.6 (5)
Sn–O(1)–C(19)	112.8 (4)	C(2)–C(3)–C(4)	111.7 (5)
O(1)–C(19)–O(2)	123.3 (6)	C(3)–C(4)–C(5)	111.4 (5)
O(1)–C(19)–C(20)	114.5 (6)	C(4)–C(5)–C(6)	111.6 (5)
O(2)–C(19)–C(20)	122.1 (7)	C(5)–C(6)–C(1)	110.8 (5)
C(19)–C(20)–C(21)	107.6 (5)	C(6)–C(1)–C(2)	110.7 (5)
C(20)–C(21)–C(22)	125.9 (7)	C(7)–C(8)–C(9)	111.8 (5)
C(21)–C(22)–N	109.6 (7)	C(8)–C(9)–C(10)	112.3 (6)
C(22)–N–C(23)	109.4 (6)	C(9)–C(10)–C(11)	111.6 (6)
C(22)–N–H(1)	125 (4)	C(10)–C(11)–C(12)	110.2 (6)
C(23)–N–H(1)	125 (4)	C(11)–C(12)–C(7)	112.0 (5)
N–C(23)–C(24)	106.9 (6)	C(12)–C(7)–C(8)	110.5 (6)
C(23)–C(24)–C(21)	108.0 (7)	C(13)–C(14)–C(15)	111.1 (5)
C(24)–C(21)–C(22)	106.2 (7)	C(14)–C(15)–C(16)	111.1 (5)
C(24)–C(21)–C(20)	127.7 (7)	C(15)–C(16)–C(17)	111.6 (5)
C(23)–C(24)–C(25)	118.2 (7)	C(16)–C(17)–C(18)	110.2 (5)
		C(17)–C(18)–C(13)	111.5 (5)
		C(18)–C(13)–C(14)	109.5 (5)
Intermolecular Angles			
N–H1–O_2′[b]	163 (4)	H1–O2′–C19′	158 (4)

[a] Estimated standard deviations of the last significant digit are given in parentheses. [b] Primed atoms represent transformed coordinates of the type $-1 - x$, $^1/_2 + y$, $-^1/_2 - z$.

Results and Discussion

The local geometry at tin in the asymmetric unit is shown in Figure 1, and the bond lengths pertinent to the discussion of this structure are given in Table V, along with

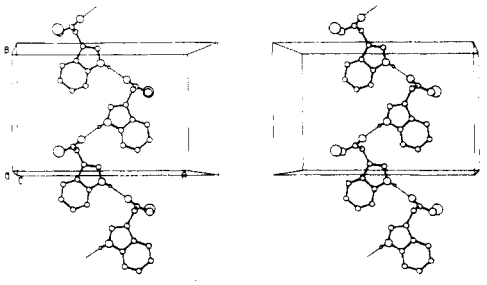

Figure 3. Stereoview of the helix, viewed down the z axis (plotting range; x, 0.0–1.0; y, −1.0 to 1.0; z, 0.0–0.5). The cyclohexyl groups bound to tin have been omitted for clarity.

Table V. Structural Data (Å) for Selected Organotin Carboxylates[a]

compd	Sn–O(1)	Sn–O(2)	O(2)–O(19)–O(1)	CO···N
(C_8H_6N)-CH_2CO_2H[b]			1.223, 1.298	2.665[c]
$(C_6H_{11})_3SnO_2$-$CCH_2(C_8H_6N)$[d]	2.086 (3)	2.929[e]	1.213 (7), 1.302 (7)	2.851[f]
$(C_6H_{11})_3SnO_2CCH_3$	2.12 (3)	3.84[h]	1.25 (9), 1.39 (8)	
$(C_6H_{11})_3SnO_2)$-CCF_3	2.08 (4)	3.70[h]	1.20 (5), 1.28 (4)	
$(C_6H_5)_3SnO_2C$-$C_6H_4(N_2R$-$o)$[j]	2.070 (5)	2.463 (7)[e]	1.224 (8), 1.2.96 (8)	2.94 (1)[c,k]
$(CH_3)_3SnO_2C$-CH_2NH_2[l]	2.21 (1)	3.23 (2)[e]	1.23 (3), 1.34 (3)	2.74 (3)

[a] A fuller listing of organotin carboxylate data is given in ref 7. [b] Reference 12. [c] CO···O. [d] This work. [e] Intramolecular. [f] N–H(1) = 0.88 (6) Å; H(1)–O(2′) = 2.00 (6) Å; ∠N – H(1)–O(2′) = 163 (4)°. If N–H(1) is extended along its vector to 1.03 Å, the remaining values above become 1.85 Å and 162°, respectively. [g] Reference 13. [h] Intermolecular. [i] Reference 14. [j] Reference 15; R = 2-hydroxy-5-methylphenyl. [k] The structure also includes N···OH and CO···N interactions at 2.58 (1) Å, forming a three-center hydrogen bond. [l] Reference 17.

selected data for other organotin carboxylates for comparison. The environment of the metal is best described in terms of a tetrahedral arrangement of ligating atoms in which the carboxylate group bonds in a monodentate fashion. The intramolecular spacial disposition of the carbonyl oxygen O(2), 2.929 Å, from tin is within the sum of the respective van der Waal's radii (3.70 Å) and moreover is almost certainly in part responsible for the opening of the ∠C(1)–Sn–C(13) to 124.9 (2)°. However, we believe that this distortion arises from steric rather than electronic factors and that the number of bonds to tin does not expand beyond four. The following three arguments support this assertion. First, despite the opening of the ∠C(1)–Sn–C(13), there is no *systematic* change in bond angles which would indicate conversion to a trigonal bipyramidal (tbp) geometry with O(2) and C(7) in the axial sites and O(1), C(1), and C(13) forming the equatorial girdle. For example, the angles C(7)–Sn–C(1) and C(7)–Sn–C(13) would both be expected to close from 109°28′ toward 90° but in fact open slightly to 113.7 (2) and 110.6 (2)°, respectively. In fact, all the angles about tin can be rationalized simply in terms of an isovalent rehybridization at the metal which concentrates p orbital character in the bond to the more electronegative O(1) and s character in the bonds to carbon, resulting in a closing of those angles involving O(1) (94.2, 101.7, 105.9°) and concomitant opening of the angles between carbon atoms (110.6, 113.7, 124.9°). In addition, the Sn–C(7) bond ostensibly trans to the approach of O(2) [∠C(7)–Sn–O(2) = 142.9°] is the shortest [2.147 (5) Å] of the three Sn–C interactions rather than the longest as would be expected from an axial tbp site. Secondly, the sum of the angles at tin involving O(1), C(1), and C(13) totals 332.5°, compared with values of 328.5° and 360° for regular tetrahedral and tbp geometries, respectively. Finally, the C(19)—O(1) [1.302 (7) Å] and C(19)=O(2) [1.213 (7) Å] bonds retain the integrity of their single- and double-bond character consistent with the strength of the Sn—O(1) bond [2.086 (3) Å] which is at the short end of the range for such interactions (2.07–2.21 Å[7]). In fact, the C(19)=O(2) bond is even shorter than in the parent 3-indolylacetic acid (1.223 Å),[12] where a stronger array of hydrogen bonds operates (vide infra).

Comparison can be drawn with two other tricyclohexyltin carboxylates, $Cy_3SnO_2CCH_3$[13] and $Cy_3SnO_2CCF_3$.[14] Both of these compounds are associated in the solid state by a bridging, bidentate carboxylate moiety,[15] to form polymers of flattened "S" (class 3[16]) construction. Although the intermolecular interactions are weak (Table V), they clearly distort the bond angles at tin systematically toward tbp geometry, in which the axial sites are occupied by the two oxygen atoms of the bridging ligand. A closer analogy to the molecular structure of the title compound is that of $Ph_3SnO_2CC_6H_4(NR_2$-$o)$ (R = 2-hydroxy-5-methylphenyl),[15] which forms discrete, five-coordinate, *cis*-R_3SnO_2 monomeric units, in which the bidentate carboxylate group spans axial and equatorial sites of the tbp geometry. The Sn–O(2) intramolecular interaction in this compound is significantly stronger [2.463 (7) Å] than in the 3-indolylacetic acid derivative, presumably a consequence of an enhanced Lewis acidity at tin resulting from bonds to three electron-withdrawing phenyl groups rather than three electron-donating cyclohexyl units in our system.

The only other organotin carboxylate structure incorporating a monodentate RCO_2 moiety is $(CH_3)_3SnO_2CCH_2NH_2$,[17] but a tbp geometry at tin still arises by virtue of a bridging N:→Sn bond. We believe that the structure of the title compound thus represents the first crystallographically authenticated example of a genuine tetrahedral organotin carboxylate.

The lattice structure of $(C_6H_{11})_3SnIAA$ comprises of chains of molecules linked intermolecularly by hydrogen bonds which join NH···O=C subunits of the 3-indolylacetate ligand (Figure 2). The resulting polymer propagates through the crystal in a helical fashion along the 2_1 axis parallel to b (Figure 3), and whose construction is aided by the intra- and intermolecular dihedral angles between C_8H_6N and CCO_2 planes of 102° and 66°, respectively (Table VIII, supplementary material). The N–H(1) and H(1)–O(2′) distances are found experimentally to be 0.88 (6) and 2.00 (6) Å and are not colinear, the ∠N–H(1)–O(2′) being 163 (4)°. However, if the N–H(1) bond length is "normalized"[18] by moving H(1) along the N–H(1) vector to a standard N–H bond length (1.03 Å), the H(1)–O(2′) length becomes 1.85 Å and the ∠N–H(1)–O(2′) = 162°. The hydrogen bond is thus quite strong as measured in comparison to the average intermolecular H···O distance of 1.895 Å (for 1112 organic compounds

(12) Karle, I. L.; Britts, K.; Gum, P. *Acta Crystallogr.* **1964**, *17*, 496.
(13) Alcock, N. W.; Timms, R. E. *J. Chem. Soc. A.* **1968**, 1876.
(14) Calogero, S.; Ganis, P.; Peruzzo, V.; Tagliavini, G. *J. Organomet. Chem.* **1980**, *191*, 381.
(15) Harrison, P. G.; Lambert, K.; King, T. J.; Magee, B. *J. Chem. Soc., Dalton Trans.* **1983**, 363.
(16) Molloy, K. C.; Quill, K. *J. Chem. Soc., Dalton Trans.* **1985**, 1417.
(17) Ho, B. Y. K.; Molloy, K. C.; Zuckerman, J. J.; Reidinger, F.; Zubieta, J. A. *J. Organomet. Chem.* **1980**, *187*, 213.
(18) Jeffrey, G. A.; Lewis, L. *Carbohydr. Res.* **1978**, *60*, 179.

surveyed), while the angle of approach of the two halves of the bond is typical (mean ∠N–H···O = 163.5°) of such systems.[19] The effect of organostannylation of 3-indolylacetic acid on the latter's lattice structure is thus to convert a dimeric OH···OC (O–O = 2.665 Å[11]) moiety into a NH···OC polymer from which the $(C_6H_{11})_3Sn$ moiety is pendant.

It is worth concluding by emphasizing the effect of hydrogen bonding on the structure of organotin compounds and in particular in the present context organotin carboxylates. The structure which dominates this compound class is that of a carboxylate-bridged polymer, propagating in a "S" fashion through the lattice. Several variations within this theme exist, such as weak ($Cy_3SnO_2CH_3$[13]) or strong ($Me_3SnO_2CH_3$[20]) bridging bonds and coordination numbers at tin of either five[20] or six ($Ph_3SnO_2CCH_3$,[7] $Me_2ClSnO_2CCH_3$[21]). Of the structures which deviate from this theme, hydrogen bonding involving the carbonyl oxygen is commonly observed. For example, in addition to $Me_3SnO_2CCH_2NH_2$[17] which retains a polymeric structure through $H_2N{:}\rightarrow Sn$ bridges, a number of five-coordinated triphenyltin complexes embodying a chelating carboxylate group have now been characterized, namely, $Ph_3SnO_2CC_6H_4(N_2R\text{-}o)$,[15] and more recently $Ph_3SnO_2CC_6H_4X$ (X = *o*-OH,[22] *o*-NH_2,[23] *p*-NH_2[23]),[24] all of which incorporate this feature. While we are not suggesting that hydrogen bonding is a prerequisite for a non-carboxylate-bridged structure, indeed three structures now contradict such a requirement and form five-coordinate, carboxylate-chelated triphenyltin species, [$Ph_3SnO_2CC_6H_4X$; X = *o*-OMe,[22] *o*-NMe_2,[23] *p*-SMe[22]],[24] it clearly plays a major role in influencing the final crystal and molecular structure.

Acknowledgment. T.G.P. thanks the Department of Education (Ireland) for support in the form of a studentship. The work of H.S. is supported by the Deutsche Forschungsgemeinschaft and the Fonds der Chemischen Industrie. The work of J.J.Z. is supported by the Office of Naval Research. We would like to thank Dr. S. Blunden (International Tin Research Institute, Greenford) for recording the ^{119}Sn NMR spectrum.

Registry No. 1, 87-51-4; $(C_6H_{11})_3SnOC(O)CH_2(C_8H_6N)$, 98737-09-8; tricyclohexyltin(IV) hydroxide, 13121-70-5.

Supplementary Material Available: Tables of thermal parameters (Table VI), hydrogen atom positions (Table VII), and least-squares planes (Table VIII) and a listing of observed and calculated structure factor amplitudes (15 pages). Ordering information is given on any current masthead page.

(19) (a) Taylor, R.; Kennard, O.; Werner, V. *J. Am. Chem. Soc.* **1983**, *105*, 5761. (b) Taylor, R.; Kennard, O.; Werner, V. *J. Am. Chem. Soc.*, **1984**, *106*, 244.

(20) Chih, H.; Penfold, B. R. *J. Cryst. Mol. Struct.* **1973**, *3*, 285.

(21) Allen, D. W.; Nowell, I. W.; Brooks, J. S.; Clarkson, R. W. *J. Organomet. Chem.* **1981**, *219*, 29.

(22) Vollano, J. F.; Day, R. O.; Rau, D. N.; Chandrasekhar, V.; Holmes, R. R. *Inorg. Chem.* **1984**, *23*, 3153.

(23) Swisher, R. G.; Vollano, J. F.; Chandrasekhar, V.; Day, R. O.; Holmes, R. R. *Inorg. Chem.* **1984**, *23*, 3147.

(24) The authors describe all the stated compounds as having five-coordinate tin atoms in the solid state and, by consistency of the infrared spectra as Nujol mulls or CCl_4 solutions, in solution also. Our interpretation of these data is that distortions from tetrahedral geometries are minor, although the relevant bond angles at tin do not follow a simple rehydridization within a tetrahedral geometry either. While the data appear more ambiguous in the assignment of coordination number at the metal than in the title compound, ^{119}Sn NMR data for representative samples, e.g., $Ph_3SnO_2CC_6H_4OMe$, δ −119.9[25] are consistent with a coordination number at tin of four in solution and, by implication from the infrared data, the solid state as well.

(25) Molloy, K. C.; Quill, K.; Blunden, S. J.; Hill, R. *Polyhedron*, in press.

Synthesis and Characterization of Bis(diphenylphosphido)bis(pentamethylcyclopentadienyl)-thorium(IV), $[(\eta^5\text{-}C_5(CH_3)_5]_2Th(PPh_2)_2$

Debra A. Wrobleski, Robert R. Ryan,* Harvey J. Wasserman, Kenneth V. Salazar, Robert T. Paine, and David C. Moody

Los Alamos National Laboratory, University of California, Los Alamos, New Mexico 87545

Received April 23, 1985

The first diorganophosphido actinide complexes $Cp^*_2Th(PR_2)_2$ ($Cp^* = \eta^5\text{-}C_5(CH_3)_5$, R = Ph, Cy, Et) have been prepared by reaction of $Cp^*_2ThCl_2$ with $LiPR_2$. These complexes have been characterized spectroscopically, and $Cp^*_2Th(PPh_2)_2$ has been structurally characterized by a complete single-crystal X-ray diffraction study. This compound crystallizes in the space group $P2_1/c$ with a = 35.071 (8) Å, b = 15.203 (6) Å, c = 21.840 (11) Å, β = 92.97 (2)°, at T = -95 °C, and V = 11629.3 Å^3 and Z = 12 (Mo Kα_1 radiation, λ = 0.709 30 Å). The structure refined to R_F = 0.08 and R_{wF} = 0.07. There are three crystallographically independent molecules in the asymmetric unit. All three molecules exhibit pseudotetrahedral geometry about the thorium atom with the pentamethylcyclopentadienyl ligands and two diphenylphosphido groups occupying the four coordination sites. While the angles about the phosphorus atoms are far from the tetrahedral, there is no evidence for significant Th–P multiple bonding. The average Th–P distance is 2.87 (2) Å.

Introduction

The recent literature reflects a burst of activity in the area of heterobimetallic complexes.[1] Incentives to study this area of chemistry include, for example, the desire to understand the difference in selectivity observed for mixed bimetallic heterogeneous catalysts compared to their homometallic analogues.[2] A second commonly stated goal is to activate small oxygen-containing molecules, e.g., CO, CO_2, SO_2, etc., toward unusual reactivity patterns. The use of phosphido ligands to form bridges between dissimilar metal centers, e.g., early and late transition metals, has been especially fruitful, and many such complexes have now been reported.[3]

Two distinct routes to the preparation of heterobimetallic complexes with bridging phosphido ligands have proven successful. Perhaps the most commonly used route involves the deprotonation of a coordinated secondary phosphine[3] followed by metathesis with a metal halide to form the heterobimetallic complex. A second route requires metathesis of a coordinated halide using $M(PPh_2)$[4] (M = Na, Li) to form the neutral phosphido transition-metal compound. The resulting complex contains a terminal phosphide that displays many of the properties of a tertiary phosphine including simple displacement reactions with transition-metal complexes containing labile ligands to form the desired bimetallic complex. Especially intriguing to us was the recent appearance of several reports of group 4[19] metal phosphido complexes with an attendant rich chemistry toward low-valent transition-metal fragments.[5] In some cases, metal–metal bonding has been strongly implicated for the resulting heterobimetallic complexes. Our interest in the preparation of bimetallic actinide–transition metal complexes has led us to investigate the phosphido coordination chemistry of the actinide metals, a previously unexplored area. We report here the synthesis and molecular structure of the first diorganophosphido actinide complex $Cp^*_2Th(PPh_2)_2$ [$Cp^* = \eta^5\text{-}C_5(CH_3)_5$]. The preparation of the first heterobimetallic phosphido complex via coordination of the Ni(CO)$_2$ fragment to the molecular species reported here has recently been communicated.[6] The Th–Ni distance was found to be significantly shorter than that expected for a nonbonded contact, and a bonding interaction is strongly implied.

Experimental Section

Materials and Methods. All compounds described herein are highly air- and moisture-sensitive in the solid state. Syntheses were routinely conducted under a nitrogen atmosphere using Schlenk techniques. Toluene was freshly distilled from sodium benzophenone ketyl under nitrogen and transferred to reaction vessels via high vacuum techniques. $ThCp^*_2Cl_2$[7] and $LiPR_2$ (R = Et, Cy)[8] were prepared according to published procedures. $LiPPh_2$ was purchased from Alfa Products and used without further purification.

Infrared spectra were recorded on a Perkin-Elmer 683 spectrophotometer as Nujol mulls using KBr plates. UV-visible spectra were obtained on a Perkin-Elmer 330 spectrophotometer in toluene. Proton and $^{31}P\{^1H\}$ NMR spectra were obtained on a Bruker WM 300 wide-bore spectrometer at 300 and 121.5 MHz, respectively. Benzene-d_6 was used as a lock solvent for most spectra. Phosphorus chemical shifts (δ) are reported relative to external 85% H_3PO_4. Positive chemical shifts are assigned to resonances (at higher frequency) downfield from the reference. Elemental analyses were obtained from Schwarzkopf Microanalytical Laboratory.

(1) (a) Bruno, J. W.; Huffman, J. C.; Green, M. A.; Caulton, K. G. *J. Am. Chem. Soc.* **1984**, *106*, 8310. (b) Casey, C. P.; Jordan, R. F.; Rheingold, A. L. *Ibid.* **1983**, *105*, 665. (c) Wrobleski, D. A.; Day, C. S.; Goodman, B. A.; Rauchfuss, T. B. *Ibid.* **1984**, *106*, 5464. (d) Rosenburg, S.; Whittle, R. R.; Geoffroy, G. L. *Ibid.* **1984**, *106*, 5934. (e) Breen, M. J.; Shulman, P. M.; Geoffroy, G. L.; Rheingold, A. L.; Fultz, W. C. *Organometallics* **1984**, *3*, 782. (f) Regragui, R.; Dixneuf, P. H.; Taylor, N. J.; Carty, A. J. *Ibid.* **1984**, *3*, 814. (g) Chandler, D. J.; Jones, R. A.; Stuart, A. L.; Wright, T. C. *Ibid.* **1984**, *3*, 1830.

(2) Sinfelt, J. H. "Bimetallic Catalysts"; Wiley: New York, 1983.

(3) Roberts, D. A.; Geoffroy, G. L. In "Comprehensive Organometallic Chemistry"; Wilkinson, G., Stone, F. G. A., Abel, E. W., Eds.; Pergamon Press: Oxford, 1982; Vol. 6, Chapter 40.

(4) Wade, S. R.; Wallbridge, M. G. H.; Willey, G. R. *J. Chem. Soc., Dalton Trans.* **1983**, 2555 and references therein.

(5) Baker, R. T.; Tulip, T. H.; Wreford, S. S. *Inorg. Chem.* **1985**, *24*, 1379.

(6) Ritchey, J. M.; Zozulin, A. J.; Wrobleski, D. A.; Ryan, R. R.; Wasserman, H. J.; Moody, D. C.; Paine, R. T. *J. Am. Chem. Soc.* **1985**, *107*, 501.

(7) Fagan, P. J.; Manriquez, J. M.; Maatta, E. A.; Serjam, A. M.; Marks, T. J. *J. Am. Chem. Soc.* **1981**, *103*, 6650.

(8) $LiPR_2$ (R = Et, Cy) were prepared in hexane from PR_2H and *n*-BuLi: Issleib, K.; Tzachach, A. *Chem. Ber.* **1959**, *92*, 1118.

0276-7333/86/2305-0090$01.50/0

Table I. Crystal Data and Data Collection[a]

formula	$C_{44}H_{50}P_2Th$	crystal system	monoclinic
a, Å	35.071 (8)	space group	$P2_1/c$
b, Å	15.203 (6)	Z	12
c, Å	21.840 (11)	V, Å^3	11629.1
β, deg	92.97 (2)	ρ (calcd), g/cm^3	1.50
radiation, Å	Mo Kα_1, 0.709 30	mol wt	872.9
monochromator	graphite	abs coeff, cm^{-1}	40.0
scan method	θ–2θ	scan speed	variable
2θ limit, deg	0–50	no. of reflctns	14518
temp, °C	−95	reflctns obsd $I \geq 2\sigma(I)$	7764

[a] $R_F = \sum||F_o| - |F_c||/\sum|F_o| = 0.07$. $R_{wF} = \sum w||F_o| - |F_c||/\sum|F_o| = 0.08$. $\sigma(F^2) = \sigma_c(F^2) + 0.02\,F^4$. $\sigma_c(F^2)$ = error due to counting statistics. Two standards every 2 h.

Preparation of Bis(pentamethylcyclopentadienyl)bis(diphenylphosphido)thorium(IV), $Cp^*_2Th(PPh_2)_2$ (1). Treatment of $Cp^*_2ThCl_2$ (1.7 g, 3 mmol) in 35 mL of toluene with an excess of $LiPPh_2$ (1.73 g, 9 mmol) in 65 mL of toluene results in a rapid color change to dark purple. Following filtration to remove excess $LiPPh_2$ and LiCl and concentration to 5 mL, addition of hexane (100 mL) and cooling the solution to −30 °C affords a deep purple crystalline product (67% yield) which is extremely moisture- and air-sensitive. ^{1}H NMR: δ 7.9–7.0 (m, 20 H, Ph), 1.925 (s, 30 H, $C_5(CH_3)_5$). $^{31}P\{^1H\}$ NMR (121.5 MHz, C_6H_6): δ +144 (s). IR (Nujol mull): 1575 (m) cm^{-1}. UV–vis (toluene): 570 (4440), 498 nm (sh, 2740 cm^{-1} M^{-1}). Anal. Calcd for $C_{44}H_{50}P_2Th$: C, 60.53; H, 5.77; P, 7.10; Th, 26.60. Found: C, 60.34; H, 5.85; P, 7.12; Th, 26.88.

Preparation of Bis(pentamethylcyclopentadienyl)bis(diethylphosphido)thorium(IV), $Cp^*_2Th(PEt_2)_2$ (2). Treatment of $Cp^*_2ThCl_2$ (3.44 g, 6 mmol) with $LiPEt_2$ (1.15 g, 12 mmol) in toluene (125 mL) resulted in a rapid color change to deep cherry red. Following filtration, the solvent was removed in vacuo. Hexane (20 mL) was added and cooled to −78 °C to give dark red crystals which were isolated (ca. 60% yield) by filtration and drying the product in vacuo. ^{1}H NMR: δ 2.419 (dq, 8 H, CH_2CH_3, J_{H-H} = 7.5 Hz, J_{P-H} = 2.35 Hz), 2.133 (s, 30 H, $C_5(CH_3)_5$), 1.384 (dt, 12 H, CH_2CH_3, J_{P-H} = 12.8 Hz). $^{31}P\{^1H\}$ NMR: δ 136 (s).

Preparation of Bis(pentamethylcyclopentadienyl)bis(dicyclohexylphosphido)thorium(IV), $Cp^*_2Th(PCy_2)_2$ (3). Treatment of $Cp^*_2ThCl_2$ (287 mg, 0.5 mmol) with $LiPCy_2$ (204 mg, 1.0 mmol) results in a slow color change to burgundy red over the period of 2 days. Following filtration, the solvent was removed in vacuo to give a red oil. Due to its high solubility in organic solvents, 3 was characterized in solution. ^{1}H NMR: δ 2.246 (s, br, Cy), 2.233 (s, Cy), 2.139 (s, $C_5(CH_3)_5$), 2.110 (s, Cy), 2.058 (s, Cy), 2.013 (s, Cy). $^{31}P\{^1H\}$ NMR: δ 205 (s).

Crystal Structure Analysis. Cell and intensity data are given in Table I. X-ray quality crystals of $Cp^*_2Th(PPh_2)_2$ were obtained by slow cooling of a hot hexane solution of 1. A crystal (0.2 × 0.2 × 0.3 mm) was selected and mounted in a glass capillary in an inert-atmosphere drybox. The capillary was sealed with epoxy, removed from the box, and flame sealed. Data were collected at −95 °C on an Enraf-Nonius CAD4 diffractometer equipped with an Isotherm boil-off flowing N_2 low-temperature system, using variable speed θ–2θ scans. Two standard reflections were monitored after every 2 h and were used to correct for long-range intensity variations. A correction for the effects of absorption was derived from the intensity variation of a reflection near χ = 90° which was measured as a function of ψ. A spherical correction was superimposed on the resulting curve.

The structure was solved by using standard Patterson and Fourier methods. There are three crystallographically independent $Cp^*_2Th(PPh_2)_2$ molecules in the asymmetric unit. The refinements were carried out using neutral atom scattering factors and appropriate anomalous scattering terms.[9] Because of the size of the problem, i.e., three molecules in the asymmetric unit, rigid-body constraints were applied to all phenyl and Cp* groups. The phenyl rings were assumed to have D_{6h} symmetry with d(C–C) = 1.39 Å. For the Cp* groups $d(C\text{–}C)_{int}$ = 1.42 Å and $d(C\text{–}C)_{ext}$ = 1.53 Å were used and held fixed in the refinements, and D_{5h} symmetry was assumed in the starting model. However, in the refinements the symmetry constraint was relaxed to C_{5v} and a distance parameter between the two planes, one defined by the five internal carbon atoms and the other by the five external carbons, refined to 0.25 Å. All carbon atom thermal parameters were allowed to refine independently. Anisotropic thermal parameters were included for the three independent thorium atoms and the six independent phosphorus atoms. A secondary extinction parameter[10] was refined, but no hydrogen atoms were included. The final model with 141 atoms, 324 parameters refined to R_F = 0.08 and R_{wF} = 0.07.

Results and Discussion

The metathesis reaction of $Cp^*_2ThCl_2$ with $LiPR_2$ (R = Ph, Et, Cy) in toluene yields the highly air-sensitive thorium complexes $Cp^*_2Th(PR_2)_2$. The rate of substitution of the phosphido group with the chloride is dependent on the steric bulk of the R groups. When R = Ph and Et, the substitution proceeds within minutes while the cyclohexyl reaction requires days. Because of its high solubility in nonpolar organic solvents, the cyclohexyl derivative was not isolated as a solid but was characterized spectroscopically. A unique feature of this class of thorium complexes is their intense purple/red color. This is highly unusual for Th(IV) organometallic complexes since most are colorless[11] although there is some evidence for highly colored Th(III) compounds such as $ThCp_3$.[12] We attribute the transitions (λ_{max} = 570, 498 nm for 1) in the visible region to phosphido ligand-to-metal charge-transfer bands.

An ORTEP projection of molecule 1 is shown in Figure 1. Fractional coordinates and selected distances and angles are given in Table II and Table III, respectively. Clearly, all three molecules are conformationally equivalent. While some related distances and angles differ significantly, from a statistical point of view, it would be difficult to claim that any chemical difference can be inferred from these. Structures which contain three identical molecules in the asymmetric unit are extremely uncommon. The reason for this unusual behavior is unclear in the present case. Inspection of intramolecular distances and of the packing diagram show no unusual interactions which would indicate incipient trimerization. All three molecules exhibit the pseudotetrahedral geometry which is ubiquitous among structures of the type $Cp^*_2MX_2$, where M is an early transition metal and X is a halide or pseudohalide. Although many structures containing bridging phosphido ligands have now been reported, reports of structures with a terminal PR_2 ligand are rare.[13,14] An early-transition-metal complex analogous to ours, viz., $Cp_2Hf(PEt_2)_2$, has been structurally characterized.[14] Its structure differs from the present one in one important respect: the conformation about the phosphorus atoms. The hafnium structure exhibits one phosphorus atom with pyramidal geometry while the other is planar, indicative of pπ–dπ ligand to metal bonding. In the present structure

(9) Cromer, D. T.; Waber, J. T. "International Tables for X-ray Crystallography"; Kynoch Press: Birmingham, England, 1974; Table 2.2A. Cromer, D. T. *Ibid.*, Table 2.3.1.

(10) (a) Zachariasen, W. H. *Acta Crystallogr.* **1967**, *23*, 558–564. (b) Larson, A. C. *Ibid.* **1967**, *23*, 664–665.

(11) See, for example: (a) Marks, T. J.; Wachter, W. A. *J. Am. Chem. Soc.* **1976**, *98*, 703. (b) Sonnenberger, D. C.; Mintz, E. A.; Marks, T. J. *J. Am. Chem. Soc.* **1984**, *106*, 3484.

(12) (a) Kanellakopulos, B.; Dornberger, E.; Baumgartner, F. *Inorg. Nucl. Chem. Lett.* **1974**, *10*, 155. (b) Bruno, J. W.; Kalina, D. G.; Mintz, E. A.; Marks, T. J. *J. Am. Chem. Soc.* **1982**, *104*, 1860.

(13) (a) Domaille, P. J.; Foxman, B. M.; McNeese, T. J.; Wreford, S. S. *J. Am. Chem. Soc.* **1980**, *102*, 4114. (b) Rocklage, S. M.; Schrock, R. R.; Churchill, M. R.; Wasserman, H. J. *Organometallics* **1982**, *1*, 1332. (c) Baker, R. T.; Krusic, P. J.; Tulip, T. H.; Calabrese, J. C.; Wreford, S. S. *J. Am. Chem. Soc.* **1983**, *105*, 6763.

(14) Baker, R. T.; Whitney, J. F.; Wreford, S. S. *Organometallics* **1983**, *2*, 1049.

Table II. Positional Parameters for $Cp^*_2Th(PPh_2)_2$

atom	x	y	z	atom	x	y	z
Th(1)	0.23884 (3)	0.22505 (7)	0.37695 (4)	Th(2)	0.57800 (3)	0.28022 (7)	0.60160 (4)
Th(3)	0.90987 (3)	0.18799 (6)	0.41272 (4)	P(1)	0.2909 (2)	0.3336 (5)	0.3142 (3)
P(2)	0.2086 (2)	0.3690 (5)	0.4457 (3)	P(3)	0.6234 (2)	0.1573 (5)	0.6738 (3)
P(4)	0.5504 (2)	0.1423 (5)	0.5204 (3)	P(5)	0.8913 (2)	0.3094 (5)	0.5051 (3)
P(6)	0.9548 (2)	0.3186 (5)	0.3561 (3)	C(1)	0.2016 (3)	0.1358 (7)	0.2814 (5)
C(2)	0.1959 (3)	0.2256 (7)	0.2654 (4)	C(3)	0.1702 (3)	0.2625 (6)	0.3065 (5)
C(4)	0.1602 (3)	0.1954 (7)	0.3480 (4)	C(5)	0.1795 (3)	0.1173 (6)	0.3325 (5)
C(6)	0.1720 (4)	0.0260 (7)	0.3584 (7)	C(7)	0.1285 (4)	0.2021 (9)	0.3933 (6)
C(8)	0.1513 (4)	0.3526 (7)	0.2999 (7)	C(9)	0.2090 (4)	0.2695 (9)	0.2072 (6)
C(10)	0.2218 (4)	0.0677 (9)	0.2434 (7)	C(11)	0.2590 (3)	0.1112 (7)	0.4705 (5)
C(12)	0.2815 (3)	0.1865 (6)	0.4855 (4)	C(13)	0.3104 (3)	0.1928 (6)	0.4424 (5)
C(14)	0.3056 (3)	0.1214 (7)	0.4008 (4)	C(15)	0.2739 (3)	0.0710 (7)	0.4181 (5)
C(16)	0.2625 (4)	−0.0192 (8)	0.3925 (7)	C(17)	0.3340 (4)	0.0943 (10)	0.3535 (6)
C(18)	0.3446 (4)	0.2549 (9)	0.4471 (7)	C(19)	0.2797 (4)	0.2406 (9)	0.5441 (6)
C(20)	0.2290 (4)	0.0712 (10)	0.5103 (7)	C(21)	0.6044 (3)	0.3997 (7)	0.5202 (5)
C(22)	0.6246 (3)	0.3220 (7)	0.5060 (5)	C(23)	0.6518 (3)	0.3052 (7)	0.5550 (5)
C(24)	0.6484 (3)	0.3726 (7)	0.5994 (4)	C(25)	0.6192 (3)	0.4309 (7)	0.5780 (5)
C(26)	0.6103 (4)	0.5201 (8)	0.6061 (7)	C(27)	0.6762 (7)	0.3886 (11)	0.6545 (5)
C(28)	0.6838 (4)	0.2371 (9)	0.5544 (7)	C(29)	0.6225 (4)	0.2750 (10)	0.4442 (5)
C(30)	0.5771 (4)	0.4499 (10)	0.4761 (6)	C(31)	0.5384 (3)	0.3684 (7)	0.6903 (5)
C(32)	0.5288 (3)	0.2787 (7)	0.6992 (4)	C(33)	0.5047 (3)	0.2516 (6)	0.6484 (5)
C(34)	0.4995 (3)	0.3246 (7)	0.6083 (4)	C(35)	0.5203 (3)	0.3966 (6)	0.6341 (5)
C(36)	0.5176 (4)	0.4916 (7)	0.6116 (7)	C(37)	0.4707 (4)	0.3292 (10)	0.5533 (5)
C(38)	0.4826 (4)	0.1652 (7)	0.6438 (7)	C(39)	0.5368 (4)	0.2263 (9)	0.7580 (5)
C(40)	0.5584 (4)	0.4280 (9)	0.7381 (6)	C(41)	0.8630 (3)	0.1285 (7)	0.3180 (4)
C(42)	0.8561 (3)	0.2205 (6)	0.3176 (4)	C(43)	0.8354 (3)	0.2414 (6)	0.3699 (4)
C(44)	0.8296 (3)	0.1621 (6)	0.4024 (4)	C(45)	0.8466 (3)	0.0925 (6)	0.3705 (4)
C(46)	0.8417 (4)	−0.0054 (6)	0.3836 (7)	C(47)	0.8033 (4)	0.1516 (9)	0.4557 (5)
C(48)	0.8165 (4)	0.3297 (6)	0.3821 (6)	C(49)	0.8631 (4)	0.2828 (8)	0.2645 (5)
C(50)	0.8787 (4)	0.0757 (9)	0.2654 (6)	C(51)	0.9361 (3)	0.0470 (7)	0.4811 (5)
C(52)	0.9603 (3)	0.1175 (7)	0.5008 (4)	C(53)	0.9848 (3)	0.1371 (6)	0.4528 (5)
C(54)	0.9756 (3)	0.0787 (7)	0.4035 (4)	C(55)	0.9456 (3)	0.0231 (7)	0.4209 (5)
C(56)	0.9313 (4)	−0.0585 (9)	0.3861 (6)	C(57)	0.9989 (4)	0.0668 (10)	0.3468 (5)
C(58)	1.0194 (4)	0.1980 (9)	0.4580 (6)	C(59)	0.9644 (4)	0.1538 (10)	0.5660 (5)
C(60)	0.9099 (4)	−0.0047 (10)	0.5216 (6)	C(61)	0.3823 (5)	0.2304 (13)	0.1870 (8)
C(62)	0.3915 (4)	0.2930 (14)	0.2317 (10)	C(63)	0.3637 (6)	0.3222 (11)	0.2702 (8)
C(64)	0.3269 (5)	0.2887 (12)	0.2639 (7)	C(65)	0.3177 (4)	0.2261 (12)	0.2192 (9)
C(66)	0.3454 (6)	0.1969 (11)	0.1807 (7)	C(67)	0.2395 (5)	0.5704 (9)	0.2054 (8)
C(68)	0.2668 (5)	0.5192 (12)	0.1784 (6)	C(69)	0.2822 (4)	0.4463 (11)	0.2093 (8)
C(70)	0.2702 (5)	0.4248 (9)	0.2671 (8)	C(71)	0.2429 (5)	0.4761 (11)	0.2941 (6)
C(72)	0.2275 (4)	0.5489 (11)	0.2633 (8)	C(73)	0.0957 (4)	0.3283 (12)	0.5408 (7)
C(74)	0.1274 (5)	0.2781 (10)	0.5593 (6)	C(75)	0.1621 (4)	0.2919 (10)	0.5328 (7)
C(76)	0.1651 (3)	0.3557 (11)	0.4877 (7)	C(77)	0.1334 (5)	0.4058 (9)	0.4692 (6)
C(78)	0.0987 (4)	0.3921 (10)	0.4957 (8)	C(79)	0.2944 (5)	0.5229 (11)	0.5712 (8)
C(80)	0.3033 (4)	0.4968 (12)	0.5126 (8)	C(81)	0.2768 (5)	0.4503 (11)	0.4759 (6)
C(82)	0.2413 (4)	0.4299 (11)	0.4977 (8)	C(83)	0.2324 (4)	0.4560 (12)	0.5563 (8)
C(84)	0.2589 (5)	0.5025 (12)	0.5930 (6)	C(85)	0.5540 (5)	−0.0583 (10)	0.7695 (8)
C(86)	0.5827 (5)	−0.0137 (12)	0.8030 (6)	C(87)	0.6036 (4)	0.0513 (11)	0.7751 (8)
C(88)	0.6585 (5)	0.1959 (12)	0.7339 (7)	C(89)	0.5671 (5)	0.0273 (12)	0.6802 (6)
C(90)	0.5462 (4)	−0.0378 (11)	0.7081 (8)	C(91)	0.7131 (5)	0.2436 (14)	0.8246 (8)
C(92)	0.6776 (6)	0.2842 (11)	0.8217 (8)	C(93)	0.6503 (4)	0.2604 (12)	0.7764 (9)
C(94)	0.5958 (5)	0.0719 (10)	0.7137 (8)	C(95)	0.6941 (6)	0.1552 (10)	0.7368 (8)
C(96)	0.7214 (4)	0.1791 (13)	0.7822 (10)	C(97)	0.4415 (4)	0.2059 (12)	0.4000 (7)
C(98)	0.4745 (5)	0.2547 (9)	0.3923 (7)	C(99)	0.5080 (4)	0.2337 (10)	0.4259 (7)
C(100)	0.5086 (4)	0.1640 (11)	0.4671 (7)	C(101)	0.4756 (5)	0.1152 (9)	0.4748 (7)
C(102)	0.4421 (4)	0.1362 (11)	0.4412 (8)	C(103)	0.6336 (5)	−0.0283 (10)	0.4160 (8)
C(104)	0.5991 (5)	−0.0029 (12)	0.3870 (6)	C(105)	0.5739 (4)	0.0495 (12)	0.4177 (8)
C(106)	0.5830 (4)	0.0765 (10)	0.4775 (8)	C(107)	0.6175 (5)	0.0511 (11)	0.5065 (6)
C(108)	0.6428 (4)	−0.0013 (11)	0.4758 (8)	C(109)	0.9785 (4)	0.4742 (10)	0.6210 (7)
C(110)	0.9425 (5)	0.4585 (11)	0.6426 (6)	C(111)	0.9163 (3)	0.4073 (11)	0.6085 (7)
C(112)	0.8486 (3)	0.3018 (10)	0.5501 (6)	C(113)	0.9621 (5)	0.3877 (10)	0.5312 (6)
C(114)	0.9883 (3)	0.4388 (11)	0.5653 (7)	C(115)	0.7824 (4)	0.2858 (12)	0.6139 (7)
C(116)	0.8103 (5)	0.2208 (9)	0.6190 (7)	C(117)	0.8434 (4)	0.2288 (9)	0.5871 (7)
C(118)	0.9261 (4)	0.3719 (10)	0.5528 (7)	C(119)	0.8207 (5)	0.3667 (8)	0.5449 (7)
C(120)	0.7876 (4)	0.3587 (10)	0.5768 (8)	C(121)	0.8901 (5)	0.5648 (9)	0.2821 (8)
C(122)	0.8832 (4)	0.5306 (11)	0.3395 (8)	C(123)	0.9032 (5)	0.4570 (11)	0.3612 (6)
C(124)	0.9878 (4)	0.2881 (10)	0.2958 (6)	C(125)	0.9370 (4)	0.4519 (11)	0.2681 (7)
C(126)	0.9170 (5)	0.5254 (11)	0.2464 (6)	C(127)	1.0382 (5)	0.2368 (12)	0.2083 (7)
C(128)	0.9992 (5)	0.2222 (11)	0.1981 (6)	C(129)	0.9741 (3)	0.2479 (11)	0.2419 (8)
C(130)	0.9301 (4)	0.4177 (9)	0.3255 (8)	C(131)	1.0268 (5)	0.3027 (11)	0.3059 (6)
C(132)	1.0520 (3)	0.2770 (13)	0.2621 (8)				

the angles about the phosphorus atoms have values which are far from tetrahedral; the largest variations are exhibited for Th–P–C angles. Included in Table IIID are the angles between the Th–P vectors and the normal to the C–P–C′ plane (144.7° for tetrahedral geometry). The most notable of these is that associated with P(5) (110.4°) which is also associated with the shortest Th–P distance (2.834 Å). However, since no significant correlation can be found

Table III. Interatomic Distances (Å) and Angles (deg) for $Cp^*_2Th(PPh_2)_2$[a,b]

A. Distances from the Thorium Atoms

Th(1)-P(1)	2.861 (7)	Th(2)-P(3)	2.873 (7)	Th(3)-P(5)	2.834 (7)
-P(2)	2.887 (8)	-P(4)	2.883 (7)	-P(6)	2.857 (7)
-C(1)	2.76 (1)	-C(21)	2.74 (1)	-C(41)	2.73 (1)
-C(2)	2.80 (1)	-C(22)	2.79 (1)	-C(42)	2.78 (1)
-C(3)	2.84 (1)	-C(23)	2.86 (1)	-C(43)	2.85 (1)
-C(4)	2.84 (1)	-C(24)	2.84 (1)	-C(44)	2.84 (1)
-C(5)	2.78 (1)	-C(25)	2.77 (1)	-C(45)	2.77 (1)
-C(11)	2.74 (1)	-C(31)	2.78 (1)	-C(51)	2.74 (1)
-C(12)	2.80 (1)	-C(32)	2.81 (1)	-C(52)	2.76 (1)
-C(13)	2.86 (1)	-C(33)	2.85 (1)	-C(53)	2.83 (1)
-C(14)	2.85 (1)	-C(34)	2.84 (1)	-C(54)	2.86 (1)
-C(15)	2.77 (1)	-C(35)	2.81 (1)	-C(55)	2.80 (1)
-Cp(1)	2.54	-Cp(3)	2.52	-Cp(5)	2.53
-Cp(2)	2.54	-Cp(4)	2.55	-Cp(6)	2.53

B. Phosphorus-Carbon Distances

P(1)-C(64)	1.85 (1)	P(3)-C(88)	1.85 (1)	P(5)-C(112)	1.84 (1)
-C(70)	1.85 (1)	-C(94)	1.86 (1)	-C(118)	1.83 (1)
P(2)-C(76)	1.83 (1)	P(4)-C(100)	1.85 (1)	P(6)-C(124)	1.86 (1)
-C(82)	1.83 (1)	-C(106)	1.82 (1)	-C(130)	1.85 (1)

C. Angles about the Thorium Atoms

P(1)-Th-P(2)	94.2 (2)	P(3)-Th-P(4)	91.4 (2)	P(5)-Th-P(6)	90.4 (2)
Cp(1)-Th-Cp(2)	134.9	Cp(3)-Th-Cp(4)	133.7	Cp(5)-Th-Cp(6)	132.9
Cp(1)-Th-P(1)	110.3	Cp(3)-Th-P(3)	100.5	Cp(5)-Th-P(5)	101.9
Cp(1)-Th-P(2)	100.1	Cp(3)-Th-P(4)	109.8	Cp(5)-Th-P(6)	111.5
Cp(2)-Th-P(1)	99.9	Cp(4)-Th-P(3)	111.5	Cp(6)-Th-P(5)	111.1
Cp(2)-Th-P(2)	110.5	Cp(4)-Th-P(4)	102.3	Cp(6)-Th-P(6)	101.2

D. Angles about the Phosphorus Atoms[c]

Th(1)-P(1)-C(64)	123.0 (7)	Th(2)-P(4)-C(100)	119.1 (6)
Th(1)-P(1)-C(70)	117.2 (6)	Th(2)-P(4)-C(106)	121.1 (6)
C(64)-P(1)-C(70)	101.9 (8) [127.1]	C(100)-P(4)-C(106)	105.9 (8) [123.6]
Th(1)-P(2)-C(76)	121.0 (6)	Th(3)-P(5)-C(112)	124.3 (6)
Th(1)-P(2)-C(82)	118.2 (7)	Th(3)-P(5)-C(118)	124.9 (6)
C(76)-P(2)-C(82)	104.9 (8) [125.9]	C(112)-P(5)-C(118)	105.5 (8) [110.4]
Th(2)-P(3)-C(88)	120.9 (7)	Th(3)-P(6)-C(124)	120.8 (6)
Th(2)-P(3)-C(94)	115.1 (6)	Th(3)-P(6)-C(130)	117.7 (6)
C(88)-P(3)-C(94)	103.4 (8) [130.7]	C(124)-P(6)-C(130)	104.2 (8) [127.3]

[a] Cp denotes the centroid for the Cp* ring calculated from the inner carbon atom positions. [b] Atoms listed in this table are numbered in molecules 2 and 3 in the same sequence as in molecule 1. Carbon atom numbers are incremented by 24 between molecules 1 and 2 and between molecules 2 and 3; $\Delta n = 2$ for phosphorus atoms; and Cp(1) corresponds to Cp(4) and Cp(6) while Cp(2) corresponds to Cp(3) and Cp(5). [c] Brackets [ ] denote angle between the Th-P bond and the C-P-C′ plane normal.

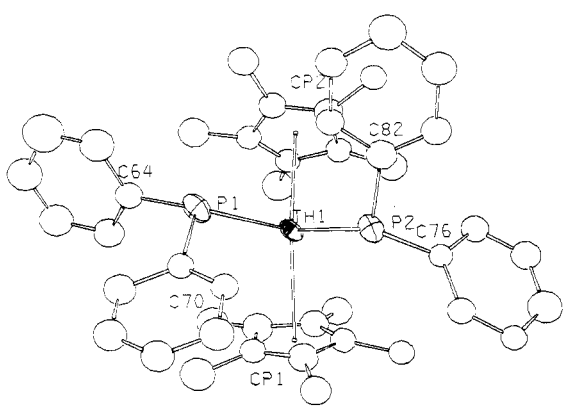

Figure 1. ORTEP view of molecule 1 of $[(\eta^5\text{-}C_5(CH_3)_5]_2Th(PPh_2)_2$.

among the remaining distances and the corresponding angles, no conclusions regarding possible multiple bonding effects can be drawn.

The $^{31}P\{^1H\}$ NMR spectrum for the thorium complexes consists of a singlet between δ +136 and δ +205 at 25 °C, similar to that observed for early transition complexes with terminal phosphido ligands.[14] The low-temperature spectrum (−120 °C, toluene-d_8/methylcyclohexane) of 1 shows no evidence of line broadening, indicating that the phosphido ligands are equivalent on the NMR time scale, in agreement with the solid-state structure. This contrasts with the $^{31}P\{^1H\}$ NMR spectrum of $Cp_2Hf(PCy_2)_2$ which reveals two resonances at low temperature supporting the structural evidence for single and double M–P bonds.[14] It is interesting that the zirconium and hafnium systems achieve an 18-electron count with one single and one double M–P bond while the thorium system exhibits no multiple Th–P bonding in spite of its formal 16-electron count. We note, however, that the electron count for other thorium complexes ranges from 16e in $Cp^*_2Th(CH_3)_2$[15] to 24e in Cp_4Th.[16]

The Th–P distance, averaged over all six linkages, is 2.87 (2) Å, a value which compares well with the Hf–P(pyramidal) distance (Hf–P = 2.682 Å) in $Cp_2Hf(PEt_2)_2$ when proper allowance is made for the difference in ionic radii.[17] In addition, this distance is only slightly shorter than the Th–P distance of 2.884 (2) Å in the Th–Ni complex[6] mentioned above. The structure of a *thorium–phosphine* complex, $Th(CH_2Ph)_4(Me_2PCH_2CH_2PMe_2)$, has recently appeared[18] in which the average thorium–phosphorus

(15) Manriquez, J. M.; Fagen, P. J.; Marks, T. J. *J. Am. Chem. Soc.* **1978**, *100*, 3939.
(16) Fischer, E. O.; Triebner, A. *Z. Naturforsch., B: Anorg. Chem., Org. Chem., Biochem., Biophys., Biol.* **1962**, *17B*, 276.
(17) Shannon, R. D. *Acta Crystallogr., Sect. A: Cryst. Phys., Diffr., Theor. Gen. Crystallogr.* **1976**, *A32*, 751.
(18) Edwards, P. G.; Anderson, R. A.; Zalkin, A. *Organometallics* **1984**, *3*, 293.

distance is considerably longer, at 3.155 (10) Å as would be expected for a Lewis acid–base interaction.

The chemistry of the $Cp^*_2Th(PR_2)_2$ complexes and other actinide analogues, in combination with a number of late-transition-metal fragments, is currently under investigation in our laboratory. Preliminary results, including the preparation of the above-mentioned nickel complex, indicate that a large number of bimetallic complexes can be successfully prepared.

Acknowledgment. This work was performed under the auspices of the U.S. Department of Energy and, in part, under the auspices of the Division of Chemical Energy Sciences, Office of Basic Energy Sciences, U.S. Department of Energy.

Registry No. 1, 93943-04-5; 2, 98720-31-1; 3, 98720-32-2; Cp^*ThCl_2, 67506-88-1; $LiPPh_2$, 4541-02-0; $LiPEt_2$, 19093-80-2; $LiPCy_2$, 19966-81-5.

Supplementary Material Available: Tables of anisotropic thermal parameters as well as tables of observed and calculated structure factors and isotropic thermal parameters (45 pages). Ordering information is given on any current masthead page.

(19) In this paper the periodic group notation is in accord with recent actions by IUPAC and ACS nomenclature committees. A and B notation is eliminated because of wide confusion. Groups IA and IIA become groups 1 and 2. The d-transition elements comprise groups 3 through 12, and the p-block elements comprise groups 13 through 18. (Note that the former Roman number designation is preserved in the last digit of the new numbering: e.g., III→3 and 13.)

η^2-Vinyl and η^2-Ketenyl Ligands as Analogues of Four-Electron Alkyne Ligands

Douglas C. Brower, Kurt R. Birdwhistell, and Joseph L. Templeton*

W. R. Kenan, Jr. Laboratory, Department of Chemistry, University of North Carolina, Chapel Hill, North Carolina 27514

Received April 29, 1985

The donor and acceptor properties of $[\eta^2\text{-HC=CH}_2]^-$ and $[\eta^2\text{-HC=CO}]^-$ ligands resemble those of η^2-RC≡CR ligands. In monomeric complexes requiring four-electron donation from an alkyne unit, the role of the $\pi_\perp$ electron pair of the alkyne can be fulfilled by related filled orbitals in $[HC=CH_2]^-$ and $[HC=CO]^-$ (the charge provides a closed shell for the atoms in the free ligand). The two anionic C_2-based fragments also have empty π-acceptor orbitals which behave analogously to the $\pi_\parallel^*$ and π^* functions of alkynes and alkenes, respectively. Extended Hückel molecular orbital calculations suggest that in coordination spheres containing π-acids the orientation of η^2-ketenyl ligands is determined by frontier orbital interactions, whereas the orientation of η^2-vinyl ligands is dictated largely by steric effects.

Introduction

Comparing the electronic structures of new or unsymmetrical ligands with simpler or more thoroughly studied cases often aids in rationalizing molecular structures and predicting chemical reactivity;[1] this is the essence of Hoffmann's isolobal analogy.[2] Metallacyclopropene complexes, 1 (also called η^2-vinyl derivatives or cyclic alkylidenes, see Scheme I), and metallacyclopropenone complexes, 2 (also called η^2-ketenyl derivatives), are two examples of metal-stabilized organic fragments which have been prepared by metal-mediated ligand reactions. Conversion of metal-bound alkynes to η^2-vinyl ligands has been accomplished by nucleophilic attack at an alkyne carbon with hydride reagents,[3] thiols or thiolates,[4] nitrogen[5] and phosphorus[6] reagents, and isonitriles.[7] η^2-Ketenyl ligands

Scheme I

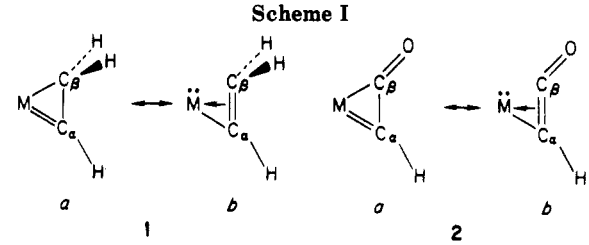

Table I. Extended Hückel Parameters

orbital	$H(i,i)$, eV	exponents ζ_1	exponents ζ_2
H	−13.6	1.3	
C_{2s}	−21.4	1.625	
C_{2p}	−11.4	1.625	
O_{2s}	−32.3	2.275	
O_{2p}	−14.8	2.275	
W_{5d}	−10.37	4.982 (0.6685)	2.068 (0.5424)
W_{6s}	−8.26	2.341	
W_{6p}	−5.17	2.309	

have been prepared by coupling reactions between carbyne and carbonyl ligands[8] and by rearrangement of η^1-ketenyl ligands after loss of another ligand.[9] We now show,

(1) (a) Pettit, R.; Sugahara, H.; Wristers, J.; Merk, W. *Discuss. Faraday Soc.* **1969**, *47*, 71. (b) Mango, F. D.; Schachtschneider, J. H. *J. Am. Chem. Soc.* **1971**, *93*, 1123. (c) Kostić, N. M.; Fenske, R. F. *Organometallics* **1982**, *1*, 974. (d) Albright, T. A. *Tetrahedron* **1982**, *38*, 1339.

(2) (a) Hoffmann, R. *Angew. Chem., Int. Ed. Engl.* **1982**, *21*, 711. (b) Stone, F. G. A. *Angew. Chem., Int. Ed. Engl.* **1984**, *23*, 89 and references therein.

(3) (a) Green, M.; Norman, N. C.; Orpen, A. G. *J. Am. Chem. Soc.* **1981**, *103*, 1267. (b) Allen, S. R.; Green, M.; Orpen, A. G.; Williams, I. D. *J. Chem. Soc., Chem. Commun.* **1982**, *826*. (c) Allen, S. R.; Beevor, R. G.; Green, M.; Norman, N. C.; Orpen, A. G.; Williams, I. D. *J. Chem. Soc., Dalton Trans.* **1985**, 435.

(4) (a) Davidson, J. L.; Shiralian, M.; Manojlović-Muir, L.; Muir, K. W. *J. Chem. Soc., Dalton Trans.* **1984**, 2167. (b) Carlton, L.; Davidson, J. L.; Miller, J. C.; Muir, K. W. *J. Chem. Soc., Chem. Commun.* **1984**, *11*. (c) Davidson, J. L. *J. Chem. Soc., Chem. Commun.* **1979**, 597.

(5) (a) Davidson, J. L.; Murray, I. E. P.; Preston, P. N.; Russo, M. V. *J. Chem. Soc., Dalton Trans.* **1983**, 1783. (b) Davidson, J. L.; Murray, I. E. P.; Preston, P. N.; Russo, M. V.; Manojlović-Muir, L.; Muir, K. W. *J. Chem. Soc., Chem. Commun.* **1981**, 1059.

(6) Davidson, J. L.; Wilson, W. F.; Manojlović-Muir, L.; Muir, K. W. *J. Organomet. Chem.* **1983**, *254*, C6.

(7) (a) Davidson, J. L.; Vasapollo, G.; Manojlović-Muir, L.; Muir, K. W. *J. Chem. Soc., Chem. Commun.* **1982**, 1025. (b) Morrow, J. R.; Tonker, T. L.; Templeton, J. L., manuscript in preparation.

(8) (a) Kreissl, F. R.; Sieber, W. J.; Alt, H. G. *Chem. Ber.* **1984**, *117*, 2527. (b) Fischer, E. O.; Filippou, A. C.; Alt, H. G.; Ackermann, K. *J. Organomet. Chem.* **1983**, *254*, C21. (c) Birdwhistell, K. R.; Tonker, T. L.; Templeton, J. L. *J. Am. Chem. Soc.* **1985**, *107*, 4474.

0276-7333/86/2305-0094$01.50/0

distance is considerably longer, at 3.155 (10) Å as would be expected for a Lewis acid–base interaction.

The chemistry of the $Cp^*_2Th(PR_2)_2$ complexes and other actinide analogues, in combination with a number of late-transition-metal fragments, is currently under investigation in our laboratory. Preliminary results, including the preparation of the above-mentioned nickel complex, indicate that a large number of bimetallic complexes can be successfully prepared.

Acknowledgment. This work was performed under the auspices of the U.S. Department of Energy and, in part, under the auspices of the Division of Chemical Energy Sciences, Office of Basic Energy Sciences, U.S. Department of Energy.

Registry No. 1, 93943-04-5; 2, 98720-31-1; 3, 98720-32-2; Cp^*ThCl_2, 67506-88-1; $LiPPh_2$, 4541-02-0; $LiPEt_2$, 19093-80-2; $LiPCy_2$, 19966-81-5.

Supplementary Material Available: Tables of anisotropic thermal parameters as well as tables of observed and calculated structure factors and isotropic thermal parameters (45 pages). Ordering information is given on any current masthead page.

(19) In this paper the periodic group notation is in accord with recent actions by IUPAC and ACS nomenclature committees. A and B notation is eliminated because of wide confusion. Groups IA and IIA become groups 1 and 2. The d-transition elements comprise groups 3 through 12, and the p-block elements comprise groups 13 through 18. (Note that the former Roman number designation is preserved in the last digit of the new numbering: e.g., III→3 and 13.)

η^2-Vinyl and η^2-Ketenyl Ligands as Analogues of Four-Electron Alkyne Ligands

Douglas C. Brower, Kurt R. Birdwhistell, and Joseph L. Templeton*

W. R. Kenan, Jr. Laboratory, Department of Chemistry, University of North Carolina, Chapel Hill, North Carolina 27514

Received April 29, 1985

The donor and acceptor properties of $[\eta^2\text{-HC=CH}_2]^-$ and $[\eta^2\text{-HC=CO}]^-$ ligands resemble those of η^2-RC≡CR ligands. In monomeric complexes requiring four-electron donation from an alkyne unit, the role of the $\pi_\perp$ electron pair of the alkyne can be fulfilled by related filled orbitals in $[HC=CH_2]^-$ and $[HC=CO]^-$ (the charge provides a closed shell for the atoms in the free ligand). The two anionic C_2-based fragments also have empty π-acceptor orbitals which behave analogously to the $\pi_\parallel^*$ and π^* functions of alkynes and alkenes, respectively. Extended Hückel molecular orbital calculations suggest that in coordination spheres containing π-acids the orientation of η^2-ketenyl ligands is determined by frontier orbital interactions, whereas the orientation of η^2-vinyl ligands is dictated largely by steric effects.

Introduction

Comparing the electronic structures of new or unsymmetrical ligands with simpler or more thoroughly studied cases often aids in rationalizing molecular structures and predicting chemical reactivity;[1] this is the essence of Hoffmann's isolobal analogy.[2] Metallacyclopropene complexes, 1 (also called η^2-vinyl derivatives or cyclic alkylidenes, see Scheme I), and metallacyclopropenone complexes, 2 (also called η^2-ketenyl derivatives), are two examples of metal-stabilized organic fragments which have been prepared by metal-mediated ligand reactions. Conversion of metal-bound alkynes to η^2-vinyl ligands has been accomplished by nucleophilic attack at an alkyne carbon with hydride reagents,[3] thiols or thiolates,[4] nitrogen[5] and phosphorus[6] reagents, and isonitriles.[7] η^2-Ketenyl ligands

Scheme I

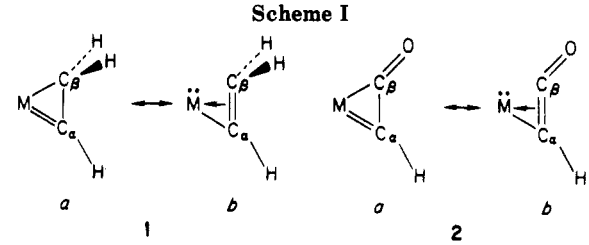

Table I. Extended Hückel Parameters

orbital	$H(i,i)$, eV	exponents ζ_1	exponents ζ_2
H	−13.6	1.3	
C_{2s}	−21.4	1.625	
C_{2p}	−11.4	1.625	
O_{2s}	−32.3	2.275	
O_{2p}	−14.8	2.275	
W_{5d}	−10.37	4.982 (0.6685)	2.068 (0.5424)
W_{6s}	−8.26	2.341	
W_{6p}	−5.17	2.309	

have been prepared by coupling reactions between carbyne and carbonyl ligands[8] and by rearrangement of η^1-ketenyl ligands after loss of another ligand.[9] We now show,

(1) (a) Pettit, R.; Sugahara, H.; Wristers, J.; Merk, W. *Discuss. Faraday Soc.* **1969**, *47*, 71. (b) Mango, F. D.; Schachtschneider, J. H. *J. Am. Chem. Soc.* **1971**, *93*, 1123. (c) Kostić, N. M.; Fenske, R. F. *Organometallics* **1982**, *1*, 974. (d) Albright, T. A. *Tetrahedron* **1982**, *38*, 1339.

(2) (a) Hoffmann, R. *Angew. Chem., Int. Ed. Engl.* **1982**, *21*, 711. (b) Stone, F. G. A. *Angew. Chem., Int. Ed. Engl.* **1984**, *23*, 89 and references therein.

(3) (a) Green, M.; Norman, N. C.; Orpen, A. G. *J. Am. Chem. Soc.* **1981**, *103*, 1267. (b) Allen, S. R.; Green, M.; Orpen, A. G.; Williams, I. D. *J. Chem. Soc., Chem. Commun.* **1982**, *826*. (c) Allen, S. R.; Beevor, R. G.; Green, M.; Norman, N. C.; Orpen, A. G.; Williams, I. D. *J. Chem. Soc., Dalton Trans.* **1985**, 435.

(4) (a) Davidson, J. L.; Shiralian, M.; Manojlović-Muir, L.; Muir, K. W. *J. Chem. Soc., Dalton Trans.* **1984**, 2167. (b) Carlton, L.; Davidson, J. L.; Miller, J. C.; Muir, K. W. *J. Chem. Soc., Chem. Commun.* **1984**, *11*. (c) Davidson, J. L. *J. Chem. Soc., Chem. Commun.* **1979**, 597.

(5) (a) Davidson, J. L.; Murray, I. E. P.; Preston, P. N.; Russo, M. V. *J. Chem. Soc., Dalton Trans.* **1983**, 1783. (b) Davidson, J. L.; Murray, I. E. P.; Preston, P. N.; Russo, M. V.; Manojlović-Muir, L.; Muir, K. W. *J. Chem. Soc., Chem. Commun.* **1981**, 1059.

(6) Davidson, J. L.; Wilson, W. F.; Manojlović-Muir, L.; Muir, K. W. *J. Organomet. Chem.* **1983**, *254*, C6.

(7) (a) Davidson, J. L.; Vasapollo, G.; Manojlović-Muir, L.; Muir, K. W. *J. Chem. Soc., Chem. Commun.* **1982**, 1025. (b) Morrow, J. R.; Tonker, T. L.; Templeton, J. L., manuscript in preparation.

(8) (a) Kreissl, F. R.; Sieber, W. J.; Alt, H. G. *Chem. Ber.* **1984**, *117*, 2527. (b) Fischer, E. O.; Filippou, A. C.; Alt, H. G.; Ackermann, K. *J. Organomet. Chem.* **1983**, *254*, C21. (c) Birdwhistell, K. R.; Tonker, T. L.; Templeton, J. L. *J. Am. Chem. Soc.* **1985**, *107*, 4474.

0276-7333/86/2305-0094$01.50/0

Table II. Bond Distances

ligand	linkage	dist, Å	ref
alkyne	C–C	1.324	13
	W–C	2.008	13
alkene	C–C	1.374	14
	W–C	2.247	13
vinyl	C–C	1.432	3a
	W–C_α	1.950	3a
	W–C_β	2.300	3a
ketenyl	C–C	1.300	8c
	C–O	1.262	8c
	W–C_α	1.997	8c
	W–C_β	2.175	8c
carbonyl	C–O	1.180	8c
	W–C	1.910	8c
all	C–H	1.090	14
	W–H	1.800	*a*

[a] Collman, J. P.; Hegedus, L. S. "Principles and Applications of Organotransition Metal Chemistry"; University Science Books: Mill Valley, CA, 1980; Chapter 3.

through extended Hückel calculations, that these C_2-based ligands $[HC{=}CH_2]^-$ and $[HC{=}CO]^-$, resemble acetylene in their interactions with a single metal center. This analogy has also been recently elaborated for η^2-vinyl ligands by Allen et al.[3c]

Computational Details

The extended Hückel method was employed in this study.[10,11] The parameters we used are summarized in Table I.[12] Bond lengths are tabulated in Table II. Metal–carbon distances for the alkene and alkyne calculations were derived from the X-ray diffraction structure of $W(\eta^2\text{-MA})(\eta^2\text{-PhC}_2\text{H})(\text{detc})_2$ (MA = maleic anhydride; Ph = phenyl; detc = diethyl dithiocarbamate).[13] The olefin geometry was matched to a neutron diffraction structure of Zeise's salt (i.e., the angle between the normals to the H–C–H planes was 32°).[14] The H–C–C angle in the alkyne ligand was set at 135°, similar to the angle between the ipso carbon of the phenyl ring and the distal alkyne carbon in the tungsten complex cited above. The bond distances and geometry of the ketenyl ligand were taken from the molecular structure of $W(CO)(dppe)(detc)(C,C\text{-}\eta^2\text{-OC}{=}CCH_2Ph)$ (dppe = 1,2-bis(diphenylphosphino)-ethane).[8c] The O–C–C angle was 154°, and the C–C–H angle was 135°. The geometry and distances were idealized for the alkylidene fragment.[3a] The C_β–C_α–H angle was 130°, both C_α–C_β–H angles were 120°, and the H–C_β–H angle was 114°. In model complexes, all cis hydride angles were fixed at 90°, and each C_2 fragment was bound so that the *z* axis bisected the C–C bond. When a carbon monoxide ligand was used, it replaced the hydride bound along the *x* axis.

Results and Discussion

Molecular Orbitals of C_2-Based Fragments. Examination of planar vinyl and linear ketenyl fragments readily reveals frontier orbitals which, apart from degeneracies, are reminiscent of an alkyne. This is not surprising, since

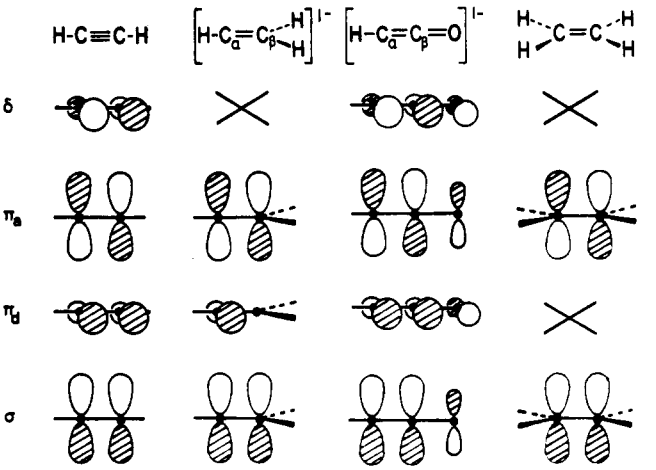

Figure 1. Analogies between the π systems of free acetylene, vinyl anion, ketenyl anion, and ethylene (cross indicates no analogy).

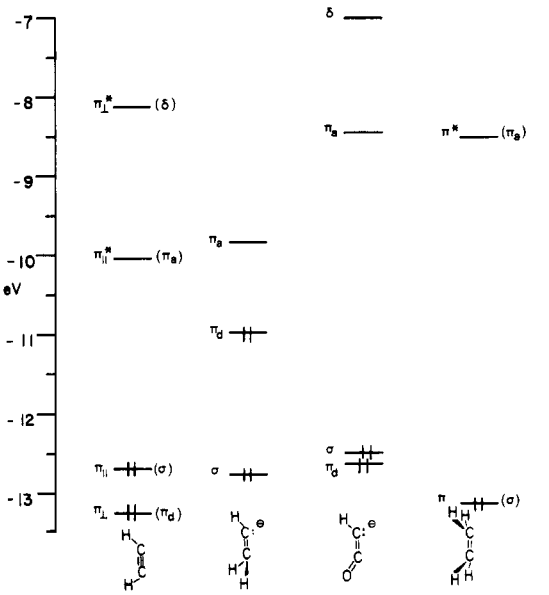

Figure 2. Orbital energy diagram for distorted ligands ready-for-bonding. (Left-hand labels for acetylene and ethylene follow conventional notations. Right-hand labels, in parentheses, use the same system as Figure 1 and Table III.)

Table III. Distribution of Density (%) in Frontier Orbitals of the Fragments

	π_d		σ		π_a		δ	
ligand	C_α	C_β	C_α	C_β	C_α	C_β	C_α	C_β
alkyne	50	50	50	50	44	44	50	50
ketenyl	59	24	67	20	26	58	38	56
vinyl	92	0	54	45	39	55		

the π systems of these C_2 moieties have much in common. The basic idea is illustrated in Figure 1 where the oribtal correlation among acetylene, vinyl anion, and ketenyl anion is set forth with ethylene included for reference purposes. The labels refer to the manner in which the orbitals would interact with a metal center when bound through both carbon atoms. The frontier orbitals change in both shape and energy as the substituents on these C_2 linkages are bent back in preparation for coordination to a transition metal, and though the extent of orbital restructuring depends on the degree of distortion, the essential analogy is retained (Figure 2 and Table III). Note that well-known C_3 organic rings result from combining these bent C_2 fragments with $[CH]^+$: cyclopropenium ion (i), cyclopropene (ii), and cyclopropenone (iii). The methyne cation—with two electrons, one σ orbital, and two π

(9) (a) Uedelhoven, W.; Eberl, K.; Kreissl, F. R. *Chem. Ber.* **1979**, *112*, 3376. (b) Kreissl, F. R.; Friedrich, P.; Huttner, G. *Angew. Chem., Int. Ed. Engl.* **1977**, *16*, 102.
(10) Hoffmann, R. *J. Chem. Phys.* **1963**, *39*, 1397.
(11) We wish to thank Professor Hoffmann for providing us with copies of programs ICONS and FMO.
(12) Kubáček, P.; Hoffmann, R. *J. Am. Chem. Soc.* **1981**, *103*, 4320.
(13) Morrow, J. R.; Tonker, T. L.; Templeton, J. L. *J. Am. Chem. Soc.*, in press.
(14) Love, R. A.; Koetzle, T. F.; Williams, G. J. B.; Andrews, L. C.; Bau, R. *Inorg. Chem.* **1975**, *14*, 2653.

Scheme II

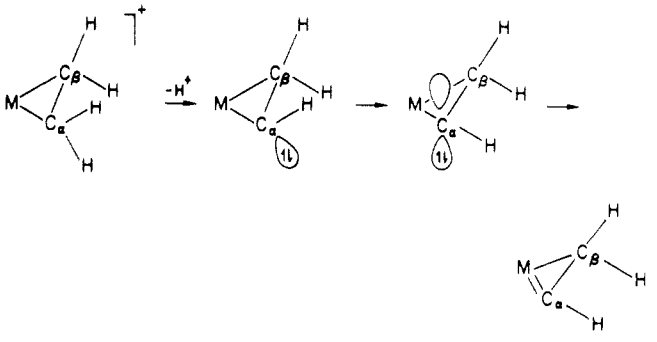

Scheme III

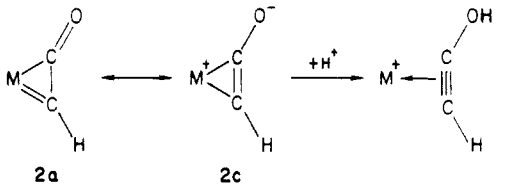

2a 2c

orbitals—is suggestive of ML_5 d^4 fragments, which can also present two electrons, one σ and two $d\pi$ orbitals to incoming ligands.

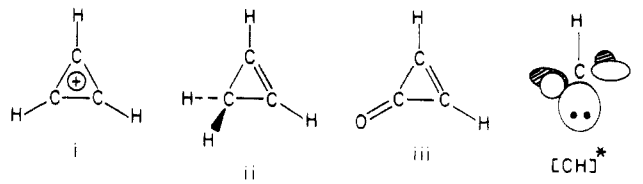

For $[H_2C{=}CH]^-$ and $[O{=}C{=}CH]^-$, the orbitals labeled σ and π_a in Figure 2 correlate with the $\pi_\parallel$ and $\pi_\parallel{}^*$ orbitals of HC≡CH and π and π^* of $H_2C{=}CH_2$. These orbitals account for σ donation to the metal and π acceptance from the metal as found in the Dewar–Chatt–Duncanson description of metal–olefin bonding.[15,16] Note that η^1-vinyl or η^1-ketenyl ligands use the orbital labeled π_d for forming their lone metal–carbon σ bond in the plane of the HC_2X fragment (see **3** and **4**).

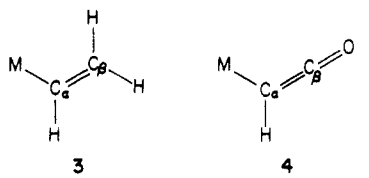

3 4

Numerous alkyne complexes are known in which the filled $\pi_\perp$ orbital provides substantial electron density to a vacant metal $d\pi$ orbital.[17] This occupied alkyne orbital has vinyl and ketenyl anion counterparts (Figure 2) which set these C_2 moieties apart from olefins since the olefins have no analogous filled orbital. The presence of an additional pair of electrons for metal complexation can be

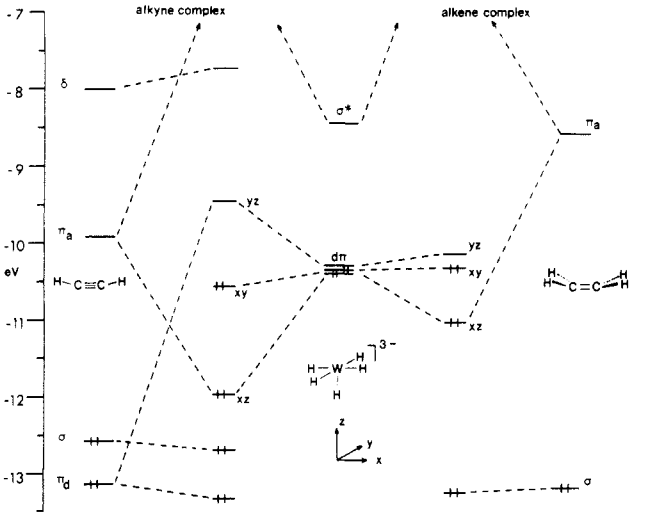

Figure 3. Energy level diagram for $[H_5W(\eta^2\text{-}H_2C{=}CH_2)]^{3-}$ and $[H_5W(\eta^2\text{-}HC{\equiv}CH)]^{3-}$.

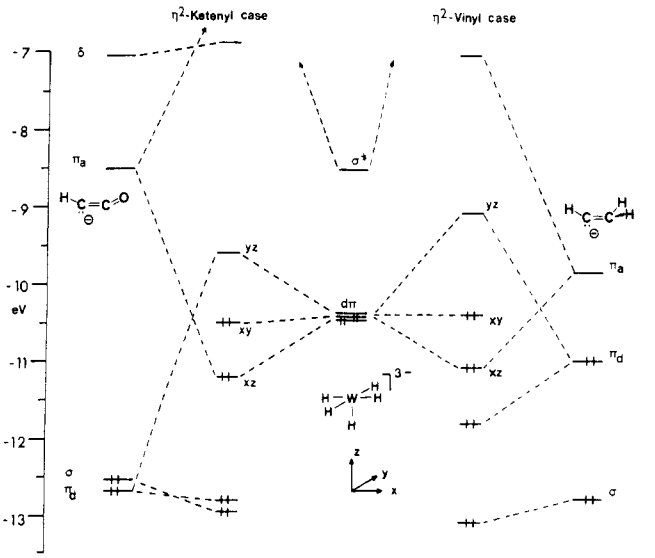

Figure 4. Energy level diagram for $[H_5W(\eta^2\text{-}H_2C{=}CH)]^{4-}$ and $[H_5W(\eta^2\text{-}HC{=}CO)]^{4-}$.

visualized for the η^2-vinyl case by imagining deprotonation of a metal–ethylene fragment (Scheme II). The metallacyclopropane valence bond picture then leads to a carbanion which can be rehybridized to sp^2 while the M–CH_2–C geometry is retained. Feeding the C_α p electrons to the metal completes the picture. Structural results reveal that the C_β substituents are located above and below the MC_2 plane as expected.[3-6]

The isolobal analogy between an η^2-ketenyl ligand and an alkyne ligand is emphasized in valence bond representation **2c** (Scheme III). The synthetic relationship between the two confirms their kinship. As with cyclopropenone itself,[18] the oxygen atom is nucleophilic and protonation[19] or alkylation[20] readily converts η^2-ketenyl ligands to hydroxyalkynes or alkoxyalkynes.

Valence bond pictures **1b** and **2b** (Scheme I) do not require the metal to donate a pair of electrons to a vacant ligand orbital. We expect back donation into π_a to be sufficiently important, however, that η^2-vinyl and η^2-ketenyl complexes will be isolated only when a metal

(15) (a) Dewar, M. J. S. *Bull. Soc. Chim. Fr.* **1951**, *18*, C71. (b) Chatt, J.; Duncanson, L. A. *J. Chem. Soc.* **1953**, 2939.
(16) (a) Albright, T. A.; Hoffmann, R.; Thibeault, J. C.; Thorn, D. L. *J. Am. Chem. Soc.* **1979**, *101*, 3801. (b) Tatsumi, K.; Hoffmann, R.; Templeton, J. L. *Inorg. Chem.* **1982**, *21*, 466.
(17) (a) King, R. B. *Inorg. Chem.* **1968**, *7*, 1044. (b) Ward, B. C.; Templeton, J. L. *J. Am. Chem. Soc.* **1980**, *102*, 1532. (c) Alt, H. G.; Hayen, H. I. *Angew. Chem. Suppl.* **1983**, 1364. (d) Theopold, K. H.; Holmes, S. J.; Schrock, R. R. *Angew. Chem. Suppl.* **1983**, 1409. (e) Cotton, F. A.; Hall, W. T. *J. Am. Chem. Soc.* **1979**, *101*, 5094. (f) Ricard, L.; Weiss, R.; Newton, W. E.; Chen, G. J.-J.; McDonald, J. W. *J. Am. Chem. Soc.* **1978**, *100*, 1318. (g) Davidson, J. L.; Green, M.; Stone, F. G. A.; Welch, A. J. *J. Chem. Soc., Dalton Trans.* **1976**, 738. (h) Winston, P. B.; Burgmayer, S. J. N.; Templeton, J. L. *Organometallics* **1983**, *2*, 167.
(18) Potts, K. T.; Baum, J. S. *Chem. Rev.* **1974**, *74*, 189.
(19) (a) Jeffery, J. C.; Laurie, J. C. V.; Moore, I.; Stone, F. G. A. *J. Organomet. Chem.* **1983**, *258*, C37. (b) Reference 8c.
(20) (a) Kreissl, F. R.; Sieber, W.; Wolfgruber,, M. *Angew. Chem., Int. Ed. Engl.* **1983**, *22*, 493. (b) Reference 8c.

electron pair is available. Structural and ^{13}C NMR data support the assignment of carbenoid character to C_α, as Davidson, Muir, and co-workers have recently pointed out.[4a] These two metal electrons merge with the four ligand-based electrons to fill three bonding combinations which result from the interaction of the C_2 ligand with a metal fragment (see next section).

Model Octahedral Complexes with HC≡CH, [HC=CH$_2$]$^-$, and [HC=CO]$^-$ Ligands. The primary bonding features of these C_2-based ligands in octahedral d^4 metal complexes can be illustrated by attaching them to the hypothetical $[H_5W]^{3-}$ fragment. Coordination of ethylene to the $[H_5W]^{3-}$ moiety is presented (Figure 3) as a reference point. The $[H_5W(\eta^2\text{-HC≡CH})]^{3-}$ diagram, also presented in Figure 3, sets the course which is roughly followed by the molecular orbitals of the metallacyclopropene and $[\eta^2\text{-HC=CO}]^-$ complexes (Figure 4).

The filled σ orbital interacts strongly with the d_{z^2}-dominated metal acceptor orbital in each case. The vacant π_a orbital overlaps, and hence stabilizes, the metal d_{xz} orbital in the coordinate system shown. Donation from π_d destabilizes d_{yz} and completes the analogy between η^2-vinyls, η^2-ketenyls, and four-electron-donor alkyne ligands. Although there are four orbitals present in the free alkyne π system, the $\pi_\perp^*$ orbital is not a crucial component of transition metal–alkyne bonding. It is of δ symmetry relative to the metal–C_2 linkage, and it interacts only weakly with d_{xy}, so three orbitals are adequate for constructing effective isolobal ligand relationships with alkynes.[21]

The calculated energies of the three metal $d\pi$ orbitals, the t_{2g} set of true octahedra, provide a crude probe of the simultaneous π-donor and π-acceptor strength of these C_2 derivatives toward a metal center. A d^4 configuration, common for alkyne complexes,[17] reflects the divergence of the $d\pi$ levels as bonding, nonbonding and antibonding. When the incoming C_2 ligand approaches along the z axis, the d_{xy} orbital, virtually unchanged in the environment of five π-innocent hydride ligands, is the HOMO1 for these model d^4 compounds. It is only slightly perturbed by C_2 δ-type orbital combinations. The HOMO1 – LUMO gap between d_{xy} and d_{yz} reflects the C_2 π-donor strength while the HOMO1 – HOMO2 difference between d_{xy} and d_{xz} depends on the π-acidity of the C_2 ligand. Some experimental data relevant to the HOMO1–LUMO energy variation for $M(CO)(\eta^2\text{-alkyne})(S_2CNR_2)_2$ (M = Mo, W) compounds as a function of the alkyne ligand substituents has been provided by electronic spectra and electrochemical measurements.[22]

Our calculations indicate that π_d destabilization of d_{yz} produces HOMO1 (d_{xy}) – LUMO (d_{yz}) separations of 1.33, 1.10, and 0.91 eV for $[HC=CH_2]^-$, HC≡CH, and [HC=CO]$^-$, respectively. The superior strength of the vinyl anion as a π donor is in accord with the substantially higher energy of π_d as seen in Figure 2. The energies of the π_d orbitals of acetylene and the ketenyl fragment are much closer to one another, with the ketenyl π_d orbital slightly higher in energy (Figure 2). The lesser π-donor ability of the ketenyl fragment reflects poorer overlap of π_d with the metal and competing delocalization of the C_α lone pair into the C=O system. These substantial HOMO1 – LUMO gaps, all approximately 1 eV, are invariably increased by replacing H^- by a π-acid ligand which stabilizes the d_{xy} HOMO1 orbital. In contrast, the absence of a π_d orbital on ethylene produces a corresponding gap of only 0.15 eV in the $[H_5W(\eta^2\text{-H}_2C=CH_2)]^{3-}$ reference complex.

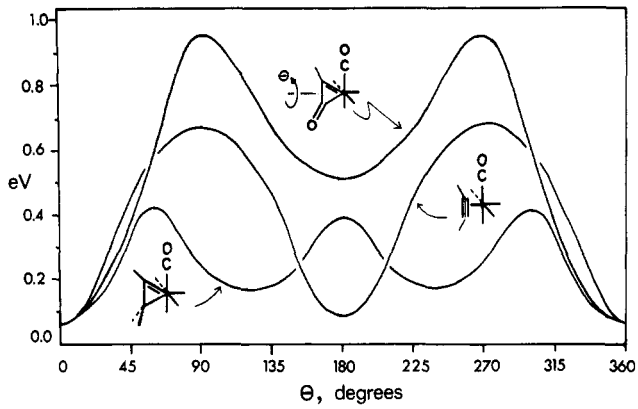

Figure 5. Rotational profiles for $[H_4(CO)W(\eta^2\text{-HC=CO})]^{3-}$, $[H_4(CO)W(\eta^2\text{-HC≡CH})]^{2-}$, and $[H_4(CO)W(\eta^2\text{-H}_2C=CH)]^{3-}$. The zero of energy is arbitrary.

The HOMO2 (d_{xz}) – HOMO1 (d_{xy}) energy differences of 1.36, 1.31, and 0.72 eV for HC≡CH, $[HC=CH_2]^-$, and [HC=CO]$^-$ indicate significant back-donation from metal to ligand in each case. The strong π_a interactions of the alkyne and vinyl ligands result from the proximity in energy of the acceptor orbitals to the $d\pi$ levels of the metal and from the hybridization of π_a which directs the carbon atomic orbitals involved toward the metal.

Rotational Properties of HC≡CH, [HC=CH$_2$]$^-$, and [HC=CO]$^-$ Ligands. Because the $d\pi$ orbitals in the $[H_5W]^{3-}$ fragment are degenerate, the energy of octahedral complexes will be nearly independent of the rotational orientation of the sixth ligand. Linear combinations of d_{xz} and d_{yz} will fulfill the roles of metal π-acceptor and π-donor orbitals for every rotamer. Placing a cylindrically symmetrical π-acid in the xy plane will break the degeneracy of d_{xz} and d_{yz} and lead to rotational preferences, as seen for alkyne ligands in d^4 *cis*-$L_4M(CO)(\eta^2\text{-alkyne})$ complexes.[23] Related analyses for d^2 metal complexes of group 6 with cylindrically symmetrical π donors have been presented (e.g., $(\pi\text{-}C_5H_5)Mo(O)(SR)(\eta^2\text{-alkyne})$,[24] $W(O)(\eta^2\text{-alkyne})(S_2CNR_2)_2$)[25], and $W(S)(\eta^2\text{-alkyne})(S_2CNR_2)_2$[26]).

It is observed in W(CO)(dppe)(detc)(*C,C*-η^2-OC=CCH_2Ph) and in other structurally characterized monocarbonyl ketenyl complexes[8b,9b] that the C_2 moiety is oriented with C_β proximal to CO and the C_α–C_β bond lies parallel to the M–carbonyl axis, i.e., $\theta = 0°$. The C_2 rotational energy profile for *cis*-$[H_4(CO)W(\eta^2\text{-HC=CO})]^{3-}$ indeed has a global minimum at $\theta = 0°$ (Figure 5). The contour is reminiscent of the one obtained for the η^2-alkyne case, but the local minimum at $\theta = 180°$ for the ketenyl ligand, with C_α proximal to CO, lies more than 10 kcal mol^{-1}, above the ground-state orientation. The destabilization at $\theta = 180°$ results from cooperative steric and electronic effects. Congestion is induced by placing C_α next

(21) Templeton, J. L.; Winston, P. B.; Ward, B. C. *J. Am. Chem. Soc.* **1981**, *103*, 7713.

(22) Templeton, J. L.; Herrick, R. S.; Morrow, J. R. *Organometallics* **1984**, *3*, 535.

(23) Rotational barriers for the alkyne ligand in a number of such complexes have been determined by NMR spectroscopy: (a) Allen, S. R.; Baker, P. K.; Barnes, S. G.; Green, M.; Trollope, L.; Manojlović-Muir, L.; Muir, K. W. *J. Chem. Soc., Dalton Trans.* **1981**, 873. (b) Reference 17b. (c) Winston, P. B.; Burgmayer, S. J. N.; Templeton, J. L. *Organometallics*, accepted for publication.

(24) Howard, J. A. K.; Stansfield, R. F. D.; Woodward, P. *J. Chem. Soc., Dalton Trans.* **1976**, 246.

(25) (a) Templeton, J. L.; Ward, B. C.; Chen, G. J.-J.; McDonald, J. W.; Newton, W. E. *Inorg. Chem.* **1981**, *20*, 1248. (b) Newton, W. E.; McDonald, J. W.; Corbin, J. L.; Ricard, L.; Weiss, R. *Inorg. Chem.* **1980**, *19*, 1997.

(26) Morrow, J. R.; Tonker, T. L.; Templeton, J. L. *Organometallics* **1985**, *4*, 745.

to the carbonyl (the distance between C_α and C_{CO} is small, 2.30 Å); moreover, the total energy of the system drops when when the carbonyl ligand is bent away from the η^2-ketenyl moiety, although the $d\pi$ orbitals are destabilized by this distortion. When $\theta = 0°$, the C_β–C_{CO} distance is 2.41 Å and the total energy increases when the carbonyl is bent away, consistent with partial destruction of the three-center two-electron bond formed between d_{xz}, CO π^*, and ketenyl π_a orbitals.

In addition to stabilizing d_{xy} and d_{xz}, the carbonyl ligand in $[H_4(CO)W]^{2-}$ causes the metal to hybridize these orbitals by mixing metal p_y and p_z character into the d functions. Hoffmann and Kubacek recently utilized this phenomenon in rationalizing the geometries of distorted-octahedral d^4 complexes of Mo(II) and W(II).[12] For the metal fragment treated here, d_{xz} is shaped so that more orbital density is located toward the carbonyl than away from it (see iv below). The overlap of the π_a orbital of the ketenyl fragment with this filled d orbital equals 0.205 when $\theta = 0°$ and 0.193 when $\theta = 180°$ (see v). The reason for this difference lies in the asymmetry of π_a, which has twice as much orbital density on C_β as on C_α (see v), leading to superior overlap when C_β lies over the enlarged lobe of d_{xz}.

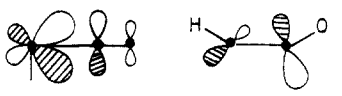

iv v

The shape of the LUMO in $[H_4(CO)W]^{2-}$, the d_{z^2} orbital, is also important in setting the geometric preference of the incoming ketenyl moiety. In the all-H metal fragment this orbital is aligned with the z axis and hybridized toward the vacant octahedral coordination site. Replacing H^- with CO along the x axis tilts this orbital, through an admixture of d_{xz}, away from the carbonyl (see vi). Since the σ-donor orbital of the ketenyl ligand is heavily weighted toward C_α (see Table III and vii), the $\theta = 0°$ orientation allows the greatest interaction between σ and d_{z^2}. The relevant overlap integral is 0.290 when $\theta = 0°$ and 0.240 when $\theta = 180°$.

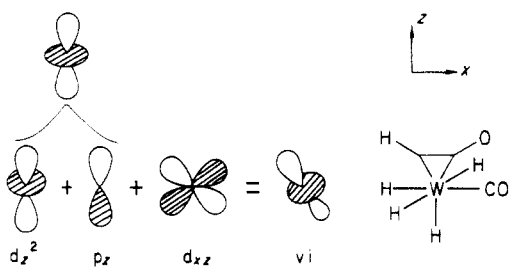

d_{z^2} p_z d_{xz} vi

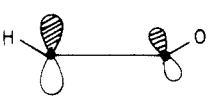

vii

The d_{yz} orbital is unaffected in shape and energy when CO replaces H^- along the x axis, and therefore interactions of d_{yz} with π_d are equivalent at $\theta = 0°$ and 180°; indeed the d_{yz} LUMO is only slightly stabilized (0.006 eV) when $\theta = 0°$. The δ interaction with d_{xy} is not significant. Overall the calculations suggest that rotation of the η^2-ketenyl ligand may be accessible on the NMR time scale with a barrier near 20 kcal mol^{-1}, but since only the $\theta = 0°$ isomer will ever by sufficiently populated for NMR observation, no rotational process will be observable in these systems.

The rotational profile for the η^2-vinyl case also has a global minimum at $\theta = 0°$ (Figure 5), but while the orientation at $\theta = 180°$ is an energy minimum for the alkyne and ketenyl complexes, it is a maximum for $[H_4(CO)W(\eta^2\text{-}HCCH_2)]^{3-}$ with a trough near $\theta = 120°$ and another maximum at $\theta = 60°$. This rotational behavior results from competing steric and electronic effects. As in the ketenyl case, steric crowding is introduced by locating C_α proximal to CO in the model complex: the carbon–carbon distance is extremely short, 2.19 Å.

The frontier orbitals of the vinyl fragment are similar to those of the ketenyl moiety, since π_a has greater density on C_β and σ is weighted toward C_α, but there is much less polarization (Table III). Furthermore, there is a greater difference in metal–carbon distances in the model η^2-vinyl complex compared to the ketenyl case (Table II). These factors are reflected in the overlap integrals for the frontier orbitals. That π_a overlap with d_{xz} is better when $\theta = 180°$ seems strange given the shapes of these orbitals, but C_α is so close to the metal that it brings its share of π_a into greater contact with d_{xz} than does C_β. The overlap between σ and d_{z^2} is better when $\theta = 0°$, as in the ketenyl case, but the difference is smaller (0.269 at 0° and 0.235 at 180°).

This analysis shows that steric crowding and relative metal–carbon distances should be important in determining the geometries of real η^2-vinyl complexes. In fact, distances and geometries vary widely for η^2-vinyl complexes. Tungsten–C_β distances vary by about 0.15 Å for a series of $[(\pi\text{-}C_5H_5)W(F_3CC{\equiv}CCF_3)(\eta^2\text{-vinyl})L]$ complexes, depending on the nature of L (chloride or thiolate) and the identity of the nucleophile employed to generate the η^2-vinyl moiety (phosphine or isonitrile).[4a] The variation in W–C_α is smaller, about 0.07 Å, in this series. There is also a startling variety of orientations for the η^2-vinyl ligands. In $(\pi\text{-}C_5H_5)Mo(F_3CC{\equiv}CCF_3)(\eta^2\text{-}F_3CC{=}CCF_3(PEt_3))Cl$[6] the η^2-vinyl ligand is parallel to the alkyne, analogous to the geometry adopted by the alkyne ligands in the tungsten bis(alkyne) precursor complex.[27] In $(\pi\text{-}C_5H_5)W(F_3CC{\equiv}CCF_3)(\eta^2\text{-}F_3CC{=}CCF_3(CNBu))Cl$, however, the η^2-vinyl ligand is nearly perpendicular to the alkyne.[7a] Finally, the η^2-vinyl moiety in $(\pi\text{-}C_5H_5)W(CO)_2(\eta^2\text{-}F_3CC{=}CCF_3(COSMe)$ lies about 30° away from the best orientation for W–C_α π bonding.[4a] These structural results are compatible with the soft energy surface, spanning less than 10 kcal mol^{-1}, calculated for rotation of the η^2-vinyl ligand in our model system. Similar conclusions were drawn by Allen et al., who showed that η^2-vinyl rotation is facile in $(\pi\text{-}C_5H_5)Mo(P(OCH_3)_3)_2(\eta^2\text{-vinyl})$ complexes.[3c]

Acknowledgment. This work was generously supported by the donors of the Petroleum Research Fund, administered by the American Chemical Society. We wish to thank Dr. D. M. P. Mingos for helpful discussions of this work.

Registry No. $W(\eta^2\text{-MA})(\eta^2\text{-}PhC_2H)(detc)_2$, 98735-53-6; $W(CO)(dppe)(detc)(c,c\text{-}\eta^2\text{-}OC{=}CCH_2Ph)$, 96454-70-5.

(27) Davidson, J. L.; Green, M.; Stone, F. G. A.; Welch, A. J. *J. Chem. Soc., Dalton Trans.* **1976**, 738.

Ligand Substitution Kinetics of the Triruthenium Hydride Ion $HRu_3(CO)_{11}^-$

Douglas J. Taube and Peter C. Ford*[1]

Department of Chemistry, University of California, Santa Barbara, California 93106

Received April 26, 1985

A kinetics investigation of the substitution of CO on $HRu_3(CO)_{11}^-$ by PPh_3 in tetrahydrofuran solution is described. The reversible reaction $HRu_3(CO)_{11}^- + PPh_3 \rightleftharpoons HRu_3(CO)_{10}PPh_3^- + CO$ is shown to have the equilibrium constant $K = 0.23$ at 25 °C. The rate of carbonyl substitution by PPh_3 shows a ligand concentration independent limiting rate constant k_1 (2.1 s^{-1} at 25 °C, $\Delta H^\ddagger = 16.0$ kcal/mol, $\Delta S^\ddagger = -1.9$ cal/(mol deg)). These data are interpreted in terms of a unimolecular CO dissociation as the first step in the substitution mechanism. The rate constant k_2 for the reverse reaction, also concluded to occur via a unimolecular ligand dissociation step, is 0.46 s^{-1} (25 °C, $\Delta H^\ddagger = 18.2$ kcal/mol, $\Delta S^\ddagger = 1.0$ cal/(mol deg)). The limiting rate constants for the reaction of $HRu_3(CO)_{11}^-$ with PPh_3 in 2-methyltetrahydrofuran solution and for the reaction of tri-*n*-butylphosphine with $HRu_3(CO)_{11}^-$ in THF were found to be nearly the same as the k_1 noted above in further support of the proposed dissociative mechanism. The activation parameters for these reactions are about 10 kcal/mol lower than for analogous reactions of neutral triruthenium carbonyl clusters. Possible mechanisms are discussed.

Introduction

The trinuclear ruthenium hydride ion $HRu_3(CO)_{11}^-$ (A)

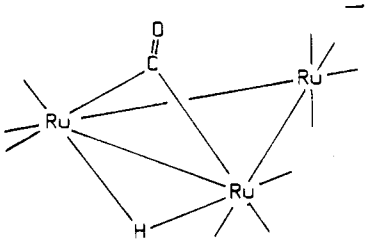

(A)

was first reported as the product of the reaction of triruthenium dodecacarbonyl, $Ru_3(CO)_{12}$, with tetrahydrofuran (THF) solutions of $NaBH_4$[2] or with aqueous KOH.[3] This anionic cluster has drawn considerable recent attention as a prominent species in homogeneous solution-phase catalysts for the water gas shift reaction (based on ruthenium carbonyl in alkaline solutions)[3-5] and for the hydrogenation, hydroformylation, and hydrosilation of alkenes.[6] In the course of investigating the reactivity of $HRu_3(CO)_{11}^-$ and its potential roles in such catalytic cycles, this ion was found to be remarkably more labile toward ligand substitution (eq 1) than the parent neutral carbonyl

$$HRu_3(CO)_{11}^- + L \underset{}{\overset{K}{\rightleftharpoons}} HRu_3(CO)_{10}L^- + CO \quad (1)$$

$Ru_3(CO)_{12}$ under similar conditions. Reported here is a quantitative investigation of the kinetics of the reaction of $HRu_3(CO)_{11}^-$ with triphenylphosphine in THF (eq 1; L = PPh_3).

Experimental Section

All manipulations were carried out by using standard Schlenk techniques. All gases (Linde), C.P. grade CO, 10% CO (90% N_2), 25% CO (75% N_2), and N_2, were used as received. Triphenylphosphine and tri-*n*-butylphosphine (Aldrich) were used as received. Tetrahydrofuran was distilled from sodium benzophenone under N_2, and 2,5-dimethyltetrahydrofuran (Aldrich) was distilled from sodium under N_2. The hydride salt $[PPN][HRu_3(CO)_{11}]$ was prepared by literature procedures.[2] All solutions were degassed by using several freeze–pump–thaw cycles to remove adventitious air and then saturated with the appropriate gas.

Infrared spectra were obtained on a Perkin-Elmer 683 spectrophotometer. UV–visible spectra were obtained on a Cary 118 recording spectrophotometer in 1.0-cm path length quartz cells. ^1H spectra were obtained on a Nicolet 300-MHz FT-NMR spectrometer with THF-d_8 (Aldrich), distilled from CaH_2, as an internal lock. Samples were referenced to the residual protons in the solvent.

Equilibrium and kinetic studies of the rates of carbonyl substitution were carried out with a Durrum-Gibson D110 stopped-flow spectrophotometer. The drive syringes and observation block were thermostated to ±0.1 °C with a Haake FS-S circulator bath. The solutions were temperature equilibrated for 15 min before analysis, and all solutions were prepared and transferred to the spectrophotometer under deaerated conditions. All the kinetic runs for reactions involving PPh_3 were monitored at 430 nm where the largest spectral differences between the monosubstituted and unsubstituted hydride complexes were observed. For the reactions with PBu_3 the disappearance of $HRu_3(CO)_{11}^-$ was monitored at 376 nm given complications at longer wavelengths from the subsequent formation of disubstituted complexes at high [PBu_3]. Traces of absorbance vs. time were recorded with a Biomation Model 805 waveform recorder. These data were then transferred digitally to a Hewlett-Packard 86 computer for mathematical analysis.[7] Rate data were analyzed from ln ($A_t - A_\infty$) vs. time plots (linear least-squares fit) or from the kinetic over-relaxation method (KORE) of Swain et al.[8]

Kinetics of the forward reaction were run under the following conditions. A 1.2×10^{-4} M solution of $[PPN][HRu_3(CO)_{11}]$ in THF, under various gas mixtures (N_2, 10% CO (90% N_2), 25% CO (75% N_2), or 100% CO) all at 1.0 atm was placed in drive syringe A. Drive syringe B contained a THF solution of PPh_3 (under the identical gas mixture) at various concentrations (0.0022–0.01 M). Kinetics of the reverse reaction were run starting with $HRu_3(CO)_{10}PPh_3^-$ in drive syringe A. The substituted cluster was made in situ by the addition of PPh_3 (0.0011–0.0047 M) to

(1) Reported in part at the 183rd National Meeting of the American Chemical Society, Las Vegas, NV, Apr 1982; American Chemical Society: Washington, D.C., 1982. INORG 93.

(2) Johnson, B. F. G.; Lewis, J.; Raithby, P. R.; Suss, G. *J. Chem. Soc., Dalton Trans.* **1979**, 1356.

(3) Ungermann, C.; Landis, V.; Moya, S. A.; Cohen, H.; Walker, H.; Pearson, R. G.; Rinker, R. G.; Ford, P. C. *J. Am. Chem. Soc.* **1979**, *101*, 5922.

(4) Ford, P. C. *Acc. Chem. Res.* **1981**, *14*, 31.

(5) (a) Bricker, J. C.; Nagel, C. C., Shore, S. G. *J. Am. Chem. Soc.* **1982**, *104*, 1444. (b) Bricker, J. C.; Nagel, C. C.; Bhattacharyya, A. A.; Shore, S. G. *Ibid.* **1985**, *107*, 377.

(6) (a) Suss-Fink, G. *Angew. Chem., Int. Ed. Engl.* **1982**, *21*, 73. (b) Suss-Fink, G.; Ott, J.; Schmidkonz, B.; Guldner, K. *Chem. Ber.* **1982**, *115*, 2487. (c) Suss-Fink, G.; Reiner, J. *J. Mol. Catal.* **1982**, *16*, 231.

(7) Trautman, R.; Gross, D. C.; Ford, P. C. *J. Am. Chem. Soc.* **1985**, *107*, 2355–2362.

(8) Swain, C. G.; Swain, M. S.; Berg, L. F. *J. Chem. Inf. Comput. Sci.* **1980**, *20*, 47.

0276-7333/86/2305-0099$01.50/0

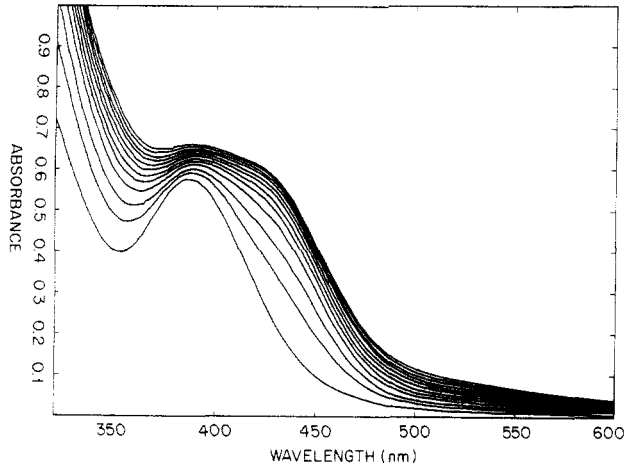

Figure 1. Spectral changes observed upon the sequential addition of 8.0×10^{-4} M aliquots of PPh_3 in THF to 8.0×10^{-5} M [PPN][$HRu_3(CO)_{11}$] in THF under N_2. Curve A was obtained for [PPh_3] = 0.00 M; curve L represents [PPh_3] = 5.0×10^{-4} M.

THF solutions of [PPN][$HRu_3(CO)_{11}$] (1.2×10^{-4} M) under N_2. The solutions were degassed by four freeze–pump–thaw cycles to remove the resultant CO. THF solutions equilibrated with 10% CO (90% N_2), 25% CO (75% N_2), or 100% CO, all at 1.0 atm, were used in drive syringe B. Mixing of the two solutions led to the partial reformation of $HRu_3(CO)_{11}^-$ with the [$HRu_3(CO)_{10}PPh_3^-$]/[$HRu_3(CO)_{11}^-$] ratio dependent upon [CO] and [PPh_3].

Results

THF solutions of [PPN][$HRu_3(CO)_{11}$] under 1.0 atm of N_2 display a strong absorption maximum in the electronic spectrum at 387 nm (ϵ 6900 M^{-1} cm^{-1}) along with a broad absorption centered at 505 nm (ϵ 400 cm^{-1}). Sequential additions of PPh_3 led to the spectral changes shown in Figure 1, with new absorptions at higher wavelengths. The limiting spectrum, obtained upon the addition of excess PPh_3, showed a broad flat peak with a maximum at 420 nm (ϵ 7300 M^{-1} cm^{-1}) along with a shallow minimum at 370 nm (ϵ 6900 M^{-1} cm^{-1}). Rapid acidification of the final solution leads to the appearance of a new band centered at 416 nm, which has been attributed to $Ru_3(CO)_{11}PPh_3$.[9] Thus, it may be concluded that the 420-nm band belongs to [PPN][$HRu_3(CO)_{10}PPh_3$]. When CO was bubbled through a THF solution of [PPN][$HRu_3(CO)_{10}PPh_3$] under N_2, the bright yellow solution immediately became pale and the absorption band associated with [PPN][$HRu_3(CO)_{11}$] quantitatively appeared. When N_2 was then bubbled through the same solution, the spectrum of [PPN][$HRu_3(CO)_{10}PPh_3$] was reproduced. These observations clearly indicate the reversible reaction shown in eq 1 (L = PPh_3).

$$K = \frac{[HRu_3(CO)_{10}PPh_3^-][CO]}{[HRu_3(CO)_{11}^-][PPh_3]} \qquad (2)$$

The reaction of [PPN][$HRu_3(CO)_{11}$] with PPh_3 was also followed by infrared spectroscopy (Figure 2). A THF solution of [PPN][$HRu_3(CO)_{11}$] under N_2 shows infrared bands[2] in the ν_{CO} region at 2072 (w), 2006 (s), 1983 (s), and 1948 (m) cm^{-1}. When PPh_3 was sequentially added, new bands attributed to [PPN[($HRu_3(CO)_{10}PPh_3$] grew in at 2044 (m), 1995 (s), 1973 (m), 1960 (s), 1938 (m), and 1916 (w) cm^{-1}. Throughout the reaction, isosbestic points at 2018, 1998, 1990, 1975, and 1952 cm^{-1} were maintained. The isosbestic points indicate that intermediates, if produced during the reaction, were not formed in concentrations detectable under these conditions.

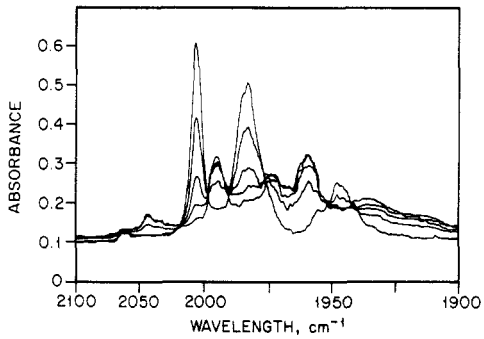

Figure 2. Infrared spectral changes observed upon the sequential addition of 8.0×10^{-3} M PPh_3 aliquots to a THF solution of 2.5×10^{-3} M [PPN][$HRu_3(CO)_{11}$] under N_2. Curve A was obtained for [PPh_3] = 0.00 M; curve E represents [PPh_3] = 4.0×10^{-3} M.

The equilibrium constant for eq 1 was determined by ^1H NMR and UV–visible absorbance changes. For the NMR experiment, a THF-d_8 solution of [PPN][$HRu_3(CO)_{11}$] (0.0065 M) with PPh_3 (0.091 M) was saturated with 10% CO (90% N_2) and allowed to equilibrate at 25 °C. The hydride region of the ^1H NMR showed two resonances, a singlet at −12.50 ppm for $HRu_3(CO)_{11}^-$ and a doublet at −11.91 ppm (J_{P-H} = 5.4 Hz) for $HRu_3(CO)_{10}PPh_3^-$. Integration of the hydride resonances gave their relative concentrations, and from these data the concentration of PPh_3 was calculated. The CO concentration was varied by bubbling the equilibrium mixture with 25% CO (75% N_2) and then with 100% CO. Equilibrium constant values calculated according to eq 2 were 0.24 ± 0.12 for the above solutions. The uncertainty in K measured in this manner was attributed to uncertainty in concentrations of various species owing to incomplete equilibrium with CO and to evaporation of the solvent upon bubbling. However, the appearance of only two resonances in the hydride region did indicate that the only substituted hydride cluster formed was the monophosphine derivative $HRu_3(CO)_{10}PPh_3^-$.

The equilibrium constant determined from absorbance changes was measured by using the stopped-flow spectrophotometer. Solutions containing a fixed amount of [PPN][$HRu_3(CO)_{11}$] but varied [PPh_3]/[CO]ratios were mixed and then allowed to equilibrate at 25 °C. The resulting absorbances were plotted according to eq 3, where

$$A_{eq} = 1/K(A_0 - A_{eq})([CO]/[PPh_3]) + A_\infty \qquad (3)$$

A_{eq} is the equilibrium absorbance at 430 nm for the corresponding [PPh_3]/[CO] ratio, A_0 and A_∞ are the absorances of the pure reactants and products, and K is the equilibrium constant or eq 1. A typical plot is shown in Figure 3, where the inverse of the slope (determined using a least squares program) is equal to K. Equilibrium constant measurements were made by using 10% CO (90% N_2) and 25% CO (75% N_2) so that there was a wide range in equilibrium mixtures upon the addition of PPh_3. The values for the equilibrium constant K measured under these conditions were 0.20 ± 0.02 and 0.23 ± 0.02, respectively, well within the range obtained by ^1H NMR. The value of K = 0.23 ± 0.02 (25 °C) was used in all further calculations described below. Static electronic absorption spectral experiments at other temperatures gave the K values 0.20 ± 0.01 at 9.0 °C and 0.26 ± 0.01 at 37.3 °C and thus the $\Delta H°$ and $\Delta S°$ values of 1.5 ± 0.1 kcal/mol and 2.2 ± 0.2 cal/(mol deg), respectively.

Stopped-flow kinetics of the forward reaction (eq 1) were run under "pseudo-first-order" conditions where [PPh_3]

(9) Bruce, M. I.; Shaw, G.; Stone, F. G. A. *J. Chem. Soc., Dalton Trans.* **1972**, 2094.

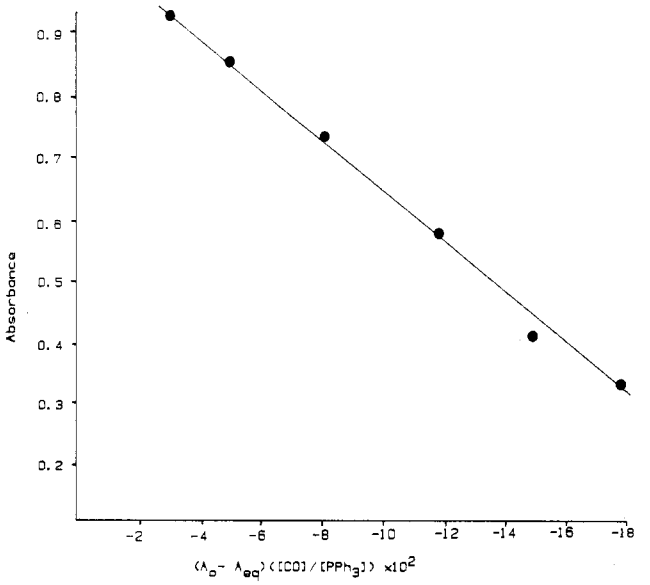

Figure 3. Equilibrium constant plot of eq 3 for the reaction of $HRu_3(CO)_{11}^-$ + PPh_3 ⇌ $HRu_3(CO)_{10}PPh_3^-$ + CO in THF under 25:75 CO/N_2 at 25 °C.

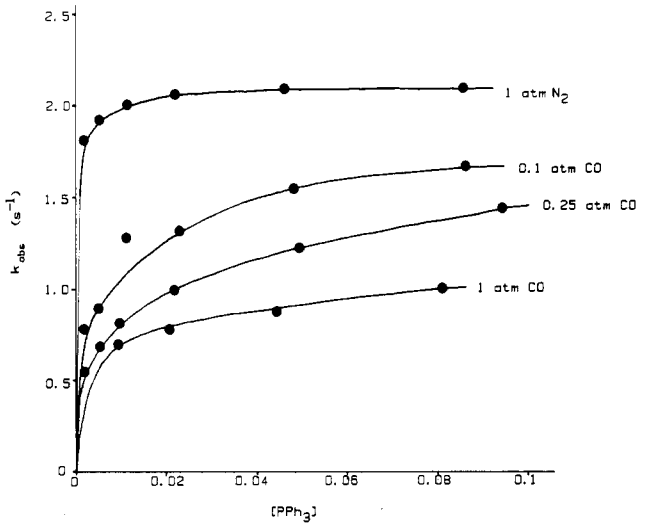

Figure 4. Plots of k_{obsd} vs. $[PPh_3]$ for the reaction of $HRu_3(CO)_{11}^-$ plus PPh_3 in THF under varied P_{CO} at 25 °C (curves drawn for illustrative purposes only).

≫ $[HRu_3(CO)_{11}^-]$. The reaction was monitored by the decrease in absorbance at 430 nm. Plots of ln $(A - A_\infty)$ vs. time were linear for more than 3 half-lives, indicating that the reaction is first order with respect to cluster concentration. Experiments were carried out varying $[PPh_3]$ over the range 0.0022–0.1 M and [CO] over the range 0.0016–0.016 M (0.10–1.0 atm).[10] Plots of k_{obsd} vs. $[PPh_3]$ were nonlinear and leveled to limiting values at high $[PPh_3]$. At fixed $[PPh_3]$, the observed rate constant increased upon decreasing [CO] (Figure 4). This behavior suggests a mechanism proceeding via CO dissociation:

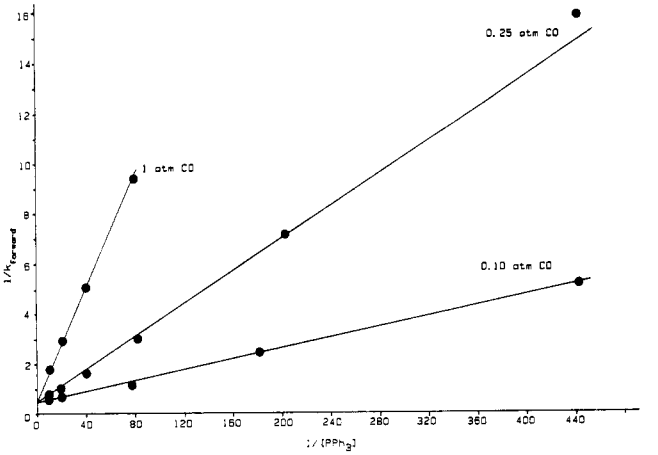

Figure 5. Double reciprocal plots of $1/k_f$ vs. $1/[PPh_3]$ according to eq 10 for the reaction of $HRu_3(CO)_{11}^-$ plus PPh_3 in THF at 25 °C.

Scheme I

$$HRu_3(CO)_{11}^- \underset{k_{-1}}{\overset{k_1}{\rightleftharpoons}} HRu_3(CO)_{10}^- + CO \quad (4)$$

$$HRu_3(CO)_{10}^- + PPh_3 \underset{k_{-2}}{\overset{k_2}{\rightleftharpoons}} HRu_3(CO)_{10}PPh_3^- \quad (5)$$

If the steady-state approximation for $[HRu_3(CO)_{10}^-]$ is made, Scheme I predicts the following relationships for k_{obsd} and K:

$$k_{obsd} = \frac{k_1k_2[PPh_3] + k_{-1}k_{-2}[CO]}{k_{-1}[CO] + k_2[PPh_3]} \quad (6)$$

$$K = \frac{k_1k_2}{k_{-1}k_{-2}} \quad (7)$$

In the absence of added CO, a limiting value of 2.1 ± 0.1 s^{-1} is quickly reached for k_{obsd} (Figure 4). Under these conditions $k_1k_2[PPh_3] \gg k_{-1}k_{-2}[CO]$ and $k_2[PPh_3] \gg k_{-1}[CO]$, and thus eq 5 simplifies to $k_{obsd} = k_1$.

The rate constant k_1 can also be obtained under less than limiting conditions (e.g., 10:90 CO/N_2 or 25:75 CO/N_2) by the use of the following analysis. The rate expression in eq 6 can be broken into forward and reverse contributions[11] (eq 8).

$$k_{obsd} = \frac{k_1k_2[PPh_3]}{k_{-1}[CO] + k_2[PPh_3]} + \frac{k_{-1}k_{-2}[CO]}{k_{-1}[CO] + k_2[PPh_3]} \quad (8)$$

For simplicity the term on the left will be defined as "k_f" and the right as "k_r". The value of k_f can be calculated from the following relationship.[11]

$$k_f = \frac{k_1k_2[PPh_3]}{k_{-1}[CO] + k_2[PPh_3]} = \frac{k_{obsd}}{1 + ([CO]/[PPh_3])K^{-1}} \quad (9)$$

If the mechanism shown in Scheme I applies, then a double reciprocal plot of $(k_f)^{-1}$ vs. $[PPh_3]^{-1}$ should be linear according to eq 10

$$k_f^{-1} = \frac{k_{-1}[CO]}{k_1k_2[PPh_3]} + \frac{1}{k_1} \quad (10)$$

with an intercept of $(k_1)^{-1}$ and a slope of $k_{-1}[CO]/k_1k_2$. Figure 5 represents such plots for three different values

(10) "Solubilities of Inorganic and Metal Organic Compounds"; 4th ed.; Seidell and Linke, Eds.; D. Nostrand Co.: Princeton NJ, 1958. [**Note added in proof**: Carbon monoxide concentrations were calculated by using the *assumption* that the solubility of CO in THF is the same as in diethyl ether (0.016 mol/L atm at 25 °C). We have been unable to find a literature value for this parameter, but further consideration has led us to conclude that this is too large a value for CO solubility in THF. The use of solution theory ("Encyclopedia of Chemical Technology", 3rd ed.; Wiley: New York, 1978; Vol 21, p 377) gives an estimated CO solubility of 0.0084 mol/L atm. Use of this latter estimate instead would change several of the parameters calculated from the experimental data. The key changes would be for the equilibrium constant K (eq 2) which would assume the values 0.11 ± 0.1 (9.0 °C), 0.12 ± 0.01 (25.0 °C), and 0.14 ± 0.01 (37.3 °C). The other changes would be the rate constant ratio k_{-1}/k_2 (eq 4 and 5), which would assume the values 29 ± 5 for L = PPh_3 and 27 ± 4 for L = PBu_3. These new values lead to no substantive changes in the conclusions drawn in this paper.]

(11) Doeff, M. M.; Sweigart, D. A. *Inorg. Chem.* **1981**, *20*, 1683.

Table I. Rate Data for the Forward Reaction of $HRu_3(CO)_{11}^-$ Plus PPh_3 As Calculated According to the Kinetic Analysis Described for Scheme I

solv	temp, °C	atm	k_1, s^{-1}	$k_{-1}[CO]/k_1k_2$[a]
THF	25.0	100% CO	2.1 ± 0.1[b]	0.108
THF	25.0	25% CO	2.3 ± 0.2[b]	0.0321
THF	25.0	10% CO	2.0 ± 0.2[b]	0.0106
THF	9.4	N_2	0.36 ± 0.01[c]	
THF	25.0	N_2	2.1 ± 0.1[c]	
THF	37.6	N_2	5.1 ± 0.1[c]	
$\Delta H^\ddagger$ = 16.0 ± 1.7 kcal/mol; $\Delta S^\ddagger$ = −1.9 ± 3.0 cal/(deg mol)				
DMTHF	8.1	N_2	0.26 ± 0.02[c]	
DMTHF	25.0	N_2	1.6 ± 0.1[c]	
DMTHF	38.1	N_2	5.8 ± 0.1[c]	
$\Delta H^\ddagger$ = 17.9 ± 0.3 kcal/mol; $\Delta S^\ddagger$ = 2.7 ± 0.8 cal/(deg mol)				

[a] Slopes of plots in Figure 5. [b] Calculated from the inverse of the intercepts of plots as in Figure 5. [c] Limiting k_{obsd} values measured at high $[PPh_3]$.

of P_{CO} with intercepts independent of P_{CO} and slopes linearly dependent on P_{CO} as predicted. From these plots an average value of k_1 = 2.1 ± 0.1 is derived, consistent with the limiting k_{obsd} measured under dinitrogen (Table I). Given that [CO] = 0.016 M in 25 °C THF[10] under P_{CO} = 1.0 atm, the ratio k_{-1}/k_2 = 15 ± 4 can be calculated from the slopes of these plots. This represents the discrimination of the intermediate (presumably $HRu_3(CO)_{10}^-$) toward reaction with CO relative to reaction with PPh_3.

Kinetics of the forward reaction were run under N_2 for the temperatures 9.4 and 37.6 °C as well. The k_1 values obtained from k_{obsd}(limiting) at these temperatures (0.36 and 5.1 s^{-1}, respectively) were plotted according to the Eyring equation to give the activation parameters for k_1 in THF: $\Delta H^\ddagger$ = 16.0 ± 1.7 kcal/mol and $\Delta S^\ddagger$ = −1.9 ± 3.0 cal/(deg mol).

One possible explanation for the reactively low value of $\Delta H^\ddagger$ would be that this reflects an associative reaction of a solvent molecule with $HRu_3(CO)_{11}^-$ to labilize a carbonyl. This possibility was explored by using a similar, but more sterically hindered and less coordinating solvent[12] 2,5-dimethyltetrahydrofuran (DMTHF). The reaction conditions for studying the forward reaction were otherwise identical to those in THF. The kinetics, followed spectrophotometrically at 430 nm, gave linear ln $(A - A_\infty)$ vs. time plots. The k_1(DMTHF) values derived from the intercepts of plots of $(k_{obsd})^{-1}$ vs. $[PPh_3]^{-1}$ at 8.0, 25.0, and 38.1 °C were found to equal 0.26 ± 0.02 s^{-1}, 1.6 ± 0.1 s^{-1}, and 5.8 ± 0.1 s^{-1}, respectively. These values gave activation parameters of $\Delta H^\ddagger$ = 17.9 ± 0.3 kcal/mol and $\Delta S^\ddagger$ = 2.7 ± 0.8 cal/(deg mol). It is notable that the k_1 values are only marginally different in DMTHF than in THF and that the activation parameters in DMTHF are within experimental uncertainity to those obtained for k_1 in THF.

Rates of the reverse reaction were obtained for the reaction of $[PPN][HRu_3(CO)_{10}PPh_3]$ with CO in THF. The substituted cluster $[PPN][HRu_3(CO)_{10}PPh_3]$ was prepared in situ by the addition of a 10–40-fold excess of PPh_3 to solutions of $[PPN][HRu_3(CO)_{11}]$ under N_2. The solutions were degassed by four freeze–pump–thaw cycles to remove the resultant CO. The reactions were then monitored by observing the decrease in absorbance at 430 nm upon mixing with solvent containing CO. Plots of ln $(A - A_\infty)$ vs. time obtained over the [CO] range of 0.0008–0.008 M were linear for more than 3 half-lives showing the reaction to be first order in $[HRu_3(CO)_{10}PPh_3^-]$. Plots of k_{obsd} vs. [CO] at constant $[PPh_3]$ were nonlinear, but limiting k_{obsd} values were not obtained even at the highest P_{CO} employed. The k_r term defined above (eq 8) can be written as

$$k_r = \frac{k_{-1}k_{-2}[CO]}{k_{-1}[CO] + k_2[PPh_3]} = \frac{k_{obsd}}{1 + ([PPh_3]/[CO])(K)} \quad (11)$$

A plot of $(k_r)^{-1}$ vs. $[PPh_3]/[CO]$ is linear with a nonzero intercept, $(k_{-2})^{-1}$ (Figure 6). The value of k_{-2} obtained at 25 °C is 0.46 ± 0.02 s^{-1}. The reverse reaction was run at 10.5, 25.0, and 37.6 °C, and the rate constants k_{-2} determined for these tempertures were 0.11 ± 0.02 s^{-1}, 0.46 ± 0.02 s^{-1}, and 2.0 ± 0.2 s^{-1}, respectively. The activation parameters for the loss of PPh_3 from $[PPN][HRu_3(CO)_{10}PPh_3]$ in THF are $\Delta H^\ddagger$ = 18.2 ± 1.2 kcal/mol and $\Delta S^\ddagger$ = 1.0 ± 4.0 cal/(deg mol).

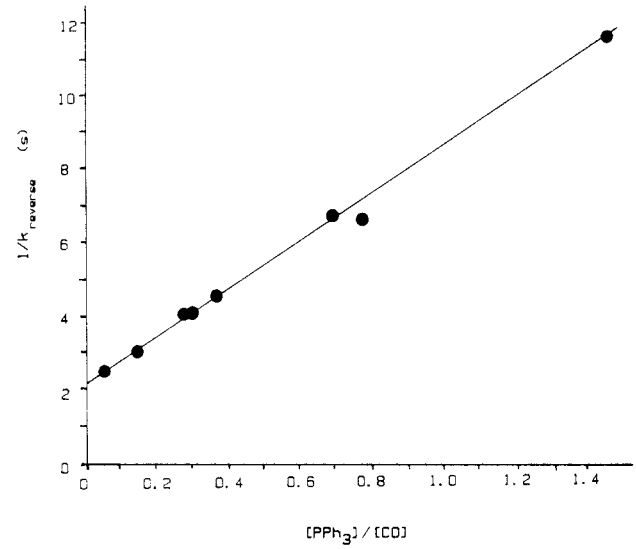

Figure 6. Plot of $1/k_r$ vs. $[PPh_3]/[CO]$ according to eq 11 for the reaction of $HRu_3(CO)_{10}PPh_3^-$ plus CO in THF at 25 °C.

The dissociative mechanism proposed in Scheme I predicts the limiting k_1 values to be independent of the nature of the incoming ligand L. This prediction was tested by examining the kinetics for the reaction of $HRu_3(CO)_{11}^-$ with excess PBu_3 (0.007–0.10 M) in THF under a 10% CO (90% N_2) atmosphere. First-order rate behavior was observed by following the disappearance of $HRu_3(CO)_{11}^-$ at 376 nm (25 °C). The double reciprocal plot, k_{obsd}^{-1} vs. $[PBu_3]^{-1}$, was found to be linear as predicted by Scheme I with slope and intercept virtually identical with those observed for reaction with PPh_3 under the same conditions. The k_1 value, 2.1 ± 0.2 s^{-1} (intercept)$^{-1}$, so calculated is identical with the value found for PPh_3, as would be expected for the proposed dissociative mechanism. Notably, the k_{-1}/k_2 value for PBu_3, calculated as above, is 14 ± 2, within experimental uncertainty the same as found for PPh_3. Thus, it appears that while the suggested intermediate $HRu_3(CO)_{10}^-$ is roughly an order of magnitude more reactive with CO than with either phosphine, it differentiates little between PPh_3 and PBu_3.

Discussion

The substitution of a carbonyl on $HRu_3(CO)_{11}^-$ by PPh_3 in THF solution is a particularly facile process occurring at rates conveniently measured with a stopped-flow spectrophotometer and displaying a relatively low activation enthalpy. The reverse reaction has similar characteristics. These properties contrast strongly with the analogous substitution reactions of the neutral clusters $Ru_3(CO)_{12}$ and $Ir_4(CO)_{12}$ which are orders of magnitude less labile toward substitution.[13,14] Another key difference is

(12) Gutmann, V. *Coord. Chem. Rev.* **1976**, *18*, 225.

the reluctance of the hydride triruthenium core to undergo multiple substitutions in the presence of PPh_3. However, spectral changes indicating the formation of disubstitution products were observed in the presence of excess PBu_3, and trisubstitution products were observed in the presence of excess $P(OCH_3)_3$.[1]

In eq 4 and 5 it was suggested that the reaction kinetics, especially the inhibition of CO substitution by excess CO, could be interpreted in terms of a mechanism involving CO dissociation to give the unsaturated intermediate $HRu_3(CO)_{10}^-$ which would undergo competitive addition with CO or PPh_3. The rate law is fully consistent with this mechanism as is the observation that the identical limiting k_1 value was measured for the reaction of $HRu_3(CO)_{11}^-$ with PBu_3. However, the kinetic data would be equally consistent with an alternative mechanism proceeding via an unimolecular step giving an intermediate subject to competitive trapping by these two ligands. An example of such an alternative would be the associative reaction with solvent to displace the leaving group and form a solvento intermediate complex, e.g., eq 12, followed by

$$HRu_3(CO)_{11}^- + S \rightarrow HRu_3(CO)_{10}S^- + CO \quad (12)$$

nucleophilic attack by either CO or PPh_3 to give $HRu_3(CO)_{11}^-$ or $HRu_3(CO)_{10}PPh_3^-$, respectively. The limiting "unimolecular" rate constant k_1 would be for eq 12, since solvent would not appear in the rate law. However, the values and activation parameters for k_1 are nearly identical for reactions run in THF and DMTHF (Table I), a strong indication that the solvent is not as intimately involved as suggested by eq 12.

Another alternative for the k_1 step would be a unimolecular isomerization to give a more reactive species of the same chemical composition, e.g., eq 13. Such an isomer

$$HRu_3(CO)_{11}^- \rightarrow \text{"}HRu_3(CO)_{11}^-\text{"} \quad (13)$$

could be one where a metal–metal bond has been broken simultaneous with motion of a ligand to or from a bridging configuration[13a,15] (e.g., B) or one where migration of the hydride to a carbonyl has occurred to give a formyl complex[5,16] (e.g., C), in each case opening a coordination site

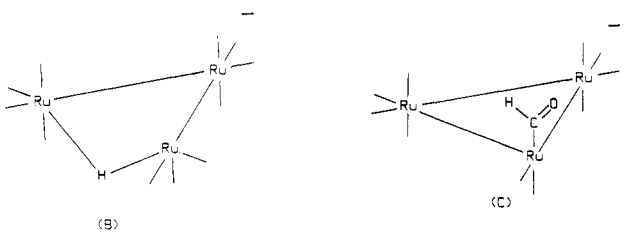

to reaction with a two-electron donor. Rate behavior of the type described here would be duplicated if the intermediate "$HRu_3(CO)_{11}^-$" were quenched by reacting irreversibly with CO or proceeded along the forward reaction coordinate by reacting with PPh_3, first to give a new intermediate, "$HRu_3(CO)_{11}PPh_3^-$", and then the product, *and* if the analogous intermediate formed by isomerization of $HRu_3(CO)_{10}PPh_3^-$ were quenched by reacting with PPh_3 or proceeded along the back reaction coordinate by reacting with CO to give the "$HRu_3(CO)_{11}PPh_3^-$" intermediate. Although such a mechanism involving at least five different intermediates can be constructed without violating the principle of microscopic reversiblity, there appears to be no evidence at present supporting so detailed a hypothesis. Furthermore, the pathways for which cluster intermediates of the type depicted in B or C have been proposed[5,13] are concerned with cluster fragmentation or displacement of the hydride, and there is no indication of either of these processes occurring in the present case.

Thus, we believe that a dissociative mechanism as indicated in eq 4 and 5 is the most likely explanation of the observed substitution rate behavior. However, the high lability and low activation enthalpy of the reactions of both $HRu_3(CO)_{11}^-$ and $HRu_3(CO)_{10}PPh_3^-$ need to be addressed in the context of rate studies other triruthenium clusters. For example, investigation of the substitution reactions of $Ru_3(CO)_{12}$ in hydrocarbon solutions have concluded that two mechanisms are operative, a dissociation mechanism analogous to eq 4 and 5 and a second-order mechanism. The k_1 value of the former pathway (1.1×10^{-5} s^{-1} at 40 °C) is more than 5 orders of magnitude less than that for $HRu_3(CO)_{11}^-$ and has activation enthalpy 14 kcal/mol larger.[13] Even more significant is the report[17] that methylation of the bridging CO of $HRu_3(CO)_{11}^-$ to give $HRu_3(\mu\text{-}COCH_3)(CO)_{10}$ leads to reduced lability toward first-order CO labilization by roughly 5 orders of magnitude ($k_{obsd} = 3.2 \times 10^{-5}$ s^{-1} in heptane at 24 °C for 0.010 M PPh_3 under N_2 atmosphere) with a corresponding increase in ΔH^* (27 kcal/mol).[17] Notably even the presence of alkali-metal cations (rather than PPN^+) as the counterion to $HRu_3(CO)_{11}^-$ has been shown[18] to slow the exchange between coordinated and solution CO in THF, a result which can be attributed to formation of tight ion pairs at the bridging CO, the most negative site on the cluster.[19]

Several rationalization can be offered for the high lability of $HRu_3(CO)_{11}^-$ toward CO dissociation. For example, the structure of this anion displays elongated Ru–CO bonds for those carbonyls trans to bridging carbonyl[2] suggesting some ground state destabilizing contribution to the CO dissociation. However, similar elongations are seen in other $HRu_3(\mu\text{-}CX)(CO)_{10}$ derivatives (X = OCH_3 or $N(CH_3)_2$),[20] yet there is no correlation between the extent of such bond lengthening and the observed substitution rates.

The low ΔH^* values for $HRu_3(CO)_{11}^-$ are likely to reflect a lowering of the barrier for ligand dissociation owing to some special stabilization of the intermediate "$HRu_3(CO)_{10}^-$". A likely structure for such an intermediate is D. However, it is not clear why an analogous species formed via CO dissociation from other $HRu_3(\mu\text{-}CX)(CO)_{10}$ derivatives would not be equally stabilized, unless the reason lies in the tendency of anionic complexes to favor species with bridging carbonyls.[21]

(13) (a) Poe, A.; Twigg, M. V. *J. Chem. Soc., Dalton. Trans.* **1974**, 1860. (b) Malik, S. K., Poe, A. *Inorg. Chem.* **1978**, *17*, 1484 and references therein.

(14) (a) Karel, K. J.; Norton, J. R. *J. Am. Chem. Soc.* **1974**, *96*, 6812. (b) Sonnenberger, D. C.; Atwood, J. D. *Inorg. Chem.* **1981**, *20*, 3243. (c) Sonnenberger, D. C.; Atwood, J. D. *J. Am. Chem. Soc.* **1982**, *104*, 2113. (d) Darensbourg, D. J.; Baldwin-Zuschke, B. J. *J. Am. Chem. Soc.* **1982**, *104*, 3906.

(15) (a) A similar mechanism has been suggested for several photochemical reactions of polynuclear metal compounds including photofragmentation reactions of $Ru_3(CO)_{12}$.[15] (b) Desrosiers, M. F.; Ford, P. C. *Organometallics* **1982**, *1*, 1715. (c) Malito, J.; Markiewicz, S.; Poe, A. *Inorg. Chem.* **1982**, *21*, 4335.

(16) Pearson, R. G.; Walker, H. W.; Mauermann, H.; Ford, P. C. *Inorg. Chem.* **1981**, *20*, 2741.

(17) Dalton, D. M.; Barnett, D. J.; Duggan, T. P.; Keister, J. B.; Malik, P. T.; Modi, S.; Shaffer, M. R.; Smeski, S. A.; submitted for publication.

(18) Shore, S. G.; Bricker, J. C.; Bhattacharyya, A. A.; Nagel, C. C., reported at the 1984 International Chemical Congress of Pacific Basin Societies, Symposium on Metal Cluster chemistry, Honolulu, HI, Dec 1984; Paper 07N07.

(19) Keister, J. B. *J. Organomet. Chem.* **1980**, *190*, C36.

(20) (a) Johnson, B. F. G.; Lewis, J.; Guy Orpen, A.; Raithby, P. R.; Suss, G. *J. Organomet: Chem.* **1979**, *173*, 187. (b) Churchill, M. R.; Beanan, L. R.; Wasserman, H. J.; Bueno, C.; Abdul Rahman, Z.; Keister, J. B. *Organometallics* **1983**, *2*, 1179. (c) Churchill, M. R.; DeBoer, B. G.; Rotella, F. J. *Inorg. Chem.* **1976**, *15*, 1843.

(21) Avanzino, S. C.; Jolly, W. L. *J. Am. Chem. Soc.* **1976**, *98*, 6505.

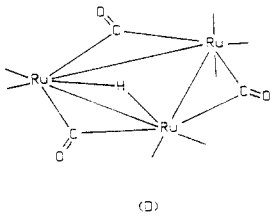

(D)

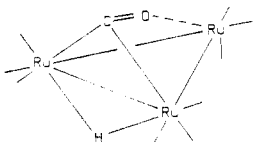

(E)

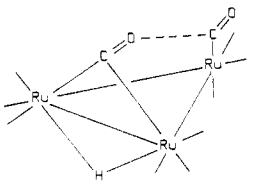

(F)

Another attractive proposal was the suggestion by Keister[17] that the ligand substitution in the $HRu_3(\mu\text{-}CX)(CO)_{10}$ series may reflect an internal nucleophilic attack of the X group on the unique ruthenium center, displacing a CO to give an intermediate such as E. The higher reactivity of $HRu_3(CO)_{11}^-$ could then be attributed to the more nucleophilic character of the oxygen of the bridging CO relative to, for example, the oxygen of the μ-$COCH_3$ group of $HRu_3(\mu\text{-}COCH_3)(CO)_{10}$. In support of such a proposal, there is ample precedent for the interaction of a bridging ligand with all three metals of a triangular cluster to form stable η^2-μ_3 complexes.[22] However, the recent demonstrations that nucleophiles capable of forming adducts with coordinated CO are particularly effective catalysts for the ligand substitution reactions of metal clusters[23,24] suggest an alternative possible role of the μ-CO group, namely, nucleophilic attack on an axial CO of the unique ruthenium rather than at the metal center itself.[25] The resulting intermediate F would then be expected to undergo rapid ligand dissociation given the lability of such nucleophilic adducts.[23]

In summary, it is clear that the hydride anion $HRu_3(CO)_{11}^-$ is dramatically more reactive toward carbonyl substitution than the neutral carbonyl clusters $Ru_3(CO)_{12}$ or $HRu_3(\mu\text{-}COCH_3)(CO)_{10}$. The substitution kinetics suggest a dissociative mechanism, and the low $\Delta H^\ddagger$ value may indicate an unusually stabilized transition state and/or intermediate for CO dissociation. However, the present information is not sufficient to characterize the precise nature of such an intermediate.

Acknowledgment. This work was supported by a U.S. Department of Energy (office of Basic Energy Sciences) contract to P.C.F.. We thank Johnson-Matthey Inc. for a loan of ruthenium and Dr. J. Keister (SUNY—Buffalo) for communicating a copy of ref 17 prior to publication. D.J.T. thanks Dr. M. M. Doeff for many helpful discussions.

Registry No. $HRu_3(CO)_{11}^-$, 60496-59-5; PPh_3, 603-35-0; PBu_3, 998-40-3.

(22) (a) Kaesz, H. D.; Knobler, C. B.; Andrews, M. A.; van Busbird, G. *Pure Appl. Chem.* **1982**, *54*, 131. (b) Schink, K. P.; Jones, N. L.; Sekula, P.; Bosag, N. M.; Labinger, J. A.; Kaesz, H. D. *Inorg. Chem.* **1984**, *23*, 2204. (c) Barner-Thorsen, C.; Rosenberg, E.; Saatjian, G.; Aime, S.; Milone, L.; Osella, D. *Inorg. Chem.* **1981**, *20*, 1592.

(23) Anstock, M.; Taube, D.; Gross, D. C.; Ford, P. C. *J. Am. Chem. Soc.* **1984**, *106*, 3696.

(24) (a) Morris, D. E.; Basolo, F. *J. Am. Chem. Soc.* **1968**, *90*, 2536. (b) Brown, T. L.; Bellus, P. A. *Inorg. Chem.* **1978**, *17*, 3726. (c) Darensbourg, D. L.; Gray, R. L.; Pala, M. *Organometallics* **1984**, *3*, 1928. (d) Lavigne, G.; Kaesz, H. D. *J. Am. Chem. Soc.* **1984**, *106*, 4647.

(25) In this context it is notable that according to the atomic coordinates given in ref 2, the μ-CO oxygen of A is ~0.9 Å closer to the carbon of the axial CO than to the metal atom of the unique $Ru(CO)_4$ group.

Diamagnetic Anisotropy of Organometallic Moieties: χ Values for $M(CO)_3$ (M = Cr, Mo, W) and for Ferrocene

Michael J. McGlinchey,*† Robert C. Burns,† Roger Hofer,† Siden Top,‡ and Gérard Jaouen‡

Department of Chemistry, McMaster University, Hamilton, Ontario, L8S 4M1, Canada, and Ecole Nationale Supérieure de Chimie, 75231 Paris Cedex 05, France

Received May 30, 1985

Proton NMR chemical shifts are profoundly influenced by their proximity to metal carbonyl moieties. It is shown that the McConnell relationship can be used to evaluate the diamagnetic anisotropy of carbonyl ligands in $M(CO)_3$ fragments, where M = Cr, Mo, and W. The 500-MHz ^1H NMR spectra of the α- and β-$Cr(CO)_3$ complexes of an estradiol derivative reveal that protons proximate to the tripod are deshielded relative to their resonance positions when they are distal to the metal carbonyl moiety. The chemical shift differences together with the geometric terms yield a χ value of -490×10^{-36} m^3/molecule for a chromium carbonyl ligand. Analogous calculations are presented for molybdenum and tungsten carbonyls and also for the ferrocene molecule.

Introduction

The effect of the anisotropy in diamagnetic susceptibility of certain organic functional groups upon the NMR chemical shifts of neighboring nuclei in the molecule is a well-established phenomenon. Perhaps the clearest examples are provided by the alkyne and benzene systems. In the first case, one can readily envisage that when the applied magnetic field B_0 is along the molecular axis, there is no hindrance to circulation of the electrons in the C≡C bond and so the temperature-independent paramagnetic term will be zero. In contrast, when B_0 is perpendicular to the axis, the nuclei hinder the circulation and the paramagnetic effect is strong.[1]

† McMaster University.
‡ Ecole Nationale Supérieure de Chimie.

(1) Harris, R. K. "Nuclear Magnetic Resonance Spectroscopy"; Pitman: London, England, 1983; p 193.

0276-7333/86/2305-0104$01.50/0

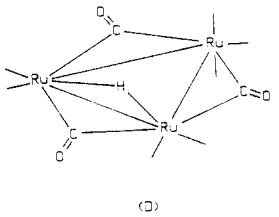

(D)

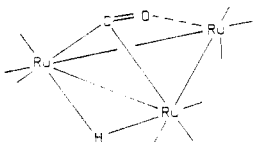

(E)

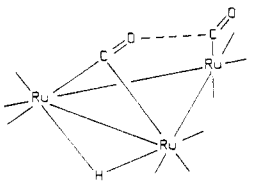

(F)

Another attractive proposal was the suggestion by Keister[17] that the ligand substitution in the $HRu_3(\mu\text{-}CX)(CO)_{10}$ series may reflect an internal nucleophilic attack of the X group on the unique ruthenium center, displacing a CO to give an intermediate such as E. The higher reactivity of $HRu_3(CO)_{11}^-$ could then be attributed to the more nucleophilic character of the oxygen of the bridging CO relative to, for example, the oxygen of the μ-$COCH_3$ group of $HRu_3(\mu\text{-}COCH_3)(CO)_{10}$. In support of such a proposal, there is ample precedent for the interaction of a bridging ligand with all three metals of a triangular cluster to form stable η^2-μ_3 complexes.[22] However, the recent demonstrations that nucleophiles capable of forming adducts with coordinated CO are particularly effective catalysts for the ligand substitution reactions of metal clusters[23,24] suggest an alternative possible role of the μ-CO group, namely, nucleophilic attack on an axial CO of the unique ruthenium rather than at the metal center itself.[25] The resulting intermediate F would then be expected to undergo rapid ligand dissociation given the lability of such nucleophilic adducts.[23]

In summary, it is clear that the hydride anion $HRu_3(CO)_{11}^-$ is dramatically more reactive toward carbonyl substitution than the neutral carbonyl clusters $Ru_3(CO)_{12}$ or $HRu_3(\mu\text{-}COCH_3)(CO)_{10}$. The substitution kinetics suggest a dissociative mechanism, and the low $\Delta H^\ddagger$ value may indicate an unusually stabilized transition state and/or intermediate for CO dissociation. However, the present information is not sufficient to characterize the precise nature of such an intermediate.

Acknowledgment. This work was supported by a U.S. Department of Energy (office of Basic Energy Sciences) contract to P.C.F.. We thank Johnson-Matthey Inc. for a loan of ruthenium and Dr. J. Keister (SUNY—Buffalo) for communicating a copy of ref 17 prior to publication. D.J.T. thanks Dr. M. M. Doeff for many helpful discussions.

Registry No. $HRu_3(CO)_{11}^-$, 60496-59-5; PPh_3, 603-35-0; PBu_3, 998-40-3.

(22) (a) Kaesz, H. D.; Knobler, C. B.; Andrews, M. A.; van Busbird, G. *Pure Appl. Chem.* **1982**, *54*, 131. (b) Schink, K. P.; Jones, N. L.; Sekula, P.; Bosag, N. M.; Labinger, J. A.; Kaesz, H. D. *Inorg. Chem.* **1984**, *23*, 2204. (c) Barner-Thorsen, C.; Rosenberg, E.; Saatjian, G.; Aime, S.; Milone, L.; Osella, D. *Inorg. Chem.* **1981**, *20*, 1592.

(23) Anstock, M.; Taube, D.; Gross, D. C.; Ford, P. C. *J. Am. Chem. Soc.* **1984**, *106*, 3696.

(24) (a) Morris, D. E.; Basolo, F. *J. Am. Chem. Soc.* **1968**, *90*, 2536. (b) Brown, T. L.; Bellus, P. A. *Inorg. Chem.* **1978**, *17*, 3726. (c) Darensbourg, D. L.; Gray, R. L.; Pala, M. *Organometallics* **1984**, *3*, 1928. (d) Lavigne, G.; Kaesz, H. D. *J. Am. Chem. Soc.* **1984**, *106*, 4647.

(25) In this context it is notable that according to the atomic coordinates given in ref 2, the μ-CO oxygen of A is ~0.9 Å closer to the carbon of the axial CO than to the metal atom of the unique $Ru(CO)_4$ group.

Diamagnetic Anisotropy of Organometallic Moieties: χ Values for $M(CO)_3$ (M = Cr, Mo, W) and for Ferrocene

Michael J. McGlinchey,*† Robert C. Burns,† Roger Hofer,† Siden Top,‡ and Gérard Jaouen‡

Department of Chemistry, McMaster University, Hamilton, Ontario, L8S 4M1, Canada, and Ecole Nationale Supérieure de Chimie, 75231 Paris Cedex 05, France

Received May 30, 1985

Proton NMR chemical shifts are profoundly influenced by their proximity to metal carbonyl moieties. It is shown that the McConnell relationship can be used to evaluate the diamagnetic anisotropy of carbonyl ligands in $M(CO)_3$ fragments, where M = Cr, Mo, and W. The 500-MHz ^1H NMR spectra of the α- and β-$Cr(CO)_3$ complexes of an estradiol derivative reveal that protons proximate to the tripod are deshielded relative to their resonance positions when they are distal to the metal carbonyl moiety. The chemical shift differences together with the geometric terms yield a χ value of -490×10^{-36} m^3/molecule for a chromium carbonyl ligand. Analogous calculations are presented for molybdenum and tungsten carbonyls and also for the ferrocene molecule.

Introduction

The effect of the anisotropy in diamagnetic susceptibility of certain organic functional groups upon the NMR chemical shifts of neighboring nuclei in the molecule is a well-established phenomenon. Perhaps the clearest examples are provided by the alkyne and benzene systems. In the first case, one can readily envisage that when the applied magnetic field B_0 is along the molecular axis, there is no hindrance to circulation of the electrons in the C≡C bond and so the temperature-independent paramagnetic term will be zero. In contrast, when B_0 is perpendicular to the axis, the nuclei hinder the circulation and the paramagnetic effect is strong.[1]

† McMaster University.
‡ Ecole Nationale Supérieure de Chimie.

(1) Harris, R. K. "Nuclear Magnetic Resonance Spectroscopy"; Pitman: London, England, 1983; p 193.

0276-7333/86/2305-0104$01.50/0

A simple classical model would suggest that, upon application of a magnetic field, induced electron circulation about the C_∞ axis can occur. The consequently induced field will oppose the applied field so that protons along the molecular axis require a larger applied field to bring them into resonance. As a corollary, one would expect protons close to the horizontal plane to be deshielded; this is in fact the case.[2] A simple mathematical model, proposed by McConnell,[3] relates the chemical shift increment, σ, and the molar diamagnetic anisotropy, χ, through the geometric term in eq 1, where R is the distance from the

$$\sigma = \frac{\chi}{N}\frac{(1 - 3\cos^2\theta)}{3R^3} \quad (1)$$

electrical center of gravity of the bond to the proton and θ is the angle made by R with the multiple-bond axis. For the present case, where the bond is cylindrically symmetrical, χ is the difference between the longitudinal susceptibility ($\chi_\parallel$; along the bond axis) and the transverse principal susceptibilities ($\chi_\perp' = \chi_\perp''$; perpendicular to the bond).

To evaluate χ for a particular functional group, it is necessary to position two protons (whose chemical shifts would be identical in the absence of the anisotropic group) in different geometric dispositions with respect to the center of anisotropy. Thus, for two otherwise equivalent nuclei with chemical shifts σ_1 and σ_2 and geometric terms G_1 and G_2, respectively, the diamagnetic anisotropy can be evaluated via eq 2.

$$(\sigma_1 - \sigma_2) = \chi(G_1 - G_2) \quad (2)$$

A more extreme range of shifts is seen for protons near arene rings, and the concept of an aromatic ring current with its shielding and deshielding zones is frequently invoked in organic chemistry.[4] Similarly, χ values for other organic functional groups, such as C≡C, C=O, and N=O, have been tabulated.[5] In contrast, the diamagnetic anisotropic contributions attributable to organometallic moieties have been little investigated. As was pointed out by San Filippo some years ago,[6] metal–metal multiple bonds should be decidedly anisotropic and the NMR chemical shifts of protons situated proximate to such functionalities should be markedly dependent upon their geometric disposition with respect to the metal–metal multiple-bond axis. Calculation of the diamagnetic anisotropy of metal–metal triple bonds became possible recently when Cotton and Chisholm reported that the dimethylamino groups of $(Me_2N)_3Mo{\equiv}Mo(NMe_2)_3$ exhibited slow rotation about the Mo—N bond at low temperatures. Thus, the proximal methyl groups were deshielded by 1.88 ppm relative to their distal partners.[7] This chemical shift difference, together with a knowledge of the molecular geometry, allowed the evaluation of χ for the Mo≡Mo bond.[8] This in turn led to a rationalization of other proton shifts in the vicinity of metal–metal triple bonds.[9]

Table I. ^{1}H NMR Chemical Shifts (δ) of (Estradiol)Cr(CO)$_3$ Complexes

hydrogen	α-complex	β-complex
6α	2.76	2.44
6β	2.56	3.01
7α	1.61	1.11
7β	1.72	1.90
8β	1.17	1.80
9α	2.15	1.85
11α	1.93	1.97
11β	1.27	1.95

We now present data extending our original ideas to other organometallic fragments, viz., carbonyl ligands in $M(CO)_3$ groups, where M = Cr, Mo, and W, and also for the ferrocene system.

Results and Discussion

It is well-known that the π-complexation of an arene to a $Cr(CO)_3$ unit leads to an upfield shift of 1.5–2 ppm; this has been attributed to a variety of effects such as the diminution of the ring current, the magnetic anisotropy of the metal arene bond, or the electron-withdrawing effect of the metal carbonyl moiety.[10] However, it is rather difficult to attempt a separation of these effects to see which, if any, of them are significant. More recently, it has been pointed out that changes in the local anisotropic terms associated with the aromatic ring carbons can account for at least part of this shielding.[11] As described above, one approach to evaluating the diamagnetic anisotropic contribution of a $Cr(CO)_3$ group would be to site otherwise equivalent protons in differing geometric positions relative to the tripodal moiety. Fortuitously, this criterion is beautifully fulfilled by some molecules synthesized in our laboratories in connection with our bioorganometallic endeavors.

In our quest for organometallic derivatives of steroidal hormones which might be of use in monitoring the hormonal dependence of breast cancer,[12] we synthesized the $Cr(CO)_3$ derivatives of β-estradiol and several related complexes. The tripodal fragment can complex either to the α- or the β-face of the hormones giving rise to diastereomeric pairs. After separation of these stereoisomers, they were examined by ^{1}H NMR spectroscopy at 500 MHz, and, with the full armamentarium of two-dimensional proton–proton and proton–carbon correlation techniques, we were able to identify unambiguously all the protons in the steroid skeleton.[13] In particular, one can now see clearly the effect on each proton of placing the $Cr(CO)_3$

(2) Agarwal, A.; McGlinchey, M. J. *Can. J. Chem.* **1978**, *56*, 959.
(3) McConnell, H. M. *J. Chem. Phys.* **1957**, *27*, 226.
(4) Haigh, C. W.; Mallion, R. B. *Prog. Nucl. Magn. Reson. Spectrosc.* **1980**, *13*, 303.
(5) (a) Reddy, G. S.; Goldstein, J. H. *J. Chem. Phys.* **1963**, *39*, 2644. (b) Jackman, L. M.; Sternhell, S. "Applications of NMR Spectroscopy in Organic Chemistry", 2nd ed.; Pergamon Press: Oxford, England, 1969; pp 76–94 and references therein.
(6) San Filippo, J. *Inorg. Chem.* **1972**, *11*, 3140.
(7) (a) Chisholm, M. H.; Cotton, F. A.; Freng, B. A.; Reichert, W. W.; Shive, L. W.; Stults, B. R. *J. Am. Chem. Soc.* **1976**, *98*, 4469. (b) Chisholm, M. H.; Cotton, F. A.; Extine, M. W.; Stults, B. R. *J. Am. Chem. Soc.* **1976**, *98*, 4477.
(8) McGlinchey, M. J. *Inorg. Chem.* **1980**, *19*, 1392.
(9) Chetcuti, M. J.; Chisholm, M. H.; Folting, K.; Haitko, D. A.; Huffman, J. C.; Janos, J. *J. Am. Chem. Soc.* **1983**, *105*, 1163.
(10) (a) Deubzer, B.; Fritz, H. P.; Kreiter, C. G.; Öfele, K. *J. Organomet. Chem.* **1967**, *7*, 289. (b) Carroll, D. G.; McGlynn, S. P. *Inorg. Chem.* **1968**, *7*, 1285. (c) Brown, D. A.; Rawlinson, R. W. *J. Chem. Soc. A* **1969**, 1530. (d) McFarlane, W.; Grim, S. O. *J. Organomet. Chem.* **1966**, *5*, 147. (e) Fritz, H. P.; Kreiter, C. G. *J. Organomet. Chem.* **1967**, *7*, 427. (f) Price, J. T.; Sorenson, T. S. *Can. J. Chem.* **1968**, *46*, 515. (g) Emmanuel, R. V.; Randall, E. W. *J. Chem. Soc. A* **1969**, 3002. (h) Wu, A.; Biehl, E. R.; Reeves, P. C. *J. Chem. Soc., Perkin Trans. 2* **1972**, 449. (i) Khandkarova, V. S.; Gubin, S. P.; Kvasov, B. A. *J. Organomet. Chem.* **1970**, *23*, 509. (j) Siedle, A. R.; Bodner, G. M. *Inorg. Chem.* **1972**, *11*, 3108. (k) Langer, E.; Lehner, H. *J. Organomet. Chem.* **1979**, *173*, 47. (l) Keller, L. S. *Tetrahedron Lett.* **1978**, 2361.
(11) Maricq, M. M.; Waugh, J. S.; Fletcher, J. L.; McGlinchey, M. J. *J. Am. Chem. Soc.* **1978**, *100*, 6902.
(12) (a) Top, S.; Vessières, A.; Abjean, J.-P.; Jaouen, G. *J. Chem. Soc., Chem. Commun.* **1984**, 428. (b) Jaouen, G.; Top, S.; Laconi, A.; Couturier D.; Brochard, J. *J. Am. Chem. Soc.* **1984**, *106*, 2207. (c) Jaouen, G.; Vessières, A.; Top, S.; Ismail, A. A.; Butler, I. S. *C.R. Acad. Sci., Ser. 2* **1984**, *298*, 683.
(13) Top, S.; Jaouen, G.; Vessières, A.; Abjean, J.-P.; Davoust, D.; Rodger, C. A.; Sayer, B. G.; McGlinchey, M. J. *Organometallics* **1985**, *4*, 2143.

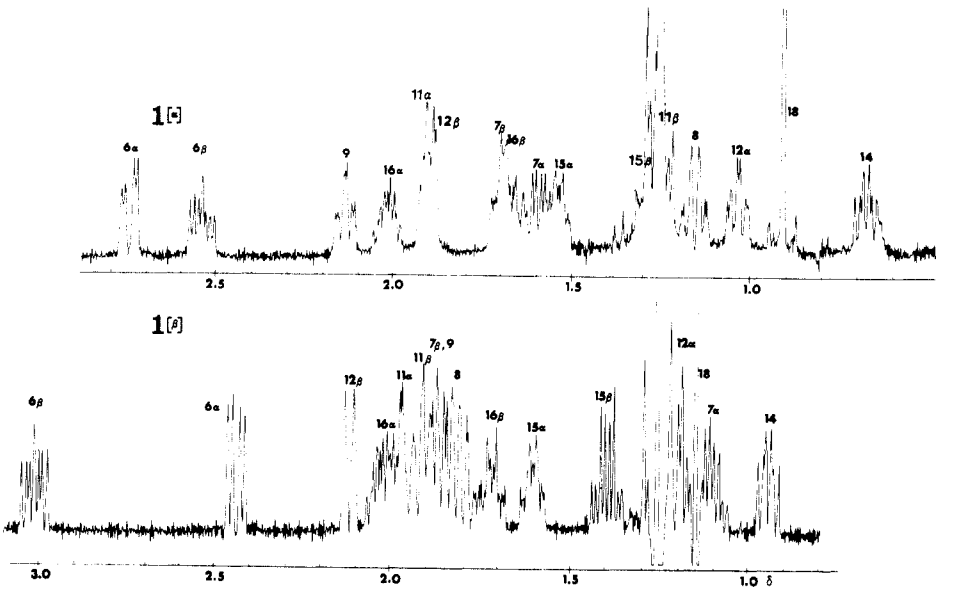

Figure 1. Sections of the 500-MHz ^{1}H NMR spectra of the (steroid)$Cr(CO)_3$ complexes 1[α] and 1[β].

unit either proximal or distal to it. It is obvious that the inherent shift of, for example, the 7α proton should not change depending on the site of complexation of the organometallic functionality. **[Note added in proof:** Strictly speaking, this condition will not always hold. It has very recently been shown that the shifts of exo and endo protons in organometallic π-complexes can be affected slightly differently by very highly anisotropic solvents.[29]] The electron-withdrawing effect of the $Cr(CO)_3$ group and its perturbation of the arene ring current should be the same whether it is bonded to the α- or to the β-face of the steroid. Thus, all other extraneous effects having been compensated for, the incremental chemical shift for a given proton environment must be dependent only on its geometric disposition with respect to the anisotropic group. We note also that crystallographic data for the noncomplexed steroid[14] and for a chromium complex[15] show that distortions of the steroid skeleton are minimal. The vicinal coupling constants ($^3J_{H-H}$) are also virtually identical in the free and complexed ligands;[13] this again indicates that the steroid structure does not change to any appreciable extent upon coordination.

Figure 1 shows sections of the 500-MHz ^{1}H NMR spectra of the α- and β-$Cr(CO)_3$ complexes of a diprotected estradiol, 1, where R = benzyl and R′ = dimethyl-*tert*-butylsilyl. The assignments, which were obtained via two-dimensional COSY and SECSY experiments,[16] are listed in Table I. It is immediately apparent that siting the chromium on the α- or the β-face causes dramatically different effects on the protons in the B ring of the steroid. As would be expected for a geometric term involving an inverse cube dependence on distance, the effect on the nuclei in the C and D rings is rather small. We, therefore, focussed our attention on the protons at C-6, C-7, C-8, C-9, and C-11. The most striking feature which emerges from these spectra is that protons proximal to the metal carbonyl group are deshielded relative to their resonance positions when the $Cr(CO)_3$ is distal. Thus, if one were to move the metal from the α-face to the β-face, 6α, 7α, and 9α become shielded while 6β, 7β, 8, and 11β become deshielded. This is not the effect one might initially have predicted; protons directly bonded to low oxidation state metals show very large low-frequency (upfield) shifts, and it could have been argued that proximity to a chromium atom should result in at least a modest shielding. We shall return to this point later.

To get an estimate of χ for the $Cr(CO)_3$ unit requires a knowledge of the chemical shift difference between the resonance positions *of the same proton* in the α-$Cr(CO)_3$ complex and in the β-complex and also the change in the geometry terms. While the former are directly obtainable from the spectra, the latter are less obviously available. The simplest approach is to place the center of anisotropy at the chromium atom and to evaluate the geometric term, $G(Cr)$, by taking R as the distance from Cr to H and θ as the angle made by R with the Cr to ring center axis.[17] Now

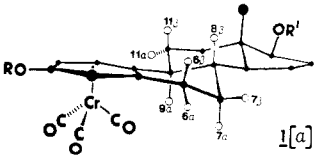

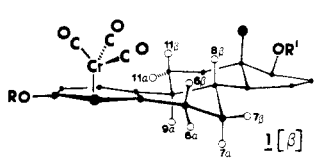

(14) (a) Busetta, B.; Hospital, M. *Acta Crystallogr., Sect. B: Struct. Crystallogr. Cryst. Chem.* **1972**, *B28*, 560. (b) Busetta, B.; Courseille, C.; Geoffre, S.; Hospital, M. *Acta Crystallogr., Sect. B: Struct. Crystallogr. Cryst. Chem.* **1972**, *B28*, 1349. (c) Duax, W. L. *Acta Crystallogr., Sect. B: Struct. Crystallogr. Cryst. Chem.* **1972** *B28*, 1864.

(15) Louër, M., unpublished results.

(16) (a) Benn, R.; Günther, H. *Angew. Chem., Int. Ed. Engl.* **1983**, *22*, 350. (b) Hull, W. E. "Two-Dimensional NMR"; Bruker Analytische Messtechnik: Karlsruhe, 1982. (c) Bax, A.; Freeman, R. *J. Magn. Reson.* **1981**, *42*, 164. (d) Bax, A.; Freeman, R. *J. Magn. Reson.* **1981**, *44*, 542. (e) Freeman, R.; Morris, G. A. *Bull. Magn. Reson.* **1978**, *1*, 5.

(17) The structural data for the estradiol complexes were adapted from those of the estradiol urea compound;[14c] averaged distances and angles for the $Cr(CO)_3$ moiety were taken from appropriate structures given in: Sneeden, R. P. A. "Organochromium Compounds"; Academic Press: New York, 1975. The distance from chromium to the centroid of the complexed ring was 1.731 Å, Cr–CO and C–O distances were 1.832 and 1.150 Å, respectively, and the centroid–Cr–CO angle was 126°. In our geometry, the $Cr(CO)_3$ unit was placed such that the chromium was approximately equidistant from all six carbon atoms in the complexed arene ring, although this is not always a feature of experimentally observed structures. The errors introduced in the geometric terms for the hydrogen atoms using this idealized geometry are, however, negligible.

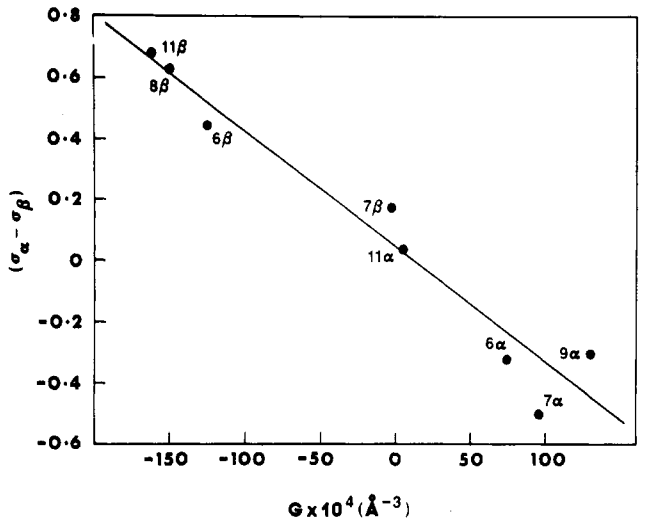

Figure 2. Plot of the ^1H NMR chemical shift differences for the indicated protons in the complexes 1[α] and 1[β] vs. the differences in geometry terms. See text.

a plot of $[\sigma_\alpha - \sigma_\beta]$ vs. $[G(Cr)_\alpha - G(Cr)_\beta]$ for the eight protons 6α, 6β, 7α, 7β, 8, 9α, 11α, and 11β should yield a straight line of slope χ. In fact, the correlation coefficient of such a plot is only 0.92, indicating that the center of anisotropy was not well chosen.

A second approach recognizes that the anisotropy most probably arises from the carbonyl ligands whose electronic charge distribution must in some ways resemble that of an alkyne. Hence, the center of anisotropy was placed midway along the C–O bond, R taken as the distance from this point to the proton and θ as the angle made by R with the Cr–C–O axis.[17] It is, of course, necessary to take account of the contributions from all three carbonyls to each proton and so generate a composite geometric term of the type

$$G(CO) = \sum_{i=1-3} \frac{(1 - 3\cos^2\theta_i)}{3R_i^3} \qquad (3)$$

Furthermore, the tripodal moiety is certainly rotating about the Cr to ring center axis and so the geometric term used was the average of $G(CO)$ where the tripod was rotated in 10° increments. For this purpose a short program was written so that proton coordinates could be input and the rotationally averaged $G(CO)_\alpha$ and $G(CO)_\beta$ values obtained. A plot of $[\sigma_\alpha - \sigma_\beta]$ vs. $[G(CO)_\alpha - G(CO)_\beta]$ for the eight previously designated protons appears as Figure 2. The resulting straight line has a correlation coefficient of 0.980 and, considering all the assumptions built into the model, is surprisingly good. An interesting result which emerges is the positions of the zero shift surfaces between the shielding and deshielding zones for the total anisotropy in diamagnetic susceptibility for the chromium tricarbonyl group. Since the geometric term goes to zero when θ = 54.7° and the angle made by the carbonyl ligands with the C_3 axis is 54°, then the net result for an individual carbonyl moiety is to generate a zero shift contour line parallel to the C_3 axis and passing through the center of the C–O bond. However, the actual surface swept out by the rotating $Cr(CO)_3$ tripod causes this cylindrical contour to be flared out at the ends as shown in Figure 3.

The final model examined was based on the idea that the carbonyls could be resolved into a "super-carbonyl" along the C_3 axis. This time, the center of anisotropy was determined empirically by moving it down the $Cr(CO)_3$ axis in increments of 0.1 Å until the best least-squares fit for the $\Delta\sigma$ vs. $\Delta G(CrCO)$ plot was found. It transpires that

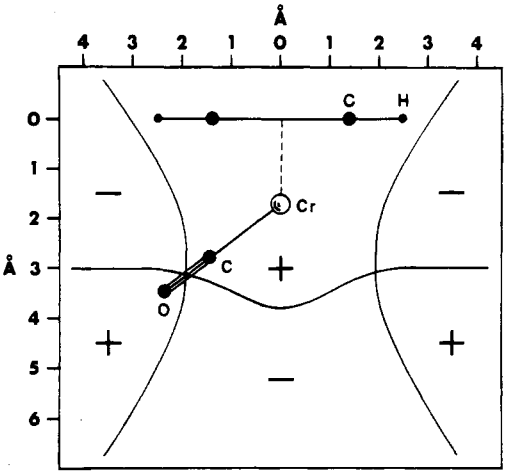

Figure 3. The shielding and deshielding zones associated with the diamagnetic anisotropy of a rapidly rotating $Cr(CO)_3$ group. The positions of the carbons and protons of an arene ring π-bonded to the tripod are also shown. A positive sign indicates a shielding region, and a negative sign indicates a deshielding region.

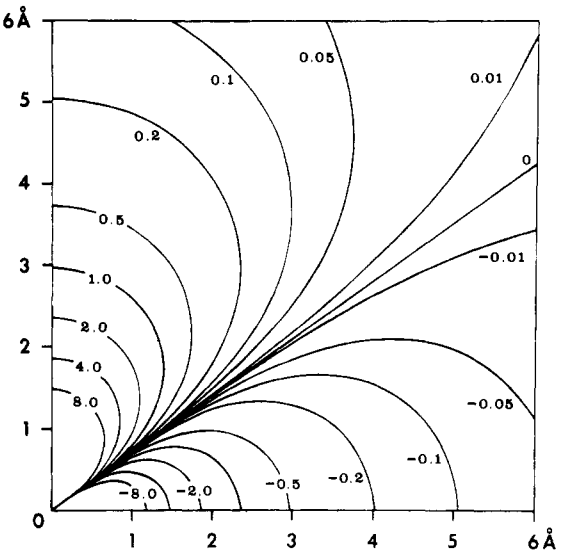

Figure 4. Incremental shifts (in ppm) of a nucleus positioned near a *single* chromium carbonyl ligand. The plot represents one quadrant of a plane containing the C_∞ axis; the origin is at the center of the C–O bond which lies along the vertical axis. A positive sign corresponds to an upfield (i.e., low-frequency) shift.

the best fit line occurs when the center of anisotropy is almost exactly midway between chromium and oxygen. Effectively, the model seems to be fitting itself to a Cr=C=O moiety whereby the shielding effect arises from the circulation of electrons back-donated from Cr 3d into the carbonyl π^* orbitals. However, one must not over-interpret data from a model which, although it gives a simple picture and a single geometry term, is based on a physically unrealistic premise. Since both the second and third models fit the data quite adequately, we prefer to invoke the one closer to the physical reality of the situation; i.e., we regard each proton as experiencing the induced magnetic field attributable to three rotating carbonyl groups. The numerical value of $\chi(CO)$ obtained from Figure 2 is -490×10^{-36} m^3/molecule which is approximately 44% greater than the value of -340×10^{-36} m^3/molecule normally quoted for the alkyne linkage.[5]

Figure 4 shows a series of contour plots of the incremental chemical shift induced by a single chromium carbonyl ligand as calculated by using this second model. The origin of the graph is the center of the C–O bond which

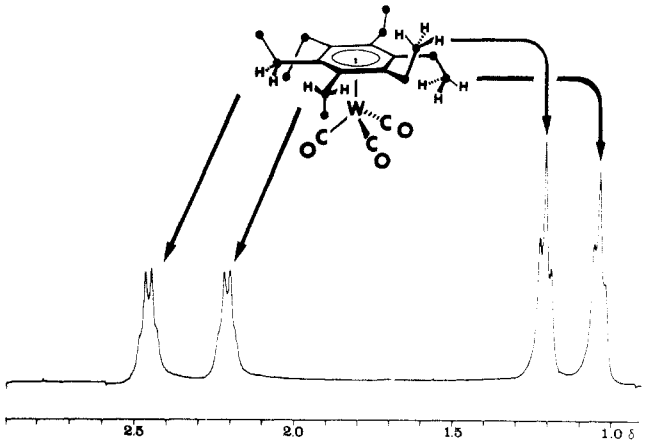

Figure 5. 400-MHz ^1H NMR spectrum of (hexaethylbenzene)-tricarbonyltungsten(0) in CD_2Cl_2 at −70 °C. At this temperature rotation of the ethyl groups and of the $W(CO)_3$ tripod is slow on the NMR time scale and so the single ethyl resonance seen at room temperature is split as shown.

is aligned along the vertical axis. Clearly, protons close to the carbonyl axis will be markedly shielded whereas nuclei near to the horizontal plane orthogonal to the axis are deshielded. Comparison with the analogous plot for the alkyne unit[2] shows the effect of the carbonyl group to be noticeably larger.

One must emphasize that the second model gives a value for χ(CO) specific for a single carbonyl ligand bonded to chromium; this value must be used in conjunction with a composite geometric term associated with a rotating tripodal moiety. In contrast, the third model for which χ-($Cr(CO)_3$) is −2124 m^3/molecule, gives a value for a $Cr(CO)_3$ entity with the center of anisotropy 3.3 Å below the chromium where the three anisotropic carbonyls are projected onto the threefold axis giving rise to a "super-carbonyl".

A short comment is in order here concerning units. These have been problematical in many calculations of this type. Even the justly famous ring current model based upon the circulation of π-electron density above and below the benzene ring plane was originally in error by a factor of $4\pi/10$. The McConnell equation[3] gives χ in units of cubic centimeters per mole when σ is given in parts per million and R is in centimeters. To convert to the SI unit, it is necessary to multiply by $(4\pi/N) \times 10^{-6}$ (= 2.086×10^{-29}). In the original paper[8] evaluating χ for the Mo≡Mo and W≡W linkages the factor 4π required for the conversion from electromagnetic units to SI was inadvertantly omitted. Consequently, the quoted values are too small by this factor. The corrected values have been incorporated into Table II. This in no way invalidates the conclusions originally drawn.[8] The calculated geometries and chemical shift increments are correct; it is merely the units of χ which are in error.

With these data in hand, it should be possible to rationalize the chemical shifts of a variety of protons in the neighborhood of a $Cr(CO)_3$ moiety. Thus in molecules such as **2** through **5**,[18,19] in which the incorporation of a chromium tripod yields diastereomeric products and renders the faces nonequivalent, we see that the exo methyls are shielded relative to those in their endo epimers; this is in accord with the data presented earlier on the steroid complexes. To show the quantitative reliability of the model, we note that use of the McConnell equation (1) and

Table II. χ Values[a] for Some Triple-Bonded Organometallic Moieties

mol fragment	χ	mol fragment	χ
C≡C[b]	−340	(Mo)-C≡O[d]	−572
Mo≡Mo[c]	−1784	(W)-C≡O[d]	−649
W≡W[c]	−1960	$Cr(CO)_3$[e]	−2124
(Cr)-C≡O[d]	−490		

[a] In units of 10^{-36} m^3/molecule; realistic error limits are probably ±10%. [b] From ref 5a. [c] From ref 8. [d] Value quoted is for a single carbonyl group bonded to the appropriate metal. [e] Value quoted is for a "super-carbonyl" group; see text.

the composite geometric term of eq 3 together with a χ-(CO) value of -490×10^{-36} m^3/molecule predicts that the exo methylene proton of the complexed heterocycle **6** should be 0.315 ppm more shielded than its endo partner. This is in remarkably good agreement with the literature spectrum.[20]

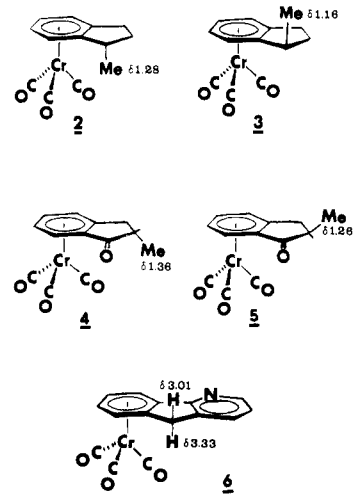

2 **3** **4** **5** **6**

Another particularly pleasing example is provided by our earlier work on (hexaethylbenzene)$Cr(CO)_3$ in which tripodal rotation can be slowed on the NMR time scale at low temperature.[21] It has been shown that the arene has approximate D_{3d} symmetry[22] and this is relatively little changed on complexation.[23] Thus, there are two types of methylene proton; one set is proximal and should thereby be deshielded relative to the distal set. The inherent shifts of these protons should be identical since any ring current effects should be the same. The calculation reveals that the chemical shift separation should be 0.25 ppm; the experimental difference is 0.20 ppm.

We can extend this result to the molybdenum and tungsten congeners of $(C_6Et_6)M(CO)_3$ which exhibit similar ^1H spectra at low temperature. The chemical shift differences between proximal and distal methylene protons are 0.23 and 0.25 ppm for Mo and W, respectively.[21] A typical spectrum appears as Figure 5 which depicts the 400 MHz ^1H spectrum of $(C_6Et_6)W(CO)_3$ at −70 °C. The identity of the distal and proximal methylene and methyl protons were established by homonuclear and heteronuclear (^1H–^{13}C) decoupling experiments. These shifts, in conjunction with the published structural data for the molybdenum complex,[23] yield χ values of −572 and −649

(18) Gracey, D. E. F.; Jackson, W. R.; McMullen, C. H.; Thompson, N. *J. Chem. Soc. B* **1969**, 1197.
(19) Jaouen, G.; Meyer, A. *J. Am. Chem. Soc.* **1975**, *97*, 4667.
(20) Thoma, T.; Pleshakov, V. G.; Prostakov, N. S.; Ustynyuk, Y. A.; Nesmeyanov, A. N.; Ustynyuk, N. A. *J. Organomet. Chem.* **1980**, *192*, 359.
(21) McGlinchey, M. J.; Bougeard, P.; Sayer, B. G.; Hofer, R.; Lock, C. J. L. *J. Chem. Soc., Chem. Commun.* **1984**, 789.
(22) Pal, H. K.; Guha, A. C. *Z. Kristalogr., Kristalgeom., Kristalphys., Kristalchem.* **1935**, *A92*, 393.
(23) Iverson, D. J.; Hunter, G.; Blount, J. F.; Damewood, J. R., Jr.; Mislow, K. *J. Am. Chem. Soc.* **1981**, *103*, 6073.

$\times 10^{-36}$ m^3/molecule for carbonyls bonded to Mo and W, respectively. As with metal–metal triple bonds, there is an increase in the value of χ as one descends group 6.

The diamagnetic anisotropy of ferrocene has been discussed by Turbitt and Watts.[24] In the course of a series of elegant deuterium labeling studies, the resonance positions of the exo and endo protons of several [3](1,2)-ferrocenophane derivatives, **7** through **9**, were established.

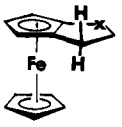

7; X = CH_2
8; X = C=O
9; X = C=CH_2

As with the $M(CO)_3$ group, the distal nuclei were shielded relative to their proximal partners. The average chemical shift difference between the methylene protons is 0.36 ppm, and this value, in conjunction with the structural parameters,[25] leads to a χ value of -494×10^{-36}/m^3/molecule for the ferrocene unit with the center of anisotropy positioned on the iron atom.[26] This result is in complete accord with the measurements of Mulay and Fox who determined the principal magnetic susceptibilities of the molecule.[27] They found that the susceptibility along the molecular axis perpendicular to the planes of the cyclopentadienyl rings and passing through their center of mass was much greater than those along the axes in the plane containing the iron atom and parallel to the planes of the rings. Similarly, solid-state ^{59}Co NMR studies[28] on the cobalticinium ion revealed a large anisotropy in the same sense as for ferrocene.

In his NMR studies on the ferrocene system, Watts[24] noted that when a proton is sited particularly close to the iron atom, it was shielded in the same way as a metal hydride and he postulated the existence of a shielding zone round the metal atom. It is noteworthy that in the (hexaethylbenzene)$M(CO)_3$ systems the proximal methyl group is somewhat more shielded than would have been expected. One could argue that as the methyl protons rotate, they pass so close to the metal atom that they are encroaching on the shielding zone round the metal. However, it is also important to realize that the model developed by McConnell is based merely on a dipole approximation. For it to be valid, the magnitude of R (the direct distance from the center of anisotropy to the proton under investigation) should be considerably larger than the radius of circulation of the electronic charge which gives rise to the induced field.

To conclude, it has been demonstrated that a simple model relating proton NMR chemical shifts and the anisotropy in diamagnetic susceptibility can be successfully applied to organometallic molecules. The organometallic fragments are found to have large χ values compared to commonly encountered organic moieties and thus have profound effects on the shifts of neighboring nuclei. Extension of these concepts to other organometallic fragments will be reported elsewhere.

Acknowledgment. We thank the Natural Sciences and Engineering Council of Canada for financial support. R.H. was the recipient of a post-doctoral fellowship from the Stiftung für Stipendien auf dem Gebiete der Chemie (Switzerland). M.J.M. thanks the France–Canada scientific exchange program for a visiting professorship.

Registry No. 1[α], 88729-93-5; 1[β], 88765-18-8; $(C_6Et_6)W(CO)_3$, 88077-04-7; $(C_6Et_6)Mo(CO)_3$, 78672-26-1; ferrocene, 102-54-5.

(24) Turbitt, T. D.; Watts, W. E. *Tetrahedron* **1972**, *28*, 1227.

(25) Structural data were based on the corresponding distances and angles reported for (−)-Fe(η-C_5H_5)-[η-$C_5H_3CH_2CH$(Me-*exo*)CH_2C(O)]. Lecomte, C.; Dusausoy, Y.; Protas, J.; Gautheron, B.; Broussier, R. *Acta Crystallogr., Sect. B: Struct. Crystallogr. Cryst. Chem.* **1973**, *B29*, 1504.

(26) A similar calculation for the exo and endo methyls in the same molecules produces a χ value of −1100 m^3/molecule, but this is unrealistic since the puckering of the noncomplexed five-membered ring containing the methyls renders them nonequivalent. Their inherent chemical shifts are no longer identical since they are not symmetrically disposed with respect to the aromatic ring and so experience different ring current effects.

(27) Mulay, L. N.; Fox, M. E. *J. Chem. Phys.* **1963**, *38*, 760.

(28) Spiess, H. W.; Haas, H.; Hartmann, H. *J. Chem. Phys.* **1969**, *50*, 3057.

(29) Ustynyuk, N. A.; Novikova, L. N.; Bel'skii, V. K.; Oprunenko, Yu. F.; Malyugina, S. G.; Trifonova, O. I.; Ustynyuk, Yu. A. *J. Organomet. Chem.* **1985**, *294*, 31.

Excitation wavelength dependence of photodissociation and the secondary laser pulse photolysis of dimanganese decacarbonyl

Takayoshi. Kobayashi, Hiroyuki. Ohtani, Hisanao. Noda,
Shosuke. Teratani, Hiroshi. Yamazaki, and Katsutoshi. Yasufuku

Organometallics, **1986**, 5 (1), 110-113• DOI: 10.1021/om00132a019 • Publication Date (Web): 01 May 2002

Excitation Wavelength Dependence of Photodissociation and the Secondary Laser Pulse Photolysis of Dimanganese Decacarbonyl†

Takayoshi Kobayashi,*[1a] Hiroyuki Ohtani,[1a,d] Hisanao Noda,[1b] Shosuke Teratani,[1c] Hiroshi Yamazaki,[1b] and Katsutoshi Yasufuku[1c]

Department of Physics, the University of Tokyo, Hongo, Bunkyo-ku, Tokyo 113, Japan, Institute of Physical and Chemical Research, Wako-shi, Saitama 351, Japan, and Tokyo Gakugei University, Koganei-shi, Tokyo 184, Japan

Received May 22, 1985

The transient spectroscopy technique was applied for the determination of the quantum yields for the following two processes, and their dependences on the excitation wavelength were found. The quantum yield for process I, Y_1, increases with the excitation wavelength while that of process II, Y_2, decreases. The ratio $R = Y_1/Y_2$ obtained for different excitation wavelengths (λ_{ex}) is as follows: $R = 0.19 \pm 0.05$ (λ_{ex} = 266 nm), $R = 0.43 \pm 0.02$ (λ_{ex} = 337 nm), and $R = 1.1 \pm 0.2$ (λ_{ex} = 355 nm). The sum of Y_1 and Y_2 were

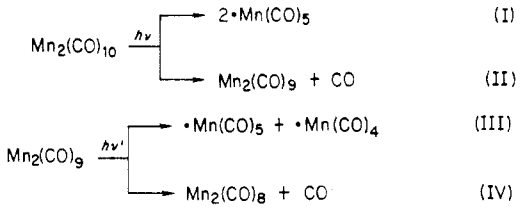

found to be unity for 355-, 337-, and 266-nm excitations. These results are discussed in terms of the properties of their excited states. Using two Q-switched Nd:YAG lasers, the following successive photolysis of $Mn_2(CO)_9$ by the second pulse was found to result in further CO elimination (process IV).

Introduction

The photochemistry of $Mn_2(CO)_{10}$ in solution has been studied by a number of groups and is generally taken as a prototype for photoreactions of organometallic compounds containing metal–metal bonds.[2-4] However, recently two primary photochemical reaction pathways in the photolysis of $Mn_2(CO)_{10}$ have been established: metal–metal bond cleavage to produce $\cdot Mn(CO)_5$ radicals (eq 1) and dissociative loss of CO to give $Mn_2(CO)_9$ without metal–metal bond cleavage (eq 2). These have been

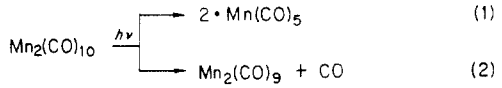

demonstrated by flash photolysis with UV–vis detection[5-7] or IR detection[8] and by conventional photolysis in low-temperature matrices.[9] The IR spectroscopic studies[8,9] have revealed that $Mn_2(CO)_9$ has an unsymmetrically bridged CO in solvents which have no coordinating ability.

In the framework of a simple one-electron diagram of the dinuclear metal carbonyl,[10] $M_2(CO)_{10}$, the photoexcitation of a metal–metal bonding (σ) electron to the antibonding σ^* orbital results in metal–metal bond cleavage (eq 1). However, as these findings show, the $\sigma \rightarrow \sigma^*$ excitation also causes dissociation of the metal–CO bond (eq 2) as well as process 1. Thus, it is of great interest to study the effect of excitation wavelength on the two primary processes. Only two reports have appeared so far on the dependence of wavelength on quantum yields for CO photodissociation and metal–metal bond cleavage in $[CpFe(CO)_2]_2$[11] and $Ru_3(CO)_{12}$.[12,13]

In this paper, we report the first known real-time measurement of the branching ratio between the two processes 1 and 2 at different excitation wavelengths by means of nanosecond spectroscopy. Furthermore double-flash experiment on $Mn_2(CO)_{10}$ in cyclohexane is reported to clarify the photochemistry of the ligand-unsaturated intermediate $Mn_2(CO)_9$. In the double-flash study, the first flash (355 nm, 5-ns fwhm) is used to produce $Mn_2(CO)_9$ and $\cdot Mn(CO)_5$ and the second flash (532 nm, 20-ns fwhm) is used to excite $Mn_2(CO)_9$.

Experimental Section

Materials. $Mn_2(CO)_{10}$ was synthesized by the method described in the literature[14] and purified by sublimation. Cyclohexane stored on a K–Na alloy was volumetrically added to the sample compartment in vacuo. The sample solutions were de-

† This work was supported in part by a Grant-in-Aid from the Ministry of Education, Science and Culture of Japan, Toray Science and Technology Foundation, and Kurata Science Foundation to T.K. This work was in part supported by grants of "Solar energy conversion by means of photosynthesis" given to Riken (IPCR) by the Science and Technology Agency.

(1) (a) Department of Physics, the University of Tokyo. (b) Institute of Physical and Chemical Research. (c) Tokyo Gakugei University. (d) Visiting research fellow from Hamamatsu Photonics K.K. to the Department of Physics, the University of Tokyo.

(2) Geoffroy, G. L.; Wrighton, M. S. "Organometallic Photochemistry"; Academic Press: New York, 1978. Geoffroy, G. L. *J. Chem. Educ.* **1983**, *60*, 861.
(3) Wegman, R. W.; Olsen, R. J.; Gard, D. R.; Faulkner, L. R.; Brown, T. L. *J. Am. Chem. Soc.* **1981**, *103*, 6089.
(4) Wrighton, M. S.; Ginley, D. S. *J. Am. Chem. Soc.* **1975**, *97*, 2065.
(5) Yesaka, H.; Kobayashi, T.; Yasufuku, K.; Nagakura, S. *Reza Kagaku Kenkyu* **1981**, *3*, 97; *J. Am. Chem. Soc.* **1983**, *105*, 6249.
(6) Rothberg, L. J.; Cooper, N. J.; Peters, K. S.; Vaida, V. *J. Am. Chem. Soc.* **1982**, *104*, 3536.
(7) Herrick, R. S.; Brown, T. L. *Inorg. Chem.* **1984**, *23*, 4550.
(8) Church, S. P.; Herman, H.; Grevels, F.-W.; Schaffner, K. *J. Chem. Soc., Chem. Commun.* **1984**, 785.
(9) Hepp, A. F.; Wrighton, M. S. *J. Am. Chem. Soc.* **1983**, *105*, 5934.
(10) Levenson, R. A.; Gray, H. B. *J. Am. Chem. Soc.* **1975**, *97*, 6042.
(11) Tyler, D. R.; Schmidt, M. A.; Gray, H. B. *J. Am. Chem. Soc.* **1983**, *105*, 6018.
(12) Malito, J.; Markiewicz, S.; Poë, A. *Inorg. Chem.* **1981**, *21*, 4337.
(13) Desroslers, M. F.; Ford, P. C. *Organometallics* **1982**, *1*, 1715.
(14) King, R. B.; Stokes, J. C.; Korenowski, T. F. *J. Organomet. Chem.* **1968**, *11*, 641.

0276-7333/86/2305-0110$01.50/0

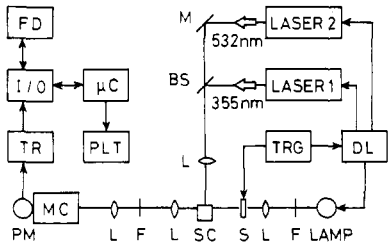

Figure 1. Block diagram of nanosecond time-resolved spectroscopy apparatus. The symbols for the abbreviation are as follows: TRG, main trigger circuit; DL, digital delay circuit; BS, beam splitter; F, filter; M, mirror; L, lens; S, mechanical shutter; SC, sample cell; MC, monochromator; PM, photomultiplier; TR, transient recorder; I/O, input/output unit; FD, floppy disk driver; μC, microcomputer; PLT, X-Y plotter.

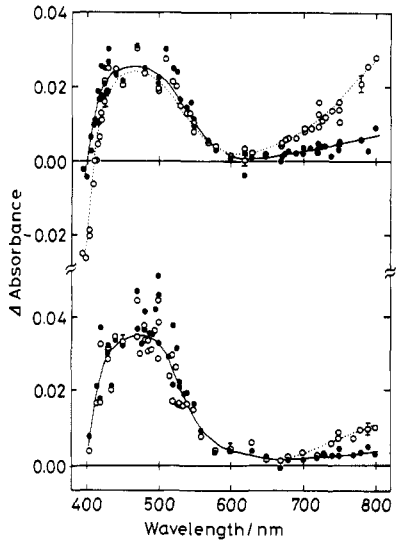

Figure 2. Transient difference absorption spectra of $Mn_2(CO)_{10}$ in cyclohexane 3 (open circles) and 30 μs (closed circles) after excitation. Excitation wavelengths are 355 (top) and 266 nm (bottom).

gassed after five freeze–thaw cycles and were hermetically sealed. Then, Ar or CO gas was admitted through a side arm with a Teflon stopcock.

Excitation Wavelength Dependence on the Quantum Yield. A nanosecond spectroscopic experiment was performed at 20–22 °C with the fourth (266 nm, 5-ns fwhm, 0.1 MW) and third (355 nm, 5-ns fwhm, 0.4 MW) harmonics of a Q-switched Nd:YAG laser (Quanta-Ray, DCR-1A). The concentrations of $Mn_2(CO)_{10}$ in cyclohexane are 8×10^{-4} mol dm^{-3} for the 266-nm excitation and 4×10^{-4} mol dm^{-3} for the 337- and 355-nm excitations. The intensity of the probe light was detected with a photomultiplier (Hamamatsu Photonics, R666S), and the output signal of the photomultiplier was digitized with a transient recorder (Iwatsu, DM901) and was averaged with a microcomputer (NEC, PC8001).

Double-Flash Experiment. The excitation light sources of the first and the second flashes are a third harmonic (355 nm, 5-ns fwhm, 0.4 MW) of the Q-switched Nd:YAG laser (Quanta-Ray, DCR-1A) and a second harmonic (532 nm, 20-ns fwhm, 0.6 MW) of a Q-switched Nd:YAG laser (Quantel, YG472), respectively. The time interval of the two excitation light pulses was adjusted by a digital delay circuit with a time resolution of 10 ns.[15] Figure 1 shows the block diagram of the nanosecond time-resolved double-flash excitation apparatus. The two excitation beams are colinear to each other.

Results and Discussion

Excitation Wavelength Dependence. Figure 2 shows the excitation wavelength dependence on the photodissociation processes of $Mn_2(CO)_{10}$ in cyclohexane. The absorbance with λ_{max} at 800 nm is due to the photogenerated radicals which decay in the following recombination process (1B). The second-order rate constant, k_1, in cyclohexane was estimated for both 266- and 355-nm excitations to be 8.5×10^8 mol^{-1} dm^3 s^{-1}, which is very close to the previously reported value for the 337-nm excitation (8.8×10^8 mol^{-1} dm^3 s^{-1}).[5] The photogenerated $Mn_2(CO)_9$ and $\cdot Mn(CO)_5$ do not appreciably disappear within 30 ns after excitation. Therefore the present nanosecond experiment allows the direct real-time observation of the initial amounts of both primary photoproducts under the conditions without the subsequent bimolecular recombination reaction of $\cdot Mn(CO)_5$ (process 1B) and/or a probable secondary photoreaction of $Mn_2(CO)_9$.[16]

$$2 \cdot Mn(CO)_5 \xrightarrow{k_1} Mn_2(CO)_{10} \qquad (1B)$$

The absorbance at 500 nm is due to $Mn_2(CO)_9$,[5] and the bimolecular rate constant for the reaction of $Mn_2(CO)_9$ with CO has been estimated to be on the order of 10^{5-6} mol^{-1} dm^3 s^{-1}.[5-8] The quantum yield, Y_1 or Y_2, is determined from the comparison of the absorbance change at 500 nm due to $Mn_2(CO)_9$ or that at 780 nm due to $\cdot Mn(CO)_5$ with that of benzophenone in the triplet state at 530 nm as a standard.[17] In this experiment the photolyses of benzophenone and $Mn_2(CO)_{10}$ were performed under the same optical geometry, excitation density, and absorbance at the excitation wavelength. The molar extinction coefficient of $Mn_2(CO)_9$ at 500 nm (ϵ_{500}) was taken to be 900 mol^{-1} dm^3 cm^{-1} from both the reported values.[5,7] The molar extinction coefficient of $\cdot Mn(CO)_5$ at 780 nm (ϵ_{780}) was determined to be 800 mol^{-1} dm^3 cm^{-1} from both the reported spectral shape and ϵ_{830} value.[18] Here ϵ_{830} was taken to be 875 mol^{-1} dm^3 cm^{-1} which is an averaged value of ϵ_{830}'s reported by Waltz et al. (800 ± 80 mol^{-1} dm^3 cm^{-1})[19] and by Walker et al. (950 mol^{-1} dm^3 cm^{-1}).[18] The measured quantum yields are shown in Table I.[20] It is noted that the sum of Y_1 and Y_2 is unity for each excitation wavelength.

Table I. Quantum Yields of Processes 1 and 2, Y_1 and Y_2, Respectively, and the Excitation Wavelength λ_{ex}[a]

λ_{ex}/nm	solvent	Δt[b]	Y_1	Y_2
266	cyclohexane	5 ns	0.16 ± 0.02	0.84 ± 0.10
337	cyclohexane	10 ns	0.30 ± 0.02	0.70 ± 0.00
347[c]	ethanol	25 ps	0.33[d]	0.67[d]
355	cyclohexane	5 ns	0.49 ± 0.05	0.44 ± 0.03

[a] Reference 20. [b] Excitation pulse width (fwhm). [c] Reference 6. [d] Calculated on the assumption that their sum of Y_1 and Y_2 is equal to unity.

The value Y_1 thus estimated increases with the excitation wavelength as shown in Table I. The electronic absorption spectrum of $Mn_2(CO)_{10}$ has been assigned as

(15) Kobayashi, T.; Koshihara, S. *Chem. Phys. Lett.* **1984**, *104*, 174.

(16) (a) The experiment of excitation by pulses longer than 1 μs or by ordinary light sources may suffer from a possible subsequent reaction following CO cleavage (eq 2) as follows:[16b]

$$Mn_2(CO)_9 \rightarrow \cdot Mn(CO)_5 + \cdot Mn(CO)_4$$

(b) Coville, N. J.; Stolzenberg, A. M.; Muetterties, E. L. *J. Am. Chem. Soc.* **1983**, *105*, 2499.

(17) Bensasson, R.; Land, E. J. *Trans. Faraday Soc.* **1971**, *67*, 1904.

(18) Walker, H. W.; Herrick, R. S.; Olsen, R. J.; Brown, T. L. *Inorg. Chem.* **1984**, *23*, 3748.

(19) Waltz, W. L.; Hackelberg, O.; Dorfman, L. M.; Wojciki, A. *J. Am. Chem. Soc.* **1978**, *100*, 7259.

(20) (a) The ratio Y_1/Y_2 has been preliminary reported.[20b] In this paper the measurement of the quantum yields has been improved. (b) Kobayashi, T.; Yasufuku, K.; Iwai, J.; Yesaka, H.; Noda, H.; Ohtani, H. *Coord. Chem. Rev.* **1985**, *64*, 1.

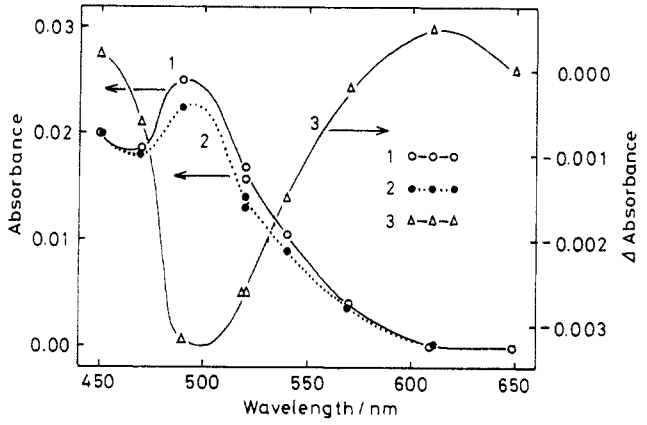

Figure 3. Transient absorption spectra of $Mn_2(CO)_{10}$ in cyclohexane following 355-nm excitation: curve 1, 5 μs before the second pulse (532-nm) excitation; curve 2, 3 μs after the second pulse excitation; curve 3, difference spectrum of curve 2 minus curve 1.

follows: 374 nm ($d\pi-\sigma^*$), 336 nm ($\sigma-\sigma^*$), 303 nm ($\sigma-\pi^*$), and 266 nm ($d\pi-\pi^*_{CO}$).[10] This clearly shows that the rate of the internal conversion is smaller than the reaction rate. The value Y_1/Y_2 shows that in the case of the $d\pi \rightarrow \pi^*_{CO}$ excitation, metal–CO cleavages are more efficient than metal–metal fissions by a factor of 5. It is worth mentioning that the CO cleavage occurs as efficiently as radical formation even by the lower energy σ^* excitation. Thus both the $\sigma \rightarrow \sigma^*$ (337 nm) excitation and the $d\pi \rightarrow \pi^*_{CO}$ (266 nm) excitation have reaction channels to (1) and (2). However it should also be noted that the irradiation of light induces the fission of the metal–metal bond. This is in contrast with the thermal reaction in which the absence of metal–metal bond cleavage has recently been verified.[16a] A different value of Y_1/Y_2 (about 2) was estimated by the competition reaction method[9] and a flash photolysis with a 35-μs pulse.[7] We consider that their experiments may have suffered from complications due to a stationary or longer pulse excitation by polychromatic lamp whose spectrum extends to the longer wavelength region. Kidd and Brown measured the total quantum yield for the disappearance of $Mn_2(CO)_{10}$ to be 0.81–0.94 by the photolysis of $Mn_2(CO)_{10}$ with the stationary light irradiation at 350 nm in the presence of phosphorus bases (P).[21] Their results can be reinterpreted along with our new results obtained by the 355-nm excitation as follows. The disappearance yield of $Mn_2(CO)_{10}$ for reaction 3 is estimated to be 0.44 in our recent study. The difference

$$Mn_2(CO)_9 + P \rightarrow Mn_2(CO)_9P \quad (3)$$

between the disappearance yield of $Mn_2(CO)_{10}$ (0.81–0.94) and the residue yield of 0.37–0.50 is interpreted by invoking mechanism 4 suggested by Kidd and Brown.[21]

$$\cdot Mn(CO)_5 + P \rightarrow Mn(CO)_4P + CO \quad (4)$$

They also reported that the yield for the disappearance of $Mn_2(CO)_{10}$ decreases to 0.66–0.76 in the presence of both phosphorus bases and CO. The result can be explained as follows. Reaction 3 competes with the back reaction of process 2 which reproduces $Mn_2(CO)_{10}$ from $Mn_2(CO)_9$ and externally adds CO.

Double-Flash Excitation. Figure 3 shows the transient absorption of $Mn_2(CO)_{10}$ in cyclohexane under 1 atm of Ar following double-flash excitation. The secondary excitation of the sample by the 532-nm light pulse was performed 30 μs after the first excitation by the 355-nm excitation light pulse. Curves 1 and 2 show the transient absorption spectra 5 μs before and 3 μs after the second excitation, respectively. Curve 3 shows the difference absorption spectrum (curve 2 minus curve 1). The spectrum resembles the absorption due to $Mn_2(CO)_9$. Therefore, the decrease in the absorbance around 500 nm is caused by the disappearance of $Mn_2(CO)_9$ induced by the second excitation light at 532 nm. On analogy with the photoreaction of $Mn_2(CO)_{10}$, eq 5 and 6 may be the two possible processes. In process 6, there may be other disproportionations such as $\rightarrow Mn_2(CO)_7 + 2CO$ and $\rightarrow Mn_2(CO)_6 + 3CO$ and so on.

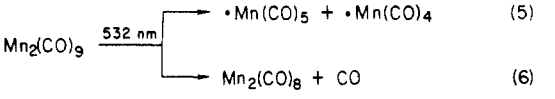

(5)

(6)

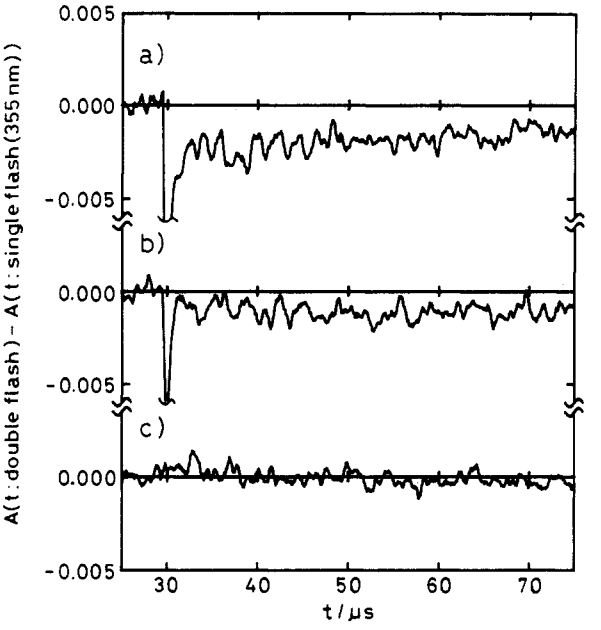

Figure 4. Kinetics of the absorbance change of $Mn_2(CO)_{10}$ in cyclohexane, A(t; double-flash) – A(t; single flash (355 nm)). The 532-nm light was irradiated at the sample solution 30 μs after the 355-nm excitation pulse: (a) under 1 atm of Ar measured at 500 nm, (b) under 1 atm of CO measured at 500 nm, and (c) under 1 atm of Ar measured at 780 nm.

Parts a and b of Figure 4 show the kinetics of the absorbance changes, $A(t$; double flash) – $A(t$; single flash (355 nm)), of $Mn_2(CO)_{10}$ in cyclohexane under 1 atm of Ar and CO, respectively, at 500 nm. The intense spikes at 30 μs shown in parts a and b of Figure 4 are due to scatterings of the 532-nm excitation light. The 355-nm excitation was performed 30 μs before the 532-nm excitation. The absorbance change due to the disappearance of $Mn_2(CO)_9$ is smaller under 1 atm of CO than Ar, since the back reaction of process 6 may be rapid due to higher CO concentration. Figure 4c shows the kinetics of the absorbance change at 780 nm. If cleavage of the Mn–Mn bond of $Mn_2(CO)_9$ takes place, the radical $\cdot Mn(CO)_5$ is expected as one of the species in process 5.[16a] However, no detectable signal was observed at 780 nm where the molar extinction coefficient of $\cdot Mn(CO)_5$ is nearly equal to that of $Mn_2(CO)_9$ at 500 nm. The molar concentration (C_5) of $\cdot Mn(CO)_5$ formed through process 5 is estimated to be 3×10^{-6} mol dm^{-3} by assuming that the absorbance change shown in Figure 4b is solely due to the loss of $Mn_2(CO)_9$ by process 5. The expected absorbance change due to the formation of $\cdot Mn(CO)_5$ thus should be 7×10^{-4}, which is lower than the detectable absorbance change (0.001; see Figure 4c). The ratio of the quantum yield for processes 5 and 6, Y_5/Y_6, is estimated

(21) Kidd, D. R.; Brown, T. L. *J. Am. Chem. Soc.* **1978**, *100*, 4095.

from eq 7 and 8. Here the upper limit of C_5 is 3×10^{-6}

$$Y_5/Y_6 = C_5/C_6 \quad (7)$$

$$C_5 + C_6 \geq \Delta A(t)/\epsilon_{500}(Mn_2(CO)_9)l \quad (8)$$

mol dm^{-3} and C_6 is the molar concentration of $Mn_2(CO)_8$. The equality relationship in (8) is satisfied when $Mn_2(CO)_8$ and other species such as $Mn_2(CO)_7$ do not have absorptions at that wavelength. Inequality in (8) is due to any absorbance of these species. The optical path length (l) is 0.3 cm in this double-pulse experiment. The absorbance change, $\Delta A(t)$ (0.002), is shown in Figure 4a. The ratio Y_5/Y_6 is therefore estimated to be lower than 0.7. The yield for process 5, which was proposed by Coville et al.,[16a] is, therefore, concluded to be low even if it is present. The major process in $Mn_2(CO)_9$ photolysis is not the cleavage of the metal–metal bond but of the Mn–CO bond (process 6). The steady-state irradiation at low temperature is in progress to clarify the products of the photoreaction of $Mn_2(CO)_9$. The recombination of $Mn_2(CO)_8$ with CO following the second flash has not been studied because of the complicated kinetics and the small absorbance change. Advanced studies will be published in another paper.

Acknowledgment. We wish to express thanks to Prof. A. Poë for his helpful discussions on the wavelength dependence. They also thank Mr. J. Iwai for his help in the early stage of the study.

Registry No. $Mn_2(CO)_{10}$, 10170-69-1; $Mn(CO)_5$, 54832-42-7; $Mn_2(CO)_9$, 86728-79-2; $Mn(CO)_4$, 71518-80-4; CO, 630-08-0.

A New General Route to Diphosphenes via Germylated Compounds

Claude Couret, Jean Escudie, Henri Ranaivonjatovo, and Jacques Satgé*

Laboratoire de Chimie des Organominéraux, UA du CNRS No. 477, Université Paul Sabatier, 31062 Toulouse, France

Received April 10, 1985

Several (trichlorogermyl)phosphines RP(H)$GeCl_3$ (**3**) are prepared by two different routes: (i) from primary phosphines RPH_2 and germanium tetrachloride and (ii) from dichlorophosphines $RPCl_2$ and the dichlorogermylene–dioxane complex, $GeCl_2 \cdot C_4H_8O_2$. Subsequent addition of **3** to an excess of DBU (1,5-diazabicyclo[5.4.0]undec-5-ene) affords the corresponding diphosphenes RP=PR. This method appears conveniently and generally applicable to the synthesis of diphosphenes. This reaction involves formation of chlorophosphine intermediates RP(H)Cl (**2**). Stable diphosphenes **1c**, bis(2,4,6-tri-*tert*-butylphenyl)diphosphene, and **1e**, bis[bis(trimethylsilyl)methyl]diphosphene, can be isolated in excellent yield. Unstable dienophilic diphosphenes were characterized by cycloaddition with 1,3-dienes. Cycloadduct **12d**, obtained by reaction of di-*tert*-butyldiphosphene with cyclopentadiene, is a clean precursor of di-*tert*-butyldiphosphene, **1d**.

Introduction

Since the report by Yoshifuji et al. describing the synthesis and characterization of the first stable compound with a P=P bond, bis(2,4,6-tri-*tert*-butylphenyl)diphosphene,[1] this new class of unsaturated compounds has been of current interest.[2-10]

Diphosphenes have been obtained by several routes from reactions of the corresponding dichlorophosphines with various reagents: magnesium,[1,3] sodium,[4] or lithium derivatives,[5] bis(trimethylsilyl)mercury,[6] divalent species of group IVA[7] (14),[30] primary phosphines (dehydrochlorination in the presence of amines),[8] and silylphosphines (dechlorosilylation).[3,9] However, although all these methods are convenient for the preparation of some kinds of diphosphenes, there is currently no generally applicable methodology for the preparation of *all* diphosphenes.

In a preceding paper, we described the synthesis of bis[bis(trimethylsilyl)methyl]diphosphene via organogermanium compounds,[10] which is presently the only existing route to this diphosphene. Herein, we describe the

(1) (a) Yoshifuji, M.; Shima, I.; Inamoto, N.; Hirotsu, K.; Higuchi, T., *J. Am. Chem. Soc.* **1981**, *103*, 4587; (b) *Ibid.* **1982**, *104*, 6167.

(2) For recent reviews see: Cowley, A. H. *Polyhedron* **1984**, *3*, 389–432. Cowley, A. H.; Kilduff, J. E.; Lasch, J. G.; Mehrotra, S. K.; Norman, N. C.; Pakulski, M.; Whittlesey, B. R.; Atwood, J. L.; Hunter, W. E. *Inorg. Chem.* **1984**, *23*, 2582–2593.

(3) Smit, C. N.; Van der Knaap, T. A.; Bickelhaupt, F. *Tetrahedron Lett.* **1983**, *24*, 2031.

(4) Cowley, A. H.; Kilduff, J. E.; Newman, T. H.; Pakulski, M. *J. Am. Chem. Soc.* **1982**, *104*, 5820. Cowley, A. H.; Kilduff, J. E.; Pakulski, M.; Stewart, C. A. *Ibid.* **1983**, *105*, 1655.

(5) (a) Bertrand, G.; Couret, C.; Escudié, J.; Majid, S.; Majoral, J. P. *Tetrahedron. Lett.* **1982**, *23*, 3567. (b) Couret, C.; Escudié, J.; Satgé, J. *Ibid.* **1982**, *23*, 4941. Escudié, J.; Couret, C.; Ranaivonjatovo, H.; Satgé, J.; Jaud, J. *Phosphorus Sulfur* **1983**, *17*, 221. Niecke, E.; Rüger, R. *Angew. Chem.* **1983**, *95*, 154; *Angew. Chem., Int. Ed. Engl.* **1983**, *22*, 155. Niecke, E.; Rüger, R.; Lysek, M.; Pohl, S.; Schoeller, W. *Angew. Chem.* **1983**, *95*, 495; *Angew. Chem., Int. Ed. Engl.* **1983**, *22*, 486; *Angew. Chem. Suppl.* **1983**, 639. Schmidt, H.; Wirkner, C.; Issleib, K. *Z. Chem.* **1983**, *23*, 67. Cetinkaya, B.; Hudson, A.; Lappert, M. F.; Goldwhite, H. *J. Chem. Soc., Chem. Commun.* **1982**, 609, 691.

(6) Romanenko, V. D.; Klebalskii, E. O.; Markovskii, L. N. *Zh. Obshch. Khim.* **1984**, *54*, 465.

(7) Veith, M.; Huch, V.; Majoral, J. P.; Bertrand, G.; Manuel, G. *Tetrahedron Lett.* **1983**, *24*, 4219.

(8) (a) Cowley, A. H.; Kilduff, J. E.; Mehrotra, N. C.; Norman, N. C.; Pakulski, M. *J. Chem. Soc., Chem. Commun.* **1983**, 528. (b) Yoshifuji, M.; Shibayama, K.; Inamoto, N.; Matsushita, T.; Nishimoto, K. *J. Am. Chem. Soc.* **1983**, *105*, 2495.

(9) Escudié, J.; Couret, C.; Andriamizaka, J. D.; Satgé, J. *J. Organomet. Chem.* **1982**, *228* C76.

(10) Escudié, J.; Couret, C.; Ranaivonjatovo, H.; Satgé, J. *J. Chem. Soc., Chem. Commun.* **1984**, *24*, 1621.

0276-7333/86/2305-0113$01.50/0

from eq 7 and 8. Here the upper limit of C_5 is 3×10^{-6}

$$Y_5/Y_6 = C_5/C_6 \quad (7)$$

$$C_5 + C_6 \geq \Delta A(t)/\epsilon_{500}(Mn_2(CO)_9)l \quad (8)$$

mol dm^{-3} and C_6 is the molar concentration of $Mn_2(CO)_8$. The equality relationship in (8) is satisfied when $Mn_2(CO)_8$ and other species such as $Mn_2(CO)_7$ do not have absorptions at that wavelength. Inequality in (8) is due to any absorbance of these species. The optical path length (l) is 0.3 cm in this double-pulse experiment. The absorbance change, $\Delta A(t)$ (0.002), is shown in Figure 4a. The ratio Y_5/Y_6 is therefore estimated to be lower than 0.7. The yield for process 5, which was proposed by Coville et al.,[16a] is, therefore, concluded to be low even if it is present. The major process in $Mn_2(CO)_9$ photolysis is not the cleavage of the metal–metal bond but of the Mn–CO bond (process 6). The steady-state irradiation at low temperature is in progress to clarify the products of the photoreaction of $Mn_2(CO)_9$. The recombination of $Mn_2(CO)_8$ with CO following the second flash has not been studied because of the complicated kinetics and the small absorbance change. Advanced studies will be published in another paper.

Acknowledgment. We wish to express thanks to Prof. A. Poë for his helpful discussions on the wavelength dependence. They also thank Mr. J. Iwai for his help in the early stage of the study.

Registry No. $Mn_2(CO)_{10}$, 10170-69-1; $Mn(CO)_5$, 54832-42-7; $Mn_2(CO)_9$, 86728-79-2; $Mn(CO)_4$, 71518-80-4; CO, 630-08-0.

A New General Route to Diphosphenes via Germylated Compounds

Claude Couret, Jean Escudie, Henri Ranaivonjatovo, and Jacques Satgé*

Laboratoire de Chimie des Organominéraux, UA du CNRS No. 477, Université Paul Sabatier, 31062 Toulouse, France

Received April 10, 1985

Several (trichlorogermyl)phosphines RP(H)$GeCl_3$ (**3**) are prepared by two different routes: (i) from primary phosphines RPH_2 and germanium tetrachloride and (ii) from dichlorophosphines $RPCl_2$ and the dichlorogermylene–dioxane complex, $GeCl_2{\cdot}C_4H_8O_2$. Subsequent addition of **3** to an excess of DBU (1,5-diazabicyclo[5.4.0]undec-5-ene) affords the corresponding diphosphenes RP=PR. This method appears conveniently and generally applicable to the synthesis of diphosphenes. This reaction involves formation of chlorophosphine intermediates RP(H)Cl (**2**). Stable diphosphenes **1c**, bis(2,4,6-tri-*tert*-butylphenyl)-diphosphene, and **1e**, bis[bis(trimethylsilyl)methyl]diphosphene, can be isolated in excellent yield. Unstable dienophilic diphosphenes were characterized by cycloaddition with 1,3-dienes. Cycloadduct **12d**, obtained by reaction of di-*tert*-butyldiphosphene with cyclopentadiene, is a clean precursor of di-*tert*-butyldiphosphene, **1d**.

Introduction

Since the report by Yoshifuji et al. describing the synthesis and characterization of the first stable compound with a P=P bond, bis(2,4,6-tri-*tert*-butylphenyl)diphosphene,[1] this new class of unsaturated compounds has been of current interest.[2-10]

Diphosphenes have been obtained by several routes from reactions of the corresponding dichlorophosphines with various reagents: magnesium,[1,3] sodium,[4] or lithium derivatives,[5] bis(trimethylsilyl)mercury,[6] divalent species of group IVA[7] (14),[30] primary phosphines (dehydrochlorination in the presence of amines),[8] and silylphosphines (dechlorosilylation).[3,9] However, although all these methods are convenient for the preparation of some kinds of diphosphenes, there is currently no generally applicable methodology for the preparation of *all* diphosphenes.

In a preceding paper, we described the synthesis of bis[bis(trimethylsilyl)methyl]diphosphene via organogermanium compounds,[10] which is presently the only existing route to this diphosphene. Herein, we describe the

(1) (a) Yoshifuji, M.; Shima, I.; Inamoto, N.; Hirotsu, K.; Higuchi, T., *J. Am. Chem. Soc.* **1981**, *103*, 4587; (b) *Ibid.* **1982**, *104*, 6167.

(2) For recent reviews see: Cowley, A. H. *Polyhedron* **1984**, *3*, 389–432. Cowley, A. H.; Kilduff, J. E.; Lasch, J. G.; Mehrotra, S. K.; Norman, N. C.; Pakulski, M.; Whittlesey, B. R.; Atwood, J. L.; Hunter, W. E. *Inorg. Chem.* **1984**, *23*, 2582–2593.

(3) Smit, C. N.; Van der Knaap, T. A.; Bickelhaupt, F. *Tetrahedron Lett.* **1983**, *24*, 2031.

(4) Cowley, A. H.; Kilduff, J. E.; Newman, T. H.; Pakulski, M. *J. Am. Chem. Soc.* **1982**, *104*, 5820. Cowley, A. H.; Kilduff, J. E.; Pakulski, M.; Stewart, C. A. *Ibid.* **1983**, *105*, 1655.

(5) (a) Bertrand, G.; Couret, C.; Escudié, J.; Majid, S.; Majoral, J. P. *Tetrahedron. Lett.* **1982**, *23*, 3567. (b) Couret, C.; Escudié, J.; Satgé, J. *Ibid.* **1982**, *23*, 4941. Escudié, J.; Couret, C.; Ranaivonjatovo, H.; Satgé, J.; Jaud, J. *Phosphorus Sulfur* **1983**, *17*, 221. Niecke, E.; Rüger, R. *Angew. Chem.* **1983**, *95*, 154; *Angew. Chem., Int. Ed. Engl.* **1983**, *22*, 155. Niecke, E.; Rüger, R.; Lysek, M.; Pohl, S.; Schoeller, W. *Angew. Chem.* **1983**, *95*, 495; *Angew. Chem., Int. Ed. Engl.* **1983**, *22*, 486; *Angew. Chem. Suppl.* **1983**, 639. Schmidt, H.; Wirkner, C.; Issleib, K. *Z. Chem.* **1983**, *23*, 67. Cetinkaya, B.; Hudson, A.; Lappert, M. F.; Goldwhite, H. *J. Chem. Soc., Chem. Commun.* **1982**, 609, 691.

(6) Romanenko, V. D.; Klebalskii, E. O.; Markovskii, L. N. *Zh. Obshch. Khim.* **1984**, *54*, 465.

(7) Veith, M.; Huch, V.; Majoral, J. P.; Bertrand, G.; Manuel, G. *Tetrahedron Lett.* **1983**, *24*, 4219.

(8) (a) Cowley, A. H.; Kilduff, J. E.; Mehrotra, N. C.; Norman, N. C.; Pakulski, M. *J. Chem. Soc., Chem. Commun.* **1983**, 528. (b) Yoshifuji, M.; Shibayama, K.; Inamoto, N.; Matsushita, T.; Nishimoto, K. *J. Am. Chem. Soc.* **1983**, *105*, 2495.

(9) Escudié, J.; Couret, C.; Andriamizaka, J. D.; Satgé, J. *J. Organomet. Chem.* **1982**, *228* C76.

(10) Escudié, J.; Couret, C.; Ranaivonjatovo, H.; Satgé, J. *J. Chem. Soc., Chem. Commun.* **1984**, *24*, 1621.

0276-7333/86/2305-0113$01.50/0

general applicability of this method to the synthesis of almost all diphosphenes including very hindered, but stable diphosphenes, as well as unhindered and reactive diphosphenes. The major focus of this new method is the use of readily available precursors: primary phosphines, commercially available germanium tetrachloride, and 1,5-diazabicyclo[5.4.0]undec-5-ene (DBU).

Results and Discussion

In our experiments, we have observed that chlorophosphines **2** afford almost quantitatively diphosphenes **1** by dehydrochlorination with DBU. This reaction is illustrated employing the relatively stable chlorophosphine **2c** (eq 1). However, chlorophospines of type **2** are stable[11] only when bulky substituents are attached to phosphorus. Thus, it is necessary in other cases to use precursors of these compounds such as (trichlorogermyl)phosphines **3**, which also afford chlorophosphines **2** by reaction with DBU (eq 2) and thus can be used as in situ reagents for RP(H)Cl.

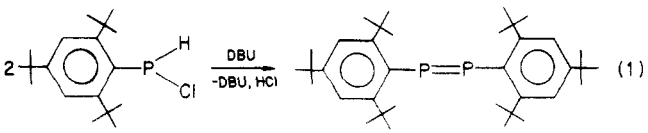

(1)

2c **1c**

$$RP(H)GeCl_3 \xrightarrow{DBU} RP(H)Cl + DBU\cdot GeCl_2 \quad (2)$$

3 **2**

(Trichlorogermyl)phosphines **3** are themselves easily prepared in excellent yield by two different routes, i and ii. (i) The addition of germanium tetrachloride to primary phosphines gives, after spontaneous evolution of hydrogen chloride, trichlorogermylphosphines in nearly quantitative yield (eq 3). This method appears especially convenient for the synthesis of (trichlorogermyl)phosphines, since these rapidly precipitate from the reaction mixture and can be easily isolated as the pure substances. (ii) Heating dioxane solution of dichlorogermylene–dioxane complex[12] and a dichlorophosphine at reflux gives, unexpectedly, the same (trichlorogermyl)phosphines **3** in variable yield (20–95%), depending of the substituent R (see Experimental section) (eq 4).

$$RPH_2 + GeCl_4 \xrightarrow[-HCl]{C_6H_6 \text{ (or } Et_2O)} RP(H)GeCl_3 \quad (3)$$

9a-e **3a-e**

a, R = Ph; **b**, Mes; **c**, 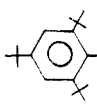 ; **d**, *t*-Bu; **e**, $(Me_3Si)_2CH$

$$RPCl_2 + GeCl_2\cdot C_4H_8O_2 \xrightarrow[110\ ^\circ C]{C_4H_8O_2} RP(H)GeCl_3 \quad (4)$$

4 **3**

The mechanism of formation of **3** by the latter route probably involves initial formation of the germylene–phosphine complex **5** (eq 5). Germylene–phosphine complexes have been described in the literature,[13] and they are generally obtained simply by mixing a germylene with a phosphine. Complex **5**, presumably would give the intermediate chloro(trichlorogermyl)phosphine **6**, corresponding to an insertion of $GeCl_2$ into the P–Cl bond of **5** (eq 6), consistent with the observation of Du Mont and Schumann of the reaction between di-*tert*-butylchlorophosphine and the dichlorogermylene–dioxane complex.[13d] Under these experimental conditions, we suggest germylphosphine **6** is thermally labile and undergoes decomposition by α-elimination with formation of germanium tetrachloride and a phosphinidene, **8** (eq 7). The latter then abstracts two hydrogen atoms from the solvent to afford phosphine **9**, which then reacts with germanium tetrachloride according to the already described reaction i (vide supra).

$$RPCl_2 + GeCl_2\cdot C_4H_8O_2 \xrightarrow[-C_4H_8O_2]{} [RPCl_2\cdot GeCl_2] \quad (5)$$

4 **5**

$$[RPCl_2\cdot GeCl_2] \xrightarrow[C_4H_8O_2]{110\ ^\circ C} [RP(Cl)GeCl_3] \quad (6)$$

5 **6**

$$[RP(Cl)GeCl_3] \xrightarrow[C_4H_8O_2]{110\ ^\circ C} [RP:] + GeCl_4 \xrightarrow{\text{solv}} RPH_2 + GeCl_4 \quad (7)$$

6 **8** **9**

$$RPH_2 \xrightarrow{-HCl} RP(H)GeCl_3$$

3

In the experimental conditions, primary phosphines **9** and $GeCl_4$ react immediately to give **3**; but their formation is unambiguously proved by recent results (not yet published): in the reaction between $RPCl_2$ and $GeCl_2\cdot C_4H_8O_2$ (R = 2,4-bis(trifluoromethyl)phenyl) quantitative formation of phosphine **9** and $GeCl_4$ have been observed because, in this case, reaction between these two derivatives is very difficult (heating at 110 °C for 24 h).

Synthesis and Characterization of Diphosphenes

The addition of (trichlorogermyl)phosphines **3**, in benzene solution, to an excess (100%) of DBU gives immediately the corresponding diphosphenes and a mixture of solid materials identified as the hydrochloride DBU·HCl and the complex $DBU\cdot GeCl_2$[14] (eq 8).

$$2RP(H)GeCl_3 \xrightarrow{DBU} RP{=}PR + 2DBU\cdot GeCl_2 + 2DBU\cdot HCl \quad (8)$$

3 **1**

When R is a bulky substituent, monomeric diphosphenes are obtained: **1c** (R = 2,4,6-tri-*tert*-butylphenyl) and **1e** (R = bis(trimethylsilyl)methyl). With other substituents, oligomers $[(RP)_n]$ **1a** (R = phenyl, n = 5), **1b** (R = 2,4,6-trimethylphenyl, n = 3, 4), and **1d** (R = *tert*-butyl, n = 3, 4) are the major products.

(a) Mechanism of Formation of Diphosphenes. Our mechanistic ideas on the formation of diphosphenes from

(11) Halophosphines RP(H)X are generally unstable and lose HX to afford the corresponding cyclopolyphosphines. The only exception was trifluoromethylhalophosphines $CF_3P(H)X$: Dobbie, R. C.; Gosling, P. D.; Straughan, B. P. *J. Chem. Soc., Dalton Trans.* **1975**, 2368.

(12) Kolesnikov, S. P.; Shiryaev, V. I.; Nefedov, O. M. *Izv. Akad. Nauk SSSR, Ser. Khim.* **1966**, 584.

(13) (a) King, R. B. *Inorg. Chem.* **1963**, *2*, 199. (b) Escudié, J.; Couret, C.; Rivière, P.; Satgé, J. *J. Organomet. Chem.* **1977**, *124*, C45. (c) Schumann, H.; Du Mont, W. W. *J. Organomet. Chem.* **1975**, *85*, C45. (d) Du Mont, W. W.; Neudert, B.; Rudolph, G.; Schumann, H. *Angew. Chem.* **1976**, *88*, 303; *Angew. Chem., Int. Ed. Engl.* **1976**, *15*, 308.

(14) The complex $DBU\cdot GeCl_2$ can be obtained by a direct synthesis from DBU and $GeCl_2\cdot Et_2O$. It has been identified by mass spectroscopy (field desorption (^{74}Ge, ^{35}Cl), m/e 296 (M^+)).

3 are derived specifically from the use of **3c** (where R = 2,4,6-tri-*tert*-butylphenyl) owing to the stability of the intermediate **2c**. Indeed, the first step of the reaction between (trichlorogermyl)phosphine **3c** and DBU is the formation of the chlorophosphine **2c** and the DBU·$GeCl_2$ complex. This process has been demonstrated by using a stoichiometric amount of DBU. Further addition of a 100% excess of DBU gives diphosphene **1c** in virtually quantitative yield (see eq 9, route a).

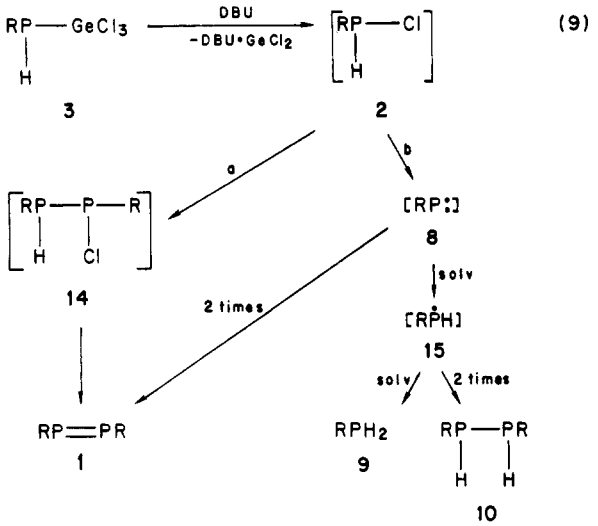

(9)

With other substituents, formation of diphosphenes **1** with minor quantities of phosphines **9** and diphosphines **10** are observed. For example, when R is the bis(trimethylsilyl)methyl group, the product ratio of **1e**/**9e**/**10e** is 55/25/20. Formation of these three compounds from **2** can be explained by pathways a and b (eq 9). Route a leads to the expected diphosphene via an intermolecular dehydrochlorination with formation of intermediate **14**. Route b leads to **9** and **10** via an intramolecular dehydrochlorination giving the phosphinidene **8** which we postulate is the precursor of radical intermediate **15**. Phosphine **9** and diphosphine **10** arise from intermediate **15** by hydrogen abstraction from the solvent or by dimerization, respectively. Dimerization of phosphinidene **8** to diphosphene **1** cannot be excluded.

(b) Characterization of Diphosphenes. Stable diphosphenes **1c** and **1e** have been isolated and unambiguously identified by their characteristic δ (^{31}P) NMR resonance at very low field; **1c** at +493 ppm;[1b] **1e** at + 517 ppm.[10] Unstable diphosphenes **1a**, **1b**, and **1d** have been characterized by trapping reactions with 2,3-dimethylbuta-1,3-diene or cyclopentadiene (eq 10).

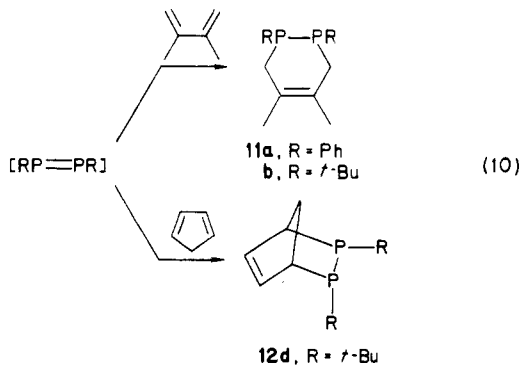

(10)

Cycloadduct **12d** has been isolated and characterized and has been prepared by an independent synthesis. For example, the reaction between *tert*-butyldichlorophosphine and *tert*-butylbis(trimethylsilyl)phosphine using cyclopentadiene as solvent gives **12d** according to a procedure previously described for the synthesis of **11d**[9] (eq 11). The

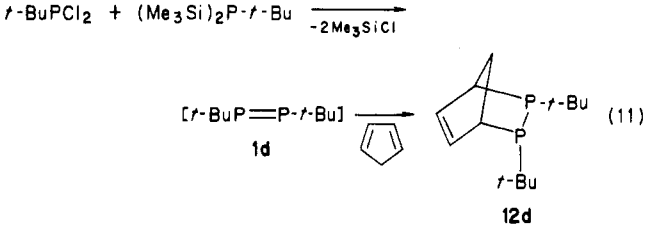

(11)

retro-Diels–Alder decomposition of **12d** should afford **1d**. Evidence for such thermal decomposition of **12d** with formation of **1d** was obtained by the novel "diene exchange". Thus, heating **12d** in the presence of 2,3-dimethylbuta-1,3-diene affords **11d** in good yields (85%) (eq 12). Small amounts of phosphine **9d** (thermal decomposition of **10d**[29]) and diphosphine **10d** (from diradical **13d**) also were obtained in this reaction.

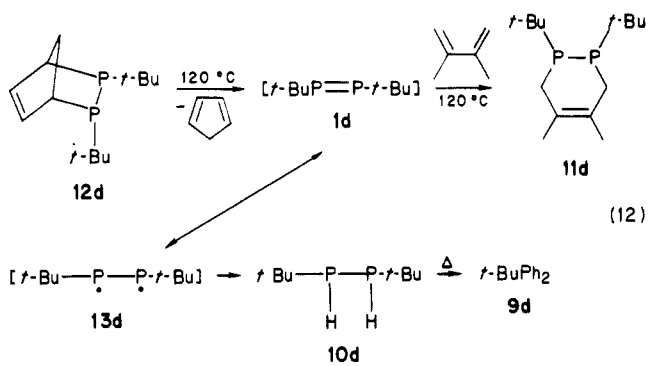

(12)

When R is a mesityl group, the trapping reaction of dimesityldiphosphene (**1b**) by cyclopentadiene gives the diphosphine **10b** in quantitative yield. We rationalize this reaction by assuming that the low thermal stability of the cycloadduct **12b** at room temperature results in formation of cyclopentadiene and **13b**. **13b**, which we write as a diradical, then abstracts two hydrogen atoms from the solvent (eq 13).

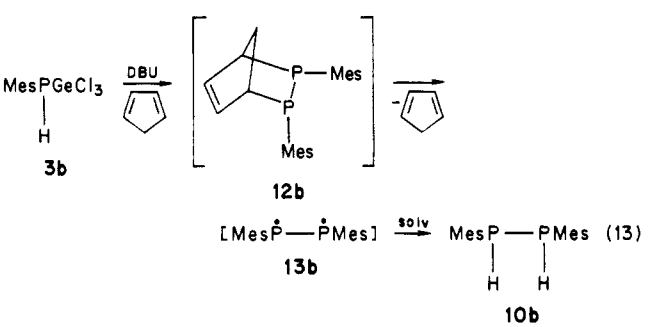

(13)

In summary, this organogermanium route to diphosphenes appears to be a general one; it has allowed in particular the synthesis of a very interesting diphosphene, bis[bis(trimethylsilyl)methyl]diphosphene which, while stable, also is reactive and was not accessible by other ways. This new diphosphene should allow an extensive investigation of the reactivity of the diphosphenes, which, until now, is only poorly developed.

Experimental Section

General Comments. All syntheses were performed under an atmosphere of dry nitrogen using standard Schlenk or high-vacuum line techniques. Solvents were dried by distillation from sodium benzophenone ketyl immediately prior to use. Commercial 2,3-dimethylbuta-1,3-diene, cyclopentadiene, and 1,5-diazabicy-

clo[5.4.0]undec-5-ene (DBU) were freshly distilled under nitrogen. $GeCl_4$ was purchased from Sogemet and $PhPCl_2$ from Fluka. The complex $GeCl_2{\cdot}C_4H_8O_2$ was prepared according to the method of Kolesnikov.[12]

Dichlorophosphines **4** were prepared by reaction of PCl_3 with Grignard or lithio compounds: **4b**,[15] **4c**,[1a] **4d**,[16] **4e**.[17] Primary phosphines **9** were obtained by reduction of corresponding dichlorophosphines **4** by $LiAlH_4$: **9a**,[18] **9b**,[19] **9c**,[20] **9d**,[21] **9e**.[10]

^1H NMR spectra were recorded on a Varian EM 360 A at 60 MHz and Bruker WH 90 at 90 MHz. ^{31}P NMR spectra were recorded on a Bruker WH 90 at 36.44 MHz. Chemical shifts are reported in parts per million from internal Me_4Si for ^1H and from external 85% H_3PO_4 for ^{31}P. Downfield shifts are noted positive in all cases. Infrared spectra were recorded on a Perkin-Elmer 457 grating spectrometer. Mass spectra were performed on a Varian MAT 311 A spectrometer (EI) and a Ribermag R 1010 spectrometer (desorption). For (trichlorogermyl)phosphines, experimental molecular peaks patterns were assigned after comparison with theoretical peaks patterns calculated on a Tektronics 4051.

Melting points were determined on a Reichert apparatus and are uncorrected. Elemental analyses were done by the "Service Central de Microanalyse du CNRS", Vernaison, France.

Synthesis of (Trichlorogermyl)phosphines 3.[22] **(a) From Primary Phosphines 9 and Germanium Tetrachloride.** The (trichlorogermyl)phosphines **3** (except **3c**) were synthesized according to the experimental procedure which we describe in detail below for the case of **3a**. The 100-mL three-necked flask used for the reaction was connected to a trap cooled to −196 °C. To a stirred solution of **9a** (4.4 g, 40.0 mmol) in benzene (50 mL) was added slowly a large excess of $GeCl_4$ (25 g, 300% excess) at room temperature. A white precipitate appeared immediately. The reaction mixture was stirred for 30 min and then frozen to 0 °C. Hydrogen chloride then was eliminated in vacuo from the reaction mixture, trapped in a receiver cooled to −196 °C, and titrated with a 1 N solution of NaOH. Yield of HCl: 95%. The reaction mixture was allowed to warm to room temperature. Filtration afforded white crystals of **3a**; yield 10.0 g (87%).

In the case of **3c**, 24-h stirring with periodical elimination of HCl from the solution, in vacuo, was necessary for completion of the reaction.

3a: mp 69–72 °C dec; ^1H NMR (C_6D_6) δ 4.66 (d, $^1J(PH)$ = 198 Hz, 1 H, PH); $^{31}P\{^1H\}$ NMR (C_6D_6) δ −67.8; IR (KBr) ν(PH) 2290 cm^{-1}; mass spectrum (field desorption, ^{35}Cl, ^{74}Ge), m/e 288 (M^+)). Anal. Calcd for $C_6H_6Cl_3GeP$: C, 25.21; H, 2.10; Cl, 36.93. Found: C, 24.87; H, 2.01; Cl, 37.12.

3b: mp 23–25 °C; ^1H NMR (C_6D_6) δ 1.96 (s, 3 H, *p*-Me), 2.23 (s, 6 H, *o*-Me), 4.65 (d, $^1J(PH)$ = 210 Hz, 1 H, PH), 6.63 (br s, 2 H, aromatic H); $^{31}P\{^1H\}$ NMR (C_6D_6) δ −94.8; IR (KBr) ν(PH) 2320 cm^{-1}; mass spectrum (desorption, ^{35}Cl, ^{74}Ge), m/e 330 (M^+). Anal. Calcd for $C_9H_{12}Cl_3GeP$: C, 32.76; H, 3.66; Cl, 32.22. Found: C, 33.01; H, 3.89; Cl, 31.86.

3c: mp 150–155 °C dec; ^1H NMR (C_6D_6) δ 1.23 (s, 9 H, *p*-*t*-Bu), 1.50 (s, 18 H, *o*-*t*-Bu), 5.90 (d, $^1J(PH)$ = 212 Hz, 1 H, PH), 7.51 (br s, 2 H, aromatic H); $^{31}P\{^1H\}$ NMR (C_6D_6) δ −59.6; IR (KBr) ν(PH) 2270 cm^{-1}; mass spectrum (field desorption, ^{35}Cl, ^{74}Ge), m/e 456 (M^+). Anal. Calcd for $C_{18}H_{30}Cl_3GeP$: C, 47.37; H, 6.63; Cl, 23.31. Found: C, 47.41; H, 6.76; Cl, 23.11.

3d: mp 49–52 °C dec; ^1H NMR (C_6D_6) δ 1.26 (d, $^3J(PH)$ = 13.0 Hz, 9 H, *t*-Bu), 3.86 (d, $^1J(PH)$ = 193 Hz, 1 H, PH); $^{31}P\{^1H\}$ NMR (C_6D_6) δ −21.4; IR (KBr) ν(PH) 2270 cm^{-1}; mass spectrum (field desorption, ^{35}Cl, ^{74}Ge), m/e 456 (M^+). Anal. Calcd for $C_4H_{10}Cl_3GeP$: C, 17.92; H, 3.76; Cl, 39.68. Found: C, 18.07; H, 3.97; Cl, 39.92.

3e:[10] mp 46–49 °C dec; ^1H NMR (C_6D_6) δ 0.15 (s, 18 H, Me_3Si), 3.58 (d, $^1J(PH)$ = 185 Hz, ^1H, PH); $^{31}P\{^1H\}$ NMR (C_6D_6) δ −72.5; IR (KBr) ν(PH) 2268 cm^{-1}; cryoscopy (C_6H_6) calcd 370.1, found 366. Anal. Calcd for $C_6H_{20}Cl_3GePSi_2$: C, 22.70; H, 5.44; Cl, 28.72. Found: C, 23.02; H, 5.76; Cl, 29.08.

(b) From Dichlorophosphines 4 and the Dichlorogermylene–Dioxane Complex. All reactions were performed according to the same procedure. A solution of the alkyl- or aryldichlorophosphine **4** (10 mmol), dichlorogermylene–dioxane complex (10 mmol), and 1,4-dioxane (20 mL) was heated at 110 °C for 1 h. Analysis of the reaction mixture, performed by ^1H and ^{31}P NMR, showed the formation of the (trichlorogermyl)-phosphines **3**, previously prepared (see above). Dioxane was eliminated in vacuo and replaced by benzene. A white precipitate of **3** appeared immediately; filtration afforded pure **3**. Other products were sometimes obtained in these reactions and were identified on the basis their literature data (^1H and ^{31}P NMR).

Derivatives obtained from **4** and the dichlorogermylene–dioxane complex and yields calculated by NMR: from **4a**, **3a** (20%), $(PhP)_5$[23] (70%); from **4b**, **3b** (85%); from **4c**, **3c** (70%), **9c** (20%);[5a,20,24] from **4d**, **3d** (40%), $(t\text{-BuP})_4$[25] (10%) [$^{31}P\{^1H\}$ NMR (C_6D_6) δ −58], other unidentified products; from **4e**, **3e** (85%).

Synthesis of 1c. (a) Characterization of Chlorophosphine 2c. To a suspension of **3c** (3.50 g, 7.7 mmol) in 15 mL of C_6H_6 was slowly added a stoichiometric quantity of DBU (1.17 g, 7.7 mmol). The reaction mixture was stirred for 30 min at room temperature, and then benzene was evaporated in vacuo and replaced by pentane (10 mL). After elimination of complex DBU·$GeCl_2$ by centrifugation, ^1H and ^{31}P NMR analysis of the solution showed the nearly quantitative formation of chlorophosphine **2c**: ^{31}P NMR (C_6D_6) δ + 21.3 ($^1J(PH)$ = 216 Hz). **2c** has recently been obtained by Cowley.[26]

(b) Preparation of 1c. Addition of an excess of DBU (100%) to the mixture of chlorophosphine **2c** and the DBU·$GeCl_2$ complex gives immediately a light yellow precipitate and an orange solution. Benzene was removed in vacuo, and 20 mL of pentane was added to allow complete precipitation of DBU·HCl and DBU·$GeCl_2$. After filtration, the orange solution was evaporated and the residue was chromatographed on silica gel with pentane (R_f ~0.7) to afford an orange solid (1.65 g, yield 78 %), identified as **1c** according to its physicochemical data,[1] particularly its very low-field ^{31}P NMR chemical shift, +493 ppm.[1b]

1c can also be obtained in one step by reaction of (trichlorogermyl)phosphine **3c** with an excess of DBU. In this case, the same result was obtained by the addition of **3c** to DBU or by the addition of DBU to **3c** because of the stability of the chlorophosphine intermediate **2c**. In the other cases, since chlorophosphines **2a**, **2b**, **2d**, and **2e** are not stable, better yields of diphosphenes were obtained by addition of the corresponding (trichlorogermyl)phosphines to an excess of DBU.

Synthesis of 1e. A solution of **3e** (2.88 g, 7.8 mmol) in benzene (20 mL) was added by syringe to a solution of DBU (4.72 g, 31.2 mmol, 100% excess) in benzene (10 mL) at room temperature. The reaction mixture was stirred for 30 min at room temperature; after elimination of benzene in vacuo and addition of pentane (20 mL), filtration gave an orange solution. A ^{31}P NMR analysis showed the formation of three products in the relative percentages: **1e**, 55%; **9e**, 25%; **10e**, 20%.

These three products were identified on the basis of their literature data.[10]

1e: ^{31}P NMR (C_6D_6) δ +517; mass spectrum (field desorption), m/e 380 (M^+).

(15) Brazier, J. L.; Mathis, F.; Wolf, R. *C. R. Hebd. Acad. Sci., Ser. C* **1966**, *262*, 1393.
(16) Voskuil, W.; Arens, J. F. *Recl. Trav. Chim. Pays-Bas* **1963**, *82*, 302.
(17) Gynane, M. J. S.; Hudson, A.; Lappert, M. F.; Power, P. P.; Goldwhite, H. *J. Chem. Soc., Dalton Trans.* **1980**, 2428.
(18) Horvat, R. J.; Furst, A. *J. Am. Chem. Soc.* **1952**, *74*, 562.
(19) Kosolapoff, G. M.; Maier, L., Eds. "Organic Phosphorus Compounds"; Wiley-Interscience: New York, 1972; Vol. 1, Chapter 1.
(20) Issleib, K.; Schmidt, H.; Wirkner, C. *Z. Anorg. Allg. Chem.* **1982**, *488*, 75.
(21) Issleib, K.; Hoffmann, H. *Chem. Ber.* **1966**, *99*, 1320.
(22) Tris(trimethylsilyl)methylphosphine, $(Me_3Si)_3CPH_2$, does not react with germanium tetrachloride in refluxing benzene presumably for steric reasons.
(23) Fluck, E.; Issleib, K. *Chem. Ber.* **1965**, *98*, 2674.
(24) Zschunke, A.; Baver, E.; Schmidt, H.; Issleib, K. *Z. Anorg. Allg. Chem.* **1982**, *495*, 115.
(25) Issleib, K.; Hoffmann, M. *Chem. Ber.* **1966**, *99*, 1320.
(26) Cowley, A. H.; Kilduff, J. E.; Norman, N. C.; Pakulski, M.; Atwood, J. L.; Hunter, W. E. *J. Am. Chem. Soc.*, **1983**, *105*, 4845.

9e: ^{31}P NMR (C_6D_6) δ −149 ($^1J(PH)$ = 188 Hz); ^1H NMR (C_6D_6) δ 0.07 (s, 18 H, Me_3Si), 2.67 (dd, $^1J(PH)$ = 188 Hz) $^3J(HH)$ = 8.0 Hz, 2 H, PH).

10e: two diastereoisomers; AA'XX' systems. As the low intensity bands have not been assigned with precision, the AA'XX' system has not been completely elucidated; only the sum of the two coupling constants $^1J(PH)$ and $^2J(PH)$ has been determined. **10'e** (40%): ^{31}P NMR (C_6D_6) δ −90.0 ($^1J(PH) + {}^2J(PH)$ = 195 Hz). **10'e** (60%): ^{31}P NMR (C_6D_6) δ = −97.9 ($^1J(PH) + {}^2J(PH)$ = 183 Hz).

No trace of $[(Me_3Si)_2CH - P]_n$ (n = 3, 4) was detected. A rapid distillation on a short column afforded a mixture of **1e** and **10e** and a minor quantity of oligomers $[(Me_3Si)_2CH - P]_n$ (n = 3,[8a] 4: $^{31}P\{^1H\}$ NMR (C_6D_6) δ −17.0 (s)) (10%). The latter were formed by heating diphosphene **1e** during the distillation.

Action of DBU on (Trichlorogermyl)phosphines 3a, 3b, and 3d without Trapping Reagent. Addition of a suspension of (trichlorogermyl)phosphines **3a**, **3b**, or **3d** (10 mmol) in pentane to DBU (50% excess) results immediately in the formation of a precipitate of DBU·$GeCl_2$ and DBU·HCl. Subsequent filtration gave a colorless solution. ^{31}P NMR analysis showed, in every case, the formation in very good yield (more than 80%) of the oligomers $(RP)_n$, identified when R is a phenyl or a *tert*-butyl group by their literature data. R = Ph: $(PhP)_5$,[23] ^{31}P (C_6H_6) δ +4.4. R = *t*-Bu: $(t\text{-BuP})_3$[27] (80%), $^{31}P\{^1H\}$ NMR (C_6D_6, A_2B system) δ(A) − 71.0, δ(B) −69.6 (J(AB) = 201.1 Hz); $(t\text{-BuP})_4$[25] (20%), $^{31}P\{^1H\}$ NMR (C_6D_6) δ −58.

When R is a mesityl group, the reaction mixture was filtered and excess DBU eliminated at 80 °C (10^{-2} mmHg). The residue was crystallized from C_6H_6 to afford a mixture of $(MesP)_3$ (75%) and $(MesP)_4$ (25%). $(MesP)_3$: $^{31}P\{^1H\}$ NMR (C_6D_6, A_2B system) δ(A) −111.6, δ(B) −145.8 (J(AB) = 179 Hz). $(MesP)_4$: $^{31}P\{^1H\}$ NMR (C_6D_6) δ −45.4 (s). Mass spectrum (EI, 70 eV): m/e 600 $(MesP)_4$, 450 $(MesP)_3$.

Synthesis of 11a. A suspension of (trichlorogermyl)phosphine **3a** (3.18 g, 11.0 mmol) in pentane (20 mL) was added to a solution of DBU (6.71 g, 44.0 mmol) in 2,3-dimethylbuta-1,3-diene (15 mL) at room temperature. Immediate filtration of solid DBU·HCl and DBU·$GeCl_2$ afforded a colorless solution. ^{31}P NMR analysis showed the formation of $(PhP)_5$[23] (see above) (50%), $PhPH_2$[19] (30%), and **11a** (20%) characterized on the basis its literature data:[28] $^{31}P\{^1H\}$ NMR (C_6D_6) δ −23 (s); mass spectrum (EI, 70 eV), m/e 298 (M^+).

Synthesis of 11d. (a) From 3d and DBU. A solution of **3d** (1.80 g, 6.7 mmol) in benzene (15 mL) was slowly added to a solution of DBU (4.08 g, 26.8 mmol, 100% excess) in 2,3-dimethylbuta-1,3-diene (15 mL) at room temperature. A precipitate appeared immediately. After elimination of solvents (benzene and DMB) in vacuo, 20 mL of pentane was added, and the reaction mixture was filtered to remove DBU·$GeCl_2$ and DBU·HCl. Distillation gave pure **11d** (0.60 g, 69%) identified by its literature data:[9] bp 138–139 °C (2 mmHg); ^1H NMR (C_6D_6) δ 1.23 (pseudotriplet, $X_9AA'X'_9$ system, $(^3J(PH) + {}^4J(PH)$ = 12.2 Hz, 18 H, *t*-Bu), 1.77 (s, 6 H, MeC), 2.07–2.40 (m, 4 H, CH_2C); ^{31}P NMR (C_6D_6) δ −11.4.

(b) From 12d and 2,3-Dimethylbuta-1,3-diene. A mixture of **12d** (1.50 g, 6.2 mmol) and 2,3-dimethylbuta-1,3-diene (5.15 g, large excess) was heated in a sealed tube at 120 °C for 15 h. ^1H and ^{31}P NMR analysis of the reaction mixture showed the formation of **11d**, **9d**, and **10d** in the relative percentages of 85/10/5. No oligomers $(t\text{-BuP})_n$ were detected, demonstrating the efficient trapping of the diphosphene generated from **12d**.

9d[19] and **10d**[29] were unambiguously identified by their ^{31}P NMR data. **9d**: ^{31}P NMR (C_6D_6) δ −82. **10d**: ^{31}P NMR (C_6D_6, two diastereoisomers **10'd** and **10''d**, AA'XX' system) **10'd**, δ −62.0 ($^1J(PP)$ = −206 Hz), **10''d**, δ −60.8 ($^1J(PP)$ = −162 Hz).

Distillation of the reaction mixture gave pure **11d** identified by its physicochemical data[9] (see above) (1.20 g, 75%).

Synthesis of 12d. (a) By Me_3SiCl Elimination. A mixture of *tert*-butyldichlorophosphine (8.54 g, 53.7 mmol), *tert*-butylbis(trimethylsilyl)phosphine (12.57 g, 53.7 mmol), and cyclopentadiene (20 g, large excess) was heated in a sealed tube at 90 °C for 72 h. A rapid distillation using a short column afforded **12d**: yield 8.45 g (65%); bp 95 °C (0.02 mmHg); ^1H NMR (C_6D_6) δ 0.90 (d, $^3J(PH)$ = 13.4 Hz, 9 H, endo *t*-Bu), 1.13 (d, $^3J(PH)$ = 12.4 Hz, 9 H, exo *t*-Bu); $^{31}P\{^1H\}$ NMR (C_6D_6) (AB system) δ −1.8 and −6.1 ($^1J(PP)$ = 272 Hz). Anal. Calcd for $C_{13}H_{24}P_2$: C, 64.44; H, 9.98. Found: C, 65.01; H, 10.22.

(b) From 3d and DBU. A solution of **3d** (2.11 g, 7.9 mmol) in benzene (15 mL) was added to a solution of DBU (4.78 g, 31.6 mmol) in cyclopentadiene (15 mL) at room temperature. The precipitate that appeared immediately was filtered. After evaporation of solvents from the filtrate in vacuo, the residue was extracted with pentane. Distillation of the extracts gave **12d** (1.17 g, 61%) (see data above).

(27) Baudler, M.; Hahn, J.; Dietsch, H.; Furstenberg, G. *Z. Naturforsch., B: Anorg. Chem., Org. Chem.* **1976**, *31B*, 1305.

(28) Meriem, A.; Majoral, J. P.; Revel, M.; Navech, J. *Tetrahedron Lett.* **1983**, *24*, 1975.

(29) Baudler, M.; Gruner, C.; Tschabunin, H.; Hahn, J. *Chem. Ber.* **1982**, *115*, 1739.

(30) In this paper the periodic group notation is in accord with recent actions by IUPAC and ACS nomenclature committees. A and B notation is eliminated because of wide confusion. Groups IA and IIA become groups 1 and 2. The d-transition elements comprise groups 3 through 12, and the p-block elements comprise groups 13 through 18. (Note that the former Raman number designation is preserved in the last digit of the new numbering: e.g., III → 3 and 13.)

Lewis Acidities of Trialkylhalostannanes

J. N. Spencer, Robert B. Belser, Susan R. Moyer, Ronald E. Haines, Maria A. DiStravalo, and Claude H. Yoder*

Department of Chemistry, Franklin and Marshall College, Lancaster, Pennsylvania 17604

Received May 29, 1985

The Lewis acidities of R_3SnX (R = CH_3, C_2H_5, C_3H_7, C_4H_9, C_6H_5; X = Cl, Br, I) relative to triphenylphosphine oxide in benzene solvent were determined calorimetrically and by ^{31}P NMR. Equilibrium constants determined for the 1:1 adducts by both methods were in generally good agreement. The enthalpies and entropies of adduct formation show that the acidities decrease slightly as the size of the alkyl group increases and increase as the size of the halogen increases. These trends are discussed in terms of a model that attributes the observed trends to polarizability effects in the adduct and changes in steric congestion upon adduct formation.

Introduction

Although the organotin halides are among the most studied group 14 halides, their complexes have been thoroughly characterized for only a few systems.[1,2] In particular, for the triorganotin halides, which form 1:1 adducts with Lewis bases,[3-5] only trimethyltin chloride seems to have been the object of several investigations. Two studies have been concerned with the effect of varying alkyl chain length on the acidity of trimethyltin chloride,[3,4] one study has examined the acidity of trimethyltin iodide[6] and investigation of the adducts of $(CH_3)_3SnCl$ with various bases has been reported.[7]

The present work was undertaken to provide a systematic investigation of the effects of alkyl and halo substituents on the Lewis acidity of triorganotin halides. Both calorimetric and NMR spectroscopic techniques were employed to determine the equilibrium constants and attendant thermodynamic parameters for complexation of these acids with triphenylphosphine oxide (TPPO). TPPO was used as a reference base because of its moderate basicity and its NMR-active ^{31}P nucleus.

Experimental Section

ACS reagent grade benzene and cyclohexane were refluxed over P_2O_5 and then distilled over nitrogen or argon and stored over activated Linde type 4A molecular sieves. ACS reagent grade Me_2SO was dried over $CaCl_2$ for 24 h and then fractionally distilled under reduced pressure and collected over activated molecular sieves. Fisher Scientific gold label pyridine was refluxed over KOH for several hours, distilled under nitrogen, and collected over activated molecular sieves. Aldrich reagent grade quinuclidine was sublimed under reduced pressure and stored in vacuo. Aldrich reagent grade TPPO was dried at 110 °C for 24 h and stored in vacuo (mp 156-157 °C). Alfa or Aldrich halostannanes were sublimed or distilled in vacuo before use. The melting or boiling points of all acids were in good agreement with literature values. Carbon-13 and tin-119 NMR spectra were also used as a criterion of purity.

All reagents and solvents were handled in a glovebag or drybox under argon. Glassware was oven-dried at 110 °C and cooled either in a vacuum desiccator or in a glovebag.

All calorimetric analysis was done with a Model 450 Tronac calorimeter with ampule assembly and 25-mL reaction vessel. Ampules were oven-dried for at least 24 h, filled and capped in a glovebag, and then heat sealed.

The base concentrations varied from 0.05 to 0.3 M while the acid concentrations ranged from 0.004 to 0.04 M. Errors in concentrations are estimated to contribute less than 1% to the total experimental error.

The calorimetric data were analyzed by a least-squares technqiue. The heat change for n reactions in the reaction vessel can be given by

$$Q = \sum_i n_i, \Delta H_i$$

where n_i is the number of moles of adduct produced for a given acid and base concentration. Q is the heat for a given determination, corrected for the enthalpy of solution of the acid. A minimum of 6 runs were used to determine Q for a given reaction. Enthalpies of solution for the acids are given in Table I. The equilibrium constant and enthalpy change are found from the error square sum over the data points.

$$U(K_i,\Delta H_i) = \sum(Q - \sum_i n_i \Delta H_i)^2$$

The best values for K and ΔH are those which minimize $U(K_i,\Delta H_i)$. The error analysis is that given by Rosseinsky and Kellawi.[8]

Phosphorus-31 spectra were obtained on a JEOL FX-90Q at 25 °C in 10 mm tubes. Stock solutions of acid and base, both 0.2 M in benzene, were prepared and then mixed equally by volume in a 10-mL volumetric flask. A 5-mL aliquot was in turn diluted to 10 mL, and this was repeated until six solutions, ranging in concentrations from 0.1 to 0.001 M were prepared. A standard, trimethyl phosphate, dissolved in deuterioacetone in a 1:50 ratio was present in a coaxial tube. The equilibrium constant for formation of a 1:1 adduct can be obtained from the exchange-averaged chemical shift of some nucleus using the equation[9]

$$\Delta = \Delta_c - (\Delta_c/K)^{1/2}(\Delta/C_0)^{1/2}$$

where Δ is the difference between the chemical shift of the solution and that of the base, Δ_c is the difference between the chemical shift of the adduct and the free base, and C_0 is the initial concentration of the acid and base. The equilibrium constant is obtained from the slope of a plot of Δ vs. $(\Delta/C_0)^{1/2}$. The standard

Table I. Enthalpies of Solution in Benzene (298 K)

	$\Delta\bar{H}_s$, kcal mol^{-1}		$\Delta\bar{H}_s$, kcal mol^{-1}
$(CH_3)_3SnCl$(s)	+4.42 ± 0.20	$(C_2H_5)_3SnBr$(l)	+0.88 ± 0.21
$(CH_3)_3SnBr$(l)	+1.02 ± 0.13	$(C_3H_7)_3SnCl$(l)	+1.01 ± 0.11
$(CH_3)_3SnI$(l)	+0.49 ± 0.13	$(C_4H_9)_3SnCl$(l)	+1.27 ± 0.02
$(C_2H_5)_3SnCl$(l)	+1.17 ± 0.02	$(C_6H_5)_3SnCl$(s)	+5.21 ± 0.44

(1) (a) Satchell, D. P. N.; Satchell, R. S. *Chem. Rev.* **1969**, *69*, 251. (b) Ruidisch, I.; Schmidbaur, H.; Schumann, H. "Halogen Chemistry"; Gutmann, V., Ed.; Academic Press: New York, 1967; Vol. 2, p 233. (c) Poller, R. C. *J. Organomet. Chem.* **1965**, *3*, 321. (d) Davies, A. G.; Smith, P. J. "Comprehensive Organometallic Chemistry", Vol. 2, Wilkinson, G., Stone, F. G. A., Abel, W., Eds.; Pergamon Press: New York, 1982; Vol. 2, p 519. (e) Zubiata, J. A.; Zuckerman, J. J. *Prog. Inorg. Chem.* **1978**, *24*, 251.

(2) Guryanova, E. N.; Goldshtein, J. P.; Romm, J. P. "Donor Acceptor Bond"; Wiley: New York, 1975.

(3) Matwioff, N. A.; Drago, R. S. *Inorg. Chem.* **1964**, *3*, 337.

(4) Graddon, D. P.; Rana, B. A. *J. Organomet. Chem.* **1976**, *105*, 51.

(5) Farhangi, Y.; Graddon, D. P. *J. Organomet. Chem.* **1975**, *87*, 67.

(6) Bolles, T. F.; Drago, R. S. *J. Am. Chem. Soc.* **1966**, *88*, 5730.

(7) Bolles, T. F.; Drago, R. S. *J. Am. Chem. Soc.* **1966**, *88*, 3921.

(8) Rosseinsky, D. R.; Kellawi, H. *J. Chem. Soc. A* **1969**, 1207.

(9) Zeldin, M.; Mehta, P.; Vernon, W. P. *Inorg. Chem.* **1979**, *76*, 265.

0276-7333/86/2305-0118$01.50/0

Table II. Thermodynamic Parameters for the Formation of Adducts of Triorganotin Halides with Triphenylphosphine Oxide[a] (298 K)

	$-\Delta H°$, kcal mol^{-1}	K_{CAL}[c]	$-\Delta S°$, cal K^{-1} mol^{-1}	K_{NMR}[b]
$(CH_3)_3Sn$–Cl	8.1 ± 0.1	21.4 ± 0.5	21 ± 0.4	14
$(CH_3)_3Sn$–Br	8.3 ± 0.1	19 ± 1	22 ± 0.4	18
$(CH_3)_3Sn$–I	9.4 ± 0.3	11 ± 1	27 ± 1.0	12
$(C_2H_5)_3Sn$–Cl	8.3 ± 0.2	9.1 ± 0.4	23 ± 0.7	14
$(C_2H_5)_3Sn$–Br	8.7 ± 0.2	7.6 ± 0.5	25 ± 0.7	16
$(C_3H_7)_3Sn$–Cl	7.3 ± 0.2	5.0 ± 0.2	21 ± 0.7	10
$(C_4H_9)_3Sn$–Cl	7.6 ± 0.4	5.5 ± 0.6	22 ± 1.0	7
$(C_6H_5)_3Sn$–Cl	8.3 ± 0.1	12.6 ± 0.3	23 ± 0.3	15

[a] Benzene solvent. [b] Estimated error is ±20%. [c] Determined by calorimetric analysis.

state is molarity for both calorimetric and NMR analyses.

Results

The $\Delta H°$, $\Delta S°$, and equilibrium constants found by calorimetry are given in Table II. Also given in Table II are the equilibrium constants determined from NMR data. The equilibrium constants are given for the formation of 1:1 adducts. The formation of 1:1 adducts by the monhalotin derivatives is supported by previous isolation of 1:1 complexes,[1] X-ray structure determination[1e] of monohalo complexes and the linearity of the plot of Δ vs. $(\Delta/c)^{1/2}$. Computer simulations of 1:2 adduct formation and simultaneous formation of both 1:1 and 1:2 show that these possibilities produce curves with very marked curvature that bear no resemblance to the experimental plots.

Although the linearity of the NMR plots for 1:1 complexes was generally good as indicated by correlation coefficients of greater than 0.98, some runs produced plots with a slight concave curvature. Computer simulations of the effect of the formation of 1:2 adducts, 1:1 and 1:2 adducts, self-associated base, and associated adduct all produced Δ vs. $(\Delta/c)^{1/2}$ curves of drastically different curvature. Only the assumption of the formation of 10–20% of protonated base resulted in similar curvatures. When the acid was repurified by sublimation and even more rigorous anhydrous conditions were used, the curvature was reduced. Thus, hydrolysis of the acid is presumably responsible for this phenomena.

The thermodynamics of the formation of these 1:1 adducts can be rationalized with the following thermodynamic cycle for the interaction of an acid A with a base B:

$$A + e^- \rightarrow A\cdot \quad -EA \ (1)$$

$$B: \rightarrow B\cdot + e^- \quad IE \ (2)$$

$$A\cdot + B\cdot \rightarrow A\text{–}B \quad -BE \ (3)$$

$$A + B: \rightarrow A\text{–}B \quad \Delta H° = -EA + IE - BE$$

This gas-phase cycle has the advantage of using the homolytic bond energy (BE) as a measure of the strength of the adduct bond. The first step, the addition of an electron to the acid, is affected by the nature of the substituents on the acid moiety. Because the electron must be accommodated in an orbital eventually used to establish the A–B bond, any rehybridization and relief of steric congestion that occurs before (on) bonding to the base are also included in this step. The second step, removal of one electron from the base, can be ignored in a comparison of relative acidities. The third step is a function of the degree of overlap of A and B orbitals, π-interaction between A and B, ionic character in the A–B bond, steric repulsion between substituents on A and B, and other influences such as charge- or dipole-induced dipole interactions between substituents and the acid or base centers.

For the series of acids studied here, an increase in the size of the alkyl substituent should affect the electron affinity very little; a change from CH_3 to C_6H_5 should slightly increase the electron affinity; and a change from chloro to bromo to iodo should decrease the electron affinity of A. These predictions are supported by σ_I values: CH_3, –0.04; C_2H_5, –0.05; C_3H_7, –0.03; C_4H_9, –0.04; Cl, 0.47; Br, 0.44; I, 0.39; C_6H_5, 0.10. The similarity of the ^{119}Sn–^1H coupling constants in a series of trimethylhalostannane adducts has been cited previously as evidence that the hybridization in a variety of adducts is the same.[6]

The effect of the substituents on the homolytic bond energy is somewhat more difficult to predict. An increase in electronegativity of the substituent should lead to a decrease in energy of the tin hybrid and a consequent increase in overlap. On the other hand, the more polarizable groups should stabilize the negative formal charge on tin, but because these are also the bulkiest, they should produce increased steric repulsions.

Examination of the data in Table II shows that within experimental error $\Delta H°$ for the propyl and butyl derivatives is lower than $\Delta H°$ for the methyl and ethyl derivatives. For the halogens, there is a fairly consistent trend of increasing $-\Delta H°$ as the halogen gets larger. Within the framework of the thermodynamic model presented above, the first trend can only be explained by steric repulsions between the larger alkyl groups and the triphenylphosphine oxide and a consequent weakening of the adduct bond. Steric hindrance was also used to rationalize $\Delta H°$ for the interaction of $(CH_3)_3SnCl$ with a variety of bases.[7]

Rationalization of the second trend is more difficult because the decrease in electronegativity of the halogens from Cl to I should result in a decrease in electron affinity in step 1 and a decrease in bond strength due to less favorable overlap in step 2. On the other hand the larger halogens should produce more steric congestion between the alkyl groups in the tetrahedral molecule that can be relieved in the trigonal-bipyramidal adduct that probably contains the alkyl groups on the equatorial position.[1e] Moreover, the larger and more polarizable halogens can also stabilize the formal negative charge on the Sn of the adduct through the charge-induced dipole interaction. The $\Delta H°$ for the $(Ph)_3SnCl$ adduct can also be rationalized by the high polarizability of the phenyl group as well as its slight electron-withdrawing effect.

The large $\Delta H°$ for the $(CH_3)_3SnI$ adduct with several other bases has been previously attributed to a change in the Sn–X bond energy upon complexation. Because the Sn–I bond is weaker than the Sn–Cl bond, it was suggested that the Sn–I bond would be less affected than the Sn–Cl bond and that therefore the chloro adduct would have a lower $\Delta H°$ of complexation in spite of a greater tin–adduct bond energy.[6] This analysis adds the additional complication of a change in energy of bonds other than the adduct bond.

Indeed, the use of $\Delta H°$ as the indicator of relative acidities is problematic.[2,10] Some reviews[1a] have focused mainly on equilibrium constants, partly because of the paucity of thermodynamic parameters. For many adducts, the sensitivity of the equilibrium constant to structural effects is moderated by a linear relationship between $\Delta H°$ and $\Delta S°$. Because of this, $\Delta S°$ for adduct formation can also be used as a measure of the strength of the adduct. The change in entropy can be written as

(10) Shepp, A.; Bauer, S. H. *J. Am. Chem. Soc.* **1954**, *76*, 265.

$$\Delta S = \Delta S_{t,r} + \Delta S_v$$

where $\Delta S_{t,r}$, the change in translational and rotational entropy, is very similar for a series of acids and ΔS_v, the change in vibrational entropy, is due mainly to the new adduct bond.

Upon complex formation three degrees of translational and three degrees of rotational freedom are lost and $\Delta S_{t,r}$ must be negative. It is this loss of entropy which accounts for the negative entropy changes of Table II. However, the vibrational entropy change must be positive because six new vibrational degrees of freedom result from the association. If the bonding between the acid and base is strong, the new vibrations associated with the Sn–B bond will have a higher frequency and the entropy gain will be small. If the bond is weak the entropy gain will be correspondingly larger. Hence $\Delta S°$ may be a more unambiguous indicator of bond strength than $\Delta H°$. The linear relationship that has been shown to exist between $\Delta H°$ and $\Delta S°$ is a result of the fact that a tighter bond, as evidenced by a more negative $\Delta H°$, will produce a corresponding larger loss of entropy. The entropy decrease from $(CH_3)_3Sn-Cl$ to $(CH_3)_3Sn-Br$ to $(CH_3)_3Sn-I$ results from larger vibrational entropy loss due to increased enthalpy of bond formation. This relationship would not be expected to hold if the ligand bonds changed in less than a regular way for similar adducts or if the rehybridization enthalpy differed for each compound. This requires that the enthalpy data of Table II be interpreted as being due to a stronger bond between the tin atom and the base and not as being due to differences in the Sn–X bond energies in the complex or to rehybridization differences.

Acknowledgment. We are indebted to the National Science Foundation for support of this work and to Marjorie Samples and Scott Penfil for their assistance.

Registry No. $(CH_3)_3SnCl$, 1066-45-1; $(CH_3)_3SnBr$, 1066-44-0; $(CH_3)_3SnI$, 811-73-4; $(C_2H_5)_3SnCl$, 994-31-0; $(C_2H_5)_3SnBr$, 2767-54-6; $(c_3H_7)_3SnCl$, 2279-76-7; $(C_4H_9)_3SnCl$, 1461-22-9; $(C_6H_5)_3SnCl$, 639-58-7; $(C_6H_5)_3PO$, 791-28-6.

Approaches to the Synthesis and Detection of a Transient Palladium(0) Alkylidene

Robert A. Wanat and David B. Collum*

Baker Laboratory, Department of Chemistry, Cornell University, Ithaca, New York 14853

Received June 25, 1985

Treatment of palladium enolate $(PPh_3)_2BrPdCH_2C(O)$-*t*-Bu with *t*-BuOK in tetrahydrofuran at −63 °C affords $Ph_3P{=}CHC(O)$-*t*-Bu (**2**) in good yield. Kinetics demonstrated the reaction to involve rate-determining dissociation of phosphine. In the presence of added phosphine, the reaction exhibited fractional direct dependence on the concentration of *t*-BuOK and fractional inverse dependence on the concentration of added phosphine. Isotopic labeling studies showed that the *t*-BuOK did not function as a Brønsted base up to the rate-determining step. Crossover experiments demonstrated that the post-rate-determining step involving phosphorus–carbon bond formation occurred by an intramolecular mechanism. Reactions of (*Z*)-$BrCH{=}C(OSiMe_3)$-*t*-Bu, $Br_2CHC(O)$-*t*-Bu, (*Z*)-$BrCH{=}C(OLi)$-*t*-Bu, and $N_2CHC(O)$-*t*-Bu with $Pd(PPh_3)_4$ each provided phosphorane **2**. The mechanism for formation of **2** and the possible intermediacy of low-valent palladium alkylidenes are discussed.

Introduction

We are interested in the elucidation of the organic chemistry of highly reactive transition-metal alkylidenes.[1] Specifically, we are intrigued by the class of alkylidenes that bear potentially *destabilizing*, and thus highly activating, electron-withdrawing groups.[2,3] These species are frequently implicated as reactive intermediates derived from diazo ketones and diazo esters en route to C=C,[4] C≡C,[5] C≡N,[6] C—H,[7] C—O,[8a-c] C—S,[8c] O—H,[9] S—H,[10]

(1) Selected reviews of metal carbene/alkylidene complexes: (a) Cardin, D. J.; Cetinkaya, B.; Lappert, M. F. *Chem. Rev.* **1972**, *72*, 545. (b) Schubert, U. *Coord. Chem. Rev.* **1984**, *55*, 261. Grubbs, R. H. *Prog. Inorg. Chem.* **1978**, *24*, 1. (c) Brown-Wensley, K. A.; Buchwald, S. L.; Cannizzo, L.; Clawson, L.; Ho, D.; Stille, J. R.; Straus, D.; Grubbs, R. H. *Pure Appl. Chem.* **1983**, *55*, 1733. (d) Casey, C. P. In "Transition Metal Organometallics in Organic Synthesis"; Alper, H., Ed.; Academic Press: New York, 1976; Vol. 1, pp 189–233.

(2) In those systems in which the metal carbene moieties are stabilized by electron-donating groups (Fisher carbenes), electron-withdrawing acyl substituents should be destabilizing. However, such substituent effects will be dependent upon the electronic configuration at the metal center. For recent theoretical treatments that address the question of M=C stabilities and philicities, see ref 3.

(3) (a) Taylor, T. E.; Hall, M. B. *J. Am. Chem. Soc.* **1984**, *106*, 1576. (b) Ushio, J.; Nakatsuji, H.; Yonezawa, T. *J. Am. Chem. Soc.* **1984**, *106*, 5892.

(4) Leading references: Doyle, M. P.; Dorow, R. L.; Buhro, W. E.; Griffin, J. H.; Tamblyn, W. H.; Trudell, M. L. *Organometallics* **1984**, *3*, 44. Doyle, M. P.; Griffin, J. H.; Bogheri, V.; Dorow, R. L. *Ibid.* **1984**, *3*, 55. Anciaux, A. J.; Hubert, A. J.; Noels, A. F.; Petiniot, N.; Teyssié, P. *J. Org. Chem.* **1980**, *45*, 695. Doyle, M. P.; Wang, L. C.; Loh, K. L. *Tetrahedron Lett.* **1984**, *25*, 4087. Salomon, R. G.; Kochi, J. K. *J. Am. Chem. Soc.* **1973**, *95*, 3300. Anciaux, A. J.; Demonceau, A.; Noels, A. F.; Warin, R.; Hubert, A. J.; Teyssié, P. *Tetrahedron* **1983**, *39*, 2169. Peace, B. W.; Wulfman, D. S. *Synthesis* **1973**, 137.

(5) Petiniot, N.; Anciaux, A. J.; Noels, A. F.; Hubert, A. J.; Teyssié, P. *Tetrahedron Lett.* **1978**, 1239.

(6) Paulissen, R.; Moniotte, P.; Hubert, A. J.; Teyssié, P. *Tetrahedron Lett.* **1974**, 3311.

(7) Demonceau, A.; Noels, A. F.; Hubert, A. J.; Teyssié, P. *J. Chem. Soc., Perkin Trans. 1* **1981**, 688. Cane, D. E.; Thomas, P. J. *J. Am. Chem. Soc.* **1984**, *106*, 5295. Taber, D. F.; Raman, K. *Ibid.* **1983**, *105*, 5935. Taber, D. F.; Petty, E. H. *J. Org. Chem.* **1982**, *47*, 4808. Callot, H. J.; Metz, F. *Tetrahedron Lett.* **1982**, *23*, 4321. Taylor, E. C.; Davies, H. M. L. *Ibid.* **1983**, *24*, 5453.

(8) (a) Martin, M. G.; Ganem, B. *Tetrahedron Lett.* **1984**, *25*, 251. (b) Doyle, M. P.; Griffin, J. H.; Chinn, M. S.; van Leusen, D. *J. Org. Chem.* **1984**, *49*, 1917. (c) Kametani, T.; Kanaya, N.; Mochizuki, T.; Honda, T. *Heterocycles* **1982**, *19*, 1023. (d) Kirmse, W.; Chien, P. V. *Tetrahedron Lett.* **1985**, *26*, 197.

0276-7333/86/2305-0120$01.50/0

$$\Delta S = \Delta S_{t,r} + \Delta S_v$$

where $\Delta S_{t,r}$, the change in translational and rotational entropy, is very similar for a series of acids and ΔS_v, the change in vibrational entropy, is due mainly to the new adduct bond.

Upon complex formation three degrees of translational and three degrees of rotational freedom are lost and $\Delta S_{t,r}$ must be negative. It is this loss of entropy which accounts for the negative entropy changes of Table II. However, the vibrational entropy change must be positive because six new vibrational degrees of freedom result from the association. If the bonding between the acid and base is strong, the new vibrations associated with the Sn–B bond will have a higher frequency and the entropy gain will be small. If the bond is weak the entropy gain will be correspondingly larger. Hence $\Delta S°$ may be a more unambiguous indicator of bond strength than $\Delta H°$. The linear relationship that has been shown to exist between $\Delta H°$ and $\Delta S°$ is a result of the fact that a tighter bond, as evidenced by a more negative $\Delta H°$, will produce a corresponding larger loss of entropy. The entropy decrease from $(CH_3)_3Sn-Cl$ to $(CH_3)_3Sn-Br$ to $(CH_3)_3Sn-I$ results from larger vibrational entropy loss due to increased enthalpy of bond formation. This relationship would not be expected to hold if the ligand bonds changed in less than a regular way for similar adducts or if the rehybridization enthalpy differed for each compound. This requires that the enthalpy data of Table II be interpreted as being due to a stronger bond between the tin atom and the base and not as being due to differences in the Sn–X bond energies in the complex or to rehybridization differences.

Acknowledgment. We are indebted to the National Science Foundation for support of this work and to Marjorie Samples and Scott Penfil for their assistance.

Registry No. $(CH_3)_3SnCl$, 1066-45-1; $(CH_3)_3SnBr$, 1066-44-0; $(CH_3)_3SnI$, 811-73-4; $(C_2H_5)_3SnCl$, 994-31-0; $(C_2H_5)_3SnBr$, 2767-54-6; $(c_3H_7)_3SnCl$, 2279-76-7; $(C_4H_9)_3SnCl$, 1461-22-9; $(C_6H_5)_3SnCl$, 639-58-7; $(C_6H_5)_3PO$, 791-28-6.

Approaches to the Synthesis and Detection of a Transient Palladium(0) Alkylidene

Robert A. Wanat and David B. Collum*

Baker Laboratory, Department of Chemistry, Cornell University, Ithaca, New York 14853

Received June 25, 1985

Treatment of palladium enolate $(PPh_3)_2BrPdCH_2C(O)$-*t*-Bu with *t*-BuOK in tetrahydrofuran at −63 °C affords $Ph_3P{=}CHC(O)$-*t*-Bu (**2**) in good yield. Kinetics demonstrated the reaction to involve rate-determining dissociation of phosphine. In the presence of added phosphine, the reaction exhibited fractional direct dependence on the concentration of *t*-BuOK and fractional inverse dependence on the concentration of added phosphine. Isotopic labeling studies showed that the *t*-BuOK did not function as a Brønsted base up to the rate-determining step. Crossover experiments demonstrated that the post-rate-determining step involving phosphorus–carbon bond formation occurred by an intramolecular mechanism. Reactions of (*Z*)-$BrCH{=}C(OSiMe_3)$-*t*-Bu, $Br_2CHC(O)$-*t*-Bu, (*Z*)-$BrCH{=}C(OLi)$-*t*-Bu, and $N_2CHC(O)$-*t*-Bu with $Pd(PPh_3)_4$ each provided phosphorane **2**. The mechanism for formation of **2** and the possible intermediacy of low-valent palladium alkylidenes are discussed.

Introduction

We are interested in the elucidation of the organic chemistry of highly reactive transition-metal alkylidenes.[1] Specifically, we are intrigued by the class of alkylidenes that bear potentially *destabilizing*, and thus highly activating, electron-withdrawing groups.[2,3] These species are frequently implicated as reactive intermediates derived from diazo ketones and diazo esters en route to C=C,[4] C≡C,[5] C≡N,[6] C—H,[7] C—O,[8a-c] C—S,[8c] O—H,[9] S—H,[10]

(1) Selected reviews of metal carbene/alkylidene complexes: (a) Cardin, D. J.; Cetinkaya, B.; Lappert, M. F. *Chem. Rev.* **1972**, *72*, 545. (b) Schubert, U. *Coord. Chem. Rev.* **1984**, *55*, 261. Grubbs, R. H. *Prog. Inorg. Chem.* **1978**, *24*, 1. (c) Brown-Wensley, K. A.; Buchwald, S. L.; Cannizzo, L.; Clawson, L.; Ho, D.; Stille, J. R.; Straus, D.; Grubbs, R. H. *Pure Appl. Chem.* **1983**, *55*, 1733. (d) Casey, C. P. In "Transition Metal Organometallics in Organic Synthesis"; Alper, H., Ed.; Academic Press: New York, 1976; Vol. 1, pp 189–233.

(2) In those systems in which the metal carbene moieties are stabilized by electron-donating groups (Fisher carbenes), electron-withdrawing acyl substituents should be destabilizing. However, such substituent effects will be dependent upon the electronic configuration at the metal center. For recent theoretical treatments that address the question of M=C stabilities and philicities, see ref 3.

(3) (a) Taylor, T. E.; Hall, M. B. *J. Am. Chem. Soc.* **1984**, *106*, 1576. (b) Ushio, J.; Nakatsuji, H.; Yonezawa, T. *J. Am. Chem. Soc.* **1984**, *106*, 5892.

(4) Leading references: Doyle, M. P.; Dorow, R. L.; Buhro, W. E.; Griffin, J. H.; Tamblyn, W. H.; Trudell, M. L. *Organometallics* **1984**, *3*, 44. Doyle, M. P.; Griffin, J. H.; Bogheri, V.; Dorow, R. L. *Ibid.* **1984**, *3*, 55. Anciaux, A. J.; Hubert, A. J.; Noels, A. F.; Petiniot, N.; Teyssié, P. *J. Org. Chem.* **1980**, *45*, 695. Doyle, M. P.; Wang, L. C.; Loh, K. L. *Tetrahedron Lett.* **1984**, *25*, 4087. Salomon, R. G.; Kochi, J. K. *J. Am. Chem. Soc.* **1973**, *95*, 3300. Anciaux, A. J.; Demonceau, A.; Noels, A. F.; Warin, R.; Hubert, A. J.; Teyssié, P. *Tetrahedron* **1983**, *39*, 2169. Peace, B. W.; Wulfman, D. S. *Synthesis* **1973**, 137.

(5) Petiniot, N.; Anciaux, A. J.; Noels, A. F.; Hubert, A. J.; Teyssié, P. *Tetrahedron Lett.* **1978**, 1239.

(6) Paulissen, R.; Moniotte, P.; Hubert, A. J.; Teyssié, P. *Tetrahedron Lett.* **1974**, 3311.

(7) Demonceau, A.; Noels, A. F.; Hubert, A. J.; Teyssié, P. *J. Chem. Soc., Perkin Trans. 1* **1981**, 688. Cane, D. E.; Thomas, P. J. *J. Am. Chem. Soc.* **1984**, *106*, 5295. Taber, D. F.; Raman, K. *Ibid.* **1983**, *105*, 5935. Taber, D. F.; Petty, E. H. *J. Org. Chem.* **1982**, *47*, 4808. Callot, H. J.; Metz, F. *Tetrahedron Lett.* **1982**, *23*, 4321. Taylor, E. C.; Davies, H. M. L. *Ibid.* **1983**, *24*, 5453.

(8) (a) Martin, M. G.; Ganem, B. *Tetrahedron Lett.* **1984**, *25*, 251. (b) Doyle, M. P.; Griffin, J. H.; Chinn, M. S.; van Leusen, D. *J. Org. Chem.* **1984**, *49*, 1917. (c) Kametani, T.; Kanaya, N.; Mochizuki, T.; Honda, T. *Heterocycles* **1982**, *19*, 1023. (d) Kirmse, W.; Chien, P. V. *Tetrahedron Lett.* **1985**, *26*, 197.

0276-7333/86/2305-0120$01.50/0

N—H,[11,12] and N—N[12] bond functionalizations. Several laboratories have reported mechanistic work on the transition-metal-catalyzed olefin cyclopropanations by α-diazo esters.[4] However, acyl-substituted terminal alkylidenes have been isolated only very rarely and never in the later triads.[13] By the very nature of the high reactivities that make them spectroscopically invisible, and because of the vast number of possible modes of diazo activation[14] that do not necessarily proceed through mononuclear terminal alkylidenes,[15] inferences of their intermediacy are still conjectural.

We describe herein an approach to the synthesis and detection of an acyl-substituted palladium alkylidene in which the dominant decomposition pathway involves extrusion of the corresponding phosphorane by a process involving rapid *intramolecular* carbon–phosphorus bond formation.[16] Support for the intermediacy of an alkylidene comes from a demonstration of common modes of reactivity arising from independent approaches to this class of reactive intermediate.

Results

Our strategy to prepare acyl-substituted alkylidenes is illustrated in eq 1. Upon treatment of palladium complex

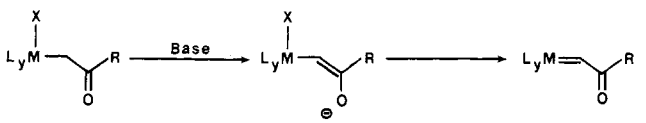

(1)

1 with 1.1 equiv of *t*-BuOK in tetrahydrofuran (THF) at −78 °C with subsequent warming to room temperature, we were able to isolate phosphorane **2**[17] from the resulting heterogeneous, black reaction mixture. The only other isolable product was an incompletely characterized palladium triphenylphosphine complex.[18] Consistent with the black material being Pd metal arising from a deficiency of ligand, reaction in the presence of 3.0 equiv of added triphenylphosphine afforded a pale yellow, homogeneous reaction mixture from which we isolated phosphorane **2** (82% yield) and tetrakis(triphenylphosphine)palladium (84% yield).

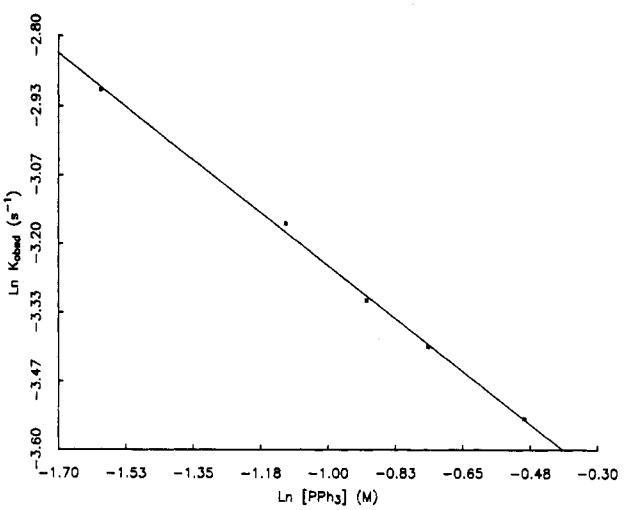

Figure 1. Dependence of ln k_{obsd} vs. ln [PPh_3]. Slope of −0.58 ± 0.02 represents reaction order in PPh_3.[20] [1] = 0.02 M; [*t*-BuOK] = 0.21 M; t = −39 °C; in THF-d_8.

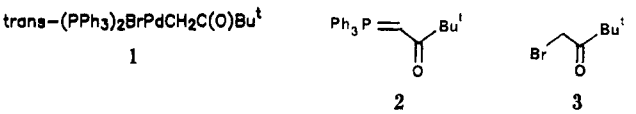

A control experiment ruled out the possibility that bromo ketone **3** was reductively eliminated and converted to **2** independent of the palladium: a mixture of PPh_3, *t*-BuOK, and ketone **3** in THF failed to give detectable quantities of **2** even after extended reaction times at room temperature.[19] Following the course of the reaction of **1** with *t*-BuOK-d_9 by ^{1}H NMR in THF-d_8 at −63 °C showed that phosphorane **2** was formed along with only traces of several *tert*-butyl-containing by-products. No intermediates could be detected. Furthermore, GC–MS analysis of the reaction contents provided no evidence for the formation of volatile organic by-products.

We investigated the efficacy of a variety of alkoxides to effect dehydrohalogenation of **1**. Lithium tertiary alkoxides and potassium phenoxides smoothly converted **1** to **2** albeit at ambient temperatures. Complex product distributions resulted from attempted dehydrohalogenations of **1** with alkoxides bearing hydrogens at the α-carbon (e.g., $KOCH_2R$). These may have arisen from facile β-hydride eliminations[20] of Pd–OCH_2R intermediates (vide infra).

One might speculate that phosphorane **2** arose from nucleophilic attack of residual triphenylphosphine on an intermediate alkylidene (e.g., ii) to provide an unstable [21]

(9) Noels, A. F.; Demonceau, A.; Petiniot, N.; Hubert, A. J.; Teyssié, P. *Tetrahedron* **1982**, *38*, 2733. Paulissen, R.; Reimlinger, H.; Hayez, E.; Hubert, A. J.; Teyssié, P. *Tetrahedron Lett.* **1973**, 2233. Yates, P. *J. Am. Chem. Soc.* **1952**, *74*, 5376. Takebayashi, M.; Ibata, T.; Kohara, H.; Kim, B. H. *Bull. Chem. Soc. Jpn.* **1967**, *40*, 2392.

(10) McKervey, M. A.; Ratananukul, P. *Tetrahedron Lett.* **1982**, *23*, 2509.

(11) Ratcliff, R. W.; Saltzmann, T. N.; Christensen, B. G. *Tetrahedron Lett.* **1980**, *21*, 31. Kametani, T.; Honda, T.; Nakayama, A.; Sasaki, Y.; Mochizuki, T. *J. Chem. Soc., Perkin Trans. 1* **1981**, 2228.

(12) Taylor, E. C.; Davies, H. M. L. *J. Org. Chem.* **1984**, *49*, 113.

(13) (a) Redhouse, A. D. *J. Organomet. Chem.* **1975**, *99*, C29. (b) Kolobova, N. E.; Ivanov, L. L.; Zhvanko, O. S.; Chechulina, I. N.; Batsanov, A. S.; Struchkov, Yu. T. *J. Organomet. Chem.* **1982**, *238*, 223. (c) Herrmann, W. A. *Angew. Chem., Int. Ed. Engl.* **1974**, *13*, 599. (d) Herrmann, W. A. *Chem. Ber.* **19775**, *108*, 486. (e) **1975**, *108*, 3412. (f) Fischer, E. O.; Schambeck, W. *J. Organomet. Chem.* **1980**, *201*, 311. (g) Fischer, E. O.; Stückler, P.; Kreissl, F. R. *J. Organomet. Chem.* **1977**, *129*, 197.

(14) Leading references to the various modes of diazoalkane coordination at one or more transition-metal centers: Hillhouse, G. L.; Haymore, B. L. *J. Am. Chem. Soc.* **1982**, *104*, 1537. Herrmann, W. A. *Angew. Chem., Int. Ed. Engl.* **1978**, *17*, 800.

(15) Herrmann, W. A.; Barnes, C. E.; Zahn, T.; Ziegler, M. L. *Organometallics* **1985**, *4*, 172 and references cited therein.

(16) Selected reviews of the transition-metal chemistry of phosphorus ylids: Weber, L. In "The Chemistry of the Metal-Carbon Bond", Patai, S., Hartley, F. R., Eds.; Wiley: New York, 1982; Chapter 3. Kaska, W. C. *Coord. Chem. Rev.* **1983**, *48*, 1. Schmidbaur, H. *Angew. Chem., Int. Ed. Engl.* **1983**, *22*, 907.

(17) Ingham, C. F.; Massy-Westropp, R. A.; Reynolds, G. D.; Thorpe, W. D. *Aust. J. Chem.* **1975**, *28*, 2499.

(18) For reports of the formation of incompletely characterized Pd–phosphine oligomers or polymers formed under phosphine-deficient conditions see: Sisaki, A.; Ungvary, F.; Kiss, G. *J. Mol. Catal.* **1983**, *18*, 223. Onishi, M., Hiraki, K.; Itoh, T.; Ohama, Y. *J. Organomet. Chem.* **1983**, *254*, 381. Fenton, D. M. *J. Org. Chem.* **1973**, *38*, 3192.

(19) In a reaction that appeared to be superficially related to the dehydrohalogenation of **1**, Stille found that reaction of $Pd(PPh_3)_4$ with 2.5 equiv of $BrCH_2COPh$ afforded $Ph_3P{=}CHCOPh$ and CH_3COPh. However, they postulated that the reaction simply involved formation of the phosphonium salt from dissociated PPh_3 and the excess of $BrCH_2COPh$ *independent* of the palladium center, followed by deprotonation mediated by an equivalent of slightly basic $(PPh_3)_2PdBrCH_2COPh$ adduct. The appropriate control experiments run in our laboratory confirmed their conclusions. Stille, J. K.; Lau, K. S. Y. *J. Am. Chem. Soc.* **1976**, *98*, 5841.

(20) Roffia, P.; Gregario, G.; Conti, F.; Pregaglia, G. F.; Ugo, R. *J. Mol. Catal.* **1977**, *2*, 191. Mayer, J. M.; Curtis, C. J.; Bercaw, J. E. *J. Am. Chem. Soc.* **1983**, *105*, 2651 and references cited therein.

(21) Zerovalent metal complexes of stabilized ylides typically undergo facile dissociation.[16]

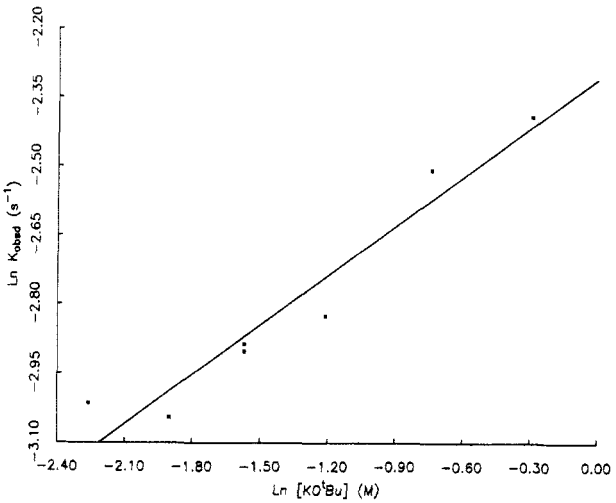

Figure 2. Dependence of ln k_{obsd} vs. ln [*t*-BuOK]. Slope of 0.35 ± 0.04 represents reaction order in *t*-BuOK.[20] [1] = 0.02 M; [PPh_3] = 0.21 M; t = −39 °C; in THF-d_8.

ylide complex. Interconversion of complexed phosphoranes (ylide complexes) and alkylidenes are well documented.[22] However, this mechanism would require somewhat surprising electrophilicity for ii since limited experimental[29] and theoretical[3,24] evidence indicates that a low-valent alkylidene in the nickel triad containing no strongly π-acidic ligands should be *nucleophilic* at the alkylidene carbon atom. Furthermore, a battery of experiments designed to trap the putative reactive alkylidene with large molar excesses of a variety of olefins and internal acetylenes failed to divert the formation of **2**.

To gain further insight into the sequence of events leading up to formation of phosphorane **2**, we conducted a kinetic study of the reaction as described below.

Kinetics. All kinetic runs were conducted under pseudo-first-order conditions in *t*-BuOK (≥10.0 molar equiv) in THF-d_8. Reaction rates were monitored by following loss of the *tert*-butyl singlet of **1** at 0.12 ppm in the 300-MHz ^{1}H NMR spectra.

Conversion of complex **1** to phosphorane **2** at −63.0 °C was found to be first order in **1** and zero order in *t*-BuOK over more than 4 half-lives (R^2 = 0.96–0.99). The reaction was inhibited by the addition of 3 equiv of PPh_3. The phosphine inhibition was not due to an associative mechanism via a pentacoordinated palladium intermediate since the added phosphine had no effect on the chemical shifts or multiplicities of the proton resonances of the low-temperature (−63 °C), slow-exchange spectrum of starting complex **1**. Upon comparison of the reaction rates for dehydrohalogenation of **1** and **1**-d_2, no appreciable kinetic isotope effect was detected (k_H/k_D = 1.06 ± 0.04). Therefore, in the absence of added phosphine, dissociation of PPh_3 from **1** appeared to be rate limiting.[25,26]

Under pseudo-first-order conditions for PPh_3 and *t*-BuOK, the reaction proceeded smoothly at −39.0 °C, exhibiting a fractional inverse dependence on [PPh_3] (Figure 1; rate ∝ $1/[PPh_3]^{0.58\pm0.02}$) and a direct fractional order dependence on [*t*-BuOK] (Figure 2; rate ∝ [*t*-BuOK]$^{0.35\pm0.04}$).[27] Upon comparing the rates of reaction of **1** and **1**-d_2 in the presence of 10 equiv of PPh_3 (conditions in which PPh_3 dissociation was not rate determining) we observed a small inverse intermolecular isotope effect (k_H/k_D = 0.80 ± 0.10). Treatment of monodeuterated **1**-*d* in THF-d_8 with 10 equiv of *t*-BuOK in the presence of 10 equiv of PPh_3 (monitored by ^{1}H NMR at −43 °C) afforded **2**-*d* to the exclusion of **2** (≤20%) showing the intramolecular isotope effect[28] to be large ($k_H/k_D \geq 4$).

trans-$(Ar_3P)_2BrPd$-R

1-d_2; R = $CD_2C(O)Bu^t$, Ar = Ph
1-*d*; R = $CHDC(O)Bu^t$, Ar = Ph
5; R = $CH_2C(O)Bu^t$, Ar = p-tolyl
5-d_2; R = $CD_2C(O)Bu^t$, Ar = p-tolyl

Ar_3P=R

2-*d*; R = $CDC(O)Bu_t$, Ar = Ph
4; R = $CHC(O)Bu^t$, Ar = p-tolyl
4-*d*; R = $CDC(O)Bu^t$, Ar = p-tolyl

Crossover Studies. A crossover experiment was run to elucidate the extent of intramolecularity of phosphorus–carbon bond formation. The 300-MHz ^{1}H NMR spectrum of triphenylphosphorane **2** in THF-d_8 exhibited a doublet for the ylidic proton centered at 3.64 ppm ($^2J_{P-H}$ = 28 Hz) that was completely resolved from the corresponding doublet of tri-*p*-tolylphosphorane **4** (3.58 ppm, $^2J_{P-H}$ = 27 Hz). In the absence of added phosphine at −63 °C in THF-d_8 (conditions in which phosphine dissociation was irreversible and proton exchange in the resulting phosphoranes was found to be slow), the reaction of a 1:1 mixture of **1** and **5**-d_2 with *t*-BuOK (10 equiv) produced phosphorane **2** (and **4**-*d*) to the exclusion of (<5%) phosphorane **4**. The complimentary experiment using **5** and **1**-d_2 provided **4** to the exclusion (<5%) of **2**. Therefore, phosphorus–carbon bond formation occurred almost exclusively by an intramolecular mechanism.

Alternative Approaches to Alkylidenes. We investigated alternative syntheses of palladium alkylidenes to gain support for such intermediates through demonstration of common modes of reactivity. In an effort generate an α-palladated alkali-metal enolate (cf. i in eq 1) that, in some as-of-yet undefined form, was a possible reactive intermediate en route to phosphorane **2**, we attempted to prepare palladated enol ether **6**. When enol ether **7** (*Z* geometry as shown by NOE experiments) and $(PPh_3)_4Pd$ were heated in benzene-d_6 at 100 °C (eq 2), we observed no sign of adduct **6**. The ^{1}H NMR spectrum of the reaction showed phosphorane **2** to account for over 90% of the

(22) Leading references: (a) Canestrari, M.; Green, M. L. H. *J. Chem. Soc., Chem. Commun.* **1982**, 1789. (b) Nakazawa, H.; Johnson, D. L.; Gladysz, J. A. *Organometallics* **1983**, *2*, 1846. (c) Choi, H. S.; Sweigart, D. A. *J. Organomet. Chem.* **1982**, *228*, 249. (d) See ref 16.

(23) Miyashita, A.; Grubbs, R. H. *Tetrahedron Lett.* **1981**, *22*, 1255. Noyori, R. *Tetrahedron Lett.* **1973**, 1691. Nakamura, A.; Yoshida, T.; Cowie, M.; Otsuka, S.; Ibers, J. A. *J. Am. Chem. Soc.* **1977**, *99*, 2108.

(24) Rappé, A. K.; Goddard, W. A. *J. Am. Chem. Soc.* **1977**, *99*, 3966; **1982**, *104*, 448. Spangler, D.; Wendoloski, J. J.; Dupuis, M.; Chen, M. M. L.; Schaefer, H. F., III *J. Am. Chem. Soc.* **1981**, *103*, 3985.

(25) The postulated predissociation of phosphine from **1** was further supported by the observation that the relatively nondissociationg bis(diphenylphosphino)ethane (dppe) and bis(trimethylphosphine) complexes corresponding to **1** required higher temperatures (−50 °C) for reaction to occur. Although we observed smooth formation of Me_3P=CHC(O)-*t*-Bu from the latter, the dppe derivative afforded a complex product distribution.

(26) For leading references to kinetic analyses for reactions of d^8 square-planar $(PR_3)_2MX_2$ species, see: (a) Reamey, R. H.; Whitesides, G. M. *J. Am. Chem. Soc.* **1984**, *106*, 81. (b) Scott, J. D.; Puddephatt, R. J. *Organometallics* **1983**, *2*, 1643. (c) Anderson, G. K.; Cross, R. J. *Chem. Soc. Rev.* **1980**, 185.

(27) The reaction orders in PPh_3 and *t*-BuOK were obtained from the general rate equations[20b] $k_{obsd} = k'[Y]^Z$ and ln k_{obsd} = ln k' + Z ln [Y]. Plots of ln k_{obsd} vs. ln [Y] (Y = PPh_3 and *t*-BuOK in Figures 1 and 2, respectively) afforded lines with slopes (Z) representing the calculated reaction orders in component Y: Frost, A.; Pearson, R. In "Kinetics and Mechanism", 2nd ed.; Wiley: New York, 1961; Chapter 3.

(28) Dai, S.-H.; Dolbier, W. R., Jr. *J. Am. Chem. Soc.* **1972**, *94*, 3946. Chipman, D. M.; Yaniv, R.; van Eikeren, P. *J. Am. Chem. Soc.* **1980**, *102*, 3244.

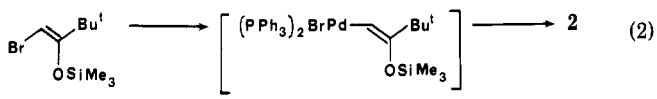

7 6

tert-butyl-containing material. Although superficially this result implicated a rate-determining oxidative addition followed by alkylidene formation via rapid (halide ion assisted?) decomposition of **6**, the mechanistic implications outlined in the Discussion are more complex.

We prepared the α-brominated palladium derivative **8** in order to investigate reductive dehalogenation routes to acyl-substituted alkylidenes (eq 2). Reaction of $Pd(PPh_3)_4$ and dibrominated ketone **9**[29] in benzene-d_6 at 25 °C for 0.5 h afforded an approximate 3:2 mixture of stereoisomers. The major isomer was shown to be *trans*-**8** by the symmetric methine triplet (J_{P-H} = 8.0 Hz) centered at 4.81 ppm and a singlet corresponding to the *tert*-butyl group at 1.02 ppm. The minor isomer (*cis*-**8**) exhibited a doublet of doublets ($J_{cis\text{-}P\text{-}H}$ = 9.5 Hz, $J_{trans\text{-}P\text{-}H}$ = 14.3 Hz) centered at 4.55 ppm and a *tert*-butyl resonance at 1.42 ppm.[30] When the mixture in benzene-d_6 was left at room temperature and monitored by ^1H NMR spectroscopy, the resonances corresponding to *cis*-**8** and *trans*-**8** disappeared with concomitant appearance of the resonances corresponding to phosphorane **2** and precipitation of a highly insoluble phosphine-containing material (presumably $[(PPh_3)_2PdBr]_2$). Conversions of M–C–X (X = halogen) species to the corresponding alkylidenes[31] (as well as the reverse reaction involving insertion of alkylidenes into metal–halogen bonds[32]) have been implicated previously.

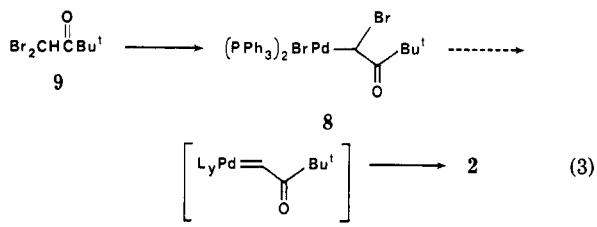

We anticipated that alternative entry to this class of alkylidenes could be obtained as depicted in eq 4. When

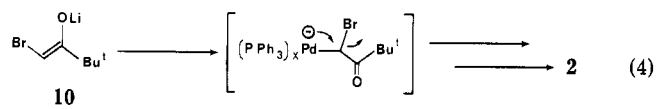

10

a 3.5:1 mixture of crystalline bromo enolate **10** and $Pd(PPh_3)_4$ (0.875 equiv of enolate/phosphine) dissolved in benzene-d_6 was held at 25 °C, phosphorane **2** was formed within 45 h (62% isolated yield). The reaction was inhibited by added phosphine with the rate of formation of phosphorane **2** accelerating as the palladium was stripped of PPh_3.[33] In the absence of palladium no reaction was observed between **10** and PPh_3. Treatment of enolate **10** with 5 mol % $Pd(PPh_3)_4$ in the presence of 1.0 equiv of added PPh_3 provided phosphorane **2** cleanly and catalytically (52% isolated yield) albeit at significantly reduced reaction rates (9 days).

In order to correlate the alkoxide-mediated chemistry of **1** with palladium-mediated diazo ketone chemistry, diazo ketone **11**[34] and 0.25 equiv[35] of $Pd(PPh_3)_4$ were heated in benzene-d_6 at 55 °C (eq 5). Within 0.5 h there

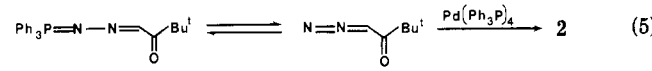

12 11

appeared a static 12:1 mixture of diazo ketone **11** and a new compound that exhibited a *tert*-butyl resonance at 1.30 ppm. Over a period of 48 h, both *tert*-butyl resonances were replaced by a *tert*-butyl resonance at 1.51 ppm that was shown to belong to phosphorane **2**. We assigned the intermediate resonance to phosphazine **12** based on well-documented phosphazine–diazoalkane equilibria.[36] When **11** and PPh_3 in benzene-d_6 were warmed to 60 °C for 3 days in the absence of palladium, the resulting mixture of **11** and **12** was not converted to **2**.[37]

Discussion

We were able to observe kinetically only a portion of the pathway in the *t*-BuOK-mediated conversion of complex **1** to phosphorane **2** (eq 6–8). In the absence of added

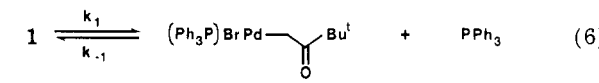

iii

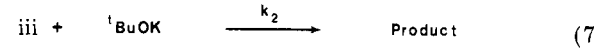

$$-d[1]/dt = \frac{k_1k_2[1][t\text{-BuOK}]}{(k_{-1}[PPh_3] + k_2[t\text{-BuOK}])} \quad (8)$$

phosphine, the dehydrohalogenation of **1** was first order in **1** and zero order in *t*-BuOK and exhibited no measurable isotope effect, indicating that phosphine dissociation from **1** (eq 6) was rate-determining ($k_{-1}[PPh_3] \ll k_2[t\text{-BuOK}]$). In the presence of added PPh_3, the direct dependence on [*t*-BuOK] and inverse dependence on $[PPh_3]$ indicated that phosphine dissociation was no longer rate-determining ($k_{-1}[PPh_3] \geq k_2[t\text{-BuOK}]$). The simplest possible mechanism would involve the rate-determining

(29) Hill, G. A.; Kropa, E. L. *J. Am. Chem. Soc.* **1933**, *55*, 2509.
(30) Ito, T.; Tsuchiya, H.; Yamamoto, A. *Bull. Chem. Soc. Jpn.* **1977**, *50*, 1319.
(31) Leading references: (a) Engelter, C.; Moss, J. R.; Niven, M. L.; Nassimbeni, L. R.; Reid, G. *J. Organomet. Chem.* **1982**, *232*, C78. (b) Feser, R.; Werner, H. *Angew. Chem., Int. Ed. Engl.* **1980**, *19*, 940.
(32) Lappert, M. F.; Poland, J. S. *Adv. Organomet. Chem.* **1970**, *9*, 397. Mango, F. D.; Dvoretzky, I. *J. Am. Chem. Soc.* **1966**, *88*, 1654. Matsumoto, K.; Odaira, Y.; Tsutsumi, S. *J. Chem. Soc., Chem. Commun.* **1968**, 832. Clark, G. R.; Roper, W. R.; Wright, A. H. *J. Organomet. Chem.* **1984**, *273*, C17. Day, V. W.; Stults, B. R.; Reimer, K. J.; Shaver, A. *J. Am. Chem. Soc.* **1974**, *96*, 1227; 4008. Herrmann, W. A.; Huber, M. *J. Organomet. Chem.* **1977**, *140*, 55. Herrmann, W. A.; Huber, M. *Chem. Ber.* **1978**, *111*, 3124. Clemens, J.; Green, M.; Stone, F. G. A. *J. Chem. Soc., Dalton Trans.* **1973**, 1620.
(33) Both enolate **10** and phosphorane **2** are carbenoid equivalents except that **10** should exhibit dramatically greater nucleophilicity. Accordingly, the conversion of the putative alkylidene to phosphorane **2** could, in principle, be reversible (cf. Sharp, P. R.; Schrock, R. R. *J. Organomet. Chem.* **1979**, *171*, 43). If so, then reaction of $Pd(PPh_3)_4$ with tolyl-substituted phosphorane **4** would effect exchange of the PPh_3 and $(p\text{-tolyl})_3P$ fragments by way of a zerovalent ylide complex $(PPh_3)_xPdCH(PAr_3)C(O)$-*t*-Bu. However, phosphorane **4** was not detected (<5%) by ^1H or ^{31}P NMR when a mixture of **2**, $Pd(PPh_3)_4$, and $(p\text{-tolyl})_3P$ were heated in C_6D_6 at 110 °C for 8 days.
(34) Yates, P.; Garneau, F. X.; Lokensgard, J. P. *Tetrahedron* **1975**, *31*, 1979.
(35) The poor solubility of $(PPh_3)_4Pd$ mandated the 4.6:1 stoichiometry of **11** and $Pd(PPh_3)_4$. Complete conversion of diazo ketone **11** to phosphorane **2** illustrates the reaction to be catalytic in Pd metal.
(36) Pudovic, A. N.; Gareev, R. D. *Zh. Obshch. Khim.* **1976**, *46*, 945; **1975**, *45*, 1847, 1717. Krommes, P.; Lorberth, J. *J. Organomet. Chem.* **1977**, *127*, 19. Guziec, F. S., Jr.; Luzzio, F. A. *J. Org. Chem.* **1983**, *48*, 2434. Ramirez, F.; Levy, S. *J. Org. Chem.* **1958**, *23*, 2036.
(37) Schramm and Ibers reported that treatment of diazocyclopentadienylidene with bis(triphenylphosphine)nickel ethylene afforded the corresponding phosphorane: Schramm, K. D.; Ibers, J. A. *Inorg. Chem.* **1980**, *19*, 2441.

reaction of three-coordinate intermediate iii with *t*-BuOK (eq 7). The observed *fractional* value for the reaction order in *t*-BuOK (0.35 order) undoubtedly derived, at least in part, from concentration-dependent alkoxide aggregation phenomena.[38,39a] However, an inverse first-order dependence on added phosphine would have been anticipated rather than the measured inverse *fractional* order dependence.[26] From crossover experiments we know that during the course of the reaction in the *absence* of added phosphine, the dissociated phosphine does not return to any of the intermediates along the reaction pathway to **2**. In the presence of added phosphine the reaction may be more complex.[40] (One possibility is that the added phosphine played a role in the presumed deaggregation of *t*-BuOK oligomers.[39]) In any event, although we were unable to obtain useful quantitative information from the rate data, the qualitative dependencies proved valuable for the interpretation of the observed isotope effects (see below).

The *t*-BuOK and PPh_3 rate dependencies were qualitatively consistent with a mechanism involving rapid phosphine predissociation followed by a slower *t*-BuOK-mediated deprotonation step. Nevertheless, the small inverse isotope effect measured at −39 °C in the presence of added PPh_3 (k_H/k_D = 0.80) was contrary to that normally observed for a primary kinetic isotope effect.[41] If, on the other hand, the deprotonation step was rapid and reversible, the resulting *equilibrium* isotope effect would be small and either normal or inverse.[42] However, the observed isotope effect was shown not to be an equilibrium isotope effect from several observations. A plot of ln [1] vs. time was linear over greater than 4 half-lives showing no autoinhibition from the presumed increase in [*t*-BuOH] over the course of the reaction. Furthermore, conversion of **1**-d_2 to phosphorane **2**-*d* in the presence of excess PPh_3 and an additional 1.0 equiv of *t*-BuO*H* showed no proton incorporation in the methylene position of **1**-d_2 at partial conversion.[43] Most importantly, the large discrepancy between the small *intermolecular* and the large *intramolecular* isotope effects indicated that kinetic deprotonation had occurred, but in a kinetically invisible, post-rate-determining step.[28]

Therefore, there must have occurred an interaction between *t*-BuOK and a palladium intermediate during (or prior to) the rate-determining step that did *not* involve deprotonation; palladate iv would be the logical intermediate (eq 9).[44] An additional step involving extrusion of bromide from palladate iv followed by a second reaction with *t*-BuOK to provide palladate v clearly cannot be dismissed at this time.

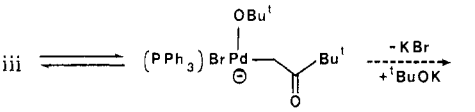

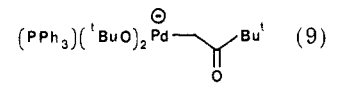

(9)

Important aspects of the mechanism, including a putative deprotonation step and the crucial carbon–phosphorus bond-forming step, remained obscure in a kinetically invisible section of the pathway. We are able to account for many of our experimental observations by invoking either of two mechanistic rationales. Although a distinction between the two pathways cannot be made at this time, close inspection shows that the two seemingly disparate mechanisms may actually be variants of the same theme.

In the following mechanistic discussions only some of the details of the metal coordination spheres can be surmised from kinetic and crossover data. Additionally, the structures may vary for conditions that provide Pd metal (no added PPh_3) vs. those that provide $Pd(PPh_3)_4$. Accordingly, only the portions of the coordination spheres that are relevant to the discussion are depicted; implicit additional ligands of undefined structure are designated as "Ly". Furthermore, with the exception of eq 10 and 11, the diagrams are not intended to imply stereochemistry at trigonal palladium centers.[45]

Alkylidene Mechanism. To argue for the intermediacy of an alkylidene in the dehydrohalogenation of **1**, we are forced to keep within several constraints. Deprotonation of the methylene group of iv or v, whether via a biomolecular or possibly a more facile unimolecular pathway (eq 10), must have occurred subsequent to the rate-determining step.[59] Secondly, crossover experiments showed a very high degree of *intramolecularity* of phosphine–alkyl coupling. In a process that bears some relationship to metal-centered couplings of alkylidene and CO fragments,[46] sliding the phosphine toward the alkylidene carbon to afford phosphacyclopropane viii could occur with only very subtle structural reorganization and minimal charge localization (eq 11). Phosphacyclopropane viii is simply a resonance structure for a coordinated ylide complex ix.

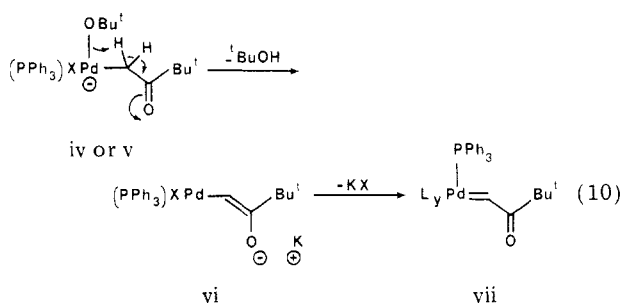

(10)

(38) Brown, T. L.; Ladd, J. A.; Newman, G. N. *J. Organomet. Chem.* **1965**, *3*, 1. Reichle, W. T. *J. Org. Chem.* **1972**, *37*, 4254. Jackman, L. M.; Lange, B. C. *Tetrahedron* **1977**, *33*, 2737. Cetinkaya, B.; Gümrükcü, I.; Lappert, M. F.; Atwood, J. L.; Shakir, R. *J. Am. Chem. Soc.* **1980**, *102*, 2086. Jackman, L. M.; DeBrosse, C. W. *J. Am. Chem. Soc.* **1983**, *105*, 4177.

(39) (a) *t*-BuOK is reported to be a tetramer in THF: Schmidt, P.; Lochmann, L.; Schneider, B. *J. Mol. Struct.* **1971**, *9*, 403. Schlosser, M.; Jan, G.; Byrne, E.; Sicher, J. *Helv. Chim. Acta* **1973**, *56*, 1630. (b) Karsch, H. H.; Appelt, A.; Müller, G. *J. Chem. Soc., Chem. Commun.* **1984**, 1415.

(40) Rearrangement of the rate equation depicted in eq 8 leads to

$$\frac{1}{k_{obsd}} = \frac{k_{-1}[PPh_3]^x}{k_1k_2[t\text{-BuOK}]^y} + \frac{1}{k_2}$$

Plots of $1/k_{obsd}$ vs. $[PPh_3]^x/[t\text{-BuOK}]^y$ proved linear only when the calculated reaction orders in PPh_3 and *t*-BuOK were used (x = 0.58, y = 0.35). This may indicate that the fractional reaction orders arose from complex preequilibria that were not directly associated with the reaction pathway.

(41) Sugimoto, N.; Sasaki, M.; Osugi, J. *J. Am. Chem. Soc.* **1983**, *105*, 7676 and references cited therein.

(42) (a) Cram, D. J.; Kingsbury, C. A.; Rickborn, B. *J. Am. Chem. Soc.* **1961**, *83*, 3688. (b) Cram, D. J.; Uyeda, R. T. *J. Am. Chem. Soc.* **1962**, *84*, 4358. (c) Hofmann, J. E.; Schreisheim, A.; Nickols, R. E. *Tetrahedron Lett.* **1965**, 1745. (d) Streitweiser, A., Jr.; Van Sickle, D. E.; Langworthy, W. C. *J. Am. Chem. Soc.* **1962**, *84*, 244. (e) Streitweiser, A., Jr.; Van Sickle, D. E.; Reif, L. *Ibid.* **1962**, *84*, 258.

(43) Even in the event of rapid, reversible deprotonation, intimate acid–base association could preclude exchange with protic materials in the reaction medium.[42b,e]

(44) For a kinetic analysis of ate complex formation from MeLi addition to $PdMe_2(PR_3)_2$ see: Nakazawa, H.; Ozawa, F.; Yamamoto, A. *Organometallics* **1983**, *2*, 241.

(45) For leading references to the stereochemistry of three-coordinate d^8 systems, see ref 26b.

(46) Fischer, H.; Weber, L. *Chem. Ber.* **1984**, *117*, 3340.

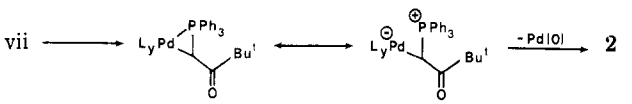

viii ix

(11)

Support for the intermediacy of an alkylidene during the dehydrohalogenation of **1** comes from the common modes of reactivity observed in the reactions of $Pd(PPh_3)_4$ with enol ether **7**, dibromo ketone **9**, enolate **10**, or diazoalkane **11**. Reactions intimately related to eq 3–5 have been postulated to provide or proceed through alkylidene intermediates.[4,15,31,47] The common product (phosphorane **2**) obtained from each of the five different approaches to alkylidenes argues in support of related reactive intermediates.

Phosphonium Salt Reductive Elimination Mechanism. We must also consider an alternative mechanism for phosphorane formation involving a rate-determining reductive elimination of a phosphonium salt (e.g., Ph_3PCH_2CO-*t*-Bu^+X^-) with subsequent deprotonation by *t*-BuOK. Product distributions that appear to arise from similar aryl and vinyl phosphonium salt reductive eliminations at elevated temperatures have been reported.[48–54] Although such a reductive elimination mechanism is consistent with the experimental results, we are troubled by a number of points. Since the reported examples of phosphonium salt reductive eliminations require elevated temperatures (75–100 °C) for extended reaction times, by crudest estimates the *t*-BuOK-mediated reaction of **1** occurred at least 10^6 times faster. It might be tempting to invoke a scenario in which formation of a *t*-BuOK ate complex (e.g., iv or v) facilitated a phosphonium salt reductive elimination. However, reductive eliminations typically proceed more slowly from electron-rich metal centers.[50] Furthermore, Kampmeier[49] provided evidence that the carbon–phosphorus bond-forming step in the

Chart I

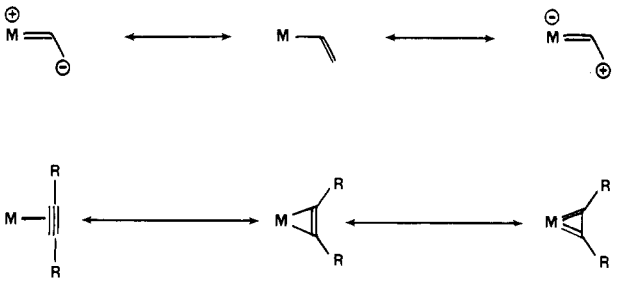

corresponding *alkyl* phosphonium reductive eliminations proceed independent of the metal centers subsequent to reductive elimination of the alkyl halide moiety; such a mechanism was unambiguously ruled out in the *t*-BuOK-mediated conversion of **1** to **2**.

The dilemma of differentiating two seemingly disparate mechanisms might be partially resolved by considering the possible mechanisms by which carbon–phosphorus bond formation occurs at transition-metal centers. Many cationic and Fischer carbene complexes[22] and cationic olefin π complexes[51] are sufficiently electrophilic to react with nucleophilic phosphines. However, there also exist examples of σ-vinyl complexes[52] and π-complexed acetylenes[53] that undergo facile P–C bond-forming reactions via mechanisms that are not necessarily so transparent. One of the common threads connecting all such reactions is that the starting materials or logical reactive intermediates can be depicted in alkylidene-like resonance structures (Chart I).[54–56] Thus, *metal-centered phosphorus–carbon bond formation may prove facile only when the transition state is stabilized by alkylidene character.* The reaction of bromoenol ether **7** with $Pd(PPh_3)_4$ to give phosphorane **2** can be represented as either a phosphonium salt reductive elimination or phosphine–alkylidene coupling, depending on whether the putative intermediate is drawn as a σ-vinyl derivative (e.g., **6**) or as the alternative alkylidene resonance structure **x** or **xi**. By depicting the intermediate palladium-bound enolate of type **vi** as the alternative alkylidene resonance structures **xii** or **xiii**, we find that it too may be represented as an alkylidene–phosphine coupling or a vinyl phosphonium salt reductive elimination analogous to those studied by Kampmeier.[49] Nevertheless, the

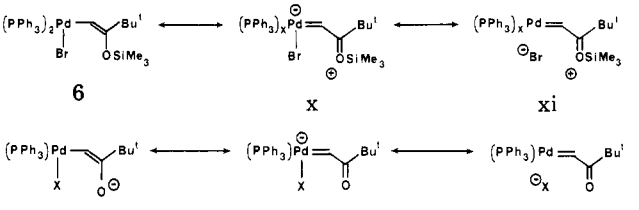

6 x xi

vi xii xiii

P–C coupling reaction from the dehydrohalogenation of **1** is extraordinarily facile given that the putative alkylidene intermediates along the pathway are unlikely to exhibit any positive character at the alkylidene carbon atom. We attribute the facility of the coupling step to the *intramolecularity* that was demonstrated by the crossover ex-

(47) For theoretical studies and leading references to the coupling of the X and Y fragments of X=M=Y species, see: Hoffmann, R.; Wilker, C. N.; Eisenstein, O. *J. Am. Chem. Soc.* **1982**, *104*, 632. Hoffmann, R.; Wilker, C. N.; Lippard, S. J.; Templeton, J. L.; Brower, D. C. *J. Am. Chem. Soc.* **1983**, *105*, 146.

(48) Horner, L.; Mummenthey, G.; Moser, H.; Beck, P. *Chem. Ber.* **1966**, *99*, 2782. Cassar, L.; Foa, M. *J. Organomet. Chem.* **1974**, *74*, 75. Heck, R. F.; Ziegler, C. B., Jr. *J. Org. Chem.* **1978**, *43*, 2941. Mitchell, R. H.; Chaudhary, M.; Dingle, T. W.; Williams, R. V. *J. Am. Chem. Soc.* **1984**, *106*, 7776. Cramer, R.; Coulson, D. R. *J. Org. Chem.* **1975**, *40*, 2267.

(49) Kampmeier, J. A.; Harris, S. H.; Rodehurst, R. M. *J. Am. Chem. Soc.* **1981**, *103*, 1478.

(50) For reductive eliminations from d^8 square-planar complexes, evidence for mechanisms involving either phosphine association or dissociation have been presented: Tatsumi, K.; Nakamura, A.; Komiya, S.; Yamamoto, A. Yamamoto, T. *J. Am. Chem. Soc.* **1984**, *106*, 8181 and references cited therein.

(51) Choi, H. S.; Sweigart, D. A. *Organometallics* **1982**, *1*, 60 and references cited therein. See also references cited in ref 49.

(52) (a) Churchill, M. R.; DeBoer, B. G. *Inorg. Chem.* **1977**, *16*, 1141. (b) Huggins, J. M.; Bergman, R. G. *J. Am. Chem. Soc.* **1979**, *101*, 4410. (c) Carmona, E.; Gutierrez-Puebla, E.; Monge, A.; Marin, J. M.; Panque, M.; Poveda, M. L. *Organometallics* **1984**, *3*, 1438. (d) Scordia, H.; Kergoat, R.; Kubicki, M. M.; Guerehais, J. E. *Organometallics* **1983**, *2*, 1681. (e) Alt, H. G.; Schwarzle, J. A.; Kreissl, F. R. *J. Organomet. Chem.* **1978**, *152*, C57. (f) Deeming, A. J.; Hasso, S. *J. Organomet. Chem.* **1976**, *112*, C39. (g) Yasufuku, K.; Hamada, A.; Aoki, K.; Yamazaki, H. *J. Am. Chem. Soc.* **1980**, *102*, 4363.

(53) Davidson, J. L.; Vasapollo, G.; Manojlovic-Muir, L.; Muir, K. L. *J. Chem. Soc., Chem. Commun.* **1982**, 1025. See also ref 13b.

(54) Acetylenes as four-electron-donating bis(carbenes): Churchill, M. R.; Wasserman, H. J.; Holmes, S. J.; Schrock, R. R. *Organometallics* **1982**, *1*, 766. Richard, R. L.; Weiss, R.; Newton, W. E.; Chen, G. J.; McDonald, J. W. *J. Am. Chem. Soc.* **1978**, *100*, 1318. Cotton, F. A.; Hall, W. T. *Ibid.* **1979**, *101*, 5094. Smith, G.; Schrock, R. R.; Churchill, M. R.; Youngs, W. J. *Inorg. Chem.* **1981**, *20*, 387. Churchill, M. R.; Youngs, W. J. *Inorg. Chem.* **1979**, *18*, 1697. Tatsumi, K.; Hoffmann, R.; Templeton, J. L. *Inorg. Chem.* **1982**, *21*, 466.

(55) Resonance relationships of M(σ-vinyl), M(σ-aryl), and M–C$^-$ species to alkylidenes: Cramer, R. E.; Maynard, R. B.; Paw, J. C.; Gilje, J. W. *Organometallics* **1982**, *1*, 869; **1983**, *3*, 1336; *J. Am. Chem. Soc.* **1981**, *103*, 3589. Baldwin, J. C.; Keder, N. L.; Strouse, C. E.; Kaska, W. C. *Z Naturforsch., B: Anorg. Chem., Org. Chem.* **1980**, *35B*, 1289. Cotton, F. A.; Schwotzer, W. *Inorg. Chem.* **1983**, *22*, 387. Brown, K. L.; Ngamelue, M. *J. Organomet. Chem.* **1983**, *243*, 339.

(56) Metallacyclopropene/σ-vinyl metal equilibria: Green, M.; Norman, N. C.; Orpen, A. G. *J. Am. Chem. Soc.* **1981**, *103*, 1267. Davidson, J. L.; Wilson, W. F.; Manojlovic-Muir, L.; Murir, K. W. *J. Organomet. Chem.* **1983**, *254*, C6 and references cited therein.

periments. We have begun to question whether the role of *intramolecularity* in alkylidene-to-phosphorane conversions has been underestimated[57] and, in turn, whether this has resulted in the importance of the alkylidene charge polarizations to be overestimated. In this connection, the calculations of Nakatsuji et al. suggest that alkylidene philicities are determined by frontier orbital control rather than charge distribution.[3b]

Experimental Section

General Data. ^{13}C and ^{31}P NMR spectra were recorded on a JEOL FX-90Q spectrometer. Routine ^1H NMR spectra were recorded on a Varian CFT-20 (80 MHz) spectrometer. The low-temperature reaction kinetics were monitored on a Brucker WP 300 spectrometer with temperature correction to within 0.1 °C. The phosphines were obtained from Strem and recrystallized prior to use. The *t*-BuOK obtained from Aldrich was purified by sublimation. The *t*-BuOK-d_9 was prepared from commercially available *tert*-butyl-d_{10} alcohol (Aldrich) with oil-free potassium hydride in THF and was sublimed before use. Tetrakis(triphenylphosphine)palladium and tetrakis(tri-*p*-tolylphosphine)-palladium were prepared by standard literature procedures.[58] Benzene, benzene-d_6, tetrahydrofuran, and tetrahydrofuran-d_8 were distilled in vacuo from sodium benzophenone ketyl by using standard vacuum line techniques. All other reagents were handled by using standard protocols, and all air-sensitive compounds were manipulated by using standard vacuum line and glovebox techniques.

1-Bromo-3,3-dimethyl-2-butanone (3). Bromo ketone **3** was prepared by using a nondescript literature procedure as follows.[29] (Note: the reaction evolves large volumes of gaseous HBr and should be performed in a well-ventilated hood.) A 500-mL round-bottom flask was charged sequentially with anhydrous $CuBr_2$ (81.2 g, 363 mmol), 220 mL of 1:1 ethyl acetate/chloroform, and 26 mL (210 mmol) of pinacolone (Aldrich). The contents were held at reflux under a $CaCl_2$ drying tube for 24 h, at which time the slurry was filtered free of solids with ethyl acetate rinsings. Concentration of the filtrate followed by fractional distillation afforded 23 g (71% yield) of **3** as a colorless oil (bp 78 °C at 11 mm): ^1H NMR (80 MHz, $CDCl_3$) δ 4.15 (s, 2 H), 1.21 (s, 9 H).

$(PPh_3)_2$(Br)PdCH$_2$C(O)-*t*-Bu (1). To a solution of $Pd(PPh_3)_4$ (1.85 g, 1.60 mmol) slurried in 40 mL of benzene under argon at 25 °C was added ketone **3** (256 μL, 1.90 mmol). After 1.0 h the clear yellow solution was concentrated in vacuo. The resulting yellow solid was washed once with hexane and then recrystallized from THF/hexane or CH_2Cl_2 to afford **1** (1.20 g, 85% yield) as a microcrystalline solvate: ^1H NMR ($CDCl_3$) δ 8.0–7.0 (m, 30 H), 2.45 (br s, 2 H), 0.25 (s, 9 H); $^{13}C\{^1H\}$ NMR ($CDCl_3$) δ 220.1 (CO), 135.1–127.9 (envelope of phenyl carbons), 44.23 (quaternary C), 31.3 (CH_2), 26.8 (CH_3); $^{31}P\{^1H\}$ NMR ($CDCl_3$) δ 27.60 (s). IR (Nujol) 1670, 1090 cm^{-1}. Anal. Calcd for $C_{46}H_{49}BrO_2P_2Pd\cdot CH_2Cl_2$: C, 57.78; H, 4.85; P, 6.94; Pd, 11.91. Found: C, 57.84; H, 4.79; P, 6.97; Pd, 12.10.

Reaction of 1 with *t*-BuOK in the Presence of PPh_3. To a 25-mL round-bottom flask charged with **1** (400 mg, 0.48 mmol), PPh_3 (393 mg, 1.50 mmol), and freshly sublimed *t*-BuOK (56 mg, 0.50 mmol) was vacuum transferred 20 mL of THF at −78 °C. After the reaction vessel was allowed to slowly warm to room temperature over 4 h, the solvent was removed from the resulting yellow slurry to afford a pale yellow solid. The yellow solid was extracted twice with diethyl ether and once with THF. The remaining solid (480 mg, 84% yield) was shown to be spectroscopically homogeneous and indistinguishable from an authentic sample of $Pd(PPh_3)_4$ prepared by a literature procedure.[58] The extracts were concentrated in vacuo and the resulting yellow solid recrystallized from ether and hexane, affording 141 mg (82% yield) of phosphorane **2** that was identical with an authentic sample prepared by a literature procedure.[17] When the reaction was run in THF-d_8 with *t*-BuOK-d_9 on an NMR scale (for the experimental procedure, see the Kinetics section), phosphorane **2** (*tert*-butyl resonance; 1.14 ppm) was formed in ≥90% purity along with minor impurities exhibiting *tert*-butyl resonances at 1.10, 1.07, and 0.88 ppm. GC–MS analysis of the reaction contents afforded no evidence of volatile organic products.

3,3-Dimethyl-1,1,1-trideuterio-2-butanone. A two-phase mixture of pinacolone (25 mL, 200 mmol), anhydrous potassium carbonate (500 mg, 3.62 mmol), and D_2O (99.8% d, 50 mL) was held at reflux for 48 h under N_2. The aqueous phase was removed, and the pinacolone was carried through two additional cycles using fresh potassium carbonate and fresh D_2O each time. After the third cycle, the organic layer was dried over anhydrous Na_2SO_4 and distilled (105 °C, 760 mm) to afford 14 g of 3,3-dimethyl-1,1,1-trideuterio-2-butanone (68% yield) with >99% deuteration at the methyl group as shown by 300-MHz ^1H NMR.

1-Bromo-1,1-dideuterio-3,3-dimethyl-2-butanone (3-d_2). Doubly deuterated **3**-d_2 was prepared in 68% yield from the trideuterated pinacolone (vide supra) by the procedure used to prepare **3** with substitution of $CDCl_3$ for $CHCl_3$ as reaction solvent. 300-MHz ^1H NMR ($CDCl_3$) showed 98% deuteration of the bromomethyl moiety of **3**-d_2.

$(PPh_3)_2$(Br)PdCD$_2$C(O)-*t*-Bu (1-d_2). Complex **1**-d_2 was prepared from **3**-d_2 by the procedure used to prepare **1**. The 300-MHz ^1H NMR showed 1.92 deuteria per methylene moiety.

1-Bromo-1-deuterio-3,3-dimethyl-2-butanone (3-d_1). To a solution of lithium diisopropylamide (3.80 mmol) in 15 mL of anhydrous THF at −78 °C under N_2 was added **1**-d_2 (405 μL, 3.00 mmol) in 1.0 mL of THF. After being stirred at −78 °C for 45 min, the contents of the reaction were transferred by cannulation into 20 mL of 1:1 THF/H_2O. Following extraction with CH_2Cl_2 (3 × 20 mL), the combined organic layers were dried (Na_2SO_4) and concentrated. Kugelrohr distillation (11 mm, 75–85 °C) afforded 470 mg (87% yield) of **3**-d_1 exhibiting 1.08 deuteria per bromomethyl moiety as shown by 300-MHz ^1H NMR spectroscopy.

$(PPh_3)_2$(Br)PdC(D)HC(O)-*t*-Bu (1-d_1). **1**-d_1 was prepared from **3**-d_1 as described above for **1**. The 300-MHz ^1H NMR analysis showed an average of 1.0 deuteria per methylene moiety.

[P(*p*-tolyl)$_3$]$_2$(Br)PdCH$_2$C(O)-*t*-Bu (5). Complex **5** was prepared analogously to **1** by starting with $(p\text{-tolyl}_3P)_4Pd$.[58] Recrystallization from hexane/ether afforded the product as off-white microcrystals (71% yield): ^1H NMR (C_6D_6) δ 7.90 (br m, 12 H), 6.97 (m, 12 H), 2.00 (s, 18 H), 0.55 (s, 9 H); $^{31}P\{^1H\}$ NMR (C_6D_6) δ 25.31; $^{13}C\{^1H\}$ NMR (C_6D_6) δ 219.0 (CO), 140–126 (envelope of aryl carbons), 44.6 (quaternary C), 32.0 (CH_2), 27.4 (CH_3), 21.2 (aryl-CH_3). Anal. Calcd for $C_{48}H_{53}BrP_2PdO$: C, 64.50; H, 5.98; P, 6.94; Pd, 11.91. Found: C, 64.43; H, 5.96; P, 7.04; Pd, 11.85.

[P(p-tolyl)$_3$]$_2$(Br)PdCD$_2$C(O)-*t*-Bu (5-d_2). **5**-d_2 was prepared as described for **5**. The 300-MHz ^1H NMR analysis showed an average of 1.90 deuteria per molecule.

Authentic Ph_3P=CHC(O)-*t*-Bu (2).[17] Phosphorane **2** prepared by a standard literature procedure exhibited the following spectroscopic characteristics: ^1H NMR (THF-d_8) δ 7.7–6.8 (m, 15 H), 3.64 (d, J_{P-H} = 28 Hz, 1 H), 0.12 (s, 9 H); ^1H NMR (C_6D_6) δ 7.85–6.80 (m, 15 H), 3.96 (d, J_{P-H} = 28 Hz, 1 H), 1.51 (s, 9 H); $^{31}P\{^1H\}$ NMR (C_6D_6) δ 15.38 (s); $^{13}C\{^1H\}$ NMR (C_6D_6) δ 199.6 (CO), 133.6–126.9 (envelope of aryl carbons), 45.9 (d, J_{P-C} = 110 Hz, CH), 40.9 (d, J_{P-C} = 12 Hz, quaternary carbon), 29.3 (CH_3).

Authentic (*p*-Tolyl)$_3$P=CHC(O)-*t*-Bu (4). A solution of 1-bromo-3,3-dimethyl-2-butanone (**3**; 135 μL, 1.0 mmol) and tri-*p*-tolylphosphine (300 mg, 1.0 mmol) in anhydrous THF under N_2 was heated at 60 °C for 3 h. After the mixture was cooled to −78 °C, 10 mL of THF followed by oil-free KH (60 mg, 1.50 mmol) was added sequentially. The solvent was removed in vacuo to afford a pale yellow oil. Recrystallization from hexane provided 280 mg of **4** (70% yield) as white crystals: ^1H NMR (THF-d_8) δ 7.72 (dd, J_{H-H} = 8.1 Hz, J_{P-H} = 12.1 Hz, 2 H), 6.88 (dd, J_{H-H} = 8.1, J_{P-H} = 2.4 Hz, 2 H), 4.04 (d, J_{P-H} = 27.5 Hz, 1 H), 1.94 (s,

(57) Although metal-centered P–C bond formation has been suspected to occur intramolecularly in several instances (cf. ref 1d, 31b, 49, 52d), we are unaware of any fully documented examples. A recent publication cites such a migration as unpublished work from R. R. Schrock's laboratories (Churchill, M. R.; Wasserman, H. J. *Inorg. Chem.* **1982**, *21*, 3913). However, the necessary control experiments had not been carried out. Schrock, R. R., personal communication.

(58) Garrou, P.; Heck, R. F. *J. Am. Chem. Soc.* **1976**, *98*, 4115. Coulson, D. R. *Inorg. Synth.* **1972**, *13*, 121.

(59) **Note Added in Proof.** Cp(CO)(NO)ReCH$_2$CN can be deprotonated (*n*-BuLi) and alkylated to give Cp(CO)(NO)ReCH(CH$_3$)CN. Crocco, G. L.; Gladysz, J. A. *J. Am. Chem. Soc.* **1985**, *107*, 4103.

9 H, Ar-Me), 1.54 (s, 9 H, *t*-Bu); $^{31}P\{^1H\}$ NMR (C_6D_6) δ 14.5 (s); $^{13}C\{^1H\}$ NMR (C_6D_6) δ 199.5 (s, CO), 142–124 (envelope of aryl carbons), 46.8 (d, J_{P-C} = 110 Hz), 41.0 (d, J_{P-C} = 10 Hz, quaternary C), 29.4 (s, CH_3), 21.3 (s, CH_3-aryl); IR (film) 1595 (m), 1525 (s), 1480 (s), 1100 (s) cm^{-1}; exact mass calcd for $C_{27}H_{31}OP$ 402.2112, found 402.2091.

Crossover Experiment. To an argon-flushed NMR tube at −95 °C were added **1** (5 mg) and **5**-d_2 (5 mg) each in 175 μL of THF-d_8, followed by *t*-BuOK-d_9 (14 mg) in 200 μL of THF-d_8. The tube was sealed under vacuum, warmed to −78 °C, agitated vigorously, and inserted in a probe of a 300-MHz NMR spectrometer held at −63 °C. Proton NMR analysis showed the growth of the doublet centered at 3.64 ppm corresponding to phosphorane **2** to the exclusion (<5%) of the doublet centered at 3.58 ppm corresponding to phosphorane **4**. When the experiment was repeated by using **5** and **1**-d_2, phosphorane **4** formed to the exclusion (<5%) of phosphorane **2**.

Kinetics: Representative Procedure. With standard glovebox and vacuum line procedures, a 5-mm NMR tube was charged with a solution containing 10 mg (0.012 mmol) of complex **1**·(CH_2Cl_2) and PPh_3 (32 mg, 0.12 mmol) in THF-d_8 (250 μL) and capped with a septum. After cooling the tube to −78 °C under argon, a solution of freshly sublimed *t*-BuOK (14 mg, 0.12 mmol) in THF-d_8 (200 μL) was syringed down the cold walls of the NMR tube. Following sealing of the tube with a torch, it was immediately placed without warming into the 300-MHz NMR probe held at −39.3 °C. (The probe temperature was checked between each run, and the temperature equilibration upon insertion of the tube occurred in ≤4 min.) The reaction was monitored for loss of the *tert*-butyl resonance of **1** at 0.12 ppm relative to a CH_2Cl_2 internal standard. All reported errors represent one standard deviation from linear, nonweighted least-squares analyses. Reaction orders were calculated as described elsewhere.[27]

(*Z*)-BrCH=C(OSiMe$_3$)Bu (7). To a solution of lithium diisopropylamide (1.00 mmol) in THF (3 mL) at −78 °C under nitrogen was added neat bromo ketone **1** (135 μL, 1.00 mmol). (Note: a procedure for the generation and isolation of the solvent free enolate **10** as a stable crystalline solid is described later.) After 0.5 h the reaction was quenched with freshly distilled trimethylsilyl chloride (130 μL, 1.10 mmol). The reaction was warmed to room temperature and partitioned between ethyl acetate and aqueous $NaHCO_3$. The organic layer was dried (Na_2SO_4), stripped to an oil, and flash chromatographed (hexane) to afford 140 mg (56% yield) of **7**. ^1H NMR (C_6D_6) δ 5.24 (s, 1 H), 0.91 (s, 9 H), 0.30 (s, 9 H); $^{13}C\{^1H\}$ NMR ($CDCl_3$) δ 162.3 (C-OMe$_3$Si), 83.0 (CHBr), 38.0 ($C(CH_3)_3$), 28.1 (CH_3 of *t*-Bu), 1.3 ($SiCH_3$); IR (film) 3120 (w), 2960 (s), 1620 (s) cm^{-1}; exact mass calcd for $C_9H_{19}BrOSi$ 250.0389, found 250.0385. Irradiation of the silyl resonance at 0.30 ppm in the ^1H NMR spectrum had no measurable affect on the vinyl resonance at 5.24 ppm. However, irradiation of the *tert*-butyl resonance at 0.91 ppm led to a 21% NOE enhancement of the vinyl resonance.

Reaction of 7 with Pd(PPh$_3$)$_4$. A solution of enol ether **7** (5 mg, 0.020 mmol) and $Pd(PPh_3)_4$ (30 mg, 0.026 mmol) in benzene-d_6 (0.5 mL) in a sealed NMR tube under N_2 was heated in a 100 °C oil bath. Aside from aromatic resonances derived from triphenylphosphine-containing materials, the only products observable by 80-MHz ^1H NMR spectroscopy were those derived from phosphorane **2** and an envelope of trimethylsilyl fragments (0.4–0.1 ppm).

Reaction of 9 with Pd(PPh$_3$)$_4$. To an NMR tube charge with $Pd(PPh_3)_4$ (30 mg, 0.026 mmol) was added dibromo ketone **9**[29] (6 mg, 0.023 mmol) in 0.5 mL of C_6D_6 at 25 °C. Rapid reaction lead to a 2:3 mixture of isomeric oxidative adducts. *cis*-**8** (minor isomer): ^1H NMR (300 MHz) δ 8.1–6.9 (br m), 4.55 (dd, J_{P-H} = 14.3 Hz, 9.5 Hz, 1 H), 1.42 (s, 9 H). *trans*-**8** (major isomer): ^1H NMR (300 MHz) δ 8.1–6.9 (br m), 4.81 (t, J_{P-H} = 8 Hz, 1 H), 1.02 (s, 9 H). Upon standing for 2 days at 25 °C *cis*-**8** and *trans*-**8** disappeared with concomitant appearance of phosphorane **2**. (See preparation of authentic **2** for NMR shifts in C_6D_6.)

Bromo Enolate 10. To a solution of $(Me_3Si)_2NH$ (1.0 mL, 4.76 mmol) in 35 mL of toluene under argon at −78 °C was added 2.2 M *n*-BuLi in hexane (4.50 mmol). After the solution was stirred at −78 °C for 15 min, bromo ketone **3** (607 μL, 4.50 mmol) in hexane (0.40 mL) was added. After an additional 1.0 h at −78 °C the vessel was warmed to 25 °C and the contents were stirred for 0.5 h. The solution was then stripped in vacuo to approximately 15 mL and diluted with 30 mL of hexane by vacuum transfer to afford white crystals. After the mixture was cooled to −78 °C, the crystals of enolate **10** were filtered and dried in vacuo (yield 570 mg, 68%): ^1H NMR (80 MHz, C_6D_6) δ 4.98 (s, 1 H), 1.06 (s, 9 H).

Addition of 10 to Pd(PPh$_3$)$_4$: Stoichiometric. An argon-flushed NMR tube was charged with $(PPh_3)_4Pd$ (40 mg, 0.035 mmol), bromo enolate **10** (23 mg, 0.12 mmol), and C_6D_6 (2.0 mL) and then sealed under vacuum with a flame. After 45 h at 25 °C proton NMR analysis showed the complete disappearance of the resonances corresponding to enolate **10** and the concomitant clean formation of resonances corresponding to phosphorane **2** (to the exclusion of significant quantities of other resonances). The resulting black reaction mixture was passed through a short column of silica gel (methanol elution) to removed the Pd metal, and the eluate was flash chromatographed (5% ethanol/ethyl acetate) on silica gel to afford phosphorane **2** (27 mg, 62% yield) that was pure by proton NMR.

Addition of 10 to Pd(PPh$_3$)$_4$: Catalytic. An NMR tube was charged with PPh_3 (46 mg, 0.176 mmol), enolate **10** (30 mg, 0.16 mmol), $(PPh_3)_4Pd$ (9 mg, 0.008 mmol), and C_6D_6 (2.0 mL) and sealed under vacuum with a flame. After 9 days at 25 °C ^1H NMR analysis showed the yellow, homogeneous solution to contain almost exclusively phosphorane **2** with approximately 5% of enolate **10** remaining. Workup as described above for the stoichiometric transformation afforded 30 mg of phosphorane **2** (52% yield; 55% yield based on 95% conversion).

Diazo Ketone 11.[34] Diazo ketone **11** was prepared by a nondescript literature procedure as follows. To a solution of pivaloyl chloride (590 mg, 4.90 mmol) in 20 mL of anhydrous diethyl ether at 0 °C under N_2 was added an excess of ethereal diazomethane. After stirring for 12 h at 25 °C, the solution was concentrated, and the resulting pale yellow oil was flash chromatographed (20% ethyl acetate in hexane) to afford diazo ketone **11** (480 mg, 78% yield) as a yellow oil: ^1H NMR (C_6D_6) δ 4.35 (s, 1 H), 0.91 (s, 9 H); $^{13}C\{^1H\}$ NMR ($CDCl_3$) δ 200.4 (CO), 51.0 (br s, CHN_2), 41.7 (quaternary C), 26.2 (CH_3); IR (film) 3000, 2100, 1630, 1480 cm^{-1}.

Reaction of 11 with Pd(PPh$_3$)$_4$. A solution of $Pd(PPh_3)_4$ (30 mg, 0.026 mmol) and diazo ketone **11** (15 mg, 0.12 mmol)[35] in benzene-d_6 under N_2 was heated in a sealed NMR tube at 55 °C with monitoring by 80-MHz ^1H NMR spectroscopy. (The reaction darkened from the deposition of Pd metal.) Minor resonances attributable to phosphazine **12** appeared: δ 1.31 (s, 9 H), 8.55 (d, J_{P-H} = 3 H; or uncoupled syn and anti isomers). These were slowly replaced with resonances corresponding to phosphorane **2** over a period of 48 h.[35] When an experiment was performed in the absence of $Pd(PPh_3)_4$, the resonances assigned to phosphazine **12** and diazo ketone **11** (approximate 1:1 ratio) persisted unchanged for up to 72 h at 60 °C/h.

Acknowledgment. We wish to thank Dr. Alfred Bader, Dr. M. Farahati, and the Eli Lilly Co. for generous financial support of this work. We also would like to thank Professors Barry K. Carpenter, Peter T. Wolczanski, and Klaus Theopold for invaluable discussions. Acknowledgment is made to the National Science Foundation Instrumentation Program (CHE 7904825 and PCM 8018643) for support of the Cornell Nuclear Magnetic Resonance Facility.

Registry No. **1**, 98991-62-9; **1**-d_1, 98991-66-3; **1**-d_2, 98991-65-2; **2**, 26487-93-4; **2**-d_9, 98991-61-8; **3**, 5469-26-1; **3**-d_1, 99016-52-1; **3**-d_2, 79275-78-8; **4**, 98991-58-3; **5**, 98991-63-0; **5**-d_2, 98991-67-4; **7**, 98991-59-4; *cis*-**8**, 98991-64-1; *trans*-**8**, 99094-65-2; **9**, 30263-65-1; **10**, 98991-60-7; **11**, 6832-15-1; **12**, 99016-51-0; $Pd(PPh_3)_4$, 14221-01-3; $(p\text{-tolyl}_3P)_4Pd$, 29032-56-2; $P(p\text{-tolyl})_3$, 1038-95-5; *t*-BuOK-d_9, 34833-83-5; D_2, 7782-39-0; pinacolone, 75-97-8; 3,3-dimethyl-1,1,1-trideuterio-2-butanone, 54699-14-8; pivaloyl chloride, 3282-30-2.

Metal Halide Catalyzed Rearrangements of Alkylcyclosilanes

Thomas A. Blinka and Robert West*

Department of Chemistry, University of Wisconsin, Madison, Wisconsin 53706

Received May 16, 1985

In the presence of an $Al(Fe)Cl_3$ catalyst ($AlFeCl_6$; the $Al(Fe)Cl_3$ notation is being used because the exact nature of the catalyst is unknown), a series of permethylcyclosilanes $(Me_2Si)_n$, n = 5–12, rearranged to form isomeric branched cyclopentasilanes or cyclohexasilanes. For each permethylcyclosilane only one rearranged product was obtained. With the same catalyst, ethylundecamethylcyclohexasilane exhibited both skeletal rearrangement and alkyl group redistribution reactions. Perethylcyclosilanes, cyclopentamethylenecyclosilanes, cyclotetramethylenecyclosilanes, and ethylmethylcyclosilanes either decomposed or did not react with the $Al(Fe)Cl_3$ catalyst, depending upon the choice of solvent used in the reaction. A mechanism involving a cyclosilane–$Al(Fe)Cl_3$ complex is proposed to explain the observed rearrangement and redistribution reactions. The branching pattern and ring size of the rearranged permethylcyclosilanes are explained by σ-conjugation effects and steric interactions.

Introduction

Lewis acid catalyzed rearrangements of alkanes are well-known and have been thoroughly reviewed.[1] In contrast, reactions of polysilanes with Lewis acids have been reported just recently. Only a handful of linear and cyclic permethylsilane rearrangements have been investigated, and the mechanistic details of the reaction have yet to be completely elucidated.[2] However, it is now clear that polysilane rearrangements are strikingly selective reactions (much more so than the analogous alkane rearrangements[1]), whose products constitute a novel class of branched polysilanes. In this paper, the metal halide catalyzed rearrangements of a series of permethylcyclosilanes $(Me_2Si)_n$, n = 5–12, are reported. The effects of replacing methyl with other alkyl groups are described, and a mechanism to account for the selective formation of the observed isomers is proposed.

Results and Discussion

Permethylcyclosilanes. Permethylcyclosilanes **1–8** were reacted with the $Al(Fe)Cl_3$ catalyst (prepared as described in the Experimental Section). The results (Figure

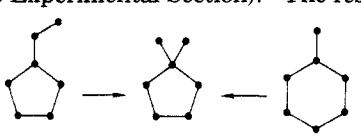

10

$(Me_2Si)_7$

3

1) are remarkable; in each reaction, a *single* isomeric product was obtained in nearly quantitative yield. Other products were not detected, but if present constitute at most 2% of the reaction mixture.[3] In addition, the same product can be obtained from the rearrangement of isomeric starting materials. If the reactions were quenched before complete consumption of the starting material, only unreacted starting material and the isomeric rearranged product were observed. Any intermediate is therefore a transient species; partially rearranged cyclosilanes were never detected. Also, the composition of the reaction mixture was unaffected by long reaction times. Reactions quenched immediately after the starting material disappeared gave the same products and yields as those allowed to continue for an additional 18 h. Thus it appears that equilibrium is rapidly established and that the observed branched products are thermodynamically favored over the starting materials.

The principal structural features of the rearranged cyclosilanes (ring size, branching pattern) were determined by analysis of the ^{29}Si NMR spectrum; ^1H NMR[4] and mass spectroscopic data were then compared for consistency with the ^{29}Si NMR data. The $(Me_2Si)_n$ rings up to n = 9 (**1–5**) rearrange to branched cyclopentasilanes, and larger rings **6–8** rearrange to branched cyclohexasilanes. In every case, the rearrangement reaction favors geminal bis(trimethylsilyl) substitution.

The ^{29}Si NMR assignments are listed in Table I. Resonances corresponding to the various types of silicon atoms (Me_3Si, Me_2Si, etc.) are well separated and appear at characteristic chemical shifts.[5] The resonances around −10 ppm are typical of trimethylsilyl groups[5] and are so assigned. Other assignments were based on the chemical shift trends observed for **1**, **9**, and **10**. Trimethylsilyl groups should have a large shielding effect on the chemical shifts of the silicons to which they are attached.[5] Consequently, Si_a of **9** is assigned to the −84.9 ppm resonance, and Si_a of **10** is assigned to the high field signal at −132.4 ppm.[6] Silicon atoms remote from the perturbing effect of the trimethylsilyl group(s) should have chemical shifts most like that of **1**. Therefore the Si_c's in **9** and **10** are assigned to the −42.6 and −40.2 ppm resonances, respectively. Silicon atoms β to the trimethylsilyl group(s) (Si_b) are shifted downfield from the reference chemical shift of **1**, about 5 ppm/β-trimethylsilyl group.

(1) (a) Pines, H.; Mavity, J. M. In "The Chemistry of Petroleum Hydrocarbons"; Brooks, B. T., Boord, C. E., Kurtz, S. S., Jr., Schmerling, L., Eds.; Rheinhold: New York, 1955; Chapter 39, pp 9–58. (b) Pines, H.; Hoffman, N. E. In "Friedel-Crafts and Related Reactions"; Ohah, G. A., Ed.; Interscience: New York, 1964; Vol. 2, Part 2, pp 1211–1252. (c) Pines, H. "The Chemistry of Catalytic Hydrocarbon Conversions"; Academic Press: New York, 1981.

(2) (a) Ishikawa, M.; Kumada, M. *Chem. Commun.* **1965**, 567. (b) Ishikawa, M.; Kumada, M. *J. Chem. Soc. D* **1970**, 157. (c) Ishikawa, M.; Iyoda, J.; Ikeda, H.; Kotake, K.; Hashimoti, T.; Kumada, M. *J. Am. Chem. Soc.* **1981**, *103*, 4845. (d) Ishikawa, M.; Watanabe, M.; Iyoda, J.; Ikeda, H.; Kumada, M. *Organometallics* **1982**, *1*, 317. (e) Kumada, M. *J. Organomet. Chem.* **1975**, *100*, 127.

(3) Estimated from ^{29}Si NMR spectra.

(4) The ^1H NMR spectra clearly differentiate between starting material and product. Unfortunately, the small chemical shift range makes accidental equivalence common and unequivocal assignments of the ^1H NMR spectra impossible.

(5) (a) Stanislawski, D. A. Ph.D. Thesis, University of Wisconsin—Madison, 1978, Chapter 2. (b) Mann, B. E. In "Spectroscopic Properties of Inorganic and Organometallic Compounds"; Chemical Society: London, 1968–1981; Vols. 1–14.

(6) The assignments are also consistent with the observed signal intensities.

0276-7333/86/2305-0128$01.50/0

Table I. ^{29}Si NMR Data (δ) for Rearranged Permethylcyclosilanes

	Me_3Si	a	b	c	d	e	f
1		-42.0					
9	-11.9	-84.9	-37.8	-42.6			
10	-7.5	-132.4	-31.6	-40.2			
11	-7.2, -7.8, -9.6	-130.8	-24.7	-80.5	-31.1	-27.2	
12	-7.1	-129.0	-1.94	-24.2			
13	-7.1	-129.0	-24.1				
14	-6.3, -6.7, -7.8, -8.8, -9.9	-120.3	-66.4	-14.3	-129.0	-24.1	-16.3
15	-9.1	-153.2	-37.7				

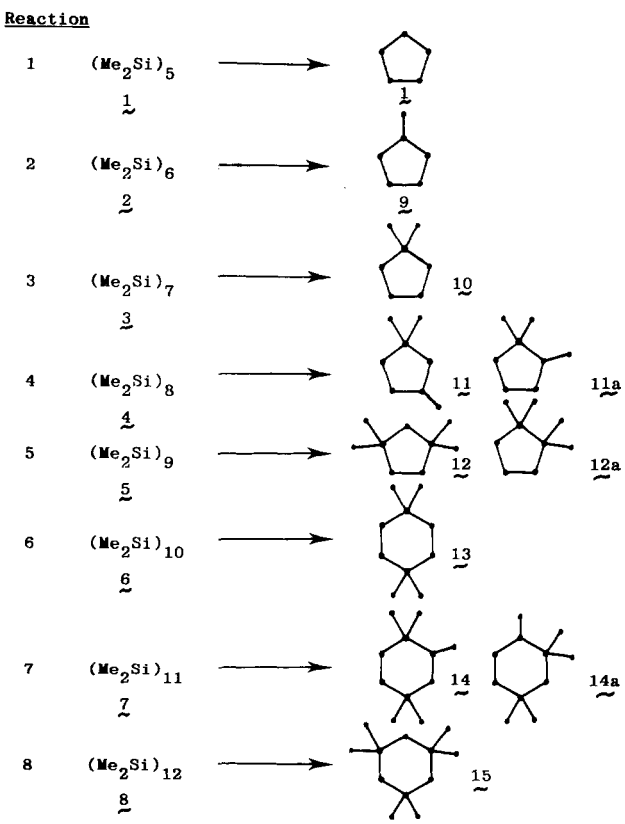

Figure 1. Al(Fe)Cl_3-catalyzed rearrangements of permethylcyclosilanes (isomers **11a**, **12a**, and **14a** were not observed).

The ^{29}Si NMR spectra of **11**, **12**, and **14** are consistent with either of two possible isomers. For example, both **11** and **11a** (Figure 1) are expected to give eight-line spectra: three trimethylsilyl resonances (Me_3Si), three dimethylsilyl resonances (Me_2Si), and one each of trisilyl-substituted (Si_3SiMe) and tetrasilyl-substituted (Si_4Si) silicon resonances.[7] The isomers are most easily differentiated on the basis of the Me_2Si chemical shifts. With use of the chemical shift trends observed in the spectra of **9** and **10**, the predicted Me_2Si resonances for **11** are -27, -32, and -37 ppm (assuming that each Me_2Si resonance is deshielded 5 ppm/β-trimethylsilyl group from the reference value of -42 ppm for **1**). Likewise, the predicted Me_2Si resonances of **11a** are -32, -37, and -42 ppm. The observed values (Table I) are closest to those predicted for isomer **11**, which is therefore assigned as the product of reaction **4** (Figure 1). Similarly, the predicted Me_2Si resonances of isomer **12** correspond more closely to the experimental values (Table I) than those predicted for **12a**. In addition, MM2 calculations[8] indicate that **12** should be more stable than **12a** by about 4 kcal/mol.

Isomers **14** and **14a** are more difficult to distinguish by ^{29}Si NMR. Because there is no ^{29}Si NMR data for poly(trimethylsilyl)-substituted cyclohexasilanes analogous to **1**, **9**, and **10**, the magnitude of the effects of branching on chemical shift cannot be determined for the branched cyclohexasilane systems. However, since **13** is unmistakably the 1,1,4,4-isomer, it seems likely that the same substitution pattern should be present in **14**. Also, MM2

(7) One might expect to rule out isomer **11a** simply because of unfavorable steric interactions between vicinal trimethylsilyl groups. However, MM2 calculations (see ref 8) show that **11** and **11a** are nearly isoenergetic. It is therefore necessary to consider both isomers as the possible product formed in reaction 4.

(8) Blinka, T. A.; West, R. *Organometallics*, following paper in this issue.

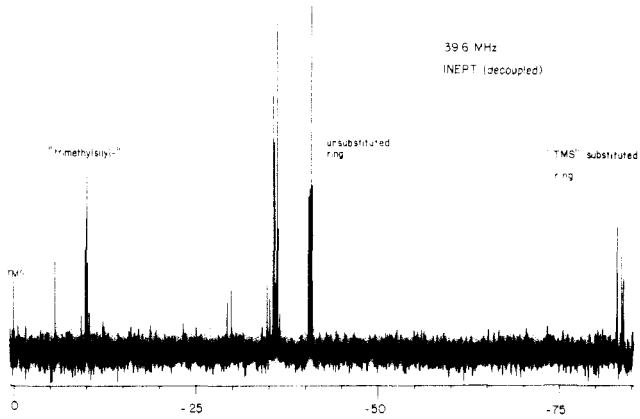

Figure 2. ^{29}Si NMR spectrum products of **21b–f** from rearrangement of ethylundecamethylcyclohexasilane.

calculations[8] predict isomer **14a** to be 2 kcal/mol less stable than **14**.

Other Alkyl-Substituted Cyclosilanes. A variety of perethyl- (**16a–f**),[9] cyclopentamethylene- (**17**),[10] cyclotetramethylene- (**18**),[10] and ethylmethylcyclosilanes (**19**)[11]

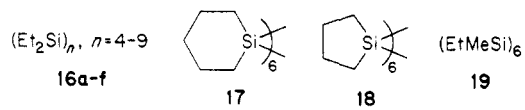

were treated with the $Al(Fe)Cl_3$ catalyst, under two sets of conditions. The reactivities of **16–19** were identical. In refluxing benzene, the cyclosilanes above decomposed completely to an uncharacterizable mixture after several hours of reaction. In refluxing cyclohexane, no reaction was observed, and the starting materials were recovered quantitatively. The difference in reactivity of **16–19** in the two solvents is probably a consequence of the greater solubility of $AlCl_3$ in benzene,[12] making the decomposition reaction much faster than in cyclohexane. Since methyl and ethyl have similar electronic properties,[13] the lack of rearrangement of **16–19** presumably results from differences in steric bulk between methyl and other alkyl groups.[14] It seems apparent that the $Al(Fe)Cl_3$-catalyzed rearrangement reaction is limited to permethylated polysilanes.

Ethylundecamethylcyclohexasilane. As an aid in probing the reaction mechanism, the rearrangement of a methylcyclohexasilane containing one ethyl group (**20**) was investigated. When **20** was subjected to the usual rearrangement conditions, a four-component reaction mixture was observed by GLC. Mass spectroscopy indicated the following molecular formulas: Si_6Me_{12} (20%), $Si_6Me_{11}Et$ (42%), $Si_6Me_{10}Et_2$ (26%), $Si_6Me_9Et_3$ (12%). Silicon-29 NMR revealed that all four components of the reaction mixture have the same (trialkylsilyl)cyclopentasilane skeleton and that the ethyl-containing components are mixtures of isomers differing by the placement of ethyl group(s) around the silicon framework (eq 1). (The ^{29}Si NMR spectrum of component **21** is shown by way of example in Figure 2.) Thus, two distinct reactions take place: intramolecular rearrangement of the silicon skeleton and intermolecular redistribution of the alkyl groups. The latter reaction undoubtedly occurs with the permethylcyclosilane systems as well.

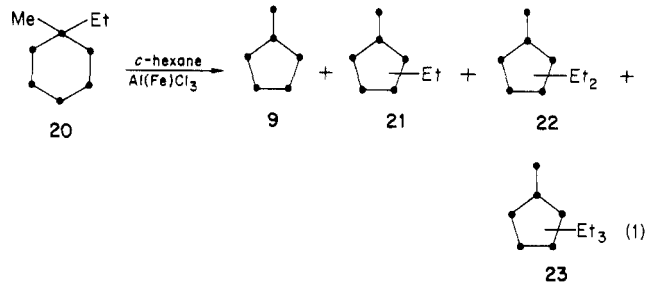

Careful examination of Figure 2 reveals an interesting phenomenon: of the six isomers possible for **21**, only five are observed. This is most easily seen the Me_3Si region of the ^{29}Si NMR spectrum (around −10 ppm). Four resonances are clustered between −9.9 and −10.3 ppm and are attributed to the Me_3Si silicons of isomers **21c–f**. A single

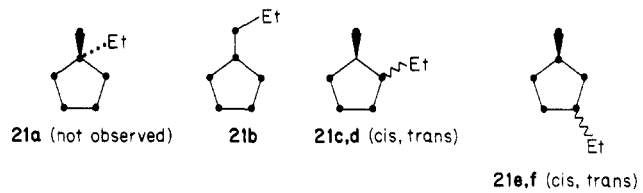

resonance is shifted downfield to −5.8 ppm and is assigned to the $EtMe_2Si$ silicon of **22b**. The Me_3Si resonance of **21a** would be expected to fall between −5.8 and −10 ppm; the absence of a sixth resonance in this region indicates that **21a** is not formed. Similarly, only five resonances are observed around −80 ppm (Si_3SiMe).

Mechanism. Ishikawa and Kumada,[2] in their pioneering studies of $AlCl_3$-catalyzed polysilane rearrangements, observed trace amounts of chlorosilanes in their reaction mixtures. They proposed a reaction mechanism in which chlorosilane intermediates, formed by initial chlorodemethylation of the starting material, rearrange and then undergo chlorine–methyl exchange[15] to complete the catalytic cycle. However, we do not observe chlorosilanes with our procedure (see Experimental Section), and even if chlorosilanes were present, they need not be intermediates in the rearrangement.

We find that the $Al(Fe)Cl_3$ catalyst which gives rapid rearrangement does not catalyze chlorodephenylation reactions (see Experimental Section). It therefore seems unlikely that an initial chlorodemethylation step would occur (or occur rapidly) in the presence of our catalyst. If chlorosilanes are necessary for rearrangement, then the deliberate addition of trace moisture to the reaction mixture should increase the amount of HCl present and hence the amount of chlorosilane generated.[16] One would thus expect an increase in the rate of rearrangement. In our hands, the addition of as little as 2 μL of water to the reaction caused decomposition but no rearrangement of **2**. These observations led us to search for a more satisfactory mechanism.

The similarities between acid-catalyzed ($HCl/AlCl_3$ or H_2SO_4) cycloalkane rearrangements[1] and $Al(Fe)Cl_3$-catalyzed cyclosilane rearrangements suggests that silyl radicals or silicenium ions (analogues of carbon radicals and car-

(9) Carlson, C. W.; Matsumura, K.; West, R. *J. Organomet. Chem.* **1980**, *194*, C5.
(10) (a) Carlson, C. W.; Zhang, X.-H.; West, R. *Organometallics* **1983**, *2*, 453. (b) Carlson, C. W.; Haller, K. J.; Zhang, X.-H.; West, R. *J. Am. Chem. Soc.* **1984**, *106*, 5521.
(11) Katti, A.; Carlson, C. W.; West, R. *J. Organomet. Chem.* **1984**, *271*, 353.
(12) "Handbook of Chemistry and Physics", 57th ed.; Weast, R. C., Ed.; CRC Press: Cleveland, OH, 1976.
(13) Ritchie, C. D.; Sager, W. F. *Prog. Phys. Org. Chem.* **1964**, *2*, 323.
(14) (a) Cartledge, F. K. *Organometallics* **1983**, *2*, 425. (b) Boe, B. *J. Organomet. Chem.* **1976**, *107*, 139. (c) Watanabe, H.; Muraoka, T.; Kageyama, M.; Yoshizumi, K.; Nagai, Y. *Organometallics* **1984**, *3*, 141.
(15) For example: Ishikawa, M.; Kumada, M.; Sakurai, H. *J. Organomet. Chem.* **1970**, *23*, 63.
(16) Ishikawa, M.; Kumada, M. *Synth. Inorg. Met.-Org. Chem.* **1971**, *1*, 191.

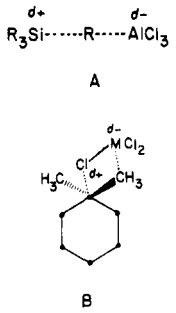

Figure 3. Possible silane–metal halide complexes.

benium ions) may be intermediates in the cyclosilane rearrangements. Silyl radicals cannot be ruled out, but seem improbable: silyl radicals do not generally react cleanly[17] and would be expected to give a variety of byproducts. Trivalent silicenium ion intermediates also seem unlikely because of the well-known reluctance of silicon to form trivalent cations in solution.[18] However, other types of silicon "cations" have been observed in solution, including pentavalent silicon cations,[19] cyclosilane cation radicals,[20] and tetracyanoethylene–cyclosilane charge-transfer complexes.[21] Reasonable intermediates could therefore include complexes or hypervalent silicon species bearing only a partial positive charge.

The finding that $Al(Fe)Cl_3$ catalyzes both rearrangement and alkyl redistribution reactions in cyclosilanes (eq 1) suggested that a common intermediate may be involved in both reactions. Previously, Russell and others[22] proposed that $AlCl_3$-catalyzed tetraalkylsilane redistribution reactions occur via a silane–$AlCl_3$ complex, A (Figure 3), in which a silicon atom bears a partial positive charge. Such an intermediate would explain not only redistribution but also rearrangement reactions. Because positively charged pentavalent silicon species are relative stable in solution,[19] we prefer a pentavalent silicon intermediate, B (Figure 3). Complex B is similar to Russell's intermediate, except that a chlorine ligand coordinates to the electron-deficient silicon atom.[23] As shown in Figure 4, intermediate B could exchange alkyl groups with uncomplexed cyclosilane or rearrange via intramolecular 1,2 silicon–silicon and silicon–carbon bond shifts to give branched cyclosilanes.

The branching in the rearrangement products should be favored by σ-conjugation.[24] Photoelectron spectra[20,25]

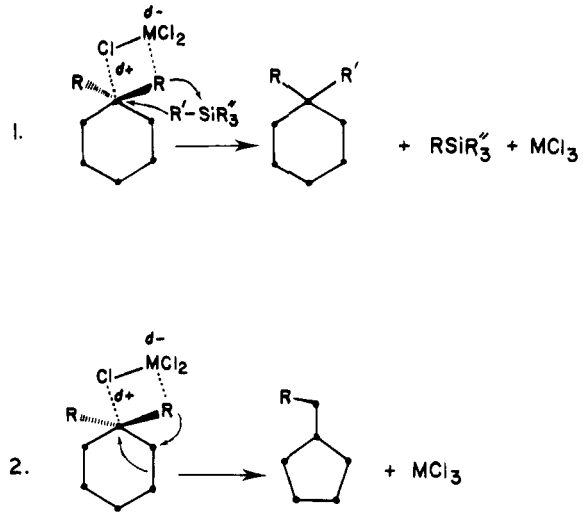

Figure 4. Mechanisms proposed for rearrangement and redistribution reactions.

show that the silicon–silicon σ-bonding orbitals of **9** are on average 0.26 eV[26] lower in energy than the corresponding orbitals of **2**. Calculations[24c] also predict the most highly branched cyclosilanes to be more stable than isomeric cyclosilanes.

During rearrangement, increased branching of a cyclosilane requires decreased ring size and hence leads to increased steric interactions. The final ring size of the rearrangement products is therefore determined by the relative magnitude of stabilizing σ-conjugation (from branching) and destabilizing steric interactions (particularly ring strain). Cyclosilanes **1–5** rearrange to branched cyclopentasilanes, since cyclopentasilanes are only marginally strained relative to cyclohexasilanes,[27] but afford more branching. (Still greater branching could be achieved by ring contraction to cyclotetrasilanes, but this would be opposed by large increases in steric interactions.) Larger rings **6–8** rearrange to branched cyclohexasilanes, to minimize steric interactions between trimethylsilyl groups.

Experimental Section

Spectroscopy. All NMR spectra were obtained by using benzene-d_6 as the solvent. The benzene signal was used as an internal standard for ^1H NMR spectra, and tetramethylsilane was used as an internal standard for ^{29}Si NMR spectra. ^1H NMR spectra were obtained with either a Bruker WP-200 (200 MHz) or WP-270 (270 MHz) spectrometer; ^{29}Si NMR spectra were obtained with a JEOL FX-200 spectrometer at 39.6 MHz, using the INEPT pulse sequence[28] (τ = 35.7 ms, Δ = 19.1 ms).

Ultraviolet spectra were obtained with a Cary 14 spectrophotometer using spectrograde cyclohexane. Mass spectra were run at 30 eV with use of a Kratos MS-80 mass spectrometer.

Chromatography. Analytical GLC analyses were obtained with a Hewlett-Packard 5720A gas chromatograph, equipped with a flame ionization detector, using a 3 ft × 1/8 in. Dexsil 400 column (5% on Chromosorb W), or a Hewlett-Packard 5890A gas chromatograph, also equipped with a flame ionization detector, using a 20-ft HP-530 μ capillary column. Preparative GLC separations were obtained by using a GOW-MAC 550P gas chromatograph equipped with a thermal conductivity detector, using a 0.4 cm × 220 cm Dexsil 400 column (10% on Chromosorb W). All GLC

(17) Brook, A. G.; Bassindale, A. R. In "Rearrangements in Ground and Excited States"; de Mayo, P., Ed.; Academic Press: New York, N. Y., 1980; Vol. 2, Essay 9. (b) Jackson, R. A. In "Advances in Free-Radical Chemistry"; Williams, G. H., Ed.; Academic Press: New York, 1969; Vol. 3, Chapter 5.

(18) (a) Corriu, R. J. P.; Henner, M. *J. Organomet. Chem.* **1974**, *74*, 1. (b) Olah, G. A.; Mo, Y. K. *J. Am. Chem. Soc.* **1971**, *93*, 4942. (c) Corey, J. Y. *J. Am. Chem. Soc.* **1975**, *97*, 3237. (d) O'Brien, D. H.; Hairston, T. J. *Organomet. Chem. Rev. A* **1971**, *7*, 95. (e) Lambert, J. B.; Schultz, W. J., Sr. *J. Am. Chem. Soc.* **1983**, *105*, 1671.

(19) (a) Corey, J. Y.; West, R. *J. Am. Chem. Soc.* **1963**, *85*, 4034. (b) Aylett, B. J.; Campbell, J. M. *Chem. Commun.* **1967**, 159.

(20) Bock, H.; Kaim, W.; Kira, M.; West, R. *J. Am. Chem. Soc.* **1979**, *101*, 7667.

(21) Traven, V. F.; West, R. *J. Am. Chem. Soc.* **1973**, *95*, 6824.

(22) Zemany, P. D.; Price, F. P. *J. Am. Chem. Soc.* **1948**, *70*, 4222. (b) Russell, G. A. *J. Am. Chem. Soc.* **1959**, *81*, 4815. (c) Russell, G. A. *J. Am. Chem. Soc.* **1959**, *81*, 4875. (d) Russell, G. A.; Nagpal, K. L. *Tetrahedron Lett.* **1961**, 421.

(23) Clegg, W.; Klingebiel, U.; Neeman, J.; Sheldrick, G. M. *J. Organomet. Chem.* **1983**, *249*, 47.

(24) (a) Dewar, M. J. S. *J. Am. Chem. Soc.* **1984**, *106*, 669. (b) Hoffman, R. *Acc. Chem. Res.* **1971**, *4*, 1. (c) Pitt, C. G. In "Homoatomic Rings, Chains and Macromolecules of Main-Group Elements"; Rheingold, A. L., Ed.; Elsevier: New York, 1977; Chapter 8.

(25) (a) Bock, H.; Ramsey, G. B. *Angew. Chem.* **1973**, *85*, 773; *Angew. Chem., Int. Ed. Engl.* **1973**, *12*, 734. (b) Bock, H.; Ensslin, W. *Angew. Chem.* **1971**, *83*, 435; *Angew. Chem., Int. Ed. Engl.* **1971**, *10*, 404.

(26) Weighted average energy of bonding Si–Si molecular orbitals: 2, 8.96 eV; 9, 8.70 eV. See ref 25.

(27) Cyclopentasilanes should have no more than 5 kcal/mol more ring strain than cyclohexasilanes. See: Burkert, U.; Allinger, N. L. In "Molecular Mechanics"; American Chemical Society: Washington, D.C., 1981.

(28) For a review, see: Blinka, T. A.; West, R. *Adv. Organomet. Chem.* **1984**, *23*, 193.

separations utilized temperature programming. HPLC separations were obtained on a Whatman M-9 ODS-2 reverse-phase semipreparative column, with a mobile phase of MeOH/THF, using a Waters Associates 6000 LC pump, and an Altex Model 153 UV detector (254 nm). Solvent programming was used, with MeOH/THF ratios varying between 4/1 and 1/1.

Methods. Cyclohexane and benzene were deolefinated with HNO_3/H_2SO_4, dried over $MgSO_4$, and then distilled from Na/benzophenone. The solvents were stored in Schlenk flasks containing activated 4-Å molecular sieves, under a dry argon atmosphere. Tetrahydrofuran was distilled before use from Na/benzophenone. Lithium wire was supplied by Alfa and stored under mineral oil. Chlorosilanes (Petrarch) were distilled from anhydrous K_2CO_3 and stored under inert atmosphere.

Catalyst. The catalyst was prepared by the sublimation of technical-grade $AlCl_3$ containing 0.1% $FeCl_3$ or the cosublimation of pure $AlCl_3$ with $FeCl_3$ (1%), in a Beers–McCarley sublimator.[29] The resulting pale yellow catalyst was stored in a Schlenck flask under dry argon. Unsublimed, technical-grade $AlCl_3$, pure sublimed $AlCl_3$, or pure $AlCl_3$ to which $FeCl_3$ was added without cosubliming did not catalyze cyclosilane rearrangements. It is likely that the active catalyst contains $AlFeCl_6$[30] which may be the actual catalytic species. However, because the exact nature of the catalyst is unknown, it is written as $Al(Fe)Cl_3$.

Attempted Chlorodephenylation[16] Using the $Al(Fe)Cl_3$ Catalyst. To a 100-mL flask equipped with a magnetic stirrer was added 5.0 g (15 mmol) of 2,2-diphenylhexamethyltrisilane, **21**, 50 mL of benzene, and approximately 1.0 g of the $Al(Fe)Cl_3$ catalyst. A rapid stream of dry HCl(g) was introduced and the solution cooled with an ice bath. The reaction was monitored by GLC. Even after 1 h of exposure to $HCl/Al(Fe)Cl_3$, only unreacted **21** was observed.

Preparation of Cyclosilanes. Permethylcyclosilanes,[31] perethylcyclosilanes,[9] cyclopentamethylenecyclosilanes,[10] cyclotetramethylenecyclosilanes,[10] and ethylmethylcyclosilanes[11] were prepared as previously reported. The particular ring sizes were isolated from the mixtures by preparative HPLC. The compounds were characterized by ^1H NMR, mass spectroscopy, and GLC retention times, which were in agreement with the literature.

Preparation of Ethylundecamethylcyclohexasilane (20). To a 250-mL flask equipped with a mechanical stirrer, reflux condenser, and a 100-mL pressure equalized addition funnel (all glassware oven-dried, apparatus maintained under Ar atmosphere), was added 0.5 g of Mg turnings (21 mmol) and 2.2 g of ethyl bromide (20 mmol) in 15.0 mL of THF. After formation of the Grignard reagent was completed, a solution of 5.0 g of chloroundecamethylcyclohexasilane[32] dissolved in 50.0 mL of THF was added dropwise at room temperature. The solution was then refluxed overnight. The reaction was quenched with 95% ethanol; salts were precipitated with 100 mL of hexane and removed by filtration. Solvent was removed at reduced pressure, giving 5.3 g of a colorless, semicrystalline solid, **20**: mp 190–192 °C; ^1H NMR (200 mHz) δ 0.024 (m, 33 H), 0.81 (q, 2 H), 1.09 (t, 3 H); ^{29}Si NMR (39.6 MHz) δ −36.79 (1 Si, SiMeEt), −41.68 (2 Si, $SiMe_2$), −41.87 (2 Si, $SiMe_2$), −41.91 (1 Si, $SiMe_2$). Anal. Calcd for $Si_6C_{13}H_{38}$: Si, 46.43; C, 43.02; H, 10.55. Found: Si, 46.36; C, 43.35; H, 10.29.

Rearrangements of Cyclosilanes. A similar procedure was employed in the rearrangements of all the cyclosilanes, except **6–8**, for which the small scale of the experiments necessitated special handling.

To a 25-mL flask equipped with a reflux condenser and a magnetic stirrer was added 10 mL of cyclohexane and approximately 5–10 mg of the $Al(Fe)Cl_3$ catalyst. The solution was purged for 10 min with a rapid stream of Ar before adding the cyclosilane. The solution was brought to reflux and monitored by GLC. When the starting material was completely consumed (usually 2–5 h), the solution was cooled to room temperature, transferred to a small silica gel column (0.7 × 3 cm), and rapidly eluted with 10–20 mL of cyclohexane. The solvent was stripped off under reduced pressure to give a colorless solid.

Rearrangement of Decamethylcyclopentasilane (1). With use of the procedure above, 0.200 g of **1** was reacted with 10 mg of $AlCl_3$ catalyst in 10.0 mL of cyclohexane. After 3 h no change in composition was noted by GLC. After workup, the product was found by ^1H NMR and mass spectroscopy to be unreacted **1**.[31]

Rearrangement of Dodecamethylcyclohexasilane (2). With use of the procedure above, 1.00 g of **2** was reacted with 10 mg of the $Al(Fe)Cl_3$ catalyst in 10.0 mL of cyclohexane. After 1 h, **2** was completely consumed. After workup, a quantitative yield of **9**, (trimethylsilyl)nonamethylcyclopentasilane,[2a,d] was obtained: UV λ_{max} (log ϵ) 280 nm (3.0); ^1H NMR (200 MHz) δ 0.150 (s, 3 H), 0.225–0.234 (m, 21 H), 0.277 (s, 6 H) 0.289 (s, 6 H); MS, *m/e* (relative intensity) 350 (14), 349 (21), 348 (49, M^+), 215 (25), 201 (41), 171 (10), 157 (16), 73 (100). Anal. Calcd for $Si_6C_{12}H_{36}$: mol wt, 348.1433. Found: mol wt, 348.1430.

Rearrangement of Tetradecamethylcycloheptasilane (3). With use the procedure above, 0.160 g of **3** was reacted with 10 mg of $AlCl_3$ catalyst in 10.0 mL of cyclohexane. After 6 h, **3** was completely consumed. After workup, 0.136 g (85%) of 1,1-bis(trimethylsilyl)octamethylcyclopentasilane, **10**,[2d] was obtained: mp 173.5–176 °C UV λ_{max} (log ϵ) 281 nm (2.9), 241 (3.9, sh); ^1H NMR (270 MHz) δ 0.25 (s, 12 H), 0.30 (s, 18 H), 0.38 (s, 12 H); MS, *m/e* (relative intensity) 408 (37), 407 (46), 406 (89, M^+), 312 (17), 73 (14). Anal. Calcd for $Si_7C_{14}H_{42}$: mol wt, 406.1672. Found: mol wt, 406.1608.

Rearrangement of Hexadecamethylcyclooctasilane (4). With use of the procedure above, 0.32 g of **4** was reacted with 10 mg of the $AlCl_3$ catalyst in 10.0 mL of cyclohexane. The solution was allowed to reflux 5 h. After workup, a quantitative yield of colorless solid 1,1,3-tris(trimethylsilyl)heptamethylcyclopentasilane, **11a**, was obtained: mp 59 °C (cloudy melt), 72 °C (clear melt); UV λ_{max} (log ϵ) 237 nm (4.2), 275 (3.3, sh); ^1H NMR (270 MHz) δ 0.19 (s, 3 H), 0.24 (s, 6 H), 0.32 (s, 27 H), 0.40 (m, 6 H), 0.47 (m, 6 H); MS, *m/e* (relative intensity) 466 (12), 465 (17), 464 (34, M^+), 73 (100). Anal. Calcd. for $Si_8C_{16}H_{48}$: Si, 48.29; C, 41.31; H, 11.14; MW 464.1910. Found: Si, 48.56; C, 41.13; H, 10.31; MW 464.1897.

Rearrangement of Octadecamethylcyclononasilane (5). With use of the procedure above, 0.310 g of **5** was reacted with 10 mg of the $AlCl_3$ catalyst in 10.0 mL of cyclohexane. The solution was allowed to reflux 5 h. After workup, a quantitative yield of colorless, semicrystalline 1,1,3,3-tetrakis(trimethylsilyl)hexamethylcyclopentasilane, **12**, was obtained: mp 142–143 °C; UV λ_{max} (log ϵ) 240 nm (4.3), 280 (3.2, sh); ^1H NMR (270 MHz) δ 0.32 (s, 36 H), 0.40 (s, 12 H), 0.58 (s, 6 H); MS, *m/e* (relative intensity) 524 (43), 523 (56), 522 (100, M^+), 429 (13), 376 (24), 73 (45). Anal. Calcd for $Si_9C_{18}H_{54}$: Si, 48.29; C, 41.31; H, 11.14; mol wt, 522.2149. Found: C, 41.06; H, 10.08.

Rearrangement of Ethylundecamethylcyclohexasilane (20). With use of the above procedure, 0.200 g of **20** was reacted with 10 mg of the $AlCl_3$ catalyst in 15 mL of cyclohexane. The reaction was monitored by GLC. After 24 h, **20** was completely consumed, and no changes were observed in the product mixture. After workup a quantitative mass recovery of a mixture of products was obtained. **9** (20%) was identified by ^1H NMR. **21** (five isomers, 43.3%): ^1H NMR (200 MHz) δ 0.15–0.35 (m, 33 H), 0.7–0.83 (m, 2 H), 1.03–1.20 (m, 3 H); ^{29}Si NMR (39.6 MHz) δ −5.78, −9.91, −10.01, −10.08, −10.26 (Me_3Si), −29.26, −29.82, −34.78, −35.13, −35.52, −35.72, −35.87, −36.03, −36.13, −36.20, −40.37, −40.54, −50.73, −40.82, −40.87, −49.90, −40.99 (Me_2Si), −82.91, −82.97, −83.52, −83.75, −83.85 (Si_3SiMe); MS, *m/e* (relative intensity) 364 (21), 363 (35), 362 (100, M^+), 259 (11), 73 (15). **22** (mixture of isomers, 25.7%): ^1H NMR (200 MHz) δ 0.13–0.36 (m, 30 H), 0.70–1.20 (m, 10 H); ^{29}Si NMR (39.6 MHz) δ −6 to −11 (Me_3Si), −29 to −30, −34 to −38, −40 to −43 (Me_2Si), −83 to −85 (Si_3SiMe); MS, *m/e* (relative intensity) 378 (22), 377 (36), 376 (100, M^+), 273 (11), 215 (16), 73 (9.0). **23** (mixture of isomers, 12.0%): ^1H NMR (200 MHz) δ 0.13–0.36 (m, 27 H), 0.7–1.20 (m, 15 H); ^{29}Si NMR (39.6 MHz) δ −5 to −12 (Me_3Si), −27 to −45 (Me_2Si), −80 to −87 (Si_3SiMe); MS, *m/e* (relative intensity) 392 (24), 391 (45), 390 (100, M^+), 321 (14), 288 (10), 274 (14), 259 (11), 73 (43).

Rearrangements of Large (p = 10–12) Permethylcyclosilanes. Because of the small scale of these reactions (due to the

(29) Jensen, W. B. Ph.D. Thesis, University of Wisconsin—Madison, 1982; p 224.
(30) Fowler, R. M.; Melford, S. S. *Inorg. Chem.* **1976**, *15*, 473.
(31) (a) Brough, L. F.; Matsumura, K.; West, R. *Angew. Chem., Int. Ed. Engl.* **1979**, *18*, 955. (b) Matsumura, K.; Brough, L. F.; West, R. *J. Chem. Soc., Chem. Commun.* **1978**, 1092.
(32) Helmer, B. J.; West, R. *J. Organomet. Chem.* **1982**, *236*, 21.

difficulty of isolating the starting materials), a special apparatus was constructed, consisting of a 2-mL flask fused directly to the bottom of a 10-cm reflux condenser. The apparatus was oven-dried at 160 °C before use, equipped with a small magnetic stirrer, and maintained throughout the reaction under dry Ar atmosphere. All details of the procedure (including workup) used for other cyclosilanes were the same with the exception that solvent volumes and the amounts of $Al(Fe)Cl_3$ catalyst employed were much smaller.

Rearrangement of Eicosamethylcyclodecasilane (6). With use of the above procedure, 23.1 mg of **6** was reacted with 2.0 mg of the $Al(Fe)Cl_3$ catalyst in 2.0 mL of cyclohexane. The solution was allowed to reflux for 2.5 h. After workup, 15.3 mg (66% mass recovery) of colorless solid 1,1,4,4-tetrakis(trimethylsilyl)octamethylcyclohexasilane, **13**, was obtained: ^1H NMR δ 0.36 (s, 36 H), 0.37 (s, 24 H). Anal. Calcd for $Si_{10}C_{20}H_{60}$: mol wt 580.2388. Found: wt 580.2391.

Rearrangement of Docosamethylcycloundecasilane (7). With use of the above procedure, 17.4 mg of **7** was reacted with 2.0 mg of the $Al(Fe)Cl_3$ catalyst in 2.5 mL of cyclohexane. The solution was allowed to reflux for 2.5 h. After workup, 12.2 mg (70% mass recovery) of a colorless oil containing 1,1,2,4,4-pentakis(trimethylsilyl)heptamethylcyclohexasilane, **14a**, was obtained: ^1H NMR δ 0.32 (m, 48 H), 0.40 (s, 6 H), 0.49 (m, 6 H), 0.62 (m, 6 H). Anal. Calcd for $Si_{11}C_{22}H_{66}$: mol wt, 638.2607. Found: mol wt, 638.2614.

Rearrangement of Tetracosamethylcyclododecasilane (8). With use of the above procedure, 14.7 mg of **8** was reacted with 2.0 mg of the $Al(Fe)Cl_3$ catalyst in 1.5 mL of cyclohexane. The solution was allowed to reflux for 2 h. After workup, 7.9 mg (54% mass recovery) of a colorless oil containing 1,1,3,3,5,5-hexakis(trimethylsilyl)hexamethylcyclohexasilane, **15**, was obtained: ^1H NMR δ 0.36 (m, br). Anal. Calcd for $Si_{12}C_{24}H_{72}$: mol wt, 696.2844. Found: mol wt, 696.2882.

Reactions of Other Cyclosilanes. Reaction of cyclosilanes **16-19** with the $Al(Fe)Cl_3$ catalyst were performed by using the procedures detailed for **1**. In all cases, unreacted starting material was recovered when the solvent employed was cyclohexane (determined by GLC retention times and spectroscopic data consistent with those reported in the literature).[9-11] When cyclohexane was replaced with benzene, using identical methodology, a complex mixture was obtained.

Acknowledgment. This research was sponsored by the Air Force Office of Scientific Research, Air Force Systems Command, USAF, under Contract No. F49620-83-C-0044, and by a grant from the 3M Co. The United States Government is authorized to reproduce and distribute reprints for governmental purposes notwithstanding any copyright notation thereon. We thank Professor J. R. Damewood, Jr., for helpful suggestions and comments.

Conformational Analysis of Branched Cyclosilanes

Thomas A. Blinka and Robert West*

Department of Chemistry, University of Wisconsin, Madison, Wisconsin 53706

Received May 16, 1985

Conformational analyses of a number of branched cyclopentasilanes and cyclohexasilanes were performed by using the empirical force field method. In comparisons of structurally similar isomers, the thermodynamically preferred isomer was usually calculated to have significantly lower steric energy. Steric energies and equilibrium constants were used to estimate relative σ-conjugation stabilizations. The magnitude of the structural distortions in the cyclopentasilane rings were dependent on the extent of trimethylsilyl substitution.

Introduction

Although conformational analysis has become a powerful tool in organic chemistry,[1] conformational principles in organosilicon chemistry are only starting to be elucidated. Conformational analyses of silanes have been limited mainly to linear molecules and symmetrically substituted rings[2,3] for which experimental structure data is available.

In the preceding paper[4] the synthesis of several branched, trimethylsilyl-substituted cyclopentasilanes and cyclohexasilanes, obtained by rearrangement of unbranched permethylcyclosilane rings, is described. The experimental results raised many questions concerning conformation, steric strain, and σ-delocalization,[5] which prompted the present study. In this paper we report calculations of steric energies (ΔH_{steric}) and structures of cyclosilanes **1-12**, using the empirical force field method.[6]

Calculational Methods and Notation

The calculations were performed by using the program MM2[7] and the full relaxation method.[8] The force field parameters used were developed previously for polysilane calculations[9] and satisfactorily reproduce electron diffraction and X-ray structure for cyclosilanes **1**[10] and **2**,[11] as well as for the branched highly strained molecule $(Me_3Si)_4Si$.[12] Input structures for the calculation of conformations for poly(trimethylsilyl)cyclopentasilanes

(1) See: Eliel, E. L.; Allinger, N. L.; Angyal, S. J.; Morrison, G. A. "Conformational Analysis"; American Chemical Society: Washington, D.C., 1981.

(2) (a) Hummel, J. P.; Stackhouse, J.; Mislow, K. *Tetrahedron* **1977**, *33*, 1925. (b) Honig, H.; Hassler, K. *Monatsh. Chem.* **1982**, *113*, 129.

(3) Shafiee, F.; Damewood, Jr., J. R.; Haller, K. J.; West, R. *J. Am. Chem. Soc.* **1985**, *107*, 0000.

(4) Blinka, T. A.; West, R. *Organometallics*, preceding paper in this issue.

(5) (a) Dewar, M. J. S. *J. Am. Chem. Soc.* **1984**, *106*, 669. (b) Hoffman, R. *Acc. Chem. Res.* **1971**, *4*, 1. (c) Pitt, C. G. In "Homoatomic Rings, Chains and Macromolecules of Main Group Elements"; Rheingold, A. L., Ed.; Elsevier: New York, 1977; Chapter 8.

(6) For reviews of the EFF method, see: (a) Williams, J. D.; Stang, P. J.; Schleyer, P. v. R. *Annu. Rev. Phys. Chem.* **1968**, *19*, 531. (b) Engler, E. M.; Andose, J. D.; Schleyer, P. v. R. *J. Am. Chem. Soc.* **1973**, *95*, 8005. (c) Kitaigorodsky, A. I. *Chem. Soc. Rev.* **1978**, *7*, 133. (d) Mislow, K.; Doughtery, D. A.; Hoonshell, W. D. *Bull. Soc. Chim. Belg.* **1978**, *87*, 555. (e) Burkert, V.; Allinger, N. L. "Molecular Mechanics"; American Chemical Society, Washington, D.C., 1981.

(7) Allinger, N. L. *QCPE* **1981**, *13*, 395, adapted for use with a Harris/7 computer by Prof. H. Whitlock.

(8) The bond lengths, bond angles, and torsion angles are adjusted to the minimum energy values for each conformation.

(9) Damewood, J. R., Jr.; West, R. *Macromolecules* **1985**, *18* (2), 158.

(10) Smith, Z.; Seip, H. M.; Hengge, E.; Bauer, G. *Acta Chem. Scand., Ser. A* **1976**, *A30*, 697.

(11) Carrell, H. L.; Donohue, J. *Acta Crystallogr., Sect. B* **1972**, *B28*, 1566.

(12) Bartell, C. S.; Clippard, F. B., Jr.; Boates, T. L. *Inorg. Chem.* **1970**, *9*, 2436.

0276-7333/86/2305-0133$01.50/0

difficulty of isolating the starting materials), a special apparatus was constructed, consisting of a 2-mL flask fused directly to the bottom of a 10-cm reflux condenser. The apparatus was oven-dried at 160 °C before use, equipped with a small magnetic stirrer, and maintained throughout the reaction under dry Ar atmosphere. All details of the procedure (including workup) used for other cyclosilanes were the same with the exception that solvent volumes and the amounts of $Al(Fe)Cl_3$ catalyst employed were much smaller.

Rearrangement of Eicosamethylcyclodecasilane (6). With use of the above procedure, 23.1 mg of **6** was reacted with 2.0 mg of the $Al(Fe)Cl_3$ catalyst in 2.0 mL of cyclohexane. The solution was allowed to reflux for 2.5 h. After workup, 15.3 mg (66% mass recovery) of colorless solid 1,1,4,4-tetrakis(trimethylsilyl)octamethylcyclohexasilane, **13**, was obtained: ^1H NMR δ 0.36 (s, 36 H), 0.37 (s, 24 H). Anal. Calcd for $Si_{10}C_{20}H_{60}$: mol wt 580.2388. Found: wt 580.2391.

Rearrangement of Docosamethylcycloundecasilane (7). With use of the above procedure, 17.4 mg of **7** was reacted with 2.0 mg of the $Al(Fe)Cl_3$ catalyst in 2.5 mL of cyclohexane. The solution was allowed to reflux for 2.5 h. After workup, 12.2 mg (70% mass recovery) of a colorless oil containing 1,1,2,4,4-pentakis(trimethylsilyl)heptamethylcyclohexasilane, **14a**, was obtained: ^1H NMR δ 0.32 (m, 48 H), 0.40 (s, 6 H), 0.49 (m, 6 H), 0.62 (m, 6 H). Anal. Calcd for $Si_{11}C_{22}H_{66}$: mol wt, 638.2607. Found: mol wt, 638.2614.

Rearrangement of Tetracosamethylcyclododecasilane (8). With use of the above procedure, 14.7 mg of **8** was reacted with 2.0 mg of the $Al(Fe)Cl_3$ catalyst in 1.5 mL of cyclohexane. The solution was allowed to reflux for 2 h. After workup, 7.9 mg (54% mass recovery) of a colorless oil containing 1,1,3,3,5,5-hexakis(trimethylsilyl)hexamethylcyclohexasilane, **15**, was obtained: ^1H NMR δ 0.36 (m, br). Anal. Calcd for $Si_{12}C_{24}H_{72}$: mol wt, 696.2844. Found: mol wt, 696.2882.

Reactions of Other Cyclosilanes. Reaction of cyclosilanes **16-19** with the $Al(Fe)Cl_3$ catalyst were performed by using the procedures detailed for **1**. In all cases, unreacted starting material was recovered when the solvent employed was cyclohexane (determined by GLC retention times and spectroscopic data consistent with those reported in the literature).[9-11] When cyclohexane was replaced with benzene, using identical methodology, a complex mixture was obtained.

Acknowledgment. This research was sponsored by the Air Force Office of Scientific Research, Air Force Systems Command, USAF, under Contract No. F49620-83-C-0044, and by a grant from the 3M Co. The United States Government is authorized to reproduce and distribute reprints for governmental purposes notwithstanding any copyright notation thereon. We thank Professor J. R. Damewood, Jr., for helpful suggestions and comments.

Conformational Analysis of Branched Cyclosilanes

Thomas A. Blinka and Robert West*

Department of Chemistry, University of Wisconsin, Madison, Wisconsin 53706

Received May 16, 1985

Conformational analyses of a number of branched cyclopentasilanes and cyclohexasilanes were performed by using the empirical force field method. In comparisons of structurally similar isomers, the thermodynamically preferred isomer was usually calculated to have significantly lower steric energy. Steric energies and equilibrium constants were used to estimate relative σ-conjugation stabilizations. The magnitude of the structural distortions in the cyclopentasilane rings were dependent on the extent of trimethylsilyl substitution.

Introduction

Although conformational analysis has become a powerful tool in organic chemistry,[1] conformational principles in organosilicon chemistry are only starting to be elucidated. Conformational analyses of silanes have been limited mainly to linear molecules and symmetrically substituted rings[2,3] for which experimental structure data is available.

In the preceding paper[4] the synthesis of several branched, trimethylsilyl-substituted cyclopentasilanes and cyclohexasilanes, obtained by rearrangement of unbranched permethylcyclosilane rings, is described. The experimental results raised many questions concerning conformation, steric strain, and σ-delocalization,[5] which prompted the present study. In this paper we report calculations of steric energies (ΔH_{steric}) and structures of cyclosilanes **1-12**, using the empirical force field method.[6]

Calculational Methods and Notation

The calculations were performed by using the program MM2[7] and the full relaxation method.[8] The force field parameters used were developed previously for polysilane calculations[9] and satisfactorily reproduce electron diffraction and X-ray structure for cyclosilanes **1**[10] and **2**,[11] as well as for the branched highly strained molecule $(Me_3Si)_4Si$.[12] Input structures for the calculation of conformations for poly(trimethylsilyl)cyclopentasilanes

(1) See: Eliel, E. L.; Allinger, N. L.; Angyal, S. J.; Morrison, G. A. "Conformational Analysis"; American Chemical Society: Washington, D.C., 1981.

(2) (a) Hummel, J. P.; Stackhouse, J.; Mislow, K. *Tetrahedron* **1977**, *33*, 1925. (b) Honig, H.; Hassler, K. *Monatsh. Chem.* **1982**, *113*, 129.

(3) Shafiee, F.; Damewood, Jr., J. R.; Haller, K. J.; West, R. *J. Am. Chem. Soc.* **1985**, *107*, 0000.

(4) Blinka, T. A.; West, R. *Organometallics*, preceding paper in this issue.

(5) (a) Dewar, M. J. S. *J. Am. Chem. Soc.* **1984**, *106*, 669. (b) Hoffman, R. *Acc. Chem. Res.* **1971**, *4*, 1. (c) Pitt, C. G. In "Homoatomic Rings, Chains and Macromolecules of Main Group Elements"; Rheingold, A. L., Ed.; Elsevier: New York, 1977; Chapter 8.

(6) For reviews of the EFF method, see: (a) Williams, J. D.; Stang, P. J.; Schleyer, P. v. R. *Annu. Rev. Phys. Chem.* **1968**, *19*, 531. (b) Engler, E. M.; Andose, J. D.; Schleyer, P. v. R. *J. Am. Chem. Soc.* **1973**, *95*, 8005. (c) Kitaigorodsky, A. I. *Chem. Soc. Rev.* **1978**, *7*, 133. (d) Mislow, K.; Doughtery, D. A.; Hoonshell, W. D. *Bull. Soc. Chim. Belg.* **1978**, *87*, 555. (e) Burkert, V.; Allinger, N. L. "Molecular Mechanics"; American Chemical Society, Washington, D.C., 1981.

(7) Allinger, N. L. *QCPE* **1981**, *13*, 395, adapted for use with a Harris/7 computer by Prof. H. Whitlock.

(8) The bond lengths, bond angles, and torsion angles are adjusted to the minimum energy values for each conformation.

(9) Damewood, J. R., Jr.; West, R. *Macromolecules* **1985**, *18* (2), 158.

(10) Smith, Z.; Seip, H. M.; Hengge, E.; Bauer, G. *Acta Chem. Scand., Ser. A* **1976**, *A30*, 697.

(11) Carrell, H. L.; Donohue, J. *Acta Crystallogr., Sect. B* **1972**, *B28*, 1566.

(12) Bartell, C. S.; Clippard, F. B., Jr.; Boates, T. L. *Inorg. Chem.* **1970**, *9*, 2436.

0276-7333/86/2305-0133$01.50/0

Table I. Structural Parameters for Decamethylcyclopentasilane (1), Cyclopentasilane, and Dodecamethylcyclohexasilane (2) (See Figure 2 for Numbering System)

	torsion angles, deg			internal angles, deg			bond lengths, pm			
structure	θ_{12}	θ_{23}	θ_{34}	ϕ_1	ϕ_2	ϕ_3	L_{12}	L_{23}	L_{34}	ref
1 (*TE*)	12.4	32.5	40.2	106.7	105.3	103.4	234.6	234.2	234.1	MM2, this paper
1 (*E*)	38.4	23.7	0.0	103.3	103.9	106.4	234.1	234.4	234.7	MM2, this paper
cyclopentasilane (*TE*)	13.3	34.8	43.6							electron diffraction[9b]
cyclopentasilane (*E*)	41.5	25.3	0.0							electron diffraction[9b]
2 (chair)		52.9	(av)		112.1	(av)		234.5	(av)	MM2, this paper
2 (chair)		53.5	(av)		111.9	(av)		233.8	(av)	X-ray[13]

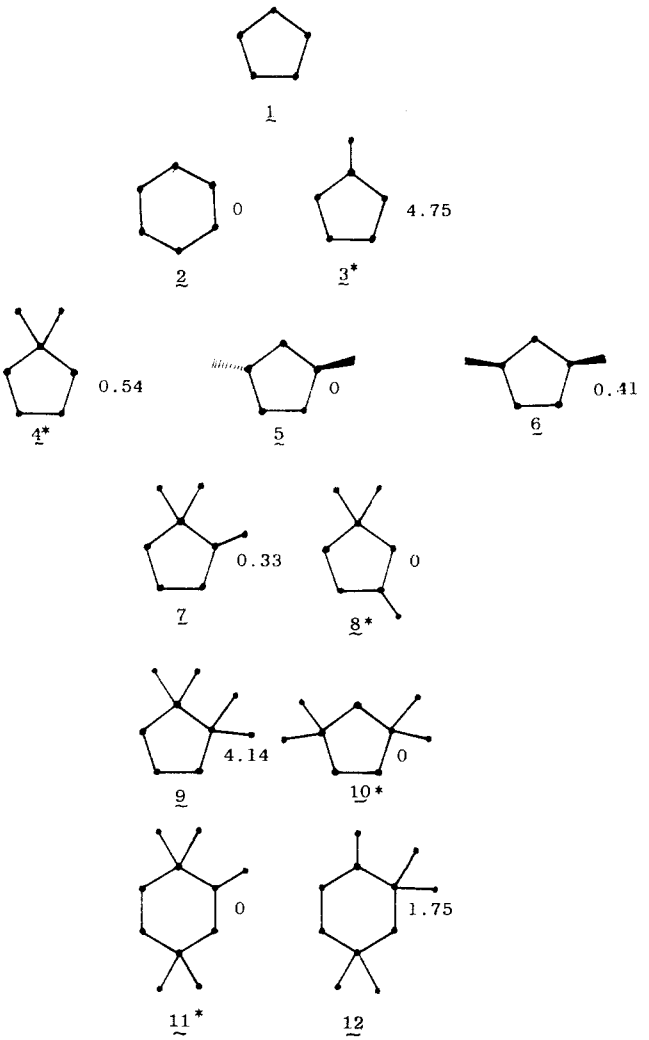

Figure 1. Cyclosilanes studied by MM2 and relative steric energies for isomeric compounds.

3–10 were derived from twist-envelope (*TE*) and envelope (*E*) conformations[2,13] (Figure 2) of decamethylcyclopentasilane, **1** (Table I). Input structures for the pentakis(trimethylsilyl)heptamethylcyclohexasilane calculations used the geometric parameters calculated for the chair conformations of **2**, with trimethylsilyl groups substituted for methyl at equatorial positions when possible.

The numbering systems for the *TE* and *E* conformations are shown in Figure 2. Conformers are designated by the position of trimethylsilyl substitution and the conformation of the ring. (For example 1ax-*E* refers to a conformer of **3** which has an envelope ring conformation and a trimethylsilyl group attached axially to silicon atom 1.) Torsion angles, bending angles, and silicon–silicon bond lengths for **1** and **2** are compared to the appropriate reference values in Table I. For all of the molecules, structural parameters such as bond lengths and bending angles involving carbon or hydrogen atoms are generally close to the strain-free values.[10] Average steric energies are

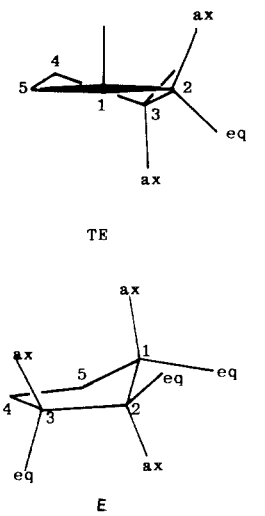

Figure 2. Twist-envelope (*TE*) and envelope (*E*) conformations of cyclopentasilanes.

weighted according to the relative Boltzmann populations of all conformers, except as noted.

Results and Discussion

Steric Energies. Figure 1 provides a general overview of the relative steric energies for isomeric cyclosilanes among **2–12**. The predominant isomer found in the equilibrium mixture is indicated by an asterisk.

As explained in the companion paper,[4] due to σ-conjugation[7] geminally branched structures are favored over 1,2- or 1,3-branching. For this reason **3** is more stable than **2**, even though, as seen from Table II, **3** is sterically destabilized by 4.75 kcal mol^{-1} compared to **2**. The magnitude of σ-conjugation stabilization of **3** cf. **2** can be estimated by formulating ΔH_f as the sum of three terms (eq 1).[14]

$$\Delta H_f = \Delta H_{bond} + \Delta H_{steric} + \Delta H_\sigma \quad (1)$$

Since at equilibrium the ratio of **3** to **2** is at least 99:1, we estimate ΔH_f to be at least 2.7 kcal mol^{-1} more negative for **3**.[15] Because **2** and **3** are isomers ΔH_{bond} is the same for both compounds. It follows that **3** is stabilized over **2** by at least 7.4 kcal mol^{-1} due to σ-conjugation.

Similarly in the $AlCl_3/FeCl_3$ catalyzed rearrangement of $(Me_2Si)_7$, **4** predominates at equilibrium, by >99:1 over all other isomers. Although the differences in ΔH_{steric} are small, **4** is also sterically destabilized compared to **5** and **6**. A lower limit for the electronic stabilization of **4** cf. **5** can be estimated as 3.2 kcal mol^{-1}.[16]

(13) *TE* and *E* correspond to the C_2 and C_2 conformations, respectively. See: Pitzer, K. S.; Donath, W. E. *J. Am. Chem. Soc.* **1956**, *78*, 3213; also ref 10.

(14) Allinger, N. L.; Tribble, M. T.; Miller, M. A.; Wertz, D. H. *J. Am. Chem. Soc.* **1971**, *93*, 1637.

(15) An equilibrium constant $K_{eq} > 99$ gives $\Delta G < -2.7$ kcal mol^{-1} at $T = 300$ K, assuming ΔS to be negligible.

(16) MM2 calculations were not done for the conformers of 1,2-bis(trimethylsilyl)cyclopentasilanes; these structures are, however, expected to be at least as strained as **5** or **6**.

Table II. Structural Data for conformers of (Trimethylsilyl)nonamethylcyclopentasilane (3)

	ring torsion angles, deg					internal ring angles, deg				
conformer	θ_{12}	θ_{23}	θ_{34}	θ_{45}	θ_{51}	ϕ_1	ϕ_2	ϕ_3	ϕ_4	ϕ_5
1-*TE*	12.6	33.5	41.7	34.1	13.3	106.2	105.6	102.7	103.7	105.2
2ax-*TE*	15.0	32.8	37.9	27.8	8.0	108.1	103.3	105.7	103.0	106.0
2eq-*TE*	7.9	28.0	37.7	32.8	15.4	107.0	104.9	104.3	103.7	106.2
3ax-*TE*	15.5	30.5	34.4	25.5	6.1	106.6	107.2	102.2	106.7	105.5
3eq-*TE*	10.7	30.7	39.4	32.4	13.4	106.9	105.6	103.7	103.7	105.3
1ax-*E*	33.4	21.4	0.4	20.7	33.1	102.1	106.9	106.0	106.3	106.8
1eq-*E*	30.6	19.9	3.7	25.9	38.3	103.6	103.9	106.3	106.7	104.5
2ax-*E*	34.2	18.9	3.0	23.8	36.4	106.0	102.8	108.1	106.5	103.3
2eq-*E*	36.3	19.6	4.5	26.8	39.2	104.0	103.9	106.9	106.3	103.4
3ax-*E*	39.3	22.8	2.1	26.1	40.0	103.0	10.4	105.4	107.0	103.1
3eq-*E*	39.3	25.2	1.5	22.7	38.3	103.1	103.9	106.1	106.5	104.1

	bond lengths, pm						
conformer	L_{12}	L_{23}	L_{34}	L_{45}	L_{51}	L_{exo}(av)	ΔH_{steric}, kcal/mol
1-*TE*	234.9	234.1	234.0	234.0	234.9	234.6	−14.4914
2ax-*TE*	234.9	234.4	234.1	234.0	234.7	234.9	−14.1558
2eq-*TE*	234.8	234.4	234.3	234.3	234.7	234.9	−14.5628
3ax-*TE*	234.5	234.5	234.4	234.4	234.4	234.6	−14.3617
3eq-*TE*	234.6	234.2	234.1	234.1	234.5	234.4	−14.6342
1ax-*E*	234.5	234.4	234.4	234.5	234.4	234.7	−14.3949
1eq-*E*	234.1	234.3	234.6	234.4	234.1	234.4	−14.6536
2ax-*E*	234.3	234.8	234.7	234.1	234.2	234.8	−14.1182
2eq-*E*	234.3	234.8	234.8	234.5	234.3	234.5	−14.5696
3ax-*E*	234.0	234.7	235.2	234.3	233.9	234.9	−14.3981
3eq-*E*	234.0	234.4	234.9	234.4	234.0	234.5	−14.6012

In the isomer pairs **7–8** and **9–10** the branching multiplicities are similar so that large differences in σ-delocalization energy are not expected. Accordingly, the sterically more stable isomers **8** and **10** are the ones formed in the rearrangement reactions. However, the rather small difference in ΔH_{steric} for **7** and **8** is insufficient to account for the fact that **8** is the preponderant (>95%) product; **8** may also be stabilized relative to **7** by electronic factors. Finally in isomer pair **11–12**, the identity of the isomer mainly formed in the rearrangement could not be decisively determined from spectral data. The calculated steric energies suggest that the more stable isomer is **11**, in agreement with the tentative assignment from ^{29}Si NMR spectra.[4]

In summary, it appears that among isomeric cyclosilanes with similar numbers and kinds of branching (**7–8**, **9–10**, and **11–12**), the isomer with lower steric energy is the one predominating at equilibrium. However when the number or kind of branches differs (**2–3** and **4–5**), electronic effects due to σ-conjugation may outweigh differences in steric energy.

Dodecamethylcyclohexasilane (2) and (Trimethylsilyl)nonamethylcyclopentasilane (3). Selected structural data and ΔH_{steric} for the *TE* and *E* conformers of **3** are listed in Table II. The conformers of **3** are nearly isoenergetic, as expected because the *TE* and *E* conformations of **1** differ by only 0.05 kcal mol^{-1}. Also, the long silicon–silicon bond lengths and small force constants[6e,9] allow the various conformers of **3** to avoid significant destabilizing steric interactions. The relationship between relative steric energy and the position of trimethylsilyl substitution in *TE* conformers of **3** is similar to that calculated for *TE* conformers of methylcyclopentane[17] (Table III), although the magnitudes of the relative energies are much smaller for **3**.

The ring torsion angles of the conformers of **3** (Table II) differed by only a few degrees from the corresponding angles in **1** (Table I). The largest deviations occurred in conformers in which the trimethylsilyl group was axial.

Table III. Relative Steric Angles of *TE* Conformers (kcal/mol) of 3 Compared to Methylcyclopentane (kcal/mol)

conformer	3	methylcyclopentane
1	0.14	0.72
2ax	0.42	1.47
2eq	0.07	0.34
2ax	0.27	0.91
3eq	0.00	0.00

The 3ax-*E* conformation is particularly distorted and is not far different from the 1ax-*E* conformation. The internal angles of the rings are also similar to those found in **1**. Internal angles having an axial trimethylsilyl group at the vertex are compressed slightly (about 1°), and silicon–silicon bonds flanking the branch points are slightly stretched (0.2–0.3 pm).

Bis(trimethylsilyl)octamethylcyclopentasilanes (4–6). Selected structural parameters and steric energies for conformers of **4–6** are listed in Tables IV–VI. Input structures for several conformers, especially those expected to have high ΔH_{steric}, did not relax to the appropriate conformations.[18]

With the exception of the 1,1-*TE* conformer (Table IV), the cyclopentasilane rings of **4–6** were slightly flatter than **1**. As observed for **3**, internal ring angles with trimethylsilyl groups attached at the vertex were slightly smaller than the corresponding angles in **1** (Table I), and silicon–silicon bonds flanking the branch point were stretched 0.2–0.7 pm. Internal ring angles with neighboring axial trimethylsilyl substituents (for example, conformer 2ax,4ax-*E*, θ_2 and θ_3, Table V) expanded several degrees relative to the corresponding angles in **1**. Such distortions in ring torsion angles, internal ring angles, and bond lengths were particularly acute for conformers of **4** (Table IV).

Tris(trimethylsilyl)heptamethylcyclopentasilanes (7 and 8). Because of the large number of possible conformations of **7** and **8** (twenty for each isomer), the com-

(17) Allinger, N. L.; Hirsch, J. A.; Miller, M. A.; Tyminski, I. J.; Van Catledge, G. A. *J. Am. Chem. Soc.* **1968**, *90*, 1199.

(18) For each of these conformers, a variety of slightly different input structures were employed, but in each case the input structure relaxed to a different conformation.

Table IV. Structural Parameters for Conformers of 1,1-Bis(trimethylsilyl)octamethylcyclopentasilane (4)

	ring torsion angles, deg					internal ring angles, deg					
conformer	θ_{12}	θ_{23}	θ_{34}	θ_{45}	θ_{51}	ϕ_1	ϕ_2	ϕ_3	ϕ_4	ϕ_5	$\phi_{exo,exo}$[a]
1,1-*TE*	14.2	35.9	43.3	35.1	12.9	104.8	105.9	102.3	102.3	106.0	110.6
2,2-*TE*	11.4	28.8	36.8	29.6	10.8	108.7	102.5	107.5	102.2	106.3	108.5
3,3-*TE*									no minimum found		
1,1-*E*	32.1	22.7	3.4	16.9	29.7	101.2	108.3	105.3	106.6	108.2	108.7
2,2-*E*									no minimum found		
3,3-*E*	39.3	21.8	4.0	28.1	40.9	102.1	105.8	103.9	107.5	103.0	109.2

	bond lengths, pm						ΔH_{steric}, kcal/mol
conformer	L_{12}	L_{23}	L_{34}	L_{45}	L_{51}	L_{exo}(av)	
1,1-*TE*	236.0	234.0	234.0	234.0	236.0	235.7	−18.9828
2,2-*TE*	235.7	235.1	234.3	233.9	234.8	235.6	−18.8849
3,3-*TE*				no minimum found			
1,1-*E*	234.9	234.5	234.2	234.7	235.2	235.4	−19.2271
2,2-*E*				no minimum found			
3,3-*E*	234.1	235.6	236.3	234.3	233.9	235.8	−18.7239

[a] Me_3Si–Si–$SiMe_3$ angle.

Table V. Structural Parameters for Conformers of *trans*-1,3-Bis(trimethylsilyl)octamethylcyclopentasilane (5)

	ring torsion angles, deg					internal ring angles, deg				
conformer	θ_{12}	θ_{23}	θ_{34}	θ_{45}	θ_{51}	ϕ_1	ϕ_2	ϕ_3	ϕ_4	ϕ_5
1,3ax-*TE*					no minimum found					
1,3eq-*TE*	12.8	32.9	40.5	32.8	12.4	106.4	105.5	103.1	103.4	105.4
2ax,4eq-*TE*					no minimum found					
2eq,4ax-*TE*	7.5	27.0	35.3	30.3	14.5	106.8	105.0	106.7	102.0	107.3
2ax,5ax-*TE*	12.6	31.1	38.5	29.8	10.6	108.9	103.7	104.8	104.5	104.1
2ax,5ax-*TE*	12.6	31.1	38.5	29.8	10.6	108.9	103.7	104.7	104.5	104.1
2eq,5eq-*TE*	8.5	29.4	39.1	33.9	15.7	106.7	105.9	103.6	103.5	105.1
1ax,3eq-*E*	33.3	20.4	1.0	22.2	33.9	101.8	107.3	105.7	106.2	106.8
1eq,3ax-*E*	37.2	22.8	0.3	23.2	36.9	103.0	105.4	105.2	107.3	104.3
2ax,4ax-*E*	36.0	23.0	1.7	20.5	35.8	105.9	101.9	108.7	105.7	104.1
2eq,4eq-*E*	38.9	25.4	2.2	21.8	37.5	103.3	103.9	106.2	106.5	104.3
3ax,5eq-*E*	33.0	16.4	6.0	26.0	37.0	105.8	103.2	108.2	106.2	103.3

	bond lengths, pm						ΔH_{steric}, kcal/mol
conformer	L_{12}	L_{23}	L_{34}	L_{45}	L_{51}	L_{exo}(av)	
1,3ax-*TE*				no minimum found			
1,3eq-*TE*	234.8	234.1	234.1	234.0	234.9	234.5	−19.6700
2ax,4eq-*TE*				no minimum found			
2eq,4ax-*TE*	234.5	234.4	234.4	234.4	234.5	234.6	−19.3314
2ax,5ax-*TE*	235.4	234.4	234.1	234.5	235.5	235.3	−18.8608
2eq,5eq-*TE*	234.7	234.2	234.1	234.1	234.5	234.4	−19.8401
1ax,3eq-*E*	234.5	234.6	234.6	234.4	234.3	234.7	−19.3251
1eq,3ax-*E*	234.4	235.0	235.3	234.4	234.2	235.0	−19.4405
2ax,4ax-*E*	234.1	234.7	235.3	234.5	234.1	234.8	−18.9173
2eq,4eq-*E*	234.1	234.3	234.9	234.5	234.1	234.4	−19.7299
2ax,5eq-*E*	234.4	234.8	234.7	234.0	234.2	234.7	−19.2173

putations were restricted to representative *TE* and *E* conformations that were expected (by inspection of molecular models) to define the high- and low-energy extremes of the steric energies of **7** and **8**. The steric energies of each conformer calculated were weighted by their relative Boltzmann populations as before, but since all of the conformations for each isomer were not calculated, the average energy obtained is only approximate.

The cyclopentasilane rings of **7** and **8** were usually slightly flatter, and the average internal ring angles were correspondingly larger than for **1**. Internal ring angles having two trimethylsilyl groups at the vertex were compressed 0.4–3.0°, while internal angles with neighboring geminal branch points expanded by as much as 4.3° (Tables VII and VIII). The silicon–silicon bond lengths in conformers of **7** average about 0.5 pm longer than those of **8**. Conformers having two axial trimethylsilyl groups, or nearly eclipsing trimethylsilyl groups, had the largest ΔH_{steric}.

Tetrakis(trimethylsilyl)hexamethylcyclopentasilanes (9 and 10). Structural and steric energy data for the calculated conformers of **9** and **10** are listed in Tables IX and X. Minimum energy structures for four conformations could not be obtained; the appropriate input structures consistently relaxed to other conformations.[14]

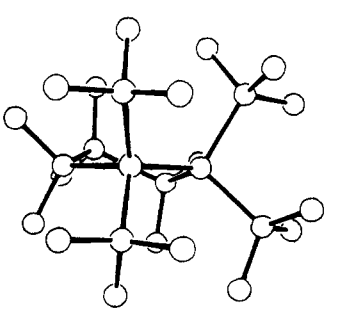

Figure 3. 1,1,2,2-*TE* conformer of **9**, illustrating deformations induced by interactions between trimethylsilyl groups (H atoms not shown).

The average steric energies for **9** and **10** are −24.21 and −28.07 kcal mol^{-1}, respectively. The higher steric energy

Table VI. Structural Parameters for Conformers of *cis*-1,3-Bis(trimethylsilyl)octamethylcyclopentasilane (6)

	ring torsion angles, deg					internal ring angles, deg				
conformer	θ_{12}	θ_{23}	θ_{34}	θ_{45}	θ_{51}	ϕ_1	ϕ_2	ϕ_3	ϕ_4	ϕ_5
1,3ax-*TE*	9.5	27.1	34.8	29.7	12.2	106.1	108.1	102.3	106.3	105.3
1,3eq-*TE*	8.0	29.9	40.4	35.7	17.1	106.1	106.3	102.9	103.5	104.8
2ax,4ax-*TE*	no minimum found									
2eq,4eq-*TE*	11.7	28.1	33.6	26.2	9.0	107.2	105.6	105.3	104.3	106.7
2ax,5eq-*TE*	13.4	30.6	36.3	27.5	8.7	107.9	104.5	105.1	104.3	105.6
2ax,5eq-*TE*	no minimum found									
1eq,3eq-*E*	35.4	19.1	4.6	26.5	38.1	103.1	105.3	106.2	106.4	104.2
2ax,4eq-*E*	34.7	21.2	0.2	21.0	35.0	106.0	102.7	108.2	106.3	104.0
2eq,4ax-*E*	37.4	22.8	0.6	23.9	38.3	103.4	103.8	107.3	105.3	104.7
3ax,5ax-*E*	no minimum found									
2eq,5eq-*E*	31.2	17.8	2.3	21.5	32.6	105.3	105.0	107.2	107.0	104.7

	bond lengths, pm						ΔH_{steric},
conformer	L_{12}	L_{23}	L_{34}	L_{45}	L_{51}	L_{exo}(av)	kcal/mol
1,3ax-*TE*	234.9	234.5	234.3	234.3	234.8	234.7	−19.3015
1,3eq-*TE*	235.0	234.2	234.0	234.0	234.8	234.6	−19.6068
2ax,4ax-*TE*	no minimum found						
2eq,4eq-*TE*	234.8	234.6	234.4	234.4	234.5	234.9	−19.4759
2ax,5eq-*TE*	235.3	234.6	234.1	234.3	235.0	235.0	−19.3677
1ax,3ax-*E*	no minimum found						
1eq,3eq-*E*	234.3	234.9	235.1	234.3	234.3	234.8	−19.5956
2a,4eq-*E*	234.3	234.7	235.0	234.2	234.2	234.7	−19.3673
2eq,4ax-*E*	234.0	234.4	235.2	234.7	234.0	234.7	−19.4869
2ax,5ax-*E*	no minimum found						
2eq,5eq-*E*	234.6	234.7	234.5	234.5	234.4	234.9	−19.481

Table VII. Structural Parameters for Conformers of 1,1,2-Tris(trimethylsilyl)heptamethylcyclopentasilane (7)

	ring torsion angles, deg							internal ring angles, deg					
conformer	θ_{12}	θ_{23}	θ_{34}	θ_{45}	θ_{51}	θ_{exo}[a]	θ_{exo}[b]	ϕ_1	ϕ_2	ϕ_3	ϕ_4	ϕ_5	ϕ_{gem}[c]
1,1,3ax-*TE*	13.5	35.2	43.0	34.5	13.1	8.0	129.3	105.2	104.5	103.9	101.7	106.5	107.0
1,1,2eq-*TE*	14.4	13.7	42.6	34.1	12.3	26.4	96.2	104.7	105.6	103.0	103.0	106.7	109.0
2eq,3,3-*TE*	15.4	29.5	33.7	25.3	5.7	39.4	87.0	106.9	108.3	100.4	108.6	104.6	108.0
1,1,2ax-*E*	30.6	19.6	0.1	20.0	31.5	23.3	143.7	102.0	106.0	108.0	105.1	108.6	105.6
1,1,2eq-*E*	30.7	20.1	0.7	19.1	30.5	40.6	81.2	101.7	107.5	106.6	105.9	108.2	108.4
1ax,2,2-*E*	31.2	17.8	2.2	21.7	33.2	30.4	150.2	105.4	103.5	108.6	106.3	105.1	106.5

	bond lengths, pm						
conformer	L_{12}	L_{23}	L_{34}	L_{45}	L_{51}	L_{exo}(av)	ΔH_{steric} kcal/mol
1,1,2ax-*TE*	237.7	234.7	233.6	233.8	236.3	236.1	−21.1300
1,1,2eq-*TE*	236.6	234.2	234.1	233.9	236.1	235.5	−23.4698
2eq,3,3-*TE*	234.9	236.0	235.2	234.3	234.0	235.4	−23.6149
1,1,2ax-*E*	237.6	236.1	234.0	234.2	235.7	236.5	−18.2872
1,1,2eq-*E*	235.8	234.8	234.0	234.4	235.5	235.5	−23.9110
1ax,2,2-*E*	236.8	235.5	234.4	234.0	235.3	236.0	−21.8262

[a] Me_3Si–Si–Si–$SiMe_3$, cis. [b] Me_3Si–Si–Si–$SiMe_3$, trans. [c] Me_3Si–Si–$SiMe_3$.

Table VIII. Structural Parameters for Conformers of 1,1,3-Tris(trimethylsilyl)heptamethylcyclopentasilane (8)

	ring torsion angles, deg					bond angles, deg					
conformer	θ_{12}	θ_{23}	θ_{34}	θ_{45}	θ_{51}	ϕ_1	ϕ_2	ϕ_3	ϕ_4	ϕ_5	ϕ_{gem}[a]
1,1,3ax-*TE*	6.7	26.5	36.1	33.5	16.1	103.8	109.7	101.5	105.5	106.2	109.1
1,1,3eq-*TE*	13.8	35.5	43.3	35.4	13.4	104.8	106.1	102.0	102.6	105.8	110.1
1ax,3,3-*TE*	6.5	23.5	32.6	29.4	13.6	106.7	109.0	101.5	108.1	104.3	108.6
1eq,3,3-*TE*	6.0	23.4	32.9	30.1	14.2	106.5	109.3	101.0	108.5	104.0	108.5
2,2,5eq-*TE*	12.6	29.9	35.6	26.5	8.8	108.8	102.5	107.6	102.7	106.5	108.6
1,1,3eq-*E*	32.2	22.7	3.1	17.3	29.8	100.7	108.9	104.7	106.8	108.3	107.9
2,2,5eq-*E*	30.9	19.7	2.0	16.8	30.3	108.6	101.7	109.1	107.3	103.5	108.1
2ax,4,4-*E*	33.1	18.4	3.4	24.1	36.4	104.6	103.3	109.5	103.7	105.9	108.8

	bond lengths, pm						
conformer	L_{12}	L_{23}	L_{34}	L_{45}	L_{51}	L_{exo}	ΔH_{steric}, kcal/mol
1,1,3ax-*TE*	236.3	234.7	234.1	234.5	235.6	235.6	−23.1834
1,1,3eq-*TE*	236.1	234.0	234.1	234.0	236.0	235.3	−24.1847
1ax,3,3-*TE*	235.1	235.2	234.8	234.4	234.3	235.2	−24.1035
1eq,3,3-*TE*	235.3	235.2	234.7	234.3	234.5	235.3	−23.7518
2,2,5eq-*TE*	235.6	235.0	234.3	233.9	234.9	235.2	−24.2217
1,1,3eq-*E*	235.0	234.7	234.4	234.7	235.1	235.2	−24.0384
2,2,5eq-*E*	235.1	235.3	234.8	234.1	234.5	235.3	−23.7955
2ax,4,4-*E*	234.2	235.0	236.1	235.2	234.2	235.6	−23.5005

[a] Me_3Si–Si–$SiMe_3$.

Table IX. Structural Parameters for Conformers 1,1,2,2-Tetrakis(trimethylsilyl)hexamethylcyclopentasilane (9)

	ring torsion angles, deg							internal ring angles, deg					
conformer	θ_{12}	θ_{23}	θ_{34}	θ_{45}	θ_{51}	θ_{exo}[a]	θ_{exo}[a]	ϕ_1	ϕ_2	ϕ_3	ϕ_4	ϕ_5	ϕ_{gem}(av)[b]
1,1,2,2-*TE*	11.0	31.8	39.8	31.8	13.2	15.4	10.7	106.2	102.8	107.2	101.2	107.5	104.2
2,2,3,3-*TE*	no minimum found												
3,3,4,4-*TE*	9.1	25.3	31.2	26.1	10.9	85.2	160.7	107.0	107.1	105.0	103.6	102.7	105.5
1,1,2,2-*E*	30.4	20.8	2.7	16.8	29.3	31.2	37.4	103.5	105.3	107.6	106.7	107.4	105.2
2,2,3,3-*E*	no minimum found												
3,3,4,4-*E*	36.9	23.5	0.6	22.4	36.0	10.9	3.6	100.9	108.3	103.8	105.4	107.3	100.9

	bond lengths, pm						ΔH_{steric},
conformer	L_{12}	L_{23}	L_{34}	L_{45}	L_{51}	L_{exo}(av)	kcal/mol
1,1,2,2-*TE*	240.2	235.5	233.8	233.6	236.6	236.9	−22.4961
2,2,3,3-*TE*	no minimum found						
3,3,4,4-*TE*	234.1	236.0	239.2	236.4	243.2	236.9	−24.1047
1,1,2,2-*E*	239.1	235.9	234.2	234.1	235.9	236.7	−24.3560
2,2,3,3-*E*	no minimum found						
3,3,4,4-*E*	234.2	236.6	241.5	237.3	233.8	238.2	−4.3528

[a] Me_3Si-Si-$SiMe_3$, cis. [b] Me_3Si—Si=$SiMe_3$.

Table X. Structural Parameters for 1,1,3,3-Tetrakis(trimethylsilyl)hexamethylcyclopentasilane (10)

	ring torsion angles, deg					internal ring angles, deg					
conformer	θ_{12}	θ_{23}	θ_{34}	θ_{45}	θ_{51}	ϕ_1	ϕ_2	ϕ_3	ϕ_4	ϕ_5	ϕ_{gem}(av)[a]
1,1,3,3-*TE*	7.8	25.8	34.5	31.6	14.0	103.7	111.1	99.8	107.7	105.7	107.9
2,2,4,4-*TE*	no minimum found										
2,2,5,5-*TE*	11.0	27.2	34.3	26.0	9.2	110.8	102.9	106.3	106.0	103.3	108.1
1,1,3,3-*E*	33.8	22.4	1.2	20.2	31.8	99.2	110.8	102.3	107.8	108.1	106.9
2,2,4,4-*E*	no minimum found										
2,2,5,5-*E*	35.0	15.9	61.9	26.2	39.2	111.6	97.1	110.8	108.5	97.5	106.9

	bond lengths, pm						ΔH_{steric},
conformer	L_{12}	L_{23}	L_{34}	L_{45}	L_{51}	L_{exo}(av)	kcal/mol
1,1,3,3-*TE*	236.7	235.6	234.5	234.4	235.6	236.0	−27.4941
2,2,4,4-*TE*	no minimum found						
2,2,5,5-*TE*	236.0	235.0	234.3	235.0	236.1	235.9	−28.2642
1,1,3,3-*E*	235.7	235.9	235.7	235.1	234.6	235.9	−26.0342
2,2,4,4-*E*	no minimum found						
2,2,5,5-*E*	239.4	236.7	235.3	235.4	238.1	238.7	9.9024

[a] Me_3Si-Si-$SiMe_3$.

Table XI. Structural Parameters for 1,1,2,4,4- and 1,2,2,4,4-Pentakis(trimethylsilyl)heptamethylcyclohexasilane (11 and 12) (See Figure 4 for Numbering Scheme)

	ring torsion angles,[a] deg								angles, deg						
compd	θ_{12}	θ_{23}	θ_{34}	θ_{45}	θ_{56}	θ_{61}	θ_{exo}[a]	θ_{exo}[b]	ϕ_1	ϕ_2	ϕ_3	ϕ_4	ϕ_5	ϕ_6	ϕ_{gem}(av)[c]
11	37.9	39.2	44.3	53.2	60.6	49.3	43.5	75.0	109.4	116.2	119.8	107.2	113.4	115.2	105.6
12	46.6	43.1	43.3	45.7	55.6	56.8	50.7	67.2	114.6	106.5	124.0	108.6	113.6	112.9	103.4

	bond lengths, pm							
compd	L_{12}	L_{23}	L_{34}	L_{45}	L_{56}	L_{61}	L_{exo}(av)	ΔH_{steric}, kcal/mol
11	237.7	237.3	235.6	235.1	234.4	236.5	236.6	−36.8383
12	237.4	237.7	237.7	234.9	234.6	235.2	236.9	−35.0879

[a] *cis*-Me_3Si-Si-Si-$SiMe_3$. [b] *trans*-Me_3Si-Si-Si-$SiMe_3$. [c] Me_3Si-Si-$SiMe_3$.

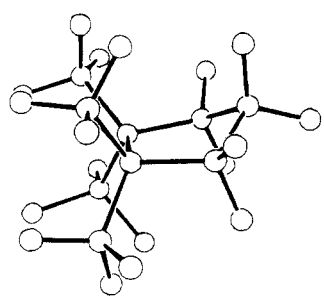

Figure 4. 3,3,4,4-*E* conformation of **9**, showing eclipsing trimethylsilyl groups (H atoms not shown).

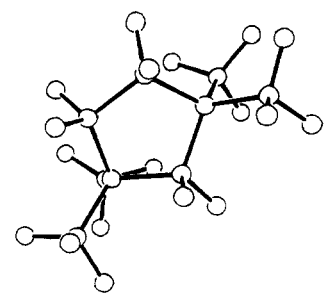

Figure 5. The 2,2,5,5-*E* conformation of **10**, showing distorted internal ring angles (H atoms not shown).

in **9** is primarily due to the long silicon–silicon bond lengths (average 236.0 pm), compressed Me_3Si-Si-$SiMe_3$ angles, and other distortions caused by interactions between vicinal trimethylsilyl groups (Figure 3). Conformers of **9** were more puckered than those of **10**, thus minimizing eclipsing interactions between trimethylsilyl groups. The

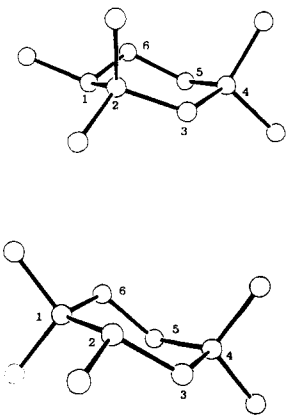

Figure 6. Calculated structures of **11** (above) and **12** (below), showing numbering system (C and H atoms not shown).

highest steric energies were obtained for conformations containing eclipsed trimethylsilyl groups (Figure 4).

The conformers of **10** exhibited a wide variation in internal ring angles (97–111.6°) and contained the most flattened cyclopentasilane rings observed in this study. The 2,2,5,5-*E* conformation (Table X) exhibits extreme variations in internal ring angles (Figure 5) and long silicon–silicon bond lengths (average 237.3 pm).

Pentakis(trimethylsilyl)heptamethylcyclohexasilanes (11 and 12). Compounds **11** and **12** were assumed to have chair ground-state conformations[2a] with maximum equatorial substitution by trimethylsilyl groups (Figure 6). The structure data and steric energies for **11** and **12** are listed in Table XI.

Compound **11** is calculated to be 1.75 kcal mol^{-1} lower in steric energy than **12**, thus supporting the assignment of **11** as the product obtained in the catalyzed rearrangement of $(Me_2Si)_{11}$.[4] The difference in steric energy arises primarily from the 1,3-diaxial interaction in **12**, which forced **12** to flatten between the two geminal bis(trimethylsilyl) branch points (θ_{23}, θ_{34}, Table XI) and expanded the internal ring angle between the branch points (θ_3, Table XI) to 124°. The silicon–silicon bond lengths are also quite long (average 2.362 Å), a consequence of accommodating five trimethylsilyl groups around the ring.

Acknowledgment. This research was sponsored by the Air Force Office of Scientific Research, Air Force Systems Command, USAF, under Contract No. F49620-83-C-0044, and by a grant from the 3M Co. The United States Government is authorized to reproduce and distribute reprints for governmental purposes notwithstanding any copyright notation thereon. We thank Professor J. R. Damewood, Jr., for helpful suggestions and comments.

Registry No. **1**, 13452-92-1; **2**, 4098-30-0; **3**, 23118-85-6; **4**, 79769-58-7; **5**, 99148-07-9; **6**, 99165-15-8; **7**, 99148-08-0; **8**, 99148-09-1; **9**, 99148-10-4; **10**, 99148-11-5; **11**, 99148-12-6; **12**, 99148-13-7; cyclopentasilane, 289-22-5.

Electron Counting in Square-Pyramidal Organo-Transition-Metal Carbides: Can a Carbon Atom Be a Vertex of a Closo Octahedral M_5C Cluster

Jean-François Halet,[†] Jean-Yves Saillard,*[†] Roland Lissillour,[†] Michael J. McGlinchey,[‡] and Gérard Jaouen[§]

Laboratoires de Chimie du Solide et Inorganique Moléculaire, LA 254, ERA 477, Université de Rennes 1, 35042 Rennes Cedex, France, Department of Chemistry, McMaster University, Hamilton, Ontario L8S 4M1, Canada, and Ecole Nationale Supérieure de Chimie, 75231 Paris Cedex 05, France

Received April 12, 1985

By use of molecular orbital calculations and the polyhedral skeletal electron pair approach, different electron counts for square-pyramidal transition-metal carbides are analyzed. Two situations are considered: either the main-group atom is situated in the center of a polyhedron and allocates all its valence electrons to the cluster bonding, as in $Fe_5(CO)_{15}C$, or it occupies a vertex of the polyhedron as in $Os_5(CO)_{15}(\mu_4\text{-}S)$. In the latter case, the main-group element retains a nonbonding lone pair which is not included in the skeleton electron count. Intermediate cases between these two extremes are described. The discussion is also extended to related species, viz., butterfly M_4C, tetrahedral M_3C, and mixed M_3C_2C clusters.

M_5C Clusters

To our knowledge, no square-pyramidal transition-metal clusters of type **1** have yet been isolated. According to the polyhedral skeletal electron pair (PSEP) theory,[1] these nido clusters, which are organometallic analogues of the borane B_5H_9,[2] should be stable for seven skeletal electron pairs (SEP) as in the hypothetical cluster $FeCo_4(CO)_{15}$. However, many square-pyramidal compounds M_5E, where E can be a carbon or a nitrogen atom, have been characterized.[3] These clusters, of which a typical example is the

[†] Université de Rennes 1.
[‡] McMaster University.
[§] Ecole Nationale Supérieure de Chimie.

(1) (a) Wade, K. *Adv. Inorg. Chem. Radiochem.* **1976**, *18*, 1. (b) Wade, K. In "Transition Metal Clusters"; Johnson, B. F. G., Ed.; Wiley-Interscience: New York, 1980; p 193. (c) Mingos, D. M. P. *Nature Phys. Sci. (London)* **1972**, *236*, 99. (d) Mingos, D. M. P. *Acc. Chem. Res.* **1984**, *17*, 311.
(2) Williams, R. E. *Adv. Inorg. Chem. Radiochem.* **1976**, *18*, 67.

0276-7333/86/2305-0139$01.50/0

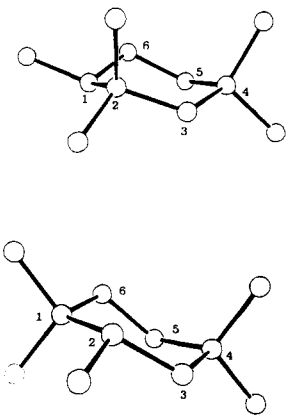

Figure 6. Calculated structures of **11** (above) and **12** (below), showing numbering system (C and H atoms not shown).

highest steric energies were obtained for conformations containing eclipsed trimethylsilyl groups (Figure 4).

The conformers of **10** exhibited a wide variation in internal ring angles (97–111.6°) and contained the most flattened cyclopentasilane rings observed in this study. The 2,2,5,5-*E* conformation (Table X) exhibits extreme variations in internal ring angles (Figure 5) and long silicon–silicon bond lengths (average 237.3 pm).

Pentakis(trimethylsilyl)heptamethylcyclohexasilanes (11 and 12). Compounds **11** and **12** were assumed to have chair ground-state conformations[2a] with maximum equatorial substitution by trimethylsilyl groups (Figure 6). The structure data and steric energies for **11** and **12** are listed in Table XI.

Compound **11** is calculated to be 1.75 kcal mol^{-1} lower in steric energy than **12**, thus supporting the assignment of **11** as the product obtained in the catalyzed rearrangement of $(Me_2Si)_{11}$.[4] The difference in steric energy arises primarily from the 1,3-diaxial interaction in **12**, which forced **12** to flatten between the two geminal bis(trimethylsilyl) branch points (θ_{23}, θ_{34}, Table XI) and expanded the internal ring angle between the branch points (θ_3, Table XI) to 124°. The silicon–silicon bond lengths are also quite long (average 2.362 Å), a consequence of accommodating five trimethylsilyl groups around the ring.

Acknowledgment. This research was sponsored by the Air Force Office of Scientific Research, Air Force Systems Command, USAF, under Contract No. F49620-83-C-0044, and by a grant from the 3M Co. The United States Government is authorized to reproduce and distribute reprints for governmental purposes notwithstanding any copyright notation thereon. We thank Professor J. R. Damewood, Jr., for helpful suggestions and comments.

Registry No. **1**, 13452-92-1; **2**, 4098-30-0; **3**, 23118-85-6; **4**, 79769-58-7; **5**, 99148-07-9; **6**, 99165-15-8; **7**, 99148-08-0; **8**, 99148-09-1; **9**, 99148-10-4; **10**, 99148-11-5; **11**, 99148-12-6; **12**, 99148-13-7; cyclopentasilane, 289-22-5.

Electron Counting in Square-Pyramidal Organo-Transition-Metal Carbides: Can a Carbon Atom Be a Vertex of a Closo Octahedral M_5C Cluster

Jean-François Halet,[†] Jean-Yves Saillard,*[†] Roland Lissillour,[†] Michael J. McGlinchey,[‡] and Gérard Jaouen[§]

Laboratoires de Chimie du Solide et Inorganique Moléculaire, LA 254, ERA 477, Université de Rennes 1, 35042 Rennes Cedex, France, Department of Chemistry, McMaster University, Hamilton, Ontario L8S 4M1, Canada, and Ecole Nationale Supérieure de Chimie, 75231 Paris Cedex 05, France

Received April 12, 1985

By use of molecular orbital calculations and the polyhedral skeletal electron pair approach, different electron counts for square-pyramidal transition-metal carbides are analyzed. Two situations are considered: either the main-group atom is situated in the center of a polyhedron and allocates all its valence electrons to the cluster bonding, as in $Fe_5(CO)_{15}C$, or it occupies a vertex of the polyhedron as in $Os_5(CO)_{15}(\mu_4\text{-}S)$. In the latter case, the main-group element retains a nonbonding lone pair which is not included in the skeleton electron count. Intermediate cases between these two extremes are described. The discussion is also extended to related species, viz., butterfly M_4C, tetrahedral M_3C, and mixed M_3C_2C clusters.

M_5C Clusters

To our knowledge, no square-pyramidal transition-metal clusters of type **1** have yet been isolated. According to the polyhedral skeletal electron pair (PSEP) theory,[1] these nido clusters, which are organometallic analogues of the borane B_5H_9,[2] should be stable for seven skeletal electron pairs (SEP) as in the hypothetical cluster $FeCo_4(CO)_{15}$. However, many square-pyramidal compounds M_5E, where E can be a carbon or a nitrogen atom, have been characterized.[3] These clusters, of which a typical example is the

[†] Université de Rennes 1.
[‡] McMaster University.
[§] Ecole Nationale Supérieure de Chimie.

(1) (a) Wade, K. *Adv. Inorg. Chem. Radiochem.* **1976**, *18*, 1. (b) Wade, K. In "Transition Metal Clusters"; Johnson, B. F. G., Ed.; Wiley-Interscience: New York, 1980; p 193. (c) Mingos, D. M. P. *Nature Phys. Sci. (London)* **1972**, *236*, 99. (d) Mingos, D. M. P. *Acc. Chem. Res.* **1984**, *17*, 311.
(2) Williams, R. E. *Adv. Inorg. Chem. Radiochem.* **1976**, *18*, 67.

0276-7333/86/2305-0139$01.50/0

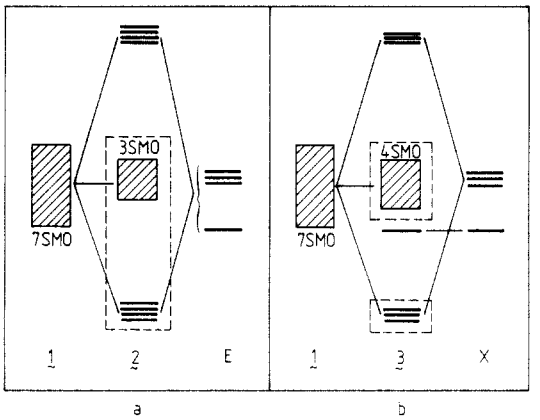

Figure 1. Simplified orbital scheme for the interaction of a carbon with a square-pyramidal M_5 framework: (a) C in the square face; (b) C as a vertex of the polyhedron.

well-known compound $Fe_5(CO)_{15}C$ (**2**),[4] have the exposed atom, C or N, situated in the middle (or very close to the middle) of the square face.

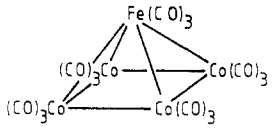

1

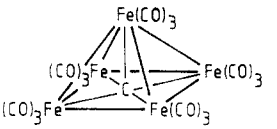

2

As the carbon atom is not a vertex of the polyhedron on which the cluster is based, all its electrons are included in the seven SEP count of structure **2** and implies that all the carbon orbitals are involved in the skeletal bonding. The simplified MO diagram in Figure 1a shows the relationship between the seven bonding skeletal molecular orbitals (SMO's) of **1** and **2**. As a consequence of this total involvement of the carbon valence orbitals in the formation of strongly bonding and antibonding molecular orbitals, it follows that (a) the carbon atom exhibits rather low reactivity[5] and (b) the introduction of a C^{4+} nucleus into a seven-SEP cluster of type **1** leads to a stabilization of some SEP's and an increase in the HOMO–LUMO gap. Thus, seven-SEP clusters of type **2** are expected to be thermodynamically more stable and kinetically more inert than seven-SEP molecules of type **1**. Such reasoning may explain why complexes such as **2** are isolable while no examples of type **1** are currently extant.[6]

On the basis of PSEP theory, octahedral clusters such as **3** are expected to be stable for seven SEP's. Here X represents a fragment having a set of frontier orbitals similar to an ML_3 or a B–H group (i.e., two π orbitals and

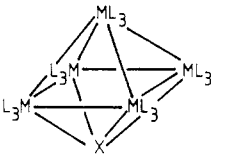

3

one σ orbital). A number of such structures have been reported, including several M_6 compounds.[7] It is also possible for X to be a main-group atom in which case only three of its valence orbitals (one σ and two π orbitals) participate in the skeletal bonding; one orbital of σ symmetry (s, p_z, or an sp hybrid) remains almost unperturbed and contains a lone pair of electrons. The simplified MO diagram depicted in Figure 1b shows the relationship between the seven bonding SMO's of **3** and the corresponding MO's of **1**.

It is apparent from a comparison of parts a and b of Figure 1 that in **2** the main-group element contributes all its valence electrons to the skeletal bonding, making a total of seven occupied SMO's. In contrast, molecules of type **3** are stable for eight occupied MO's of which seven are skeletal molecular orbitals and the eighth electron pair is essentially localized on the main-group atom.

Compounds of type **3**, where X is a main-group element, are known only for X = S.[8] At first sight, they appear to be unrealistic for X = C or N because of the relative sizes of the square face and of the carbon (or nitrogen) atom. As drawn in **3**, if X = C, it would be too far from the metal atoms but one must take into account the geometric flexibility of the M_5 cage. If the M_{basal}–C distance is kept constant at 1.9 Å, the carbon lies in the center of the square face for M–M = 2.69 Å; reduction of the M–M distance by only 12% to 2.37 Å places the carbon 0.9 Å below the basal plane. Of relevance to this discussion is the compound $Ru_5(CO)_{13}(PPh_2)(\mu_4\text{-CCPh})$ (**4**) which has recently been synthesized and structurally characterized.[9]

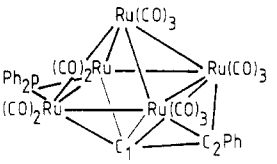

4

(3) (a) Tachikawa, M.; Muetterties, E. L. *Prog. Inorg. Chem.* **1981**, *28*, 203 and references therein. (b) Johnson, B. F. G.; Lewis, J.; Nelson, W. J. H.; Nicholls, J. N.; Vargas, M. D. *J. Organomet. Chem.* **1983**, *249*, 252. (c) Bradley, J. S. *Adv. Organomet. Chem.* **1984**, *22*, 1 and references therein. (d) Tachikawa, M.; Stein, J.; Muetterties, E. L.; Teller, R. G.; Beno, M. A.; Gebert, E.; Williams, J. M. *J. Am. Chem. Soc.* **1980**, *102*, 6648. (e) Gourdon, A.; Jeannin, Y. *C.R. Acad. Sci., Ser. 2* **1982**, *295*, 1101. (f) Blohm, M. L.; Fjare, D. E.; Gladfelter, W. L. *Inorg. Chem.* **1983**, *22*, 1004.

(4) Braye, E. H.; Dahl, L. F.; Hübel, W.; Wampler, D. L. *J. Am. Chem. Soc.* **1962**, *84*, 4633.

(5) See, for example: (a) Cooke, C. G.; Mays, M. J. *J. Organomet. Chem.* **1975**, *88*, 231. (b) Tachikawa, M.; Muetterties, E. L. *J. Am. Chem. Soc.* **1980**, *102*, 4541. (c) Bradley, J. S.; Hill, E. W. *Organometallics* **1982**, *1*, 1634. (d) Sosinsky, B. A.; Norem, M.; Shelly, J. *Inorg. Chem.* **1982**, *21*, 348. (e) Kolis, J. W.; Basolo, F.; Shriver, D. F. *J. Am. Chem. Soc.* **1982**, *104*, 5626. (f) Cowie, A. G.; Johnson, B. F. G.; Lewis, J.; Nicholls, J. N.; Raithby, P. R.; Swanson, A. G. *J. Chem. Soc., Chem. Commun.* **1984**, 637 and references therein. (g) Wijeysekera, S. D.; Hoffmann, R. *Organometallics* **1984**, *3*, 962.

(6) A capped square-pyramidal cluster $Os_6H_2(CO)_{18}$, related to the clusters of type **1** has been reported: McPartlin, M.; Eady, C. R.; Johnson, B. F. G.; Lewis, J. *J. Chem. Soc., Chem. Commun.* **1976**, 883.

(7) For M_6 octahedral clusters see: (a) Albano, V. G.; Chini, P.; Scaturin, V. *J. Organomet. Chem.* **1968**, *15*, 423. (b) Albano, V. G.; Bellon, P. L.; Chini, P.; Scaturin, V. *J. Organomet. Chem.* **1969**, *16*, 461. (c) Jackson, P. F.; Johnson, B. F. G.; Lewis, J.; McPartlin, M.; Nelson, W. J. H. *J. Chem. Soc., Chem. Commun.* **1979**, 735. (d) Corey, E. R.; Dahl, L. F.; Beck, W. *J. Am. Chem. Soc.* **1963**, *85*, 1202. (e) Albano, V. G.; Ciani, G.; Chini, P. *J. Chem. Soc., Dalton Trans.* **1974**, 195. (f) Famagalli, A.; Martinengo, S.; Chini, P.; Albatini, A.; Bruckner, S.; Heaton, B. T. *J. Chem. Soc., Chem. Commun.* **1978**, 195. (g) Churchill, M. R.; Wormald, J. *J. Am. Chem. Soc.* **1971**, *93*, 5670. (h) Eady, C. R.; Johnson, B. F. G.; Lewis, J.; Malatesta, M. C.; Machin, P.; McPartlin, M. *J. Chem. Soc., Chem. Commun.* **1976**, 945. (i) Ceriotti, A.; Ciani, G.; Garlaschelli, L.; Sartorelli, U.; Sironi, A. *J. Organomet. Chem.* **1982**, *229*, C9. (j) Demartin, F.; Manessero, M.; Sansoni, M.; Garlaschelli, L.; Sartorelli, U.; Tagliabue, F. *J. Organomet. Chem.* **1982**, *234*, C39. (k) Ciani, G.; Sironi, A.; Chini, P. *J. Organomet. Chem.* **1981**, *213*, C37. (l) Paquette, M. S.; Dahl, L. F. *J. Am. Chem. Soc.* **1980**, *102*, 6621. (m) Slovokhotov, Yu. L.; Struchkov, Yu. L.; Lopatin, V. E.; Gubin, S. P. *J. Organomet. Chem.* **1984**, *266*, 139. For $M_5(\mu_4\text{-PR})$ see: (n) Fernandez, J. M.; Johnson, B. F. G.; Lewis, J.; Raithby, P. R. *J. Chem. Soc., Chem. Commun.* **1978**, 1015; *Acta Crystallogr., Sect. B: Struct. Crystallogr. Cryst. Chem.* **1979**, *B35*, 1711. (o) Natarajan, K.; Zsolnai, L.; Huttner, G. *J. Organomet. Chem.* **1981**, *209*, 85. (p) Mays, M. J.; Raithby, P. R.; Taylor, P. L. *J. Organomet. Chem.* **1982**, *244*, C45; *J. Chem. Soc., Dalton Trans.* **1984**, 959.

(8) (a) Adams, R. D.; Horvath, I. T.; Segmüller, B. E.; Yang, L. W. *Organometallics* **1983**, *2*, 1301. (b) Adams, R. D.; Foust, D. F.; Mathur, P. *Organometallics* **1983**, *2*, 990. (c) Adams, R. D.; Horvath, I. T.; Mathur, P. *Organometallics* **1984**, *3*, 623.

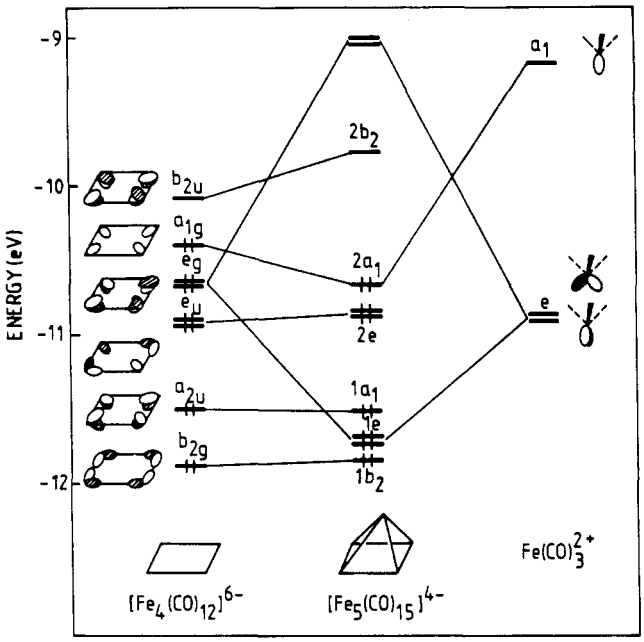

Figure 2. The orbitals of $[Fe_5(CO)_{15}]^{4-}$ built up from a square $Fe_4(CO)_{12}]^{6-}$ capped by an $[Fe(CO)_3]^{2+}$ unit. The labeling of the molecular levels was kept in the D_{4h} pseudosymmetry group for the $[Fe_4(CO)_{12}]^{6-}$ fragment and in C_{4v} pseudosymmetry for the $[Fe_5(CO)_{15}]^{4-}$ system.

In this compound, the C_1 atom lies 0.84 Å below the square face.[10] An alternative description of this structure is to view it as a closo M_5C octahedral cluster having a triangular M_2C face capped by a CPh group. According to the capping principle,[1c] to a first approximation the CR group can be seen as providing its three electrons merely to complete the seven SEP count required for a closo octahedral cluster. Thus, if we remove the CPh fragment, but not its electrons, it remains a seven-SEP framework in which the carbon atom occupies a polyhedral vertex and supplies only two electrons to the skeletal electron count. The bonding scheme could be the one depicted in Figure 1b.

In order to test this hypothesis concerning the existence of two possible geometries for M_5C clusters with two different electron counts, but the *same number of SEP's*, we have undertaken a series of calculations on M_5X and related molecules.

MO Picture of the M_5 Cage. Our basic square pyramid is $[Fe_5(CO)_{15}]^{4-}$. Its MO's can easily be derived from those of a square Fe_4 unit and those of a capping $Fe(CO)_3$ fragment (see Figure 2). The general picture is that of a group of seven bonding/nonbonding MO's below a rather low-lying π-antibonding MO preferentially localized in the iron square. From the diagram we see that a normal count of seven SEP's[1] or 74 valence electrons[11] is expected but a count of eight SEP's is not totally excluded.[12]

MO Picture of the Octahedral M_5S Cluster, 5. Figure 3 shows the frontier molecular orbital (FMO) interaction diagram of $Fe_5(CO)_{15}$ with the sulfur atom capping the square face as in **3**. This diagram is in good agreement with the simplified picture of Figure 1b. Four of the seven bonding/nonbonding MO's of the Fe_5 framework are only slightly perturbed whereas the three

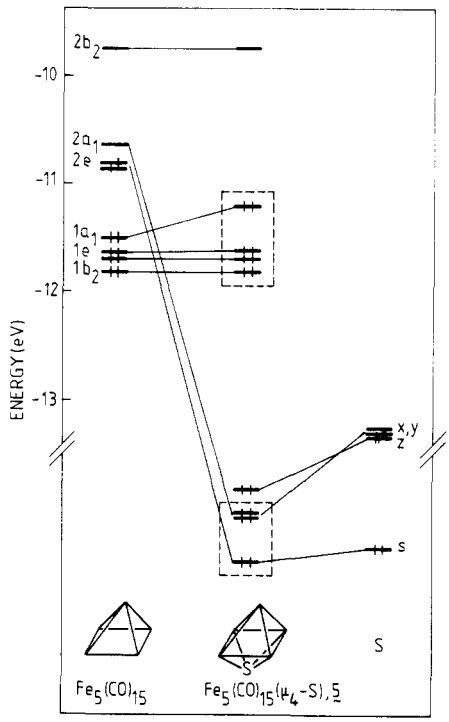

Figure 3. Orbital interaction diagram for $[Fe_5(CO)_{15}](\mu_4\text{-S})$. The SEP's are shown boxed in by dashed lines.

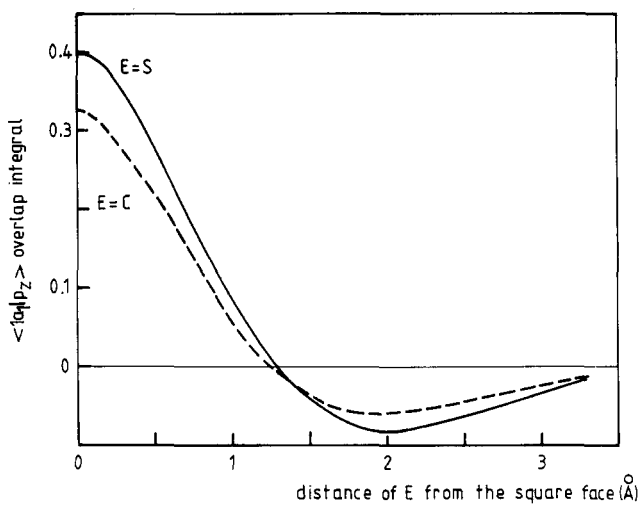

Figure 4. Evolution of the overlap between the metallic $1a_1$ FMO and the sulfur p_z AO (solid line) or the carbon p_z AO (dashed line).

others interact significantly with the three AO's of the sulfur atom leading to three bonding skeletal MO's. Surprisingly, the noninteracting AO of the sulfur atom is the p_z orbital. This orbital of a_1 symmetry is expected to interact with the FMO's of the M_5 fragment which have the "same a_1 symmetry", in particular with the metallic $1a_1$ FMO which is the closest in energy. Actually, it does not because the overlap integral $\langle 1a_1|p_z\rangle$ shown in **6** is about zero. Figure 4 shows the variation of the overlap

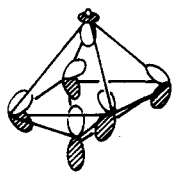

$<1a_1|p_z> = 0.001$

6

integral between the p_z orbital of the sulfur atom and the

(9) MacLaughlin, S. A.; Taylor, N. J.; Carty, A. J. *Organometallics* **1983**, *2*, 1194.
(10) Distance calculated from the published crystallographic atomic positions in ref 9.
(11) Lauher, J. W. *J. Am. Chem. Soc.* **1978**, *100*, 5305.
(12) Halet, J.-F.; Saillard, J.-Y.; Hoffmann, R. *Inorg. Chem.* **1985**, *24*, 1695.

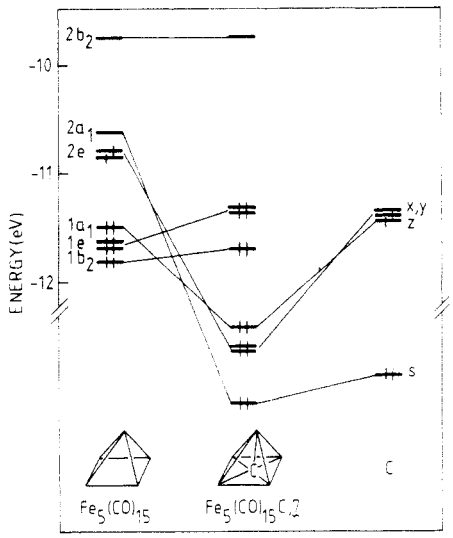

Figure 5. Orbital interaction diagram for $Fe_5(CO)_{15}C$ with the carbon in the square face.

$1a_1$ FMO of the M_5 fragment (which is of π-type symmetry in the square) as the sulfur is moved along the fourfold axis. As shown by this simplified picture, the overlap is large when the sulfur atom lies in the face, it decreases to zero, and then it changes its sign before again going to zero at infinite separation. As the intensity of the interaction varies with S_{ij}^2, it should be zero when the sulfur atom is 1.25 Å below the square face. This is almost exactly the experimental distance (1.26 Å) observed in $Os_5(CO)_{15}(\mu_4\text{-}S)$.[8]

The net result is that the sulfur p_z orbital interacts only with the $2a_1$ FMO of the metallic fragment and even then the interaction is weak since they are reasonably far separated in energy and their overlap is poor. The p_z orbital can be regarded as containing the sulfur lone pair, and these electrons are not included in the number of SEP's required for the cluster bonding. This situation is reminiscent of the nonbonding "exo-deltahedral" atomic orbitals described by Rudolph et al. in heteroboranes.[13] In contrast, the sulfur s orbital exhibits considerable overlap with the metallic $2a_1$ (and also $1a_1$) orbital and is, therefore, more perturbed than is the p_z orbital.

MO Picture of M_5C, 7. In Figure 5 we show the interaction diagram of the cluster $Fe_5(CO)_{15}C$ (**7**), in which the carbon atom is situated in the center of the metallic square face; actually, as usually observed in these systems,[3,4] the carbon is 0.1 Å below the square. The main difference between this case and that of $Fe_5(CO)_{15}S$ (**5**; see Figure 3) is that here the carbon p_z orbital interacts strongly with the metallic $1a_1$ FMO. As shown in **8**, there

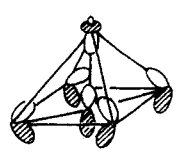

$\langle 1a_1|p_z \rangle = 0.315$

8

is a large overlap integral $\langle 1a_1|p_z \rangle$ when the carbon atom is close to the middle of the square face. Consequently, the $1a_1$ and p_z FMO's, which remained essentially nonbonding in Fe_5S, **5** (see Figure 3), now form strongly bonding and antibonding combinations. The compound

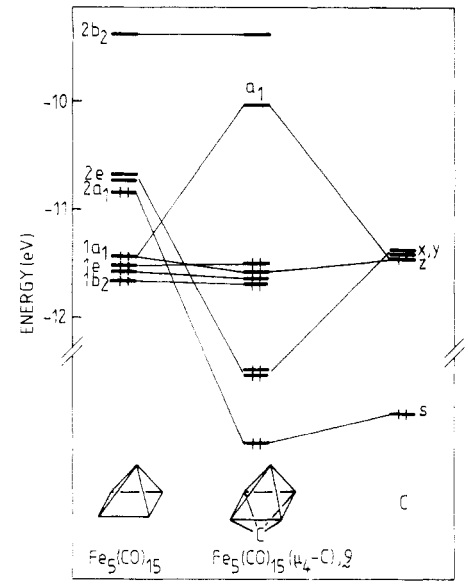

Figure 6. Orbital interaction diagram for $Fe_5(CO)_{15}(\mu_4\text{-}C)$ with the carbon occupying a vertex position.

is stable for seven SEP; the four carbon AO's participate in the cluster bonding, and all four of its valence electrons are included in the skeletal electron pair count. This orbital diagram is consistent with the simplified picture of Figure 1b.

If we now move the carbon atom away from the square face, the overlap integral $\langle 1a_1|p_z \rangle$ follows a curve similar to that for Fe_5S, **5**, as shown in Figure 4. In accordance with the preceding discussion on Fe_5S, we would expect a molecular orbital diagram comparable to that of Figure 3. That is, the $1a_1$ and p_z should be almost nonbonding when the overlap integral $\langle 1a_1|p_z \rangle$ is close to zero; at this point the carbon atom is 1.2 Å below the square face and the M_{basal}–C distance would be unrealistically long. The structure of the compound **4** seems to indicate that a compromise can exist between the M–M and M–C distances so as to put the carbon atom some considerable distance (0.84 Å) below the square plane. We thus designed a similar model, **9**, in which Fe–Fe = 2.52 Å and Fe_{basal}–C = 1.99 Å; this places the carbon 0.9 Å below the square base, and the corresponding MO diagram appears as Figure 6. The MO spectrum of the Fe_5 core is slightly perturbed by the contraction of the metallic cage. The $\langle 1a_1|p_z \rangle$ overlap is still significant (0.09) but considerably smaller than in a geometry such as **7**. Consequently, the gap between the bonding and antibonding combinations of $1a_1$ and p_z is reduced in **9** compared to **7**. Thus the MO diagram of **9** is intermediate between that of Fe_5S, **5**, (where $\langle 1a_1|p_z \rangle$ is near zero) and the one for **7** (in which there is a strong $\langle 1a_1|p_z \rangle$ overlap). The out-of-plane combination of the $1a_1$ and p_z FMO's in **9** is the first antibonding MO, and it lies at relatively low energy above the skeletal bonding/nonbonding MO group. For an electron count corresponding to occupation as far as this bonding/nonbonding block (i.e., neutral Fe_5C) the geometry **7**, with the carbon atom near the center of the square face, is obviously preferred. If we were to add two electrons, one would predict a shift of the carbon atom away from the polyhedral center so as to become a vertex as in **9**. Although such a rearrangement would lower the energy of the HOMO, the Fe_5C^{2-} cluster **9** is not likely to be very stable and it should be very susceptible to electrophilic attack at the carbon atom.

MO Picture of $[Fe_5(CO)_{15}CCH]^+$ (10). Compound **4** possesses a CPh group capping a triangular Ru_2C face. Let

(13) (a) Rudolph, R. W.; Pretzer, W. R. *Inorg. Chem.* **1972**, *11*, 1974. (b) Teo, B. K.; Longoni, G.; Chung, F. K. R. *Inorg. Chem.* **1984**, *23*, 1257.

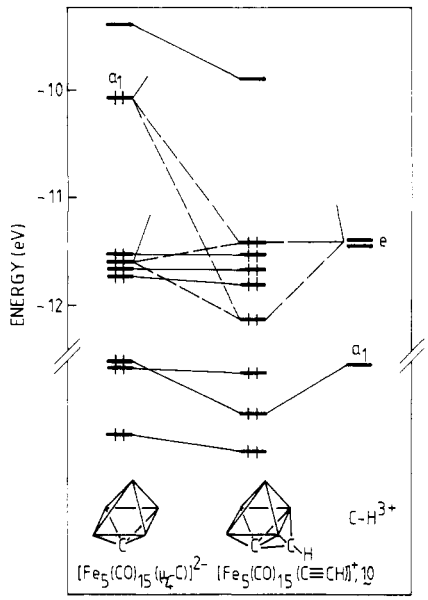

Figure 7. MO diagram for $[Fe_5(CO)_{15}(\mu_4\text{-CCH})]^+$.

us observe the role played by this moiety and its effects on the energy levels of the M_5 core. The MO diagram of **10** obtained by capping a triangular face Fe_2C of **3** by a CH^{3+} unit is shown in Figure 7. Because of the relatively low symmetry of **10**, the interactions between the FMO's are numerous and the complete MO scheme would be rather complicated; for clarity therefore, we present a somewhat simplified diagram.

Because of its large localization on the three atoms of the capped face, FMO a_1 of **9** interacts strongly with the FMO's of the capping CH^{3+} group and is thus involved in strongly bonding and antibonding molecular orbitals. **10** has the same number (7 + 1) of occupied SMO's as does **9** but, in this case, the HOMO is stabilized leading to a large HOMO–LUMO gap thus securing good stability for this molecule and related species. One may relate the electronic structure of the capped octahedron **10**, with its eight stable occupied MO's, to the situation depicted in Figure 1b. However, the carbon "lone pair" is actually being utilized in many ways—particularly in bonding interactions with the capping CH^{3+} fragment.

Related Compounds

The addition of two electrons to **4**, through a carbonyl, results in Ru–Ru cleavage and a more open structure, viz., $Ru_5(CO)_{14}(PPh_2)(\mu_5\text{-}\eta^2\text{-CCPh})$ (**11**).[9] Now, if we as before

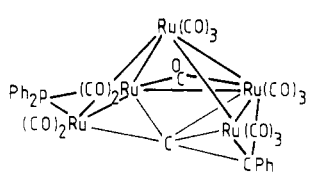

11

abstract the CPh^{3+} unit, the residual M_5C cage can be described as a nido cluster derived from a pentagonal bipyramid with a vacancy in the equatorial pentagonal plane. The carbon atom positioned 0.45 Å below the mean Ru plane occupies an apical vertex. For such a compound, PSEP theory requires an eight skeletal electron pair count; this is accomplished if we consider the carbon atom to contribute two electrons while retaining a lone pair. From our preceding discussions on the systems **7** and **9**, we would suspect this "lone pair" to be rather antibonding in **11**. As in **4**, this antibonding character is reduced by stabilizing

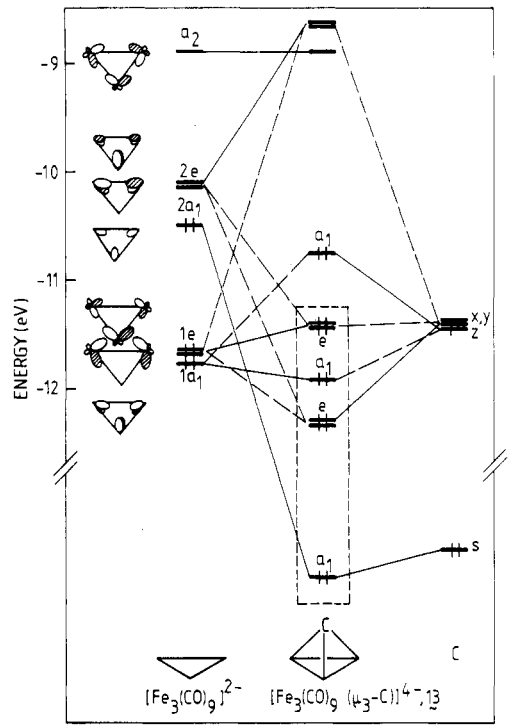

Figure 8. Orbital interaction diagram for $[Fe_3(CO)_9(\mu_3\text{-C})]^{4-}$.

interactions with the CPh^{3+} capping moiety.

We note that if one assumes the carbon atom not to be a polyhedral vertex but rather an exposed main-group element in the metallic face, it must donate all of its valence electrons and so lead to a skeletal electron pair count of nine. This would be in disagreement with the Wade–Mingos rules[1] which predict a count of eight SEP's for a five-vertex arachno M_5C cluster.[14]

At this point in the discussion, it is appropriate to mention other acetylide clusters such as **12**, which is related

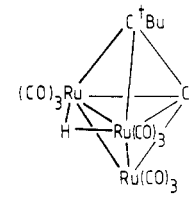

12

to **4**, but in which the C≡CPh ligand is bonded to an M_3 metallic core.[15] These closo trigonal bipyramids, in which the "naked" carbon of the acetylide ligand occupies a vertex position, have a normal electron count consistent with Figure 1b, i.e., six SEP's plus one "lone pair" on the carbon atom. This type of compound can also be viewed as a nido pseudotetrahedral M_3C cluster having an M_2C face capped by a CR group. Removal of the CR^{3+} group leaves a six-SEP M_3C framework where the carbon atom caps a trimetallic face. Calculations on the model compound $[Fe_3(CO)_9(\mu_3\text{-C})]^{4-}$ (**13**) confirm that the favored total electron pair count is seven; six of these are the normal six SEP's and the seventh is a lone pair in the $3a_1$ MO as shown in Figure 8. The $3a_1$ MO, which has mainly carbon p_z character, is somewhat metal-carbon antibonding

(14) A reviewer has pointed out that a five-vertex 9-SEP system could be regarded as a hypho eight-vertex cluster with three vertices removed from the D_{2d} dodecahedron.

(15) (a) Carty, A. J. *Pure Appl. Chem.* **1982**, *54*, 113 and references therein. (b) Sappa, E.; Tiripicchio, A.; Braunstein, P. *Chem. Rev.* **1983**, *83*, 203 and references therein.

and so the MO pictures of $M_5(\mu_4\text{-C})$, **9**, and $M_3(\mu_3\text{-C})$, **13**, are related. However, since the M–C antibonding character of the HOMO in **13** is less than is the case for **9**, the M_3C clusters are expected to be more stable than M_5C clusters such as **9**. We note that other theoretical work[5e,16] has already predicted the feasibility of such six-SEP M_3C clusters. As for $M_5(\mu_4\text{-C})$, **9**, one can stabilize the HOMO of **13** by capping an M_2C face by a CR^{3+} group and so producing stable compounds of the type **12**.

Another way of reducing the antibonding character of the HOMO's of M_3C and M_4C systems is to replace the carbon atom by an O^{2+} cation. As the $2p_z$ orbital energy of an oxygen atom is significantly lower than for the corresponding carbon orbital, its interaction with the appropriate metallic FMO's is smaller. Calculations on model **13** with an oxygen atom instead of the carbon give results comparable to those of $M_5(\mu_4\text{-S})$, **5**. Indeed, compounds with an $M_3(\mu_3\text{-O})$ core are known.[17] This leads us to suggest that syntheses of species with a μ_4-oxo capping ligand, $M_4(\mu_4\text{-O})$, are not out of the question.

In addition to the cluster carbides already mentioned, another interesting structural category is that of the butterfly M_4C carbides, such as **14**, in which the carbon atom lies halfway between the wing-tips.[3ac,18] This class of compounds has recently aroused considerable interest in the literature.[19] As shown by calculations, cluster **14**,

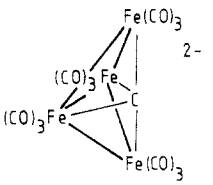

14

which adopts an arachno structure, is stable for seven SEP's. The carbido atom occupying the center of the octahedron (on which the structure is based) contributes all its AO's and all four valence electrons to the skeletal bonding. If the carbido atom moves away from the wings of the butterfly, as shown in **15**, the bonding between this carbido atom and the wing-tip iron atoms is weakened.[19] The antibonding iron–carbon MO becomes the HOMO; this is the nonbonding lone pair on carbon. Thus, the carbon allocates only two valence electrons to the cluster. We thus obtain a five-vertex closo system having the predicted electron count of six SEP's. However, the

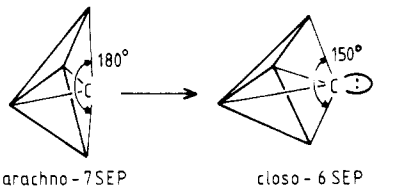

15

transformation to this closo geometry enhances the reactivity of the carbon atom toward electron acceptors.[19,20]

Mixed Clusters

Another well-known type of seven-SEP five-vertex nido cluster is the family of mixed M_3C_2 compounds well typified by $[Fe_3(CO)_9(C_2H_2)]^{2-}$ (**16**). According to the isolobal

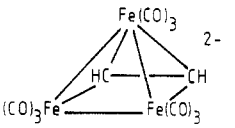

16

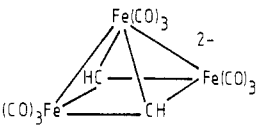

17

analogy between CR^+ and a d^8 ML_3 group like $Fe(CO)_3$,[21] M_3C_2 compounds of type **16** should have their electronic structure related to that of the hypothetical metallic cluster of type **1**. This should also hold for the as yet unsynthesized M_3C_2 nido clusters, such as **17**, where the two carbon atoms are not contiguous.[22]

As the seven-SEP carbides of type **2** are stable, we have explored the possibility of the existence of the mixed-cluster carbides of types **18** and **19**. Of course, the size

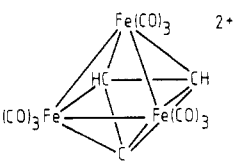

18

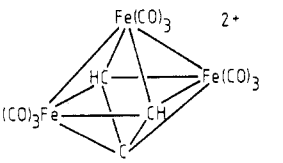

19

of the M_2C_2 square face in the models is smaller than the metallic square face of **2**, and the carbon atom cannot be positioned in (or very close to) the cluster face. Assuming "realistic" metal–carbon and carbon–carbon bond distances (1.9 Å and 1.5 Å, respectively) we have placed the exposed carbon atom 1 Å below the "square" face in **18** and 0.7 Å below in **19**. The position of the carbide atom is reminiscent of the structure of **4**.

In fact, the MO pictures of **18** and **19**, shown in Figures 9 and 10, are closely related to the one for $M_5(\mu_4\text{-C})$, **9**. The FMO's of the M_3C_2 cages, described elsewhere,[23] are labeled appropriately for the C_s point group. There is a direct relation between these FMO's and the ones of an M_5 cage. A glance at Figures 9 and 10 shows that the

(16) (a) Kolis, J. W.; Holt, E. M.; Shriver, D. F. *J. Am. Chem. Soc.* **1983**, *105*, 7307. (b) Vites, J. C.; Housecroft, C. E.; Jacobsen, G. B.; Fehlner, T. P. *Organometallics* **1984**, *3*, 1591.

(17) An X-ray structure of $[Fe_3(CO)_9(\mu_3\text{-O})]^{2-}$ has been reported: Ceriotti, A.; Demartin, F.; Longoni, G.; Manassero, M.; Masdriocchi, N.; Resconni, L.; Sansoni, M. *Congr. Naz. Chim. Inorg., [Atti], 16th* **1983**, 371. Ceriotti, A.; Resconni, L.; Demartin, F.; Longoni, G.; Manassero, M.; Sansoni, M. *J. Organomet. Chem.* **1983**, *249*, C35. For other μ_3-oxo-capped clusters see, for example: (a) Uchtman, V. A.; Dahl, L. F. *J. Am. Chem. Soc.* **1969**, *91*, 3763. (b) Goudsmit, R. J.; Johnson, B. F. G.; Lewis, J.; Raithby, P. R.; Whitmire, K. H. *J. Chem. Soc., Chem. Commun.* **1983**, 246. (c) Lavigne, G.; Lugan, N.; Bonnet, J.-J. *Nouv. J. Chim.* **1981**, *5*, 423. (d) Chisholm, M. H.; Folting, K.; Huffman, J. C.; Kirkpatrick, C. C. *J. Am. Chem. Soc.* **1981**, *103*, 5967. (e) Cotton, F. A.; Duraj, S. A.; Roth, W. J. *J. Am. Chem. Soc.* **1984**, *106*, 3527 and references therein. (f) Cotton, F. A.; Marler, D. O.; Schwotzer, W. *Inorg. Chem.* **1984**, *23*, 3671. (g) We note that a μ_3-iodo-capped triruthenium cluster has been reported: Kampa, C. E.; Boag, N. M.; Knobler, C. B.; Kaesz, H. D. *Inorg. Chem.* **1984**, *23*, 1390.

(18) There are also several reported butterfly M_4 nitrides: Fjare, D. E.; Gladfelter, W. L. *J. Am. Chem. Soc.* **1984**, *106*, 4799 and references therein.

(19) For theoretical studies on the reactivity of butterfly M_4C systems, see: (a) Reference 5g. (b) Harris, S.; Bradley, J. S. *Organometallics* **1984**, *3*, 1086. (c) Reference 5e. (d) Housecroft, C. E. *J. Organomet. Chem.* **1984**, *276*, 297.

(20) (a) Reference 3c. (b) Mlekuz, M.; Bougeard, P.; Sayer, B. G.; McGlinchey, M. J.; Faggiani, R.; Lock, C. J. L.; Jaouen, G. *Organometallics* **1985**, *4*, 2143.

(21) Hoffmann, R. *Angew. Chem., Int. Ed. Engl.* **1982**, *21*, 711.

(22) Note that closo dialkylidyne complexes have been reported: (a) Freeland, B. H.; Payne, N. C.; Stalteri, M. A.; Van Leeuven, H. *Acta Crystallogr., Sect. C: Cryst. Struct. Commun.* **1983**, *C39*, 1533. (b) Pardy, R. B. A.; Smith, G. W.; Vickers, M. E. *J. Organomet. Chem.* **1983**, *252*, 341. For theoretical studies, see: (c) Enoki, S.; Kawamura, T.; Yonezawa, T. *Inorg. Chem.* **1983**, *22*, 3821. (d) Clauss, A. D.; Shapley, J. R.; Wilker, C. N.; Hoffmann, R. *Organometallics* **1984**, *3*, 619.

(23) (a) Schilling, B. E. R.; Hoffmann, R. *J. Am. Chem. Soc.* **1979**, *101*, 3456. (b) Halet, J.-F.; Saillard, J.-Y.; Lissillour, R.; McGlinchey, M. J.; Jaouen, G. *Inorg. Chem.* **1985**, *25*, 218. (c) Busetti, V.; Granozzi, G.; Aime, S.; Gobetto, R.; Osella, D. *Organometallics* **1984**, *3*, 1510.

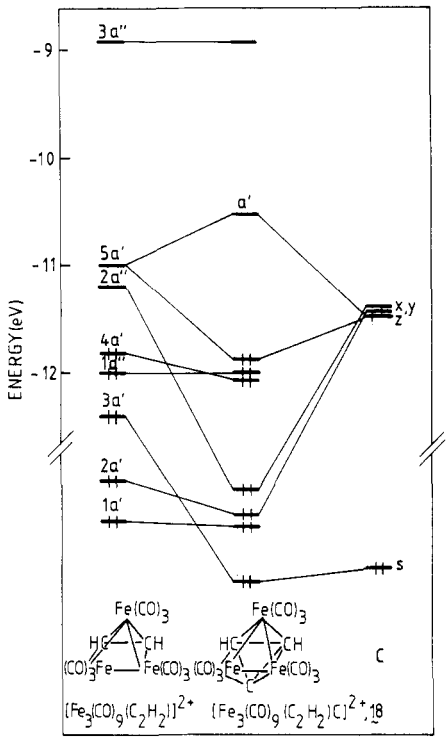

Figure 9. Orbital interaction diagram for the mixed-system $[Fe_3(CO)_9(C_2H_2)C]^{2+}$ (**18**).

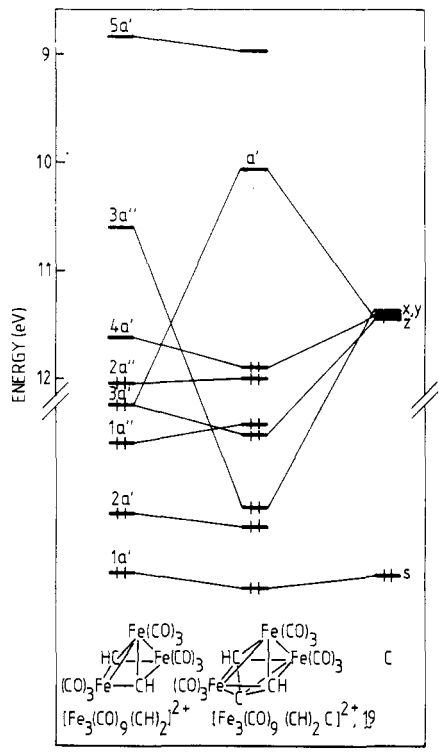

Figure 10. Orbital interaction diagram for the mixed-cluster $[Fe_3(CO)_9(CH)_2C]^{2+}$ (**19**).

interactions of the carbon AO's with the FMO's of the M_3C_2 cores are similar to the ones occurring in **9**. We are thus dealing with a group comprised of seven bonding/nonbonding SMO's below an orbital situated at an intermediate energy. This latter orbital is an out-of-phase combination of the carbon $2p_z$ orbital with metallic cage FMO's, viz., 5a' in Figure 9 and 3a' in Figure 10. As with the M_5C cluster **9**, two electron counts seem possible. If the a' molecular orbital is vacant, this would be a seven-SEP system, while if the a' MO is occupied there would be seven SEP's plus a metal–carbon antibonding electron pair. The model **18** seems to be the more stable for an eight SEP count, and one might anticipate that such a system would be susceptible to electrophilic attack. In contrast, the seven SEP count is preferred for model **19**; in this case, the carbide would be sensitive toward incoming nucleophilic reagents.

For both geometries **18** and **19**, the "7 + 1" SEP count is expected to be stabilized by capping an M_2C or MC_2 triangular face with a CR^{3+} group as in $Fe_5(\mu_4\text{-}C)$, **9**.

Table I. Parameters Used in Extended Hückel Calculations

orbital		H_{ii}, eV	ζ_1	ζ_2	c_1[a]	c_2[a]
H	1s	−13.6	1.30			
C	2s	−21.4	1.625			
	2p	−11.4	1.625			
O	2s	−32.3	2.275			
	2p	−14.8	2.275			
S	3s	−20.0	1.817			
	3p	−13.3	1.817			
Fe	3d	−12.6	5.35	1.80	0.5366	0.6678
	4s	−9.1	1.90			
	4p	−5.32	1.90			

[a] Two Slater exponents are listed for the 3d functions.

Acknowledgment. We thank the CNRS for financial support and L. Hubert for the drawings.

Appendix

All calculations were performed via the extended Hückel method[24] using weighted H_{ij}'s.[25] The parameters used are listed in Table I. The basic geometry of the five-metal systems consisted of a square-pyramidal framework with iron–iron separations of 2.70 Å and **5** and **7** and 2.52 Å in **9** and **10**. The capping sulfur atom was placed 1.28 Å below the square face, whereas the carbon was positioned 0.1 Å from the square face in **9** and **10** and 0.9 Å distant in **7**. In M_3E models, the capping ligands were placed 1.38 Å (for the carbon atom) and 1.42 Å (for the oxygen atom) above the trimetallic base. Geometry **14** was taken from the X-ray structure.[3c] In the mixed clusters, the Fe–Fe distance was taken as 2.52 Å, as in the M_3E geometry. The following distances were used: $Fe\text{–}C_{basal}$ = 1.95 Å; $Fe\text{–}C_{exposed}$ = 1.85 Å, and $C_{basal}\text{–}C_{exposed}$ = 1.5 Å. In all calculations, Fe–C(O) values were set at 1.8 Å and C–O at 1.15 Å.

Registry No. **1**, 99052-73-0; **2**, 11087-47-1; **5**, 99052-75-2; **10**, 99033-70-2; **11**, 99052-76-3; **13**, 99033-71-3; **14**, 74792-04-4; **16**, 93646-07-2; **18**, 99033-72-4; **19**, 99033-73-5; $[Fe_5(CO)_{15}]^{4-}$, 99052-74-1.

(24) (a) Hoffmann, R. *J. Chem. Phys.* **1963**, *39*, 1397. (b) Hoffmann, R.; Lipscomb, W. N. *Ibid.* **1962**, *36*, 2179, 3489; **1962**, *37*, 2872.
(25) Ammeter, J. H.; Bürgi, H.-B.; Thibeault, J. C.; Hoffmann, R. *J. Am. Chem. Soc.* **1978**, *100*, 3686.

Preparation of Cyclodisilazanes from Dimethylhydroaminosilanes, $(CH_3)_2Si(H)NHR$

Gary H. Wiseman, David R. Wheeler, and Dietmar Seyferth*

Department of Chemistry, Massachusetts Institute of Technology, Cambridge, Massachusetts 02139

Received May 8, 1985

The deprotonation of dimethylhydroaminosilanes, $(CH_3)_2Si(H)NHR$, with *n*-butyllithium and subsequent reactions of the intermediate lithium silylamide with chlorosilanes or methyl iodide in THF produced simple substitution products in high yield. However, reactions of these lithium silylamides with chlorosilanes in nonpolar solvents, e.g., hexane, produced mixtures of substitution products and cyclodisilazanes. On the basis of the results of various experiments, a mechanism is proposed for this cyclization reaction which involves the head-to-tail dimerization of an unstable "silaimine" intermediate, $(CH_3)_2Si{=}NR$. An attempt to trap the proposed intermediate was unsuccessful.

Introduction

The chemistry of silicon–nitrogen compounds has been explored in some detail, at least in part because of past interest in Si–N polymers (polysilazanes) as potential complements to polysiloxanes in high-temperature applications.[1] However, polysilazanes have never been used in such applications due to the lack of a suitable method for high molecular weight polymer synthesis and also because of the inherent hydrolytic instability of the Si–N bond.[2] Recently, interest in Si–N polymers has been renewed because of their potential use as precursors to Si_3N_4, Si_3N_4/SiC mixtures, and related ceramic materials.[3-5] In this context, we have been especially interested in polysilazanes with adjacent Si–H and N–H groups because such polymers generally have given high polymer-to-ceramic conversion yields. The synthesis of low molecular weight polymers or oligomers with the approximate structures $(-H_2SiNH-)_n$ and $(-RSiHNH-)_n$ (R = CH_3, CH_3CH_2, C_6H_5, etc.) has been the subject of previous papers from this group.[3] However, prior to the study of the reaction chemistry (for either further polymerization or derivatization) of such polymers, it was important to develop prototype chemistry using small molecules. The advantages of this approach have been pointed out by Allcock[6] and primarily derive from the ease of product purification and spectroscopic identification. Along these lines, this paper will be concerned with the deprotonation and subsequent reactions of dimethylhydroaminosilanes, $(CH_3)_2Si(H)NHR$ (R = $(CH_3)_2SiH$, $(CH_3)_2CH$, $(CH_3)_3C$), compounds which are monofunctional models for polymers with RSiHNH repeat units. Our primary goal was to investigate potentially useful Si–N bond-forming reactions which could be used to polymerize the low molecular weight oligomers described in previous publications.[3] A preliminary communication of a novel polysilazane synthesis using reaction chemistry similar to that described in this paper has been published,[3b] and full details of the polymer synthesis and polymer-to-ceramic conversion will be provided in future papers.

Results and Discussion

Aminosilazanes of type R_3SiHNR' are readily deprotonated by inorganic or organometallic bases. For example, hexamethyldisilazane, $[(CH_3)_3Si]_2NH$, reacts with phenyllithium to produce *N*-lithiohexamethyldisilazane (eq 1).[7] *N*-lithio- and *N*-sodiohexamethyldisilazane (prepared

$$[(CH_3)_3Si]_2NH + C_6H_5Li \rightarrow [(CH_3)_3Si]_2NLi + C_6H_6 \quad (1)$$

from $[(CH_3)_3Si]_2NH$ and $NaNH_2$)[8] are widely used as strong, but weakly nucleophilic bases. In reactions with trialkylchlorosilanes they act as nucleophiles to produce a trisilylamine (eq 2).[7]

$$[(CH_3)_3Si]_2NNa + R_3SiCl \rightarrow NaCl + [(CH_3)_3Si]_2NSiR_3 \quad (2)$$

The deprotonation of tetramethyldisilazane, $[(CH_3)_2SiH]_2NH$, by *n*-butyllithium and the subsequent reaction of the *N*-lithiosilazane with trimethylchlorosilane or dimethylchlorosilane has been reported to give the expected trisilylamine in good yield (eq 3).[9] The nucleophilic

$$[(CH_3)_2SiH]_2NH + n\text{-}C_4H_9Li \xrightarrow{\text{pentane}} [(CH_3)_2SiH]_2NLi + n\text{-}C_4H_{10} \xrightarrow[R(CH_3)_2SiCl,\ R = H,\ CH_3]{\text{THF, 66 °C}} [(CH_3)_2SiH]_2NSi(CH_3)_2R + LiCl \quad (3)$$

60–70%

displacement of hydride from silicon by n-C_4H_9Li was considered to be a possible side reaction but did not occur under the reaction conditions used.[9] The deprotonation was carried out in pentane, and THF was only added just prior to the addition of the chlorosilane.

We found that deprotonation of $[(CH_3)_2SiH]_2NH$ with n-butyllithium is readily achieved at −78 °C in THF so-

(1) (a) Fessenden, R.; Fessenden, J. S. *Chem. Rev.* **1961**, *61*, 361. (b) Wannagat, U. *Adv. Inorg. Chem. Radiochem.* **1964**, *6*, 225.
(2) Krüger, C. R.; Rochow, E. G. *J. Polym. Sci.: Part A* **1964**, *2*, 3179.
(3) (a) Seyferth, D.; Wiseman, G. H.; Prud'homme, C. *J. Am. Ceram. Soc.* **1983**, *66*, C-13. (b) Seyferth, D.; Wiseman, G. H. *J. Am. Ceram. Soc.* **1984**, *67*, C-132. (c) Seyferth, D.; Wiseman, G. H. In "Ultrastructure Processing of Ceramics, Glasses and Composites"; Hench, L. L., and Ulrich, D. R., Eds.; Plenum Press: New York, 1984; Chapter 22. (d) Seyferth, D.; Wiseman, G. H. In "Emergent Process Methods for High-Technology Ceramics"; Davis, R. F., Palmour III, H., Porter, R. L., Eds.; Plenum Press; New York, 1984; Vol. 17, p 263.
(4) (a) Verbeek, W. (Bayer A.-G) Ger. Offen. 2218960, 1973; *Chem. Abstr.* **1974**, *80*, P98019. (b) Verbeek, W.; Winter, G. (Bayer A.-G.) Ger. Offen. 2236078, 1974; *Chem. Abstr.* **1974**, *81*, P50911. (c) Winter, G.; Verbeek, W.; Mansmann, M. (Bayer, A.-G.) Ger. Offen. 2243527, 1974; *Chem. Abstr.* **1974**, *81*, P126134.
(5) (a) Gaul, J. H., Jr. (Dow Corning) Belg. BE 889029; *Chem. Abstr.* **1982**, *96*, 163389. (b) Gaul, J. H., Jr. (Dow Corning) Belg. BE 888787; *Chem. Abstr.* **1982**, *96*, 143567.
(6) Allcock, H. R. *Acc. Chem. Res.* **1979**, *12*, 351.
(7) (a) Wannagat, U.; Niederprüm, H. *Angew. Chem.* **1959**, *71*, 574. (b) Wannagat, U. *Adv. Inorg. Chem. Radiochem.* **1964**, *6*, 225.
(8) Fink, W. *Angew. Chem.* **1961**, *73*, 467.
(9) (a) Bush, R. P.; Lloyd, N. C.; Pearce, C. A. *J. Chem. Soc., Chem. Commun.* **1967**, 1269. (b) Bush, R. P.; Lloyd, N. C.; Pearce, C. A. *J. Chem. Soc. A* **1969**, 253. The reaction temperature was not reported.

0276-7333/86/2305-0146$01.50/0

lution. The addition of $(CH_3)_3SiCl$ to this solution of $[(CH_3)_2SiH]_2NLi$ at −78 °C produced a 100% yield of the expected $[(CH_3)_2SiH]_2NSi(CH_3)_3$ (eq 4). The intermediate

$$[(CH_3)_2SiH]_2NH + n\text{-}C_4H_9Li \xrightarrow{-78\ °C} [(CH_3)_2SiH]_2NLi \xrightarrow[\text{THF, } -78\ °C]{(CH_3)_3SiCl} [(CH_3)_2SiH]_2NSi(CH_3)_3 + LiCl \quad (4)$$

N-lithiosilazane $[(CH_3)_2SiH]_2NLi$ need not be prepared and quenched at −78 °C. In another experiment, it was generated at 0 °C and was found to be stable in refluxing THF. The $[(CH_3)_2SiH]_2NLi$ intermediate was quenched with CH_3I to produce a quantitative yield of $[(CH_3)_2SiH]_2NCH_3$.

However, the use of nonpolar solvents for such reactions produced surprisingly different results. When *n*-butyllithium was added to a solution of $[(CH_3)_2SiH]_2NH$ in *hexane* at 0 °C, a white precipitate formed immediately (this was not mentioned by Bush et al.[9]). When this reaction mixture was heated to reflux (69 °C), the precipitate disappeared, but it formed again when the solution was allowed to cool to room temperature. GLC analysis of the reaction solution showed that no volatile products were present. The solution was heated to reflux again (the precipitate disappeared again) and $(CH_3)_3SiCl$ was added. A GLC analysis of this reaction mixture now showed only a low (9%) yield of the expected silylation product $[(CH_3)_2SiH]_2NSi(CH_3)_3$ but a much higher yield (83%) of a new product, *N,N'*-bis(dimethylsilyl)tetramethylcyclodisilazane, cyclo-$[(CH_3)_2SiNSi(CH_3)_2H]_2$ (eq 5). The latter had been prepared previously by the $LiAlH_4$ reduction of *N,N'*-bis(dimethylchlorosilyl)tetramethylcyclodisilazane.[10]

$$[(CH_3)_2SiH]_2NH + n\text{-}C_4H_9Li \xrightarrow[0\ °C]{\text{hexane}} \text{white precipitate} \xrightarrow[\text{hexane, reflux}]{(CH_3)_3SiCl,} [(CH_3)_2SiH]_2NSi(CH_3)_3\ (9\%) + \underset{83\%}{\begin{matrix}(CH_3)_2Si-NSi(CH_3)_2H \\ | \\ H(CH_3)_2SiN-Si(CH_3)_2\end{matrix}} \quad (5)$$

The preparation of cyclodisilazanes by a base-induced silylamine deprotonation/hydride elimination from silicon sequence has been reported by previous workers. Such syntheses may be effected in two ways. (1) The Si–H and N–H functions can be in different starting compounds, a 1:1 mixture of which is treated with a base (eq 6).[11]

$$2R_2SiH_2 + 2R'NH_2 \xrightarrow{\text{base}} \begin{matrix}R_2Si-NR' \\ | \quad | \\ R'N-SiR_2\end{matrix} + 4H_2 \quad (6)$$

Without doubt, $R_2Si(H)N(H)R'$ is an intermediate in this reaction. A related reaction is that shown in eq 7.[12] (2)

$$Me_2Si(NHSiMe_3)_2 + PhSiH_3 \xrightarrow{[Me_3SiOK]} \begin{matrix}Me_3SiN-SiMe_2 \\ | \quad | \\ PhSi-NSiMe_3 \\ | \\ H\end{matrix} + 2H_2 \quad (7)$$

The Si–H and N–H functions can both be in the same starting compound (eq 8).[13] Various basic reagents have been used to effect this conversion: K in di-*n*-butyl ether,[13a] KOH or CH_3ONa,[13b] and Me_3SiOK.[13c]

$$2R_2Si(H)-NR'(H) \xrightarrow{\text{base}} \begin{matrix}R_2Si-NR' \\ | \quad | \\ R'N-SiR_2\end{matrix} + 2H_2 \quad (8)$$

Table I. Preparation of Substitution Products and Cyclodisilazanes from $(CH_3)_2Si(H)NHR$

$$(CH_3)_2Si(H)NHR \xrightarrow[2.\ E\text{-}X/\text{solvent}]{1.\ n\text{-BuLi}} (CH_3)_2Si(H)N(E)R + \text{cyclo-}[(CH_3)_2SiNR]_2$$

				I	II
example no.	R	solv	E-X	yields, % I	II
1[a]	$(CH_3)_2SiH$	THF	$(CH_3)_3SiCl$	100	0
2	$(CH_3)_2SiH$	THF	CH_3I	100	0
3[b]	$(CH_3)_2SiH$	THF	$(CH_3CH_2)_3SiCl$	86	0
4	$(CH_3)_2SiH$	hexane	$(CH_3)_3SiCl$	9	83
5[c]	$(CH_3)_2SiH$	benzene	$(CH_3)_3SiCl$	33	60
6	$(CH_3)_2SiH$	toluene	$(CH_3)_3SiCl$	15	79
7	$(CH_3)_2SiH$	hexane	$(CH_3)_2SiHCl$	75	trace
8[d]	$(CH_3)_2SiH$	hexane	$(CH_3CH_2)_3SiCl$	0	46
9	$(CH_3)_2SiH$	hexane	$(CH_3)_3CCl$	6 (E = H)	74
10	$(CH_3)_2CH$	THF	$(CH_3)_3SiCl$	94	0
11	$(CH_3)_2CH$	hexane	$(CH_3)_3SiCl$	5	51
12	$(CH_3)_2CH$	hexane	$(CH_3)_2SiHCl$	61	trace
13	$(CH_3)_3C$	THF	$(CH_3)_3SiCl$	57	0
14	$(CH_3)_3C$	THF	$(CH_3)_2SiHCl$	81	0
15[e]	$(CH_3)_3C$	hexane	$(CH_3)_3SiCl$	0	66
16	$(CH_3)_3C$	hexane	$(CH_3)_2SiHCl$	32	66

[a] Reaction temperature = −78 °C. [b] Deprotonation performed in hexane and insoluble lithium amide separated by filtration and then redissolved in THF–see text. [c] After addition of $(CH_3)_3SiCl$, heated at reflux 11 h. [d] After addition of $(CH_3CH_2)_3SiCl$, heated at reflux 41 h. [e] After addition of $(CH_3)_3SiCl$, heated at reflux 6 h.

In further studies of the tetramethyldisilazane/*n*-butyllithium reaction we found that the formation of the cyclodisilazane and/or the substitution product is remarkably sensitive to both reaction solvent and to the quench reagent. These results are summarized in Table I.

The addition of *n*-butyllithium to a solution of tetramethyldisilazane in benzene at 5 °C produced a white precipitate which again disappeared when the reaction mixture was heated. Trimethylchlorosilane was subsequently added to the reaction mixture, and GLC analysis of the solution showed a 33% yield of the substitution product $[(CH_3)_2SiH]_2NSi(CH_3)_3$ and a 60% yield of the cyclodisilazane $[(CH_3)_2SiNSi(CH_3)_2H]_2$ (Table I, example 5). A similar result was obtained when toluene was used as the reaction solvent (Table I, example 6).

A surprising result was obtained when the tetramethyldisilazane/*n*-butyllithium reaction mixture in hexane was treated with dimethylchlorosilane, $(CH_3)_2SiHCl$, instead of $(CH_3)_3SiCl$. Gas chromatographic analysis of this reaction mixture showed only a trace of the (expected) cyclodisilazane and a 75% yield of the substitution product tris(dimethylsilyl)amine, $[(CH_3)_2SiH]_3N$ (Table I, example 7). On the other hand, when the $[(CH_3)_2SiH]_2NH/n\text{-}C_4H_9Li$ reaction mixture in hexane was treated with triethylchlorosilane, a very slow reaction occurred. The reaction mixture was heated at reflux for 41 h, and subsequent GLC analysis showed a 46% yield of cyclo-$[(CH_3)_2SiNSi(CH_3)_2H]_2$ and a 53% yield of $(CH_3CH_2)_3SiH$ (eq 9). This experiment proved that LiH is a product of the cyclodisilazane-forming reaction and that

(10) Breed, L. W.; Budde, W. L.; Elliott, R. L. *J. Organomet. Chem.* **1966**, *6*, 676.
(11) Peake, J. S. (Minnesota Mining and Manufacturing Co.) Fr. Pat. 1 350 220, 1964; *Chem. Abstr.* **1964**, *60*, 15912.
(12) Andrianov, U. A.; Shkol'nik, M. I.; Syrtsova, Zh. S.; Petrov, K. I.; Kopylov, V. M.; Zaitseva, M. G.; Koroleva, E. A. *Dokl. Akad. Nauk SSSR* **1975**, *223*, 347.
(13) (a) Monsanto Company Neth. Appl. 6 507 996, 1965; *Chem. Abstr.* **1966**, *64*, 19677. (b) Andrianov, K. A.; Kopylov, V. M.; Khananashvili, L. M.; Nesterova, T. V. *Dokl. Akad. Nauk SSR* **1967**, *176*, 85. (c) Andrianov, K. A.; Shkol'nik, M. I.; Kopylov, V. M.; Prikhod'ko, P. L. *Dokl. Adad. Nauk SSR* **1976**, *227*, 352. (d) Further examples may be found in a review on cyclodisilazanes: Zhinkin, D. Ya.; Varezhkin, Yu. M.; Morgunova, M. M. *Russ. Chem. Rev. (Engl. Transl.)* **1980**, *49*, 1149.

$$[(CH_3)_2SiH]_2NH + n\text{-}C_4H_9Li \xrightarrow{\text{hexane}} \text{white precipitate} \xrightarrow{(CH_3CH_2)_3SiCl}$$

$$\begin{matrix}(CH_3)_2Si-NSi(CH_3)_2H \\ | \quad\quad | \\ H(CH_3)_2SiN-Si(CH_3)_2 \\ 46\%\end{matrix} + [LiH] \rightarrow (CH_3CH_2)_3SiH + LiCl \quad (9)$$

53%

it reacts with the chlorosilane quench to produce the respective Si–H compound, in this case, $(CH_3CH_2)_3SiH$.

This precipitate had to be either $[(CH_3)_2SiH]_2NLi$, which is insoluble in nonpolar solvents but soluble in THF, or LiH, the byproduct of cyclodisilazane formation. To distinguish between these two possibilities, such a *n*-butyllithium/tetramethyldisilazane in hexane reaction mixture was filtered to remove the white precipitate. The filtrate was analyzed by GLC; no volatile products were present. The white precipitate dissolved easily in THF, and this solution then was quenched with $(C_2H_5)_3SiCl$. GLC analysis of this reaction mixture showed that no cyclodisilazane or $(C_2H_5)_3SiH$ had been formed, but instead, a new compound, $[(CH_3)_2SiH]_2NSi(C_2H_5)_3$ (86% yield), had been produced (Table I, example 8). Thus the white precipitate was $[(CH_3)_2SiH]_2NLi$. The nature of the solvent apparently is important during the *quenching reaction only*, and the cyclodisilazane is not formed *until the* quench *reagent is added*. The mechanistic implications of these results will be discussed below.

An interesting and useful result was obtained when the usual $[(CH_3)_2SiH]_2SiH]_2NLi$ solution in hexane was quenched with $(CH_3)_3CCl$, which can serve as a proton source.[14] The usual reaction procedure produced a 6% yield of the starting material $[(CH_3)_2SiH]_2NH$, which arises from deprotonation of the $(CH_3)_3CCl$ by the *N*-lithiosilazane and a 74% yield of the cyclodisilazane (eq 10). If

$$[(CH_3)_2SiH]_2NH + n\text{-}C_4H_9Li \xrightarrow{\text{hexane}} \xrightarrow{(CH_3)_3CCl}$$

$$\begin{matrix}[(CH_3)_2SiH]_2NH \\ 6\%\end{matrix} + \begin{matrix}(CH_3)_2Si-NSi(CH_3)_2H \\ | \quad\quad | \\ H(CH_3)_2SiN-Si(CH_3)_2 \\ 74\%\end{matrix} + LiCl + CH_2{=}C(CH_3)_2 \quad (10)$$

a large quantity of the cyclodisilazane were desired, this would probably be the method of choice because the byproduct of this reaction $[(CH_3)_2SiH]_2NH$ would be much easier to separate from the cyclodisilazane than $[(CH_3)_2SiH]_2NSi(CH_3)_3$, which is a byproduct when the reaction mixture is quenched with $(CH_3)_3SiCl$.

Other dimethylhydroaminosilanes appear to behave similarly to tetramethyldisilazane. These materials were easily prepared in good yield by the reaction of $(CH_3)_2SiHCl$ with the appropriate amine. The addition of *n*-C_4H_9Li to a THF solution of $(CH_3)_2Si(H)NHCH(CH_3)_2$ or $(CH_3)_2Si(H)NHC(CH_3)_3$, followed by the addition of $(CH_3)_3SiCl$, produced a good yield of the expected substitution product (Table I, examples 10, 13). Several attempts to improve the yield of example 13 were unsuccessful. However, an excellent yield of the substitution product was obtained when a THF solution of $(CH_3)_2Si(H)N(Li)C(CH_3)_3$ was quenched with the less hindered $(CH_3)_2SiHCl$ instead of $(CH_3)_3SiCl$ (Table I, example 14). Cyclodisilazanes also may be prepared from these compounds using hexane as the solvent. Thus, the addition of *n*-butyllithium to a solution of $(CH_3)_2Si(H)NHCH(CH_3)_2$ or $(CH_3)_2Si(H)NHC(CH_3)_3$ in hexane, followed by the addition of $(CH_3)_3SiCl$, produced a good yield of the respective cyclodisilazane (Table I, examples 11, 15). When the $(CH_3)_2Si(H)N(Li)R$ solution in hexane was quenched with $(CH_3)_2SiHCl$, the substitution product was the major one when R was $CH(CH_3)_2$, but the cyclodisilazane was the major product when R was $C(CH_3)_3$ (Table I, examples 12, 16).

To summarize, the reaction of *n*-butyllithium with dimethylhydroaminosilanes, $(CH_3)_2Si(H)NHR$ (R = $(CH_3)_2SiH$, $CH(CH_3)_2$, $C(CH_3)_3$), produces an *N*-lithiosilazane, $(CH_3)_2Si(H)N(Li)R$. When this new lithium reagent is quenched with a chlorosilane, either a substitution product, $(CH_3)_2Si(H)N(R)SiR'_3$, or a cyclodisilazane, cyclo-$[(CH_3)_2SiNR]_2$, is formed, depending on the reaction solvent, the quench reagent, and the nature of R. Specifically, the results that must be explained are as follows. 1. When the solvent is THF, a substitution product is always produced, whereas when nonpolar solvents (e.g., hexane, benzene, toluene) are used, a mixture of the substitution product and the cyclodisilazane results. 2. When $[(CH_3)_2SiH]_2NLi$ in hexane is quenched with $(CH_3)_2SiHCl$, the substitution product is formed in 75% yield. When $[(CH_3)_2SiH]_2NLi$ in hexane is quenched with $(CH_3)_3SiCl$, the cyclodisilazane is formed in 83% yield. 3. The cyclodisilazane formed only after the chlorosilane quench has been added.

Mechanism of the Cyclodisilazane-Forming Reaction. Compounds with the general formula $R_2Si(X)NHR'$, where X is Cl or F, are known to be converted to cyclodisilazanes when they are deprotonated with *n*-butyllithium and the resulting *N*-lithiohaloaminosilane is heated. Two different mechanisms have been proposed for this conversion, one for the compounds where X = Cl and a different one for compounds with X = F. An "organometallic" mechanism was proposed by Breed and Wiley for the cyclization of *N*-lithio-1,3-dichlorotetraorganodisilazanes, $(ClSiR_2)_2NLi$.[15] This mechanism features the nucleophilic displacement of chlorine from silicon in one molecule by the amide function of another to form LiCl and a new Si–N bond. This step is then repeated within the new molecule and the ring is closed (eq 11).

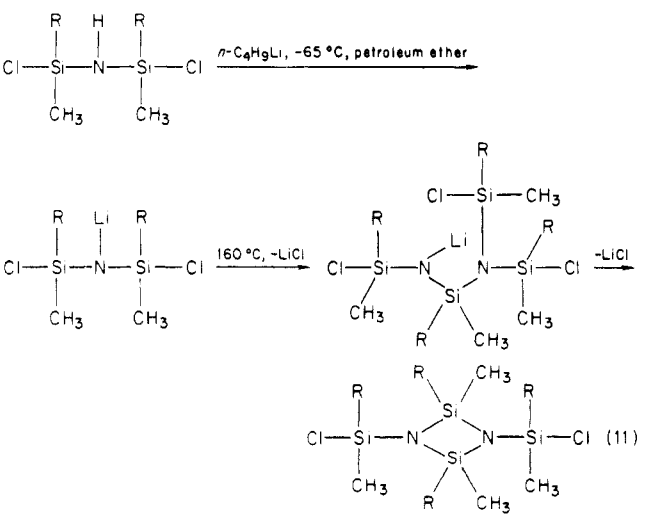

(11)

Another mechanism was proposed by Klingebiel, Bentmann, and Meller for the preparation of cyclodisilazanes from *N*-lithioaminofluorosilanes. These workers proposed that *N*-lithioaminofluorosilanes unimolecularly eliminate LiF to produce an unstable "silaimine", $R_2Si{=}NR'$, which dimerizes in head-to-tail fashion to produce the cyclodisilazane (eq 12).[16]

(14) Sommer, K. *Z. Anorg. Allg. Chem.* **1970**, *376*, 37.

(15) Breed, L. W.; Wiley, J. C., Jr. *Inorg. Chem.* **1972**, *11*, 1634.

(16) Klingebiel, U.; Bentmann, D.; Meller, A. *J. Organomet. Chem.* **1978**, *144*, 381.

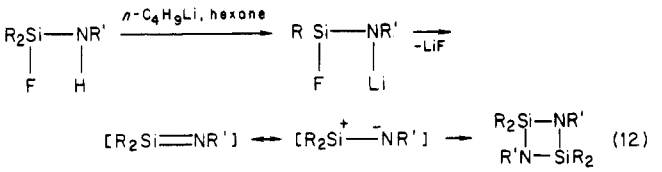

The question of which of these mechanisms can best account for our results concerning the dimerization of $R_2Si(H)N(Li)R'$ compounds was subjected to experimental scrutiny. The organometallic mechanism for this reaction is shown in (eq 13). The polar displacement of the hydride

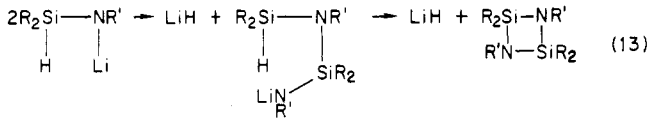

from silicon by aliphatic or aromatic lithium or sodium amides is a well-known reaction,[17,18] although it usually requires high temperatures. However, it would be difficult to explain some of our observations on the basis of this mechanism. 1. Cyclodisilazanes are produced in nonpolar solvents but not at all in THF. This is exactly the *opposite* of what would be expected for a polar nucleophilic displacement process which always occurs more readily in a polar solvent such as THF than in a nonpolar solvent. This is in part because lithium reagents are more associated and, therefore, less reactive in hydrocarbon solvents than in ether solvents.[19,20] *N*-Lithiohexamethyldisilazane, $[(CH_3)_3Si]_2NLi$, is trimeric in the solid state[21] and a dimer–tetramer equilibrium apparently obtains in hydrocarbon solvents.[22] In THF, however, a monomer–dimer equilibrium is rapidly established.[22] 2. Cyclodisilazane formation does not occur until *after* the electrophilic quench reagent is added and is very dependent on the steric requirements of the reagent which is used. The nucleophilic displacement of H from silicon by lithium amides occurs spontaneously when the two reactants are mixed and heated; i.e., the reaction mixture does not need to be quenched with anything.

Two experiments were designed to test whether the organometallic mechanism could be operating in our cyclodisilazane-forming reaction. In the first experiment, we hoped to prepare by an independent synthesis the intermediate condensation product of two $(CH_3)_2Si(H)N(Li)R$ molecules and then determine whether, under the appropriate reaction conditions, this intermediate would in fact cyclize to the cyclodisilazane. This scheme is outlined in (eq 14). Thus $(CH_3)_2Si[NHCH(CH_3)_2]_2$ was prepared

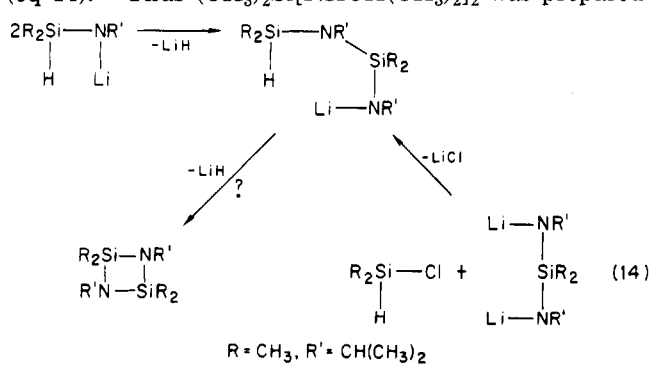

R = CH_3, R' = $CH(CH_3)_2$

from $(CH_3)_2CHNH_2$ and $(CH_3)_2SiCl_2$, and 2 equiv of *n*-C_4H_9Li were added to a solution of this bis(amino)silane in hexane at 0 °C to product $(CH_3)_2Si[N(Li)CH(CH_3)_2]_2$. At room temperature, exactly 1 equiv of $(CH_3)_2SiHCl$ was added and the reaction mixture was stirred for 1 h. Another equivalent of $(CH_3)_2SiHCl$ then was added to quench all of the lithium reagents, and the reaction mixture was examined by GLC. Two products were isolated, the cyclodisilazane, cyclo-$[(CH_3)_2SiNCH(CH_3)_2]_2$, in 46% yield, and a disubstitution product, $(CH_3)_2Si[N(Si(CH_3)_2H)CH(CH_3)_2]_2$, in 17% yield (eq 15). It is clear from this experiment that ring closure via intramolecular nucleophilic displacement of hydrogen from silicon by an N–Li function *can* occur.

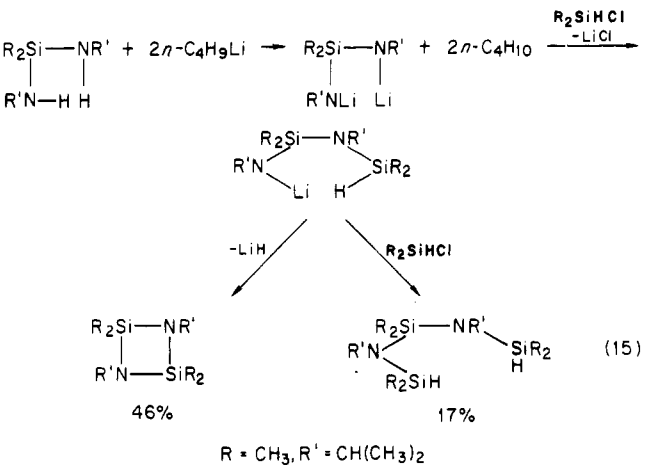

R = CH_3, R' = $CH(CH_3)_2$

Another experiment was carried out in order to determine whether the first step of the organometallic reaction can occur, that is, whether an *N*-lithiosilazane will react with an Si–H group in another aminosilane. To test this, a solution of *N*-lithiotetramethyldisilazane and 1,1,2,3,3-pentamethyldisilazane, $[(CH_3)_2SiH]_2NCH_3$ in hexane was heated at reflux. The reaction mixture than was quenched with $(CH_3)_3SiCl$ in the usual manner. The reaction scheme and the expected condensation product are shown in (eq 16). GLC analysis of the reaction mixture described above

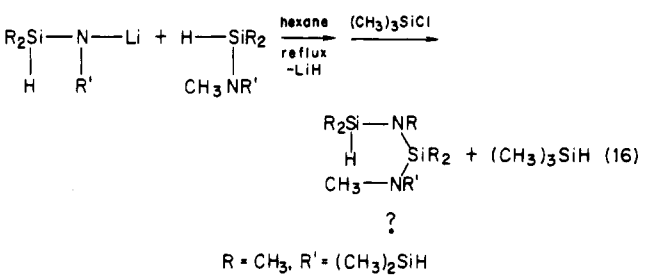

R = CH_3, R' = $(CH_3)_2SiH$

did *not* show any of the expected condensation product. Instead, the usual mixture of substitution product $[(CH_3)_2SiH]_2NSi(CH_3)_3$ (17%) and cyclodisilazane (76%) was observed, in addition to a 96% recovery of $[(CH_3)_2SiH]_2NCH_3$. It would seem that intermolecular condensation of an *N*-lithiosilazane with the Si–H bond of another silazane does *not* occur under the conditions where cyclodisilazane formation in this system is observed.

Can a "silaimine mechanism" explain the results which have been described? A scheme that has been considered is shown in eq 17.

Consider an *N*-lithiohydrosilazane in rapid equilibrium with a small amount of LiH and a silaimine. If the reverse of this reaction, i.e., the addition of LiH to a silaimine, is sufficiently fast ($k_{-1} \gg k_4$), no net chemistry (cyclodisilazane formation) would be observed until this equilibrium is perturbed. The addition of a reagent that reacts

(17) Gilman, H.; Hofferth, B.; Melvin, H. W.; Dunn, G. E. *J. Am. Chem. Soc.* **1950**, *72*, 5767.
(18) Fink, W. *Helv. Chim. Acta* **1966**, *49*, 1408.
(19) Lewis, H. L.; Brown, T. L. *J. Am. Chem. Soc.* **1970**, *92*, 4664.
(20) West, P.; Waack, R. *J. Am. Chem. Soc.* **1967**, *89*, 4395.
(21) Mootz, M.; Zinnius, A.; Bottscher, B. *Angew. Chem., Int. Ed. Engl.* **1969**, *8*, 378.
(22) Kimura, B. Y.; Brown, T. L. *J. Organomet. Chem.* **1971**, *26*, 57.

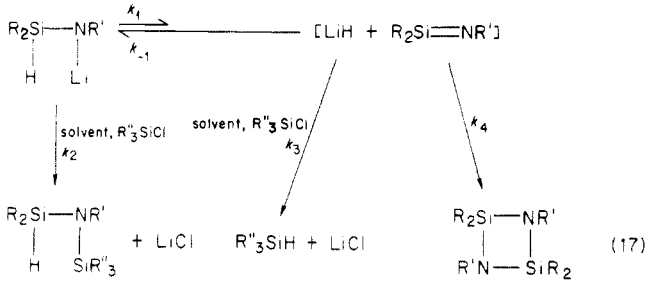

with LiH (e.g., $(CH_3)_3SiCl$) would perturb this equilibrium, however, by removing the LiH, thus forcing the reaction to the right and causing the silaimine to dimerize. Any reagent which can react with LiH also might be expected to react with the *N*-lithiosilazane. In the case of a chlorosilane quench, a substitution product would result. Thus, the varying amounts of the substitution product and the cyclodisilazane which have been observed might be the result of a *competition* between LiH and $(CH_3)_2Si(H)N(Li)R$ for the quench reagent (k_2 vs. k_3). Different solvents, different chlorosilane quenches, and different R' groups might affect the course of the reaction because they might change the relative values of k_2 and k_3. For example, when THF is the solvent, k_2 probably is relatively large in the case of all R_3SiCl because the *N*-lithiosilazane is not highly associated (probably largely monomeric). In hydrocarbon solvents, however, reactions of lithium reagents can be sluggish (k_2 = slow) because they are associated and thus the chemistry of LiH can be competative. Assuming that k_3 is fairly constant, the use of a smaller, more reactive chlorosilane (e.g., $(CH_3)_2SiHCl$) might give a value of k_2 sufficiently larger so that, as in THF medium, the simple substitution chemistry of $R_2Si(H)N(Li)R'$ would be observed. The value of k_2 would also be affected by the size of R', and this would explain why $(CH_3)_2Si(H)N(Li)CH(CH_3)_2$ when quenched by $(CH_3)_2SiHCl$ in hexane produces only the substitution product, but $(CH_3)_2Si(H)N(Li)C(CH_3)_3$ gives a mixture of the cyclodisilazane and the substitution product under the same conditions. We attempted to trap the proposed silaimine intermediate with hexamethylcyclotrisiloxane. This strained and reactive cyclotrisiloxane has been used to trap silaimines generated by the gas-phase pyrolysis of silyl azides.[23,24] The expected reaction product, the azasiloxane shown in eq 18, *was* not obtained. Instead, the usual mixture of substitution product and cyclodisilazane (in addition to a quantative recovery of the trapping reagent) was observed.

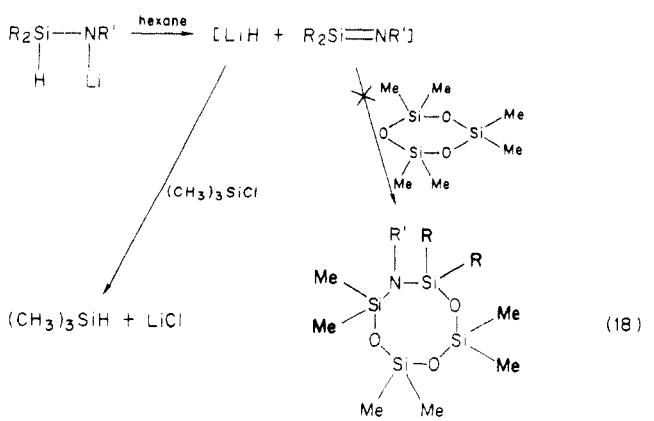

In conclusion, we can say that the dimerization of *N*-lithiohydrosilazanes to produce cyclodisilazanes is an interesting and synthetically useful reaction but is somewhat difficult to explain mechanistically. A mechanism involving the intramolecular elimination of LiH with formation of an unstable silaimine, $(CH_3)_2Si{=}NR'$, which subsequently dimerizes, can explain the effects of solvent, quench, and amine substituent (R') on the course of the reaction. This proposed silaimine intermediate has not been observed directly or trapped, however, and thus this mechanism can only be suggested as an explanation of the data. The alternative "organometallic" mechanism cannot account for the unusual variety of results which have been observed. However, it may possibly contribute to the reaction course. We have demonstrated that Si_2N_2 ring closure, the second step of this scheme, definitely can occur under the appropriate reaction conditions. The necessary first intermolecular condensation step could not be demonstrated though.

We have limited this study to the reactions of dimethylhydroaminosilanes with *n*-butyllithium. As noted earlier, sodium and potassium bases also have been used to induce such cyclodisilazane formation.[11-13] There are certain to be interesting and important cation effects in this chemistry, and these merit further study.

Experimental Section

General Comments. All reactions were carried out in flame-dried flasks under an atmosphere of pre-purified nitrogen. All solvents were reagent grade and were distilled under nitrogen from the appropriate drying agent (tetrahydrofuran, diethyl ether, benzene, and toluene from Na/benzophenone and hexane from $LiAlH_4$). Dimethylchlorosilane, trimethylchlorosilane, dimethyldichlorosilane, and triethylchlorosilane were freshly distilled from Mg filings. Methyl iodide and *tert*-butyl chloride were distilled from P_2O_5. Isopropylamine and *tert*-butylamine were distilled from CaO. Hexamethylcyclotrisiloxane and 1,1,2,3,3-pentamethyldisilazane were purchased from Petrarch and were used as received. *n*-Butyllithium (Alfa/Ventron, solution in hexane) was titrated by the method of Gilman and Cartledge.[25]

Analytical gas chromatography was performed by using a Hewlett-Packard 5750 gas chromatograph using a 6-ft SE-30 on Chromosorb P column programmed to increase in temperature from 100 to 250 °C at 6 °C/min. The internal standard method was used in yield determinations. Proton NMR spectra were obtained by using either a JEOL FX-90Q (90 MHz) or a Bruker WM-250 (250 MHz) spectrometer in $CDCl_3$ and are referenced to $CHCl_3$ at 7.24 ppm downfield from tetramethylsilane. Elemental analyses were performed by the Scandinavian Microanalytical Laboratory, Herlev, Denmark.

Deprotonation/Quenching Reactions of Dimethylhydroaminosilanes. A general procedure for the deprotonation of dimethylhydroaminosilanes by *n*-butyllithium and subsequent quenching is described below. A 50-mL, three-necked, round-bottomed flask was equipped with a gas-inlet tube, a glass stopper, a no-air rubber septum, and a stir bar and flame-dried under nitrogen. The flask was charged with 25 mL of the appropriate solvent and 5–10 mmol of the aminosilane. By syringe, 1 molar equiv of *n*-butyllithium was added and the reaction mixture was stirred at 0 °C for 1 h and then heated for 1–2 h unless otherwise noted in Table I. The appropriate electrophilic reagent was added and then the reaction mixture heated at reflux for 1–2 h unless otherwise noted. The reaction mixture was either filtered or centrifuged to remove the precipitated halide. The solution was analyzed by GC and samples of the product were collected by GC. Analytical and spectroscopic data for each of the compounds prepared in this work are given in Table II. Complete IR spectra can be found in ref 26.

Preparation of Dimethyl(isopropylamino)silane. A 1-L, three-necked, round-bottomed flask was equipped with an overhead stirrer, an addition funnel, and a Claisen adapter with a

(23) Parker, D. R.; Sommer, L. H. *J. Organomet. Chem.* **1976**, *110*, C1.
(24) Parker, D. R.; Sommer, L. H. *J. Am. Chem. Soc.* **1976**, *98*, 618.
(25) Gilman, H.; Cartledge, F. K. *J. Organomet. Chem.* **1964**, *2*, 447.
(26) Wiseman, G. H. "The Development and Application of Polysilazane Precursors to Ceramics"; Massachusetts Institute of Technology, Ph.D. Thesis, 1984.

Table II. Substitution and Cyclodisilazane Products from Dimethylhydroaminosilanes

compd	n^{20}_D (lit.)	anal. found (calcd) C	H	N	^{1}H NMR, δ
$[(CH_3)_2SiH]_2NSi(CH_3)_3$	1.4308 (1.4309)[a]				0.12 (s, 9 H, $Si(CH_3)_3$), 0.17 (d, J = 3.4 Hz, 6 H, $HSi(CH_3)_2$), 4.50 (sept, J = 3.4 Hz, 1 H, SiH)
$[(CH_3)_2SiH]_2NCH_3$	1.4123 (1.4135)[b]				0.12 (d, J = 2.9 Hz, 12 H, $HSi(CH_3)_2$), 2.47 (s, 3 H, NCH_3), 4.40 (sept, J = 2.9 Hz, 2 H, SiH)
cyclo-$[(CH_3)_2SiNSi(CH_3)_2H]_2$	1.4312 (1.4312)[c]				0.06 (d, J = 3.0 Hz, 12 H, $HSi(CH_3)_2$), 0.23 (s, 12 H, $Si(CH_3)_2$), 4.37 (sept, J = 3.0 Hz, 2 H, SiH)
$[(CH_3)_2SiH]_3N$	1.4255, n^{25}_D 1.4230 (n^{25}_D 1.4222)[d]				0.19 (d, J = 3.3 Hz, 18 H, $HSi(CH_3)_2$), 4.63 (sept, J = 3.3 Hz, 3 H, SiH)
$[(CH_3)_2SiH]_2NSi(CH_2CH_3)_3$	1.4568	48.64 (48.51)	11.70 (11.80)	5.69 (5.66)	0.19 (d, J = 3.4 Hz, 12 H, $HSi(CH_3)_2$), 0.69 (m, 6 H, $SiCH_2CH_3$), 0.90 (m, 9 H, $SiCH_2CH_3$), 4.50 (sept, J = 3.4 Hz, 2 H, SiH)
$(CH_3)_2Si(H)N[CH(CH_3)_2]Si(CH_3)_3$	1.4287	50.77 (50.72)	12.16 (12.24)	7.40 (7.39)	0.08 (s, 9 H, $Si(CH_3)_3$), 0.13 (d, J = 3.4 Hz, 6 H, $HSi(CH_3)_2$), 1.14 (d, J = 6.8 Hz, 6 H, $CH(CH_3)_2$), 3.27 (sept, J = 6.8 Hz, 1 H, $CH(CH_3)_2$, 4.50 (sept, J = 3.4 Hz, 1 H, SiH)
$[(CH_3)_2SiH]_2NCH(CH_3)_2$	1.4224	48.09 (47.93)	12.06 (12.07)	7.79 (7.98)	0.13 (d, J = 3.4 Hz, 12 H, $HSi(CH_3)_2$), 1.14 (d, J = 6.5 Hz, 6 H, $CH(CH_3)_2$), 3.27 (sept, J = 6.5 Hz, 1 H, $CH(CH_3)_2$), 4.47 (sept, J = 3.4 Hz, 2 H, SiH)
cyclo-$[(CH_3)_2SiNCH(CH_3)_2]_2$	1.4349	51.96 (52.11)	11.30 (11.37)	11.94 (12.15)	0.19 (s, 1i H, $SiCH_3$), 1.01 (d, J = 6.4 Hz, 12 H, $CHCH_3$), 3.19 (sept, J = 6.4 Hz, 2 H, $CH(CH_3)_2$)
$(CH_3)_2Si(H)N[C(CH_3)_3]Si(CH_3)_3$	1.4436	53.20 (53.13)	12.66 (12.38)	7.13 (6.88)	0.18 (s, 9 H, $Si(CH_3)_3$), 0.21 (d, J = 3.4 Hz, 6 H, $HSi(CH_3)_2$), 1.29 (s, 9 H, $C(CH_3)_3$), 4.59 (sept, J = 3.4 Hz, 1 H, SiH)
$[(CH_3)_2SiH]_2NC(CH_3)_3$	1.4358	50.62 (50.72)	12.22 (12.24)	6.84 (7.39)	0.18 (d, J = 3.4 Hz, 12 H, $HSi(CH_3)_2$), 1.26 (s, 9 H, $C(CH_3)_3$), 4.54 (sept, J = 3.4 Hz, 2 H, SiH)
cyclo-$[(CH_3)_2SiNC(CH_3)_3]_2$	mp 40–41.5 °C (35 °C)[e]	55.93 (55.75)	11.86 (11.69)	10.87 (10.83)	0.25 (s, 12 H, $Si(CH_3)_2$), 1.10 (s, 18 H, $C(CH_3)_3$)

[a] Breed, L. W.; Elliott, R. L. *J. Organomet. Chem.* **1968**, *11*, 447. [b] Andrianov, K. A.; Khananashvili, L. M.; Kopylov, V. M.; Nesterova, T. V. *Izv. Akad. Nauk SSSR, Ser. Khim.* **1968**, 351. [c] Reference 10. [d] Dennis, W. E.; Speier, J. L. *J. Org. Chem.* **1970**, *35*, 3879. [e] Reference 13a.

gas-inlet tube and a no-air rubber septum and flame-dried under nitrogen. The flask was charged with 300 mL of diethyl ether and 110 mL of isopropylamine (1.29 mol) and cooled to 0 °C. The addition funnel was charged with $(CH_3)_2SiHCl$ (0.459 mol) and an equal volume of ether. The contents of the addition funnel were added to the flask over a period of 1 h, and the reaction mixture then was stirred for an additional 30 min. The reaction mixture was filtered through a coarse-fritted Schlenk funnel, and the precipitate was washed with two 50-mL portions of ether. The ether was distilled from the filtrate through a 2-ft Vigreaux column. The product $(CH_3)_2Si(H)NHCH(CH_3)_2$ (73%) was isolated by distillation through a 1-ft Vigreaux column (bp 88.5 °C), n^{20}_D 1.3941 (lit.[27] n^{20}_D 1.3943; bp 87 °C). Anal. Calcd for $C_5H_{15}NSi$: C, 51.21; H, 12.89; N, 11.94. Found: C, 51.22; H, 12.75; N, 11.49. ^{1}H NMR: δ 0.08 (d, J = 3.4 Hz, 6 H, $SiCH_3$), 1.05 (d, J = 6.3 Hz, 6 H, $CHCH_3$), 2.84–3.16 (doublet of septets, $J(H_N)$ = 9.3 Hz, $J(H_C)$ = 6.3 Hz, 1 H, $CHCH_3$), 4.43 (sept, J = 3.4 Hz, 1 H, SiH).

Preparation of Dimethyl(*tert*-butylamino)silane. A reaction as described above between 150 mL of *tert*-butylamine (1.43 mol) and dimethylchlorosilane (0.459 mol) in 400 mL of diethyl ether produced, after distillation, a 62% yield of $(CH_3)_2Si(H)NHC(nCH_3)_3$, n^{20}_D 1.4042 (lit.[27] n^{20}_D 1.3940). Anal. Calcd for $C_6H_{17}NSi$: C, 54.89; H, 13.05; N, 10.67. Found: C, 55.04; H, 13.04; N, 10.31. ^{1}H NMR: δ 0.09 (d, J = 3.0 Hz, 6 H, $SiCH_3$), 1.14 (s, 9 H, $C(CH_3)_3$, 4.50 (sept, J = 3.0 Hz, 1 H, SiH).

Preparation of Bis(isopropylamino)dimethylsilane. A reaction as described above between 52.7 g of isopropylamine (0.892 mol) and 26.2 g of dimethyldichlorosilane (0.203 mol) in 400 mL of diethyl ether produced, after distillation through a 1-ft Vigreaux column, an 82% yield of $(CH_3)_2Si[N(H)CH(CH_3)_2]_2$, n^{20}_D 1.4150 (lit.[28] n^{20}_D 1.4158; bp 47–48 °C (11 mmHg)). ^{1}H NMR: δ −0.02 (s, 3 H, $Si(CH_3)_2$), 1.02 (d, 6 H, $CH(CH_3)_2$), 3.2 (br m, 1 H, $CH(CH_3)_2$).

Reaction of Bis(isopropylamino)dimethylsilane with *n*-Butyllithium in Hexane. Dimethylchlorosilane Quench. The standard reaction apparatus was charged with hexane (25 mL) and bis(isopropylamino)dimethylsilane (4.93 mmol) and cooled to 0 °C. By syringe, 2 equiv of n-C_4H_9Li were added (9.92 mmol) and the reaction mixture was stirred at 0 °C for 15 min and then heated at reflux for 15 min. At room temperature, 1 equiv of dimethylchlorosilane (4.95 mmol) was added and the reaction mixture was stirred for 1 h. A second equivalent of dimethylchlorosilane was added, and the reaction mixture was stirred for room temperature overnight. The usual workup and GC analysis showed the presence of two products which were

(27) Jarvie, S. W.; Lewis, D. *J. Chem. Soc.* **1963**, 4758.

(28) Wannagat, U.; Schreiner, G. *Monatsh. Chem.* **1965**, *96*, 1916.

collected and identified as cyclo-$[(CH_3)_2SiNCH(CH_3)_2]_2$ (46%) on the basis of its ^1H NMR and IR spectra and $[(CH_3)_2SiHNCH(CH_3)_2]_2Si(CH_3)_2$ (17%), n^{20}_D 1.4582. Anal. Calcd for $C_{12}H_{34}N_2Si_3$: C, 49.50; H, 11.79; N, 9.64. Found: C, 49.48; H, 11.72; N, 9.78. ^1H NMR: δ 0.17 (s, 6 H, $Si(CH_3)_2$), 0.17 (d, J = 3.4 Hz, 12 H, $HSi(CH_3)_2$), 1.15 (d, J = 6.3 Hz, 12 H, $CH(CH_3)_2$), 3.43 (sept, J = 6.3 Hz, 2 H, $CH(CH_3)_2$), 4.54 (sept, J = 3.4 Hz, 2 H, SiH).

Reaction of Tetramethyldisilazane with *n*-Butyllithium in Hexane Followed by Addition of 1,1,2,3,3-Pentamethyldisilazane. Trimethylchlorosilane Quench. The standard reaction apparatus was charged with hexane (25 mL) and tetramethyldisilazane (8.61 mmol) and cooled to 0 °C. By syringe, 8.68 mmol of n-C_4H_9Li was added (a white precipitate formed), and the reaction mixture was stirred at 0 °C for 1 h. Still at 0 °C, $[(CH_3)_2SiH]_2NCH_3$ (8.62 mmol) was added but no reaction was observed. The reaction mixture was heated at reflux for 1 h (the precipitate disappeared), but still no reaction of the $[(CH_3)_2SiH]_2NCH_3$ was evident. Trimethylchlorosilane (9.47 mmol) was added, and the reaction mixture was heated at reflux for another 11 h. The usual workup and GC analysis showed that the reaction mixture contained unreacted $[(CH_3)_2SiH]_2NCH_3$ (96%), the substitution product $[(CH_3)_2SiH]_2NSi(CH_3)_3$ (17%), and the cyclodisilazane cyclo-$[(CH_3)_2SiNSi(CH_3)_2H]_2$ (76%). All three compounds were identified by comparison of their GC retention times and ^1H NMR spectra with those of the compounds previously described.

Reaction of Tetramethyldisilazane with *n*-Butyllithium in Hexane Followed by Addition of Hexamethylcyclotrisiloxane. Trimethylchlorosilane Quench. The standard reaction apparatus was charged with hexane (25 mL) and tetramethyldisilazane (8.61 mmol) and cooled to 0 °C. By syringe, 8.67 mmol of n-C_4H_9Li was added and the reaction mixture was stirred at 0 °C for 1 h. An excess of cyclo-$[(CH_3)_2SiO]_3$ (24 mmol) was added, and the reaction mixture was heated at reflux for 30 min (a clear solution was formed). Trimethylchlorosilane (11.8 mmol) was added and the reaction mixture was heated at reflux for 30 min (a clear solution was formed). The usual workup and GC analysis showed the presence of unreacted cyclo-$[(CH_3)_2SiO]_3$ (100%) and two products $[(CH_3)_2SiH]_2NSi(CH_3)_3$ (9%) and cyclo-$[(CH_3)_2SiNSi(CH_3)_2H]_2$ (74%). All three compounds were identified by comparison of their GC retention times and ^1H NMR spectra with those of the compounds previously described.

Acknowledgment. We are grateful to the Office of Naval Research for partial support of this work and to the M.I.T. Undergraduate Research Opportunities Program for assistance to D.R.W.

Registry No. I (R = $(CH_3)_2SiH$, E = $(CH_3)_3Si$), 16642-71-0; I (R = $(CH_3)_2SiH$, E = CH_3), 19923-75-2; I (R = $(CH_3)_2SiH$, E = $(CH_3CH_2)_3Si$), 98689-72-6; I (R = $(CH_3)_2SiH$, E = $(CH_3)_2SiH$), 21331-86-2; I (R = $(CH_3)_2SiH$, E = H, 15933-59-2; I (R = $(CH_3)_2CH$, E = $(CH_3)_3Si$), 98689-73-7; I (R = $(CH_3)_2CH$, E = $(CH_3)_2SiH$), 98689-75-9; I (R = $(CH_3)_3C$, E = $(CH_3)_3Si$), 72525-59-8; I (R = $(CH_3)_3C$, E = $(CH_3)_2SiH$), 72525-61-2; II (R = $(CH_3)_2SiH$), 13270-87-6; II (R = $(CH_3)_2CH$), 98689-74-8; II (R = $(CH_3)_3C$), 5931-45-3; $[(CH_3)_2SiH]_2NCH_3$, 19923-75-2; $[(CH_3)_2SiHNCH(CH_3)_2]_2Si(CH_3)_2$, 98689-76-0; $(CH_3)_2Si(H)NH(CH_3)_2SiH$, 15933-59-2; $(CH_3)_2Si(H)NH(CH_3)_2CH$, 18135-38-1; $(CH_3)_2Si(H)NH(CH_3)_3C$, 18182-35-9; $(CH_3)_3CCl$, 507-20-0; $(CH_3)_2Si[NHCH(CH_3)_2]_2$, 6026-42-2; $(CH_3CH_2)_3SiH$, 617-86-7; $(CH_3)_3SiCl$, 75-77-4; CH_3I, 74-88-4; $(CH_3CH_2)_3SiCl$, 994-30-9; $(CH_3)_2SiHCl$, 1066-35-9; $(CH_3)_2SiCl_2$, 75-78-5; cyclo-$[(CH_3)_2SiO]_3$, 541-05-9.

Electronic Structures and Reactivity of Tricarbonyltropyliummetal Complexes

David A. Brown,* Noel J. Fitzpatrick, Michael A. McGinn, and Thomas H. Taylor

Department of Chemistry, University College, Belfield, Dublin 4, Ireland

Received April 22, 1985

The extended Hückel molelcular orbital and interaction determinant reactivity methods are used to examine the electronic structures and reactivities of the complexes $[(\eta^7\text{-}C_7H_7)M(CO)_3]^+$ (M = Cr, Mo, W). Calculated ground-state properties are compared with those of the analogous $(\eta^6\text{-}C_6H_6)M(CO)_3$ and (7-*exo*-η-1,6-$C_7H_7OCH_3)M(CO)_3$ series. Charges, frontier charge densities, and interaction energies are used to explain the recent observation of initial metal and carbonyl attack by alkoxide on the tricarbonyltropyliummetal cations at low temperatures, while extended Hückel results correlate with the isolation of the 7-exo ring adduct as the thermodynamically stable product from this reaction.

Introduction

Cations of the type $[(\eta^7\text{-}C_7H_7)M(CO)_3]^+$, where M = Cr, Mo, and W, continue to attract considerable experimental interest, and their syntheses, structures, and reactivities toward nucleophilic reagents have been extensively investigated.[1-21] Yet despite the accumulation of a wealth of data, the factors influencing the regioselectivity of such nucleophilic additions are still not clear. These reactions generally lead to isolation of 7-exo ring addition products. However, in the following paper spectroscopic evidence is reported for the formation of low-temperature adducts

(1) Brown, D. A.; Fitzpatrick, N. J.; McGinn, M. A. *J. Organomet. Chem.* **1984**, *275*, C5.
(2) Dauben, H. J.; Honnen, L. R. *J. Am. Chem. Soc.* **1958**, *80*, 5570.
(3) Munro, J. D.; Pauson, P. L. *J. Chem. Soc.* **1961** 3475, 3579, 3484.
(4) Baikie, P. E.; Mills, O. S.; Pauson, P. L.; Smith, G. H.; Valentine, J. H. *J. Chem. Soc., Chem. Commun.* **1965**, 425.
(5) Pauson, P. L.; Smith, G. H.; Valentine, J. H. *J. Chem. Soc. C* **1967**, 1057, 1061.
(6) Pauson, P. L.; Todd, K. H. *J. Chem. Soc. C* **1970**, 2315, 2636, 2638.
(7) Sneeden, R. P. A. "Organochromium Compounds"; Academic Press: New York, 1975.
(8) Khand, I. U.; Pauson, P. L.; Watts, W. E. *J. Chem. Soc. C* **1969**, 2024.
(9) Foreman, M. *J. Chem. Soc., Perkin Trans. 2* **1970**, 1141.
(10) Mohr, D.; Wienand, H.; Ziegler, M. L. *Z. Naturforsch, B.: Anorg. Chem., Org. Chem.* **1976**, *31B*, 66.
(11) Tremmel, P. O.; Wiedenhammer, K.; Wienand, H.; Ziegler, M. L. *Z. Naturforsch, B: Anorg. Chem., Org. Chem.* **1975**, *30B*, 699.
(12) Hoch, G.; Panter, R.; Ziegler, M. L. *Z. Naturforsch, B: Anorg. Chem., Org. Chem.* **1976**, *31B*, 294.
(13) Salzer, A. *Inorg. Chim. Acta* **1976**, *17*, 221.
(14) Gower, M.; John, G. R.; Kane-Maguire, L. A. P.; Odiaka, T. I.; Salzer, A. *J. Chem. Soc., Dalton Trans.* **1979**, 2003.
(15) John, G. R.; Kane-Maguire, L. A. P. *J. Chem. Soc., Dalton Trans.* **1979**, 1196.
(16) Atton, J. G.; Hassan, L. A.; Kane-Maguire, L. A. P. *Inorg. Chim. Acta* **1980**, *41*, 245.
(17) Al-Kathumi, K. M.; Kane-Maguire, L. A. P. *J. Organomet. Chem.* **1975**, *102*, C4.
(18) King, R. B.; Fronzaglia, A. *Inorg. Chem.* **1966**, *5*, 1837.
(19) Müller, J. *Angew. Chem. Int. Ed. Engl.* **1972**, *11*, 653.
(20) Müller, J.; Fenderl, K. *Chem. Ber.* **1970**, *103*, 3128.
(21) Hackett, P.; Jaouen, G. *Inorg. Chim. Acta* **1975**, L19.

0276-7333/86/2305-0152$01.50/0

collected and identified as cyclo-$[(CH_3)_2SiNCH(CH_3)_2]_2$ (46%) on the basis of its ^1H NMR and IR spectra and $[(CH_3)_2SiHNCH(CH_3)_2]_2Si(CH_3)_2$ (17%), n^{20}_D 1.4582. Anal. Calcd for $C_{12}H_{34}N_2Si_3$: C, 49.50; H, 11.79; N, 9.64. Found: C, 49.48; H, 11.72; N, 9.78. ^1H NMR: δ 0.17 (s, 6 H, $Si(CH_3)_2$), 0.17 (d, J = 3.4 Hz, 12 H, $HSi(CH_3)_2$), 1.15 (d, J = 6.3 Hz, 12 H, $CH(CH_3)_2$), 3.43 (sept, J = 6.3 Hz, 2 H, $CH(CH_3)_2$), 4.54 (sept, J = 3.4 Hz, 2 H, SiH).

Reaction of Tetramethyldisilazane with *n*-Butyllithium in Hexane Followed by Addition of 1,1,2,3,3-Pentamethyldisilazane. Trimethylchlorosilane Quench. The standard reaction apparatus was charged with hexane (25 mL) and tetramethyldisilazane (8.61 mmol) and cooled to 0 °C. By syringe, 8.68 mmol of n-C_4H_9Li was added (a white precipitate formed), and the reaction mixture was stirred at 0 °C for 1 h. Still at 0 °C, $[(CH_3)_2SiH]_2NCH_3$ (8.62 mmol) was added but no reaction was observed. The reaction mixture was heated at reflux for 1 h (the precipitate disappeared), but still no reaction of the $[(CH_3)_2SiH]_2NCH_3$ was evident. Trimethylchlorosilane (9.47 mmol) was added, and the reaction mixture was heated at reflux for another 11 h. The usual workup and GC analysis showed that the reaction mixture contained unreacted $[(CH_3)_2SiH]_2NCH_3$ (96%), the substitution product $[(CH_3)_2SiH]_2NSi(CH_3)_3$ (17%), and the cyclodisilazane cyclo-$[(CH_3)_2SiNSi(CH_3)_2H]_2$ (76%). All three compounds were identified by comparison of their GC retention times and ^1H NMR spectra with those of the compounds previously described.

Reaction of Tetramethyldisilazane with *n*-Butyllithium in Hexane Followed by Addition of Hexamethylcyclotrisiloxane. Trimethylchlorosilane Quench. The standard reaction apparatus was charged with hexane (25 mL) and tetramethyldisilazane (8.61 mmol) and cooled to 0 °C. By syringe, 8.67 mmol of n-C_4H_9Li was added and the reaction mixture was stirred at 0 °C for 1 h. An excess of cyclo-$[(CH_3)_2SiO]_3$ (24 mmol) was added, and the reaction mixture was heated at reflux for 30 min (a clear solution was formed). Trimethylchlorosilane (11.8 mmol) was added and the reaction mixture was heated at reflux for 30 min (a clear solution was formed). The usual workup and GC analysis showed the presence of unreacted cyclo-$[(CH_3)_2SiO]_3$ (100%) and two products $[(CH_3)_2SiH]_2NSi(CH_3)_3$ (9%) and cyclo-$[(CH_3)_2SiNSi(CH_3)_2H]_2$ (74%). All three compounds were identified by comparison of their GC retention times and ^1H NMR spectra with those of the compounds previously described.

Acknowledgment. We are grateful to the Office of Naval Research for partial support of this work and to the M.I.T. Undergraduate Research Opportunities Program for assistance to D.R.W.

Registry No. I (R = $(CH_3)_2SiH$, E = $(CH_3)_3Si$), 16642-71-0; I (R = $(CH_3)_2SiH$, E = CH_3), 19923-75-2; I (R = $(CH_3)_2SiH$, E = $(CH_3CH_2)_3Si$), 98689-72-6; I (R = $(CH_3)_2SiH$, E = $(CH_3)_2SiH$), 21331-86-2; I (R = $(CH_3)_2SiH$, E = H, 15933-59-2; I (R = $(CH_3)_2CH$, E = $(CH_3)_3Si$), 98689-73-7; I (R = $(CH_3)_2CH$, E = $(CH_3)_2SiH$), 98689-75-9; I (R = $(CH_3)_3C$, E = $(CH_3)_3Si$), 72525-59-8; I (R = $(CH_3)_3C$, E = $(CH_3)_2SiH$), 72525-61-2; II (R = $(CH_3)_2SiH$), 13270-87-6; II (R = $(CH_3)_2CH$), 98689-74-8; II (R = $(CH_3)_3C$), 5931-45-3; $[(CH_3)_2SiH]_2NCH_3$, 19923-75-2; $[(CH_3)_2SiHNCH(CH_3)_2]_2Si(CH_3)_2$, 98689-76-0; $(CH_3)_2Si(H)NH(CH_3)_2SiH$, 15933-59-2; $(CH_3)_2Si(H)NH(CH_3)_2CH$, 18135-38-1; $(CH_3)_2Si(H)NH(CH_3)_3C$, 18182-35-9; $(CH_3)_3CCl$, 507-20-0; $(CH_3)_2Si[NHCH(CH_3)_2]_2$, 6026-42-2; $(CH_3CH_2)_3SiH$, 617-86-7; $(CH_3)_3SiCl$, 75-77-4; CH_3I, 74-88-4; $(CH_3CH_2)_3SiCl$, 994-30-9; $(CH_3)_2SiHCl$, 1066-35-9; $(CH_3)_2SiCl_2$, 75-78-5; cyclo-$[(CH_3)_2SiO]_3$, 541-05-9.

Electronic Structures and Reactivity of Tricarbonyltropyliummetal Complexes

David A. Brown,* Noel J. Fitzpatrick, Michael A. McGinn, and Thomas H. Taylor

Department of Chemistry, University College, Belfield, Dublin 4, Ireland

Received April 22, 1985

The extended Hückel molelcular orbital and interaction determinant reactivity methods are used to examine the electronic structures and reactivities of the complexes $[(\eta^7\text{-}C_7H_7)M(CO)_3]^+$ (M = Cr, Mo, W). Calculated ground-state properties are compared with those of the analogous $(\eta^6\text{-}C_6H_6)M(CO)_3$ and (7-*exo*-η-1,6-$C_7H_7OCH_3)M(CO)_3$ series. Charges, frontier charge densities, and interaction energies are used to explain the recent observation of initial metal and carbonyl attack by alkoxide on the tricarbonyltropyliummetal cations at low temperatures, while extended Hückel results correlate with the isolation of the 7-exo ring adduct as the thermodynamically stable product from this reaction.

Introduction

Cations of the type $[(\eta^7\text{-}C_7H_7)M(CO)_3]^+$, where M = Cr, Mo, and W, continue to attract considerable experimental interest, and their syntheses, structures, and reactivities toward nucleophilic reagents have been extensively investigated.[1-21] Yet despite the accumulation of a wealth of data, the factors influencing the regioselectivity of such nucleophilic additions are still not clear. These reactions generally lead to isolation of 7-exo ring addition products. However, in the following paper spectroscopic evidence is reported for the formation of low-temperature adducts

(1) Brown, D. A.; Fitzpatrick, N. J.; McGinn, M. A. *J. Organomet. Chem.* **1984**, *275*, C5.
(2) Dauben, H. J.; Honnen, L. R. *J. Am. Chem. Soc.* **1958**, *80*, 5570.
(3) Munro, J. D.; Pauson, P. L. *J. Chem. Soc.* **1961** 3475, 3579, 3484.
(4) Baikie, P. E.; Mills, O. S.; Pauson, P. L.; Smith, G. H.; Valentine, J. H. *J. Chem. Soc., Chem. Commun.* **1965**, 425.
(5) Pauson, P. L.; Smith, G. H.; Valentine, J. H. *J. Chem. Soc. C* **1967**, 1057, 1061.
(6) Pauson, P. L.; Todd, K. H. *J. Chem. Soc. C* **1970**, 2315, 2636, 2638.
(7) Sneeden, R. P. A. "Organochromium Compounds"; Academic Press: New York, 1975.
(8) Khand, I. U.; Pauson, P. L.; Watts, W. E. *J. Chem. Soc. C* **1969**, 2024.
(9) Foreman, M. *J. Chem. Soc., Perkin Trans. 2* **1970**, 1141.
(10) Mohr, D.; Wienand, H.; Ziegler, M. L. *Z. Naturforsch, B.: Anorg. Chem., Org. Chem.* **1976**, *31B*, 66.
(11) Tremmel, P. O.; Wiedenhammer, K.; Wienand, H.; Ziegler, M. L. *Z. Naturforsch, B: Anorg. Chem., Org. Chem.* **1975**, *30B*, 699.
(12) Hoch, G.; Panter, R.; Ziegler, M. L. *Z. Naturforsch, B: Anorg. Chem., Org. Chem.* **1976**, *31B*, 294.
(13) Salzer, A. *Inorg. Chim. Acta* **1976**, *17*, 221.
(14) Gower, M.; John, G. R.; Kane-Maguire, L. A. P.; Odiaka, T. I.; Salzer, A. *J. Chem. Soc., Dalton Trans.* **1979**, 2003.
(15) John, G. R.; Kane-Maguire, L. A. P. *J. Chem. Soc., Dalton Trans.* **1979**, 1196.
(16) Atton, J. G.; Hassan, L. A.; Kane-Maguire, L. A. P. *Inorg. Chim. Acta* **1980**, *41*, 245.
(17) Al-Kathumi, K. M.; Kane-Maguire, L. A. P. *J. Organomet. Chem.* **1975**, *102*, C4.
(18) King, R. B.; Fronzaglia, A. *Inorg. Chem.* **1966**, *5*, 1837.
(19) Müller, J. *Angew. Chem. Int. Ed. Engl.* **1972**, *11*, 653.
(20) Müller, J.; Fenderl, K. *Chem. Ber.* **1970**, *103*, 3128.
(21) Hackett, P.; Jaouen, G. *Inorg. Chim. Acta* **1975**, L19.

0276-7333/86/2305-0152$01.50/0

Table I. Parameters Used in the Extended Hückel Calculations

		exponents			VOIPS, eV		
atom	n	ns	np	$(n-1)$d	ns	np	$(n-1)$d
Cr	4	1.3153	0.9239	3.1190	−6.590	−3.520	−7.785
Mo	5	1.4803	1.0724	2.6204	−6.571	−4.203	−8.394
W	6	1.7950	1.2172	3.0642	−6.571	−4.203	−8.394[a]
C	2	1.5533	1.4500				
O	2	2.1632	2.1739				
H	1	1.3000					

[a] Initial VOIPs approximated by values for molybdenum (see text).

resulting from metal and carbonyl attack during reaction of methoxide with the title complexes. Further, in several related cases in which the final product is the ring addition complex, there is evidence for the observation of low-temperature adducts resulting from initial attack at other sites, and it may be that the existence of such species is a quite general phenomenon.[22-27]

In this paper, we describe the electronic structures of tricarbonyltropyliummetal complexes and compare them with the isoelectronic tricarbonyl(benzene)metal series. We also examine the possible theoretical explanations for the existence of low-temperature adducts.

Computational Details

Molecular orbital calculations were performed by using the self-consistent charge and configuration extended Hückel method, with the FORTICON 8 computer program.[28-31] The basis functions for the transition-metal atoms comprised valence Slater-type $(n-1)$d, ns, and np atomic orbitals. 2s and 2p functions were included on carbon and oxygen atoms and 1s on hydrogens. The radial wave functions computed by Fitzpatrick and Murphy[32] as a least-squares fit to the SCF functions of Herman and Skillman[33] were chosen. A value of 1.3 was used as the exponent for the hydrogen atoms.

Valence orbital ionization potentials (VOIPs) for nine configurations of the transition-metal atoms were taken from the work of Basch, Viste, and Gray[34] for chromium and from Munita and Letelier[35] for molybdenum, as approximations to the diagonal terms of the Coulomb matrix. Initial guess VOIPs for tungsten were approximated by using those of molybdenum. This is a valid assumption, as these values are iterated upon during the calculations until a set yielding charge self-consistency is obtained. Off-diagonal Coulomb terms were computed by using the weighted Wolfsberg–Helmholz formula.[36] The parameters used are summarized in Table I.

Table II. Calculated Charges on $[(\eta^7\text{-}C_7H_7)M(CO)_3]^+$

M	metal	C(O)(av)	C(H)(av)	total CO(av)	total ring
Cr	0.566	0.107	0.066	−0.016	0.482
Mo	0.612	0.095	0.067	−0.035	0.493
W	0.626	0.093	0.067	−0.039	0.491

Geometries of the complexes were adapted from the crystal structure of $[(\eta^7\text{-}C_7H_7)Mo(CO)_3]BF_4$ determined by Clark and Palenik.[37] The structures of the molybdenum and tungsten complexes were assumed to be identical on the basis of the close similarity of the atomic covalent radii (due to the lanthanide contraction)[38] and of the structures of the corresponding hexacarbonyls.[39] For the chromium complex, the ring plane to metal, M–C(O), and C–O distances were those of tricarbonyl(benzene)chromium.[40] The structures of the *exo*-methoxy adducts were approximated by using the experimental geometries of $(C_7H_8)Mo(CO)_3$[41] and methanol.[42] Three-dimensional orbital plots were obtained by using a modified version of the PSI/77 program.[43]

Results and Discussion

Electronic Structure of the Tropylium Complexes. The known structures show that the complexes adopt an almost perfect "piano-stool" geometry, analogous to the isoelectronic tricarbonyl(benzene)metal series, which has been extensively studied by using the fragment MO[44-46] and ab initio[47] methods. Figure 1 shows a comparison between the energy level diagrams of tricarbonylbenzene and tricarbonyltropyliumchromium. The symmetry labels "s" and "a" refer to symmetric or antisymmetric behavior with respect to reflection in the plane of symmetry of the complexes.

The main difference between the two species is that the unoccupied δ-symmetry $3\pi_{a,s}$ MOs lie at much lower energy in $(C_7H_7)^+$ than in C_6H_6, improving their interaction with the $1e_{a,s}$ occupied and $3e_{a,s}$ unoccupied MOs of the $M(CO)_3$ group. This alters the character of the metal contribution to the LUMO of the complex. For $(C_6H_6)Cr(CO)_3$, the LUMO results from the $2e\text{–}2\pi$ interaction, whereas in $[(C_7H_7)Cr(CO)_3]^+$, the low-lying 3π levels allow a good

(22) Brown, D. A.; Fitzpatrick, N. J.; Glass, W, K.; Taylor, T. H. *J. Organomet. Chem.* **1984**, *275*, C9.
(23) Hooker, R. H.; Rest, A. J. *J. Organomet. Chem.* **1982**, *234*, C23.
(24) Brown, D. A.; Chester, J. P.; Fitzpatrick, N. J. *J. Organomet. Chem.* **1978**, *155*, C21.
(25) Brown, D. A.; Chester, J. P.; Fitzpatrick, N. J. *Inorg. Chem.* **1982**, *21*, 2723.
(26) Brown, D. A.; Chawla, S. K.; Glass, W. K. *Inorg. Chim. Acta* **1976**, *19*, L31.
(27) Brown, D. A.; Glass, W. K.; Hussein, F. M. *J. Organomet. Chem.* **1980**, *186*, C58.
(28) Hoffmann, R. *J. Chem. Phys.* **1963**, *39*, 1397.
(29) Hoffmann, R. *J*,; Lipscomb, W. N. *J. Chem. Phys.* **1962**, *36*, 3179, 3489.
(30) Hoffmann, R.; Lipscomb, W. N. *J. Chem. Phys.* **1962**, *32*, 2872.
(31) Howell, J.; Rossi, A.; Wallace, D.; Haraki, K.; Hoffmann, R. "FORTICON-8", *QCPE* **1977**, *No. 344*.
(32) Fitzpatrick, N. J.; Murphy, G. H. *Inorg. Chim. Acta* **1984**, *87*, 41.
(33) Herman, F.; Skillman, S. "Atomic Structure Calculations"; Prentice Hall: New Jersey, 1963.
(34) Basch, H.; Viste, A.; Gray, H. B. *Theor. Chim. Acta* **1965**, *3*, 463.
(35) Munita, R.; Letelier, J. R. *Theor. Chim. Acta* **1981**, *58*, 167.
(36) Ammeter, J. H.; Bürgi, H. B.; Thibeault, J. C.; Hoffmann, R. *J. Am. Chem. Soc.* **1978**, *100*, 3686.
(37) Clark, G. R.; Palenik, G. J. *J. Organomet. Chem.* **1973**, *50*, 185.
(38) Shannon, R. D.; Prewitt, C. T. *Acta Crysatallogr., Sect. B: Struct. Crystallogr. Cryst. Chem.* **1969**, *B25*, 925.
(39) Brockway, L. O.; Ewens, R. V. G.; Lister, M. W. *Trans. Faraday Soc.* **1938**, *34*, 1350.
(40) Chiu, N. S.; Schafer, L.; Seip, R. *J. Organomet. Chem.* **1975**, *101*, 331.
(41) Dunitz, J. D.; Pauling, P. *Helv. Chim. Acta* **1960**, *43*, 2188.
(42) "Interatomic Distances"; The Chemical Society: London, 1958.
(43) Jorgensen, W. L. "PSI/77", *QCPE* **1977**, *No.* 340.
(44) Albright, T. A.; Hofmann, P; Hoffmann, R. *J. Am. Chem. Soc.* **1977**, *99*, 7546.
(45) Albright, T. A.; Hofmann, P.; Hoffmann, R. *Chem. Ber.* **1978**, *111*, 1591.
(46) Chinn, J. W.; Hall, M. B. *J. Am. Chem. Soc.* **1983**, *105*, 4930.
(47) Guest, M. F.; Hillier, I. H.; Higginson, B. R.; Lloyd, D. R. *Mol. Phys.* **1975**, *29*, 113.

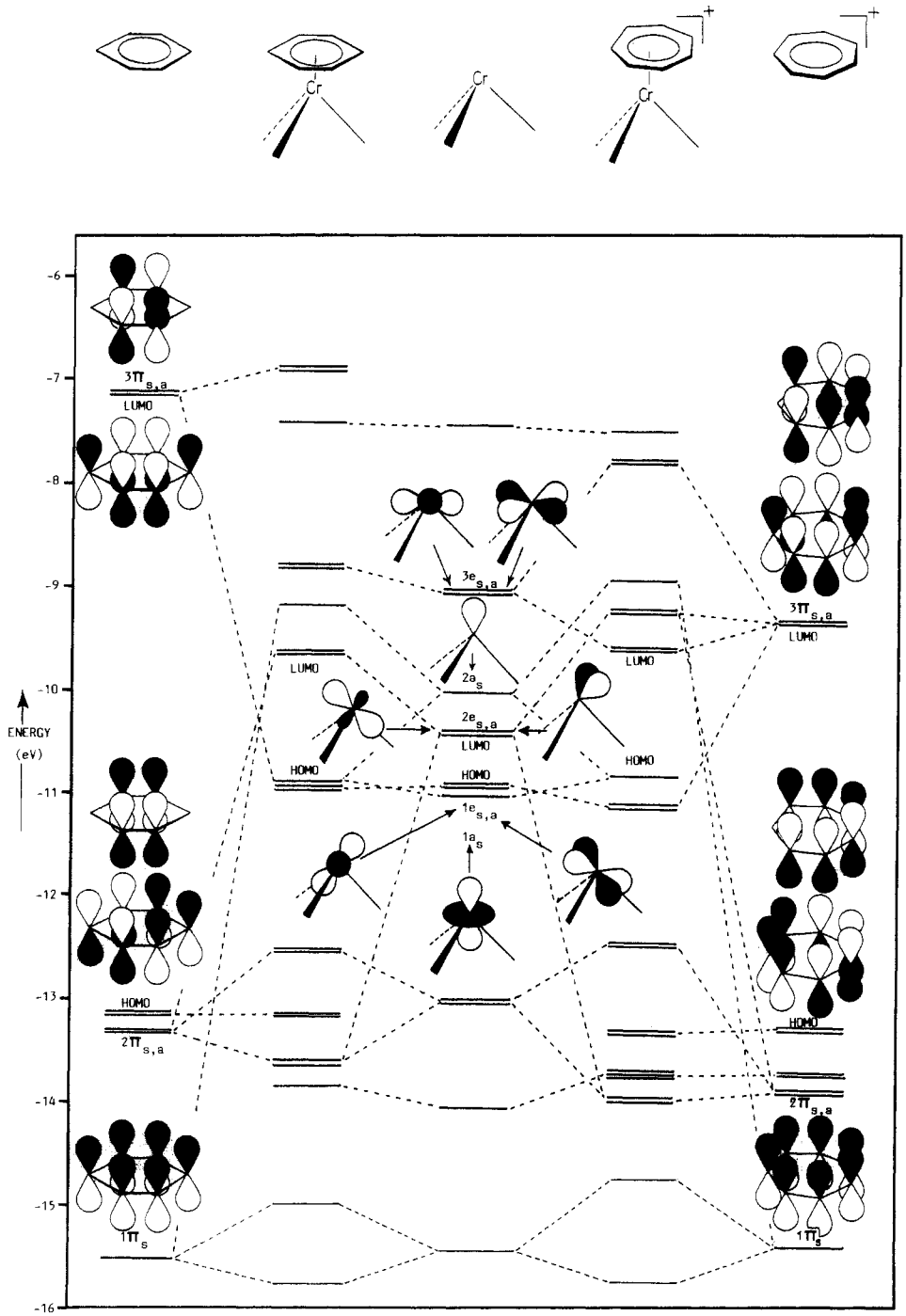

Figure 1. Energy level diagrams for $[(\eta^7\text{-}C_7H_7)M(CO)_3]^+$ and $(\eta^6\text{-}C_6H_6)M(CO)_3$ (M = Cr).

δ-overlap with $3e_{a,s}$ levels on $Cr(CO)_3$. This latter interaction gives rise to a LUMO lying below the $2e\text{–}2\pi$ antibonding MO.

Energy level diagrams of the chromium and molybdenum complexes are compared in Figure 2. The differences are traceable to the drop in energy of the occupied and a rise in energy of the unoccupied fragment MOs of $Mo(CO)_3$ relative to $Cr(CO)_3$, which increases ΔE(HOMO – LUMO). This is mirrored in the complexes, where the gap is almost three times larger for Mo than for Cr. The unoccupied MOs are the most sensitive to this change, and in the molybdenum case the LUMO results from interaction of the 3π with the 2e levels rather than the 3e. Further, the lowest "group" of unoccupied MOs in the molybdenum complex contains eight rather than five levels. This is also true in the tungsten case. We shall see that this effect has important consequences for the reactivity of the complexes.

Finally, calculated orbital and overlap populations for the complexes support the experimental observation (see following paper) from the CO stretching frequencies that $(C_7H_7)^+$ is a better π-acceptor than C_6H_6.

Reactivity toward Nucleophilic Species. We now turn to the problem of finding a theoretical foundation for the observed behavior of the tropylium complexes toward nucleophilic attack. Attempts to formulate a correlation between the charges on each possible site of attack in $[(\text{polyene})_nM(L)_m]^t$ complexes and the experimental observations of products involving exo ring addition have led many workers to the conclusion that such reactions are not charge controlled,[24,25,48–53] since the most positive site is

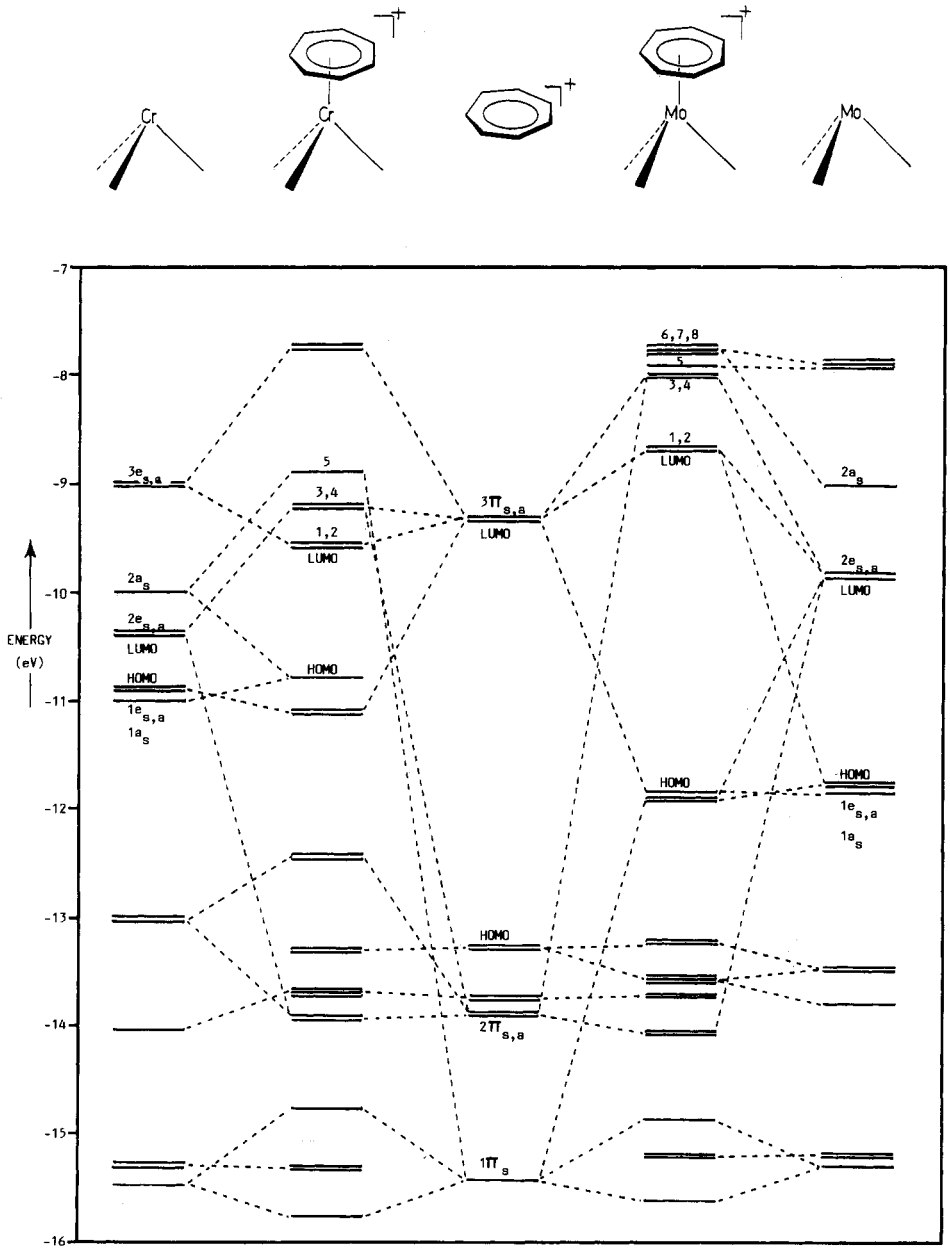

Figure 2. Energy level diagrams for $[(\eta^7\text{-}C_7H_7)M(CO)_3]^+$ (M = Cr, Mo).

invariably the metal. This is indeed the case for the tropylium complexes, as may be seen from the calculated charges (Table II). However, in the following paper experimental evidence is reported for initial metal and carbonyl attack by methoxide and ethoxide on the Mo and W cations in dichloromethane, with only the metal low-temperature adduct occurring in *n*-pentane. For the chromium cation, no metal or carbonyl low-temperature adducts were observed. This suggests that in low polarity solvents at least, the reaction may be charge-controlled. Nevertheless, this cannot be true in all cases, since the charges do not predict ring attack for chromium. Hence an orbital factor must also operate. To probe this, we consider first the application of a single reactivity index.

Some success has been achieved in the correlation of the frontier electron density, ρ^{LUMO}, computed by using semiempirical techniques, with experimental reactivities. A large number of correlations have been made for fused ring systems and Diels–Alder type additions.[54] Recently this index has been applied quite successfully to the nucleophilic addition reactions of the $AM(CO)_3$ series (AM = $(C_6H_6)Cr$, $(C_5H_5)Mn$, $(C_4H_4)Fe$, $(C_3H_5)Co$, and $(C_2H_4)Ni$).[24] Therefore, we have calculated the ρ^{LUMO} values for the metal atom, the carbonyl carbon atoms, and the ring carbon atoms of the tropylium complexes as the sum of

(48) Clack, D. W.; Monshi, M.; Kane-Maguire, L. A. P. *J. Organomet. Chem.* **1976**, *107*, C40.
(49) Clack, D. W.; Monshi, M.; Kane-Maguire, L. A. P. *J. Organomet. Chem.* **1976**, *120*, C25.
(50) Clack, D. W.; Kane-Maguire, L. A. P. *J. Organomet. Chem.* **1978**, *145*, 201.
(51) Astruc, D.; Michaud, P.; Saillard, J.; Hoffmann, R., submitted for publication.
(52) Curtis, M. D.; Eisenstein, O. *Organometallics* **1984**, *3*, 887.
(53) Kostic, N. M.; Fenske, R. F. *Organometallics* **1982**, *1*, 489.
(54) Fukui, K. "Molecular Orbitals in Chemistry, Physics and Biology"; Löwdin, P. O,, Pullman, B., Eds.; Academic Press: New York, 1964.

Table III. ρ_A^{LUMO} Values for Ring, Metal, and Carbonyl Attack on $[(C_7H_7)M(CO)_3]^+$

		$\rho_{C(H)}^{LUMO}$					$\rho_{C(O)}^{LUMO}$		
metal	summation	C_1	C_2–C_7	C_3–C_6	C_4–C_7	ρ_M^{LUMO}	CA	CB–CC	predictn
Cr	frontier[a]	0.012	0.084	0.026	0.059	1.130	0.157	0.165	M > C(O) > C(H)
	extended[b]	0.290	0.147	0.258	0.190	2.339	0.454	0.457	M > C(O) > C(H)
Mo	frontier[a]	0.589	0.487	0.557	0.505	0.230	0.291	0.307	C(H) > C(O) > M
	extended[b]	0.647	0.764	0.680	0.726	3.425	3.051	3.049	M > C(O) > C(H)
W	frontier[a]	0.583	0.488	0.553	0.504	0.216	0.299	0.312	C(H) > C(O) > M
	extended[b]	0.672	0.759	0.676	0.724	3.371	2.824	3.082	M > C(O) > C(H)

[a] Summation over the two LUMOs. [b] Summation over all MOs in the "LUMO group".

Table IV. Interaction Energies for Attack by Methoxide and Ethoxide on $[(C_7H_7)M(CO)_3]^+$

		$(\Delta E)_{RS\ orbital}$, eV		$(\Delta E)_{RS\ total}$ (ϵ^a = 2)		$(\Delta E)_{RS\ total}$ (ϵ^a = 100)	
complex	site of attack	methoxide	ethoxide	methoxide	ethoxide	methoxide	ethoxide
$[(C_7H_7)Cr(CO)_3]^+$	ring "exo"	20.3	21.6	22.4	23.8	20.3	21.6
	ring "endo"	20.4	21.7	22.9	24.2	20.5	21.7
	metal "face"	22.4	23.5	25.2	26.3	22.5	23.6
	metal "edge"	21.2	22.3	24.0	25.2	21.3	22.4
	C(O) "exo"	20.4	21.7	22.4	23.7	20.4	21.7
	C(O) "endo"	21.7	22.9	24.4	25.5	21.8	22.9
$[(C_7H_7)Mo(CO)_3]^+$	ring "exo"	19.9	21.2	22.0	23.4	19.9	21.2
	ring "endo"	20.0	21.2	22.5	23.7	20.0	21.3
	metal "face"	23.1	23.9	25.8	26.7	23.1	24.0
	metal "edge"	25.8	26.8	28.6	29.6	25.9	26.8
	C(O) "exo"	19.8	21.1	21.7	23.1	19.9	21.2
	C(O) "endo"	21.9	22.9	24.4	25.5	21.9	23.0
$[(C_7H_7)W(CO)_3]^+$	ring "exo"	21.3	22.6	23.4	24.7	21.3	22.6
	ring "endo"	21.5	22.8	24.0	25.2	21.6	22.8
	metal "face"	25.8	26.6	28.5	29.4	25.9	26.7
	metal "edge"	29.2	30.0	32.0	32.8	29.2	30.1
	C(O) "exo"	21.3	22.6	23.2	24.6	21.4	22.7
	C(O) "endo"	23.7	24.8	26.3	27.3	23.8	24.8

[a] ϵ = Dielectric constant of medium.

the squares of the atomic orbital coefficients for each atom in the LUMO, normalized to two electrons. These values are set out in Table III. In addition to the values for the LUMO itself, the densities summed over all the MOs making up the "LUMO group" for each complex are also given.

The predictions based on the frontier orbital only, i.e., of metal attack on the chromium complex and ring attack on the molybdenum and tungsten complexes, are at variance with observed behavior. Also, the "nonfrontier" or "extended" ρ^{LUMO} results reinforce the pattern of metal attack predicted by the charges. They demonstrate that for molybdenum and tungsten the M and C(O) sites are quite similar in favorability but do not explain the nonobservation of attack at these sites for the chromium complex.

Several workers have attempted to evolve equations which include the influence of solvent in the computation of an interaction energy between a nucleophile and substrate, while at the same time segregating the charge and orbital interactions into separate terms whose relative magnitudes may be analysed.[55-57] A method of computing the orbital interaction energy by solution of a determinant of frontier and near frontier MOs from the nucleophile and substrate was described in a recent note.[1]

This method has been used to calculate interaction energies for reaction of the methoxide and ethoxide with the title cations. The MOs of the "LUMO group" plus the three HOMOs arising from the interaction of the 1a and 1e MOs of $M(CO)_3$ and the 3π MOs of $(C_7H_7)^+$ (Figure 1) were included in each determinant. The relative geometries of the nucleophile–substrate system are shown in

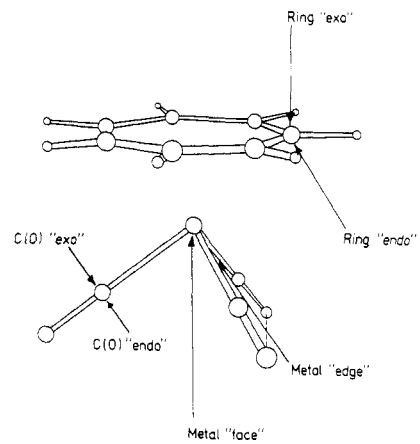

Figure 3. Geometries of the tricarbonyltropyliummetal alkoxide composite molecule corresponding to ring, metal, and carbonyl attack.

Figure 3 and correspond to various orientations of attack of methoxide at different sites on the cation. All calculations were performed at a fixed distance of 2Å between the site of attack and the oxygen atom of the alkoxide.

The calculated energies are shown in Table IV. For each complex, attack by methoxide and ethoxide is predicted to occur in the order M > C(O) > C(H) by both nucleophiles in media of all polarities. This agrees with the prediction made by using the extended summation of frontier electron density. The latter method corresponds to consideration of the high dielectric constant solvent region where the charge term, which has an inverse dependence on polarity, is small. The interaction determinant results also agree with the charge-based predictions, which correlate to the low dielectric constant region where the charge term is dominant. Once again the absence of

(55) Klopman, G.; Hudson, R. F. *Theor. Chim. Acta* **1967**, *8*, 105.
(56) Klopman, G. *J. Am. Chem. Soc.* **1968**, *90*, 223.
(57) Salem, L. *J. Am. Chem. Soc.* **1968**, *90*, 543, 553.

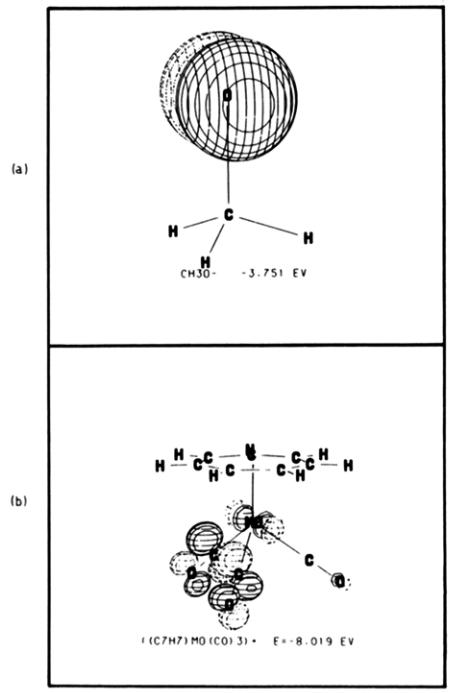

Figure 4. (a) Asymmetric occupied MO of CH_3O^- which interacts favorably with the LUMO of $[\eta^7\text{-}C_7H_7)M(CO)_3]^+$ (M = Mo) shown in (b) resulting in a preference for "edge" attack.

Table V. Extended Hückel Energies[a] for Attack by Methoxide on $[(C_7H_7)M(CO)_3]^+$

site and orientatn of attack	$[(C_7H_7)\text{-}Cr(CO)_3]^+$	$[(C_7H_7)\text{-}Mo(CO)_3]^+$	$[(C_7H_7)\text{-}W(CO)_3]^+$
ring "exo"	0.00	0.00	0.00
ring "endo"	+1.65	+1.82	+1.66
metal "face"	+6.21	+5.95	+5.69
metal "edge"	+4.97	+5.63	+5.08
C(O) "exo"	+1.92	+1.26	+1.29
C(O) "endo"	+8.45	+8.56	+8.01

[a] All values in electron volts, quoted relative to ring "exo" attack for each complex.

low-temperature adducts in the chromium case is not reproduced by the predictions. However, in the series W to Cr the difference in energy between metal and ring attack drops from 8 to 2 eV at all polarities, indicating that although it is still not predicted to occur, ring attack in the chromium case is more favorable than in the tungsten case.

The orientation of attack at a given site is dependent, in the determinant method, on the degree of overlap of the nucleophile with the LUMOs centered on that site. Hence the predicted preference for "edge" attack over "face" attack on the metal for the molybdenum complex is due to good overlap between the HOMO of the methoxide (Figure 4a) and frontier orbital "5" (see Figure 2) in the LUMO group of the complex (Figure 4b). The electron density between the carbonyl groups in this MO is greater than along the "C_3 axis", yielding better overlap in the "edge" case. Recently, extended Hückel theory was used to explain the observed site of attack of nucleophiles on (η^6-benzene)(η-1,5-cyclohexadienyl)iron(II).[51] The results of such calculations on the adduct geometries shown in Figure 3 are given in Table V. In each case, the ring exo addition product is the most stable, which correlates with the isolation of these products from reactions with alkoxide. Approaches to the metal and carbonyl groups and also the endo face of the ring are unfavorable due to repulsions between relatively low-lying occupied levels on the nucleophile and complex. This is illustrated in Figure 5 where the exo ring approach is more favorable than the "C_3" approach to the metal.

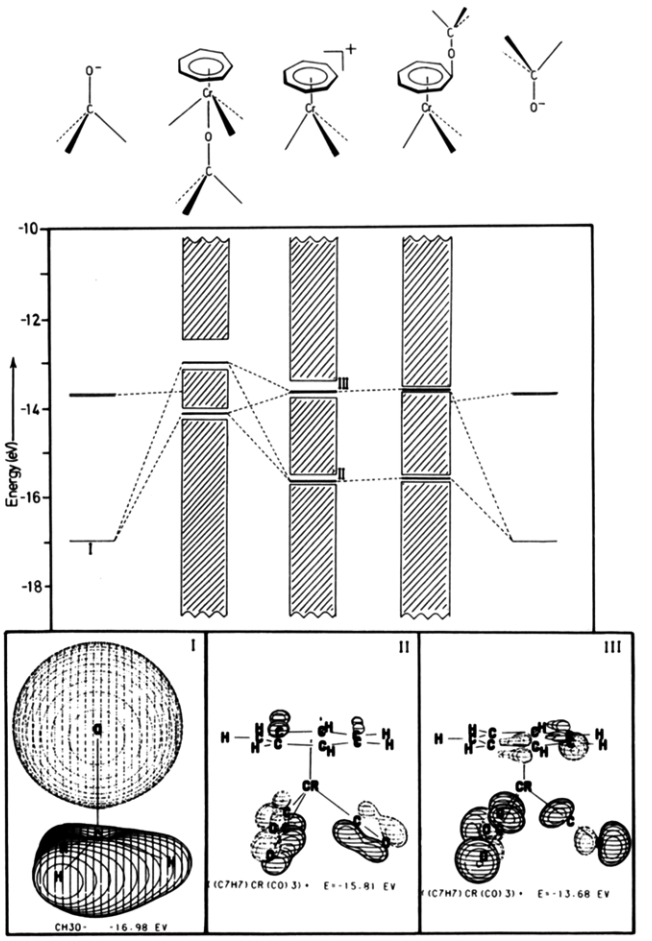

Figure 5. Energy level diagram showing "filled–filled" orbital repulsions for "C_3" attack by methoxide on $[(\eta^7\text{-}C_7H_7)M(CO)_3]^+$ (M = Cr). Shaded areas indicate occupied levels which do not differ in energy between the complexes.

Conclusions

The bonding in tricarbonyltropyliummetal complexes is similar to that observed in the isoelectronic tricarbonyl(benzene)metal species. However, the δ-symmetry 3π MOs of $(C_7H_7)^+$ lie much lower than in C_6H_6, and interact strongly with an unoccupied 3e level on $M(CO)_3$ to give rise to the LUMO.

The ΔE(HOMO – LUMO) value is much larger for the molybdenum and tungsten complexes than for the chromium, and this results in a "LUMO group" in the former which is less widely spread in energy and which contains more metal-dominated orbitals.

Energies calculated by the extended Hückel method show, in all cases, that ring "exo" attack is most favorable while a similar treatment using the interaction determinant reactivity method predicts metal attack. This suggests that the EH method correlates best with the isolation of the thermodynamically stable product whereas the interaction determinant method correlates best with initial site of attack.

Use of charge and ρ^{LUMO} values for near frontier orbitals predicts the existence of metal attack adducts for all three metals. Such species have not been observed for the chromium complex, and a more detailed investigation of the paths of attack followed by incoming nucleophiles is necessary before a complete understanding of regiospecificity in nucleophilic additions to these complexes is obtained.

Formation of Low-Temperature Adducts on Nucleophilic Addition to Tricarbonyltropyliummetal Complexes

David A. Brown,* Noel J. Fitzpatrick, William K. Glass, and Thomas H. Taylor

Department of Chemistry, University College, Belfield, Dublin 4, Ireland

Received April 22, 1985

Low-temperature spectroscopic techniques were employed to explore the reaction between the title cations and alkoxide ions. The low-temperature adducts observed were characterized by IR and NMR spectroscopy. A metal attack adduct is the initial species formed by the Mo and W cations. The initial site of attack is unaffected by changes in solvent polarity. No adducts are observed in the reaction with the chromium cation. In all cases, the thermodynamically stable product is the (7-*exo*-η-1,6-C_7H_7OR)$M(CO)_3$ complex, where R = Me and Et and M = Cr, Mo, and W, for which mass spectra, NMR, and IR data are presented. The simulated NMR spectrum of (7-*exo*-η-1,6-$C_7H_7OCH_3$)$Cr(CO)_3$ is given.

Introduction

The factors influencing the regioselectivity of nucleophilic attack on cations of the type $[(\eta^7\text{-}C_7H_7)M(CO)_3]BF_4$, where M = Cr, Mo, and W, are still unclear, but in a number of related cases, where the final product is either the ring adduct or a carbonyl substitution product, evidence has been presented for the existence of adducts involving initial attack at other sites, for example, the metal or carbonyl group.[1-3] In a recent note, we reported briefly on the existence of low-temperature, kinetically controlled, adducts observed during the reaction of alkoxide ions with $[(\eta^7\text{-}C_7H_7)M(CO)_3]BF_4$, where M = Mo and W.[4] A theoretical approach to reactivity supports the existence of such adducts since initial metal attack is predicted for these cations.[5,6]

In this paper we present detailed spectroscopic evidence for these adducts together with the preparation and spectroscopic characterization of a range of 7-*exo*-alkoxy products not reported previously.

Experimental Section

General Information. Published methods were used to prepare $[(\eta^7\text{-}C_7H_7)M(CO)_3]BF_4$, where M = Cr,[7] Mo, and W,[8] 7-*exo*- and 7-*endo*-(η-1,6-$C_7H_7OCH_3$)$Cr(CO)_3$[9,10] (I - V). Sodium alkoxide solutions were freshly prepared prior to use by dissolving the required amount of sodium in the respective alcohol. All solvents were dried and deoxygenated before use. Reactions and workup, including chromatography, were carried out under oxygen-free nitrogen. Infrared spectra were recorded on a Perkin-Elmer 283B spectrophotometer linked to a Perkin-Elmer 3500 data station. ^1H NMR spectra were recorded on JEOL PS100FT and JEOL GX270FT spectrometers. ^{13}C NMR spectra were recorded on a JEOL GX270FT spectrometer. Mass spectra were recorded on a VG micromass 7070H linked to an INCOS 2400 data system. Microanalyses were performed by the microanalytical laboratory of this department.

Preparation of (7-*exo*-1,6-$C_7H_7OCH_3$)$Mo(CO)_3$ (VI). Additon of a solution of sodium (0.1 g, 4.35 mmol) in methanol (15 mL) to a well-stirred suspension of $[(\eta^7\text{-}C_7H_7)Mo(CO)_3]BF_4$ (0.8 g, 2.24 mmol) in methanol (10 mL) gave an initial red colour before formation of an orange solution. After the solution was stirred for 10 min, the solvent was removed. Extraction of the residue with petroleum spirit (40–60 °C) and subsequent solvent removal, followed by recrystallization from hexane gave orange needles of (7-*exo*-η-1,6-$C_7H_7OCH_3$)$Mo(CO)_3$ (0.41 g, 62%). Prolonged stirring during reaction resulted in significant loss of yield. The product (VI) is stable for several months if stored at 0 °C under nitrogen.

Preparation of (7-*exo*-η-1,6-$C_7H_7OCH_3$)$W(CO)_3$ (VII). The above procedure was applied to $[(\eta^7\text{-}C_7H_7)W(CO)_3]BF_4$ (0.8 g, 1.79 mmol). Recrystallization from hexane yielded orange/red needles (0.36 g, 52%). The product was stable for short periods at room temperature and decomposed after approximately 2 weeks when stored under nitrogen at 0 °C.

Preparation of (7-*exo*-η-1,6-$C_7H_7OC_2H_5$)$Cr(CO)_3$ (VIII). A solution from sodium (0.1 g, 4.35 mmol) in ethanol (10 mL) was added to a well-stirred suspension of $[(\eta^7\text{-}C_7H_7)Cr(CO)_3]BF_4$ (0.8 g, 2.55 mmol) in ethanol (15 mL). No intermediate colors were observed. After the solution was stirred for 30 min, the solvent was removed. Extraction of the residue with petroleum spirit (40–60 °C) and recrystallization from the same solvent yielded the product as yellow/orange needles (0.35 g, 50%).

Preparation of (7-*exo*-η-1,6-$C_7H_7OC_2H_5$)$Mo(CO)_3$ (IX). The above method was applied to $[(\eta^7\text{-}C_7H_7)Mo(CO)_3]BF_4$ (1.0 g, 2.80 mmol). An initial red color was observed before formation of an orange solution. Recrystallization, at −70 °C, from petroleum spirit yielded (7-*exo*-η-1,6-$C_7H_7OC_2H_5$)$Mo(CO)_3$ as a yellow/orange powder (0.2 g, 33%). The product was stable for approximately 1 week if stored at 0 °C under nitrogen.

Attempted Preparation of (7-*endo*-η-1,6-$C_7H_7OCH_3$)$Mo(CO)_3$. 7-*endo*-$C_7H_7OCH_3$[11] (3.1 g, 25.4 mmol) was added to a solution of $(CH_3CN)_3Mo(CO)_3$ (4.0 g, 13.2 mmol) in THF (80 mL). The mixture was heated under reflux for 30 min and the solvent removed under reduced pressure. Extraction of the residue with petroleum spirit (60–80 °C)–ether (1:3) and chromatography on neutral alumina gave $(CH_3CN)Mo(CO)_5$, a yellow solid, as the major product with the dimeric complex $[(\eta^7\text{-}C_7H_7)Mo(CO)_3]_2$ as a minor product (as confirmed by microanalysis). None of the endo complex could be detected although the presence of the dimer suggests that the endo isomer is initially formed. The use of milder reaction conditions failed to give the product.

Low-Temperature Reaction of $[(\eta^7\text{-}C_7H_7)M(CO)_3]BF_4$ with $NaOCH_3$. To the cation (M = Cr, Mo, W (0.7 g)), slurried in CH_2Cl_2 (15 mL) at −15 °C was added a slurry of sodium methoxide in CH_2Cl_2 at −15 °C. The sodium methoxide was prepared freshly as a solid from sodium (1.5 g, 65.2 mmol) in CH_3OH (20 mL) and subsequent solvent removal. After the solution was stirred briefly (1 min), a sample was removed for immediate IR analysis in the

(1) Cowles, R. J.; Johnson, B. F. G.; Lewis, J. *J. Chem. Soc., Chem. Commun.* **1969**, 392.
(2) Powell, P.; Russell, L.; Styles, E.; Brown, A.; Howarth, D.; Moore, P. *J. Organomet. Chem.* **1978**, *149*, C1.
(3) Brown, D. A.; Chawla, S. K.; Glass, W. K. *Inorg. Chim. Acta* **1976**, *19*, L31.
(4) Brown, D. A.; Fitzpatrick, N. J.; Glass, W. K.; Taylor, T. H. *J. Organomet. Chem.* **1984**, *275*, C9.
(5) Brown, D. A.; Fitzpatrick, N. J.; McGinn, M. A. *J. Organomet. Chem.* **1984**, *275*, C5.
(6) Brown, D. A.; Fitzpatrick, N. J.; McGinn, M. A.; Taylor, T. H., preceding paper in this issue.
(7) Munro, J. D.; Pauson, P. L. *J. Chem. Soc.* **1961**, 3475.
(8) Tate, C. P.; Augi, J. M.; Knipple, W. R. *Inorg. Chem.* **1962**, *1*, 433.
(9) Pauson, P. L.; Smith, G. H.; Valentine, J. H. *J. Chem. Soc. C* **1967**, 1057.
(10) Pauson, P. L.; Todd, K. H. *J. Chem. Soc. C* **1970**, 2315.
(11) Doering, W. von E.; Knox, L. H. *J. Am. Chem. Soc.* **1954**, *76*, 3203.

0276-7333/86/2305-0158$01.50/0

Table I. Analyses and IR Spectra of Starter Cations, Low-Temperature Adducts, and Thermodynamically Stable Products (M = Cr, Mo, W) Formed by Reaction of Alkoxide with the Cations

complex	no.	anal. found (calcd) C	anal. found (calcd) H	IR spectra ν_{CO}, cm^{-1} CH_2Cl_2	IR spectra ν_{CO}, cm^{-1} pentane
$[(C_7H_7)Cr(CO)_3]BF_4$	I	38.2 (38.2)	2.7 (2.2)	2071, 2028, 1990	
$[(C_7H_7)Mo(CO)_3]BF_4$	II	33.5 (33.5)	2.1 (2.0)	2081, 2025, 1976	
$[(C_7H_7)W(CO)_3]BF_4$	III	26.8 (26.9)	1.5 (1.6)	2075, 2010, 1952	
7-*exo*-$(OCH_3C_7H_7)Cr(CO)_3$	IV	50.6 (51.1)	3.6 (3.9)	1987, 1922, 1896	1996, 1937, 1917
7-*endo*-$(OCH_3C_7H_7)Cr(CO)_3$	V	51.3 (51.1)	3.9 (3.9)	1983, 1918, 1885	1998, 1939, 1909
7-*exo*-$(OCH_3C_7H_7)Mo(CO)_3$	VI	43.9 (43.7)	3.4 (3.3)	1996, 1926, 1896	2000, 1941, 1919
7-*exo*-$(OCH_3C_7H_7)W(CO)_3$	VII	34.2 (33.9)	2.9 (2.6)	1991, 1919, 1889	2000, 1936, 1912
7-*exo*-$(OC_2H_5C_7H_7)Cr(CO)_3$	VIII	52.5 (52.8)	4.3 (4.4)	1983, 1919, 1891	1995, 1935, 1915
7-*exo*-$(OC_2H_5C_7H_7)Mo(CO)_3$	IX	45.7 (45.6)	3.9 (3.8)	1993, 1921, 1893	2000, 1940, 1918
$(C_7H_7)MoOCH_3(CO)_3$	X			2005, 1957	2015, 1974
$(C_7H_7)Mo(CO)_2(CO_2CH_3)$	XI			1986, 1631	
$(C_7H_7)WOCH_3(CO)_3$	XII			2002, 1955	2010, 1971
$(C_7H_7)W(CO)_2(CO_2CH_3)$	XIII			1983, 1630	
$(C_7H_7)MoOC_2H_5(CO)_3$	XIV			2004, 1957	
$(C_7H_7)Mo(CO)_2(CO_2C_2H_5)$	XV			1984, 1630	

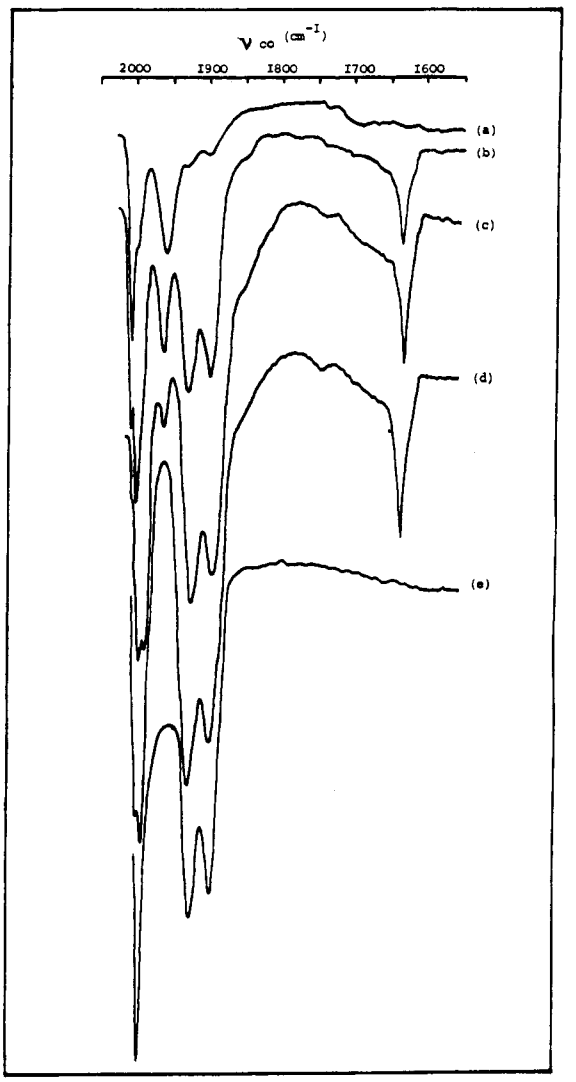

Figure 1. Low-temperature spectra of reaction between $[(\eta^7\text{-}C_7H_7)Mo(CO)_3]^+$ and $NaOCH_3$ recorded on a Perkin-Elmer 283B IR spectrometer: (a) initial spectrum after 1 min, (b) second sample after 10 min, (c) second sample after 30 min, (d) second sample after 50 min, and (e) third sample after 3 h.

region 1550–2200 cm^{-1}, using low-temperature cells. After 10 min, a second sample was removed from the reaction mixture for IR analysis. This sample was allowed to warm up in the IR cells and was rerun after 30 and 50 min. A third sample was removed after 3 h and its IR spectrum obtained.

Similar reactions were performed by (a) using pentane as solvent in place of CH_2Cl_2 and (b) using $NaOC_2H_5$ in place of $NaOCH_3$ as nucleophile.

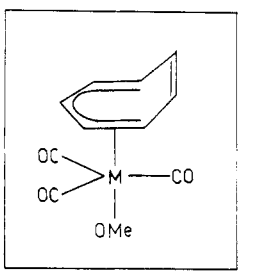

Figure 2. Possible structure of fluxional adduct resulting from metal attack.

Results and Discussion

A typical series of IR spectra are shown in Figure 1 for the low-temperature reaction between $[(\eta^7\text{-}C_7H_7)Mo(CO)_3]BF_4$ and CH_3O^- in CH_2Cl_2. Similar spectra were obtained for both cations and alkoxide ions in CH_2Cl_2 and *n*-pentane. The results are summarized in Table I.

The peaks at 2005 and 1957 cm^{-1}, which disappear within 45 min, are assigned to an alkoxymetal adduct (X) formed by direct attack (or association) of the CH_3O^- at the metal atom. This then dissociates to give both the stable 7-exo ring product VI, with peaks at 1996, 1926, and 1896 cm^{-1}, and the carbomethoxy species $(\eta^7\text{-}C_7H_7)Mo(CO)_2(CO_2Me)$ (XI), with bands at 1986 and 1631 cm^{-1}. The carbomethoxy compound XI is stable for about 24 h at low temperatures but rearranges rapidly to the ring product VI at room temperature and could not be isolated pure.

Complementary ^1H NMR studies in CD_2Cl_2 showed, at the very early stages of reaction, a sharp singlet at 5.34 ppm, assigned to X, which disappears with time to give the 7-exo ring adduct VI. No ring proton peak of XI was observed although it may be obscured by a solvent peak at 5.32 ppm, but a small singlet at 2.91 ppm may be assigned to the methoxy group of XI. The initial appearance of the sharp singlet at 5.34 ppm suggests equivalent ring protons in X, implying either rapid fluxionality of the ring (Figure 2) or possibly a 20-electron system as shown in the reaction scheme in Figure 3.

The exclusive formation of the 7-exo ring adduct VI suggests a dissociative rearrangement of X and XI since intramolecular rearrangement would yield a measurable quantity of the 7-endo ring adduct.

In the case of related complexes addition of alkoxide to $[(C_7H_9)Fe(CO)_3]BF_4$[12] and $[(C_6H_7)Os(CO)_3]BF_4$[13] results

(12) Brown, D. A.; Glass, W. K.; Hussein, F. M. *J. Organomet. Chem.* **1980**, *186*, C58.
(13) Bryan, E. G.; Burrows, A. L.; Johnson, B. F.; Lewis, J.; Schiavon, G. M. *J. Organomet. Chem.* **1977**, *129*, C9.

Table II. Proton Shifts and J Values for Cycloheptatriene, Methoxycycloheptatriene, and (η-1,6-C_7H_7OR)$M(CO)_3$

complex	chemical shift values, ppm							J values, Hz			
	$H_{3,4}$	$H_{2,5}$	$H_{1,6}$	H_7	OCH_3	OCH_2	CH_3	$J_{3,4}$	$J_{2,3=4,5}$	$J_{1,2=5,6}$	$J_{1,7=6,7}$
C_7H_8	6.6	6.2	5.4	2.2							
$C_7H_7OCH_3$	6.7	6.2	5.5	3.4	3.4			8.6	7.0	9.3	4.4
7-*exo*-$(OCH_3C_7H_7)Cr(CO)_3$	5.9	5.1	4.1	4.3	3.0			8.1	7.5	8.5	7.3
7-*endo*-$(OCH_3C_7H_7)Cr(CO)_3$	6.0	4.7	3.3	3.2	3.4			8.0	*b*	8.8	3.5
7-*exo*-$(OC_2H_5C_7H_7)Cr(CO)_3$	5.9	5.1	4.0	4.4		3.2	1.0				
7-*endo*-$(OC_2H_5C_7H_7)Cr(CO)_3$[a]	6.1	4.8	3.4	3.3		3.5	1.2				
7-*exo*-$(OCH_3C_7H_7)Mo(CO)_3$	5.9	5.2	4.2	4.3	3.1			8.1	7.8	8.5	7.3
7-*exo*-$(OC_2H_5C_7H_7)Mo(CO)_3$	5.9	5.2	4.2	4.4		3.3	1.0	7.9	*b*	8.4	7.1
7-*exo*-$(OCH_3C_7H_7)W(CO)_3$	5.9	5.1	4.2	4.3	3.1			8.1	7.6	8.5	7.4

[a] Pauson, P. L.; Todd, K. H. *J. Chem. Soc. C* **1970**, 2317. [b] Coupling constants could not be measured due to difficulties in decoupling at $H_{1,6}$.

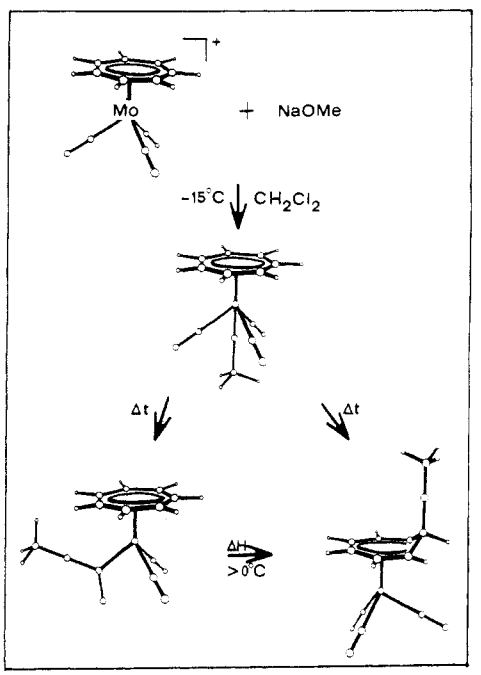

Figure 3. Reaction scheme for the low-temperature reaction between $[(\eta^7\text{-}C_7H_7)Mo(CO)_3]^+$ and $NaOCH_3$ in CH_2Cl_2 solvent.

in the formation of carboalkoxy adducts which rearrange dissociatively on heating to give the 5-exo ring adduct.

Analogous results were obtained for the $[(\eta^7\text{-}C_7H_7)W(CO)_3]^+$ cation in CH_2Cl_2. The infrared ν_{CO} peaks for the alkoxymetal XII, the carboalkoxy XIII, and the 7-exo ring product are given in Table I. The rate of reaction was faster that that of the Mo complex with peaks due to all three adducts present in the initial spectrum. The final spectrum, recorded after 35 min, showed only those peaks due to the 7-exo ring adduct VII along with some peaks due to decomposition.

In pentane the rate of reaction increased and no carbomethoxy species were observed. However, the change in solvent polarity had no effect on the initial site of attack (metal attack). The results of the analogous reaction with the tungsten cation III were similar and are given in Table I.

The reaction of ethoxide in CH_2Cl_2, at −15 °C, with the Mo cation II also gave metal (XIV), carbonyl (XV), and ring attack (VI) although the rate of reaction was faster than that of the analogous methoxide reaction.

Further qualitative evidence for adducts in the reaction between alkoxide and the Mo and W cations was observed when preparing the 7-exo-alkoxy ring products in the respective alcohols. On additon of alkoxide to the orange cation slurry in alcohol, a clear deep red color formed which persisted for approximately 20 s at room temperature before the formation of the final orange solution which is characteristic of the 7-exo ring adduct.

In contrast, no adducts were detected with $[(\eta^7\text{-}C_7H_7)Cr(CO)_3]^+$ in either CH_2Cl_2 or pentane as solvent and only the 7-*exo*-alkoxy ring product was obtained. This is consistent with the fact that metal attack products are rare for the chromium cation; i.e., no reaction occurs with halide ions whereas the Mo and W cations readily form $(\eta^7\text{-}C_7H_7)M(CO)_2I$. The anomalous behavior of the Cr cation cannot be explained by steric factors or the suggestion that the tropylium ring is more electrophilic than in the Mo and W cations which is contradicted by the charges calculated in the preceding paper (Table II). It was shown also that for the three cations $[(\eta^7\text{-}C_7H_7)M(CO)_3]^+$, where M = Cr, Mo, and W, the metal is the most favorable initial site of nucleophilic attack although the difference in interaction energies between ring and metal attack is much smaller for the Cr cation than the Mo and W analogues.

Spectroscopic Results for 7-Exo and 7-Endo Ring Adducts

Both NMR[15] and mass spectroscopy[16] have been used to distinguish between the 7-exo and (7-*endo*-η-1,6-$C_7H_7L)M(CO)_3$, where M = Cr, Mo, and W.

^{1}H NMR Spectra. The substitution of a proton by a methoxy group at the 7-position of cycloheptatriene results in little change in the ^{1}H NMR spectrum. Two-dimensional J-resolved studies projected along the F1 domain, for the 7-methoxycycloheptatriene, showed three singlets, for the olefinic protons, indicating that $H_3 = H_4$, $H_2 = H_5$ and $H_1 = H_6$. Addition of the $Cr(CO)_3$ moiety to form the (7-*endo*-η-1,6-$C_7H_7OCH_3)Cr(CO)_3$ complex does not affect the equivalence of these protons but each set of protons is shielded to a different extent. The X-ray structure of (η-1,6-$C_4H_8)Mo(CO)_3$,[17] assumed to be similar to (7-*exo*-η-1,6-$C_7H_7OR)Mo(CO)_3$, shows that the metal atom is not equidistant from the olefinic carbons with the $M\text{–}C_{3,4}$ distance 2.31 Å, $M\text{–}C_{2,5}$ distance 2.35 Å, and the $M\text{–}C_{1,6}$ distance 2.45 Å. This "ring slippage" may be a contributing factor toward the unequal shielding of the olefinic protons. Increasing the size of the metal from Cr to W in the 7-*exo*-alkoxy complexes has little or no effect on the chemical shift of any of the protons. However, comparison between the 7-exo and 7-endo chromium complexes shows a marked difference in chemical shift. This deshielding of the endo ligand has been observed previously with related complexes[18] and suggests some direct interaction between the

(14) King, R. B.; Fronzaglia, A. *Inorg. Chem.* **1966**, *5*, 1837.

(15) Pauson, P. L.; Smith, G. H.; Valentine, J. H. *J. Chem. Soc. C* **1967**, 1061.

(16) Muller, J.; Fenderl, K. *Chem. Ber.* **1970**, *103*, 3128.

(17) Dunitz, J. D.; Pauling, P. *Helv. Chim. Acta* **1960**, *43*, 2188.

Table III. ^{13}C NMR Shift Values for Cycloheptatriene, Methoxycycloheptatriene, and (η-1,6-C_7H_7OR)$M(CO)_3$

complex	chemical shifts, ppm							
	$C_{3,4}$	$C_{2,5}$	$C_{1,6}$	C_7	OCH_3	OCH_2	CH_3	$(CO)_3$
C_7H_8[a]	131.3	127.3	121.3	28.7				
$C_7H_7OCH_3$	130.9	125.3	123.0	77.8	56.3			
7-*endo*-$OCH_3C_7H_7Cr(CO)_3$	97.3	94.7	61.7	73.8	56.8			*b*
7-*exo*-$OCH_3C_7H_7Cr(CO)_3$	99.5	98.3	67.2	70.6	52.5			230.3
7-*exo*-$OC_2H_5C_7H_7Cr(CO)_3$	99.4	98.3	67.7	68.7		60.0	15.1	230.9
7-*exo*-$OCH_3C_7H_7Mo(CO)_3$	101.0	97.0	68.7	72.6	52.8			217.9

[a] Mann, B. E. *J. Chem. Soc., Chem. Commun.* **1978**, 976. [b] No resonance was observed for the carbonyl carbons.

Table IV. Mass Spectra Values for (η-1,6-C_7H_7OR)$M(CO)_3$, Where M = Cr, Mo, and W and R = CH_3 and C_2H_5

fragment	7-*endo*-($C_7H_7OCH_3$)-$Cr(CO)_3$		7-*exo*-($C_7H_7OCH_3$)-$Cr(CO)_3$		7-*exo*-($C_7H_7OCH_3$)-$Mo(CO)_3$		7-*exo*-($C_7H_7OCH_3$) $W(CO)_3$		7-*exo*-($C_7H_7OC_2H_5$)-$Cr(CO)_3$		7-*exo*-($C_7H_7OC_2H_5$)-$Mo(CO)_3$	
	amu	intens	amu	intens	amu	intens	amu	intens	amu	intens	amu	intens
$C_7H_7ORM(CO)_3^+$	258	35.48	258	13.10	304	47.80	390	53.40	272	7.20	318	20.70
$C_7H_7ORM(CO)_2^+$	230	9.74	230	7.61	276	8.30	362	8.17	244	3.30	290	2.65
$C_7H_7M(CO)_3^+$	227	0.49	227	1.26	273	18.41	359	28.80	227	2.41	273	9.79
$C_7H_7ORM(CO)^+$	202	23.70	202	4.97	248	20.49	334	16.50	216	6.17	262	6.34
$C_7H_7M(CO)_2^+$	199	0.15	199	8.51	245	25.98	331	35.52	199	6.76	245	9.68
$C_7H_7ORM^+$	174	48.77	174	15.41	220	100.00	306	81.72	188	15.96	234	18.58
$C_7H_7M(CO)^+$	171	0.85	171	11.41	217	86.95	303	53.24	171	7.13	217	11.38
$C_7H_7OM^+$	159	100.00	159	25.24	205	26.34	291	54.85	159	12.14	205	16.66
$C_7H_8M^+$	144	81.23	144	24.57	190	21.19	276	43.04	144	74.38	190	4.86
$C_7H_7M^+$	143	4.69	143	20.94	189	67.80	275	83.98	143	16.46	189	29.67
$C_7H_6M^+$	142	4.84	142	1.71	188	47.26	274	60.03	142	4.20	188	20.06
$C_7H_7^+$	91	84.25	91	100.00	91	50.91	91	100.00	91	100.00	91	100.00
$C_6H_6^+$	78	2.55	78	2.90	78	15.88	78	26.90	78	3.30	78	14.04
$C_5H_5^+$	65	13.36	65	18.89	65	14.34	65	36.57	65	32.64	65	13.13
H^+	52	82.19	52	43.31	98	11.65	184		52	28.65	98	9.36

metal and 7-*endo*-alkoxy ligand.

The main points of interest with the coupling constants involves the $J_{1,7=6,7}$ and, to a lesser extent, the $J_{1,2=5,6}$ values (Table II). These values remain unchanged at 7.33 and 8.50 Hz, respectively, for the 7-*exo*-methoxy series, irrespective of the metal.

The accuracy of the coupling constants and chemical shift values were confirmed by computer-simulated spectra using the NMRIT progam.[19] The expanded FT100 ^1H NMR spectrum of the seven ring protons of the (7-*exo*-η-1,6-$C_7H_7OCH_3$)$Cr(CO)_3$ complex and its computer-simulated spectrum are shown in Figure 4.

^{13}C NMR Spectra. Comparison of the ^{13}C NMR spectra of cycloheptatriene and 7-methoxycycloheptatriene shows that C_7 is deshielded by the methoxy group by ca. 50 ppm. In (7-*endo*-η-1,6-$C_7H_7OCH_3$)$Cr(CO)_3$ the ring carbons are shielded but, as with the proton spectra, not equally (Table III). Comparison with the exo isomer shows, once again, differences at the $C_{1,6}$ and C_7 positions with $C_{1,6}$ of the exo complex deshielded by 5.5 ppm more than the endo isomer while the C_7 is shielded by 3.2 ppm in accord with the general assumption that the metal deshields the endo ligand in metal complexes.[20] Replacement of Cr with Mo in the 7-exo series results in little change in the ring ^{13}C chemical shifts although the carbonyl carbons are shielded by 12 ppm.

Mass Spectra. The mass spectra of the exo and endo isomers of (η-1,6-$C_7H_7OCH_3$)$Cr(CO)_3$ showed that preferential elimination of the three carbonyls occurs in the endo case whereas loss of the methoxy group occurs only in the exo case. Such differences in mass spectra were proposed as a means of distinguishing the isomers.[16] In the present (7-*exo*-η-1,6-C_7H_7OR)$M(CO)_3$ series, where M = Cr, Mo, and W and R = CH_3 and C_2H_5, the preferential loss of the alkoxy ligand occurs in accordance with the above suggestion (Table IV). However, the increasing intensity of the $(M - OCH_3)^+$ fragment across the series Cr to W indicates increasing ease of removal of the CH_3O^- group, suggesting that for the endo isomers alkoxy loss may also be more significant in the Mo and W cases. Thus

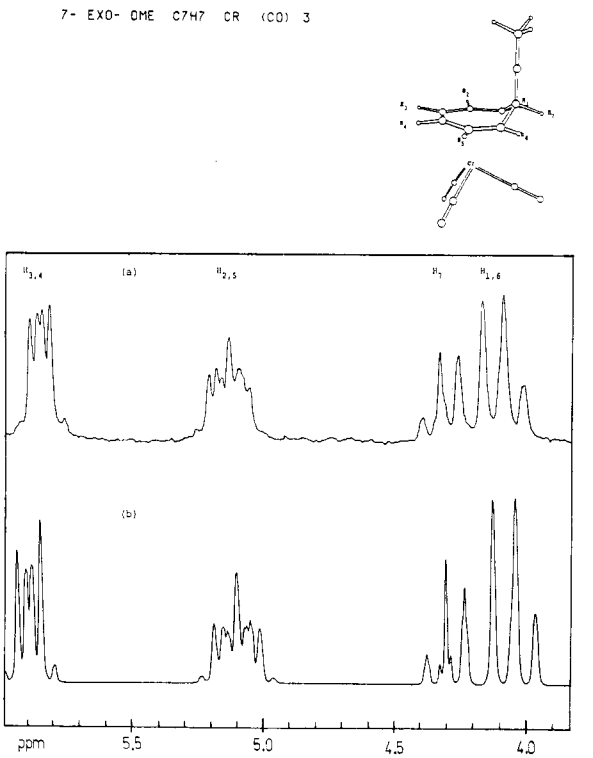

Figure 4. (a) Expanded ^1H NMR spectrum and (b) computer-simulated spectrum of (7-*exo*-η-1,6-$C_7H_7OCH_3$)$Cr(CO)_3$ showing the ring protons.

(18) Brown, D. A.; Fitzpatrick, N. J.; Glass, W. K.; Sayal, P. K. *Organometallics* **1984**, *3*, 1137.
(19) Detar, D. F. "Computer Programs for Chemistry"; W. A. Benjamin: New York, 1968; Vol. 1.
(20) Bandara, B. M. R; Birch, A. J.; Raverty, W. D. *J. Chem. Soc., Perkin Trans.* **1982**, 1745.

preferential alkoxy loss may not always be a valid criterion for distinguishing between exo and endo isomers of this type.

Conclusions

Low-temperature spectroscopic studies show that for attack of alkoxide on $[(\eta^7\text{-}C_7H_7)M(CO)_3]^+$, where M = Mo and W, in CH_2Cl_2 or pentane, the initial site of attack is the metal. Changes in solvent polarity do not affect the initial attacking site although for solvents with low dielectric constant the rate of reaction increases. No transient adducts are observed in the reaction of the analogous chromium complex. The 7-exo ring adducts are the final thermodynamically stable products in all cases, suggesting a dissociative mechanism for their formation from the transient adducts since some formation of the 7-endo adducts would be expected if the reaction proceeded by an intramolecular rearrangement.

NMR studies of the 7-*exo*-alkoxy ring adducts show that H_7 lies slightly downfield from $H_{1,6}$ and the values of $J_{1,7}$ = 7.33 and 3.5 Hz confirm exo and endo geometries, respectively. ^{13}C NMR of the exo and endo isomers show differences in chemical shift for the $C_{1,6}$ and C_7. Increasing the size of the metal does not significantly affect the shift values of the ring carbons although the carbonyl carbons are shielded.

Mass spectra show increasing ease of ionization of the exo ligand across the series from Cr to W.

A Comparison of the Reactivity of Alkoxide and Alkoxide–Alkanol Negative Ions with Alkyl- and Alkoxyboranes in the Gas Phase. An Ion Cyclotron Resonance and ab Initio Study

Roger N. Hayes, John C. Sheldon, and John H. Bowie*

Departments of Chemistry, University of Adelaide, Adelaide, South Australia 5001

Received May 15, 1985

Alkoxide ions R^1O^- react with alkylboranes $(R^2)_3B$ to effect both deprotonation of and hydride transfer to the borane. Tetrahedral adducts $(R^1O)(R^2)_3B^-$ are also formed. The decomposing form of this adduct gives $(R^2)_2BO^- + R^1R^2$. Alkanol–alkoxide ions $(R^1O^-\cdots HOR^1)$ react with alkylboranes to give only $(R^1O)(R^2)_3B^- + R^1OH$. Alkoxide ions R^1O^- react with alkoxyboranes [e.g., $(R^2O)_3B$] to produce tetrahedral species $(R^1O)(R^2O)_3B^-$: the decomposing form of which yields $R^2O^- + (R^1O)(R^2O)_2B$. In addition, the S_N2 reaction $R^1O^- + R^2\text{–}OB(OR^2)_2 \rightarrow R^1OR^2 + (R^2O)_2BO^-$ is observed. Alkanol–alkoxide ions $(R^1O^-\cdots HOR^1)$ react with alkoxyboranes in two ways: (i) to form $(R^1O)(R^2O)_3B^-$ ions and (ii) to undergo the alkoxide exchange reaction $(R^1O\cdots HOR^1) + (R^2O)_3B \rightarrow (R^1O\cdots H\cdots OR^2)^- + (R^1O)(R^2O)_2B$. When the alkanol–alkoxide reactant ion is unsymmetrical, the smaller alkoxide reacts at boron.

Introduction

The differences in reactivities and rates of chemical reactions in the gas phase and in the condensed phase have been often described (see, e.g., ref 1–4). Condensed-phase reactions are dependent in a complex manner upon solvent parameters, and it is not possible to totally mirror these parameters in gas-phase reactions. Yet it is possible to form "solvated" ions $[Nu^-(HNu)_n]$ in the gas phase and to study their reactivities.[4-7] The differences in reactivity of alkoxide ions (RO^-) and alkanol–alkoxides ($RO^-\cdots HOR$)[7] toward carbon[2,8] and silicon[3] substrates have been described. The solvated species are less basic and less nucleophilic than their unsolvated counterparts, and the reactivity of the two species is often quite different. In particular, alkanol–alkoxide ions react with alkoxysilanes[3] (and to a lesser extent with carbon ethers[8]) by reaction 1 ($R_1 \leq R_2$). Alkanol–alkoxide addition in the reverse sense is not observed in silicon systems.

$$[R^1O^-\cdots HOR^2] + Me_3SiOR^3 \rightarrow [R^2O^-\cdots HOR^3] + Me_3SiOR^1 \quad (1)$$

$$B_xH_y^- \rightarrow [B_xH_{y-2}]^- + H_2 \quad (2)$$

$$B_xH_y^- \rightarrow [B_{x-1}H_{y-3}]^- + BH_3 \quad (3)$$

$$F^- + B_2H_6 \rightarrow BH_4^- + BH_2F \quad (4)$$

$$CD_3O^- + B_2H_6 \rightarrow B_2H_6D^- + CD_2O \quad (5)$$

$$CD_3O^- + B_2H_6 \rightarrow BH_4^- + CD_3OBH_2 \quad (6)$$

In this paper we extend our studies of alkoxide and alkoxide–alkanol reactivity into the area of boron chemistry. Some aspects of the gas-phase negative ion chemistry of boron hydrides and alkylboranes have been described, and these are summarized here. Negative ions from diborane (e.g., $B_2H_6^-$· and $B_2H_5^-$) have been observed in conventional mass spectra: the decompositions of typical

(1) DePuy, C. H.; Bierbaum, V. M. *Acc. Chem. Res.* **1981**, *14*, 146.
(2) Bowie, J. H. *Mass Spectrom. Rev.* **1984**, *3*, 1.
(3) Hayes, R. N.; Bowie, J. H.; Klass, G. *J. Chem. Soc., Perkin Trans. 2* **1984**, 1167.
(4) Tanaka, J.; Mackay, G. I.; Payzant, J. D.; Bohme, D. K. *Can. J. Chem.* **1976**, *54*, 1643.
(5) Bohme, D. K.; Young, L. B. *J. Am. Chem. Soc.* **1970**, *92*, 7354.
(6) Bohme, D. K.; Mackay, G. I.; Payzant, J. D. *J. Am. Chem. Soc.* **1974**, *96*, 4027.
(7) Faigle, J. F. G.; Isolani, P. C.; Riveros, J. M. *J. Am. Chem. Soc.* **1976**, *88*, 2049 and references cited therein.
(8) Hayes, R. N.; Paltridge, R. L.; Bowie, J. H. *J. Chem. Soc., Perkin Trans. 2* **1985**, 567.

0276-7333/86/2305-0162$01.50/0

preferential alkoxy loss may not always be a valid criterion for distinguishing between exo and endo isomers of this type.

Conclusions

Low-temperature spectroscopic studies show that for attack of alkoxide on $[(\eta^7\text{-}C_7H_7)M(CO)_3]^+$, where M = Mo and W, in CH_2Cl_2 or pentane, the initial site of attack is the metal. Changes in solvent polarity do not affect the initial attacking site although for solvents with low dielectric constant the rate of reaction increases. No transient adducts are observed in the reaction of the analogous chromium complex. The 7-exo ring adducts are the final thermodynamically stable products in all cases, suggesting a dissociative mechanism for their formation from the transient adducts since some formation of the 7-endo adducts would be expected if the reaction proceeded by an intramolecular rearrangement.

NMR studies of the 7-*exo*-alkoxy ring adducts show that H_7 lies slightly downfield from $H_{1,6}$ and the values of $J_{1,7}$ = 7.33 and 3.5 Hz confirm exo and endo geometries, respectively. ^{13}C NMR of the exo and endo isomers show differences in chemical shift for the $C_{1,6}$ and C_7. Increasing the size of the metal does not significantly affect the shift values of the ring carbons although the carbonyl carbons are shielded.

Mass spectra show increasing ease of ionization of the exo ligand across the series from Cr to W.

A Comparison of the Reactivity of Alkoxide and Alkoxide–Alkanol Negative Ions with Alkyl- and Alkoxyboranes in the Gas Phase. An Ion Cyclotron Resonance and ab Initio Study

Roger N. Hayes, John C. Sheldon, and John H. Bowie*

Departments of Chemistry, University of Adelaide, Adelaide, South Australia 5001

Received May 15, 1985

Alkoxide ions R^1O^- react with alkylboranes $(R^2)_3B$ to effect both deprotonation of and hydride transfer to the borane. Tetrahedral adducts $(R^1O)(R^2)_3B^-$ are also formed. The decomposing form of this adduct gives $(R^2)_2BO^- + R^1R^2$. Alkanol–alkoxide ions $(R^1O^-\cdots HOR^1)$ react with alkylboranes to give only $(R^1O)(R^2)_3B^- + R^1OH$. Alkoxide ions R^1O^- react with alkoxyboranes [e.g., $(R^2O)_3B$] to produce tetrahedral species $(R^1O)(R^2O)_3B^-$: the decomposing form of which yields $R^2O^- + (R^1O)(R^2O)_2B$. In addition, the S_N2 reaction $R^1O^- + R^2\text{–}OB(OR^2)_2 \rightarrow R^1OR^2 + (R^2O)_2BO^-$ is observed. Alkanol–alkoxide ions $(R^1O^-\cdots HOR^1)$ react with alkoxyboranes in two ways: (i) to form $(R^1O)(R^2O)_3B^-$ ions and (ii) to undergo the alkoxide exchange reaction $(R^1O\cdots HOR^1) + (R^2O)_3B \rightarrow (R^1O\cdots H\cdots OR^2)^- + (R^1O)(R^2O)_2B$. When the alkanol–alkoxide reactant ion is unsymmetrical, the smaller alkoxide reacts at boron.

Introduction

The differences in reactivities and rates of chemical reactions in the gas phase and in the condensed phase have been often described (see, e.g., ref 1–4). Condensed-phase reactions are dependent in a complex manner upon solvent parameters, and it is not possible to totally mirror these parameters in gas-phase reactions. Yet it is possible to form "solvated" ions $[Nu^-(HNu)_n]$ in the gas phase and to study their reactivities.[4-7] The differences in reactivity of alkoxide ions (RO^-) and alkanol–alkoxides ($RO^-\cdots HOR$)[7] toward carbon[2,8] and silicon[3] substrates have been described. The solvated species are less basic and less nucleophilic than their unsolvated counterparts, and the reactivity of the two species is often quite different. In particular, alkanol–alkoxide ions react with alkoxysilanes[3] (and to a lesser extent with carbon ethers[8]) by reaction 1 ($R_1 \leq R_2$). Alkanol–alkoxide addition in the reverse sense is not observed in silicon systems.

$$[R^1O^-\cdots HOR^2] + Me_3SiOR^3 \rightarrow [R^2O^-\cdots HOR^3] + Me_3SiOR^1 \quad (1)$$

$$B_xH_y^- \rightarrow [B_xH_{y-2}]^- + H_2 \quad (2)$$

$$B_xH_y^- \rightarrow [B_{x-1}H_{y-3}]^- + BH_3 \quad (3)$$

$$F^- + B_2H_6 \rightarrow BH_4^- + BH_2F \quad (4)$$

$$CD_3O^- + B_2H_6 \rightarrow B_2H_6D^- + CD_2O \quad (5)$$

$$CD_3O^- + B_2H_6 \rightarrow BH_4^- + CD_3OBH_2 \quad (6)$$

In this paper we extend our studies of alkoxide and alkoxide–alkanol reactivity into the area of boron chemistry. Some aspects of the gas-phase negative ion chemistry of boron hydrides and alkylboranes have been described, and these are summarized here. Negative ions from diborane (e.g., $B_2H_6^-$· and $B_2H_5^-$) have been observed in conventional mass spectra: the decompositions of typical

(1) DePuy, C. H.; Bierbaum, V. M. *Acc. Chem. Res.* **1981**, *14*, 146.
(2) Bowie, J. H. *Mass Spectrom. Rev.* **1984**, *3*, 1.
(3) Hayes, R. N.; Bowie, J. H.; Klass, G. *J. Chem. Soc., Perkin Trans. 2* **1984**, 1167.
(4) Tanaka, J.; Mackay, G. I.; Payzant, J. D.; Bohme, D. K. *Can. J. Chem.* **1976**, *54*, 1643.
(5) Bohme, D. K.; Young, L. B. *J. Am. Chem. Soc.* **1970**, *92*, 7354.
(6) Bohme, D. K.; Mackay, G. I.; Payzant, J. D. *J. Am. Chem. Soc.* **1974**, *96*, 4027.
(7) Faigle, J. F. G.; Isolani, P. C.; Riveros, J. M. *J. Am. Chem. Soc.* **1976**, *88*, 2049 and references cited therein.
(8) Hayes, R. N.; Paltridge, R. L.; Bowie, J. H. *J. Chem. Soc., Perkin Trans. 2* **1985**, 567.

0276-7333/86/2305-0162$01.50/0

Table I. Partial ICR Spectra for the Reactions between R^1O^- (from R^1ONO) and R^2_3B (M)

R^1	R^2	$[R^1O^-]$	$[M + R^1O^-]$	$[M - H^+]$	$[M + H^-]^a$	$[R^2_2BO^-]$
Me	Me	100	3	23	12[b]	*b*
CD_3	Me	100	4	25	14[c,d]	*d*
Et	Me	100	1	75	45[b]	*b*
Pr	Me	100	1	45	88[b,e]	*b*
Me	Et	100	7	24	9	2
Et	Et	100	2	2	1	3
Pr	Et	100	4	3		1
t-Bu	Et	100	2	1		2
Me	Pr	100	11	24	33	6

[a] The major precursors for these ions are $[HNO^-\cdot]$ for $[M + H^-]$ or $[DNO^-\cdot]$ for $[M + D^-]$—see, e.g., Figure 1. [b] $[Me_2BO^-]$ and $[Me_3BH^-]$ are both m/z 57. [c] In this case $[M + D^-]$. [d] $[Me_2{}^{11}BO^-]$ and $[Me_3{}^{10}BD^-]$ are both m/z 57. [e] $[Me_3BH^-]$ and $[MeCH{=}CHO^-]$ (from PrO^-) are both m/z 57.

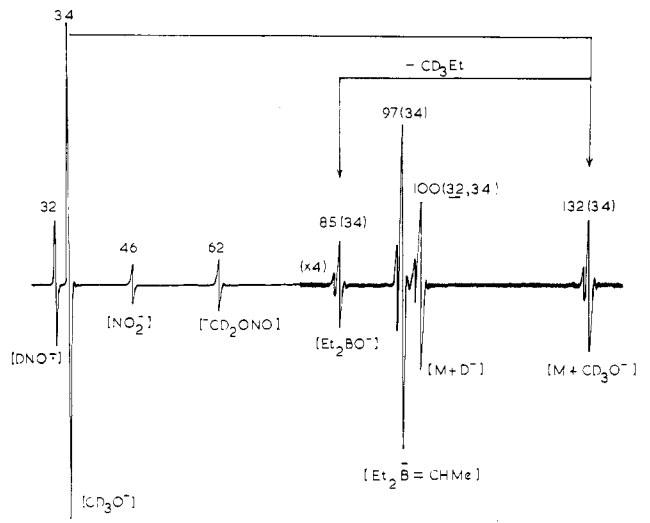

Figure 1. ICR spectrum of the system CD_3ONO/Et_3B. For experimental conditions, see Experimental Section. Numbers in parentheses refer to the masses of precursor ions as determined by cyclotron ejection.

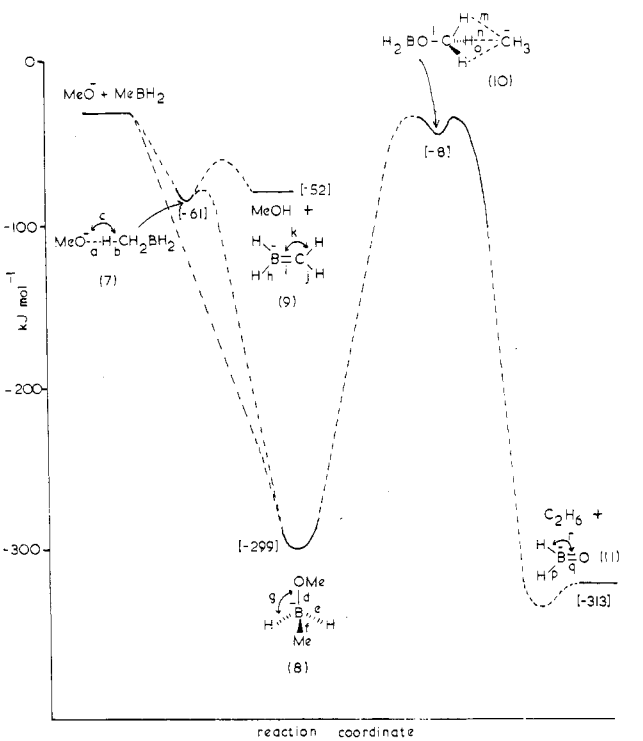

Figure 2. Ab initio calculations for reactions of MeO^- with $MeBH_2$. Calculations on **8**, **9**, and **11** performed with Gaussian 76 (4-31G) and other calculations with Gaussian 82 (4-31G level). Numbers in parentheses refer to structure numbers and numbers in brackets to energies. Solid lines refer to data obtained from fully optimized geometries. (4-31G level). Bond lengths (Å) and angles (deg) are as follows: **7**, $a = 1.75$, $b = 1.15$, $c = 178$; **8**, $d = 1.53$, $e = 1.25$, $f = 1.65$, $g = 109.4$; **9**, $h = 1.22$, $i = 1.44$, $j = 1.085$, $k = 120$; **10**, $l = 1.48$, $m = 2.56$, $n = 2.88$, $o = 2.88$; **11**, $p = 1.24$, $q = 1.295$, $r = 120$.

boron anions are summarized in sequences **2** and **3**.[9] The fluoride negative ion reacts with diborane to give a number of product ions including BH_4^- (reaction 4),[10] and it has been demonstrated that BH_4^- [unlike CH_3O^-[12] and $C_6H_7^-$[13]] does not transfer H^- to formaldehyde in gas-phase experiments.[11] Reactions **5** and **6** occur between CD_3O^- and diborane.[10] Deuterium transfer (from $DNO^-\cdot$)[10] and fluoride transfer (from NF_3, $SF_6^-\cdot$, and SF_5^-)[14,15] to trimethylborane yield Me_3BR^- (R = D or F). Alkoxide negative ions deprotonate trimethylborane to form $Me_2B^-{=}CH_2$.[10]

Results and Discussion

(A) Trialkylboranes. (1) Reactions with Alkoxide Negative Ions. The ICR spectra obtained for alkoxide ion/trialkylborane systems are recorded in Table I, and a representative spectrum (CD_3O^-/Et_3B) is shown in Figure 1.

The reactions may be summarized as follows. (i) Alkoxide ions react with trialkylboranes to give both stable and decomposing ($M + RO^-$) adducts.[16] Adducts decompose by the process $R^1O^- + R^2_3B \rightarrow R^2_2BO^- + R^1R^2$. (ii) Alkoxide ions deprotonate trialkylboranes to yield ($M - H^+$) ions. (iii) ($M + H^-$) ions are observed in the majority of spectra: these ions are shown by cyclotron ejection experiments to be formed mainly from $HNO^-\cdot$ and to a lesser extent by transfer of an α hydrogen from the alkoxide ion.

We have undertaken a study of the structures of certain reactive intermediates and product ions in the above reaction sequences using ab initio calculations (at 4-31G

(9) Enrione, R. E.; Rosen, R. *Inorg. Chim. Acta* **1967**, *1*, 169.
(10) Murphy, M. K.; Beauchamp, J. L. *J. Am. Chem. Soc.* **1976**, *98*, 1433.
(11) Kayser, M. M.; McMahon, T. B. *Tetrahedron Lett.* **1948**, *25*, 3379.
(12) Ingemann, S.; Kleingeld, J. C.; Nibbering, N. M. M. *J. Chem. Soc., Chem. Commun.* **1982**, 1009. Sheldon, J. C.; Bowie, J. H.; Hayes, R. N. *Nouv. J. Chim.* **1984**, *8*, 79; Sheldon, J. C.; Currie, G. J.; Lahnstein, J.; Hayes, R. N.; Bowie, J. H. *Nouv. J. Chim.* **1985**, *9*, 205.
(13) DePuy, C. H.; Bierbaum, V. M.; Schmitt, R. J.; Shapiro, R. H. *J. Am. Chem. Soc.* **1978**, *100*, 2920.
(14) Rhynne, T. C.; Dillard, J. G. *Inorg. Chem.* **1971**, *10*, 730.
(15) Murphy, M. K.; Beauchamp, J. L. *Inorg. Chem.* **1977**, *16*, 2437.

(16) Both "stable" and "decomposing" adducts ($M + RO^-$) are considered to have the same structure in this case, viz., tetrahedral geometry. Such adducts are formed in strongly exothermic reactions. A "stable" adduct is one which is detected as a peak in an ICR spectrum—its energy of formation has been dissipated either by collision or by some other (e.g., radiative) process. A "decomposing" adduct is one which has retained sufficient of its formation energy in order that energy barrier(s) may be surmounted, and product(s) formed.

Table II. Partial ICR Spectra for the Reactions between [RO⁻•••HOR][a] and R^1_3B (M)

R	R^1	[RO⁻]	[RO⁻···HOR]	[M + RO⁻]	[M − H⁺]	[M + H⁻][b]	[$R^1_2BO^-$]
Me	Me	100	21	15	21	12[c]	*c*
Et	Me	100	11	8	93	20[c]	*c*
Pr	Me	100	5	3	51	78[c,d]	*d*
t-Bu	Me	100	32	18	26	17[c]	*c*
Me	Et	100	20	11	20	16	4

[a] Produced by the Riveros reaction[7] between RO⁻ (from RONO) and HCO_2R. [b] The major precursor for these ions is [HNO⁻·]. [c] [Me_2BO^-] and [Me_3BH^-] are both *m/z* 57. [d] [Me_3BH^-] and [MeCH=CHO⁻] (from PrO⁻) are both *m/z* 57.

Table III. Partial ICR Spectra for Reactions R^1O^- (from R^1ONO) and $B(OR^2)_3$ (M)

R^1	R^2	[R^1O^-]	[R^2O^-]	[M + R^1O^-]	[M + R^2O^-]	[$(R^2O)_2BO^-$]
CD_3	Me	87	39	63	100	1
Et	Me	100	25	20		3
Pr	Me	100	46	22	25	1
i-Pr	Me	100	29	53	7	0.5
Bu	Me	54	100	72	57	1
t-Bu	Me	100	19	74	68	
neo-Pen	Me	18	100	67	36	1
Me	Et	100	56	29	11	1
Pr	Et	100	8	56	10	2

level[17] using Gaussian 76[18] and 82[19]). Results are shown in Figure 2 for the model system $MeO^-/MeBH_2$. If MeO⁻ approaches the neutral in the vicinity of the methyl group, a transient H-bonded species **7** is formed which is a precursor of both the deprotonated ion **9** and the tetrahedral adduct **8**. However we believe that there is also a second channel to **8**, in which MeO⁻ skirts the methyl substituent, approaches, and bonds to boron with monotonically decreasing energy.[20] Adduct **8** is formed with considerable excess energy (−299 kJ mol⁻¹, 4-31G), and in order to produce a stable form, collisional deactivation would be necessary. The decomposing form of the adduct **8** eliminates ethane to form H_2BO^- (**11**). The reaction is stepwise, proceeding through the intermediacy of solvated methyl anion **10**.[21]

In Figure 2 we indicate that the solvated ion **7** is formed by nucleophilic addition to a trialkylborane and that this species may then rearrange to tetrahedral ion **8** in a strongly exothermic process. We have been unable to identify such solvated species by solvent-exchange experiments. For example if the (M + MeO⁻) species formed from MeO⁻ and Me_3B is allowed to react with CD_3OD or EtOH, neither (M + CD_3O^-) nor (M + EtO^-) ions are produced. Stable (M + RO⁻) species are thus likely to correspond to tetrahedral structures.

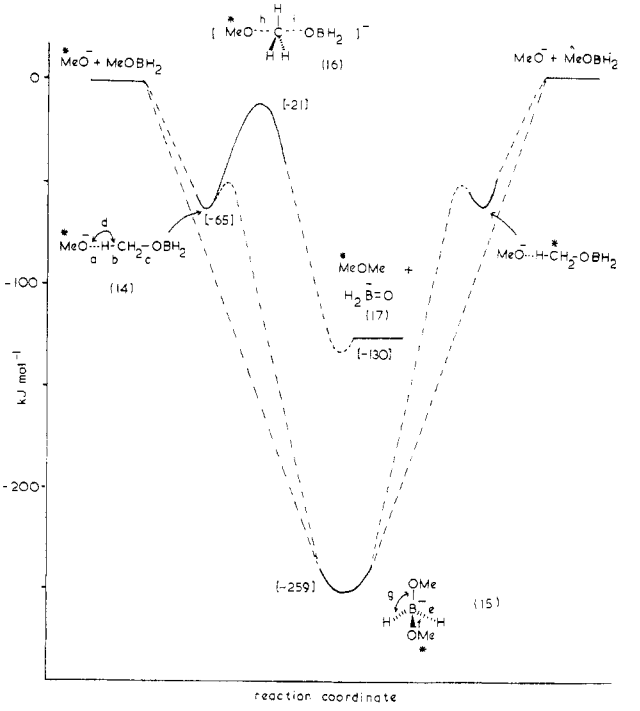

Figure 3. Ab initio calculations for reactions of MeO⁻ with $MeOBH_2$. Calculations on **15** and **17** performed with Gaussian 76 (4-31G) and other calculations with Gaussian 82. Numbers in parentheses refer to structure numbers and numbers in brackets to energies. Solid lines refer to data obtained from fully optimized geometries. Bond lengths (Å) and angles (deg) are as follows: **14**, a = 1.89, b = 1.09, c = 1.47, d = 207; **15**, e = 1.25, f = 1.49, g = 109.4; **16**, h = 2.11, i = 1.80.

(2) Reactions with Alkoxide–Alkanol Negative Ions. The ICR spectra obtained from reactions between alkoxide–alkanol negative ions and trialkylborane are listed in Table II. Alkoxide–alkanol ions (RO⁻···HOR)[7] yield stable adducts (M + RO⁻) with trialkylboranes. The relative yield of stable (M + RO⁻) ions is greater when the reactant ion is (RO⁻···HOR) rather than RO⁻, since the

(17) We recognize that accurate representation of negatively charged species requires expanded bases (Radom, L. *Mod. Theor. Chem.* **1977**, *4*, 333. Chandraseka, J.; Andrade, J. G.; Schleyer, P. v. R. *J. Am. Chem. Soc.* **1981**, *103*, 5609), preferably with a low-exponent Gausian in each set to represent the diffuse outer region of negative ions. Nevertheless we believe that systematic exploration of the relative energies of intermediates and products at a practical level of approximation is indispensable if reaction sequences (like those shown in Figure 2) are to be evaluated and characterized.

(18) Binkley, J. S.; Whitehead, R. A.; Hariharan, P. C.; Seeger, R.; Pople, J. A. *QCPE* **1978**, 368.

(19) Gordon, M. S.; Binkley, J. S.; Pople, J. A.; Pietro, W. J.; Hehre, W. J. *J. Am. Chem. Soc.* **1982**, *104*, 2797.

(20) We have not carried out calculations on this channel, but calculations on the model system $F^-/MeBH_2$ clearly show two channels, viz., the formation of an H-bonded intermediate corresponding to **7** (Figure 2) and direct attack of F⁻ on boron. A similar situation occurs for the reaction of MeO⁻ with $MeSiH_3$ (Sheldon, J. C; Hayes, R. N.; Bowie, J. H. *J. Am. Chem. Soc.* **1984**, *106*, 7711).

(21) (a) Analogous gas-phase reactions are observed in other systems, e.g., alkoxides (Tumas, W.; Foster, R. F.; Pellerite, M. J.; Brauman, J. I. *J. Am. Chem. Soc.* **1983**, *105*, 7464. Tumas, W.; Foster, R. F.; Brauman, J. I. *J. Am. Chem. Soc.* **1984**, *106*, 4053. Hayes, R. N.; Sheldon, J. C.; Bowie, J. H.; Lewis, D. E. *J. Chem. Soc., Chem. Commun.* **1984**, 1431; *Aust. J. Chem.* **1985**, *38*, 1197), tetrahedral adducts formed between alkoxide negative ions and carbonyl systems (e.g. Klass, G.; Underwood, D. J.; Bowie, J. H. *Aust. J. Chem.* **1981**, *34*, 507), and silanes (DePuy, C. H.; Bierbaum, V. M.; Flippin, L. A.; Grabowski, J. J.; Schmitt, G. K.; Sullivan, S. A. *J. Am. Chem. Soc.* **1980**, *102*, 5012. DePuy, C. H., Bierbaum, V. M.; Damrauer, R. *J. Am. Chem. Soc.* **1984**, *106*, 4051. Klass, G.; Trenerry, V. C.; Sheldon, J. C.; Bowie, J. H. *Aust. J. Chem.* **1981**, *34*, 519). There are subtle differences in the structures of the reactive intermediates (e.g., **10**, Figure 2) in the various reaction sequences. (b) A reviewer has suggested that if the alkoxy group is larger than OMe, an elimination reaction may compete with the reaction sequence analogous to **8** → **10** → **11** (Figure 2). For example in the case of the system $EtO^-/MeBH_2$ this would be $EtO^- + MeBH_2 \rightarrow (EtO)(Me)BH_2^- \rightarrow H_2BO^- + CH_4 + C_2H_4$.

Table IV. Partial ICR Spectra for Reactions between $[R^1O\bullet\bullet\bullet H\bullet\bullet\bullet OR^2]^-$ and $R^3B(OR^4)_2$ (M)

R^1	R^2	R^3	R^4	$[R^1O^-]$	$[R^2O^-]$	$[R^3O^-]$	$[R^1O\cdots H\cdots OR^2]^-$ [a]	$[R^2O\cdots H\cdots OR^4]^-$ [b]	$[R^1O\cdots H\cdots OR^4]^-$ [c]	$[M + R^1O^-]$	$[M + R^2O^-]$	$[M + R^4O^-]$
Et	Et	Me	Me	96	(96)	20	42	*d*	4[d]	100		5
Et	Bu	Me	Me	68	37	8	100[e]	1	4	23	18	*e*
Et	Et	Me	Bu	100	(100)	34	65	*d*	71[d]	21		5
Me	Pr	Et	Et	100	6	2	35	4	2	3	20	5
Me	Me	Et	Bu	100	(100)	11	39	*d*	14[d]	11		
Me	Et	Et	Bu	99	17	7	100	7	15	2	3	
Et	Et	Pr	Me	100	(100)	26	76	*d*	8[d]	2		1
Pr	Pr	Pr	Me	63	(63)	21	100	*d, f*	7[d]	13		
Et	Bu	Pr	Me	100	53	13	60	*f*	2	1	4	0.5

[a] $[R^1O\cdots H\cdots OR^2]^-$ is produced by the Riveros reaction between R^2O^- and HCO_2R^1. [b] $[R^2O\cdots H\cdots OR^4]^-$ is produced by a specific alkoxide-exchange reaction between $[R^1O\cdots H\cdots OR^2]^-$ and $R^3B(OR^4)_2$. [c] $[R^1O\cdots H\cdots OR^4]^-$ is produced by the Riveros reaction between R^4O^- and HCO_2R^1 (R^4O^- is produced by the reaction between R^2O^- and $R^3B(OR^4)_2$). [d] Since $R^1 = R^2$ in this case: $[R^1O\cdots H\cdots OR^4]^-$ is the same as $[R^2O\cdots H\cdots OR^4]^-$. [e] $[EtO\cdots H\cdots OBu]^-$ and $[M + MeO^-]$ are both *m/z* 119. [f] No alkoxide-exchange reaction is observed between $[R^1O\cdots H\cdots OR^2]^-$ and $R^3B(OR^4)_2$.

Table V. Partial ICR Spectra for Reactions between $[R^1O\bullet\bullet\bullet H\bullet\bullet\bullet OR^2]^-$ and $B(OR^3)_3$ (M)

R^1	R^2	R^3	$[R^1O^-]$	$[R^2O^-]$	$[R^3O^-]$	$[R^1O\cdots H\cdots OR^2]^-$ [a]	$[R^2O\cdots H\cdots OR^3]^-$ [b]	$[R^1O\cdots H\cdots OR^3]^-$ [c]	$[M + R^1O^-]$	$[M + R^2O^-]$	$[M + R^3O^-]$
Et	CD_3	Me	25	19	100	3		16	5	17	17
Et	Et	Me	100	(100)	95	13	*d*	10[d]	49		11
Et	Pr	Me	100	11	58	36	8	33	5	13	15
Et	*i*-Pr	Me	100	(100)	34	53	0.5	6	9	17	9
CD_3	Bu	Me	100	(100)	78	21	1	17	4	27	8
t-Bu	*t*-Bu	Me	100	(100)	38	36			36		26
Me	Me	Et	100	(100)	46	12	*d*	5[d]	88		51
Me	Pr	Et	100	24	51	49	3	33	31	72	37
Me	Me	Pr	100	(100)	6	31	*d*	5[d]	1		
Me	Et	Pr	100	29	14	43	12	22	8	7	0.4
Me	Bu	Pr	8	39	100	63	9	82	15	3	8
Me	Me	Bu	80	(80)	2	100	*d*	13[d]			
Me	Et	Bu	100	21	11	88	12	20			
Me	Pr	Bu	100	24	8	88	23	22			

[a] $[R^1O\cdots H\cdots OR^2]^-$ is produced by the Riveros reaction between R^2O^- and HCO_2R^1. [b] $[R^2O\cdots H\cdots OR^3]^-$ is produced by a specific alkoxide-exchange reaction between $[R^1O\cdots H\cdots OR^2]^-$ and $B(OR^3)_3$. [c] $[R^1O\cdots H\cdots OR^3]^-$ is produced by a Riveros reaction between R^3O^- and HCO_2R^1 (R^3O^- is produced by the reaction of R^2O^- with $B(OR^3)_3$). [d] Since $R^1 = R^2$ in this case: $[R^1O\cdots H\cdots OR^3]^-$ is the same as $[R^2O\cdots H\cdots OR^3]^-$.

eliminated molecule of ROH takes off some of the excess energy of the reaction effectively stabilizing the $(M + RO^-)$ species. Alkoxide–alkanol ions do not deprotonate trialkylboranes, they do not transfer hydride ion to the neutral, and they do not act as precursors to R_2BO^- ions.

We were able to demonstrate attachment of $(RO^-\cdots DOR)$ to hydrogen in >CH–CO– systems because of the occurence of a specific H/D equilibration reaction.[22] The analogous intermediates for $(RO^-\cdots DOR)/Me_3B$ are **12** and **13**. In an ICR experiment, the reaction between (EtO-

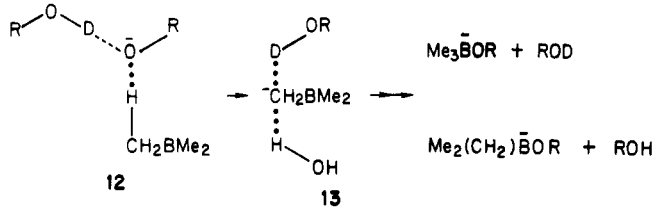

$\cdots D\cdots OPr)^-$ and Me_3B yielded $(Me_3BOEt)^-$ and $(Me_3BOPr)^-$. No H/D equilibration occurred; therefore, we can provide no experimental evidence for the intermediacy of **12** in the reaction pathway. Nevertheless we believe that ions analogous to **12** are initial intermediates in reaction sequences (of this type) which lead to four-coordinate boron negative ions (cf. also Figure 2).

(B) Alkoxyboranes. (1) Reactions with Alkoxide Negative Ions. The ICR spectra obtained from reactions between alkoxide negative ions and trialkylborates are listed in Table III. Ab initio calculations (at 4–31G level) are recorded in Figure 3 for the model system $MeO^-/(MeO)BH_2$.

An alkoxide ion approaching a methoxyborane (rotating through its center of mass) encounters the hydrogens of a methyl group and may form an initial hydrogen-bonded intermediate (e.g., **14**, Figure 3).[23] Such an intermediate is a precursor for products formed in these systems.

Products are summarized as follows. (i) Pronounced peaks corresponding to stable four-coordinate boron anions are observed for all systems studied. The reactions are strongly exothermic, and the product ion must be stabilized by collisional deactivation. The high yields of stable $(M + RO^-)$ adducts (e.g., **15**, Figure 3) in these systems should be contrasted with the small abundances of analogous peaks in trialkylborane systems. Perhaps the difference is due to the stabilizing effect of oxygen atoms of the alkoxyborane system from dative π bonding into the vacant 2p orbital.[24] (ii) Alkoxide displacement (through, e.g., **15**, Figure 3) is the major reaction of these systems. The liberated alkoxide ion also undergoes reaction with the alkoxyborane to yield a four-coordinate boron ion. (iii) All systems show the reaction $R^1O^- + (R^2O)_3B \rightarrow (R^2O)_2BO^- + R^1OR^2$. This reaction could, in principle, occur by two mechanisms, viz., a 1,2-elimination from an excited four-coordinate intermediate $[(R^2O)_3B(OR^1)]^-$ (cf. **8** → **11**, Figure 2) or an S_N2 reaction at carbon. In order

(22) Klass, G.; Sheldon, J. C.; Bowie, J. H. *Aust. J. Chem.* **1982**, *35*, 2471.

(23) There is also a strong possibility that MeO^- may directly attack boron in this system, but we have not carried out calculations on this possible reaction channel.

(24) Cotton, F. A.; Wilkinson, G. "Advanced Inorganic Chemistry. A Comprehensive Text", 3rd ed.; Wiley Interscience: New York, 1972; p 223.

Table VI. Partial ICR Spectra for the Reactions $[R^1O\bullet\bullet\bullet H\bullet\bullet\bullet OR^2]^-$ and $Et\overline{BOCH_2CH_2O}$ (M)

R^1	R^2	$[R^1O^-]$	$[R^2O^-]$	$[R^1O\cdots H\cdots OR^2]^{-a}$	$[R^1O^-\cdots HOR^1]^b$	$[M + R^1O^-]$	$[M + R^2O^-]$	$[M + (R^1O\cdots H\cdots OR^2)^-]$	$[M + (R^1O^-\cdots HOR^1)]$
Me	Me	100		44		60		2	
Me	Et	66	13	72	5	59	17	3	1
Me	Pr	84	19	100	2	68	36	4	1

[a] $[R^1O\cdots H\cdots OR^2]^-$ is produced by the Riveros reaction between R^2O^- and HCO_2R^1. [b] $[R^1O^-\cdots HOR^1]$ is produced by the Riveros reaction between R^1O^- and HCO_2R^1 (R^1O^- is produced by the reaction between R^2O^- and HCO_2R^1).

to differentiate experimentally between these two possibilities, $Me^{18}O^-$ was allowed to react with trimethoxyborane. No ^{18}O was incorporated into the peak corresponding to $(MeO)_2BO^-$: the reaction therefore proceeds by an S_N2 mechanism (e.g., **14** → **16** → **17**, Figure 3).

(2) Reactions with Alkoxide–Alkanol Negative Ions. Results obtained for reactions of $(R^1O\cdots H\cdots OR^2)^-$ with both dialkoxyboranes and alkylborates are listed in Tables IV and V. In summary: (i) alkanol–alkoxide negative ions $(R^1O\cdots H\cdots OR^2)^-$ react with alkoxyboranes to yield stable species $(M + R^1O^-)$ and $(M + R^2O^-)$; (ii) the only other reaction observed is the alkoxide exchange reaction **18** ($R^1 \leq R^2$, at least either R^1 or R^2 must be ethyl or larger and R^3 is either alkyl or OR^4).

$$(R^1O\cdots H\cdots OR^2)^- + R^3B(OR^4)_2 \rightarrow (R^2O\cdots H\cdots OR^4)^- + R^3B(OR^4)(OR^1)$$

18

$$(R^1O\cdots H\cdots OR^2)^- + R^3B(OR^4)_2 \rightarrow (R^1O\cdots H\cdots OR^4)^- + R^3B(OR^4)(OR^2)$$

19

In this reaction the smaller alkoxide ion reacts at boron and the larger alkanol forms part of the new alkanol–alkoxide ion. We were not able to detect (by cyclotron ejection experiments) addition in the reverse direction (i.e., reaction **19**).[25] This specificity is similar to that observed for analogous reactions in Si–OR systems:[3] in contrast, addition in both directions occurs for C–OR reactions with that analogous to **18** being the major process.[8] The yield of product alkanol–alkoxide ion increases with elaboration of R^1 and R^2 and decreases with elaboration of R^4 in accord with previous results in carbon[8] and silicon[3] systems.

A number of possible mechanisms can be proposed for the alkoxide-exchange reaction of alkoxyboranes, but the most plausible is that shown in sequence **20**. We have

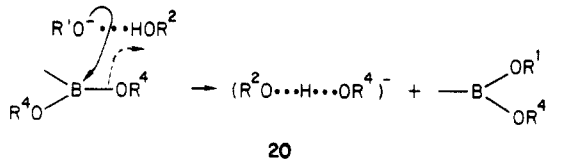

20

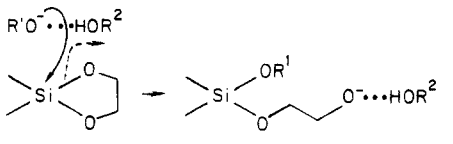

21

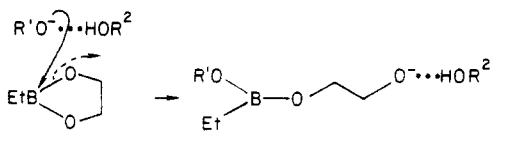

22

(25) We have not carried out ab initio calculations for this reaction. It is certainly close to thermoneutral, but we do not know if the specificity is due to internal barriers for the stepwise reactions.

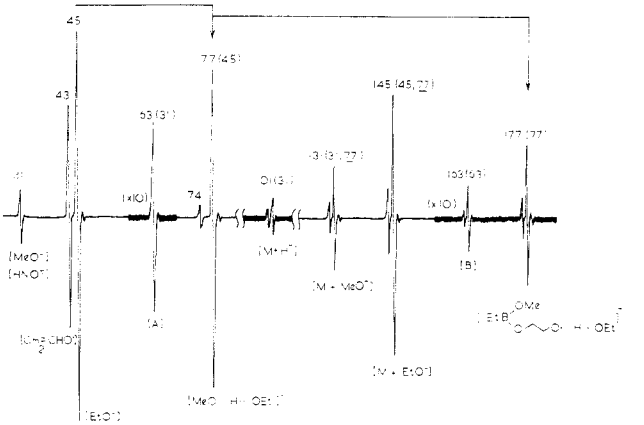

Figure 4. ICR spectrum of the system $EtONO/HCO_2Me/Et\overline{BOCH_2CH_2O}$. For experimental conditions, see Experimental Section. Numbers in parentheses refer to the masses of precursor ions as determined by cyclotron ejection: (A) $(MeO^-\cdots HOMe)$, are formed by the Riveros reaction between MeO^- and HCO_2Me; (B) $[Et(MeO)B–O(CH_2)_2O^-\cdots HOMe]$, formed by the alkoxide exchange reaction from $(MeO^-\cdots HOMe)$ (m/z 63).

already shown that analogous processes occur for carbon[8] and silicon[3] ether systems, e.g., the unsymmetrical precursor $(R^1O\cdots H\cdots OR^2)^-$ reacts with cyclic silyl ethers in the *specific* manner shown in reaction **21**. If such a mechanism (e.g., **20**) is operating in boron systems, it should be possible to observe reaction **22** for cyclic boronates.

The ICR spectra of $(R^1O\cdots H\cdots OR^2)^-$ and $Et\overline{BOCH_2CH_2O}$ systems are recorded in Table VI and Figure 4. The situation is best described by reference to Figure 4. The reactant ion $(MeO\cdots H\cdots OEt)^-$ (m/z 77, from EtO^- and HCO_2Me) reacts with the cyclic boronate to yield both $(M + MeO^-)$ and $(M + EtO^-)$ ions. In addition, it reacts to form an adduct $[M + (MeO\cdots H\cdots OEt)^-]$ (m/z 177). In order to determine the structure of m/z 177, a solvent-exchange reaction was carried out. Addition of propanol to the system resulted in solvent exchange with $[M + (MeO\cdots H\cdots OEt)^-]$ ion to form exclusively the species $[M + (MeO\cdots H\cdots OPr)^-]$. Thus *the methoxide ion is bound to boron, and the ethanol residue is hydrogen bonded to the oxy moiety* as shown in Figure 4 (cf. reactions **20** and **22**).[26]

Conclusions

Alkoxide and alkoxide–alkanol ions show quite different reactivity toward trisubstituted boranes—in summary: (i) both alkoxide and alkoxide–alkanol ions react with trisubstituted boranes to yield tetrahedral ions $RO\bar{B}R_3$, with the latter reactant ion providing the more abundant product peaks; (ii) alkoxide–alkanol ions undergo a specific alkoxide exchange reaction with alkoxyboranes, e.g.,

(26) A reviewer has suggested that the solvated product ion shown in sequence (**22**) could be in equilibrium with $(R^1O)(R^2O)EtB^-O(CH_2)_2OH$. This is possible: our "solvent-switching" experiment merely establishes the presence and identity of the solvated ion.

$(R^1O\cdots H\cdots OR^2)^- + >B–OR^3 \rightarrow (R^2O\cdots H\cdots OR^3)^- + >B–OR^1$ when $R^1 \leq R^2$; (iii) alkoxide ions react with both alkyl- and alkoxyboranes by reaction channels not available for the solvated ions: e.g., deprotonation of alkylboranes, hydride transfer to alkylboranes, 1,2-elimination reactions (e.g., $MeO^- + R_3B \rightarrow R^2BO^- + MeR$), alkoxide displacement with alkoxyboranes and S_N2 reactions with alkoxyboranes.

Experimental Section

ICR spectra were measured with a Dynaspec ICR 9 spectrometer equipped with a three-section cell. Spectra were obtained at 70 eV (primary negative ions formed by dissociative secondary electron capture). Other reaction conditions: $\omega_c/2\pi$ = 125.0 kHz, ion current in 10^{-10} A range, emission current 0.2 μA, and ion transit time 1×10^{-3} s. Precursor ions in reaction sequences were determined by the cyclotron ejection technique. Pressure conditions: (i) in RO^-/borane or borate experiments, both RONO (the precursor of RO^-) and the borane (borate) = 5×10^{-6} torr (total pressure = 1×10^{-5} torr); (ii) for (RO^-–HOR)/borane (borate) experiments, RONO = 5×10^{-6} torr, $HCO_2R = 5 \times 10^{-6}$ torr, and the borane/borate = 1×10^{-5} torr (total pressure = 2×10^{-5} torr).

Alkyl nitrites were prepared from the appropriate alcohol and sodium nitrite by a reported method.[27] Formates, including methyl [^{2}H]formate, were prepared by the method of Stevens and Van Es.[28] All boranes, boronates, and borates were prepared by reported procedures: trimethylborane,[29] triethylborane,[30] tripropylborane,[30] methyl methylboronate,[31] ethyl ethylboronate,[31] butyl ethylboronate,[32] methyl propylboronate,[32] 2-ethyl-1,3,2-dioxaborolane,[33] trimethyl borate,[34] triethyl borate,[35] and tripropyl borate.[35]

Acknowledgment. This work was carried out with the aid of a grant from the Australian Research Grants Scheme. We thank the University of Adelaide Computing Centre for facilities.

Registry No. MeO^-, 3315-60-4; CD_3O^-, 51679-31-3; EtO^-, 16331-64-9; PrO^-, 26232-83-7; *t*-BuO^-, 16331-65-0; *i*-PrO^-, 15520-32-8; BuO^-, 26232-84-8; *neo*-$PenO^-$, 55091-58-2; Me_3B, 593-90-8; Et_3B, 97-94-9; Pr_3B, 1116-61-6; $B(OMe)_3$, 121-43-7; $B(OEt)_3$, 150-46-9; $MeB(OMe)_2$, 7318-81-2; $EtB(Oet)_2$, 53907-92-9; $EtB(OBu)_2$, 3027-60-9; $PrB(OMe)_2$, 2938-87-6; $B(OPr)_3$, 688-71-1; $B(OBu)_3$, 688-74-4; $EtBOCH_2CH_2O$, 10173-38-3.

(27) Noyes, W. A. *Org. Synth.* **1936**, *16*, 108.

(28) Stevens, W.; Van Es, A. *Recl. Trav. Chim. Pays-Bas* **1964**, *83*, 1287.

(29) Brown, H. C. *J. Am. Chem. Soc.* **1945**, *67*, 374.

(30) Rosenblum, L. *J. Org. Chem.* **1960**, *25*, 1652.

(31) Wiberg, E.; Kruerke, U. *Z. Naturforsch., B: Anorg. Chem., Org. Chem., Biochem., Biophys. Biol.* **1953**, *8B*, 608.

(32) Mikhailov, B. M. and Blokhima, A. N. *Izv. Adad. Nauk SSSR, Ser. Khim.* **1962**, 827; *Chem. Abstr.* **1963**, *58*, 5706g.

(33) Laurent, J. P.; Bonnet, J. P. *C. R. Seances Acad. Sci., Ser. C* **1900**, *262*, 1109.

(34) Schlessinger, H. I.; Brown, H. C.; Mayfield, D. L.; Gilbreath, J. R. *J. Am. Chem. Soc.* **1953**, *75*, 213.

(35) Lappert, M. F. *Chem. Rev.* **1956**, *56*, 959.

Activation of Arene Carbon–Hydrogen Bonds. Highly Regioselective, Electrophilic Aromatic Metalation with Rhodium(III) Porphyrin and Subsequent Cleavage of Carbon–Rhodium Bond[1]

Yasuhiro Aoyama,* Tohru Yoshida, Ken-ichi Sakurai, and Hisanobu Ogoshi*

Department of Material Science, Technological University of Nagaoka, Kamitomioka, Nagaoka, Niigata 949-54, Japan

Received June 24, 1985

(Octaethylporphyrinato)rhodium(III) chloride, (OEP)$Rh^{III}Cl$, reacts with benzene in the presence of $AgClO_4$ or $AgBF_4$ to give the phenyl–rhodium(III) complex. Anisole, toluene, and chlorobenzene are similarly metalated exclusively at the para positions. The metalation of methyl benzoate, on the other hand, gives a 92:8 mixture of meta- and para-metalated isomers. The reactivities of arenes follow the Hammett equation with the ρ value of −5.43. The observed substituent effects both on reactivity and orientation unambiguously characterize the present reaction as an electrophilic aromatic metalation with a $[(OEP)Rh^{III}]^+$ intermediate generated from the anion exchange of (OEP)$Rh^{III}Cl$ with silver salts. The slow step in the reaction is coordination of arene to form $[(OEP)Rh(arene)]^+$, which subsequently loses a proton. Arenes thus activated with rhodium undergo photochemical homolysis of the C–Rh bond as well as its halogen-induced heterolysis. The photolysis in benzene leads to 4-substituted biphenyls and the halogenolysis gives *p*-haloarenes with extremely high regioselectivities (>99%).

The activation of chemically inert carbon–hydrogen bonds under mild conditions constitutes a rapidly growing research area in recent years.[2,3] The homogeneous activation of arene C–H bonds by metal complexes involves either oxidative or electrophilic addition of the metal to an arene C–H bond.[2] The great majority of intramolecular or intermolecular arene C–H bond activations by transition-metal species in lower oxidation states involves oxidative addition mechanisms.[3-15] Some non-transition-metal ions such as Hg^{2+}, Tl^{3+}, and Pb^{4+} are known to act as electrophiles capable of metalation of arenes.[16-18] A number of reactions of arenes are catalyzed by transition-metal ions, where arylmetal complexes are often proposed as plausible intermediates. In some cases, transition-metal *electrophiles* lead to isolable arylmetal complexes as is seen in many organic electrophilic substitution reactions; examples include intramolecular ortho metalations[14b,19,20] and intermolecular aromatic platination.[21] In the latter reaction, the observed substituent effects are different from those in classical electrophilic aromatic substitution. While the interaction of olefins with electrophilic transition-metal centers is well understood,[22,23]

(1) Preliminary accounts of this work: Aoyama, Y.; Yoshida, T.; Sakurai, K.; Ogoshi, H. *J. Chem. Soc., Chem. Commun.* **1983**, 478.

(2) (a) Halpern, J. *Discuss. Faraday Soc.* **1968**, *46*, 7. (b) Parshall, G. W. *Acc. Chem. Res.* **1970**, *3*, 139. (c) Parshall, G. W. *Chem. Tech.* **1974**, *4*, 445. (d) Parshall, G. W. *Acc. Chem. Res.* **1975**, *8*, 113. (e) Dehand, J.; Pfeffer, M. *Coord. Chem. Rev.* **1976**, *18*, 327. (f) Clarke, J. K. A.; Rooney, J. J. *Adv. Catal.* **1976**, *25*, 125. (g) Shilov, A. E.; Shteinman, A. A. *Coord. Chem. Rev.* **1977**, *24*, 97. (h) Bruce, M. I. *Angew. Chem., Int. Ed. Engl.* **1977**, *16*, 73. (i) Shilov, A. E. *Pure Appl. Chem.* **1978**, *50*. 725. (j) Parshall, G. W. "Homogeneous Catalysis"; Wiley-Interscience: New York, 1980; Chapter 7. (k) Collman, J. P.; Hegedus, L. S. "Principles and Applications of Organotransition Metal Chemistry"; University Science Books: Mill Valley, CA, 1980. (l) Puddephatt, R. J. *Coord. Chem. Rev.* **1980**, *33*, 149.

(3) For recent work on transition-metal systems capable of intermolecular oxidative addition to C–H bonds in saturated hydrocarbons, see: (a) Janowicz, A. H.; Bergman, R. G. *J. Am. Chem. Soc.* **1982**, *104*, 352. (b) Hoyano, J. K.; Graham, W. A. G. *Ibid.* **1982**, *104*, 3723. (c) Watson, P. L. *J. Chem. Soc., Chem. Commun.* **1983**, 276. References cited in ref 3a cover recent work on intramolecular oxidative addition to unactivated sp^3 C–H bonds and intermolecular oxidative addition to activated sp^3 C–H bonds.

(4) (a) Green, M. L. H.; Knowles, P. J. *J. Chem. Soc. A* **1971**, 1508. (b) Giannotti, C.; Green, M. L. H. *J. Chem. Soc., Chem. Commun.* **1972**, 1114. (c) Elmitt, K.; Green, M. L. H.; Forder, R. A.; Jefferson, I.; Prout, K. *Ibid.* **1974**, 747. (d) Fornies, J.; Green, M.; Spencer, J. L.; Stone, F. G. A. *J. Chem. Soc., Dalton Trans.* **1977**, 1006. (e) Cooper, J. N.; Green, M. L. H.; Mahtab, R. *Ibid.* **1979**, 1557. (f) Berry, M.; Elmitt, K.; Green, M. L. H. *Ibid.* **1979**, 1950.

(5) (a) Ittel, S. D.; Tolman, C. A.; English, A. D.; Jesson, J. P. *J. Am. Chem. Soc.* **1976**, *98*, 6073. (b) Ittel, S. D.; Tolman, C. A.; English, A. D.; Jesson, J. P. *Ibid.* **1978**, *100*, 7577. (c) Tolman, C. A.; Ittel, S. D.; English, A. D.; Jesson, J. P. *Ibid.* **1979**, *101*, 1742.

(6) Jones, W. D.; Feher, F. J. *J. Am. Chem. Soc.* **1982**, *104*, 4240.

(7) Bruno, J. W.; Marks, T. J.; Day, V. W. *J. Am. Chem. Soc.* **1982**, *104*, 7357.

(8) Bradley, M. G.; Roberts, D. A.; Geoffroy, G. L. *J. Am. Chem. Soc.* **1981**, *103*, 379.

(9) Tulip, T. H.; Thorn, D. L. *J. Am. Chem. Soc.* **1981**, *103*, 2448.

(10) (a) Bruce, M. I.; Goodall, B. L.; Stone, F. G. A. *J. Chem. Soc., Chem. Commun.* **1973**, 558. (b) Bruce, M. I.; Gardner, R. C. F.; Goodall, B. L.; Stone, F. G. A. *Ibid.* **1974**, 187. (c) Bruce, M. I.; Goodall, B. L.; Stone, F. G. A. *J. Chem. Soc., Dalton Trans.* **1978**, 687.

(11) Rausch, M. D.; Gastinger, R. G.; Gardner, S. A.; Brown, R. K.; Wood, J. S. *J. Am. Chem. Soc.* **1977**, *99*, 7870.

(12) Wong, K. L. T.; Thomas, J. L.; Brintzinger, H. H. *J. Am. Chem. Soc.* **1974**, *96*, 3694.

(13) (a) Barefield, E. K.; Parshall, G. W.; Tebbe, F. N. *J. Am. Chem. Soc.* **1970**, 92, 5234. (b) Tebbe, F. N.; Parshall, G. W. *Ibid.* **1971**, *93*, 3793.

(14) (a) van Baar, J. F.; Vrieze, K.; Stufkens, D. J. *J. Organomet. Chem.* **1975**, *97*, 461. (b) Hietkamp, S.; Stufkens, D. J.; Vrieze, K. *Ibid.* **1979**, *168*, 351.

(15) (a) Kleiman, J. P.; Dubeck, M. *J. Am. Chem. Soc.* **1963**, *85*, 1544. (b) Chatt, J.; Davidson, J. M. *J. Chem. Soc.* **1965**, 843. (c) Bennett, M. A.; Milner, D. L. *J. Am. Chem. Soc.* **1969**, *91*, 6983. (d) Ustynyuk, Y. A.; Barinov, I. V. *J. Organomet. Chem.* **1970**, *23*, 551. (e) Cheney, A. J.; Mann, B. E.; Shaw, B. L.; Slade, R. M. *J. Chem. Soc. A* **1971**, 3833. (f) Guss, J. M.; Mason, R. *J. Chem. Soc., Chem. Commun.* **1971**, 58. (g) Abicht, H. P.; Issleib, K. *Z. Chem.* **1977**, *17*, 1.

(16) Kitching, W. *Organomet. Chem. Rev.* **1968**, *3*, 35.

(17) McKillop, A.; Hunt, J. D.; Zelesko, M. J.; Fowler, J. S.; Taylor, E. C.; McGillivray, G.; Kienzle, F. *J. Am. Chem. Soc.* **1971**, *93*, 4841.

(18) Harvey, D. R.; Norman, R. O. C. *J. Chem. Soc.* **1964**, 4860.

(19) Cope, A. C.; Siekman, R. W. *J. Am. Chem. Soc.* **1965**, *87*, 3272.

(20) Ahmad, N.; Ainscough, E. W.; James, T. A.; Robinson, S. D. *J. Chem. Soc. D* **1973**, 1151.

(21) (a) Gol'dshleger, N. F.; Nekipelov, V. M.; Nikitaev, A. T.; Zamaraev, K. I.; Shilov, A. E.; Shteinman, A. A. *Kinet. Katal.* **1979**, *20*, 538. (b) Shul'pin, G. B.; Rosenberg, L. P.; Shibaeva, R. P.; Shilov, A. E. *Ibid.* **1979**, *20*, 1570. (c) Shul'pin, G. B.; Shilov, A. E.; Kitaigorodskii, A. N.; Krevor, J. V. Z. *J. Organomet. Chem.* **1980**, *201*, 319. (d) Shul'pin, G. B.; Kitaigorodskii, A. N. *Zh. Fiz. Khim.* **1981**, *55*, 266. (e) Shul'pin, G. B. *J. Organomet. Chem.* **1981**, *212*, 267. (f) Shul'pin, G. B. *Kinet. Katal.* **1981**, *22*, 520. (g) Shul'pin, G. B.; Nikitaev. A. T. *Izv. Akad. Nauk SSSR, Ser. Khim.* **1981**, 1416. (h) Shul'pin, G. B.; Nizova, G. V. *Kinet. Katal.* **1981**, *22*, 1061. (i) Shul'pin, G. B.; Nizova, G. V. *Izv. Akad. Nauk SSSR, Ser. Khim.* **1982**, 1172.

(22) Stern, E. W. In "Transition Metals in Homogeneous Catalysis"; Schrauzer, G. N., Ed.; Marcel Dekker: New York, 1971; pp 96–107.

(23) Sen, A.; Lai, T.-W. *J. Am. Chem. Soc.* **1981**, *103*, 4627.

0276-7333/86/2305-0168$01.50/0

Table I. Microanalyses and Yields of $(OEP)Rh^{III}C_6H_4X$

compd	X	yield, %	formula	calcd C	calcd H	calcd N	found C	found H	found N
2	p-OCH_3	46	$C_{43}H_{51}N_4ORh$	69.53	6.92	7.54	69.08	6.84	7.42
4	p-Cl	18	$C_{42}H_{48}N_4ClRh$	67.51	6.48	7.50	67.36	6.50	7.44
5	m-CO_2CH_3	22	$C_{44}H_{51}N_4O_2Rh$	68.56	6.67	7.27	68.19	6.74	6.93

it still remains to be clarified how transition-metal electrophiles compare with such electrophiles as NO_2^+ used in usual electrophilic aromatic substitution. In this study we have investigated the activation of arenes by a Rh^{III} electrophile and subsequent functionalization of the coordinated arenes.

Results

Metalation of Benzene. In the presence of a slightly greater than molar amount of $AgClO_4$ or $AgBF_4$, (octaethylporphyrinato)rhodium(III) chloride, $(OEP)Rh^{III}Cl$, readily reacted with benzene under mild conditions (≤50 °C) to give the σ-bonded phenyl–rhodium(III) complex **1** (eq 1) in yields of 40 (with $AgClO_4$) and 70% (with $AgBF_4$)

$$(OEP)Rh^{III}Cl + C_6H_5X \xrightarrow[AgBF_4]{AgClO_4\ or} (OEP)Rh^{III}C_6H_4\text{-}p\text{-}X \quad \begin{matrix}\mathbf{1},\ X=H\\ \mathbf{2},\ X=OCH_3\\ \mathbf{3},\ X=CH_3\\ \mathbf{4},\ X=Cl\end{matrix} \qquad (1)$$

after purification.[24] The product was unambiguously identified by comparison with authentic **1** obtained by the published procedure (eq 2, X = H).[25] In the absence of

$$(OEP)Rh^{III}Cl + X\text{-}p\text{-}C_6H_4Li \rightarrow (OEP)Rh^{III}C_6H_4\text{-}p\text{-}X \qquad (2)$$

a silver salt no reaction took place. The formation of **1** was completely inhibited by the presence of potential donor cosolvents such as methanol, tetrahydrofuran, and pyridine, but not by dioxygen. The TLC monitoring of the reaction indicated a facile exchange of Cl^- of $(OEP)Rh^{III}Cl$ with ClO_4^- or BF_4^- of the silver salt followed by the gradual conversion of the thus formed intermediate complex to **1**. The only noticeable side reaction was decomposition of the intermediate to some extent as independently confirmed. Treatment of $(OEP)Rh^{III}Cl$ with a silver salt in dichloromethane afforded relatively unstable and hygroscopic complexes $(OEP)Rh^{III}(ClO_4)$ and $(OEP)Rh^{III}(BF_4)$ in yields of 56 and 51%, respectively, with concomitant precipitation of AgCl. The isolated perchlorate and tetrafluoroborate species were independently shown to undergo reaction with benzene to generate **1** without the participation of a silver salt. The silver ion assisted phenylation of $(OEP)Rh^{III}Cl$ with a 1:1 mixture of benzene and benzene-d_6 gave rise to **1** and **1**-d_5 in nearly the same amounts determined from comparison of the integrated intensities of the axial phenyl and the meso protons in NMR spectrum. The present result indicates essentially no kinetic deuterium isotope effect ($k_H/k_D \simeq 1$).

Metalation of Substituted Benzenes. Anisole, toluene, and chlorobenzene reacted similarly with $(OEP)Rh^{III}Cl$ in the presence of $AgClO_4$ to give the corresponding aryl–rhodium(III) complexes **2**–**4** (eq 1). The tolyl complex **3**, obtained in 46% yield, was identified by NMR spectral comparison with authentic **3** prepared according to eq 2 (X = CH_3).[25] The yields and analytical data of new aryl–rhodium(III) complexes are shown in Table I. The highly regioselective para metalation of substituted benzenes was demonstrated by the ^1H NMR spectra of **2**–**4**, in which the aromatic proton resonances appeared as a pair of doublets in 1:1 integrated ratio for two types of protons, one being highly and the other moderately shielded due to the porphyrin ring current effect. (Table II). These were readily assigned to the ortho and meta protons respectively to rhodium on the basis of their geometrical parameters and the isoshielding map of organorhodium porphyrins.[25] Exclusive para metalation was always observed when the reaction conditions (time and temperature) were altered. Furthermore, the aryl–rhodium complexes were found to be quite stable under the present reaction conditions even in the presence of aqueous HCl or $HClO_4$. These facts are indicative of an essentially irreversible electrophilic metalation of arenes.

Table II. ^1H NMR Spectral Data for Aryl Ligands in $(OEP)Rh^{III}C_6H_4X$ (δ from Me_4Si)[a,b]

complex	ortho H	meta H	para H	CH_3
1	−0.39 (d)	4.49 (t)	5.11 (t)	
2	−0.44 (d)	~4.1[c]		2.57 (s)
3	−0.43 (d)	4.31 (d)		0.88 (s)
4	−0.49 (d)	4.43 (d)		
5	−0.19[d] (dq), 0.26[d] (q)	4.54 (t)	5.70 (dq)[d]	3.20 (s)
6	−0.26 (d)	5.18 (d)		3.13 (s)

[a] Spectra were obtained for $CDCl_3$ solutions with tetramethylsilane as standard using either 200- (for **1**, **2**, **3**, **4**, and **6**) or 270-MHz machine (for **5**): s, singlet; d, doublet; t, triplet; q, quartet; dq, double quartet. Ortho, meta, and para are in reference to rhodium. [b] J_{ortho} = 7–8 Hz. [c] Overlapping with CH_2CH_3. [d] J_{meta} = 1.7 and 2.8 Hz.

The metalation of methyl benzoate required more drastic conditions than those used for the substituted benzenes above. At 90 °C in the presence of a silver salt, the ester reacted with $(OEP)Rh^{III}Cl$ and afforded in 24% total yield a chromatography-separable mixture of two aryl–rhodium(III) complexes in a ratio of 92:8 (eq 3). The

$$(OEP)Rh^{III}Cl + C_6H_5CO_2CH_3 \xrightarrow[AgBF_4]{AgClO_4\ or} \underset{\mathbf{5}\ (92\%)}{(OEP)Rh^{III}C_6H_4\text{-}m\text{-}CO_2CH_3} + \underset{\mathbf{6}\ (8\%)}{(OEP)Rh^{III}C_6H_4\text{-}p\text{-}CO_2CH_3} \qquad (3)$$

minor one **6** was readily assigned as the para-metalated isomer from the NMR spectrum which showed an A_2B_2 aromatic proton resonance. The NMR spectrum of the major isomer **5** showed two highly shielded ortho (to rhodium) proton resonances and the two remaining proton resonances at lower field. The observed splitting and coupling patterns (Table II) were consistent with the structure in which the position meta to the methoxycarbonyl group was metalated. In Table I the analytical data are shown.

(24) Fleischer and Lavallee (Fleischer, E. B.; Lavallee, D. *J. Am. Chem. Soc.* **1967**, *89*, 7132) reported the formation of a phenylrhodium(IV) derivative, $(TPP)Rh^{IV}(C_6H_5)(Cl)$, from the reaction of tetraphenylporphyrin (TPP) and $[Rh(CO)_2Cl]_2$ in benzene. This and the present phenylation reactions may be related, but the lack of mechanistic information as well as the difference in rhodium oxidation states allows no further comparison.

(25) Ogoshi, H.; Setsune, J.; Omura, T.; Yoshida, Z. *J. Am. Chem. Soc.* **1975**, *97*, 6461.

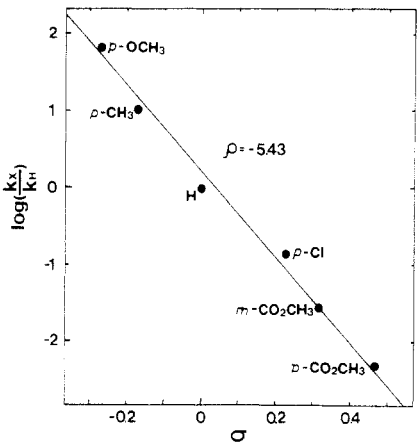

Figure 1. Hammett plots for reactivities of arenes in the Ag^+-assisted metalation with $(OEP)Rh^{III}Cl$: k_X and k_H stand respectively for the statistically corrected reactivity of an arene and benzene.

The competitive metalation reactions of C_6H_5X (X = H, OCH_3, CH_3, Cl, and CO_2CH_3) show relative rate increases with increasing electron-donating abilities of the substituents X (relative rate): OCH_3 (71.4), CH_3 (10.7), H (1 after statistical correction for 6 H), Cl (0.143), and CO_2CH_3 (0.062, statistically not corrected). The isomer distribution in eq 3 allows the respective reactivities of meta and para hydrogens of methyl benzoate to be evaluated; meta H (0.029 after statistical correction for 2 H) and para H (0.005). The logarithmic relative rates are correlated with substituent constants σ or σ^+ in the Hammett-type equations. Use of σ results in a better correlation (correlation coefficient 0.995) and gives a ρ value of −5.43 (Figure 1). Interestingly, this ρ value is comparable to that for the nitration of monosubstituted benzenes with NO_2^+,[26] a typical example of electrophilic aromatic substitution.

Cleavage of Aryl–Rhodium(III) Bonds. The present aryl–rhodium(III) complexes underwent facile cleavage of the C–Rh bond induced by halogen. Treatment of complex **1** with iodine at room temperature gave iodobenzene in nearly quantitative yield together with $(OEP)Rh^{III}I$ (eq 4).

$$(OEP)Rh^{III}C_6H_5 + I_2 \rightarrow (OEP)Rh^{III}I + C_6H_5I \quad (4)$$

Bromine and chlorine reacted similarly with **1** to afford bromobenzene and chlorobenzene in ~100 and 94% yields, respectively. Iodination and bromination of the tolyl complex **3** derived from the present metalation (eq 1) gave the corresponding *p*-halotoluenes in nearly quantitative chemical yields and with extremely high regioselectivities (>99%). This trend is also found for the bromination of the anisyl complex **2**. The regioselective para metalation shown by the analysis of ^1H NMR spectra of **2** and **3** has thus been put on a more quantitative level.

Complex **1**, like homologous organocobalt derivatives,[27-32] underwent photolysis of the carbon–metal bond. Irradiation of a degassed benzene solution of **1** led to the formation of biphenyl in 85% yield. Photolysis of **2** and **3** gave 4-methoxy- and 4-methylbiphenyl, respectively, arising from homolytic aromatic substitution[33] of the solvent benzene with the photogenerated para-substituted phenyl radicals. In neither case was 4,4′-disubstituted biphenyl detected, a product which may result from radical coupling.

Discussion

Electrophilic Aromatic Metalation. Substituent effects in electrophilic aromatic substitution have been thoroughly investigated.[34] The substituents employed in this study cover the three categories; OCH_3 and CH_3 (ortho and para orienting with activation), Cl (ortho and para orienting with deactivation), and CO_2CH_3 (meta orienting with deactivation). The observed substituent effects on both reactivity (Figure 1) and orientation (eq 1 and 3) clearly characterize the present reaction as an (ionic) electrophilic aromatic metalation with a cationic intermediate, $[(OEP)Rh^{III}]^+$, generated from the anion exchange of $(OEP)Rh^{III}Cl$ with silver salts. As in the recent catalytic transformations of olefins by $[Pd(CH_3CN)_4](BF_4)_2$,[23] the role of ClO_4^- or BF_4^- would be that of noncoordinating counteranions, thus accommodating vacant coordination sites and enhancing the electrophilicity of the central metal. This explanation is compatible with the observed inhibition of the reaction by coordinating cosolvents. The absence of an ortho attack may be due to a steric effect. Mechanisms involving radical species are not consistent with the observed large negative ρ value and regioselectivity.[35] Furthermore, there is no evidence of cleavage of potentially reactive methyl C–H bonds of toluene and anisole. The lack of an inhibitory effect by dioxygen provides further evidence for the exclusion of radical mechanisms. The substituent effects observed here are in marked contrast to those found in oxidative addition processes of lower valent transition metals to the arene C–H bonds: these reactions are facilitated by electron-withdrawing groups[5a,c] and usually give nonregioselective isomer mixtures (vide infra); in some cases metalation of alkyl side chains takes place.[4c,e,f]

An interesting comparison can be made between the present aromatic metalation and aromatic nitration with NO_2^+. Both reactions give rise to comparable Hammett ρ values and are free from kinetic deuterium isotope effects.[34] An indication of this is that $[(OEP)Rh^{III}]^+$ of a similar electrophilicity as NO_2^+ attacks the arene in the rate-determining step to form $[(OEP)Rh^{III}(arene)]^+$, which subsequently undergoes rapid loss of a proton as in nitration (eq 5). Relevant to the deprotonation step is the

$$[(OEP)Rh^{III}]^+ + C_6H_6 \xrightarrow{\text{slow}} [(OEP)Rh^{III}(C_6H_6)]^+ \xrightarrow[-H^+]{\text{fast}} \mathbf{1} \quad (5)$$

recent report of the protonation–deprotonation interconversion of σ-aryl and η^2-arene complexes of $[(\eta\text{-}C_5H_5)Re$-

(26) Nitration of monosubstituted benzenes with NO_2^+ in acetic anhydride at 18 °C gives a ρ value of −5.926: Roberts, J. D.; Stewart, R.; Caserio, M. C. "Organic Chemistry"; W. A. Benjamin: Menlo Park, CA, 1971; p 664. Also see: (a) Roberts, J. D.; Sanford, J. K.; Sixma, F. L. J.; Cerfontain, H.; Zakt, R. *J. Am. Chem. Soc.* **1954**, *76*, 4525. (b) Brown, H. C.; Okamoto, Y. *Ibid.* **1957**, *79*, 1913.

(27) (a) Mok, C. Y.; Endicott, J. F. *J. Am. Chem. Soc.* **1977**, *99*, 1276. (b) Mok, C. Y.; Endicott, J. F. *Ibid.* **1978**, *100*, 123.

(28) Pailes, W. H.; Hogenkamp, H. P. C. *Biochemistry* **1968**, *7*, 4160.

(29) Schrauzer, G. N.; Lee, L. P.; Sibert, J. W. *J. Am. Chem. Soc.* **1970**, *92*, 2997.

(30) Hogenkamp. H. P. C. *Biochemistry* **1966**, *5*, 417.

(31) (a) Pratt, J. M. *J. Chem. Soc.* **1964**, 5154. (b) Pratt, J. M.; Whitear, B. R. D. *J. Chem. Soc. A* **1971**, 252.

(32) (a) Gianotti, C.; Gaudemer, A.; Fontaine, C. *Tetrahedron Lett.* **1970**, 3209. (b) Gianotti, C.; Bolton, J. R. *J. Organomet. Chem.* **1974**, *80*, 379.

(33) Detar, D. F.; Long, R. A. J.; Bradley, J.; Duncan, P. *J. Am. Chem. Soc.* **1967**, *89*, 4051.

(34) Gould, E. S. "Mechanism and Structure in Organic Chemistry"; Henry Holt and Co.: New York, 1960; pp 412–471.

(35) Homolytic aromatic substitution usually gives considerable amounts of meta-substituted products. See, for example: (a) Hey, D. H.; Pengilly, B. W.; Williams, G. H. *J. Chem. Soc.* **1955**, 6; **1956**, 1463. (b) Cowley, B. R.; Norman, R. O. C.; Waters, W. A. *Ibid.* **1959**, 1799. (c) Kovacic, P.; Reid, C. G.; Britton, M. J. *J. Org. Chem.* **1970**, *35*, 2152. (d) Davies, D. L.; Hey, D. H.; Summers, B. *J. Chem. Soc. C* **1971**, 2681.

Table III. Isomer Distribution in Aromatic Substitution

entry	reaction	substrate C_6H_5X, X =	reagent	isomer distributn, % ortho	meta	para	ref
1	bromination	CH_3	$[(OEP)Rh^{III}]^+$, Br_2	0	<1	>99	this work
2	iodination	CH_3	$[(OEP)Rh^{III}]^+$, I_2	0	<1	>99	this work
3	bromination	OCH_3	$[(OEP)Rh^{III}]^+$, Br_2	0	<1	>99	this work
4	nitration	CH_3	NO_2^+	56.5	3.5	40	*a*
5	metalation (Hg)	CH_3	$Hg(CH_3CO_2)_2$[b]	~20	~10	~70[c]	16
6	metalation (Tl)	CH_3	$Tl(CF_3CO_2)_3$	9	4	87[d]	17
7	metalation (Pt)	CH_3	H_2PtCl_6	0	ca. 50	ca. 50	21c
8	chlorination	Cl	$PtCl_6^{2-}$	1	61–62	38–39	37
9	metalation (Fe)[e]	CH_3	$Fe(dmpe)_2$[f]	0	62	38	5c
10	metalation (Rh)[g]	CH_3	$Rh[C_5(CH_3)_5][P(CH_3)_3]$	0	67	33	6
11	metalation (Re)[h]	CH_3	$[(C_5H_5)Re(NO)(CO)]^+$	0	6	94	36
12	metalation (Re)[h]	CF_3	$[(C_5H_5)Re(NO)(CO)]^+$	0	84	16	36
13	chlorination	OCH_3	HOCl, α-CD[i]	4	0	96	*j*
14	metalation (Rh)	CO_2CH_3	$[(OEP)Rh^{III}]^+$	~0	92	8	this work
15	nitration	$CO_2CH_2CH_3$	NO_2^+	28.3	68.4	3.3	*a*
16	metalation (W)	CO_2CH_3	$(C_5H_5)_2W$[k]	0	26	74	4f

[a] Reference 26, p 568. [b] Under perchloric acid catalysis. [c] Isomer distribution extraporated to zero reaction time. The distribution changes with reaction time to approach a statistical distribution of the three. [d] At 22 °C. At higher temperatures, thermally induced reorientation results in predominant meta substitution: Taylor, E. C.; Kienzle, F.; Robey, R. L.; McKillop, A.; Hunt, J. D. *J. Am. Chem. Soc.* **1971**, *93*, 4845. [e] Isomer distribution from exchange reaction of $HFe(C_{10}H_7)(dmpe)_2 + C_6H_5CH_3 \rightleftharpoons HFe(C_6H_5CH_3)(dmpe)_2 + C_{10}H_8$. [f] dmpe = $(CH_3)_2PCH_2CH_2P(CH_3)_2$. [g] Isomer distribution from oxidative addition to coordinated toluene in a η^2 fashion. [h] Isomer distribution from deprotonation of η^2-arene complex of $[(C_5H_5)Re(NO)(CO)]^+$. [i] α-Cyclodextrin (9.39×10^{-3} M). [j] Breslow, R.; Campbell, P. *J. Am. Chem. Soc.* **1969**, *91*, 3085. [k] Photochemically generated from $(C_5H_5)_2WH_2$.

$(NO)(CO)]^+$.[36] Such a formulation of a cationic η^2-arene complex, rather than an η^1-arenium cation, may apply to the present intermediate in eq 5, and this might also explain, at least partially, a better correlation of reactivities with substituent constants σ (r = 0.995) than with σ^+ (r = 0.979), in contrast to usual electrophilic aromatic substitution.

Electrophilic interactions of transition-metal ions may be involved in a number of reactions of arenes[2j] including metal-catalyzed hydrogen isotope exchange[37-39] and oxidation of arenes.[37] A class of facile, intramolecular aromatic metalations is known as ortho metalation or cyclometalation.[14b,19,20] However, these intramolecular reactions preclude a systematic study on the substituent effects as presented here, and in most of metal-catalyzed reactions aryl–metal complexes only have been proposed as intermediates. In some cases, reductive elimination follows initial oxidative addition so that the metal retains its original formal valency.[14b] When simple transition-metal salts or complexes are used, further complexities arise from facile ligand exchanges; this may lead to many species usually not readily identified unambiguously and may leave many mechanistic possibilities.[37] In this respect the rigid porphyrin ligand has a great significance.

Regioselectivity. In Table III are summarized the isomer distributions in aromatic substitutions. The crucial factors in the extremely regioselective (>99%) para substitution (metalation and subsequent halogenation) of toluene and anisole (entries 1–3) are (1) the electrophilic attack of the central metal and (2) the planar and bulky porphyrin ligand which effectively prevents otherwise facile ortho substitution (entry 4). A steric inhibition of ortho attack due to inclusion complex formation has been noted (entry 13). The mercuration and thallation are predominantly para orienting (entry 5 and 6) (but see footnotes *c* and *d* of Table III). The platination of arenes with $H_2Pt^{IV}Cl_6$ may involve an electrophilic mechanism on the basis of reactivity correlation:[21d] ρ = −3.6 which should be compared with the present ρ of −5.43. Aromatic auration might proceed through a similar mechanism.[40] However, the observed meta/para ratio in the platination of toluene (entry 7) is apparently not consistent with the electrophilic mechanism. A similar trend has been reported for the aromatic chlorination with $PtCl_6^{2-}$ (entry 8), where aryl–platinum complexes are intermediates.[21h,37] In fact the latter reaction gives the meta/para ratio very close to the statistical one (meta/para = 2:1), and this is also characteristic of the oxidative addition processes of lower valent transition metals (entries 9 and 10). The platination might also involve similar mechanisms.[41] Furthermore, it is interesting to compare the isomer distributions in the case of meta-directing alkoxycarbonyl substituents (entries 14–16). This brief survey of the substituent effects is intended to show that the hitherto known metalation reactions of arenes with transition-metal species are rather nonregioselective, irrespective of the mechanisms involved. There is, however, at least one clear example of electrophilic aromatic metalation that follows the directive effects of electrophilic aromatic substitution (entries 11 and 12), as in the present case.

A significance of homogeneous C–H bond activation by transition metals lies in further conversion of the resulting C–M bonds.[42,43] The present system provides a way to the functionalization of arenes via activation by transition metals. For simple arenes, there is no precedent for such a high regioselectivity as observed here for the halogenation of toluene and anisole. The present halogenolysis of the carbon–rhodium bond probably takes place in a similar

(36) Sweet, J. R.; Graham, W. A. G. *J. Am. Chem. Soc.* **1983**, *105*, 305.
(37) Garnett, J. L.; West, J. C. *Aust. J. Chem.* **1974**, *27*, 129 and references therein.
(38) Preece, M.; Robinson, S. D. *Inorg. Chim. Acta* **1978**, *29*, L199 and references therein.
(39) Garnett, J. L.; Long, M. A.; Vining, R. F. W. *J. Chem. Soc., Chem. Commun.* **1972**, 1172.
(40) (a) Kharasch, M. S.; Isbell, H. S. *J. Am. Chem. Soc.* **1931**, *53*, 3053. (b) Kharasch, M. S.; Bech, P. M. *Ibid.* **1934**, *56*, 2057. (c) Nizova, G. V.; Shul'pin, G. B. *React. Kinet. Catal. Lett.* **1982**, *20*, 69.
(41) In the isotope exchange and oxidation reactions of arenes with Pt^{IV} halides, the active catalyst is shown to be a Pt^{II} species which forms aryl–Pt^{II} complexes as intermediates.[37] Furthermore, the aryl–Pt^{II} complexes formed from reactions of arenes with Na_2PtCl_4 undergo oxidation with H_2PtCl_6 to give aryl–Pt^{IV} complexes.[21h]
(42) The formation of aryl–metal complexes was proposed in a number of reactions of arenes with palladium salts such as oxidative coupling, arene–olefin coupling, and carboxylation. See, for example: (a) Moritani, I.; Fujiwara, Y. *Synthesis* **1973**, 524. (b) Fujiwara, Y.; Kawauchi, T.; Taniguchi, M. *J. Chem. Soc., Chem. Commun.* **1980**, 220.
(43) For organic syntheses via arylthallium complexes, see: Taylor, E. C.; McKillop, A. *Acc. Chem. Res.* **1970**, *3*, 338.

manner as reported for the electrophilic cleavage of the carbon–cobalt bond with halogen.[44,45] In fact, a close similarity of the electronic spectra of (OEP)Rh^{III}aryl and (OEP)$Rh^{III}Cl$ indicates a significant carbanion character of the coordinated aryl ligands.

In principle it seems to be possible to carry out the present functionalization of arenes in a catalytic manner with respect to rhodium porphyrin. Various functionalizations of the C–Rh bond other than halogenation also seem promising, since rhodium is homologous to cobalt and there is a rich chemistry in organocobalt complexes.

Concluding Remarks

From the mechanistic viewpoint, this work provides an unambiguous example of intermolecular electrophilic aromatic metalations with transition metals in a single step. On all the criteria we stand on, except for a rather minor difference in the reactivity correlation with σ vs. σ^+, the present Rh^{III} electrophile behaves quite similarly to NO_2^+, a typical electrophile in classical electrophilic aromatic substitution; there is no special metal effect. From the synthetic viewpoint, the arenes thus activated by Rh^{III} indeed undergo extremely regioselective functionalization.

Experimental Section

General Analyses. IR spectra were obtained by using KBr disks on a Hitachi 260-10 spectrophotometer. ^1H NMR spectra were taken on a JEOL JNM-PMX 60, JNM-FX 200, or JNM-GX 270 spectrometer using tetramethylsilane as internal reference. Electronic spectra were recorded on a Hitachi 200-10 or 320 spectrophotometer. Elemental analyses were performed at the Microanalysis Center of Kyoto University. Gas chromatographic analyses were made with a Shimadzu GC-4C gas chromatograph using helium as a carrier gas. Identification of the reaction products was performed by coinjection with authentic samples on columns of poly(ethylene glycol) 60M, silicone SE-30, and azoxydianisole SG. Column chromatographic separations were carried out with silica gel (Wakogel C-200) and alumina (Merck 90, activity II-III). Silica gel 60 F_{254} (Merck) was used for analytical and preparative thin-layer chromatography (TLC).

Materials. (Octaethylporphyrinato)rhodium(III) chloride [(OEP)$Rh^{III}Cl$] was prepared by a slight modification of the published procedure.[25] A mixture of octaethylporphyrin (1 g) and $[Rh(CO)_2Cl]_2$ (1.2 g) in benzene (1 L) was stirred at room temperature for 6 h. About 700 mL of the solvent was removed, and the concentrated solution left was refluxed for 2 h. Usual workup and chromatographic (silica gel) purification followed by recrystallization from dichloromethane–hexane afforded the rhodium porphyrin in yields of 75–80%. Silver salts ($AgClO_4$ and $AgBF_4$) were dried at 80 °C in vacuo for 1–2 h just before use. Thiophene-free benzene was crystallized three times; one-fourth was discarded each time as unfrozen liquid. It was then dried over calcium hydride and finally distilled through a 35-cm Vigreux column. Toluene, anisole, chlorobenzene, and methyl benzoate were also purified by standard procedures.

Metalation of Arenes. A dried 200-mL three-necked flask equipped with a reflux condenser, N_2 inlet, addition funnel, and a magnetic stirring bar was charged with a solution of $AgClO_4$ or $AgBF_4$ (10 mg) in an arene (50 mL). To this was added a solution of (OEP)$Rh^{III}Cl$ (20 mg) in the arene (50 mL) over a period of 2 h at 50 °C (for benzene, toluene, anisole, and chlorobenzene) or 90 °C (for methyl benzoate). The mixture was further stirred at room temperature for 48 h. The solvent was removed in vacuo, and the residue was chromatographed first on alumina and then on silica gel. The reddish orange fraction eluted with benzene–hexane (4:1 by volume) (for **1**, **3**, and **4**) or with benzene (for **2** and mixture of **5** and **6**) was evaporated to dryness. The residue was further purified by recrystallization from dichloromethane–methanol to give reddish orange needles of phenyl- (**1**, 8.5 mg (40%) with $AgClO_4$ and 14.9 mg (70%) with $AgBF_4$), *p*-anisyl- (**2**, 10.2 mg (46%) with $AgClO_4$), *p*-tolyl- (**3**, 10.0 mg (46%) with $AgClO_4$), and *p*-chlorophenyl-Rh^{III} (**4**, 4.0 mg (18%) with $AgClO_4$) complexes. The isomeric mixture of (methoxycarbonyl)phenyl-Rh^{III} complexes **5** and **6** was separated by means of preparative TLC using benzene–hexane (85:15 by volume) as eluant: **5** (R_f 0.23; 5.1 mg (22%) with $AgClO_4$) and **6** (R_f 0.15; 0.5 mg (2%) with $AgClO_4$). The electronic spectra for solutions in CH_2Cl_2 showed λ_{max} (log ϵ) as follows: **1**, 394 nm (5.00), 509 (3.96), 542 (4.58); **2**, 393 nm (5.09), 510 (4.08), 542 (4.66); **3**, 394 nm (5.11), 508 (4.12), 542 (4.70); **4**, 394 nm (5.09), 509 (4.06), 544 (4.69); **5**, 394 nm (5.22), 510 (4.16), 543 (4.69).

Competition Reactions. A 1:1 molar mixture of anisole (standard) and C_6H_5X (X = H, CH_3, or Cl) was subjected to $AgClO_4$-assisted metalation with (OEP)$Rh^{III}Cl$ as above. After the workup as described above, the product mixture was chromatographed on silica gel. (OEP)$Rh^{III}C_6H_4$-*p*-X (**1**, **3**, or **4**) was eluted with benzene–hexane (1:1 by volume) and (OEP)-$Rh^{III}C_6H_4$-*p*-OCH_3 (**2**) with benzene–hexane (4:1 by volume); the separation was complete in every case. Since the reactivity of methyl benzoate was too low to compete with anisole, chlorobenzene was taken as a second standard. The competitive metalation of a 1:1 mixture of chlorobenzene and methyl benzoate was carried out under the conditions required for that of methyl benzoate. Chlorophenyl (**4**) and (methoxycarbonyl)phenyl (**5** and **6**) derivatives were separated by TLC. The relative reactivities of arenes were based on the amounts (determined by electronic spectroscopy) of the isolated aryl-Rh^{III} complexes in respective competition runs. The molar extinction coefficients of **6** were assumed to be the same as those of its isomer (**5**). Independent experiments indicated that all of aryl-Rh^{III} complexes are stable under the condition of metalation reaction and chromatographic manipulation.

The competitive metalation of benzene and benzene-d_6 (Merck, minimum 99%) was carried out similarly. The ratio of light and heavy phenyl complexes was determined from the ^1H NMR spectrum. An integrated ratio of 4:1 of the meso-proton signal to that of phenyl meta protons to rhodium indicated that (OEP)$Rh^{III}C_6H_5$ and (OEP)$Rh^{III}C_6D_5$ had been formed in approximately equal amounts.

(OEP)$Rh^{III}(ClO_4)$ and (OEP)$Rh^{III}(BF_4)$. A solution of (OEP)$Rh^{III}Cl$ (20 mg) and $AgClO_4$ or $AgBF_4$ (10 mg) in 100 mL of dichloromethane dried with CaH_2 was stirred at room temperature under nitrogen for 2 days. Deposition of microprecipitates of AgCl was observed. The solvent was removed, and the residue was chromatographed on silica gel. Elution with a mixed solvent of dichloromethane and ethyl acetate (9:1 by volume) followed by recrystallization from dichloromethane–hexane afforded (OEP)$Rh^{III}(ClO_4)$ (12.9 mg, 56%) or (OEP)$Rh^{III}(BF_4)$ (11.5 mg, 51%) as the dihydrated form. These complexes are hygroscopic, and they pick up water during manipulation of chromatography on silica gel.

For the perchlorate complex: IR 1155, 1115, 1092 cm^{-1} (ν_{ClO});[46] ^1H NMR (CD_2Cl_2) δ 10.49 (br s, 4 H, meso H), 4.19 (m, 16 H, CH_2), 1.92 (t, 24 H, CH_3); electronic spectrum in CH_2Cl_2, λ_{max} (log ϵ) 396 nm (5.00), 516 (4.20), 549 (4.54). Anal. Calcd for $C_{36}H_{54}ClN_4O_4Rh\cdot 2H_2O$: C, 56.07; H, 6.27; N, 7.26. Found: C, 56.25; H, 6.44; N, 7.20.

For the tetrafluoroborate complex: IR 1115, 1089, 1070, 1060 cm^{-1} (ν_{BF});[46] ^1H NMR (CD_2Cl_2) δ 10.46 (br s, 4 H, meso H), 4.22 (m, 16 H, CH_2), 1.97 (t, 24 H, CH_3); electronic spectrum in CH_2Cl_2, λ_{max} (log ϵ) 396 nm (5.26), 514 (4.20), 548 (4.51). Anal. Calcd for $C_{36}H_{54}BF_4N_4Rh\cdot 2H_2O$: C, 57.01; H, 6.37; N, 7.38. Found: C, 57.35; H, 6.42; N, 7.42.

A solution of the purified perchlorate or tetrafluoroborate complex in benzene was stirred at room temperature. The gradual formation of **1** was ascertained by TLC and absorption spectroscopy.

Halogenation. A solution of **1** (20 mg) in dichloromethane–benzene (10:1 by volume, 30 mL) containing iodine (50-molar

(44) Dodd, D.; Jhonson, M. D. *J. Chem. Soc., Chem. Commun.* **1971**, 571.

(45) Jensen, F. R.; Madan, V.; Buchanan, D. H. *J. Am. Chem. Soc.* **1971**, *93*, 5283.

(46) Nakamoto, K. "Infrared and Raman Spectra of Inorganic and Coordination Compounds", 3rd ed.; Wiley: New York, 1977; p 136, pp 242–243.

excess) was stirred at room temperature under nitrogen for 3 days. The solution was washed three times with aqueous $Na_2S_2O_4$ or $NaHSO_3$ solution. The organic layer was dried (Na_2SO_4), and the solvent was carefully removed in vacuo. The residue was chromatographed on silica gel. Elution with benzene afforded iodobenzene and $(OEP)Rh^{III}I$. These products were identified by comparison of their chromatographic and spectral behavior with those of authentic samples.[47] Similarly, the iodination of **3** and bromination of **1**, **2**, and **3** with a 50-molar excess of bromine in benzene (30 mL) were carried out. In the chlorination of **1**, chlorine gas was introduced with a stream of nitrogen into a solution of **1** in benzene (30 mL) for 30 min, and the mixture was worked up as described above. Gas chromatography was applied to determine the analytical yields of haloarenes and isomer distributions therein, on columns of azoxydianisole SG (for halotoluenes) and poly(ethylene glycol) 60M (for haloanisoles) with durene as an internal standard.

Photolysis. A solution of **1** (5 mg) in benzene (25 mL) in a Pyrex flask was irradiated with a 100-W high-pressure mercury lamp for 12 h. The solution was analyzed by gas chromatography. The photolyses of **2** and **3** were carried out similarly. The organic products, isolated by column chromatography on silica gel using benzene–hexane (4:1 by volume), showed ^1H NMR spectra identical with those of 4-methoxy- and 4-methylbiphenyl, respectively.

Acknowledgment. This work was supported by a Grant-in-Aid for Scientific Research from the Ministry of Education, Science, and Culture of Japan (Subject No. 57550533) and by the Asahi Glass Foundation for Industrial Technology. We are indebted to Dr. S. Matsugo (Niigata College of Pharmacy) and JEOL Ltd. for measurements of 200- and 270-MHz ^1H NMR spectra.

(47) Abeysekera, A. M.; Grigg, R.; Trocha-Grimshaw, J.; Viswanatha, V. *J. Chem. Soc., Perkin Trans. 1* **1977**, 1395.

Communications

Silicon-Containing Carbene Complexes. 6.[1] Stable 16-Electron Carbonyl Carbene Complexes of Tungsten(0), Molybdenum(0), and Chromium(0)

Ulrich Schubert,* Wolfgang Hepp, and Johannes Müller
Institut für Anorganische Chemie der Universität
D-8700 Würzburg, Germany

Received August 14, 1985

Summary: On warming $(CO)_5W{=}C(NR_2)SiPh_3$ (NR_2 = NMe_2, **1a**, NC_5H_{10}, **1b**) under vacuum, a CO ligand is eliminated and 16-electron carbene complexes $(CO)_4W{=}C(NR_2)SiPh_3$ (**2a,b**) are formed as stable compounds. Analogous chromium and molybdenum complexes $(CO)_4M{=}C(NC_5H_{10})SiPh_3$ (M = Mo, **2c**, Cr, **2d**) are already formed during the preparation of $(CO)_5M{=}C(NC_5H_{10})SiPh_3$ (**1c,d**). The reaction is readily reversed on bubbling CO through solutions of **2**. X-ray structure determination of $(CO)_4W{=}C(NC_5H_{10})SiPh_3$ (**2b**) shows that the vacant coordination site at the metal is capped by a phenyl group of the $SiPh_3$ substituent. However, the long W–C(phenyl) distances exclude strong bonding interaction. The driving force for the conversion of **1** to give **2** seems to be relaxation of the steric strain within the carbene ligand.

The dissociative loss of a carbonyl ligand is the initial step in many reactions of Fischer-type carbene complexes $(CO)_5M{=}C(YR)R'$ (M = Cr, Mo, W; YR = OR, SR, NR_2, etc.), cis CO's being particularly labile.[2] Some $(CO)_5Cr{=}C(NEt_2)X$ complexes (X = Cl, Br, I, SeR, TeR, $SnPh_3$, $PbPh_3$) rearrange spontaneously to give *trans*-$X(CO)_4Cr{\equiv}CNEt_2$ by an intramolecular process probably involving concerted dissociation of a CO ligand and C,Cr-migration of the group X.[3] In the synthetically important reactions of $(CO)_5M{=}C(OR)R'$ with alkenes or alkynes, CO dissociation is the rate-determining first step, which is followed by addition of the unsaturated molecule to the vacant coordination site.[4] In no case have the 16-electron $(CO)_4M{=}C(YR)R'$ intermediates been observed directly.

We have now been able to isolate such complexes. If solid $(CO)_5W{=}C(NMe_2)SiPh_3$ (**1a**)[5,6] or $(CO)_5W{=}C(NC_5H_{10})SiPh_3$ (**1b**)[6] (but not $(CO)_5W{=}C(NEt_2)SiPh_3$[7]) are warmed to 110 °C at 0.1–0.2 torr in a Schlenk tube, the color changes from yellow to orange-red and the 16-electron complexes $(CO)_4W{=}C(NMe_2)SiPh_3$ (**2a**) or $(CO)_4W{=}C(NC_5H_{10})SiPh_3$ (**2b**) are obtained as major products.[8] They can be separated from byproducts and unreacted **1a,b** by column chromatography on silica at −20 °C (pentane/ether, 25:1). Contrary to **2a** and **2b** the

$$(CO)_5M{=}C(NR_2)SiPh_3 \rightleftharpoons \underset{\textbf{1a–d}}{} CO + \underset{\textbf{2a–d}}{(CO)_4M{=}C(NR_2)SiPh_3} \quad (1)$$

a, M = W, NR_2 = NMe_2; **b**, M = W, NR_2 = NC_5H_{10}; **c**, M = Mo, NR_2 = NC_5H_{10}; **d**, M = Cr, NR_2 = NC_5H_{10}

analogous complexes of molybdenum (**2c**) and chromium

(1) Part 5: Hörnig, H.; Walther, E.; Schubert, U. *Organometallics* **1985**, *4*, 1905.
(2) Casey, C. P.; Cesa, M. C. *Organometallics* **1982**, *1*, 87.
(3) Fischer, H.; Motsch, A.; Märkl, R.; Ackermann, K.; *Organometallics* **1985**, *4*, 726 and references cited therein.
(4) Fischer, H. In "Transition Metal Carbene Complexes"; Dötz, K. H., Fischer, H., Hofmann, P., Kreissl, F. R., Schubert, U., Weiss, K.; Verlag Chemie: Weinheim/Bergstr., Germany, 1983. Casey, C. P.; Shusterman, A. J.; *Organometallics* **1985**, *4*, 736 and references cited therein.
(5) Fischer, E. O.; Hollfelder, H.; Friedrich, P.; Kreissl, F. R.; Huttner, G. *Chem. Ber.* **1977**, *110*, 3467.
(6) **1a** was prepared by reaction of $(CO)_5W{=}C(OEt)SiPh_3$[5] with $HNMe_2$ in THF at +20 °C analogous to that of ref 5 and **1b–d** by reaction of the corresponding $(CO)_5M{=}C(OEt)SiPh_3$[5] with neat piperidine at +20 °C.
(7) Schubert, U.; Hörnig, H.; Erdmann, K.-U.; Weiss, K. *J. Chem. Soc. Chem. Commun.* **1984**, 13.
(8) Anal. Calcd for $C_{25}H_{21}NO_4SiW$ (**2a**): C, 49.11; H, 3.46; N, 2.29. Found: C, 49.35; H, 3.43; N, 1.87. Anal. Calcd for $C_{28}H_{25}NO_4SiW$ (**2b**): C, 51.62; H, 3.87; N, 2.15. Found: C, 51.62; H, 3.73; N, 1.72. Mass spectrum of **2b** (70 eV): *m/e* (relative intensity) 651 (1, M^+), 595 (25, M − 2CO), 567 (18, M − 3CO), 539 (31, M − 4CO), 507 (36), 446 (24), 259 (51, $SiPh_3$), 182 (100, $SiPh_2$), 105 (66, SiPh).

0276-7333/86/2305-0173$01.50/0

Silicon-containing carbene complexes. 6. Stable 16-electron carbonyl carbene complexes of tungsten(0), molybdenum(0), and chromium(0)

Ulrich. Schubert, Wolfgang. Hepp, and Johannes. Muller

Organometallics, **1986**, 5 (1), 173-175• DOI: 10.1021/om00132a031 • Publication Date (Web): 01 May 2002

excess) was stirred at room temperature under nitrogen for 3 days. The solution was washed three times with aqueous $Na_2S_2O_4$ or $NaHSO_3$ solution. The organic layer was dried (Na_2SO_4), and the solvent was carefully removed in vacuo. The residue was chromatographed on silica gel. Elution with benzene afforded iodobenzene and (OEP)$Rh^{III}I$. These products were identified by comparison of their chromatographic and spectral behavior with those of authentic samples.[47] Similarly, the iodination of **3** and bromination of **1**, **2**, and **3** with a 50-molar excess of bromine in benzene (30 mL) were carried out. In the chlorination of **1**, chlorine gas was introduced with a stream of nitrogen into a solution of **1** in benzene (30 mL) for 30 min, and the mixture was worked up as described above. Gas chromatography was applied to determine the analytical yields of haloarenes and isomer distributions therein, on columns of azoxydianisole SG (for halotoluenes) and poly(ethylene glycol) 60M (for haloanisoles) with durene as an internal standard.

Photolysis. A solution of **1** (5 mg) in benzene (25 mL) in a Pyrex flask was irradiated with a 100-W high-pressure mercury lamp for 12 h. The solution was analyzed by gas chromatography. The photolyses of **2** and **3** were carried out similarly. The organic products, isolated by column chromatography on silica gel using benzene–hexane (4:1 by volume), showed ^1H NMR spectra identical with those of 4-methoxy- and 4-methylbiphenyl, respectively.

Acknowledgment. This work was supported by a Grant-in-Aid for Scientific Research from the Ministry of Education, Science, and Culture of Japan (Subject No. 57550533) and by the Asahi Glass Foundation for Industrial Technology. We are indebted to Dr. S. Matsugo (Niigata College of Pharmacy) and JEOL Ltd. for measurements of 200- and 270-MHz ^1H NMR spectra.

(47) Abeysekera, A. M.; Grigg, R.; Trocha-Grimshaw, J.; Viswanatha, V. *J. Chem. Soc., Perkin Trans. 1* **1977**, 1395.

Communications

Silicon-Containing Carbene Complexes. 6.[1] Stable 16-Electron Carbonyl Carbene Complexes of Tungsten(0), Molybdenum(0), and Chromium(0)

Ulrich Schubert,* Wolfgang Hepp, and Johannes Müller

Institut für Anorganische Chemie der Universität
D-8700 Würzburg, Germany

Received August 14, 1985

Summary: On warming $(CO)_5W{=}C(NR_2)SiPh_3$ (NR_2 = NMe_2, **1a**, NC_5H_{10}, **1b**) under vacuum, a CO ligand is eliminated and 16-electron carbene complexes $(CO)_4W{=}C(NR_2)SiPh_3$ (**2a,b**) are formed as stable compounds. Analogous chromium and molybdenum complexes $(CO)_4M{=}C(NC_5H_{10})SiPh_3$ (M = Mo, **2c**, Cr, **2d**) are already formed during the preparation of $(CO)_5M{=}C(NC_5H_{10})SiPh_3$ (**1c,d**). The reaction is readily reversed on bubbling CO through solutions of **2**. X-ray structure determination of $(CO)_4W{=}C(NC_5H_{10})SiPh_3$ (**2b**) shows that the vacant coordination site at the metal is capped by a phenyl group of the $SiPh_3$ substituent. However, the long W–C(phenyl) distances exclude strong bonding interaction. The driving force for the conversion of **1** to give **2** seems to be relaxation of the steric strain within the carbene ligand.

The dissociative loss of a carbonyl ligand is the initial step in many reactions of Fischer-type carbene complexes $(CO)_5M{=}C(YR)R'$ (M = Cr, Mo, W; YR = OR, SR, NR_2, etc.), cis CO's being particularly labile.[2] Some $(CO)_5Cr{=}C(NEt_2)X$ complexes (X = Cl, Br, I, SeR, TeR, $SnPh_3$, $PbPh_3$) rearrange spontaneously to give *trans*-$X(CO)_4Cr{\equiv}CNEt_2$ by an intramolecular process probably involving concerted dissociation of a CO ligand and C,Cr-migration of the group X.[3] In the synthetically important reactions of $(CO)_5M{=}C(OR)R'$ with alkenes or alkynes, CO dissociation is the rate-determining first step, which is followed by addition of the unsaturated molecule to the vacant coordination site.[4] In no case have the 16-electron $(CO)_4M{=}C(YR)R'$ intermediates been observed directly.

We have now been able to isolate such complexes. If solid $(CO)_5W{=}C(NMe_2)SiPh_3$ (**1a**)[5,6] or $(CO)_5W{=}C(NC_5H_{10})SiPh_3$ (**1b**)[6] (but not $(CO)_5W{=}C(NEt_2)SiPh_3$[7]) are warmed to 110 °C at 0.1–0.2 torr in a Schlenk tube, the color changes from yellow to orange-red and the 16-electron complexes $(CO)_4W{=}C(NMe_2)SiPh_3$ (**2a**) or $(CO)_4W{=}C(NC_5H_{10})SiPh_3$ (**2b**) are obtained as major products.[8] They can be separated from byproducts and unreacted **1a,b** by column chromatography on silica at −20 °C (pentane/ether, 25:1). Contrary to **2a** and **2b** the

$$(CO)_5M{=}C(NR_2)SiPh_3 \underset{\textbf{1a–d}}{\rightleftharpoons} CO + (CO)_4M{=}C(NR_2)SiPh_3 \underset{\textbf{2a–d}}{} \quad (1)$$

a, M = W, NR_2 = NMe_2; **b**, M = W, NR_2 = NC_5H_{10}; **c**, M = Mo, NR_2 = NC_5H_{10}; **d**, M = Cr, NR_2 = NC_5H_{10}

analogous complexes of molybdenum (**2c**) and chromium

(1) Part 5: Hörnig, H.; Walther, E.; Schubert, U. *Organometallics* **1985**, *4*, 1905.
(2) Casey, C. P.; Cesa, M. C. *Organometallics* **1982**, *1*, 87.
(3) Fischer, H.; Motsch, A.; Märkl, R.; Ackermann, K.; *Organometallics* **1985**, *4*, 726 and references cited therein.
(4) Fischer, H. In "Transition Metal Carbene Complexes"; Dötz, K. H., Fischer, H., Hofmann, P., Kreissl, F. R., Schubert, U., Weiss, K.; Verlag Chemie: Weinheim/Bergstr., Germany, 1983. Casey, C. P.; Shusterman, A. J.; *Organometallics* **1985**, *4*, 736 and references cited therein.
(5) Fischer, E. O.; Hollfelder, H.; Friedrich, P.; Kreissl, F. R.; Huttner, G. *Chem. Ber.* **1977**, *110*, 3467.
(6) **1a** was prepared by reaction of $(CO)_5W{=}C(OEt)SiPh_3$[5] with $HNMe_2$ in THF at +20 °C analogous to that of ref 5 and **1b–d** by reaction of the corresponding $(CO)_5M{=}C(OEt)SiPh_3$[5] with neat piperidine at +20 °C.
(7) Schubert, U.; Hörnig, H.; Erdmann, K.-U.; Weiss, K. *J. Chem. Soc. Chem. Commun.* **1984**, 13.
(8) Anal. Calcd for $C_{25}H_{21}NO_4SiW$ (**2a**): C, 49.11; H, 3.46; N, 2.29. Found: C, 49.35; H, 3.43; N, 1.87. Anal. Calcd for $C_{28}H_{25}NO_4SiW$ (**2b**): C, 51.62; H, 3.87; N, 2.15. Found: C, 51.62; H, 3.73; N, 1.72. Mass spectrum of **2b** (70 eV): *m/e* (relative intensity) 651 (1, M^+), 595 (25, M − 2CO), 567 (18, M − 3CO), 539 (31, M − 4CO), 507 (36), 446 (24), 259 (51, $SiPh_3$), 182 (100, $SiPh_2$), 105 (66, SiPh).

0276-7333/86/2305-0173$01.50/0

Table I. Selected Bond Lengths (pm) and Angles (deg) for 2b

	Bond Lengths		
W-C1	214.7 (9)	W-C2	193.5 (10)
C1-N	131.1 (12)	W-C3	200.4 (10)
C1-Si	187.7 (9)	W-C4	199.6 (10)
W-C21	268.8 (8)	W-C5	199.5 (11)
W-C22	329.0 (9)	C21-C26	138.8 (13)
W-C26	301.4 (9)	C21-C22	139.3 (12)
	Bond Angles		
C1-W-C2	103.9 (3)	W-C1-Si	101.2 (4)
C1-W-C3	89.4 (4)	W-C1-N	138.0 (7)
C1-W-C4	92.7 (4)	Si-C1-N	120.8 (7)
C1-W-C5	166.9 (4)	C1-N-C6	121.6 (8)
C2-W-C3	84.0 (4)	C1-N-C10	127.5 (8)
C2-W-C4	86.8 (4)	C6-N-C10	110.6 (7)
C2-W-C5	89.2 (4)	C1-Si-C11	112.3 (4)
C3-W-C4	169.3 (3)	C1-Si-C21	101.7 (4)
C3-W-C5	90.4 (4)	C1-Si-C31	112.9 (4)
C4-W-C5	89.6 (4)	C2-W-C21	175.2 (3)

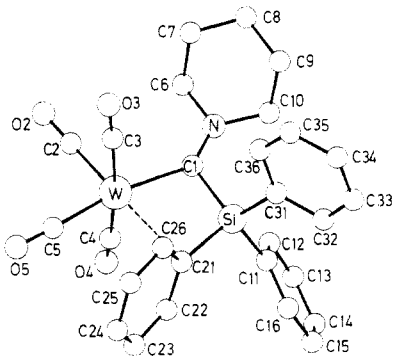

Figure 1. A perspective drawing of $(CO)_4W{=}C(NC_5H_{10})SiPh_3$ (**2b**). Hydrogen atoms have been omitted for clarity.

(**2d**) are already formed to some extent according to eq 1 during the preparation of **1c** and **1d**.[6] While complexes **2** are stable in the solid state, they slowly decompose in solution to give **1**, $M(CO)_6$, and other, unidentified products. On bubbling CO through a pentane solution of **2**, reaction 1 can be reversed.

The X-ray structure determination of **2b**[9] (Table I and Figure 1) reveals that the unique complexes **2** are stabilized by the steric bulk of the carbene ligand. One of the phenyl groups (C21–C26) of the $SiPh_3$ moiety acts like a lid and screens the empty coordination site at tungsten (trans to C2). The shortest distance between the metal atom and the carbon atoms of this phenyl group (W–C21 = 268.8 (8) pm) is much longer than W–C(olefin) distances in *cis*-$(CO)_4$(olefin)W(carbene) complexes (238.1–251.9 pm, mean 243 pm)[10] or W–C(π-aromatic) distances.

Chart I

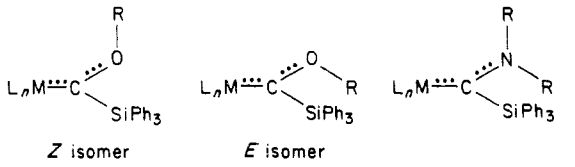

We have previously shown that bond angles at the carbene carbon atom depend on steric rather than electronic effects.[11,12] In a series of octahedral rhenium complexes containing $C(OR)SiPh_3$ ligands the optimal Re–C(carbene)–O angle in *Z* isomers (Chart I) (steric interaction between R and L_nM) is about 135°, while the optimal Si–C(carbene)–O angle in *E* isomers (steric interaction between R and $SiPh_3$) is about 115°. (Dialkylamino)carbene complexes may be regarded sterically as a superposition of an (*E*)- and a (*Z*)-alkoxycarbene complex (Chart I). In (dialkylamino)(triphenylsilyl)carbene complexes we therefore would expect a M–C(carbene)–N bond angle of about 135° (see also ref 13) and a Si–C(carbene)–N bond angle of about 115°, if only steric interactions of the dialkylamino substituent are considered. In the 18-electron complexes **1** bond angles of this magnitude are impossible, because they would cause severe steric interactions between the $SiPh_3$ group and the $M(CO)_5$ moiety. However, they become possible, if one CO ligand is removed from the metal. In fact, the W–C1–N and Si–C1–N bond angles in **2b** correspond to the optimal values.

We therefore believe that relaxation of the steric strain within the carbene ligand is the driving force for the formation of **2** from **1**. Consequently, CO elimination is favored in **1c** and **1d** compared with **1a** and **1b**, because the former complexes are even more crowded due to shorter M–C distances. Interestingly, $(CO)_5Cr{=}C(NEt_2)SnPh_3$ (C(carbene)–Sn is much longer than C(carbene)–Si) does not give a 16-electron complex on heating but rearranges to *trans*-$Ph_3Sn(CO)_4Cr{\equiv}CNEt_2$ by loss of CO.[13,14]

The following experimental findings agree with our notion that coordination around the metal atom in **2** is not severely influenced by the missing CO ligand and that the main difference between complexes **1** and **2** is a sterically relaxed carbene ligand: (i) the bond distances around the carbene carbon in **2b** are not different than those in comparable 18-electron carbene complexes[10-12] and bond angles within the $(CO)_4W$ moiety are hardly distorted; (ii) the ν(CO) absorptions in the infrared spectra of **2**[15] are similar to those in complexes *cis*-$(CO)_4LM{=}C(OMe)R$ (R = Me, Ph; L = PR'_3,[16] MeCN, THF, PhCCPh);[17] (iii) δ[C(carbene)] in the ^{13}C NMR spectra of **1a**[5] (285.90 ppm, acetone-d_6, −20 °C) and **2a** (290.67 ppm, acetone-d_6, −30 °C) are very similar (δ[C(CO)]: **1a**,[5] 204.77, 199.27 ppm; **2a**, 218.88, 217.21 ppm).

Acknowledgment. We thank the Deutsche Forschungsgemeinschaft and the Fonds der Chemischen Industrie for financial support and Wacker-Chemie GmbH for a gift of chemicals.

(9) Crystal structure of **2b**: crystals grown from pentane/ether at −78 °C; orthorhombic; a = 1253.8 (3) pm, b = 1871.4 (7) pm, c = 2273.7 (11) pm; $V = 5335 \times 10^6$ pm^3; space group *Pcab* (nonstandard setting of *Pbca*) (Z = 8); d(calcd) = 1.62 g/cm^3; 4391 independent reflections ($2° \le 2\theta \le 50°$, Mo K_α radiation, Syntex $P2_1$ diffractometer); empirical absorption, Lorentz and polarization corrections; solution of the structure by the Patterson method (Syntex XTL); hydrogen positions calculated according to ideal geometry. Full-matrix least-squares refinement with anisotropic thermal parameters for all non-hydrogen atoms (hydrogen parameters were not refined) led to R = 0.047 and R_w = 0.036 ($1/w = \sigma^2 + 0.000025F_o^2$) for 3078 structure factors with $F_o \ge 3\sigma(F_o)$.

(10) Toledano, C. A.; Levisalles, J.; Rudler, M.; Rudler, H.; Daran, J. C.; Jeannin, Y. *J. Organomet. Chem.* **1982**, *228*, C7. Casey, C. P.; Shusterman, A. J.; Vollendorf, N. W.; Haller, K. J. *J. Am. Chem. Soc.* **1982**, *104*, 2417. Toledano, C. A.; Parlier, A.; Rudler, H.; Daran, J. C.; Jeannin, Y. *J. Chem. Soc., Chem. Commun.* **1984**, 576. Toledano, C. A.; Rudler, H.; Daran, J. C.; Jeannin, Y. *J. Chem. Soc., Chem. Commun.* **1984**, 574. Casey, C. P.; Vollendorf, N. W.; Haller, K. J. *J. Am. Chem. Soc.* **1984**, *106*, 3754. Angermund, K.; Grevels, F.-W.; Krüger, C.; Skibbe, V. *Angew. Chem.* **1984**, *96*, 911; *Angew. Chem., Int. Ed. Engl.* **1984**, *23*, 904.

(11) Schubert, U. *Coord. Chem. Rev.* **1984**, *55*, 261.

(12) Schubert, U.; Ackermann, K.; Rustemeyer, P. *J. Organomet. Chem.* **1982**, *231*, 323.

(13) Fischer, E. O.; Pardy, R. B. A.; Schubert, U. *J. Organomet. Chem.* **1979**, *181*, 37.

(14) Fischer, E. O.; Fischer, H.; Schubert, U.; Pardy, R. B. A., *Angew. Chem.* **1979**, *91*, 929; *Angew. Chem., Int. Ed. Engl.* **1979**, *18*, 872.

(15) ν(CO) (cm^{-1}, pentane): **2a**, 2013 (m), 1931 (s), 1914 (vs), 1860 (m); **2b**, 2011 (m), 1929 (s), 1911 (vs), 1857 (m); **2c**, 2015 (m), 1937 (s), 1919 (s), 1859 (m); **2d**, 2006 (m), 1934 (vs), 1919 (s), 1860 (m).

(16) Fischer, E. O.; Fischer, H. *Chem. Ber.* **1974**, *107*, 657.

(17) Foley, H. C.; Strubinger, L. M.; Targos, T. S.; Geoffroy, G. L. *J. Am. Chem. Soc.* **1983**, *105*, 3064.

Supplementary Material Available: Listings of final atomic parameters, bond lengths and angles, and observed and calculated structure factors (38 pages). Ordering information is given on any current masthead page.

Trisubstituted Heteropolytungstates as Soluble Metal Oxide Analogues. 2.[1] 1,2,3-β-$SiW_9V_3O_{40}^{7-}$ Supported $CpTi^{3+}$, $(Bu_4N)_4[CpTi{\cdot}SiW_9V_3O_{40}]$

Richard G. Finke* and Brian Rapko

Department of Chemistry, University of Oregon
Eugene, Oregon 97403

Peter J. Domaille

Central Research and Development
E. I. duPont de Nemours and Company
Experimental Station, Wilmington, Delaware 19898[†]

Received August 13, 1985

Summary: $(Bu_4N)_4[CpTi{\cdot}SiW_9V_3O_{40}]$ has been synthesized and fully characterized by elemental analysis, FAB mass spectroscopy, IR, and ^{29}Si, ^{183}W, $^{183}W\{^{51}V\}$, and 2-D INADEQUATE $^{183}W\{^{51}V\}$ NMR; the significance of these results to the developing area of vanadium-substituted polyoxoanions in homogeneous and heterogeneous catalysis is discussed.

Transition-metal or organo-transition-metal complexes supported on organic solvent solubilized, vanadium(V)-containing heteropolyanions[2] have not been previously described[3] despite the special interest such species accrue due to the role of vanadium-substituted polyoxoanions in catalytic oxidations.[4] Moreover, only three previous organic solvent soluble, κ^3-*O*-oxide support[1f] polyoxoanions have been described, a major reason why the very promising area of catalysis by polyoxoanion-supported metals has yet to flourish. Note the distinction made here[1f] between support (covalent attachment) of organometallic groups to a polyoxoanion surface and direct incorporation of organometallics into the polyoxoanion lattice. The three reported *support* systems are $(Bu_4N)_4Nb_2W_4O_{19}$ and

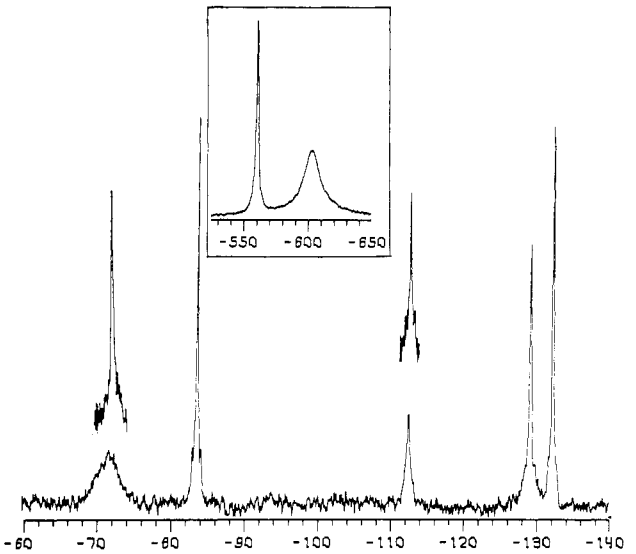

Figure 1. Five-line ^{183}W NMR (15 MHz) of 2:2:1:2:2 relative intensity of 0.28 M $(Bu_4N)_4[CpTi{\cdot}SiW_9V_3O_{40}]$ in 2:1 DMF/CD_3CN recorded on a Nicolet NT-360 NMR at 21 °C in 10-mm sample tubes, $\pi/2$ pulse of 70 μs, LB = 1, and 100 000 pulses collected over 23 h. Chemical shifts in parts per million are negative toward higher field and are referenced to saturated Na_2WO_4 in D_2O at 21 °C using the substitution method. The significant sharpening of the −83 ppm peak as well as that of the −112 ppm peak upon ^{51}V decoupling (obtained as previously described)[12] is shown as insets over these peaks. The ^{51}V (95-MHz) NMR is shown as a boxed inset and was recorded on a 0.09 M sample at 21 °C, LB = 25 Hz in a 12 mm sample tube, and referenced to neat $VOCl_3$ using the substitution method. Chemical shifts are in parts per million and are negative toward higher field.

[†] Contribution no. 3880.

(1) (a) Part 1: Finke, R. G.; Droege, M. W. *J. Am. Chem. Soc.* **1984**, *106*, 7274. (b) Part 3: Finke, R. G.; Rapko, B.; Saxton, R. J.; Domaille, P. "Trisubstituted Heteropolytungstates as Soluble Metal Oxide Analogues. 3. The Synthesis, Characterization, ^{31}P, ^{29}Si, ^{51}V, and ^{183}W NMR, Deprotonation, and H^+ Mobility Studies of Organic Solvent Soluble Forms of $H_3SiW_9V_3O_{40}^{4-}$ and $H_4P_2W_{15}V_3O_{62}^{5-}$", *J. Am. Chem. Soc.*, in press. (c) Part 4: Finke, R. G.; Rapko, B. "Trisubstituted Heteropolytungstates as Soluble Metal Oxide Analogues. 4. $CpTi{\cdot}SiW_9V_3O_{40}^{4-}$ and $CpTi{\cdot}P_2W_{15}V_3O_{62}^{6-}$", unpublished results. (d) Part 5: Finke, R. G.; Edlund, D. J.; Saxton, R. J. "Trisubstituted Heteropolytungstates as Soluble Metal Oxide Analogues. 5. The Synthesis and Characterization of Organic Solvent Soluble $(Bu_4N)_9P_2W_{15}Nb_3O_{62}$ and Its Organometallic Derivatives $(Bu_4N)_7[(C_5Me_5)Rh{\cdot}P_2W_{15}Nb_3O_{62}]$ and $(Bu_4N)_7[(C_6H_6)Ru{\cdot}P_2W_{15}Nb_3O_{62}]$", manuscript in preparation. (e) For earlier work showing that higher valent metals and A-type lacunary polyoxoanions lead to the desired trisubstituted polyoxoanions while lower valent metals and B-type lacunary polyoxoanions tend to give disubstituted dimers, see: Finke, R. G.; Droege, M. W. *Inorg. Chem.* **1983**, *22*, 1006. Finke, R. G.; Droege, M. W.; Hutchinson, J. R.; Gansow, O. W. *J. Am. Chem. Soc.* **1981**, *103*, 1587. (f) An important conceptual difference here, that we point out in response to a reviewer's comments, is the difference between metals supported *on*, as opposed to metals incorporated *into*, a polyoxoanion. By polyoxoanion-*supported* metals, we mean species that are firmly attached to a κ^3-O site of *surface* oxygens of a polyoxoanion analogous to the envisioned situation of at least some oxide-supported heterogeneous catalysts. This situation is quite different from the more common one of metals or organometallics *incorporated into* a vacancy in the polyoxoanion *framework* by four, approximately square-planar O^{2-} ligands, e.g., $CpTi^{3+}$ incorporated into $PW_{11}O_{39}^{7-}$ or $Mo_5O_{18}^{6-}$ as $PW_{11}O_{39}(CpTi)^{4-}$ and $Mo_5O_{18}(CpTi)^{3-}$, respectively, or the incorporated Nb^{5+} in $NbW_5O_{19}^{3-}$, $Nb_2W_4O_{19}^{3-}$, or $SiW_9Nb_3O_{40}^{7-}$. Metals supported on a polyoxoanion surface (but not incorporated metals) can have cis-coordination sites, greater coordinative unsaturation, and perhaps mobility on the oxide surface—all leading to reactions and mechanisms unavailable to incorporated metals and thus to distinctive catalytic chemistries. Also worth distinguishing here are organometallics bound by a single, *labile* bridging oxygen,[3b] cases where the polyoxoanion behaves like a simple alkoxide, RO^-, e.g., $RO{-}U(Cp)_3{-}OR$ ($-OR = -OMW_5O_{19}^{3-}$; M = Ta^{5+}, Nb^{5+})[3b] rather than as a tight binding, κ^3-O ligand or support.

(2) Pope, M. T. In "Hetero- and Isopoly Oxometalates"; Springer-Verlag: New York, 1983.

(3) For lead references to the extensive and pioneering studies of Klemperer, Day, and co-workers in the area of polyoxoanion κ^3-O-supported[14] organometallics, using primarily $Nb_2W_4O_{19}^{4-}$, see: (a) Day, V. W.; Klemperer, W. G. *Science (Washington, D.C.)* **1985**, 228, 533 and references therein to their earlier work. (b) Day, V. W.; Klemperer, W. G.; Maltbie, D. J. *Organometallics* **1985**, *4*, 104. (c) Besecker, C. J.; Day, V. W.; Klemperer, W. G.; Thompson, M. R. *Inorg. Chem.* **1985**, *24*, 44. (d) Besecker, C. J.; Day, V. W.; Klemperer, W. G.; *Organometallics* **1985**, *4*, 564. (e) Besecker, C. J.; Day, V. W.; Klemperer, W. G.; Thompson, M. R. *J. Am. Chem. Soc.* **1984**, *106*, 4125. (f) Che, T. M., Day, V. W.; Francesconi, L. C.; Fredrich, M. F.; Klemperer, W. G.; Shum, W. "Synthesis and Structure of the $[CpTi(Mo_5O_{18})]^{3-}$ and $[(CpTi)W_5O_{18}]^{3-}$ Anions", submitted for publication. We thank Professor Klemperer for providing us with a preprint of this full version of their earlier work: *J. Am. Chem. Soc.* **1981**, *103*, 3597; *J. Chem. Soc., Chem. Commun.* **1979**, 60.

(4) (a) Kozhevenikov, I. V.; Matveev, K. I. *Appl. Catal.* **1983**, *5*, 15; *Russ. Chem. Rev. (Engl. Transl.)* **1982**, *51*, 1075. (b) Tarabanko, V. E.; Kozhevenkov, I. V.; Matveev, K. I. *Kinet. Katal.* **1978**, *19*, 1160. (c) Kozhevenikov, I. V.; Tarabanko, V. E.; Matveev, K. I.; Vardanyan, V. D. *React. Kinet. Catal. Lett.* **1977**, *7*, 297. (d) Ogawa, H.; Fujinami, H.; Taya, K. *J. Chem. Soc., Chem. Commun.* **1981**, 1274. (e) Davison, S. F.; Mann, B. E.; Maitlis, P. M. *J. Chem. Soc., Dalton Trans.* **1984**, 1223. (f) Murtha, T. P.; Shioyama, T. K. U.S. Patent 4 434 082, 1984, assigned to Phillips Petroleum Co. (g) Akimoto, M.; Ikeda, H.; Okabe, A.; Echigoya, E. *J. Catal.* **1984**, *89*, 196 and references therein. (h) Ai, M. *J. Catal.* **1984**, *85*, 324 and references therein. (i) Konishi, Y.; Sakata, K.; Misono, M.; Yoneda, Y. *J. Catal.* **1982**, *77*, 169.

0276-7333/86/2305-0175$01.50/0

Supplementary Material Available: Listings of final atomic parameters, bond lengths and angles, and observed and calculated structure factors (38 pages). Ordering information is given on any current masthead page.

Trisubstituted Heteropolytungstates as Soluble Metal Oxide Analogues. 2.[1] 1,2,3-β-$SiW_9V_3O_{40}^{7-}$ Supported $CpTi^{3+}$, $(Bu_4N)_4[CpTi{\cdot}SiW_9V_3O_{40}]$

Richard G. Finke* and Brian Rapko

Department of Chemistry, University of Oregon
Eugene, Oregon 97403

Peter J. Domaille

Central Research and Development
E. I. duPont de Nemours and Company
Experimental Station, Wilmington, Delaware 19898†

Received August 13, 1985

Summary: $(Bu_4N)_4[CpTi{\cdot}SiW_9V_3O_{40}]$ has been synthesized and fully characterized by elemental analysis, FAB mass spectroscopy, IR, and ^{29}Si, ^{183}W, $^{183}W\{^{51}V\}$, and 2-D INADEQUATE $^{183}W\{^{51}V\}$ NMR; the significance of these results to the developing area of vanadium-substituted polyoxoanions in homogeneous and heterogeneous catalysis is discussed.

Transition-metal or organo-transition-metal complexes supported on organic solvent solubilized, vanadium(V)-containing heteropolyanions[2] have not been previously described[3] despite the special interest such species accrue due to the role of vanadium-substituted polyoxoanions in catalytic oxidations.[4] Moreover, only three previous organic solvent soluble, κ^3-*O*-oxide support[1f] polyoxoanions have been described, a major reason why the very promising area of catalysis by polyoxoanion-supported metals has yet to flourish. Note the distinction made here[1f] between support (covalent attachment) of organometallic groups to a polyoxoanion surface and direct incorporation of organometallics into the polyoxoanion lattice. The three reported *support* systems are $(Bu_4N)_4Nb_2W_4O_{19}$ and

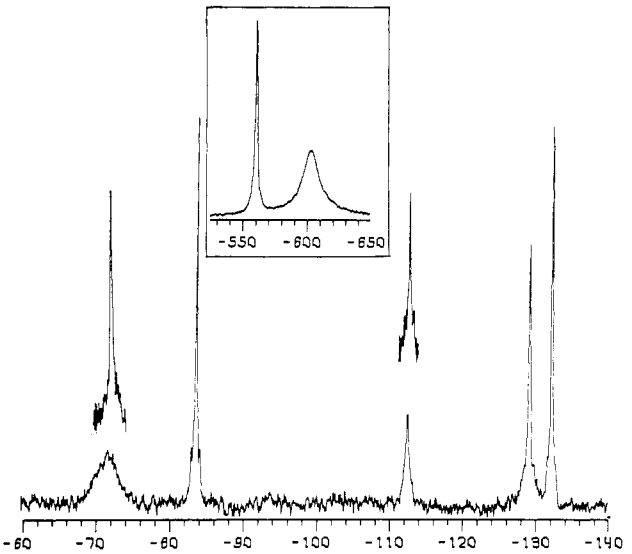

Figure 1. Five-line ^{183}W NMR (15 MHz) of 2:2:1:2:2 relative intensity of 0.28 M $(Bu_4N)_4[CpTi{\cdot}SiW_9V_3O_{40}]$ in 2:1 DMF/CD_3CN recorded on a Nicolet NT-360 NMR at 21 °C in 10-mm sample tubes, $\pi/2$ pulse of 70 μs, LB = 1, and 100 000 pulses collected over 23 h. Chemical shifts in parts per million are negative toward higher field and are referenced to saturated Na_2WO_4 in D_2O at 21 °C using the substitution method. The significant sharpening of the −83 ppm peak as well as that of the −112 ppm peak upon ^{51}V decoupling (obtained as previously described)[12] is shown as insets over these peaks. The ^{51}V (95-MHz) NMR is shown as a boxed inset and was recorded on a 0.09 M sample at 21 °C, LB = 25 Hz in a 12 mm sample tube, and referenced to neat $VOCl_3$ using the substitution method. Chemical shifts are in parts per million and are negative toward higher field.

† Contribution no. 3880.

(1) (a) Part 1: Finke, R. G.; Droege, M. W. *J. Am. Chem. Soc.* **1984**, *106*, 7274. (b) Part 3: Finke, R. G.; Rapko, B.; Saxton, R. J.; Domaille, P. "Trisubstituted Heteropolytungstates as Soluble Metal Oxide Analogues. 3. The Synthesis, Characterization, ^{31}P, ^{29}Si, ^{51}V, and ^{183}W NMR, Deprotonation, and H^+ Mobility Studies of Organic Solvent Soluble Forms of $H_3SiW_9V_3O_{40}^{4-}$ and $H_4P_2W_{15}V_3O_{62}^{5-n}$", *J. Am. Chem. Soc.*, in press. (c) Part 4: Finke, R. G.; Rapko, B. "Trisubstituted Heteropolytungstates as Soluble Metal Oxide Analogues. 4. $CpTi{\cdot}SiW_9V_3O_{40}^{4-}$ and $CpTi{\cdot}P_2W_{15}V_3O_{62}^{6-n}$", unpublished results. (d) Part 5: Finke, R. G.; Edlund, D. J.; Saxton, R. J. "Trisubstituted Heteropolytungstates as Soluble Metal Oxide Analogues. 5. The Synthesis and Characterization of Organic Solvent Soluble $(Bu_4N)_9P_2W_{15}Nb_3O_{62}$ and Its Organometallic Derivatives $(Bu_4N)_7[(C_5Me_5)Rh{\cdot}P_2W_{15}Nb_3O_{62}]$ and $(Bu_4N)_7[(C_6H_6)Ru{\cdot}P_2W_{15}Nb_3O_{62}]$", manuscript in preparation. (e) For earlier work showing that higher valent metals and A-type lacunary polyoxoanions lead to the desired trisubstituted polyoxoanions while lower valent metals and B-type lacunary polyoxoanions tend to give disubstituted dimers, see: Finke, R. G.; Droege, M. W. *Inorg. Chem.* **1983**, *22*, 1006. Finke, R. G.; Droege, M. W.; Hutchinson, J. R.; Gansow, O. W. *J. Am. Chem. Soc.* **1981**, *103*, 1587. (f) An important conceptual difference here, that we point out in response to a reviewer's comments, is the difference between metals supported *on*, as opposed to metals incorporated *into*, a polyoxoanion. By polyoxoanion-*supported* metals, we mean species that are firmly attached to a κ^3-O site of *surface* oxygens of a polyoxoanion analogous to the envisioned situation of at least some oxide-supported heterogeneous catalysts. This situation is quite different from the more common one of metals or organometallics *incorporated into* a vacancy in the polyoxoanion *framework* by four, approximately square-planar O^{2-} ligands, e.g., $CpTi^{3+}$ incorporated into $PW_{11}O_{39}^{7-}$ or $Mo_5O_{18}^{6-}$ as $PW_{11}O_{39}(CpTi)^{4-}$ and $Mo_5O_{18}(CpTi)^{3-}$, respectively, or the incorporated Nb^{5+} in $NbW_5O_{19}^{3-}$, $Nb_2W_4O_{19}^{3-}$, or $SiW_9Nb_3O_{40}^{7-}$. Metals supported on a polyoxoanion surface (but not incorporated metals) can have cis-coordination sites, greater coordinative unsaturation, and perhaps mobility on the oxide surface—all leading to reactions and mechanisms unavailable to incorporated metals and thus to distinctive catalytic chemistries. Also worth distinguishing here are organometallics bound by a single, *labile* bridging oxygen,[3b] cases where the polyoxoanion behaves like a simple alkoxide, RO^-, e.g., $RO{-}U(Cp)_3{-}OR$ (−OR = $-OMW_5O_{19}^{3-}$; M = Ta^{5+}, Nb^{5+})[3b] rather than as a tight binding, κ^3-O ligand or support.

(2) Pope, M. T. In "Hetero- and Isopoly Oxometalates"; Springer-Verlag: New York, 1983.

(3) For lead references to the extensive and pioneering studies of Klemperer, Day, and co-workers in the area of polyoxoanion κ^3-O-supported[14] organometallics, using primarily $Nb_2W_4O_{19}^{4-}$, see: (a) Day, V. W.; Klemperer, W. G. *Science* (*Washington, D.C.*) **1985**, 228, 533 and references therein to their earlier work. (b) Day, V. W.; Klemperer, W. G.; Maltbie, D. J. *Organometallics* **1985**, *4*, 104. (c) Besecker, C. J.; Day, V. W.; Klemperer, W. G.; Thompson, M. R. *Inorg. Chem.* **1985**, *24*, 44. (d) Besecker, C. J.; Day, V. W.; Klemperer, W. G.; *Organometallics* **1985**, *4*, 564. (e) Besecker, C. J.; Day, V. W.; Klemperer, W. G.; Thompson, M. R. *J. Am. Chem. Soc.* **1984**, *106*, 4125. (f) Che, T. M., Day, V. W.; Francesconi, L. C.; Fredrich, M. F.; Klemperer, W. G.; Shum, W. "Synthesis and Structure of the $[CpTi(Mo_5O_{18})]^{3-}$ and $[(CpTi)W_5O_{18}]^{3-}$ Anions", submitted for publication. We thank Professor Klemperer for providing us with a preprint of this full version of their earlier work: *J. Am. Chem. Soc.* **1981**, *103*, 3597; *J. Chem. Soc., Chem. Commun.* **1979**, 60.

(4) (a) Kozhevenikov, I. V.; Matveev, K. I. *Appl. Catal.* **1983**, *5*, 15; *Russ. Chem. Rev.* (*Engl. Transl.*) **1982**, *51*, 1075. (b) Tarabanko, V. E.; Kozhevenkov, I. V.; Matveev, K. I. *Kinet. Katal.* **1978**, *19*, 1160. (c) Kozhevenikov, I. V.; Tarabanko, V. E.; Matveev, K. I.; Vardanyan, V. D. *React. Kinet. Catal. Lett.* **1977**, *7*, 297. (d) Ogawa, H.; Fujinami, H.; Taya, K. *J. Chem. Soc., Chem. Commun.* **1981**, 1274. (e) Davison, S. F.; Mann, B. E.; Maitlis, P. M. *J. Chem. Soc., Dalton Trans.* **1984**, 1223. (f) Murtha, T. P.; Shioyama, T. K. U.S. Patent 4 434 082, 1984, assigned to Phillips Petroleum Co. (g) Akimoto, M.; Ikeda, H.; Okabe, A.; Echigoya, E. *J. Catal.* **1984**, *89*, 196 and references therein. (h) Ai, M. *J. Catal.* **1984**, *85*, 324 and references therein. (i) Konishi, Y.; Sakata, K.; Misono, M.; Yoneda, Y. *J. Catal.* **1982**, *77*, 169.

0276-7333/86/2305-0175$01.50/0

$CpTiM_5O_{18}^{3-}$ (M = Mo and W and with Ti^{4+} incorporated[1f] into the $M_6O_{19}^{n-}$ framework) described by Klemperer and Day and our[1a] $(Bu_4N)_7SiW_9Nb_3O_{40}$. Only the latter ion (and now $(Bu_4N)_7SiW_9V_3O_{40}$, vide infra) exhibits a single, regiospecific site for the κ^3-O attachment[1f] of transition-metal catalysts or catalysts precursors[3] without the aid of steric blocking groups such as the Cp in[3f] $CpTiM_5O_{18}^{3-}$.

Herein we report the synthesis and characterization by elemental analysis, FAB mass spectroscopy, IR, and ^{29}Si, ^{51}V, ^{183}W, $^{183}W\{^{51}V\}$ and 2-D INADEQUATE $^{183}W\{^{51}V\}$ NMR of $(Bu_4N)_4[CpTi{\cdot}SiW_9V_3O_{40}]$. Such previously unknown, polyoxoanion κ^3-O-supported[1f] Ti^{4+} species represent the first step toward the possible development of Ziegler–Natta like polymerization[5] or Ti^{4+}/SiO_2 type olefin epoxidation[6] catalysts. In addition, the characterization in solution of $(Bu_4N)_4[CpTi{\cdot}SiW_9V_3O_{40}]$ without the powerful[3] but slow, disorder-prone, and often problematic—but often essential[7f] —technique of polyoxoanion X-ray crystallography[3c,e,7] represents another important, required step toward the development of polyoxoanion-supported homogeneous and heterogenous catalysts.

Analytically pure $(Bu_4N)_4[CpTi{\cdot}SiW_9V_3O_{40}]$ was prepared by the dropwise addition with stirring under N_2 of a moist-air-sensitive, yellow solution of $CpTi(CH_3CN)_n(NO_3)_3$[8] (3.6 mmol, in a minimum of CaH_2 dried CH_3CN) to a cherry red, CH_3CN solution of $(Bu_4N)_7SiW_9V_3O_{40}$[1b] (15 g, 3.6 mmol). The resultant, dark orange solution was gently refluxed under N_2 for 1 h, the solvent was removed under vacuum, the residue was extracted with 20-mL portions of $CHCl_3$ until a clear $CHCl_3$ phase resulted (removing any unreacted starting material), and the residual solid[9a] was crystallized from $CHCl_3/CH_3CN$ by vapor diffusion techniques[9b] to yield dark orange product. The elemental analysis (including oxygen) establishes the empirical formula as $(Bu_4N)_4[CpTi{\cdot}SiW_9V_3O_{40}]$ and accounts for all of its mass. Anal. Calcd for $C_{69}H_{149}N_4TiSiW_9V_3O_{40}$ (Found): C, 23.29 (23.10); H, 4.22 (4.25); N, 1.57 (1.65); Ti, 1.35 (1.09); Si, 0.79 (0.78); W, 46.5 (46.4); V, 4.26 (4.60); O, 18.0 (18.2); total, 100.0 (100.07). The compound's molecular formula was established both by a positive ion FAB mass spectrum,[10a] which showed the expected most abundant mass ion at $(M + H)^+ = m/z$ 3559 and the characteristic cationization and fragmentation processes,[10a,b] as well as in CH_3CN solution by ultracentrifugation molecular weight measurements[11] (calcd for CpTi·

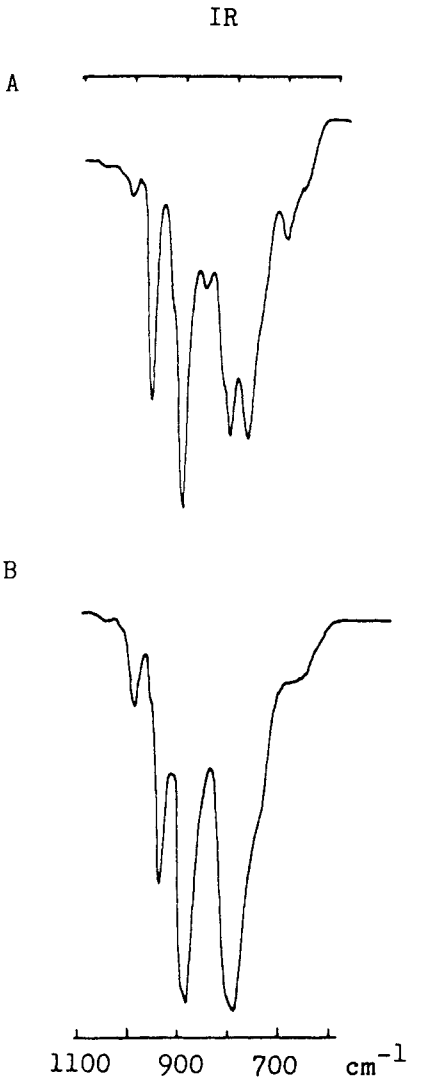

Figure 2. IR of $(Bu_4N)_4[CpTi{\cdot}SiW_9V_3O_{40}]$ (A), obtained with matched NaCl cells in CH_3CN vs. a CH_3CN reference, showing the 35 cm^{-1} splitting of the 800 cm^{-1} band assigned[13] to a ν_{asym} (M–O–M) between edge-sharing MO_6 octahedra. The IR of $(Bu_4N)_7SiW_9V_3O_{40}$ is shown in B for comparison.

(5) (a) Sinn, H.; Kaminsky, W. *Adv. Organomet. Chem.* **1980**, *18*, 99. (b) Boor, J., Jr. "Ziegler-Natta Polymerization"; Academic Press: New York, 1979.

(6) Sheldon, R. A.; Kochi, J. K. In "Metal-Catalyzed Oxidations of Organic Compounds"; Academic Press: New York, 1981; Chapter 9.

(7) (a) Problems apparent from the important, cornerstone[14b] X-ray crystallographic investigations to date of the relative small, more optimum $Nb_2W_4O_{19}^{4-}$ system[7b] include problems obtaining good, strongly diffracting crystals,[7c] problems with the occurrence of noncentrosymmetric space groups,[7d] disorder problems (e.g., Nb/W disorder in $Nb_2W_4O_{19}^{4-}$ or disorder of Bu_4N^+ cations),[3c,e] the inherent problems of a large number of heavy atoms such as W or Nb (a problem exacerbated in the larger polyoxoanions, e.g., in Keggin $XW_{12}O_{40}^{n-}$ or Dawson $X_2W_{12}O_{62}^{m-}$ polyoxoanions, with their associated larger unit cells), and the other problems that led to the reinterpretation of five recent crystal structures of heteropoly and isopoly compounds.[7e] Despite such problems, polyoxoanion crystallography often proves essential.[7f] (b) "X-ray Structural Studies of Novel Polyoxoanionic Organometallic Complexes"; 185th National Meeting of the American Chemical Society, Seattle, WA, March 1983; American Chemical Society: Washington, D.C., 1983; INOR 232. (c) In ref 3b, the authors note that "marginally acceptable" crystals of $[(C_5H_5)_3U(NbW_5O_{19})_2](Bu_4N)_5$ were grown "after more than a dozen unsuccessful attempts". Our own attempts to grow crystallographic quality single crystals of the readily crystallized $(Bu_4N)_4[CpTi{\cdot}SiW_9V_3O_{40}]$ have been unsuccessful to date; attempts with other cations are in progress. (d) Reference 3e documents these problems in the case of $(Bu_4N)_2[(C_5Me_5)Rh{\cdot}Nb_2W_4O_{19}]$ and how initial attempts to solve this structure in a centrosymmetric space group led to an apparent $M_{10}O_{28}^{n-}$ structure. (e) Evans, H. T., Jr.; Pope, M. T. *Inorg. Chem.* **1984**, *23*, 501. (f) In our own very recent studies, preliminary evidence suggests a C_s, rather than the expected C_{3v}, symmetry structure for $CpTi^{3+}$ supported on both B-type $P_2W_{15}V_3O_{62}^{9-}$ and B-type 1,4,9-$PW_9V_3O_{40}^{6-}$. Attempts at the required X-ray diffraction structural studies are in progress.[17]

(8) (a) A $CpTi(CH_3CN)_n(NO_3)_3$[8b] solution in CH_3CN was prepared by dissolving 0.79 g (3.6 mmol) of vacuum-sublimed $CpTiCl_3$[8c] in a minimum of dry CH_3CN under N_2, adding 1.83 g (10.8 mmol) of $AgNO_3$ in dry CH_3CN dropwise with stirring. Filtration of the 1.50 g of AgCl (1.55 g expected) and washing this solid until the washings were clear provided a yellow $CpTi(CH_3CN)_n(NO_3)_3$ solution with a single ^1H NMR C_5H_5 peak (in CD_3CN) at 7.14 ppm (C_5H_5). (b) Evidence for Ti^{4+}/NO_3^- bonding exists, hence the $CpTi(CH_3CN)_n(NO_3)_3$ formulation; see: Wailes, P. C.; Coutts, R. S. P.; Weigold, H. "Organometallic Chemistry of Titanium, Zirconium, and Hafnium"; Academic Press: New York, 1974. (c) Prepared from $TiCl_4$ and Cp_2TiCl_2 (Alfa): King, R. B. "Organometallic Synthesis, Vol I: Transition Metal Compounds"; Academic Press: New York, 1965; p 78.

(9) (a) The crude yield is 3.2–4.1 g (27–35%) and is low, at least in part, due to ca. 25% decomposition of $(Bu_4N)_7SiW_9V_3O_{40}$ by OH^-.[1b] For $(Bu_4N)_9P_2W_{15}V_3O_{62}$, which is not decomposed by $Bu_4N^+OH^-$ in CH_3CN at room temperature the yield of $CpTi{\cdot}P_2W_{15}V_3O_{62}^{6-}$ is much higher, ≥80%. (b) Often, even after one recrystallization, small amounts of an additional specie(s), possibly $HSiW_9V_3O_{40}^{6-}$,[1b] can be detected by ^{51}V or ^{183}W NMR. Suspension/washing of the product in/with CH_3OH or EtOH, to remove this more soluble impurity, followed by an additional recrystallization from $CHCl_3/CH_3CN$ affords pure product.

(10) (a) Finke, R. G.; Droege, M. W.; Cook, C. J.; Suslick, K. S. *J. Am. Chem. Soc.* **1984**, *106*, 5750. (b) Suslick, K. S.; Cook, J. C.; Rapko, B.; Droege, M. W.; Finke, R. G. *Inorg. Chem.*, in press.

(11) Reference 1a, supplementary material provided therein including a discussion of the errors involved in this method.

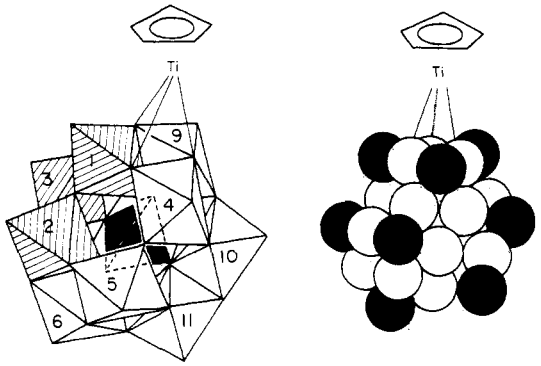

Figure 3. Proposed structure of $CpTi{\cdot}SiW_9V_3O_4O^{4-}$ shown with the polyoxoanion presented as its idealized corner and edge-sharing polyhedra representation (A) and as its more realistic, closed-packed oxide representation (B). In the polyhedra representation (A), the VO_6 octahedra are numbered 1–3, the WO_6 octahedra 4–12, and the central dark tetrahedron is the SiO_4 group. In the close-packed oxide presentation (B), the open circles represent bridging oxygens while the solid ones represent terminal, multiply bonded oxygens. The $CpTi^{3+}$ group is shown attached to three bridging oxygens of a B-type (V_1, W_4, W_9; edge-sharing) triad of octahedra although its attachment to a slightly different, C_s symmetry site composed from the V–O terminal oxygen plus the V_1–O–W_9 and V_1–O–W_4 bridging oxygens cannot be rigorously excluded on the basis of the present data.

$SiW_9V_3O_{40}^{4-}$, 2588; found, 3470 (ca. 34% high as generally observed;[11] Figure 1, supplementary material).

The product's homogeneity and its further characterization are provided by the single ^{29}Si NMR resonance at −83.2 ppm (0.09 M compound in CD_3CN at 21 °C vs. a Me_4Si/acetone-d_6 reference), the single ^1H NMR C_5H_5 resonance in CD_3CN at 6.90 ppm compared to the earlier 7.14 ppm resonance for $CpTi(CD_3CN)_n(NO_3)_3$, and the two resonances of 2:1 relative intensity at −604 ($\Delta\nu_{1/2}$ = 1096 Hz) and −561 ppm ($\Delta\nu_{1/2}$ = 146 Hz), respectively, in the ^{51}V NMR (0.09 M in CD_3CN at 21 °C, neat $VOCl_3$ reference; Figure 1, boxed inset). The ^{51}V NMR demonstrates a symmetry change from C_{3v} for the $SiW_9V_3O_{40}^{7-}$ starting material to C_s for the $CpTi{\cdot}SiW_9V_3O_{40}^{4-}$ product. The ^{183}W NMR confirms the product's C_s symmetry by exhibiting a five-line, relative intensity 2:2:1:2:2 spectrum (Figure 1) with lines at −75.1, −83.2, −112.3, −129.3, and −132.2 ppm, respectively. The ^{51}V-decoupled ^{183}W NMR shows sharpened resonances at −71.5 and −112.3 ppm (Figure 1, insets above these two peaks) indicating that broadening in the coupled spectrum occurs by scalar relaxation of W coupled to adjacent V.[12]

A comparison of the CH_3CN solution IR's of $(Bu_4N)_4[CpTi{\cdot}SiW_9V_3O_{40}]$ (Figure 2A) and $(Bu_4N)_7SiW_9V_3O_{40}$ (Figure 2B) shows a 35 cm^{-1} splitting (Figure 2A) of the 800 cm^{-1} band (Figure 2B) assigned to a ν_{asym} M–O–M vibration of edge-shared octahedra.[13] This as well as the preferred "piano stool" geometry at $CpTi^{3+}$ [8b] supports the C_s symmetry structure proposed (Figure 3), where the $CpTi^{3+}$ group is covalently and regiospecifically bonded to a κ^3-*O* site[14] formed by a triad of edge-sharing octahedra $V_1W_4W_9$ (or equivalently $V_2W_5W_6$ or $V_3W_7W_8$) rather than

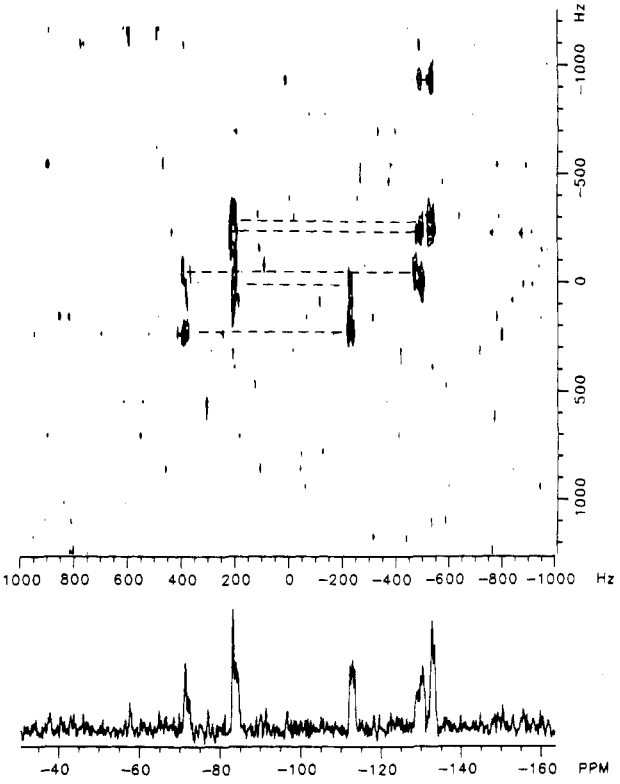

Figure 4. ^{51}V-decoupled 2-D INADEQUATE ^{183}W NMR of 0.17 M $(Bu_4N)_4[CpTi{\cdot}SiW_9V_3O_{40}]$ (30 °C, 12 160 transients, 32 files of 2K words, 72 h), obtained in a 20-mm sideways tube as previously described.[12] Coupled sites are connected by horizontal lines; connections between single "ovals" are characteristic of edge couplings[15] and those between "dumbbells" are indicative of corner couplings.[15]

at the other C_s symmetry sites $V_1W_4W_5V_2$, $W_4W_5W_{10}W_{11}$, or $W_4W_9W_{10}$.[14] This IR result confirms the strictly analogous 30 cm^{-1} splitting observed, and the structural assignment made, for $[(C_5Me_5)Rh{\cdot}SiW_9Nb_3O_{40}]^{5-}$,[1a] where it was noted that steric repulsions between the C_5Me_5 (or Cp in the present, $CpTi^{3+}$, case) and the protruding, terminal M=O (M = Nb, V) oxygens prevent attachment at the C_{3v} site ($M_1M_2M_3$, Figure 3, M = Nb, V).

The W-to-W connectivities and hence the W framework of $CpTi{\cdot}SiW_9V_3O_{40}^{4-}$ as shown in Figure 3 were unambiguously established by using ^{51}V decoupled 2-D INADEQUATE ^{183}W NMR[12,15e] Figure 4. Beginning with the unique, intensity one resonance in Figure 4 at −112 ppm (W_{10}, Figure 3), a W–O–W edge coupling[15] to the −83 ppm resonance (W_{11},W_{12}) as well as a corner coupling[15] to the −72 ppm resonance (W_4,W_9) are observed. Additional corner coupling of the W_4,W_9, −72 ppm resonance to the −129 ppm resonance allows assignment of W_5,W_8 to the −129 ppm peak. Inspection of Figure 3 indicates that the W_5,W_8, −129 ppm resonance should be further coupled via an edge coupling to W_6,W_7. This connection is apparent in the upper right hand part of Figure 4 to the −132 ppm resonance (W_6,W_7). The 2-D INADEQUATE ^{183}W NMR is consistent *only* with the basic "SiW_9V_3" skeleton shown in Figure 3, illustrating the A-type[16] (1,2,3-trivanadium)

(12) Domaille, P. J. *J. Am. Chem. Soc.* **1984**, *106*, 7677 and references therein.

(13) (a) Rocchiccioli-Deltcheff, C.; Fournier, M.; Franck, R.; Trouvenot, R. *Inorg. Chem.* **1983**, *22*, 207. (b) Thouvenot, R.; Fournier, M.; Franck, R.; Rocchiccioli-Deltcheff, C. *Inorg. Chem.* **1984**, *23*, 598.

(14) (a) The first evidence that polyoxoanions could serve as a κ^3-*O* site is due to Flynn and Stucky who obtained structures on $Cr(en)^{3+}$ and Mn^{4+} bound to $Nb_6O_{19}^{8-}$: Flynn, C. M.; Stucky, G. D. *Inorg. Chem.* **1969**, *8*, 178, 335. (b) Precedent for the polyoxoanion serving as a κ^3-O ligand is also provided by crystallographically characterized $(C_5Me_5)Rh{\cdot}Nb_2W_4O_{19}^{2-}$, $(OC)_3Re{\cdot}Nb_2W_4O_{19}^{3-}$, and related complexes.[3]

(15) (a) Corner coupling means $^2J_{W\text{-}O\text{-}W}$ coupling between corner-sharing octahedra, typically 13–30 Hz[12,15b-e] while edge couplings indicate coupling between edge-sharing octahedra, $^2J_{W\text{-}O\text{-}W}$ generally 5–12 Hz.[12,15b-e] The former appear, therefore, as "dumbbells" while the latter appear as "single ovals" in 2-D INADEQUATE spectra. (b) LeFebvre, J.; Chauveau, F.; Doppelt, P.; Brevard, C. *J. Am. Chem. Soc.* **1981**, *103*, 4589. (c) Knoth, W. H.; Domaille, P. J.; Roe, D. C. *Inorg. Chem.* **1983**, *22*, 198. (d) Domaille, P. J.; Knoth, W. H. *Inorg. Chem.* **1983**, *22*, 818. (e) Brevard, C.; Schimpf, R.; Tourne, G.; Tourne, C. *J. Am. Chem. Soc.* **1983**, *105*, 7059.

and β[16] isomer (β = W_{10}, W_{11}, W_{12} as shown).

The physical properties of CpTi·$SiW_9V_3O_{40}^{4-}$ further indicate the strong, covalent $CpTi^{3+}$ attachment to the close-packed, surface oxygens of $SiW_9V_3O_{40}^{7-}$. Although $CpTi(CH_3CN)_n(NO_3)_3$ is quite sensitive to even atmospheric moisture, once supported, CpTi·$SiW_9V_3O_{40}^{4-}$ is stable to the atmosphere for >1 month either in the solid state or in CH_3CN solution (by solution ^{51}V and ^{183}W NMR). An orange CH_3CN solution of $(Bu_4N)_4$[CpTi·$SiW_9V_3O_{40}$] passes unaltered (^1H NMR, IR) through a Amberlyst 15 cation-exchange column while a control shows that organometallic cations like $CpTi(CH_3CN)_n^{3+}(NO_3)_3^{3-}$ are retained on the top of the column. Conversely, all the color of the anionic CpTi·$SiW_9V_3O_{40}^{4-}$ remains with an Amberlyst A-27 anion-exchange column in the Cl^- form, with no visible $CpTiCl_3$ elution from this top band.

Preliminary experiments indicate that it will be possible to prepare $SiW_9V_3O_{40}^{7-}$ supported $TiCl^{3+}$, a more reactive, better catalyst precursor, and that CpTi·$P_2W_{15}V_3O_{62}^{6-}$ and CpTi·1,4,9-$PW_9V_3O_{40}^{3-}$ can be prepared;[7f] these latter two complexes will allow a comparison of 1,2,3 (or A-type) vs. 1,4,9 (or B-type) trivanadium-substituted polyoxoanions. These experiments, continuing attempts[17] at obtaining crystals of CpTi·$SiW_9V_3O_{40}^{4-}$ suitable for X-ray crystallography,[7c] and other experiments aimed at using polyoxoanion-supported Ti^{4+} as Ziegler–Natta polymerization and olefin epoxidation catalysts will be reported in due course.

Acknowledgment. Support from NSF Grant CHE-8313459 and from Dreyfus Teacher-Scholar, Alfred P. Sloan, and Guggenheim (1984–1985) fellowships to R.G.F. are gratefully acknowledged. High-resolution fast-atom-bombardment mass spectra were obtained in the Mass Spectrometry Laboratory, School of Chemical Sciences, University of Illinois at Urbana-Champaign, supported in part by a grant from the National Institute of General Medical Sciences (GM27029), and with the assistance of Professor K. S. Suslick, whose help it is a pleasure to acknowledge. The ZAB-SE mass spectrometer was purchased in part with grants from the Division of Research Resources, National Institutes of Health (RR01575), the National Science Foundation (PCM 81-21494), and the National Institute of General Medical Sciences (GM27029).

Supplementary Material Available: A plot of the ultracentrifugation, sedimentation equilibrium molecular weight measurement in CH_3CN for $(Bu_4N)_4$[CpTi·$SiW_9V_3O_{40}$] (1 page). Ordering information is given on any current masthead page.

(16) (a) Massart, R.; Contant, R.; Fruchart, J. M. Ciabrini, J. P.; Fournier, M. *Inorg. Chem.* **1977**, *16*, 2916. (b) Hervé, G.; Tézé, A. *Inorg. Chem.* **1977**, *16*, 2115. (c) See also ref 1e and the discussion and references therein.

(17) Day, V. W.; Finke, R. G.; Rapko, B., experiments in progress.

Photoinduced Ring Expansion of a Cyclobutyliron σ Complex: An Example of Rearrangement of an Alkyl Group from Saturated Carbon to a Transition Metal To Give a Carbene Complex

Yngve Stenstrøm and W. M. Jones*

Department of Chemistry, University of Florida Gainesville, Florida 32611

Received September 20, 1985

Summary: Photolysis of either dicarbonyl(η^5-cyclopentadienyl)(1-methoxycyclobutane-1-carbonyl)iron (**8**) or its corresponding σ-complex dicarbonyl(η^5-cyclopentadienyl)(1-methoxycyclobutyl)iron (**9**) gives the rearranged carbene complex **11**. The carbene complex reacts with CO at room temperature and low pressure (ca. 6.5 atm) to give the ring-contracted dicarbonyl(η^5-cyclopentadienyl)(2-methoxycyclobutyl)iron (**12**). Photolysis of **12** regenerates the carbene complex **11**. It is suggested that these rearrangements involve both rearrangement from saturated carbon to iron to give a carbene complex and its reverse.

Theory predicts that the rearrangements generalized in the following equation should be facile.[1]

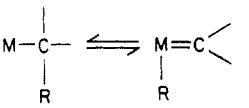

And, indeed, rearrangement in both directions in which hydrogen is the rearranging group are now commonplace[2,3] as are rearrangements of both alkyl and aryl groups from metal to carbene carbon[4] (rearrangement from right to left). In contrast, rearrangement of alkyl groups from saturated carbon to metal to give new carbene complexes are exceedingly rare[5] and aryl rearrangement has yet to be reported.

We recently reported that photolysis of **1** or **2** gives **5** for which we suggested the mechanism outlined in Scheme I.[6,8] We further suggested that the driving force for this rearrangement is a combination of relief of ring strain[8a] (**5** is less strained than **3**) and stabilization of the carbene (**5** is stabilized by electron donation from the methoxy more than **3**), a suggestion that is consistent with Green's hypothesis that the paucity of 1,2-rearrangements of alkyl or aryl groups from saturated carbon to metals is thermodynamic in origin.[3,9]

(1) Berke, H.; Hoffmann, R. *J. Am. Chem. Soc.* **1978**, *100*, 7224. Goddard, R. J.; Hoffmann, R.; Temmis, E. D. *J. Am. Chem. Soc.* **1980**, *102*, 7667.

(2) Schrock, R. R. *Acc. Chem. Res.* **1979**, *12*, 98. Schultz, A. J.; Williams, J. M.; Schrock, R. R.; Rupprecht, J. A.; Fellmann, J. *J. Am. Chem. Soc.* **1979**, *101*, 1593. Canestrani, M.; Green, M. L. H. *J. Chem. Soc., Dalton Trans.* **1982**, 1789. Calderon, N.; Lawrence, J. P.; Ofstead, E. A. *Adv. Organomet. Chem.* **1979**, *17*, 449. Foley, P.; Whitesides, G. *J. Am. Chem. Soc.* **1979**, *101*, 2732. Empsall, H. D.; Hyde, E. M.; Markham, M.; McDonald, W. S.; Norton, M. C.; Shaw, B. L.; Weeks, B. *J. Chem. Soc., Chem. Commun. 1977*, 589. Kemball, C. *Catal. Rev.* **1971**, *5*, 33. Light, J. R. C.; Zeiss, H. H. *J. Organomet. Chem.* **1970**, *21*, 391. Sneedon, R. P. A.; Zeiss, H. H. *J. Organomet. Chem.* **1971**, *26*, 101. Farady, L.; Marko, L. *J. Organomet. Chem.* **1972**, *43*, 51. Ahmed, K. J.; Chisholm, M. H.; Rothwell, I. P.; Huffman, J. C. *J. Am. Chem. Soc.* **1982**, *104*, 6453. Chamberlain, L. R.; Rothwell, A. P.; Rothwell, I. P. *J. Am. Chem. Soc.* **1984**, *106*, 1847. Green, J. C.; Green, M. L. H.; Morley, C. P. *Organometallics* **1985**, *4*, 1302.

(3) Cooper, N. J.; Green, M. L. H. *J. Chem. Soc., Dalton Trans.* **1979**, 1121.

(4) Thorn, D. L.; Tulip, T. H. *J. Am. Chem. Soc.* **1981**, *103*, 5984. Thorn, D. L. *Organometallics* **1985**, *4*, 192. Hayes, J. C.; Pearson, G. D. N.; Cooper, N. J. *J. Am. Chem. Soc.* **1981**, *103*, 4648. Jernakoff, P.; Cooper, N. J. *J. Am. Chem. Soc.* **1984**, *106*, 3026. Hayes, J. C.; Cooper, N. J. *J. Am. Chem. Soc.* **1982**, *104*, 5570. Threlkel, R. S.; Bercaw, J. E. *J. Am. Chem. Soc.* **1981**, *103*, 2650. Barger, P. T.; Bercaw, J. E. *Organometallics* **1984**, *3*, 278. van Leeuwen, P. W. N. M.; Roobeek, C. F.; Huis, R. *J. Organomet. Chem.* **1977**, *142*, 243. Taggle, R. M.; Weaver, D. L. *J. Am. Chem. Soc.* **1970**, *92*, 5523.

(5) Prior to our first report[6] on this subject, in only one case[7] had evidence accrued for such a rearrangement and in no case had the rearranged carbene been isolated and characterized.

(6) Lisko, J. R.; Jones, W. M. *Organometallics* **1985**, *4*, 944.

(7) Miyashita, A.; Grubbs, R. H. *J. Am. Chem. Soc.* **1978**, *100*, 7418.

(8) An alternate possibility is a photoinduced single step rearrangement from **2** to **5**. However, we consider this to be unlikely in view of the results reported herein. (a) Bly (Bly, R. S.; Hossain, M. M.; Lebioda, L. *J. Am. Chem. Soc.* **1985**, *107*, 5549) has recently suggested relief of ring strain as a driving force for rearrangement of alkyl from carbon to the carbene carbon of an iron(II) alkylidene.

0276-7333/86/2305-0178$01.50/0

and β[16] isomer (β = W_{10}, W_{11}, W_{12} as shown).

The physical properties of CpTi·$SiW_9V_3O_{40}^{4-}$ further indicate the strong, covalent $CpTi^{3+}$ attachment to the close-packed, surface oxygens of $SiW_9V_3O_{40}^{7-}$. Although $CpTi(CH_3CN)_n(NO_3)_3$ is quite sensitive to even atmospheric moisture, once supported, CpTi·$SiW_9V_3O_{40}^{4-}$ is stable to the atmosphere for >1 month either in the solid state or in CH_3CN solution (by solution ^{51}V and ^{183}W NMR). An orange CH_3CN solution of $(Bu_4N)_4$[CpTi·$SiW_9V_3O_{40}$] passes unaltered (^1H NMR, IR) through a Amberlyst 15 cation-exchange column while a control shows that organometallic cations like $CpTi(CH_3CN)_n^{3+}(NO_3)_3^{3-}$ are retained on the top of the column. Conversely, all the color of the anionic CpTi·$SiW_9V_3O_{40}^{4-}$ remains with an Amberlyst A-27 anion-exchange column in the Cl^- form, with no visible $CpTiCl_3$ elution from this top band.

Preliminary experiments indicate that it will be possible to prepare $SiW_9V_3O_{40}^{7-}$ supported $TiCl^{3+}$, a more reactive, better catalyst precursor, and that CpTi·$P_2W_{15}V_3O_{62}^{6-}$ and CpTi·1,4,9-$PW_9V_3O_{40}^{3-}$ can be prepared;[7f] these latter two complexes will allow a comparison of 1,2,3 (or A-type) vs. 1,4,9 (or B-type) trivanadium-substituted polyoxoanions. These experiments, continuing attempts[17] at obtaining crystals of CpTi·$SiW_9V_3O_{40}^{4-}$ suitable for X-ray crystallography,[7c] and other experiments aimed at using polyoxoanion-supported Ti^{4+} as Ziegler–Natta polymerization and olefin epoxidation catalysts will be reported in due course.

Acknowledgment. Support from NSF Grant CHE-8313459 and from Dreyfus Teacher-Scholar, Alfred P. Sloan, and Guggenheim (1984–1985) fellowships to R.G.F. are gratefully acknowledged. High-resolution fast-atom-bombardment mass spectra were obtained in the Mass Spectrometry Laboratory, School of Chemical Sciences, University of Illinois at Urbana-Champaign, supported in part by a grant from the National Institute of General Medical Sciences (GM27029), and with the assistance of Professor K. S. Suslick, whose help it is a pleasure to acknowledge. The ZAB-SE mass spectrometer was purchased in part with grants from the Division of Research Resources, National Institutes of Health (RR01575), the National Science Foundation (PCM 81-21494), and the National Institute of General Medical Sciences (GM27029).

Supplementary Material Available: A plot of the ultracentrifugation, sedimentation equilibrium molecular weight measurement in CH_3CN for $(Bu_4N)_4$[CpTi·$SiW_9V_3O_{40}$] (1 page). Ordering information is given on any current masthead page.

(16) (a) Massart, R.; Contant, R.; Fruchart, J. M. Ciabrini, J. P.; Fournier, M. *Inorg. Chem.* **1977**, *16*, 2916. (b) Hervé, G.; Tézé, A. *Inorg. Chem.* **1977**, *16*, 2115. (c) See also ref 1e and the discussion and references therein.

(17) Day, V. W.; Finke, R. G.; Rapko, B., experiments in progress.

Photoinduced Ring Expansion of a Cyclobutyliron σ Complex: An Example of Rearrangement of an Alkyl Group from Saturated Carbon to a Transition Metal To Give a Carbene Complex

Yngve Stenstrøm and W. M. Jones*

Department of Chemistry, University of Florida Gainesville, Florida 32611

Received September 20, 1985

Summary: Photolysis of either dicarbonyl(η^5-cyclopentadienyl)(1-methoxycyclobutane-1-carbonyl)iron (**8**) or its corresponding σ-complex dicarbonyl(η^5-cyclopentadienyl)(1-methoxycyclobutyl)iron (**9**) gives the rearranged carbene complex **11**. The carbene complex reacts with CO at room temperature and low pressure (ca. 6.5 atm) to give the ring-contracted dicarbonyl(η^5-cyclopentadienyl)(2-methoxycyclobutyl)iron (**12**). Photolysis of **12** regenerates the carbene complex **11**. It is suggested that these rearrangements involve both rearrangement from saturated carbon to iron to give a carbene complex and its reverse.

Theory predicts that the rearrangements generalized in the following equation should be facile.[1]

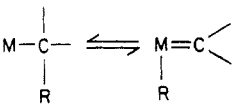

And, indeed, rearrangement in both directions in which hydrogen is the rearranging group are now commonplace[2,3] as are rearrangements of both alkyl and aryl groups from metal to carbene carbon[4] (rearrangement from right to left). In contrast, rearrangement of alkyl groups from saturated carbon to metal to give new carbene complexes are exceedingly rare[5] and aryl rearrangement has yet to be reported.

We recently reported that photolysis of **1** or **2** gives **5** for which we suggested the mechanism outlined in Scheme I.[6,8] We further suggested that the driving force for this rearrangement is a combination of relief of ring strain[8a] (**5** is less strained than **3**) and stabilization of the carbene (**5** is stabilized by electron donation from the methoxy more than **3**), a suggestion that is consistent with Green's hypothesis that the paucity of 1,2-rearrangements of alkyl or aryl groups from saturated carbon to metals is thermodynamic in origin.[3,9]

(1) Berke, H.; Hoffmann, R. *J. Am. Chem. Soc.* **1978**, *100*, 7224. Goddard, R. J.; Hoffmann, R.; Temmis, E. D. *J. Am. Chem. Soc.* **1980**, *102*, 7667.

(2) Schrock, R. R. *Acc. Chem. Res.* **1979**, *12*, 98. Schultz, A. J.; Williams, J. M.; Schrock, R. R.; Rupprecht, J. A.; Fellmann, J. *J. Am. Chem. Soc.* **1979**, *101*, 1593. Canestrani, M.; Green, M. L. H. *J. Chem. Soc., Dalton Trans.* **1982**, 1789. Calderon, N.; Lawrence, J. P.; Ofstead, E. A. *Adv. Organomet. Chem.* **1979**, *17*, 449. Foley, P.; Whitesides, G. *J. Am. Chem. Soc.* **1979**, *101*, 2732. Empsall, H. D.; Hyde, E. M.; Markham, M.; McDonald, W. S.; Norton, M. C.; Shaw, B. L.; Weeks, B. *J. Chem. Soc., Chem. Commun. 1977*, 589. Kemball, C. *Catal. Rev.* **1971**, *5*, 33. Light, J. R. C.; Zeiss, H. H. *J. Organomet. Chem.* **1970**, *21*, 391. Sneedon, R. P. A.; Zeiss, H. H. *J. Organomet. Chem.* **1971**, *26*, 101. Farady, L.; Marko, L. *J. Organomet. Chem.* **1972**, *43*, 51. Ahmed, K. J.; Chisholm, M. H.; Rothwell, I. P.; Huffman, J. C. *J. Am. Chem. Soc.* **1982**, *104*, 6453. Chamberlain, L. R.; Rothwell, A. P.; Rothwell, I. P. *J. Am. Chem. Soc.* **1984**, *106*, 1847. Green, J. C.; Green, M. L. H.; Morley, C. P. *Organometallics* **1985**, *4*, 1302.

(3) Cooper, N. J.; Green, M. L. H. *J. Chem. Soc., Dalton Trans.* **1979**, 1121.

(4) Thorn, D. L.; Tulip, T. H. *J. Am. Chem. Soc.* **1981**, *103*, 5984. Thorn, D. L. *Organometallics* **1985**, *4*, 192. Hayes, J. C.; Pearson, G. D. N.; Cooper, N. J. *J. Am. Chem. Soc.* **1981**, *103*, 4648. Jernakoff, P.; Cooper, N. J. *J. Am. Chem. Soc.* **1984**, *106*, 3026. Hayes, J. C.; Cooper, N. J. *J. Am. Chem. Soc.* **1982**, *104*, 5570. Threlkel, R. S.; Bercaw, J. E. *J. Am. Chem. Soc.* **1981**, *103*, 2650. Barger, P. T.; Bercaw, J. E. *Organometallics* **1984**, *3*, 278. van Leeuwen, P. W. N. M.; Roobeek, C. F.; Huis, R. *J. Organomet. Chem.* **1977**, *142*, 243. Taggle, R. M.; Weaver, D. L. *J. Am. Chem. Soc.* **1970**, *92*, 5523.

(5) Prior to our first report[6] on this subject, in only one case[7] had evidence accrued for such a rearrangement and in no case had the rearranged carbene been isolated and characterized.

(6) Lisko, J. R.; Jones, W. M. *Organometallics* **1985**, *4*, 944.

(7) Miyashita, A.; Grubbs, R. H. *J. Am. Chem. Soc.* **1978**, *100*, 7418.

(8) An alternate possibility is a photoinduced single step rearrangement from **2** to **5**. However, we consider this to be unlikely in view of the results reported herein. (a) Bly (Bly, R. S.; Hossain, M. M.; Lebioda, L. *J. Am. Chem. Soc.* **1985**, *107*, 5549) has recently suggested relief of ring strain as a driving force for rearrangement of alkyl from carbon to the carbene carbon of an iron(II) alkylidene.

0276-7333/86/2305-0178$01.50/0

Scheme I

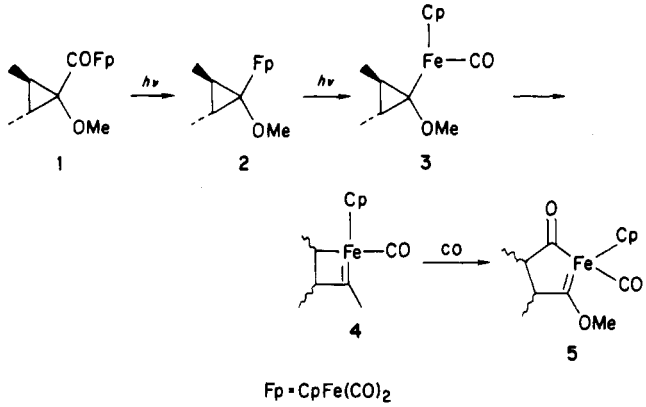

Scheme II[a]

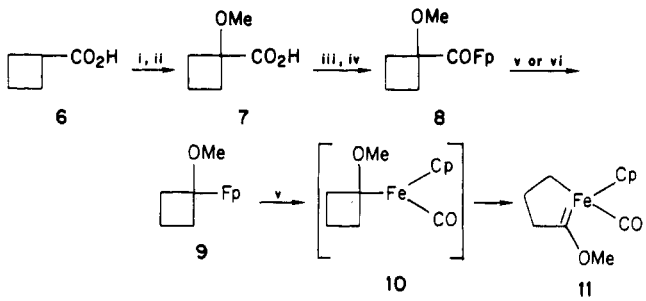

[a] (i) 3 equiv of LDA, THF, 25 °C, 16 h, then O_2, 20 °C, 2 h; (ii) 3 equiv of NaH, 3 equiv of MeI, THF, 36 h, Kugelrohr distillation; (iii) $(COCl)_2$, Et_2O, 10 h; (iv) KFp, THF, 0 °C → 25 °C, 12 h; (v) $h\nu$, C_6D_6, -CO; (vi) $[(PPh_3)_2RhCl]_2$, CH_3CN, 50 h.

Cyclobutane is nearly as strained as cyclopropane[10] and the strain in **5** and **11** should be comparable. We therefore reasoned that if the rearrangement in Scheme I were driven by relief of strain and carbene stabilization, then photolysis of the methoxycyclobutane **8** might also lead to rearrangement. At this time we report that this is indeed the case.

As in the cyclopropane system,[6] we began with the acyl complex **8** which was synthesized as depicted in Scheme II. Reacting cyclobutanecarboxylic acid with 3 equiv of LDA followed by O_2 in a slight modification of previously published procedures[11] gave a quantitative yield of α-hydroxycyclobutanecarboxylic acid. The crude acid was methylated[12] to give **7**[13] in 80% overall yield. Reaction of **7** with oxalyl chloride gave the acid chloride which was converted to the acyl complex **8**[14] in 71% yield after flash chromatography over silica gel (230–400 mesh; methylene chloride–hexane, 60:40 v/v, and then ethyl acetate–hexane, 50:50 v/v).

Scheme III[a]

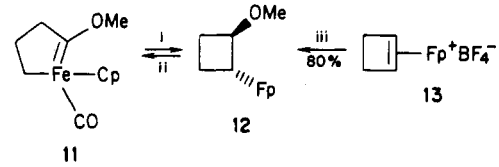

[a] (i) 6.5 atm CO, C_6D_6, 25 °C, 4–50 h; (ii) $h\nu$, C_6D_6, -CO; (iii) MeOH (excess), Na_2CO_3, 2 h.

Photolysis of a benzene solution of **8** under a N_2 atmosphere with a 450-W Hanovia medium-pressure lamp followed by flash chromatography over silica gel (230–400 mesh; EtOAc–hexane, 10:90 v/v) yielded **11** as a dark red, extremely air-sensitive oil (48% isolated, 55% NMR). The structure is based on MS, IR, and ^1H and ^{13}C NMR.[15] The most characteristic features are the relatively low-field methoxy methyl (δ 3.72) in the ^1H NMR, the relatively high-field methylene carbon (δ 13.6 ppm) bonded to iron and the very low-field carbene carbon (δ 344.28) in the ^{13}C NMR, the single CO resonance in the ^{13}C NMR, and the single terminal CO absorption and the absence of bridging carbonyl in the IR.

When photolysis of the acyl complex **8** was followed by ^1H NMR, along with other resonances, a new resonance grew in at δ 3.00 and then gradually disappeared. This was assigned to the methoxy of the σ-complex **9**, an assignment that was confirmed by isolation (flash chromatography over silica gel, 230–400 mesh; ethyl acetate–hexane, 10:90 v/v) from an incomplete reaction.[16] The same compound was also prepared by chemical decarbonylation of **8** with $[(Ph_3P)_2RhCl]_2$.[17] Photolysis of the σ-complex also gave **11** as the major product.

To explore the reversibility of rearrangement of **9** to **11**, a sample of the latter was dissolved in benzene-d_6 and sealed in an NMR tube under 6.5 atm of CO (ca. 10 molar equiv). After less than 4 h at room temperature the color of the solution had changed to light orange and both NMR (^1H and ^{13}C) and TLC indicated that a single new compound had formed in practically quantitative yield.[18] To our surprise, the new compound, which was isolated by flash chromatography over silica gel (230–400 mesh; ethyl acetate–hexane, 20:80 v/v), was not the starting σ-complex but was an isomer. This isomer was characterized by chemical analysis, spectral characteristics, and alternate synthesis (Scheme III) and is assigned structure **12**.[19,20]

(9) The contribution of strain relief to the exothermicity of the conversion of **3** to **4** in this mechanism is not known and, in fact, if carbocycles were used as models the change in strain would actually retard the reaction since cyclobutene is a bit more strained than cyclopropane.[10] However, cyclobutene is probably a poor model and, regardless, the metallocyclopentenone **5** is certainly less strained than the cyclopropane in **3**.

(10) Greenberg, A.; Liebman, J. F. "Strained Organic Molecules"; Academic Press: New York, 1978.

(11) Moersch, G. W.; Zwiesler, M. L. *Synthesis* **1971**, 647. Kouen, D. A.; Silbert, L. S.; Pfeffer, P. E. *J. Org. Chem.* **1975**, *40*, 3253.

(12) Stoochnoff, B. A.; Benoiton, N. L. *Tetrahedron Lett.* **1973**, 21.

(13) 1-Methoxycyclobutanecarboxylic acid (**7**): mp 68–69 °C; IR (KBr) 3200–2500, 1695, 1415, 1300, 1230, 1125, 1025, 945, 755 cm^{-1}; ^1H NMR (100 MHz, $CDCl_3$) δ 1.8–2.5 (m, 6 H), 3.24 (s, 3 H), 10.24 (s, 1 H); ^{13}C NMR (25 MHz, $CDCl_3$) δ 12.91 (CH_2), 30.50 (CH_2 × 2), 52.29 (CH_3O), 79.97 (C—O), 178.96 (C=O).

(14) Dicarbonyl(η^5-cyclopentadienyl)(1-methoxycyclobutyl-1-carbonyl)iron (**8**): mp 52–53 °C; IR ($CDCl_3$) 2005, 1960, 1640 cm^{-1}; ^1H NMR (60 MHz, C_6D_6) δ 1.1–2.4 (m, 6 H), 2.85 (s, 3 H), 4.35 (s, 5 H); ^{13}C NMR (25 MHz, C_6D_6) δ 11.91 (CH_2), 28.77 (CH_2 × 2), 51.10 (CH_3O), 86.67 (Cp), 92.62 (C–O), 215.92 (terminal CO), 256.66 (bridging CO); mass spectrum, *m/e* 290 (M^+), 262 (M^+ – CO), 234 (M^+ – 2CO), 205 ($FpCO^+$), 85 (M^+ – FpCO, 100%). Anal. Calcd for $C_{13}H_{14}FeO_4$: C, 53.82; H, 4.86. Found: C, 53.87; H, 4.90.

(15) 1-Carbonyl-1-(η^5-cyclopentadienyl)-2-methoxy-1-ferracyclopentene (**11**): IR ($CDCl_3$) 1925 cm^{-1}; ^1H NMR (100 MHz, C_6D_6) δ 1.6–2.6 (m, 6 H), 3.67 (s, 3 H), 4.26 (s, 5 H); ^{13}C NMR (25 MHz, C_6D_6) δ 13.58 (CH_2), 30.05 (CH_2), 60.17 (CH_2), 64.36 (CH_3O), 84.92 (Cp), 222.64 (CO), 344.28 (carbene C); mass spectrum, *m/e* 234 (M^+), 206 (M^+ – CO), 152, 122 ($FeCpH^+$, 100%), 121 ($FeCp^+$). While indefinitely stable in carefully degassed solvents, removal of the solvent gives a nearly black oil that was too unstable to permit reliable elemental analyses.

(16) Dicarbonyl(η^5-cyclopentadienyl)(1-methoxycyclobut-1-yl)iron (**9**): IR ($CDCl_3$) 2005, 1960 cm^{-1}; ^1H NMR (60 MHz, C_6D_6) δ 1.1–2.4 (m, 6 H), 3.00 (s, 3 H), 4.22 (s, 5 H); ^{13}C NMR (25 MHz, C_6D_6) δ 15.63 (CH_2), 46.33 (CH_2 × 2), 51.79 (CH_3O), 87.36 (Cp), 95.64 (C–O), 218.45 (CO). The compound was too unstable for reliable elemental analyses.

(17) Kuhlmann, E. J.; Alexander, J. J. *J. Organomet. Chem.* **1979**, 174, 81.

(18) When the reaction was run with only 1.5 molar equiv of CO (6.5 atm), the reaction required about 50 h to reach completion but the resultant reaction mixture was the same.

(19) Dicarbonyl(η^5-cyclopentadienyl)(*trans*-2-methoxycyclobut-1-yl)iron (**12**): IR ($CDCl_3$) 2000, 1945 cm^{-1}; ^1H NMR (100 MHz, C_6D_6) δ 1.3–1.7 (m, 1 H), 1.8–2.2 (m, 3 H), 2.3–2.6 (m, 1 H), 3.07 (s, 3 H), 3.4–3.7 (m, 1 H), 4.27 (s, 5 H); ^{13}C NMR (25 MHz, C_6D_6) δ 27.22 (CH_2), 28.00 (CH), 33.65 (CH_2), 55.00 (CH_3O), 84.92 (Cp), 88.24 (CH), 217.47 (CO), 217.86 (CO); mass spectrum, *m/e* 262 (M^+), 234 (M^+ – CO), 206 (M^+ – 2CO), 177 (Fp^+), 85 (M^+ – FpCO, 100%). Anal. Calcd for $C_{11}H_{14}FeO_2$: C, 54.99; H, 5.38. Found: C, 54.91; H, 5.41.

Scheme IV

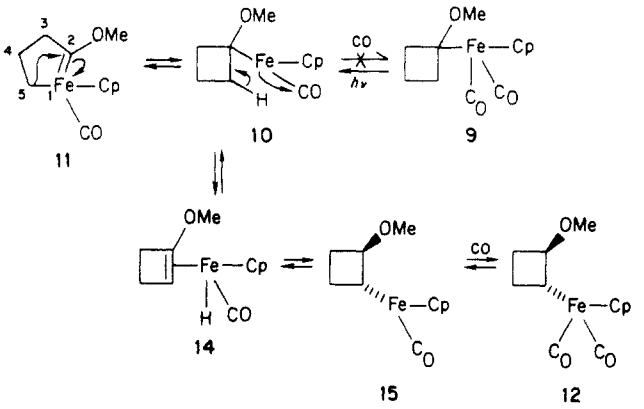

Equally surprising, the reaction is reversible; photolysis of **12** regenerates the carbene complex **11** as the primary product.

A reasonable mechanism for the interconversion of **11** and **12** is suggested in Scheme IV. The significant features and evidence to date for this mechanism are as follows: (1) The first step is a thermally induced reverse of the proposed 1,2-rearrangement, a reaction that must be occurring even in the absence of added CO since the only sensible role of the carbon monoxide is to trap **15**. Evidence for this equilibrium is the finding that treatment of **11** with a trace of CD_3O^- in CD_3OD led to rapid exchange of four ring hydrogens (followed by slower exchange of methoxide) despite the fact that only the two at C3 should be acidic. Exchange of four hydrogens would be expected if **11** were in thermal equilibrium with **10** since C3 and C5 become equivalent in the latter. (2) If **11** and **10** equilibrate at room temperature (as suggested by the deuterium exchange) but not rapidly enough for **11** to show fluxionality in the ^1H NMR, the maximum energy separating **10** from **11** can be no more than about 25 kcal/mol nor less than about 15 kcal/mol. (3) The equilibrium between **10** and **15** must favor the latter and/or CO attack on **15** must be faster than on **10** because **12** was observed to the exclusion of **9** (probably for steric reasons). (4) This mechanism requires exclusive trans stereochemistry in **12** which is observed.

In conclusion it should be noted that conversion of **10** to **11** is the first example of rearrangement of alkyl from saturated carbon to metal in which the primary rearrangement product has been isolated. It also shows that the special bonding in the cyclopropane ring of **3** is not required for rearrangement to occur.

Acknowledgment. This work was partially supported by the National Science Foundation to whom the authors are grateful. Acknowledgment is also made to the donors of the Petroleum Research Fund, administered by the American Chemical Society, for partial support of this research. The support from the Norway-America Association for Thanks to Scandinavia Scholarship to Y.S. is greatly acknowledged. High-field NMR spectra were obtained on a Nicolet NT-300 spectrometer, operating at a field of 7 T; therefore acknowledgment is made to the Instrument Program, Chemistry Division, National Science Foundation, for financial assistance in the purchase of the instrument.

(20) Assignment of the trans stereochemistry is based on the known[21] trans addition of nucleophiles to Fp^+ π-complexes. However the cis isomer has not been synthesized for final confirmation.

(21) Davies, S. G. "Organotransition Metal Chemistry: Applications to Organic Synthesis"; Pergamon Press: New York, 1982; pp 128–135. Lennon, P.; Madhavarao, M.; Rosan, A.; Rosenblum, M. *J. Organomet. Chem.* **1976**, *108*, 93.

(22) Careful examination of the ^1H NMR from photolysis of **8** reveals the growth and decline of a small resonance corresponding to the methoxy methyl of **12**, which could also be isolated in small quantities as an impure sample from an incomplete reaction mixture.

Regiospecific Reactions of Cobalt–Rhodium Mixed-Metal Clusters. Unprecedented, Facile and Reversible Tetranuclear–Dinuclear Transformations Involving Diphenylacetylene and/or Carbon Monoxide

István T. Horváth*

Department of Industrial and Engineering Chemistry
Swiss Federal Institute of Technology
ETH-Zentrum, CH-8092 Zürich, Switzerland

László Zsolnai and Gottfried Huttner

Fakultät für Chemie der Universität Konstanz
Postfach 5560
D-7750 Konstanz, Federal Republic of Germany

Received October 2, 1985

Summary: $Co_2Rh_2(CO)_{12}$ (**1**) reacts with alkynes (RC_2R, R = C_6F_5 (**2a**), R = Ph (**2b**)) via specific insertion into the cobalt–cobalt bond to give $Co_2Rh_2(CO)_{10}(\mu_4\text{-}\eta^2\text{-}RC_2R)$ (**3a,b**). **3a** was characterized by a single-crystal X-ray diffraction analysis: space group $P2_1/c$ (No. 14), a = 11.286 (8) Å, b = 17.37 (1) Å, c = 16.65 (1) Å, β = 126.32 (5)°, V = 2630 (5) Å^3, Z = 4, D_{calcd} = 2.43 g/cm^3. A total of 2479 reflections ($I \geq 2\sigma$) of 3215 reflections were used to give R_F = 5.2% and R_{F^2} = 5.6%. Reaction of **3a** with CO and **2a** results in regiospecific fragmentation to give $CoRh(CO)_6(\mu\text{-}\eta^2\text{-}F_5C_6C_2C_6F_5)$ (**4a**) exclusively. **3b** undergoes facile, reversible, and regiospecific fragmentation when treated with PhC_2Ph (**2b**) and carbon monoxide to give $CoRh(CO)_6(\mu\text{-}\eta^2\text{-}PhC_2Ph)$ (**4b**). Medium-pressure in situ IR studies have revealed that **3b** reacts with carbon monoxide in a reversible and regiospecific reaction to give the 1:1 mixture of $CoRh(CO)_7$ (**5**) and **4b**.

The chemistry of mixed-metal cluster compounds is of current interest.[1] The reactions of mixed-metal clusters and alkynes can result in either substitution or degradation of the cluster to lower nuclearity complexes.[2] Two interesting questions arise. First, at which site does the substitution take place, and second, what is the metal distribution in the fragmentation products.

Reversible fragmentation of transition-metal clusters involving ligand addition and elimination is rarely observed, and the few studied examples are limited to clusters containing only carbonyl and hydride ligands.[3] We now wish to report a facile, reversible, and regiospecific fragmentation of $Co_2Rh_2(CO)_{10}(\mu_4\text{-}\eta^2\text{-}PhC_2Ph)$ (**3a**) affected by diphenylacetylene and/or carbon monoxide.

The reaction of $Co_2Rh_2(CO)_{12}$ (**1**)[4] and 1 equiv of alkyne

(1) Gladfelter, W. L.; Geoffroy, G. L. *Adv. Organomet. Chem.* **1980**, *18*, 207. Roberts, D. A.; Geoffroy, G. L. In "Comprehensive Organometallic Chemistry"; Wilkinson, G., Stone, F. G. A., Abel, E., Eds.; Pergamon Press: Elmsford, NY, 1982; Chapter 40.

(2) Sappa, E.; Tiripicchio, A.; Braunstein, P. *Chem. Rev.* **1983**, *83*, 203.

(3) Whyman, R. *J. Chem. Soc., Dalton Trans.* **1972**, 1375. Whyman, R. *J. Chem. Soc., Chem. Commun.* **1970**, 1194. Ungváry, F. *J. Organomet. Chem.* **1972**, *36*, 363. Oldani, F.; Bor, G. *J. Organomet. Chem.* **1983**, *246*, 309.

0276-7333/86/2305-0180$01.50/0

Scheme IV

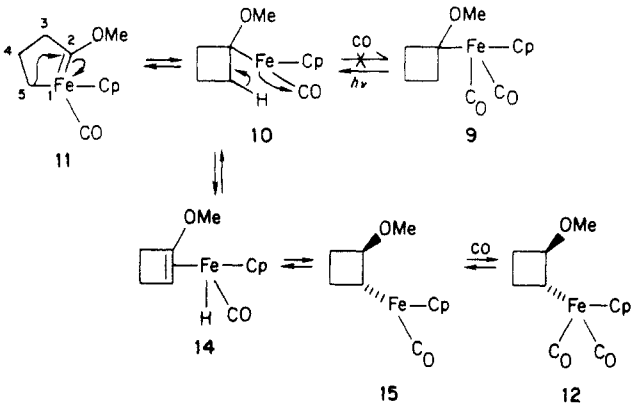

Equally surprising, the reaction is reversible; photolysis of **12** regenerates the carbene complex **11** as the primary product.

A reasonable mechanism for the interconversion of **11** and **12** is suggested in Scheme IV. The significant features and evidence to date for this mechanism are as follows: (1) The first step is a thermally induced reverse of the proposed 1,2-rearrangement, a reaction that must be occurring even in the absence of added CO since the only sensible role of the carbon monoxide is to trap **15**. Evidence for this equilibrium is the finding that treatment of **11** with a trace of CD_3O^- in CD_3OD led to rapid exchange of four ring hydrogens (followed by slower exchange of methoxide) despite the fact that only the two at C3 should be acidic. Exchange of four hydrogens would be expected if **11** were in thermal equilibrium with **10** since C3 and C5 become equivalent in the latter. (2) If **11** and **10** equilibrate at room temperature (as suggested by the deuterium exchange) but not rapidly enough for **11** to show fluxionality in the ^1H NMR, the maximum energy separating **10** from **11** can be no more than about 25 kcal/mol nor less than about 15 kcal/mol. (3) The equilibrium between **10** and **15** must favor the latter and/or CO attack on **15** must be faster than on **10** because **12** was observed to the exclusion of **9** (probably for steric reasons). (4) This mechanism requires exclusive trans stereochemistry in **12** which is observed.

In conclusion it should be noted that conversion of **10** to **11** is the first example of rearrangement of alkyl from saturated carbon to metal in which the primary rearrangement product has been isolated. It also shows that the special bonding in the cyclopropane ring of **3** is not required for rearrangement to occur.

Acknowledgment. This work was partially supported by the National Science Foundation to whom the authors are grateful. Acknowledgment is also made to the donors of the Petroleum Research Fund, administered by the American Chemical Society, for partial support of this research. The support from the Norway-America Association for Thanks to Scandinavia Scholarship to Y.S. is greatly acknowledged. High-field NMR spectra were obtained on a Nicolet NT-300 spectrometer, operating at a field of 7 T; therefore acknowledgment is made to the Instrument Program, Chemistry Division, National Science Foundation, for financial assistance in the purchase of the instrument.

(20) Assignment of the trans stereochemistry is based on the known[21] trans addition of nucleophiles to Fp^+ π-complexes. However the cis isomer has not been synthesized for final confirmation.

(21) Davies, S. G. "Organotransition Metal Chemistry: Applications to Organic Synthesis"; Pergamon Press: New York, 1982; pp 128–135. Lennon, P.; Madhavarao, M.; Rosan, A.; Rosenblum, M. *J. Organomet. Chem.* **1976**, *108*, 93.

(22) Careful examination of the ^1H NMR from photolysis of **8** reveals the growth and decline of a small resonance corresponding to the methoxy methyl of **12**, which could also be isolated in small quantities as an impure sample from an incomplete reaction mixture.

Regiospecific Reactions of Cobalt–Rhodium Mixed-Metal Clusters. Unprecedented, Facile and Reversible Tetranuclear–Dinuclear Transformations Involving Diphenylacetylene and/or Carbon Monoxide

István T. Horváth*

Department of Industrial and Engineering Chemistry
Swiss Federal Institute of Technology
ETH-Zentrum, CH-8092 Zürich, Switzerland

László Zsolnai and Gottfried Huttner

Fakultät für Chemie der Universität Konstanz
Postfach 5560
D-7750 Konstanz, Federal Republic of Germany

Received October 2, 1985

Summary: $Co_2Rh_2(CO)_{12}$ (**1**) reacts with alkynes (RC_2R, R = C_6F_5 (**2a**), R = Ph (**2b**)) via specific insertion into the cobalt–cobalt bond to give $Co_2Rh_2(CO)_{10}(\mu_4\text{-}\eta^2\text{-}RC_2R)$ (**3a,b**). **3a** was characterized by a single-crystal X-ray diffraction analysis: space group $P2_1/c$ (No. 14), a = 11.286 (8) Å, b = 17.37 (1) Å, c = 16.65 (1) Å, β = 126.32 (5)°, V = 2630 (5) Å^3, Z = 4, D_{calcd} = 2.43 g/cm^3. A total of 2479 reflections ($I \geq 2\sigma$) of 3215 reflections were used to give R_F = 5.2% and R_{F^2} = 5.6%. Reaction of **3a** with CO and **2a** results in regiospecific fragmentation to give $CoRh(CO)_6(\mu\text{-}\eta^2\text{-}F_5C_6C_2C_6F_5)$ (**4a**) exclusively. **3b** undergoes facile, reversible, and regiospecific fragmentation when treated with PhC_2Ph (**2b**) and carbon monoxide to give $CoRh(CO)_6(\mu\text{-}\eta^2\text{-}PhC_2Ph)$ (**4b**). Medium-pressure in situ IR studies have revealed that **3b** reacts with carbon monoxide in a reversible and regiospecific reaction to give the 1:1 mixture of $CoRh(CO)_7$ (**5**) and **4b**.

The chemistry of mixed-metal cluster compounds is of current interest.[1] The reactions of mixed-metal clusters and alkynes can result in either substitution or degradation of the cluster to lower nuclearity complexes.[2] Two interesting questions arise. First, at which site does the substitution take place, and second, what is the metal distribution in the fragmentation products.

Reversible fragmentation of transition-metal clusters involving ligand addition and elimination is rarely observed, and the few studied examples are limited to clusters containing only carbonyl and hydride ligands.[3] We now wish to report a facile, reversible, and regiospecific fragmentation of $Co_2Rh_2(CO)_{10}(\mu_4\text{-}\eta^2\text{-}PhC_2Ph)$ (**3a**) affected by diphenylacetylene and/or carbon monoxide.

The reaction of $Co_2Rh_2(CO)_{12}$ (**1**)[4] and 1 equiv of alkyne

(1) Gladfelter, W. L.; Geoffroy, G. L. *Adv. Organomet. Chem.* **1980**, *18*, 207. Roberts, D. A.; Geoffroy, G. L. In "Comprehensive Organometallic Chemistry"; Wilkinson, G., Stone, F. G. A., Abel, E., Eds.; Pergamon Press: Elmsford, NY, 1982; Chapter 40.

(2) Sappa, E.; Tiripicchio, A.; Braunstein, P. *Chem. Rev.* **1983**, *83*, 203.

(3) Whyman, R. *J. Chem. Soc., Dalton Trans.* **1972**, 1375. Whyman, R. *J. Chem. Soc., Chem. Commun.* **1970**, 1194. Ungváry, F. *J. Organomet. Chem.* **1972**, *36*, 363. Oldani, F.; Bor, G. *J. Organomet. Chem.* **1983**, *246*, 309.

0276-7333/86/2305-0180$01.50/0

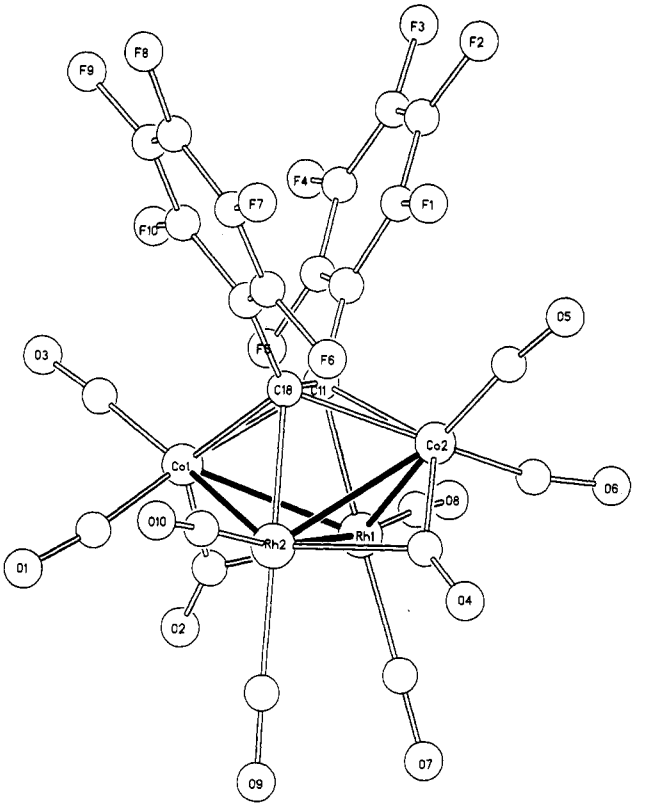

Figure 1. The molecular structure of **3a**. Selected bond lengths (Å): Rh(1)–Rh(2), 2.700 (3); Rh(1)–Co(1), 2.539 (3); Rh(1)–Co(2), 2.513 (2); Rh(2)–Co(1), 2.515 (2); Rh(2)–Co(2), 2.541 (3); C(11)–C(18), 1.369 (23); Co(1)–C(2), 1.820 (15); Rh(1)–C(2), 2.133 (11); Co(2)–C(4), 1.825 (16); Rh(2)–C(4), 2.123 (12); Co(1)–C(1), 1.723 (19); Rh(2)–C(1), 2.566 (12); Co(2)–C(6), 1.724 (19); Rh(1)–C(6), 2.561 (11). Selected bond angles (deg): Rh(1)–Co(1)–Rh(2), 64.6 (1); Co(1)–Rh(1)–Co(2), 92.3 (1); C(11)–Co(1)–C(18), 37.2 (6); C(12)–C(11)–C(18), 127.9 (11); C(11)–C(18)–C(19), 126.1 (11); Co(1)–C(1)–O(1), 169.4 (10); Co(2)–C(6)–O(6), 165.6 (10). Dihedral angle (deg) between the Co(1)–Rh(1)–Rh(2) and Co(2)–Rh(1)–Rh(2) planes: 116.9.

Scheme I

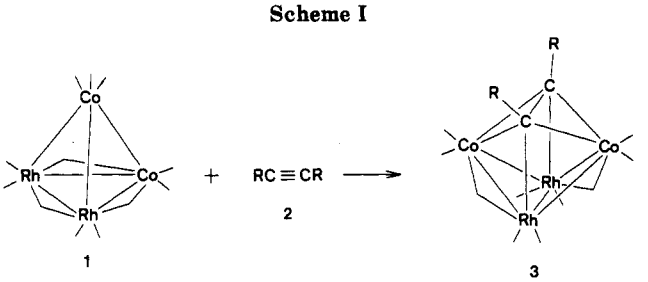

(RC_2R', R = C_6F_5 (**2a**), R = Ph (**2b**)) in *n*-hexane resulted in formation of the purple clusters $Co_2Rh_2(CO)_{10}(\mu_4\text{-}\eta^2\text{-}RC_2R)$ (**3a,b**) in high yield (Scheme I).[5] **3a,b** were characterized by IR and NMR spectroscopic methods[6] and

Scheme II

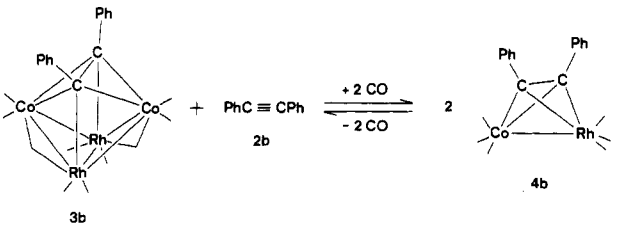

Scheme III

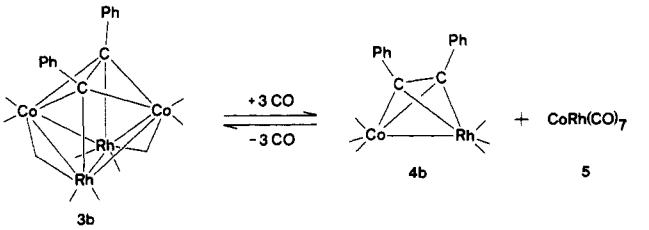

elemental analysis.[7] The molecular structure of **3a** was determined by a single-crystal X-ray diffraction analysis,[8] and its structure is shown in Figure 1. The molecule contains a butterfly cluster of two cobalt and two rhodium atoms with the cobalt atoms in the wing-tip position. The alkyne coordinates to all metal atoms to form a distorted *closo*-$Co_2Rh_2C_2$ octahedron. Overall, there are 10 carbonyl ligands; each cobalt atom and each rhodium atom is bonded to one linear terminal carbonyl ligand and two linear terminal carbonyl ligands, respectively. There are two semibridging and two bridging carbonyl ligands along the hinge-to-wing-tip cobalt–rhodium bonds. Structurally **3a** is very similar to the related $Co_4(CO)_{10}(\mu_4\text{-}\eta^2\text{-}RC_2R)$ (R = Et,[9] H[10]) and to the analogous compounds containing a *closo*-M_4C_2 framework.[11,12]

The formation of **3** has occurred apparently via specific insertion into a cobalt–cobalt bond accompanied by the loss of two carbonyl ligands. Although metal-specific insertion of alkynes have recently been reported for $Co_2Ru_2(CO)_{13}$[12] and $Cp_2W_2Ir_2(CO)_{10}$,[13] this is the first example of metal specificity between metals of the same group in the periodic table.

Upon addition of another mole of **2a** to **3a** in the presence of carbon monoxide, highly regiospecific fragmentation occurs to give $CoRh(CO)_6(\mu\text{-}\eta^2\text{-}F_5C_6C_2C_6F_5)$ (**4a**) in 98% yield.[14] The structure of **4a** was established by

(4) Martinengo, S.; Chini, P.; Albano, V. G., Cariati, F.; Salvatori, T. *J. Organomet. Chem.* **1973**, *59*, 379.

(5) Compounds **3a,b** are purple and were isolated by column chromatography (silica gel, *n*-hexane eluent) in 98 and 99% yield, respectively.

(6) For **3a**: mp 178 °C dec; IR (ν(CO) in hexane) 2102 m, 2076 s, 2058 m, 2050 s, 1986 w, br, 1898 m cm^{-1}. For **3b**: mp 192 °C dec; IR (ν(CO) in *n*-hexane) 2094.5 m, 2069 s, 2049 m, 2035 m, sh, 2029 s, 1978 w, br, 1889 m cm^{-1}; ^1H NMR (in CD_2Cl_2) 7.15–7.00 (m, 10 H) ppm; ^{13}C NMR spectrum of ^{13}CO-enriched **3b** exhibits three resonances at 202.1 (s), 187.2 (d, J_{Rh-C} = 60 Hz), and 176.8 (d, J_{Rh-C} = 62 Hz) ppm of relative intensity 6:2:2 between 25 and −80 °C. This is in agreement with the structure of **3a** and suggests that the rhodium-bonded terminal carbonyl ligands are still rigid at 25 °C and the cobalt-bonded terminal and the semibridging and bridging carbonyl ligands are exchanging evenly at −80 °C. Similar results have been reported for the analogous $Co_4(CO)_{10}(\mu_4\text{-}\eta^2\text{-}PhC_2Ph)$ compound: Evans, J.; Johnson, B. F. G.; Lewis, J.; Matheson, T. W.; Norton, J. R. *J. Chem. Soc., Dalton Trans.* **1978**, 626.

(7) All new compounds gave satisfactory elemental analysis.

(8) Crystal data: $C_{24}Co_2F_{10}O_{10}Rh_2$, M_r = 961.92, monoclinic, space group $p2_1/c$ (No. 14), a = 11.286 (8) Å, b = 17.37 (1) Å, c = 16.65 (1) Å, β = 126.32 (5)°, V = 2630 (5) Å^3, Z = 4, D_{calcd} = 2.43 g/cm^3. Data were measured on a Syntex P3 diffractometer with graphite-monochromated Mo K_α (λ = 0.71073 Å) radiation using the ω scan technique. The structure was solved by direct methods. Solution and refinement were performed by using the SHELXTL system (Sheldrick, G. M. "Crystallographic Computing System", Revision, 1982, University of Göttingen, FRG). A total of 2479 reflections ($I \geq 2\sigma$) of 3215 reflections were used to give R_F = 5.2% and R_{F^2} = 5.6%.

(9) Dahl, L. F.; Smith, D. L. *J. Am. Chem. Soc.* **1962**, *84*, 2450.

(10) Gervasio, G.; Rossetti, R.; Stanghellini, P. L. *Organometallics*, **1985**, *4*, 1612.

(11) Johnson, B. F. G.; Lewis, J.; Reichter, B. E.; Schorpp, K. T.; Sheldrick, G. M. *J. Chem. Soc., Dalton Trans.* **1977**, 1417. Fox, J. P.; Gladfelter, W. L.; Geoffroy, G. L.; Taranaiepour, I.; Abdel-Mequid, S.; Day, V. W. *Inorg. Chem.* **1981**, *20*, 3230.

(12) Roland, E.; Vahrenkamp, H. *Organometallics* **1983**, *2*, 183.

(13) Shapley, J. R.; McAteer, C. H.; Churchill, M. R.; Biondi, L. V. *Organometallics* **1984**, *3*, 1595.

(14) Compound **4a** is orange and was isolated by column chromatography (silica gel, n-hexane eluent).

single-crystal X-ray analysis[15] and by spectroscopic analyses.[16]

3b reacts similarly with 1 mol of diphenylacetylene and 2 mol of carbon monoxide to form $CoRh(CO)_6(\mu\text{-}\eta^2\text{-}PhC_2Ph)$ (**4b**)[17] according to Scheme II. Surprisingly, the reaction is fully reversible, such that upon bubbling N_2 into the reaction mixture **3b** reforms quantitatively.[18] Since **3b** does not react with **2b** in the absence of carbon monoxide, we have assumed that **3b** reacts first with CO and then with **2b**. This was evidenced by the reaction of **3b** with CO, performed in a medium-pressure (2–16 bar) glass autoclave connected to a high-pressure IR cell[19] using CO:N_2 (1:9).[20] At 0.3-bar partial CO pressure and 10 °C **3b** reacts with CO to give an equilibrium mixture[21] of **3b**, **4b**, and $CoRh(CO)_7$ (**5**).[22] By increasing the partial pressure of CO to 2 bar, **3b** disproportionates almost completely (>99.5%) to a 1:1 mixture of **4b** and **5**. Upon slowly removing the pressure and purging the solution with N_2, **4b** and **5** recombine to give **3b** quantitatively (Scheme III).

To best of our knowledge the reversible fragmentation of **3b** to **4b** (Scheme II) is the first example for a reversible tetranuclear–dinuclear transformation involving an "alkyne cluster", free alkyne, and carbon monoxide. Mechanistically, it is clear that **3b** reacts first with **CO**, which probably results in an unobserved intermediate such as $[Co_2Rh_2(CO)_{11}(PhC_2Ph)]$ (**6**). It is not apparent whether **6** is first attacked by CO or by free PhC_2Ph. However, if **6** is attacked first by carbon monoxide, **4b** and **5** can be formed according to Scheme III; **5** can subsequently react with the free PhC_2Ph to result in the "second" mole of **4b**. The most striking feature of Scheme II is the facile loss of the PhC_2Ph ligand and the regiospecific reformation of **3b**. Currently, there is no clear explanation for this unprecedented ligand loss.

Finally, it should be stressed that no spectroscopic evidence has been obtained for the existence of homonuclear cobalt or rhodium carbonyls in these reactions. This could mean that the heteronuclear metal–metal bond is stronger than the homonuclear bonds.

Acknowledgment. Portions of this research were supported by the "Schweizerischer Nationalfonds zur Förderung der wissenschaftlichen Forschung", No. 5.521.330.784/2. I.T.H. is grateful to Professors Piero Pino and György Bor for their helpful discussions.

Supplementary Material Available: Tables of bond distances and angles, positional and thermal parameters, and observed and calculated structure factors and an ORTEP drawing of **4a** (34 pages). Ordering information is given on any current masthead page.

(15) Crystal data: $C_{20}CoF_{10}O_6Rh$, M_r = 688.04, monoclinic, space group $p2_1/c$ (No. 14), a = 9.812 (6) Å, b = 15.582 (9) Å, c = 17.82 (1) Å, β = 127.85 (4)°, V = 2151 (5) Å^3, Z = 4, D_{calcd} = 1.83 g/cm^3. A total of 2121 reflections ($I \geq 2\sigma$) of 2578 reflections were used to give R_F = 12.6% and R_{F^2} = 12.7%. During the refinement it became clear that the cobalt and rhodium atoms are mutually disordered within the $CoRhC_2$ tetrahedron framework. The X-ray analysis cannot decide between the disorder of Co and Rh positions within the individual molecules in the crystal and a mixed-crystal containing Co_2C_2 or Rh_2C_2 cores. This later possibility was, however, ruled out by the significant differences between the spectroscopic data[16] of **4a** and $Co_2(CO)_6(\mu\text{-}\eta^2\text{-}F_5C_6C_2C_6F_5)$: Birchall, J. M.; Bowden, F. L.; Haszeldine, R. N.; Lever, A. B. P. *J. Chem. Soc. A* **1967**, 747. Thus, the molecule of **4a** consists of a sawhorse type of $CoRhC_2$ tetrahedral framework, and each metal atom is bonded to three linear terminal carbonyl ligands.

(16) For **4a**: MS, m/e 660 $(M - CO)^+$ plus ions corresponding to the loss of five CO ligands; IR (ν(CO) in *n*-hexane) 2110 m, 2077 vs, 2063 s, 2053 s, 2033 m cm^{-1}; ^{19}F NMR (in $CDCl_3$, in ppm from $CFCl_3$) −137.1 (q, 4 F), −154.5 (t, 2 F), −161.5 (m, 4 F).

(17) For **4b**: IR (ν(CO) in *n*-hexane) 2095 m, 2060 vs, 2044 s, 2034.5 s, 2015 m, 2009.5 m cm^{-1}; ^{1}H NMR (in CD_2Cl_2) 7.60–7.25 (m, 10 H) ppm.

(18) Repeating the reaction several times, **4b** can be recovered in 100% yield.

(19) Dietler, U. K. Ph.D. Thesis, No. 5428, ETH-Zürich, 1974.

(20) Before each spectrum was scanned, the cell was flushed with 5–10 mL of a fresh solution from the autoclave by opening a discharge valve placed after the cell. The total pressure and temperature were kept constant.

(21) K = [**3b**][CO]^3/[**4b**][**5**] = 3.3 × 10^{-4} mol^2 L^{-2} at 10 °C.

(22) Spindler, F.; Bor, G.; Dietler, U. K.; Pino, P. *J. Organomet. Chem.* **1981**, *213*, 303. Horváth, I. T.; Bor, G.; Garland, M.; Pino, P. *Organometallics*, submitted for publication.

Photolysis of Organopolysilanes. Photochemical Behavior of 3-Phenyl-4-[phenyl(trimethylsilyl)methylene]-1,1,2-tris(trimethylsilyl)-1-silacyclobut-2-ene and Molecular Structure of a Photoproduct

Mitsuo Ishikawa,* Hiroshi Sugisawa, and Shigeji Matsuzawa

Department of Synthetic Chemistry
Faculty of Engineering, Kyoto University
Kyoto 606, Japan

Ken Hirotsu and Taiichi Higuchi*

Department of Chemistry
Faculty of Science, Osaka City University
Sugimotocho, Sumiyoshi-ku, Osaka 558, Japan

Received August 27, 1985

Summary: The photolysis of 3-phenyl-4-[phenyl(trimethylsilyl)methylene]-1,1,2-tris(trimethylsilyl)-1-silacyclobut-2-ene produced 4,5-benzo-1,3-bis(trimethylsilyl)-2-[1-phenyl-2,2-bis(trimethylsilyl)ethenyl]-1-silacyclopenta-2,4-diene (**2**), via a 1-silabicyclo[2.1.0]pent-3-ene intermediate, which could be trapped by methanol. Similar photolysis of 1,4,4-trimethyl-3,6-diphenyl-1,2,5-tris(trimethylsilyl)-1,4-disilacyclohexa-2,5-diene also afforded compound **2**. Preliminary results of an X-ray diffraction study of **2** are also described.

Small ring compounds involving one or two silicon atoms in the ring are interesting because of their high-strain energy.[1-5] In this communication, we report novel photochemical behavior of 3-phenyl-4-[phenyl(trimethylsilyl)methylene]-1,1,2-tris(trimethylsilyl)-1-silacyclobut-2-ene (**1**), which can be prepared from the reaction of 3-phenyl-1,1,2-tris(trimethylsilyl)-1-silacyclopropene or (phenylethynyl)tris(trimethylsilyl)silane with phenyl(trimethylsilyl)acetylene in the presence of a nickel catalyst.[6,7]

When a solution of **1** (0.8483 g, 1.62 mmol) in 100 mL of dry benzene was irradiated for 70 min, with a high-

(1) (a) Ishikawa, M.; Sugisawa, H.; Kumada, M.; Higuchi, T.; Matsui, K.; Hirotsu, K.; Iyoda, J. *Organometallics* **1983**, *2*, 174. (b) Ishikawa, M.; Sugisawa, H.; Kumada, M.; Kawakami, H.; Yamabe, T. *Organometallics* **1983**, *2*, 974.

(2) Masamune, S.; Murakami, S.; Tobita, H. *J. Am. Chem. Soc.* **1983**, *105*, 7776.

(3) (a) Seyferth, D.; Duncan, D. P.; Shannon, M. L. *Organometallics* **1984**, *3*, 579. (b) Seyferth, D.; Goldman, E. W.; Escudie, J. *J. Organomet. Chem.* **1984**, *271*, 337.

(4) Seyferth, D.; Shannon, M. L.; Vick, S. C.; Lim, T. F. O. *Organometallics* **1985**, *4*, 57.

(5) Ishikawa, M.; Matsuzawa, S. *J. Chem. Soc., Chem. Commun.* **1985**, 588.

(6) Ishikawa, M.; Matsuzawa, S.; Hirotsu, K.; Kamitori, S.; Higuchi, T. *Organometallics* **1984**, *3*, 1930.

(7) Ishikawa, M.; Matsuzawa, S.; Higuchi, T.; Kamitori, S.; Hirotsu, K. *Organometallics* **1985**, *4*, 2040.

0276-7333/86/2305-0182$01.50/0

single-crystal X-ray analysis[15] and by spectroscopic analyses.[16]

3b reacts similarly with 1 mol of diphenylacetylene and 2 mol of carbon monoxide to form $CoRh(CO)_6(\mu\text{-}\eta^2\text{-}PhC_2Ph)$ (**4b**)[17] according to Scheme II. Surprisingly, the reaction is fully reversible, such that upon bubbling N_2 into the reaction mixture **3b** reforms quantitatively.[18] Since **3b** does not react with **2b** in the absence of carbon monoxide, we have assumed that **3b** reacts first with CO and then with **2b**. This was evidenced by the reaction of **3b** with CO, performed in a medium-pressure (2–16 bar) glass autoclave connected to a high-pressure IR cell[19] using CO:N_2 (1:9).[20] At 0.3-bar partial CO pressure and 10 °C **3b** reacts with CO to give an equilibrium mixture[21] of **3b**, **4b**, and $CoRh(CO)_7$ (**5**).[22] By increasing the partial pressure of CO to 2 bar, **3b** disproportionates almost completely (>99.5%) to a 1:1 mixture of **4b** and **5**. Upon slowly removing the pressure and purging the solution with N_2, **4b** and **5** recombine to give **3b** quantitatively (Scheme III).

To best of our knowledge the reversible fragmentation of **3b** to **4b** (Scheme II) is the first example for a reversible tetranuclear–dinuclear transformation involving an "alkyne cluster", free alkyne, and carbon monoxide. Mechanistically, it is clear that **3b** reacts first with **CO**, which probably results in an unobserved intermediate such as $[Co_2Rh_2(CO)_{11}(PhC_2Ph)]$ (**6**). It is not apparent whether **6** is first attacked by CO or by free PhC_2Ph. However, if **6** is attacked first by carbon monoxide, **4b** and **5** can be formed according to Scheme III; **5** can subsequently react with the free PhC_2Ph to result in the "second" mole of **4b**. The most striking feature of Scheme II is the facile loss of the PhC_2Ph ligand and the regiospecific reformation of **3b**. Currently, there is no clear explanation for this unprecedented ligand loss.

Finally, it should be stressed that no spectroscopic evidence has been obtained for the existence of homonuclear cobalt or rhodium carbonyls in these reactions. This could mean that the heteronuclear metal–metal bond is stronger than the homonuclear bonds.

Acknowledgment. Portions of this research were supported by the "Schweizerischer Nationalfonds zur Förderung der wissenschaftlichen Forschung", No. 5.521.330.784/2. I.T.H. is grateful to Professors Piero Pino and György Bor for their helpful discussions.

Supplementary Material Available: Tables of bond distances and angles, positional and thermal parameters, and observed and calculated structure factors and an ORTEP drawing of **4a** (34 pages). Ordering information is given on any current masthead page.

(15) Crystal data: $C_{20}CoF_{10}O_6Rh$, M_r = 688.04, monoclinic, space group $p2_1/c$ (No. 14), a = 9.812 (6) Å, b = 15.582 (9) Å, c = 17.82 (1) Å, β = 127.85 (4)°, V = 2151 (5) Å^3, Z = 4, D_{calcd} = 1.83 g/cm^3. A total of 2121 reflections ($I \geq 2\sigma$) of 2578 reflections were used to give R_F = 12.6% and R_{F^2} = 12.7%. During the refinement it became clear that the cobalt and rhodium atoms are mutually disordered within the $CoRhC_2$ tetrahedron framework. The X-ray analysis cannot decide between the disorder of Co and Rh positions within the individual molecules in the crystal and a mixed-crystal containing Co_2C_2 or Rh_2C_2 cores. This later possibility was, however, ruled out by the significant differences between the spectroscopic data[16] of **4a** and $Co_2(CO)_6(\mu\text{-}\eta^2\text{-}F_5C_6C_2C_6F_5)$: Birchall, J. M.; Bowden, F. L.; Haszeldine, R. N.; Lever, A. B. P. *J. Chem. Soc. A* **1967**, 747. Thus, the molecule of **4a** consists of a sawhorse type of $CoRhC_2$ tetrahedral framework, and each metal atom is bonded to three linear terminal carbonyl ligands.

(16) For **4a**: MS, m/e 660 $(M - CO)^+$ plus ions corresponding to the loss of five CO ligands; IR (ν(CO) in *n*-hexane) 2110 m, 2077 vs, 2063 s, 2053 s, 2033 m cm^{-1}; ^{19}F NMR (in $CDCl_3$, in ppm from $CFCl_3$) −137.1 (q, 4 F), −154.5 (t, 2 F), −161.5 (m, 4 F).

(17) For **4b**: IR (ν(CO) in *n*-hexane) 2095 m, 2060 vs, 2044 s, 2034.5 s, 2015 m, 2009.5 m cm^{-1}; ^{1}H NMR (in CD_2Cl_2) 7.60–7.25 (m, 10 H) ppm.

(18) Repeating the reaction several times, **4b** can be recovered in 100% yield.

(19) Dietler, U. K. Ph.D. Thesis, No. 5428, ETH-Zürich, 1974.

(20) Before each spectrum was scanned, the cell was flushed with 5–10 mL of a fresh solution from the autoclave by opening a discharge valve placed after the cell. The total pressure and temperature were kept constant.

(21) K = [**3b**][CO]^3/[**4b**][**5**] = 3.3 × 10^{-4} mol^2 L^{-2} at 10 °C.

(22) Spindler, F.; Bor, G.; Dietler, U. K.; Pino, P. *J. Organomet. Chem.* **1981**, *213*, 303. Horváth, I. T.; Bor, G.; Garland, M.; Pino, P. *Organometallics*, submitted for publication.

Photolysis of Organopolysilanes. Photochemical Behavior of 3-Phenyl-4-[phenyl(trimethylsilyl)methylene]-1,1,2-tris(trimethylsilyl)-1-silacyclobut-2-ene and Molecular Structure of a Photoproduct

Mitsuo Ishikawa,* Hiroshi Sugisawa, and Shigeji Matsuzawa

Department of Synthetic Chemistry
Faculty of Engineering, Kyoto University
Kyoto 606, Japan

Ken Hirotsu and Taiichi Higuchi*

Department of Chemistry
Faculty of Science, Osaka City University
Sugimotocho, Sumiyoshi-ku, Osaka 558, Japan

Received August 27, 1985

Summary: The photolysis of 3-phenyl-4-[phenyl(trimethylsilyl)methylene]-1,1,2-tris(trimethylsilyl)-1-silacyclobut-2-ene produced 4,5-benzo-1,3-bis(trimethylsilyl)-2-[1-phenyl-2,2-bis(trimethylsilyl)ethenyl]-1-silacyclopenta-2,4-diene (**2**), via a 1-silabicyclo[2.1.0]pent-3-ene intermediate, which could be trapped by methanol. Similar photolysis of 1,4,4-trimethyl-3,6-diphenyl-1,2,5-tris(trimethylsilyl)-1,4-disilacyclohexa-2,5-diene also afforded compound **2**. Preliminary results of an X-ray diffraction study of **2** are also described.

Small ring compounds involving one or two silicon atoms in the ring are interesting because of their high-strain energy.[1-5] In this communication, we report novel photochemical behavior of 3-phenyl-4-[phenyl(trimethylsilyl)methylene]-1,1,2-tris(trimethylsilyl)-1-silacyclobut-2-ene (**1**), which can be prepared from the reaction of 3-phenyl-1,1,2-tris(trimethylsilyl)-1-silacyclopropene or (phenylethynyl)tris(trimethylsilyl)silane with phenyl(trimethylsilyl)acetylene in the presence of a nickel catalyst.[6,7]

When a solution of **1** (0.8483 g, 1.62 mmol) in 100 mL of dry benzene was irradiated for 70 min, with a high-

(1) (a) Ishikawa, M.; Sugisawa, H.; Kumada, M.; Higuchi, T.; Matsui, K.; Hirotsu, K.; Iyoda, J. *Organometallics* **1983**, *2*, 174. (b) Ishikawa, M.; Sugisawa, H.; Kumada, M.; Kawakami, H.; Yamabe, T. *Organometallics* **1983**, *2*, 974.

(2) Masamune, S.; Murakami, S.; Tobita, H. *J. Am. Chem. Soc.* **1983**, *105*, 7776.

(3) (a) Seyferth, D.; Duncan, D. P.; Shannon, M. L. *Organometallics* **1984**, *3*, 579. (b) Seyferth, D.; Goldman, E. W.; Escudie, J. *J. Organomet. Chem.* **1984**, *271*, 337.

(4) Seyferth, D.; Shannon, M. L.; Vick, S. C.; Lim, T. F. O. *Organometallics* **1985**, *4*, 57.

(5) Ishikawa, M.; Matsuzawa, S. *J. Chem. Soc., Chem. Commun.* **1985**, 588.

(6) Ishikawa, M.; Matsuzawa, S.; Hirotsu, K.; Kamitori, S.; Higuchi, T. *Organometallics* **1984**, *3*, 1930.

(7) Ishikawa, M.; Matsuzawa, S.; Higuchi, T.; Kamitori, S.; Hirotsu, K. *Organometallics* **1985**, *4*, 2040.

0276-7333/86/2305-0182$01.50/0

Scheme I

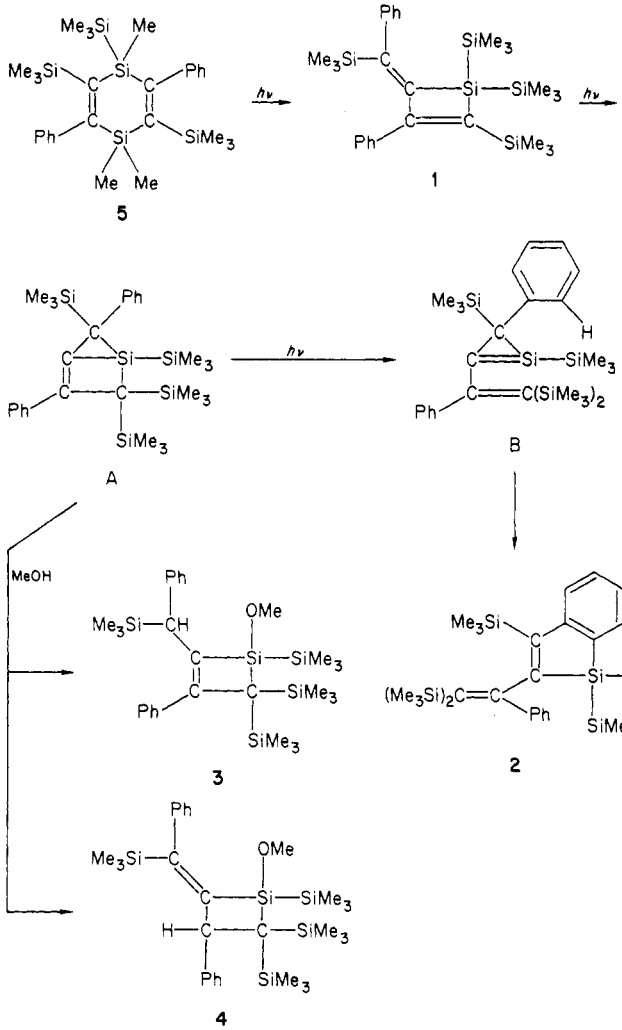

pressure mercury immersion lamp bearing a quartz filter under a nitrogen atmosphere, almost all the starting silacyclobut-2-ene **1** was cleanly photolyzed to give a white crystalline compound, 4,5-benzo-1,3-bis(trimethylsilyl)-2-[1-phenyl-2,2-bis(trimethylsilyl)ethenyl]-1-silacyclopenta-2,4-diene (**2**) (0.5983 g, 70% yield), as the sole product (Scheme I). The structure of **2** was confirmed by spectroscopic analysis[8] as well as an X-ray crystallographic analysis (see below). The IR spectrum of the product **2** shows a strong band at 2110 cm^{-1}, due to the stretching vibration of an Si–H bond. The fact that in the similar photolysis of **1** in deuteriobenzene, no product which contains an Si–D bond is detected by spectroscopic analysis indicates that hydrogen on the silicon atom must come from a phenyl group but not from the solvent used.

Next, we investigated the photochemical reaction of **1** in the presence of methanol, in order to trap the reactive species which would be formed in the photolysis. Thus, irradiation of **1** in the presence of a large excess of methanol in benzene under similar conditions afforded a 1:1 mixture of two methoxysilanes, 1-methoxy-3-phenyl-2-[phenyl(trimethylsilyl)methyl]-1,4,4-tris(trimethylsilyl)-1-silacyclobut-2-ene (**3**) and 1-methoxy-3-phenyl-2-[phenyl(trimethylsilyl)methylene]-1,4,4-tris(trimethylsilyl)-1-silacyclobutane (**4**), in 60% combined yield. No other products were detected by either HPLC or spectroscopic analysis. Products **3** and **4** thus formed could be readily isolated by medium-pressure liquid chromatography. Mass and ^1H, ^{13}C, and ^{29}Si NMR spectra obtained for **3** and **4** are wholly consistent with the proposed structure.[9,10]

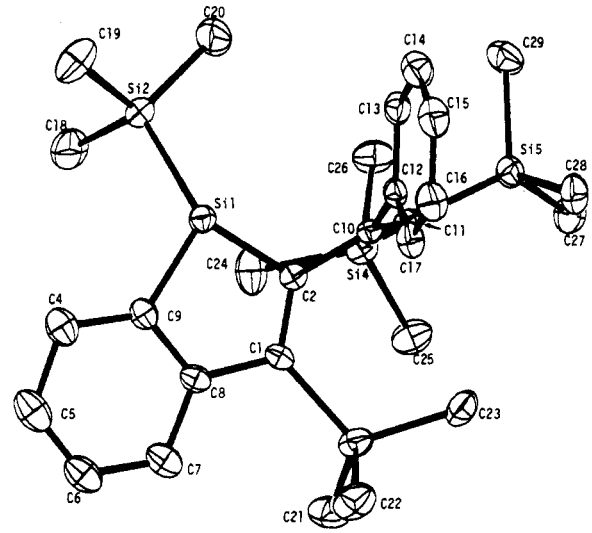

Figure 1. Molecular structure of **2** showing the atom numbering scheme. Selected bond distances (Å) and angles (deg): Si1–Si2 = 2.346 (4), Si1–C2 = 1.899 (9), Si1–C9 = 1.847 (10), C2–C10 = 1.507 (13), C1–C2 = 1.354 (12), Si3–C1 = 1.897 (9), C1–C8 = 1.484 (14), C8–C9 = 1.406 (13), C10–C11 = 1.334 (13), Si4–C11 = 1.909 (9), Si5–C11 = 1.908 (10); C9–Si1–C2 = 90.7 (4), C9–Si1–Si2 = 115.2 (3), Si2–Si1–C2 = 125.1 (3), Si1–C2–C1 = 110.2 (7), Si1–C2–C10 = 119.5 (6), C1–C2–C10 = 129.4 (8), C2–C1–C8 = 113.4 (8), C2–C1–Si3 = 127.5 (7), Si3–C1–C8 = 118.9 (6), C1–C8–C9 = 117.2 (8), C8–C9–Si1 = 107.9 (7).

The formation of **3** and **4** can be best understood by the reaction of 1-silabicyclo[2.1.0]pent-3-ene (**A**), produced photochemically from **1**, via a 1,2-shift of a trimethylsilyl group, with methanol. Direct evidence for the production of **A** has not yet been obtained. However, the photochemical 1,2-silyl shift to the unsaturated carbon atom in alkenyl- and alkynyldisilane systems is well-known.[11,12]

(8) Compound **2**: mp 158 °C; IR 2110 cm^{-1}; mass spectrum, *m/e* 522 (M^+); ^1H NMR δ (ppm in CCl_4) –0.11 (9 H, s, Me_3Si), 0.14 (9 H, s, Me_3Si), 0.23 (9 H, s, Me_3Si), 0.47 (9 H, s, Me_3Si), 3.56 (1 H, s, HSi), 6.8–7.6 (9 H, m, ring protons); ^{13}C NMR δ (ppm in $CDCl_3$) –0.4 (CH_3SiSi), 2.6 ($CH_3SiC{=}C$), 3.1 ($CH_3SiC(Si){=}$), 4.6 ($CH_3SiC(Si){=}$), 125.3, 126.1, 127.8 (two peaks), 129.0 (two peaks), 132.6, 136.9, 137.6, 146.4, 152.8, 154.5, 162.0, 168.9 (olefinic and ring carbons); ^{29}Si NMR δ (ppm in $CDCl_3$) –29.4 (SiH, $^1J_{Si-H}$ = 86.5 Hz), –17.3 (Me_3SiSiH), –7.5 ($Me_3SiC(SiMe_3){=}$), –7.3 ($Me_3SiC(SiMe_3){=}$), –6.5 (Me_3Si-C=). Anal. Calcd for $C_{28}H_{46}Si_5$: C, 64.29; H, 8.86. Found: C, 64.05; H, 8.83.

(9) Compound **3**: mp 170–172 °C; IR 1010, 1105, 1250, 1495, 1603 cm^{-1}; mass spectrum, *m/e* 554 (M^+); ^1H NMR δ (ppm in CCl_4) –0.11 (9 H, s, Me_3Si), –0.09 (9 H, s, Me_3Si), 0.13 (9 H, s, Me_3Si), 0.36 (9 H, s, Me_3Si), 2.99 (3 H, s, MeO), 3.29 (1 H, s, HC), 6.8–7.4 (10 H, m, phenyl ring protons); ^{13}C NMR δ (ppm in $CDCl_3$) –1.3 ($CH_2SiSi(OMe)$), 1.5 ($CH_3SiC(SiMe_3)$), 2.5 ($CH_3SiC(SiMe_3)$), 3.3 ($CH_3SiCH(Ph)$), 35.5 ($C(SiMe_3)_2$), 40.8 (CH(Ph)), 53.0 (CH_3O), 140.7 and 159.3 (olefinic carbons), 124.5, 126.7, 127.7, 128.1, 128.4, 128.7, 143.6, 145.6 (phenyl ring carbons); ^{29}Si NMR δ (ppm in $CDCl_3$) –20.0 ($Me_3SiSi(OMe)$), –2.6 ($Me_3SiCH(Ph)$), 0.8 ($Si(OMe)SiMe_3$), 2.9 ($Me_3SiC(SiMe_3)$), 3.1 ($Me_3SiC(SiMe_3)$). Anal. Calcd for $C_{29}H_{50}OSi_5$: C, 62.74; H, 9.08. Found: C, 62.76; H, 8.96. The structure for **3** is also supported by an X-ray crystallographic analysis: Higuchi, T.; Kamitori, S.; Hirotsu, K., to be submitted for publication.

(10) Compound **4**: mp 175–177 °C; IR 1010, 1100, 1250, 1495, 1603 cm^{-1}; mass spectrum, *m/e* 554 (M^+); ^1H NMR δ (ppm in CCl_4) –0.26 (9 H, s, Me_3Si), –0.24 (9 H, s, Me_3Si), –0.01 (9 H, s, Me_3Si), 0.28 (9 H, s, Me_3Si), 3.44 (1 H, s, HC), 3.68 (3 H, s, MeO), 7.0–7.4 (10 H, m, phenyl ring protons); ^{13}C NMR δ (ppm in $CDCl_3$) –1.8 ($CH_2SiSi(OMe)$), 1.4 ($CH_3SiC(SiMe_3)$), 2.4 ($CH_3SiC(SiMe_3)$), 3.4 ($CH_3SiC(Ph){=}$), 35.5 ($C(SiMe_3)_2$), 40.9 (CH(Ph)), 52.9 (CH_3O), 140.6 and 155.1 (olefinic carbons), 124.4, 126.8, 128.0 (br), 128.5, 128.8, 144.5, 148.1 (phenyl ring carbons); ^{29}Si NMR δ (ppm in $CDCl_3$) –19.2 ($Me_3SiSi(OMe)$), –7.8 ($Si(OMe)SiMe_3$), –2.8 ($Me_3SiC(Ph){=}$), 1.2 ($Me_3SiC(SiMe_3)$), 4.6 ($Me_3SiC(SiMe_3)$). Anal. Calcd for $C_{29}H_{50}OSi_5$: C, 62.74; H, 9.08. Found: C, 62.70; H, 8,89.

(11) Ishikawa, M.; Fuchikami, T.; Kumada, M. *J. Organomet. Chem.* **1978**, *149*, 37.

(12) Ishikawa, M.; Sugisawa, H.; Fuchikami, T.; Kumada, M.; Yamabe, T.; Kawakami, H.; Fukui, K.; Ueki, Y.; Shizuka, H. *J. Am. Chem. Soc.* **1982**, *104*, 2872.

The production of 4,5-benzo-1-silacyclopenta-2,4-diene **2** can be explained as a result of isomerization of a 1-silabutadiene derivative (B) generated photochemically from the intermediate A. The photochemical ring opening of a 1-silacyclobutene producing a 1-silabutadiene intermediate has been reported in the photolysis of 1,1-dimethyl-2-phenyl-1-silacyclobutene.[13]

Surprisingly, the photolysis of 1,4,4-trimethyl-3,6-diphenyl-1,2,5-tris(trimethylsilyl)-1,4-disilacyclohexa-2,5-diene[6,7] (**5**) in benzene again afforded compound **2** in 60% yield. Monitoring the photochemical reaction of **5** by ^{1}H NMR revealed that signals of the trimethylsilyl groups attributed to **2** increase as those of the starting **5** decrease. Furthermore, resonances with low intensities due to the trimethylsilyl groups of **1** are also observed during the photolysis, showing that photochemical isomerization of **5** to **1** is involved in this reaction. In fact, similar photolysis of **5** in the presence of methanol gave a 1:1 mixture of **3** and **4** in 60% combined yield.

Compound **2** crystallizes in the triclinic space group $P\bar{1}$ with cell dimensions a = 12.476 (1) Å, b = 12.074 (1) Å, c = 11.053 (1) Å, α = 88.10 (1)°, β = 91.80 (1)°, γ = 95.97 (1)°, V = 1654.4 (2) Å^3, D_{calcd} (Z = 2) = 1.050 Mg m^{-3}, and μ(Mo Kα) = 2.3 cm^{-1}. Intensity data were collected on a Philips PW1100 diffractometer with graphite-monochromated Mo Kα radiation. A total of 4077 independent reflections were obtained for a θ range of 2.0–20.0° using the ω-scan mode with speed of 3.6°/min, of which 2401 [$I_o > 2\sigma(I_o)$] were used in the least-squares refinement. The structure was solved by MULTAN.[14] Refinement for all non-hydrogen atoms, assigned anisotropic temperature factors, converged to an R value of 0.079. Figure 1 shows the molecular structure of **2** which involves a condensed ring system (silaindenyl ring). The silaindenyl ring is nearly planar (<0.04-Å deviation), with the exception of the C2 atom with a deviation of 0.09 Å. In the five-membered ring, the bonding around the Si1 atom can be viewed as a highly distorted tetrahedron where the bond angles of C2–Si1–C9, Si2–Si1–C9, and Si2–Si1–C2 are 90.7 (4), 115.2 (3), and 125.1 (3)°, respectively. The length of the Si1–C9 (aromatic carbon) bond is shorter than those of the silicon–carbon bonds in which the silicon atoms bond to the aliphatic unsaturated carbon atoms, the Si1–C2, Si3–C1, Si4–C11, and Si5–C11 bonds. A hydrogen atom bonded to the Si1 atom is revealed in a difference-Fourier map, H–Si1–X (X = C2, C9, and Si2) = 108 ± 2° and Si1–H = 1.39 Å. The geometry around the C2 atom is almost trigonal. Two double bonds, C1–C2 and C10–C11, are twisted to each other by 76.7° with respect to the C2–C10 bond, that is, the plane defined by atoms C1, C2, and C10 intersects the C2, C10, C11 plane with a dihedral angle of 76.7°.

Acknowledgment. We are indebted to the Computation Centers of Osaka City University and Osaka University and to the Crystallographic Research Center, Institute for Protein Research, Osaka University, for computer calculations.

Supplementary Material Available: A listing of observed and calculated structure factors and tables of positional and anisotropic thermal parameters, deviation of atoms from the least-squares plane, and bond lengths and angles (14 pages). Ordering information is given on any current masthead page.

(13) Tzeng, D.; Fong, R. A.; Soysa, H. S. D.; Weber, W. P. *J. Organomet. Chem.* **1981**, *219*, 153.
(14) Germain, G.; Woolfson, M. M. *Acta Crystallogr., Sect. B: Struct. Crystallogr. Cryst. Chem.* **1968**, *24B*, 91.

Book Reviews

Inorganic Syntheses. Vol. 23. S. Kirschner, editor-in-chief. Wiley, New York. 1985. xxii + 257 pages. $39.95.

The latest addition to this well-established and highly valued series starts off with a 46-page chapter on organometallic compounds: the syntheses of (substituted thiourea)Cr(CO)$_5$ complexes; dicarbonylnitrosyl[tris(3,5-dimethylpyrazolyl)hydroborato]molybdenum(III) compounds; diisocyanide complexes of Mo(0) and W(0) and derived aminocarbyne complexes; η^5-pentamethylcyclopentadienyl cobalt complexes (including the very useful η^5-$Me_5C_5Co(C_2H_4)_2$); diphenyltin dibromide; carbonyl(pentafluorophenyl)cobalt(I) and -(II) complexes; potassium (μ-hydrido)bis[pentacarbonylchromium(0)] and -bis[pentacarbonyltungsten(0)]; [Mn(CO)$_4$X]$_2$; Na[Nb(CO)$_6$]; disubstituted derivatives of Cr(CO)$_6$ and (OC)$_5$ReX. Quite a mixture, but every one of these syntheses will be of use to someone—the sheer volume of organometallic research going on these days will ensure that. In addition, organometallic chemists will find syntheses of interest in the fourth chapter which is devoted to bridge and cluster compounds and in the fifth chapter in which syntheses of unusual ligands and compounds are provided. Other chapters cover syntheses of compounds of biological interest and of stereoisomers (the latter topic no surprise in view of the research interests of the editor).

The value of the Inorganic Syntheses volumes lies in their clear exposition of synthetic procedures which have been tested by workers other than the submitters. Useful hints and, just as important, potential hazards are given.

The inorganic/organometallic community is indebted to the editor, the submitters, and the checkers for another useful Inorganic Syntheses volume.

Dietmar Seyferth, *Massachusetts Institute of Technology*